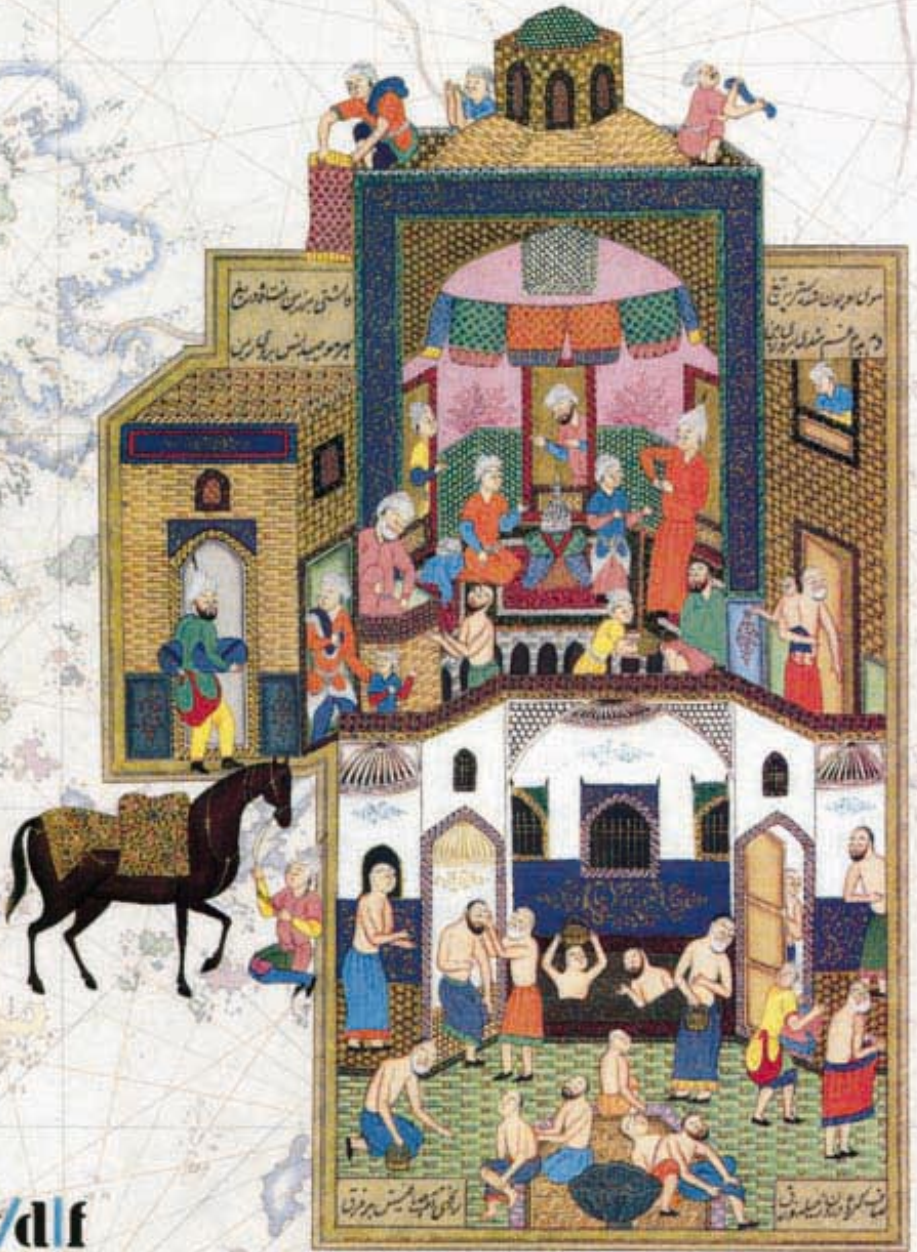
Active Tectonics of Northwestern Anatolia – The MARMARA Poly-Project

A Multidisciplinary Approach
by Space-Geodesy,
Geology, Hydrogeology,
Geothermics and Seismology



v/d/f

Die Deutsche Bibliothek - CIP-Einheitsaufnahme

Conrad Schindler, Martin Pfister (eds.)

Active Tectonics of Northwestern Anatolia - The MARMARA Poly-Project
A Multidisciplinary Approach by Space-Geodesy, Geology, Hydrology, Geothermics and Seismology

Das Werk einschließlich aller seiner Teile ist urheberrechtlich geschützt. Jede Verwertung außerhalb der engen Grenzen des Urheberrechtsschutzgesetzes ist ohne Zustimmung des Verlags unzulässig und strafbar. Das gilt insbesondere für Vervielfältigungen, Übersetzungen, Mikroverfilmungen und die Einspeicherung und Verarbeitung in elektronischen Systemen.

ISBN 3- 7281-2425-7
© 1997, vdf Hochschulverlag AG an der ETH Zürich

Table of contents

Preface V
CONRAD SCHINDLER

Main contributors and authors: IX

Theme 1: Introduction **1**

The MARMARA Poly-Project: an introduction 3
MARTIN PFISTER AND CONRAD SCHINDLER

Theme 2: Plate tectonics **11**

Plate tectonic situation in the Anatolian-Aegean region 13
STEPHAN MUELLER, HANS-GERT KAHLE AND AYKUT BARKA

Theme 3: General overview **29**

Geology of Western Anatolia 31
YÜCEL YILMAZ

Neotectonics of the Marmara region 55
AYKUT BARKA

Seismic investigations of the Marmara region 89
BALAMİR ÜÇER, HALUK EYIDOĞAN, CEMİL GÜRBÜZ, AYKUT BARKA AND ŞERIF BARIŞ

Activities for the determination of crustal movements in Turkey 101
AHMET AKSOY AND RASIM DENİZ

Geothermal potential in Northwestern Turkey 111
ŞAKİR ŞİMŞEK

Hydrogeology of Northwestern Turkey 125
ERDOĞAN YÜZER

Theme 4: Recent investigations in geology and hydrogeology **139**

Stratigraphic evolution and tectonics in an area of high seismicity:
Akyazı/Adapazarı (Pontides, Northwestern Turkey) 141
EMIL GREBER

Deep circulation of CO_2-rich paleowaters in a seismically active zone
(Kuzuluk/Adapazarı, Northwestern Turkey) 161
EMIL GREBER

Observed pressure variations and their causes in the geothermal field of
Kuzuluk / NW Turkey 185
SILVIO TSCHUDI

The thermal springs of the Armutlu peninsula (NW Turkey) and their
relationship to geology and tectonic 197
THOMAS EISENLOHR

Environmental isotope study and 2-D-modelling of cold and thermal karst within the Gemlik (Bursa) area of Northwestern Turkey 229
THOMAS EISENLOHR, MARTIN PFISTER AND WERNER BALDERER

Geology of Mount Uludağ with emphasis on the genesis of the Bursa thermal waters, Northwest Anatolia, Turkey 239
THOMAS IMBACH

Hydraulic level variations in a thermal water well: Impact of precipitation on the Çekirge thermal water system 267
EMIL GREBER, MARTIN PFISTER AND THOMAS IMBACH

Hydrogeological investigation of the Gönen and Ekşidere thermal waters (NW Turkey) 275
TOLGA YALÇIN

Nature and origin of the thermal springs in the Tuzla area, Western Anatolia, Turkey 301
STEFAN MÜTZENBERG

Regional investigation of cold groundwater for the determination of recharge conditions in geothermal areas of Northwestern Turkey 321
THOMAS EISENLOHR, CHRISTOF JECKELMANN, WERNER BALDERER, STEFANO BERNASCONI, WALTER RAUERT AND PETER TRIMBORN

Theme 5: Regional contributions **327**

Geology of Northwestern Turkey: Results of the MARMARA Poly-Project 329
CONRAD SCHINDLER

Mechanisms and processes of groundwater circulation in tectonically active areas 375
WERNER BALDERER

Recent crustal deformation and strain accumulation in the Marmara sea region, NW Anatolia, inferred from repeated GPS measurements 417
CHRISTIAN STRAUB AND HANS-GERT KAHLE

Seismicity and seismotectonics of the Bursa region 449
SOUAD SELLAMI, NAZARIO PAVONI, DIETER MAYER-ROSA, STEPHAN MUELLER, HALUK EYIDOĞAN, MUSTAFA AKTAR, CEMİL GÜRBÜZ, ŞERİF BARİŞ, ORHAN POLAT AND NAMİK YALCIN.

Gravimetric studies of the Marmara sea region 487
EMILE KLINGELÉ AND FAUSTO MEDICI

Geothermal reconnaissance of the Marmara sea region 503
MARTIN PFISTER, LADISLAUS RYBACH AND ŞAKİR ŞİMŞEK

Theme 6: Synthesis **537**

Synthesis of the MARMARA Poly-Project 539
MARTIN PFISTER, WERNER BALDERER, EMIL GREBER, HANS-GERT KAHLE, DIETER MAYER-ROSA, STEPHAN MUELLER, LADISLAUS RYBACH, CONRAD SCHINDLER, SOUAD SELLAMI AND CHRISTIAN STRAUB

Index **567**

Preface

CONRAD SCHINDLER

In 1988, a new kind of scientific concept was created at the ETH Zürich, a so-called "Poly-Project". The idea was to study complex scientific subjects using an interdisciplinary approach also involving foreign universities. Thus, the idea for the "MARMARA Poly-Project" began with a draft project submitted in July 1988, followed by a final draft in October 1989 and the official start in January 1990. The project included three periods of two years, ending in December 1995. However, saved research money allowed us to continue work until Spring 1997. During this additional time the last two doctoral theses were completed, a synthesis was made and the final publication was prepared.

Northwestern Anatolia, including the Marmara sea region, proved to be, for Earth sciences, the ideal opportunity for an efficient collaboration of representatives from different disciplines. In this part of Turkey, active crustal movements take place, combined with very high seismicity and numerous outflows of thermal waters and gas outputs. Previous work in Turkey by N. Pavoni and C. Schindler and existing contacts with Turkish scientists were very favourable for the initiation of scientific investigations in Turkey. Work and progress would never have been possible without the logistic and scientific support of Turkish universities, research centres and state owned organisations, our main partner being the Technical University of İstanbul (İTÜ). The first enthusiastic promoter of the MARMARA project on behalf of the İTÜ was the outstanding engineering geologist Kemal Erguvanli. Unfortunately he died soon after the work had begun.

The main *aim of the MARMARA Poly-Project* was to study tectonic activities and their relationship to the circulation of normal and geothermal waters, the distribution of zones with elevated seismicity and the spatial heat flow pattern. All of the scientists involved worked, in different disciplines such as Geology, Hydrogeology, Geodesy, Geothermics and Seismology and were dependent on each other. For this reason, information was exchanged periodically in conferences held in Zürich and seminars in İstanbul completed by shared field trips in Turkey. The contacts between Turkish and Swiss scientists were also intensified through the exchange of students and advisers for PhD theses. Parallel to the increasing knowledge concerning the investigated objects, co-operation between the research groups became very close and peaked during the period when this final report had to be drafted and written. Additional scientists from Switzerland and Turkey who helped to complete or add to the previous work of the MARMARA project with their contributions were contacted during this period.

Evolution of the project

Not all participants in Switzerland and Turkey began their work at the same time. The first group, *Geology and Hydrogeology*, already started work in Turkey in 1986, four years before the MARMARA project was launched. Through this, a reliable basis was created for the groups which followed. Up to the end of the project, a total of five Swiss and one Turkish student worked on separate areas of special geological and geothermal interest, including detailed mapping at the scale of 1:25,000. These studies were able to be completed by previous work done for petroleum research in the years 1956 – 1959 by two of the authors (Pavoni and Schindler), however, no additional studies were made, as thermal springs do not exist in these areas.

In order to confirm crustal movements along fault lines as suggested by the geologists, some 50 GPS-stations were installed all over NW Turkey by the *Geodesy* group according to the indications of the geologists. The first measurements were made in 1990, steadily improving in quality during the campaigns of 1992, 1994 and 1996. Besides the groups from the ETH and the İTÜ, the General Command of Mapping (GCM) participated in this project. The GPS stations were concentrated in tree large areas, each covering the North Anatolian Fault Zone system and reaching the more stable areas to the south and to the north. 10 of our GPS stations were measured again in 1996, this in the context of an international project covering large parts of the Eastern Mediterranean.

In 1991, the *Geothermics* group made borehole measurements over the entire research area, including the Ergene basin in Thrace. The purpose was to establish a heat flow map covering a large area of NW Turkey and to find correlations with the results of the other disciplines. Based on data provided by the Geology and Hydrogeology group, numerical models of selected thermal water systems were developed.

The *Seismology* group started their work in 1992. The main subject of the scientists from the ETH, the İTÜ, the Observatory of Kandilli and Tübitak was the investigation of the region of Bursa. Twelve new seismic stations were installed there in 1992. Attention was also paid to the seismicity and its relationships with neotectonics for the other areas where the MARMARA project was underway. However, the database used there was completely furnished from the Turkish stations.

All field studies of the MARMARA project were finished by the end of 1995 (except Seismology). An extensive synthesis of the results of each group started at that time. Concurrently, Turkish scientists worked on Theme 3 which synthesises the actual state of the knowledge in Earth sciences in Western Turkey outside of the MARMARA project.

Organisation

Even though the project was guided and co-ordinated by C. Schindler, the various groups and especially their leaders, were responsible for their own work. The organisation at the ETH had a counterpart at the İTÜ, directed by E. Yüzer, with one or more representatives of each group. Apart from these direct partners, co-operation was also established with other scientists in Turkey, as well as in other countries. The names of all the persons involved appear in the respective themes.

For the co-ordination of the groups, for the work on a general synthesis and for the preparation of the final report a full time postdoctoral fellow was at the disposal of the MARMARA project co-operating closely with C. Schindler. This key job was carried out by Th. Imbach (1992-1994) and for the final stage by M. Pfister (1995-1997), both former PhD students of the project.

Remarks on the final report

The present publication contains, in a condensed form, contributions from many authors. They alone are responsible for the content of their papers. Included are summaries from the ETH dissertations carried out in the framework of the MARMARA project. They were printed in full in German or English, but are available only in limited numbers, copies, as well as the complete database, are available for consultation at ETH-Hönggerberg.

Current knowledge concerning stratigraphy, tectonics, geothermics and the structure of the lithosphere in NW Turkey lies at a much lower level than in Central Europe, for example, where Earth science research began more than 100 years ago. In addition, good outcrops and long sequences of stratigraphic profiles are missing over large areas and fossiliferous series are sparse. As neotectonics often obliquely cut older structures and disturb them intensively, the reconstruction of pre-tertiary development becomes very difficult. Therefore, it is not surprising that large differences exist not only in the interpretation of age and tectonic history of the series older than Upper Cretaceous, but also for many other questions. Controversies can be observed between older and more recent publications and also among current interpretations. Therefore, some controversial interpretations can be recognised if different papers of the final report are compared. As many problems can not be currently solved in a definitive way, different opinions were expressed in the hope that the future will bring clear answers. The external conditions in the working field of the MARMARA project may be difficult. On the other hand, they are fascinating and a challenge to everyone concerned.

This final report starts with an introduction (Theme 1) to the investigated Marmara sea region and to the main aims and problems of the Poly-Project. It is followed by a general view of Eastern Mediterranean plate tectonics in Theme 2. Turkish colleagues give a condensed overview of the actual knowledge in the different research disciplines for the area of Western Turkey (Theme 3). Different papers from the extensive Geology and Hydrogeology groups are collected in Theme 4. These studies were carried out in locally restricted areas. Condensed regional evaluations of the results according to single disciplines follow in Theme 5. These contributions are representative of the Turkish-Swiss collaboration under the guidance of the different group leaders. The articles of Theme 4 and 5 show interdisciplinary aspects already and results as they were written after intensive mutual contacts. In the last part of the final report (Theme 6), an attempt is made by a few persons included in the MARMARA Poly-Project to pursue the interdisciplinary approach even farther and to obtain results from the large field existing between the specialists – a very difficult and uncommon task. The proposed results may open the way for many further discussions.

Acknowledgements

The MARMARA Poly-Project was financed and supported by the Swiss Federal Institute of Technology (ETH Zürich). I would like to thank Vicepresident R. Hütter and the research commission of the school for their broadmindedness and confidence. The very effective and straightforward assistance was of great help during all stages of the project. Similar generous support came from the İstanbul Technical University: on one hand the project was sponsored by the research fund (İTÜ araştırma fonu), and on the other hand the entire infrastructure of the İTÜ, the always ready guesthouse and various invitations helped the project to survive.

Thanks go to all colleagues at the ETH and the İTÜ involved within the MARMARA Poly-Project. I remember intensive and agreable collaboration, fruitful and intense discussions and shared adventures, not only with my PhD students, but also with all the other research group members or leaders, in Turkey as well as in Switzerland.

Special thanks go my colleague E. Yüzer of the İTÜ: he organised numerous seminars, diverse social events, excursions and prepared the necessary political contacts within the diverse investigation areas. I also remember fondly our former colleague K. Erguvanli who was our project partner and pathfinder during the first years. M. Vardar, O. Dumlu (İTÜ) and O. Eroskay (İstanbul University) contributed valuable assistance, help and scientific knowledge to the project, and prepared an atmosphere of friendship. Thanks to you all of you!

St. Mueller supported with all his forces, his experience and wisdom our project until his premature death in February 1997. We remember him for ever with great respect and appreciation.

Numerous persons and institutions supported the project:
in Switzerland: E. Klingelé, R. Gysin, S. Tschudi, P. Smith, M. Spühler, M. Gurtner, P. Signer, M. Grünenfelder, L. Martinenghi, J. McKenzie (ETH Zürich); Institutions: EAWAG (Dübendorf), WSL (Birmenstorf), Institutes of Geophysics, Geology and Geodesy at ETH Zürich.
in Germany: H. Woith (GfZ Potsdam); Institutions: gsf (Neuherberg, Munich).
in Turkey: E. Saker and H. Tezel (DSİ Bursa), O. Öztuncer (Yeni Kaplıca Bursa), G. Dikmen (Köy Hizmetleri Balıkesir), İ. Kınık (GCM); Institutions: DSİ (State department for water resources), MTA (State department for mining purposes), GCM (General Command of Mapping in Ankara), Kandilli Observatory, Tübitak Organisation, Köy Hizmetleri (State department for rural purposes).

My wife Ursula often took part in our excursions, establishing personal contacts and pointing our attention to the fascinating living Turkey around us after endless scientific discussions.

Finally, I would like to thank the Turkish people for their hospitality and generosity. The warm welcome and help will never be forgotten; we experienced an eventful and beautiful time.

Main contributors and authors:

Name	Institution	Adress	e-mail
Prof. Dr. A. Aksoy	İnşaat Fakültesi İTÜ	İTÜ Ayazağa Kampüsü TR-80626 Maslak, İstanbul	aksoy@ sariyer.cc.itu.edu.tr
Prof. Dr. M. Aktar	TÜBİTAK Research Centre	TÜBİTAK Marmara Araştirma Merkezi, PK 21 TR-4170 Gebze Kocaeli	aktar@mam.gov.tr
PD Dr. W. Balderer	Engineering Geology ETH Zürich	ETH Hönggerberg CH-8093 Zürich	balderer@ erdw.ethz.ch
Dr. Ş. Bariş	Kandilli Rasathanesi ve Deprem Araştirma Enstitüsü	Boğaziçi Üniversitesi TR-Çengelköy, İstanbul	baris@ hamlin.cc.boun.edu.tr
Prof. Dr. A. Barka	Maden Fakültesi İTÜ	İTÜ Ayazağa Kampüsü TR-80626 Maslak, İstanbul	barka@ sariyer.cc.itu.edu.tr
Dr. R. Deniz	İnşaat Fakültesi İTÜ	İTÜ Ayazağa Kampüsü TR-80626 Maslak, İstanbul	
Dr. Th. Eisenlohr	H. Jäckli AG Zürich, Switzerland	Bettenstr. 44 (private) CH-8400 Winterthur	
Prof. Dr. H. Eyidoğan	Jeofizik Mühendisliği Bölümü İTÜ	İTÜ Ayazağa Kampüsü TR-80626 Maslak, İstanbul	mdeyido@ cc.itu.edu.tr
Dr. E. Greber	Geoform Winterthur, Switzerland	Dienerstr. 36 (private) CH-8004 Zürich	
Prof. Dr. C. Gürbüz	Kandilli Rasathanesi ve Deprem Arastirma Enstitüsü	Boğaziçi Üniversitesi TR-Çengelköy, İstanbul	gurbuz@ hamlin.cc.boun. edu.tr
Dr. Ch. Jeckelmann	CSD Aarau, Switzerland	Hönggerstr. 41 (private) CH-8037 Zürich	
Dr. Th. Imbach	H. Jäckli AG Zürich, Switzerland	Limmatstr. 211 (private) CH-8005 Zürich	101744.2744@ com-puserve.com
Prof. Dr. H.-G. Kahle	Institute of Geodesy ETH Zürich	ETH Hönggerberg CH-8093 Zürich	hans-gert.kahle@ geod. ethz.ch
Prof. Dr. E. Klingelé	Institute of Geophysics ETH Zürich	ETH Hönggerberg CH-8093 Zürich	emile.klingele@ geod.ethz.ch
Dr. D. Mayer-Rosa	Institute of Geophysics ETH Zürich	ETH Hönggerberg CH-8093 Zürich	mayer-rosa@ seismo.ifg. ethz.ch
Prof. Dr. St. Mueller †	Institute of Geophysics ETH Zürich	Frohburgstr. 138 (private) CH-8057 Zürich	
Dr. St. Mützenberg	H. Jäckli AG Zürich, Switzerland	Pfaffenzielstr. 16 (private) CH-5300 Ennetturgi	
Dr. N. Pavoni	Institute of Geophysics ETH Zürich	Sonnenbergstr. 11 (private) CH-8134 Adliswil	
Dr. M. Pfister	GSF München, Insitute of Hydrology	Palmstrasse 4 (private) D-80496 München	martin.pfister@gsf.de
Prof. Dr. L. Rybach	Institute of Geophysics ETH Zürich	ETH Hönggerberg CH-8093 Zürich	rybach@ geo.phys.ethz.ch
Prof. Dr. C. Schindler	Engineering Geology ETH Zürich	Schwerzestr. 7 (private) CH-8616 Oetwil am See	
Dr. S. Sellami	Institute of Geophysics ETH Zürich	ETH Hönggerberg CH-8093 Zürich	sellami@ seismo.ifg.ethz.ch
Dr. Ch. Straub	Institute of Geodesy ETH Zürich	Weihermattstr. 3 (private) CH-8902 Urdorf	christian_straub@union-re.com

X Main contributors and authors:

Name	Institution	Adress	e-mail
Prof. Dr. Ş. Şimşek	UKAM Hacettepe Üniversitesi	Beytepe Kampüsü TR-06532 Beytepe, Ankara	ukam@ jeo.hun.edu.tr
S. Tschudi	Institute of Particle Physics ETH Zürich	ETH Hönggerberg CH-8093 Zürich	tschudi@ particle.phys. ethz.ch
Dr. B. Üçer	Kandilli Rasathanesi ve Deprem Araştirma Enstitüsü	Boğaziçi Üniversitesi TR-Çengelköy, İstanbul	
Prof. Dr. N. Yalcın	TÜBİTAK Research Centre	TÜBİTAK Marmara Araştirma Merkezi, PK 21 TR-4170 Gebze Kocaeli	yalcin@ mam.gov.tr
T. Yalcın	Maden Fakültesi İTÜ	İTÜ Ayazağa Kampüsü TR-80626 Maslak, İstanbul	kocak@ sariyer.cc.itu.edu.tr
Prof. Dr. E. Yüzer	Maden Fakültesi İTÜ	İTÜ Ayazağa Kampüsü TR-80626 Maslak, İstanbul	kocak@ sariyer.cc.itu.edu.tr
Prof. Dr. Y. Yılmaz	Maden Fakültesi İTÜ	İTÜ Ayazağa Kampüsü TR-80626 Maslak, İstanbul	yilmaz@ sariyer.cc.itu.edu.tr

THEME 1

Introduction

The MARMARA Poly-Project: an introduction

MARTIN PFISTER AND CONRAD SCHINDLER

The Marmara region in Northwestern Anatolia represents an area of major earthquake occurrence caused by recent tectonic activity of the Earth's crust and accompanied by numerous thermal springs and geothermal fields. The possibility to observe an ongoing deformation of the Earth's crust with such an intensity is unique and, therefore, extremely promising.

As a consequence of the collision of the Arabian with the Eurasian plate, other plates – including the Turkish plate – are moving away from the Caucasus. Because of this structural lithospheric setting, the sinistral East Anatolian and the dextral North Anatolian strike-slip faults have been neotectonically active. The North Anatolian Fault Zone (NAFZ) is the dominant feature in the research area and forms a tectonic connection between the East Anatolian convergent zone and the Hellenic trench, where the motion is compensated by the consumption of oceanic crust (Şengör 1979).

The strong seismic activity of the research area is triggered mainly by the westward moving Turkish plate (McKenzie 1972) combined with the southward extension of the Aegean and westernmost Anatolian realm. More to the east, the NAFZ is characterised by quite a narrow strike-slip zone with occasional pull-apart basins, but in the project realm it progressively splits up to the west. The pure strike-slip regime changes into a stress regime with additional N-S extension.

The NAFZ is characterised by elongated valleys, rift morphology, isolated hills, pull-apart basins, tectonic breccias, crushed tectonic lenses, fault scarps, landslides, diverted river courses, as well as high seismicity and hot springs. South of the NAFZ, Horst-Graben like structures developed in the research area due to the extensional forces of the Aegean system.

The Geology exhibits a complex interplay of various, partly metamorphic or magmatic, rocks recalling changing tectonic regimes as far as back to Variscan orogenies. To understand the present conditions, the past has to be analysed. This is a difficult, but fascinating, task. Besides, new space geodetic developments have had a great impact on geodynamic theories since they have measured the rates of moving lithosphere over long distances (hundreds of kilometers) even though the displacements are relatively small (<150mm/a).

Interrelations between surface ruptures, groundwater and earthquakes in history

Looking back into history, earthquakes and surface ruptures of the Earth's crust have always fascinated philosophers and natural scientists. In ancient Greece, the philosopher Democrites from Milet (south of current day İzmir on the western coast of Turkey) explained in the Pleiade the cause for earthquakes by water transport or 'wind' in the underground (Democrites, 2000 BP). Nowadays, we cannot imagine any air turbulence in the Earth's underground, but the influence of fluid circulation on the release of earthquakes has developed as a key problem of modern geoscience.

In the 19th century AD, important observations about fluids in the Earth's crust were presented in literature. Among these, observations were also made in Northwestern Anatolia: the large earthquakes on April 4th, 1850, and on April 11th, 1855, in the environs of the beau-

tiful city of Bursa, a former sultan's capital, caused enormous destruction and visible displacements of the Earth's crust. The occurrence of new hot springs in Çekirge and Kükürtlü, two thermal spa districts in Bursa dating back to Byzantine times, were documented (Palmerston 1851, Sandison 1855, see also Imbach this volume). These new springs subsequently partly disappeared, the old ones remained and some of them slightly changed their outflow characteristics, but the main portion could still be used for thermal spa purposes. Kluge (1858) described the important earthquakes of the years 1855 and 1856 in his article "Die Reaktion des Erdinnern gegen die Erdoberfläche in den Jahren 1855 und 1856". He too recognised significant changes in the thermal spring behaviour in Bursa caused by these large earthquakes. But without the knowledge of plate tectonics at that time, he postulated an active zone of elevated seismicity parallel to the equator going around the world in the northern hemisphere.

Based on observations of rocks exposed at the surface which show fractures as well as ductile deformations, new conclusive questions were established. If we can assume fluid circulation within the crust, how deep do these fluids circulate and how deep do the fractures reach? And further, is the whole crust fractured or where does a so-called ductile zone begin? Is fracturing the only generating process for earthquakes? During the year 1912, Frank D. Adams wrote an article entitled 'An experimental contribution to the question of the depth of the zone of flow in the Earth's crust'. According to him, 'this subject has an interest and importance, not only as bearing many problems in geology, but also on one question at least of direct importance in mining, namely, that of the depth to which mineral bearing fissures may extend in the Earth's crust'. This depth range was thought to be a gradual zone, where the brittle behaviour changes into a ductile one. The model of a brittle, fractured upper crust with a change in rheology at greater depths to a zone of flow (ductile regime) was also proposed by the geologist Albert Heim, 30 years previously, from observations in the Swiss Alps. Finally, the main conclusions of Adams were the possible presence of fluids up to depths of 11 miles below the surface and the importance of water in the crust for the release of earthquakes.

Methods used in the MARMARA Poly-Project

This collection of historical quotations outlines the complex interplay between active tectonics, groundwater circulation, seismicity and the thermal state of the Earth's crust. Modern reflections speak about interrelations of physical, structural and chemical factors which control faulting of the crust. Main controlling factors are probably geological conditions, geophysical parameters or geochemical composition (structural orientation, rock fabric, grain size, strain localisation, age and total displacement of fault zones, temperature, stress, strain rate, crack size, fault roughness, porosity, fluid pressure, permeability, mineral assemblage, pore-fluid chemistry).

Data concerning these factors had to be collected in NW Turkey, this forcing various research disciplines to carry out detailed observations. The geoscience endeavour was therefore to combine the results of individual disciplines into an overall picture, a multidisciplinary synthesis. In the following, we shall try to explain some of the key research aspects of the different single disciplines, as well as give a short outlook on the multidisciplinary approach.

Geology The geological study serves as a basis for all other disciplines: a thorough comprehension of local and regional tectonic/geological evolution is essential. Special attention should be paid to fault phenomena of the neotectonic stress regime, including the deformation behaviour of different rock types. However, tectonic events and structures older than Miocene were also studied in detail, as they might have had an influence on the circulation

patterns of normal or thermal groundwater, on the orientation of neotectonic disturbances and the modern stress field. From these tectonic studies, a better understanding of the actual crustal motion pattern was obtained, which will be compared with the geodetic and seismic observations.

Hydrogeology The hydrogeological study tries to explain the existence of thermal and mineral waters within the local normal groundwater circulation system. Every step of groundwater evolution between infiltration and exfiltration area needs to be reconstructed. All of the different processes of water evolution, such as rock-water-gas interaction, gas exchange, heating and mixing, must be the subject of thorough investigation. The interpretation of thermal and mineral waters as a product of groundwater evolution requires a detailed study of the local normal groundwater system.

Geodesy Applying GPS (Global Positioning System) technology, large geodetical networks over distances of hundreds of kilometres can be constructed and measured in short time. Second and third measurements of the same network after several years allow the interpretation of coordinate differences by geodynamic explanations. The motion of upper crust blocks due to plate tectonics is characterised by the calculated velocity field and strain rate pattern.

Geothermics Terrestrial heat flow as a main boundary condition of geodynamic processes is calculated using the following two observable quantities. First, a geothermal gradient is determined by geophysical logging of existing drillholes; second, thermal conductivity of the main lithologies is measured on rock samples in the laboratory. Interpolation of the irregularly distributed point determinations leads to the regional surface heat flow field. Furthermore, numerical modelling of coupled thermohydraulic processes is able to describe groundwater flow and the special conditions for the presence of thermal springs. Geothermal methods, therefore, provide a powerful tool for investigating deep-reaching groundwater circulation systems on the one hand, and to interpret the spatial pattern of seismicity in terms of crustal rheology on the other.

Seismology Distinct seismoactive structural features have to be defined to establish the relationship between local tectonics and seismicity, based on the precise distribution of microearthquakes and the types of observed focal mechanisms. This allows scientists to gain insight into the present strain and stress state of the crust.

Gravimetry The Earth's gravity field and its anomalies indicate mass lows and highs. Significant anomalies can be interpreted as thinning or thickening processes of the crust or lithosphere. These findings will be major indications for a possible extensional neotectonic process.

The picture of the present neotectonic activity and its influence on different observable quantities such as seismicity, groundwater circulation and terrestrial heat flow should be presented. This has to be performed through a combination of all research results and working hypotheses of the above-mentioned single disciplines.

The first step of the *multidisciplinary synthesis* should integrate the different geological research results of the local areas (stratigraphy, structural geology) into an overall valid model of the geological evolution of the Marmara region. This evolution ends with the definition of the present neotectonic activity and its surface appearance (e.g. faults). Furthermore, so-called "Key observable quantities" of other disciplines, e.g. present day terrestrial heat flow density or 3D seismicity distribution, have to be defined and investigated.

The second step is mainly concerned with the interpretation of these key observable quantities. This involves the definition of physical and chemical models and processes. Finally, a combination of these models can lead to answers for some of the following questions:

What is the influence of older tectonic and geologic structures on the modern neotectonic activity?

Are the present faults completely newly developed or do they follow mainly old structures?

The occurrence of thermal springs is bound to which kind of faults and what are the conditions to bring about thermal water outflow at surface?

How deep do these waters circulate and is the historically supposed triggering effect on the release of earthquakes quantifiable with modern measuring methods?

Do we recognise any different levels of the Earth's crust or the lithosphere?

Which processes may be involved with the release of earthquakes and where do we observe them?

What is the interpretation of repeated GPS measurements at the Earth's surface in the context of plate tectonic motions?

General map of NW Turkey (Figure 1)

The region covered by this map has a size of approximately 100,000km^2. A first look at the map shows the dominating features of the Marmara sea and the city of İstanbul, the historical Byzantine capital Constantinople. The important Black sea – İstanbul – Marmara sea – Aegean sea – Mediterranean sea trade route crosses the investigation area of the project from northeast to the southwest. Modern İstanbul and the Bosporus symbolises the bridge between Europe and Asia. The second largest city is Bursa with over 1 million citizens. Small towns with a history dating back to ancient times are Bergama (Pergamon: Hellenistic and Roman province capital, 3rd to 1st century BC) and also İznik (Nicea: city of the first Christian council, 7th century AD). The Dardanelles, connecting the Marmara and the Aegean seas, are well known today under the ancient Greek expression Hellespont, where nearby probably the most famous ancient city Troia was discovered on the Biga peninsula.

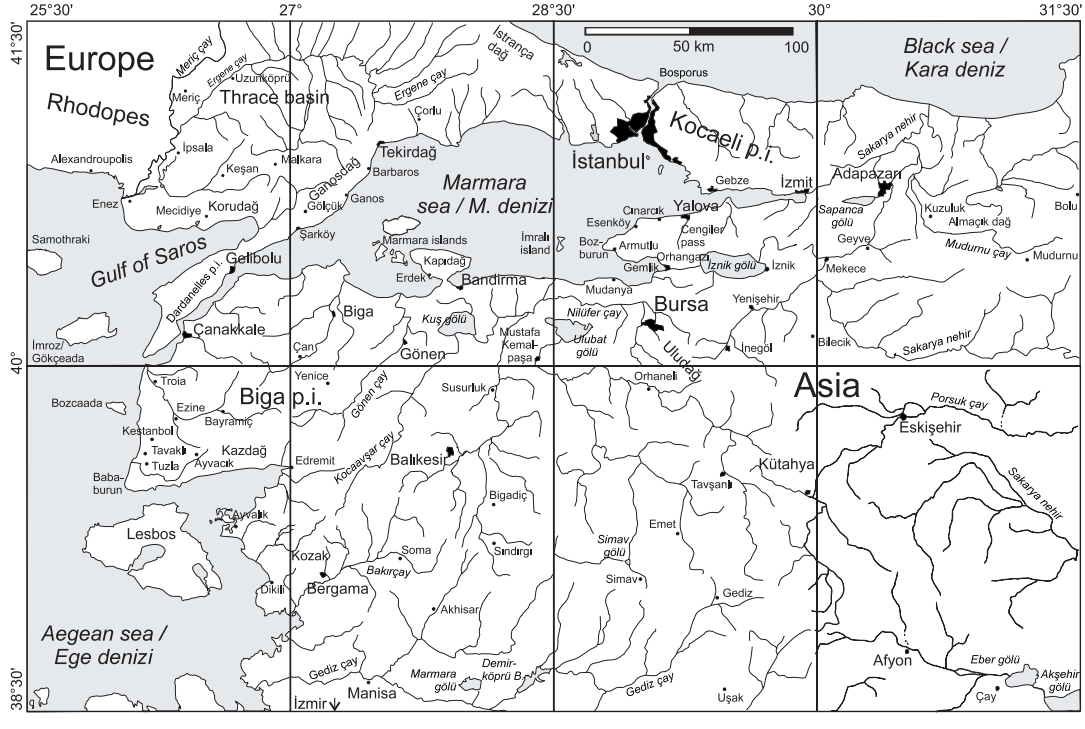


Figure 1: Geographical map of the Marmara sea region

Numerous rivers and some large freshwater lakes are characteristic for the region. The abundance of water serves for irrigation of large agricultural plains. Very significant are the river systems of the Ergene çay in the Thrace basin area, of the Sakarya nehir, as well as the Gönen çay. Famous agricultural areas are the plains of Bursa, the plains between the Kuş and Ulubat lakes, the plains in the vicinity of Biga and Bergama, as well as the plains of İzmit-Adapazarı. Most of the area, however, is hilly, relief being moderate, without sharp cut ridges. Prominent are two large massives, Kazdağ at 1710m (ancient Ida) and Uludağ at 2543m (ancient Bythinian Olymp). Some of the most commonly used Turkish words with a geographical meaning are given below in Table 1.

English	Turkish
Marmara sea	Marmara deniz
Black sea	Kara deniz
Aegean sea	Ege deniz
Mediterranean sea	Akdeniz
plain	ova
island	ada
mountain	dağ
city	şehir, kent
village	köy
spring	kaynak
thermal spa, hot spring	kaplıca, ılıca
hot water	sıcak su
river	nehir
brook, creek	çay, dere
lake	göl

Table 1: Most commonly used Turkish words with a geographical meaning

Topography and bathymetry of NW Turkey (Figure 2)

Due to moderate erosion and deep-reaching weathering processes, the topography generally is quite smooth and rises from west to east, reaching 2000m a.s.l. in some points. The bathymetry is dominated by basins over 2000m deep in the Marmara sea, the Black sea (only partly visible) and the gulf of Saros.

Topography and especially bathymetry reveals first impressions of a possible influence of the neotectonic activity of the NAFZ. The deep basins in the Marmara sea and the gulf of Saros show sharp borders and trace the continuation of the NAFZ to the west and into the Aegean sea. This picture demonstrates that the clear strike-slip regime of the NAFZ has changed into a combination of strike-slip and extension. The Gelibolu peninsula and its prolongation to the northeast interrupts the connection between the two deep troughs as a topographical local high. At this point, a local zone with a compressional stress regime can be supposed. The northern zone of the NAFZ shows the most significant influence on topography.

Valleys and rivers in the eastern part of the research area show an enhanced east-west directed appearance. The Sakarya river (compare Figure 1) and its valley structure especially indicate a right lateral displacement of the southern part versus the northern part along the NAFZ. Furthermore, in the region south of the E-W oriented plain connecting the Kuş and Ulubat lakes, the landscape is dominated by NE-SW oriented valleys and ridges. From Edremit to the southeast, large plains or depressions oriented W-E to WSW-ENE become frequent, which likely can be brought into correlation with the actual Aegean extensional stress regime, indicating a NNE-SSW instead of a N-S directed extension in this area.

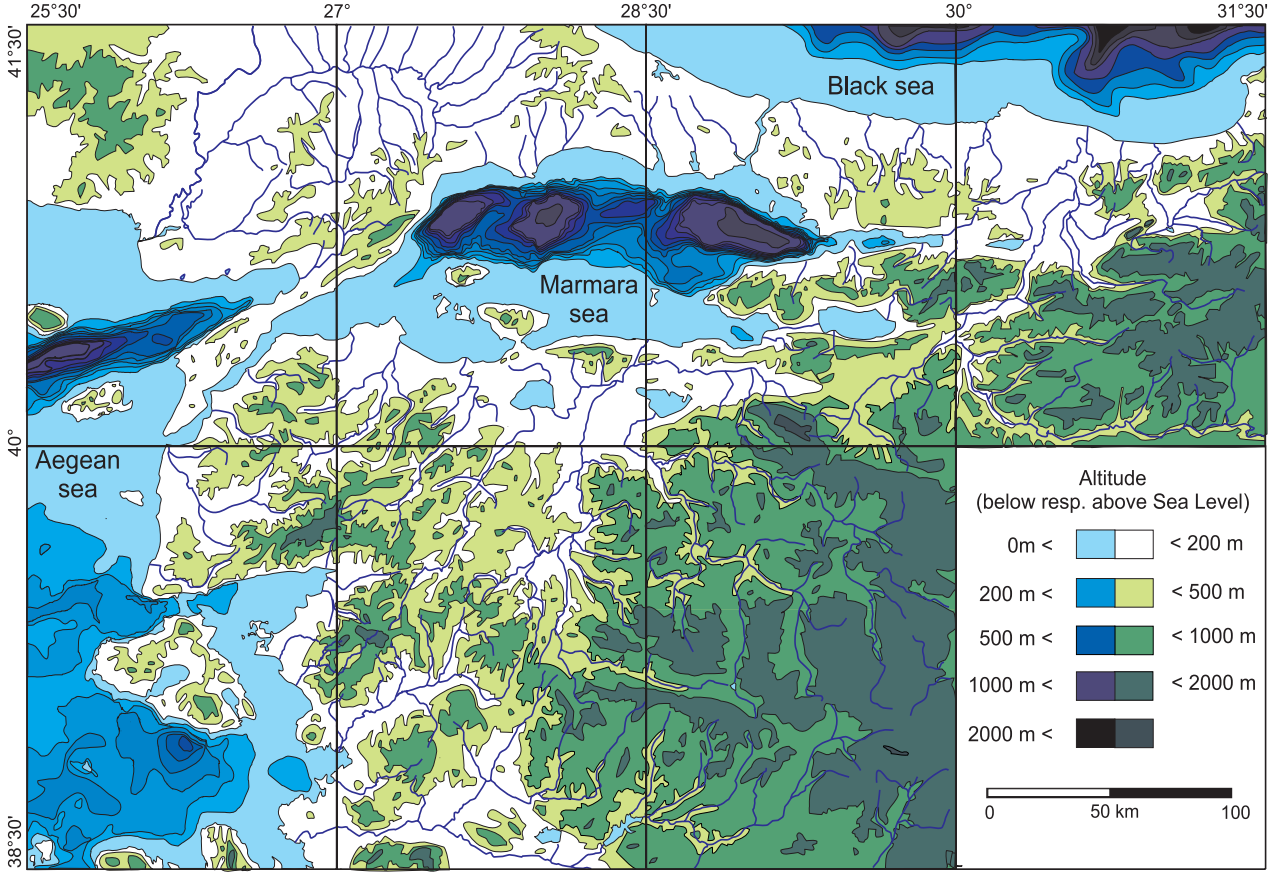


Figure 2: Topographic and bathymetric map

Investigation areas of the research disciplines (Figure 3)

A total of 9 geological working areas were differentiated and these areas are distributed over the entire Marmara sea region: Kuzuluk in the east directly located on the NAFZ, Bursa, Yalova-Armutlu-Gemlik, Yenice-Gönen, Tuzla-Kestanbol, Bergama-Kozak, Şarköy, Tekirdağ and Uzunköprü. Except Şarköy, Tekirdağ and Uzunköprü north of Marmara sea, all these regions show significant thermal spring occurrence and were investigated by the Hydrogeology group, too.

Five GPS networks were set up, directly related to the geological research areas. The measurement points were selected in collaboration with the geologists on relevant rock underground. All five networks together were combined into a unifying large geodetic network to determine the overall displacement field.

Geothermal research was mainly driven by the search for reliable drillholes which could be used for heat flow determination. These drillholes, distributed over the whole Marmara sea region, are necessary for a regional interpretation. Furthermore, thermal spring modelling studies were concentrated in the region of Bursa and Yalova-Armutlu-Gemlik, where a MARMARA project seismological network was installed. A large and frequent thermal spring occurrence, high seismicity and distinctive distribution of active faults were favourable here. On the other hand, the well developed infrastructure of the area aided our field activities immensely.

Not indicated on Figure 3 but covering the whole Marmara sea region on land are Turkish measurements of Bouger gravity anomalies. Unfortunately, offshore data are very rare for all disciplines involved in our project but would contribute precious significant knowledge. The only relevant offshore data at present are recent seismic investigations of the sediments in the Marmara sea (Wong et al. 1995, Ergün and Özel 1995) and some geothermal measurements in oil wells.

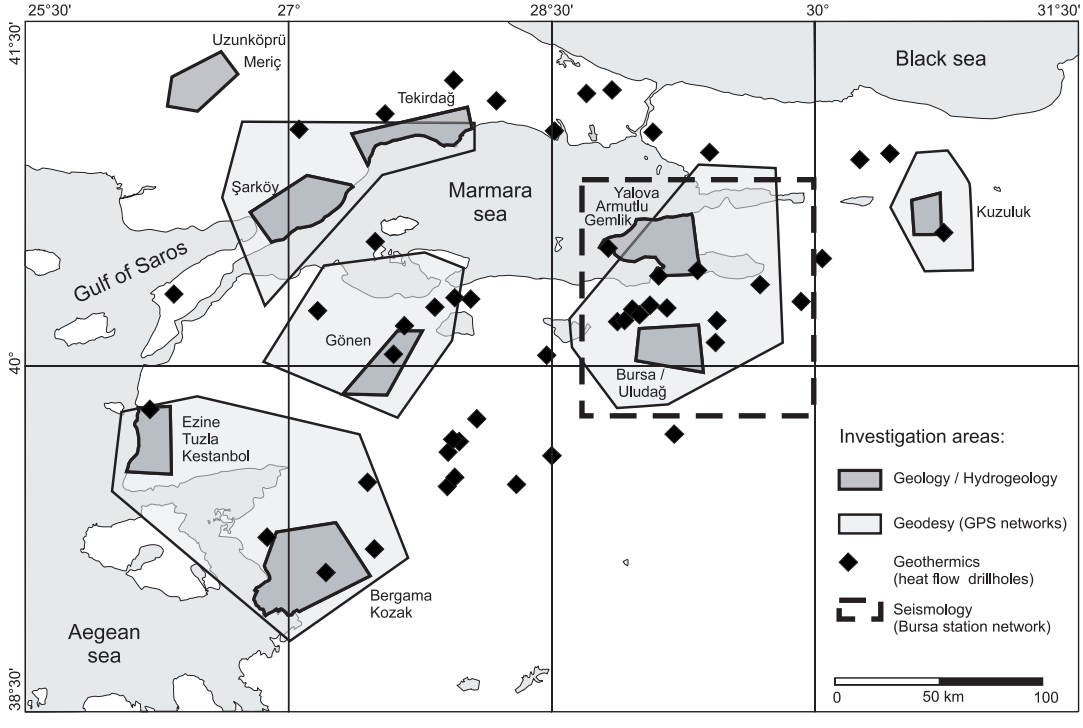


Figure 3: Map of investigation areas of the MARMARA Poly-Project.

References

Adams, F.D., 1912, An experimental contribution to the question of the depth of the zone of flow in the Earth's crust, The Journal of Geology, Vol. XX, No. 2, February-March, 97-118.

Demokrit, 2000y B.P., Bibliothèque de la Pléiade, Les Présocratiques, XCVIII, Editions Gallimard, pages 794-795, 1988.

Ergün, M. and Özel, E., 1995, Structural relationship between the Sea of Marmara Basin and the North Anatolian Fault Zone, Terra Nova, 7, 278-288.

Imbach, Th., this volume, Geology of Mount Uludağ with emphasis on the genesis of the Bursa thermal waters, Northwest Anatolia.

Kluge, E., 1858, Die Reaktionen des Erdinnern gegen die Erdoberfläche in den Jahren 1855 u. 1856, in: Mittheilungen aus Justhus Perthes' geographischer Anstalt Über wichtige neue Erforschungen auf dem Gesammtgebiete der Geographie, von Dr. A. Petermann, Gotha: Justus Perthes, 236-251.

McKenzie, D.P., 1972, Active tectonics of the Mediterranean region, Geophys. J. R. Astr. Soc., 30, 109-185.

Palmerston, ?. Viscount, 1851, Notice of the occurrence of an earthquake at Brussa, in: The quarterly journal of the geological society of London, volume the seventh, part the first, proceedings of the geological society, 19-19.

Sandison, D., 1855, Notice of the earthquakes at Brussa, in: The quarterly journal of the geological society of London, volume the eleventh, part the first, proceedings of the geological society, 543-544.

Şengör, A.M.C., 1979, The North Anatolian transform fault: its age, offset and tectonic significance, J. Geol. Soc. Lond., 136, 269-282.

Wong, H.K., Lüdmann, T., Ulug, A. and Görür, N., 1995, The sea of Marmara: a plate boundary sea in an escape tectonic regime, Tectonophysics, 244, 231-250.

THEME 2

Plate tectonics

Plate tectonic situation in the Anatolian-Aegean region

STEPHAN MUELLER, HANS-GERT KAHLE AND AYKUT BARKA

Abstract

The Eastern Mediterranean region marks the tectonically most active part of the broad transition zone between the African/Arabian and Eurasian plates. Its present activity is clearly marked by a most conspicuous earthquake belt surrounding the Aegean Sea. While this belt follows the subduction zone along the Hellenic arc in the Ionian and Aegean Seas it forms a triangle in the central and southern part of western Anatolia. The various regional features associated with the seismotectonic framework indicated by the seismicity are discussed from the Near East (Anatolia) through the Aegean Sea to the Ionian Sea. The crustal and upper mantle structure is described by using p- and s-wave tomography sections. The dynamic processes are elucidated by examining heat flow data, helium distribution in crustal fluids and recent space geodetic results. The current rates of crustal deformation provide a detailed pattern of vectors constraining the westward motion of NW Anatolia to 22mm/a, relative to Eurasia.

Introduction

The tectonic activity in the Eastern Mediterranean is caused by the very complex lithospheric regime which evolved since the break-up of the Tethys belt and which can still be surmised from the present bathymetry and topography of this region. In a simplified scheme the formation of the present-day tectonic framework can be understood as a consequence of the counter-clockwise rotation of the African plate since the last 92m.y. which has led to a lithospheric shortening rate increasing from west to east. For the last 10 to 9m.y. the Eurasian / African plate contact is to a large extent under SE-NW directed compression (Dewey et al. 1989). This paper is intended to give an overview of the current knowledge of the plate-tectonic setting of this region. It also describes the apparent relationship between the deep structure of the lithosphere-asthenosphere system, deduced from seismological data, with the kinematic field derived from space geodetic observations and with the present stress pattern, as well as with heat flow estimates and helium isotope distribution.

Seismicity and seismotectonics

The earthquake activity observed around the Aegean Sea comprising large parts of Greece and Western Anatolia has been the most conspicuous geodynamic phenomenon in the Eastern Mediterranean region (Fig. 2) during this century (Ambraseys and Finkel 1991). At a first glance the clearest seismicity feature is associated with the Hellenic arc forming an almost perfect "semicircle" from the Ionian islands in the west to the central part of western Anatolia in the east, with endpoints at about 38°N / 20°E and 38°N / 32°E. A closer inspection reveals,

however, that southwest of the Peloponnesus and particularly south of the island of Crete the Hellenic arc is transected by clusters of earthquakes which are oriented perpendicular to the arc (cf. also Fig. 1). Noticeable is also the clear offset of the seismicity of about 220km to the NNW between the islands of Karpathos and Rhodes which is probably due to an irregularity in the crust and upper mantle.

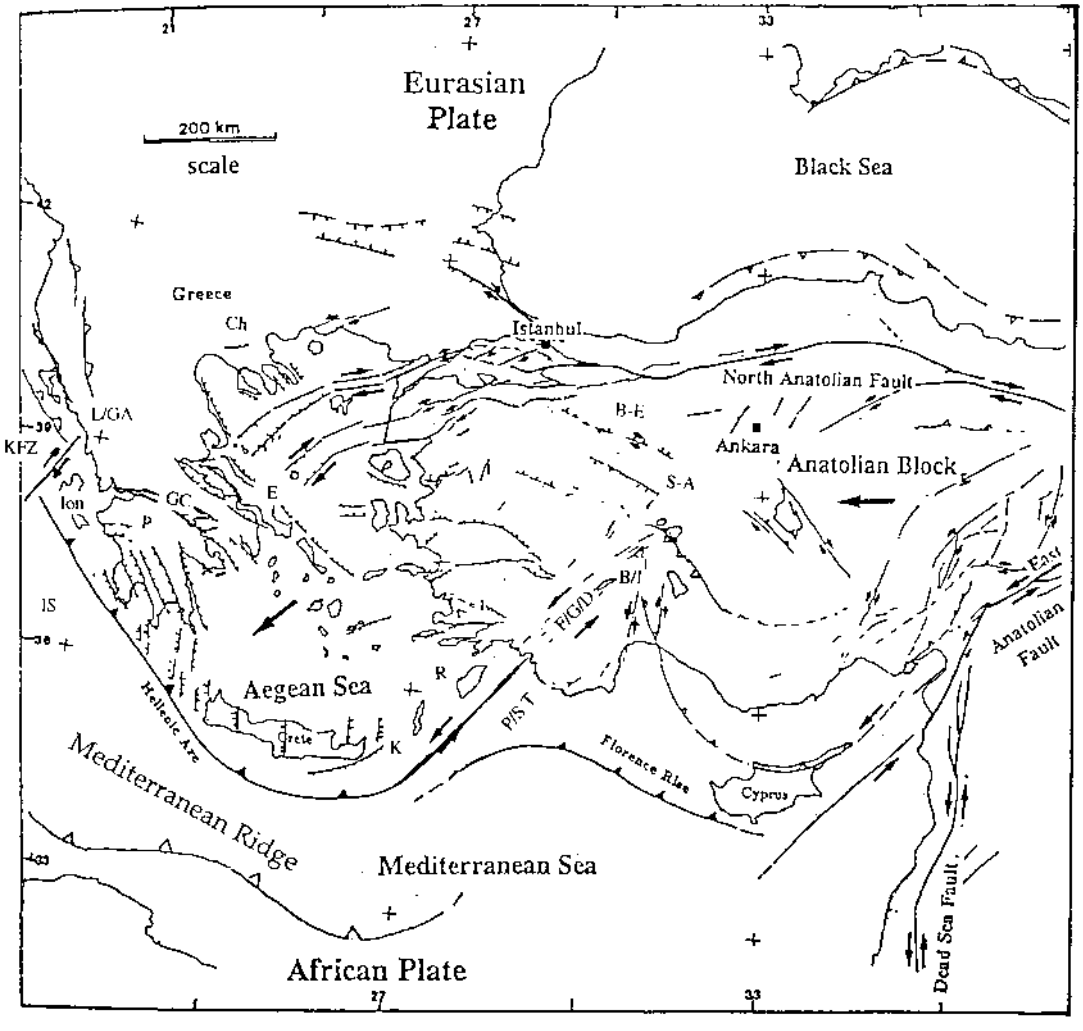


Figure 1: *Tectonic sketch map of the Aegean-Anatolian region, after Barka (1992). B-E: Bursa – Eskişehir fault, S-A: Simav – Afyon fault, F/G/D: Fethiye / Gökova – Burdur / Dinar zone, B/I: Burdur / İsparta, K: Karpathos, Ion: Ionian islands, P: Peloponnesus, R: Rhodes, KFZ: Kephalonia fault zone, P/S T: Pliny / Strabo trench, IS: Ionian Sea, L/GA: Levkada / Gulf of Arta, GC: Gulf of Corinth, E: Evia, Ch: Chalkidike.*

North of the Hellenic arc, proceeding from west to east, the right-lateral Kephalonia Fault Zone (KFZ) dominates the activity in the Ionian Sea (Anderson and Jackson 1987). The maximum strain values (180 nanostrain/a) were found in the area of Levkada / Gulf of Arta, and the strain energy reaches a maximum of 0.004J/m^3 (Müller 1995). The central part of Greece is characterised by two parallel west-east trending seismicity belts: a southern one along the Gulf of Corinth and a northern one from the Gulf of Arta to the Gulf of Evia. Three clear SW-NE striking earthquake lineaments can be traced across the northern Aegean Sea (Fig. 2). They can be considered as southwestward prolongation of the seismicity of the North Anatolian Fault Zone (NAFZ). The northernmost belt extends from Cape Kanastraion at the tip of

Kassandra peninsula (Chalkidike peninsula) into the Gulf of Saros with the three most recent larger earthquakes, namely 1975 (Magnitude M = 6.7), 1982 (M = 7.1) and 1983 (M = 6.9). Between central Evia and the Dardanelles a second belt can be located with the strongest recent earthquake 1968 (M = 7.2). Similarly, a third zone is identifiable between southern Evia across Lesbos island towards the Gulf of Edremit; two large earthquakes happened there in 1981 (M = 7.2 and 6.5).

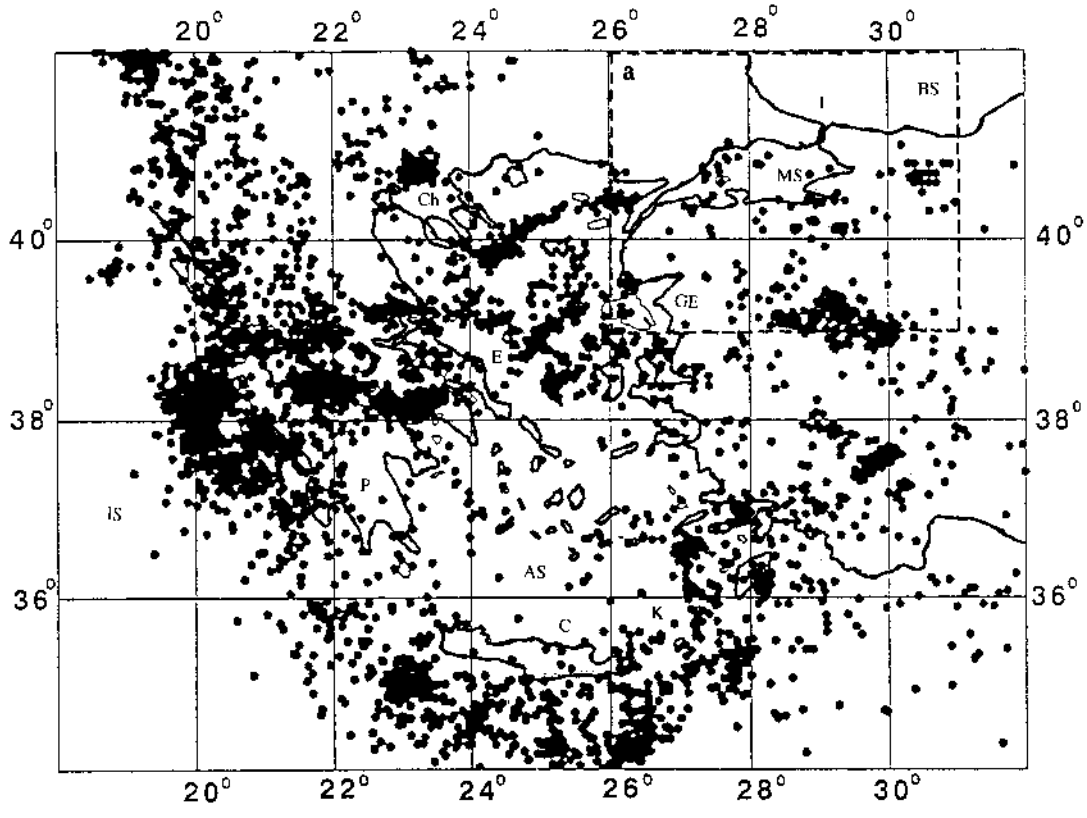


Figure 2: *Seismic activity in the Aegean Sea and neighbouring regions reported by the USGS in the period 1963 to 1987, probably complete down to magnitudes 4.5. Inset (a) shows the seismic activity in the Marmara Sea region, after Ambraseys and Finkel (1991). IS: Ionian Sea, AS: Aegean Sea, MS: Marmara Sea, BS: Black Sea, C: Crete, R: Rhodes, Ch: Chalkidike, K: Karpathos, P: Peloponnesus, E: Evia, GE: Gulf of Edremit, I: İstanbul.*

The seismicity in westernmost Anatolia for M > 4.5 is considerably lower than that in the northern part of the Aegean. At this point it should be mentioned that the moderate seismic activity in the Marmara Sea region is being dealt with in the context of neotectonics (Barka this volume) which is enlarged especially in the region around the city of Bursa (Sellami et al. this volume).

South of Bursa (at about 39°N) a striking seismicity feature is located. It has the shape of a NW-SE oriented extended active cluster from the small town of Sindirgi (NE of Akhisar) as far as Cay (SE of Afyon) (Fig. 2) which is obviously related to the Simav-Afyon fault zone and not to the Bursa-Eskişehir fault which has not been significantly affected by major earthquakes in the recent past. At its western end this zone is cut by a SW-NE directed seismically moderate lineament which goes past the Mudanya (NW of Bursa) region, the Gulf of Gemlik and terminates at Yalova. Further south segments of the seismic activity associated with the broad Fethiye – Burdur zone (F/G/D in Fig. 1) of parallel faults can be identified. They are most likely affected by the offset of seismicity between the islands of Rhodes and Karpathos as has been

mentioned earlier. Also clearly visible in Fig. 2 is the SE-NW oriented short active segment between the Burdur / İsparta and the Dinar regions. Details have recently been published by Eyidoğan and Barka (1996). In summary it can be stated that the recent and present seismicity in the Aegean-Anatolian region is much more complex than it appears from descriptions in the current literature.

Kinematic fault plane solutions (FPS) of earthquakes provide insight into the processes and causes associated with the seismicity pattern described in the previous section and the tectonic framework outlined in the first section. They are illustrated by lower hemisphere projections of the seismic rays traced back from distant observation stations to the sphere which encompasses the earthquake focus. In Fig. 3b the principal stresses $\sigma_1 > \sigma_2 > \sigma_3$ are indicated (from left to right) as thrust motion (reverse faulting), lateral strike-slip motion (non-unique, could either be right or left lateral), and rifting (normal faulting). “Pure” deformations as described in the previous examples are usually rare. Mixed mechanisms are the more likely case. For the region under consideration (Fig. 3a) there are quite a number of fault plane studies available (see e.g. Kiratzi and Papazachos 1995). The distribution of focal mechanisms of the stronger shallow earthquakes shows thrust faulting along the Dalmatian coast of Croatia and Montenegro. The main shock and the largest aftershock of the 1979 Montenegro sequence exhibit almost pure thrust mechanisms with nodal planes striking parallel to the coast. This belt of thrust faulting continues south along the coastal region of western Albania and also along the westernmost part of the mainland of Greece. It can be assumed that the above-mentioned zone of thrust faulting is due to the collision of two continental lithospheric plates, i.e. the Adriatic with the Eurasian plate. There is no evidence of subduction along this part of the plate boundary.

Thrusting continues southward along the coastal regions of Northwestern Greece up to the island of Kephalonia. The rather frequent earthquake activity there revealed dextral strike-slip movement on SW-NE striking nodal planes. This belt of dextral strike-slip faulting is generally considered as the western termination of the Hellenic subduction zone. Along the convex side of the Hellenic arc the distribution of focal mechanisms (with depths less than 40km) indicates the existence of low-angle thrust faulting with the shallow dipping plane ascribed to the active fault plane in the subduction process (McKenzie 1978). The trend of the compressional (P) axis is perpendicular to the Hellenic arc in its western and southern part, keeping the same pattern to become parallel to the arc in the Pliny and Strabo trenches (with left-lateral strike-slip motion) at the eastern end of the arc.

The focal mechanisms of intermediate-depth events, i.e. with foci between 40 and 100km depth, all in the southern Aegean, north and south of Crete, are characterised by thrust faulting with a significant strike-slip component – not shown in Fig. 3a (Papazachos et al. 1991). It seems that the shallow seismicity along the external part of the Hellenic arc is coupled to the deeper-reaching intermediate activity. In this depth range all the big earthquakes (with magnitudes up to M = 8) occur. At a depth of around 100km the slope of the dipping Benioff zone increases from 23° to 38° (Papazachos 1990). As can be seen in Fig. 3a normal faulting is dominating most of the Greek mainland as well as the western part of Turkey. The study of recent seismic sequences has illustrated that the normal faults with predominantly west-east striking nodal planes are in most cases listric faults limited to relatively shallow depths (10 to 15km).

Central Greece and in particular the region north of the Gulf of Corinth is governed by extensional focal mechanisms which interrupt the right-lateral strike slip regime between the Kephalonia fault in the west and a corresponding segment across the northern Aegean in the northeast. A joint interpretation of the neotectonic features (Fig. 1) and the seismotectonic pattern (Fig. 3) suggests that this wide extensional zone in central Greece is actually repre-

senting a large-scale transtensional “pull-apart” structure as has been proposed some time ago by Reuther et al. (1993). Along the northernmost branch of seismicity in the northern Aegean (Fig. 2) a change from dextral strike-slip to normal faulting is observed when the Gulf of Saros is approached. This explains the differential rifting and thus the opening of the gulf.

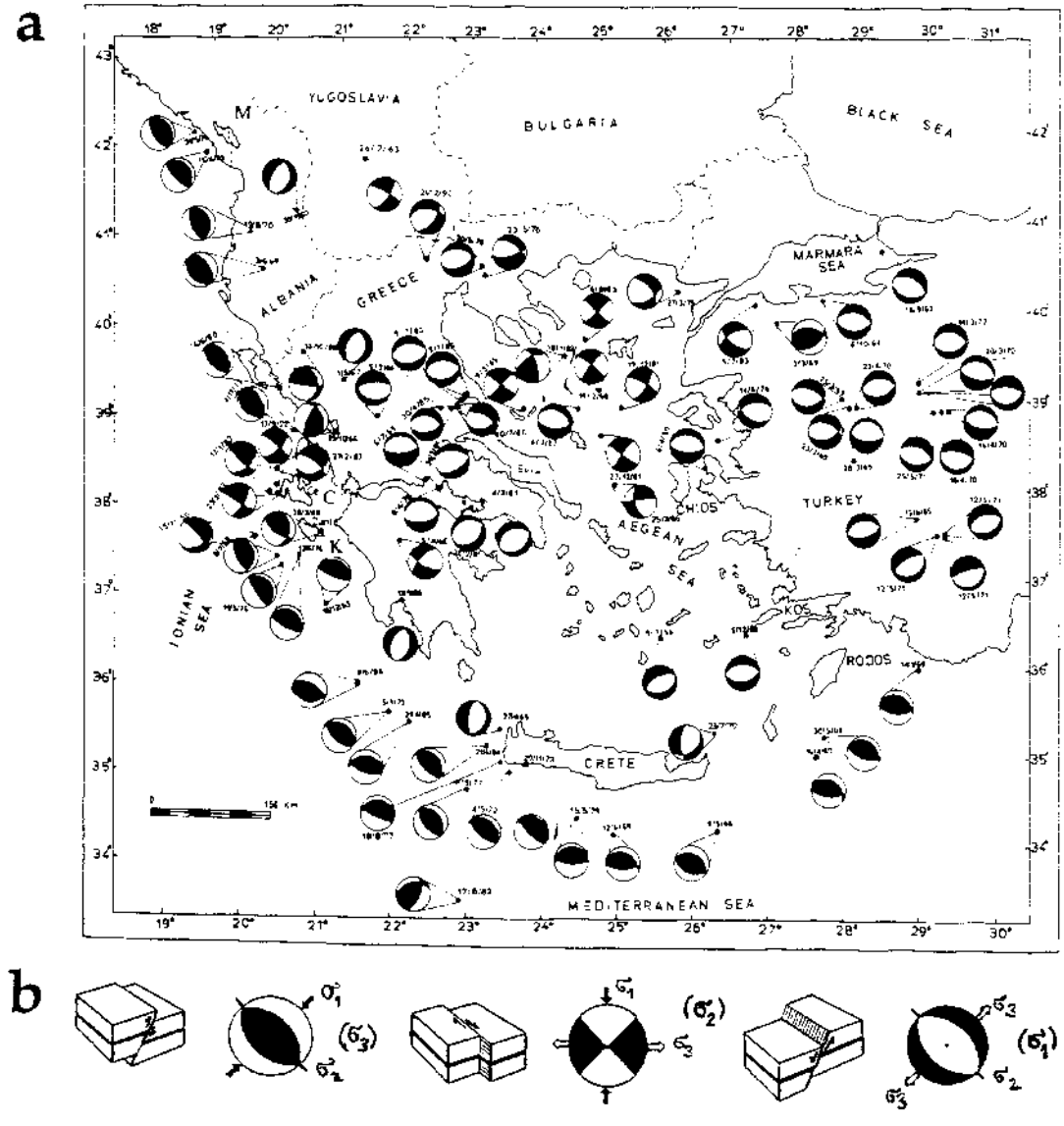


Figure 3: *The distribution of the focal mechanisms. (a) The Aegean area and the surrounding lands, after Kiratzi and Papazachos (1995). (b) Fault plane solutions and respective fault models. M: Montenegro, C: island of Cephalonia, K: Karpathos.*

As has been mentioned before the most conspicuous seismicity feature in Western Anatolia is obviously associated with the Simav-Afyon fault zone (Fig. 2). It is characterised by normal faulting and a sporadic right-lateral strike-slip component with predominantly NNE oriented nodal planes (Fig. 3a). The same focal mechanism pattern was listed in a catalogue by Udias et al. (1989) and has been refined on a much more detailed scale by Zanchi and Angelier (1993). A somewhat different situation is encountered in the broad Fethiye – Burdur tectonic zone (Eyidoğan and Barka 1996) where the normal faulting is more distributed with a strongly pronounced left-lateral strike-slip component (cf. Fig. 1). Based on this evidence it can be sur-

mised that the central and southern part of Western Anatolia forms a triangle which is pulled out to the west and at the same time possibly rotated counter-clockwise as indicated by the shape of the gulf inlets along the west coast of Anatolia.

Crustal and upper mantle structure

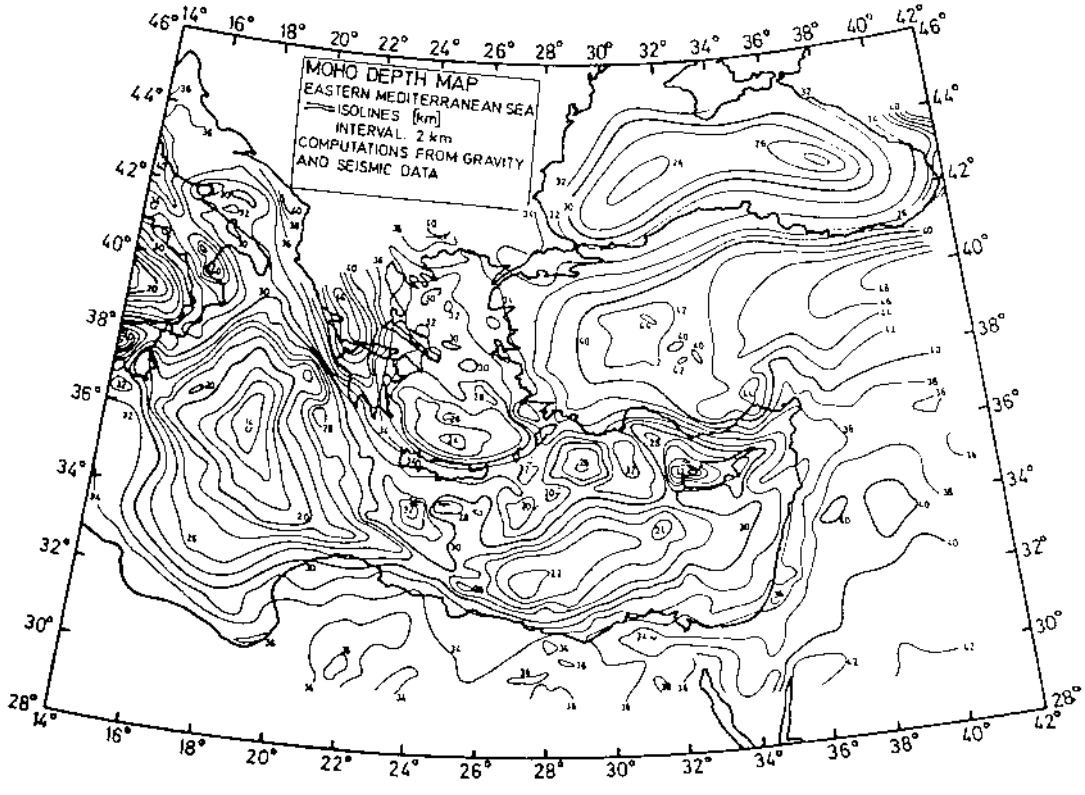


Figure 4: *Contour map of depth (in kilometers) to the crust-mantle boundary, i.e. the Moho discontinuity, in the Eastern Mediterranean and adjacent regions (after Makris und Stobbe 1984). The Moho depth map has been deduced from seismically constrained gravity data.*

From the presently available data the Aegean region is underlain by a thinned continental crust, having a mean thickness of 28-32km and a minimum thickness of 24km north of Crete. Beneath the Peloponnesus and Western Anatolia the continental crust reaches a maximum thickness of about 40km (Fig. 4), (cf. Makris 1978, Makris and Stobbe 1984).

The upper mantle of the European-Mediterranean region has been the subject of many recent tomographic studies with the aim to determine the velocity-depth distribution of seismic p- and s-waves in an attempt to obtain quantified images of the lithosphere-asthenosphere system. Our knowledge about the variations in the physical state and chemical composition of the upper mantle is still rather limited. The availability of accurate velocity data for both p-waves and the geophysically more significant s-waves would provide answers to the question whether the observed velocity information are primarily caused by regional stress conditions, temperature variations (cf. Yan et al. 1989) or differences in composition. Most likely it is an interaction of all these factors, particularly in complex regimes, such as the Anatolian-Aegean region.

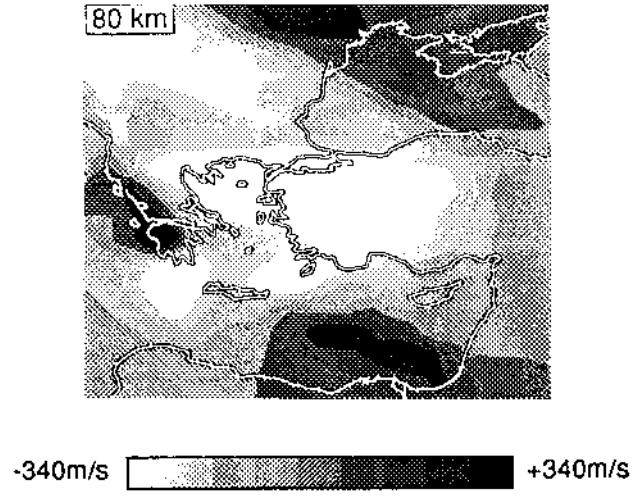


Figure 5: Horizontal s-wave tomographic cut (at 80 km depth), after Zielhuis (1992).

The most comprehensive study so far of the three-dimensional (3-D) s-wave velocity field below Europe based on delay-time and waveform inversions has been carried out by Zielhuis (1992). Assuming the reference values of Yan et al. (1989) for the s-wave velocity and temperature at 150km depth (4.5km/s and 1300°C, respectively) which are representative for the eastern European craton, the low s-wave velocities in the depth range from 80 to 140km beneath the Pannonian basin, the northern Aegean and the Anatolian region (Fig. 5) can only be explained by partial melting in the asthenosphere. It should be noted here that the p-wave velocity model of Spakman et al. (1993) with variations of 2% correlates reasonable well with respect to the sign of the s-wave anomalies, but the amplitudes of the s-wave velocity variations are significantly larger (7.5%).

A vertical section to a depth of 700km extending from central Greece to the Crimea (Fig. 6, after Zielhuis 1992) illustrates the subducting lithospheric slab in the Hellenic collision zone and the adjoining low-velocity asthenosphere reaching to a depth of 140km between the northern Aegean Sea, Thrace and the Black Sea coast (Fig. 6). That part of the tomographic model is the one with the highest resolution, because there the coverage by s-wave paths has the highest density.

For the central Mediterranean region also an estimate of the present p-wave velocity structure exists derived from delay-time tomography (Spakman et al. 1988 and 1993). These tomographic results describe the three-dimensional (3-D) mantle structure from the surface down to a depth of 800km and provide a qualitative handle on the possible causes of the complicated velocity field. In Fig. 7a the recent seismic activity between the Tyrrhenian sea and Western Anatolia is depicted illustrating once more the same basic seismicity features as shown in Fig. 2.

The vertical cross-section of Fig. 7b clearly shows the earthquakes associated with the Tyrrhenian (Calabric) and Hellenic subduction zones which are superimposed on the p-wave tomographic velocity structure (De Jonge et al. 1994).

A surprising new tomographic feature is the deep-reaching mantle plume in the Ionian Sea which separates the two subduction slabs and is capped by a high-velocity lid in the upper part of the mantle (above 200km depth). The seismic activity in the central Aegean and Western Anatolia is restricted to the lithosphere, but at the eastern end of the mantle profile in Turkey a clearly defined subduction zone seems to exist which dips westward reaching to a depth of about 200km.

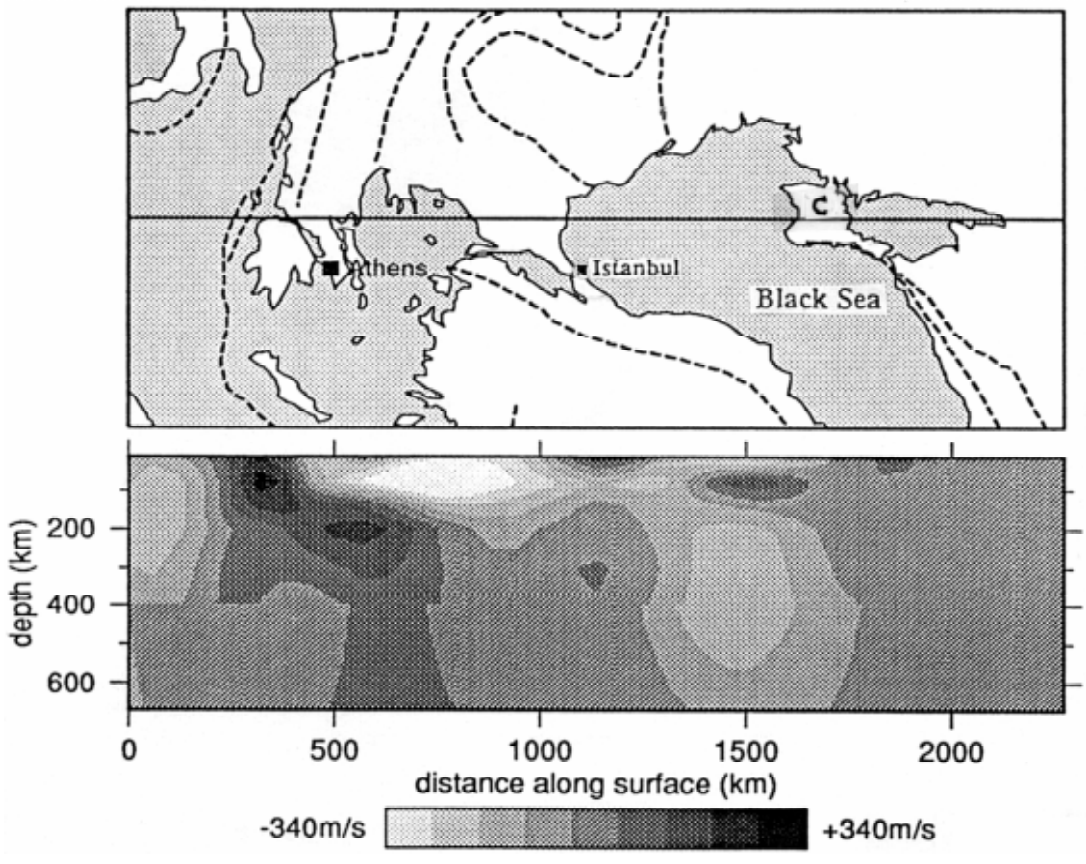


Figure 6: *Vertical cross section by s-wave tomography (down to 700km depth), after Zielhuis (1992). C: Crimea.*

The heat flow map presented in Fig. 8 (Tezcan and Turgay 1991) is based on 204 not evenly distributed temperature soundings in oil, gas and coal wells (Thrace and SE-Turkey) and especially in Western and central Anatolia in deep geothermal wells. Since there are no in-situ thermal conductivity measurements available a typical standard value of $2.1 Wm^{-1}K^{-1}$ has been used in all the heat flow calculations. In Fig. 8 it can be seen that the general level of heat flow in Western Anatolia may be much higher (100 to $120 mWm^{-2}$) than that in the Eastern Mediterranean Sea and the Black Sea with values of 20 to $30 mWm^{-2}$. Also the heat flow in the north Aegean trough, the Biga peninsula and the “horst and graben” structures (metamorphic core complexes, misleadingly called “massifs”) in the central part of Western Anatolia points to elevated heat flow values if compared with the remainder of the Turkish territory.

If an attempt is made to relate the pattern of heat flow to the observed seismicity (cf. Fig. 2) a strikingly similar picture becomes visible which exhibits the same structural “triangular” configuration. It also coincides with the region of increasing crustal thickness (from W to E) and lower average crustal velocities as well as a decreased sub-Moho (p_n) velocity, indicating that the high heat flow is not only caused by a crustal contribution, but that it must also contain a sizeable mantle component.

Additional evidence of a strong crust-mantle interaction in Western Anatolia is provided by the results of measurements aimed at a determination of the $^3He/^4He$-isotope ratio in crustal fluids (Gülec 1988). Samples from natural springs and one drilling hole were collected and analysed. The majority of samples are from groundwater discharges associated with the faults bounding the well-mapped graben structures in Western Anatolia. In Figure 3 of the

Poly-Project synthesis (Theme 6 this volume) sampling locations in NW Anatolia are shown with the measured He-isotope ratios. It is customary to express the He-isotope composition relative to that of a standard atmosphere, i.e. $(^3He/^4He)_{sample} / (^3He/^4He)_{atm} = R / R_a$.

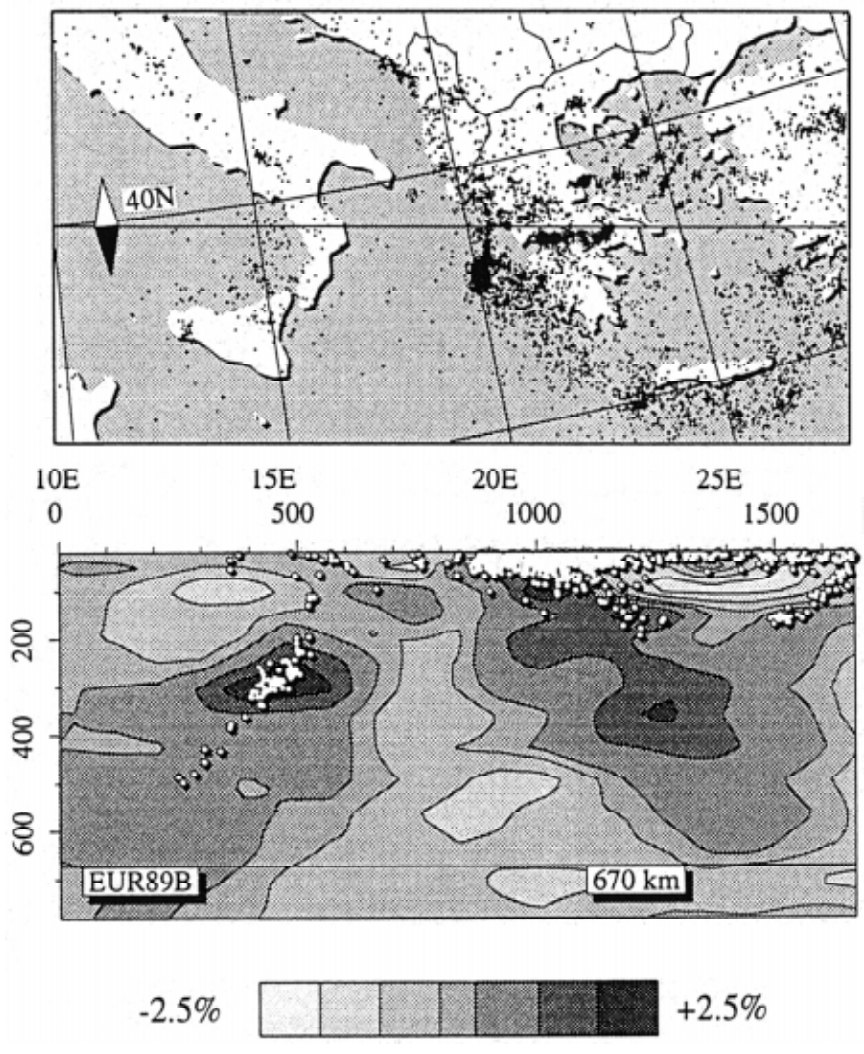


Figure 7: *Vertical section by p-wave tomography crossing both the Tyrrhenian (left) and Hellenic (right) subduction zones (down to 700km depth), after De Jonge et al. (1994).*

Detailed geophysical surveys carried out in some continental rift systems, such as the Rhine-graben, the east African, Rio Grande, Baikal, and Oslo rifts (cf. Olsen 1995), have revealed the presence of anomalous zones of low seismic velocities in combination with high electrical conductivity within the crust and uppermost mantle. These anomalies have been interpreted as magma accumulations assuming that these partial melts also play an efficient role in transporting mantle-helium e.g. into the Western Anatolian crust, where extension is prevailing since about Upper Miocene time, i.e. in the last 20m.y. Since mantle helium is widely distributed in the western part of Turkey extensive melt additions to the lithosphere are apparently taking place. The fault structures have presumably aided the escape of mantle helium through crustal channel ways to the surface. There is no obvious evidence for a related distribution between mantle helium and surface volcanism which suggests that helium is degassing from plutons emplaced deeper in the crust and upper mantle.

Dynamic processes

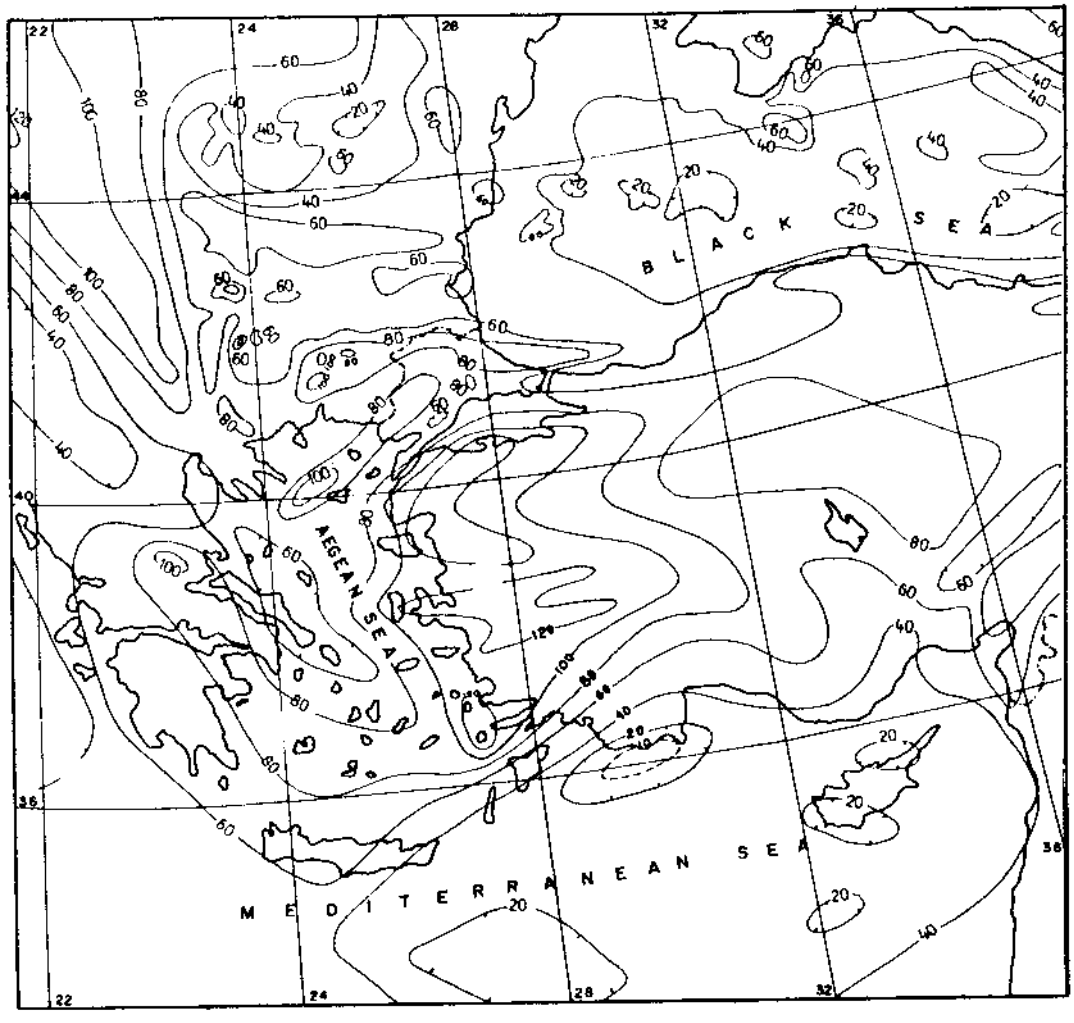


Figure 8: *Heat flow in Western and Central Anatolia and the surrounding areas [mW/m2], compiled from Tezcan und Turgay (1991) and heat flow map of Europe (Cermak and Rybach (eds.) 1979).*

The rates of crustal motion were initially measured by Satellite Laser Ranging (SLR) using permanent and mobile tracking equipment (Smith et al. 1994, Noomen et al. 1995, Robbins et al. 1996). The SLR data have been used by Oral et al. (1995) and LePichon et al. (1995) to model the velocity field of the Anatolian region as a counter-clockwise rigid rotation about a pole located in northern Egypt. The SLR solutions give a good pattern of the large-scale deformation in the Eastern Mediterranean. The northward motion solution for Diyarbakır reflects the movement of the Arabian plate (19mm/a N and 8mm/a W). The westward motion of the Anatolian block is seen in the solutions for the motion of Yozgat and Melengiclik. Three stations (Rhodes, Roumeli and Chrisokellaria, Greece) located on the leading edge of the overriding Aegean plate show SW oriented motion with rates of nearly 40mm/a, relative to a Europe-fixed reference system. The solutions for the sites in the Italian part of the network suggest that the motion there is similar to the Europe-fixed sites.

Since 1988 Global Positioning System (GPS) networks have been used to measure the motion between Italy and Turkey to assess the fine structure of the kinematic field. From west to east these networks are: the Calabrian arc (Zerbini et al. 1994, Kaniuth et al.1995), the West Hellenic arc (Kahle et al. 1993), Central Greece (Denys et al. 1995), the Aegean Sea (Kastens et al. 1997), the Anatolian plate (Oral 1994), and the Marmara Sea (Straub and Kahle 1995, Straub 1996). A first combination of the motion vectors of the four networks was presented by Reilinger et al. (1995).

The kinematic field of Western Greece, relative to Matera, Apulia (S. Italy), is characterised by a negligible motion north of the Kephalonia fault zone (KFZ), and a homogeneous southwest oriented motion of SW Greece reaching rates of 40mm/a. The stations in the southern part of the Aegean Sea, south of a line from Evia to Chios are moving essentially together at about 40-45mm/a to the SW relative to the Eurasian plate.

The Marmara Sea (MS) network covers the northwestern part of the boundary between Eurasia and Anatolia. The continuation of the single North Anatolian Fault Zone (NAFZ) is divided into several so-called strands when traversing the region from east to west (Barka and Kadinsky-Cade 1988). In the analysis discussed later we will introduce a different division of the Marmara Sea region, instead of strands separating it into two different zones (compare Theme 5 and 6 of this volume). The results of the MS network are summarised in Straub and Kahle (1995) (compare also Straub and Kahle this volume). The average westward motion of the Anatolian plate in the Marmara Sea region is 22mm/a relative to the Eurasian plate. West of 27.5°E the motion turns to ENE-WSW. Most of the deformation occurs along the northern zone which passes through the northern Marmara Sea. A detailed description of the data analysis, the crustal motion derived, and models constructed, are given in Straub(1996).

The results of the network on the Anatolian plate are summarised and discussed by Reilinger et al. (1997). The velocities for the sites located south of the Bitlis suture zone in Eastern Anatolia indicate NNW to NW oriented motion relative to Eurasia (18mm/a). Stations located north of the Bitlis suture zone in eastern and central Turkey show velocities similar to those to the south of it. The stations bridging the Caucasus mountains in Armenia, Georgia, and Russia indicate shortening across the Caucasus (10mm/a). Sites north of the NAFZ and north of the Greater Caucasus show insignificant motion in the Europe-fixed reference frame.

Sites west of the Karliova triple junction have a tendency to a more westerly directed motion which becomes progressively more pronounced to the W-WSW with stations indicating SW oriented rates in southwestern Turkey (Reilinger et al. 1997).

The principal axes of the strain rate tensor and the principal values of compressional and extensional strain rates calculated from the GPS deformation field (Kahle et al. 1996) yield insights into the major features: In the western part of Turkey as well as in central and southern Greece, N-S oriented extensional strain rates dominate, accompanied by normal faulting earthquake mechanisms (cf. Fig. 3a). They are most likely due to trans-tensional type of active processes in the Aegean graben system.

New GPS campaigns were recently commenced in the Eastern Mediterranean area including the Balkan region and northern Africa. In addition, a permanent network has been installed, which is designed to monitor the ongoing deformation across the KFZ and the West Hellenic arc (Peter et al. 1997). The new data will help to connect the networks and fill significant gaps in the knowledge of the crustal deformation pattern in the Eastern Mediterranean.

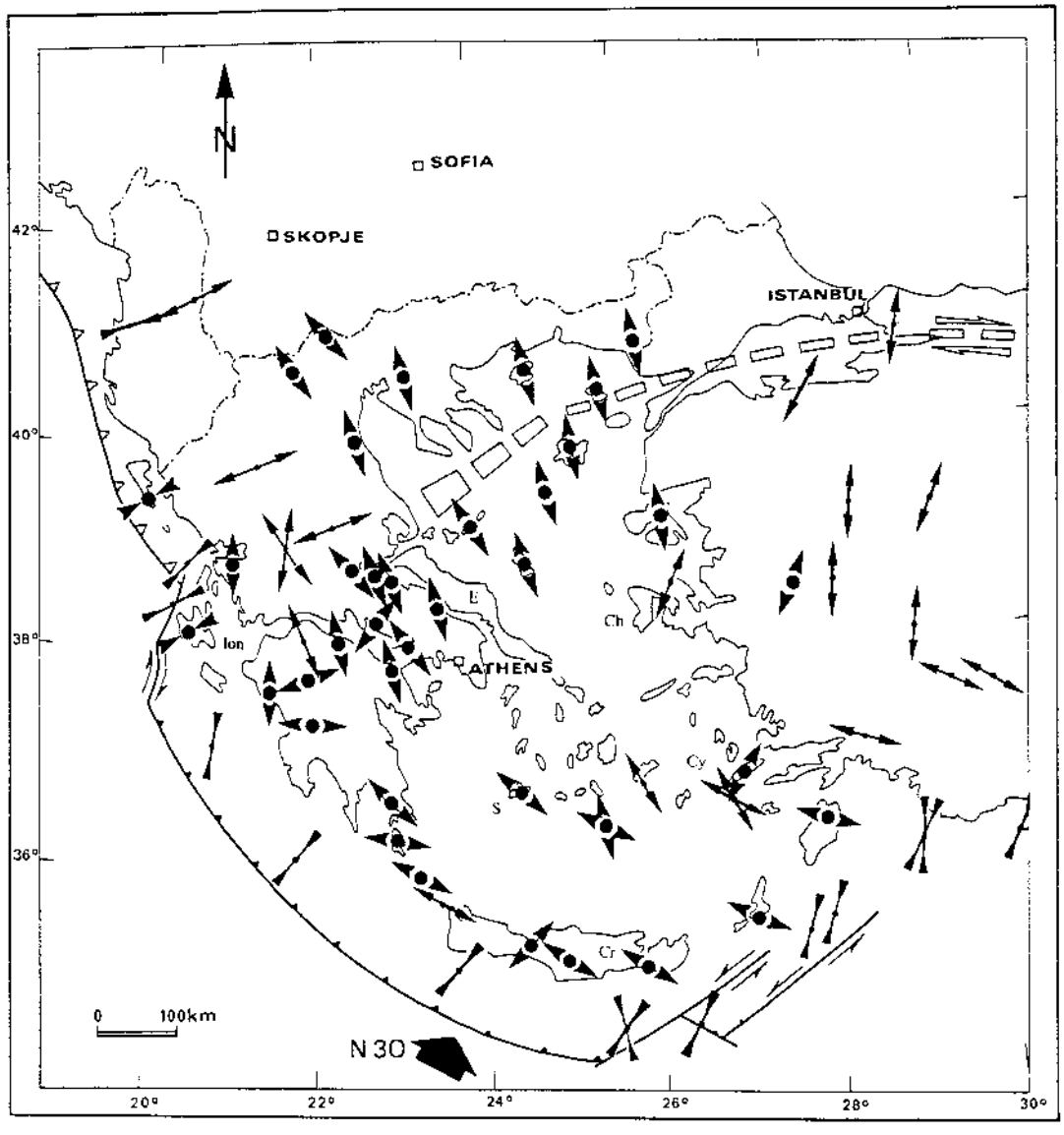


Figure 9: *Seismic stress pattern from FPS and structural analysis of faults, after Mercier et al. (1987). E: Evia, Ch: Chios, S: Santorin, Cr: Crete, Ion: Ionian islands, Cy: Cyclades.*

Conclusions

In this paper we have made an attempt to present a summary of the dominant structural and dynamic features that characterise the broad contact zone between the African / Arabian and European plates in the Eastern Mediterranean. The discussion is based on geodetic, geological and geophysical data available on the Anatolian/Aegean region. Our main conclusions are set forth below:

1) A detailed analysis of the focal mechanisms of earthquakes, and of structural field work, has produced evidence that the state of stress in the Aegean region has changed several times in the last 9m.y. (Mercier et al. 1987). The Hellenic arc exhibits geophysical and geological characteristics ascribed to those of island arcs. From the Hellenic trench towards

the northeast a subduction zone dips as deep as 180 to 200km. Its curvature is outlined by the calc-alkaline volcanic arc of the Cyclades and the southern Aegean sedimentary arc. The southern part of the Aegean Sea represents a back-arc basin, termed the Southern Aegean Trough, between Santorin (Thira) and Crete.

2) The Hellenic arc is located between the Arabia-Africa / Eurasia collision in the east and the Africa-Adria / Eurasia collision in the west. It is there, in the region of the Ionian islands, that the transition from the Hellenic arc to the Adriatic collision zone takes place (cf. Fig. 1). Northeast of the volcanic arc of the Cyclades, the back-arc basin transforms laterally into a zone of different intracontinental deformation which influences the tectonics in the central Aegean Sea and the adjoining western region of Anatolia. The northern Aegean Sea is dominated by the western continuation of the NAFZ.

3) Along the edge of the Hellenic arc which borders the deep-sea trench, the present-day tectonic regime is compressional whereas in the southern Aegean Sea region it is extensional. Since the Lower Pliocene, two compressional events have affected the Aegean domain. It would therefore appear that the neotectonics is characterised by an alternation of long-lived extensional periods – as at the present time – and short-lived compressional events (Mercier et al. 1987). In the last few decades numerous data have been collected revealing the principal directions of extension and compression during these four tectonic phases. It seems likely that compressional tectonics dominated briefly during the Lower to Middle Pleistocene (about 1m.y. ago). Following this short interval up until the present day, the internal Aegean domain has again been under extension (Fig. 9), whereas compressional structures have formed along the Hellenic arc. The focal mechanisms of the Aegean earthquakes agree with both these tectonic manifestations.

4) The upper mantle structure deduced from p- and s-wave tomography is dominated by the subduction of the African lithosphere along the Calabrian and Hellenic arcs. The corresponding two subducting slabs are separated by a deep-reaching mantle plume in the Ionian Sea.

5) In addition to the well-known seismicity belt following the subducting slabs, a dominant cluster of earthquakes exists in southern and western Anatolia. It has a triangular shape and it is surmised that this part of Anatolia is being pulled out to the southwest and at the same time being rotated counter-clockwise, as indicated by the shape of the gulf inlets along the west coast of Anatolia. It should also be noted that there is a clear offset of the seismicity of about 220km to the NNW, between the islands of Karpathos and Rhodes, which is probably due to an irregularity in the crust and upper mantle related to the triangular feature.

6) The level of heat flow in western Anatolia is much higher (100 to 120mWm^{-2}) than that in the Eastern Mediterranean Sea and the Black Sea, with values of 20 to 30mWm^{-2}. In addition, the heat flow in the North Aegean Trough, the Biga Peninsula and the “horst and graben” structures in the central part of western Anatolia clearly shows considerably elevated heat flow values when compared with the remainder of the Turkish territory. The heat flow pattern is similar to the observed seismicity which exhibits the structural “triangular” configuration.

7) Recent GPS results obtained in extensive GPS campaigns (Reilinger et al. 1997, Straub and Kahle 1996) constrain the crustal motion of western Anatolia to rates of about 22mm/a, relative to a Europe fixed reference system. The Aegean region is characterised by rates reaching SW oriented velocities of about 40mm/a at the leading edge of the Hellenic arc. The driving mechanism of this spatial acceleration is as yet unkown.

References

Ambraseys N.N. and Finkel, C.F., 1991, Long-term seismicity of İstanbul and the Marmara Sea region, Terra Nova 3, 527-539.

Anderson, H. and Jackson, J., 1987, Active tectonics of the Adriatic region, Geophys. J. R. astr. Soc., 91, 937-983.

Barka, A. and Kadinsky-Cade, K., 1988, Strike-slip fault geometry in Turkey and its influence on earthquake activity, Tectonics, 7, 3, 663-684.

Barka, A., 1992, The North Anatolian Fault Zone, Annales Tectonicae, Suppl. to Vol. VI: 164-195.

Barka, A.A., 1997, Neotectonics of the Marmara Sea region, this volume.

Cermak, V. and Rybach, L., (eds.) 1979, Terrestrial heat flow in Europe, Springer Verlag Berlin.

De Jonge, M.R., Wortel, M.J.R. and Spakman, W., 1994, Regional scale tectonic evolution and the seismic velocity structure of the lithosphere and upper mantle: The Mediterranean region, J. Geophys. Res., Vol. 99, 12091-12108.

Denys, P., Cross, P., Veis, G., Billiris, H., Paradissis, D., Ashkenazi, V., Bingley, R., England, P., Clarke, P., Kahle, H.-G. and Mueller, M.V., 1995, GPS networks for determining the accumulation of current crustal strain in central Greece, Proceedings of 1st Turkish International Symposium on deformations, Vol. 2, 748-758.

Dewey, J.F., Helman, M., Turco, E., Hutton, D. and Knott, S., 1989, Kinematics of the Western Mediterranean, in: Alpine Tectonics, edited by: M. Coward, D. Dietrich and R. Park, Spec. Publ. Geol. Soc., London, 45, 265-283.

Eyidoğan, H. and Barka, A., 1996, The 1 October 1995 Dinar earthquake, SW Turkey, Terra Nova, 8, 479-485.

Güleç, N., 1988, Helium-3 distribution in Western Turkey, Mineral Res. Expl. Bull., 108, 35-42.

Kahle, H.-G., Müller, M.V., Mueller, St., Veis, G., Billiris, H., Paradissis, D., Drewes, H., Kaniuth, K., Stuber, K., Tremel, H., Zerbini, S., Corrado, G. and Verrone, G., 1993, Monitoring West Hellenic Arc Tectonics and Calabrian Arc Tectonics ("WHAT A CAT") Using the Global Positioning System, in: Contribution of Space Geodesy to Geodynamics, edited by: D. Smith and D. Turcotte, AGU Geodynamics Series, Vol. 23, 417-429.

Kahle, H.-G., Straub, C., Müller, M.V., Kastens, K., Gilbert, L., Hurst, K., Veis, G., Billiris, H. and Paradissis, D., 1996, Estimates of strain rates in the Eastern Mediterranean, inferred from GPS measurements, Abstract, American Geophysical Union (AGU), EOS Supplement, April 23, 1996, Vol. 77, No. 17, S73.

Kaniuth, K., Drewes, H., Stuber, K., Tremel, H., Zerbini, S., Pezzoli, L., Corrado, G., Kahle, H.-G., Müller, M.V., Mueller, St., Veis, G., Billiris, H., and Paradissis, D., 1995, GPS based deformation estimates in the Calabrian and West Hellenic Arcs, *XXI IUGG General Assembly. Boulder*, Colorado, USA. Abstract Volume A, 32.

Kastens, K., Gilbert, L., Hurst, K., Veis, G., Paradissis, D., Billiris, H., Schlüter, W. and Seeger, H., 1997, GPS evidence for arc-parallel extension along the Hellenic Arc, Greece, Tectonophysics, in press.

Kiratzi, A. and Papazachos, C.B., 1995, Active crustal deformation from the Azores triple junction to the Middle East, Tectonophysics, 243, 1-24.

Le Pichon, X., Chamot-Rooke, N., Lallemant, S., Noomen, R. and Veis, G., 1995, Geodetic determination of the kinematics of Central Greece with respect to Europe: Implications for Eastern Mediterranean Tectonics, J. Geophys. Res., 100, B7: 12'675-12'690.

Makris, J., 1978, The crust and upper mantle of the Aegean region from deep seismic soundings, Geophysics, 46, 269-284.

Makris, J. and Stobbe, C., 1984, Physical properties and state of the crust and upper mantle of the Eastern Mediterranean Sea deduced from geophysical data, in: Geological and geodynamical aspects on the Mediterranean, edited by: C. Morelli, Marine Geology, Vol. 55, No 3/4. Special Issue, 347-363.

McKenzie, D.P., 1978, Active tectonics of the Alpine-Himalayan belt: The Aegean and surrounding regions, Geophys. J. R. astr. Soc., 55, 217-254.

Mercier, J., Sorel, D. and Simeakis, K., 1987, Changes in the state of stress, Ann. Tectonicae, 1, 20-39.

Müller, M.V., 1995, Satellite Geodesy and Geodynamics: Current deformation along the West Hellenic Arc, PhD. thesis ETH Zürich, No. 11'358.

Noomen, R., Springer, T., Ambrosius, B., Herzberger, K., Kuijper, D., Mets, G., Overgaauw, B. and Wakker, K., 1995, Crustal deformations in the Mediterranean area computed from SLR and GPS observations, J. Geodynamics, 21, 1, 73-96.

Olsen, K.H., (ed.), 1995, Continental rifts: evolution, structure, tectonics, Developments in Geotectonics, Elsevier.

Oral, B., GPS measurements in Turkey (1988-1992), 1994, Kinematics of the Africa-Arabia-Eurasia plate collision zone, PhD thesis, Massachusetts Institute of Technology, 344p.

Oral, M., Reilinger, R., Toksöz, M., King, R., Barka, A., Kinik, I. and Lenk, O., 1995, GPS offers evidence of plate motions in E. Mediterranean, EOS Trans., 76, 9-10.

Papazachos, B., 1990, Seismicity of the Aegean and surrounding area, Tectonophysics, 178, 287-308.

Peter, Y., Kahle, H.-G., Cocard, M., Veis, G., Paradissis, D. and Felekis, S., 1997, Establishment of a permanent GPS-network across the Kephalonia Fault Zone, Greece, Proceedings 7th WEGENER General Assembly, University of Porto, Portugal, Tectonophysics, in press.

Papazachos, B., Kiratzi, A. and Papadimitriou, E., 1991, Regional focal mechanism for earthquakes in the Aegean Sea, Pageoph., 136, No. 4, 405-420.

Reilinger, R., McClusky, S., Kahle, H.-G., Müller, M.V., Straub, C., Kastens, K., Gilbert, L., Hurst, K., Veis, G., Paradissis, D. and Barka, A., 1995, GPS evidence for westward continuation of dextral strike-slip motion from the North Anatolian Fault Zone across the North Aegean and North-Central Greece, Abstract, Fall Meeting American Geophysical Union (AGU), EOS, Supplement, Nov. 7: F620-F621.

Reilinger, R., McClusky, S., Oral, B., King, R., Toksöz, M., Barka, A., Kinik, I., Lenk, O. and Sanli, I., 1997, GPS measurements of present-day crustal movements in the Arabia-Africa-Eurasia Plate collision zone, J. Geophys. Res., 102, B5, 9983-9999.

Reuther, C.-D., Ben-Avraham, Z. and Grasso, M., 1993, Origin and role of major strike-slip transfers during plate collision in the Central Mediterranean, Terra Nova, 5, 249-257.

Robbins, J., P. J. Dunn, M. H. Torrence and Smith, D.E., 1996, Deformation in the Eastern Mediterranean, Proceedings of the First Turkish International Symposium on Deformations 1994, edited by: M. Sahin and P.A. Cross, 738-745.

Sellami, S., Pavoni, N., Mayer-Rosa, D., Mueller, St., Aktar, M., Eyidoğan, H., Gürbüz, C., Bariş, Ş and Yalcin, N. 1997, Seismicity and Seismotectonics of the Bursa region, this volume.

Smith, D.E., Kolonkiewicz, R., Robbins, J.W., Dunn, P. and Torrence, M., 1994, Horizontal crustal motion in the central and Eastern Mediterranean inferred from satellite laser ranging measurements, Geophys. Res. Letters, 21, 18, 1979-1982.

Spakman, W., Wortel, M.J.R. and Vlaar, N.J., 1988, The hellenic subduction zone: A tomographic image and its geodynamic implications, Geophysical Research Letters, Vol. 15, No. 1, 60-63.

Spakman, W., Van der Lee, S. and Van der Hilst, R., 1993, Travel-time tomography of the European-Mediterranean mantle down to 1400km, Physics of the Earth and Planetary Interiors, 79, 3-74.

Straub, C. and Kahle, H.-G., 1995, Active crustal deformation in the Marmara Sea region, NW Anatolia, inferred from GPS measurements, Geophysical Research Letters, 22, 18, 2'533-2'536.

Straub, C., 1996, Recent crustal deformation and strain accumulation in the Marmara Sea region, N.W. Anatolia, inferred from GPS measurements, PhD thesis, ETH Zürich.

Straub, Ch. and Kahle, H.-G., this volume, Recent crustal deformation and strain accumulation in the Marmara Sea region, N.W. Anatolia, inferred from repeated GPS measurements.

Tezcan, A.K. and Turgay, M.I., 1991, Geothermal atlas of Europe, catalogue of heat flow density data: Turkey, in: Geothermal Atlas of Europe, edited by: E. Hurtig, V. Cermák, R. Haenel and V. Zui, 84-85.

Udias, A., Buforn, E. and Ruiz, J., 1989, Catalogue of focal mechanisms of European earthquakes, Dept. of Geophysics, Universidad Complutense, Madrid, 274p.

Wortel, R. and Spakman, W., 1992, Structure and dynamics of subducted lithosphere in the Mediterranean region, Proc. Kon. Ned. Akad. v. Wetensch., 95, 325-347.

Yan, B., Graham, E.K. and Furlong, K.P., 1989, Lateral variations in upper mantle thermal structure inferred from three dimensional seismic inversion models, Geophys. Res. Letters, 16, 449-452.

Zanchi, A. and Angelier, J., 1993, Seismotectonics of Western Anatolia: Regional stress orientation from geophysical and geological data, Tectonophysics, 222, 259-274.

Zerbini, S., Billiris, H., Corrado,G., Drewes, H., Kahle, H.-G., Kaniuth, K., Müller, M., Pezzoli, L., Stuber, K., Tremel, H. and Veis, G., 1994, Monitoring crustal deformation in the West Hellenic Arc and Calabrian Arc using GPS, Abstract, Spring Meeting American Geophysical Union (AGU), EOS, Supplement, April 19, 115-116.

Zielhuis, A., 1992, S-wave velocity below Europe from delay-time and waveform inversion, PhD thesis, University of Utrecht, Dept. of Earth Sciences, No. 88, 148p.

Zielhuis, A. and Nolet, G., 1994, Shear-wave velocity variations in the upper mantle beneath central Europe, Geophys. J. Int., 117, 695-715.

Geology of Western Anatolia

YÜCEL YILMAZ

Introduction

The sequence of Western Anatolia may be divided into two parts: the lower association and the upper association. The lower association is a tectonic mosaic consisting of the different tectonic entities. From north to the south these are: the Sakarya continent, the İzmir-Ankara ophiolitic suture, the Menderes massif and the Taurides (Figure 1).

The Sakarya continent is a narrow continental fragment that is delimited along the northern and the southern boundaries by the ophiolitic suture zones. The İzmir-Ankara ophiolitic suture zone is the remnant of the Tethyan ocean that was totally consumed between the Sakarya continent and the Taurides. The Menderes massif is a metamorphic complex that represents the northern margin of Gondwanaland.

The rocks which will be described as the upper association or the cover make up the succession which was formed following the final amalgamation of the tectonic entities mentioned above, and are post Oligocene rocks which consist essentially of continental deposits and associated widespread volcanic rocks. The lower association and the upper association will be briefly outlined in the following pages.

The lower association

The tectonic units of the lower association of Western Anatolia will be described below, starting from the northern areas.

The Sakarya continent

The Sakarya continent between the Intra-Pontide suture and the İzmir-Ankara suture extends from the Biga peninsula to the Ankara region and even further east (Figure 1). It consists of metamorphic and non-metamorphic Palaeozoic rocks at the base and Mesozoic and Cenozoic rocks as the cover.

Across the Biga peninsula and Bilecik region, there are widespread outcrops of a Pre-liassic basement complex. A large proportion of this basement is formed of Permian and Triassic tectonostratigraphic units which have previously been grouped together and referred to as the "Karakaya complex" (Bingöl et al. 1973).

The distribution of the Preliassic basement and the major tectonic elements of Northwestern Anatolia are shown in Figure 2. From the map, it is seen that these rocks outcrop mainly within the cores of antiformal culminations, which have subsequently been stripped of their Postliassic cover successions.

In the Sakarya continent, there are two distinctly different basement associations which are separated from one another by normal faults or thrusts. They will be referred to here as the Uludağ group and the Yenişehir metamorphic complex. The Uludağ group has a high-grade

metamorphic basement and a Permo-Triassic cover succession. The Yenişehir metamorphic complex consists of metalavas and associated low-grade metasediments, and a slab of a metamorphosed ophiolite, which was wedged tectonically into the metamorphic rocks.

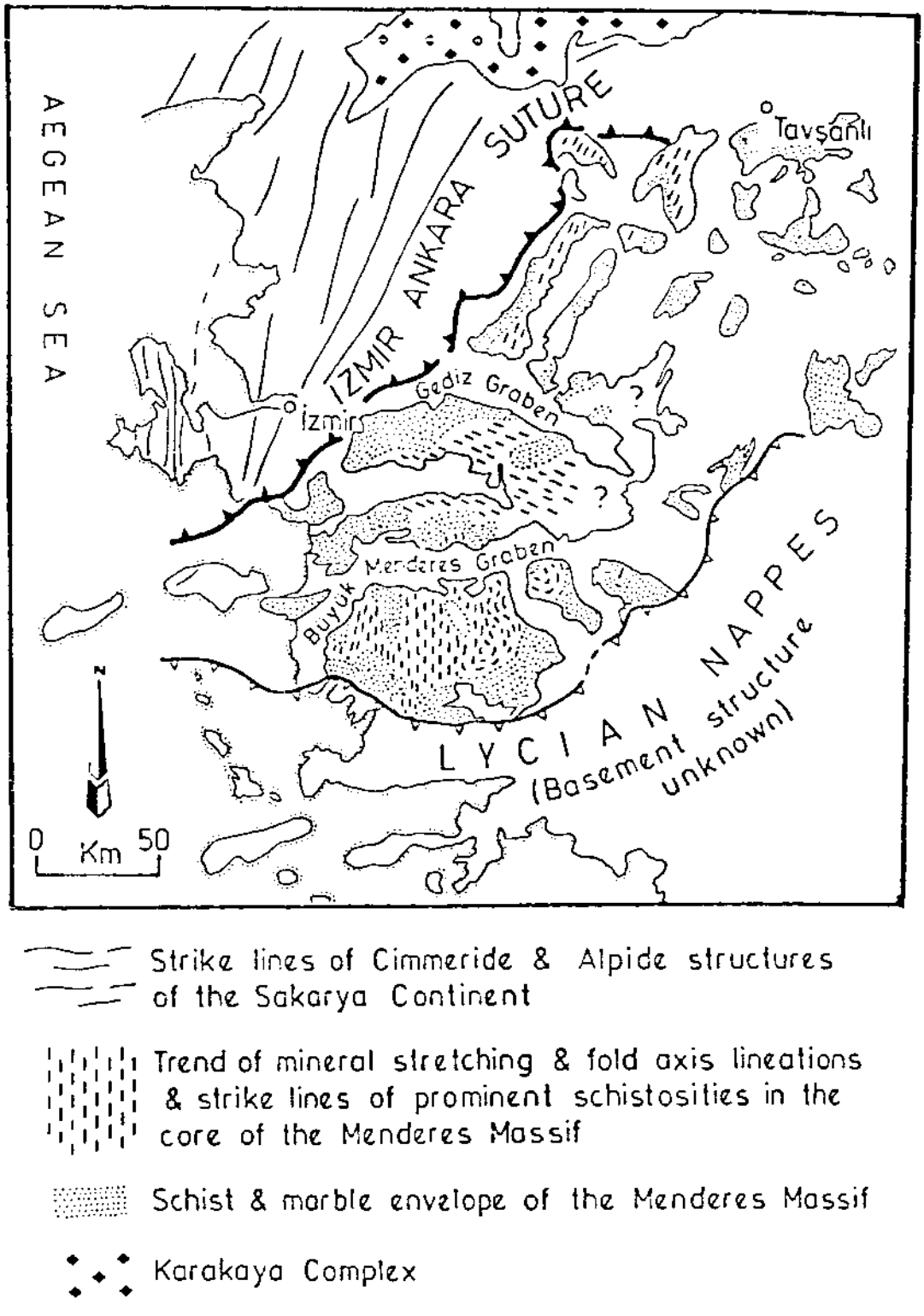


Figure 1: Tectonic map of Western Anatolia.

The Uludağ group outcrops predominantly around the towns of Bursa and Bilecik. The Yenişehir metamorphic complex outcrops mostly around the towns of Yenişehir, Boğaz, Ezine and along the Göksu river valley. In the following paragraphs the basement units will be described, beginning with the Uludağ group.

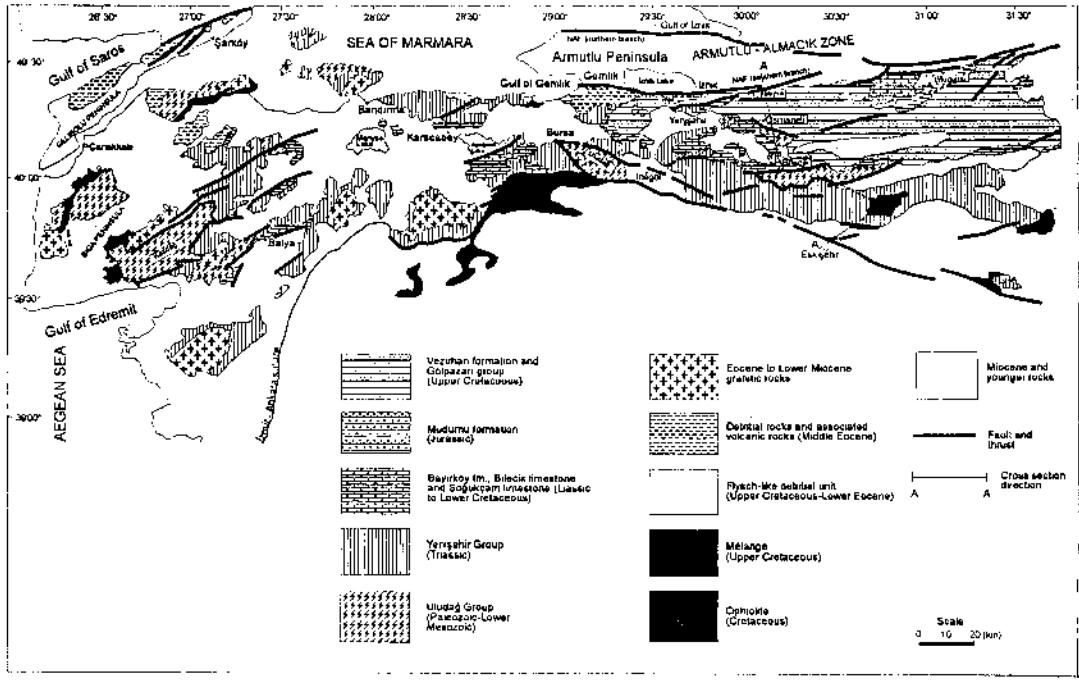


Figure 2: Geological map of the Sakarya continent of Western Anatolia.

The Uludağ group

The Uludağ group is best exposed in the Uludağ and the Bilecik areas. It consists of amphibolite facies, metamorphic gneisses, schists and migmatites and overlying green schists and phyllites (Ketin 1947, Yılmaz 1977). These metamorphic rocks are metapelitic in origin and represent the Paleozoic and older continental fragment. The metamorphic association is intruded by a post tectonic granitic pluton (Yılmaz 1977) that has been dated at about 272±3m.y. old (Çoğulu 1967), corresponding to Carboniferous-Early Permian. These metamorphic associations are overlain by a sedimentary cover succession.

The lowermost lithologies of the sedimentary succession are arkosic conglomerates and sandstones with a disconformable relationship with the Pre-Carboniferous metamorphic complex. These sandstones and conglomerates pass laterally and vertically into a richly fossilifereous neritic limestone of Permo-Carboniferous age (Altınlı 1973, Saner 1977). The limestone gives way to a flysch-like succession of the same age.

However authochthonous, the Permo-Carboniferous sedimentary successions are very rare in Northwestern Anatolia. Most of the Permo-Carboniferous rocks are more commonly observed as blocks and debris hosted with the overlying Triassic rocks. This suggests that Carboniferous and Permian successions were largely removed by erosion prior to and during the deposition of the Triassic. As a result of this, initial products of the Permo-Triassic transgression rest upon the Pre-Carboniferous metamorphic complex rather than the Carboniferous sedimentary rocks. However, in spite of erosion, there are a few scattered remnants of the in-situ Permo-Carboniferous succession beneath the Triassic. The Göksu gorge, the Karasu

valley, the area to the north of the town of Osmaneli and north and east of the town of Ezine are the areas where this can be recognised. A generalised stratigraphic section of the Triassic successions is shown in Figure 3, where two major groups may be distinguished in the sequence: a lower basal detritial unit and a partly overlapping upper unit which is a lava-sediment alternation. Between these successions, rapid lateral and vertical transitions are observed.

The cover rocks display two different types of contact with the underlying metamorphic rocks: either a normal stratigraphic contact or a tectonic contact along which the cover sedimentary rocks were displaced as a decollement.

The lower unit is a basal arkosic sandstone and conglomerate. These white or pink basal rocks pass vertically into alternations of dark gray siltstone and marl (Figure 3), which display severe deformation. There are moderately thin (<50m), neritic limestone lenses also occurring within this lower unit. Petrographically, this unit contains arkose, lithic arenite and orthoquartzite. These lithologies are derivatives from a granitic and quartzo-feldspathic metamorphic source.

The age of this basal unit has been established as Upper Permien-Lower Triassic, according to the fossil assemblage (Kaya 1991)

The basal clastic rocks pass laterally and vertically to the lava sediment association. This commonly begins as an internally chaotic sediment and volcanic assemblage which becomes less chaotic upwards. The volcanic rocks comprise partly spilitised basaltic lavas and pyroclastic rocks such as tuffs and agglomerates. Amongst the sedimentary lithologies, in decreasing order of abundance, there are graywackes, quartz-rich sandstones, micaceous siltstones and different varieties of limestones.These sediments gradually give way to deep-sea sedimentary and volcanic rocks, including pelagic red mudstone, radiolarian and ribbon cherts, and tholeiitic basalts, which are thought to be Middle-Upper Triassic in age (Kaya 1991, Okay et al. 1990).

The lower detritial rocks of the Triassic succession are regarded as representing a transgressive sequence beginning with continental and/or shallow marine sediments, progressively succeeded by relatively deepening marine sedimentary units. The upper part of these sequences are represented by pelagic rocks, including radiolarian chert, shale, mudstone, micritic pink limestone and intercalated, locally pillowed basaltic lavas. However, within the upper pelagic succession, there are also abundant blocks and fragments derived from the Carboniferous and Permian limestones and an ophiolite. Therefore, due partly to the rapid influx of foreign material and frequently developed olistostromes, the lower, as well as the upper parts of the Triassic successions are internally chaotic. The middle part is well-ordered. This suggests that an active tectonic environment governed the development of the Triassic units at the beginning, and the final stages. The lower basaltic lavas display alkaline affinity and compare favourably with rift-type basaltic rocks (Genç 1993, Yılmaz 1977). The upper basalts are either mildly alkaline or tholeiitic.

The data outlined above indicate that the Triassic sequence of the Uludağ group is bounded by two angular unconformities developed during the pre-late Permian and the Early Liassic. The sequence may result from deposition in a short-lived basin that existed during the Triassic. The lower part of the sequence is interpreted as having formed in a continental environment which evolved subsequently into a deep marine basin, as evidenced by the upper part of the succession containing the pelagic sedimentary rocks and associated tholeiitic basalts. The large quantities of olistostromes, blocks and fragments of the top of the succession is interpreted as indicating the tectonic phase which led to the closure of the basin and compressional deformation of the basin fill.

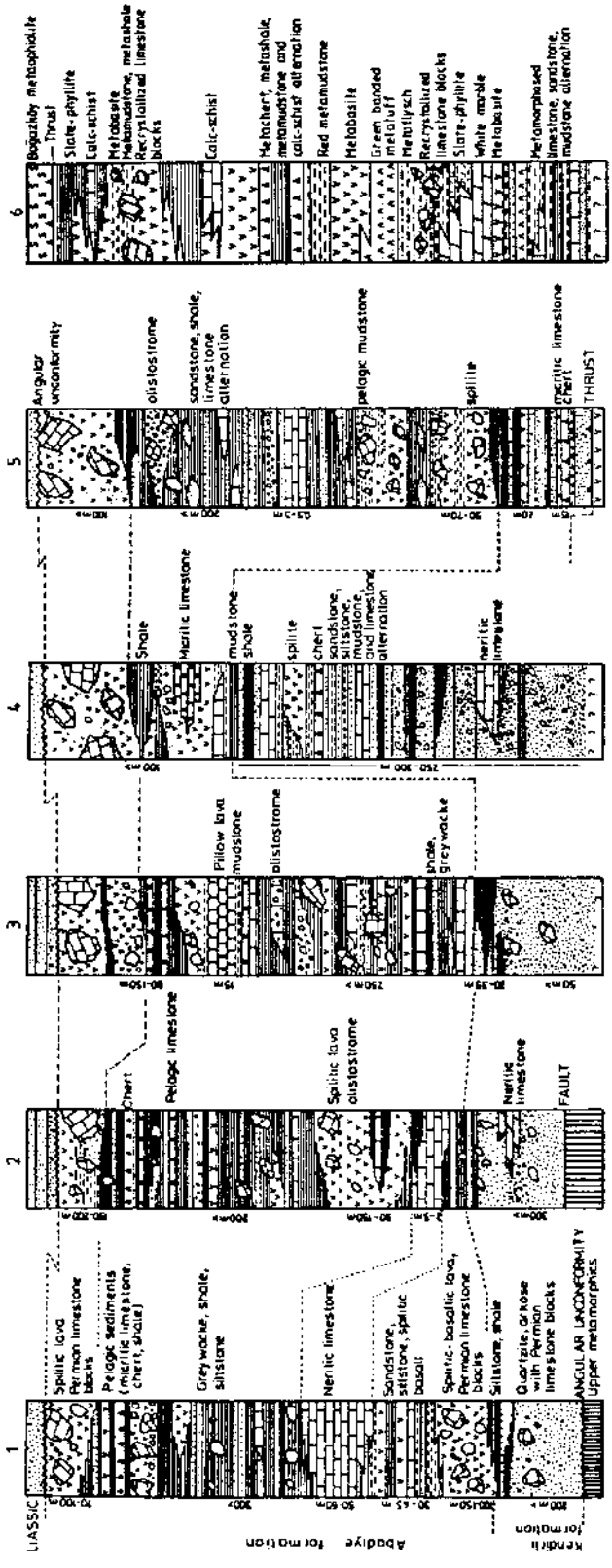


Figure 3: Triassic stratigraphic sections of Northwestern Anatolia.

The Yenişehir metamorphic complex

In this rock association, two different rock groups are differentiated. These are regional metamorphic rocks and an ophiolitic slice. The former is a polyphase metamorphic assemblage, in which metabasic rocks dominate. The latter is represented by a thin (<200m) slice of an ordered ophiolite. Within the variety of metamorphic rocks, basic lavas, pyroclastic rocks, such as meta-tuffs and meta-sedimentary rocks including mudstone, chert and limestone, dominate. Also, in this association there are abundant blocks and fragments of marbles and recrystallised limestones of various sizes.

The age of this group may be estimated from available stratigraphical data; there are fossiliferous Upper Permian recrystallised limestone blocks within these rocks, which, in turn, are overlain by Liassic basal sandstones. This evidence clearly places the age of this group of rocks in the Triassic. The Triassic age estimation is further supported by two lines of evidence: (1) The rock units of the Yenişehir metamorphic complex correlate closely with the non-metamorphic cover association of the Uludağ group which is Middle – Upper Triassic in age, (2) Triassic fossils were obtained from similar rocks (Okay et al. 1990).

The ophiolite, which is tectonically mixed with the Triassic units, is seen as a tectonic wedge in the Yenişehir area and in the Bandırma-Erdek region. The ophiolite in these areas is seen as a thin (>500m thick) slice and is represented by an ordered ophiolite, represented by ultramafic rocks (particulary in the Kazdağ) and layered gabbros (the Erdek area), gabbroes (the Erdek and Yenişehir areas) and spilitised lavas. The have undergone greenshist facies metamorphism, possibly together with the enclosing metasedimentary rocks (Genç and Yılmaz 1994, Genç 1993).

In addition to the ordered ophiolite, there are also some ophiolitic melange associations. They outcrop in the south of the Bayramiç graben and to the south of the Armutlu peninsula, between İznik and Geyve (Figure 2). The melange displays greenschist facies metamorphism and consists mainly of spilitised basic volcanic rocks, radiolarian red cherts, marbles, metagraywackes and pyroclastic rocks.

Within the phyllitic hosts, there are number of ophiolitic blocks. They crop out mainly in the Gemlik, Geyve and Körfez areas.

In the Biga peninsula, there are few granitic stocks which cut the Yenişehir metamorphic complex. These are possibly Late Triassic in age, because they intruded into the Triassic rocks following their regional metamorphism and are overlain unconformably by the Liassic basal detritials. They outcrop south of Biga and south of Körfez. These data lead to the conclusion that, prior to the Latest Triassic deformation and the metamorphism of the Yenişehir metamorphic complex, these two assemblages were assembled together to form the amalgamated tectonostratigraphic unit.

When the Permo-Triassic rocks that cover the Uludağ metamorphic assemblage in normal stratigraphic contact are compared to the Yenişehir metamorphic complex, a close similarity between the two is apparent. However, the former is non-metamorphic and the latter is metamorphosed. Both assemblages show similar depositional histories and the facies, in both their upper and lower parts, were governed by an active tectonic regime. This supports a genetic link between the two groups. Both of these assemblages are covered collectively by the Liassic (Hettangian-Pliensbachian) basal detritial succession (the Bayırköy formation). The post-metamorphic cover succession is illustrated in Figures 2, 4A, 4B and 5. The basal detritial rocks are overlain by a thick neritic limestone succession that is known as Bilecik limestone (Altınlı 1973). This begins at the base with oolithic or terrigeneous limestones of Bathonian-Oxfordian age (Granit and Tintant 1960, Altınlı 1973, Saner 1977, Yılmaz 1981, 1990a, b, Altıner and Koçyiğit 1992). Nowhere is the contact between the basal clastic rocks and the

succeeding shallow marine limestone an angular unconformity, despite a stratigraphic break corresponding to the Dogger interval, which has been identified locally based on fossil findings (Granit and Tintant 1960, Altınlı 1973, Altıner and Koçyiğit 1992). The Jurassic limestones are laterally and vertically replaced by a cherty, thinly-bedded, white limestone of Early Cretaceous age (Soğukçam limestone). These limestones pass upward into a reddish pelagic limestone, radiolarite, mudstone unit of Cenomanian-Turonian age. After that, the uniform and continuous Cretaceous pelagic limestone succession is replaced by units showings wide lateral facies changes. In the southern areas, the limestone is followed initially by a carbonate flysch and then by a flysch. The northern areas consist of a coeval basal sandstone and/or limestone unit which overlies a variety of older rocks, including the basement metamorphic rocks (Figure 5). The basal clastic rocks, or carbonate rocks, pass upward into a flysch sequence, identical to the flysch extending from the continuous succession of the southern areas. Thus, the continuous and deeply-eroded successions both underlain by the same flysch blanket suggest that part of the region was elevated and eroded prior to the flysch deposition during the Coniacian-Santonian. The post-erosional flysch yields Campanian-Maastrichtian age.

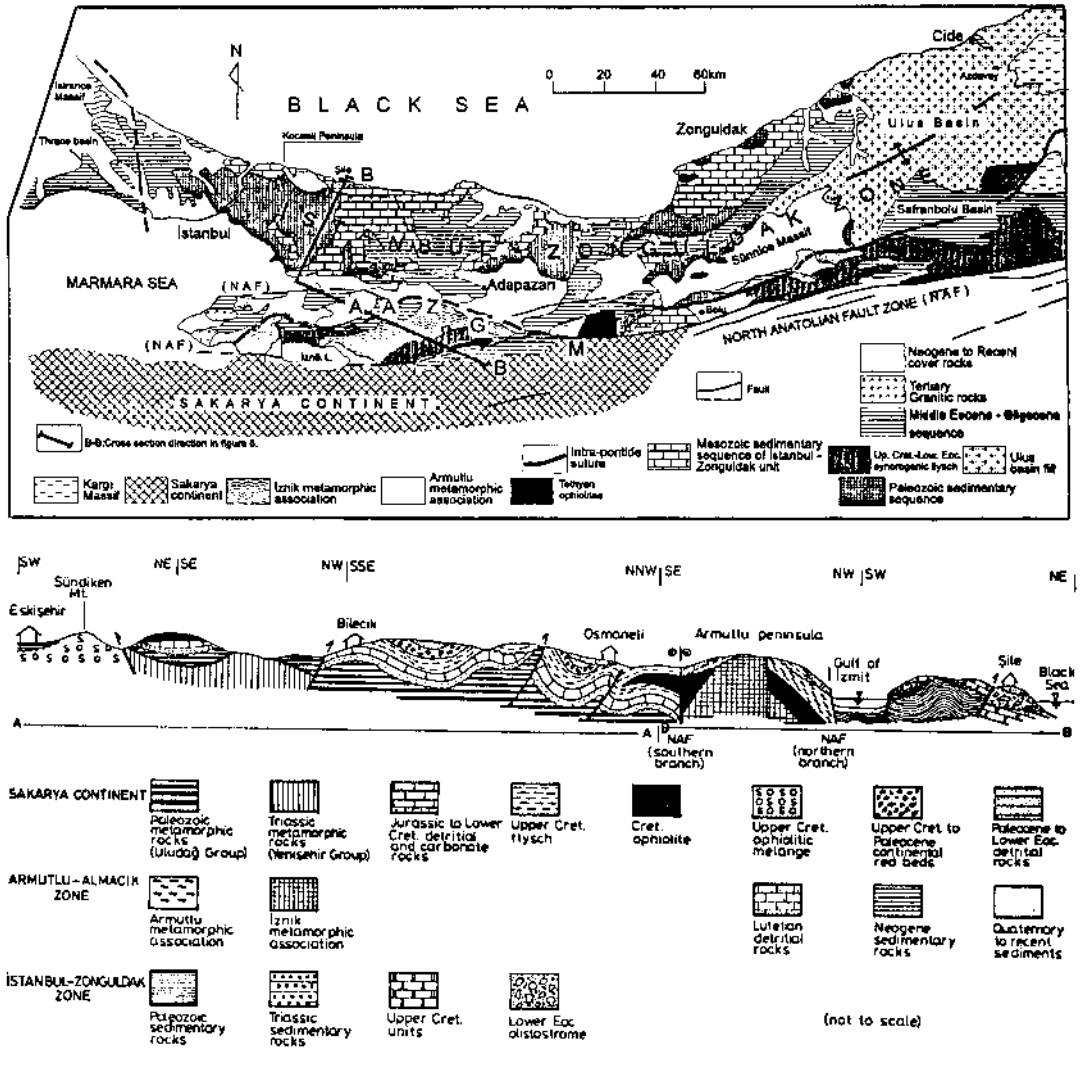


Figure 4: *Geological map (Fig. 4A) and accompanying geological cross section (Fig. 4B) of the western Pontide, NW Turkey (after Yılmaz et al. in press).*

There are abundant blocks, olistostromes and fragments of the older units, comprising debris flow deposits within the flysch. Among the older unit fragments, the upper Jurassic and lower Cretaceous limestones predominate. There are also blocks and fragments of an ophiolite, ophiolitic melange association and blue-schist metamorphic rocks, within the flysch succession.

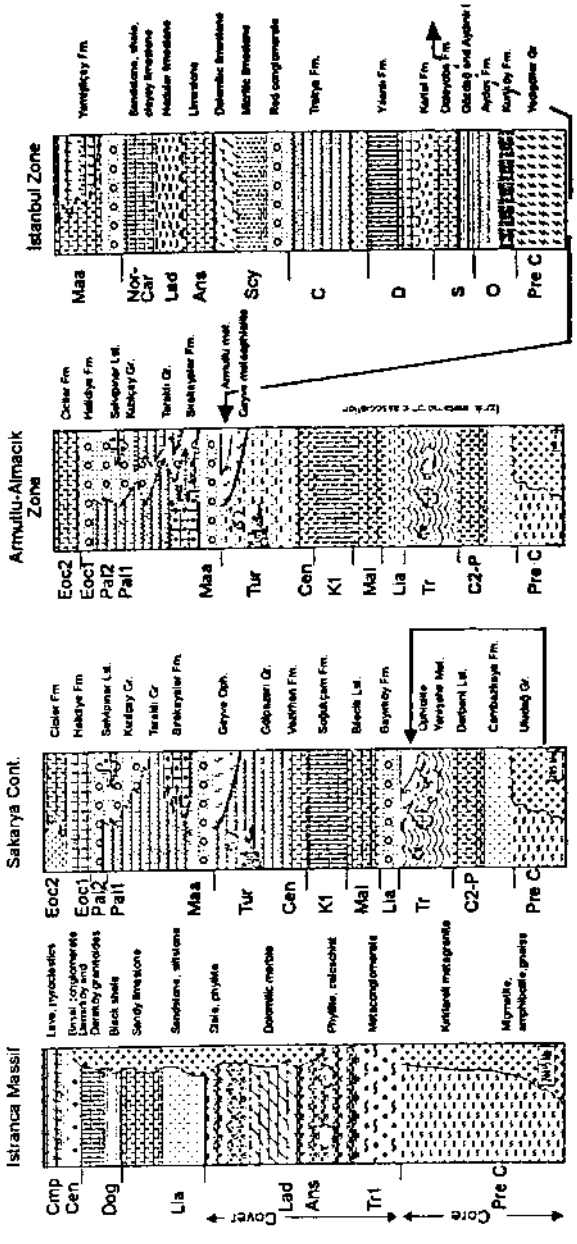


Figure 5: *Generalised stratigraphic sections from the Sakarya continent and adjacent regions (after Yılmaz et al. in press).*

Following the incorporation of the olistostromes and blocks, the depositional environment changed from deep sea to shallow sea (Yılmaz 1981, Yılmaz 1990a, b), as evidenced by the gradual replacement of the flysch with shallow marine sandstone and reefal limestone (Altınlı 1973, Yılmaz 1990a, b). This change occurred during the Maastrichtian (Yılmaz 1990a, b).

The regressive succession was then overlain by continental red beds that formed during the Maastrichtian-Palaeocene transition (Altınlı 1973, Bargu 1982, Yılmaz 1990a. b). Around the Geyve and Taraklı areas, an ophiolite slice rests on the flysch which, in turn, is overlain by the lower Maastrichtian shallow marine sediments. The sediment deposition continued until the end of the Early Eocene period along roughly E-W oriented depressions; i.e. the Osmaneli area (Fig. 2). The whole region was then gradually elevated and eroded prior to the deposition of the new region wide transgression in the Middle Eocene (Fig. 5). These shallow marine sedimentary rocks are accompanied by widespread intermediate volcanics that were formed in fault-bounded interconnected basins governed by a regional extensional system. The marine environment and volcanism survived to the Late Eocene. It then gradually gave way to the continental red beds in the Oligocene period due to the new compressional tectonics and consequent region wide deformation.

The İzmir-Ankara suture zone

The İzmir-Ankara suture divides the Sakarya continent from the Taurid system (Figures 1 and 2). It consists of a metamorphic and nonmetamorphic ophiolitic melange association and a peridotite nappe. Therefore, it is regarded as the remnant of an oceanic realm that was consumed between the two continents.

The İzmir-Ankara suture displays different geological features in different areas. From Orhaneli eastward to the Yunak area, it displays HP/LT metamorphism. The width of this belt (30-100km) decreases westwards and terminates to the west of Orhaneli. The contact between this belt and the Sakarya continent is presently a high angle, young fault which cuts and obscures the original contact, which is a low-dipping thrust, along which the basement metamorphic rocks of the Sakarya continent rest on the ophiolitic melange (Figure 4B). The thrust is well exposed around Orhaneli. To the west of Orhaneli, rare outcrops of an ophiolitic melange occur, but it is either non-metamorphic or a green schist facies metamorphic unit. Along this suture zone olistostromes of ophiolitic rocks embedded in a flysch matrix also occur. Outcrops of this unit extend from the İzmir region in the west to the Eskişehir and Konya areas to the east.

The matrix of the melange is a strongly tectonised volcano-sedimentary association. These rocks are spilitised basic lavas, shales and graywackes. Among the blocks, there are radiolarian cherts, pelagic limestones, manganifereous cherts, neritic limestone olistoliths, marble blocks and serpentinite lenses. The sedimentary rocks were tectonically intercalated with ophiolitic rocks. Some eclogites are reported from the İzmir-Ankara suture zone (Çoğulu 1967, Okay 1984).

The age of generation of the blue schists in the suture zone occurred over a period from 108 to 88m.y., according to the radiometric age-dating data (Harris et al. 1994). However, generation of the ophiolitic tectonic melange definitely lasted to the Late Cretaceous, because the melange also contains Upper Cretaceous pelagic sedimentary rocks, such as red pelagic limestones.

The Menderes massif

The Menderes massif is the major metamorphic culmination of Western Anatolia (Figure 1). It extends from the İzmir-Ankara suture in the north to the Kale -Tavas molasse basin in the south. It is roughly elliptical, with a NE-SW oriented long axis. The massif has a complex internal structure and lithological distribution. Despite this, there are high grade (the amphibolite facies) gneisses and schists, commonly regarded as the core of the massif (Şengör et al.

1984). The lower grade (the greenschist facies) schists, marbles and phyllites, and the lowest grade (the lower greenschist facies) recrystallised limestones and associated metasedimentary rocks surround the core rocks. The low grade rocks are considered to be representing the cover rocks that envelope the core.

There are a number of radiometric and paleontologic data obtained from the metamorphic rocks, and during the recent years a number of detailed studies were conducted on the massif. Despite these, age, generation and development of the massif are still widely debated. The radiometric ages obtained from the high grade gneisses show a wide scatter varying from 1.2b.y., 900m.y., 500m.y., 470m.y (Şengör et al. 1984, Satır and Friedrichsen 1986), up to 56, 37, 35, 25 and even to 10 to 5m.y. (Şengör et. al. 1984).

Erdoğan and Güngör (1992) demonstrated a relatively well ordered cover succession dominated by the carbonate rich rocks and listed fossil assemblages covering a wide range from Carboniferous to the Upper Cretaceous. These data alone indicate that the main metamorphic phase occurred between the latest Cretaceous and the Early Miocene interval, because the Late Oligocene continental red beds rests stratigraphically on the metamorphic rocks along the southern margin of the massif.

The tectonic history of the Menderes massif involves a major regional dynamothermal metamorphism, which reached amphibolite-facies at the so-called core rocks. This event is referred to as the main Menderes metamorphism, which resulted from burial under the nappe stack of the Lycian nappes during the compressional regime which affected the region from the Late Cretaceous to Miocene interval.

This Barrowian regional metamorphism has been dated to be 35±5m.y. (Şengör et al. 1984, Satır and Friedrichsen 1986) corresponding to Oligocene.

The regional metamorphism was followed by thermal doming during the Early Miocene and then the Menderes dome collapsed, creating a region wide extensional system all around the massif. This is thought to have triggered development of the first fault-bounded basins, prior to the E-W oriented Aegean grabens.

The Menderes massif is regarded as the northern margin of the Taurides (Şengör and Yılmaz 1981). This assumption is based on the close similarities of the Mesozoic successions that are recorded in the Taurus and the Menderes massif. The rock units common to the two tectonic entities cover the entire Mesozoic section, including the Upper Cretaceous.

The ophiolitic nappes which were emplaced on the platform successions during the Late Cretaceous ceased further development of the Tauride passive margin. From then on, the Menderes and the Taurus began having different geological evolutions. The former underwent regional metamorphism, while the latter remained as a sedimentary succession. This may be related to the progressive burial of the nappe-laden northern edge of the Taurus passive margin.

The upper association

The rocks that rest on the different tectonic entities of Western Anatolia (the Sakarya continent, the İzmir-Ankara suture, the Menderes massif and the Taurus), as the first common cover unit began to form during the Late Oligocene-Early Miocene period. This suggests that final development of the present tectonic configuration of Western Anatolia coincides with the Oligocene period. This conclusion is further supported by the radioactive ages obtained from the Menderes massif; the main Menderes metamorphism occurred approximately 35m.y. ago. According to this evidence, the high grade rocks of the massif were not yet unroofed and were still buried under a 15-20km rock pile during the Late Eocene – Early Oligocene period (Şengör et al. 1984, Akkök 1979).

This suggests that the massif was elevated and unroofed at a later period, possibly during the Late Oligocene – Early Miocene interval.

The removal of the envelope rocks of the Menderes massif may have been due to exhumation of the lower crustal rocks, accompanied by subordinate degrees of erosion, because the amount of sedimentary infill in the present Neogene basins around the Menderes massif cannot account for the obliteration of a 15-18km thick rock column. This rules out erosion as the single mechanism which is responsible for the complete removal of the envelope rocks.

Starting from the final tectonic amalgamation, Western Anatolia began to be covered by a region wide common cover of sediments and associated volcanic rocks. The sediments were formed mostly in the continental basins.

Figure 6 shows the generalised stratigraphic sections of the cover successions of Western Anatolia. In the following paragraphs, the cover successions will be summarised starting from the sedimentary assemblages.

According to the sedimentary successions recorded in the different areas of the region, two consecutive, major stages of the basin development may be distinguished. This is seen clearly in the Edremit-Ayvacık area (Fig. 6A), the Bergama-Korucu-Soma area (Fig. 6) and the Uşak area. The first stage corresponds to Late Oligocene(?) – Early Miocene and is represented dominantly by lacustrine limestone and associated fine-grained detritial depositions such as limestones, marls, and siltstones. These sediments were deposited mostly in a low energy environment. The following succession begins mainly with coarse detritial rocks and passes up into sandstones and conglomerates alternating with porous, lacustrine limestones. This new environment of deposition was tectonically more active and represented by the rocks of a higher energy environment.

In some areas, such as the Bayramiç graben and the southern part of the Bergama graben, these major phases of basin development were followed by yet a third phase, which corresponds to the Pliocene period.

The first phase of sedimentation occurred in continental basins, mostly in interconnected lake basins (Benda 1971). These rocks are not confined to the present graben system and apparently are independent from the grabens, as they outcrop more extensively, covering the horsts as well as the graben areas.

These lake basins appear to have covered very large areas in Western Anatolia. They extended from the Çanakkale area in the north down to the Muğla area in the south. There is a debate on the age of development and the tectonic regime during which the lake basins were formed. Seyitoğlu and Scott (1991a, b) suggested that these rocks were developed within the grabens that were formed due to a N-S extensional regime. Some other workers have suggested that the Early Miocene lake basins were developed over a region wide peneplain surface during the late phase of the compressional system (Şengör and Yılmaz 1981). Accordingly, this phase occurred prior to the formation of the present graben system.

The second phase began following a new tectonic phase, as evidenced by the following data:

1) A commonly angular unconformity is observed between the succession of the first phase of deposition and the rocks of the second phase.
2) The second phase begins with rapidly accumulated coarse clastic rocks, suggesting that the previous low energy environment ended and a new environment began with the development of irregular structural and morphological features.
3) The new phase of sedimentation is confined to narrow basins that correspond roughly to the graben systems.

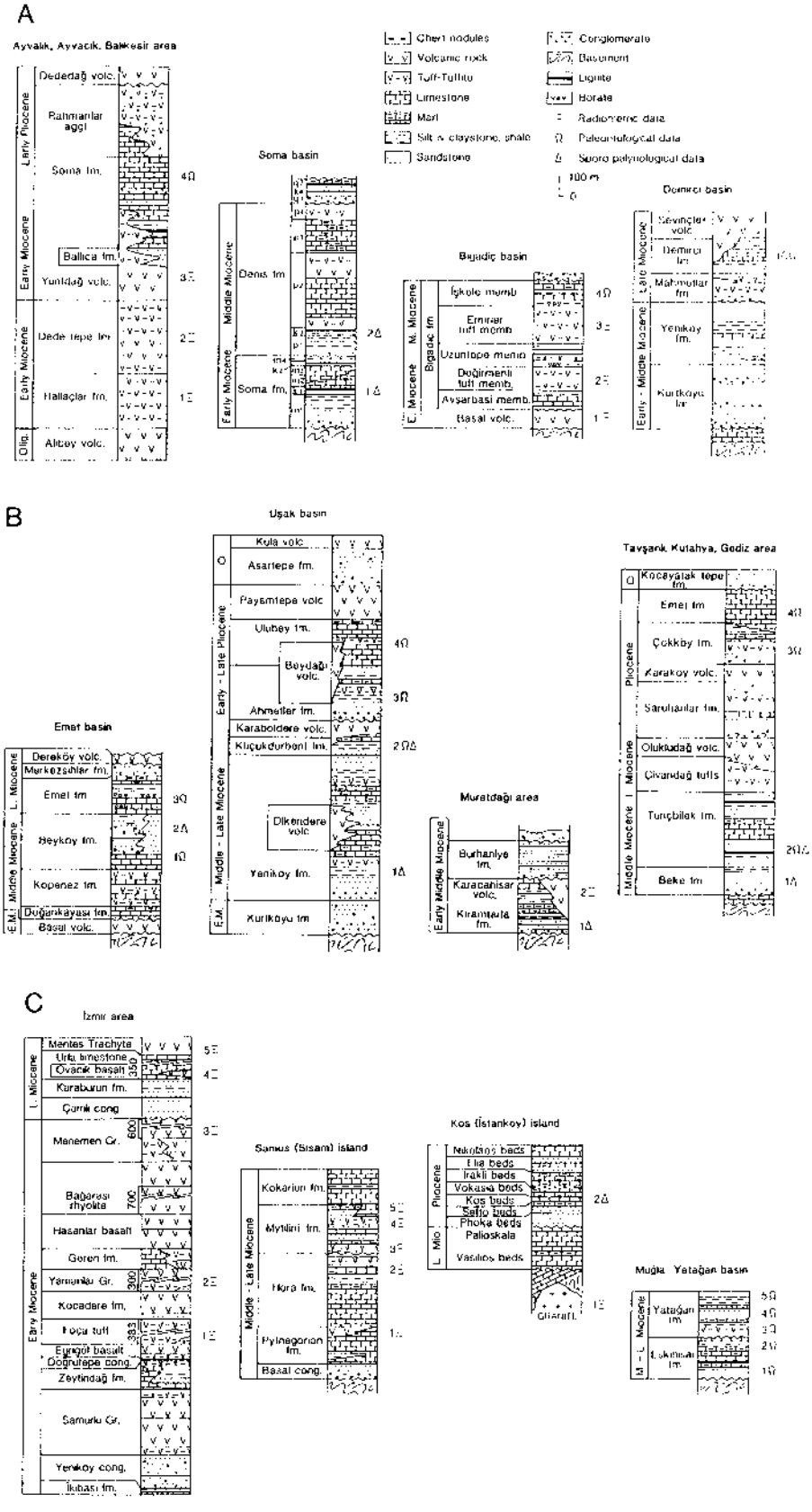


Figure 6: *Generalised stratigraphic sections from the Miocene successions of Western Anatolia (after Seyitoğlu and Scott 1991a, b).*

The sediment deposition in this phase began approximately during the Late Miocene, and restricted to fault-bounded basins.

The latest (the third) phase may be regarded as the reactivation of the horst graben system. During this phase, the graben and horst morphology became more distinct and, consequently, new continental deposition began in front of the newly elevated horst blocks. The scree deposits and debris flow deposits were commonly formed in this phase, and rate of the sediment infill increased.

In some graben areas, such as the Bayramiç graben, a much narrower and deeper graben began to form within the previously formed broad graben area. The major phase of uplift of the Kazdağ horst corresponds to this phase, which began in the Pliocene and continued during the Quaternary.

The magmatic rocks

The Neogene geological evolution of Western Anatolia involves a widespread magmatism producing intrusive, as well as extrusive rocks. The spatial and temporal relations of the magmatic rocks of Western Anatolia are shown in Figures 7 and Table 1. It is seen from Table 1 that the magmatism started at the Oligocene, intensified during the Early Miocene and waned in the Late Miocene-Pliocene. The only exception to this occurred in the Kula area, where volcanic activity continued until prehistorical times.

In the region, three different groups of rocks may readily be distinguished: a granitoid plutonic association, an intermediate volcanic association and a basaltic association. The plutonic rocks are dated from 35 to 20m.y. The intermediate volcanic rocks were partly formed contemporaneously with the plutonic rocks and are dated from 30 to 15m.y. These two groups also show close spatial association. There appears to be a brief nonvolcanic interval between 15m.y and 10m.y. The magmatic activity was rejuvenated approximately 10m.y. ago for a further 6m.y., continued until 4m.y. ago and then disappeared completely. During the latest phase, the basaltic lavas which were nearly absent previously, were formed as the dominant lavas.

The granitic plutonic associations are composed mainly of granodiorites and monzonites with subordinate amounts of adamellites, leucogranites and syenites (i.e. the Kestanbol pluton) (Karacık 1995).

The plutonic assemblage is commonly accompanied by hypabissal rocks, as exemplified by the granodiorite porphyry sheet intrusions in the Kozak granite (Altunkaynak and Yılmaz 1995). Some plutons display gradational contact with the surrounding volcanic rocks, as is the case in the Kestanbol pluton. This indicates that the granitic magmas were emplaced in shallow levels in the crust. This observation is further supported by the data that some plutonic bodies are surrounded by rhyolitic lava domes, ignimbrite flows and felsic pumiceous fall deposits. They all appear to be associated with one another in space and time, and connected collectively with shallow level intrusion in a caldera collapse environment.

The intermediate volcanic rocks display a large variety of composition including basaltic andesite, andesite, trachyandesite, latite and dacite. These rocks vary in the field from a dark-coloured, basalt-like lavas to light-coloured, felsic varieties. The pyroclastic rocks dominate this association. They display almost all of the pyroclastic rock varieties that were formed as the products of pyroclastic fall deposits, flow deposits and surge deposits. Lahar breccias and volcanogenic mud flow deposits are also common.

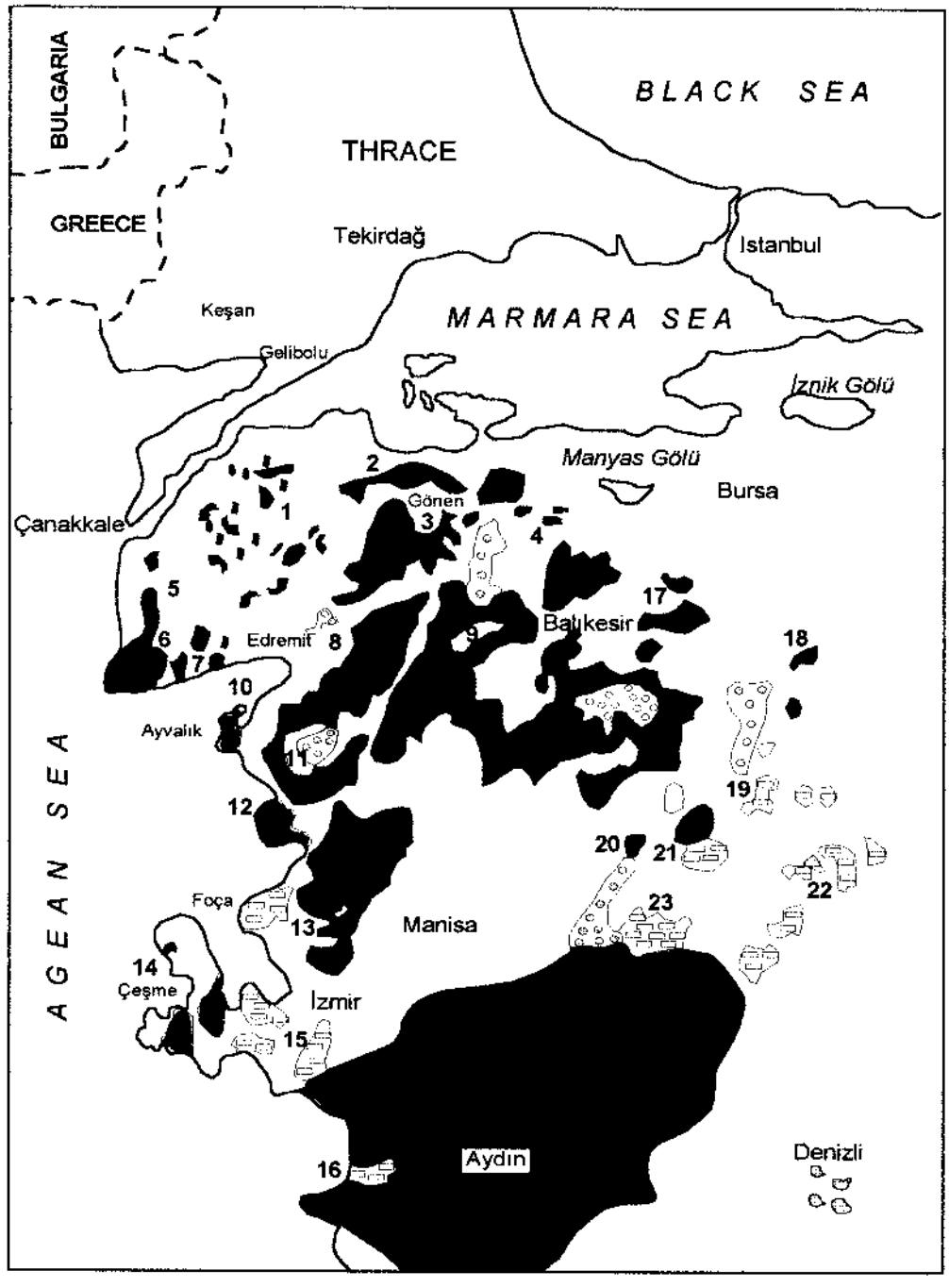


Figure 7: *Distribution of young volcanic and plutonic rocks in Western Anatolia. Numbers indicate the locations shown in Table 1.*

The volcanic layers are often intercalated with lacustrine sedimentary rocks, suggesting that the lavas or the pyroclastic rocks have, in places, been deposited in the lakes. As a consequence of this, welding of the pumiceous pyroclastic flows are only very rarely observed.

In Western Anatolia, two geochemically distinct phases of magmatic activities are distinguished. These are calc-alkaline and alkaline varieties. The early phase that produced the granitic plutons and associated intermediate volcanic rocks are commonly calc-alkaline in composition. Alkaline rock varieties during this period are rare. The late phase that produced basaltic lavas are generally alkaline or transitional. The basic extrusive rocks are nearly

absent in the early phase. This does not mean that the basaltic magma in this period was totally missing, because the intermediate lavas of this phase include basaltic xenoliths, suggesting that the basic magmas were formed but were greatly modified before reaching the surface.

The calc-alkaline association has high volatile content, enriched in LIL elements and the isotope composition. All of this geochemical evidence suggest a hybrid origin, mantled derived magmas contaminated and/or mixed with crustal materials (Yılmaz 1989). The granitic sequence of rocks has much higher isotope ratios but still occupies an intermediate position between the mantle field and the continental values (Yılmaz 1989, 1990a, b).

The alkaline association is predominantly represented by the locally developed basalts and subordinate mugaerites, trachytes and hawaiites. On the petrological basis, two different sequences of alkaline rocks may be distinguished: a) a transitional sequence and b) a distinctly alkaline sequence. The former is the group that shows many similar features to the calk-alkaline volcanic group and is intricately intermixed with it. In this assemblage, the andesitic sequence intersperse with or grade into the dark, but silica enriched, mildly alkaline basaltic lavas. The latter, which is represented by basalts, are distinctly alkaline. This group show geochemical features of a typically mantle-derived magma composition (Yılmaz 1990a, b).

Referenz to the locations cited in fig. 7	Time/Stratigraphy	Lithology	Geochemical Affinity	Radiometric Age (m.y.)
Çanakkala- Bayramiç-Ezine 1,5	Late Pliocene Late Miocene (?) Early Miocene	Basalt Basalt Andesite-dacite-rhyodacite	A A CA	3.85 8.4-9.7-11 31.1
Biga 2	Late Pliocene Late Miocene (?) Early Miocene	Basalt Basalt Andesite-dacite-rhyodacite-rhyolite	A CA	
Gönen 3	Late Pliocene Early Pliocene (?) Early Miocene	Basalt Andesite Andesite-tuff-agglomerate	A CA	
Susurluk 4	Late Pliocene Early Pliocene (?) Early Miocene	Basalt Andesite Andesite-tuff-agglomerate	A CA	
Gülpınar 6	Middle Miocene Early Miocene	Andesite-dacite- rhyolite	CA	18.5 19.5
Ayvacik 7	Late Miocene Middle Miocene Early Miocene	Basalt Rhyolite-ignimbrite Andesite- dacite-rhyolite	A CA CA	7 - 9.9 20.3 - 20.8 21.9 -23.6
Edremit-Burhaniye-Korucu 8	Early Pliocene Early Miocene Late Oligocene Early Miocene	Tuff-agglomerate Dacite-rhyolite Andesite-trachyandesite-dacite-tuff	CA CA CA	19.5 - 19.9 20.3 - 20.8 21.9 - 23.6
Balikesir-Bigadıç 9	Late Miocene (?) Middle Miocene-Early Miocene Late Oligocene-Early Miocene	Basalt Rhyolite Andesite-Latite-dacite Dacite-Rhyolite-tuff Andesite-trachyandesite-dacite-tuff	A CA CA-SH CA	13.0 17.6 - 18.3 19.5 - 20.3 22.3 - 23.6
Ayvalik 10	Late Miocene Early Miocene Late Oligocene-Early Miocene	Basalt Rhyolite- dacite-andesite Andesite- dacite	A CA CA	 16.0 31.4
Bergama 11	Late Pliocene Late Miocene Middle Miocene	Basalt Dacite- rhyolite (lava-tuff) Andesite (lava-pyroclast)	A CA CA	 13.6 14.6, 15.2-15.6

Referenz to the locations cited in fig. 7	Time/Stratigraphy	Lithology	Geochemical Affinity	Radiometric Age (m.y.)
Dikili-Çandarlı 12	Late Pliocene Late Miocene Middle Miocene	Basalt Andesite (lava-pyroclast)	A CA	14.1-16.7 17.3-17.6
Menemen-Foça Izmir 13	Middle Miocene Early Miocene	Basalt- hawaiite- mugearite Latite-latitic andesite- rhyolite	A SH CA	 16.5-17.0 21.5
Çeşme-Karaburun 14	Middle Miocene Early Miocene	Andesite-latitic andesite- dacite-rhyodacite	CA	11.5-12 17-17.3- 18.2 19.2- 21.3
Urla-Cumaovası- Seferihisar 15	Middle Miocene	Basalt- hawaiite- mugearite- trachyte Alkali rhyolite	A	11.3-11.9- 12.5
Söke 16	Late Pliocene Early Pliocene- Late Miocene Miocene (?)	Basalt Trachybasalt Andesite latitic andesite- latite- dacite	A A CA	 6.99
Dursunbey- Orhaneli 17	Late Pliocene Late Miocene- Middle Miocene	Basalt Andesite- dacite- rhyolite	A CA	
Tavşanli 18	Pliocene Late Miocene (?)- Middle Miocene	Basalt Andesite (lava-pyroclast)	A CA	
Simav 19	Late-Middle Pliocene Late-Middle Miocene	Trachybasalt- hawaiite-mugearite- rhyolite Andesite- dacite- rhyolite	A CA	
Gördes 20	Late Miocene	Dacite-rhyolite-rhyodacite	CA	
Selendi 21	Quaternary- Late Pliocene Early Pliocene- Middle Miocene	Basalt-hawaiite Andesite- dacite- rhyolite	A CA	
Uşak 22	Late Pliocene Late Miocene Middle Miocene	Basalt Andesite-trachyandesite- dacite- rhyodacite Rhyolite (lava-tuff)	A CA CA	8.3-12.2
Kula 23	Quaternary- recent Pliocene	Basalt- hawaiite-tephritetuff Andesite	A CA	10.000- 300.000 1.4
Salarya granite	Early Miocene Late Oligocene	 Granodiorite	CA	23.5 20.3
Eybek granite	Late Oligocene	Granodiorite-quartzmonzonite Granite	CA	35.33-30.5 24.2-23.9 23.6
Kozak granite	Miocene- Late Oligocene	Granodiorite-monzonite- granite	CA	16.5-19.5 25.7-24.2- 22.1 20.2
Alaçam granite	Early Miocene Late Oligocene	Monzogranite- monzonite Siyeno- monzogranite	CA CA A(?)	20.3 18.0-25.1
Eğrigöz granite	Early Miocene	Monzogranite	CA A(?)	20 21.2, 24.6

Table 1: Young volcanic and plutonic centres, the rock association, radiometric dating data from Western Anatolia.

Discussion and geological evolution

The major tectonic zones of Western Anatolia are displayed in Figure 1. The figure shows that the northern continental fragment, the Sakarya continent (Figure 2) and the southern continental fragment, the Tauride Anatolide platform of Şengör and Yılmaz (1981) are separated from one another by the remnant of the ocean floor (the Neotethys) that is known as the İzmir-Ankara melange zone. It sutures the two continental masses. According to the data available, the following geological evolution may be envisaged: during the Late Cretaceous, the Neo-Tethyan ocean floor began to be consumed by northward subduction under the Sakarya continent (Figure 9). It created a weakly-developed magmatic chain on the Sakarya continent, and a well-developed high pressure metamorphic belt, together with accretionary melange association, in front of the Sakarya continent. During this phase, the ophiolite slabs moved onto the leading edge of the Taurus platform. The ophiolites, which are presently observed on the metamorphic rocks of the Menderes massif and on the Tauride carbonate platform succession, are the remnant of this southernly transported nappe. The ophiolite nappe transport continued until the Eocene. The evidence for this is seen in the coarse-ophiolitic debris which were shed into the basin lying in front of the nappes. Later, the ophiolite were also moved and thrust onto this clastic succession.

The metamorphism of the Menderes massif may, in part, be ascribed to this obduction event (Fig. 8) resulting from the descent of the Tauride Anatolide platform (Şengör and Yılmaz 1981) into progressively hotter regions. Thus the radiometric age data show a spread of ages beginning with 60m.y. (Şengör et al. 1984).

Following the collision, the convergence between the two continents continued until the Miocene. Consequently, the platform began to be internally imbricated and the continental crust was shortened and thickened to reached over 60km. (Şengör et al. 1984).

Further burial of the platform unit created the peak metamorphism (the main Menderes metamorphism) 35m.y. ago. The grade of metamorphism reached to the amphibolite facies or perhaps even extended into the granulite facies (Akkök 1979, Ashworth and Evirgen 1984, Bozkurt and Park 1994, Candan et al. 1994). Southward thrust propagation continued in the Lycian Taurus in the Early Miocene.

As a result of the increasing tightening, the structure in Western Anatolia is dominated by composite nappe systems that become progressively younger in the direction of transport. The high grade core metamorphic rocks possibly thrust onto the low grade envelope rocks during this phase (Dora et al. 1992).

Some of these thrust planes may be the surface expression of the zone of separation between the lower and upper continental crust, which propagated to the surface as listic thrusts (Figure 8). An active example of this may be the low velocity zones in the cores of the orogens, as is the case beneath the central Alps (Mueller et al. 1976).

Thickness of the continental crust of Western Anatolia is calculated to be about 28-32km by different methods (Ezen 1993, Meissner et al. 1987, Makris and Stobbe 1984). Akkök (1979) estimates that at least a 15km envelope of rocks of the Menderes massif have been removed from its outer parts since its uplift.

Penecontemporaneous with the main metamorphic phase of the massif, anatectic melts were generated in the high metamorphic zones and formed migmatitic rocks (Dora et al. 1992). The granitic instrusions rose into shallow levels in the crust, where they formed shallow level and hypabissal intrusives (the granites are dated 30-35m.y). Partly coevally with these events, the first phase of young volcanic activity began in the region (dated 30m.y.) and wide-

spread intermediate volcanic rocks of hybrid nature were formed as a result. These simultaneous events show clearly that the magma ascended through the potentially wide zone of anatexis at the lower levels in the crust.

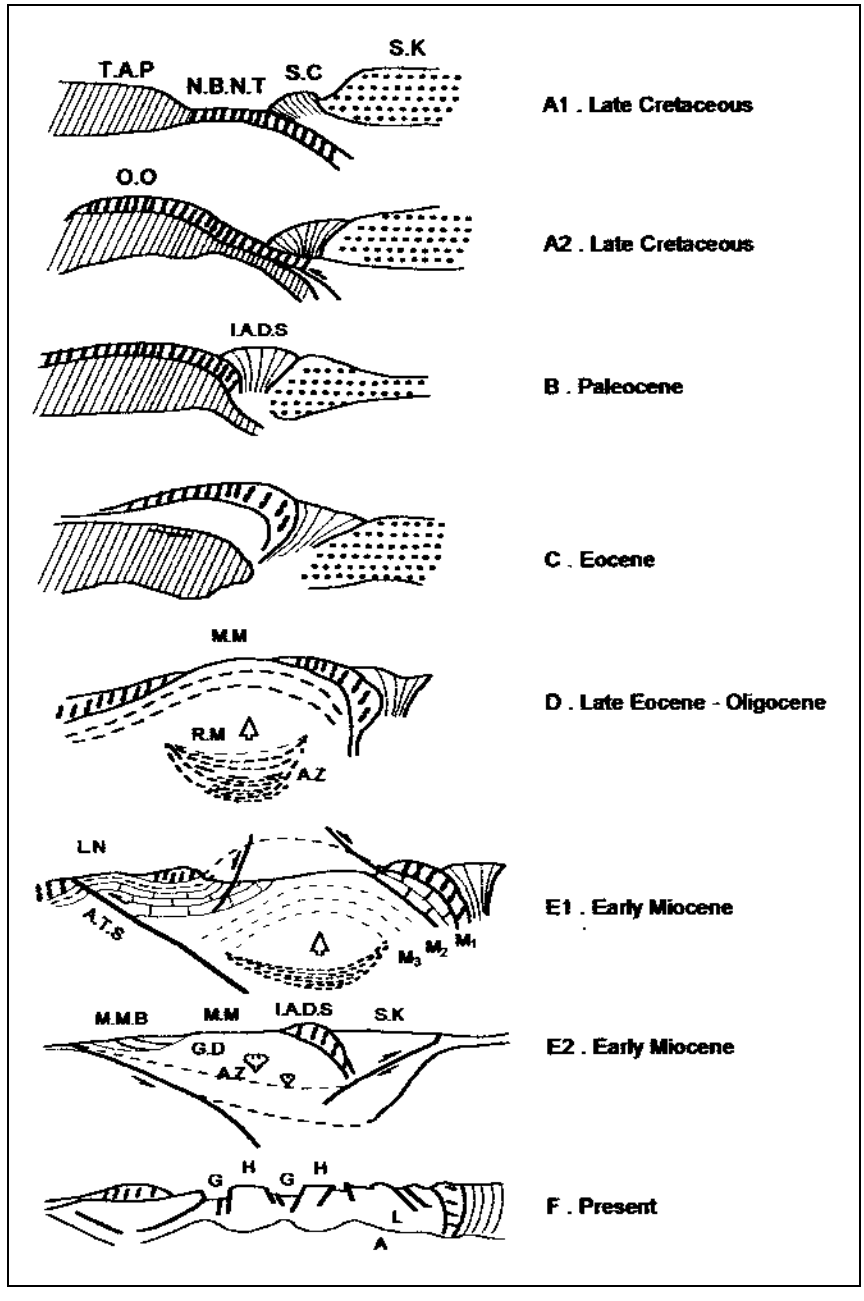


Figure 8: *Schematic sequential cross sections showing Late Mesozoic to the present, tectonic evolution of Western Anatolia.*
Abbreviations: TAP : Tauride-Anatolide platform, NBNT: northern branch of the neo-Tethyan ocean, SK: Sakarya continent, SC: subduction-acreation complex, OO: ophiolite obduction onto the Taurus carbonate platform, IADS: İzmir-Ankara ophiolitic suture zone MM: Menderes massif, AZ: zone of anatexis, RM: core rocks of the Menderes massif, M1, M2, M3: envelopes of the Menderes massif, GD: granitic diapirs, L: lithosphere, A: asthenosphere, G: graben, H: horst, LN: Lycian nappes, MMB: Miocene molasse basins.

During the ascent, this magma affected the continental crust and was itself affected by it. The main influence of the magma in the crust is thought to be an increase of the thermal gradient and a promotion of the crustal anatexis at progressively shallower levels. The sialic crust, on the other hand, affects the rising magma as a density filter and promotes the differentiation. This contributes to the higher silica mode of rocks, as attested to by the great variety of rocks from basic andesite to the dacite. As the magma ascended through it, the thickened continental crust may have permitted the magma to be selectively contaminated, in particular by radiogenic isotopes (Güleç 1991, Yılmaz 1989).

Extrusion of the intermediate magmas lasted to the end of the compressional regime and possibly extended to the beginning of the extensional regime, and then gradually died out with the beginning of the middle Miocene (approximately 15m.y. ago).

The Western Anatolian extensional regime followed the compressional system. This regime has been continuing since the middle Miocene and, as a result of this, the present structural features, represented by about 10 E-W oriented grabens, were developed.

The grabens are the most prominent morphological features of Western Anatolia. They control the drainage pattern and, thus, the sedimentation.

The N-S extension is calculated to be about 30 to 40mm/y by a variety of methods, including GPS measurements. The width of the most advanced grabens (i.e. the Büyük Menderes and Gediz graben) is only about 10km across. The graben sedimentary fills are about 2 to 2.8km thick (unpublished T.P.A.O. data). Using the different sets of data, the stretching factor has been calculated as varying from 1.3 to 1.5.

There is a debate concerning the age of development of the E-W trending graben system in Western Anatolia. Contrary to the earlier suggestion of Şengör and Yılmaz (1981), Seyitoğlu and Scott (1991a, b) claim that the extension began during the Late Oligocene and has been continuing since then for the last 35m.y. They also suggested that all of the magmatic rocks that were formed from the Oligocene onwards were generated under the extensional regime. Seyitoğlu and Scott base their main arguments on the observations that the earliest sedimentary rocks resting on the metamorphic rocks of the Menderes massif date back to the Early Miocene.

In the light of such conflicting views, the development of the E-W trending grabens will be evaluated using three lines of evidence:

- direct evidence (the data derived from the present E-W oriented graben system) (a).
- direct evidence dating the final phase of the previous N-S compressional regime of Western Anatolia (b).
- indirect evidence, taking into consideration the rate of the active tectonic processes and making inferences from this set of data (c).

a) The sampling from the earliest sedimentary fills of the E-W oriented graben system is presently difficult because they are mostly under the younger sedimentary cover. The data presented from the Büyük Menderes graben and Gördes graben to document age of the graben's opening seem to be dubious because it is uncertain that these sediments are the product of E-W oriented graben infill, as they outcrop more extensively than the graben areas. Therefore, their relations to the present graben systems have not been established with relevant data.

b) The first phase of the cover sedimentary units of Western Anatolia has no apparent relation to the present graben system. The final phase of the compressional system of Western Anatolia, as exemplified by the Lycian nappe emplacement, lasted to the middle Miocene and ceased in the Langhian (Hayward 1984). Previously, the Kale-Tavas basin fills, which are re-

garded to seal the thrust contact between the Lycian nappes and the Menderes massif (Delaune-Mayere et al. 1977), have been re-examined (Gutnic et.al. 1979) and it has been concluded that the so-called seal units were transported passively on the massif during its southward movement. It has now been shown that the Tortonian coarse clastic rocks are the real seal, formed after the thrusting (Hayward 1984). The compressional structural features of the Aegean islands, agreeing with data of Western Anatolia, also occurred during the Early Miocene (Robertson and Dixon 1984) until the Langhian (Bonneau 1984). Immediately after the regional metamorphism, the Menderes massif was thermally domed and its cover began to be removed by erosional processes. This phase was possibly followed by the thermal collapse of the regional dome, as suggested by Dewey et al. (1986). This is believed to have created an initial extensional regime producing radially distributed grabens with respect to the centre of the dome. Maybe it was during this phase that the first fault-bounded basins of Western Anatolia began to develop. Therefore, this phase of basin development is independent of that of the N-S extension related late grabens. The younger grabens cut and were partly superimposed upon the older grabens. The Akhisar and Gördes grabens may be examples of the older grabens and the Gediz graben of the major young graben.

c) When the initiation of the extension in Western Anatolia is estimated using the various geophysical data, the total amount of the extension may be calculated to have taking place during the last 5m.y. The data for this are the paleomagnetic rotations around the graben systems (Kissel and Laj 1988), the relationship between the strain rate (β1,5) and total amount of the extension (≅10km), the kinematic approach (Le Pichon and Angelier 1981) and seismic moment rates (Main and Burton 1989).

The direct and indirect evidence discussed above do not favour initiation of the E-W grabens in the Oligocene-early Miocene period. Our on-going research in the extreme north (the Bayramiç graben) in the centre (the Bergama-Bakırçay graben) and in the extreme south (the Kerme graben; Görür et al. 1995) of Western Anatolia reveal, partly in agreement with the geophysical data, that the present E-W oriented graben system began very late, possibly after the middle Miocene period. The field evidence indicates that the grabens were mainly developed during the Late Miocene-Pliocene period.

During the N-S extension regime, the Menderes massif together with the surrounding regions, were extended considerably. The total extension is estimated of more than 50% since its beginning (Şengör et al. 1984). Such an extension is thought to have been accommodated by regional shear zones, along which high-grade metamorphic rocks were produced. They were accompanied by syntectonically formed anatectic melts (Verge, personnel communication, 1994).

During the more advanced stage of the extension, under the subhorizontal flow regime, basaltic melts were liberated from the underlying mantle, possibly due to the adiabatic upwelling of the mantle and extension-induced pressure release. For this, small melt fraction is thought to have played an important role in enriching the source region in the upper "lithospheric" mantle (Mc Kenzie and Yılmaz 1991). The wide diversity in geochemical composition of this late phase of basaltic magmas (Yılmaz 1989) may be related to the heterogeneous source region, which has in part been metasomatised prior to or during extension.

References

Akkök, R., 1979, Petrology of gneisses and schists in the Menderes Massif, Derbent, Alaşehir,Turkey, PhD. Thesis, Uni. London.

Altıner, D., and Koçyiğit, A., 1992, Kuzeybatı Anadolu güneyinin Jura-Erken Kretase'de paleocoğrafik evrimi, Doğa, Türk Yerbilimleri Dergisi, 1, 1-11.

Altınlı, İ.E., 1973, Orta Sakarya Jeolojisi, Cumhuriyetin 50. Yılı Yerbilimleri Kongr. Tebliğler, MTA Inst., Ankara, 159-191.

Altunkaynak, Ş. and Yılmaz, Y., 1995, Geology of the Kozak dağı magmatic complex, Int. Earth Sci Coll. on The Aegean region, 1995 IESCA Program and Abstracts, 4.

Ashworth, J.R. and Evirgen, M.M, 1984, Garnet and associated minerals in the Southern Margin of the Menderes Massif, south-west Turkey, Geol. Mag., 121, 323-327.

Bargu, S., 1982, The geology of the İznik Yenişehir (Bursa)-Osmaneli (Bilecik) area, İstanbul Earth Sc. Rev., 3, 191-234.

Benda, L., 1971, Principles of the palynologic subdivision of the Turkish Neogene, Newsletter Stratigraphy, 1-3, 23-26.

Bingöl, E., Akyürek, B., ve Korkmazer, B., 1973, Biga yarımadasının Jeolojisi ve Karakaya formasyonunun bazı Özellikleri, Cumhuriyetin 50.yılı Yerbilimleri Kong. Tebliğleri, MTA Inst. Ankara, 70-77.

Bonneau, M., 1984, Correlation of the Hellenides nappes in the South east Aegean and tectonic reconstruction, in: The Geological Evolution of the Eastern Mediterranean, edited by: J.E. Dixon and A.H.F. Robertson, Geol. Soc. London Spec. Publ., 17, 517-528.

Bozkurt, E. and Park, R.G., 1994, Southern Menderes Massif: an incipient metamorphic core complex in Western Anatolia, Turkey. Jour. Geol. Soc. London., 151, 213-216.

Candan, D., Dora, Ö., Dürr, H. and Oberhänsli, R., 1994, Erster Nachweis von Granulit- und Eklogitrelikten im Menderes-Massif/Türkei, 5. TSK Symposium, Göttingen, 25, 3.

Çoğulu, E., 1967, Etude petrographique de la region de Mihaliçcik (Turquie), Bull. Suisse Min. Pet., 47, 683-824.

Delaune-Mayere, M., Marcoux, J., Parrot, J.,F. and Poisson, A., 1977, Modèle d'évolution Mésozoique de la Paléo-marge tethysienne au niveau des nappes radiolaritiques et ophiolitiques du Taurus lycien, d'Antalya et du Bear-Bassid, in: Structural history of the Mediterranean basins, edited by: B. Biju-Duval and L. Montadiert, Editions Technip, Paris, 79-94.

Dewey, J.F, Hempton, M.R., Kidd, W.S.F., Şaroğlu, F, and Şengör, A.M.C., 1986, Shortening of continental lithosphere: the neotectonics of Eastern Anatolia – a young collision zone, in: Collision Tectonics, edited by: M.P. Coward and A.C. Ries, Geological Society, London, Special Publication, No 29., 91-105.

Dora, O.Ö., Kun, N. and Candan, O., 1992, Menderes Masifinin metemorfik tarihçesi ve jeoteknik konumu, Türkiye Jeol. Bült., 35, 1-14.

Erdoğan., B. and Güngör, T., 1992, Menderes Masifinin kuzey kanadının stratigrafisi ve tektonik evrimi, TPJD Bülteni, C. 4/I, 9-34.

Ezen, Ü., 1993, Kuzey ve doğu Anadolu'da zone dalgalarının dispersiyonu ve Yer kabuğu yapısı, Deprem Araştırma Enstitüsü Bülteni, 43, 42-62.

Genç, S.C., 1993, İznik-İnegöl (Bursa) arasındaki tektonik birliklerin jeolojik ve petrolojik incelemesi, PhD. Thesis, İstanbul Teknik Üniv., 521.

Genç, S.C and Yılmaz, Y., 1994, Evolution of the Triassic continental margin, Northwestern Anatolia, Tectonophysics, 243, 193-207.

Görür, N., Şengör, A.M.C., Sakinç, M., Tüyüsüz O., Akkök, R., Yiğitbaş, E., Oktay, F.Y., Barka, A., Sarıca, N., Ecevitoğlu, B., Demirbağ, E., Ersoy Ş., Algan, O., Güneysu, C. and Aykola, A., 1995, Rift formation in the Gökova region, Southwest Anatolia, implications for the opening of the Aegean Sea, Geol. Mag., 132(6), 637-650.

Granit, Y. and Tintant, H., 1960, Observations preliminaires sur le Jurassique de la région de Bilecik (Turquie), C.R. Accad. Sci., 251, 1801-1803.

Gutnic, M., Monod, O., Poisson, A. and Dumont, F.-D., 1979, Geologie des Taurides occidentales (Turquie), Mem. Soc. Geol. Francais, 58,112.

Güleç., N., 1991, Crust-Mantle interaction in Western Turkey: implications from Sr and Nd isotope geochemistry of Tertiary and Quaternary volcanics, Geol. Mag., 128, 417-435.

Harris, N., Kelly, S. and Okay, A.I, 1994, Post-collision magmatism and tectonics in northwest Anatolia, Contrib. Mineral. Petrol., 117, 241-252.

Hayward, A.B., 1984, Miocene clastic sedimentation related to the emplacement of the lycian Nappes and the Antalya complex, SW Turkey, in: The Geological Evolution of the Eastern Mediterranean, edited by: J.E. Dixon and A.H.F. Robertson, Geol. Soc. London, Spec.Publ., 17, 287-300.

Karacık, Z., 1995, Ezine-Ayvacık (Çanakkale) dolayında genç volkanizma plütonizma ilişkileri, İTü Fen. Bil Ens., Doktora Tezi, 342.

Kaya, O., 1991, Stratigraphy of the Pre-Jurassic sedimentary rocks of the western parts of Turkey: Type area study and tectonic considerations, Newsl. Stratigr., 23(3), 123-140.

Ketin, İ., 1947, Uludağ Masifinin Teknoniği hakkında, TJK Bült., Cilt 1, S.1, Ankara.

Kissel, L. and Laj, L., 1988, The Tertiary geodynamic evolution of the Aegean area: a paleomagnetic reconstruction, Tectonophysics, 146, 183-201.

Le Pichon, X. and Angelier, J., 1981, The Aegean sea, Philosophical Transactions of the Royal Society of London, A 300, 357-372.

Main, I.G. and Burton, P.W., 1989, Seismotectonics and the earthquake frequency magnitude distribution in the Aegean area, Geophysical Journal of the Royal Astronomical Soc., 98, 575-586.

Makris, J. and Stobbe, C., 1984, Physical properties and state of the crust and upper mantle of the Eastern Mediterranean Area, Tectonophysics, 60, 1-42.

Mc Kenzie, D.P. and Yılmaz, Y., 1991, Deformation and volcanism in Western Turkey and the Aegean, Bull-Tech. Univ. İstanbul, 44, 343-375.

Meissner, R., Wever, Th. and Flüh, E.R., 1987, The Moho in Europe: implications for crustal development, Annales Geophysicae, 513, 357-364.

Mueller, St., Egloff, R. and Ansorge, J., 1976, Struktur des tieferen Untergrundes entlang der Schweizer Geotraverse, Schweiz. Min. Pet. Mitt., 56, 685.

Okay, A.I., 1984, Distribution and characteristics of the Northwestern Turkish blueschists, Geol. Soc. London, Spec. Publ., 17, 455-466.

Okay, A., Siyako, M. and Bürkan, K.A., 1990, Biga yarımadasının jeolojisi ve tektonik evrimi, TPJD Bült. 2(1), 83-121.

Robertson, A.H.F. and Dixon, J.E., 1984, Introduction: Aspects of geological evolution of the Eastern Mediterranean, in: The Geological Evolution of the Eastern Mediterranean, edited by: J.E. Dixon and A.H.F. Robertson, Geol.Soc. London, Spec. Publ.17, 1-74.

Satır, M. and Friedrichsen, H., 1986, The origin and evolution of the Menderes Massif, W-Turkey – A rubidium/strontium and oxygen isotope study, Geologische Rundschau, 75/3, 703-714.

Saner, S., 1977, Geyve-Osmaneli Gölpazarı – Taraklı alanının jeolojisi: Eski Çökelme ortamları ve Çökelmenin evrimi, PhD. Thesis, İstanbul Üniv., 312.

Şengör, A.M.C. and Yılmaz, Y., 1981, Tethyan evolution of Turkey: A plate tectonic approach, Tectonophysics, 75, 181-241.

Şengör, A.M.C., Yılmaz, Y. and Sungurlu, O., 1984, Tectonics of the Mediterranean Cimmerids: Nature and evolution of the western termination of Paleo Tethys, in: Geological Evolution of the Eastern Mediterranean, edited by: J.E. Dixon and A.H.F. Robertson, Geol. Soc. London, Spec.Publ., 17, 77-112.

Seyitoğlu, G. and Scott, B., 1991a, Late Cenozoic basin development in west Turkey: Gördes basin: tectonics and sedimentation, Geol. Mag., 131, 631-637.

Seyitoğlu, G. and Scott, B., 1991b, Late Cenozoic crustal extension and basin formation in Western Turkey, Geol. Mag., 128, 155-166.

Yılmaz, Y., 1977, Bilecik-Söğüt dolayındaki "Eski Temel Karmaşığı" nın petrojenik evrimi, Doçentlik Tezi., İstanbul Üniversitesi Fen Fakültesi, Tatbiki Jeolojisi Kürsüsü, 169.

Yılmaz, Y., 1981, Sakarya kıtası güney kenarının tektonik evrimi, İstanbul Yerbilimleri İstanbul Üniv. 1-2, 33-52.

Yılmaz,Y., 1989, An approach to the origin of volcanic rocks of Western Turkey, in: Tectonic evolution of the Tethyan region, edited by: A.M.C. Şengör, Kluwer, The Hague, 159-189.

Yılmaz, Y., 1990a, Comparison of young volcanic associations of Western and Eastern Anatolia formed under the compressional regime, a review, Jour. Volcan, Geotherm. Res., 44, 69-87.

Yılmaz, Y., 1990b, Allochthonous terranes in the Tethyan Middle East: Anatolia and surrounding region, Philos. Trans R. Soc. London, Ser. A, 331, 611-624.

Yılmaz,Y., Tüysüz, O., Yiğitbaş, E., Genç, Ş.C. and Şengör, A.M.C., in press, Geology and tectonic evolution of the Pontides, A.A.P.G.

Neotectonics of the Marmara region

AYKUT BARKA

Abstract

The North Anatolian Fault Zone (NAFZ) splays into three strands in the Marmara and north Aegean regions. Each strand consists of NE-SW trending short strike-slip fault segments which form pull-apart structures, particularly in the Marmara regions. The fault plane solutions of recent earthquakes and GPS measurements indicate that the dominant motion along these strands is strike-slip. All strike-slip fault segments strike ENE -WSW and/or NE- SW while the regional slip vector is almost E-W, causing a thrust component along the strike-slip segments. Microseismic activities are mostly located to the pull-apart basins, thus normal faults, while strike-slip segments have almost no macro-seismic activity except aftershock activity. Paleogeographical maps indicate that the initiation of the north Anatolian is about Pliocene. The long term seismicity and GPS measurements and geological data suggest that the northern strand of the fault zone is more active than the other two southern strands. Both restoration of the Karamürsel basin and the amount of extension deduced from the Çınarcık basin from the Marathons seismic profile-16 reveal about 10-15km total offset along the northern strand. This value give rise to a long term slip rate of 2-4mm/y if we consider that the fault zone initiated 3-4m.y. ago. On the other hand, GPS measurements give a slip rate of approximately 10-15mm/y for the northern strand. Historical and paleoseismological data indicate that the recurrence interval of clusters of large earthquakes is 1200 years in the İzmit bay area, 500-800 years along the Gaziköy-Saros segments and more than 2000 years along the Geyve-Gemlik section of the middle strand. The return period for large earthquakes, Intensity>VIII, for the south of İstanbul varies between 100-1000 years, depending on the size of earthquakes. The GPS rate for the northern strand is much higher than that obtained from historical earthquake records and geological data. The central Marmara ridge needs further detailed studies, as it is considered to be a major source of large earthquakes for the İstanbul region. The last major large earthquake on this ridge was probably in 1509AD. The return period for these earthquakes can be 225-1000 years, depending on slip rate considered (GPS= 15mm/y, geological=2-4 mm/y).

Introduction

In the Marmara sea region, the North Anatolian Fault Zone (NAFZ), the northern boundary of the westward moving Anatolian block, splays into several strands and it forms a diffused boundary between the Anatolian block and the Black sea (Fig. 1). Because these strands are not continuous and are made up of small fault segments, there has been a conflict of ideas whether the southern strands should be considered within the NAFZ representing a diffused boundary or an internal deformation of Western Anatolia. Although some sections of each strand have ruptured during twentieth century earthquakes, the seismicity pattern of the Marmara sea region does not illustrate a clear picture of strands except for the northern one. This paper will, first, present general characteristics of bathymetry, morphology and paleogeographic evolution of the Marmara sea region in relation to the NAFZ and, second, focus on some key areas, such as İzmit bay, İznik-Gemlik, Gaziköy-Saros and Biga peninsula, where there are more detailed neotectonic data available, including seismic reflection profiles, GPS, seismicity and historical earthquake records.

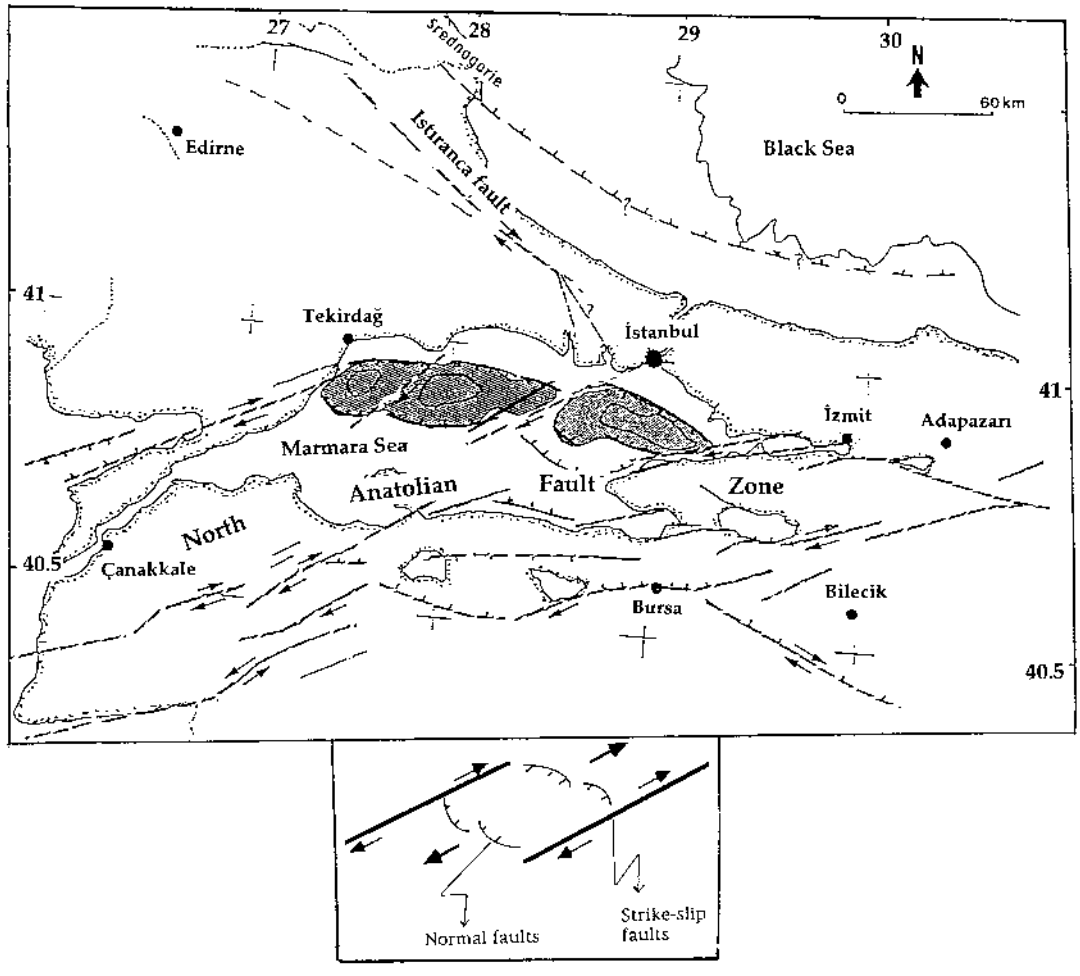


Figure 1: *Extent of the three strands of the NAFZ in the Marmara region from Barka and Kadinsky-Cade (1988), Barka (1991 and 1992). Inset map shows the pull-apart mechanism which is the characteristic structure of the Marmara sea region.*

Previous studies

During the last fifty years, a large number of studies have focused on the NAFZ within and around the Marmara sea. Some of these works have suggested that the NAFZ ends in the eastern Marmara region and that, to the west, the Marmara sea and north Aegean regions are considered to be under a purely extensional regime as a northern extent of the extensional regime of Western Anatolia and Aegean (e. g. Allen 1969, Ambraseys 1970, Kıyak 1986). However, particularly following the 1981, 1982 and 1983 north Aegean earthquakes, Taymaz et al. (1991), Barka (1992) and many others, even before these events proposed that the NAFZ continues through Marmara and north Aegean (e. g. McKenzie 1972 and 1978, Alptekin 1973, Dewey and Şengör 1979, Şengör 1979, LePichon and Angelier 1981, Lyberis 1984, Şengör et al. 1985, Barka and Kadınsky-Cade 1988), (Fig. 2). More recently, there are studies indicating that the NAFZ continues to the Hellenic arc through the Cephalonia fault (Reilinger et al. 1995, Le Pichon et al. 1995).

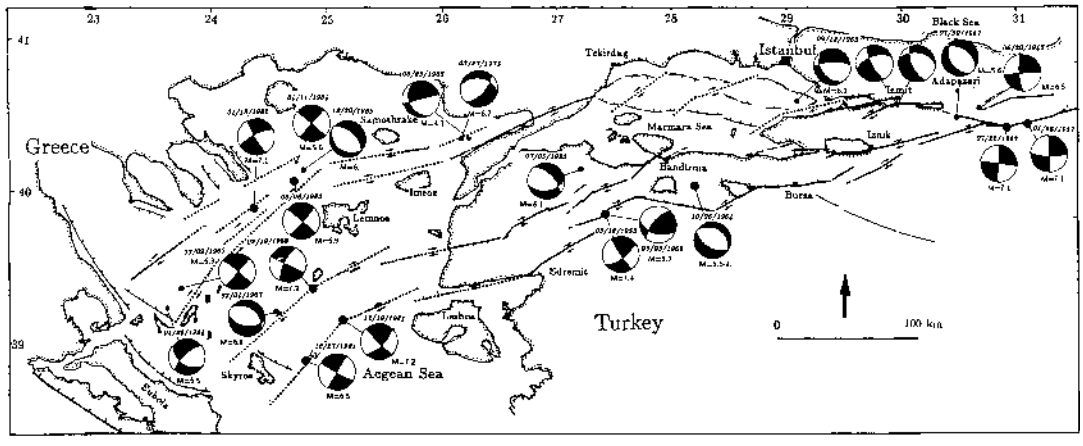


Figure 2: *Fault plane solutions of the significant earthquakes along the strands of the NAFZ in the Marmara sea and north Aegean region (Barka 1992). Fault plane solutions are from McKenzie (1972 and 1978), Jackson and McKenzie (1984), Crampin and Üçer (1987) and ISC (1981-1983).*

The geometry and distribution of active faults belonging to the NAFZ in the Marmara sea has been an other controversial issue. Before seismic reflection data, Pınar (1943) suggested that two strands of the NAFZ crossed the Marmara sea, the northern one going through the basins of northern Marmara and the southern one running through the Gemlik and Bandırma bays (Fig. 3a). Pfannenstiel (1944) drew attention to the importance of the NE-SW trending ridges in the northern Marmara sea and included NE-SW faults in his model (Fig. 3b). He also studied the Plio-Quaternary evolution of the region and suggested that the lakes around the Marmara sea were once (Late Pleistocene) connected to the Marmara sea. Crampin and Evans (1986) interpreted northern Marmara as an E-W trending single graben (Fig. 3c) and they also introduced a wedge-shaped Marmara block by looking at seismicity patterns of the region. They considered that this Marmara block escapes westward along the ophiolitic suture zone extending from İzmir and Eskişehir. However, this idea has not evidently been confirmed by fault mechanisms along the suture zone. Şengör (1987) located only one strand in the Marmara sea, and he showed that the Çınarcık basin is a pull-apart structure (Fig. 3d). Barka and Kadınsky-Cade (1988) and Barka (1991 and 1992) suggested that the NAFZ has at least three continuous strands in the Marmara region and that the north Aegean trough can be considered as forming a diffuse boundary (Fig. 3e). The northern strand has several pull-apart stepping which forms the basins of the northern half of the Marmara sea. This pull-apart model has been slightly modified by Wong et al. (1995) and Ergün and Özel (1995), (Fig. 3f), who studied the shallow seismic reflection data. Both papers identified 4 units in the profiles which will be described in more detail in the following sections. Smith et al. (1995), who studied high resolution sparker seismic profiling, observed mostly E-W, WNW-ESE trending normal faults and suggested that the faults that occur in the northern half of the Marmara sea have clearer morphology since the sedimentation rate is less relative to the southern Marmara shelf.

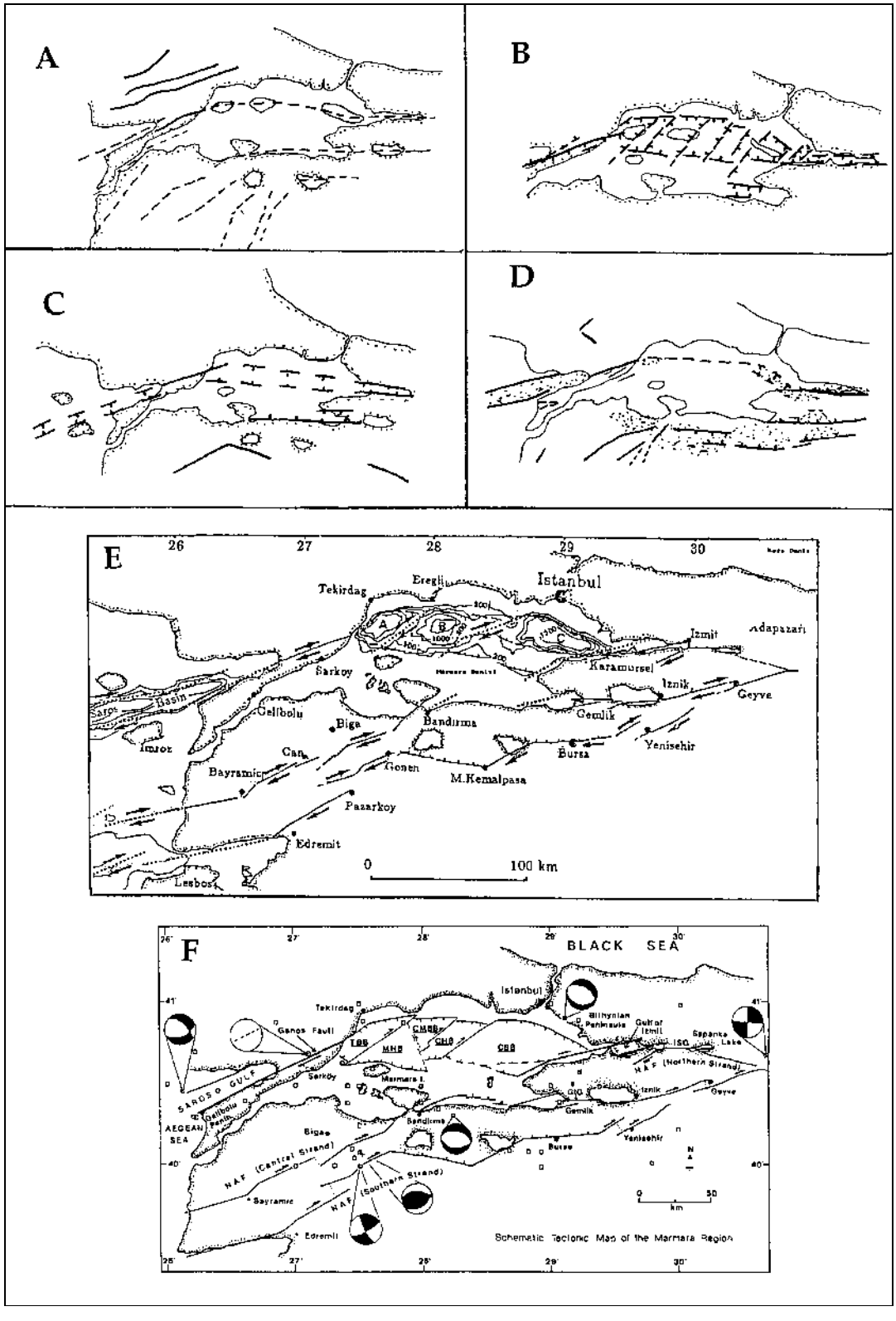


Figure 3: *Comparison of the structural models suggested for the Marmara region. (a) Pınar (1943), (b) Pfannenstiel (1944), (c) Crampin and Evans (1986), (d) Şengör (1987), (e) Barka and Kadınsky-Cade (1988), f) Wong et al. (1995), Ergün and Özel (1995).*

Bathymetry of the Marmara sea and morphological features of the onshore areas

Since the bathymetry of the Marmara sea has not been obtained by using modern techniques, with the existing ones, 1:250,000 scale, only large features can be identified (Fig. 4). Thus, the Marmara sea can be divided into two parts, the northern and southern, by an E-W trending line in the middle. The northern part basically consists of three basins, the eastern or Çınarcık basin, the central basin and the western basin. The basins are approximately 1200m deep and are separated by two NE-SW trending ridges. The depth of the ridges varies between 500-700m. The central ridge is wider than the western ridge and they both have complicated morphologies. The central ridge has a small basin and a high, while the western one has two small highs. Barka and Kadınsky-Cade (1988), who studied bathymetry, microseismicity, seismic reflection profiles (Marathon Oil 1975) and extrapolated onshore fault geometry to offshore areas, suggested that the northern Marmara sea is a large releasing stepover which was formed between the 1944-1967 (Bolu-Mudurnu) and the 1912 (Gaziköy-Saros segments) ruptures. However, this large stepover does not form a large pull-apart basin, instead it is divided into smaller basins by NE-SW trending strike-slip faults, forming a series of smaller pull-apart basins between the Sapanca lake and Saros bay. Very similar structures exist along the middle and southern strands (e.g. Bursa and Manyas-Karacabey basins). Wong et al. (1995) and Ergün and Özel (1995) emphasised the northern and southern slopes as northern and southern boundary faults.

The southern half of the Marmara sea consists of a wide shelf less than 100m deep. Seismic profiles on the southern shelf show NE-SW trending basins and ridges covered by young sediments. These basins are already filled up by the sediments, and the vertical offsets of the bounding faults are much smaller than in the northern half (Marathon Oil 1975). Smith et al. (1995) have suggested that the width of the southern shelf is due to three major rivers flowing into the Marmara sea from the south, namely the Biga, Gönen and Simav/Nilüfer rivers. The southern half of the Marmara sea and Gemlik, Bandırma and Erdek bays are considered as shallow basins, their maximum depths being slightly over 100m.

Figure 4 shows the areas around the Marmara sea with an altitude greater than 200m. This map also illustrates that the terrain to the north and northwest (Thrace) of the Marmara sea differs from that to the east and south in two ways: a) elevations are much lower in the north (Thrace), and b) only a few small rivers drain from the north into the Marmara sea while at least three major rivers enter from the south. This map also shows the uplifted areas along the course of the strands of the NAFZ, such as Ganos dağ (700-900m), the Biga peninsula (700-1700m), the Armutlu peninsula (900-1600m), İmranlı island, the Kapıdağ peninsula (782m) and Marmara island (700m). An E-W trending uplifted basement has been detected on the offshore seismic profiles between the Armutlu peninsula and Marmara island. The elevation difference between this ridge and the Armutlu peninsula is related to the fault kinematics, these uplifts are related to the hanging wall uplift of E-W trending normal faults forming northern and southern boundary of pull-aparts (Fig. 5), whereas, the high elevation of Armutlu, Biga peninsula and Ganos dağ are associated with the compressional component of the strike-slip segments. Overall, the morphology of the Marmara sea shows that the northern basins are more developed (larger and deeper) that the southern ones, indicating that the rate of tectonic activity is higher along the northern than along the southern strands.

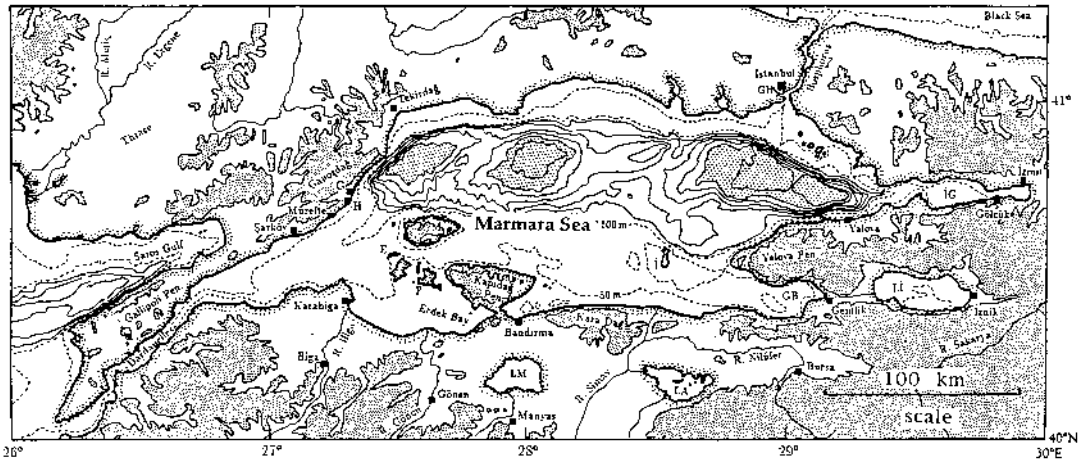


Figure 4: *Bathymetry of the Marmara sea and morphology of the Marmara sea region from Smith et al. (1995).*

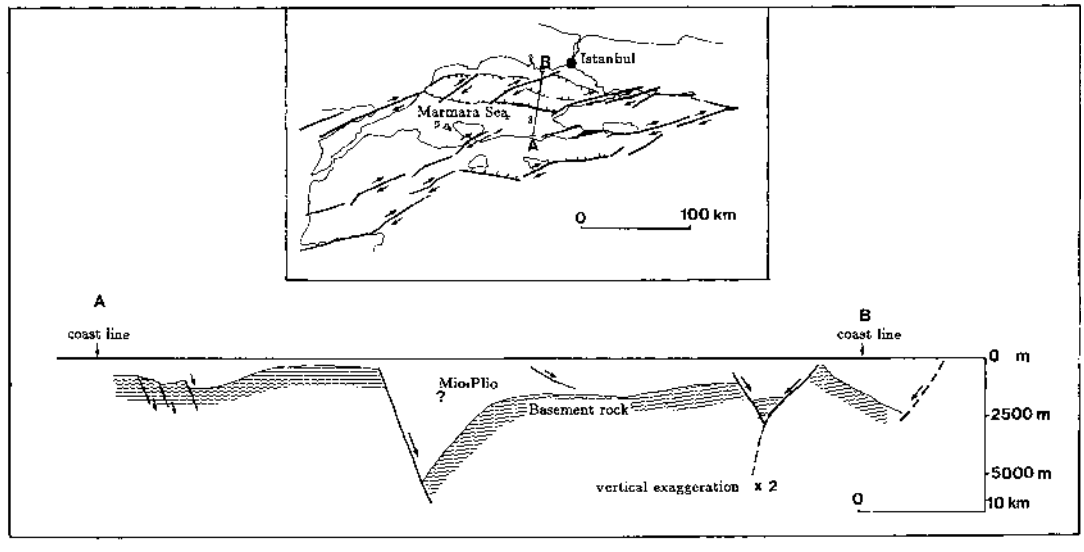


Figure 5: *N-S trending deep seismic reflection profile-16 from Marathon Oil (1975) obliquely crossing the Çınarcık basin. Note the rollover structure and uplift of the footwall at the southern boundary fault. The thickness of the sediments filling the rollover is about 5,500m.*

Paleogeographic evolution of the Marmara sea region

The Marmara region has been subjected to two stages of extension since the Middle Eocene. The first stage was related to the opening of the Thrace basin between the Middle Eocene and Miocene period. The second stage was related to the NAFZ (Late Miocene?-Plio-Quaternary). Borehole data and seismic reflection profiles reveal that the Thrace and Marmara basins were a single basin during the period of Middle Eocene-Miocene (e.g. Doust and Arıkan 1974). The total thickness of all sediments filling these basins reached about 5-5.5km in places (Marathon Oil 1975).

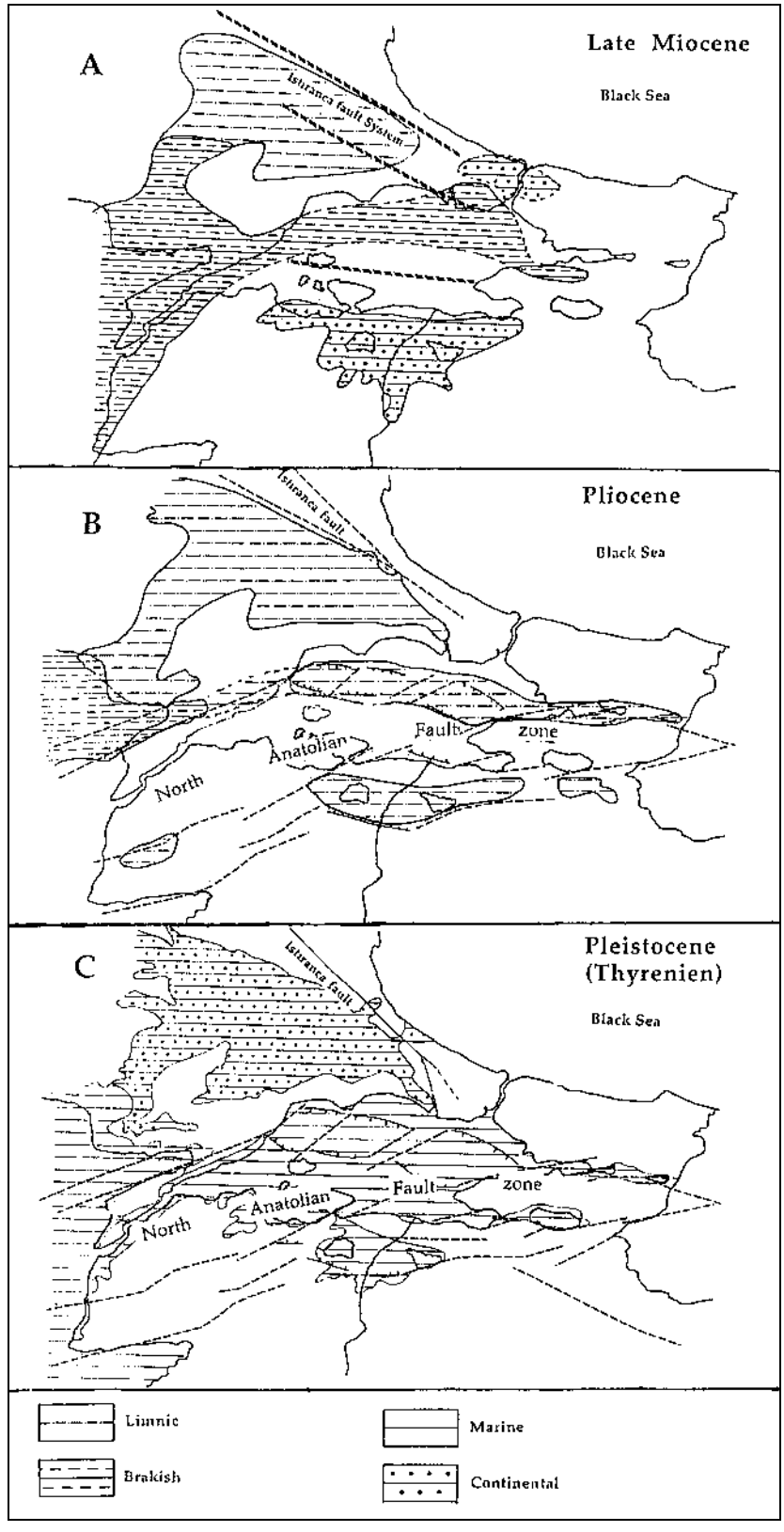


Figure 6: *A three stage paleogeographic evolution of the Marmara sea region. a) Late Miocene, b) Pliocene, and c) Pleistocene. Documented mainly from Lüttig and Steffens (1979), Sakınç and Yaltırak (1995a, b) and Meriç et al. (1995).*

Figure 6 shows a three stage of paleogeographic evolution in the Marmara sea region, from Late Miocene-Late Pleistocene. These maps were documented mainly from Doust and Arıkan (1974), Lüttig and Steffens (1979), Sakınç and Yaltırak (1995a, b), Sakınç et al. (1995), Wong et al. (1995), Ergün and Özel (1995), Erol (1992), Erol and Çetin (1995), Meriç et al. (1995). The Late Miocene paleogeographic map illustrates that there was a brackish seaway connection between the Marmara sea and Aegean, however, the Black sea connection is not very well known yet (Sakınç 1996, pers. com.). The Late Miocene age continental and shallow marine sediments have been correlated around the western part of İstanbul, Gelibolu, Çanakkale and Yalova regions. These sediments are gently folded in the İstanbul area and contain some thrusts in the Ganos, Gelibolu and Yalova areas. Distribution of the Late Miocene deposits in offshore areas there has not been well documented, except Wong et al.'s (1995) seismic unit 2. The Marathon Oil's seismic reflection profiles along the southern shelf show that, on the southern shelf, there are a number of small graben structures which are covered by Plio-Quaternary sediments. It is presumed that some of the basin fill sediments might be Late Miocene in age. Kurtuluş (1985) described Neogene sediments in the Gemlik bay basin, however, this needs further studies. In the southern Marmara region, between Biga, Mustafakemalpaşa and the Bursa area, fluvial sediments are intercalated with volcanoclastics and limnic facies while the Biga peninsula has dominantly volcanogenic facies. In the Thrace basin, limnic-fluvial deposits are dominant. The Late Miocene paleogeographic map indicates that only the northern shelf of the Marmara sea might have existed and that the southern shelf might have remained as land area, including İzmit, Gemlik and the Bandırma bay areas. The pattern of the distribution of sediments indicates that the NAFZ may not have existed yet, since we can not directly relate the deposition of sediments and present day distribution of the active fault strand of the NAFZ in the İstanbul area and the Yalova basin. The Late Miocene paleographic map indicates that the sedimentation might have been still controlled by two fault systems; the İstranca fault, a right-lateral fault zone (Çağlayan et al. 1988, Perinçek 1991, Turgut et al. 1991) in the north, and the southern Marmara sea ridge in the south, both of which were responsible for the opening of the Thrace basin.

The Pliocene paleogeographic map of the Marmara sea region (Fig. 6b) is much simpler. The limnic-fluvial deposition continued in the Thrace basin. Sea existed west of the Saros bay and sea probably entered the Marmara sea basins in the Late Pliocene (Erol and Çetin 1995, Meriç et al. 1995, Sakınç 1996, pers. com.). Shallow seismic reflection data within the Marmara sea basins and including the İzmit, Gemlik and Bandırma bays (Kavukçu 1990, Wong et al. 1995, Ergün and Özel 1995) indicate that the basins probably began to form during this period and received initial limnic-fluvial deposits. These deposits may be equivalent to units, 3a, 3b and 3c in Wong et al. (1995), as they considered unit 3 as hemipelagic turbidity deposits. The Pliocene paleogeographic map indicates the initiation of the NAFZ.

There are an abundance of uplifted marine terraces along the Marmara coastline (Erinç 1956, Göney 1964, Sakınç and Bargu 1989, Sakınç 1993, Sakınç and Yaltırak 1995a, b), (Fig. 6c). These terraces are mostly located on the southern side of main strike-slip segments of the northern strand, such as Gaziköy and Karamürsel. These Ostrea-rich terraces are approximately 250,000 years old (known as Thyrenien age) and have been studied since the beginning of the century (e.g. English 1904). According to recent studies on O^{18} isotopes in the oceans (e.g. La Joie 1986), during the Late Quaternary interglacial periods, sea level has never been higher than at the present time. Thus, the origin of the marine terraces are all tectonic uplift. Pfannenstiel (1944) suggested that, due to high sea level in Thyrenien, there was a sea invasion in the lowlands particularly in the areas where the present day lakes are located in the east (Sapanca and İznik lakes) and south Marmara region (Ulubat and Manyas lakes). During the Thyrenien, these areas were lower in elevation than at present, and since then, these areas have been uplifted. During the last glacial period (100,000-8000a), the water level dropped to -90m and during the Holocene increased to the present level (Pfannenstiel 1944).

Geometry, kinematics and earthquake activity of the strands of the North Anatolian Fault Zone (NAFZ) in the Marmara sea region

Segmentation and earthquake activity of the NAFZ in the Marmara sea region has been studied in detail by Barka and Kadinsky-Cade (1988). Figure 1 shows the geometry and the distribution of active fault segments belonging to each strand. For the onshore areas, the data were obtained from aerial photographs, field observations, existing literature (e.g. Ketin 1969, Siyako et al. 1989, Herece 1990) and the extents of the surface ruptures of large earthquakes (e.g. Ketin and Roesli 1953, Ketin 1969, Ateş and Tabban 1976, Ambraseys and Finkel 1987). Since the details of each fault and rupture segment have already been given by Barka and Kadinsky-Cade (1988), these will be not be repeated here. Instead, some key areas, including İzmit bay, İznik-Gemlik, Ganos-Saros and the Biga peninsula, will be investigated in terms of geology, geomorphology and seismicity.

The İzmit bay area

In earlier studies, the bay area was considered as a graben structure (i. e. Crampin and Evans 1986) and some others thought that a single southern strike-slip fault with a vertical component had formed the bay (i.e. Ketin 1969, Şaroğlu et al. 1987). On the other hand, Barka and Kadınsky-Cade (1988) and Barka and Gülen (1988) introduced a pull-apart model in which they claimed that instead of considering a single segment occurring along the southern shore, en echelon strike-slip segments stepping up westward can give rise to open small basins, such as the İzmit and Karamürsel basins, as pull-apart structures (Fig. 7). Bargu and Yüksel, (1993), Akgün and Ergün (1995) and Koral and Öncel (1995), who studied seismic reflection profiles and onshore geological structures, also concluded that the İzmit bay area consists of a few en echelon strike-slip fault segments and that they form pull-apart basins such as the İzmit and Karamürsel basins. Özhan et al. (1985) and Kavukçu (1990) studied shallow seismic reflection profiles in the bay area and they pointed out that the bay area is not a single graben and that there are two basins separated by basement rocks where the Hersek delta lies over. Thus, it can be suggested that the northern strand of the NAFZ consists of at least three en echelon strike-slip fault segments which form the İzmit bay area (Figs. 7-9). These are the Sapanca-Gölcük, İzmit Karamürsel and Yarımca-Yalova segments. Between these segments, the İzmit and Karamürsel basins open as pull-part basins.

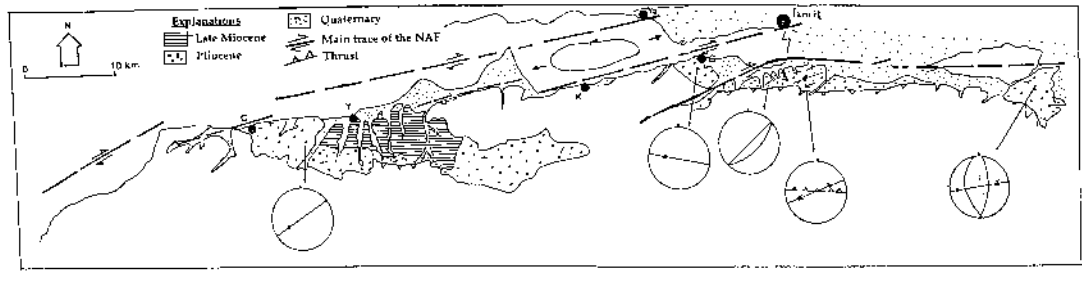


Figure 7: Neotectonic map of the Sapanca-İzmit bay area from Barka and Gülen (1988). Stereonets show fold axis, thrusts and normal faults. Ya, Yarımca, Y, Yalova, C, Çınarcık, K, Karamürsel, G, Gölcük.

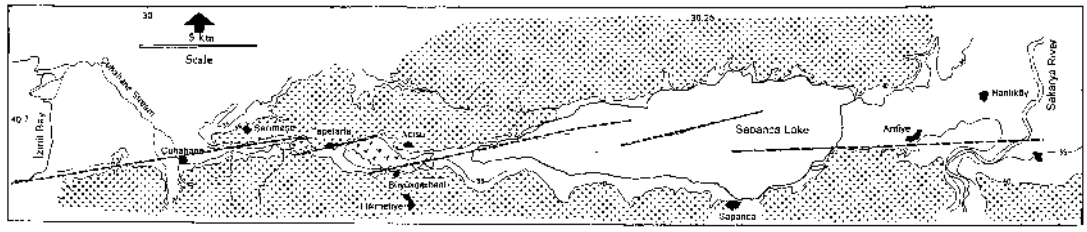


Figure 8: *Geometry and segmentation of the northern strand of the NAFZ between Sapanca lake and İzmit bay. Triangles are the areas with contours above 50m.*

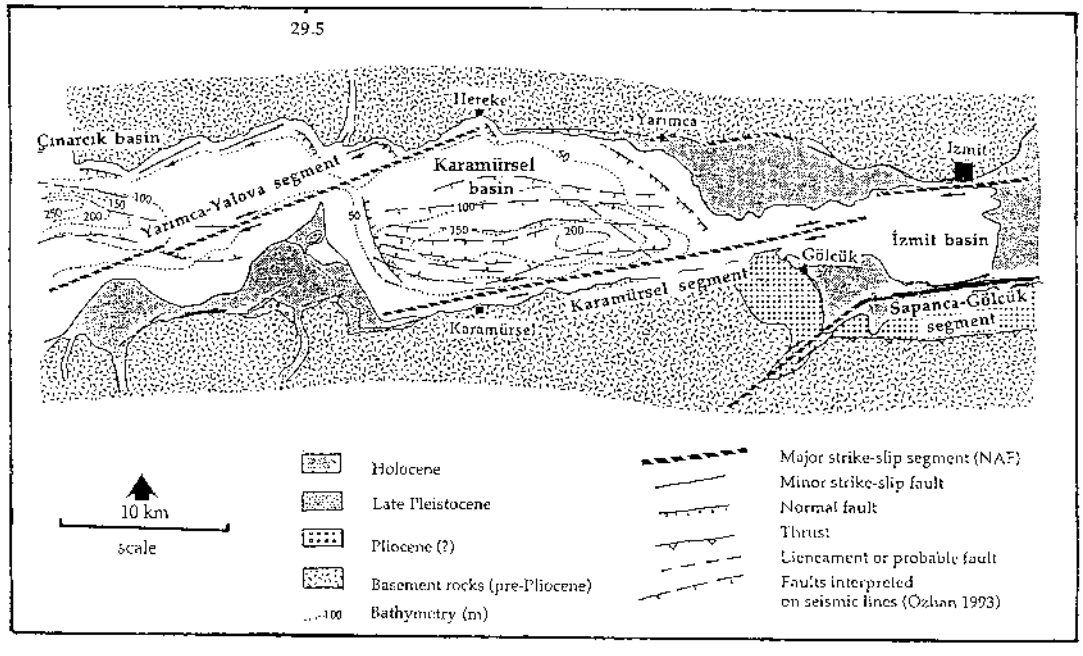


Figure 9: *Neotectonic map of the İzmit bay area.*

The İzmit basin opens between the Sapanca-Gölcük and Karamürsel segments. The E-W trending Sapanca-Gölcük segment extends between Sapanca lake and İzmit bay with en echelon geometry (Fig. 8) and then it changes direction abruptly to southwestward south of Gölcük. The high elevations in the southern block are related to the compressional component of this segment. These mountains are also the main source of the Hersek delta. The shore line between the Hersek delta and Gölcük is very straight, indicating a near shore strike-slip fault (Fig. 7). This segment is named the Karamürsel segment and it initiates near the city of İzmit and extends to the southeastern corner of the Hersek delta (Figs. 9 and 10). A 1:35,000 and 1:10,000 scale aerial photograph study revealed that the Karamürsel segment may not extend to the west of the Hersek delta. Along the southern margin of the delta, it steps to the north and continues to the west as discontinuous small segments. Near Topçular, strike-slip (with thrust component) morphology is well developed for short distances and this extends to Taşköprü village. However, the elevations of the Late Pleistocene shallow marine deposits on the Hersek delta and south of Altınova are comparable (27/20-30m), indicating that the major fault segment should occur north of the delta (Fig. 10). A DSİ borehole near Altınova cut the bedrock at 46m, indicating that the basement under the delta is shallow (Fig. 10). Thus, this may suggest that the delta moves with the southern block, otherwise we could expect a greater depth for the bedrock under the delta.

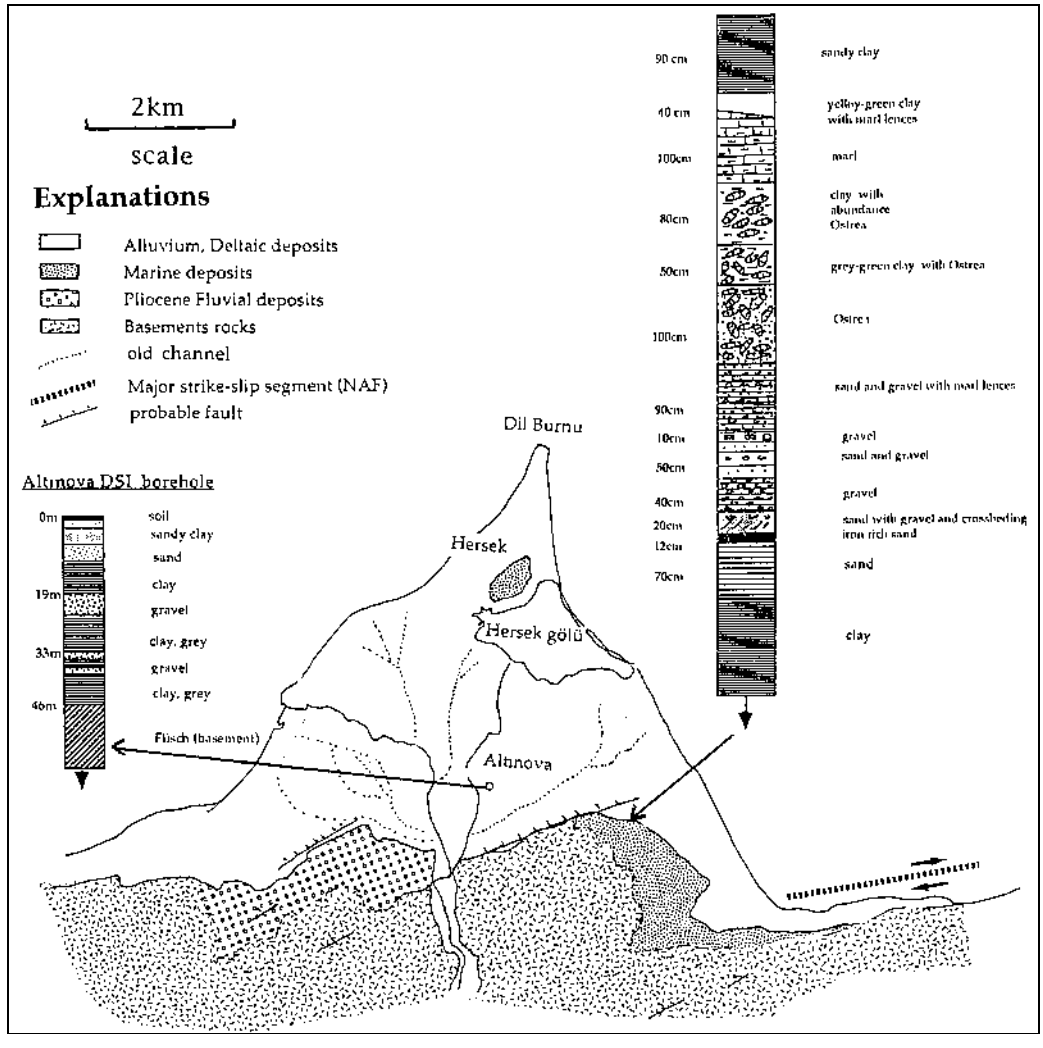


Figure 10: Neotectonic map of the Hersek delta. The longer stratigraphic column shows the stratigraphy of the Thyrenien deposits and the shorter one is DSİ's Altınova borehole log.

The northern margin of the Karamürsel basin is formed by the Yarımca-Yalova segment. East of Yarımca, this segment consists of small faults trending approximately E-W. Between Yarımca and Hereke the shore is fairly straight, trending again E-W, and aerial photographs illustrate many triangular facets along the shoreline. Then this segment trends WSW-ENE and extends towards Çınarcık, delimiting the northern apex of the Hersek delta (Figs. 9 and 11). The NE-SW trending shoreline between Hereke and Gebze suggests that the shoreline may have been formed by secondary en echelon strike-slip faults.

A restoration of the geological map of the İzmit bay area by closing the pull-part basin reveals about 15km of total slip (Figs. 12a and b). From the Marathon Oil's (1975) N-S trending seismic reflection profile 16 (Fig. 5), one can estimate the stretching in the eastern Marmara sea basin to be about 10-15km. This value is similar to that obtained from the Karamürsel basin. This has given rise to a 2-4mm/y slip rate along the northern strand for the last 3-4m.y. (since the initiation of the NAFZ). However, recent GPS measurements reveal a slip rate of about 15mm/y along this strand (Reilinger et al. 1995, Straub 1996).

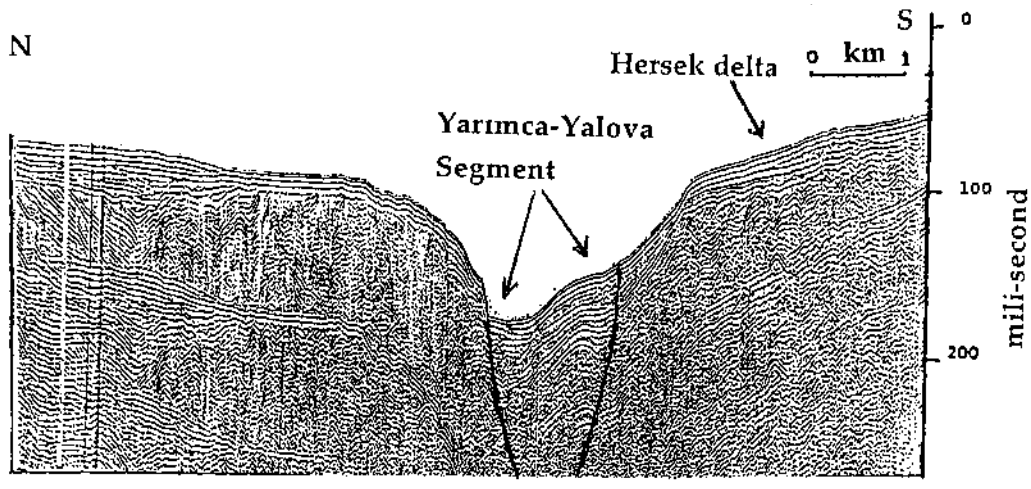
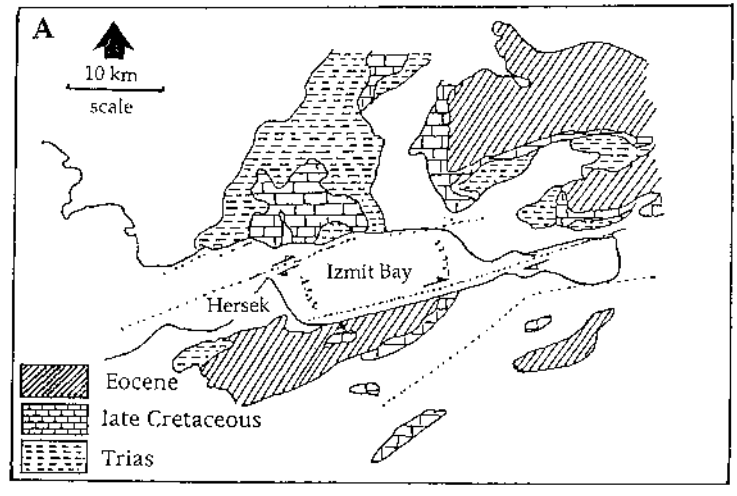


Figure 11: *A shallow seismic reflection profile of the MTA 1983 crossing the Hersek delta from Özhan et al. (1985). Note the transtensional fault expressions in the central part of the profile.*



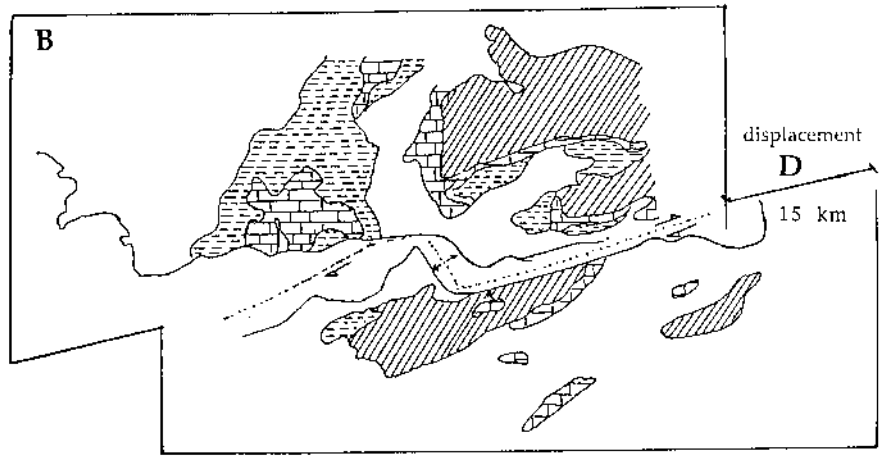


Figure 12: *A restoration of the İzmit bay area by closing the Karamürsel basin along the pull-apart. This reveals an offset of about 15km along the northern strand of the NAFZ.*

Furthermore, Pliocene deposits, which are located between Gölcük and south of the Sapanca lake, are deformed by folding (Ikeda et al. 1989, 1991) and local thrusting (Akartuna 1968), (Fig. 7). This suggest that the trends of the segments are slightly oblique to the slip vectors. Straub (1996) reported that according to the GPS measurements in the area, the velocity vectors have an E-W trending, and this is consistent with the fault plane solution of major earthquakes such as these in 1943, 1957 and 1967 (Fig. 13). This result is consistent with the compressional deformation along the strike-slip fault segment.

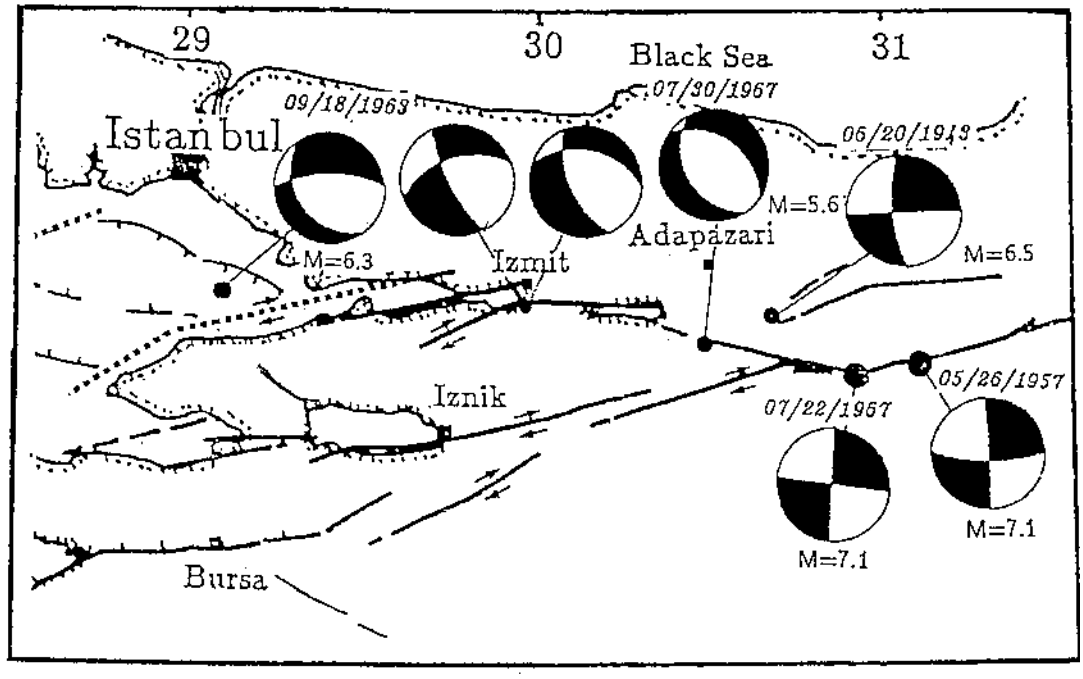


Figure 13: Fault plane solutions of the significant earthquakes in the eastern Marmara region modified from Barka (1992). Fault plane solutions are from McKenzie (1972, 1978). Two solutions in the İzmit region are composite solutions taken from Üçer (1990).

Geyve, İznik lake and Gemlik areas

Figure 14 shows the extent of the middle strand between Geyve and Gemlik. This strand has been studied in detail by Sipahioğlu and Matsuda (1986), Tsukuda et al. (1988), Ikeda et al. (1989, 1991) and Barka (1993). There is abundant evidence of morpho-tectonic features along this section of middle strand. Fault expressions are well developed in Mekece and south of İznik lake. The Geyve-Pamukova basin has been interpreted as a pull-apart basin (Tsukuda et al. 1988, Koçyiğit 1988, Barka 1993). In this basin, the Sakarya river has about 14-21km right-lateral offset (Sipahioğlu and Matsuda 1986, Koçyiğit 1988). İznik lake is a pull-apart depression formed between İznik and Sölöz. Between İznik lake and Gemlik bay this strand splays into two faults; the NE-SW trending one is called Gençali fault (Tsukuda et al. 1988), (Fig. 15). The Gençali fault extends to Mudanya and forms the southern boundary of the Gemlik basin (Fig. 16). The Gemlik bay area was studied by Kurtuluş (1985), who interpreted the structures from high resolution shallow (effective to 300m) seismic reflection profiles which were obtained by MTA Sismik-1 in 1984. According to the bathymetric map, the maximum depth was about 110m and was located NE of Mudanya. The long axis of the low area trends NW-SE (Fig. 16). The pattern of active fault segments, both those interpreted from seismic profiles in Gemlik bay and onshore areas and offsets along them, suggest that the Gemlik bay area is a pull-part structure. Figure 16 shows fault geometry between the Gemlik and Bandırma bays which is identical with the northern (Çınarcık basin) and southern strand (Karacabey basin) at the same longitudes (see also Figure 1).

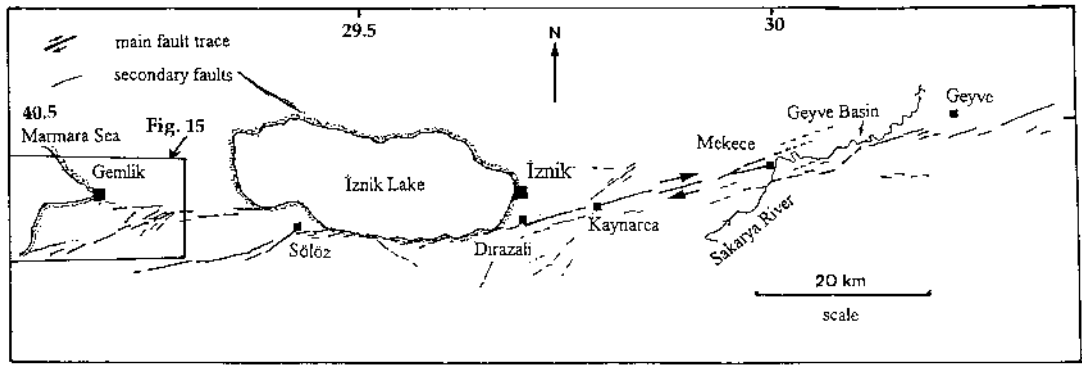


Figure 14: *The extent of the fault traces between Geyve and Gemlik obtained from 1:60,000 scale aerial photographs from Barka (1993).*

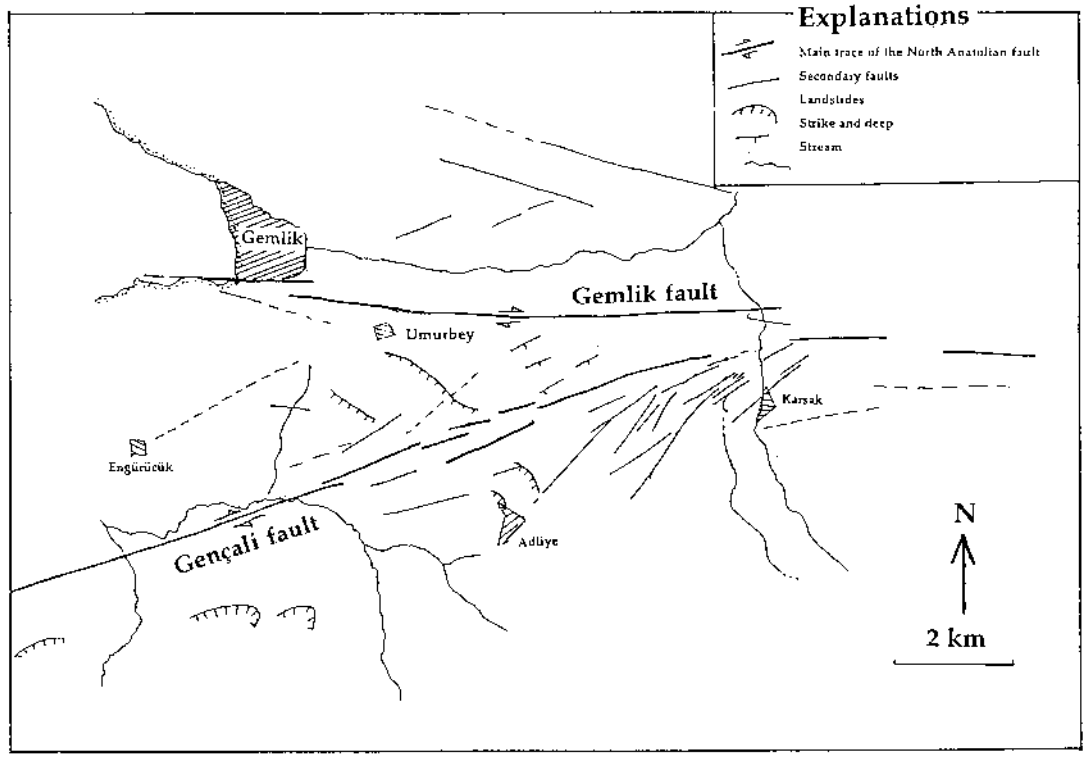


Figure 15: *Fault segments between İznik lake and Gemlik bay from Tsukuda et al. (1988).*

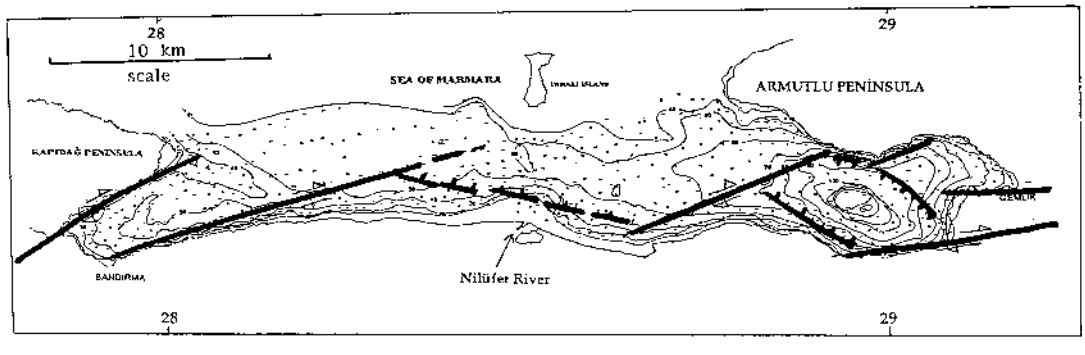


Figure 16: *Distribution of the active fault segments between Gemlik and Bandırma bays from Barka and Kuşçu (1996).*

The Orhangazi-Yalova fault (Akartuna, 1968) is a NW-SE trending fault connecting the middle strand and northern strand. This fault has well-developed right-lateral strike-slip faults with normal component expressions such as offset streams and linear fault line scarp. Nevertheless, this fault has not been studied in detail (Fig. 1).

Earthquake activity in the İzmit bay and İznik areas

Figure 17a shows the distribution of large historical earthquakes in the İzmit and İznik regions after Ambraseys and Finkel (1991). Figure 17b shows the time distribution of historical earthquakes for the northern strands between Adapazarı and İzmit bay. From the time distribution of earthquakes, it can be seen that there are two clusters of large events: the first 5 centuries AD and the 18^{th} and 19^{th} centuries. In between, over 12 centuries only a few events occurred in the region. The distribution of M>3.9 events for this century shows relatively low earthquake activity, except for a few moderate earthquakes (Fig. 18). On the other hand, microseismic earthquakes recorded from 1976-1990 show higher activity in the İzmit-Gölcük area (Fig. 19). The same data illustrate that two major parallel segments, Karamürsel and Yarımca-Yalova and Karamürsel basin, have almost no activity. This may be interpreted that these strike-slip segments are locked. Even though the 1719 and 1754 earthquakes occurred in this area, the large earthquake storms (length of period and amount of events) of the first 5 centuries and the 18-19^{th} centuries are compared one can suggest that more large earthquake activity would be expected in the area. This may correspond most possibly where there is no micro seismic activity at present.

There has been an extensive trenching effort along the İznik-Mekece section of the middle strand (Ikeda et al. 1989, 1991, Barka 1993) in order to find out the time elapsed since the last earthquake and the recurrence interval of large earthquakes along this section of the middle strand of the NAFZ. This effort was mostly related to the earthquake prediction studies along the İznik-Mekece segment undertaken by Boğaziçi University. However, the results obtained from these studies have not been conclusive. Ikeda et al. (1989, 1991) reported that there was an earthquake occurring between 300-500BP. On the other hand, Barka (1993) concluded that the last earthquake might have occurred between 700AD and 250BC, this earthquake was about the only earthquake within the last 4000 years. According to historical documents the 29AD event is the only large earthquake known in the İznik area which is consistent with Barka's (1993) results. Yoshioka and Kuşçu (1994) recognised one event along the Geyve segment of the middle strand which occurred about 2300 years BP. Guidoboni et al. (1994) reported that the 29AD, 362 and 368AD events were important events for the İznik area. Ambraseys and Finkel (1991) who studied the last 2000 years, reported that there may be two events which can be associated with this section of the middle strand: in 128 west of İznik lake and in 1419 in the Geyve-Pamukova area. Ikeda et al. (1989, 1991) found a natural exposure of thrust faulting with a small offset west of Iznik lake which led them suggest that there was one event in the 19^{th} century. This faulting might be correlated to the 1857 earthquake which occurred in this region (Ambraseys and Finkel 1991). The main conclusion from the above discussion is that both the historical earthquakes and trench results may indicate that the recurrence interval of large earthquakes for the Geyve-Gemlik section of the middle strand is probably in the vicinity of 2000 years or more. As far as instrumental data is concerned, there has not been any significant earthquake in this area. There is only a micro-earthquake activity occurring in the Gemlik bay area for the last 15 years.

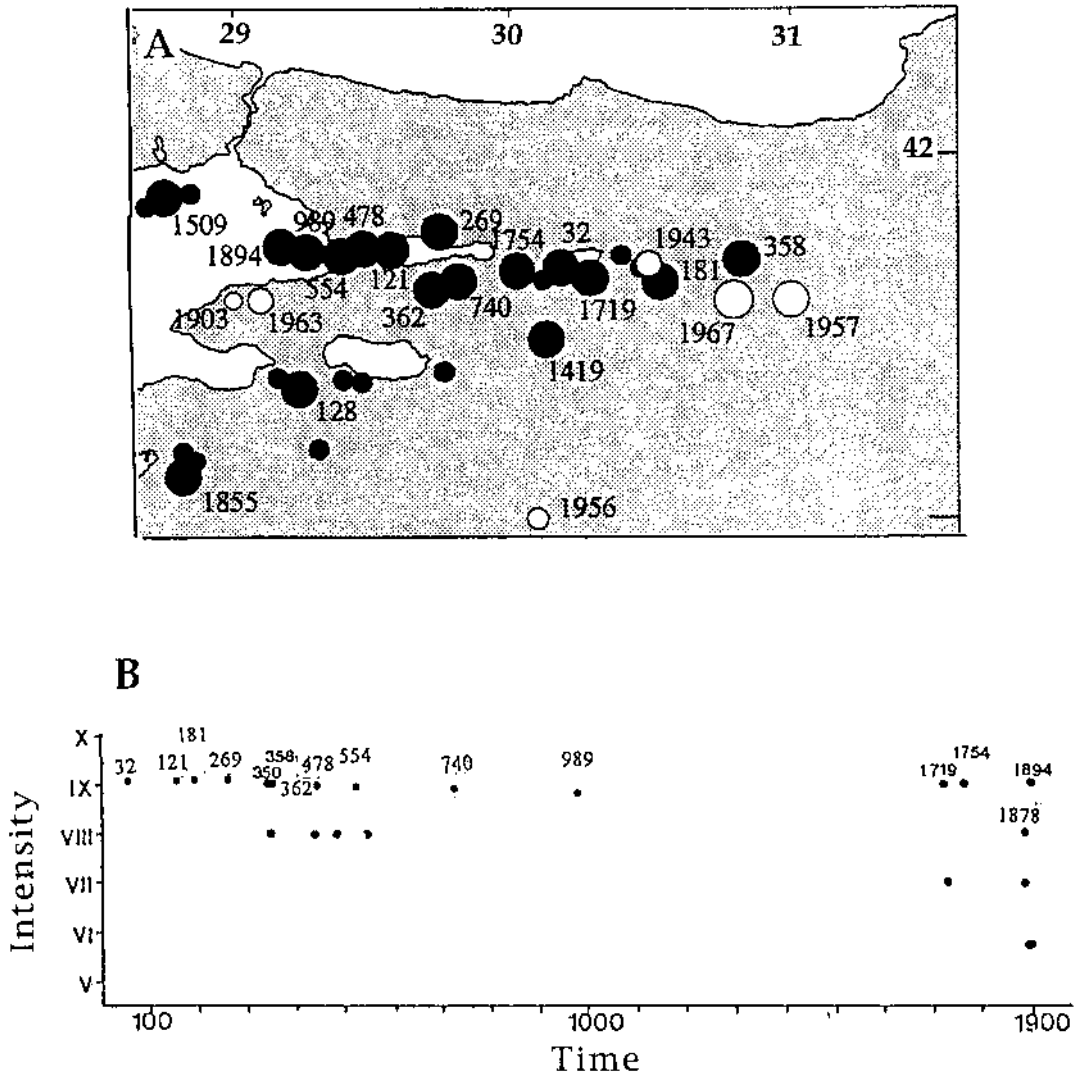


Figure 17: *Distribution of the historical earthquakes over the last 2000 years in the eastern Marmara region from Ambraseys and Finkel (1991), taken from Straub (1996). b) Time and intensity distributions of the historical earthquakes in the İzmit bay area documented from Ambraseys and Finkel (1991).*

GPS data show that most of the motion along the fault, about 10-15mm/y, is taken up by the northern strand (Straub 1996). This is consistent with both paleoseismological data and historical earthquake records. Stein et al. (1997), who modelled failure stress distributions of the migrating earthquakes along the NAFZ between 1939-1967, reported that high failure stress accumulation on both strands of the fault, Sapanca-İzmit and Geyve-İznik. However, from the above results it appears that the northern strand has more potential than the middle strand.

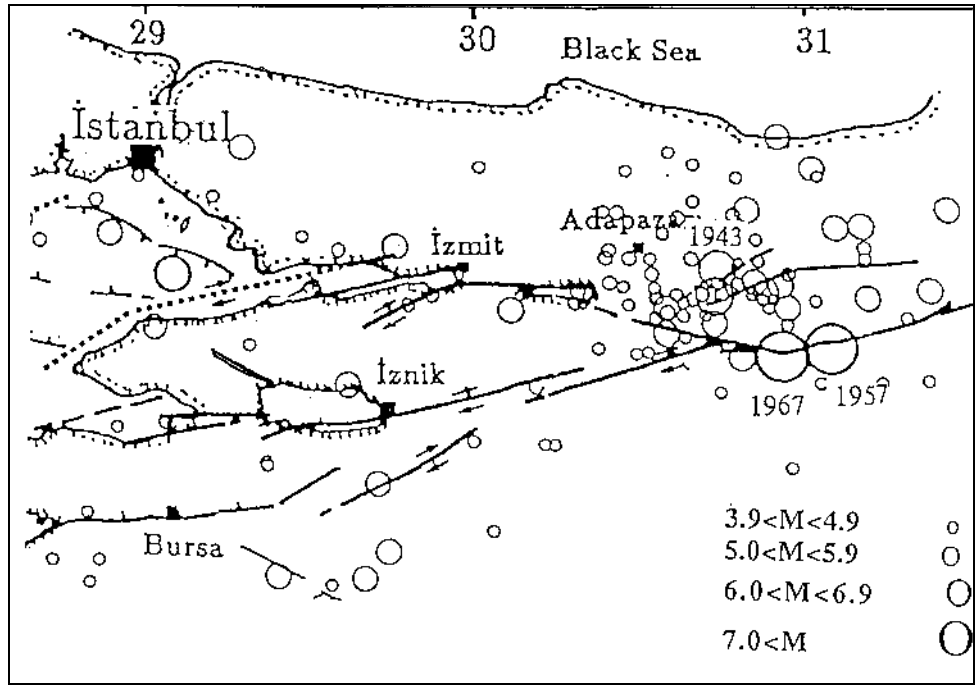


Figure 18: *Seismicity map of the eastern Marmara region, earthquakes M>3.9 between 1900-1990. Documented from Crampin and Üçer (1975), Dewey (1976) and ISC (1964-1984).*

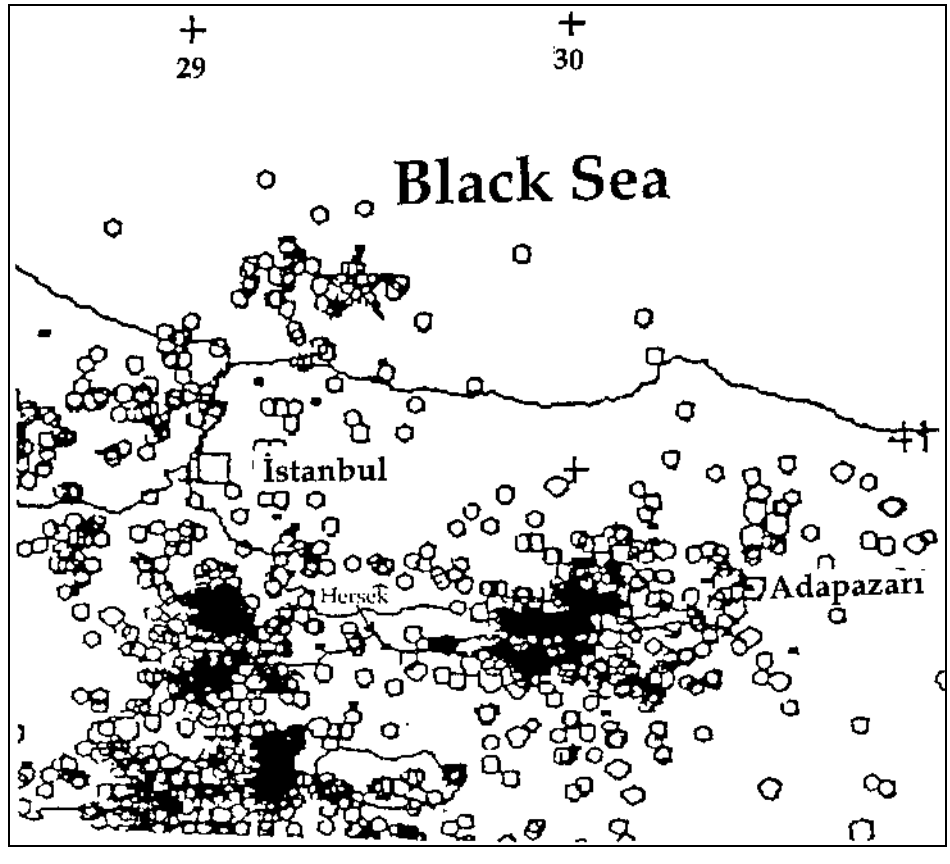


Figure 19: *Distribution of microseismicity in the eastern Marmara sea region for the period from 1976 to 1990 (Records from Kandilli Observatory).*

The Ganos-Saros region

In the northwestern Marmara sea, the northern strand extends from Gaziköy to Saros bay and is approximately 100km long, connecting the Marmara pull-apart basins to the Saros basin (Fig. 20). The geological studies in the area revealed that the Late Miocene units on the southern block are folded and some thrusting has been also identified subparallel to the main trace of the northern strand, both in the Şarköy area and also on the Gelibolu peninsula (Saner 1985, Önal 1986, Sümengen et al. 1987, Yaltırak 1995). Uplifted shorelines exist all along the Gaziköy to the Gelibolu peninsula (English 1904, Erol 1992, Sakınç and Yaltırak 1995a, b). Figure 21 is a spot image showing the active fault morphology of the central part of the main trace between Saros and Gaziköy, illustrating the linear fault line scarp and right-laterally dragged stream valleys and some linear ridges. The 1912 earthquake occurred along this part and it created right-lateral surface breaks which can be documented from Macovei (1912), Mihalinoviç (1927), Ateş and Tabban (1976), Ateş (1982), Ambraseys and Finkel (1987), Öztin (1987) and Eyidoğan et al. (1991), (Fig. 22). Ambraseys and Finkel (1987) also reported that some parts of the shoreline in the Şarköy area were uplifted. Although some of the Mihalinovic (1927) photographs show extensional features resulting from the 1912 earthquake, these could be related to landslides. Otherwise, active fault morphology and geological structures indicate that this earthquake should have had dominantly right-lateral strike-slip with a thrust component.

GPS data show that most of the motion along the fault, about 10-15mm/y, is taken up by the northern strand (Straub 1996). This is consistent with both paleoseismological data and historical earthquake records. Stein et al. (1997), who modelled failure stress distributions of the migrating earthquakes along the NAFZ between 1939-1967, reported that high failure stress accumulation on both strands of the fault, Sapanca-İzmit and Geyve-İznik. However, from the above results it appears that the northern strand has more potential than the middle strand.

A study of the Ganos dağ area is particularly important, because this section of the fault could be used as an analogue for Marmara sea ridges occurring along the northern strand in order to understand the structure, active fault morphology and earthquake activity of the strike-slip origins of the NE-SW trending ridges. Figure 20 shows the morpho-tectonic map of the Gaziköy-Saros area indicating the Enez-Ganos and Ganos-Gelibolu highs and the Saros and Marmara sea basins. Simple boundary element modelling (Bilham and King 1989) was carried out to test the kinematics of the faults. The results of the modelling illustrated that the segments extending from Uçmakdere to Gelibolu should have a thrust component of at least 50% (Fig. 23). This modelling agrees with a kinematic model produced from GPS measurements (Straub 1996). This model also is consistent with the seismicity pattern of the region, for example, the extensional areas (pull-parts) show continuos seismic activity (Fig. 28), while the strike-slip segments with thrust components have infrequent large earthquakes as reported by Ambraseys and Finkel (1991). This thrust component is also supported by a few moderate thrust earthquake (Fig. 24, Kalafat 1995).

Historical earthquakes in the area (Figs. 25 and 26) (Ambraseys and Finkel 1991) show that the repeat time of large earthquakes may change 570-800 years along the Gaziköy-Saros segment, which may include the western Marmara sea and the gulf of Saros.

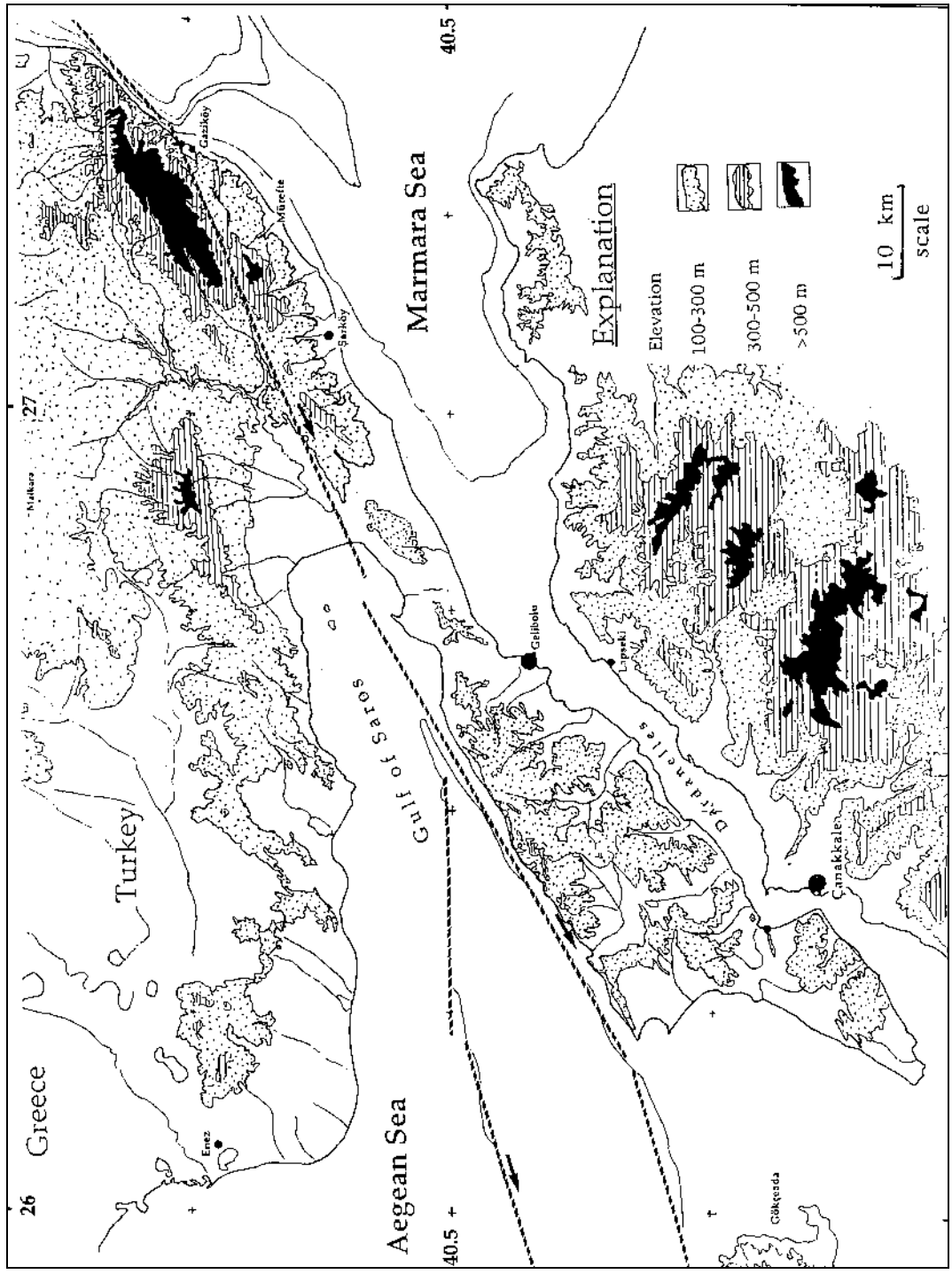


Figure 20: Morphotectonic map of the Gaziköy-Saros area along the northern strand of the NAFZ.



Figure 21: *A spot image of the central part of the Gaziköy-Saros segment, arrows show the main trace of the strike-slip segment.*

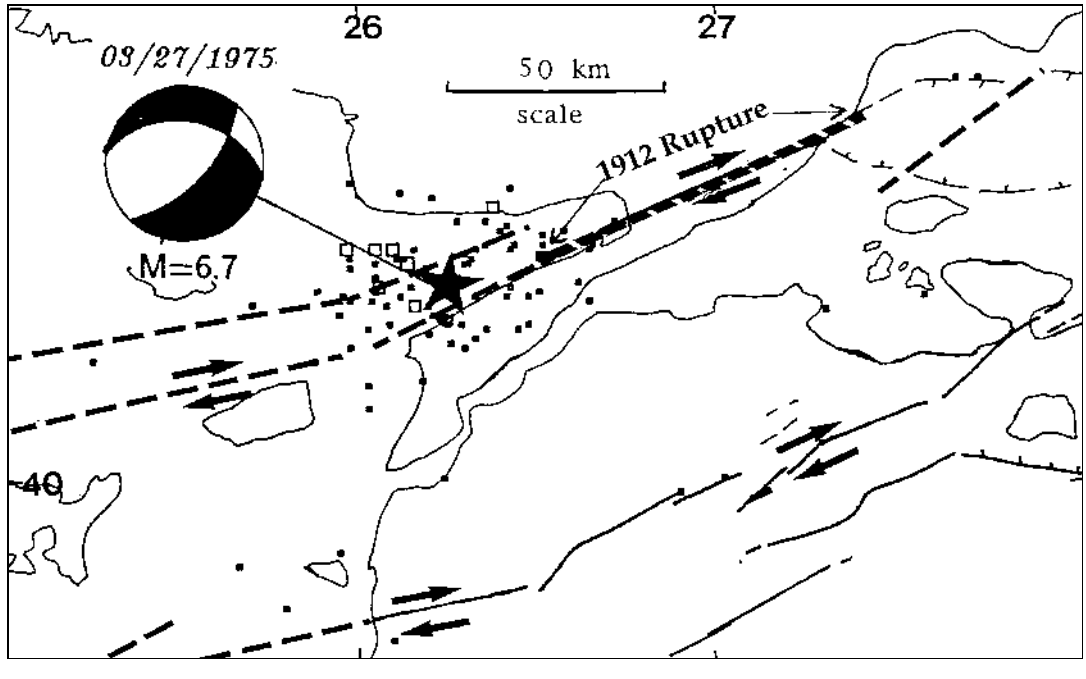


Figure 22: *The Saros earthquake of 03/27/1975 and its aftershock distribution from ISC data and approximate extent of the 1912 rupture zone.*

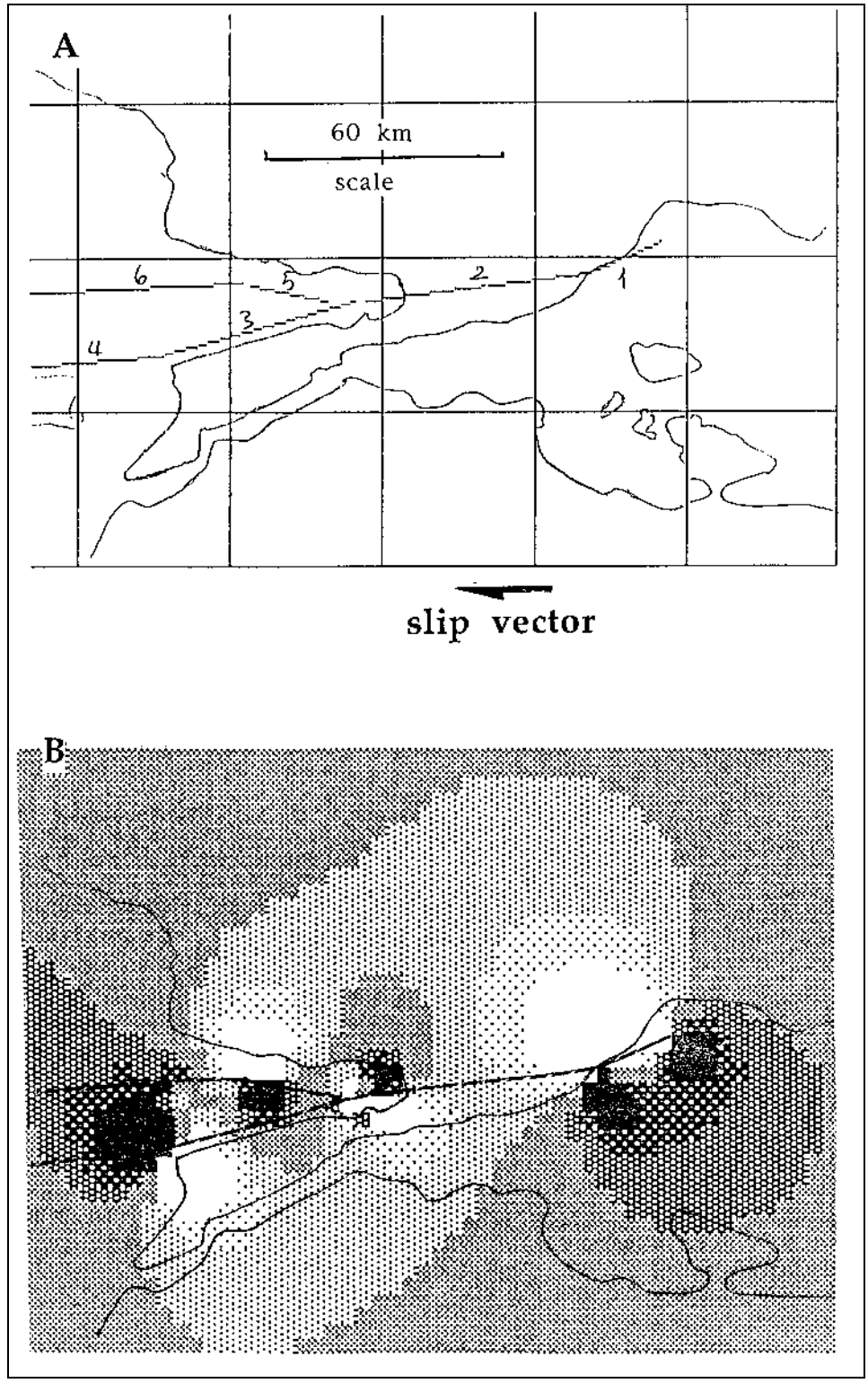


Figure 23: *a) Fault segments and slip vectors in the Ganos-Saros section of the NAFZ which were used for the boundary element modelling. b) Boundary element modelling of the fault kinematics in the Ganos-Saros region along the northern strand of the north Anatolian. White areas are the compressional areas which coincide with uplifted areas, black areas are the dilatational areas which coincide with basins. To obtain this modelling, 50% thrust components were added to segments 1, 2 and 3.*

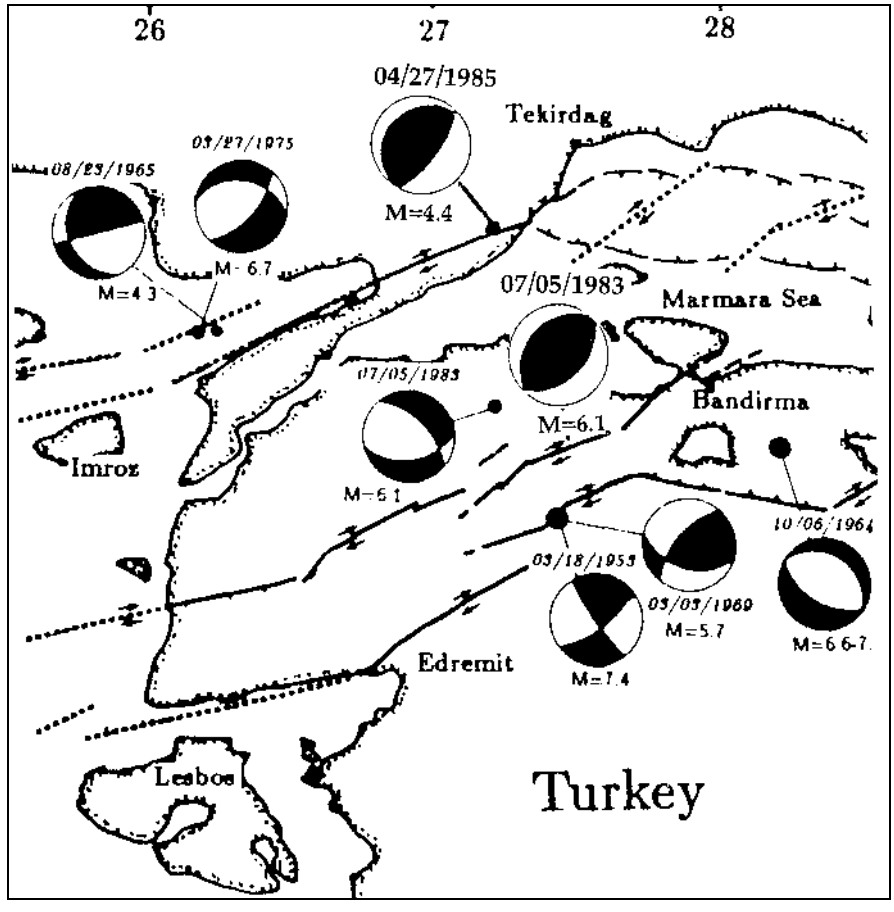


Figure 24: *Fault plane solutions of the significant earthquakes in the western Marmara region, compiled from McKenzie (1972 and 1978), Jackson and McKenzie (1984), Alsan et al. (1984), Kıyak (1986) and Kalafat (1995).*

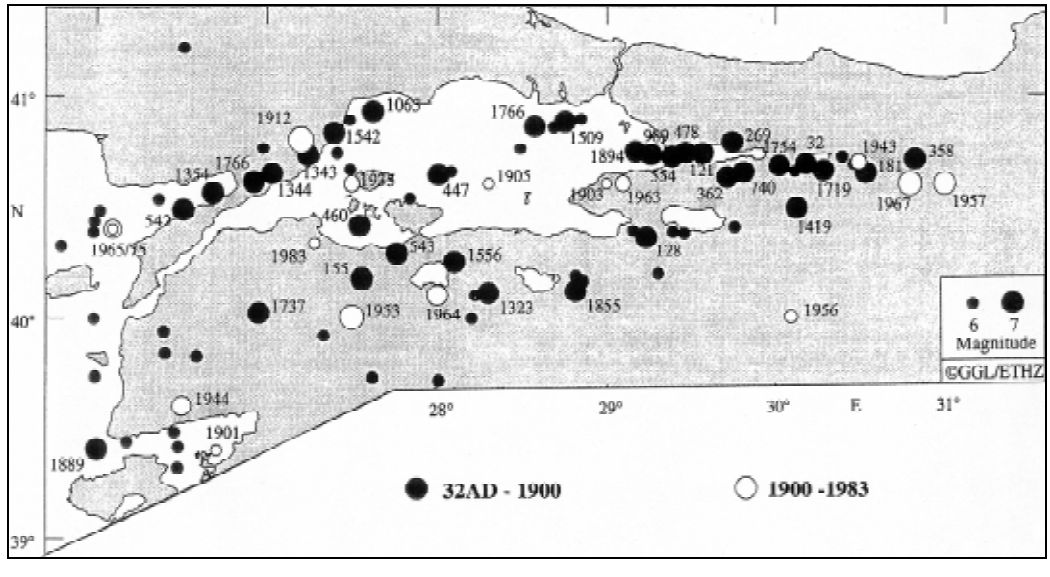


Figure 25: *Historical earthquakes in the Marmara sea region, originally from Ambraseys and Finkel (1991), taken from Straub (1996).*

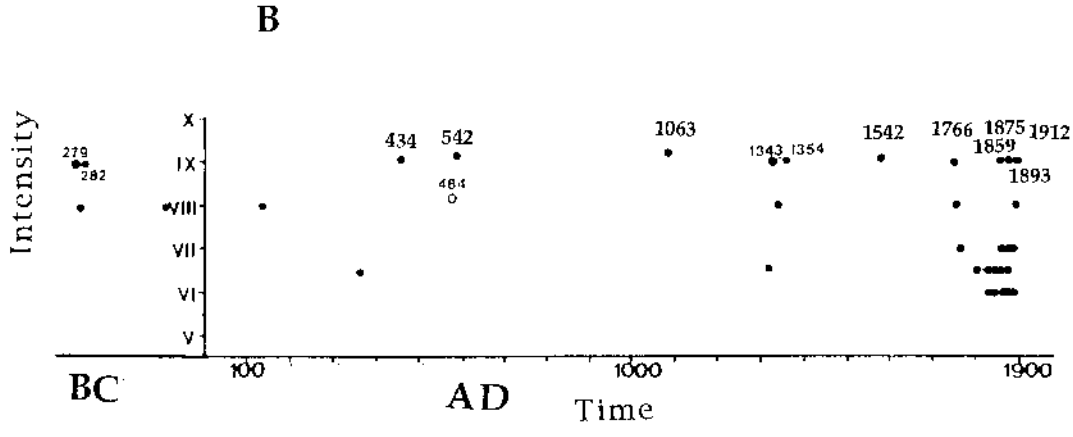


Figure 26: Time and intensity distributions of the historical earthquakes, documented from Ambraseys and Finkel (1987 and 1991).

The Biga peninsula

Barka and Kadınsky-Cade (1988), Siyako et al. (1989), Herece (1990), Barka (1992) and Şaroğlu et al (1987) described active faults in the Biga peninsula (Figs. 1 and 24). In this area, there are several NE-SW trending strike-slip faults parallel to each other, also showing en echelon geometry giving rise to a few pull-apart basins, such as the Aşağıinova, Bayramiç-Ezine and Yenice basins. Between basins, the area is morphologically elevated. In the Biga peninsula, the southern strand continues to Aegean via Gönen, Yenice and Edremit bay, while the middle strand goes through Sarıköy, Çan, Bayramiç and Ezine. The area between Ezine and Aegean sea has not been studied for active faults and recent studies did not show the continuity of the fault. Whether the fault does not continue further southwest, or, whether these studies failed to recognise the fault is not clear. However, the 1968, M=7.2, earthquake in the Aegean may indicate that this strand continues toward the Aegean sea. As far as historical earthquakes are concerned, the 155, 543 and 1737 earthquakes and a few other moderate to large events can be associated with this strand (Fig. 25). Nevertheless, during the present century, this strand has been seismically quiet. The 1953 Yenice-Gönen earthquake, M=7.4, along the southern strand formed the NE-SW trending strike-slip rupture zone with 3.5m maximum right-lateral motion (Ketin and Roesli 1953). The 1969 Gönen earthquake, M=5.7, had a dominant thrust component, indicating that the Biga peninsula has been uplifted by a thrust component (Fig. 24), (e. g. Taymaz et al. 1991). The 1983 Biga earthquake, M=6.1, has a controversial solution, between thrust and normal faulting: the ISC solution reveals dominant normal faulting while solution obtained by Alsan et al. (1984) and Kıyak (1986) suggest dominantly thrust, very similar to the solution of the 1966 earthquake which occurred in Ganos region. The direction of thrust being similar the strike-slip faults suggest also that there is a slip partitioning (e.g. Molnar 1992) along these segments including the Gaziköy-Saros segment where oblique faulting is taken up by two different faults: strike-slip and thrusts which are parallel to each other.

Herece (1990) reported about 8km offset in the Karacabey-Manyas basin since the Late Pliocene. He also documented a 2.8km total dextral offset along the Yenice-Gönen segment.

The central Marmara sea ridge

The northern half of the Marmara sea has two NE-SW trending ridges located in the area between İstanbul and the Kapıdağ peninsula, and Ereğli and Marmara island. The eastern one is known the central Marmara sea ridge. The central Marmara sea ridge separates the Çınarcık and Silivri-Ereğli basins, located east and west respectively. This ridge is particularly important to study for earthquake risks in the İstanbul metropolitan area. The detailed morphology of this ridge is poorly known except for a small basin in the northwest. From the overall fault patterns of the Marmara sea region, it can easily be suggested that this central Marmara ridge is similar to the Ganos-Saros ridge. However, the Gaziköy-Saros segment is longer. Figure 27 shows a shallow seismic profile across these ridges. From these profiles, this ridge can be interpreted as having a positive flower structure. In the northern half of the Marmara sea, E-W trending normal faults appear to dominate to the NE-SW trending strike-slip faults, two possible reasons: first, their dipslip motions create assertive morphology, and second, the ends of the NE-SW trending major strike-slip faults would be concealed by the prograding shelfs. However, it is not very clear yet, why the central and western ridges have lower elevations (600-700m below sea level). This might be due to the fact that the strike-slip faults here in these ridges are secondary, possibly having been formed during the progressive motion along the northern strand as a result of the distortion of the large pull-part (from İzmit bay to the Gaziköy-Saros segment) bounded by northern and southern boundary faults. Thus, these ridges require detailed bathymetric studies to better understand the kinematics and morphological expressions of the active fault segments.

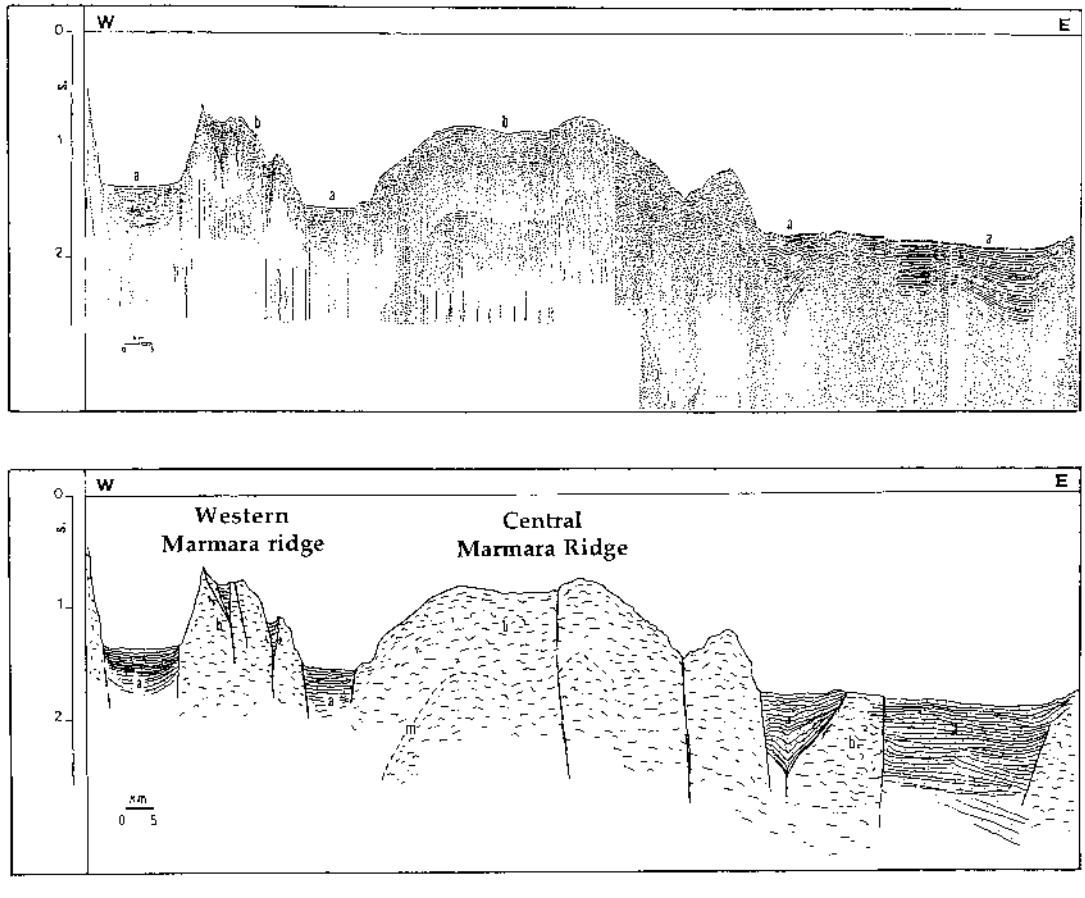


Figure 27: Shallow seismic reflection profile across the central ridge in the Marmara sea, from Ergün and Özel (1995).

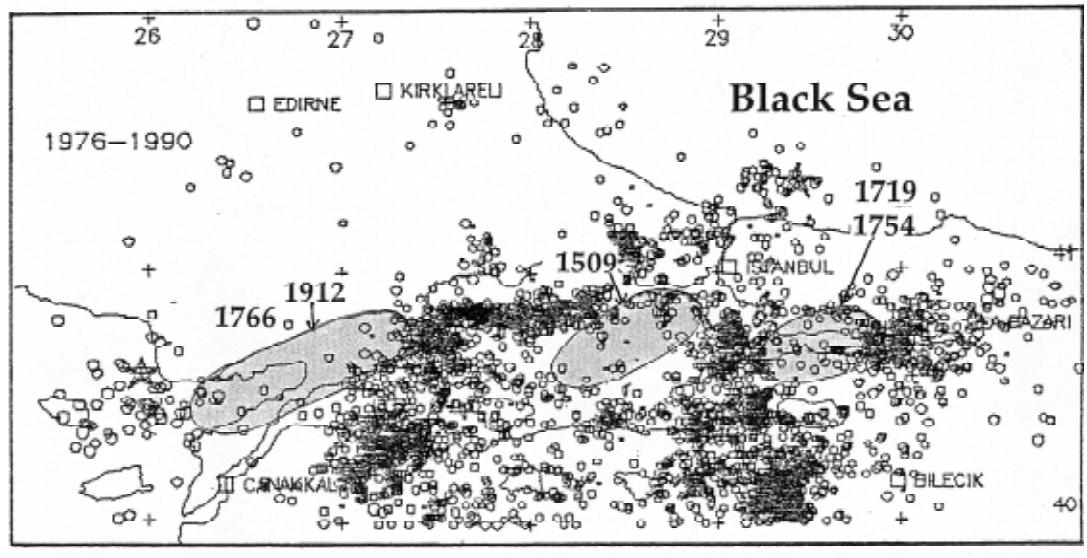


Figure 28: *Seismicity of the Marmara sea region between 1976-1990 (Kandilli Observatory records). Three ellipses emphasise the areas where there is a lack of seismicity, which coincides with major strike-slip segments. Dates are the dates of the last large events at these sites.*

At each side of the central Marmara ridge, there are two pull-apart basins, bounded by approximately E-W trending normal faults. A 1976-1990 seismicity map of the Marmara sea (Fig. 28) illustrates that the pull-apart basins have continuous seismic activity while the ridges have very little or no activity, such as the gulf of İzmit, central Marmara sea ridge and Gaziköy-Saros region. This can be interpreted that there are two different fault systems: normal faults forming southern and northern margins of the pull-aparts and strike-slip faults forming the ridges between the pull-aparts. In terms of seismic activity, we can suggest that the pull-apart basins have earthquakes M<7, while the ridges have the ability of creating M>7 earthquakes. For example, the 1963, 1964, and 1975 events were all M<7 and they occurred in the basins having normal solutions (e.g. McKenzie 1972, Taymaz et al. 1991) while the 1912 and 1953 had strike-slip mechanisms and they all occurred along the ridges or strike-slip segments.

Studies of historical earthquakes (Eginitis 1895, Sieberg 1932, Pınar 1943, Ergin et al. 1967, Ambraseys and Zatopek 1969, Karnik 1971, Ambraseys 1971, 1975 and 1988, Sipahioğlu 1984, Ambraseys and Finkel 1987, 1990, 1991 and 1995, Öztin and Bayülke 1990) indicate that there have been an abundance of large earthquakes, Intensity>VIII, in the İstanbul area. This high activity is not very surprising if we considered the active fault pattern in the Marmara sea. The normal faults bounding both basins on each side of the central Marmara ridge are responsible for frequent moderate to large earthquakes (e.g. the 1894 and 1963 earthquakes) and continuous microactivity (Fig. 28). The central ridge might be responsible for creating mostly the less frequent but larger earthquakes (such as the 1509 earthquake). The other important source of large earthquakes for the İstanbul region is the İzmit bay area. From historical earthquake records it is clear that most of the İzmit bay area earthquakes created considerable damage in the İstanbul area (e.g. 1754).

From the list of the historical earthquakes documented by Ambraseys and Finkel (1991) for the last 2000 years (Fig. 29), it appears, that earthquakes which create considerable damage in the İstanbul area, Intensity=VIII, occur approximately every 100 years, while the earthquakes, Intensity=IX have an average recurrence interval of 250 years. According to historical records, both periods will be completed presently. The last significant earthquake in this

area was in 1894, the intensity in İstanbul was IX. From the damaged area, it is postulated that the earthquake might have been created by the eastern part of the eastern pull-apart structure. The last moderate earthquake is the 09/18/1963 with M=6.3. The fault plane solution of this event illustrates dominant normal faulting and confirms the direction of pull-apart opening (Fig. 2).

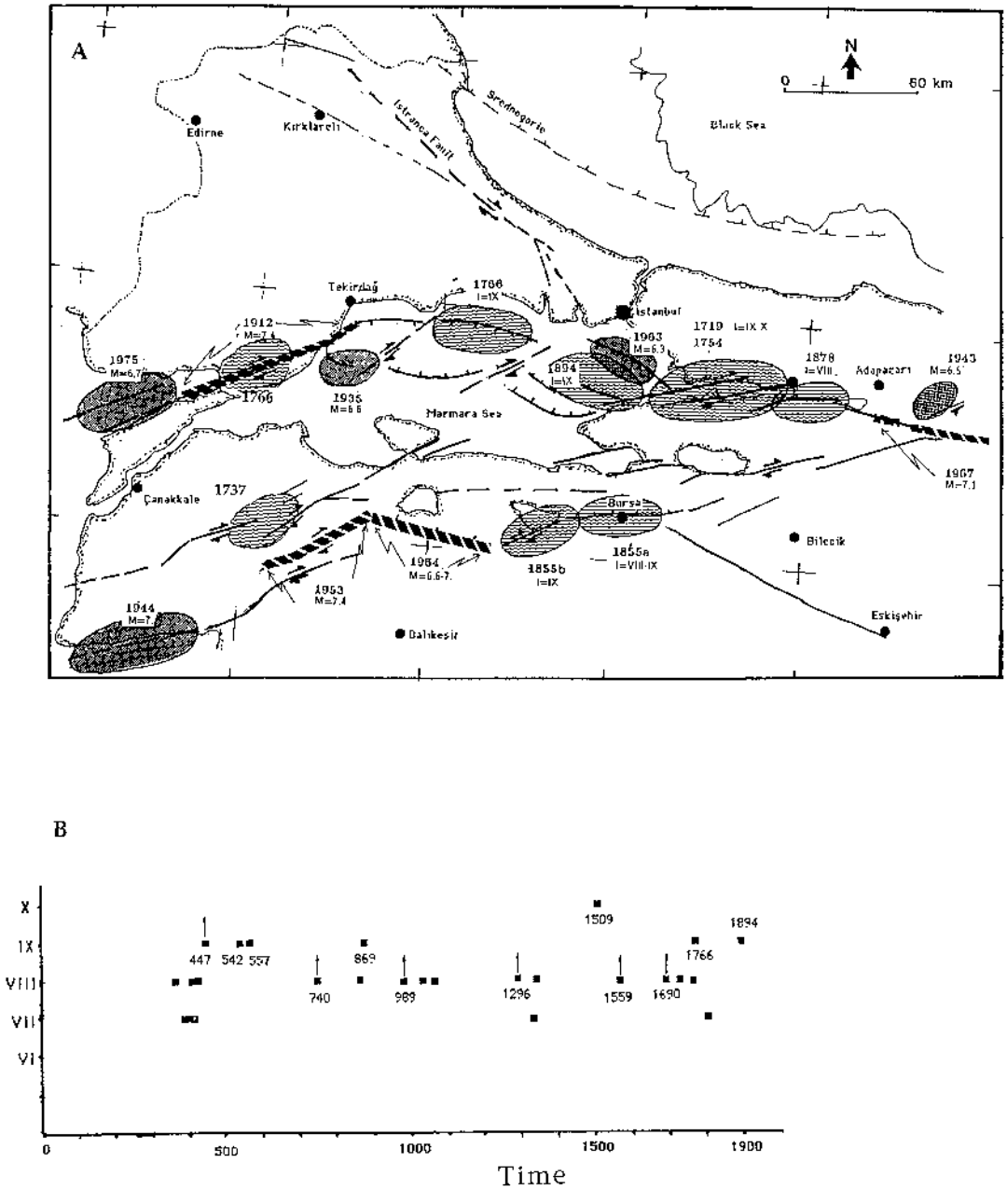


Figure 29: Distribution of large earthquakes in the Marmara sea region over the last 300 years. Wavy pattern shows historical events, dashed lines are surface breaks of the 20th century earthquakes and doted areas show the aftershock distribution of the recent earthquakes (last 50 years), documented from Öztin and Bayülke (1990), Ambraseys and Finkel (1991). b) Time and intensity distribution of earthquakes for the İstanbul region documented from Ambraseys and Finkel (1991).

Segments that have the potential of creating large earthquakes

The lack of microseismicity located between the 28°-29° longitudes on the central Marmara ridge is related to the major NE-SW trending strike-slip fault segment(s) (Barka and Toksöz 1989, Barka 1991 and 1992). The last known significant earthquake in the region was the 1894 İstanbul earthquake, Intensity=IX, (Eginitis 1895, Gündoğdu et al. 1991). According to Eginitis (1895) and Ambraseys and Finkel (1991), the earthquake was effective between İstanbul and İzmit and it was probably located in the Çınarcık basin. Ambraseys and Finkel (1987) reported that the 1766 event occurred near the 1509 earthquake in the northern central Marmara sea (Fig. 25). The 1509 earthquake on the other hand (Ambraseys and Finkel 1990 and 1991) was probably the largest earthquake to have occurred since the 5th century AD in the area and it is also the most possible earthquake that can be attributed to this gap. The area affected by this earthquake lays between İstanbul and Gelibolu (Ergin et al. 1967, Soysal et al. 1981, Ambraseys and Finkel 1991) and caused extensive damage in İstanbul and the death of 13,000 people in the region (Eginitis 1895). Eginitis (1895) also reported that a large ground fissure opened in the Topkapı Palace area and swallowed many people and horses. The other significant earthquakes which occurred in 554 and 447 are the other two events that are known to have caused great damage and loss of life in the İstanbul area (Ambraseys and Finkel 1991). From this data, it appears that the recurrence interval of great earthquakes is about 1000 years (Eginitis 1895, Ambraseys 1971, Ambraseys and Finkel 1991). A return period of 1000 years for the largest earthquakes with a 2-4m slip along the central Marmara ridge may be considered to be consistent with the long-term slip rate calculated from geological data of about 2-4mm/y. This time interval is comparable to the quiescence periods obtained from the historical data covering the İzmit and Ganos-Saros regions. However, the slip rate obtained from GPS measurements, ~15 mm/y, appears to be 4-7 times higher than this value.

Figure 29 shows the distribution of large earthquakes in the Marmara sea region for the last 300 years. From this figure, it is clear that the northern strand appears to create more large earthquakes than the other two strands, even though there has been significant activity along the southern strand for the last 100 years in the southern Marmara and north Aegean (e.g. 1982 events). Toksöz et al. (1979) suggested a possible seismic gap between the 29° and 30° longitudes. Even though, this part of the northern strand was subjected to several large earthquakes during the 18th and 19th centuries such as in 1719, 1754, 1878 and 1894. Two recent studies, modelling the 1944-1967 earthquakes that occurred along the NAFZ, indicate an increase of failure stress in this region. GPS measurements reveal, that the slip rate along the northern strand is 10-15mm/y, suggesting that the region of lake Sapanca and gulf of İzmit might still have potential of large earthquakes.

In spite of active morphological expressions along the middle strand from the Mudurnu valley (from the 1967 earthquake) to the Aegean sea (to the 02/19/1968 earthquake area), there are only a few possible historical earthquakes for the last 1000 years which can be associated with this strand. These are the 1419 and 1737 events (Ambraseys and Finkel 1991). Thus, almost the entire middle strand can be considered as a potential site for large earthquakes.

During the last two centuries, the greatest part of the southern strand has been ruptured as a result of large earthquakes (Fig. 29). However, two possible seismic gaps still exist: the Pazarköy-Edremit and the Yenişehir gaps. The Pazarköy-Edremit gap is 60km long, has a double bend geometry and is separated from the 1953 rupture segment by about a 12km wide restraining stepover. The Yenişehir gap, on the other hand, has pull-apart geometry.

From the data presented above, it appears that the motion along the fault zone has been taken up by the northern and southern strands. It is difficult to know when the middle strand will take over the activity.

Conclusions

1- The NAFZ splays into three strands in the Marmara and north Aegean regions. Each strand consists of NE-SW trending short strike-slip fault segments which form pull-apart structures, particularly in the Marmara region.

2- The northern strand follows the Marmara basins and the north Aegean trough, which includes the Saros and Sporados basins. The middle strand runs along the southern shore of the Marmara sea, cuts through the Biga peninsula and ends at the western end of the Skyros basin. The southern strand forms the Bursa and Manyas-Karacabey basins and then runs parallel to the middle strand and ends in the Skyros basin.

3- The geometry of the three strands are identical and parallel to each other. It seems that they follow the pre-existing structures in the region.

4- The fault plane solutions of recent earthquakes and GPS measurements indicate that the dominant motion along these strands is strike-slip.

5- In the Marmara sea region all strike-slip fault segments strike ENE-WSW and/or NE-SW, while the regional slip vector is almost E-W, causing a thrust component along the strike-slip segments.

6- Microseismic activity is mostly located to the pull-apart basins, thus normal faults, while strike-slip segments have almost no micro-seismic activity except aftershock activity.

7- Paleogeographical maps indicate that the initiation of the north Anatolian is about Pliocene.

8- The long term seismicity and GPS measurements and geological data suggest that the northern strand of the fault zone is more active than the other two southern strands.

9- Both restoration of the Karamürsel basin and the amount of extension from the Çınarcık basin, deduced from the Marathons seismic profile-16, reveal about 10-15km total offset along the northern strand. This value gives rise to a long term slip rate of 2-4mm/y, if we consider that the fault zone initiated 3-4m.y. ago. On the other hand, GPS measurements give a slip rate of approximately 10-15mm/y for the northern strand.

10- Historical and paleoseismological data indicate, that the recurrence interval of clusters of large earthquakes is 1200 years in the İzmit bay area, 500-800 years along the Gaziköy-Saros segments and more than 2000 years along the Geyve-Gemlik section of the middle strand. The return period for large earthquakes, Intensity>VIII, for the south of İstanbul varies between 100-1000 years, depending on the size and the mechanism of earthquakes. The GPS rate for the northern strand is much higher than that obtained from historical earthquake records and geological data.

11- The central Marmara ridge needs further detailed studies, as it is considered to be a major source of large earthquakes for the İstanbul region. The last major large earthquake on this ridge was probably in 1509AD. The return period for these earthquakes can be 225-1000 years, depending on slip rate considered (GPS = 15mm/y, geological = 2-4mm/y).

Acknowledgement

I would like to thank C. Schindler, St. Mueller and M. Pfister for inviting me to write this article. I would like to thank for long discussions that I had with C. Straub, M. Sakınc, O. Tüysüz and Yığıtbaş. This research was supported in part by TYDABÇAG-237-G, National Marine Geology and Geophysics Programme (Coordinator Nacı Görür) and Glotek unit, both supported by TÜBiTAK.

References

Akartuna, M., 1968, Armutlu yarımadasının Jeolojisi, Ist. Üni. Fen Fak. Monog., 20, 105p.

Akgün, M. ve Ergün, M., 1995, İzmit Körfezinin yapısı ve Kuzey Anadolu fayı (KAF) ile ilişkisinin irdelenmesi, Jeofizik, 9, 71-78.

Allen, C.R., 1969, Active faulting in northern Turkey, Contr. No. 1577, Div. Geol. Sci. Calif. Inst. Tech., 32p.

Alptekin, Ö., 1973, Focal mechanisms of earthquakes in Western Turkey and their tectonic implications, Ph.D Thesis, New Mexico Inst. Mining and Technology, Socrro, New Mexico, 95p.

Alsan, E., Tezuçan, L., Başarır, E., Ayhan, E. and Sancaklı, N., 1984, Temmuz 1983, Biga depremi ve artçı deprem etkinliği, Deprem Araştırma Bülteni, 46, 50-75.

Ambraseys, N.N., 1970, Some characteristic features of the North Anatolian fault zone, Tectonophysics, 9, 143-165.

Ambraseys, N.N., 1971, Value of historical earthquakes, Nature, 232, 375-379.

Ambraseys, N.N., 1975, Studies in historical seismicity and tectonics, in: Geodynamics of Today, The Royal Soc. London, 7-16.

Ambraseys, N.N., 1988, Engineering seismology, Earthquake Engineering and Structural Dynamics, 17, 1-105.

Ambraseys, N.N. and Finkel, C.F., 1987, The Saros-Marmara earthquake of 9 August 1912, Earthq. Engin. and Struc. Dynam., 15, 189-211.

Ambraseys, N.N. and Finkel, C.F., 1990, Marmara sea earthquake of 1509, Terra Motae, 167-174.

Ambraseys, N.N. and Finkel, C.F., 1991, Long-term seismicity of İstanbul and of the Marmara region, Engin. Seis. Earthq. Engin.Report, 91/8, Imperial College.

Ambraseys, N.N. and Finkel, C.F., 1995, Seismicity of Turkey and Adjacent Areas, A historical Review, 1500-1800. Eren Yayıncılık ve Kitapçılık Ltd., 224p.

Ambraseys, N.N. and Zatopek, A., 1969, The Mudurnu valley, West Anatolia, Turkey, earthquake of 22 July 1967, Bull. Seism. Soc. Amer., 59, 521-589.

Ateş, R. and Tabban, A., 1976, Preliminary report for the Şarköy-Mürefte earthquake of 9th August, 1912, Publ. Earth. Res. Inst., 24p.

Ateş, R., 1982, Earthquake activity on the North Anatolian fault zone, in: Progress in Earthquake Prediction, edited by: A.M. Işıkara and A. Vogel, Friedr.Vieweg and Sohn, FGR, 95-113.

Bargu, S. and Yüksel, A., 1993, İzmit Körfezi Kuvaterner deniz dibi çökellerinin stratigrafik ve yapısal Özellikleri ile kalınlıklarının dağılımı, TJK Bülteni, 8, 169-187.

Barka, A.A., 1991, İstanbul'un Depremselliğini oluşturan tektonik yapılar ve İstanbul için bir mikro-bölgelendirme denemesi, "İstanbul ve Deprem Sempozyumu" Inşaat Müh. Odası, 35-56.

Barka, A.A., 1992, The North Anatolian Fault, Annales Tectonicae, 6, 164-195.

Barka, A.A., 1993, Kuzey Anadolu Fayının Sapanca- İzmit ve Geyve- İznik Kolları Üzerinde Paleosismik Araştırmalar, Proje No: YBAG-4/7551, 85p.

Barka, A.A., and Gülen, L., 1988, New constraints on age and total offset of the North Anatolian fault zone: Implications for tectonics of the Eastern Mediterranean region, METÜ J. Pure Appl. Sciences, 21, 39-64.

Barka, A.A. and Kadınsky-Cade, K., 1988, Strike-slip fault geometry in Turkey and its influence on earthquake activity, Tectonics, 7, 663-684.

Barka, A.A. and Kuşçu, İ, 1996, Extents of the North Anatolian fault in the İzmit, Gemlik and Bandırma bays, Turkish J. Marine Sci., 2, 93-106.

Barka, A.A. and Toksöz, N. M., 1989, Seismic gaps along the North Anatolian Fault, Özet, IASPEI meeting in İstanbul, Turkey, S9-1.

Bilham, R. and King, G., 1989, The morphology of strike-slip faults: Examples from the San Andreas fault, California, J. Geophys. Res., 94, 10204-10216.

Crampin, S. and Evans, R., 1986, Neotectonics of the Marmara sea region of Turkey, J. Geol. Soc. London, 143, 343-346.

Crampin, S. and Üçer, B., 1975, Seismicity of the Marmara sea region of Turkey, J. R. Astr. Soc., 40, 269-288.

Çaglayan, A.M., Şengün, M. and Yurtsever, A., 1988, Main Fault Systems shaping the İstranca massif, Turkey, METÜ, J. Pure Appl. Sciences, 21, 145-154.

Dewey, J.W., 1976, Seismicity of Northern Anatolia, Bull. Seism. Soc. Am., 66, 843-868.

Dewey, J.F. and Şengör, A.M.C., 1979, Aegean and surrounding regions: Complex multiplate and continuum tectonics in a convergent zone, Geological Society of America Bulletin, 90, 84-92.

Doust, H. and Arıkan, Y., 1974, The geology of the Thrace basin, in: Proceedings of the Second Petroleum Congress of Turkey, edited by: H. Okay and E. Dileköz, Assoc. Turkish Petrol. Geologists, 119-136.

Eginitis, M.D., 1895, Le tremblement de terre de Constantinople du 10 Juillet.1884, Ann. Georg., 4, 151-165.

English, T., 1904, Eocene and Later Formations Surrounding the Dardanelles, Quart. Journ. Geol. Soc., 58, 309-390.

Ergin, K., Güçlü, U. and Uz, Z., 1967, A catalogue of earthquakes for Turkey and surrounding area, Publ. Ist. Techn. Univer. Mining Fac., 24, l89p.

Ergün, M. and Özel, E., 1995, Structural relationship between the sea of Marmara basin and the North Anatolian fault, Terra Nova, 7, 278-288.

Erinç, S., 1956, Yalova civarında Pleistosen depoları ve taraçaları, Türk Coğrafya Dergisi, 15-16, 188-190.

Erol, O., 1992, Çanakkale Yöresinin Jeomorfolojisi ve Tektoniği, TPJD Bülteni, 4, 1, 147-165.

Erol, O. and Çetin, O., 1995, Evolution of the Marmara sea from Late Miocene to Holocene, in: Quaternary sequence in the gulf of İzmit, edited by: E. Meriç, 313-341.

Eyidoğan, H., Güçlü, U., Utku, Z. and Değirmenci, E., 1991, Türkiye büyük depremleri makro-sismik rehberi, ITÜ, Maden Fakültesi, Jeofizik Bölümü yayını, 198p.

Göney, S., 1964, Karamürsel civarında Pleyistosen'e ait bazı eski kıyı izleri, Y.Ü. Coğ. Ens. Derg., 14, 200-208.

Guidoboni, E., Comastri, A. and Traina, G., 1994, Catalogue of ancient earthquakes in the Mediterranean area up to the 10th century, ING, Italy, 504p.

Gündoğdu, O., Altınok, Y., Özer, N. and Kolçak, D., 1991, 1894 depremi ve İstanbul, Türkiye 12. Jeofizik Kurultayı Bildiri Özetleri, 41.

Herece, E., 1990, The Yenice-Gönen earthquake of 1953 and some examples of recent tectonic events in the Biga peninsula of northwestern Turkey, Bull. Min. Res. and Expl. Inst. of Turkey, 111, 1-15.

Ikeda, Y., Suzuki, Y., and Herece, E., 1989, Late Holocene activity of the North Anatolian fault zone in the Orhangazi plain, Northwestern Turkey, in: Multidisciplinary research on fault activity in the western part of the North Anatolian fault zone, edited by: Y. Honkura and A. Işıkara, 16-30.

Ikeda, Y., Suzuki, Y., Herece, E., Şaroğlu, F., Işıkara, A.M. and Honkura, Y., 1991, Geological evidence for the last two faulting events on the North Anatolian fault zone in the Mudurnu Valley, western Turkey, Tectonophysics, 193, 335-345.

Jackson, J.A. and Mckenzie, D., 1984, Active tectonics of the Alpine-Himalayan belt between western Turkey and Pakistan, Geophysical Journal of the Royal Astronomical Society, 77, 185-264.

Kalafat, D., 1995, Anadolu'nun tektonik yapıların deprem mekanizmaları açışından irdelenmesi, PhD. Thesis, Istanbul Üniversitesi, Deniz Bilimleri ve İşletmeciliği Enstitüsü, 217p.

Karnik, V., 1971, Seismicity of the European area, part 2, D. Riedel Publ. Co., Dordreet-Holland, 225p.

Kavukçu, S., 1990, Active fault investigation in İzmit bay, Bandırma bay and Erdek bay of Marmara sea. Proceedings " Historical seismicity and seismotectonics of the Mediterranean region", Turkish Atomic Energy Authority, 238-266.

Ketin, İ., 1969, Über die nordanatolische Horizontalverschiebung, Bull. Mineral Res. Explor. Inst. Turkey, 72, 1-28.

Ketin, İ. and Roesli, H., 1953, Makroseismische Untersuchungen über das Nordwest Anatolische Beben vom 18. März 1953, Eclogae. Helv., 462.

Kıyak, U., 1986, Kuzey Anadolu Fay zonunun Batı Uzantılarının İncelenmesi, Ph.D Thesis, İstanbul Üniversitesi Müh. Fak. Jeofizik Böl., 175p.

Koçyiğit, A., 1988, Tectonic setting of the Geyve basin: Age and total displacement of the Geyve fault zone, in: 1987 Melih Tokay Symposium, METÜ, J. Pure Appl. Sciences, 21, 81-104.

Koral, H. ve Öncel, A.O., 1995, İzmit körfezinin yapısal ve sismolojik özellikleri, Jeofizik, 9, 1-2, 79-82.

Kurtuluş, C., 1985, Gemlik Körfezi yüksek ayrımlı sığ sismik etüdü raporu, MTA, Jeofizik Etüdler Dairesi, 735, 6p.

La Joie, ?, 1986, Coastal tectonics, in: Active tectonics, Washington D. C. National Academy Press, 483-486.

Le Pichon, X. and Angelier, J., 1981, The Aegean sea, Philosophical Transactions of the Royal Society of London, A 300, 357-372.

Le Pichon, X., Cahmot-Rooke, N., Lallememnt, S., Noomen, R. and Veis, G., 1995, Geodetic determination of the kinematics of central Greece with respect to Europe: Implications for Eastern Mediterranean tectonics, J. Geophys. Res., 100, 12675-12690.

Lüttig, G. and Steffens, P., 1979, Explanatory notes for the paleogeographical Atlas of Turkey from Oligocene to Pleistocene, Hannover, 64p.

Lyberis, N., 1984, Tectonic evolution of the North Aegean trough, in: The Geological Evolution of Eastern Mediterranean, edited by: J.E. Dixon and A.H.F. Robertson, Geological Society, London, Special Publication, No. 17., 709-725.

Macovei, G., 1912, Sur le tremblement de terre de la mer de Marmara le 9 août 1912, Bull. Sect. Sci. Acad. Roumanie, Bukarest, 1/1, 1-10.

Marathon Oil, 1975, Marmara-1, Final well report, Turkey, 26p.

McKenzie, D.P., 1972, Active tectonics of the Mediterranean Region, Geophys. J.R. Astr. Soc. 30, 109-185.

McKenzie, D.P., 1978, Active tectonics of the Alpine-Himalayan belt: the Aegean sea and surrounding regions (tectonics of Aegean region), Geophys. J.R. Astr. Soc., 55, 217-254.

Meriç, E., Yanko, V., Avşar, N. Nazik, A. and Koral, H., 1995, Kuvaterner döneminde Akdeniz ile Marmara Denizi arasındaki deniz bağlantıları, in: İzmit Körfezi Kuvaterner istifi, edited by: E. Meriç, University of İstanbul, 285-295.

Mihalinoviç, J., 1927, Grandes catastrophes seismiques dans la mer de Marmara, Inst. Seismo. Univ. de Beograd, 350p.

Molnar, P., 1992, Brace-Goetze strength profiles, the partitioning of strike-slip and thrust faulting at zones of oblique convergence and the stress-heat flow paradox of the San Andreas fault, in: Fault Mechanics and transport properties of rocks, Acad. Pres. Ltd. 436-459.

Önal, M., 1986, Gelibolu Yarymadası'nın orta bölümünün, çökelme istifleri ve tektoniği, kuzeybatı Anadolu ve Türkiye, İTÜ Mühendislik Fakültesi Yerbilimleri Dergisi, 5, 1-2, 21-38.

Özhan, G., Kavukçu, S., Çete, M., Kurtuluş, C., 1985, Marmara Denizi İzmit Körfezi, yüksek ayrımlı sığ sismik etüdü raporu, MTA, Jeofizik Etüdler Dairesi, 15p.

Öztin, F., 1987, 9 Ağustos 1912 Şarköy-Mürefte depremi, deprem Araştırma Bült., 56, 91-127.

Öztin, F. and Bayülke, N., 1990, Historical earthquakes of İstanbul, Kayseri and Elazığ, Report, Earthquake Research Department, General Directorate of Disaster Affairs, Ministry of Public Works and Settlement, Ankara, 85-95.

Perinçek, D., 1991, Possible strand of the North Anatolian fault in the Thrace basin – an interpretation, AAPG 75/2, 241-257.

Pfannenstiel, M., 1944, Diluviale Geologie des Mittelmeergebietes: Die diluvialen Entwicklungsstadien und die Urgeschichte von Dardanellen, Marmara Meer und Bosphorus, Geol. Rundschau., 34, 342-334.

Pınar, N., 1943, Marmara Denizi basenlerinin jeolojisi, sismisitesi ve meteorolojisi, İst. Üni. Fen. Fak. Mec., 7, 314p.

Reilinger, R., Toksöz, N., King, R., McClusky, S., Oral, B., Kınık, I., Lenk, O., Sanlı, I., Barka, A., Prilepin, M., Mishin, A., Balassanian, S., Veis, G., Paradisis, D. Taeleb, A., Melzer, Y., Normandeau, J. and Mencin, D., 1995, GPS measurements in Turkey and surrounding areas of the E. Mediterranean/Middle East, Abstracts, IUGG XXI General Assembly, Boulder, USA.

Sakınç, M., 1993, Marmara kıyılarynda denizel Üst pleyistosen-Holosen çökellerinin-stratigrafik Özellikleri, Türkiye Kuvaterneri Workshop Bildiri Özleri,17-19 Kasım, İstanbul, 69-71.

Sakınç, M. and Bargu, S., 1989, İzmit körfezi güneyindeki Geç Pleyistosen (Tireniyen) çökel stratigrafisi ve bölgenin neotektonik özellikleri, TJK Bült., 32, 51-64.

Sakınç M. and Yaltırak, C., 1995a, Güney Trakya Sahillerinin Denizel Pleistosen Çökelleri ve Paleocoğrafyası, Trakya Havzası Jeolojisi Sempozyumu, TPAO ve Ozan Sungurlu Bilim ve Egitim Vakfı, Bildiri Özetleri, 38-39.

Sakınç, M. and Yaltırak, C., 1995b, Güney Trakya Sahillerinin Denizel Pleistosen Çökelleri ve Paleocoğrafyası, Trakya Havzasının Jeolojisi Sempozyumu, 30 Mayıs – 3 Haziran, Bidiriler Kitabı, in press.

Sakınç, M., Yaltırak, C. ve Örçen, S., 1995, Trakya'nın Neojen Paleocoğrafyası ve Evrimi, Trakya Havzasy Jeolojisi Sempozyumu, 30 Mayıs – 3 Haziran Lüleburgaz-Kırklareli, 35.

Saner, S., 1985, Saroz körfezi dolayının çökelme istifleri ve tektonik yerleşimi, Kuzeydoğu Ege Denizi, Türkiye, Türkiye Jeoloji Kurumu Bülteni, 28, 1-10.

Şaroğlu, F., Boray, A. and Emre, O., 1987, Active faults of Turkey, Mineral Res. Explor. Inst. Turkey, Unpubl. Report 8643, 394p.

Şengör, A.M.C., 1979, The North Anatolian transform fault: its age, offset and tectonic significance, J. Geol. Soc., 136, 269-282.

Şengör, A.M.C., 1987, Cross-faults and differential stretching of hanging walls in regions of low angle normal faulting: Examples from Western Turkey, in: Continental extensional tectonics, edited by: M.P. Coward, J.F. Dewey and P.L. Hancock, Geological Society, London, Special Publication, No. 28. 575-89.

Şengör, A.M.C., Görür, N. and Şaroğlu, F., 1985, Strike-slip faulting and related basin formation in zones of tectonic escape: Turkey as a case study, in: Strike-slip Faulting and Basin Formation, edited by: K.T. Biddle and N. Christie-Blick, Society of Econ. Paleont. Min. Sp. Publ., 227-264.

Sieberg, A., 1932, Erdbebengeographie, in: Handbuch der Geophysik, edited by: B. Gutenberg, Band IV, Borntrager, Berlin, 527-1005.

Sipahioğlu, S., 1984, Seismo-tectonic features of the North Anatolian fault zone, Bull. Earthq. Res. Inst. Turkey, 45, 5-139.

Sipahioğlu, Ş. and Matsuda, T., 1986, Geology and Quaternary fault in the İznik-Mekece area, in: Electric and Magnetic Research on active faults in the North Anatolian fault zone, edited by: A.M. Işıkara and Y. Honkura, 25-42.

Siyako, M., Bürkan, A.K. and Okay, A.I., 1989, Biga ve Gelibolu yarımadalarıõnın Tersiyer jeolojisi ve hidrokarbon olanakları, TPJD Bülteni, 1(3), 183-199.

Smith, A. D., Taymaz, T., Oktay, F., Yüce, H., Alpar, B., Başaran, H., Jackson, A. J., Kara, S. and Şimşek, U., 1995, High resolution seismic profiling in the sea of Marmara (NW Turkey: Late Quaternary sedimentation and sea level changes, GSA Bull. 107/8, 923-936.

Soysal, H., Sipahioglu, S., Kolçak, D. and Altınok, Y., 1981, Türkiye tarihsel deprem kataloğu, TÜBİTAK Project No: TBAG 341.

Stein, R., Barka, A. and Dieterich, J., 1997, Progressive failure on the North Anatolian fault since 1939 by earthquake stress triggering, Geophys. J. Int., submitted.

Straub, C., 1996, Recent crustal deformation and strain accumulation in the Marmara sea region, NW Anatolia, inferred from GPS Measurements, PhD Thesis, ETH, 122p.

Sümengen, M., Terlemez, I., Şentürk, K., Karasöse, C., Erkan, E. N., Ünay, E., Gürbüz, M. and Atalay, Z., 1987, Gelibolu Yarımadası ve Güneybatı Tersiyer havzasının stratigrafisi, sedimentolojisi ve Tektoniği, MTA Jeoloji Etüdleri Dairesi Raporu No.8128. 213p.

Taymaz, T., Jackson, J. and McKenzie, D.P., 1991, Active tectonics of the north and central Aegean, Geophys. J. Int, 106, 433-490.

Toksöz, M. N., Shakal, A.F., and Michael, A.J., 1979, Space-time migration of earthquakes along the North Anatolian fault zone and seismicity gaps, Pure Appl. Geophy., 117, 1258-1270.

Tsukuda, E., Herece, E. and Kuşçu, I., 1988, Some geological evidence on activity of the western North Anatolian fault, Geyve, İznik, Gemlik area, ITIT project 8513, 68-91.

Turgut, S., Türkaslan, M. and Perinçek, D., 1991, Evolution of the Thrace Sedimentary Basin and its Hydrocarbon Prospectivity, in: Generation, accumulation and production of Europe's Hydrocarbons, edited by: A.M. Spencer, Special Publication of the European Assoc. Petrol. Geoscientists, No. 1, Oxford University Press., Oxford, 415-437.

Üçer, B., 1990, Marmara bölgesinin deprem etkinliği ve aktif tektonik ile ilişkisi, PhD Thesis, Uni. İstanbul, 142p.

Wong, H. K., Lüdman, T., Uluğ, A. and Görür, N., 1995, The sea of Marmara: a plate boundary in an escape tectonic regime, Tectonophysics, 244, 231-250.

Yaltırak, C., 1995, Gelibolu Yarımadasıõnda Pliyo-Kuvaterner Sedimantasyonunu Denetleyen Tektonik Mekanizma, Nezihi Canitez Sempozyumu,İstanbul, Jeofizik,10, 103-106.

Yoshioka, T. and Kuşçu, İ., 1994, Late Holocene faulting events on the İznik-Mekece fault in the western part of the North Anatolian fault zone, Turkey. Bull. Geol. Surv. Japan, 45, 677-685.

Seismic investigations of the Marmara region

BALAMIR ÜÇER, HALUK EYIDOĞAN, CEMIL GÜRBÜZ, AYKUT BARKA AND ŞERIF BARIŞ

Abstract

Based on historical and instrumental earthquake records, the Marmara sea region is one of the most seismically active regions of the Eastern Mediterranean. In this essay, we aimed to investigate the patterns of the earthquake distribution in time and space for the period of 1976-1995. For the Marmara region, we also examined the patterns of seismicity for longer time periods, including historical (pre-1900) and instrumental (1900-1975) earthquake records for the Marmara sea region.

Introduction

Based on historical and instrumental earthquake records, the Marmara sea region is one of the most seismically active regions of the Eastern Mediterranean. The earthquake mechanism solutions (Fig. 1), strain rate calculations, GPS measurements (Straub and Kahle 1994, Reilinger et al. 1995) and neotectonic studies (Barka 1992) show that the Marmara region is under the influence of the western part of the North Anatolian Fault Zone (NAFZ) and the N-S extensional regime of Western Turkey. The parameters of the earthquake mechanism solutions are given in Table 1. The NAFZ splays into a number of branches in and around the Marmara sea region. The northernmost branch forms a graben and follows the gulf of İzmit, connecting with the Çınarcık-Yalova pull-apart basin in the Marmara sea region. According to seismological studies (Crampin and Üçer 1975, Eyidoğan 1988, Üçer 1990) the Marmara region shows different seismotectonic characteristics than the main part of the NAFZ and Aegean grabens.

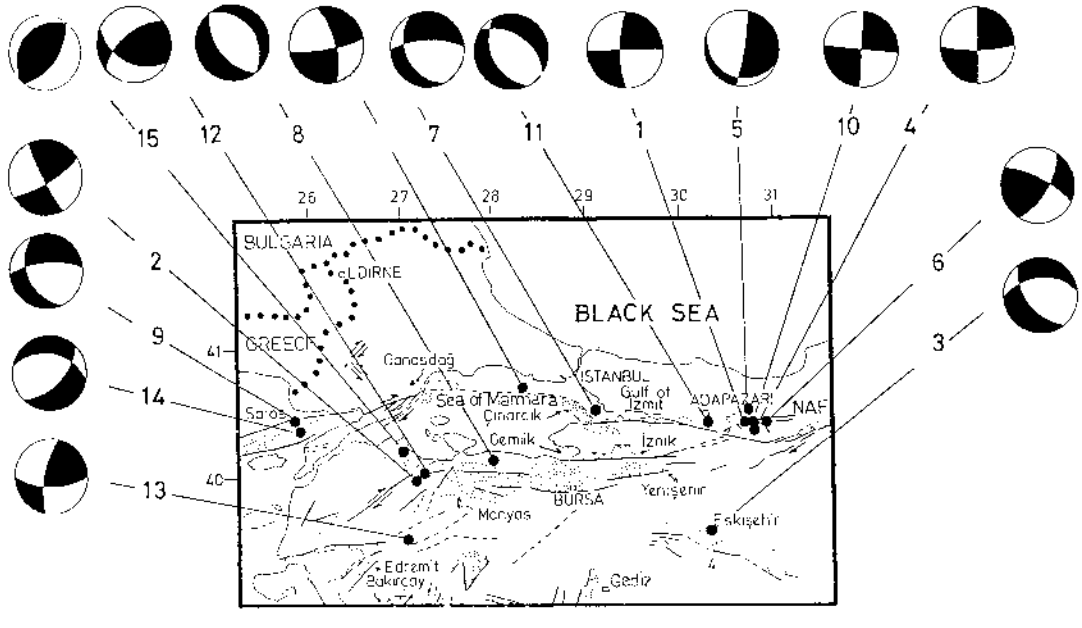


Figure 1: Tectonic map of the Marmara region and fault plane solutions of major earthquakes. The numbers indicate the earthquakes listed in Table 1. The mechanism solutions are plotted for a lower hemisphere projection.

In this essay, we aimed to investigate the patterns of the earthquake distribution in time and space for the period of 1976-1995. For the Marmara region, we also examined the patterns of seismicity for longer time periods, including historical (pre-1900) and instrumental (1900-1975) earthquake records for the Marmara sea region. The detection level of microearthquakes since 1976 has considerably increased with the installation of the sensitive seismographic stations in the Marmara region. The developments of instrumentation in the region helped us to recognise that the region could be characterised by a number of earthquake clusterings. For the period of 1976-1988, Üçer (1990) pointed out fifteen earthquake clusterings located in Northwestern Turkey, including the Marmara sea and the northern part of Western Turkey.

The crustal structure model used to locate the earthquakes was also improved after 1986. This model was obtained by determining seismic P_g and P_n velocity variations and layering within the crust from the travel-time data of local earthquakes, quarry blasts and explosions. Figure 2 shows the locations of the seismic refraction profiles obtained from the recording of quarry blast and explosion experiments. The travel times of the local earthquakes recorded mainly by the Marnet stations are grouped according to the back azimuth intervals of 0E-180E, 90E-270E, 180E-360E, 0E-90E, 270E-360E. This gave a variation of seismic P_g and P_n wave velocities with azimuth (Kuleli et al. 1996). Travel time distance graphs are constructed for the back azimuths.

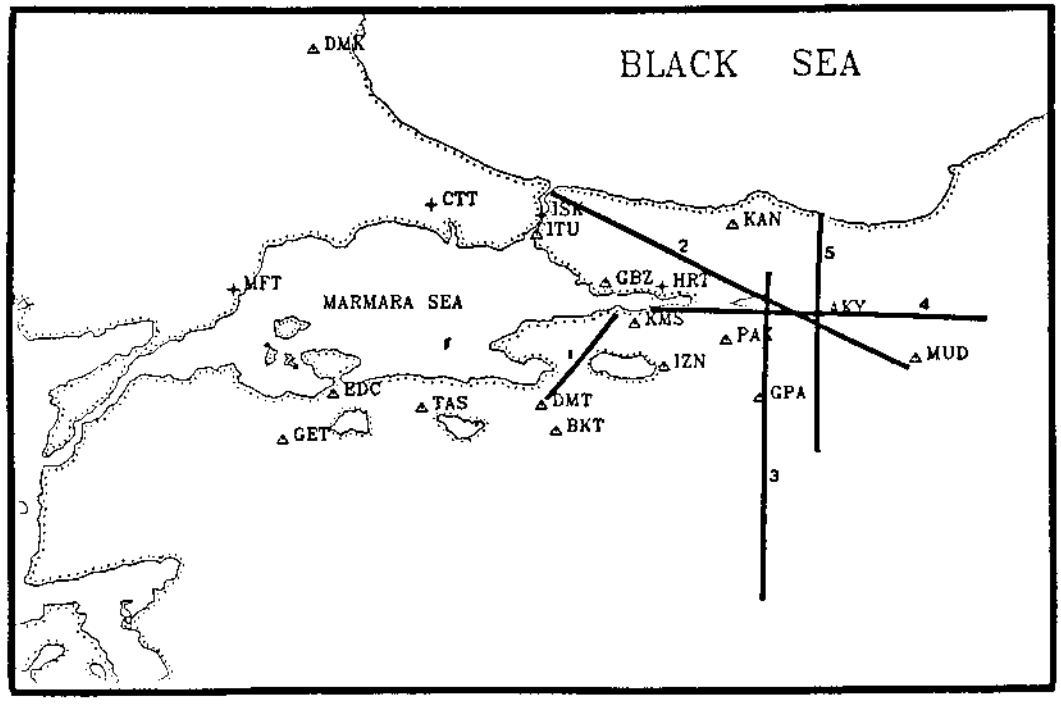


Figure 2: Location of seismic stations (triangles) and refraction profiles (solid lines) which were used for the quarry blast and explosion recordings in the Marmara region. 1- Kestel, 2- Anadolu Kavağı, 3-Adapazarı, 4 and 5- Turkish-German refraction project.

Similar studies were carried out by Necioğlu et al. (1981), Kalafat et al. (1987) and Gürbüz et al. (1992) in the Marmara region and Western Turkey by obtaining conventional travel time-distance graphs from all azimuths for each station.

According to the above modelling, P_g and P_n velocity values are calculated as being in the range of 5.3-6.2km/s and 8.0km/s, respectively. It was also noticed that P_n velocities have azimuthal dependence. P_n velocities show higher values in the Marmara region relative to those

calculated for Western Turkey and the Aegean sea. Our modelling also suggested that the thickness of the crust in the Marmara region varies between 28 and 33km and these values decrease towards the Black sea.

Historical seismicity

The first descriptive catalogue of historical earthquakes in Turkey was prepared by Pınar and Lahn (1952). Later, Ergin et al. (1967) prepared a catalogue in the form of seismological meaning, including earthquakes between 1100-1964AD. Soysal et al. (1981) prepared a catalogue of historical earthquakes that occurred between 2100BP and 1900AD by studying the Selçuk, Byzantium and Ottoman documents. Recently, Ambraseys and Finkel (1991, 1995) have presented more reliable and complete earthquake records, especially for the destructive earthquakes which occurred in the Marmara sea region, for the period between 0-1900AD. From these more reliable studies, we can suggest that the recurrence interval of I_o=VIII earthquakes is about 100 years, while this value is about 250 years for I_o=IX earthquakes. The last I_o=VIII earthquake occurred in this region in 1894.

Seismicity during the instrumental period

There have been several efforts made (Crampin and Üçer 1975, Alsan et al. 1975, Makropoulos and Burton 1981) to relocate earthquakes which occurred pre-1964, when ISC data became more reliable. In most cases, it was observed that these relocated epicenters are consistent with the macro-seismic epicenters. At the same time, magnitude determinations in recent catalogues are more homogeneous than in the previous studies, and most were determined as surface wave magnitudes (M_S).

Event	Date (d.m.y.)	Origin Time (h:m:s)	Lat (N°)	Long (E°)	M_S	h (km)	ϕ(°)	δ(°)	Ref
1	20.6.43	15:32:54	40.85	30.51	6.5	10	86	90	a
2	18.3.53	19:06:16	39.99	27.36	7.2	10	59	76	a
3	20.2.56	20:31:44	39.89	30.49	6.4	40	140	56	a
4	26.5.57	06:33:35	40.67	31.06	7.1	10	87	78	a
5	26.5.57	09:36:37	40.80	30.80	6.0	--	114	24	b
6	27.5.57	11:01:27	40.70	31.00	5.5	--	293	74	b
7	18.9.63	16:58:15	40.77	29.12	6.3	40	268	70	c
8	6.10.64	14:31:23	40.30	28.23	6.7	8	302	36	a
9	23.8.65	14:08:59	40.50	26.02	5.6	33	261	70	d
10	22.7.67	16:56:58	40.67	30.69	7.2	4	93	90	a
11	30.7.67	01:31:02	40.70	30.40	5.6	16	301	50	a
12	03.3.69	00:59:11	40.12	27.43	5.8	4	107	50	a
13	23.2.71	19:41:23	39.62	27.32	5.5	10	86	66	e
14	27.3.75	05:15:08	40.45	26.12	6.7	15	41	60	f
15	05.7.83	12:01:27	40.33	27.23	5.8	10	218	32	g
16	24.4.88	20:49:33	40.88	28.24	5.1	18	356	71	h

*Table 1: Parameters of earthquake mechanism solutions, * ϕ and δ are the strike and dip angle of the fault plane in degrees, respectively. H is the focal depth. References: a-McKenzie (1972); b- Canitez and Üçer (1967); c- Jackson and McKenzie (1988); d- Kocaefe and Ataman (1976); e- Papadopoulos et al. (1986); f- McKenzie (1978); g- Kiyak (1987); h- NEIS.*

In this study, the earthquakes which occurred during the instrumental period (1900-1995) have been recompiled mainly from Ayhan et al. (1987), ISC monthly catalogues and the Kandilli observatory data base. In the following paragraphs the characteristics of seismicity in the region have been studied for two periods: 1900-1975 (pre-MARNET) and 1976-1995 (during the MARNET operation).

Observation period between 1900-1975

From the examination of the existing catalogues (Üçer et al. 1976) it was shown that the error in epicentral determinations was found to be as high as 140km within the first 10 years after 1918. This error was reduced to 45km between 1948-1958 and it was further reduced to about 10km between 1959-1963. Large errors in epicentral determinations in the early years of instrumental period are due to insufficient number and poor azimuthal distribution of seismic stations. With the recent instrumental developments, errors in epicentral determinations have been reduced to less than 10km. Üçer (1990) applied a completeness test to the earthquakes that occurred between 1900-1988 in the Marmara sea region and showed that the earthquake data for magnitudes 6.0 or greater is complete since 1900, while the earthquakes for magnitudes 4.5 or greater is complete since 1960. Table 2 gives the list of earthquakes with magnitudes greater than 6.0.

Date D. M. Year	**Time** h. m. s.	**Lat**. North	**Lon**. East	**Depth** km	**Mag**. M_s	**Int**. MSK	Locality
09 08 1912	01:29	40.60	27.20	16	7.3	X	Mürefte
10 08 1912	09:23	40.60	27.10	15	6.3	--	Aftershock
18 11 1919	21:54:50	39.26	26.71	10	7.0	VIII	Soma
02 05 1928	21:54:32	39.64	29.14	10	6.1	VIII	Emet
04 01 1935	14:41:30	40.40	27.49	30	6.4	IX	Marmara
04 01 1935	16:20:04	40.30	27.45	20	6.3	VIII	Aftershock
22 09 1939	00.36.36	39.07	26.94	10	6.6	VIII	Dikili
15 11 1942	17:01:23	39.55	28.58	10	6.1	VIII	Bigadiç
20 06 1943	15:32:54	40.85	30.51	10	6.5	IX	Hendek
06 10 1944	02:34:49	39.48	26.56	40	6.8	VIII	Ayvacık
18 03 1953	19:06:16	39.99	27.36	10	7.2	IX	Yenice
20 02 1956	20:31:44	39.89	30.49	40	6.4	VIII	Soğut
26 05 1957	06:33:35	40.67	31.00	10	7.1	X	Abant
18 09 1963	16:58:15	40.77	29.12	40	6.3	VIII	Yalova
06 10 1964	14:31:23	40.30	28.23	8	7.0	IX	Manyas
22 07 1967	16:56:58	40.67	30.69	4	7.2	X	Mudurnu
23 03 1969	21:08:42	39.14	28.48	9	6.0	--	Demirci
25 03 1969	13:21:34	39.25	28.44	37	6.0	VIII	Demirci
28 03 1970	21:02:23	39.21	29.51	18	7.2	IX	Gediz
27 03 1975	05:15:08	40.45	26.12	15	6.7	VII	Saroz bay

Table 2: List of earthquakes with magnitude greater than 6.0 (after Soysal et al. 1981, Ambraseys and Finkel 1991).

Observation period between 1976 and 1995

In the Marmara sea region, after 1976, the earthquake detection level was greatly improved through the installation of permanent stations and the radio-linked seismic station networks in the Marmara sea (MARNET) and the İznik regions (İZİNET) (Fig. 3). The networks in these regions are able to record the microearthquakes down to a magnitude of M=2.4. The MARNET and İZİNET stations can detect the earthquakes both in analogue and digital form. Most of the permanent stations have short-period vertical seismometers. During the period 1976-1995, more than 20,000 microearthquakes were located in the Marmara region bounded by 39-42N (latitude) and 25.5-31E (longitude). 4900 earthquakes with magnitude greater than 3.0 were located during the same period. The epicentral distribution of these well-located earthquakes shows several earthquake clusterings in the Marmara sea region (Fig. 4 on next page)

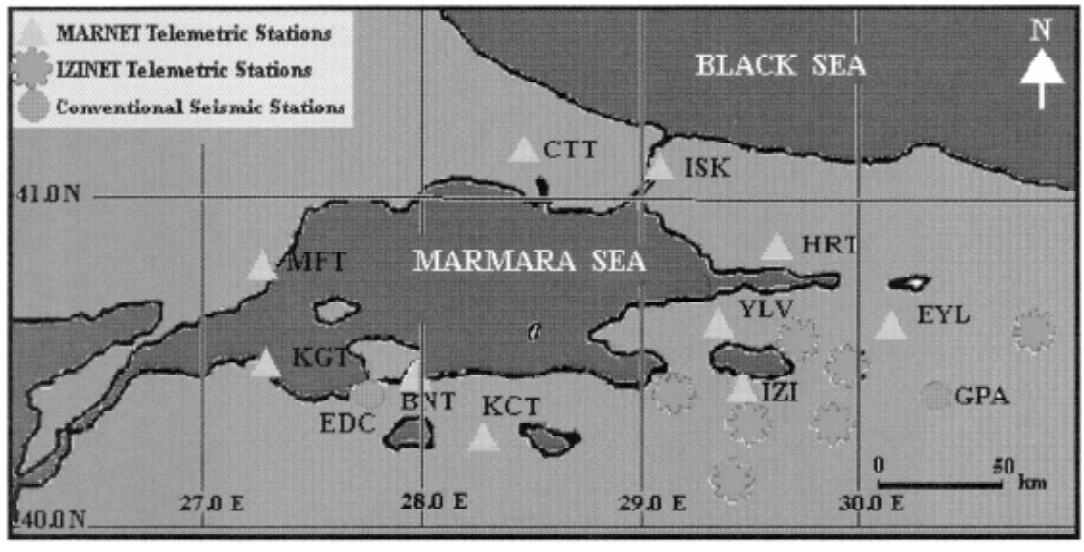


Figure 3: *Location of MARNET, İZİNET and conventional seismic stations in the Marmara region.*

Earthquake clusterings

The earthquake clusterings identified since 1976 in the Marmara sea region were examined by using strain energy release and the number of earthquakes per 0.2° cells were determined according to the method given by Üçer (1990). Seven earthquake clusterings were recognised in the Marmara region (north of latitude 39.5) as illustrated in Fig. 4, and the characteristic parameters of the clusterings are given in Table 3. The earthquake activity in the Saros and Yalova-Çınarcık basins and the Biga region are typical aftershock sequences taking place after the March 27, 1975 Saroz earthquake (M_S=6.7), September 18, 1963 Çınarcık earthquake (M_S=6.3) and July 5, 1983 Biga earthquake (M_S=5.8), respectively (Fig. 5). It is suggested that the clusterings which occurred in these regions were related to the post-seismic activity associated with dominantly normal fault mechanisms (Fig. 1). A foreshock activity was observed almost a year before the Biga earthquake of July 5, 1983 (M_S=5.8). In the İnegöl region, the October 21, 1983 İnegöl earthquake, which can be associated with the Eskişehir fault (e.g. Barka 1991), created an aftershock clustering.

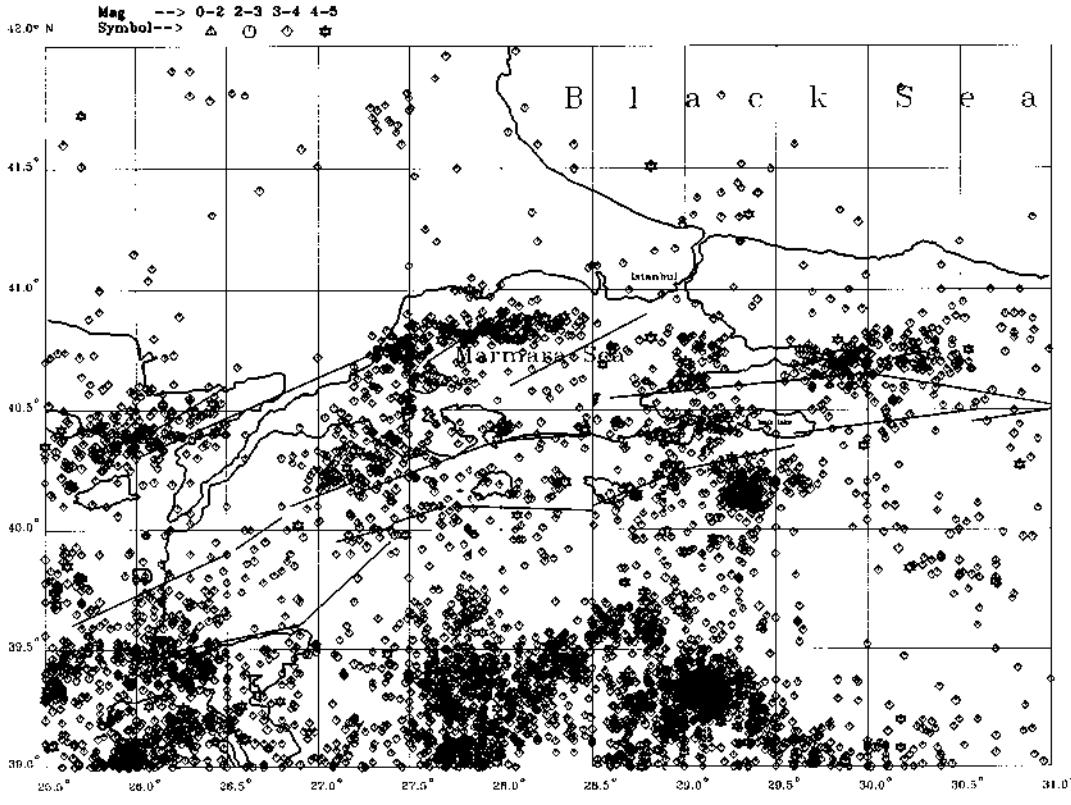


Figure 4: *Seismicity map of the Marmara region in the interval of 1976-1995 for the earthquakes with magnitudes greater than 3. Letters indicate the seismic clusterings given in Table 3.*

The earthquake sequence which occurred in the same region in 1979 could be considered as the foreshock activity of this 1983 event. The earthquake clustering observed in the İzmit-Sapanca area (Fig. 5) displays a characteristic swarm (no moderate or large event before the cluster) type activity. İzmit swarm has been extensively studied by Crampin et al. (1985) and Evans et al. (1987).

	Cluster area				
Locality	Lat.	Long.	Num. of events	Str. [E10]	Mag [max]
Marmara region	39.0-42.0	25.5-31.0	20040		
a: Saroz bay	40.2-40.8	25.5-26.5	406	3.03	4.5
b: Marmara sea	40.6-41.0	27.2-28.5	1363	5.45	5.0
c: Yalova-Cınarcık	40.5-41.0	28.7-29.2	612	1.98	4.8
d: İzmit	40.5-40.9	29.6-31.0	1171	4.14	4.0
e: İznik-Gemlik	40.3-40.5	27.8-29.6	961	3.27	4.4
f: Biga	40.1-40.6	27.0-27.6	699	3.22	5.8
g: İnegöl	40.0-40.4	29.1-29.6	1171	4.36	4.9

Table 3: *Characteristics of the selected clusterings in the Marmara region.*

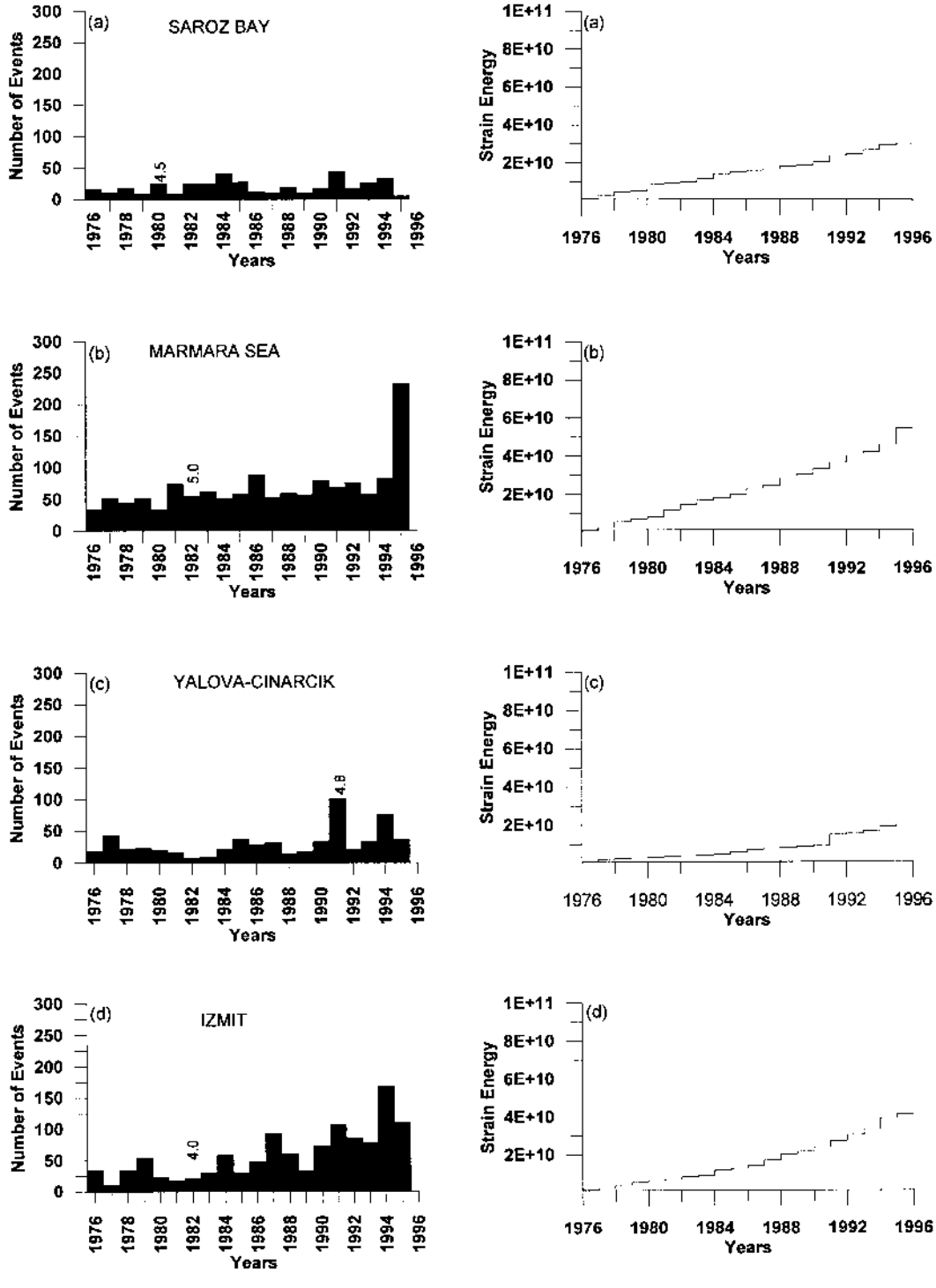


Figure 5a: *Number of events and strain energy release diagrams for the interval of 1976-1995 at (a) Saroz bay, (b) Marmara sea, (c) Yalova-Cınarcık and (d) İzmit clusterings.*

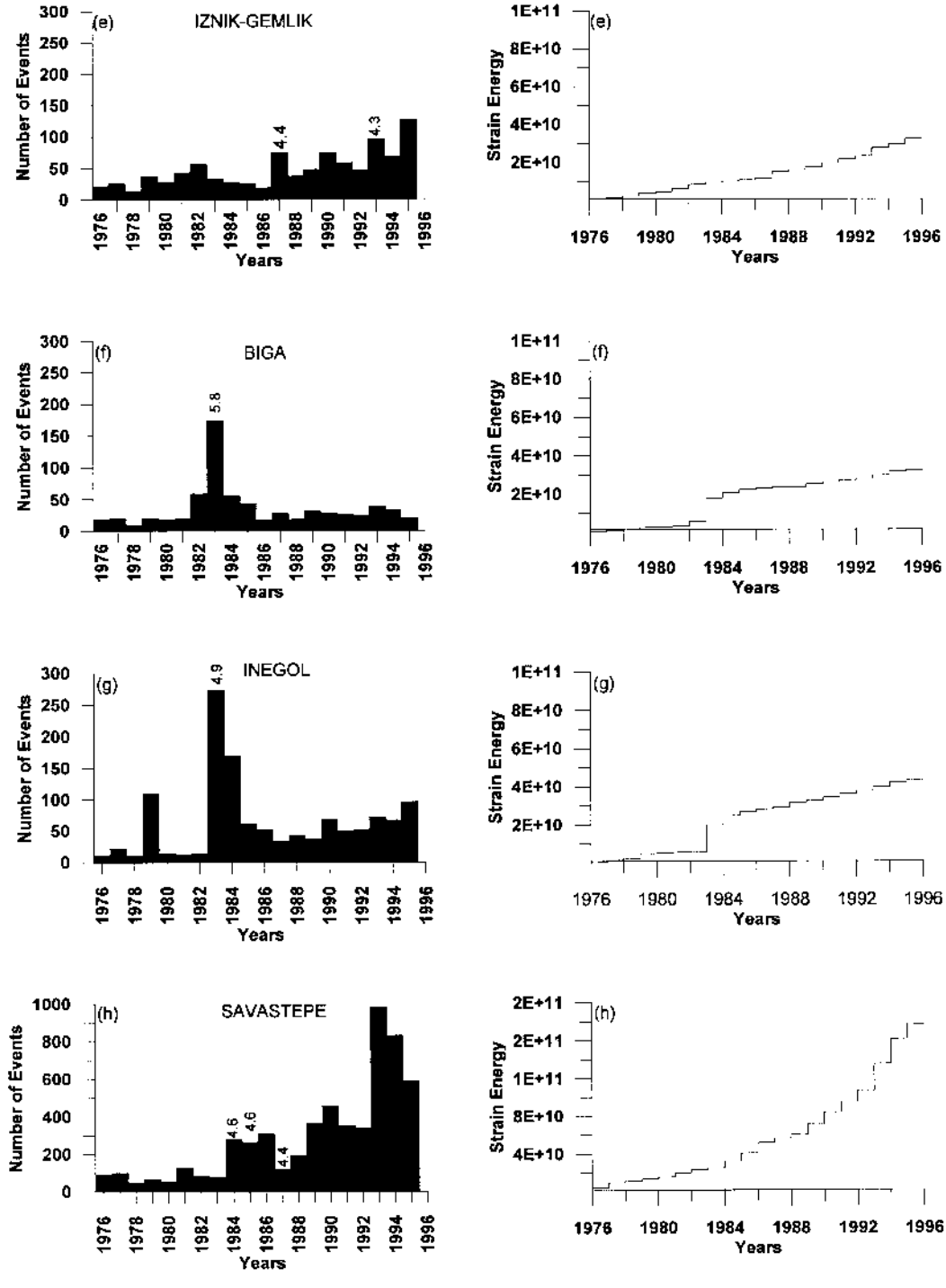


Figure 5b: *Number of events and strain energy release diagrams for the interval of 1976-1995 at (e) İznik-Gemlik, (f) Biga, (g) İnegöl and (h) Savaştepe clusterings.*

Discussion and conclusions

The earthquake data of the Marmara sea region for different periods illustrate, that for I_0>VIII earthquakes the data relatively are complete for the last 800 years. However, for the lower intensities, there is a need for more information. The epicenter location of historical earthquakes shows scatter and does not always correspond with the well-known fault zones. For these scattered events, there is a need for more detailed studies. For the instrumental period between 1900-1995, we have rather complete earthquake catalogues for M>4.5.

Seven earthquake clusterings were recognised in the period between the years 1976-1995 in the Marmara region. Four clusterings have been distinguished along the northern strand of the NAFZ, namely Saros bay, Marmara sea, Yalova-Çınarcık and İzmit clusterings. The Saros bay and Yalova-Çınarcık clusterings display aftershock activity. The middle and southern strands of the NAFZ have relatively lower seismic activity. The İzmit clustering shows a distinct character and can be assigned a typical swarm-type activity during this study period. The seismic activity in the west of the İznik-Gemlik area is relatively higher than in the east of the area, suggesting that the İznik-Mekece fault is not very active. An earthquake sequence occurred in the İnegöl area, along the Eskişehir fault, and is associated with a remarkable foreshock-mainshock pattern. Two additional swarms (Savaştepe and Emet) exist in the south of the Marmara region, which is not considered as a part of the study area. 4852 earthquakes with magnitudes greater than M_L=3.0 have been reported during the observation period.

We suggest that there is a close correspondence between the earthquake clusterings and the pull-apart structures (Barka and Kadinsky-Cade 1988) of the strands of the NAFZ in the Marmara sea region. Most of the clusterings are located within the pull-apart basins such as Saros, Çınarcık and İzmit. The areas that lie between the clusterings can be associated with the strike-slip segments of the strands and can be described as seismic gaps.

Three seismic gaps have been identified based on the existing seismicity pattern and tectonic information along the northern strand of the NAFZ, namely the Saros-Ganos, the northern central Marmara sea and the Karamürsel gaps (Barka and Toksöz 1989, Barka 1991, 1992). The fourth gap is located on the middle strand of the NAFZ in the İznik-Mekece area (Üçer 1990). Toksöz et al. (1979) also pointed out the seismic gap occurring between Sapanca and Yalova along the northern strand of the NAFZ by using the space and time distribution of the earthquakes which occurred during the instrumental period between 1910-1975. The Saros gap experienced the 1912 Mürefte-Şarköy earthquake, M=7.4, and the Karamürsel gap had two historical earthquakes in 1719 and 1754. The central Marmara sea gap has not experienced a significant earthquake according to the existing catalogues. Thus, this gap requires special attention for the earthquake risk assessments for the İstanbul region.

References

Alsan, E., Tezuçan, L. and Bath, M., 1975, An earthquake catalogue for Turkey for the interval 1913-1970, Publ. Seism. Int. Univ. Uppsala, No: 7/75, Uppsala.

Ambraseys, N.N. and Finkel, C.F., 1991, Long-term seismicity of İstanbul and of the Marmara sea region, Terra,3, Oxford, 527-539.

Ambraseys, N.N. and Finkel, C.F., 1995, The seismicity of Turkey and adjacent areas, a historical Review, 1500-1800, Eren Yayıncılık Ltd. Sti., 240p.

Ayhan, E., Alsan, E., Sancaklı, N. and Üçer, B., 1987, Earthquake Catalogue for Turkey and surrounding area, 1881-1980. Publ. of Kandilli Observatory, Space and Earth Sciences Research and Development Centre.

Barka, A., 1991, İstanbul'un depremselliğini oluşturan tektonik yapılar ve İstanbul için bir mikrobölgleme denemesi, İstanbul ve Deprem Sempozyumu, 4 Mayıs 1991, TMMOB İnsaat Mühendisleri Odası İstanbul Şubesi, 35-56.

Barka, A., 1992, The North Anatolian Fault zone, Annales Tectonicae, Special Issue, Supplement to volume 6, 164-195.

Barka, A. and Kadinsky-Cade, K., 1988, Strike-slip fault geometry in Turkey and its influence on earthquake activity, Tectonics, 7, 663-684.

Barka, A. and Toksöz, M.N., 1989, Seismic gaps along the North Anatolian Fault, Abstract, IASPEI Meeting in İstanbul Turkey, S9-1.

Canitez, N. and Üçer, B., 1967, Computer determinations for the fault plane solutions in and near Anatolia, Tectonophysics, 4, 235-244.

Crampin, S. and Üçer, B., 1975, The seismicity of the Marmara sea region of Turkey, Geophys. J. R. astr. Soc., 40, 269-288.

Crampin, S., Evans, R. and Üçer, B., 1985, Analysis of record of local earthquakes: the Turkish dilatancy project (TDP1_TDP2), Geophys. J. R. Astr. Soc,83, 11-16.

Ergin, K., Güçlü, U. and Uz, Z., 1967, Türkiye ve civarının deprem katoloğu (M.S. 11 yılından 1964 sonuna kadar). İTÜ Maden Fak. Arz Fiziği Enst., No. 24, İstanbul.

Evans, R., Beamish, D., Crampin, S. and Üçer, B., 1987, Turkish Dilatancy Project (TDP3): Multidisciplinary studies of a potential earthquake source region, Geophys. J. R. astr. Soc., 91, 2, 265-286.

Eyidoğan, H., 1988, rates of crustal deformation in Western Turkey as deduced from major earthquakes, Tectonophysics, 148, 83-92.

Gürbüz,C., Püskülcü, S. and Üçer, S., 1992, A study of crustal structure in the Marmara region using earthquake data, in: Multidisciplinary Research on Fault Activity in the Western Part of the North Anatolian Fault Zone (4), edited by: A.M. İşıkara and Y. Honkura, 29-42.

Jackson, J. and McKenzie, D.P., 1988, The relationship between plate motions and seismic moment tensors, and the rates of active deformation in the Mediterranean and Middle East, Geophysical Journal, 93, 45-73.

Kalafat, D., Gürbüz, C. and Üçer, B., 1987, Batı Türkiyede kabuk ve Üst manto yapısının araştırılmasi. Deprem Araştırma Bülteni, 14 (59), 43-64.

Kiyak, Ü., 1987, Kuzey Anadolu Fay zonunun batı uzantısının araştırılmasi, Doktora Tezi, İstanbul Üniversitesi, Fen Bilimleri Enstitüsü, İstanbul.

Kocaefe, S. and Ataman, G., 1976, Anadolu'da sismotektonik olaylar-1: Antalya-Fethiye-Denizli Ücgeni icinde yeralan bölgenin incelenmesi, İÜ Yer Bilimleri yayın organı, C.2, No:1, 55-70.

Kuleli,S., Gürbüz, C. and Toksöz,M.N., 1996, Seismic velocity distribution in the Aegean region, in: IESCA Proceedings, in press.

Makropoulos, K.C. and Burton, P.W., 1981, A catalogue of seismicity in Greece and adjacent areas, Geophys. J.R. astr. Soc., 65, 741-762.

McKenzie, D.P., 1972, Active tectonics of the Mediterranean region, Geophys. J. Roy. Astr. Soc., 30, 109-185.

McKenzie, D.P., 1978, Active tectonics of the Alpine-Himalayan belt: the Aegean sea and surrounding regions, Geophys. J. Roy. Astr. Soc., 55, 217-254.

Necioğlu, A., Maddison, B. and Türkelli, N., 1981, A study of crustal and upper mantle structure of Northwestern Turkey, Geophysical Research Letters, 8, 33-35.

Papadopoulos,G.A., Kondopoulou, D.P., Leventakis, G.A. and Pavlides, S.B., 1986, Seismotectonics of the Aegean region, Tectonophysics, 124,67-84,

Pınar, N. and Lahn, E., 1952, Türkiye depremleri izahlı kataloğu, Yapı ve İmar İsleri Reisliği yayını, Seri 6, No: 6, Ankara.

Reilinger, R., Toksöz, N., King, R., McClusky, S., Oral, B., Kınık, I., Lenk, O., Sanlı, I., Barka, A., Prilepin, M., Mishin, A., Balassanian, S., Veis, G., Paradisis, D. Taeleb, A., Melzer, Y., Normandeau, J. and Mencin, D., 1995, GPS measurements in Turkey and surrounding areas of the E. Mediterranean/Middle East, Abstracts, IUGG XXI General Assembly, Boulder, USA.

Soysal, H., Sipahioğlu, S., Kolçak, D. and Altınok, Y., 1981, Türkiye ve Çevresinin Tarihsel Deprem Katoloğu, TüBıTAK, Proje No. TBAG 341.

Straub, Ch. and Kahle, H.G., 1994, Global Positioning System (GPS) estimates of crustal deformation in the Marmara sea region, Northwestern Anatolia, Earth and Planet. Sci. Lett., 121, 495-502.

Toksöz, M. N., Shakal, A.F. and Michael, A.J., 1979, Space-time migration of earthquakes along the North Anatolian Fault zone and seismic gaps, Pageophys, 117, 1258-1270.

Üçer, S. B., 1990, Marmara bölgesinin deprem etkinliği ve aktif tektonikle ilişkisi, İ.Ü.Fen Bilimleri Enstitüsü, Doktora Tezi, 142.

Üçer, S. B., Alsan, E. and Ayhan, E., 1976, Preliminary statistical results for the preparation of a seismic zoning map of Anatolia, UNDP/UNESCO, Project of Survey of the Seismicity of Balkan Region, Seminar on Seismic Risk and Seismic Zoning, May 1976, Skopje.

Activities for the determination of crustal movements in Turkey

AHMET AKSOY AND RASIM DENİZ

Abstract

It is well known that, in Turkey, neotectonic activities originated following the collision of the Arabian and Anatolian land masses during the Middle Miocene. As a result of that collision, the escape of the Anatolian block towards the west introduced E-W compression in Western Turkey, which began to be relieved by N-S extension.

The basic element of multi-disciplinary and multifunctional "geodynamic" studies is the determination of changes in the horizontal and vertical movements, as well as in the gravity field, in the Earth's crust. In Turkey, the first studies for the determination of crustal movements using geodetic methods were started in the western section of the North Anatolian Fault Zone (NAFZ), in 1972. So far, individual activities and studies coordinated by multidisciplinary projects have been realised in this region. The first studies, coordinated and supported by multidisciplinary projects, were started under the coordination and financial support of the Earthquake Research Office in 1981. In 1984, with the participation of various disciplines from German Universities, the national project mentioned above was enlarged to the German-Turkish Project on Earthquake Prediction Research, as well as geodetic control research.

Here, a general review on the topic of the NAFZ and the undertakings in local measurements and analyses in the microgeodetic networks in İsmetpaşa, Taşkesti and Gerede are given. From the measurements and their evaluation, no periodical movement was found in the Gerede network. Significant movements were detected in the İsmetpaşa network, with d=9.6mm/a on the average in the southern part compared to the northern part in the direction t=243.0gon with respect to the north, and in the Taşkesti network, d=2.7mm/a, in the direction t=294.6gon, respectively.

Introduction

As part of the Alpine-Himalayan orogenic belt, Anatolia is a region of high complexity. Its geologic and tectonic evolution has been dominated by long-term cycles of openings and closings of Paleozoic and Mesozoic oceans. Continent-continent collision zones, extensional provinces, transform faults and subduction zones have formed an assemblage of lithospheric blocks with a wide range of thicknesses and rheologies. Tectonic processes are accompanied by the northerly movement of the Arabian Plate towards Eurasia. As a result of that collision, the escape towards the west of the Anatolian block introduced E-W compression in Western Turkey, which began to be relieved by N-S extension (Şengör et al. 1985*)*. No doubt, Turkey is one of the important natural laboratories offering study fields for increasing knowledge related to earthquakes, since the movements of these plates are reflected in the movements of the active fault zones in northern and eastern Anatolia, which are among the most

active zones in the world. The rates of motion along this fault estimated by several authors are in the range of 4 to 29mm/a.

In Turkey, the first studies for the determination of crustal movements using geodetic methods were started in the western section of the NAFZ, in 1972. In that year, two microgeodetic networks were established in İsmetpaşa and Gerede by the General Directorate of Mapping (Fig. 1). The distances and angles of both networks were measured for the periods 1972 and 1973. From the evaluation of these measurements, significant movement was not found (Uğur 1974). In the section which covers the İsmetpaşa and Gerede areas of the Turkish first-order triangulation and levelling networks, which crosses the fault perpendicularly, the measurements performed in 1942, 1945, 1946 and 1972 were evaluated to determine crustal movements, but because the precision of the measurements was not high enough, a significant result was not found.

The İsmetpaşa network was measured again in 1982 (Eren 1983) and in 1992 by the İstanbul Technical University (İTÜ) Geodesy Working Group. The other activity, related to the determination of crustal movements, was started by the Office for Mineral Research in the Mudurnu Valley in 1976. At the beginning, a network of 4 points was established and then this network was enlarged to 11 points in 1977 (Fig. 1). In the different sections of the network mentioned, distance and angle measurements were repeated in 1976, 1979, 1980, 1982, 1984 and 1986. No significant movements were detected from the measurements for the period 1976-1986 (Öztürk et al. 1987).

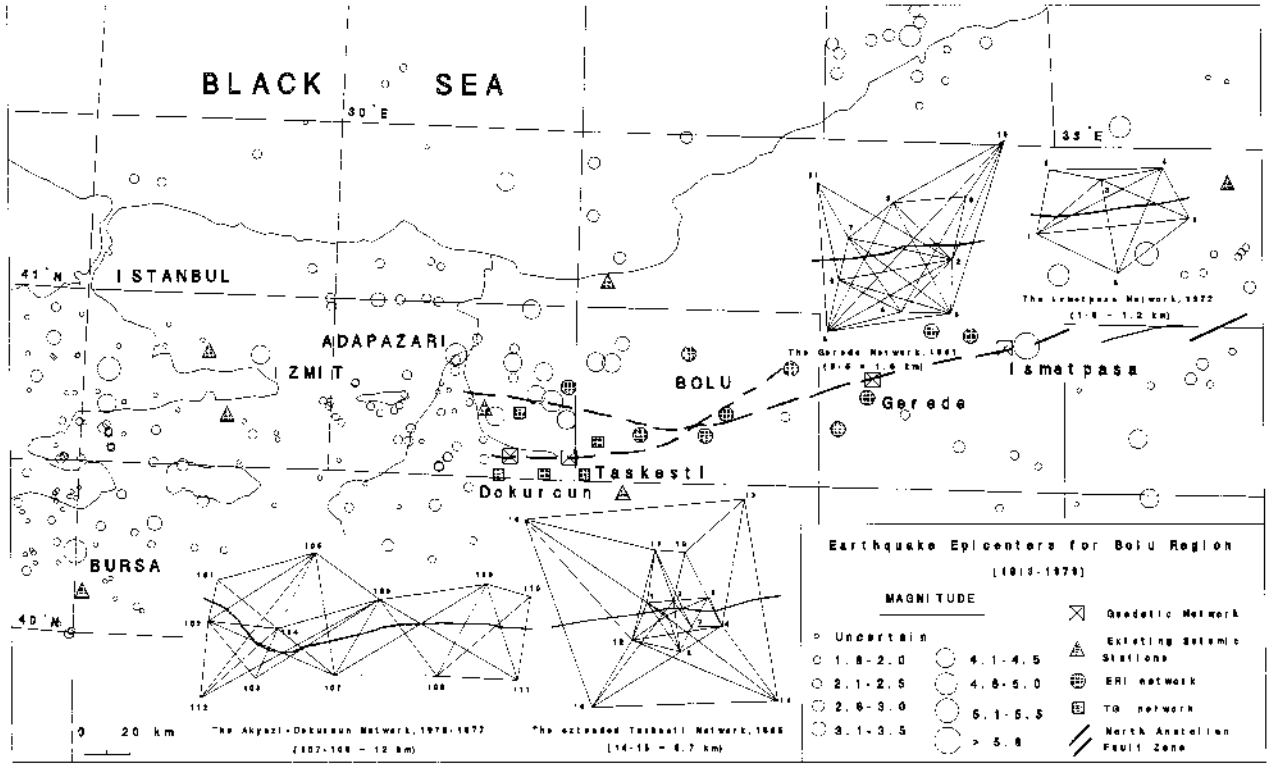


Figure 1: The position of geodetic networks where activities have been carried out (Deniz et al. 1993).

Activities of the İTÜ geodesy working group

After the individual projects mentioned above, the first geodetic studies coordinated and supported by multidisciplinary projects were started under the coordination and financial support of the Earthquake Research Office and the Geodesy Working Group of the İTÜ. In the East and North Anatolian Fault Zones, the task of determining crustal movements by geodetic methods was given to the Geodesy Working Group as the "National Project on Earthquake Hazards".

At the beginning, the networks established according to the project were:

- The Taşkesti microgeodetic network of 10 check points at distances up to 3km, on both flanks of the Mudurnu Valley.
- The Gerede microgeodetic network of 8 check points, three of which had been installed previously as mentioned above.
- The Yeniçağ (Bolu) microgravimetric network to monitor the vertical component of crustal movement.

The Taşkesti geodetic network was measured by the İTÜ Geodesy Working Group for the periods 1981, 1982, 1983 and 1984 (Aksoy 1983). In 1984, with the participation of various disciplines from Federal Germany Universities, the national project mentioned above was enlarged to the German-Turkish Project on Earthquake Prediction Research. In this project, it was decided to carry out geodetical studies with the collaboration of the İTÜ, the Department of Geodesy for the Turkish side and the University of Bonn, the Institute of Geodesy for the German side, in 1985. From 1988, the Institute for applied Geodesy (IfaG) in Frankfurt has also funded this project. The Taşkesti network was extended to 14 points at distances of up to 10km (Fig. 1) and periodic measurements have been carried out since 1985 (Franke et al., 1991a, 1991b).

The periodic measurements of the Gerede network were carried out by the İTÜ Geodesy Working Group in 1982, 1983, 1984 and 1985. In 1986 and 1987, no observations were made. In 1988, the work was started again by the project named "Geodetic Control Measurements". This project was funded by the İTÜ, as well as the Berlin Technical University and the Volkswagen Foundation. For this period, point 9 was established instead of the destroyed point 1 and the observations were repeated using this new point. In 1989, the network was extended towards the north by adding two points, 10 and 11 (Fig. 1), and observations were carried out at the 8 points from 1990 until 1992.

The microgravimetric network installed in Yeniçağa was extended towards Akyazı along the fault. Periodic gravimetric measurements and evaluations in this network were realised by Darmstadt University, the İTÜ Geodesy Working Group and Yıldız University, Geodesy Department (Aksoy et al. 1988). So far, a significant vertical point movement has not been found from these measurements. The Yeniçağa network was connected to that of the Berlin Technical University (Aksoy et al. 1994, 1995).

In addition to the studies mentioned above, the Bosphorous University, Earthquake Research Institute, Geodesy Department, started a new project in 1990. In the vicinity of the Sapanca and İznik Lakes, two microgeodetic networks, which cover the NAFZ, were installed and the measurements were realised by this department.

In Turkey, in addition to the conventional geodetic studies summarised above, geodynamic projects using geodetic space techniques were put into practice more recently. These are:

- the Wegener-Medlas project, which aims at the determination of crustal movements of the Asia-Europa and Africa plates by the satellite laser ranging method.
- the Geodynamic project, which is managed by the Massachusetts Institute of Technology and Turkish Institutes, aims at the determination of crustal movements in the East Anatolian Fault Zone.
- the GPS project, which is managed in collaboration with Durham University, Eylül University and the General Mapping Command, aims at the determination of crustal movements in western Anatolia.
- the SLR and GPS measurements projects which are managed by the IfaG and the General Directorate of Mapping, aim at the determination of crustal movements in the North Anatolian Fault Zone (Seeger et al. 1993).
- the MARMARA Poly-Project "Tectonic Activity and its Interactions with Groundwater Circulation, Geothermics and Seismicity" which is managed by the İTÜ and the Swiss Federal Institute of Technology (ETH Zurich), also aims at the determination of active plate movements in Northwestern Turkey (this volume).

Adjustment and deformation analysis

The adjustment and deformation analysis of the repeated measurements of the geodetic networks, made by the İTÜ Geodetic Working Group in the İsmetpaşa, Taşkesti and Gerede networks, were based on a linear hypothesis test in implicit form in the "Gauss-Markoff Model with constraints" and were carried out using the following steps:

- outliers were selected by the Poppe method.
- the existence of scale inconsistencies between the distances measured by different distance measurement instruments over the same period were investigated.
- a global test was applied to find out if there were significant movements within the network and at both sites from the estimated fault line.
- when significant movement was found, unstable and stable points were distinguished by applying localisation tests.
- after the stable points were determined, these points were taken as common points for both periods and all measurements in both periods were adjusted by taking a double coordinate unknown for common (stable) points and two double coordinate unknown for all other points.
- deformation vectors and confidence ellipses were calculated for the moving points.

Strain analysis

For the strain analysis, the method proposed by Vanicek and Nagy (1981) was used. Strain was computed for each point in the network using the following equations:

$$\begin{Vmatrix} df \\ \dots \\ C \end{Vmatrix} = \begin{Vmatrix} B^T P_{\Delta x} B & B^T P_{\Delta x} F \\ F^T P_{\Delta x} B & F^T P_{\Delta x} F \end{Vmatrix}^{-1} \begin{Vmatrix} B^T \\ \dots \\ F^T \end{Vmatrix} P_{\Delta x} \Delta x \qquad [1]$$

where:

$\Delta x = \| dx \quad dy \|^T$ = deformation vector

$C = \begin{Vmatrix} dx_0 \\ dy_0 \end{Vmatrix}$ = translation vector

$P_{\Delta x}$ = weight matrix of deformation vector

$$B = \begin{Vmatrix} 1 & 0 \\ 0 & 1 \end{Vmatrix} \quad , \quad F = \begin{Vmatrix} x & y & 0 & 0 \\ 0 & 0 & x & y \end{Vmatrix}$$

$$df = \| f_{xx} \quad f_{xy} \quad f_{yx} \quad f_{yy} \|$$

The strain tensor elements can be obtained by:

$$e = \begin{Vmatrix} f_{xx} & \frac{1}{2}(f_{xy} + f_{yx}) \\ \frac{1}{2}(f_{xy} + f_{yx}) & f_{yy} \end{Vmatrix} = \begin{Vmatrix} e_{xx} & e_{xy} \\ e_{yx} & e_{yy} \end{Vmatrix} \qquad [2]$$

Then, principal strain rates may be calculated by:

$$E_{\max} = \frac{1}{2}(e_{xx} + e_{yy}) + \frac{1}{2}[(e_{xx} - e_{yy})^2 + (e_{xy} + e_{yx})^2]^{\frac{1}{2}}$$
$$E_{\min} = \frac{1}{2}(e_{xx} + e_{yy}) - \frac{1}{2}[(e_{xx} - e_{yy})^2 + (e_{xy} + e_{yx})^2]^{\frac{1}{2}} \qquad [3]$$

and the bearing of the direction of the maximum strain rate, counterclockwise from the y-axis(east) by

$$\theta = \frac{1}{2} \arctan \frac{e_{xy} + e_{yx}}{e_{xx} - e_{yy}} \qquad [4]$$

The results of the analysis

The İsmetpaşa network:

The average position precisions (m_p) estimated for each period are given below.

period	1972	1982	1992
average m_p [mm]	3.3	3.7	3.0

The results of the deformation and strain analyses are summarised in Table 1.

Point Nr	1972-1982		1982-1992		1972-1992				
	d (mm)	t (gon)	d (mm)	t (gon)	d (mm)	t (gon)	E_{max}	E_{min}	θ (gon)
1	104.5	256.5	90.0	254.5	194.5	244.4	230.7	-51.9	87.2
2									
3									
4									
5	121.5	230.0							
6	107.9	263.9	84.2	251.6	191.2	241.5	230.8	-51.9	87.2
Average	111.2	250.1	87.1	253.1	192.9	243.0	230.8	-51.9	87.2

Table 1: *Summary of the analysis of the İsmetpaşa network (relative to points 2,3,4) d = deformation vector t = azimuth of the deformation vector with respect to the north.*

The Gerede network:

The maximum position precisions (m_p) estimated for each period are:

period	1982	1983	1984	1985	1988	1989	1990	1991	1992
maximum m_p [mm]	2.3	1.5	1.6	1.4	1.6	0.9	1.3	1.8	2.4

In the Gerede network, as a result of the analyses, local significant deformation vectors were found. The results obtained from the analyses are given in Table 2. The deformation vectors and their confidence ellipses with a significance level of 0.05 in the Gerede network for the period 1988-1991 are shown in Fig. 2.

Point Nr	1982-1988		1988-1989		1988-1990		1988-1991		1990-1992	
	d (mm)	t (gon)	d (mm)	t (gon)	d (mm)	t (gon)	d (mm)	t (gon)		t (gon)
2	10.2	21.2	1.6	73.2	2.4	54.2	0.9	126.2	4.5	372.2
3										
4										
5										
6										

Point Nr	1982-1988		1988-1989		1988-1990		1988-1991		1990-1992	
	d (mm)	t (gon)	d (mm)	t (gon)	d (mm)	t (gon)	d (mm)	t (gon)		t (gon)
7	5.8	390.0	4.8	130.6	5.4	140.5	5.3	156.9	3.6	261.6
8	7.7	33.5	2.1	133.6	5.6	173.9	5.7	194.0	5.3	354.9
9			7.8	142.3	7.4	153.1	7.4	191.5	4.6	318.0
10									3.5	256.9
11									8.2	242.9

Table 2: *The local significant displacement vectors (relative to points 3, 4, 5, 6 in the south) obtained for the complete Gerede network.*

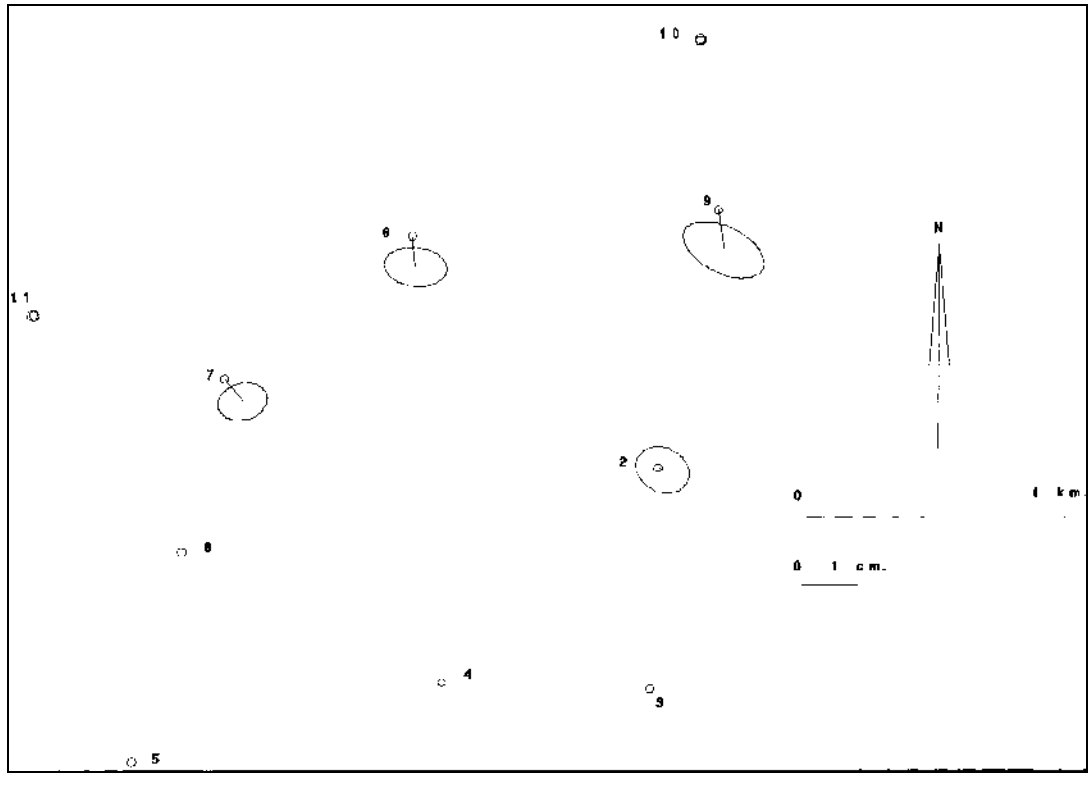


Figure 2: *Horizontal displacement vectors for the period 1988-1991 relative to points 3, 4, 5, 6 on the southern side of the Gerede network.*

The Taşkesti network:

The results of the measurements carried out before 1986 did not show any significant movement, but the results obtained in the enlarged Taşkesti network showed significant crustal movement. The maximum position precisions (m_p) estimated in the enlarged net for the period 1986-1993 are:

period	1986	1987	1988	1989	1990	1991	1992	1993
maximum m_p [mm]	4.3	3.8	2.0	3.4	2.2	2.8	2.1	2.3

The results obtained from the deformation and strain analyses are listed in Table 3. The deformation vectors and their confidence ellipses with a significance level of 0.05 in the enlarged Taşkesti network for the period 1986-1993 are shown in Fig. 3.

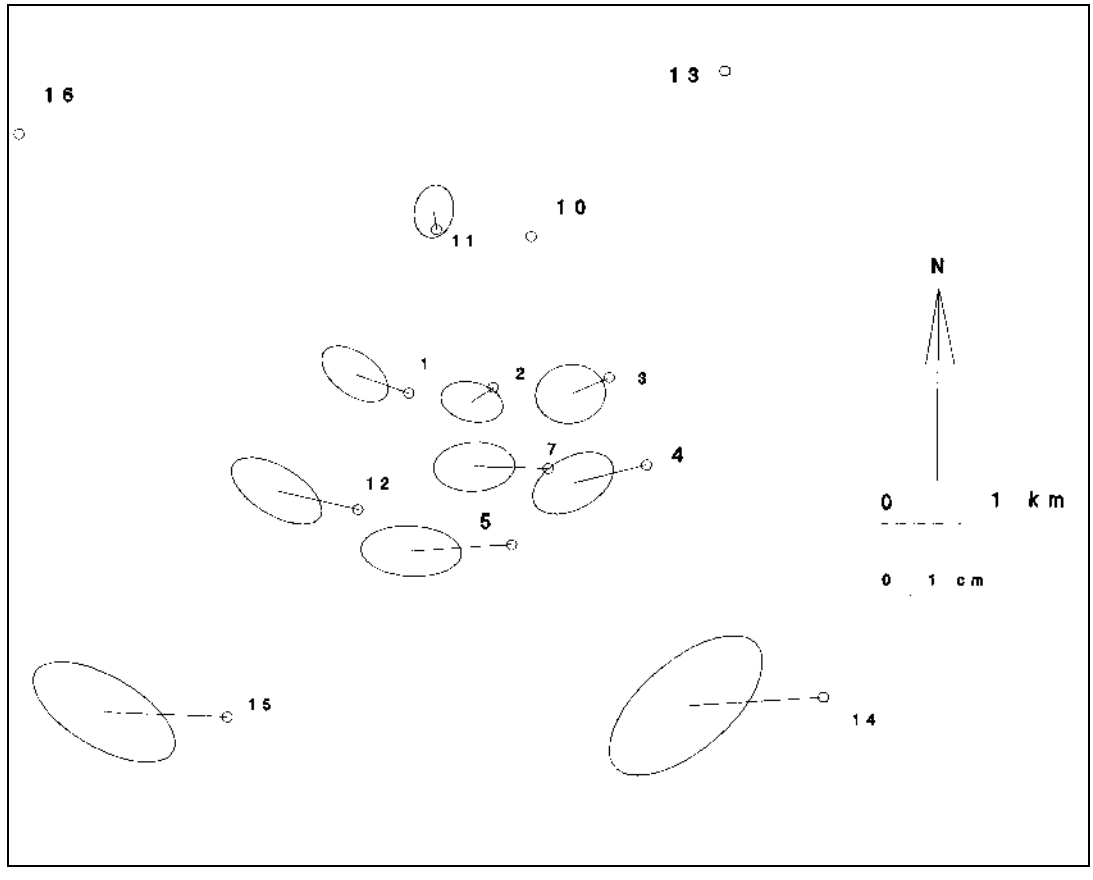


Figure 3: *Horizontal displacement vectors for the period 1986-1993 relative to points 10, 13, 16 on the northern side of the Taşkesti network. The ellipses are confidence ellipses with the level 0.05. As can be seen, the southern part moved westwards by about 3cm in 7 years with respect to the northern block.*

Point Nr	1986-1988		1986-1989		1986-1990		1986-1991		1986-1992		1986-1993		1986-1993		
	d (mm)	t (gon)	d (mm)	t (gon)	d (mm)	t (gon)	d (mm)	t (gon)	d (mm)	t (gon)	d (mm)	t (gon)	E_{max}	E_{min}	θ (gon)
1	6.5	303.2	6.9	327.8	10.1	318.4	9.4	315.7	11.8	313.8	13.7	322.2			
2	6.1	252.3	4.5	276.4	7.1	279.7	7.2	250.2	6.7	244.3	6.1	261.1	0.0	-0.2	63.32
3	4.9	204.6	3.5	244.9	6.1	270.7	5.5	267.6	8.1	270.6	10.0	273.8			
4	8.9	238.4	8.6	265.6	11.5	274.7	10.6	281.8	15.7	278.2	18.0	284.5			
5	11.2	257.1	12.3	288.7	16.4	288.3	15.9	290.7	21.6	290.1	24.0	295.7			
7	7.8	275.8	9.3	301.1	12.4	299.3	10.7	301.4	15.7	297.1	17.6	301.7			
8	5.0	207.8	1.3	196.4	14.3	302.2	11.3	304.2	12.5	280.6					
10															
11	1.6	302.7	0.2	12.4	3.4	338.6	3.8	38.8	4.1	386.0	4.4	391.4			
12	9.0	284.7	10.1	307.2	14.5	313.1	13.5	313.5	18.1	314.9	20.0	314.5	1.3	-1.0	66.2

Point Nr	1986-1988		1986-1989		1986-1990		1986-1991		1986-1992		1986-1993		1986-1993		
	d (mm)	t (gon)	d (mm)	t (gon)	d (mm)	t (gon)	d (mm)	t (gon)	d (mm)	t (gon)	d (mm)	t (gon)	E_{max}	E_{min}	θ (gon)
13													1.0	-1.1	277.7
14	10.7	301.5	19.8	293.6	25.4	294.5	25.8	295.1	31.3	296.1	32.7	295.8	-0.2	-1.2	329.6
15	14.3	269.5	15.7	298.4	21.9	303.2	22.0	299.9	24.8	301.6	29.4	302.5	0.4	-2.0	91.55
16													0.8	-0.1	167.84
17													1.7	-0.5	280.28

Table 3: Difference vectors in the Taşkesti control network (relative to points 10, 13, 16 in the north).

Conclusions

In the network established to determine crustal movement, the average deformation characteristics, such as horizontal movement rate and strain rate at certain periods of time, are much more meaningful than single point movements. Therefore, average significant movement rates and strain rates were calculated as follows:

- for the İsmetpaşa network (1972-1992): d=9.6mm/a (average crustal movement), t=243.0gon (azimuth of d), E_{max} = 11.5μs/a, E_{min} = 2.6μs/a, Θ = 87.2gon
- for the Taşkesti network (1986-1993): d=2.7mm/a, t=294.6gon

The results show that the Anatolian plate has a westward motion. The motion of the fault is becoming slower towards the west.

References

Aksoy, A., 1983, Measurements and computation in microgeodetic nets established on the North Anatolian Fault Zone for the purpose of earthquake prediction research in Turkey, IASPEI Symposium 6, XVIII, IUGG Gen. Assembly, 15.-17.8. 1983 Hamburg.

Aksoy, A., Groten, E., Becker, M. and Demirel, H., 1988, Präzisionsschweremessungen zur Überwachung von Vertikalbewegungen in der nordanatolischen Verwerfungszone, Deutsche Geodätische Kommission, Reihe B, Heft 287.

Aksoy, A., Bautsch, P. and Hirsch, O., 1994, Geodetic Control Measurements at the North-Anatolian Fault-Zone near Gerede (Turkey), contributed paper to the 1st International Symposium on Deformations in Turkey, September 5-9 1994.

Aksoy, A., Bautsch, P. and Hirsch, O., 1995, Geodätische Messungen in der Nordanatolischen Verwerfungszone, AVN 11-12/95, 423-434.

Deniz, R., Aksoy, A., Yalin, D., Seeger, H. and Hirsch, O., 1993, Determination of Crustal Movement in Turkey by Terrestrial Geodetic Methods, Journal of Geodynamics, 13-22.

Eren, K., 1983, Strain Analysis Along the North Anatolian Faulty by Using Geodetic Survey, Geodetic Bulletin, 1983.

Franke, P., Altiner, Y. and Deniz, R., 1991a, Messungen mit Mikrometer 5000 im Rahmen der Geodätisch-Geophysikalischen Untersuchungen entlang der Nordanatolischen Störzone, Vermessungswesen und Raumordnung, 53. Jahrgang, Heft 2, April, 65-77.

Franke, P. et al., 1991b, Measurements with Mekometer ME-5000 at the North Anatolian Fault Zone, contributed paper to 6th International FIG Symposium on Deformation Measurements, Hannover 24-28 November 1991.

Öztürk, E., Atasoy, V., Bektaş, S., Uysal, K. and Karahan, Z., 1987, Akyazı-Dokurcan Vadisinde kurulan Jeodezik Ağda Yatay Kabuk Hareketlerinin Araştırılmas, Türkiye 1. Harita Bilimsel ve Teknik Kurultayı, Ankara.

Seeger, H., Altiner, Y. and Franke, P., 1993, Geodynamic Projects of IFAG in the area of Turkey, contributed paper to the Prof. Wolf Geodesy Symposium, 3-5 November 1993, İstanbul.

Şengör, A.M.C., Görür, N. and Şaroğlu, F., 1985, Strike-slip faulting and related basin formation in zones of tectonic escape: Turkey as a case study, in: Strike-Slip Deformation, Basin Formation and Sedimentation, Society of Economic Palaeontologists and Mineralogists Special Publication No. 37, 227-264.

Uğur, E., 1974, Kuzey Anadolu Fay Kuşağının Gerede-Çerkes Bölümünde Yerkabuğu Hareketlerinin Jeodezik Yöntemlerle incelenmesi, Harita Gn. Md. Matbaası, Ankara.

Vanicek, P. and Nagy, D., 1981, On the compilation of the map of contemporary vertical crustal movements in Canada, Tectonophysics, 71, 1-4, 75-86.

Geothermal potential in Northwestern Turkey

ŞAKİR ŞİMŞEK

Abstract

Hacettepe University, the International Research and Application Center for Karst Water Resources (UKAM) and the Swiss Federal Institute of Technology (ETH Zurich) have signed an agreement concerning geothermal investigations in the Marmara region under the coordination of the MARMARA Poly-Project, Reg. Nr. 08818/41-3199.5, "Tectonic activity and its interactions with groundwater circulation, geothermics and seismicity – study area NW Turkey". This study consists of a general geothermal potential evaluation of Northwestern Turkey using various methods and data.

Turkey is situated in the Mediterranean sector of the Alpine-Himalayan tectonic belt which is still active. The neotectonic and Tertiary magmatic (volcanic) activity provide the basis for important geothermal potential in Turkey.

More than 90 hotsprings, up to 19 gradient, 24 shallow and 5 deep exploration wells in geothermal areas show the enormous potential of the Marmara region. This is closely related to the presence of various pervious and impervious formations that build up the reservoir and cap rock possibility. The total potential of natural thermal springs is about 80MWt. After drilling, the capacity increased to 180MWt. Most of the geothermal areas are convenient for multipurpose applications. According to the results of the studies which have been carried out so far, it seems possible to increase the production of geothermal fluids. The first important application has been realised in Balıkesir-Gönen. At present, 1600 residences and 2000m^2 of greenhouses are heated by using geothermal fluid at 90l/s and 82°C.

Of the 13 geothermal fields explored by drillings, 8 are suitable for district heating (Gönen, Pamukçu, Sındırgı, Tuzla, Kestanbol, Hıdırlar, Kuzuluk, Dikili), 12 for heating greenhouses, 8 for industrial applications, 6 for cooling and all of them for tourism and bathing possibilities.

Introduction

Turkey has a high potential for geothermal energy as a result of its suitable geological situation: the presence of young volcanism, extensional tectonics (horst-graben systems) and hydrothermally altered areas. There are a total of about 1000 thermal and mineral water spring groups in Turkey (İ.Ü. 1975, MTA 1980, Canik and Başkan 1983, Şimşek 1985a, b, 1988, 1990, 1995). It is possible to consider four main geothermal provinces, namely the Western Anatolia horst-graben system, the Northern Anatolian Fault Zone (NAFZ) and the areas affected by Upper Tertiary recent volcanic activity localised mainly in Central and Eastern Anatolia (Figure 1).

The geothermal activity of Western Anatolia is believed to be a result of tensional forces that resulted due to rigid behaviour during the Neogene and Quaternary and the development of extended near-coastal grabens. Identified and explored geothermal areas lie mainly along the following grabens: Büyük Menderes, Gediz, Bakırçay (Dikili-Bergama) and Edremit grabens. Up to 123 hot springs were identified and 36 geothermal areas were named. The

highest measured (reservoir) temperatures observed in these grabens are the Aydın-Germencik (232°C), the Denizli-Kızıldere (212°C), the Çanakkale-Tuzla (174°C), the Aydın-Salavatlı (171°C) and the Dikili-Kaynarca (130°C) fields.

The NAFZ is a major structural unit and marks the continental margin of the Eurasian plate. The NAFZ developed as a transcurrent structures as the overthrust of the crystalline massif in eastern Taurus occurred during the Pliocene and the Quaternary. Up to 94 hotwater springs and 11 geothermal sites have been identified near the 1500km long NAFZ (Şimşek 1990).

Widespread volcanic events in Eastern Anatolia occurred during the Pliocene and the Quaternary. For geothermal energy assessment, seven areas were identified and, recently, two areas were studied, namely the Nemrut and the Zilan geothermal prospects.

In Central Anatolia, widespread young volcanism and hydrothermal alteration is observed and about 44 thermal springs exist. General tectonics are in the east-west and northwest-southeast directions. Two young volcanoes (Hasandağ and Erciyes) are present.

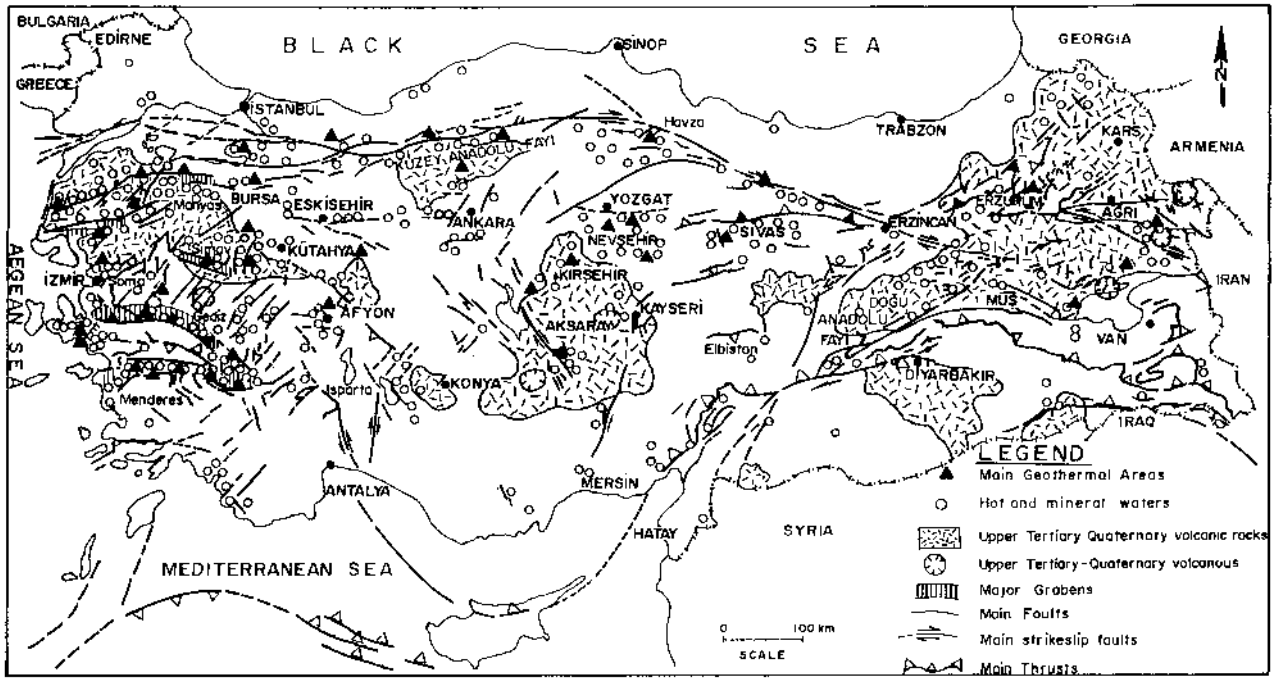


Figure 1: Main neotectonic lines and hot spring distribution of Turkey.

Approximately 400 wells have been drilled in geothermal areas of Turkey (240 gradient, 40 deep and 120 shallow wells) by MTA, TPAO and DSİ authorities as a result of different drilling activities (exploration and production etc.). The utilisation of geothermal energy in Turkey in the form of electricity and for other commercial purposes started as a consequence of studies that have been carried out since 1962.

The first important project was conducted by UNDP-MTA at the Denizli-Kızıldere area (Western Turkey) in 1968. As a result of these project, a geothermal field (212°C) was discovered and a first 20MW pilot power plant was installed in 1984 by the Turkish Electricity Authority. Also, many fields such as Aydın-Germencik (232°C), Çanakkale-Tuzla (174°C) and Kütahya-Simav (162°C) have been discovered.

At present, an equivalent of 27,000 residences (185MWt) and 120,000m^2 greenhouses are heated by geothermal energy (20MWt). Also heating system for 120,000 residences are under construction and under feasibility study (Mertoğlu et al. 1993, Şimşek 1995). On the other hand, an installation for the production of CO_2 with a capacity of 40,000 tons/year was established in 1986.

Hacettepe University, the International Research and Application Center for Karst Water Resources (UKAM) and the Swiss Federal Institute of Technology (ETH Zurich) have signed an agreement concerning "Geothermal investigations in the Marmara region" under the coordination of the MARMARA Poly-Project, Reg. Nr. 08818/41-3199.5, "Tectonic activity and its interactions with groundwater circulation, geothermics and seismicity – study area NW Turkey". This study also includes a general geothermal potential evaluation of NW Turkey by using various methods and data.

There are numerous documents to assist geothermal studies of the Marmara region. Among these are the following:

Remote sensing studies: Henden (1981);

Geological studies: Bingöl et al. (1975), Şengör and Yılmaz (1981), Akyürek and Soysal (1983), Evans et al. (1985), Şengör et al. (1985), Crampin and Evans (1986), Şengör (1987), Okay et al. (1990), Zanchi et al. (1990), Erkal (1991), Şaroğlu et al. (1994), Westaway (1994);

Studies of magmatism and volcanic activities: Ercan et al. (1982), Ercan et al. (1985), Ercan et al. (1990), Ertürk et al. (1990), Ergin and Güleç (1990), Savaşcın (1990), Savaşcın and Güleç (1990), Tankut et al. (1990), Ercan (1992);

Studies of geomorphology: Erol (1992);

Gravity studies: Ekingen (1971, 1978), Makris (1978a, b), Özelçi (1978);

Resistivity studies: Demirörer (1971), Tezcan (1979);

Seismicity and micro earthquake evaluations: Evans et al. (1985), Alptekin et al. (1990);

Thermal water inventory studies: İ.Ü. (1975), MTA (1980), Canik and Başkan (1983);

Geothermal studies: Jongsma (1974), İlkışık (1989), Koçak (1990), Staroste (1990), Stiros (1991), Tezcan (1979), Tezcan and Turgay (1991), Tezcan (1995).

The present study consists of a general geothermal potential evaluation of the northwestern part of Turkey. One of the important geothermal exploration methods is that of heat flow survey. This method helps establish the thermal boundary conditions for further geothermal modelling. The heat flow study in the Marmara region (Pfister et al. this volume) presents new information based on measurements of geothermal gradient as well as of rock thermal conductivity.

Distribution of thermal springs and geothermal characteristics of the investigation area

Turkey is situated in the Mediterranean sector of the Alpine-Himalayan tectonic belt, which is still active. The northward motion of the African and Arabian plates moved the Anatolian plate towards the west. Thus, it created the arc shaped northern Anatolian strike-slip fault and the extensional terrain features such as grabens in the east-west direction located in Western Anatolia. Subduction of the African plate beneath the Aegean-Anatolian plate caused an increase of temperature in the crust in this region.

The neotectonic and Tertiary magmatic (volcanic) activities provided the basis for significant variations in heat flow in Turkey (Tezcan 1995). Moreover, the proper hydraulic conditions and the presence of reservoir and caprocks led to the formation of numerous geothermal manifestations.

The main effects of the fault systems are determined as follows:

a) Northern Anatolian Fault Zone: mainly E-W right direction strike slip faults are dominant.

b) Aegean graben system: mainly E-W graben faults are dominant.

c) South Marmara system: mainly NE-SW strike slip and E-W oblique and normal fault system.

The special distribution of the thermal springs implies that the Edremit bay, the Edremit-Gönen, the Uludağ, the İznik-Gemlik and the Gemlik bay tectonic zones, which tend to be E-W and NE-SW in direction, are important locations for geothermal potential. Locally increased geothermal gradients occur.

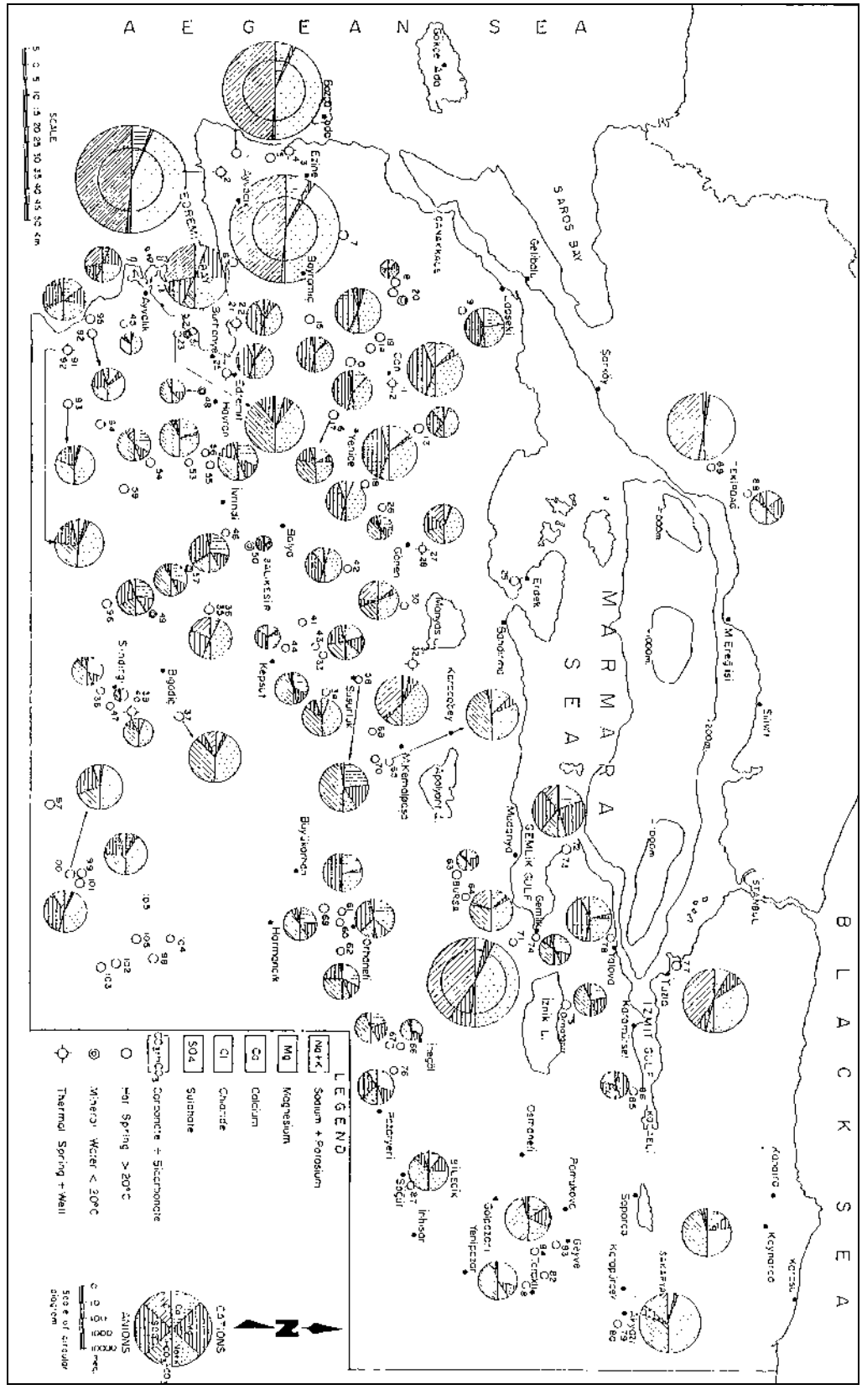
As result of extensive tectonics and former volcanic activity in the Marmara region, various types of rock units are encountered, hydrothermal systems with low to medium and even high temperature have developed and, in turn, numerous thermal springs have been formed.

On the contrary, in the Thrace basin (Ergene basin), which is located far from the NAFZ, thermal springs with low temperatures exist only at two locations due to the basin-type structure. Since fault systems that may provide deep groundwater circulation are not well-developed, only low temperature aquifers are expected to exist in this region. Numerous oil and gas fields are characteristic for the Thrace basin (Nazikoğlu et al. 1978, Ünalan 1979).

Up to 92 thermal springs, with temperatures ranging from 20°C to 102°C, have been located within the study area. The distribution of the thermal springs and the total of 13 well locations in the geothermal areas (in parentheses) by 11 provinces is as follows: Çanakkale 16, (4); Balıkesir 33, (6); Bursa 16, (1); İstanbul 2; Sakarya 5, (1); Kocaeli 2; Bilecik 1; Tekirdağ 2; İzmir 5, (1); Manisa 2; Kütahya 8. The total discharge rate of all of these springs and wells is approximately 1050l/s.

The classification of the thermal waters according to the chemical analyses (Figure 2) is as follows: 23 Na-SO_4 hotsprings, 20 $NaHCO_3$ hotsprings, 14 $CaHCO_3$ hotsprings, 13 NaCl hotsprings, 6 $CaSO_4$ hotsprings,1 CaCl hotspring.

The amount of TDS in the thermal waters is as follows: 26 areas have less than 1000ppm, 36 areas have between 1000-5000ppm, 2 areas have more than 5000ppm, Çanakkale-Tuzla has the highest amount of TDS (62,000ppm).


A E G E A N S E A
MARMARA SEA
B L A C K S E A
SAROS BAY
GEMLIK GULF
IZMIT GULF
Gelibolu
Saroy
Erdek
Bandırma
Gemlik
Iznik L.
Yalova
Karamürsel
Adapazarı
Kocaeli
Sapanca
Akyazı
Geyve
Pamukova
Çerkeş
Çankırı
Yenipazar
Inhisar
Bozüyük
Söğüt
Osmaneli
Mudanya
Bursa
Kemalpaşa
Kepsut
Sındırgı
Bigadiç
Susurluk
Havran
Balıkesir
Gönen
Manyas L.
Kuş L.
Edremit
Ayvalık
Burhaniye
Ezine
Bayramiç
Çanakkale
Ayvacık
Yenice
İvrindi
Bolyd
Kerrcoobey
Sındırgı
Buyukmenderes
Harmancık
Osmaneli
Pazaryeri
Silecik
Inhisar
Pamukova
Geyve
Çerkeş
Çankırı
Yenipazar
Sapanca
Kocaeli
Akyazı
Adapazarı
Karamürsel
Yalova
İzmit
İstanbul
Tekirdağ
Marmara Ereğlisi
Şarköy
Gelibolu
Erdek
Bandırma
Gemlik
Mudanya
Bursa
Iznik L.
Kuş L.
Manyas L.
Edremit
Ayvalık
Burhaniye
Ezine
Bayramiç
Çanakkale
Ayvacık
Yenice
İvrindi
Bolyd
Gönen
Balıkesir
Kepsut
Susurluk
Sındırgı
Bigadiç
Kerrcoobey
Buyukmenderes
Harmancık
Osmaneli
Pazaryeri
Silecik
Inhisar
Söğüt
Bozüyük

Geophysical surveys

Regional and some detailed gravity (Figure 3) as well as geoelectrical studies have been carried out for geothermal exploration by the MTA General Directorate in the Marmara region.

Gravity data

As a result of Bouguer anomalies (Ekingen 1971, 1978), some evaluations of the Marmara sea region may be made in relation to hot springs and geothermal field distributions (Figure 3). The general direction of isogals corresponds to the strike of the formation which is in the NE-SW direction. Young tectonic lines with anomalies in the E-W direction are seen in the eastern part of the region. Formations older than Tertiary are indicated with a positive gravity axis.

From the point of view of regional gravity, the peninsula is divided into two parts by the gravity gradient belt extending between Edremit and Erdek bays. A major part of the numerous hot springs included in the peninsula are either in the above mentioned gradient belt or adjacent to it. Anomalies most probably indicate a series of deep faulting or lithologic contrasts. Such a geological structure contributes to uprising thermal groundwater activity and forms a favourable possibility for geothermal energy.

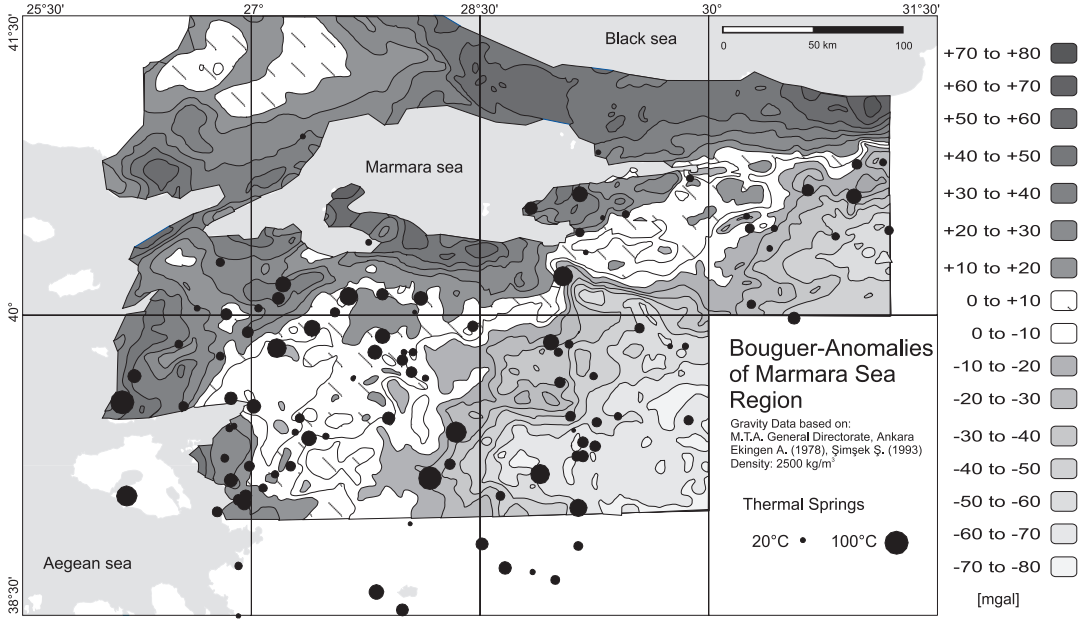


Figure 3: *Bouguer gravity anomalies and thermal spring distribution (outflow temperatures), region of NW Turkey.*

Geoelectrical anomalies

Geoelectrical studies for geothermal exploration have been carried out locally and regionally in the Marmara region. According to these studies, especially low resistivity anomalies (2-10Ωm) have been observed in some of the geothermal areas (Demirörer 1971, Tezcan 1979, 1990).

The reservoir extensions have been determined from these anomalous low values, for example in the Çanakkale-Tuzla, Kestanbol, Balıkesir-Gönen, Sındırgı, Kepekler, Sakarya-Kuzuluk and Bursa geothermal fields.

Evaluation of the data obtained from wells in geothermal areas

In the investigated region, the geothermal energy exploration and thermal water production studies have been carried out by the MTA since the 1960's. In addition, the TPAO (Turkish Petroleum Agency) has carried out geothermal research studies in the Balıkesir-Sındırgı area. Moreover, thermal waters were encountered in groundwater exploration studies carried out by the DSİ in the Edremit plain. There are also several private wells, from which thermal water is exploited.

In 13 geothermal survey areas, 19 gradient, 24 shallow exploration and production and 5 deep exploration wells have been drilled so far. Temperatures ranging from 20 to 174°C were observed in the exploration and production wells.

The thermal springs' discharge rate, which previously was in total 833.5l/s, increased to 1238.5l/s after the development of these wells. Various cap and reservoir rocks have been identified using the well logs. The reservoir rocks show a great variety, such as andesite and ignimbrite in Çanakkale-Tuzla, Balıkesir-Kepekler and Balıkesir-Sındırgı, schists in Çanakkale-Çan, granite in Hıdırlar, syenite, granite and gneisses in Kestanbol, calcschist and quartzite in Bursa-Armutlu, "mélange" (limestone and diabase) in Gönen, crystalline limestone in Akyazı-Kuzuluk and volcanic rocks in İzmir-Dikili (Şimşek 1991, 1993a). The cap rocks comprise mostly volcanic tuffs and sedimentary series of Neogene age. The geochemical properties of the thermal springs and well waters present almost similar characteristics (Table 1).

The utilisation possibilities from geothermal fields in the region

There is an important potential based on the temperatures and flow rates of the springs and wells in the geothermal fields in the region (Tables 2 and Appendix). Çanakkale-Tuzla (22MWt), Balıkesir-Gönen (23MWt), Sakarya-Kuzuluk (9.6MWt), Balıkesir-Sındırgı (15.8MWt) and 11 further fields where wells have been drilled up to the present time yield a total of 180.13MWt energy. Table 3 shows the present potential of the city provinces based on the total discharges of the springs and wells (basis of calculation $T=T_W$-30°C).

The total flow rate from 11 cities with 92 hot springs was equal to 833.5l/s and the capacity was 78.18MWt. After drilling, flow rates increased to 1238.5l/s and the capacity reached 180.13MWt. So far, the most important geothermal application is district heating in Gönen with existing geothermal potential. This heating system includes 1600 residences with no negative experiences. On the other hand, this potential is important for industrial and balneological applications (Table 2). It is important to develop the geothermal potential for purposes other than heating in the future. These applications will be very beneficial for the economy, the environment and public health.

Table 1: Information about some geothermal fields in the MARMARA Poly-Project area.

Location	Temp [°C]		Flow rate [l/s]			Present	Geology	Geo-	Wells		Utilisation possibilities						
Fields	Hs	W	Est	Hs	W	Capacity (MWt)		physics	No.	Depth (m)	Elect	DisH	GreH	Ind	Cool	Baln	Tour
BALIKESIR																	
GÖNEN	77	77-86	90	15	75	23	X	X	4	133-534	-	A	A	A	AP	A	A
PAMUKÇU	54	60	70	3	40	4.3	X		2	50-193	-	AP	AP	AP	-	A	A
KEPEKLER	60	64	100	8	15	3.1	X	X	1	390	-	-	AP	-	-	IAP	IAP
HAVRAN	57	50-60		0.5	30	3	X		4	30-122	-	-	A		-	PU	PU
GÜRE	54	42	75	10	2	1.1	X	X	1	400	-	-	AP	-	-	A	AP
SINDIRGI	98	100	165	30	25	15.8	X	X	1	881	-	AP	PU	IAP	IAP	A	AP
BURSA																	
ARMUTLU	55	77	80	10	20	5	X			500	-	-	IAP	-	-	A	AP
ÇANAKKALE																	
TUZLA	102	174	230	20	30	22	X	X	8 \2	49-150\820-1020	AP	AP	IAP	IAP	AP	IAP	IAP
KESTANBOL	73	75	100	3	15	3.1	X	X	1	290	-	AP	A	AP		PU	IAP
HIDIRLAR	40-81	75	100	8	2	2	X	X	1	380	-	IAP	IAP	IAP	IAP	IAP	IAP
ÇAN	32	47	50	0.3	5	0.4	X		2	100-300	-	-	-	-	-	A	AP
SAKARYA																	
KUZULUK	41-51	84	98	5	42	9.6	X	X	2	160-250	-	IAP	IAP	AP	AP	PU	AP
IZMIR																	
DIKILI	30-90	130	180	200		20	X	X	14	50-600\1500	AP	IAP	IAP	IAP	IAP	IAP	IAP

Explanation:

Hs:Hot Spring
W:Well
Est:Estimated
Cool: Cooling
Baln: Balneology
Tour: Touristic
Elect: Electricity Production
DisH: District Heating
GreH: Greenhouse Heating
Ind: Industrial Application

A Application at Present
PU Partly Utilization
AP Application Possibility
IAP Important Application Possibility

P = c m (T_w-30°C) [with P: energy output (W), c: heat capacity (J/kg K), m: mass flow (kg/s), T_w: temperature of water (°C)]

Table 2: General characteristics of drilled geothermal fields in the project area.

No:	Fields:	Number of well			Well Depth	Reservoir Rock	Thickness	Cap Rock	Thickness	Geochemical Properties	
		Shallow		Deep							
		Gr.	Exp.	Exp.	(m)	Lithology:	(m)	Lithology:	(m)	Spring	Well
1	BALIKESİR			NO:		Lms, Dia		S.R.		HCO3>SO4>Cl	HCO3>Cl>SO4
	GÖNEN		5		133-534.1	(Ne+Me)	200	(Ne)	123-296	Ca>Mg>Na	Na>K>Ca
2	BALIKESİR					An		S.R.		Cl>HCO3>SO4	Cl>HCO3>SO4
	KEPEKLER		1		390.3	(Mg)	176	(Ne)	22	Na>Ca>Mg>K	Na>Ca>Mg>K
3	BALIKESIR					Al		Al		HCO3>Cl>SO4	HCO3>Cl>SO4
	HAVRAN		5		30-122	Q	20	Q	10-100	Na>Ca>K	Na>Ca>K
4	BALIKESIR					Mr,Sp		S.R.		SO4>Cl>HCO3	HCO3>Cl>SO4
	PAMUKÇU		2		50-193	(Pz)	170	(Ne)	30	Na>Ca>K>Mg	Na>Ca>K
5	BALİKESİR							S.R.		SO4>Cl>HCO3	
	GÜRE		2		400	Cong	20	(Ne)		Na>Ca>K	
6	BALIKESIR					An		Tf.An		HCO3>Cl>SO4	
	SINDIRGI			1	881				355	Na>Ca>Mg	
7	BURSA					Mr		Sch.		SO4>HCO3>Cl	SO4>HCO3>Cl
	ARMUTLU			1	500		20		200	Na>Ca>Mg	Na>Ca>Mg
8	ÇANAKKALE					1. An, Ign(My)		Ign. SS		Cl>SO4>HCO3	Cl>SO4>HCO3
	TUZLA	8		2	820-1020	2. Mr(Pz)	215-760	(My)	54-465	Na>Ca>K	Na>Ca>K
9	ÇANAKKALE					Gr,Gns,Sy		S.R.		Cl>HCO3>SO4	Cl>HCO3>SO4
	KESTANBOL		1		290.7	(Pz)	52	(Ne)	238	Na>Ca>K	Na>Ca>K
10	ÇANAKKALE					Gr		Gr		SO4>HCO3>Cl	
	HIDIRLAR		1		380		370		10	Na>Ca>Mg	
11	ÇANAKKALE					S.R.		S.R.		SO4>Cl>HCO3	
	ÇAN		2		100-300		100		145	Na>Ca>Mg	
12	IZMIR				100-600	An		An		HCO3>SO4>Cl	
	DİKİLİ	11	2	1	1500		140		580	Na>Ca>Mg	
13	SAKARYA					Lms				HCO3>Cl>SO4	HCO3>Cl>SO4
	KUZULUK		3		160-250		100			Na>Ca>Mg	Na>Mg>K

Exp: Exploration	S.R.: Sedimentary Rocks	Al:Alluvium (Quaternary)	Sy:Syenite	My:Miocene
GR: Gradient	Sp: Serpentinite	Dia: Diabase	Gr:Granite	Ne:Neogene
	Cong:Conglomerate	Ign:Ignimbrite	Lms:Limestone	Me: Mesozoic
	Mr:Marble	Gns:Gneisse	An: Andesite	Pz: Palaeozoic

Fields	Spring Flow [l/s]	MWt	Well Flow [l/s]	MWt	Total Flow [l/s]	Total MWt
ÇANAKKALE	61	9	52	22	113	30
BALIKESIR	146	21	193	36	339	57
BURSA	229	9	20	4	249	13
ISTANBUL	25	3			25	3
SAKARYA	13	0,3	40	9	53	10
KOCAELI	5	0,01			5	0,01
BILECIK	6	0,08			6	0,08
TEKIRDAG	0,5				0,5	
IZMIR	15	0,75	100	31	115	32
MANISA	2	0,04			2	0,04
KÜTAHYA	131	15			131	15
Total	630	58	405	102	1040	160

Table 3: Present potential of the city provinces according to total discharges of springs and wells.

Summary of results

The evaluation of the geothermal potential for NW Turkey has been prepared on the basis of various data. Young tectonic activity in the region has affected the geomorphology and normal and strike-slip fault lines could clearly be followed. According to the results of the gravity study, gravity anomalies were correlated with main tectonic lines and the hot spring distribution. The resistivity survey of some areas characterised geothermal areas with resistivity values as low as 3-10Ωm. As a result of evaluation within the MARMARA Poly-Project, it has been shown that this region has an important geothermal energy potential. This potential is closely related to the presence of various fault zones and pervious and impervious formations which make up the reservoir and cap rocks.

The northwestern part of Turkey comprises up to 94 hot springs. In 13 geothermal areas there are 19 gradient, 24 shallow and 5 deep exploration wells. The total potential of the existing thermal spring waters was about 78.18MWt. After drilling, capacity increased to 180.13MWt. According to the results of the studies that have been carried out so far, it seems possible to further increase the production of geothermal fluids.

The region is characterised by mainly low enthalpy areas. There are only a few medium enthalpy areas, such as Çanakkale-Tuzla (174°C). Generally, these areas are convenient for multipurpose applications.

The first important application has been realised in Balıkesir-Gönen. At the present time, 1600 residences and 2000m^2 of greenhouses are heated by geothermal fluid at 90l/s and 82°C.

From the 13 areas which were drilled, 8 areas are suitable for district heating (Gönen, Pamukcu, Sındırgı, Tuzla, Kestanbol, Hıdırlar, Kuzuluk and Dikili), 12 areas for heating greenhouses, 8 areas for industrial applications, 6 areas for cooling and all areas which were drilled are suitable for tourism and bathing possibilities.

Acknowledgements

Ş.Ş. would like to express his great thanks to Prof. Gültekin Günay (Director-Hacettepe University International Research and Application Center for Karst Water Resources UKAM) for providing scientific and logistic support both in the field and laboratory. Also, Ş.Ş. would like to thank the Swiss part of the MARMARA Poly-Project: Prof. C. Schindler as the project coordinator; Prof. L. Rybach, W. Balderer, M. Pfister and all Poly-Project members for the close cooperation and discussion in Switzerland as well as in Turkey. And also, thanks to Prof. E. Yüzer for the coordination of the Turkish group and organising several scientific seminars in Istanbul. Ş.Ş. expresses his gratitude to the General Directorate of Mineral Research and Exploration of Turkey (MTA) for permitting the use and supplying some of the data for this study. Ş.Ş. expresses his appreciation to M.Ş. Doğdu, H. Çelik and K. Çolpan who assisted in this work.

References

Alptekin, S., İlkışık, O.M., Ezen, Ü. and Üçer. S.B., 1990, Heat Flow, Seismicity and the Crustal Structure of Western Anatolia, International Earth Sciences Congress on Aegean Regions, Proceedings, V.2, 1-13, İzmir.

Akyürek, B. ve Soysal, Y., 1983, Biga Yarımadası Guneyinin (Savaştepe-Kırkağac-Bergama-Ayvalık) Temel Jeolojik Özellikleri, MTA Dergisi, 95/96, 1-13.

Bingöl, E., Akyürek, B. ve Korkmazer, B., 1975, Biga Yarımadası'nın Jeolojisi ve Karakaya Formasyonu'nun Bazı Özellikleri, Cumhuriyet' in 50. Yılı Yerbilimleri Kongresi Tebliğleri, MTA Yayını, 70-77.

Canik, B. and Başkan, E.M., 1983, IAH Map of Mineral and Thermal Waters of Turkey Aegean Region, MTA Publ., No.189.

Crampin, S. and Evans, R., 1986, Neotectonics of the Marmara Sea Region of Turkey, Journal of Geological Society, London, V.143, 343-348.

Demirörer, M, 1971, Geophysical survey of Çanakkale Tuzla area, MTA Report.

Ekingen, A., 1971, Gravimetric Method in Geothermal Field Explorations and its Application in Turkey, Proceedings of I. Geothermal Energy Symposium of Turkey, 60-74.

Ekingen, A., 1978, Gravity Gradient of Biga Peninsula, Geothermal Energy Assoc. Publ. No. 6, MTA Ankara, 2-6.

Ercan, T., 1992, Trakyadaki Senozoyik Volkanizması ve Bölgesel Yayılımı, Jeoloji Mühendisliği TMMOB Jeoloji Mühendisleri Odası Yayın Organı, 37-50.

Ercan, T., Erol, O., Savaşçın, Y. and Şengör, A., 1982, Batı Anadolu'nun Genç Tektoniği ve Volkanizması, TJK Bulteni, 4-72.

Ercan, T., Satir, M., Kreuzer, H., Türkecan, A., Günay, E., Çevikbaş, A., Ateş, M. and Can, B., 1985, Interpretation of New Chemical, Isotopic and Radiometric Data on Cenozoic Volcanics of Western Anatolia, TJK Bulletin, 121-137.

Ergin, M.Y. and Güleç, N., 1990, Relationship Between Magmatic and Tectonic Activities in Western Turkey, International Earth Sciences Congress on Aegean Regions Proceedings, V.2, 28-40, İzmir.

Ercan, T., Ergül, E., Akçaören, F., Çetin, A., Granit, S. ve Asutay, İ., 1990, Balıkesir-Bandırma Arasının Jeolojisi, Tersiyer Volkanizmasının Petrolojisi ve Bölgesel Yayılımı, MTA Yayını, No.110, 113-130.

Erol, 1992, Geomorphological map, MTA publication.

Erkal, T., 1991, Some Approaches on the Occurrence of the Normal Faults Developed within the North Anatolian Transform Fault Zone, Thrace, Turkey, TAPG Bulletin, Vol.3, No.1, 87-99.

Ertürk, O., Dinçöz, E. and Alaygut, D., 1990, Petrology of the Cenozoic Volcanics in the Biga Peninsula, NW Turkey, International Earth Sciences Congress on Aegean Regions Proceedings, V.2, 368-385, İzmir.

Evans, R., Asudeh, I., Crampin Stuart, C. and Üçel, B., 1985, Tectonics of the Marmara Sea Region of Turkey: New Evidence from Micro-Earthquake Fault Plane Solution, Geophysical J.R. Astr. Soc. V.83, 47-60.

Henden, İ., 1981, Uzay Görüntülerinden Türkiye Çizgisellik Haritası ve Maden Aramaları için Hedef Sahaların Seçilmesi, Bölgesel Çizgiselliklerin Deprem ve Sıcaksu Kaynakları ile İlişkisi, MTA Bul., No 95-96, 68-77.

İlkışık, O.M., 1989, Heat Flow Pattern of Northwest Anatolia, Geophysic Bull., No.3, 83-91.

İ.Ü., 1975, Hot and Mineral Water Inventory, İst. Univ. Tıp. Fak. Vol. 2; Marmara.

Jongsma, D., 1974, Heat Flow in the Aegean Sea, Geophysical J.R. Astr. Soc., 37, 337-346.

Koçak, A., 1990, An Approach to Occurence of the Geothermal Systems in Western Anatolia, International Earth Sciences Congress on Aegean Regions Proceedings, Vol. 2, 148-160, İzmir.

Makris, J., 1978a, The Crust and Upper Mantle of the Aegean Region Obtained From Deep Seismic Sounding Tectonophysics, 46, 269-284.

Makris, J., 1978b, Some Geophysical Consideration on the Geodynamic Situation in Greece, Tectonophysics 46. 251-268.

Mertoğlu, O., Mertoğlu, M. and Başarır, N., 1993, Direct Use Applications in Turkey, Geothermal Resources Council Transactions. Vol. 17, 19-22.

MTA, 1980, Hot and Mineral Water Inventory, MTA Rap., Ankara.

Nazikoğlu, Z., Uygur, N. and Öngür, T., 1978, Isotemperature Map For 1000m Depth of Turkey, Geothermal Energy Assoc. Publ., No. 6, 23-26.

Okay, I.A., Siyako, M. and Burkan, K.A., 1990, Geology and Tectonic Evolution of the Biga Peninsula, TAPG Bulletin, V.2/1, 83-121.

Özelçi, F., 1978, A Suggestion on the Possible Significance of Volcanic Activity in the Tectonic Development of the Eastern Mediterranean Region, Tectonophysics, 46, 227-237.

Pfister, M., Rybach, L. and Şimşek, Ş., this volume, Geothermal reconnaissance of the Marmara sea region.

Savaşcın, M.Y. and Güleç, N., 1990, Relationship between magmatic and tectonic activities in Western Turkey, International Earth Sciences Congress on Aegean Regions Proceedings, Vol. 2, 300-314, İzmir.

Savaşcin, M.Y., 1990, Magmatic Activities of Cenozoic Compressional and Extensional Tectonic Regimes in Western Anatolia, International Earth Sciences Congress on Aegean Regions Proceedings, Vol. 2, 420-435, İzmir.

Staroste, E., 1990, Atlas of Geothermal Resources in the European Community, Austria and Switzerland, Geothermal Resources Council Transactions, Vol. 14, Part II, 979- 982.

Stiros, S.C., 1991, Heat Flow and Thermal Structure of the Aegean Sea and the Southern Balkans, Terrestrial Heat Flow and Lithosphere Structure, Springer Verlag Publ. 395-416.

Şaroğlu, F., Emre, İ. and Kuşcu, I., 1994, Active Fault Map of Turkey, MTA Publication, Ankara.

Şengör, A.M.C., 1987, Cross-faults and Differential Stretching of Hanging Walls in Regions of Low-Angle Normal Faulting: Examples from Western Turkey, 575-588.

Şengör, A.M.C. and Yılmaz, Y., 1981, Tethyan Evolution of Turkey: A Plate Tectonic Approach, Tectonophysics, International Earth Sciences Congress on Aegean Regions Proceedings, 75, 181-241, İzmir.

Şengör, A.M.C., Görür, N. and Şaroğlu, F., 1985, Strike-Slip Deformation and related Basin Formation and Sedimentation, in: Zones of Tectonic Escape: Turkey As A Case Study, Society of Economic Paleontologists and Mineralogists, Special Publication, No.37, 227-260.

Şimşek, Ş., 1985a, Geothermal Model of Denizli, Sarayköy-Buldan Area, Geothermics, V.14, No.2-3, 393-417.

Şimşek, Ş., 1985b, Present Status and Future Developments of the Denizli- Kızıldere Geothermal Energy Field of Turkey, International Symposium on Geothermal Energy, International Volume, 203-210.

Şimşek, Ş., 1988, Importance of Geothermal Energy in Turkey, Proceedings of International Mediterranean Congress on Solar and Other New and Renewable Energy Resources, 623-636, Antalya.

Şimşek, Ş., 1990, Geothermal Energy Development in Turkey, International Symposium on Geothermal Energy, Hawaii, Geothermal Resources Council Transactions, V.14, Part I, 257-261.

Şimşek, Ş., 1991, Reservoir and Cap Rock Characteristics of Some Geothermal Fields in Turkey and Encountered Problems Based on Lithology, Journal of the Geothermal Research Society of Japan, V.13, No.3, 191-204.

Şimşek, Ş., 1993a, Karstic Hot Water Aquifers. Hydrogeological Processes in Karst Terranes (Proceedings of the Antalya Symposium and Field Seminar October 1990). IAHS Publication No.273, 173-184.

Şimşek, Ş., 1993, Gravity map of Marmara sea region, MTA Ankara.

Şimşek, Ş., 1995, Present Status and Future Development Possibilities of Geothermal Energy in Turkey, the Second International Conference on New Energy Systems and Conversions, İstanbul.

Tankut, A., Akıman, O., Türkmenoğlu, A., Güleç, N. and Göker, T., 1990, Tertiary Volcanic Rocks in Northwest Central Anatolia, International Earth Sciences Congress on Aegean Regions, 450-467, İzmir.

Tezcan, A.K., 1979, Geothermal Studies, Their Present Status and Contribution to Heat Flow Contouring in Turkey,Terrestrial Heat Flow in Europe, Springer Verlag, Berlin, Heidelberg and New York, 283-292.

Tezcan, A.K., 1990, Investigated Geothermal Fields in Turkey, Geothermal Atlas of Europe , Int. Assoc. for Seismology and Physics of the Earth's Interior, Int. Heat Flow Commission Publication, 84-85.

Tezcan, A.K., 1995, Geothermal explorations and heat flow in Turkey, in: Terrestrial heat flow and geothermal energy in Asia, edited by: L. Mohan, Gupta and Makoto Yamano, A.A. Balkema / Rotterdam, 23-42.

Tezcan, A.K. and Turgay, M.I., 1991, Geothermal atlas of Europe, catalogue of heat flow density data: Turkey, in: Geothermal Atlas of Europe, edited by: E. Hurtig, V. Cermák, R. Haenel and V. Zui, 84-85.

Ünalan, G., Öngür, T., 1979, Geothermal Gradient and Temperature Investigation at 1000m Depth at Some of Basins of Turkey, Geocome-I First Geological Congress of the Middle East, 637-650.

Westaway, R., 1994, Present-day Kinematics of the Middle East and Eastern Mediterranean, Journal of Geophysical Research, Vol.99, No. B6, 12071-12090.

Zanchi, A., Kissel, C, and Tapırdamaz, C., 1990, Continental Deformation in Western Turkey: A Structural and Paleomagnetic Approach, International Earth Sciences Congress on Aegean Regions Proceedings, 357-368, İzmir.

Appendix

No:	City No:	Name:	T [°C]	No:	City No:	Name:	T [°C]
ÇANAKKALE				BURSA			
1	Ç-1	TUZLA-GAYZER	45-102	60	Bu-1	AGAÇHISAR	36
2	Ç-2	T1-T2 WELLS	174	61	Bu-2	KAYA-SADA	47-68
3	Ç-3	KESTANBOL	73	62	Bu-3	KOCAKAVACIK	35
4	Ç-4	K-1 WELL	73	63	Bu-4	ÇEKIRGE GR.	28-45
5	Ç-5	AKÇAKEÇILI	33-37	64	Bu-5	KÜKÜRTLÜ GR.	79-83.7
6	Ç-6	KÜÇÜKÇETMI	41	65	Bu-6	DÜMBÜLDEK	47
7	Ç-7	PALAMUTOVA	34	66	Bu-7	ILICA INEGÖL	21.5
8	Ç-8	KIRAZLI	25	67	Bu-8	KARACAKAYA	27
9	Ç-9	KOCABASLAR	37	68	Bu-9	ÇINAR ILICASI	32
10	Ç-10	OZANCIK-ÇAN	65	69	Bu-10	ILICASU	45.5
11	Ç-11	ÇAN(PAZARKÖY)	32	70	Bu-11	ÇAMASIRLIK	24
12	Ç-12	Ç1-Ç2 WELLS	47	71	Bu-12	ADLIYE KÖYÜ	21
13	Ç-13	KIRKGEÇIT	52-58	72	Bu-13	ARMUTLU	55
14	Ç-14	KARA(TEPEKÖY)	48	73	Bu-14	A1 WELL	77
15	Ç-15	KÜLCÜLER	34.5	74	Bu-15	GEMLIK	36
16	Ç-16	HIDIRLAR	40-81	75	Bu-16	KERAMET KÖYÜ	30
17	Ç-17	H1 WELL	75	76	Bu-17	OYLAT	40
18	Ç-18	KUM(TOPAKLAR)	69				
19	Ç-19	ETILI	31.6	ISTANBUL			
20	Ç-20	BALABAN	15.9	77	I-1	YALOVA	66.2
BALIKESIR				78	I-2	TUZLA	22
21	B-1	GÜRE	36				
22	B-2	G1-G2 WELLS	42	SAKARYA			
23	B-3	KARAAGAÇ(UYUZ)	31	79	S-1	KUZULUK	51
24	B-4	DERMAN(HAVRAN)	59.5	80	S-2	AK1-2 WELLS	86
25	B-5	D1 WELL	50-60	81	S-3	KIL-TARAKLI	38
26	B-6	EKSIDERE	41-44	82	S-4	ILICA	26.5
27	B-7	GÖNEN	77	83	S-5	GEYVE ALI BABA	25
28	B-8	G1-2-3-4-5 WELLS	74-86	84	S-6	GEYVE ILICAKÖY	27
29	B-9	ZEYTINLIADA	26				
30	B-10	KIZIKKÖYÜ	45.5-51	KOCAELI			
31	B-11	KEPEKLER	60	85	K-1	BAHÇECIK	30.5
32	B-12	K1-WELL	64	86	K-2	YENIKÖY	30
33	B-13	ÖMERKÖY	32	BILECIK			
34	B-14	YILDIZDAG(SALUCAK)	47	87	Bi-1	ÇALTI	36
35	B-15	PAMUKÇU	54.5	TEKIRDAG			
36	B-16	P1-P2 WELLS	56	88	T-1	YARABSIN ÇAMURU	24
37	B-17	HISARKÖY	88	89	T-2	AVSAR	22
38	B-18	EMENDERE	47				
39	B-19	HISARALAN(SINDIRGI)	98	IZMIR			
40	B-20	H1-H2 WELLS	100	90	Iz-1	NEBÜLER GR.	55-57
41	B-21	YENIKÖY	46	91	Iz-2	DIKILI KAPLICASI	42-64
42	B-22	DAGLICASI BALYA	58-63	92	Iz-3	DIKILI WELL	130
43	B-23	GÖKÇEDERE	26	93	Iz-4	GÜZELLIK KAPLICASI	35
44	B-24	ILICA-KEPSUT ESELER	28	94	Iz-5	MAHMUDIYE ILICASI	26
45	B-25	TÜRKÖZÜ-AYVALIK	34	95	Iz-6	DEGIRMEN ILICASI	35
46	B-26	KIRAZKÖY(SAVASTEPE)	40				
47	B-27	ÇATAK	27.1	MANISA			
48	B-28	DUTLUCA	17.4	96	M-1	KINIK IÇMECESI	18
49	B-29	AKÇAKISRAK	16.9	97	M-2	ESKIHISAR ILICASI	39
50	B-30	ACISUDERESI	17.2				
51	B-31	PELITKÖY ILICASI	25.9	KÜTAHYA			
52	B-32	PELITKÖY IÇMECESI	19.9	98	Kü-1	EMET KAPLICALARI	43-47
53	B-33	BÜYÜK ILICA-IVRINDI	36-39	99	Kü-1	NASA KAPLICALARI	43-52
54	B-34	GÖMELI-IVRINDI	28	100	Kü-3	ÇITGÖL ILICASI	96
55	B-35	BOZÖREN	27	101	Kü-4	EYNAL KAPLICALARI	66-78
56	B-36	ESKISU-IVRINDI	21.6	102	Kü-5	YONCAAGAC ILICASI	38-39
57	B-37	KIRAZ	19	103	Kü-6	HAMAMKÖYÜ KAP.	51
58	B-38	DEREKÖY	20	104	Kü-7	SAMRIK ILICASI	43
59	B-39	MENTES	63	105	Kü-8	DERELI ILICASI	39-41

Appendix 1: The list of thermal and mineral springs.

Hydrogeology of Northwestern Turkey

ERDOĞAN YÜZER

Introduction

This article has been prepared as a part of the final volume of the MARMARA Poly-Project and presents hydrogeologic information about Northwestern Turkey obtained from various reports and studies.

The area covered by this report is situated in NW Turkey, around the Marmara sea. The boundaries of the studied region are the Greek and Bulgarian borders and the Aegean sea to the west; the Black sea to the north, the Sakarya river to the east and the line Bakırçay valley-Soma-Sındırgı to the south. The surface area of the region is about 67,000km^2. The main part of the studied area belongs to the Marmara region.

Topography and climate

The region has mountain ranges that are neither very high nor continuous. The hills and mountains of the region are the Yıldız (İstranca) and Samanlı mountains, the Uludağ (2543m a.s.l.), the Kazdağ (1774m a.s.l.) and the Çatalca and Kocaeli hills. The lowlands are the Ergene basin; Adapazarı, Pamukova, Bursa, Gönen, İnegöl and Yenişehir plains; bottom of the Marmara sea; İzmit and Gemlik gulfs; Ulubat, Manyas, İznik and Sapanca lakes.

The Marmara type climate prevails around the Marmara sea, i.e. a transitive climate between the Mediterranean and the Black sea climates. The effect of the Mediterranean climate decreases from south to east. A steppe climate is seen in Bilecik and the Ergene basin. The climate of the Balkans and inner Anatolia prevails from time to time because of the discontinuous mountain ranges. The climate, in general, is hot and dry in the summer and cold and wet in the winter. The annual average snowy days are less than 10, but in Uludağ more than 60. In Sarıyer (İstanbul), the annual average precipitation is 752mm and the average temperature is 13.8°C. In Kırklareli, the annual average precipitation is 576mm and average temperature is 13.2°C. The Mediterranean climate is hot and dry in the summer, warm and wet in the winter. In Bergama, the annual precipitation is 755mm and the average temperature is 16.1°C. The Black sea climate is wet and warm in the summer and wet and cold in the winter. In Bartın (Zonguldak), the annual average precipitation is 1071mm and the average temperature is 13.1°C. Figure 1 shows the average precipitation of the region.

Penman's water budget of Kartal (İstanbul) and Thornthwaite's water budget of Bursa and Bergama are given in Appendices 1, 2 and 3.

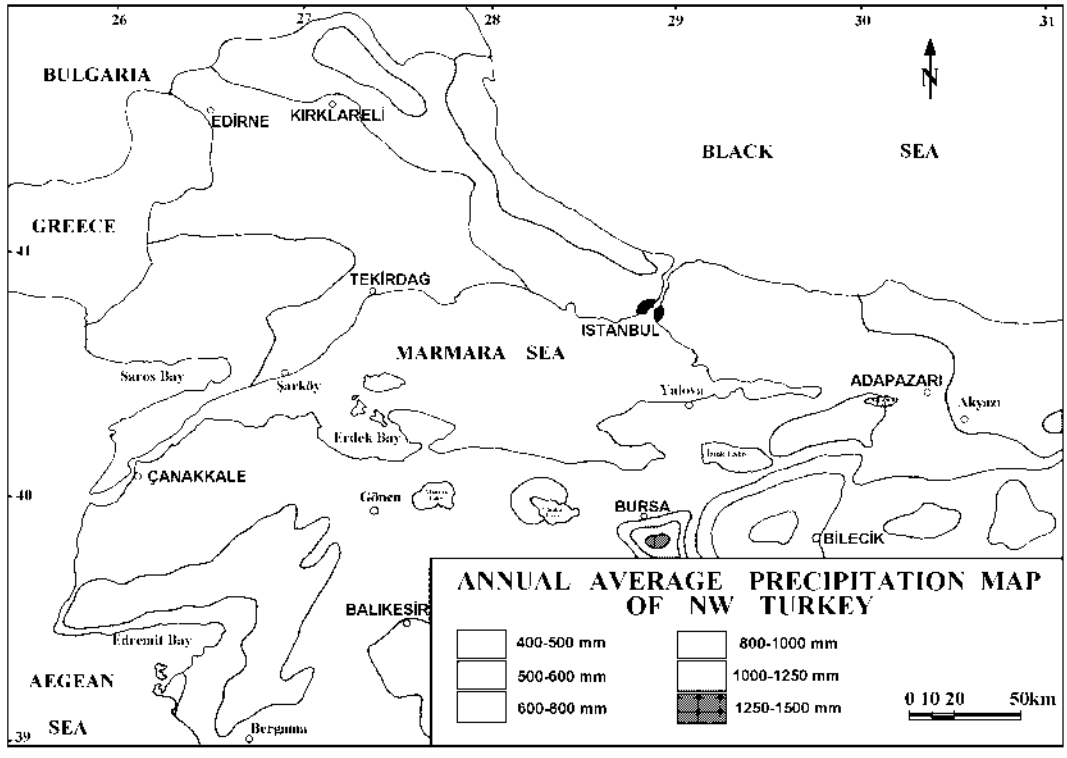


Figure 1: Annual average precipitation map of Northwestern Turkey.

Hydrogeology

The hydrogeological setting of the Marmara region is summarised in this section.

Hydrology

Streams and lakes

The main streams that drain the important plains and lakes in the Marmara region are shown in Appendix A and listed in Appendices 4 and 5. The Ulubat and Manyas lakes are situated in the southern part and the İznik and Sapanca lakes are situated in eastern part of the Marmara region. The Büyük Çekmece and Küçük Çekmece lakes are situated within the boundary of İstanbul.

Wells and springs

The ranges of depth and yield for the drilled wells are given in Appendix 6 and their chemical characteristics are given in Appendix 7. Some cold water springs in the Marmara region, their average yields and their chemical characteristics are listed in Appendix 8. The location of all wells and cold water springs mentioned in Appendices 7 and 8 can be found in Appendix B.

Geological conditions

The Marmara region is covered by a wide variety of igneous, sedimentary and metamorphic rocks ranging in age from Paleozoic to Quaternary.

Paleozoic formations cover a wide area in the Marmara region, such as the Kapıdağ peninsula, Balıkesir, Bursa, İstanbul, the Kocaeli peninsula and Adapazarı-Çamdağ. The Paleozoic formations that are located at both sides of the Bosphorus and Kocaeli peninsula begin with Ordovician and end with Carboniferous. The Ordovician units are composed of some clastic rocks referred to as the Arkose or Kocaeli series. The Silurian units are composed of limestone and shale. The Çarboniferous units are composed of claystone, siltstone and sandstone, which are known as the Trakya (Thrace) series.

The Paleozoic stratification at Çamdağ, that is located between Adapazarı and Düzce, is composed of Ordovician-Silurian age clastic sediments, such as arkose, subarkose and arkosic conglomerates and Devonian age sedimentary oolitic iron deposits. Devonian age rocks overlie the Ordovician-Silurian aged rocks transgressively.

Mesozoic formations are seen from the Triassic to the Upper Cretaceous in the Marmara region. The Paleozoic aged rocks are overlain by the Triassic age rocks unconformably. Also, the Triassic age rocks are overlain by the Cretaceous aged rocks unconformably. The Triassic-Jurassic age rocks begin with a series of red coloured conglomerate-sandstone that is 50-1000m thick at the south of Gebze and Hereke. This series is overlain by yellow coloured clay and fossiliferous limestone. This limestone is overlain by grey coloured and intercalated limestone that has a thickness of 100-300m. Green-grey coloured shales overlie all of these formations.

The Triassic-Jurassic units are transgressively overlain by the Upper Cretaceous age units with an angular unconformity. The Upper Cretaceous age units begin with a 50-100m thick conglomerate and Rudist containing limestone. This unit is overlain by a 150-300m thick white coloured marl intercalated with shale, which in turn is overlain by a 55m thick sandy limestone.

Cenozoic formations are widely seen in the Marmara region, especially in the Thrace basin. The sequence begins with Paleocene that overlies the İstranca massif unconformably. The Paleocene age rocks consist of sandstone, sandy-clay and fossiliferous limestone. Widespread sedimentation is seen in the Eocene. It generally consists of limestone. The Neogene formations are seen in most of the Marmara region which may be seen in continental facies. The thickness of sediments in the Thrace basin reaches up to 6000m.

The *Quaternary age rocks* are mostly seen as alluvium composed of sand, silt and clay.

The *intrusive rocks* of Northwestern Anatolia are generally acidic. They are seen in the İstranca, Uludağ, Çataldağ, Eğrigöz and Kozak massifs, the Kocaeli and Kapıdağ peninsulas and between Balıkesir and Bursa.

The *metamorphic rocks* of the İstranca massif are composed of metagranite, micaschist, marble, calcschist, quartzite and phyllite. The metamorphic rocks seen in Uludağ are gneiss, amphibolite, calcschist and marble overlain by phyllite and recrystallised limestone metamorphosed in greenschist facies The Kazdağ massif is composed of marble, gneiss and amphibolite.

Water bearing properties of rocks

Water bearing properties of the rocks seen in the Marmara region are summarised in the following section and shown on the hydrogeologic map of the region. (Figure 2).

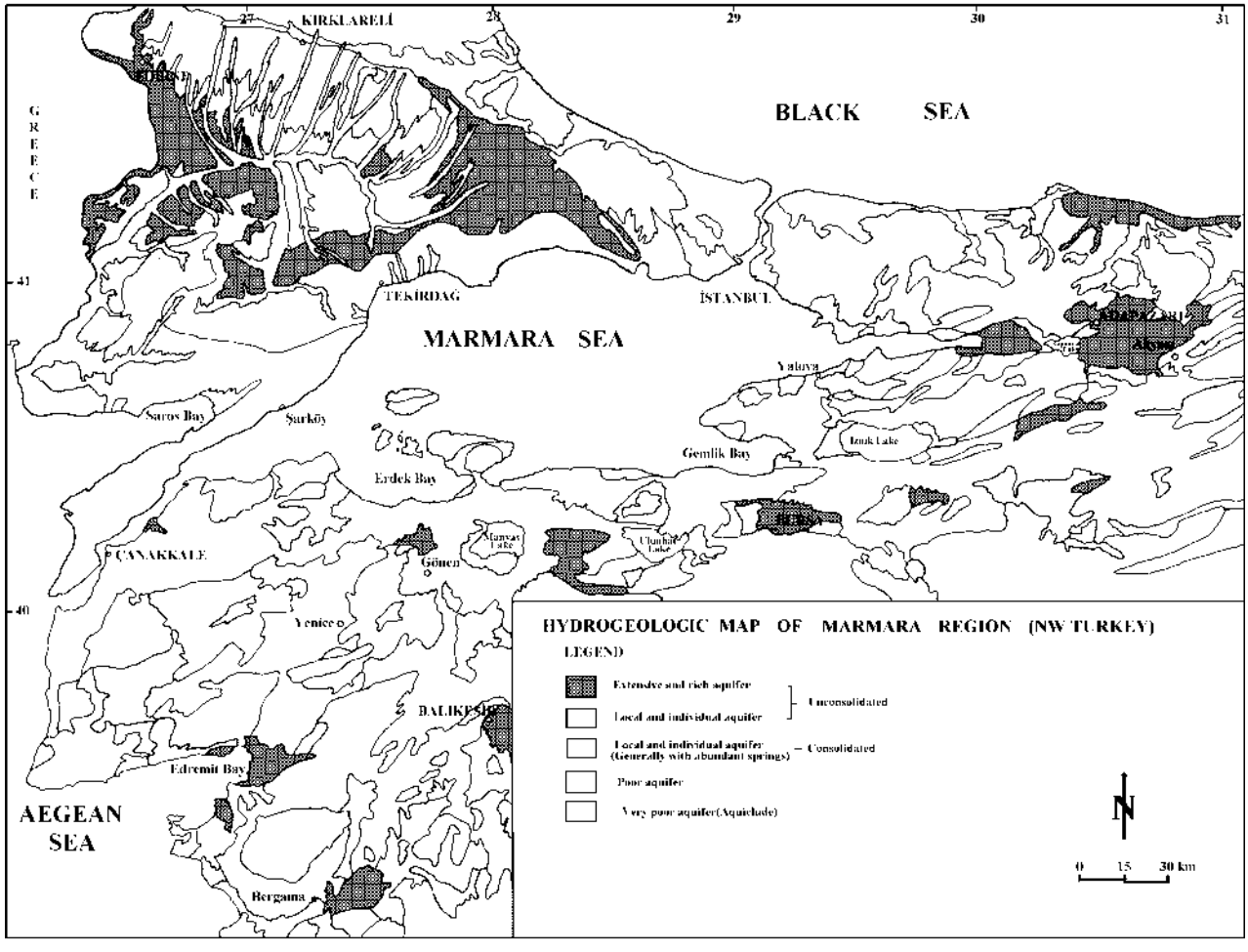


Figure 2: Hydrogeologic map of the Marmara sea region.

Rich and extensive aquifers

Unconsolidated formations (nonindurated sediments), such as Quaternary-Pliocene age alluviums, are generally extensive and rich aquifers. Their groundwater productivities are good. Specific capacities of the wells drilled in these formations are greater than 2l/s/m.

The most important alluvium aquifer of the region is in the Ergene basin. The transmissibility of this aquifer has a range of between 200-2000m/day. Other important alluvium aquifers of the region are seen in Sakarya, Bakırköy (İstanbul), İznik-Orhangazi, Yenişehir, İnegöl, Bursa, Karacabey, Sarıköy-Gönen, Gümüşçay, Yalova, Gemlik and the Kocaeli plains.

Local and individual aquifers

Some Quaternary age alluvia and Neogene age sand-gravel, as unconsolidated formations, and different ages of sandstone, conglomerate, flysch, limestone, marble, tuff, agglomerate, andesite, granite, gabbro, as consolidated formations, are local and individual aquifers. Their groundwater productivities are medium. Specific capacities of the wells drilled in these formations vary between 0.5-2l/s/m.

Poor aquifers

Quaternary, Pliocene-Quaternary and Neogene age clay-sand-gravel as unconsolidated formations, Neogene age sandstone, conglomerate, marl, limestone, tuff and agglomerate, as consolidated formations are poor aquifers. Their groundwater productivities are poor. Specific capacities of the wells drilled in these formations vary between 0.1-0.5l/s/m.

Very poor aquifers

Quaternary, Pliocene-Quaternary age clays and Neogene age clay-sand-gravel as unconsolidated formations, and different ages of well-cemented sandstone and conglomerate, marl, limestone, ophiolitic rocks, schist, quartzite, granite, andesite, peridodite, as consolidated formations are very poor aquifers. Their groundwater productivity is very poor. Specific capacities of the wells drilled in these formations are less than 0.1l/s/m.

Water quality

The electrical conductivity (EC) values of streams and lakes are given in Appendix 9 in order to give information concerning the water quality. The groundwater quality of the pilot wells is given in Appendix 7 and that of the springs in Appendix 8. Groundwater quality is generally suitable for irrigation and domestic use in the Marmara region. But, because of overpumping, groundwater has become salty (saline) in some coastal aquifers such as İstanbul-İzmit, Bakırköy-K.çekmece and the Yalova-Hersek plains. It is also partly contaminated in large cities (such as İstanbul and İzmit) because of leakage from sewers.

In the İznik-Orhangazi-Gemlik plain, the dominant anions are HCO_3-CO_3, hardness is between 13.5-40°fH and EC is 274-1387μS/cm. At the north of Orhangazi the groundwater is corrosive.

In the Silivri-Enez plain, EC is generally between 600-2250μS/cm inland but, at the sea shore and in deep wells, it is greater than 15,000μS/cm. pH values are greater than 7 and hardness is between 3-30°fH. For drinking water, bacteriological analyses are necessary because of high nitrite in some locations.

In the Gölpazarı plain, groundwater quality is sufficient for drinking, domestic use and irrigation.

In the Bursa-Çayırköy plain, the dominant anions are HCO_3-CO_3 and partly incrustative. EC is greater than 1150μS/cm for deep wells.

In the north Ergene plain, the dominant cation and anion are Ca-HCO_3. EC is between 240-700μS/cm, pH 6.8-7.8 and hardness 10-36°fH.

In the Edremit plain, EC is between 250-1500μS/cm, pH 7.5-8.4 and average hardness 20°fH.

Safe yields of the plains

The safe yields of the plains are given in Appendix 10. Because of overpumping, lowering of groundwater level and seawater intrusion are observed in İstanbul-İzmit, Bakırköy-K.çekmece and the Yalova-Hersek plains.

References

Atalay, E., 1977, Ergene Kuzeyi Hidrojeolojik Etüd Raporu, DSİ, Ankara.

DSİ, 1994, Türkiye Akarsu Havzaları Maksimum Akımlar Frekans Analizi, DSİ, Ankara.

EİE, 1994, 1990 Water Year Discharges, EİE Yayın no:94-16, Ankara.

Eisenlohr, T., 1995, Die Thermalquellen der Armutlu-Halbinsel (NW-Türkei) und deren Beziehung zu Geologie und Tektonik. PhD Thesis ETH Zürich Nr. 11340, 165.

Göçmen, M., 1973, Bursa ve Çayırköy Ovaları Hidrojeolojik Etüt Raporu, DSİ, Ankara.

Göçmen, M., Göral, M., and Keleş, N., 1974, İznik, Orhangazi ve Gemlik Ovaları Hidrojeolojik Etüt Raporu, DSİ, Ankara.

Greber, E., 1992, Das Geothermalfeld von Kuzuluk/Adapazarı (NW-Türkei) Geologie, aktive Tektonik, Hydrogeologie, Hydrochemie, Gase und Isotope, Diss. ETHZ, Nr. 9984, 213p.

Imbach, Th., 1992, Thermalwässer von Bursa. Geologische und hydrogeologische Untersuchungen am Berg Uludağ (NW-Türkei), Diss. ETHZ, Nr. 9988, 178p.

Kılıç, R., 1977, İstanbul-İzmit Arası Kıyı Ovaları Hidrojeolojik Etüt Raporu, DSİ, Ankara.

Koç, F., 1976, Bakırçay Havzası Hidrojeolojik Etüt Raporu, DSİ, Ankara.

Murat, M., 1982, İstanbul Boğazı-K.çekmece Arasındaki Önemli Kaynak Suları ve Sarıyer Kaynaklarının Hidrojeolojisi, İTÜ Bsc Thesis, İstanbul.

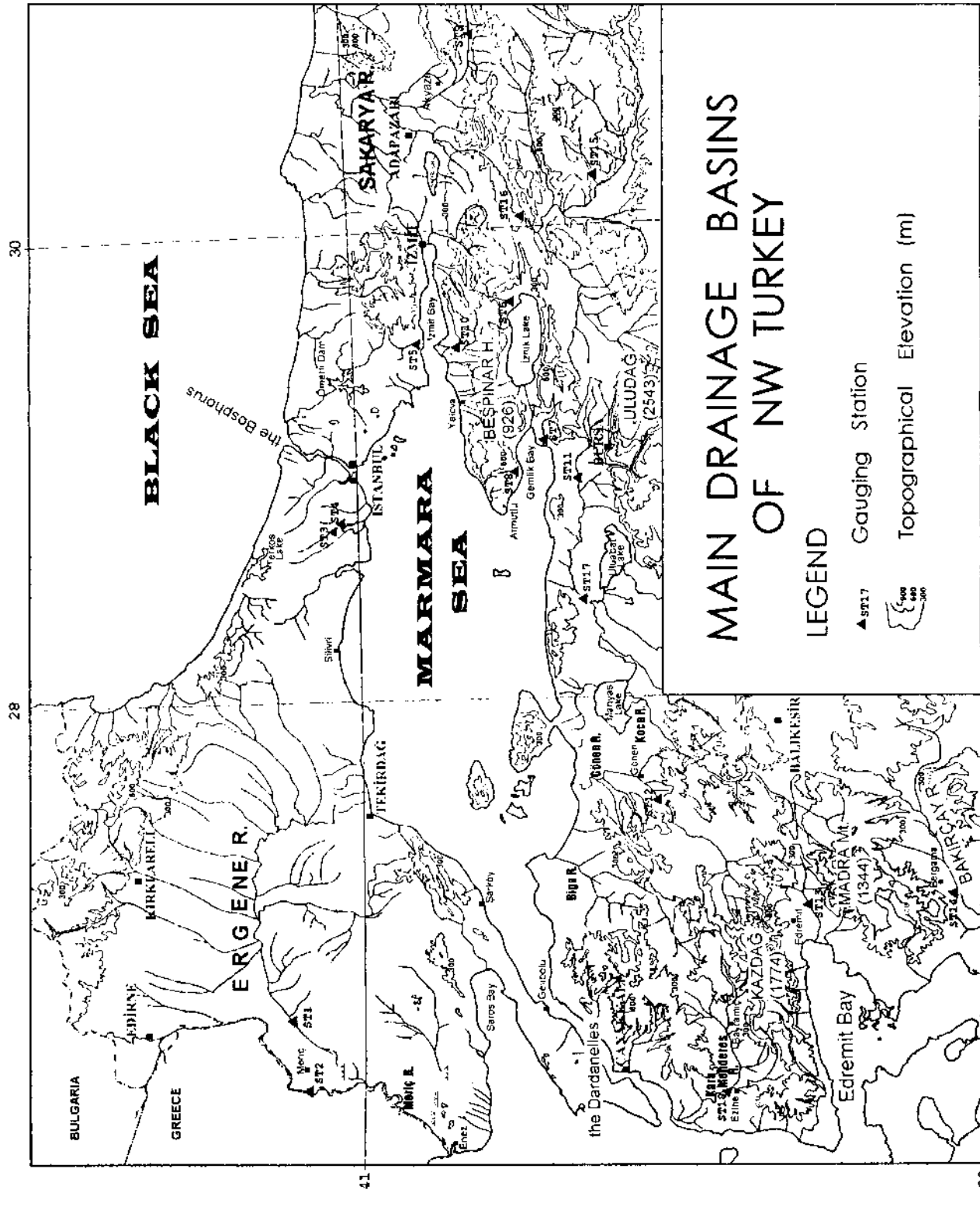
Mützenberg, S., 1991, Westliche Biga Halbinsel (Çanakkale, Türkei): Beziehung zwischen Geologie, Tektonik und Entwicklung der Thermalquellen, Mitt. aus dem geolog. Inst. Der ETHZ und der Univ. Zürich, Neue Folge, Nr. 287, 161p.

Özhan, N., 1977, Edremit ve Armutova (Gömeç) Ovaları Hidrojeolojik Etüt Raporu, DSİ, Ankara.

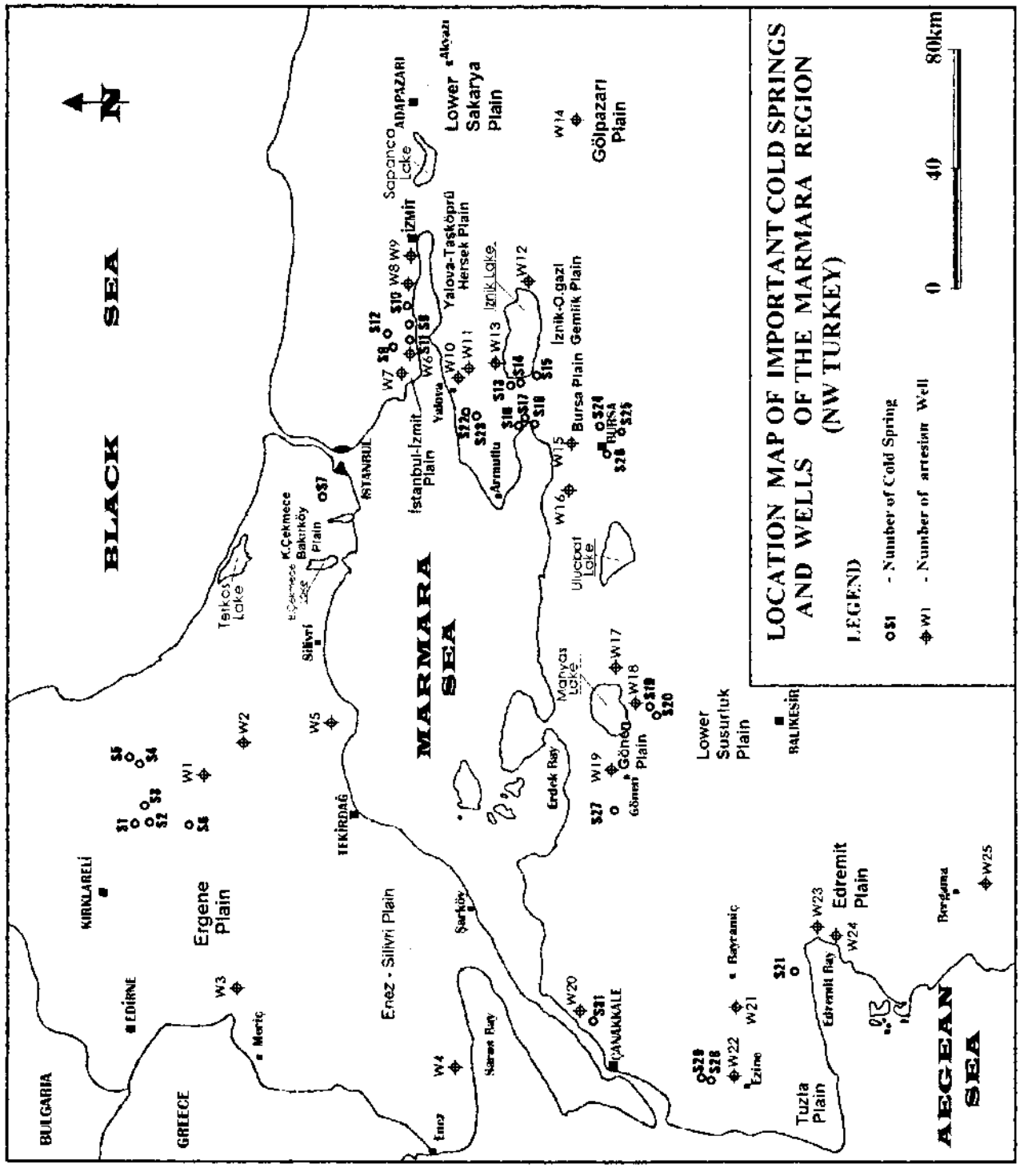
Sökeli, T., 1982, İstanbul-Kemerburgaz-Hamidiye Kaynak Suyu ve Dolayının Hidrojeolojisi, İTÜ BSc Thesis, İstanbul.

Ural, R. and Mumcu, N., 1974, Gölpazarı Ovası Hidrojeolojik Etüt Raporu, DSİ, Ankara.

Appendices



Appendix A: Main drainage basins of Northwestern Turkey.



Appendix B: Location map of important cold springs and wells of the Marmara sea region.

Months	I	II	III	IV	V	VI	VII	VIII	IX	X	XI	XII	annual
Temperature, t, (°C)	6.5	7.0	7.8	12.6	17.2	21.6	24.0	24.2	21.1	16.4	12.6	9.0	15.0
Pot. evapotranspiration ,Ep,(mm)	13.1	21.7	36.6	57.7	84.5	114.8	144.3	123.4	73.1	35.8	21.0	13.8	739.8
Precipitation, P,(mm)	96.5	79.0	71.3	47.7	30.5	19.2	19.9	18.7	46.8	59.8	82.0	109.7	678.1
P-Ep (mm)	83.4	57.3	34.7	-13.0	-54.0	-95.6	-124.4	-104.7	-26.3	24.0	61.0	95.9	-61,7
Reserve water	100.0	100.0	100.0	87.0	33.0	0.0	0.0	0.0	0.0	24.0	85.0	100.0	
Real evapotranspiration, Er, (mm)	13.1	21.7	36.6	57.7	84.5	52.2	19.9	18.7	46.8	35.8	21.0	13.8	421.8
Deficient water (mm)	0.0	0.0	0.0	0.0	0.0	62.6	124.4	104.7	26.3	0.0	0.0	0.0	318.0
Excess water (mm)	83.4	57.3	34.7	0.0	0.0	0.0	0.0	0.0	0.0	0.0	0.0	80.9	256.3
Flow (mm)	62.0	59.6	47.1	23.6	11.8	5.9	3.0	1.5	0.7	0.4	0.2	40.5	256.3
Deficiency of flow according to the precipitation	34.5	19.4	24.2	21.1	18.7	13.3	16.9	17.2	46.1	59.4	81.8	69.2	421.8

Appendix 1: Penman's water budget of Kartal -Istanbul (Kiliç 1977).

Months	I	II	III	IV	V	VI	VII	VIII	IX	X	XI	XII	annual
Temperature, t, (°C)	5.3	5.9	8.0	12.6	17.3	21.6	24.2	23.9	19.7	15.5	11.4	7.5	14,4
Temperature index	1.1	1.3	2.0	4.0	6.5	9.0	11.0	11.0	8.0	5.4	3.4	1.8	5.0
Gross evapotranspiration (mm)	16	19	28	50	75	100	120	118	90	65	45	25	60
Precipitation (mm)	91	85	72	57	56	30	30	16	42	57	77	97	709
Fluctuation of reserve water (mm)	0	0	0	0	-37	-63	0	0	0	0	+40	+77	
Reserve water (mm)	100.0	100.0	100.0	100.0	63	0	0	0	0	0	40	100	
Real evapotranspiration (mm)	13	16	29	55	93	93	30	16	42	57	37	20	388
Deficient water (mm)	0	0	0	0	0	32	121	123	52	5	0	0	333
Excess water (mm)	78	69	43	2	0	0	0	0	0	0	0	17	209
Flow (mm)	43	56	49	25	12	6	3	2	1	0	0	8	209
Deficiency of flow according to the precipitation	48	29	23	32	44	24	7	14	41	57	77	89	388

Appendix 2: Thornhwaite's water budget of Bursa (Göçmen 1973).

Months	I	II	III	IV	V	VI	VII	VIII	IX	X	XI	XII	annual
Temperature, t, (°C)	7.5	8.3	9.7	13.8	18.5	23.1	25.3	25.0	21.3	16.8	13.2	9.6	16.0
Temperature index	1.85	2.15	2.73	4.65	7.25	10.15	11.64	11.44	8.97	6.26	4.35	2.69	74.13
Gross evapotranspiration (mm)	16	19	25	45	75	108	122	118	94	63	42	25	752
Precipitation (mm)	146	94	72	46	40	17	7	5	14	50	109	150	750
Fluctuation of reserve water (mm)	0	0	0	-4	-52	-44	0	0	0	0	+74	+26	
Reserve water (mm)	100	100	100	96	44	0	0	0	0	0	74	100	
Real evapotranspiration (mm)	14	16	26	50	92	61	7	5	14	50	35	21	391
Deficient water (mm)	0	0	0	0	0	73	147	134	84	10	0	0	448
Excess water (mm)	132	78	46	0	0	0	0	0	0	0	0	103	359
Flow (mm)	92	85	66	33	17	8	4	2	1	0	0	51	359
Deficiency of flow according to the precipitation	54	9	6	13	23	9	3	3	13	50	109	99	391

Appendix 3: Thornthwaite's water budget of Bergama (Koç 1976).

Nr.	Name of Stream	Name of Plain	Catchment Area(km^2)	Average Discharge (m3/sec)	Observation Period (year)
ST1	Ergene (Uzunköprü)	Ergene	10194	25.84	22
ST2	Meriç (Meriç Bridge)	Ergene	27250	150	22
ST3	Sazlıdere	K.Çekmece - Bakırköy	84	0.89	11
ST4	Nakkaş	K.Çekmece - Bakırköy	43	0.25	21
ST5	Tavşanlı	İstanbul - İzmit	125	1.125	1
ST6	Karadere	İznik -Orhangazi - Gemlik	220	1.708	18
ST7	Kocadere	İznik -Orhangazi - Gemlik	77	0.7	24
ST8	Olukdere	İznik -Orhangazi - Gemlik	74	0.674	10
ST9	Mudurnu (Dokurcan)	Lower Sakarya (Akyazı)	1072	7.9	34
ST10	Yalakdere	Yalova-Taşköprü - Hersek	262	2.1	17
ST11	Nilüfer (Geçit)	Bursa	1290	16	32
ST12	Gönen (Kumköy)	Gönen	1192	14.6	19
ST13	Havran	Edremit	534	0.988	22
ST14	Bakırçay (Eğrigöl)	Bergama	2887	16	29
ST15	Akçay	Gölpazarı	37	0.13	2
ST16	Sakarya (Mekece)	Sakarya Basin	52372	170	4
ST17	Kocadere	Lower Susurluk Basin	21611	135	38
ST18	Karamenderes (Ezine)	Çanakkale-Bayramiç	1584	12.845	29

Appendix 4: The main streams of the Marmara region.

Nr.	Name of lake	Area of lake (km^2)
L1	İznik	300
L2	Uluabat	240
L3	Manyas	200
L4	Sapanca	60
L5	B.Çekmece used as reservoir	23

Appendix 5: The lakes of the Marmara region.

Name of plain	Depth range (m)	Yield range (lt/sec)
Ergene	30-450	0-40
Bursa	20-300	24-51
İstanbul-İzmit	32-236	0-10
İznik-Orhangazi-Gemlik	10-237	2-53
Yalova-Taşköprü-Hersek	16-243	0-25
Gönen	10-534	0-15
Edremit	33-102	2.5-60
Lower Sakarya-Adapazarı	80-120	20-22
Tuzla	814-1020	0-10
Gölpazarı	18-294	4-16
Bergama	50-250	0.1-36.8
Çanakkale-Bayramiç	31-159	8.1-39.8
K.Çekmece	10-400	0-40
Çanakkale-Lapseki	73-139	17.3-26.7
İzmit-Sapanca	10-180	1-23
Lower Susurluk	28-300	0-40

Appendix 6: Depth and yield ranges of wells in the Marmara region.

Well no	Name of plain	pH	EC (µS/cm)	Na^+	K^+	Ca^{++}	Mg^{++}	$HCO_3^- + CO_3^=$	Cl^-	SO_4^{2-}
W1	Ergene (Ahmetbey)	6.7	570	1.5	21.1	4.2		3.3	0.9	1.5
W2	Ergene (Beyazköy)	7.9	470	1.5	0.6	3.2		3.5	0.8	0.5
W3	Ergene (Pehlivanköy)	8.3	700	5.1	0.1	1.1		0.5	4.4	1.4
W4	Enez	8.3	600	1.4	0.06	4.8		3.9	1.2	1.0
W5	Silivri	7.4	2225	13.2	0.25	8.4		5.1	9.4	7.4
W6	İstanbul-İzmit (Çayırova)	7.9	600	1.6		2.8		4.8	1.1	0.1
W7	İstanbul-İzmit (Dilovası)	8.2	700	2.6		4.9		6.1	0.4	0.9
W8	İstanbul-İzmit (Yarımca)	8.2	740	2.5		6.2		4.7	1.8	2.2
W9	İstanbul-İzmit (Derince)	7.9	500	0.7		4.6		2.9	0.7	1.7
W10	Yalova-Taşköprü-Hersek	-	370	1.1		2.8		2.4	0.4	1.0
W11	Yalova-Taşköprü-Hersek	-	1600	13.0		2.4		7.0	7.0	1.6
W12	İznik-Orhangazi-Gemlik (İznik)	-	800	1.3		4.2	2.9	6.9	0.5	1.3
W13	İznik-Orhangazi-Gemlik (Orhangazi)	-	456	2.3		2.9		4.2	0.5	0.5
W14	Gölpazarı	-	620	1.6		3.3	1.1	5.0	0.3	0.4
W15	Bursa-Çayırköy (Bursa)	-	1150	2.5	0.1	8.0		4.5	3.0	4.5
W16	Bursa-Çayırköy (Çayırköy)	-	530	0.7	0.1	5.0		5.0	0.3	0.8
W17	Lower Susurluk (Karacabey)	7.5	560	1.8	0.0	1.7	1.9	4.0	0.5	1.2
W18	Lower Susurluk (Manyas)	8.2	730	4.2	0.0	2.2		5.3	1.3	0.8
W19	Gönen	7.9	400	0.7	0.07	2.3	1.1	3.5	0.3	0.3
W20	Çanakkale-Lapseki	8.2	1800	8.7	0.2	5.7	3.3	4.0	10.6	5.2
W21	Çanakkale-Bayramiç	8.1	700	1.0	0.1	4.7	1.0	5.4	0.9	0.4
W22	Çanakkale-Bayramiç	7.9	680	1.7	0.1	3.7	1.2	4.9	1.1	0.6
W23	Edremit	7.3	860	4.2	0.1	4.1	0.3	2.7	1.1	4.8
W24	Edremit	8.1	1000	3.5	0.1	4.2	2.9	5.8	1.0	4.0
W25	Bergama	7.3	660	1.3		5.5		5.4	0.6	0.8

Appendix 7: Chemical characteristics of drilled wells by DSİ (values in mval/l).

Spring no	Name of Spring	Name of plain	Average yield of spring (lt/sec)	pH	EC (µS/cm)	Na^{+}	K^{+}	Ca^{++}	Mg^{++}	$HCO_3^{-} + CO_3^{=}$	Cl^{-}	SO_4^{2-}
S1	Kaynarca	North Ergene	480	7.5	530	0.70	0.02		5.00	4.10	0.80	0.87
S2	Pınarhisar	North Ergene	65	7.1	530	0.50	0.04		5.00	4.30	0.68	0.56
S3	Poyralı	North Ergene	95	7.3	540	0.60	0.06		4.80	4.20	0.68	0.58
S4	Karpuzkaldıran	North Ergene	80	7.4	550	0.41	0.04		5.10	4.60	0.56	0.39
S5	Balkaya	North Ergene	350	7.5	600	0.36	0.03		5.70	5.40	0.41	0.25
S6	Kocakaynak	Ergene	357-560	8.2	500	0.58	0.11		4.20	3.40	0.68	0.81
S7	Altınşehir	K.Çekmece-Bakırköy	35	7.3	450	0.70	0.00	3.90	0.05	1.00	0.94	1.66
S8	Ovabaşı	İstanbul-İzmit(Dilovası)	24	7.5	670	0.30	0.04		6.60	6.31	0.40	0.23
S9	Küplü	İstanbul-İzmit(Dilovası)	17	7.4	510	0.16	0.04		4.90	4.68	0.24	0.18
S10	Ulupınar	İstanbul-İzmit(Dilovası)	100	7.1	800	0.94	0.02		6.90	5.86	1.08	1.15
S11	Ballıkaya	İstanbul-İzmit(Dilovası)	13	7.8	360	0.31	0.03		3.50	3.06	0.36	0.42
S12	Çayıraçma	İstanbul-İzmit(Dilovası)	28	7.6	630	0.21	0.05		6.40	6.08	0.36	0.22
S13	Nadir	İznik-Orhangazi-Gemlik	100	6.8	380	0.12	0.01	3.98	0.38	4.10	0.11	0.12
S14	Gedelek	İznik-Orhangazi-Gemlik	130	6.8	460	0.13	0.01	4.77	0.39	4.90	0.11	0.12
S15	Karsak	İznik-Orhangazi-Gemlik	2	7.0	595	0.34	0.03	5.70	0.64	5.96	0.44	0.26
S16	İlıpınar	İznik-Orhangazi-Gemlik	100	6.5	560	0.34	0.04	5.35	0.70	5.19	0.27	0.21
S17	Kumla	İznik-Orhangazi-Gemlik	100	6.3	344	0.15	0.02	3.21	0.47	3.54	0.11	0.13
S18	Cihatlı	İznik-Orhangazi-Gemlik	40	7.2	500	0.23	0.01	5.00	0.60	4.92	0.22	0.38
S19	Hacıyakup	Lower Susurluk	173	7.7	470	0.31	0.04		3.70	3.24	0.40	0.41
S20	Değirmenboğazı	Lower Susurluk	100-150	8.0	350	0.41	0.05		2.70	2.36	0.54	0.26
S21	Güre	Edremit	150	7.5	186	-	-		2.10	1.70	0.40	-
S22	Sellimandıra1	Yalova-Taşköprü-Hersek	20	8.3	480	1.55	0.66		3.50	2.10	0.50	2.50
S23	Sellimandıra2	Yalova-Taşköprü-Hersek	20	-	-	-	-	-	-	-	-	-
S24	Karapınar	Bursa	276-2383	7.2	353	0.09	0.06	3.20	0.66	3.30	0.13	0.52
S25	Pınarbaşı	Bursa	43-582	6.8	502	0.30	0.05	2.65	1.25	3.52	0.21	0.31
S26	İnkaya	Bursa	50	7.4	484	0.22	0.03	3.80	1.66	4.65	0.16	0.73
S27	Hafızhüseyinbey	Gönen	7	7.3	600	0.26	0.04	3.80	1.07	4.50	0.32	0.20
S28	Pınarbaşı	Çanakkale-Bayramiç	600-1500	-	-	-	-	-	-	-	-	-
S29	Kokana	Çanakkale-Bayramiç	50	-	-	-	-	-	-	-	-	-
S30	Akpınar	Çanakkale-Lapseki	10	-	-	-	-	-	-	-	-	-

Appendix 8: Chemical characteristics and average yields of springs (values in mval/l).

Nr.	EC(μS/cm)
ST5	540
ST6	400-680
ST10	500
ST11	290-500
ST12	400
ST13	400-480
L1	1150-1300
L2	<1500
L3	<1500

Appendix 9: Electric conductivity (EC) values of some streams and lakes.

Name of plain	Safe yield ($x10^6$ m^3/year)
North Ergene	45.5
Ergene	274
İstanbul-İzmit	10
Gönen	29
İznik-Orhangazi-Gemlik	39.5
Yalova-Taşköprü-Hersek	15
Bursa	40
Edremit-Armutova	64.5
Lower Sakarya(Akyazı)	65
Bakırçay-Bergama	45
Gölpazarı	2.45
Lower Susurluk	72.5
Çanakkale-Bayramiç	26
Enez-Silivri	17.5
K.Çekmece-Bakırköy	11
İzmit-Sapanca	37

Appendix 10: The estimated safe yields (by DSİ) of some plains of the Marmara region.

THEME 4

Recent investigations in geology and hydrogeology

Stratigraphic evolution and tectonics in an area of high seismicity: Akyazı/Adapazarı (Pontides, Northwestern Turkey)

EMIL GREBER

Abstract

In the western Keremali mountains (southernmost İstanbul zone), the metamorphic basement is overlain by Upper Cretaceous to probably Miocene sediments and volcanics. The complex geological situation is, to some extent, due to paleo-Alpine (Late Cretaceous-Paleocene) syn-sedimentary tectonics. Typical features are locally restricted occurrences of lithologies, rapid lateral and vertical changes in the stratigraphic columns, neighbouring zones of erosion and accumulation and the predominance of coarse clastic sediments. This paleo-Alpine phase was followed by the main-Alpine phase (Early Eocene), which is related to the juxtaposition of the İstanbul and Sakarya zone and the consumption of the Intra-Pontide ocean. This phase is associated with a regional uplift combined with a tilting and slight folding of the strata and widespread volcanism in the study area. Relicts of the Intra-Pontide ocean in the form of serpentinite lenses are exposed in the southernmost study area (Civek zone). The neotectonic (Miocene-present) North Anatolian Fault Zone (NAFZ) overprinted the whole study area and reactivated the Intra-Pontide suture as a right-lateral fault zone.

Introduction

In the framework of the MARMARA Poly-Project, an area of some 120km^2 was mapped in the western Keremali mountains (Figs. 1 and 2) during the summer months of 1989 to 1991 (Greber 1992).

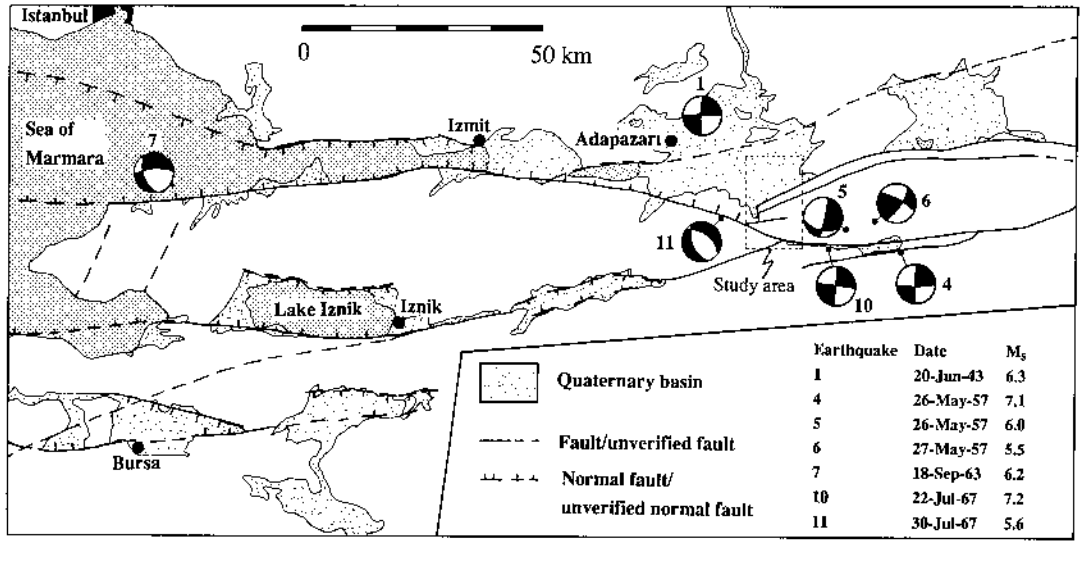


Figure 1: Tectonic overview of the western North Anatolian Transform Fault. Numbers of fault mechanism solutions refer to Fig. 1 and Table 1 in Eyidoğan (1988).

Little previous geological field work has been carried out in the area of Akyazı in the province of Sakarya. The first known geological studies were carried out by Lucius (1929). His work, however, was concentrated on a very limited area around the Kuzuluk thermal springs. The first geological map, including the closer surroundings of the Kuzuluk thermal field, was drawn up by Rupprecht (1955). Detailed, more regional studies of the western Keremali mountains have never been published.

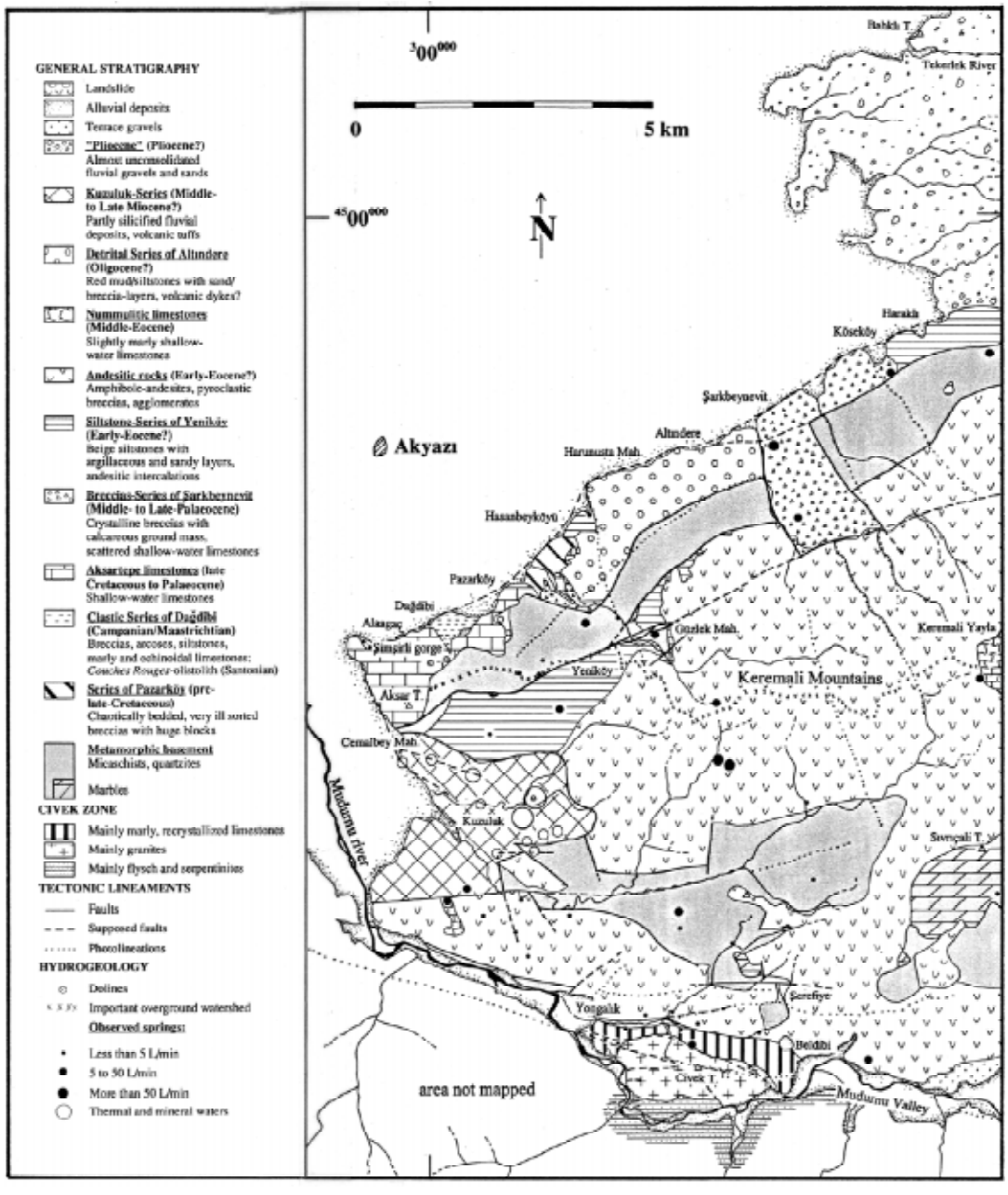


Figure 2: Geological map of the Akyazı/Adapazarı area.

During the author's field work, the stratigraphic and tectonic relationships soon turned out to be of extraordinary complexity. Many stratigraphic units were encountered that had never been described before. Dating of some of these units helped considerably to clarify the stratigraphic charts.

The study area is of special geological interest as it covers two different tectonic zones, mostly the southern İstanbul zone and a small part of the northern Sakarya zone, which are separated by a complex suture zone, the Intra-Pontide suture (e.g. Şengör et al. 1985, Okay 1989). The *İstanbul zone* is characterised by an Ordovician to Carboniferous sedimentary sequence of passive continental margin affinity, which rests unconformably on a Precambrian metamorphic basement and which was deformed during the Permian-Carboniferous. These sediments are overlain with a major angular unconformity by uppermost Permian to Paleocene sediments (Okay 1989, Okay et al. 1994). The *Sakarya zone* contains no in situ Paleozoic sedimentary rocks and underwent strong deformation and metamorphism in the Late Triassic (Şengör and Yılmaz 1981, Okay 1989). This metamorphosed complex is unconformably overlain by Liassic to Paleocene sediments (Okay 1989). The *Intra-Pontide suture*, which separates the İstanbul from the Sakarya zone, is the remnant of the Mesozoic Intra-Pontide ocean, which was at least 300km wide during Albian-Cenomanian time according to Okay et al. (1994). Today, it is marked by slivers of serpentinite, blueschist, basic volcanic rock and Upper Cretaceous to middle Paleocene pelagic limestone (Şengör and Yılmaz 1981). Outcrops of such an ophiolite suite are found in the Mudurnu valley, just some 10km east of the study area (Yılmaz et al. 1982). Adamia et al. (1981), however, interpret the scattered ophiolite outcrops of the Mudurnu valley as relicts of a Paleozoic ocean.

The area of Akyazı is also well-known as a zone of high seismicity. These tectonic activities are related to the westward movement of the continental escape wedge of the Turkish plate (McKenzie 1972) or Anatolian block (Barka 1992) along the *North Anatolian Fault Zone* (NAFZ) (Barka 1992, Şengör 1979).

This paper emphasises the stratigraphic situation of the western Keremali mountains, including some new age determinations. In addition, a preliminary tectonic evaluation is given.

Stratigraphy

Introduction

Low-grade metamorphic rocks, belonging to an east-west striking crystalline lens measuring roughly 45km in length and 20km across (MTA 1964), are overlain by non-metamorphic Late Cretaceous and younger sediments and volcanic rocks (Fig. 2). The stratigraphic columns vary considerably from place to place, especially at the northwestern slope of the Keremali mountains. For this reason, an idealised stratigraphic composite section is presented in Fig. 3. As many new stratigraphic units were encountered which cannot be correlated with neighbouring areas up to now, an informal categorisation of the units was chosen. The denominations of the series were taken from local villages.

Metamorphic basement

The metamorphic basement mainly consists of micaschists, and, to a lesser amount, of quartzites, recrystallised limestones and marbles. Based on newly-formed minerals, such as chlorite, muscovite and quartz as well as on the well accentuated parallel texture, a low-grade greenschist metamorphism can be attributed to these metasediments. The age of this metamorphism, however, is controversial. Whereas Yılmaz et al. (1982) report Middle Devonian fossils in recrystallised limestones of the basement some 10km east of the study area, Abdüsselamoğlu (1959) found non-metamorphic sediments of Devonian age in the same area. If the more supraregional works (Brinkmann 1976, Van der Kaaden 1971, Kalafatçıoğlu and Uysallı 1964) are taken into account, an old Caledonian or even older metamorphism also seems reasonable.

The metamorphic basement is overlain with a disconformity by younger, non-metamorphic series. During the Late Cretaceous and Early Tertiary times it mainly acted as a major zone of erosion.

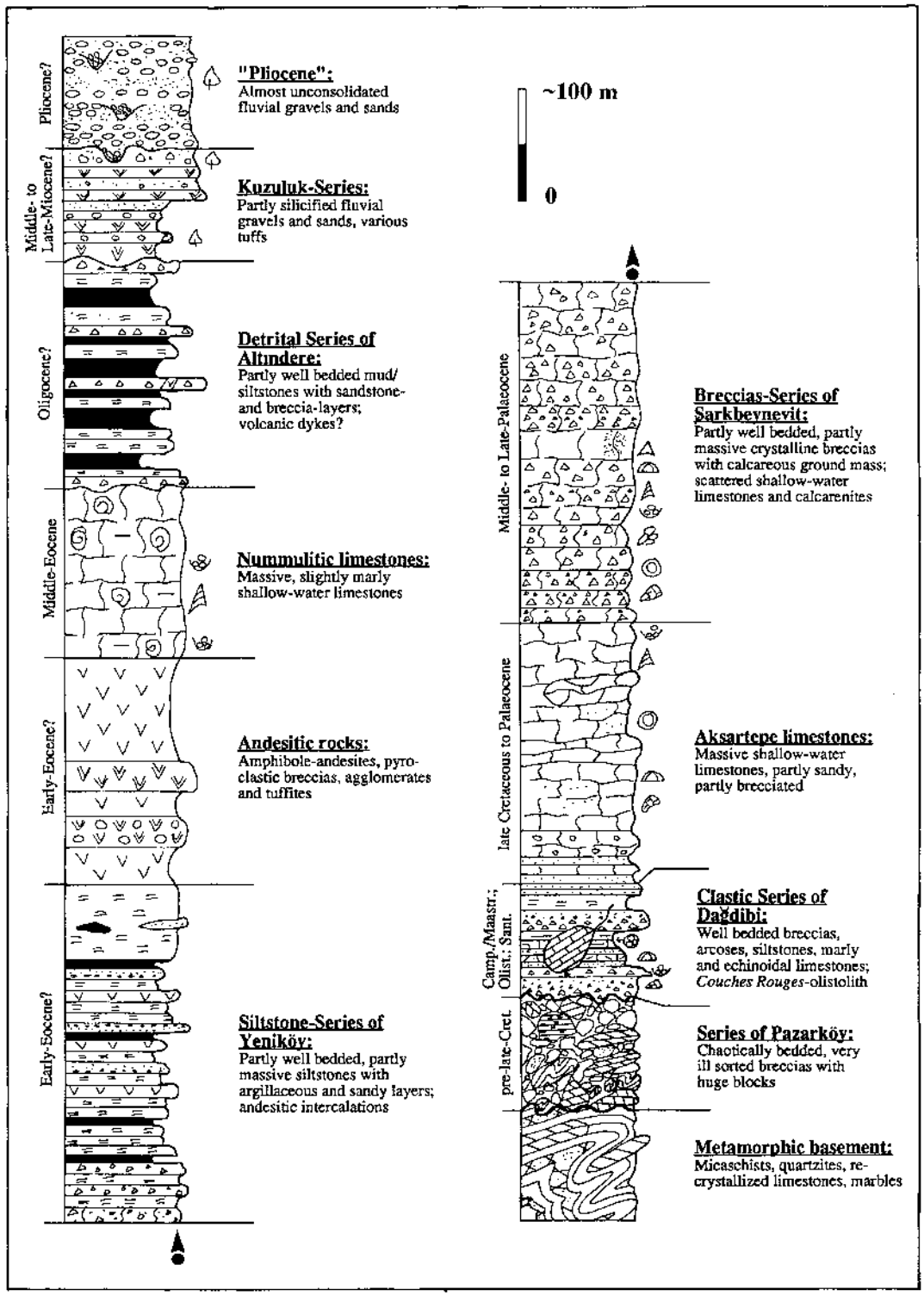
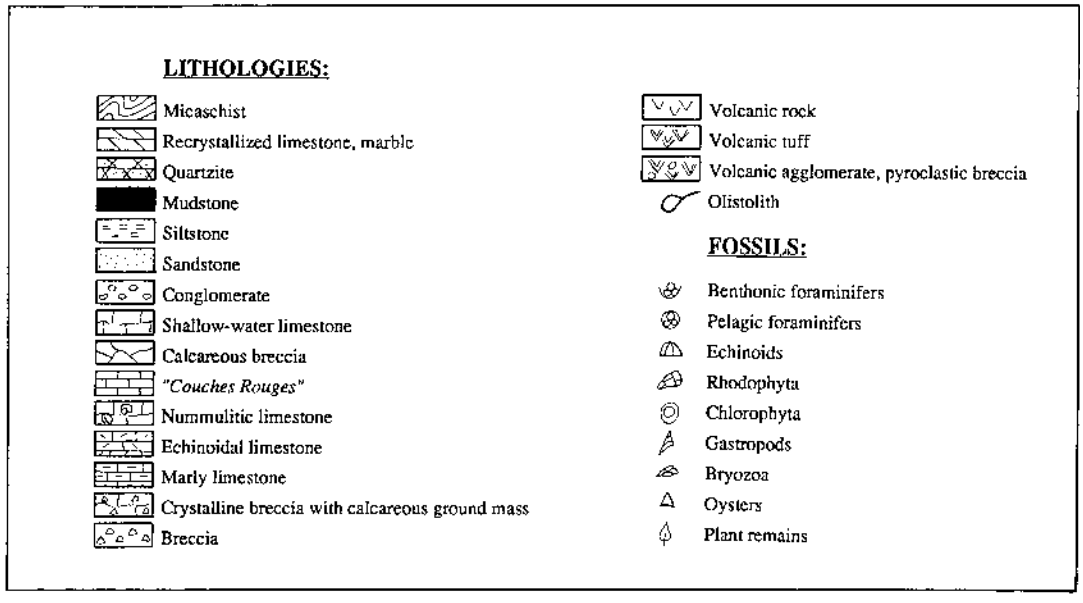


Figure 3: Idealised stratigraphic composite section of the Akyazı/Adapazarı area.



Legend of Figure 3.

The Pazarköy series

This series consists of very coarsely blocked, polymictic mega-breccias. Among the heterogenic, poorly sorted components are dark, recrystallised limestones, larger parts of micaschists, up to metre-thick white, fine-grained marbles, low-grade metamorphic sandy marbles and brown, slatey siltstones. In the upper part, sandstones with clasts of fine-crystalline marbles and sandy, calcareous slates predominate in addition to dark, recrystallised limestones. A groundmass is virtually missing in the whole series. Based on the rather chaotic character of this series, the material must have been transported rapidly over a short distance only. A sedimentological origin – although perhaps released by a tectonic event – seems to be more probable than a tectonic one. The occurrence of the series is solely local.

The series is overlain with a disconformity by the Upper Cretaceous to Paleocene Aksartepe limestones. Thus, the series must be older than Late Cretaceous.

The Dağdibi clastic series

This series is a heterolithic succession of mostly well-bedded fine-grained breccias with crystalline components, echinoidal limestones, arkoses, quartzitic sandstones, siltstones and marly limestones. Whereas the base is unknown, the series shows a transition zone of about 10m thickness into the overlying Aksartepe limestones (Şimşirli gorge, 140 to 150m above sea level). The following fossils were determined by Dr. J.-P. Beckmann, ETH Zürich:

- in echinoidal limestones: fragment of *Orbitoides* (Campanian-Maastrichtian) and *Lepidorbitoides ?* (Maastrichtian)
- in fine-grained breccias: *Siderolites*, *Lepidorbitoides* (both Maastrichtian) and fragments of *rudists* (typical for Late Cretaceous)

The series thus contains fragments of Campanian and Maastrichtian age. It is, in turn, concordantly overlain by Aksartepe limestones, which were deposited at the Cretaceous/Tertiary transition time. From this, a Late Cretaceous age, probably Campanian/Maastrichtian, can be postulated for the series.

Within this series, an olistolith measuring some 100m^3 was encountered, consisting of reddish to dark-grey biomicrites very similar to the Penninic Couches Rouges limestones of the Swiss Alps. The olistolith was dated by means of planktonic foraminifera by Prof. Dr. M. Caron, University of Fribourg:

- one fragment of *Dicarinella concavata* (Late Coniacian to Early Santonian)
- one fragment and one well-preserved specimen of *Dicarinella asymetrica* (Late Santonian)

A Late Santonian age is thus attributed to the olistolith.

The mostly crystalline detritus may have originated from a tectonically uplifted erosion ridge situated to the south, where the metamorphic basement is denuded or overlain by Eocene andesites only.

The rather small outcrops of this series might be correlated with rocks of similar age and facies in the area of Mudurnu (Abdüsselamoğlu 1959). Biomicrites comparable to those of the encountered olistolith are reported from the area between Gemlik and Bursa (Erk 1942). Couches Rouges were also observed in southern Thrace by Schindler (in Kopp et al. 1969).

Aksartepe limestones

The Aksartepe limestones are grey extra-pel-bio-micrites that overlie different, older series: (1) In the region of the Aksartepe, a disconformity is observed between the crystalline basement and the limestones. In a 250m thermal water well within the tectonic Kuzuluk basin (see below), micaschists are also overlain discordantly by approximately 95m of Aksartepe limestones. The same relationship may exist in a small outcrop of about 400m^2 of Aksartepe limestones, just some 400m northeast of the well in the same basin. (2) At Dağdibi a stratigraphic transition from the clastic Dağdibi series to the Aksartepe limestones over a short vertical distance of 10m is observed. (3) Near Pazarköy, the Aksartepe limestones overlie the Pazarköy series with a pronounced disconformity.

The fossil assemblages, including Rhodophyta, Chlorophyta, Textulariina, Miliolidae, Rotaliidae, Gastropods and Echinoidea, clearly indicate a lagoonal depositional environment. Clastic material is restricted to the base of the series. Age determinations using especially calcareous algae were carried out by Dr. J.-P. Beckmann, ETH Zürich:

- at the base of the Aksartepe limestones in fine-grained sandstones near Dağdibi: reworked *Globotruncana* (Campanian, possibly Early Maastrichtian)
- outcrop within the Kuzuluk basin: *Glomalveolina primaeva ?* (Late Paleocene), *Distichoplax biserialis* (Paleocene to Early Eocene) and *Parachaetetes* (probably Eocene)
- near Aksartepe: poorly-preserved calcareous algae showing somewhat older ages than the limestones in the Kuzuluk basin

Near Pazarköy, the Aksartepe limestones are concordantly overlain by the Middle to Upper Paleocene breccias series of Şarkbeynevit. From this, a Late Cretaceous to Early Paleocene age is postulated for the Aksartepe limestones in this area. For the Aksartepe limestones in the Kuzuluk basin, however, ages up to Late Paleocene cannot be excluded.

As clastic material is restricted to the base of the series, the Early Paleocene was probably a tectonically quiet period. Shallowing, or even complete drying of the marine basins were also observed in the surrounding areas (Yılmaz et al. 1982, Abdüsselamoğlu 1959, Kalafatçıoğlu and Uysallı 1964).

Breccias series of Şarkbeynevit

This series consists mainly of grain-supported, well-bedded breccias, that are consolidated with slightly sandy micrite or pseudosparite. Among the components are predominantly quartz pebbles, fine-grained marbles and micaschists and also, in small amounts, marly limestones, crystal fragments of quartz and feldspar, micritic intraclasts and reddish, marly to sandy limestones with poorly-preserved pelagic foraminifera.

The occurrence of this series is restricted to the areas southeast of Pazarköy and south of Şarkbeynevit. Whereas near Pazarköy the breccias are well-bedded and most layers are well sorted, they are massive, only moderately to poorly sorted and with additional biomicrite layers without any extraclasts near Şarkbeynevit.

In the area of Pazarköy, the breccias cover concordantly Aksartepe limestones and are probably discordantly overlain by the distinctly younger Altındere detrital series. The stratigraphic base of the breccias does not outcrop in the area of Şarkbeynevit. Southwest of Haraklı, they are overlain by the siltstone series of Yeniköy.

The breccias contain numerous fossils such as Rhodophyta, Chlorophyta, Gastropods and Echinoidea. Because of good preservation and lack of encrustation, these fossils can be considered as being only slightly reworked. The following age determinations were carried out by Dr. J.-P. Beckmann:

- *Planorbulina cretae* sp. (Santonian to Early Eocene)
- *Parachaetetes* sp. (Paleocene to Early Eocene)
- *Lithothamnium* sp. (probably since Campanian)
- *Planorbulina cretae* sp.? (Santonian to Early-Eocene)
- *Daviesina* sp.? (Latest Cretaceous to Paleocene)
- *Discocyclina* sp. (Middle Paleocene to Eocene)
- *Miscellanea* sp.? (Paleocene, possibly Earliest Eocene)

From this, the breccias must be younger than Middle Paleocene. From the geological context, a Middle to Upper Paleocene age seems to be most probable.

The breccias were deposited in a lagoonal environment similar to that of the Aksartepe limestones, but the sedimentation was disturbed by the supply of detritus. The predominantly crystalline nature of the components indicate erosion in the metamorphic hinterland, possibly caused by tectonic uplifts.

The breccias might be correlated with lagoonal sediments southwest of Mudurnu (Abdüsselamoğlu 1959) and terrestrial detrital sediments with volcanic layers in the region of Nallihan (Kalafatçıoğlu and Uysallı 1964). The Paleocene of that region is thus characterised by shallow marine basins, terrestrial depressions and wide, denuded areas.

Yeniköy siltstone series

In the triangle Kuzuluk-Yeniköy-Güzlek-Mah., this series consists of beige, well-bedded siltstones with some sandy and clayey layers. The layer thicknesses vary between several centimetres and a few decimetres. Furthermore, several andesitic layers are intercalated within this series, representing the first signs of volcanic activity in this region. Here, the series most probably overlies the metamorphic basement with a disconformity, indicated by calcareously cemented breccias in the lower part of the series (800m NNE of Cemalbey Mah.). The contact, however, is exposed nowhere. Towards the southeast, the series is overlain by Eocene andesites.

Near Hasanbeyköyü, the Yeniköy siltstone series is encountered between two disconformities: above the Pazarköy series and below the Altındere detrital series. Here, the basal part of the series is sandy to breccious. The main part, however, is dominated by well-bedded siltstones. No volcanic layers were encountered in this area.

Between Köseköy and Haraklı, the Yeniköy siltstone series is found above the breccias series of Şarkbeynevit. The contact in-between is not clear, but may well be of stratigraphic nature. Siltstones with sporadic sandstone and fine-grained breccia layers dominate here as well. But, in contrast to the other regions, their texture is massive. The thicknesses of the Yeniköy siltstone series vary from place to place, with maximum thicknesses in the area Kuzuluk-Yeniköy-Güzlek-Mah. of several hundred metres.

The fine-grained and quietly-bedded sediments of the Yeniköy siltstone series that do not show any erosional feature represent a calm sedimentation in a marine basin protected from coarse detritus. Probably at the end of the Paleocene, a change in paleogeography occurred. In comparison to the sedimentary environment of the Aksartepe limestones and the breccias series of Şarkbeynevit, a slight subsidence occurred that also affected former erosional areas. The volcanic layers may be best interpreted as intruded sills.

Although the series lacks fossils, an Early Eocene age may be postulated from stratigraphic relations (see above). The Early Eocene was characterised by wide-spread flysch sedimentation in Northwestern Turkey. Although the Yeniköy siltstone series shows rather few features of a classical flysch sequence, its lithological similarities to the wide flysch areas (e.g. south of the Mudurnu river, north of lake Sapanca) are obvious. Furthermore, very similar, fine-grained sediments are also found in the southernmost study area, namely in the Civek zone just north of the Mudurnu river. In contrast to the north, however, the succession here is dominated by breccious slumps, thus showing much more affinity to a typical flysch sequence.

Andesitic rocks

Large areas of the study area are covered by volcanic rocks that overlie discordantly the Yeniköy siltstone series along the northern belt of the Keremali mountains and the metamorphic basement more to the south. Up on the Keremali Yayla, the volcanic rocks are overlain by Nummulitic limestones, from which they are separated by a probably rather weak disconformity.

Mostly reddish or green-beige amphibole-andesites predominate, whereas pyroclastic breccias and agglomerates are less frequent. At the Yaylamın Tepe, the basement is covered by a volcanic breccia with reworked quartzite and micaschist fragments.

The presence of lapillis, the predominant red colours and missing signs of submarine deposition indicate a partly explosive, subaerial volcanism. The rocks belong to a calc-alkalic series typical for orogenic mountain chains. The volcanism can be attributed either to the closing of the Intra-Pontide ocean situated south of the İstanbul zone and north of the Sakarya zone as postulated by Şengör and Yılmaz (1981, see also Okay et al. 1994) or to the north-vergent subduction of the İzmir-Ankara ocean.

As the volcanic rocks are overlain on the Keremali Yayla and in Topcusırtı Mah. (Kuzuluk) by Middle Eocene Nummulitic limestones, an Early Eocene age can be postulated. Similar volcanic rocks cover large parts of Northwestern Turkey, especially southeast of Bolu and south of Zonguldak (see geological map of Zonguldak: MTA 1964).

Nummulitic limestones

The highest peaks of the Keremali mountains (maximum elevation: Keremali Tepe with 1543m a.s.l.) consist of Nummulitic limestones that cover the volcanic rocks. In Topcusırtı (Kuzuluk), a rather small outcrop of Nummulitic limestones that also overlie volcanic rocks was encountered. Here, the stratigraphic contact, which is of slightly discordant nature, is 1000m closer to sea level than in the Keremali mountains.

The series consists of poorly-bedded, grey, slightly marly shallow-water limestones. Among the macrofossils are Assilines, Nummulites and Gastropods. Prof. Dr. R. Herb, University of Bern, determined the age of the Nummulitic limestones by *Assilina spira* and Nummulites as Early to middle Lutetian (Middle Eocene). In the Keremali mountains, the thickness of the series is estimated to be in the range of several hundred metres.

The deposition of these limestones occurred in a shallow basin of probably less than 200m water depth. Nummulitic limestones are a typical facies type of the northern Tethys realm of that geologic period (Trümpy 1980). These limestones testify a last transgression in the Middle Eocene after which the sea retreated definitively from that part of Turkey. It may be argued that at no other geological period since the Late Cretaceous such vast areas of the western Keremali mountains were flooded. Other Nummulitic limestones are found south of the Mudurnu river (northernmost Sakarya zone), where they cover siltstones with breccious intercalations, south of Gemlik/lake İznik (Erk 1942) or in southern Thrace (Kopp et al. 1969).

Altındere detrital series

The occurrence of this series is restricted to an area in the northern Keremali mountains on the mountainside facing the villages Hasanbeyköyü, Harunusta Mah. and Altındere. Smaller outcrops are found south of Pazarköy. The series overlies discordantly either the metamorphic basement, the Pazarköy series, the Aksartepe limestones, the breccias series of Şarkbeynevit or the Yeniköy siltstone series.

The Altındere detrital series is a reddish, well-consolidated, predominantly fine-grained and calcareous-poor succession consisting mainly of clay- and siltstones with intercalations of sandstones and breccias. The latter are poorly-sorted and grain-supported. The most frequent components with mean sizes around 1cm are micaschists and quartzites; black claystones are of a subordinate order. In some places, strongly weathered volcanic dikes, presumably of andesitic composition, were encountered. The series is subject to very intense weathering. The best outcrops are found along the Pazarköy-Güzlek-Mah. mountain road. Because of very bad outcrop conditions, the thickness of the series is difficult to estimate but probably exceeds 100m.

The reddish colour of the series indicates a predominantly oxidising milieu during deposition and diagenesis. Taking the predominance of fine-grained sediments and the sporadic breccia layers into consideration, the marginal realm of a lacustrine delta seems to be the most probable depositional environment. As in the surrounding areas no similar sediments occur, the sediments of this series are considered to infill a local basin structure. The series lacks fossils but must be younger than the Early Eocene from stratigraphic relations (see above). Based on facies comparisons with continental Oligocene outcrops along the Bursa-Gemlik highway (Erk 1942), an Oligocene age is proposed.

Kuzuluk series

The occurrence of this series is restricted to a well-accentuated depression of less than 5km^2 at the western edge of the Keremali mountains in the small village of Kuzuluk (Fig. 4). The base of the series is displaced by faults, as indicated by geoelectrical studies (Şentürk and Demirel 1987) and a large horst structure within the Kuzuluk basin (see below) of less than a few hundred square metres, consisting of Aksartepe limestones and standing out from surrounding rocks of the Kuzuluk series. Only 400m south-west of this outcrop, the same limestones were encountered in the two 160 and 250m thermal water wells, but at a level at least 90m deeper (Şentürk and Demirel 1987).

Regardless of the rather small size of the Kuzuluk structure, the basin infill is of a very heterogeneous nature (Fig. 5), which gives rise to the suspicion that some vertical displacements also took place during and/or after the deposition of the Kuzuluk series.

Roughly, the Kuzuluk series can be divided into a lower and an upper part. The lower part consists of soft white volcanic tuffs that are intercalated with fluviatile gravels and sands. Very good outcrops of this section are found near the old mill at the waterfall (No. 2 in Fig. 4 and 5), where the Kuzuluk series is overlain discordantly by very loose sandy gravels which strongly resemble Pliocene gravels at some other locations within the study area.

Near the old bath (Eski Hamam, No. 1 in Figs. 4 and 5), an important fossil location with silicified wood was discovered within predominantly unconsolidated gravels. The following wood specimens were determined by Prof. Dr. A. Selmeier, University of Munich (Selmeier in press):

Gymnosperms:

- Taxodiaceae: *Taxodioxylon* sp. (7 specimens, partly very well-preserved)
- Taxaceae: *Taxoxylon* sp. (2 specimens)

Dicotyledones:

- Betulaceae: *Alnoxylon* sp. (1 specimen, very well-preserved)
- Casuarinaceae: *Casuarinoxylon greberi* n.sp. (1 specimen, very well-preserved; third find in the world!)

Based on these determinations, a clear ecological interpretation can be made. Among the probable biotopes of these woods are humid locations in swampy lowlands, on the one hand, and very dry areas as indicated by the occurrence of *Casuarinoxylon greberi* n.sp., on the other. From this, a fluviatile depositional environment within the Kuzuluk basin and dry locations on the surrounding hills can be concluded. This paleobotanic interpretation is in good agreement with the sedimentary facies encountered.

The upper part of the Kuzuluk series is made up of an intercalation of fluviatile sediments with hard grey welded tuffs. This upper part is cut by mostly vertical NNW-SSE striking chalcedony fissure fillings. The best outcrops are found in Orta Mah. (No. 3 in Figs. 4 and 5).

The rather unconsolidated fluviatile sediments of the whole Kuzuluk series are locally silicified, which is attributed to an early high-temperature stage of the geothermal system of Kuzuluk (Greber 1992, 1994 and this volume).

In the southern and southwestern part of the Kuzuluk basin, especially in Topcusırtı Mah. (No. 6 in Figs. 4 and 5), the sedimentary infill is rather different from those described above. Here, almost unconsolidated and chaotically textured coarse gravels and up to 50cm large blocks with a matrix of all grain sizes dominate. Because of sporadic volcanic tuff layers, they are thought to be roughly of the same age as the other parts of the basin infill. Whereas the chaotic texture, the large size of the components and the predominance of probable local andesites indicate a local origin, the good roundness, the occurrence of biotite-gneisses, which were not encountered elsewhere in the study area, and the present gentle topography make a long distance transport more probable. The rocks of Topcusırtı Mah. are hard to explain with the present morphology and river system.

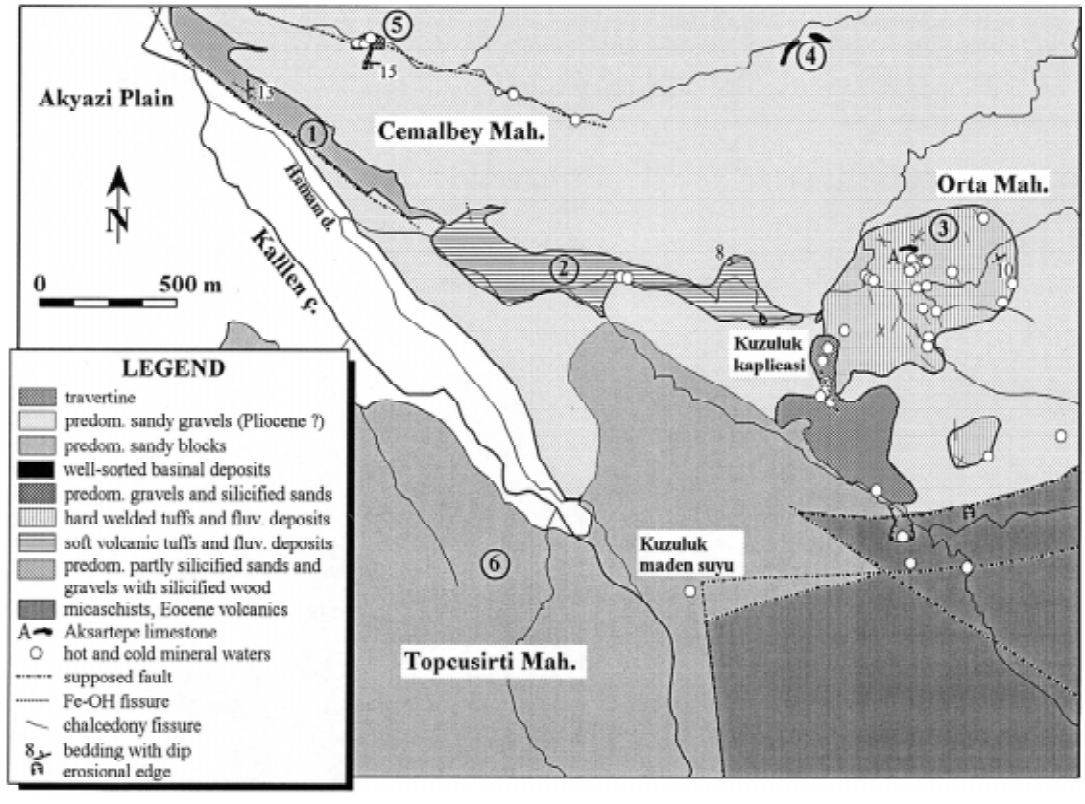


Figure 4: Geological map of the Kuzuluk basin.

The Early and Middle Miocene are considered to have been tectonically quiet periods in Anatolia. The Pontides were a low mountainous belt with shallow intramontane basins (Erol 1981). At the end of the Middle Miocene, Arabia collided with Eurasia and the neotectonic stress regime was about to establish itself (Şengör et al. 1983). During the Late Miocene, major fault lines such as the right-lateral NAF and the left-lateral *East Anatolian Fault* were formed, accompanied by some volcanism (Brinkmann 1976, Yalcın this volume). As a consequence, the landmass broke up into smaller blocks that developed independently, just like most sedimentary basins (Erol 1981). From the structural and lithological point of view, a Late Miocene age of the Kuzuluk basin sedimentary/volcanic infill seems to be rather plausible. Furthermore, the Kuzuluk series are discordantly overlain by probably Pliocene gravels near the mill at the waterfall (No. 2 in Figs. 4 and 5).

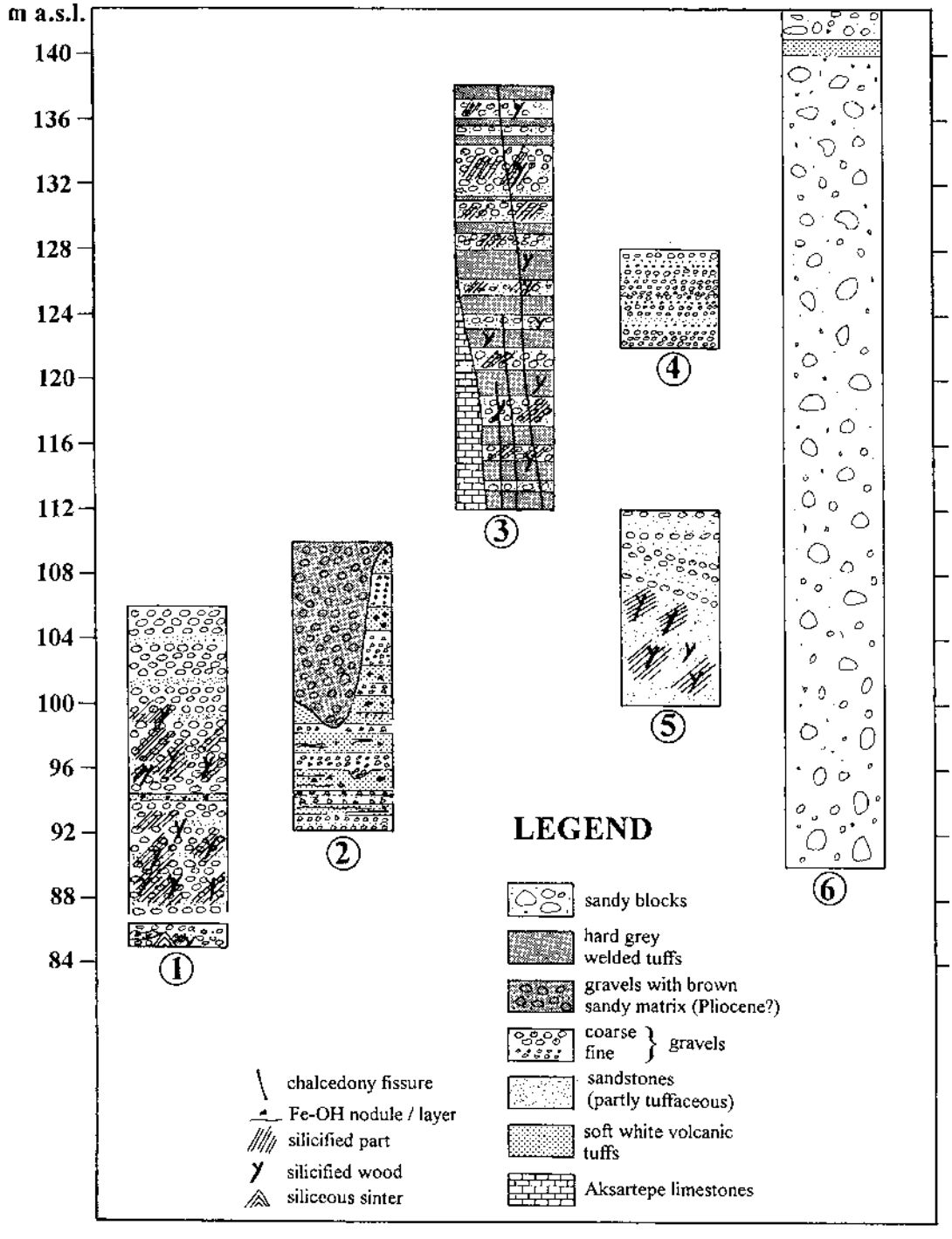


Figure 5: *Stratigraphy of the Kuzuluk basin fill (numbers of stratigraphic columns refer to locations in Fig. 4).*

"Pliocene" gravels

Almost unconsolidated gravels and sands form a low mountainous topography to the north of Haraklı. The best outcrops are found along the Haraklı-Hendek road, just south of the Tekerlek river. Here, the series consists of about one half gravel and the other half sand. The well-rounded gravel shows a mean size of 8 to 10cm and consists nearly exclusively of multicoloured volcanic rocks. Some cross-bedded channel-fill deposits clearly indicate a fluviatile depositional environment. The sandy parts are often fine-laminated.

Just across the Tekerlek river, about 100m from the outcrops described above, the gravel consists not only of volcanic rocks but also of quartzitic sandstones, white and red quartzites, high-grade metamorphic basic rocks and gneisses rich in mica. Here, the fluviatile sediments are cut by steep faults striking 77 to 90° and dipping south with 64 to 68°. Slickensides dip with about 12° to the west. From this, a relative upward movement to the east of the northern block is concluded.

At the cemetery hill south of Alaağaç, the series consists mainly of gravels with a brown sandy matrix. The very heterogeneous pebbles are well-rounded, well-sorted and well-oriented. Another outcrop, 500m ENE of the Açma tepe near Haraklı, is worth mentioning. Here, the texture is very chaotic and the sorting very poor. Many boulders are more than several decimetres across and some of them, mostly volcanic, even more than 80cm. Besides the dominating volcanic boulders, there are also Nummulitic limestones, flysch sandstones, gneisses rich in mica and poorly consolidated conglomerates with volcanic components.

Although no dating of the series exists in the study area, a Pliocene age seems to be most probable. During the Pliocene, the tectonic movements began to concentrate along the main fault structures, however, the relative uplift of mountain blocks and deepening of basins continued (Erol 1981). Along the NAFZ, deep and narrow depressions were formed and filled up with fluviatile sediments like the ones described above.

Rocks of the Civek zone

In the *Civek zone*, south of the Yongalik-Beldibi line (Fig. 6), the stratigraphic situation is rather unclear and most contacts are of a tectonic nature. For this reason, the contribution of this zone to the stratigraphy is minor and the description of its rocks is kept short.

This region, within a Mudurnu river bend, is neotectonically completely crushed and sheared off. The dominant granites and recrystallised limestones with subordinate different limestones, flysch, slates, serpentinites and siltstones are found at no other place in the study area. Only a very characteristic variety of hardly weathered andesite with large amphiboles exposed here was also observed outside the Civek zone, in the near village of Şerefiye. The high complexity of the Civek zone is probably only partly due to the NAF stress regime. The serpentinites exposed here can be interpreted as remnants of an old ocean floor, i.e. the Intra-Pontide ocean, that closed after the Middle Paleocene period (Okay et al. 1994).

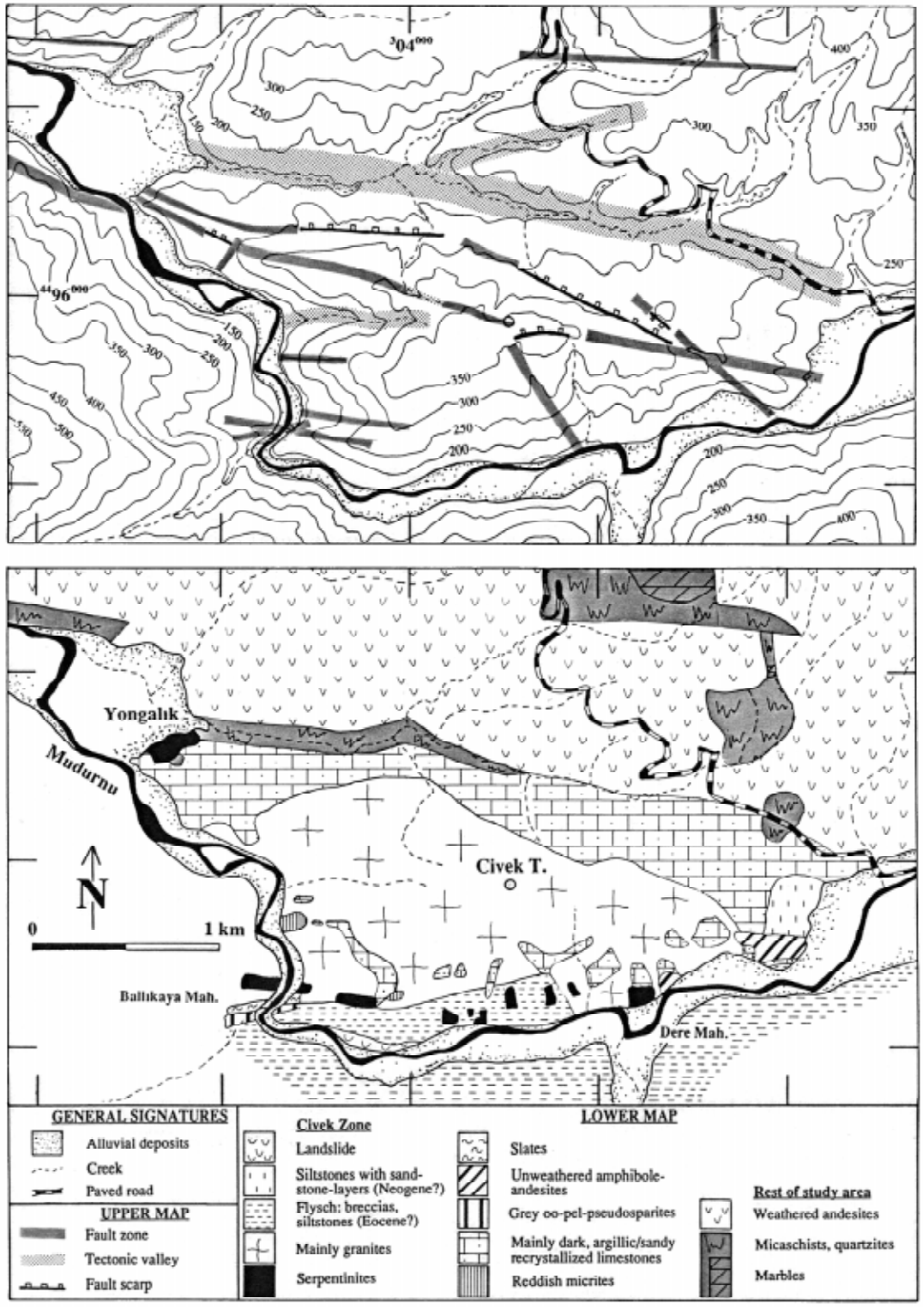


Figure 6: *Geological map of the neotectonically strongly disturbed Civek zone, a probable remnant of the Intra-Pontide ocean.*

Tectonics

Introduction

The study area lies within the Alpine-Himalayan orogenic belt. It is commonly accepted that the Alpine orogeny in Turkey started with the onset of subduction of oceanic crust during the Cretaceous and is still active at present. The Alpine orogeny is characterised by different tectonic phases. In the study area, at least two different Alpine phases can be postulated: (1) The *"main-Alpine phase"* is related to the juxtaposition of the İstanbul and Sakarya zones after the Middle Paleocene time (Okay et al. 1994). (2) Older tectonics are tentatively attributed to a *"paleo-Alpine phase"* that started from the Late Cretaceous onward and which is rather dominant in the study area. Still active *neotectonic movements* along the NAFZ- associated with high seismicity – caused a severe overprint locally. The effects of these tectonic phases are sometimes difficult to attribute to a certain phase, as reactivation of older structures has to be considered.

Paleo-Alpine tectonics

The rather complex stratigraphic situation and geologic pattern, especially along the northern slope of the Keremali mountains, may be explained by Late Cretaceous to Paleocene tectonics. This hypothesis is supported by the following points: (1) Many lithologies of solely local occurrence are found, especially at the northwestern slope of the Keremali mountains. (2) Besides lateral variations in facies, there are also significant differences in the stratigraphic successions of different areas. (3) Zones of denudation are found close to zones of accumulation where locally derived detritus was deposited. (4) The stratigraphic sequences give indications of rapid, differential vertical movements. (5) A prevailing part of the sediments consists of clastics, especially breccias. (6) The same sediments and volcanic rocks show partly varying thicknesses at different places. (7) Identical sediments were not necessarily deposited at all places over the same time range.

The sedimentary environment was thus not homogeneous but divided into swells and basins at least since the Late Cretaceous.

Main-Alpine tectonics

Considering that no Alpine metamorphism took place in the study area, the main-Alpine orogeny must have been rather weak. The main effects of the orogeny seem to have been a regional uplift, combined with a tilting and slight folding of the strata. Furthermore, the Early Eocene andesitic volcanism is closely related to a continent-continent collision. Again, it must be pointed out that main-Alpine activities are hard to distinguish from neo-Alpine ones.

Neotectonics

The NAFZ, as a major plate boundary fault zone, shows a rather complex fault pattern in the study area, as some fault lines bifurcate and others join (Fig. 7). The Keremali mountains belong to the western end of the uplifted *Almacık lens*, measuring roughly 20km across and 50km in length. This tectonic lens, with its metamorphic core and its local sedimentary and volcanic cover, is limited by the plains of Akyazı and Düzce to the north and by the Mudurnu valley to the south. Three NAFZ main branches can be distinguished: the *Haraklı*, *Cemalbey* and *Mudurnu* faults.

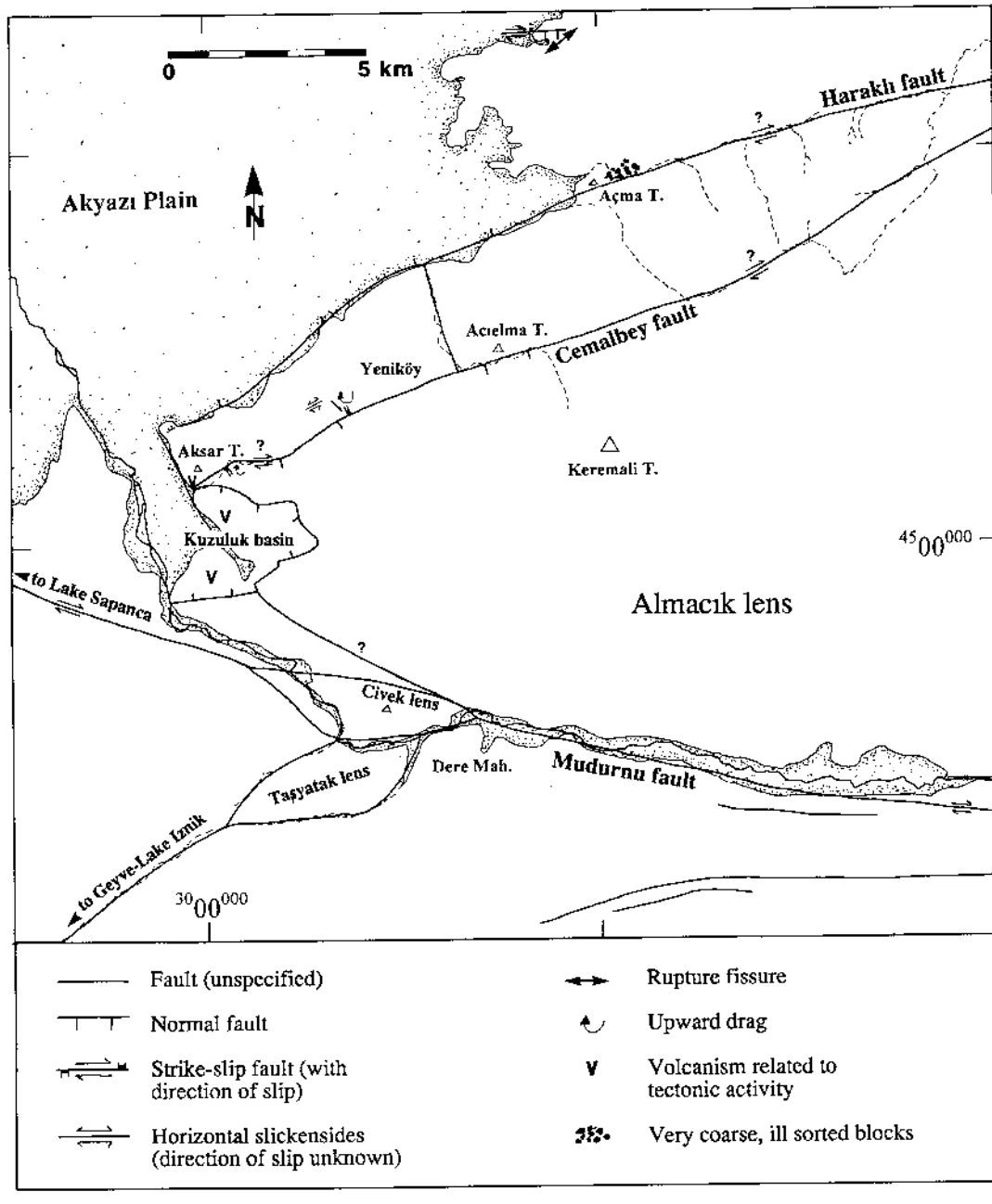


Figure 7: *Tectonic sketch map of the Akyazı/Adapazarı area. Broken lines are creeks dominated by fault lines.*

The *Haraklı fault* (in the study area, identical with the *northern strand* of Şengör et al. (1985)) separates the Almacık lens from the Akyazı plain and Pliocene gravels. In the east of the study area, two creek courses are controlled by the Haraklı fault. Very poorly-sorted gravels and boulders near Haraklı are interpreted to be strong evidence of the rapid*neotectonic* uplift of the Almacık lens. To the west of this outcrop, the pre-Pliocene rocks disappear under the thick alluvial deposits of the Akyazı plain. South of Alaağaç, very close to the Haraklı fault, Pliocene gravels are down-faulted towards the plain along secondary step faults striking in the same direction as the main fault and dipping NNW about 80°. The visible displacement is rather slight and probably does not exceed a few decimetres. It is not clear if the Haraklı fault, covered by alluvial deposits, continues to the west and joins the Mudurnu fault or if it is cut by another postulated NNW striking fault line.

The Haraklı fault is thus an important structure with very significant vertical displacements; lateral movements are probable but hard to prove. The Haraklı fault is supposed to be a rather old structure, probably of pre-Pliocene age. This presumption is based on the observations that no Pliocene rocks are found within the Almacık lens and that the Pliocene gravels were deposited in narrow depressions along the Haraklı fault. According to Şengör et al. (1985), this *northern strand* originated during the Middle to Early Late Miocene.

The *Cemalbey fault* runs roughly parallel to the northern Haraklı fault. Several creek courses are controlled by this fault line. The Cemalbey fault is not restricted to creek ravines, but also cuts hills, e.g. the dome of Yeniköy. There is one excellent outcrop at the western Cemalbey fault in Cemalbey Mah. (Kuzuluk), where the fault consists of fault breccias and kakirites more than 20m thick, intruded by a volcanic dike.

A relative uplift of the NNW-block is indicated by upward drags in siltstones (Yeniköy siltstone series) within the southern fault block and by the observation that the older rocks occur on the northern fault block. Additionally, a lateral displacement must be postulated, as the stratigraphic successions of each fault side do not match. A dextral offset of about 4km would explain the present geological pattern. If the above mentioned volcanic dike that intruded into the kakirites is related to the volcanism of the Kuzuluk series, a Late Miocene age of the Cemalbey fault seems to be plausible. The area between the Haraklı and Cemalbey fault is characterised by differentially uplifted blocks and slices along secondary fault structures, some of which may well be related to paleo-Alpine tectonics.

The Almacık lens is restricted to the south by the *Mudurnu fault*. The epicentres of two major earthquakes in 1957 (M_S=7.1) and 1967 (M_S=7.2) were located within this zone. The Mudurnu fault is the most important of the three main faults in the study area. To the east, it continues beyond the lake Abant and the southern margin of the Bolu plain and even further eastward. To the west, it bifurcates into two fault branches: a northern one (*northern strand* of Şengör et al. 1985), very active during the 1967 earthquake (Ambraseys and Zatopek, 1969), that continues to the southern shore of the lake Sapanca and the gulf of İzmit, and a southern one (*southern strand* of Şengör et al. 1985) that runs in the direction of Geyve, Lake İznik and the gulf of Gemlik. The latter branch has been seismically more or less quiet for a longer time, but – based on radon measurements – is supposedly reactivated at present (Pekdeger and Woith 1992).

The dominating morphological feature of the Mudurnu fault is the "rift" morphology in the Mudurnu valley, which might be related to the erosion of the tectonically crushed rocks by the Mudurnu river. The most important tectonic structure of the Mudurnu fault zone in the study area is the tectonic *Civek lens*, an uplifted elongated hill (Fig. 6). A striking Mudurnu river deviation can be interpreted as a result of this uplift. The Civek lens is an extremely transpressional zone. Zones of displacement are not restricted to incompetent rocks, such as serpentinites or slates. Also, granites and small tectonic lenses of limestones were repeatedly tectonised. All rocks are heavily crushed and sheared off. The zone is also rich in morphological features typical for active strike-slip zones, e.g. elongated hills, narrow tectonic valleys, fault scarps and deviated creek courses.

The *Kuzuluk basin* is an extensional structure separated by faults from the mountains in the north, east and south. There are some indications that the Kuzuluk series, which partly fills up the Kuzuluk basin, is also tectonically limited by young alluvial deposits at its western margin: the supposed NNW striking fault could (near the Eski Hamam) be demonstrated locally with a CO_2 gas profile (Greber 1992), and mineral springs flowing out along a tectonic line striking in the same direction were observed at the western end of the basin before the 1967 earthquake (Rupprecht 1955).

The Kuzuluk basin must be considered as a small, but significant, deep structure. This is indicated by the following: (1) All three main faults, and many secondary faults, converge around the Kuzuluk basin. (2) The youngest volcanism (probably in the Late Miocene) occurs in this area. (3) Circulation depths of at least 3km are postulated for the thermal waters arising in the Kuzuluk basin (Greber 1992 and this volume). (4) Helium and probably carbon dioxide from the earth's mantle could be detected (Kipfer 1991, Greber 1992 and this volume).

It might be argued, with good reason, that the Kuzuluk basin is still subsiding at present, as the morphology of the structure is still astonishingly well preserved.

Conclusions

The investigated western Keremali mountains are an area of high geological complexity. The Upper Cretaceous to Miocene cover has been influenced by a paleo-Alpine phase (Late Cretaceous-Paleocene), a main-Alpine phase (Early Eocene) and a neotectonic phase (Miocene-present). Whereas large parts of these mountains acted as zones of denudation between the Late Cretaceous and the Early Tertiary, the north-western flank was a realm of sedimentary accumulation which was controlled by paleo-Alpine tectonics at least from the Late Cretaceous onwards. The complex stratigraphic situation shows many affinities to a strike-slip related setting (as defined by Mitchell and Reading 1978). It is open for discussion if these transtensional and transpressional features are related to the southward movement of the İstanbul zone as a small continental fragment (”terrane” in North American terms) during the Late Cretaceous-Paleocene (Okay et al. 1994, Robinson et al. 1996).

Although there are no older sediments than Upper Cretaceous, the largest part of the study area with its metamorphic basement probably belongs to the İstanbul zone. Paleozoic and/or Lower Mesozoic sediments eventually were eroded before the Late Cretaceous time.

The Civek zone with its tectonic serpentinite lenses may be interpreted as the remnant of the (Early Eocene?) Intra-Pontide suture. This suture has been tectonically reactivated by the neotectonic NAFZ since the Miocene or Pliocene time.

The southernmost part of the study area, which consists mainly of widespread siltstones and subordinate Nummulitic limestones without any Paleozoic sediments or older crystalline basement rocks, can be attributed to the Sakarya zone.

Acknowledgements

This contribution is dedicated to the farmers of the beautiful Keremali mountains. Their hospitality will never be forgotten!

This contribution previously appeared with the same title but in a slightly different form in the Turkish Journal of Earth Sciences, TÜBİTAK, Turkey (Greber 1996).

References

Abdüsselamoğlu, M.S., 1959, Almacıkdagı ile Mudurnu ve Göynük civarını jeolojisi, İstanbul Üniversitesi Fen Fakültesi Monografileri, Sayı 14, 94p.

Adamia, S.A., Chkhotua, T., Kekelia, M., Lordkipanidze, M., Shavishvili, I. and Zakariadze, G., 1981, Tectonics of the Caucasus and adjoining regions: Implications for the evolution of the Tethys ocean, J. Struct. Geol., Vol. 3, No. 4, 437-447.

Ambraseys, N.N. and Zatopek, A., 1969, The Mudurnu valley, West Anatolia, Turkey, earthquake of 22 July 1967, Bull. Seismol. Soc. Am., Vol. 59, 521-589.

Barka, A.A., 1992, The North Anatolian fault zone, Annales Tectonicae, Special Issue – supplement to Vol VI, 161-195.

Brinkmann, R., 1976, Geology of Turkey, Ferdinand Enke Verlag, Stuttgart, 158.

Erk, A.S., 1942, Etude géologique de la région entre Gemlik et Bursa (Turquie), PhD., Univ. of Basel, 295p.

Erol, O., 1981, Neotectonic and geomorphological evolution of Turkey, Zeitschrift für Geomorphologie, Neue Folge, Supplement Band Vol. 40, 193-211.

Eyidoğan, H., 1988, Rates of crustal deformations in Western Turkey as deduced from major earthquakes, Tectonophysics, Vol. 148, 83-92.

Greber, E., 1992, Das Geothermalfeld von Kuzuluk/Adapazarı (NW-Türkei) – Geologie, aktive Tektonik, Hydrogeologie, Hydrochemie, Gase und Isotope, PhD thesis, ETH Zürich, 213p.

Greber, E., 1994, Deep circulation of CO_2-rich palaeowaters in a seismically active zone (Kuzuluk/Adapazarı, Northwestern Turkey), Geothermics, Vol. 23, No. 2, 151-174

Greber, E., 1996, Stratigraphic evolution and tectonics in an area of high seismicity: Akyazı/Adapazarı (Pontides, Northwestern Turkey), Tr. J. of Earth Sciences, Vol. 5, No. 2, 63-79.

Greber, E., this volume, Deep circulation of CO_2-rich palaeowaters in a seismically active zone (Kuzuluk/Adapazarı, Northwestern Turkey).

Kalafatçıoğlu, A. and Uysallı, H., 1964, Geology of the Beypazarı-Nallıhan-Seben region, Bull. Min. Res. Explor. Inst. Turkey, Vol. 62, 1-11.

Kipfer, R., 1991, Primordiale Edelgase als Tracer für Fluide aus dem Erdmantel, PhD thesis, ETH Zürich, 223p.

Kopp, K.-O., Pavoni, N. and Schindler, C., 1969, Geologie Thrakiens IV: Das Ergene-Becken, Beih. geol. Jb., Hannover, 136p.

Lucius, M., 1929, Kuzuluk (Akyazı) thermo-mineral suları hakkında rapor, MTA Derleme No: 558 unpublished, Ankara.

McKenzie, D.P., 1972, Active tectonics of the Mediterranean region, Geophys. J. Roy. Astron. Soc., Vol 30, 109-185.

Mitchell, A.H.G. and Reading, H.G., 1978, Sedimentation and Tectonics, in: Sedimentary Environments and Facies, edited by: H.G. Reading, Blackwell Scientific Publications, Oxford, 439-476.

MTA, 1964, Maden Teknik ve Arama Enstitüsü, Geological map of Turkey 1:500,000, – Map Zonguldak.

Okay, A., 1989, Tectonic units and sutures in the Pontides, Northern Turkey, in: Tectonic Evolution of the Tethyian Region, edited by: A.M.C. Şengör, NATO Advanced Science Institute (ASI) series, C259, 109-116.

Okay, A.I., Şengör, A.M.C. and Görür, N., 1994, Kinematic history of the opening of the Black Sea and its effect on the surrounding regions, Geology, Vol. 22, 267-270.

Önder, I., 1987, Sakarya-Akyazı Kuzuluk kaplıcası sıcak su aramaları resistivite etüt raporu, MTA-Report unpublished.

Pekdeger, A. and Woith, H., 1992, Radon in groundwater: A contribution to the joint German-Turkish Earthquake Prediction Research Project, in: Radon et Gaz Rares dans les Sciences de la Terre et de l'Environnement, edited by: P. Doremus, L. Dejonghe and J.-M. Charlet, Actes du Colloque International sur la Géochimie des Gaz (Mons 3-6 octobre 1990 – Belgique), 171-179.

Robinson, A.G., Rudat, J.H., Banks, C.J. and Wiles, R.L.F., 1996, Petroleum geology of the Black Sea, Marine and Petroleum Geol., Vol. 12, No. 2, 195-223.

Rupprecht, K.H., 1955, Kuzuluk-Aziziye mevkii'nin Cemalbey mahallesinde bulunan kaplıcaların jeolojik etüdü, MTA Derleme No. 2329, unpublished, Ankara.

Şengör, A.M.C. and Yılmaz, Y., 1981, Tethyan evolution of Turkey: a plate tectonic approach, Tectonophysics, Vol. 75, 181-241.

Şengör, A.M.C., 1979, The North Anatolian Transform Fault: its age, offset and tectonic significance, J. Geol. Soc. Lond., Vol. 136, 269-282.

Şengör, A.M.C., Büyükasıkoğlu, S. and Canıtez, N., 1983, Neotectonics of the Pontides: Implications for "incompatible" structures along the North Anatolian Fault, J. Struct. Geol., Vol. 5, No. 2, 211-216.

Şengör, A.M.C., Görür, N. and Saroğlu, F., 1985, Strike-Slip faulting and related basin formation in zones of tectonic escape: Turkey as a case study, The Soc. of Econ. Paleont. and Min., Vol. 37, 227-264.

Şentürk, N. and Demirel, Z., 1987, Akyazı (Sakarya) Kuzuluk kaplıcasi hidrojeoloji incelemesi, MTA Report, unpublished.

Selmeier, A., Silicified Taxus woods from the geothermal field of Kuzuluk (NW Turkey), in: Pflanzen der geologischen Vergangenheit, edited by O.H. Storch, Daber-Festschrift.

Trümpy, R., 1980, Geology of Switzerland, Schweiz. Geol. Komm., Wepf Basel, 104p.

Van der Kaaden, G., 1971, Basement rocks of Turkey, in: Geology and History of Turkey, edited by: A.S. Campbell, The Petroleum Exploration Society of Libya on the occasion of the thirteenth annual field conference, Tripoli, Libya, 192-209.

Yalçın, T., this volume, Hydrogeological investigation of the Gönen and Ekşidere thermal waters (NW Turkey).

Yılmaz, Y., Gözübol, A.M. and Tüysüz, O., 1982, Geology of an area in and around the Northern Anatolian Transform Fault Zone between Bolu and Akyazı, in: Multidisciplinary Approach to Earthquake Prediction, edited by: A.M. Işikara and A. Vogel, Vieweg, Wiesbaden, 45-65.

Deep circulation of CO_2-rich paleowaters in a seismically active zone (Kuzuluk/Adapazarı, Northwestern Turkey)

EMIL GREBER

Abstract

The upflow zone of more than 40 cold and hot mineral springs of Na-(Ca)-(Mg)-HCO_3-Cl type is restricted to an extensional structure within the seismically active North Anatolian Fault Zone (NAFZ). The chemistry of the waters, which are probably more than 10,000 years old, is influenced effectively in a low temperature environment by the CO_2 originating from the decomposition of marine carbonates and outgassing of the earth mantle. This gas is thus attributed to the interaction of the minor plates of Turkey and the Black sea in this area. A strong positive ^{18}O-shift is due to water-rock interaction with very long contact times, rather than to isotopic influence of the CO_2 on the $\delta^{18}O$-value of the waters.

Introduction

CO_2-dominated mineral waters are very special water types that occur at many places in the world. Up to now, the discussion about their origin has been controversial (Fouillac 1983). These waters have to be considered as "immature" as their chemical composition corresponds to a steady state between isochemical dissolution of aquifer rocks and equilibration of the fluid with the thermodynamically stable mineral assemblages (Giggenbach 1988, Giggenbach and Goguel 1989). Many questions arise in this context. The main themes of this paper are the influence of the uprising CO_2 on the chemical properties of the circulating waters and the possible isotopic interaction between CO_2 and water.

CO_2 discharges are mainly concentrated along zones of increased seismicity and are related to fundamental tectonic processes (Barnes et al. 1978). Knowledge about the origin of this CO_2 can provide useful indications on the nature of plate contacts.

As in many other geothermal systems, the circulation of hot and cold mineral waters at Kuzuluk, Northwestern Turkey, is closely related to major fracture zones. In contrast to other systems, however, the tectonic structures around Kuzuluk are still seismically very active, which enables us to study the influence of *active* tectonics on the circulation of deep waters.

More than 40 cold (~20°C) and hot (up to 55°C) mineral waters emerge in the small village of Kuzuluk, which is situated 150km ESE of İstanbul and 50km south of the Black sea. The springs are restricted to a basin (~115m a.s.l.) surrounded to the north, east and south by the Keremali mountains (highest peak: 1543m a.s.l.). At present, only the small but very picturesque Çökek hamamları are used as thermal baths. However, a new spa, expected to generate more than just regional interest, is now under construction. For this purpose, two boreholes were drilled, resulting in artesian water with a temperature of more than 80°C.

Kuzuluk lies in a very fertile region of Northwestern Turkey. Hazelnut plantations predominate on the hills, up to elevations of about 500m a.s.l. Large parts are covered by dense forest. Numerous species of vegetable and fruit are cultivated on the Akyazı plain (~50m a.s.l.), north of the Keremali mountains. The climate of Kuzuluk is influenced by the humid belt running along the Turkish Black sea coast, as well as the semi-arid climate of the Anatolian plateau. The mean annual precipitation of Akyazı is 871.5mm, most of it rain, with some snow during the winter. The mean annual temperature at Adapazarı is 14.2°C. The largest river in this area is the Mudurnu, with a mean annual discharge of 4873m^3/s (DSİ 1983). The Keremali mountains are drained all year long by deep-cutting creeks.

Geological setting

Low-metamorphic micaschists, quartzites and marbles are overlain by Upper Cretaceous or younger sediments and volcanic rocks (Fig. 1). The sedimentary environment was divided into swells and basins at least from the Late Cretaceous on. For this reason, the regional geological pattern is affected by numerous lateral and vertical changes in the stratigraphic sequence.

The Keremali mountains are a complicated link within the Alpine-Himalayan orogenic belt. Significant Alpine orogenic movements took place during the Eocene and Oligocene (Ketin 1959).

The tectonic setting is dominated by the dextral North Anatolian strike-slip fault, which has been active as a transform fault separating the two minor plates of the Black sea and Turkey since the Late Miocene (McKenzie 1972, Şengör 1979). The study area is situated at the western end of the east-west-striking, uplifted tectonic "Almacık lens" (Greber 1992, this volume), which extends roughly 50km in length and 20km in width. All the cold and hot mineral waters rise within the morphologically well-accentuated subsidence basin of Kuzuluk, which is partly filled with locally silicified fluviatile deposits and volcanic tuffs ("Kuzuluk series") of probably Middle or Late Miocene age. Around this extensional structure, the earth's crust seems to be weakened and deeply fractured.

In the most seismically active zone along the Mudurnu river (last severe earthquake in 1967 with M_S=7.2) there is no upflow of mineral waters at all. This can be explained by field observations (Greber this volume, Schindler 1993) that show how this zone is dominated by a transpressional stress regime (Harland 1971).

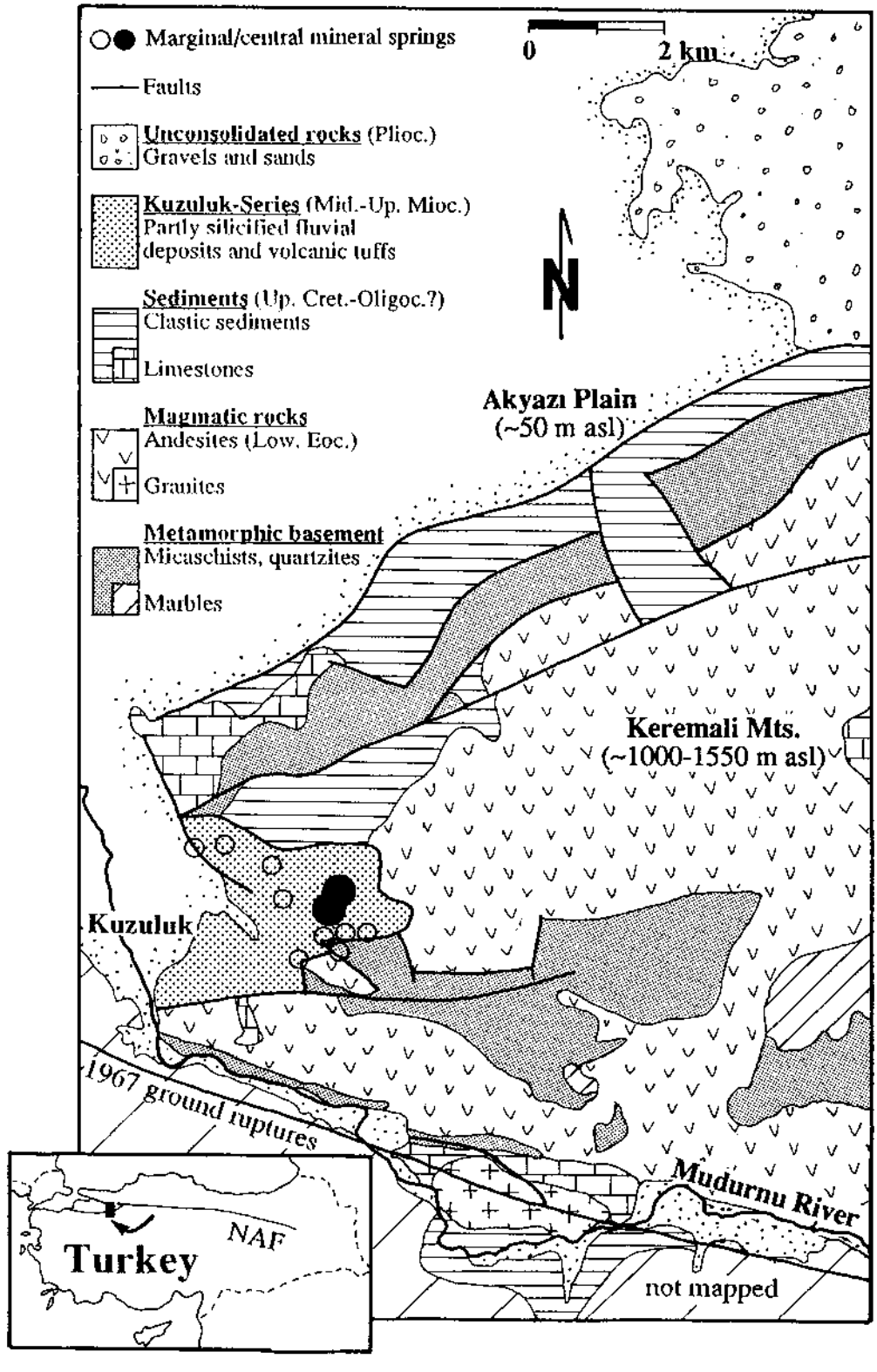


Figure 1: *Geological map of the western Keremali mountains (simplified after Greber 1992). Ground ruptures were opened during the Mudurnu earthquake on 22 July 1967 (MS=7.2, Ambraseys and Zatopek 1969; NAF = North Anatolian Fault Zone).*

Hydrogeological setting

Normal groundwaters

The area around the Kuzuluk basin is rich in normally mineralised spring waters of essentially Ca-HCO_3 type. Only a few dry out during the summer or autumn. The typical movement of humid air masses in the Black sea area is southwards towards the study area. Thus, the biggest springs, Ser (425m a.s.l.) and Kon (455m a.s.l.), occur on the northwestern slopes of the Keremali mountains, where precipitation is more abundant than in the Mudurnu valley. The most important aquifer rocks are andesites and micaschists. Both lithologies are locally deeply weathered but show high secondary permeabilities due to joints and tectonic fissures. Karstified limestones, especially in the uppermost Keremali mountains, are considered to be significant infiltration areas. As only two minor karstic springs (Ke2 and K27) were encountered, percolation into deeper lithologies and direct intake to alluvial sediments of the Akyazı plain in the northwestern Keremali mountains must be assumed.

Hot and cold mineral waters

All of the approximately 40 mineral waters are restricted to the Kuzuluk basin, an area of less than 3km^2 without any low mineralised cold spring water. Most mineral waters emerge within small ponds exhibiting conspicuous outgassing phenomena. Two boreholes (160 and 250m) found artesian water (up to 6 bar and 2.5 bar) at more than 80°C in limestones and micaschists beneath 90m cap rocks consisting of low permeable sediments and volcanic rocks (Şentürk and Demirel 1987).

The Kuzuluk mineral waters can be divided into "marginal" and "central" waters for geographical (Fig. 1) and chemical/physical reasons (Tables 1 and 2). The marginal springs emerge at the margin of the Kuzuluk basin and are characterised by fairly low temperatures but high electrical conductivities. The central waters (including the borehole samples Kuz1 and Kuz2) show higher temperatures but lower conductivities. The total discharge of all the springs is rather small, about 103l/min; the artesian outflow of the up to now unutilised and closed thermal water wells, at 2520l/min, is very high compared to the natural spring outflow and it may only be a short-term discharge.

	Normal groundwaters	Marginal springs	Central springs	Central drillings
Mean temperature(°C)	13.6	24.2	40.8	>80
Mean electrical conductivity (µS/cm)	410	4110	3200	3540
Mean discharge (l/min)	17	3.0	2.4	1260
Mean gas flux (l/min)	-	0.7	1.1	-
Total discharge Q_{tot} (l/min)	>620	35.6	67.3	2520[a]
Total gas flux G_{tot} (l/min)	-	5.0	25.0	-
Q_{tot}/G_{tot}	-	7.1	2.7	-

[a] Due to artesian overpressure

Table 1: Comparison of physical parameters between normal groundwaters and central and marginal mineral waters.

	Marginal springs	Central waters
Water types	Na-HCO_3-Cl	Na-HCO_3-Cl
	Na-Mg-(Ca)-HCO_3-Cl	Na-(Ca)-HCO_3-Cl
	Na-(Mg)-(Ca)-HCO_3-Cl	
	Na-(Ca)-HCO_3-Cl	
	Na-(Ca)-(Mg)-HCO_3-Cl	
Mean H_2CO_3*-concentration (mmol/l)	24.1	9.1
Mean total dissolved solids (mg/l)	4997	3536

Table 2: Some chemical characteristics of the Kuzuluk mineral waters (H_2CO_3= CO_2(aq) + H_2CO_3, chemical classification: all ions >10meq% are mentioned; underlined: >50meq%; in parentheses: <20meq%).*

Except for the cold, highly mineralised spring Aci2, which flows up through micaschists, all the mineral waters reach the surface through the Kuzuluk series. There are some indications that tectonic fissures serve as dominant flow paths. KapA, an old capture tunnel of the former Kuzuluk kaplıca (="spa"), consists of some 15 gas and water inflows all along a straight line of 21m. This is most probably a tectonic line, and can be followed for about 60m to another three springs.

Useful information about flow paths can be obtained from a comparison of present outflow characteristics and historical records of this century (Lucius 1929, Rupprecht 1955, Bistritschan 1957). Changes in flow rates and temperatures can be demonstrated. The earthquake in 1967 (M_S=7.2) triggered considerable changes in the thermal system of Kuzuluk: at the Eski hamam (="old bath"), six springs along a fault line with a total discharge of more than 100l/min disappeared completely. At Kuzuluk kaplıca the decrease in discharge was so drastic that the spa had to be closed. The flow path system of Kuzuluk is thus very vulnerable and susceptible to the frequent tectonic movements occurring in this seismically very active zone.

Evolution from a high-temperature to a low-temperature thermal field

A geothermal system is often subject to important changes over geological times. In Kuzuluk the heterogeneous Kuzuluk series represents an ideal sequence for studying these phenomena.

In the soft, white volcanic tuff of the lower part of the series, layers of hydroxide and iron concretions are common. Locally the fluviatile sediments are solidified by silica precipitations, and relics in the form of chalcedony layers of a former hot water spring outlet were found. An important fossil locality with silicified wood was also discovered (Greber 1992, this volume). The upper part of the Kuzuluk series, consisting of hard, grey tuff and fluviatile sediments, is penetrated by thin well-oriented, vertical chalcedony fissure fillings. As in the lower part, large parts of the gravels and sands are solidified by chalcedony cementation. One can therefore conclude that in a very early phase of the Kuzuluk thermal system, the main constituent of the circulating waters was silica. This is an indication for underground temperatures above 180°C (White et al. 1956, Fournier and Rowe 1966, White 1970). These high temperatures are evidently related to the strong volcanic activity of that time (probably Middle to Late Miocene).

The relics of this early phase are locally overlain by extended travertine layers. Carbonatic remains of former ascent channels of CO_2 - rich waters can be localised. These tectonic fractures and the travertines are indications of periods of increased tectonic and seismic activity

with cooler underground temperatures (White 1970). Seismically active zones are often associated with major CO_2-outputs (Barnes et al. 1978).

Main characteristics of the springs

Physical characteristics

The electrical conductivity of the central and marginal mineral waters is considerably higher than that of the normal groundwaters (Table 1; Greber 1992).

The gas/water-ratios are rather high as the discharges of the mineral springs are low. Gas outputs are observed in the entire Kuzuluk basin, but are more concentrated in its centre.

Chemical characteristics

The chemistry of all the normal groundwaters is dominated by Ca^{2+} and HCO_3^-, but their minor constituents are extremely variable. All of the mineral waters are dominated by Na^+ and HCO_3^- (Table 2; Greber 1992). Compared to the central waters, the marginal springs are characterised by higher portions of the alkaline earth metals Ca^{2+} and Mg^{2+}, higher amounts of dissolved CO_2 and lower SO_4^{2-} concentrations.

Soil gas characteristics

The gas phase consists of 95.2-100% CO_2 (Greber 1992). As the gas is almost free of atmospheric contamination, it originates from the earth's interior.

Isotopic characteristics

All $\delta^{18}O$- and δ^2H-values of the normal groundwaters plot between the meteoric water lines of central Anatolia (d=10; Şentürk et al. 1970) and of the Eastern Mediterranean (d=22). Tritium contents are between 16.3 and 27.6TU. The δ^2H- and $\delta^{18}O$-values of the central waters are similar and, compared to the normal groundwaters, more negative inδ^2H and more positive in $\delta^{18}O$. All tritium concentrations are close to or below detection limits. The marginal springs show more scattering. Compared to the central waters they have even more positive$\delta^{18}O$-values and slightly more positive δ^2H-values (exception: Aci2). The δ^2H-value of Mad5 is in the range of the normal groundwaters. Tritium is detectable in low concentrations (up to 7.6TU) in many marginal spring waters. Isotope data are listed in Greber (1992).

Processes within the outflow zone

The outflow area of the central and marginal mineral waters is sharply separated from that of the normal groundwaters by deep faults limiting the Kuzuluk basin.

Mineral waters rising from depth partly lose their original characteristics due to overprinting by the normal groundwater cycle and contact with the atmosphere (Truesdell and Hulston 1980).

Mixing with young normal groundwater

The upflow system of Kuzuluk is susceptible to mixing with young shallow groundwater, particularly at its margin. Many marginal waters contain tritium contents higher than 1.3TU. This can be explained by afflux of young creek water (Mad1, Mad8, Mad5), of slope water infiltrated at the margin of the Kuzuluk basin (KuzMin) and of young water from a small superficial travertine aquifer (Mad4).

As monthly measurements of temperature, electrical conductivity and discharge show, the mixing processes seem hardly to be influenced by seasonal effects: no correlation between temperature and conductivity/discharge was observed (Greber 1992).

Based on helium, neon and tritium isotope measurements, the samples diluted by young water components can be interpreted as simple mixing of two endmembers in a closed system: a shallow groundwater with atmospheric $^3He/^4He$-, $^{20}Ne/^4He$- and $^3H/^4He$-ratios and a deep, almost tritium-free groundwater with a very low $^{20}Ne/^4He$-ratio and an $^3He/^4He$-ratio of 0.866 $x10^{-6}$ (Kipfer 1991, Greber 1992).

In contrast to the marginal waters, almost all the central waters reach the surface without having undergone any mixing with young water components.

The observation that mixing processes occur especially at the margin of the upflow zone is not surprising as the flat Kuzuluk basin is surrounded on three sides by steep hills with normal groundwater aquifers.

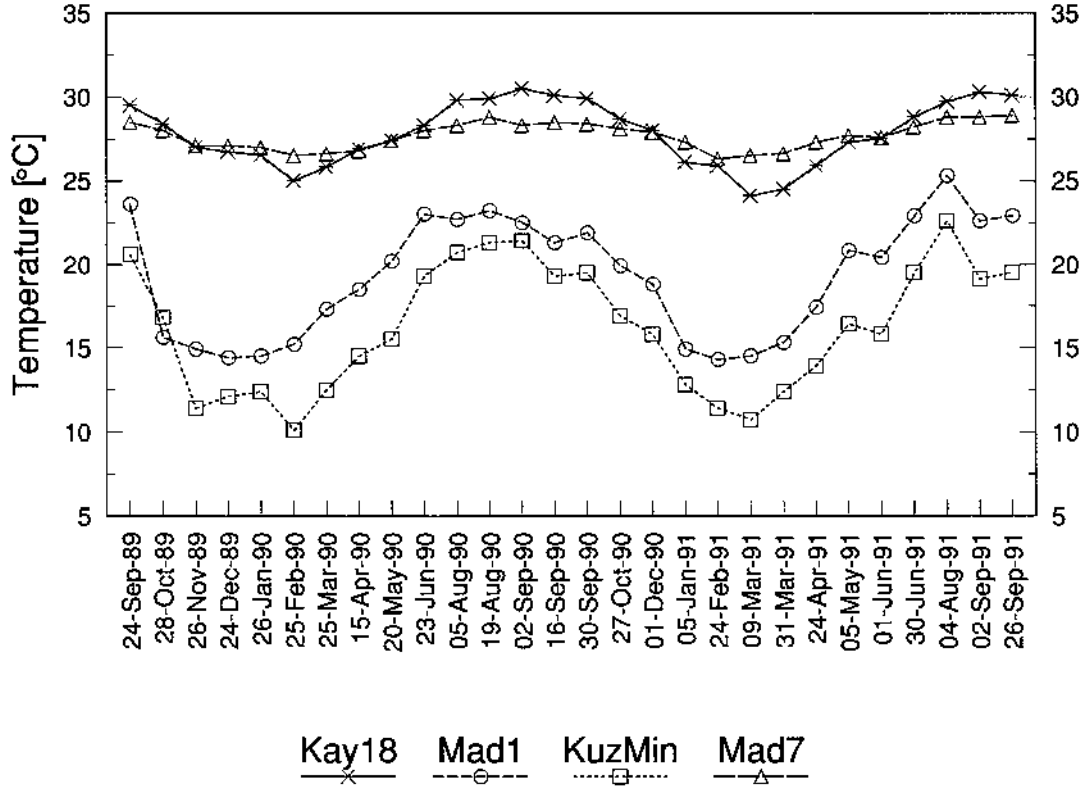


Figure 2: From seasonal temperature variations, heat exchange at shallow depths between water and atmosphere must be assumed for these springs.

Heat transfer by conduction at shallow depths

Two different kinds of temperature fluctuations were observed: periodical and non-periodical. The central waters Ort6 and Ort9 and the marginal waters Kay18, Mad1, KuzMin and Mad7 (Fig. 2) show well-accentuated seasonal temperature fluctuations of 1 to 6°C that are synchronous with regional air temperature fluctuations. As tritium analyses show, these fluctuations cannot be attributed to mixing with cold shallow groundwater. Therefore, a heat exchange between water and aquifer/atmosphere at shallow depths of less than a few meters must be assumed.

The temperatures of the marginal springs Mad4, Mad5, Mad8 and Aci2 are quite constant, indicating rapid movement of the water through the uppermost layers, whereas the temperature behaviour of the central springs Beç1 and KapD (Fig. 3) seems to be totally irregular and is affected by temperature variations of up to 10°C. Besides these long-term characteristics, the latter two springs also show abrupt temperature increases and decreases within a few seconds, often coupled with temporally intensified outgassing. Short-term gas-flux maxima may be related to sudden elastic stress changes in upper crustal levels, triggered by minor tectonic movements.

Some heat is lost by conductive heat transfer during the ascent of the central waters through 90m of low permeable andesites and layers of the Kuzuluk series. The two borehole samples Kuz1 and Kuz2, coming from a depth of 90m with temperatures of 84°C, differ neither chemically nor isotopically from central spring waters with temperatures between 36 and 55°C. Therefore, a heat loss of about 40°C occurs during their ascent through the cap rocks.

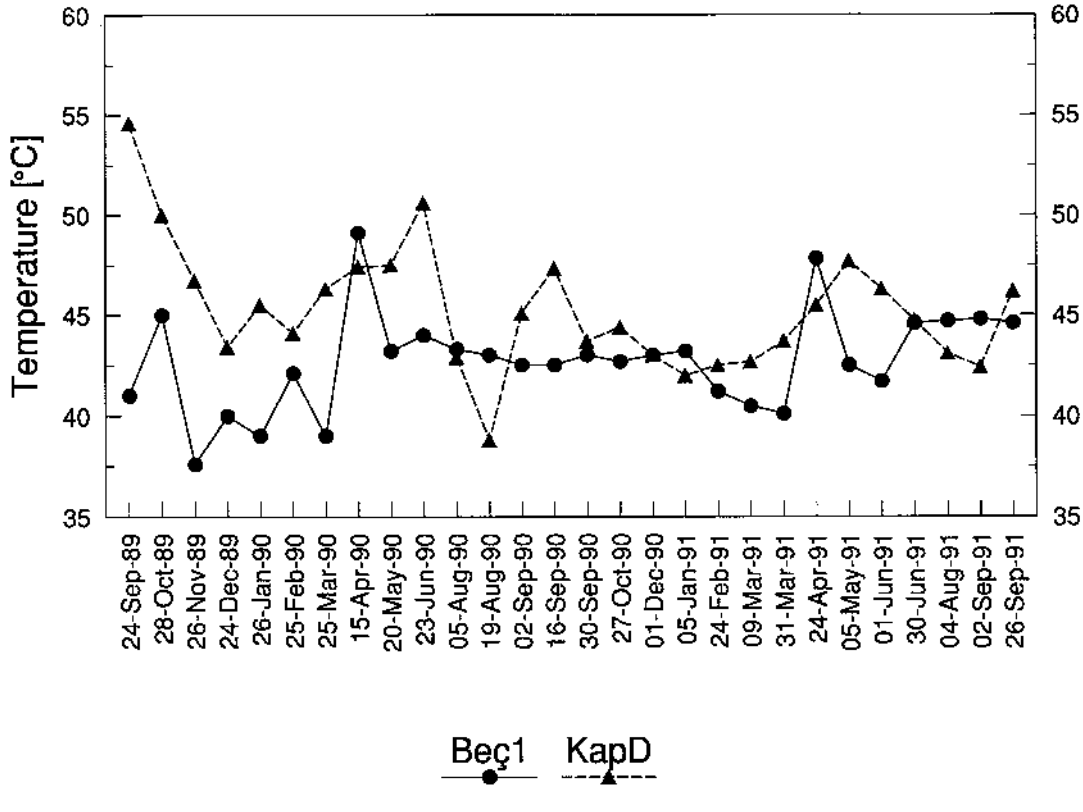


Figure 3: Irregular temperature variations of these springs are indications of rapid passing of the uppermost soil layers.

Process of mineralisation in a CO_2-dominated system

Water-rock interaction is based on the thermodynamic instability of even very low soluble minerals in the presence of water and gas under changed pressure and temperature conditions.

Role of carbonate dissolution

The dissolution of calcite can be written by the following chemical reaction:

$H_2O + CO_{2(g)} + CaCO_{3(s)} = 2HCO_3^- + Ca^{2+}$

Half of the HCO_3^- comes from the CO_2, the other half from calcite. The resulting electroneutrality $[HCO_3^-] = 2[Ca^{2+}]$ can be drawn as a straight line in a logarithmic Ca^{2+}-HCO_3^--diagram (Fig. 4).

The chemistry of the normal groundwaters is dominated by the dissolution of calcite, so that the samples plot close to the line of electroneutrality. The pressure that is exerted in this process exceeds the atmospheric CO_2-pressure considerably in all cases except for some immature, very low mineralised waters that lie below the calcite saturation line at 25°C and $10^{-3.5}$atm.

In contrast to the shallow groundwaters, the data of the central and marginal mineral waters plot far from the line of electroneutrality. For this reason, the dissolution of calcite is not considered to be a major process in the mineralisation of the mineral waters. The deviation from the line of electroneutrality also indicates that much less than one half of the HCO_3^- originates from the dissolution of calcite. Most HCO_3^- must be attributed to the dissolution of CO_2 in water.

The CO_2-pressure of the mineral waters exceeds the atmospheric pressure of $10^{3.5}$atm even more than in the normal groundwaters (Fig. 4). CO_2-pressures were calculated with different methods (Greber 1992). Calculated CO_2-pressures vary between 0.9 and 5.5atm (mean values of central waters: 2.0atm, marginal springs: 2.2atm). These pressures are much higher than the atmospheric and root-zone CO_2-pressures. The gas must therefore ascend from greater depths.

Hydrolysis under normal pressure and temperature conditions (normal groundwaters)

Regardless of aquifer lithology, all of the shallow groundwaters are dominated by the cations Ca^{2+} and Mg^{2+} and the anion HCO_3^- (Fig. 5), from which we can postulate the presence of some carbonate in all the aquifers. Besides this dominating process of calcite dissolution, the minor effects of hydrolysis or simple rock leaching are observed.

The waters from the volcanic areas are characterised by quite high Na^+-contents, and in part also by increased Cl^-- and SO_4^{2-}-concentrations. Na^+ probably originates from the decomposition of albite, SO_4^{2-} from the oxidation of metal sulphides and Cl^- is rather easily released from crystal surfaces and microfissures in the rock (Ellis and Mahon 1964, 1967).

High SO_4^{2-}-contents are typical for waters from granitic aquifers, whereas Na^+-concentrations are surprisingly low. The SO_4^{2-} may originate from pegmatitic zones that were observed in the field.

The similarity between the waters from carbonate and micaschist/quartzite aquifers underlines the low solubility of quartz and micas under normal conditions.

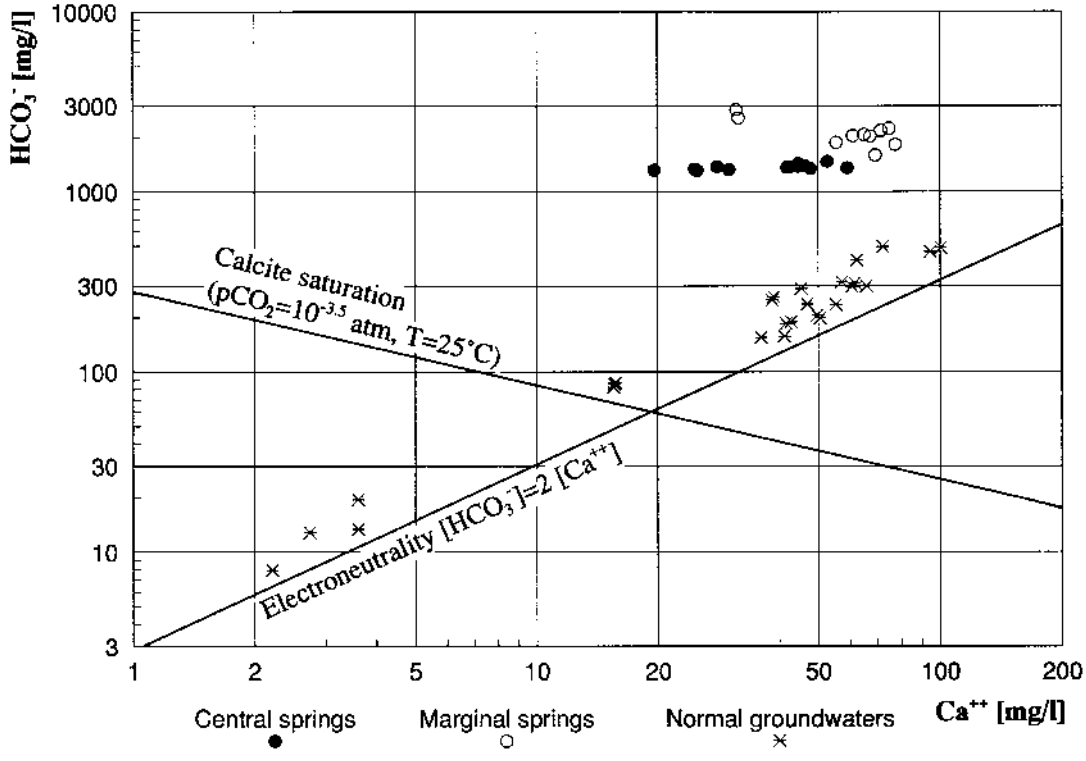


Figure 4: *In contrast to the normal groundwaters, the process of calcite dissolution is of subordinate importance for the central and marginal mineral waters. Instead of that, they are dominated by hydrolysis processes controlled by large amounts of dissolved CO_2.*

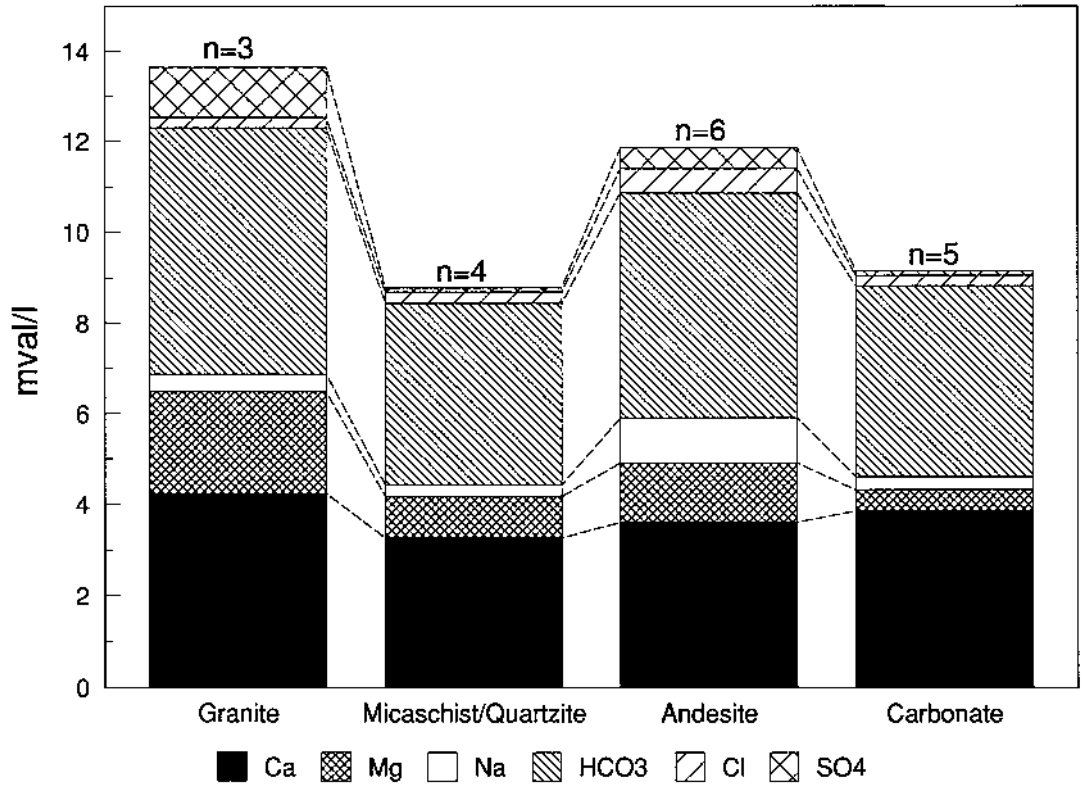


Figure 5: *Comparison of the main chemical constituents of normal groundwaters from different aquifer rocks.*

Hydrolysis under high CO_2-pressure: CO_2 versus temperature (mineral waters)

In many geothermal systems a high temperature is the dominant factor in water-rock interaction, because the solubility of most minerals (except for alkaline earth metals) increases with rising temperatures. This is not the case in CO_2-dominated systems, as can be shown with a SiO_2-temperature diagram (Fig. 6).

Regardless of temperature, all central waters show very similar SiO_2 contents. The difference in temperature between the central springs and the central boreholes Kuz1 and Kuz2, which are all isotopically and chemically identical, is attributed to conductive heat loss of the spring waters during ascent through the cap rocks. Originally, the SiO_2-content of all the central waters was probably controlled by the chalcedony solubility.

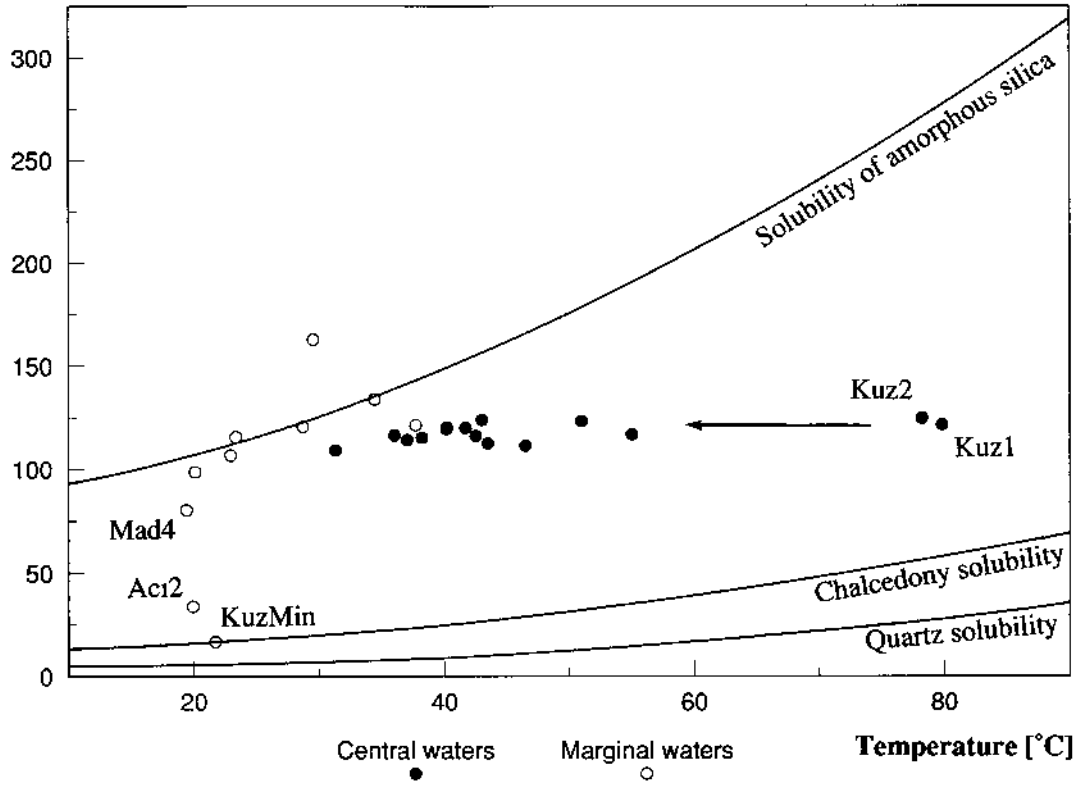


Figure 6: *The low temperature of the central waters compared to the borehole samples Kuz1 and Kuz2 are explained by heat loss by conduction flowing through the cap rocks. As the highest mineralised waters Mad4, Aci2 and KuzMin show very low SiO_2-concentrations and silica deposition may not be expected at these low temperatures, water-rock interaction is* not *dominated by very high temperatures. (Solubility of amorphous silica from Fournier (1981), that of chalcedony from Truesdell (1975) and that of quartz from Fournier and Truesdell (1974)).*

Most marginal waters plot close to the solubility curve of amorphous silica and are therefore probably controlled by this silica phase. The three marginal springs with the highest mineralisation of all the waters (KuzMin, Aci2 and Mad4) are conspicuous by their lowSiO_2-contents. The SiO_2-content of KuzMin seems to be controlled by the solubility of chalcedony and most probably that of Aci2 and Mad4 was also originally controlled by the same silica phase. Because precipitation of chalcedony or quartz is very rare at these low temperatures (Fournier

1981, Stumm and Morgan 1981), the low SiO_2-contents cannot be attributed to silica deposition during ascent of the mineral waters. They are therefore a clear indication for rather low water-rock interaction temperatures.

In the geothermal system of Kuzuluk, water-rock interaction is mainly governed by CO_2 rather than by high temperatures. This is also indicated by quite a good correlation between Cl^- (as marker for water-rock interaction) and ΣCO_2 (Fig. 7).

Hydrolysis is significantly influenced by CO_2: e.g. the solubility of albite increases considerably with rising partial pressure of CO_2 (Stumm and Morgan 1981). This reaction seems to be especially important as Na^+ is the most frequent cation.

Because the solubility of CO_2 in water increases with decreasing temperature, water-rock interaction is favoured by low temperatures in a CO_2-dominated system. This explains the higher mineralisation of the colder marginal waters compared with the hotter central waters.

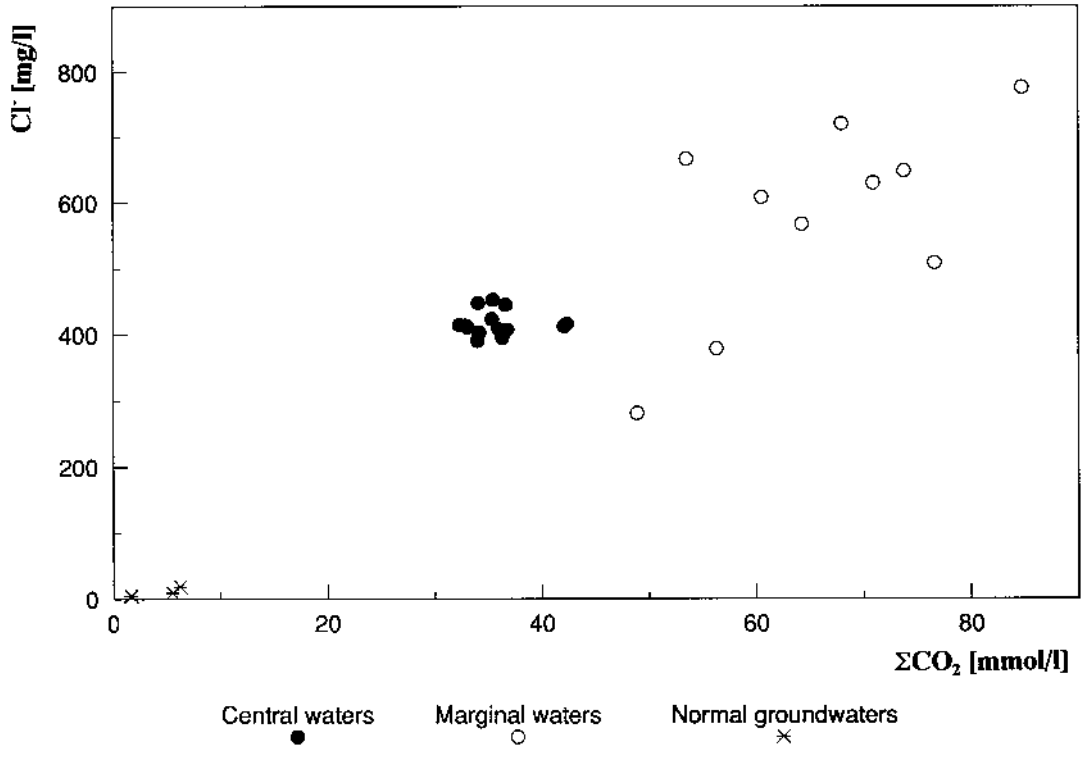


Figure 7: *The rather good correlation between the chemical tracer chloride and the sum of CO_2 (Σ CO_2 = $CO_{2(aq)}$ + H_2CO_3 + HCO_3^-) elucidates the importance of CO_2-pressure on hydrolysis reactions.*

Positive ^{18}O-shift: influence of $\delta^{18}Oco_{2(g)}$ or water-rock interaction with very long contact times?

In geothermal systems the δ^2H and $\delta^{18}O$-values of mineral waters often do not fit the meteoric water line. A positive ^{18}O-shift of up to 15‰ (Hoefs 1987) is usually attributed to water-rock interaction at elevated temperatures (T>150°C). There are two possibilities to explain the distinct ^{18}O-shift of the Kuzuluk mineral waters (Fig. 8):

(1) As gases have a strong influence on the chemical character of the mineral waters, oxygen-exchange between $H_2O_{(l)}$ and $CO_{2(g)}$ has to be taken into consideration. The central spring KapA, e.g., has, under surface conditions, a fairly low volumetric discharge/gas-flux ratio of 0.3, which corresponds to an oxygen atomic ratio r of CO_2/H_2O of about 0.5%. This ratio seems to be quite low at first sight (see IAEA 1983, p. 53), but it has to be kept in mind that gas-flux measurements yield only minimum values, probably falling considerably short of the real gas-flux.

Under equilibrium conditions, an oxygen fractionation dependent on the temperature between $H_2O_{(l)}$ and $CO_{2(g)}$ is adjusted. One proper gas sample, Kuz2, was analysed for oxygen isotopes: the $\delta^{18}O$-value was +22.65‰$_{SMOW}$. The $\delta^{18}O$-value of the corresponding H_2O was -9.16‰$_{SMOW}$. The resulting additive fractionation factor $\varepsilon_{CO2(g)-H2O(l)}$ of 31.81‰ corresponds to the oxygen isotope fractionation between water and CO_2 at 80°C (Friedman and O'Neil 1977). This temperature is almost identical to the measured temperature of 79.8°C at sampling. The $H_2O_{(l)}$ and $CO_{2(g)}$ thus seem to be in equilibrium as far as oxygen isotopes are concerned. However, as the oxygen atomic ratio of CO_2/H_2O is rather small, it is maybe more likely that the $\delta^{18}O$-value of the CO_2 is determined by the $\delta^{18}O$-value of the water rather than vice versa.

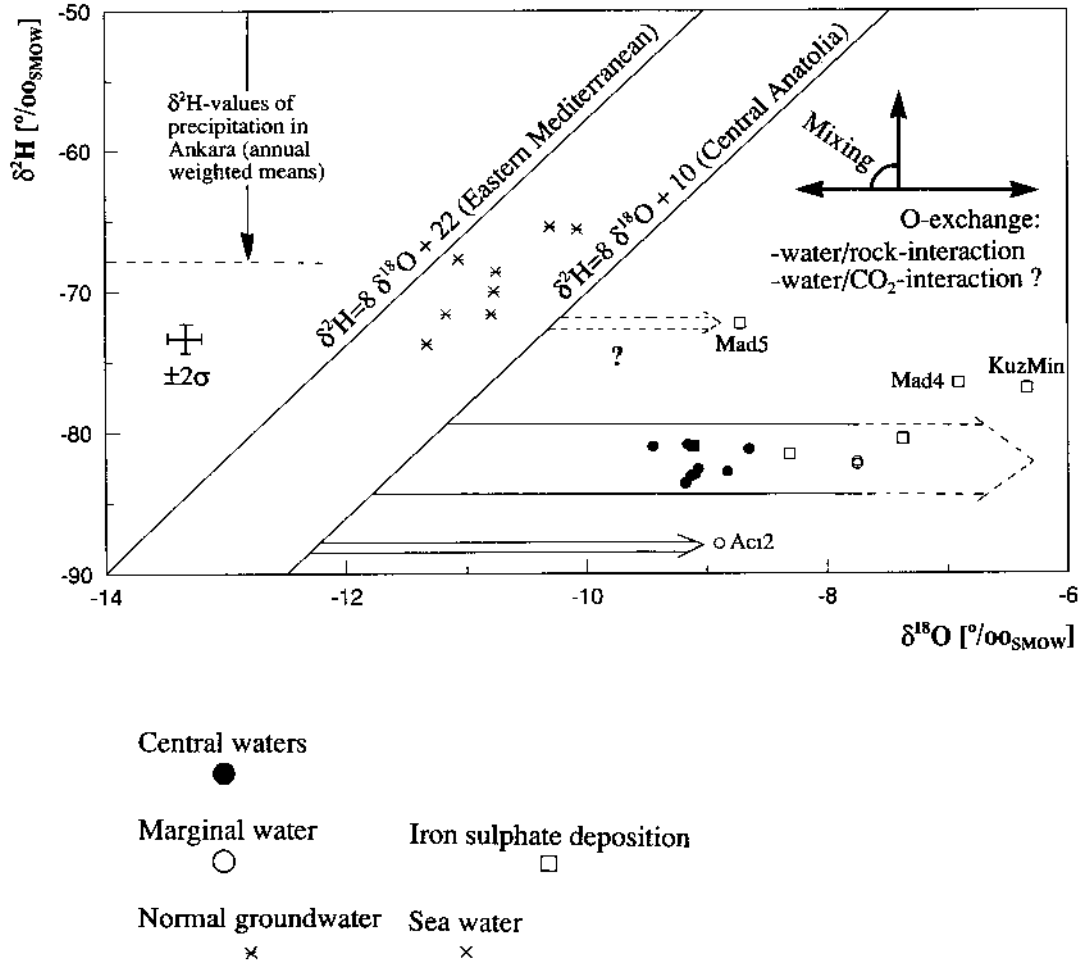


Figure 8: *The very negative δ^2H-values of the central and marginal waters are attributed to a distinctly colder climate during infiltration. Only Mad5 may be a part of the present meteoric cycle. The positive ^{18}O-shift is probably due to water-rock interaction, but an isotopic influence of the CO_2-oxygen cannot be excluded. Stable isotope analysis by W. Rauert and P. Trimborn, gsf Neuherberg, Germany.*

(2) As stated before, the ^{18}O-shift cannot be attributed to very high water-rock interaction temperatures. In low-temperature environments a long contact time between water and minerals is needed for a significant oxygen-exchange to take place and equilibrium is rarely reached (IAEA 1983, pp. 44-57). As the mineral waters of Kuzuluk are probably paleowaters (see below), very long residence times can be assumed.

Consequently, the positive ^{18}O-shift is most probably related to water-rock interaction at low temperatures and very long contact times rather than to domination ofCO_2. For further confirmation, however, additional measurements would be needed.

Sulphur sources and redox reactions

Absence of evaporites and rather low sulphate concentrations in the normal and mineral waters exclude salt deposits as a possible sulphur source. In the following, a model with metal sulphides as the source is proposed (Fig. 9).

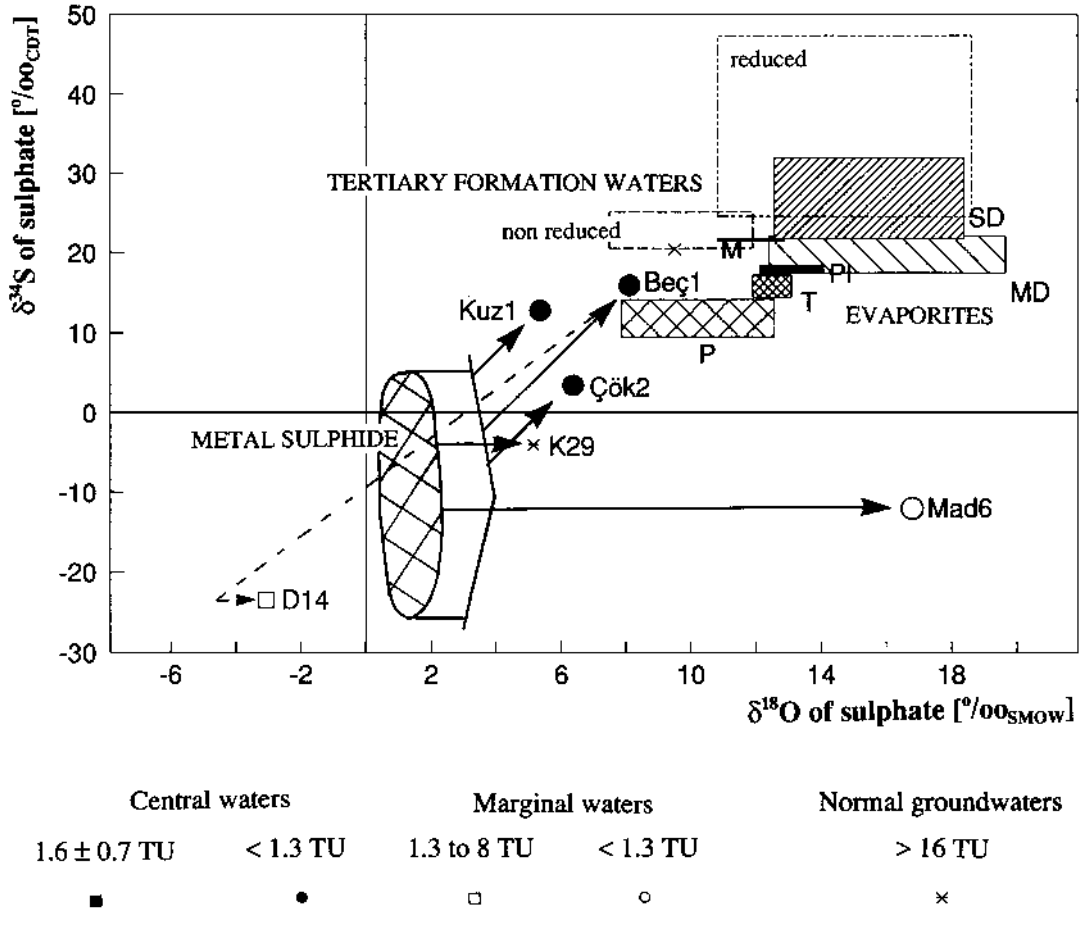


Figure 9: *All sulphate probably originates from metal sulphides (see text for further explanation). (Evaporite data from Claypool et al. (1980); MD = Middle Devonian, SD = Late Devonian, P = Permian, T = Triassic, M = Miocene, PI = Pliocene; Tertiary formation water data from Zak et al. (1980)). Sulphate isotope analysis by Bureau of Stable Isotope Analysis BSIA, Brentford, England.*

(1) K29 is a normal groundwater of Ca-Na-(Mg)-HCO_3-(Cl)-(SO_4) type with a small infiltration area in andesitic rocks. Its sulphate isotopes can be explained by inorganic or bacterial oxidation of metal sulphides. This process is combined with little sulphur fractionation. The$\delta^{18}O$-

value of the newly formed sulphate, however, is more positive than in the water because, apart from the oxygen from water, heavy oxygen from the atmosphere or the root zone may be involved in the oxidation process (Kroopnick and Craig 1976).

(2) The sulphur isotopes of the central waters Kuz1, Beç1 and Çök2 can also be explained by oxidation of metal sulphides, but a subsequent bacterial reduction of the dissolved sulphates must have occurred (Fig. 10). By this latter process the remaining sulphate is enriched in ^{34}S and ^{18}O. The H_2S-gas that was noted at the central springs can be interpreted as the reduced species. Bacterial reduction is a kinetic reaction. With the following mass-balance equation (IAEA 1983, p. 81) it is possible to check the process of bacterial reduction:

$$f \times \delta_f + (1-f)(\delta_f - \Delta_f) = \delta_i$$

where f is the remaining fraction of SO_4^{2-} (in this case: 0.5); δ_f is δ^{34} S-value of remaining SO_4^{2-} ($\delta^{34}S\text{-value}_{Beç1}$ = 15.7‰$_{CDT}$); δ_i is initial $\delta^{34}S$-value before reduction started ($\delta^{34}S\text{-value}_{K28}$ = -3.9‰$_{CDT}$) and Δ_f is $\delta^{34}S$-difference between remaining fraction of SO_4^{2-} and of the reduced species H_2S. With this equation a Δ_f -value of 39‰ is calculated. This value is very close to the predicted value of about 40‰ by Claypool et al.(1980).

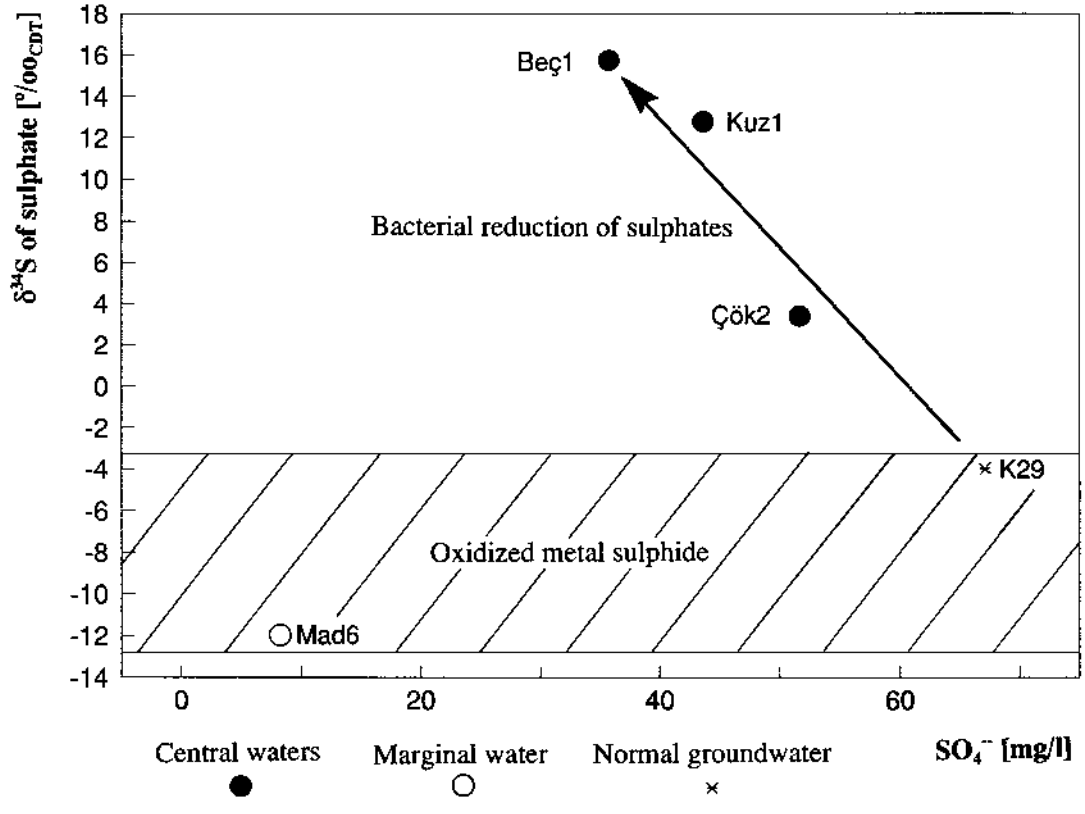


Figure 10: The negative correlation between the SO_4^{2-}-content of the waters and their $\delta^{34}S$-value is explained by progressive bacterial reduction of sulphates.

(3) The sulphate isotopes of the marginal water Mad6 can be explained by the oxidation of metal sulphides. In contrast to the normal groundwater K29, however, the oxygen must originate mostly from the root zone, where the oxygen is characterised by very positive $\delta^{18}O$-values. Another possible explanation is an oxygen equilibrium fractionation between SO_4^{2-} and H_2O, which would afford very long residence times.

(4) D14 is a yellow, partly amorphous precipitation near the central spring Beç1. Quite negative $\delta^{34}S$- and $\delta^{18}O$-values indicate a first precipitation in the form of iron sulphide by bacterial reduction of dissolved sulphates, which is combined with a $\delta^{18}O$-depletion of about 10‰ and a $\delta^{34}S$-depletion of 40‰. Later, the precipitation was probably re-oxidised to the present iron sulphate due to air exposition.

Storage of the mineral waters at depth

Is there a reservoir?

In diagrams with chemical tracers (Fig. 11) and stable isotopes (Fig. 8), the data relative to the central waters form a cluster, which indicates a common reservoir for these waters. The marginal waters have a higher chemical tracer content than the central waters and show slightly differing tracer ratios (Fig. 11). The stable isotope data are widely scattered (Fig. 8). It is thus postulated that each mineral spring had a separate flow path and evolution.

An evolution of the marginal waters from the central waters can be excluded: Aci2 has too low Li^+- and H_3BO_3-contents, KuzMin a too low Li^+-content, Mad5 and Mad6 are too weakly mineralised and the other marginal waters have too low Na^+- and K^+-concentrations. Considering the chemical tracer and stable isotope data, Mad4 is the only marginal water that could have evolved from the central waters; the SiO_2-content, however, contradicts this hypothesis.

Reservoir rocks

A rather shallow reservoir, or at least one channel of it, was penetrated by the two thermal water wells Kuz1 and Kuz2 at depths of 85 and 95m, respectively. The artesian water was found in limestones and underlying micaschists and quartzites (Şentürk and Demirel 1987). The very high Na^+-contents of all the mineral waters are hard to understand without assuming the presence of some volcanic rocks rich in Na-feldspars in a deeper part of the reservoir. This speculation is not inept as the geological situation is indeed very complicated. In addition, it is an interesting fact that even normal groundwaters from volcanic aquifers are characterised by rather high Na^+-contents (Fig. 5).

Reservoir temperatures of the central waters

In order to estimate the potential of a geothermal field, it is important to have some indication of possible reservoir temperatures. Unfortunately, CO_2-dominated waters are not really suitable for the application of classical cation geothermometers. Giggenbach (1988) showed that such waters mostly simulate unreasonably high temperatures. They have to be considered as "immature waters" as they occupy steady-state positions between simple rock dissolution and full equilibration with a thermodynamically stable mineral assemblage. For CO_2-rich waters in particular (Fouillac and Michard 1981, Fouillac 1983), the Na/Li- and Li-geothermometers are recommended. The temperatures calculated for the mineral waters of Kuzuluk by these geothermometers are, however, abnormally high and for this reason questionable.

The most reliable reservoir temperatures can be calculated with a chalcedony geothermometer (Truesdell 1975) for the central waters that have very similar SiO_2-contents. The calculated temperatures are about 120°C.

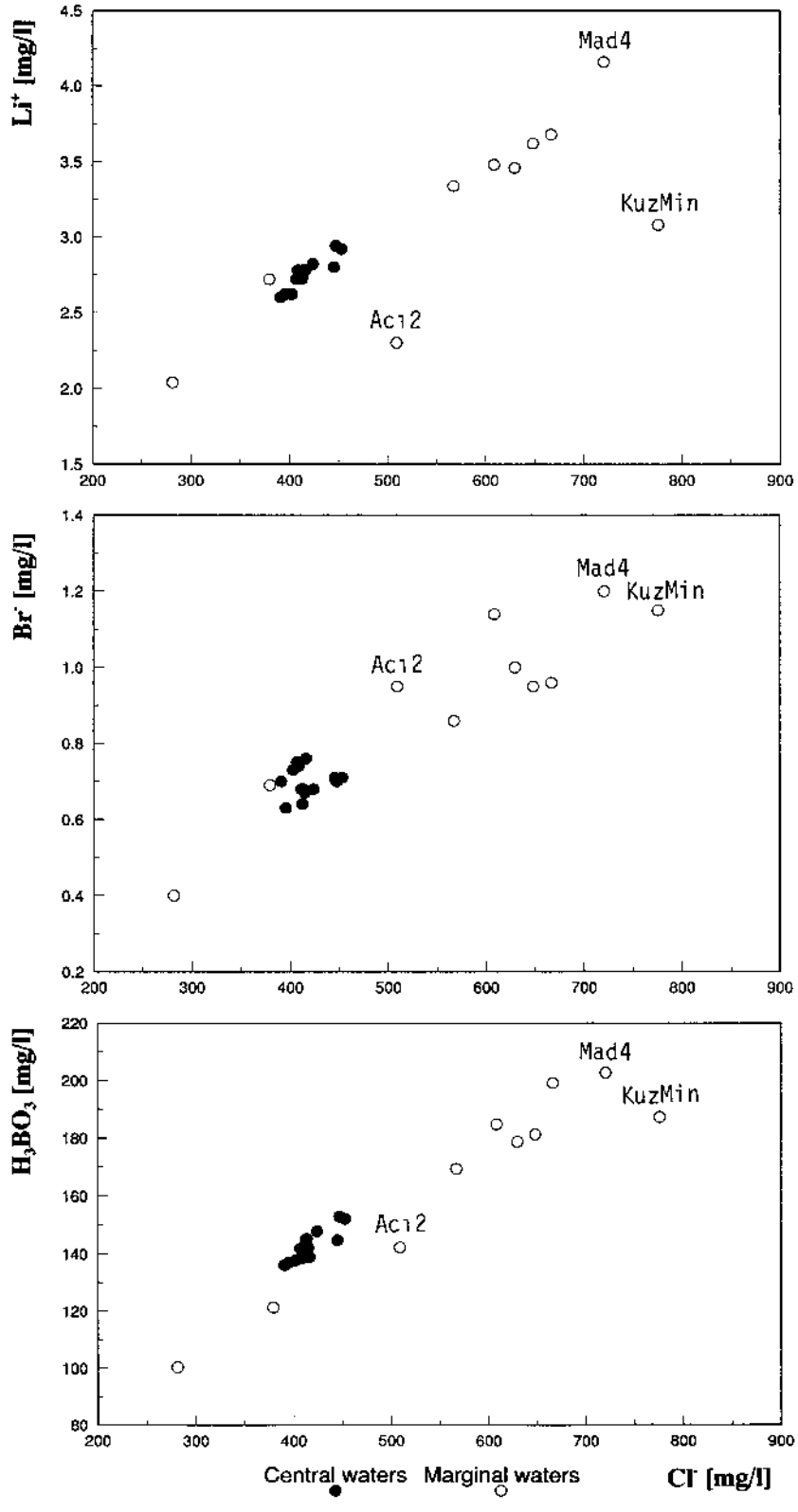


Figure 11: *Plots with chemical tracers. The central waters form a cluster which indicates a common reservoir. From slightly different tracer ratios of the marginal waters, separate flow paths and individual evolution are concluded. Mixing between central and marginal waters or a common origin can be excluded.*

Origin of CO_2-gas

Carbon-dioxide discharges are concentrated along major zones of seismicity such as the circum-Pacific belt and the Alpine belt of southern Europe and Asia Minor (Barnes et al.1978). The same authors expect the CO_2 to originate from the metamorphism of marine carbonates in convergent zones such as subduction zones, and from the earth's mantle where plates are divergent, such as along mid-ocean ridges or deep continental rift zones.

Each of the main CO_2-sources is characterised by different, partly overlapping $\delta^{13}C$-ranges (Fig. 12). $\delta^{13}C$-measurements were made on one CO_2 gas sample and on dissolved carbon species to determine the CO_2-source of the Kuzuluk mineral waters. The $\delta^{13}C$-value of the gas sample Kuz2 is -0.63 ‰$_{PDB}$, and the $\delta^{18}0$-value is 22.65‰$_{SMOW}$. The isotope measurements of the dissolved carbon species are given in Table 3.

For a better understanding of these measurements, the sampling and analysis techniques will be described briefly (Antonsen 1992). Water samples with dissolved and free gases were taken at the springs. In the laboratory, the free gases were removed from the remaining liquid phase. Subsequently, the dissolved carbon was passed into the CO_2 phase by adding air-free HCI. Part of this gas was transferred to another sample bottle and then analysed by the author for ^{13}C and ^{18}O.

In order to compare all the different measurements, the $\delta^{13}C$-values of the corresponding CO_2 phase were calculated on the dissolved carbon species (Table 3), using fractionation curves (Friedman and O'Neil 1977) and sampling temperatures. Comparison between the *calculated* $\delta^{13}C$-values of borehole samples Kuz2 (+1.43 and +1.67‰$_{PDB}$) with the *measured* $\delta^{13}C$-value of gas sample Kuz2 from the same borehole (-0.63‰$_{PDB}$) shows that the *calculated* $\delta^{13}C$-values seem to be, in general, too positive.

		Dissolved carbon species				CO_2-gas
Sample	Sampling date	Measured $\delta^{18}O$ (‰SMOW)	Measured $\delta^{13}C$ (‰PDB)	Temperature (°C)	Additive fractionation factor $\varepsilon_{diss.C-CO_{2(g)}}$	Calculated $\delta^{13}C$ (‰PDB)
Mad7	19-Aug-91	33.76	6.42	28.8	7.2	-0.78
Mad8	19-Aug-91	33.21	6.59	34.7	6.6	-0.01
Mad5	19-Aug-91	31.51	5.10	38.2	6.2	-1.10
Mad5	19-Aug-91	31.77	5.27	38.2	6.2	-0.93
Beç	19-Aug-91	32.08	5.75	50 (?)	5.2	+0.55
Kuz2	20-Sep-91	32.35	5.73	79.8	4.3	+1.43
Kuz2	20-Sep-91	32.83	5.97	79.8	4.3	+1.67
KapD	20-Aug-91	33.16	6.11	43.1	5.8	+0.31
KapD	20-Aug-91	33.16	5.82	43.1	5.8	+0.02
Aci2	20-Sep-91	31.95	2.74	19.8	8.0	-5.26
Aci2	20-Sep-91	32.32	2.92	19.8	8.0	-5.08

Table 3: Measured $\delta^{13}C$- and $\delta^{18}O$-values of dissolved carbon and calculated $\delta^{13}C$-values of corresponding CO_2 at sampling temperatures.

This difference cannot be explained by erroneous temperature values. The temperatures used cannot be too low, as the fractionation decreases with rising temperatures and the differences between the calculated and the measured values would thus become even higher.

Nor can the temperatures used be too high, as spring temperatures have to be considered as minimum values. The difference can probably be attributed to the following effect. The original gas phases with relatively light carbon isotopes were removed from the water phases before $\delta^{13}C$ -measurements were carried out (see above). This effect may have intensified because of the pressure drop during sampling.

Although the calculated $\delta^{13}C$-values are considered to be about 2‰ too positive, almost all of them fall in the (left) range of decomposition of marine carbonates (Fig. 12). Only the marginal spring Aci2 shows strong indications of some mantle-CO_2: even without considering that the calculated value is probably too positive, it still falls outside the range of marine carbonates. Thus, besides an origin from marine carbonates, a (minor?) contribution of CO_2 from degassing of the earth's mantle has to be seriously taken into consideration, although it cannot be proven with the available data. This hypothesis, however, is also supported by the helium isotope measurements (Kipfer 1991, Greber 1992). Up to 8.5% of total helium originates from the earth's mantle. The CO_2 is thought to be its carrier, transporting it into upper crustal levels (Kipfer 1991). The influence of the mantle confirms the importance of the NAFZ as a major plate boundary in general, and that of the Kuzuluk basin as a deep zone of weakness in a locally extensional regime in particular. In addition, the CO_2 coming from the decomposition of marine carbonates may be closely related to actively interacting lithospheric plates, caused by friction processes along their plate boundaries.

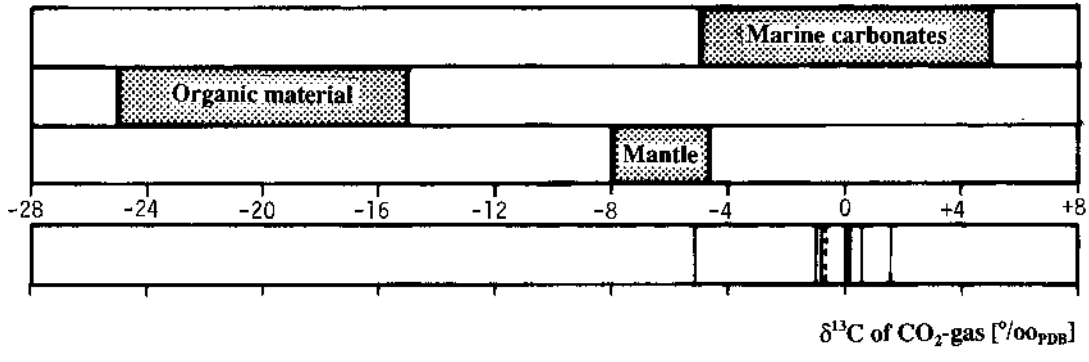


Figure 12: Measured (broken line) and calculated $\delta^{13}C$-values of Kuzuluk mineral waters are compared with main CO_2-sources. The calculated values are generally too positive. Thus, apart from CO_2 from the decomposition of marine carbonates, some minor amounts of mantle-CO_2 may be present. ($\delta^{13}C$-range of organic material from Deines (1980), other ranges from Barnes et al. (1978)).

Recharge

As most of the mineral waters have tritium contents below detection limit, their infiltration must have occurred before worldwide nuclear tests started in 1952. Another indirect indication about recharge is provided by the δ^2H-data. The δ^2H-values of the mineral waters are distinctly more negative than those of the shallow groundwaters (Fig. 8), although the latter include samples from the most elevated springs containing partly melted water. Even the δ^2H-values of the shallow groundwaters in the Bursa-Uludağ area, with infiltration areas up to 2543m a.s.l. are in the same range as the shallow groundwaters around Kuzuluk (Imbach 1992, this volume). Consequently, the negative δ^2H-values of the mineral waters cannot be attributed to altitude effects (Yurtsever and Gat 1981). The Kuzuluk mineral waters cannot be isotopically derived from present-day meteoric water or shallow groundwater except for the marginal spring Mad5.

The negative δ^2H-values can be explained only by recharge during a distinctly colder climate. Only the rather weakly mineralised marginal spring Mad5 can be interpreted as part of the present meteoric cycle. All the other mineral waters have to be considered as paleowaters (Gat 1983) that probably infiltrated during the last Ice Age. Indications for the last Ice Age in the Eastern Mediterranean were reported by Gat and Magaritz (1980). Similar paleowaters with ^{14}C-ages between 9000 and 13,000 years, indicating 5°C lower mean annual temperatures than at present, are reported from the southern Urals (Ferronsky et al 1983). As a consequence, very long residence times of more than 10,000 years must be postulated. This requires either stagnant conditions within the deeper part of the system or long and deep flow paths. A renewal of the present spring outflow is thus uncertain.

As δ^2H-data do not allow any estimation of infiltration altitudes, the original infiltration areas are difficult to identify. Nevertheless there are some indications that they were (or are still) situated in the higher Keremali mountains or in the Almacık mountains even further to the east: (1) The Nummulitic limestones of the higher Keremali mountains are intensely karstified and almost barren of vegetation; (2) by assuming an elevated infiltration area, the potential difference with the upflow area becomes maximum; (3) a westward migration of the mineral waters at depth is indicated by the fact that the Kuzuluk mineral springs are situated in a basin right at the western end of the Almacık lens (Greber 1992, this volume) and not further to the west; and (4) the NAFZ in this area consists mainly of ENE to NE striking faults, that can serve as circulation paths between the infiltration and upflow area.

Hydrogeological circulation model

The main features of the geothermal field of Kuzuluk can be summarised in a schematic circulation model (Fig. 13). Meteoric water probably infiltrated the upper Keremali mountains during the last Ice Age. During extremely long residence times in upper crustal levels, the circulating waters were mineralised by water-gas-rock interactions governed by elevated CO_2-pressures in a low-temperature environment. The decomposition of marine carbonates as well as mantle outgassing are considered to be the origin of the large amounts of CO_2. Only the central waters seem to originate from a common reservoir (maximum reservoir temperature about 120°C) made up of fractured carbonates, micaschists and probably andesites. Each marginal water uses its own separate flow path. The upflow of all the mineral waters occurs along tectonic fissures in a regional tectonic extensional structure. This is facilitated by the CO_2, which reduces the density of the waters. The upflow zone is covered by cap rocks consisting of silicified gravel, volcanic tuff and andesite. In the uppermost layers, mixing occurs with young shallow groundwaters at the margins of the basin, as well as heat exchange between small shallow aquifers and the atmosphere.

Conclusions

The influence of active tectonics on the circulation of the Kuzuluk mineral waters is variable. Firstly, the upflow area is restricted to a zone of extension that is probably still subsiding. Quite small-scale zones of alternating extension and compression are a typical feature of major strike-slip fault systems (Reading 1980). Secondly, the short-term flowpath system of tectonic fissures is very unstable in its response to releases of seismic energy. However, it is surprising that the present low-temperature system developed in the same area and in a very similar stress regime (Greber 1992) as the early volcanic high-temperature system. This may be at-

tributed to a pattern of more or less constant motion of the lithospheric plates in the Near East since the Late Miocene. Thirdly, the release of large amounts of CO_2 is probably related to seismically active tectonics, such as the interaction of the Black sea and Turkey plates. Fourthly, the ascent of the mineral waters is facilitated by the CO_2, which reduces their density.

In contrast to high-temperature systems, water-rock interaction in CO_2-dominated systems is favoured by high CO_2-pressures and low temperatures. The chemistry of the waters is influenced effectively by the dissolution of CO_2. An isotopic influence of the CO_2 on the oxygen isotopes of the waters, however, is rather unlikely.

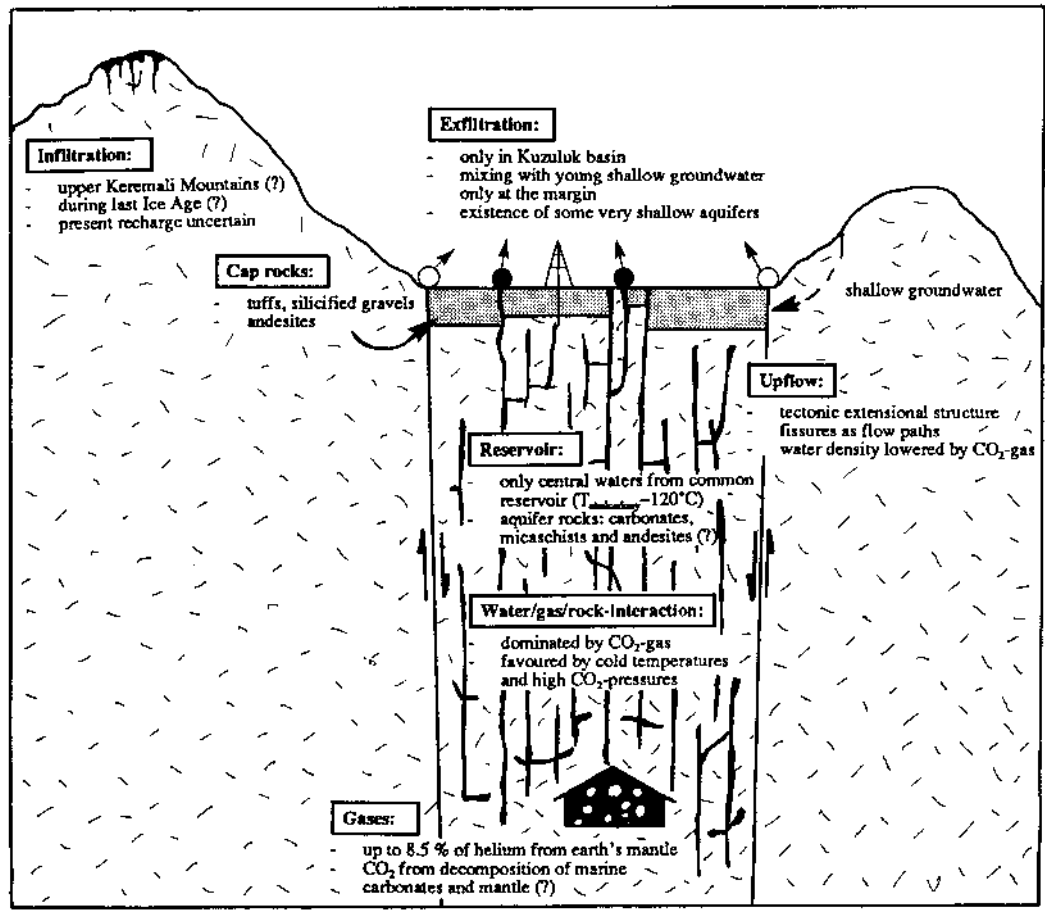


Figure 13: Schematic circulation model of the Kuzuluk mineral waters.

Note

This contribution previously appeared with the same title but in a slightly different form in the Journal *Geothermics* (Greber 1994) and was published within this volume with the agreement of *Geothermics*.

References

Ambraseys, N. N. and Zatopek, A., 1969, The Mudurnu valley, West Anatolia, Turkey, earthquake of 22 July 1967, Bull. Seismol. Soc. Am., 59, 521-589.

Antonsen, 0., 1992, Beitrag zum Projekt "Tektonische Aktivität und ihre Wechselbeziehungen zu Grundwasserzirkulation, Geothermie und Seismizität – Studiengebiet NW-Türkei", ETHZ, TU-İstanbul. Untersuchungsbericht 1/92, Paul Scherrer Institut PSI, 4 (+2 Tab.).

Barnes, I., Irwin, W. P. and White, D. E., 1978, Global distribution of carbon dioxide discharges and major zones of seismicity, U.S. Geological Survey Water Resources Investigations 78-39, Open-File Report, 12p.

Bistritschan, K., 1957, Sakarya vilayetindeki sıcaksu ve maden suyu kaynakları, MTA Derleme No. 2621, Ankara (in Turkish with summary in German, unpubl.).

Claypool, G. E., Holster, W. T., Kaplan, I. R., Sakai, H. and Zak, I., 1980, The age curve of sulphur and oxygen isotopes in marine sulphate and their mutual interpretation, Chem. Geol. 28, 199-260.

Deines, P., 1980, The isotopic composition of reduced organic carbon, in: Handbook of Environmental Isotope Geochemistry 1, The Terrestrial Environment, A., edited by: P. Fritz and J.C. Fontes, Elsevier, Amsterdam, 329-406.

DSİ, 1983, Devlet Su İşleri, Aşağı Sakarya ovası hidrojeolojik etüd raporu, Eskişehir (unpubl.).

Ellis, A. J. and Mahon, W. A. J., 1964, Natural hydrothermal systems and experimental hot-water/rock interactions, Geochim. cosmochim. Acta, 28, 1323-1357.

Ellis, A. J. and Mahon, W. A. J., 1967, Natural hydrothermal systems and experimental hot-water/rock interactions (part 2), Geochim. cosmochim. Acta, 31, 519-539.

Ferronsky, V. I., Vlasova, L. S., Esikov, A. D., Polyakov, V. A., Seletsky, Yu, B., Punning, Ya.-M. K. and Vajkmyaeh, R. A., 1983, Relationships between climatic changes and variations in isotopic composition of groundwater, precipitation and organic soil matter in the Quaternary period, in: Palaeoclimates and Palaeowaters: A Collection of Environmental Isotope Studies. Proc. Advisory Group Meeting, IAEA Vienna, 25-28 Nov. 1980, 13-35.

Fouillac, C., 1983, Chemical geothermometry in CO_2-rich thermal waters. Example of the French Massif Central, Geothermics, 12(2/3), 149-160.

Fouillac, C. and Michard, G., 1981, Sodium/lithium ratio in water applied to geothermometry of geothermal reservoirs, Geothermics, 10, 55-70.

Fournier, R. 0., 1981, Application of water geochemistry to geothermal exploration and reservoir engineering, in: Geothermal Systems: Principles and Case Histories, edited by: L. Rybach and L. J. P. Muffler, Wiley, Chichester, 109-143.

Fournier, R. 0. and Rowe, J. J., 1966, Estimation of underground temperature from the silica content of water from hot springs and wet-steam wells, Am. J. Sci., 264, 685-697.

Fournier, R. 0. and Truesdell, A. H., 1974, Geochemical indicators of subsurface temperature, 2. Estimation of temperature and fraction of hot water mixed with cold water, U.S. Geol. Surv. J. Res., 2, 263-270.

Friedman, I. and O'Neil, J. R., 1977, Compilation of stable isotope fractionation of geochemical interest, Data of Geochemistry (6^{th} edn), U.S. Geological Survey Professional Paper, 440-KK.

Gat, J. R., 1983, Precipitation, groundwater, and surface waters: Control of climate parameters on their isotopic composition and their utilisation as palaeoclimatological tools, in: Palaeoclimates and Palaeowaters: a Collection of Environmental Isotope Studies, Proc. Advisory Group Meeting, IAEA Vienna, 25-28 Nov. 1980, 3-12.

Gat, J. R. and Magaritz, M., 1980, Climatic variations in the Eastern Mediterranean sea area, Naturwissenschaften, 67, 80.

Giggenbach, W. F., 1988, Geothermal solute equilibria. Derivation of Na-K-Mg-Ca-geoindicators, Geochim. cosmochim. Acta, 52, 2749-2765.

Giggenbach, W. F. and Goguel, R. L., 1989, Collection and analysis of geothermal and volcanic water and gas discharges, Report No. CD2401, Fourth Edition, Chemistry Division, Department of Scientific and Industrial Research, Petone, New Zealand, 81p.

Greber, E., 1992, Das Geothermalfeld von Kuzuluk/Adapazarı (NW-Türkei) – Geologie, aktive Tektonik, Hydrogeologie, Hydrochemie, Gase und Isotope, Ph.D. thesis, ETH Zürich, 213p.

Greber, E., 1994, Deep circulation of CO_2-rich palaeowaters in a seismically active zone (Kuzuluk/Adapazarı, Northwestern Turkey), Geothermics, Vol. 23, No. 2, 151-174

Greber, E., this volume, Stratigraphic evolution and tectonics in an area of high seismicity: Akyazı/Adapazarı (Pontides, Northwestern Turkey).

Harland, W. B., 1971, Tectonic transpression in Caledonian Spitzbergen, Geol. Mag., 108, 27-42.

Hoefs, J., 1987, Stable isotope geochemistry, Minerals and Rocks *9* (3rd edn), Springer, Berlin, 241p.

Imbach, Th., 1992, Thermalwässer von Bursa. Geologische und hydrogeologische Untersuchungen am Berg Uludağ (NW-Türkei), PhD thesis, ETH Zürich, 178p.

Imbach, Th., this volume, Geology of Mount Uludağ with emphasis on the genesis of the Bursa thermal waters, Northwest Anatolia, Turkey.

IAEA, 1983, Isotope techniques in the hydrogeological assessment of potential sites for the disposal of high-level radioactive wastes, Technical Reports Series No. 228, International Atomic Energy Agency IAEA, Vienna, 151p.

Ketin, I., 1959, The orogenic evolution of Turkey, Bull. Min. Res. Explor. Inst. Turkey, *53,* 82-88.

Kipfer, R., 1991, Primordiale Edelgase als Tracer für Fluide aus dem Erdmantel, Ph.D. thesis, ETH Zürich, 223p.

Kroopnick, P. M. and Craig, H., 1976, Oxygen isotope fractionation in dissolved oxygen in the deep sea, Earth Planet. Sci. Lett., 32, 375-388.

Lucius, M., 1929, Kuzuluk (Akyazı) thermo-mineral suları hakkında rapor, MTA Derleme No. 558, Ankara (in Turkish with summary in German, unpubl.).

McKenzie, D. P., 1972, Active tectonics of the Mediterranean region, Geophys. J. R. Astron. Soc., 30, 109-185.

Reading, H. G., 1980, Characteristics and recognition of strike-slip systems, in: Sedimentation in Oblique-Slip Mobile Zones, edited by: P.F. Ballance and H.G. Reading, Spec. Publ. Int. Ass. Sediment, 7-26.

Rupprecht, K. H., 1955, Kuzuluk-Aziziye mevkii'nin Çemalbey Mahallesinde bulunan Kaplicaların jeolojik etüdü, MTA Derleme No. 2329, Ankara (in Turkish with summary in German, unpubl.).

Schindler, C., 1993, The MARMARA Poly-Project: Tectonics and recent crustal movements revealed by space-geodesy and their interaction with the circulation of groundwater, heat flow and seismicity in Northwestern Turkey, Terra Nova *5,* 164-173.

Şengör, A. M. C., 1979, The North Anatolian transform fault: its age, offset and tectonic significance, J. Geol. Soc. Lond., 136, 269-282.

Şentürk, N. and Demirel, Z., 1987, Akyazı (Sakarya) Kuzuluk kaplicası hidrojeoloji inçelemesi, MTA-Report (in Turkish, unpubl.).

Stumm, W. and Morgan, J. J., 1981, Aquatic Chemistry-An Introduction Emphasizing Chemical Equilibria in Natural Waters (2nd edn), Wiley-Interscience, New York, 780p.

Truesdell, A. H., 1975, Summary of section III-Geochemical techniques in exploration, Second United Nations Symposium on the Development and Use of Geothermal Resources, San Francisco, May 1975, 1, 1iii-1xiii.

Truesdell, A. H. and Hulston, J. R., 1980, Isotopic evidence on environments of geothermal systems, in: Handbook of Isotope Geochemistry. Vol. 1. The Terrestrial Environment, edited by: P. Fritz and J.C. Fontes, Elsevier, Amsterdam, 179-225.

White, D. E., Brannock, W. W. and Murata, K. J., 1956, Silica in hot spring waters, Geochim. cosmochim. Acta, 10, 27-59.

White, D. E., 1970, Geochemistry applied to the discovery, evaluation and exploitation of geothermal energy resources, Geothermics, Special Issue 2(1), 58-80.

Yurtsever, Y. and Gat, J. R., 1981, Atmospheric waters, in: Stable Isotope Hydrology Deuterium and Oxygen-18 in the Water Cycle, Technical Reports Series No. 210, IAEA, Vienna, 103-142.

Zak, I., Sakai, H. and Kaplan, I. R., 1980, Factors controlling the $^{18}O/^{16}O$ and $^{34}S/^{32}S$ isotope ratios of ocean sulfates, evaporites and interstitial sulfates from modern deep sea sediments, in: Isotope Marine Chemistry, edited by: E.D. Goldberg, Y. Horbie and K. Saruhashi, Geochem. Res. Ass., Tokyo, Japan, 339-373.

Observed pressure variations and their causes in the geothermal field of Kuzuluk / NW Turkey

SILVIO TSCHUDI

Abstract

Piezometers installed at two geothermal drillings at Kuzuluk (NW Turkey) gave the opportunity to monitor pressure variations in an active hydrothermal system. Both wells, each with a temperature of >80°C, were overpressured with 2.5 bar and 6 bar, respectively. An accelerometer was installed near the two piezometers to record occurring earthquakes. The main aim of this investigation was to identify tectonic influences on pressure variations in a hydrothermal system. Human noise and other effects on the pressure regime had to be estimated and removed before an identification of the tectonic influence could be performed. The pressure variations recorded at the well Kuz1 are dominated by at least two main processes. Beside low-frequency and often saw tooth-like variations over an interval of ±0.3 bar within a few hours and days, regular and high frequency spikes with relative pressure deflections of up to ±0.5 bar within a few minutes were obvious. The high frequency events show a strong regularity over 24hrs. Thus, direct and indirect human influences must be seriously considered. The low frequency variations were tested on several known processes, such as meteorological influences and tidal forces, but neither tidal components nor barometric correlation could be found. Strong dynamic system behaviour seems to overprint the weak external forces. Only the atmospherical tides S_1 and S_2 were prominent in the spectra. The whole hydrothermal system is dominated by a strong CO_2 outgassing phenomenon. The varying pressure in Kuz1 is probably controlled by a complex geological valve system. Cold CO_2 at the top of the hot water column builds up gas pressures which are higher than the mechanical resistance of the valve. This system seems to be sensitive to heavy rainfall, since the response level of the valve decreases by intercepting meteoric water. Other parameters of the hydrothermal system of Kuzuluk also react to rainfall. It seems that the discharging regime is strongly dependent on meteoric rainfall since also other parameters of the hydrothermal system of Kuzuluk react to it. During dry periods closed flow paths could be opened and unconsolidated fillings, which react as valves, could undergo changes in their mechanical properties by entering meteoric water. Tectonic influence on the pressure in Kuz1 could unfortunately not be identified. Several reasons could be given for this: No larger tectonic event occurred during the investigation period between spring 1991 and autumn 1992 in the area around Kuzuluk. Weak and near events could not be identified on the accelerometer recordings, since the noise level was too high. The dynamic system behaviour, controlled and dominated by strong CO_2 outgassing, seems to overprint tectonic influence.

Introduction

The observation of physical parameters in wells (e.g. pressure, temperature, electrical conductivity, pH and others) has a long tradition in hydrology, geology and geophysics. Under special conditions, an estimate of rock parameters of the aquifer can be given (e.g. Bredehoeft 1967, Van der Kamp and Gale 1983, Rojstaczer and Agnew 1989). These parameters

(e.g. permeability, porosity, specific storage, poroelastic properties), which can be computed and estimated by using tidal and barometric effects on the aquifer, are important for the use of groundwater.

Furthermore, changes in pressure, flow rate, colour, taste, smell and chemical composition have been observed as hydrologic precursors to earthquakes. Many authors described well level variation as a possible seismic precursor (e.g. Albarello et al. 1991, Kissin and Grinevsky 1990). Roeloffs (1988) gives a good overview of the methods for analysing well level variations with regard to earthquake prediction. Confined fluids can also be used as strain meters (Bodvarsson 1970) or even as seismometers (Schenk and Krauss 1972b).

The wells described in this paper lie in an active geothermal system at Kuzuluk, in Northwestern Turkey. More then 40 cold (about 20°C) and hot (up to 55°C) mineral waters emerge at this site. In addition, artesian hot water (>80°C) was found in two boreholes. The geothermal system is closely related to an active tectonic structure, the North Anatolian Fault Zone (NAFZ). This fault zone is seismically still very active; the last severe earthquake near Kuzuluk occurred in 1967 (with M_S=7.2). This enables the study of the influence of active tectonics on the circulation of deep waters. For this reason, two wells, drilled for industrial purposes, were equipped with piezometers. A vertical accelerometer was also installed next to the borehole Kuz2. This instrumentation registered data from spring 1991 until autumn 1992, when lightening destroyed the electronic equipment. It is important to keep in mind that the measurement of only two parameters (e.g. well pressure and acceleration) is not sufficient to make any statement concerning tectonic correlation or triggering. Also, meteorological influences (e.g. barometric pressure, precipitation) must be considered to determine anomalies in the different time series of pressure variations.

The thermal waters of the observed boreholes, Kuz1 and Kuz2 with a depth of 250m and 160m, respectively, have a temperature of about 80°C and an average pressure of 2.5 bar. Both waters are CO_2 dominated (Greber 1992 and this volume) and they show typical outgassing phenomena. The pressure of Kuz2 is attenuated by a trapped gas phase lying on the hot water column. In contrast to Kuz2, Kuz1 shows no attenuation effects.

Well description and data acquisition

The two wells described in this paper lie in the eastern part of Kuzuluk at 40° 38' northern latitude and 30° 39' eastern longitude. The elevation above mean sea level is about 158m. Small cabins provide protection from meteoric influences. The distance between the two boreholes Kuz1 and Kuz2 is about 25m. Near the well positions, a road of local interest passes by (Figure 1). The boreholes lie 400m south of the German multiparameter station 'Çökek Hamamları' (Woith 1995). To the south of the wells, the mineral water factory of Kuzuluk ('Kuzuluk maden suyu') commercially bottles mineral water. At some distance, a power line strikes subparallel to the Mudurnu valley.

The boreholes, each 8 inches in diameter, were drilled in 1987 and supervised by the MTA (Şentürk and Demirel 1987). Technical information about the borehole casing, the state of the space outside the casing and the depth of the open parts of the well are, unfortunately, not known. This information would be of great interest for the investigation of the pressure behaviour of the hydrothermal system of Kuzuluk. The drillings are most probably cased from top to bottom and it seems that only a small part is open to the aquifer at the bottom. A brief physical characterisation of the encountered lithologies and their hydrogeological importance is given in Table 1.

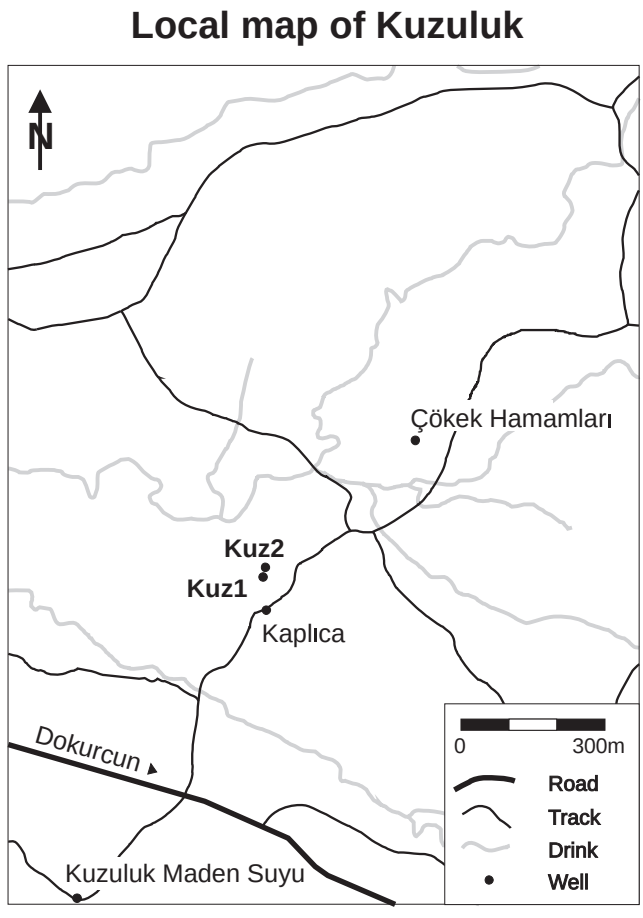


Figure 1: Detailed map of Kuzuluk with the relevant wells Kuz1, Kuz2, Çökek Hamamları (German multiparameter station) and the Kuzuluk Maden Suyu (Kuzuluk Mineral Waters).

Lithology	Hydrogeological description	Hydrogeological category
Kuzuluk Series	Partly impermeable tuffs, silicified gravels	Aquiclud
Andesites	Fractured aquifer	Aquiclud
Aksartepe Limestone	Joints, partly highly carstified but often sealed with red clays	Aquifer
Metamorphics	Fractured aquifer	Aquifer

Table 1: Hydrogeological properties of the Kuz1 and Kuz2 lithologies (after Greber 1992)

Hydrothermal fluid circulation in the upper crust is mostly controlled by the regional heat regime. The Kuzuluk hydrothermal system shows typical features of an active hydrothermal system: Under a fractured cover of travertine/silicified gravel and tuff, permeable rocks (limestone, metamorphics) provide a hydrothermal reservoir, whose temperature was determined by quartz and chalcedon methods to lie at about 180°C. The Kuzuluk area does not show an extensive high heat flow. Pfister (1995) determined the heat flow at Samanpazarı, a village near Kuzuluk, to be 74±14mW/m^2. The hot waters of Kuzuluk rise rapidly through higher permeable rocks and transport heat from greater depths to the surface.

Instrumentation

An MC-2 unit manufactured by SIG SA, Switzerland, was used for the measurements and registration of the two well pressures and the seismicity. This unit provides a combination of amplification electronics for three channels (Kuz1, Kuz2 and seismic signal), peak detection for the seismic channel and a line recorder 'Linax 7k2' (Camille Bauer, Switzerland). The MC-2 unit and the seismic sensor were installed in the cabin of the well 'Kuz2'. Power supply was provided by 220V AC and two rechargeable batteries, Günther SG 110, of a lead acid maintenance-free type. The capacity of 100Ah and 12V provides a full function of the registration unit during a power cut. The amplifiers have a total error of±2.3%. The error of the piezometric sensors was assumed to be ±3%. The seismic sensor reacts only to vertical shocks and it was used as a peak detector with a total error of about±15.3%. The three signals were recorded on a three pen analogue servo-line recorder Linax 7k2 with a maximum basic error of ±0.5%. An additional temperature error ranges between ±0.25% per 10°C. The observed time error ranges over an interval of±5 minutes per 30 days. Data was recorded from the 28th of April, 1991 until the 1st of September, 1992 (Table 2), but only Kuz1 recordings could be used for further investigation.

Availability of data (Kuz1, Kuz2, accelerometer, seismo)

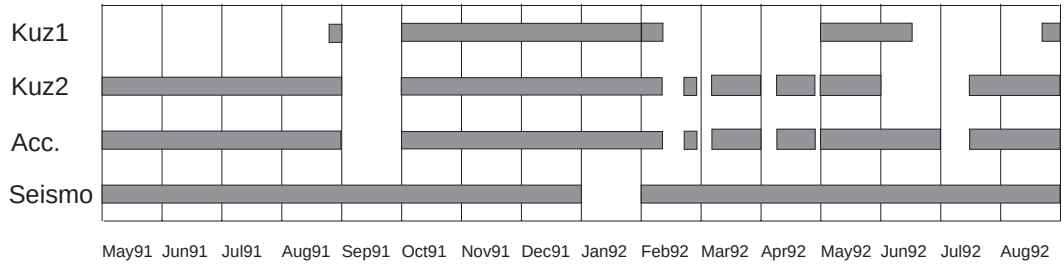


Table 2: Availability of data during the whole period of investigation

Discussion

Accelerometer

The recordings of the accelerometer were statistically analysed to check whether or not the data were regular distributed over 24hrs. It turned out that the accelerometer data were not homogeneously distributed over the whole day. The distribution encountered points to a large amount of human noise in the records. Only one cluster of recorded peaks could be clearly identified as having originated from earthquakes (March 24, 1992, 20:00 [UTC] at 40.66N / 30.61E with a magnitude of 2.1. Revised Earthquake Catalogue 1992, Mudurnu Valley, Frankfurt am Main). The noise-dominated accelerometer data were not used for further examination.

High frequency events (HFE)

Although both wells seemed to come out of the same reservoir, pressure registration of Kuz1 and Kuz2 show few similarities. One common feature is the appearance of sharp and asymmetrical pressure releases at both wells. These releases do not appear as isolated peaks, but as a group of several fast pressure deflections (Figure 2). These clusters of high frequency

variations can be defined as events. In the following, they are called 'high frequency events' (HFE). The size of a single peak of a HFE ranges between 0.1 and 0.7 bar. Pressure dropped instantaneously and was balanced up to the previous value within less than a minute.

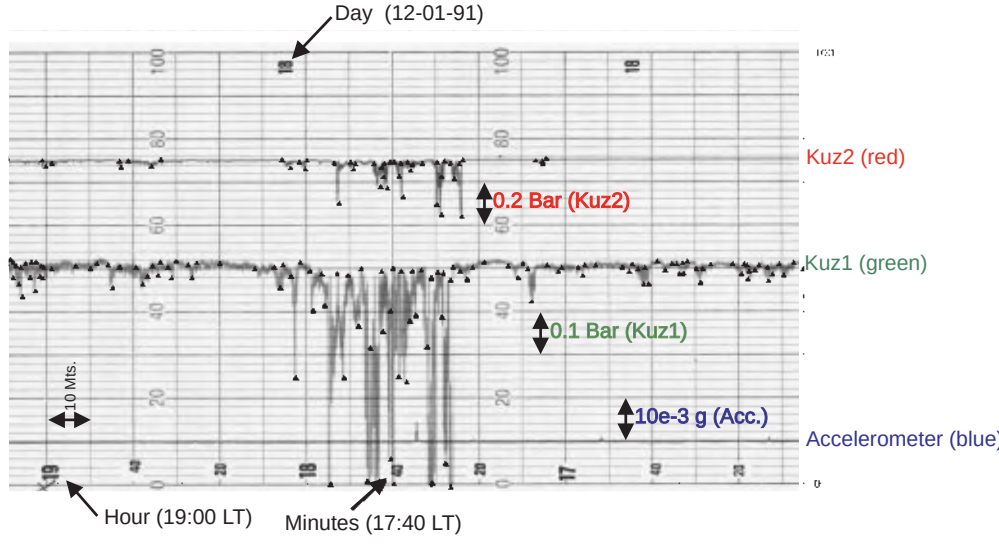


Figure 2: *Typical record of the three parameters Kuz2, Kuz1 and Accelerometer. Horizontal axis is (local) time, increasing from the right to the left. Pressure (Kuz1 and Kuz2) is recorded from 0 to 100 as relative values. The average of Kuz1 (≈50) is equal to ≈2.5 bar overpressure. Kuz2 oscillated around 75, which is equal to (4.5 bar overpressure. It is worth mentioning that the high frequency oscillation of Kuz1 and Kuz2 (between 17:25 and 18:10) only deflect downwards. Triangles represent digitised points.*

The recordings of both wells show HFE. They seem to be triggered by the same physical event. HFE do not occur at arbitrary times. For each digitised section, a statistical analysis was carried out. The compilation (Figure 3) was computed based on several histograms and it shows a significant clustering of HFE during particular time periods. Apart from calm hours (after midnight till 0500AM and from 0900AM to 0300PM, LT), periods of a much higher density of digitised points and therefore HFE exist.

The high frequency trembling of the pressure registration is probably not a reaction to a true pressure variation in the hydrothermal system of Kuzuluk, since the HFE occur regularly in time. A regular repetition of events, especially with a rhythm of 24hrs, is a strong reference to human activity. Direct human manipulations (e.g. manual pressure release) can almost be excluded, since both wells, separated by a distance of 25m, react to the same phenomena simultaneously.

The occurrence of HFE could be explained by irregularities in the power supply of the Kuzuluk well site. Both time periods of increased density of digitised points could also be time periods of increased power consumption. This consumption could be controlled by power consuming equipment in the Mudurnu valley (e.g. industrial production during 'cheap' hours, intensive cooking). Although battery packs were in place, variations in electricity could influence the analogue electronic equipment used.

Thus, it was decided to remove the HFE from the recorded time-series before further investigations were performed.

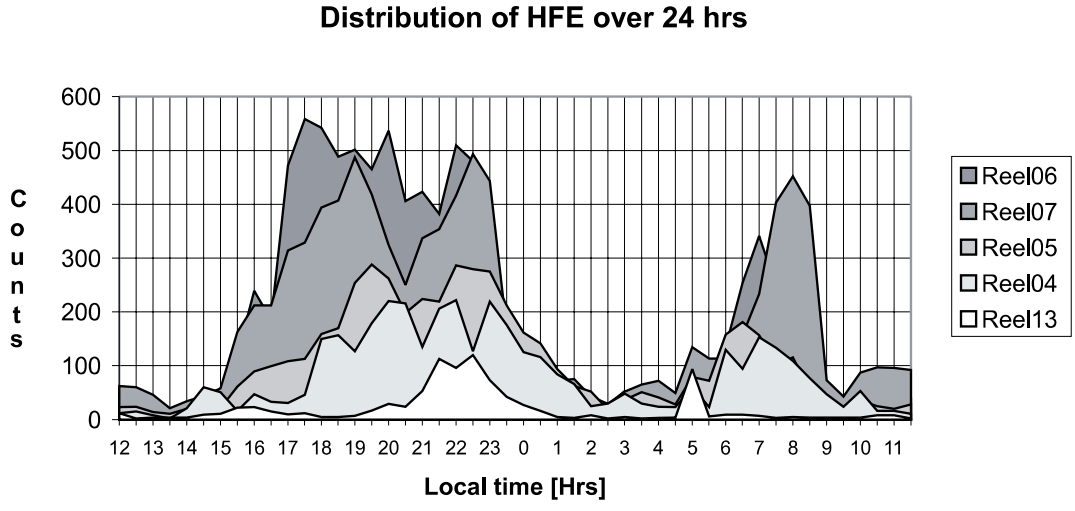


Figure 3: *Compilation of the HFE distribution over a day. Histograms with 48 bins were used to compute the counts. It is obvious that HFE are not arbitrary distributed over 24hrs. Several maxima are obvious: One during the night from the late afternoon to midnight, a second around 0500AM and a third group of HFE from 0600AM till 0900AM.*

Non tectonic influences on the Kuz1 pressure variations

Meteorological processes often strongly influence the behaviour of the well and pressure registration. Woith (1995), who investigated radon variations in ground air and ground water at the Mudurnu valley, mentioned that over 95% of his recorded parameter variations were controlled by meteorological effects. Spectral analysis would provide an estimation of possible regular processes, such as astronomical or atmospheric tides.

Direct temperature influence

The power spectral density showed in Figure 4 is a typical example for frequency characteristics of Kuz1 well recordings. Peaks at 1, 2, 3 etc. cycles per day can clearly be identified as atmospheric tides, usually known as S_1, S_2, S_3 etc. (Melchior 1983, Evans et al. 1991). The atmospheric tides are induced by solar (S) radiation and they influence, among others, atmospheric temperature and atmospheric pressure. The temperature-induced pressure variations range over ±0.05 bar relative to the absolute pressure value of 2.5 bar at the well Kuz1, which is equal to ±2% of the recorded pressure variations. Atmospherical tides influence the pressure variations of Kuz1 in a neglectable way.

Barometric influence

Barometric influence on the hydrothermal system of Kuzuluk seems to be low. Neither graphical estimation and correlation, nor theoretical and statistical approaches lead to parallelism between the two parameters. The heterogeneous and complex geology at Kuzuluk, and the dynamic behaviour of the well itself, probably prevents visible influences by atmospheric pressure changes.

Earth tides

Confined wells are often influenced by tidal processes of the earth, the sun and the moon. Bredehoeft (1967) gives a good historical overview of past scientific investigations of tidal influences. Melchior (1983) made a number of investigations concerning tidal fluctuations in

wells. The spectrum of each time series was compared with the theoretical spectra of tidal forces. Particular astronomical tides, such as M_2 or O_1 (Melchior 1983), are, in comparison with theoretical tides, not significant and almost absent.(Figure 4)

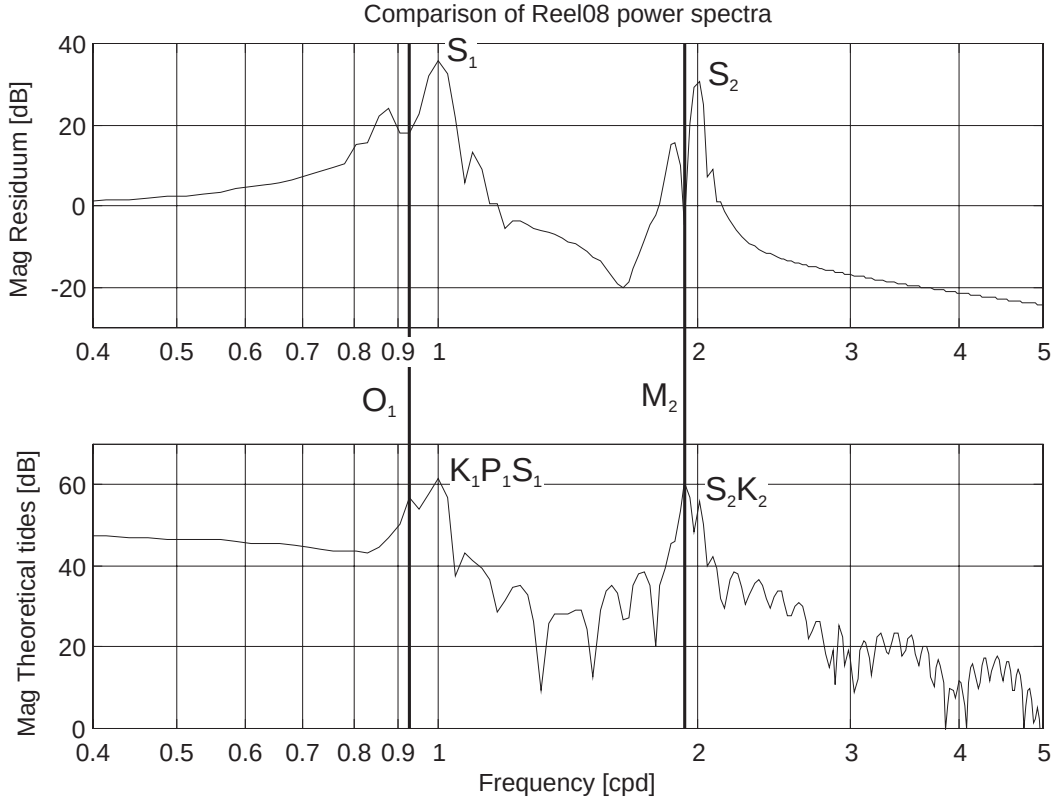


Figure 4: *Typical spectra of Kuz1 residual and of theoretical astronomical tides. Note that typical astronomical tides, such as O1 and M2, are absent in the Kuz1 spectrum. Both spectra were computed over the same time period of 29 days (which is equal to 2935 values, zero padded up to 4096) with no overlap.*

Precipitation

At the end of November 1991, both amplitude and frequency of pressure variation dramatically changed (Figure 5). After November 1991, pressure at Kuz1 did not reach the same level as previously. If Kuz1 pressure data are compared with precipitation data (kindly made available by Lühr, Westerhaus and Woith, GFZ Potsdam), a correlation between heavy rainfall and a change in the amplitude and frequency behaviour of the well Kuz1 is possible. The precipitation records from the end of November 1991 mark the beginning of the rainy season in the Mudurnu valley, NW Turkey. The pressure behaviour of the Kuzuluk hydrothermal system seems to be sensitive to continuous and heavy rainfall. How can this correlation be explained?

The waters of Kuz1 are very rich in CO_2 (Greber 1992) and it can be presumed that the CO_2 input was constant at depth during the time of investigation. The CO_2 rises together with the hot waters to the Earth's surface. At a certain, not estimated depth, boiling occurs and CO_2 bubbles create a separate gaseous phase. If the system is sealed at the top (like Kuzuluk), gas bubbles are not able to leave the hydrothermal system and enter the atmosphere. Due to that tailback, gas pressure increases and, at a certain critical level, a (not yet defined) valve, either natural or technical, opens and gas pressure decreases by outgassing into the atmosphere. The Kuz1 pressure recordings reflect such a saw tooth-like behaviour. (Figure 5).

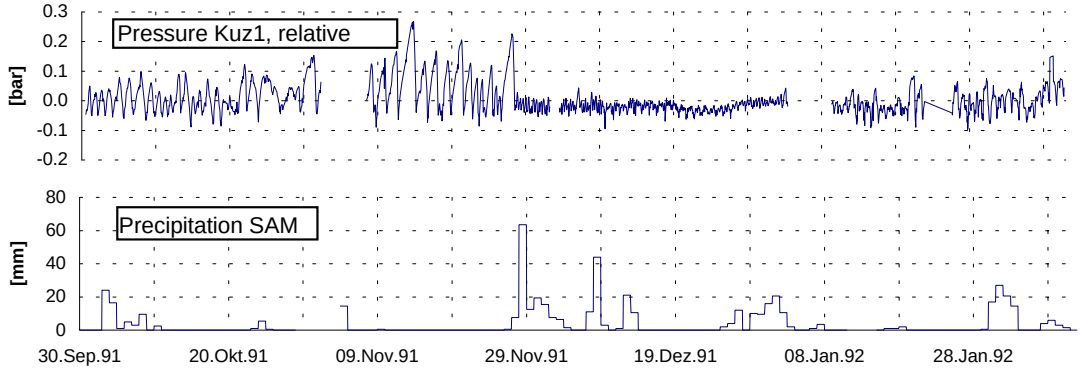


Figure 5: *Meteoric precipitation measured at German multiparameter stations in the Mudurnu valley (Samanpazarı) in comparison with pressure data of the Kuzuluk well site Kuz1. The time series were kindly made available by Lühr, Westerhaus and Woith of the GFZ Potsdam. The heavy rainfall at the end of November 1991 seems to mark the beginning of the rainy season in the Mudurnu valley. Note the obvious change of amplitude and frequency of the Kuz1 pressure variations at the end of November 1991. Heavy rainfall seems to control pressure variations at Kuz1. Infiltrated water could influence the 'valve' behaviour of the hydrothermal system by changed soil and fracture properties.*

The critical gas pressure level, at which the valve of the Kuzuluk hydrothermal system responds, is not constant in time and varies over an interval of 2.4 to 2.72 bar. The maximum values were reached just before the end of November 1991. The fall in pressure is characterised by a gradient of average values over an interval of -1.8 bar/day to -0.2 bar/day.

It is likely that the drillings of Kuz1 and Kuz2 are cased from the top of the well down to the bottom and that only a small part of the borehole is open to the reservoir. Thus, the measured pressures at Kuz1 and Kuz2 represent the characteristics of one single spot at a depth of 250m and 160m, respectively. The hot fluids of these particular spots may follow one or several unknown flow paths to the surface. These paths, fracture and joint dominated, could be controlled by a set of similar valves. The geological situation at Kuzuluk is indeed too complex to make any statement about the kind of interconnection between these paths. Although both thermal waters come out of the same reservoir (Greber 1992), their discharge behaviour tends to be different, since both wells represent different spots at the hydrothermal system, which are separated by a lateral distance of 25m and a difference in altitude of 90m.

Valve-like behaviour due to unconsolidated packer

A hydrothermal valve could be specified as a narrow joint in the uppermost part of the stiff and silicified cap rock which is partly filled with brecciated and silicified sand, gravel and crushed precipitated calcite (Figure 6).

This filling could be slightly consolidated by precipitated $CaCO_3$, but its mechanical properties would be similar to those of unconsolidated rocks.

Situated at an approximate depth of at most 10m, the unconsolidated packer could be responsible for the valve-like behaviour of the particular joint and, thus, for the total pressure below the packer is the sum of gas pressure and fluid pressure. If this pressure reaches a critical value at which the mechanical resistance of the filling is attained, the packer opens slightly into a small path and pressure decreases by discharging gas (i.e. CO_2). This process allows gas and hot water to discharge into the open joint and the atmosphere. But what would happen if hot water was passing through the unconsolidated packer? Confined water, like groundwater or hydrothermal fluid, has the physical ability to erode unconsolidated rocks.

This erosion could wear away the filling of the joint and the valve, built by this filling, would be destroyed. A repetitive function of the valve, with changing intervals of opened and closed periods, could not be provided. But the time series of Kuz1 only show repetitive behaviour. Thus, the valve would be closed before the hot water, which could easily erode the unconsolidated packer, passes through (the system would run 'dry').

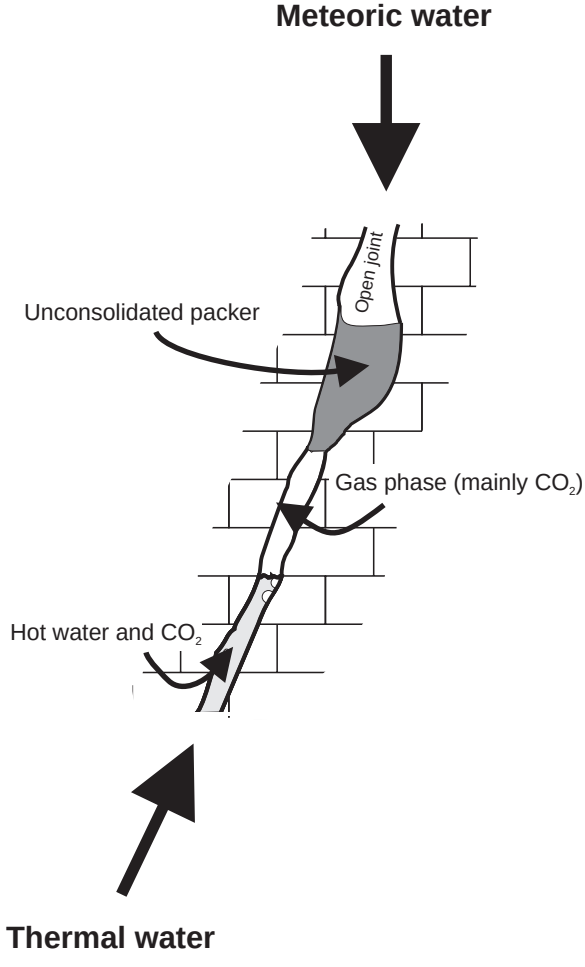


Figure 6: *Schematic of an unconsolidated packer in an open joint. Below an unconsolidated packer the hot hydrothermal water is separated in two phases. A cold gas cap (mainly CO_2) builds up gas pressure. If this pressure reaches a critical level, the unconsolidated packer fails and the gas can discharge into the atmosphere. The valve will close again after pressure has reached a normal level below the critical value. The hot hydrothermal water must not pass the valve, otherwise the unconsolidated packer would be eroded. Meteoric water changes the mechanical properties of the packer by infiltration processes. Due to that, the responding level of the valve is changed (i.e. decreased).*

Sensitivity to rainfall

Meteoric water infiltrates locally through porous soil and open joints or fractures. Since soil is almost absent at the Kuzuluk well site, meteoric water infiltrates quite rapidly. Infiltrating meteoric water could also reach the hydrothermal valve of the well Kuz1. The physical properties of unconsolidated material, proposed as forming the involved packer, are normally sensitive to water. A changing water content could influence the mechanical properties of the valve,

and increasing water saturation of the unconsolidated packer by infiltrated meteoric water could decrease the mechanical resistance. The responding level of the valves would decrease as a cause of the increasing water content of the unconsolidated packer.

Indeed, observed geological phenomena contradict the proposed discharge mechanism. Hot springs near the Kuz1 and Kuz2, which are related to the hydrothermal system of Kuzuluk (Greber 1992), show irregular CO_2 outgassing. Here, muddy ground provides in the function of a natural valve. These valves react to pressures which are far below the observed 'critical gas pressures levels' of the described Kuz1 system. It should be mentioned that the valve involved in the well Kuz1 could be located at a certain unknown distance from the wells and, thus, away from the observed hot springs. The discharge mechanisms of the different springs could easily vary within the hydrothermal field.

The geological and mechanical settings of the hydrothermal valve are uncertain since the involved packer is not directly observable. The only available information about the valve and its behaviour is the analogue pressure registration at the wells Kuz1 and Kuz2. Questions about its physical properties have to be raised:

- How could the packer be fixed at a certain depth?
- How could its reversible behaviour be explained?
- Is it realistic to postulate a 'dry' valve system?
- What are its mechanical and physical properties?

These questions cannot be answered without direct observation or obtaining experimental data for similar valve systems. Further discussion about the unconsolidated hydrothermal packer is of little benefit as long as these pertinent questions remain unanswered. The proposed mechanism could be a possible cause of the observed pressure variations, but it remains hypothetical.

Conclusions

The hydrothermal system at Kuzuluk lies near the North Anatolian Fault Zone. This system is still active and tectonic influence on the hydrothermal activity is likely. Earthquakes can influence the discharge system by changing flow paths. Changes of the discharge behaviour of springs of the hydrothermal system of Kuzuluk due to earthquakes are reported. Springs, described by Lucius (1929) have disappeared or their discharge of water and gas have changed dramatically.

Before possible tectonic influences can be investigated, undesired noise must be removed. The influence of this noise on the Kuz1 pressure recordings seems to be much higher than expected. Woith (1995) mentioned that over 95% of the recorded variations in his ground water parameters in the Mudurmu valley are caused by meteorological events. In his recordings, tectonically caused anomalies can hardly be identified and distinguished from noise.

The situation at the Kuz1 well site, a few hundred meters away from the German station, cannot be expected to be much different from the situation at the spring of the Çökek Hamamları. The Kuz1 pressure variations seem to be dominated by the continuous CO_2 input at depth. The rising CO_2 controls the pressure at the top of the hot water column by continuous outgassing phenomenon. This gas phase is probably released by a hydrothermal valve. Tectonically caused pressure variations would be strongly overprinted by this valve system and an identification of the responses of the well to tectonic stress is almost impossible. Tectonic stress

could eventually have an influence on the mechanical properties of the hydrothermal valves of the system and on the CO_2 input at depth. To check this assumption, further investigations, especially on rock properties and on the amount of outgassing CO_2, would have to be carried out.

A second important fact must be taken into account. During the short time period in which the quality of the signal was sufficient to perform investigations, no large earthquake occurred in the area around Kuzuluk. The maximum local magnitude, which was reached in 1991 and 1992, was only 3.1 on the 26th of March 1992. Unfortunately the Kuz1 pressure values were out of the range of the data recording system during this event. A larger event would perhaps provide the identification of long-term changes before an earthquake occurs. It would be interesting to observe the well behaviour just before, during and after earthquake shocks. These observations were unfortunately not possible. The question of tectonic influence on the well behaviour cannot be answered at this time.

Acknowledgements

I would like to thank Prof. C. Schindler, N. Deichmann, Prof. E. Klingelé, S. Sellami, E. Greber, W. Balderer, C. Jeckelmann, M. Pfister, B. Lühr, M. Spühler, M. Westerhaus, H. Woith, D. Estoppey, R. Hofmann, M. Löffler, S. Rudaz for their guidance and assistance. I also thank Ludmilla Good for her patient correction of the text.

References

Albarello, D., Ferrari, G., Martinelli, G and Mucciarelli, M., 1991, Well-level variation as a possible seismic precursor: a statistical assessment from Italian historical data, Tectonophysics, 193, 385-395.

Bodvarsson, G., 1970, Confined fluids as strain meters, Journal of geophysical research, Vol. 75, No. 14, 2711-2718.

Bredehoeft, J.D., 1967, Response of well-aquifer systems to earth tides, Journal of geophysical research, Vol. 72, No. 12, 3075-3087.

Evans, K., Beavan, J., Mousa, S. and Simpson, D., 1991, Estimating aquifer parameters from analysis of forced fluctuations in well level: an example from the Nubian formation near Aswan, Egypt (1. Diffusity estimates for saturated and unsaturate zone, 2. Hydrogeological background and large-scale permeability estimates, 3. Poroelastic properties), Journal of geophysical research, Vol. 96, NO. B7, 12127-12191.

Greber, E., 1992, Das Geothermalfeld von Kuzuluk/Adapazarı, Dissertation ETHZ, No. 9984.

Greber, E., this volume, Deep circulation of CO_2-rich palaeowaters in a seismically active zone (Kuzuluk/Adapazarı, Northwestern Turkey).

Kissin, I.G. and Grinevsky, A.O., 1990, Main features of hydrogeodynamic earthquake precursors, Tectonophysics, 178, 277-286.

Lucius, M., 1929, Kuzuluk (Akyazı) thermo-mineral suları hakkında rapor, MTA Derleme No. 558, Ankara (in Turkish with summary in German, unpubl.).

Melchior, P., 1983, The tides of the planet earth, 2nd edition, Pergamon Press.

Pfister, M., 1995, Geothermische Untersuchungen in der Region Marmara (NW – Türkei), Dissertation ETHZ, No. 11054.

Roeloffs, E., 1988, Hydrologic precursors to earthquakes: a review, Pure and applied geophysics, Vol. 126, Nos. 2-4, 177-209.

Rojstaczer, S. and Agnew, D., 1989, The influence of formation material properties on the response of water levels in wells to earth tides and atmospheric loading, Journal of geophysical research, Vol. 94, No. B9, 12’403-12'411.

Schenk, E. and Krauss, I., 1972b, Hydroseismische Beobachtungen an Grundwasserbeobachtungsbrunnen im Festgestein und ihre hydrogeologische Bedeutung, Z. Deutsch. Geol. Ges., Band 123, 15-27.

Şentürk, N. and Demirel, Z., 1987, Akyazı (Sakarya) Kuzuluk Kaplıcası Hidrojeoloji Incelemesi, MTA Report (Turkish, unpubl.).

Van der Kamp, G. and Gale, J.E., 1983, Theory of earth tide and barometric effects in porous formations with compressible grains, Water Resources Research, Vol. 19, No. 2, 538-544

Woith, H., 1995, Spatial and temporal variations of radon in ground air and ground water within the Mudurnu valley, NW Turkey, A contribution to the Turkish-German, joint project on earthquake research, Dissertation Christian-Albrechts-Universität Kiel.

The thermal springs of the Armutlu peninsula (NW Turkey) and their relationship to geology and tectonic

THOMAS EISENLOHR

Abstract

Within the framework of the MARMARA Poly-Project of the ETH-Zürich the thermal springs of the Armutlu peninsula (Bursa, NW Turkey) and their geological surroundings have been investigated.

The tectonic horst zone of the Armutlu peninsula consists mainly of metamorphic rocks. On top of an amphibolite-gneiss unit, greenschist metamorphic and a low grade metamorphic sequences follow. The oldest non-metamorphic rocks belong to the Upper Cretaceous. A granitic intrusion took place in the Upper Cretaceous – Paleocene period. After significant uplift and erosion an andesitic volcanism and a simultaneous flysch sedimentation developed in the Eocene. Locally, evaporitic sediments indicate a coastal facies during the Oligocene. The Neogene consists of marl, shallow water limestone, lignite, sand and gravel. By means of structural investigations it was possible to identify several ductile deformation events. The youngest, Early Alpine event caused an intensive stretching and thrusting in the southeastern direction. In the rocks younger than the Upper Cretaceous only brittle deformation is documented. The dextral Northern Anatolian Fault Zone (NAFZ) established itself in the Miocene (Şengör 1979). Two different fault patterns were observed on the peninsula. The older system consists of E-W striking dextral faults of the NAFZ and N-S to NE-SW striking sinistral faults which divide the peninsula in several blocks. NW-SE striking normal faults represent a younger system which is well in accordance with the recent regional extension in NE-SW direction. This extensional movement tears up the strike-slip faults and causes deep reaching zones of high hydraulic permeability. Since the geothermal heat flow is not generally increased in the study area (Pfister et al. this volume) the high geothermal activity is to be explained by this tectonic evolution.

The thermal springs of the peninsula were investigated by means of field measurements, chemical analyses and isotope investigations. Generally, two main groups can be distinguished: (1) The thermal waters of Yalova (65°C) and Armutlu (60-75°C) are dominated by the ions Na^{+}, Ca^{2+} and SO_4^{2-}. The magmatic and metamorphic rocks of the peninsula act most probably as reservoir rocks. In opposition to Yalova the water of Armutlu is characterised by further water-rock interaction with carbonates. Several geothermometers indicate reservoir temperatures of 70 to 100°C in Yalova and 100 to 130°C in Armutlu. The stable isotopes point to a possible recharge with recent rain and snow melt. The residence time of the waters must be longer than 40 years. The upflow zones are located at intersections of tectonic faults. (2) In contrast with Yalova and Armutlu the slightly mineralised springs of Gemlik, Orhangazi, Soğucak and Keramet yield temperatures between 20 and 37°C and can be classified as sub-thermal and thermal karstic springs. They represent "bottom outlets" of karstic systems in the marble unit of this area. It was possible to evaluate the different infiltration areas and the flow paths by stable isotope analyses. Tritium analyses and numerical modelling indicate a mixing between hot stagnant water and cold young water within the deeper part of the karstic systems.

Introduction

Within the framework of the MARMARA Poly-Project, the Armutlu peninsula, between İstanbul and Bursa (NW Turkey), was investigated. The main topic of this project of the Swiss Federal Institute of Technology Zürich is the relationship among active crustal movements, seismicity, heat flow and characteristics of the deep circulation of thermal water. The Armutlu peninsula is one of seven areas where detailed geological and hydrogeological investigations have been carried out (Eisenlohr 1995). The results of these investigations are summarised in the presented paper.

The E-W striking mountain range of the Armutlu peninsula is up to 960m high and surrounded by the eastern Marmara sea. Deep marine basins in the gulf of İzmit, just north of the peninsula, reach a depth of 1300m below sea level. The rest of the Marmara sea is less than 200m deep. The first modern and comprehensive geological study of the Armutlu peninsula was carried out by Akartuna (1968). More recently, several geologists have studied the peninsula in the light of modern plate tectonics (Şengör and Yılmaz 1981, Yılmaz et al. 1995 and others). Başkan (1981) investigated the geothermal area of Armutlu in detail. There is only limited information available concerning the other geothermal areas.

Geology

Geological setting

The geological evolution of Northwestern Turkey is very complicated and remains controversial in the literature. The stratigraphic sequence of the older mesozoic rocks, for example, vary intensively from north to south in the Marmara region. A thick non-metamorphic sedimentary sequence starting from the Ordovician can be observed in the İstanbul region (Ternek et al. 1987). On the investigated part of the Armutlu peninsula, the oldest non-metamophic rocks belong to the Upper Cretaceous. Non-metamorphic, fossiliferous permian limestones cover discordantly a highly deformed rock sequence in the region of Bursa some 30km to the south (Imbach this volume). Şengör and Yılmaz (1981) have explained the great stratigraphic variety by several micro-continents which were joined together along sutures during several orogenic stages. According to their work, the Armutlu peninsula represents a part of the Intra-Pontide suture which separates the Rhodope-Pontide fragment (part of Laurasia) from the Sakarya continent (part of Gondwana). Yılmaz (1995) went into much more detail and assigned the northwestern part of the peninsula to the Rhodope-Pontide fragment and the southeastern part to the Sakarya continent. Other geologists localise this suture zone in the north of the Armutlu peninsula (e.g. Wong et al. 1995). Not only the geographical localisation, but also the age of the closure of this suture is very controversial in the literature (Yılmaz et al. 1995: Upper Cretaceous; Şengör and Yılmaz 1981: Paleocene-Eocene; Wong et al. 1995: Lower Eocene). The neotectonic evolution is much better known. A prominent fault zone called "The Northern Anatolian Fault Zone" (NAFZ) established itself along northern Turkey in the Middle Miocene due to a westerly motion of the Turkish plate relative to Eurasia (Şengör 1979). In the Marmara region, the NAFZ splits up into several faults. The Armutlu peninsula is situated between the northern and the southern zone. In addition, the Aegean extensional regime extends its influence on the Marmara region, which caused the development of pull-apart basins and horst zones. The Armutlu peninsula represents a horst zone between the grabens of İzmit and Gemlik (Fig. 1).

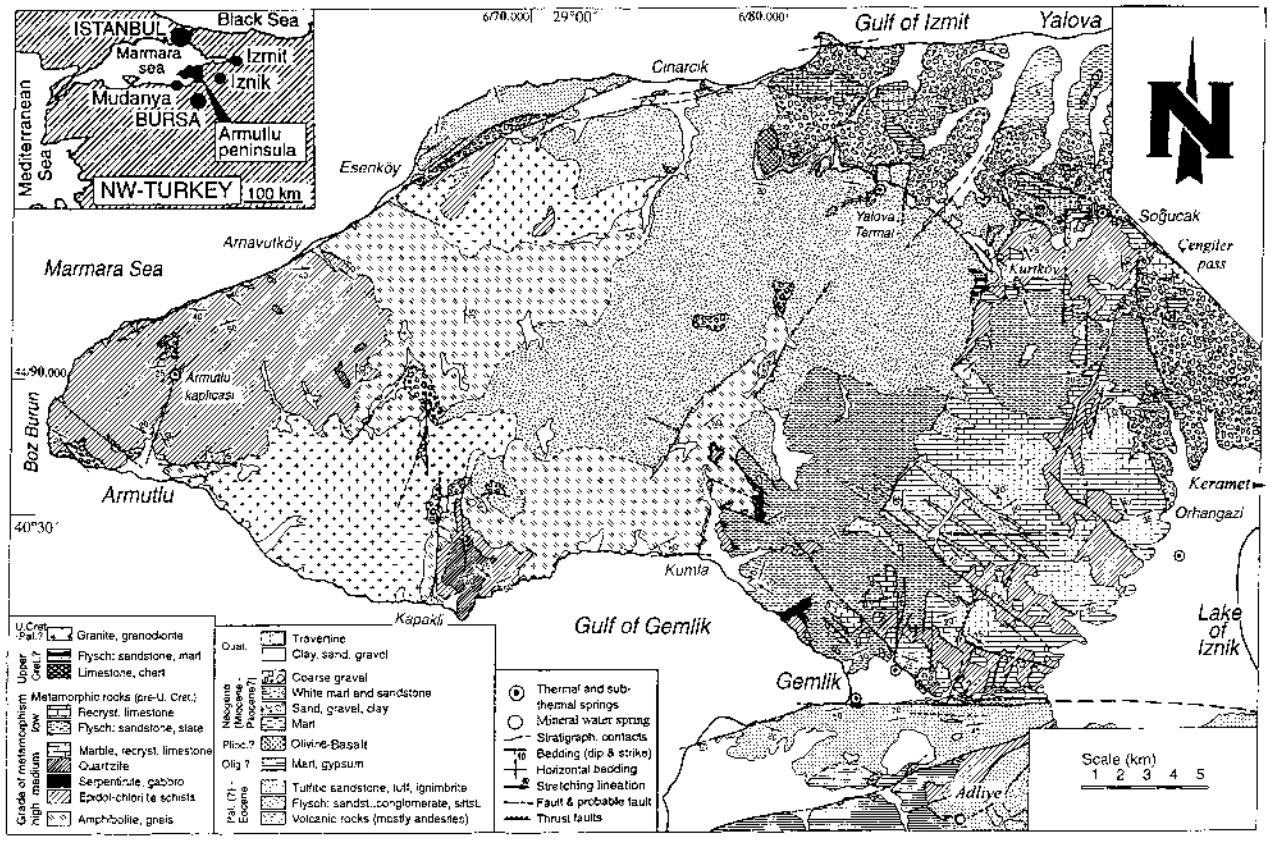


Figure 1: Geological map of the Armutlu peninsula.

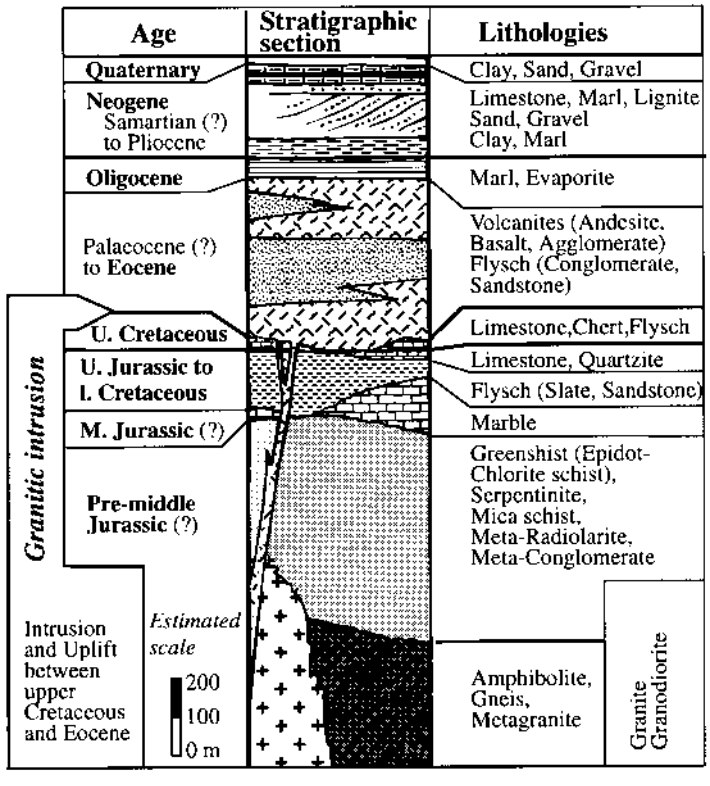


Figure 2: Generalised stratigraphic section of the Armutlu peninsula.

Stratigraphy (see Fig. 1 and 2)

The oldest rocks on the peninsula consist of amphibolite, gneiss and mica schists. The mineral assemblage of hornblende s.s., albite and quartz characterises the amphibolite *metamorphic facies*. Chlorite and epidote minerals which are typical for greenschist metamorphism overgrow the older fabric retrogradely. The age of the unit is uncertain – it must at least be older than the Jurassic.

On top of the amphibolite-gneiss unit follows a *greenschist metamorphic sequence*, consisting of meta-volcanites and meta-sediments. The most common lithologies are greenschists such as epidote-chlorite-schists, actinolite-chlorite schists and mica schists. Often, pillow structures can be observed. Perfectly preserved pillow structures where found at the cap *Boz burun* west of Armutlu (Fig. 3). Interbedded radiolarite layers occur in the surroundings of Gemlik and Armutlu. The greenschists cover a serpentinised ultramafic body north of Gemlik. Mostly quartzitic meta-conglomerates were recognised in the area north of Gemlik as well as in Kapaklı (SE Armutlu). In Kapaklı, the conglomerates follow discordantly on top of the amphibolite-gneiss unit. In the eastern part of the peninsula the greenschists are overlain by the Orhangazi marble (Kaya and Kozur 1987). The partly reddish marble is up to 100m thick and contains dolomitic layers. Kaya and Kozur (1987) dated the upper part of the marble unit as Middle Jurassic. On the outer peninsula calcareous rocks are almost missing. Only some rare marble lenses occur in the area of Arnavutköy northeast of Armutlu.

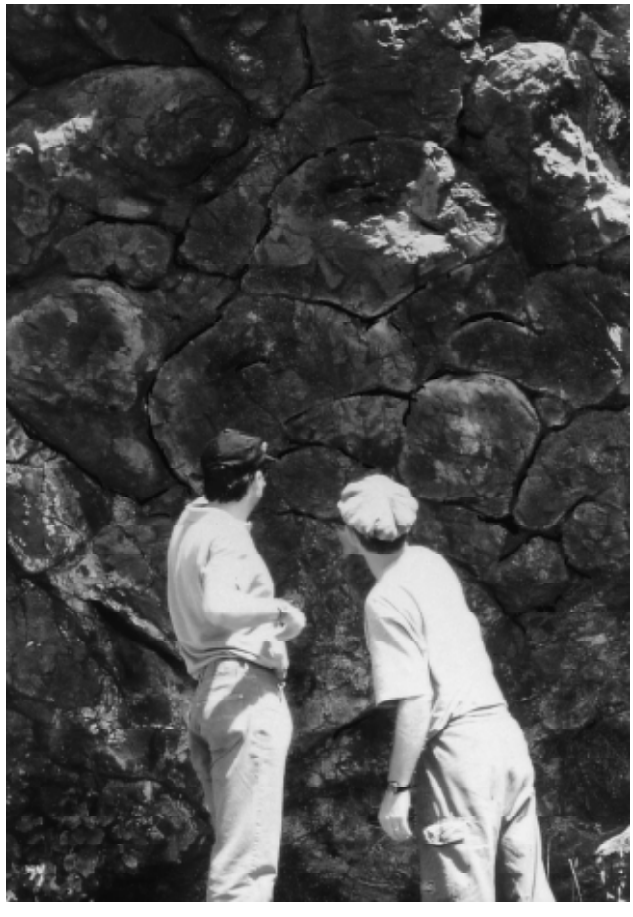


Figure 3: Well preserved pillow structures in the greenschist metamorphic sequence at Boz burun east of Armutlu.

A *low metamorphic sequence* consisting of flysch sediments (Gemlik flysch unit, up to 300m), recrystallised limestone (30m) and greenish quartzite (20m) follows on top of the Orhangazi marble in the eastern part of the study area. Thin layers of radiolarian cherts in the flysch were dated by Kaya and Kozur (1987) as Upper Jurassic to Lower Cretaceous.

The ultramafic rocks, the pillow basalts and the radiolarian cherts of the greenschist metamorphic unit are typical lithologies of an ophiolitic complex and oceanic crust, respectively. This finding shows good agreement with the localisation of the Intra-Pontide suture on the Armutlu peninsula (Şengör and Yılmaz 1981). However, the fact that all of the specific lithologies of the greenschist metamorphic unit were found in the whole area investigated does not permit the distinction of two different paleotectonic units as proposed by Yılmaz (1995). The main differences between the proposed units are the rocks below and above the greenschists. The absence of the low grade metamorphic unit in the northwestern part can be explained by a period of erosion. Eocene volcanites follow directly on top of the amphibolites and greenschists. The fact that amphibolites and gneiss are not exposed in the southeastern part does not necessarily prove that this unit does not exist below the greenschists. Therefore, an exposure of different sections of the same stratigraphic sequence is more evident in the two zones. The contact of the two zones consists of an Early Alpine overthrust (see below). Amphibolite-bearing gneiss is thrust on top of low grade metamorphic rocks. This confirms a huge uplift of the northwestern part during Cretaceous.

The oldest *non-metamorphic rocks* are reddish limestones and cherts in the Gemlik area which look very similar to the rocks of the "Couches Rouges" in the western Alps. Erk (1942) dated their radiolarian fauna as Upper Cretaceous (Turonian-Maestrichtian). Similar rocks were also recognised in southern Thrace (Schindler in Kopp et al. 1969), in the Gemlik-Bursa area (Erk 1942) and in the Kuzuluk/Adapazarı area (Greber this volume (a)). Calcareous flysch sediments near Kurtköy (15km south of Yalova) were dated by microfossils (*Globotruncana*) as Upper Cretaceous.

A *granitic to granodioritic intrusion* cuts amphibolite and greenschist metamorphic rocks on the outer peninsula. However, there exists no radiometric dating. Contrary to the metamorphic rocks, the grain fabric of the granite shows no signs of ductile deformation (see below). Erguvanlı (1949) described a contact metamorphism in Upper Cretaceous limestones on the island İmralı about 20km east of Armutlu. Granitic bolders, which are lithologically identical to the intrusion, occur in the Eocene flysch at the NW coast. Therefore, the age of the intrusion and its uplift (plus erosion) is most probably younger than Upper Cretaceous and older than Eocene.

Volcanic rocks are very widely exposed on the peninsula. They consist mainly of andesites, agglomerates and secondarily of rhyolite, ignimbrite, tuff and basalt. Volcanic dikes cut all of the metamorphic rocks and the granitic intrusion. Thick flysch sediments and volcanic deposits are interlocked. Microfossils (*nummulites, discocyclina*) in the flysch indicate an Eocene age. Most of the detritic components consist of volcanic rocks, secondary amphibolite, mica schist, granite and limestone. The conglomerate and sandstone benches yield various sediment structures which are typical for turbidite flows. Ripple marks indicate an E-W orientated flow direction during deposition. The spatial distribution of the Eocene flysch in the northern Marmara region indicates the existence of E-W striking basins (Kopp et al. 1969, Erk 1942).

A sedimentary sequence containing *marls* and *gypsum* is exposed south of Gemlik. Hydrogeological observations (see below) point to salt deposits in the evaporites. According to lithological comparisons and the stratigraphic position, Erk (1942) dated these sediments as *Oligocene*.

Neogene sediments mainly occur in the flat lands south of Yalova and in the basins of Orhangazi and Gemlik. They overlie discordantly the metamorphic and magmatic rocks. A stratigraphic section observed south of Yalova is characterised by a great variety of shallow marine, coastal, brackish and continental sediments (Table 1). Akartuna (1968) dated the sequence as Middle Miocene (? Sarmatian) to Pontian. Isolated coarse gravel deposits occur on the peninsula at higher altitudes of up to 500m a.s.l. A comparison with similar deposits in the Marmara region (Kopp et al. 1969, Akartuna 1968) makes it possible to estimate their age as Pliocene.

Lithology	Thickness	Fossils, sediment structures	Facial interpretation	Age
Gravel	> 5m	-	Continental	Pliocene ?
White limestone	~ 20m	Oncoids, birds eyes	Marine, intertidal	Pontian
White marl with lignite seams	30m	Gastropodes (Panorbis, Melanopsis) Vertebrate fossils *(according to Akartuna 1968)*	Brackish to sweat water	Pontian*(according to Akartuna 1968)*
Yellow sandstone	~ 150m	Molluscs (Cardium), foresets	Marine, delta sediments	U. Miocene ?
Brown marl, clay	> 50m	-	Marine	Sarmatian ? *(according to Akartuna 1968)*

Table 1: Stratigraphic section, facial interpretation and age of the Neogene south of Yalova.

Structural geology

Generally, two main types of rock deformation can be distinguished. All metamorphic rocks show ductile structures such as folding, cleavage and stretching. Ductile deformation and metamorphism indicate temperature and pressure conditions which can be expected at a depth of several kilometers. Rocks younger than the Upper Cretaceous were affected only by brittle deformation. Brittle structures, such as joints and faults, are typical for deformation close to the surface.

Ductile deformation

At least two generations of isoclinal folds were recognised in the amphibolite-gneiss unit. The fold axes tend mostly to be N-S to NE-SW in direction. The deformation events took place during amphibolite metamorphic conditions. The greenshist metamorphic unit is characterised by a rather inhomogenous grade of deformation. While the pillow structures at the*Boz burun* kept their original shape, the same pillows are strongly stretched one kilometer to the north. The components of the meta-conglomerates of Kapaklı are stretched as well by a factor of 5 to 10. Generally the stretching lineations tend to be southeastern in direction (Fig. 4). The greenschist-mineral actinolite shows a syncinematic growth parallel to the stretching lineation. This regional deformation event is best documented in the low grade metamorphic rocks. The slates and sandstones of the flysch are strongly stretched as well in the southeastern direction. The limestones show a dynamic recrystallisation partly even with the mylonitic fabric. Several shear direction criteria indicate the transport of the upper units to the southeast. Furthermore, it was possible to map an over-thrust with the same shear direction north of Kumla (Fig. 4). Amphibolite-bearing gneiss is thrust on top of slates of the flysch unit. A late phase of this regional deformation event is documented in the marbles and limestones by kinks and stylolites which represent the change between ductile and brittle deformation. The age of the event must be younger than the Gemlik flysch (Upper Jurassic to Lower Cretaceous) and older than the non-metamorphic rocks (Turonian to Maestrichtian), which is well in accordance with observations of Yılmaz (1995).

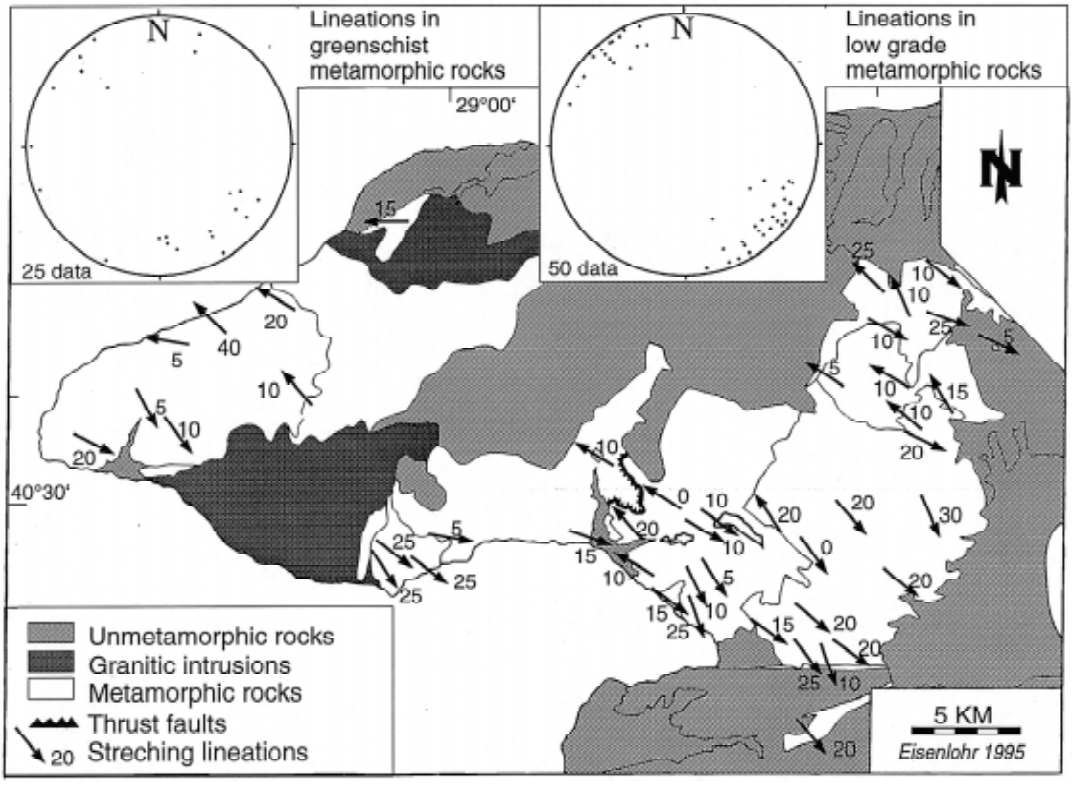


Figure 4: *Stretching lineations in the low grade and greenschist metamorphic rocks indicate a regional deformation event during the Middle to Upper Cretaceous. Amphibolite-bearing gneiss is thrust on top of low grade metamorphic slates north of Kumla (geological units see Fig. 2). The higher tectonic units were transported in a southeastern direction.*

Brittle deformation

The time period between the Upper Cretaceous and the Miocene is characterised by important tectonic events: uplift and erosion of granitic intrusion, andesitic volcanism, E-W striking flysch basins and so on. Several authors date the orogenic phase which closes the Intra-Pontide ocean in this period (e.g. Şengör and Yılmaz 1981, Wong et al. 1995). Unfortunately, meso- and small-scale structures of this period are very rare on the Armutlu peninsula because of sedimentary hiatus and the fact that the Eocene and Oligocene rocks are only exposed in zones strongly affected by neotectonic movements. At least the E-W striking flysch basins and NW-SE to E-W striking groups of volcanic dikes point to a N-S orientated extensional component in the stress field of the Eocene. The NAFZ was established in northern Turkey during the Middle Miocene (Şengör 1979). The different faults of the NAFZ follow more or less older tectonic structures in the Marmara region (e.g. Intra-Pontide suture, Eocene flysch basins).

Since the *neotectonic fault structures* are of special interest for the hydrogeology, the orientation and the inclination of almost 200 fault planes (meso-scale) were measured during the field work. Due to the bad outcrop conditions, it was often difficult to evaluate the direction, the type and the amount of displacement. Nevertheless, it was possible to obtain a complete data set for about 50 faults.

More than 70% of the measured faults on the peninsula are steeper than 70°. More than 50% of the faults with known direction of displacement are characterised by sub-horizontal movements (pitch 0-30°). Both parameters – the inclination and the pitch – indicate that the major-

ity of the faults are typical strike-slip faults. Observed normal faults with sub-vertical displacement (pitch 60-90°) are often steeper than expected from theoretical considerations. The orientation of all measured faults shows strong scatter which precludes all interpretation. In spite of this, the selection of the faults with known direction and displacement direction permits the distinguishing of three main types: (A) Dextral strike-slip faults (pitch 0-30°) striking mostly in an E-W to NW-SE direction, (B) sinistral strike-slip faults (pitch 0-30°) striking in a N-S to NE-SW direction and (C) typical normal faults (pitch 60-90°) striking mostly in a NW-SE direction. The mapping of large-scale faults (Fig. 5), joint measurements and the evaluation of air photos confirm this distinction.

The fault type (A) fits very well in the framework of the dextral, E-W striking Northern Anatolian Fault Zone (NAFZ), which is split in several strands in this region. In analogy to synthetic experiments (e.g. Riedel 1929) the fault type (B) may represent antithetic Riedel-faults in a wide shear zone. Since the initial orientation of the Riedel-faults in an E-W striking dextral shear zone would be NNW-SSE a clockwise rotation can be assumed for the NE-SW striking sinistral faults on the peninsula. Block rotations have been observed in other large-scale shear zones, such as the San Andreas fault (e.g. Nur et al. 1989). Paleomagnetic measurements in Eocene volcanites on the eastern prolongation of the Armutlu peninsula proved a clockwise rotation at least of 14° (Tatar et al. 1995). Outcrops with conjugated fault systems allow the reconstruction of the paleo-stress field (Fig. 6). The compressional stress axis is almost horizontal and SE-NW striking – the intermediate axis is vertical. This pattern is typical for a dextral E-W striking shear zone without an extensional component. The age of this stress field is very difficult to evaluate. As mentioned previously, the initiation of the NAFZ is generally dated as Middle Miocene (Şengör 1979).

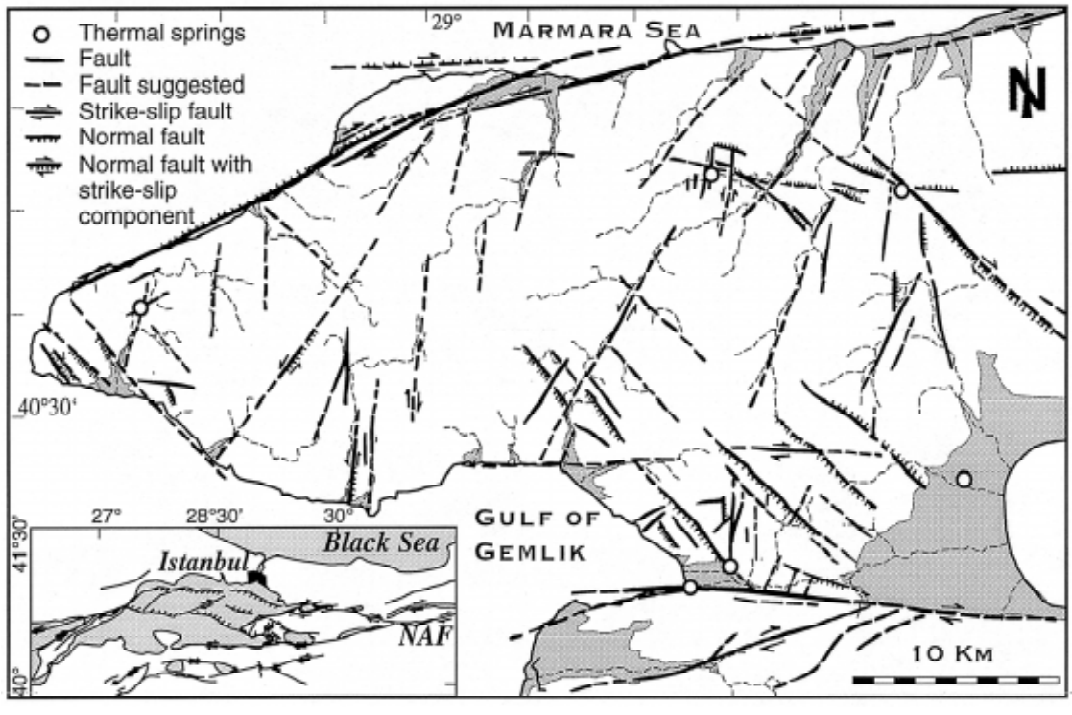


Figure 5: Neotectonic map of the Armutlu peninsula (according to field observations and air photos) and the Marmara region (small map). Most of the thermal springs are located on intersections of major fault systems. (NAF = Northern Anatolian Fault Zone).

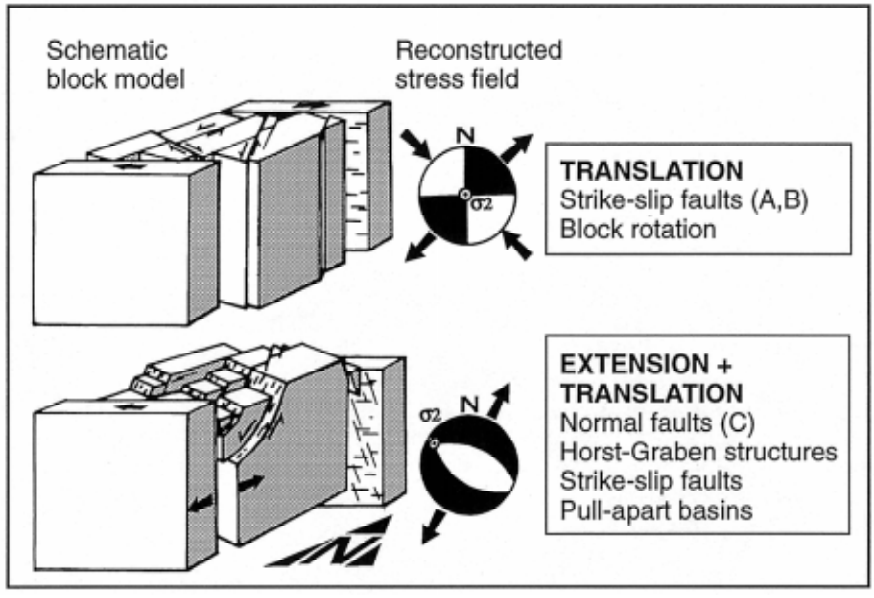


Figure 6: Schematic sketch of two stages of the neotectonic evolution derived from statistic fault measurements and the mapping of large scale structure. The paleo-stress field has been reconstructed from conjugated fault systems in the meso-scale.

The normal faults (C) cannot be explained by this stress field. The reconstructed paleo-stress of conjugated normal faults indicates maximum extension in the NE-SW direction with a certain dextral component. The intermediate axis of this stress field is now almost horizontal (Fig. 6) which shows good agreement with actual observations from earthquakes (McKenzie 1972) and remote geodesy (Straub and Kahle this volume). The transtensional tectonic regime is also visible in the large-scale structures of this region (Fig. 5). Several pull-apart basins build deep marine basins (up to 1300m deep) in the northern Marmara sea. Actually, the initiation of these basins possibly can be traced back to the Eocene (Wong et al. 1995). The Armutlu peninsula represents a tectonic horst zone. Usually two different conjugated fault systems occur in extensional regimes. On the Armutlu peninsula normal faults, which lower the northeastern part, are almost missing. On the other hand, strike-slip faults often are characterised by a corresponding vertical component of movement. Two generations of striae on the fault plains point to the reactivation of former strike-slip faults as normal faults. This indicates that the fault type (C) is most probably younger than (A) and (B), (Fig. 6). According to Şengör (1979) the influence of the Aegean extensional regime on the Marmara region intensified during the Pliocene.

This neotectonic evolution has a significant influence on the deep groundwater circulation. The recent extensional movement tears up the older, deep-reaching strike-slip faults of the NAFZ, which creates vertical zones of high hydraulic permeability and concentrated upflow path for the thermal water, respectively. Most of the thermal springs of the Armutlu peninsula occur at intersections of fault zones. Strong earthquakes may have an influence on the outflow rate of thermal springs (see below), which indicates as well that the thermal water follows tectonic fault zones to the surface.

Hydrogeology

Introduction

Several different geothermal areas occur on the Armutlu peninsula. According to the discharge temperatures, two main groups may be distinguished. In the northwestern part, the thermal springs of Yalova and Armutlu register temperatures between 60 and 70°C. By way of contrast, several poorly-known thermal springs occur in the southeastern part (Gemlik, Orhangazi, Keramet and Soğucak), which are characterised by lower temperatures between 20 and 40°C. Since these springs have very high discharges, the total amount of the emitted heat energy is as high as in Yalova and Armutlu. In addition, a cold mineral water spring has been investigated at Adliye (SE of Gemlik).

Boundary conditions of the deep groundwater circulation

For a fundamental understanding of the deep groundwater circulation, the boundary conditions of the system have to be known. Therefore, a short description of the parameters climate, shallow groundwater and heat flow is first necessary.

The Armutlu peninsula is situated in a transition zone bordered on by the climatic zones of the Mediterranean, Eastern Europe and the Black sea. In addition, the surrounding Marmara sea has a significant influence on the local climate. Rainfall enters this region mostly from a western to northern direction (Erinc and Sungur 1964). Therefore, the mean annual precipitation in Yalova (749mm), at the northern shore, is higher than in Gemlik (684mm) at the southern coast. More than 70% of the annual precipitation falls during the winter period of October-March. The mean annual temperature in Yalova is 14.3°C and in Gemlik it is 14.9°C. Considering the topography an approach based of a water balance of the peninsula is proposed in Table 2 (mean values, see also Eisenlohr 1995).

Temperature (dependent from altitude):	~13°C	
Precipitation (dependent from altitude):	~800mm	~100%
Evapotranspiration (calculated according to formula of Turc 1954):	~320mm	~40%
Surface runoff (calculated from runoff of 4 rivers on the peninsula):	~400mm	~50%
Groundwater recharge (according to the water balance):	~80mm	~10%

Table 2: Approach using a water balance of the Armutlu peninsula considering the topography (mean annual values).

Shallow groundwaters give good information about the recharge of the deep groundwater. Therefore, more than one hundred cold springs were investigated in addition to the thermal springs. Due to altitude effects, circulation patterns and atmospheric influences, the temperature of the cold springs on the peninsula (>2l/min) varies between 11 and 19°C in September and between 8 and 16°C in April. Most of the springs present an electrical conductivity between 200 and 700µS/cm. Only the springs in areas with ultramafic rocks (e.g. serpentinite) are more highly mineralised (800 to 1200µS/cm). Chemically, almost all of the spring waters are dominated by the ions Ca^{2+} and HCO_3^-. The solution of calcite seems to be the most common water-rock interaction, even in magmatic and metamorphic rocks. Nevertheless, the different aquifer lithologies control the secondary ions Mg^{2+}, Na^+, Cl^- and SO_4^{2-}. Karstic springs represent the purest Ca-HCO_3 water type. Ultramafic rocks cause a significant en-

richment in $Mg^{2+}$and SO_4^{2-}. The springs in metamorphic and magmatic rocks are characterised by a relative enrichment in Mg^{2+}, Na^+, Cl^- and SO_4^{2-}. Volcanic aquifer rocks bring out an enrichment in Na^+. In spite of this relationship between aquifer lithology and water chemistry the chlorine content is controlled by another factor. Due to the sea spray from the surrounding Marmara sea, cold springs close to the shore line yield high chlorine contents (up to 100mg/l). With increasing distance from the shore line and increasing altitude the concentrations decrease to values around 4mg/l in the highlands. Not only the water chemistry but also the isotopic composition of the shallow groundwater is highly affected by the local and regional meteorological regime (see Eisenlohr et al. this volume (a)).

An increased geothermal heat flow is the most popular explanation for the occurrence of thermal springs. Pfister et al. (this volume) measured geothermal gradients between 1.0 and 2.5°C/100m in drill holes (80 and 90m deep) in the areas of Orhangazi, Gemlik and Armutlu. This indicates that the geothermal heat flow on the peninsula is rather low compared to an average continental heat flow.

General description of the thermal and mineral waters of the Armutlu peninsula

Thermal springs of Yalova

The thermal springs of Yalova are situated on the northern slope of a mountain range about 10km south of Yalova. The thermal water has been utilised for bathing since classical times when this place was called *Sotiropolis* (Hotz 1989). At the present time, "Yalova Termal" is one of the most famous thermal baths of Turkey. The springs are bound to a slightly northward dipping detritic layer in the volcanic rocks and to N-S striking, sinistral faults (Fig. 7). An additional WNW-ESE striking fault system was observed in the valley north of the geothermal area (Gökçedere). The main spring (*Esas kaynağı*) yields a temperature of 65°C and an electrical conductivity of 1920µS/cm. Temperature and electrical conductivity are rather constant during the seasons. The measured discharge in August 1994 (19l/sec) was significantly higher than in April 1994 (13l/sec). The strong earthquake of Cinarcik on the 18th of September 1963 (M_S = 6.2) caused a significant decrease of the discharge (personal communication of the technical staff). Along the creek several small springs emerge. The famous "*Göz suyu*" (60°C, 15l/min) is applied to eye diseases. The total discharge of the small springs can be estimated at about 15l/sec by measurements of the creek runoff. This would give for the whole geothermal area a discharge between 25 and 30l/sec. In the surroundings of the spa several small cold and sub-thermal springs (0.1-5l/min, 11-19°C in April) with high mineralisation (900-3100µS/cm) have been observed (Fig. 7).

Geothermal area of Armutlu

The geothermal area of Armutlu on the outer peninsula is much less developed than Yalova. Some fifty thermal springs with discharges between 1 and 200l/min emerge from greenschist metamorphic rocks (epidot-chlorite schists) along a creek in a narrow valley (Fig. 8). Field investigations and the evaluation of air photos indicate a NNE-SSW striking fault system along the main valley and an additional WSW-ENE striking fault system in the spring area. The central springs show the highest electrical conductivites (up to 2970µS/cm) and temperatures (up to 68°C). A borehole (507m deep) drilled by MTA in 1973 (Başkan 1981) yielded artesian water with a temperature of 75°C and an electrical conductivity of 2850µS/cm. Periodic measurements showed that the temperatures of the well (8) and the springs *Mide suyu* (1) and *Nuri paşa kaynağı* (9) are constant during the year. Some of the other springs, e.g. *Gicik kaynağı* (82) are affected by dilution with creek water and cold shallow groundwater. In contrast with Yalova, travertine deposition is well developed in this area. Since most of the

springs have very diffuse outflow, the total discharge of the geothermal field is difficult to measure. The runoff of the creek increased from 30l/min above the springs to 1080l/min below the springs in summer 1992 (September). Considering the input of cold water (drinking water, creek water, waste water) and the output of thermal water (pipeline from the well to the village of Armutlu) the total discharge of the geothermal area can be estimated at 20 to25l/sec.

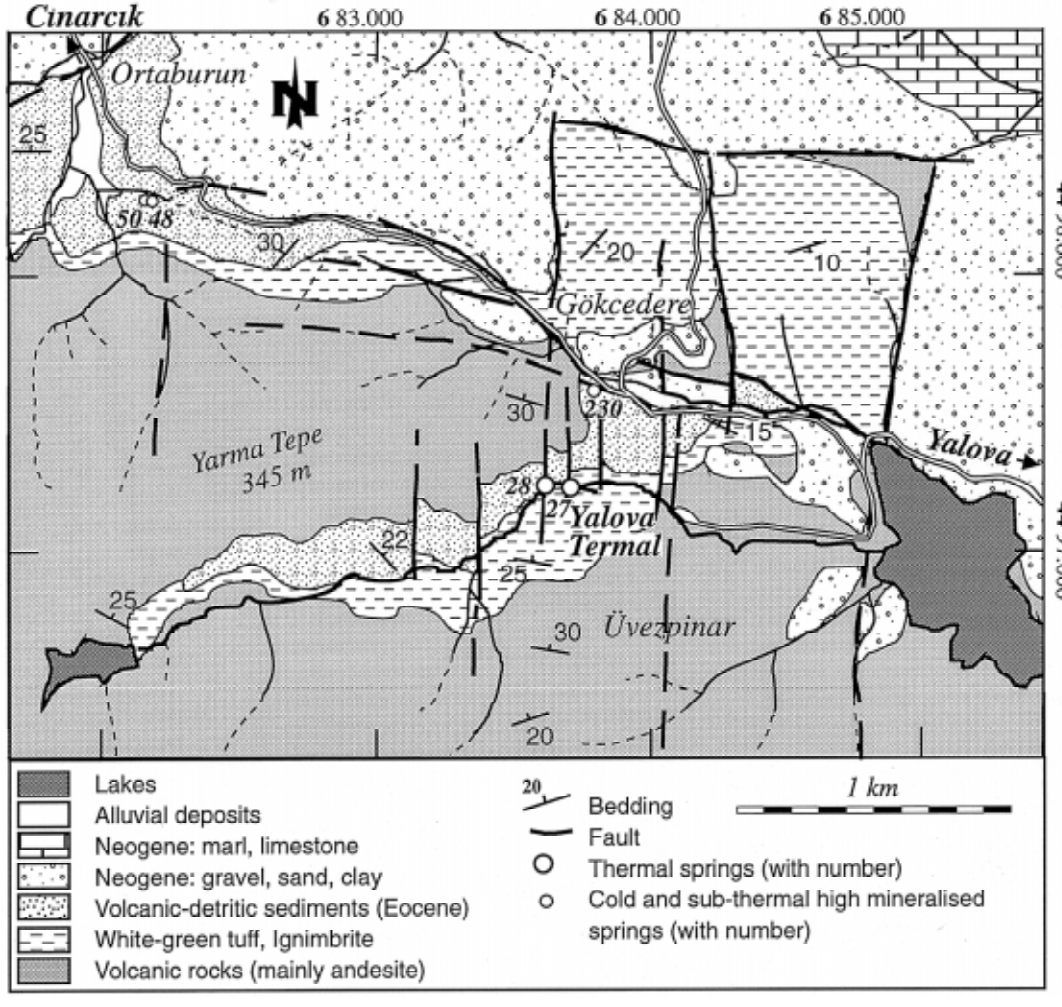


Figure 7: *Geological map of the Yalova geothermal area (Yalova Termal). In addition to the thermal springs (No. 27 and 28), small cold and sub-thermal springs with high mineralisation have been observed in Gökçedere (No. 230) and Ortaburun (No. 48 and 50).*

Gemlik and Orhangazi (see also Eisenlohr et al. this volume (b))

The mountains north of Gemlik consist of greenschists at the bottom and a marble unit and flysch sediments on top of it. Due to tectonic deformation the schists dip on each side to the surrounding plains. Several cold karstic springs (*Kumla*, *Beşpınar*, *Nadır*, *Gedelek* and *Cihatlı*) with temperatures between 12 and 16°C occur in this mountain area (Fig. 9). All of these originate directly from the marble plate. In addition several sub-thermal (17-25°C) and thermal (>25°C) springs emerge in the alluvial plains of Gemlik and Orhangazi. Since these plains border in the east, in the south and in the west on areas with completely different, highly mineralized waters (lake of İznik (1000µS/cm), the mineral water of Adliye (see below) and Marmara sea), all spring water must originate from the Gemlik mountains.

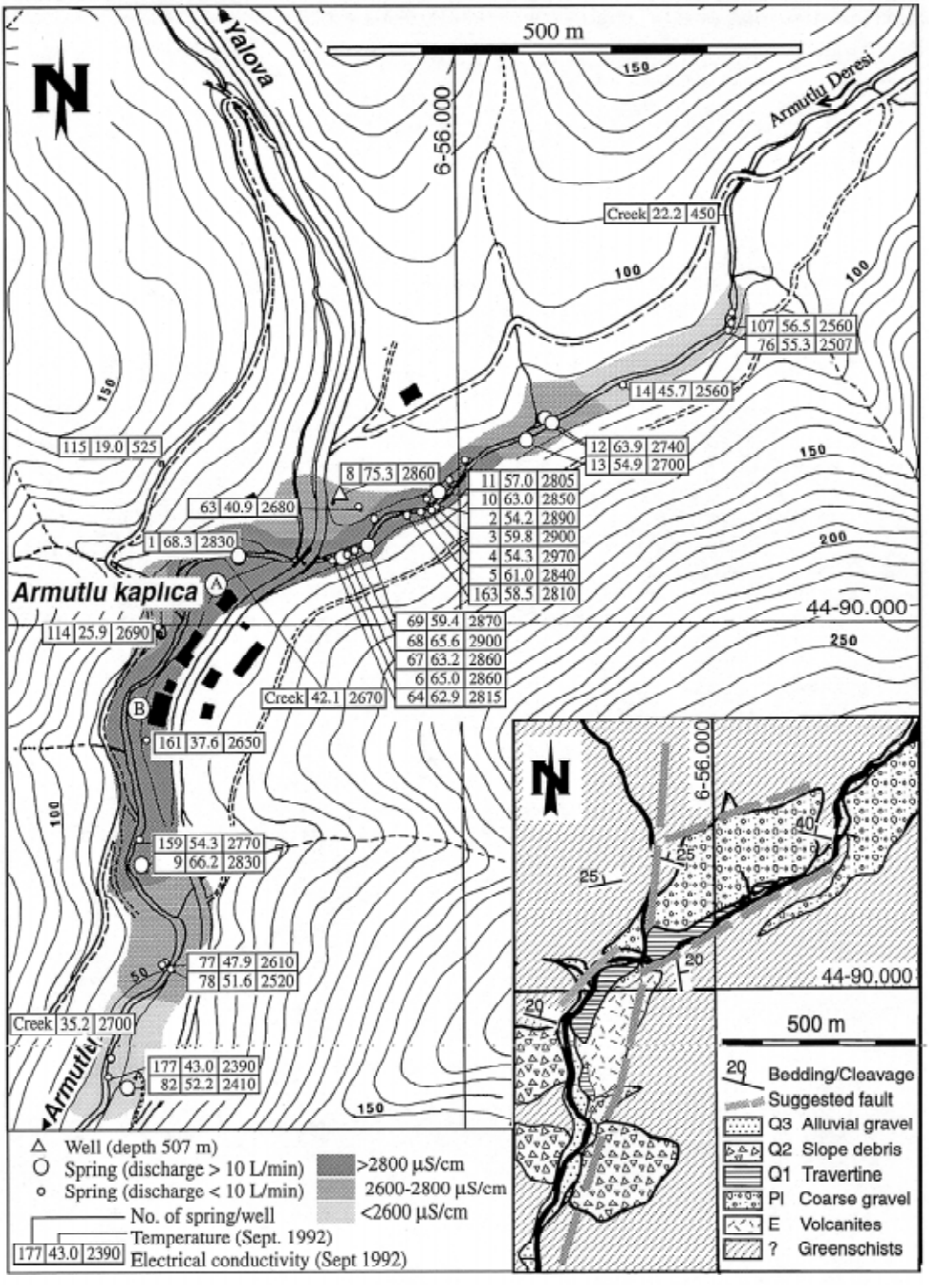


Figure 8: *Hydrogeological and geological map of the Armutlu geothermal area. The springs in the central dark shaded area are characterised by the highest electrical conductivities and the highest temperatures. (A = public spa, B = Erdilli hotel).*

Within the *plain of Gemlik* three different outflow zones can be distinguished: (1) Artesian thermal water with a temperature of 37°C emerges from quaternary sediments in the southwestern plain. Shallow wells (30-40m) collect the water for the public spa (*Gemlik kaplıca*,

200l/min) and a car wash. The southern border of the Gemlik plain is characterised by a dominant E-W striking fault zone (Geyve-İznik-Gemlik fault). By the means of soil gas measurements it was possible to localise this fault zone in the area of the spa (Eisenlohr 1995). In spite of the short distances to the Marmara sea (500m, 39000µS/cm) and to the highly polluted *Gölyağı* river (some meters, >1000µS/cm) the thermal water is clean and very slightly mineralised (415µS/cm). (2) Another artesian upflow zone is situated at a marginal alluvial fan in the northern plain (*Gemlik north*). Its water is characterised by similar electrical conductivities (370-450µS/cm) but lower temperatures (up to 25°C). Drill holes in the central part of the plain indicate that the quaternary and neogene filling of the plain consists of an intensive layering of impermeable clay and permeable gravel. The uppermost clay layer is 30m thick and prevents any mixing between the thermal water and the polluted surface water. It seems that the fault zone in the south and the alluvial fan in the north disturb the horizontal layering. (3) The third thermal outflow represents the *İlıpınar* spring (*Gemlik İlıpınar,* 21°C, 540µS/cm) which flows out of the southwards plunging marble unit at the northern edge of the plain. The DSİ (Devlet Su İşleri) has estimated a discharge of 100l/sec in 1974 (DSİ-Ankara 1974).

Another large spring with the name *"İlıpınar"* emerges in the alluvial *plain of Orhangazi* (Fig. 9). According to the results of excavations by Dutch archaeologists the mound (*hüyük*) next to the spring consists of a pre-historic human settlements. The oldest cultural layers of the mound have been dated by radiocarbon method as being 7000 years B.P (Roodenberg et al. 1990). The main spring emerges from the bottom of an artificial pool. The upflow zones are characterised by the highest temperatures (up to 22°C), the lowest mineralisation(530µS/cm) and the occurrence of gas bubbles. The smaller spring (17°C, 630µS/cm, about 100l/min) at the northeastern edge of the pool represents a mixture between the water of the main spring and that of the shallow groundwater (15.4°C, 890µS/cm) which emerges from the slope of the mound. The total discharge was roughly measured as 75l/sec in September 1993 and 230l/sec in March 1993.

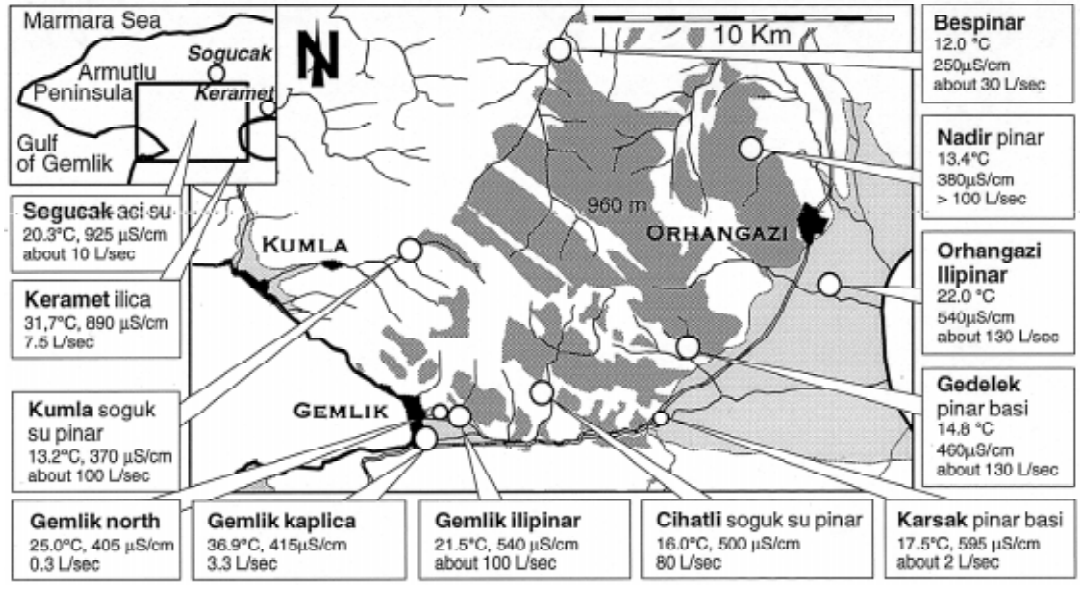


Figure 9: Geographical situation and raw data of the karstic springs of Gemlik, Orhangazi, Soğucak and Keramet (summer, 1992). The marble outcrops are shown by dark and the alluvial plains by lightly shaded areas.

Keramet and Soğucak

Another thermal spring called *Keramet İlıca* emerges from the slope of a terrace consisting of neogenous marls and sandstones at the northern shore of lake İznik (Fig. 9). The spring yields a temperature of 31°C and an electrical conductivity of 890µS/cm. As in Orhangazı gas bubbles rise from the sandy ground of the spring pool. The measured discharge was 75l/sec in September 1992 and April 1993. The E-W striking terraces in the spring area are caused by a large-scale tectonic fault zone which can be followed along the northern border of the lake İznik graben system over the Çengiler pass to the *village of Soğucak* (8km SE of Yalova). Soğucak is built on an impressive travertine complex. The spring responsible for the travertine precipitation emerges at the southeastern edge of the village. The water is not drinkable (*acı su* = bitter water, 920µS/cm) and yields a temperature of 20°C over the entire year.

Mineral water of Adliye

In addition to these thermal springs, mineral water has been investigated at *Adliye*, southeast of Gemlik. The small spring (3l/min, 15.3°C) emerges in the small valley of the *acı su deresi* creek south of the village. Its electrical conductivity of 65mS/cm is higher than that of sea water (Marmara sea: 39mS/cm). Adliye is situated in a tectonic "mélange" zone with mainly Eocene and Oligocene rocks. Quarries in the surroundings of the springs remain from a former gypsum mining.

Chemical composition

Introduction

The chemical composition of the springs confirms the preliminary distinction of two main groups of thermal springs and mineral water (Fig. 10). The "high temperature" springs of Yalova and Armutlu are characterised by higher mineralisation and the dominance of the ions Na^+, Ca^{2+} and SO_4^{2-}. On the other hand the mineralisation of the "low temperature" springs of Gemlik, Orhangazi, Keramet and Soğucak is much lower and dominated by the ions Ca^{2+}, Mg^{2+} and HCO_3^-. Finally, the mineral water of Adliye is very highly mineralised and represents a NaCl-type.

Yalova and Armutlu

The chemical composition of the different springs of Yalova is almost identical and constant during the year. Based on the main constituents, the water can be classified as $\underline{Na}Ca\underline{SO_4}$. The sulphate concentration amounts to 730mg/l. The concentrations of HCO_3^- and Mg^{2+} are very low – even lower than in the surface water or the shallow groundwater. Therefore any interaction with calcareous rocks can be excluded. Actually the chemistry is rather typical for waters in crystalline rocks. Similar waters have been observed in the crystalline basement of Switzerland (Pearson et al. 1991).

In Armutlu some of the springs show a significant dilution effect due to mixing with creek water. The other springs and the well are characterised by almost the same chemical composition. The total mineralisation of 2140mg/l is significantly higher than in Yalova (1300mg/l). The water can be classified as a $\underline{Ca}Na\underline{SO_4}HCO_3$(Cl)-type. The ions Ca^{2+}, Mg^{2+} and HCO_3^- show the highest enrichment compared to Yalova. The ionic balance of Ca+Mg and HCO_3 points to the dissolution of calcite and dolomite. The geological section of the well confirms calcareous schists at a depth of between 300 and 500m (Başkan 1981). The secondary enrichment of Na^+ and Cl^- could be affected by a further water-rock interaction with magmatic and metamorphic rocks. Due to the Na/Cl and B/Cl ratios sea water intrusion can be excluded.

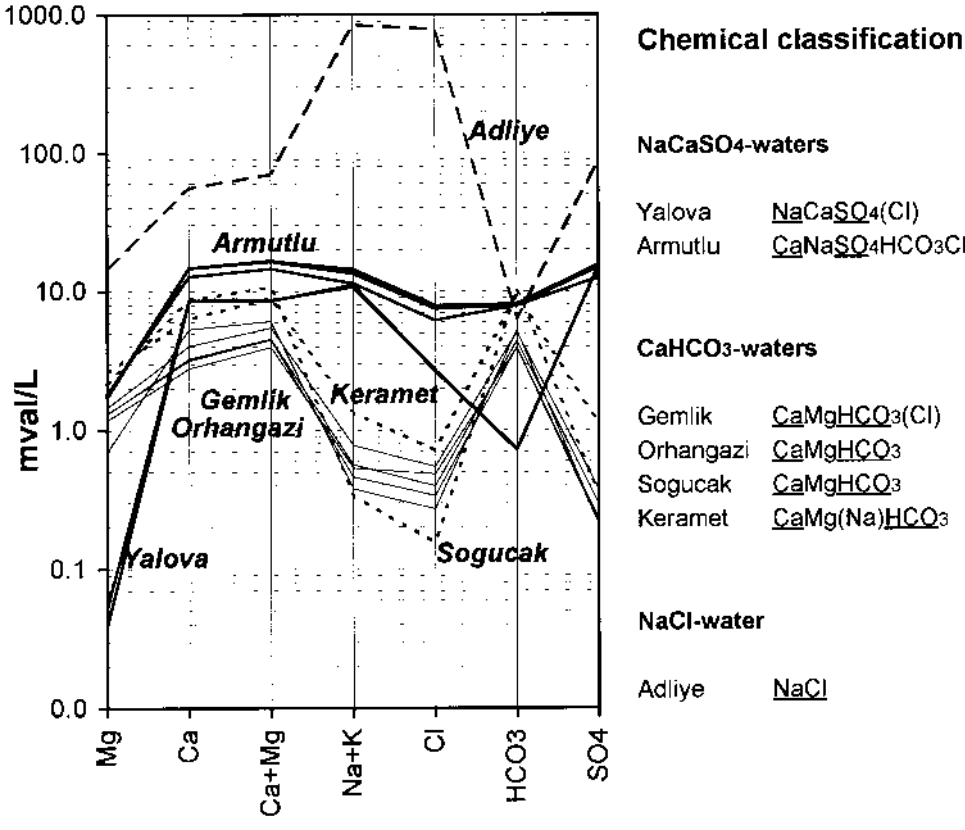


Figure 10: *Schoeller diagram and chemical classification (according to Michel 1963) of the thermal and mineral waters of the study area. According to the water chemistry three main groups can be distinguished.*

In conclusion, the thermal waters of Yalova and Armutlu both represent deep crystalline groundwater. In opposition to Yalova the water of Armutlu underwent an additional water-rock interaction with calcareous rocks. Actually it is not clear whether both waters originated from a common reservoir or if they just evolved in a similar way.

Sub-thermal and thermal springs of Gemlik, Orhangazi, Keramet and Soğucak

The springs of Gemlik, Orhangazi, Keramet and Soğucak are dominated by the ions Ca^{2+}, Mg^{2+} and HCO_3^- which indicate the dissolution of calcite and dolomite. Other processes of water-rock interactions are secondary. Considering the field investigations, the chemical composition and the gas composition (see below), all of these springs can be characterised as karstic springs – although some of them emerge from the alluvial plains. The marble unit of this region acts as a main aquifer.

The waters of Keramet and Soğucak which both precipitate calcite travertine, are characterised by a higher mineralisation (860mg/l and 880mg/l TDS respectively) than that of the thermal springs of the Gemlik-Orhangazi area (340 – 490mg/l TDS). These latter show a slight enrichment in Mg^{2+}, Na^+, Cl^- (Fig. 11c), SO_4^{2-} and silica compared to the cold springs of this area (Fig. 11d) which may be caused by increasing water-rock interaction. On the other hand, the concentration of Ca^{2+} and HCO_3^- decreases with increasing temperature (Fig. 11a,b). A suggested precipitation of calcite would explain this rather unusual behaviour. According to Matthes (1990) the potential of calcite precipitation or dissolution of a water can be estimated from chemical balance calculations. The calculated balance values of pH and dissolved CO_2 (acidity) of the chemical analyses have been compared with the direct measurements at the

spring site (Fig. 12). Lower field-pH and higher field-CO_2 values indicate a potential for calcite dissolution, higher field-pH and lower field-CO_2 values indicate a potential for calcite precipitation. The cold karstic springs (12-15°C) yield a significant potential for calcite dissolution. The sub-thermal and thermal springs of Gemlik and Orhangazi (21-37°C) show a slight potential for calcite precipitation. As expected Keramet and Soğucak are characterised by the highest potential for precipitation.

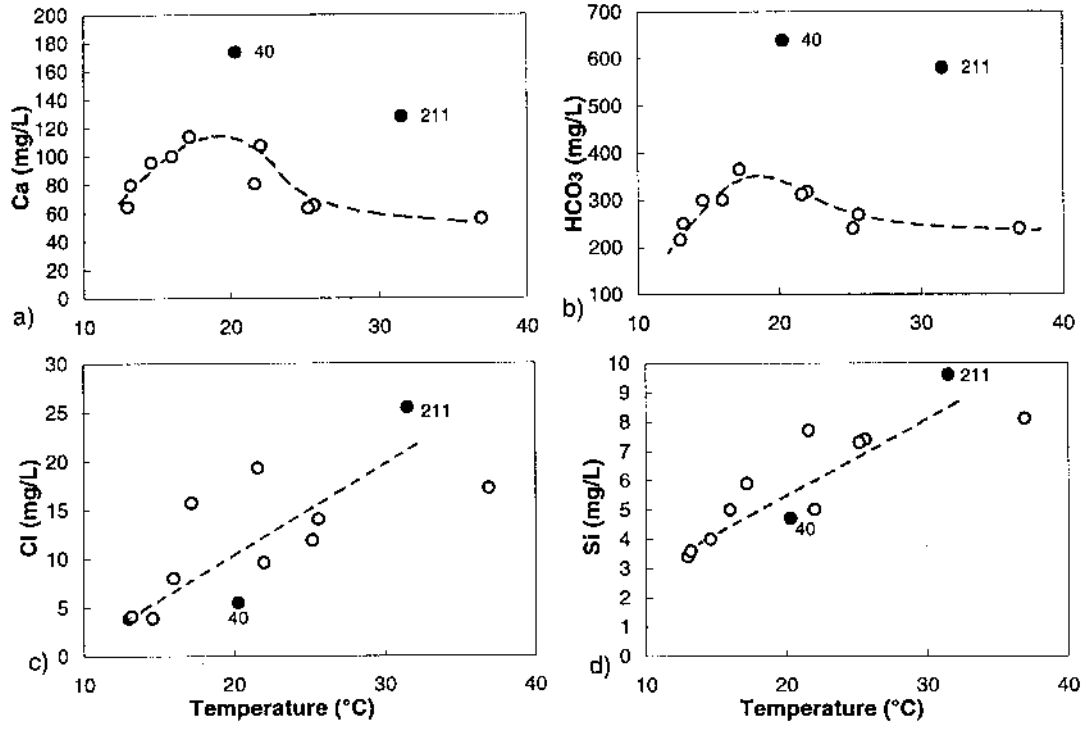


Figure 11a-d: Relationship between the temperature and the concentration of Ca^{2+}, HCO^{3-} Cl^- and Si (Keramet = 211, Soğucak = 40, Gemlik-Orhangazi area = open symbols). The thermal waters are generally enriched in Cl^- and Si. The Ca^{2+} and HCO_3^- contents of the thermal springs of Gemlik and Orhangazi are slightly decreased compared to those of the cold springs. A suggested calcite precipitation in the underground would explain this behaviour (see Fig. 12). Keramet (211) and Soğucak (40) are significantly more highly mineralised due to uprising CO_2 gas.

Geothermometer calculations

Geothermometer calculations are based on a chemical balance in the measured spring waters. Since this assumption is not correct for all thermal waters, unrealistic temperatures often result. In order to obtain an idea about the state of a thermal system, Giggenbach (1988) introduced the maturity index MI. According to this classification, only the water of Yalova is mature (MI = 2.3). All of the other waters are not mature which makes the application of geothermometers, based on Ca, Mg, Na and K, useless. The silica geothermometer is much more reliable. Nevertheless different temperatures result for the different silica species quartz, chalcedony and amorphous silica. According to their different solubilities the silica content of Armutlu and Yalova is most probably controlled by chalcedony. Chalcedony veins have been observed in both geothermal areas. The silica geothermometer is rather unreliable for the karstic springs due to the low silica concentrations and mixing processes. Another geothermometer for geothermal systems with a long residence time and relative high temperatures is the equilibration between $\delta^{18}O$ in SO_4 and H_2O (Mizutani and Rafter 1969). The re-

sults of the geothermometer calculations are summarised in Table 4. The highest reservoir temperatures of 100 to 130°C result for the geothermal field of Armutlu. In Yalova, the temperature is a little lower with 70 to 100°C. The most reliable information about the reservoir temperature of the karstic springs can be derived from the tritium data (see below). The hot mixing endmember of these springs is characterised by temperatures between 40 and 50°C.

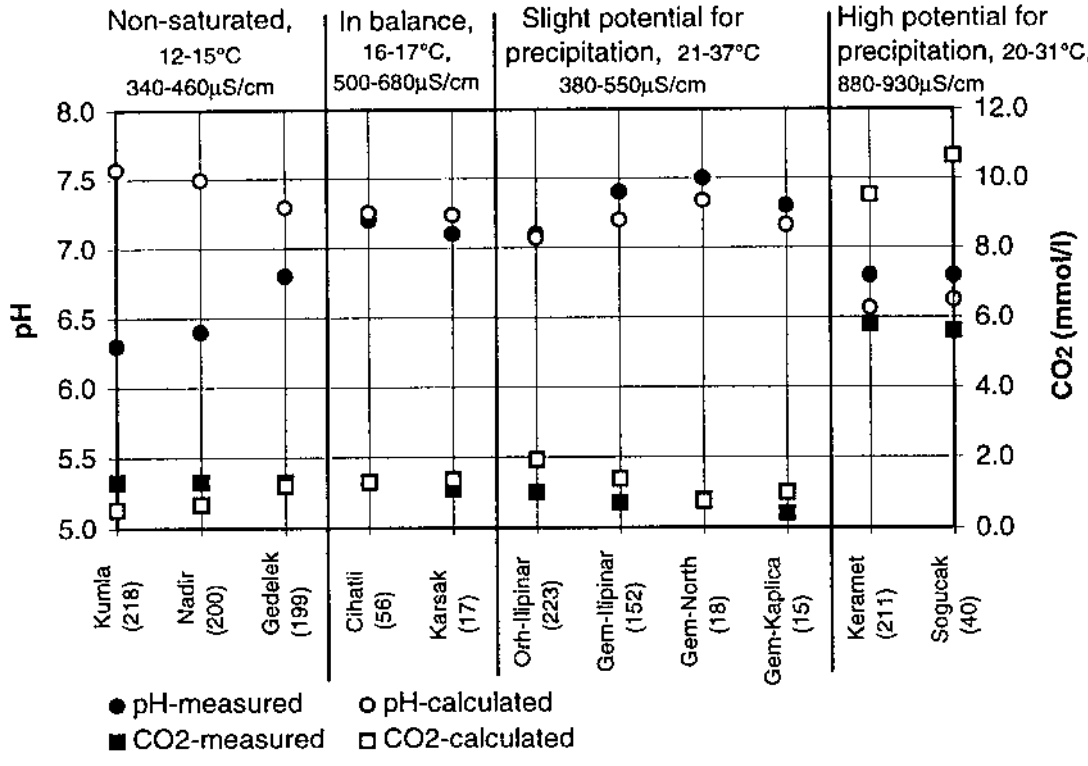


Figure 12: A comparison of the calculated balance values and measured values of pH and CO_2 indicates the potential for carbonate dissolution or precipitation (Matthes 1990). While the cold springs are aggressive the warm waters show a slight (Orhangazi, Gemlik) to high (Keramet, Soğucak) potential of calcite precipitation.

Adliye mineral water

The mineral water of Adliye represents a typical NaCl-type water. The total mineralisation of 53g/l is higher than that of normal sea water (35g/l) or that of the Marmara sea (24g/l). Apart from Na^+ and Cl^-, the concentration of Ca^{2+}, HCO_3^- and SO_4^{2-} is significantly increased compared to sea water. This can be explained by the dissolution of gypsum and calcite in the Oligocene rocks. There are two possibilities to explain the origin of the salt mineralisation. On the one hand, recent meteoric water could dissolve suggesting salt deposits within the evaporitic sequence. On the other hand, the water could represent a fossil sea water, e.g. a Tertiary formation water such as in Tuzla/Çanakkale (Mützenberg this volume). This question will be answered by the means of isotopic investigations.

Gas analyses

Gas samples were collected with evacuated glass bottles at the spring sites (see Eisenlohr 1995). Due to the specific outflow conditions, it was not possible to measure the gas flux. According to a qualitative judgement in the field the highest gas flux was expected in Armutlu. In

Yalova almost no gas flux has been observed. In the artificial pools of Keramet and Orhangazi gas bubbles rise periodically from the ground. The gas/water proportions of the samples confirm this subjective impression.

The chemical composition of the gas samples shows good correspondence with the findings from the field investigations and the chemical water analyses. The samples from Armutlu (well and two springs) consist mainly of CO_2 (80-98%). This corresponds with the high amounts of dissolved HCO_3^- in the water. Secondary nitrogen (1-19%), argon (0.1-0.3%) and methane (0.1-1.1%) have been detected. None of the samples from Armutlu contain oxygen. 93% of the gas collected in Yalova consists of nitrogen. The small amount of CO_2 (3%) corresponds well with the very low HCO_3^- values in the water. Furthermore, the samples contained argon (2.3%) and methan (7%). Oxygen was not detected. All of the samples from the karstic springs showed a composition similar to that of the atmosphere, which is well in accordance with their karstic origin. The samples *Gemlik spa* and *Gemlik north* are moderately enriched with CO_2 (29 and 43%, respectively). The origin of the CO_2 will be discussed later on.

Isotopic composition

In order to improve the knowledge about the geothermal systems, the following isotopes have been determined: $\delta^{18}O$, δD and tritium in H_2O and $\delta^{34}S$, $\delta^{18}O$ in SO_4, $\delta^{13}C$ in CO_2 and $^{3,4}He$ and $^{20,22}Ne$ of noble gases.

Deuterium and oxygen-18

The deuterium and $\delta^{18}O$ values of the cold springs of the entire Marmara region align on a regional meteoric waterline determined by the equation $\delta D = 8 \times \delta^{18}O + 15$ (Eisenlohr et al. this volume (a)). The thermal and mineral waters of the Armutlu peninsula plot on this meteoric waterline as well, more or less in the range of the cold springs (Fig. 13). This indicates that the waters belong to a recent water cycle. By way of contrast, formation waters and waters with a very intensive water-rock or water-gas interaction do not plot on the meteoric waterline (Mützenberg this volume, Greber this volume (b)).

With the cold shallow springs a local correlation between deuterium values and infiltration altitude was determined (Eisenlohr et al. this volume (a)). This correlation allows an estimation of the infiltration altitude of the deep groundwater. The thermal waters of Armutlu and Yalova are characterised by the very negative deuterium values which point to infiltration areas higher than 800m a.s.l. Since only small parts of the outer peninsula are higher than 800m a.s.l., a paleo-climatic effect (see Greber this volume (b)) cannot be excluded. Another, maybe more obvious explanation for the depleted values would be the infiltration of snow melting (this has not been sampled). The fit between the local altitude correlation of the cold springs and the subthermal and thermal karstic waters of Gemlik and Orhangazi is much better. It was possible to evaluate infiltration altitudes of 500 to 900m a.s.l. for the waters of Gemlik and 200 to 500m a.s.l. for the waters of Orhangazi, respectively (Eisenlohr et al. this volume (b)). The isotopic composition of the mineral water of Adliye indicates an infiltration altitude higher than 800m a.s.l. The infiltration area is most probably situated in the Kurban dağ mountains east of Adliye.

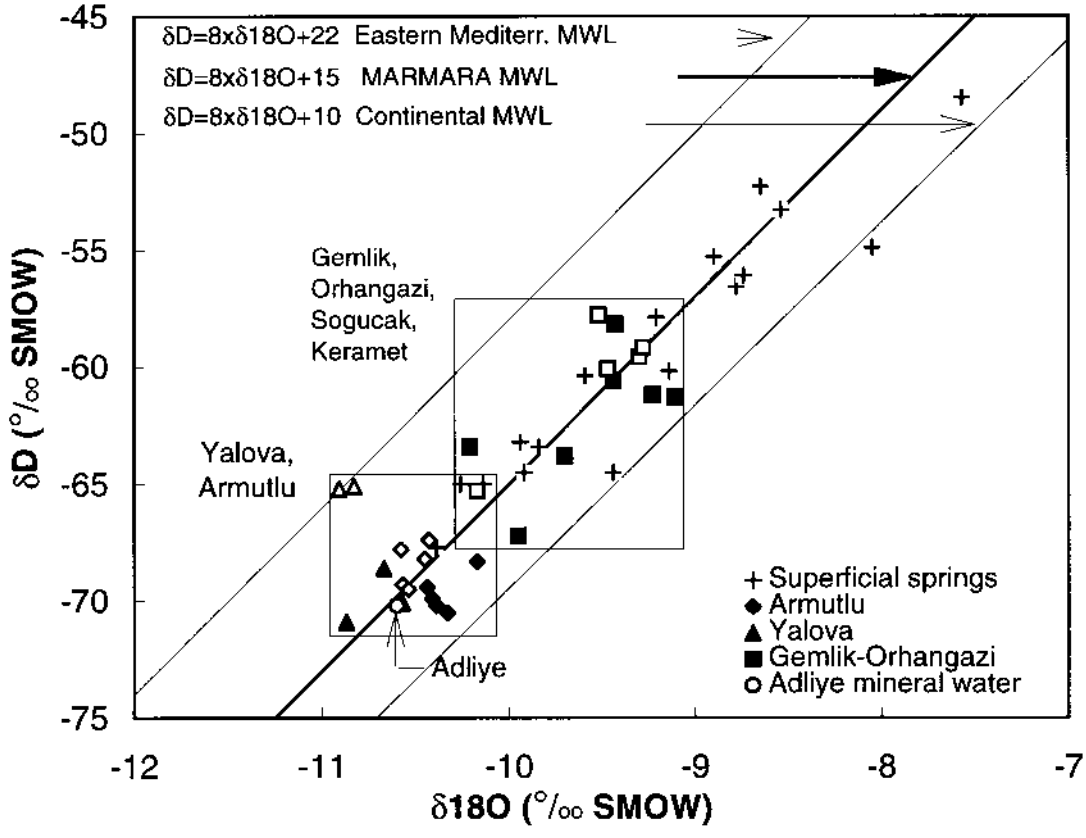


Figure 13: *δD-$\delta^{18}O$ diagram (solid symbols: summer, open symbols spring). The values of cold, sub-thermal and thermal springs plot on the local meteoric waterline (MWL) determined by cold shallow springs of the Marmara region (see Eisenlohr et al. this volume (a)).*

Tritium

Tritium is a radiogenic isotope of water with a half-life of 12.4 years. Due to atomic bomb tests in the Fifties and Sixties, the tritium concentration increased by a factor of one hundred or more in the atmosphere and the water cycle. At the present time, the concentration is decreasing to values around those of natural production. All samples were taken and analysed in 1992 and 1993.

The tritium concentration in the thermal waters of Yalova and Armutlu is below the limit of detection (<1TU). Therefore, these waters must have infiltrated before the bomb tests some 30 to 40 years ago. This gives a lower limit for the residence time in the underground. By way of contrast, the karstic springs contain between 4 and 18TU (Fig. 14). The cold karstic springs are characterised by tritium contents between 14 and 18TU. The tritium contents decrease in sub-thermal and thermal springs with increasing temperature. The lowest concentrations have been measured in Gemlik kaplıca (5TU) and Keramet (4TU). There are two different ways to explain this depletion. On the one hand, it may represent a proper decay age (*piston flow model*) which would lead to a mean residence time of about 30 – 40 years for Gemlik kaplıca. However, the numerical Finite Element models of these springs (Pfister et al. this volume, Eisenlohr et al. this volume (b)) clearly showed this time to be too short for the heat exchange. On the other hand, the depletion may be caused by the mixing of cold karstic water with a water which contains none or only very little tritium (*exponential model*). According to the chemical analyses, highly mineralised deep groundwater can be excluded as a main mixing endmember. Therefore, a mixture between cold karstic water (12-15°C, 250-450µS/cm)

and hot, stagnant karstic water (40-50°C, 300-400µS/cm) is proposed. Finally, the mineral water of Adliye contains 4TU. This can be explained either by a residence time of 20 to 30 years or by a mixture between a shallow groundwater and a slowly circulating deep groundwater. According to the stable isotopes (see above) formation water can be excluded as an old mixing endmember.

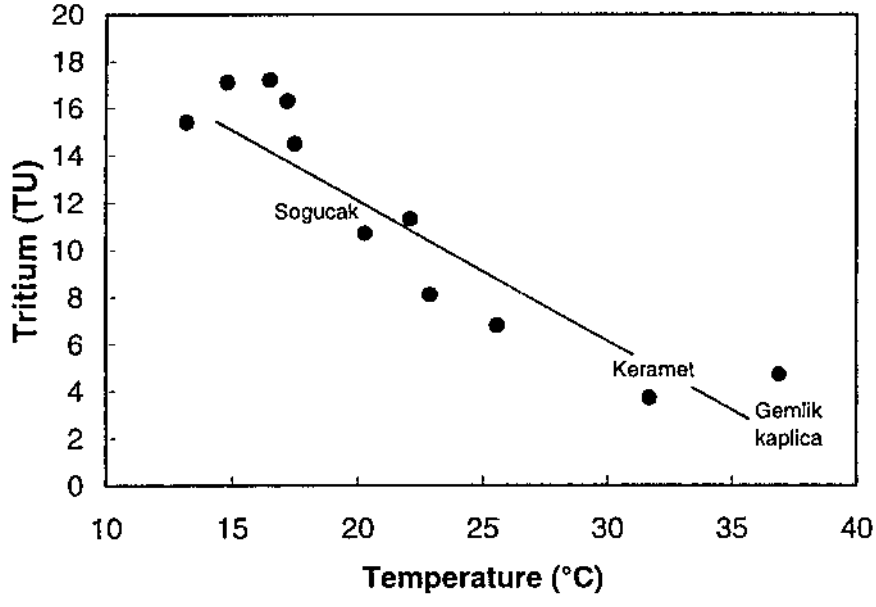


Figure 14: *Tritium-temperature plot. The tritium concentration of the karstic springs decreases with increasing temperature, which can be explained either by mixing processes or by an evolution of the water. The tritium contents of Armutlu and Yalova are below the limit of detection.*

$\delta^{34}S$ and $\delta^{18}O$ in sulphate

The origin of the sulphate in the thermal waters of Armutlu and Yalova is a very important question concerning its mineralisation and flow path. On the one hand, the sulphate may originate from "marine sources" such as sea water (~2g/l SO_4^{2-}), formation water (fossil sea water) and the dissolution of evaporites (e.g. gypsum). On the other hand sulphide minerals (e.g. pyrite) in the magmatic and metamorphic rocks may be oxidised. All of these sources are characterised by typical $\delta^{34}S$ and $\delta^{18}O$ values (Fig. 15). $\delta^{18}O$ values higher than 7 to 8‰ SMOW (Claypool et al. 1980) are typical for marine sulphate. The dissolved SO_4^{2-} in the thermal waters of Yalova and Armutlu shows significantly lower $\delta^{18}O$ values of about 5‰ SMOW. Since the anorganic oxidation of sulphide causes an isotopic fractionation to higher $\delta^{18}O$ values, it is more obvious to trace the sulphate back to sulphide minerals. The typical crystalline waters of Switzerland determine a $\delta^{34}S$ and $\delta^{18}O$ range which includes Yalova and Armutlu. Geological observations confirm this finding as well; the outer peninsula consists of magmatic and metamorphic rocks, evaporites occur only south of Gemlik. In addition to the mineral water of Adliye a gypsum sample from these evaporites has been analysed. Both plot close to each other within the "marine field". This confirms the relationship between the evaporites and the mineral water. The SO_4^{2-} concentration of the karstic springs is too small to make a reliable statement.

$\delta^{13}C$ of CO_2 gas

In analogy to the sulphate isotopes, the $\delta^{13}C$ value may yield information about the origin of the CO_2. $\delta^{13}C$ has been measured in the CO_2 of the gas samples. The samples from the karstic springs of Gemlik and Orhangazi are characterised by $\delta^{13}C$ values between -19 and

-13‰ PDB which is rather typical for the decompositon of organic material (Fig. 16). Most of the CO_2 in these waters originates from the soil in the infiltration area. The value at Keramet (-11‰ PDB) cannot be explained only by organic CO_2. Since this karstic spring is situated on a significant fault zone a certain component of CO_2 from the metamorphism of marine carbonates in the Earth's crust or from outgassing of the Earth's mantle can be expected (values from Barnes et al. 1978). The $\delta^{13}C$ values of the well and the *mide suyu* spring in Armutlu are significantly higher than those of the other samples and they plot in the transition zone between mantle CO_2 and CO_2 from marine carbonates. As mentioned previously, tectonic fault zones are responsible for the upflow of the thermal water of Armutlu. On the other hand, calcarous schists were found in the drilling in a depth of 300-500m. Therefore, a mixture of CO_2 from marine carbonates and mantle CO_2 is proposed.

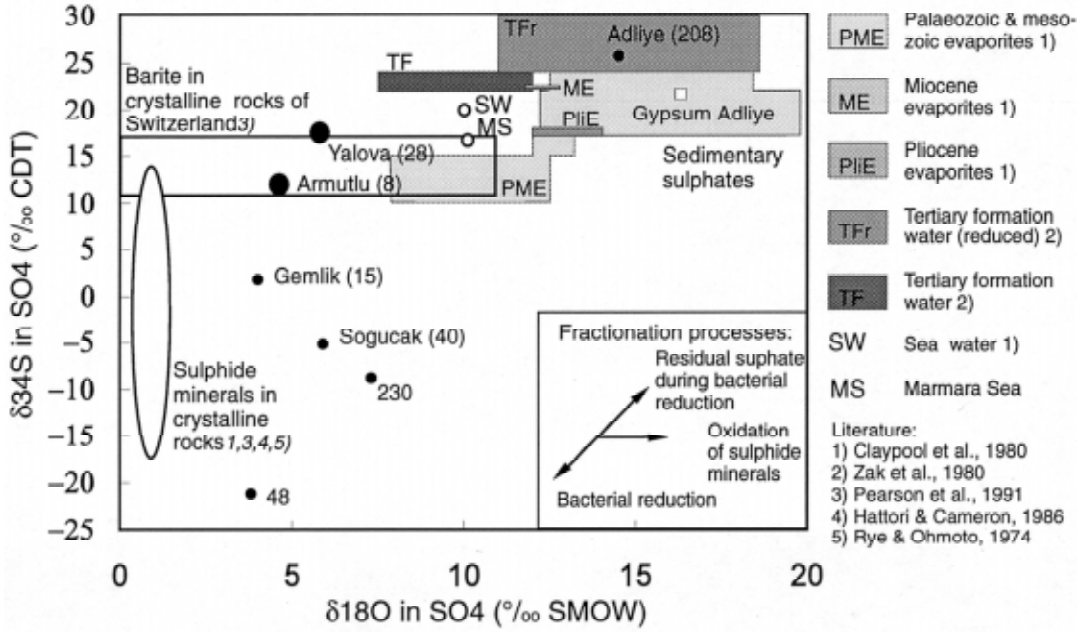


Figure 15: *$\delta^{34}S - \delta^{18}O$ diagram. According to the isotopic composition, a sedimentary origin of the sulphate of the thermal springs of Yalova (28) and Armutlu (8) can be excluded. Therefore, a water-rock interaction with metal sulphides in the crystalline rocks can be suggested. The marginal springs of Yalova (48, 230) and the waters of Gemlik kaplıca (15) and Soğucak (40) are most probably affected by bacterial processes. The mineral water of Adliye (208) plots in the field of tertiary formation waters and close to the gypsum sample from this region.*

Isotopes of noble gases ^3He, ^4He, ^{20}Ne and ^{22}Ne

Due to the conservative behaviour of noble gases and their characteristic isotopic composition in the atmosphere, the Earth's crust and the Earth's mantle can be used as natural tracers for these reservoirs. The samples were taken at the spring sites by squeezing the ends of copper pipes and were then analysed in the laboratory of the Institute of Mineralogy and Petrography / ETH Zürich.

The $^3He/^4He$ and $^{20}Ne/^4He$ ratios of the cold karstic Gedelek spring are in the range of the values for the atmosphere and air saturated water (Fig. 17) which points to an equilibration with the atmosphere. The ratios of the samples from Gemlik kaplıca and Orhangazi İlıpınar are closer to the ratio which results from the radiogenic production of helium in the Earth's crust (values from Andrew 1985). Nevertheless, they still contain a certain atmospheric component. By way of contrast, the samples from Armutlu and Yalova show no atmospheric influ-

ence concerning the origin of ^{4}He. The $^{3}He/^{4}He$ ratios indicate a slight influence of the Earth's mantle (ratio from Mamyrin and Tolstikhin 1984) for all of the samples with the exception for the karstic spring Gedelek. Since the ratio of $^{20}Ne/^{22}Ne$ of all samples is equal to the ratio in the atmosphere, almost all of the measured neon must originate from the atmosphere (infiltration). Considering the neon concentrations, the amounts of ^{3}He and ^{4}He from the different reservoirs can be estimated (Kipfer 1991). The neon correction was related to the Gedelek sample. The suggested $^{3}He/^{4}He$ ratios of the different reservoirs allow a rough quantification of the proposed helium origin (Table 3).

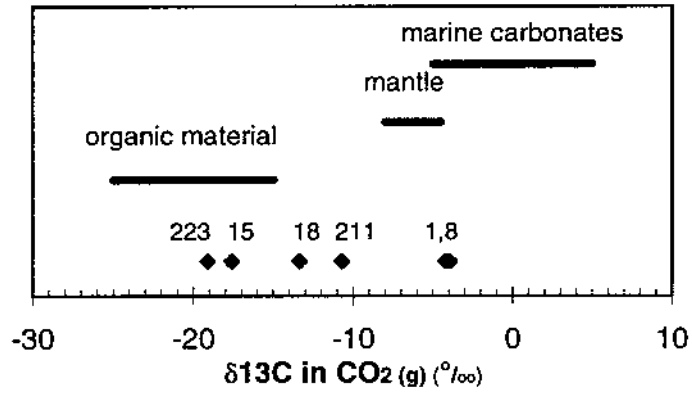


Figure 16: *$\delta^{13}C$-values of CO_2-gas. The CO_2 of Armutlu plots in a transitional range between the mantle outgassing and the metamorphic decomposition of marine carbonates. In opposition, the karstic springs (223, 15, 18 and 211) contain mostly organic CO_2. (Isotope values for CO_2 of organic material, Earth's mantle and marine carbonates from Deines (1980) and Barnes et al. (1978)).*

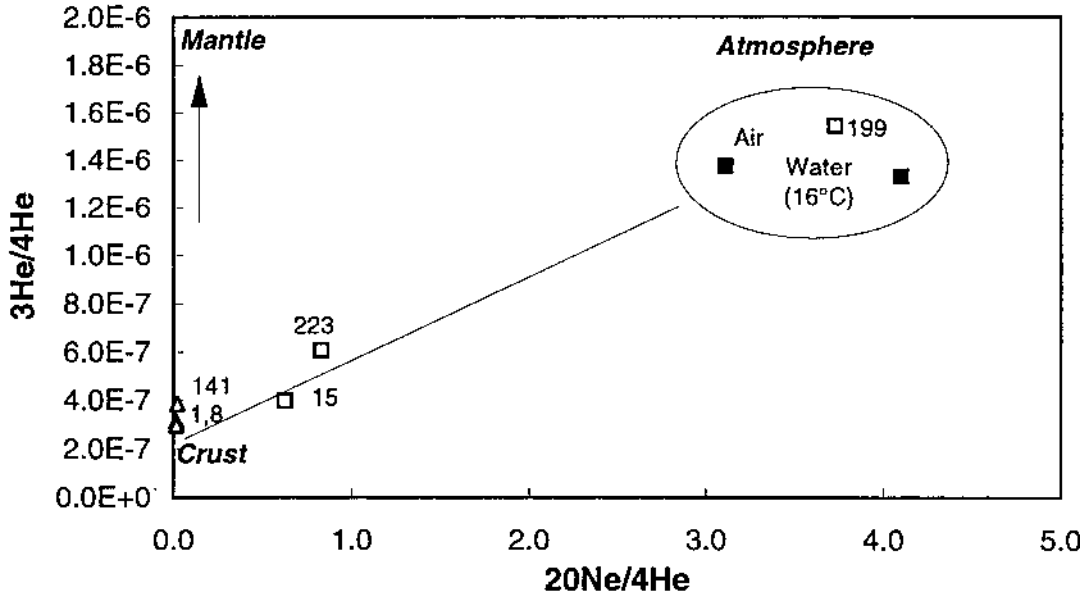


Figure 17: *$^{3}He/^{4}He$-against $^{20}Ne/^{4}He$. The cold karstic spring 199 is equilibrated with the atmosphere. All other samples indicate a mixture mainly between atmospheric and radiogenic noble gases. Nevertheless, a small component of premordial helium (from the Earth's mantle) can be observed. (Isotopic ratios and concentrations of noble gas from atmosphere, Earth's mantle and crust from Ozima and Podesek (1983) Mamyrin and Tolstikhin (1984) and Andrews (1985)).*

Sample	Atmosphere	Mantle	Crust
Yalova (spring)	0.6%	3.6%	95.8%
Armutlu (well/spring)	0.4%	3.0%	96.6%
Gemlik spa	16.7%	1.2%	82.1%
Orhangazi İlıpınar	22.2%	2.4%	75.4%
Gedelek (per definition)	100%	0%	0%

Table 3: Rough quantification of the different helium sources: atmosphere, crust and mantle. Calculations according to Kipfer (1991), see also Eisenlohr (1995).

Conclusions

Based on the geological setting and the hydrogeological investigations, it has been possible to characterise the circulation pattern of the thermal and mineral waters on the peninsula. The conceptual flow models are summarised in Table 4.

	Yalova / Armutlu	Gemlik/Orhangazi/Keramet/ Soğucak	Adliye mineral water
Infiltration	Actual recharge with snow melting (?) possible on the peninsula (>800m a.s.l.)	Actual recharge by precipitation in altitudes of 600-900m (Gemlik) and 300-600m a.s.l. (Orhangazi) resp.	Actual recharge by precipitation >1000m a.s.l.
Reservoir	Joints and fractures metamorphic and magmatic rocks; additional interaction with calcareous rocks in Armutlu	Karstic systems in the Orhangazi marble. Mixing between cold, young water and warm, stagnant water in the karstic system. Calcite precipitation suggested	Oligocene evaporites (gypsum and suggested salt deposits) and Eocene flysch
Temperature	70-100°C / 100-130°C	40-50°C (mixing endmember)	-
Residence time	> 40 years	Cold endmember: months to years, thermal endmeber: >30 years	Mixing component older than 30 years
Upflow	Intersections of fault zones	Fault zones, marble unit	Fault zone
Surface processes	Cooling, mixing with creek water in Armutlu	Cooling, mixing with shallow groundwater	-

Table 4: Conceptual flow models of the thermal and mineral waters of the Armutlu peninsula derived from geological and hydrogeological investigations.

Thermal springs are a very common feature of the Marmara region. The density of geothermal areas is higher in this area than in the southern, central and eastern parts of Turkey. The explanation of this phenomenon is one of the main aims of the MARMARA Poly-Project. Since the geothermal heat flow is not generally increased in this area (Pfister et al. this volume) a regional heat anomaly can be excluded as a possible explanation. As mentioned previously, the tectonic model derived from the structural investigations on the Armutlu peninsula, would explain the accumulation of thermal springs very well. Since the western end of the NAF is split up in a complex fault system which covers almost the entire Marmara region, this local tectonic model is most probably also applicable for the whole Marmara region.

Acknowledgements

The multidisciplinary MARMARA Poly-Project was financed by the ETH Zürich, Switzerland. I am very thankful to the coordinator of this project Prof. Dr. C. Schindler, to PD Dr. W. Balderer and to all of the other members of the project for their support. I also thank Prof. Erdoğan Yüzer for the opportunity to carry out this study in Turkey and to get in closer touch with a fascinating culture. Thanks also to the staffs of the isotopic laboratories of the Mineralogical and Petrographic Institute (IMP) and the Geological Institute of the ETH Zürich for analysing our strange samples.

References

Akartuna, M., 1968, Armutlu yarımdasının jeolojisi (turkish), İst. Üniv. Fen Fak. Monogr., 20, 105p.

Andrews, J.N., 1985, The isotopic Composition of Radiogenic Helium and its Use to Study Groundwater movement in Confined Aquifers, Chemical Geology, 49, 339-351.

Barnes, I., Irwin, W. P. and White, D. E., 1978, Global distribution of Carbon Dioxide, Discharges and Major Zones of Seismicity. U.S: Geological Survey Water Resources Investigations 78-79, Open-File Report, 12.

Başkan, E., 1981, Gemlik-Armutlu kaplıcası sıcak su kaynaklarınım hidrojeoloji incelemesi, unpubl. report, Konya, 51p.

Claypool, G. E., Holster, W. T., Kaplan, I. R., Sakai, H. and Zak, I., 1980, The Age Curve of Sulfur and Oxygen Isotopes in marine Sulfate and their Mutual Interpretation, Chem. Geol., 28, 99-260.

Deines, P., 1980, The Isotopic Composition of Reduced Organic Carbon, in: Handbook of Environmental Isotope Geochemistry 1. The Terrestrial Environment, edited by: P. Fritz and J.C. Fontes, Elsevier, Amsterdam, 329-406.

DSİ-Ankara, 1974, İznik, Orhangazi and Gemlik Plains, Hydrogeological Investigation Report, 41p.

Eisenlohr, T., 1995, Die Thermalquellen der Armutlu-Halbinsel (NW-Türkei) und deren Beziehung zu Geologie und Tektonik, Diss. ETH Zürich Nr. 11340, 165p.

Eisenlohr, T., Jeckelmann, C., Balderer, W., Bernasconi, S., Rauert, W. and Trimborn, P., this volume (a), Regional investigations of cold groundwater for determination of the recharge conditions in geothermal areas of Northwestern Turkey.

Eisenlohr, T., Pfister, M. and Balderer, W., this volume (b), Environmental isotope study and 2-D-modelling of cold and thermal karst within the Gemlik (Bursa) area of Northwestern Turkey.

Erguvanlı, K., 1949, İmralı Adasının Jeolojisi, Türkiye Jeoloji Kurumu bülteni (turkish), Cilt II, Sayı 1, 118-125.

Erinc, S. and Sungur, K, 1964, Monthly Sequence and Frequencies of Weather Types in İstanbul, Rev. Geograph. Inst. Univ. İstanbul, No. 9-10, 85-106.

Erk, A.S., 1942, Etude géologique de la région entre Gemlik et Bursa (Turquie), Diss. Univ. Basel, 295.

Giggenbach, W.F., 1988, Geothermal Solute Equilibra, Derivation of Na-K-Mg-Ca-Geoindicators, Geochim. Cosmochim. Acta, 52, 2749-2765.

Greber, E., this volume (a), Stratigraphic evolution and tectonic activities in an area of high seismicity: Akyazı/Adapazarı (Pontides, NW Turkey).

Greber, E., this volume (b), Deep circulation of CO_2-rich paleowaters in a seismically active zone (Kuzuluk/Adapazarı, NW Turkey).

Hattori, K. and Cameron, E.M., 1986, Archaean Magmatic Sulphate, Nature, 319/60482, 45-47.

Hotz, W., 1989, Die Mittelmeerküsten Anatoliens: Handbuch der Kunstdenkmäler, Wissensch. Buchges. Darmstadt.

Imbach, T., this volume, Geology of Mount Uludağ with emphasis on the genesis of the Bursa thermal waters, Northwestern Anatolia, Turkey.

Kaya, O. and Kozur, H., 1987, A new and different Jurassic to early Cretaceous sedimentary assemblage in Northwestern Turkey (Gemlik, Bursa): Implications for the pre-jurassic to early cretaceous tectonic evolution, Bull. of Earth Sc. Appl. and Res. Centre of Haceteppe University, 14, 253-268.

Kipfer, R., 1991, Primordiale Edelgase als Tracer für Fluide aus dem Erdmantel, Diss. ETH-Zürich.

Kopp, K., Pavoni, N. and Schindler, C., 1969, Geologie Thrakiens IV: Das Ergene-Becken, Beiheft geol. Jb., Hannover, 136.

Mamyrin, B.A. and Tolstikhin, I.N., 1984, Helium Isotopes in Nature, in: Developments in Geochemistry, Vol.3, edited by: W.S.Fyfe, Elsevier, 273p.

Matthess, G., 1990, Die Beschaffenheit des Grundwassers, Lehrbuch der Hydrogeologie, Band 2, 2. Auflage, Gebrüder Borntraeger, Berlin-Stuttgart, 498.

McKenzie, D.P., 1972, Active Tectonics of the Mediterranean Region, Geophys. J. Roy. Aston. Soc., 30, 109-185.

Michel, G., 1963, Untersuchung Über die Tiefenlage der Grenze Süsswasser-Salzwasser im nördlichen Rheinland und anschliessenden Teilen Westfalens, Forschbericht. Nordrhein-Westfalen, 1239.

Mizutani, Y. and Rafter, T.A., 1969, Oxygen Isotopic Composition of Sulphates – Part 3. Oxygen Isotopic Fractionation in the Bisulphate Ion-Water System, New Zealand, J. of Sc., 12.

Mützenberg, S., this volume, Nature and origin of the thermal springs in the Tuzla area, Western Anatolia, Turkey.

Nur, A., Ron, H. and Scotti, O., 1989, Mechanics of distributed fault and block rotation, in: Paleomagnetic and continental deformation, edited by: C. Kissel and C. Laj, 209-228.

Pearson, F.J., Balderer, W., Loosli, H.H., Lehmann, B.E., Matter, A., Peters, T.J., Schmassmann, H. and Gautschi, A., 1991, Applied Isotope Hydrogeology – A Case Study in Northern Switzerland, Technical Report 88-01, NAGRA, 5401 Baden.

Ozima, M. and Podesek, F.A., 1983, Noble Gas Geochemistry, Cambridge University Press, Cambridge, 367p.

Pfister, M., Rybach, L. and Şimşek, Ş., this volume, Geothermal reconnaissance of the Marmara sea region.

Riedel, W., 1929, Zur Mechanik geologischer Brucherscheinungen, Zb. Miner. Geol. Paleont. Abh. B., 354-368.

Roodenberg, J., Thissen, L. and Buitenhuis, H., 1990, Preliminary Report on the Arechaeological Investigations at Ilipinar in NW Anatolia, Anatolica, XVI, 1989-1990, 61-120.

Rye, R.O. and Ohmoto, H., 1974, Sulphur and Carbon Isotopes and Ore Genesis: a Review, Econ. Geology, 69, 826-842.

Şengör, A.M.C, 1979, The North Anatolian Transform Fault: its Age, Offset, and Tectonic Significance, J. geol. Soc. Lond., 136, 269-282.

Şengör, A.M.C and Yılmaz, Y., 1981, Tethyan Evolution of Turkey: a Plate Tectonic Approach, Tectonophysics, 75, 181-241.

Straub, Ch. and Kahle, H.-G., this volume, Recent crustal deformation and strain accumulation in the Marmara sea region, NW Anatolia, inferred from repeated GPS measurements.

Tatar, V., Ponat, E. and Işıkara, A.M., 1995, Paleomagnetism of Volcanic Rocks in the Armutlu Peninsula and Almacık Mountain, Symp. 12-14 April, İstanbul. Jeofizik, 9/1-2, 219-228.

Ternek, Z., Erentöz, C., Pamir, H.N. and Akyürek, B., 1987, Explanatory text of the Geological Map of Turkey, İstanbul, Maden Tetkik Arama (MTA), Ankara.

Wong, H.K., Lüdmann, T., Ulug, A. and Görür, N., 1995, The sea of Marmara: a plate boundary sea in an escape tectonic regime, Tectonophysics, 244, 231-250.

Yılmaz, Y., Genç, Ş., Yiğitbaş, E., Bozcu, M. and Yılmaz, K., 1995, Geological evolution of the late Mesozoic continental margin of Northern Anatolia, Tectonophysics, 243, 155-171.

Zak, I., Sakai, H. and Kaplan, 1980, Factors Controlling the $^{18}O/^{16}O$ and $^{34}S/^{32}S$ Isotope Ratios of Ocean Sulphates, Evaporites and Interstitial Sulphates from Modern Deep sea Sediments, Isotope Marine Chemistry, 339-373.

Appendices

Appendix 1 Thermal spa of Yalova (Yalova kaplıcaları)

Name	No.	Coordinates	Altitude	Purpose	User
Esas kaynağı (main spring)	28	**6** 83 650/**44** 97 230	120m a.s.l.	Spa, consumption	Turban Termal
Göz suyu (eye water)	27	**6** 83 750/**44** 97 210	115m a.s.l.	Eye compresses	Turban Termal
Small spring in creek	141	**6** 83 670/**44** 97 230	117m a.s.l.	-	-

Name	Description of spring site
Esas kaynağı	The main spring flows out of several N-S striking faults on the northern side of the creek. The thermal water is collected in a covered reservoir. The water level of the reservoir is about 1 to 2m above the creek. From the captage reservoir the water flows naturally in a channel to a main reservoir next to the post office. All bathes and the fountain of the "stomach water" (mide suyu) get their water by pumps from this reservoir. Between 11pm and 6am the reservoir is full. During this time the thermal water flows over non-utilised into a waste water channel. This allowed the measurement of discharge with a 110L-barrel at this overflow.
Göz S.	This spring is captured from a N-S orientated fault on the southern side of the creek.
Creek springs	Between the main spring and the uppermost spa (Sultan banyo) several small springs occur at joints in the bed of the creek. The spring 141 is situated under the small bridge between Göz suyu and Esas kaynağı.

Field measurements	**Date** Summer	**Date** Spring	**T_{Su}** *°C*	**T_{Sp}** *°C*	**EC_{Su}** *µS/cm*	**EC_{Sp}** *µS/cm*	**Q_{Su}** *l/min*	**Q_{Sp}** *l/min*	**pH**	**O_2** *mg/l*	Alcalinity *mmol/l*	Acidity *mmol/l*
Esas kay.	3.8.93	11.4.93	65.6	65.3	1920	1910	1020	790*	7.5	0.3	0.9	0.6
Göz suyu	4.9.92	11.4.93	59.6	59.2	1900	1915	15	15	7.5	0.3	0.9	0.7
Creek spring	28.8.92	-	63.1	-	1880	-	~3	-	7.4	-	-	-
Creek above 28	3.8.93	11.4.93	20.2	8.1	282	111	72	5000	-	10.3	0.8	0.3
Creek below 27	3.8.93	-	44.7	-	1660	-	~600	-	-	-	-	-

Chemical analyses			
No.	28	27	141
Date	Sept.92	Sept.92	Sept.92
	mg/l	*mg/l*	*mg/l*
Ca^{2+}	171	172	168
K^{+}	4.8	4.4	4.3
Li^{+}	0.12	0.13	0.13
Mg^{2+}	0.5	0.6	0.6
Na^{+}	252	246	246
Cl^{-}	96.1	94.3	93.6
HCO_3	44.5	44.0	43.9
SO_4^{2-}	737	730	727
NO_3^{-}	0.0	2.0	1.1
Σ	1305	1290	1200
SiO_2	59.1	58.1	58.1

Gas analyses		
Creek spring, 141		
2. Sept. 1992		
	mg/kg	*Vol%*
H_2	n.d.	0
He	0.002	0.08
CH_4	0.16	1.7
C_2H_6	-	-
N_2	15.2	93
O_2	n.d.	0
Ar	0.53	2.3
H_2S	0.02	0.08
CO_2	0.9	2.9
Gas	13.1	*cm^3/kg*
Water	164	*g*

Isotope analyses				
		28	27	141
		Sep.92	*Sep.92*	*Sept92*
Isotope	*in*			
δ^2H ‰ *SMOW*	H_2O	-70.8	-68.6	-70.1
$\delta^{18}O$ ‰ *SMOW*	H_2O	-10.87	-10.67	-10.57
^3H *TU*	H_2O	< 0.8	< 0.9	< 0.8
$\delta^{34}S$ ‰ *CDT*	SO_4^{2-}	17.4	-	-
$\delta^{18}O$ ‰ *SMOW*	SO_4^{2-}	5.8	-	-
^3He *(ccSTP/g)*	He (g)	-	-	2.1E-12
^4He *(ccSTP/g)*	He (g)	-	-	5.5E-06
^{20}Ne *(ccSTP/g)*	Ne (g)	-	-	1.2E-07
$\delta^{13}C$ ‰ *PDB*	CO_2(g)	-	-	-
$\delta^{18}O$ ‰ *SMOW*	CO_2(g)	-	-	-

Appendix 2 Armutlu geothermal area (Armutlu kaplıcaları)

Name	No.	Coordinates	Altitude	Purpose	User
Sondaj (well)	8	**6** 55 880/**44** 90 130	70m a.s.l.	Spa, drinking water	Belediye, MIT, ER-Hotel
Mide suyu (stomach w.)	1	**6** 55 770/**44** 90 070	60m a.s.l.	Drinking water	public
Küpeli kaynağı	3	**6** 55 995/**44** 90 230	65m a.s.l.	Drinking water	public
Nuri paşa kaynağı	9	**6** 55 655/**44** 89 750	55m a.s.l.	Spa, drinking water	B.Toker
Gicik kaynağı	82	**6** 55 650/**44** 89 510	50m a.s.l.	Spa, drinking water	Belediye, MIT (Secret service)
Ormancı kaynağı	12	**6** 56 100/**44** 90 205	70m a.s.l.	Spa, drinking water	Forest agency

Name	Description of spring site
Sondaji	Well drilled by MTA in 1973 (depth 507m, artesian) is nowadays strongly corroded and leaky. The local spas (Belediye, Erdilli-Hotel) get their water by two small pipes, a bigger pipline transmits water to Armutlu village 10km to the south (village hamam, spa of turkish secret service).
Mide S.	Emerges from gravel deposits next to the creek. The water is said to heal stomach problems (*mide* = stomach).
Küpeli	Small springs emerge from joints (No. 3 on the soutern side of the creek). The former main spring was on the northern side (travertine), it dried out after the drilling of the well 1973.
Nuri paşa	The springs emerge from gravel south of the Erdilli-hotel. A new drainage and a pipeline to a projected sanatorium some 500m to the south was made in 1993. Until 1994 the water has not been used.
Gicik	Bellow the street. The water is collected and joined to the pipline to Armutlu.
Ormancı kay.	Main spring emerges from a NS-striking fault next to the creek (No.12 southern side). The water is pumped to a recreation camp of the forest agency on top of the travertine. Several small springs occur some meters below.

Field measurements	Date Summer	Date Spring	T_{Su} °C	T_{Sp} °C	EC_{Su} µS/cm	EC_{Sp} µS/cm	Q_{Su} l/min	Q_{Sp} l/min	pH	O_2 mg/l	Alcalinity mmol/l	Acidity mmol/l
Sondaj/well	7.9.92	8.4.93	75.3	75.2	2860	2850	~500	~500	6.2	0.8	7.9	5.4
Mide suyu	2.9.92	9.4.93	68.3	67.2	2830	2815	~ 50	40	6.4	0.2	7.9	5.2
Küpeli kay.	7.9.92	11.4.92	59.8	58.4	2900	2850	~ 2	~ 2		3.5	7.9	3.4
Nuri pasa	7.9.92	11.4.92	66.2	65.9	2830	2790	35	~ 20	6.2	0.2	8.0	5.1
Gicik kaynağı	7.9.92	8.4.93	52.2	51.6	2410	2450	200	200	6.5	2.1	7.8	4.7
Ormancı kay.	2.9.92	8.4.93	63.9	62.8	2740	2705	~ 20	~ 20	6.5	0.3	7.9	6.4
Creek above	28.7.93	8.4.93	22.2	10.7	450	140	40	47000				

Chemical analyses			
No.	8	1	82
Date	Sept.92	Sept.92	Sept.92
	mg/l	*mg/l*	*mg/l*
Ca^{2+}	294	293	255
K^{+}	28.7	28.3	22.6
Li^{+}	1.28	1.25	0.98
Mg^{2+}	21.0	20.8	22.3
Na^{+}	306	303	249
Cl^{-}	274	273	219
HCO_3	483	487	480
SO_4^{2-}	755	740	604
NO_3^{-}	0.0	0.0	0.0
Σ	2140	2145	1850
SiO_2	110.4	109.1	95.4

Gas analyses		
Well, 8		
25. Aug. 1991		
	mg/kg	*Vol%*
H_2	n.d.	0
He	nd.	0
CH_4	3.0	1.1
C_2H_6	-	-
N_2	87.3	18.7
O_2	0.03	0.01
Ar	2.00	0.3
H_2S	n.d.	0
CO_2	590	79.9
Gas	374.0	*cm^3/kg*
CO_2	118	*g*

Isotope analyses				
		8	1	82
		Sep.92	*Sep.92*	*Sept92*
Isotope	*in*			
δ^2H ‰ *SMOW*	H_2O	-69.4	-68.3	-66.4
δ^{18}O ‰ *SMOW*	H_2O	-10.44	-10.17	-10.03
^{3}H *TU*	H_2O	< 1.0	< 1.0	2.7±0.7
δ^{34}S ‰ *CDT*	SO_4^{2-}	12.0	-	-
δ^{18}O ‰ *SMOW*	SO_4^{2-}	4.6	-	-
^{3}He *(ccSTP/g)*	He (g)	4.0E-12	4.0E-13	
^{4}He *(ccSTP/g)*	He (g)	1.2E-05	1.3E-06	
^{20}Ne *(ccSTP/g)*	Ne (g)	2.0E-07	2.1E-08	
δ^{13}C ‰ *PDB*	CO_2(g)	-4.2	-3.9	-
δ^{18}O ‰ *SMOW*	CO_2(g)	31.5	32.7	-

Appendix 3 Thermal water in the plain of Gemlik (and some cold karstic springs)

Name	No.	Coordinates	Altitude	Purpose	User
Gemlik Kaplıca	15	**6** 83 250/**44** 77 200	3m a.s.l.	Spa, drinking water	Gemlik Belediye
Gemlik North	18	**6** 84 250/**44** 78 450	7m a.s.l.	Irrigation	Gemlik Belediye
Gemlik- Ilıpınar	152	**6** 84 850/**44** 78 500	15m a.s.l.	Industrial use	Chemical industry
Cihatlı soguk su pn.	56	**6** 87200/**44** 79 220	138m a.s.l.	Drinking water / irrigatioon	Cihatlı köyü
Kumla soguk su pn.	218	**6** 82 600/**44** 83 850	220m a.s.l.	Drinking water	Kücük Kumla
Beşpınar	231	**6** 88 000/**44** 91 600	250m a.s.l.	Drinking water / irrigatioon	Kurtköy

Name	Description of spring site
Gemlik Kaplıca	The water of an artesian well (depth 37m, potential water level 1.7m above ground) is used for the public spa. Some thermalwater emerges naturally in the garden of the spa. Another well some 20m NW is sealed by concrete. The artesian water of two other wells about 100m to the west is used for car washing.
Gemlik north	Well (age and depth unknown) northeast of Gemlik. Between the pumping periods the water flows out by artesian pressure. In the surroundings high amounts of groundwater discharge into a drainage system
Gemlik Ilıpınar	This spring is collected at the bottom of the mountain slope east of Gemlik North. It flows out of the karstified marble unit. The water is transmitted by a pipline across the plain to a chemical industry south of Gemlik. The sampling was only possible by a hand pump from the drainage reservoir. A hand pump some 25m to the SW brings warm water out of alluvial deposits (No.151).
Cihatlı	The spring emerges from a ESE-WNW striking fault next to the creek east of the village Cihatlı.
Kumla	Karstic spring in the upper valley of Kücük Kumla. A part of the water is collected by several pipes.
Beşpınar	Karstic spring in the upper valley of Kurköy (8km south of Yalova).

Field measurements	**Date** Summer	**Date** Spring	**T** $_{Su}$ *°C*	**T** $_{Sp}$ *°C*	**EC** $_{Su}$ *µS/cm*	**EC** $_{Sp}$ *µS/cm*	**Q** $_{Su}$ *l/min*	**Q** $_{Sp}$ *l/min*	**pH**	**O**$_2$ *mg/l*	Alcalinity *mmol/l*	Acidity *mmol/l*
Gem-Kaplıca	3.9.92	7.4.93	36.9	36.8	415	415	200	200	7.3	5.5	3.8	0.4
Gem-north	26.8.91	6.4.93	25.4	25.0	370	405	~20	18	7.5	6.0	4.0	0.8
No.151	3.9.92	-	25.6	-	463	-	-	-	-	-	-	-
Gem- Ilıpınar	3.9.92	7.4.93	22.1	21.1	545	540	6000	-	7.4	7.5	4.9	0.7
Cihatlı	20.8.92	10.4.92	16.5	15.4	500	495	1200	4000	7.2	6.5	5.0	1.3
Kumla	29.9.92	17.4.93	13.2	12.8	370	345	4800	8000	6.3	6.4	3.9	6.4
Beşpınar	-	13.4.93	-	10.3	-	241	-	2000	-	-	-	-

Chemical analyses			
No.	15	18	152
Date	Sept.92	Sept.91	Sept.92
	mg/l	*mg/l*	*mg/l*
Ca^{2+}	55.7	63.3	80.4
K^+	1.1	1.5	1.1
Li^+	<0.1	< 0.1	<0.1
Mg^{2+}	14.3	16.0	17.7
Na^+	11.7	9.8	17.3
Cl^-	17.2	11.9	19.3
HCO_3	239	239	311
SO_4^{2-}	10.1	10.9	17.8
NO_3^-	0.8	1.4	6.6
Σ	350	360	480
SiO_2	17.4	15.6	16.5

Gas analyses		
Kaplıca, 15		
25. Aug. 1991		
	mg/kg	*Vol%*
H_2	n.d.	0
He	nd.	0
CH_4	n.d.	0
C_2H_6	-	-
N_2	20.3	57.6
O_2	5.0	12.5
Ar	0.68	1.4
H_2S	n.d.	0
CO_2	17.6	28.6
Gas	28.2	*cm^3/kg*
Water	174	*g*

Isotope analyses				
		15 *Sep.92*	151 *Sep.92*	152 *Sept92*
Isotope	*in*			
δ^2H ‰ *SMOW*	H_2O	-63.4	-63.8	-60.6
δ^{18}O ‰ *SMOW*	H_2O	-10.21	-9.7	-9.44
^{3}H *TU*	H_2O	4.7±0.7	6.8±0.7	11.3±0.9
δ^{34}S ‰ *CDT*	SO_4^{2-}	-5.2	-	-
δ^{18}O ‰ *SMOW*	SO_4^{2-}	5.9	-	-
^{3}He *(ccSTP/g)*	He (g)	1.5E-13	-	
^{4}He *(ccSTP/g)*	He (g)	3.7E-07	-	
^{20}Ne *(ccSTP/g)*	Ne (g)	2.3E-07	-	
δ^{13}C ‰ *PDB*	CO_2(g)	-17.6	-	-
δ^{18}O ‰ *SMOW*	CO_2(g)	30.6	-	-

Appendix 4 Sub-thermal springs in the plain of Orhangazi and cold karstic springs

Name	No.	Coordinates	Altitude	Purpose	User
Orh- Ilıpınar main spring	223	**6** 96 500/**44** 82 450	100m a.s.l.	Irrigation	Belediye Orhangazi
Orh Ilıpınar upper spring	202	**6** 96 480/**44** 82 470	101m a.s.l.	Irrigation	Belediye Orhangazi
Shallow groundwater	222	**6** 96 470/**44** 82 480	101m a.s.l.	Irrigation	-
Karsak pınar başı	17	**6** 91 050/**44** 78 500	100m a.s.l.	Consumption / irrigation	Restaurant
Nadır pınar	200	**6** 93 850/**44** 87 450	190m a.s.l.	Consumption / irrigation	Belediye Orhangazi
Gedelek pinar başı	199	**6** 91 750/**44** 80 600	180m a.s.l.	Irrigation	Gedelek köyü

Name	Description of spring site
Orh-Ilıpınar	The artificial pool of the spring ilipinar is situated SE of Orhangazi. The main spring (No.223) emerges from the the sandy bottom of the pool. A smaller spring (No.202) is situated about 50cm higher than the water level of the pool at the northwestern margin. Cold groundwater discharges in spring time from the slope above 222.
Karsak	Two springs are collected for a restaurant next to the highway north of the Karsak gorge.
Gedelek	This karstic spring flows out of marbles at the northern edge of the village of Gedelek.
Nadır	The river Nadır suyu originates from this huge karstic spring north of Orhangazi. The water emerges from the bottom of a marble slope. It is used for the water supply of the city of Orhangazi.

Field measurements	**Date** Summer	**Date** Spring	**T_{Su}** *°C*	**T_{Sp}** *°C*	**EC_{Su}** *µS/cm*	**EC_{Sp}** *µS/cm*	**Q_{Su}** *l/min*	**Q_{Sp}** *l/min*	**pH**	**O_2** *mg/l*	Alcalinity *mmol/l*	Acidity *mmol/l*
Ilıpınar (223)	5.9.93	5.3.93	22.9	20.2	530	560	4500	14000	7.1	6.8	5.4	1.0
Ilıpınar (202)	24.9.92	5.3.93	17.2	17.0	630	655	~100	~100	7.0	6.8	6.0	3.1
Ilıpınar (222)	-	7.4.93	-	15.4	-	895	-	6	-	6.8	6.7	1.2
Karsak	5.9.93	10.4.92	17.5	17.1	595	675	35	~100	7.0	6.5	5.7	1.1
Gedelek	24.9.92	6.4.93	14.8	14.4	460	465	4500	12000	6.8	8.2	4.9	1.3
Nadır	24.9.92	5.3.93	13.4	12.9	380	375	~3000	~20000	6.4	8.9	4.0	1.0

Chemical analyses			
No. Date	223 Sept.92	202 Sept.91	199 Sept.92
	mg/l	*mg/l*	*mg/l*
Ca^{2+}	107	131	95.5
K^+	1.5	0.9	0.4
Li^+	<0.1	< 0.1	<0.1
Mg^{2+}	8.4	4.6	4.7
Na^+	7.8	7.9	3.0
Cl^-	9.6	12.9	3.9
HCO_3	317	376	299
SO_4^{2-}	10.2	14.5	5.8
NO_3^-	10.2	15.6	3.5
Σ	475	570	420
SiO_2	10.7	9.2	8.6

Gas analyses		
Orhangazi ılıpınar, 223 *25. Aug. 1991*		
	mg/kg	*Vol%*
H_2	-	0
He	-	0
CH_4	-	0
C_2H_6	-	-
N_2	-	80.6
O_2	-	15.2
Ar	-	1.1
H_2S	-	0
CO_2	1.0-	3.4
Gas	-	*cm^3/kg*
Water	-	*g*

Isotope analyses				
		223 *Apr.93*	202 *Apr.93*	199 *Sep.92*
Isotope	*in*			
δ^2H ‰ *SMOW*	H_2O	-60.1	-59.2	-64.5
$\delta^{18}O$ ‰ *SMOW*	H_2O	-9.47	-9.28	-9.92
^3H *TU*	H_2O	8.1±0.7	16.3±1.2	17.1±1.3
$\delta^{34}S$ ‰ *CDT*	SO_4^{2-}	-	-	-
$\delta^{18}O$ ‰ *SMOW*	SO_4^{2-}	-	-	-
^3He *(ccSTP/g)*	He (g)	1.4E-12	-	7.5E-14
^4He *(ccSTP/g)*	He (g)	2.2E-06	-	4.9E-08
^{20}Ne *(ccSTP/g)*	Ne (g)	1.9E-06	-	1.8E-07
$\delta^{13}C$ ‰ *PDB*	CO_2(g)	-19.1	-	-
$\delta^{18}O$ ‰ *SMOW*	CO_2(g)	22.5	-	-

Appendix 5 Keramet ılıca (warm spring) & Soğucak acı su (bitter water)

Name	No.	Coordinates	Altitude	Purpose	User
Keramet Ilıca	211	**7** 09 950/**44** 86 100	120m a.s.l.	Bathing/irrigation	Keramet Belediye
Soğucak acı su	40	**6** 92 700/**44** 96 350	160m a.s.l.	Irrigation	-

Name	Description of spring site
Keramet Ilıca	The spring flows out of a travertine complex which lies on top of Neogene sediments. Swimming in the artificial pool of the spring is very popular for the local people. The main spring flows out from the sandy ground at the southeastern part of the pool.
Soğucak acı su	A drainage system collects the water from a SE-NW striking fault zone at the southwestern part of the travertine plateau of Soğucak. The samples have been collected some 15m away from the main spring. Because of its high mineralisation the water can not be used as drinking water (acı su = bitter water).

Field measurements	Date Summer	Date Spring	T_{Su} °C	T_{Sp} °C	EC_{Su} µS/cm	EC_{Sp} µS/cm	Q_{Su} l/min	Q_{Sp} l/min	pH	O_2 mg/l	Alcalinity mmol/l	Acidity mmol/l
Keramet	26.9.92	14.4.93	31.7	31.2	890	880	4600	4500	6.8	2.6	9.5	5.8
Soğucak	5.9.93	5.3.93	20.3	20.2	925	915	180	800	6.4	4.6	10.2	5.6

Chemical analyses

No. Date	211 Sept.93	40 Sept.92	41 Sept.91
	mg/l	*mg/l*	*mg/l*
Ca^{2+}	128	173	78
K^{+}	2.9	1.6	1.1
Li^{+}	<0.1	< 0.1	<0.1
Mg^{2+}	31.6	26.1	1.5
Na^{+}	28.9	6.7	3.2
Cl^{-}	25.4	5.5	8.1
HCO_3	580	638	232
SO_4^{2-}	52.9	16.1	4.4
NO_3^{-}	0.7	0.0	2.6
Σ	860	880	230
SiO_2	20.6	10.1	9.0

Gas analyses

Keramet ılıca, 211
2. Sept. 1993

	mg/kg	*Vol%*
H_2	-	0
He	-	0
CH_4	-	0
C_2H_6	-	-
N_2	-	78.8
O_2	-	19.0
Ar	-	0.9
H_2S	-	-
CO_2	-	1.4
Gas	-	*cm^3/kg*
Water	-	*g*

Isotope analyses

		211 *Sep.92*	40 *Sep.92*	
Isotope	*in*			
δ^2H ‰ *SMOW*	H_2O	-67.2	-58.2	
$\delta^{18}O$ ‰ *SMOW*	H_2O	-9.95	-9.43	
^3H *TU*	H_2O	3.7±0.7	10.7±0.9	
$\delta^{34}S$ ‰ *CDT*	SO_4^{2-}	-	-5.2	-
$\delta^{18}O$ ‰ *SMOW*	SO_4^{2-}	-	-5.9	-
^3He *(ccSTP/g)*	He (g)	-	-	-
^4He *(ccSTP/g)*	He (g)	-	-	-
^{20}Ne *(ccSTP/g)*	Ne (g)	-	-	-
$\delta^{13}C$ ‰ *PDB*	CO_2(g)	-19.1	-	-
$\delta^{18}O$ ‰ *SMOW*	CO_2(g)	22.5	-	-

Appendix 6 Mineral water of Adlıye

Name	No.	Coordinates	Altitude	Purpose	User
Adlıye köy acı suyu	208	**6** 87 550/**44** 72 350	260m a.s.l.	-	-

Name	Description of spring site
Adlıye acı su	The spring emerges from a fault zone on the northern side of the small creek (*acı su deresi*). The rocks around the spring are covered by salt minerals.

Field measurements	Date Summer	Date Spring	T_{Su} °C	T_{Sp} °C	EC_{Su} µS/cm	EC_{Sp} µS/cm	Q_{Su} l/min	Q_{Sp} l/min	pH	O_2 mg/l	Alcalinity mmol/l	Acidity mmol/l
Adl.- acı su	25.9.92		15.3		1650		3		6.4	1.0	4.3	1.0

Chemical analyses		
No.	208	Marmara Sea*
Date	Sept.92	Sept.93
	mg/l	*mg/ll*
Ca^{2+}	1120	294
K^{+}	65	312
Li^{+}	0.25	0.09
Mg^{2+}	173	838
Na^{+}	19400	6960
Cl^{-}	27750	12530
HCO_3	384	207
SO_4^{2-}	4190	2630
NO_3^{-}	-	–
Σ	53000	24000
SiO_2	22.7	–

Gas analyses		
-		
-		
	mg/kg	*Vol%*
H_2	-	-
He	-	-
CH_2	-	-
C_2H_6	-	-
N_2	-	-
O_2	-	-
Ar	-	-
H_2S	-	-
CO_2	-	-
Gas	-	*cm^3/kg*
Water	-	*g*

Isotope analyses				
		208 *Sep.92*	Gypsum *Sep.92*	
Isotope	*in*			
δ^2H ‰ *SMOW*	H_2O	-70.2		
δ^{18}O ‰ *SMOW*	H_2O	-10.56		
^{3}H *TU*	H_2O	4.1±0.7		
δ^{34}S ‰ *CDT*	SO_4^{2-}	25.7	21.7	-
δ^{18}O ‰ *SMOW*	SO_4^{2-}	14.5	16.3	-
^{3}He *(ccSTP/g)*	He (g)	-	-	-
^{4}He *(ccSTP/g)*	He (g)	-	-	-
^{20}Ne *(ccSTP/g)*	Ne (g)	-	-	-
δ^{13}C ‰ *PDB*	CO_2(g)	-	-	-
δ^{18}O ‰ *SMOW*	CO_2(g)	-	-	-

Environmental isotope study and 2-D-modelling of cold and thermal karst within the Gemlik (Bursa) area of Northwestern Turkey

THOMAS EISENLOHR, MARTIN PFISTER AND WERNER BALDERER

Abstract

In the Gemlik-Orhangazi area (Armutlu peninsula, NW Turkey) cold and thermal karstic springs with discharges between 2 and 160l/sec have been studied by field measurements, chemical and isotope analyses and 2-D-numerical modelling. The aquifer rock of all springs is strongly karstified marble unit, which has a very high hydraulic conductivity compared to the low permeable country rock below and above. According to their temperature the springs can be divided into the following groups: cold springs (<17°C), sub-thermal springs (17-25°C) and thermal springs (>25°C). Chemically all springs can be belong to the $\underline{Ca}Mg\underline{HCO_3}$ type. Their infiltration area can be located in the mountain area north of Gemlik. By means of stable isotope analyses an estimation of the mean infiltration altitudes was possible. After infiltrating, the water flows in karstic systems of the marble unit dissolving calcite and dolomite. Chemical and isotope investigations indicate mixing processes between cold, fast circulating karstic water and hot, stagnant karstic water in the lower parts of the karstic system. This conceptual model has been verified by 2-D-quantitative numerical models. The calculation of the two independent parameters 'temperature' and 'tritium' allowed to verify physical parameters such as 'hydraulic conductivity'. A successful distinction between cold, sub-thermal and thermal waters could be achieved regarding the temperature as well as the tritium content of all the springs.

Introduction

The main goal of the interdisciplinary MARMARA Poly-Project of the ETH Zurich (Switzerland) is the investigation of the relationship between deep groundwater circulation, active crustal movements, seismicity and heat flow in the Marmara region (Northwestern Turkey) (Schindler 1993). Hydrogeological investigations have been focused on six limited areas with high geothermal activity (Bergama (Jeckelmann 1996), Tuzla (Mützenberg 1991 and this volume), Gönen (Yalçın this volume), Bursa (Imbach 1992 and this volume), Armutlu (Eisenlohr 1995 and this volume) and Kuzuluk (Greber 1992 and this volume). By geological mapping, field measurements, chemical and isotope analyses conceptual models of the deep groundwater flow have been evaluated. In Gemlik (Armutlu peninsula) the conceptual model has been verified by 2-D-quantitative numerical models (Pfister 1995, Pfister et al. this volume).

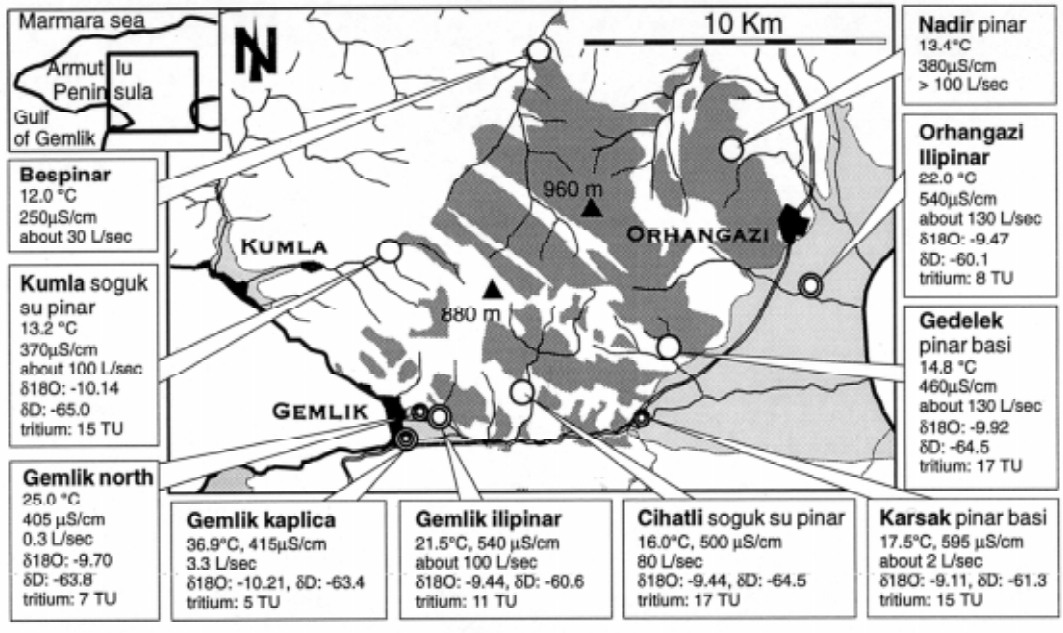


Figure 1: Geographic situation and data set (mean values of temperature, electrical conductivity, discharge, stable isotope (‰ SMOW) and tritium) of the investigated springs in the Gemlik-Orhangazi area. Marble outcrops are characterised by dark shaded areas.

Geological and hydrogeological investigations

Gemlik is situated between İstanbul and Bursa, in the southeastern part of the Armutlu peninsula (Fig. 1). The peninsula is a horst-zone between two branches of the North Anatolian Fault Zone (NAFZ). The mountains north of Gemlik consist of a metamorphic sequence which is cut by younger volcanic dikes and faults. The metamorphics consist of greenschists at the bottom, a marble unit, which is up to 100m thick, and flysch sediments (slates and sandstones) on the top (Fig. 2). Due to tectonic deformation the schists dip on each side of the mountains parallel to the slope down to the surrounding plains.

Seven karstic springs with discharges between 2 and 160l/sec have been investigated in the mountain area north of Gemlik (Fig. 1). All of them originate from the marble plate where it disappears below impermeable rocks. Due to the topographic potential the infiltration area of the karstic springs can be located in the the central part of the Gemlik mountains. In the alluvial plain of Orhangazi the spring *Orhangazi İlıpınar* (= warm spring) flows out at the bottom of a shallow pond. In shallow wells in the Gemlik-plain artesian groundwater rises to the surface (*Gemlik kaplıca* (= spa) and *Gemlik north*). The plains of Orhangazi and Gemlik border in the east, in the south and in the west to areas with completely different, high mineralised waters: lake of İznik (Eisenlohr 1995), mineral water of Adliye köy (Eisenlohr 1995) and Marmara sea. Therefore the infiltration area of the springs *Orhangazi İlıpınar*, *Gemlik north* and *Gemlik kaplıca* is most probably located in the Gemlik mountains as well.

The springs *Kumla, Beşpınar, Nadır, Gedelek* and *Cihatlı* yield temperatures between 12° and 16°C which is typical for karstic springs in Northwestern Turkey. Since the mean annual temperature is around 15°C in this area, the springs *Karsak* (17°C), *Gemlik İlıpınar* (21°C), *Orhangazi İlıpınar* (22°C), *Gemlik north* (25°C) and specially *Gemlik kaplıca* (37°C) show a

clear thermal influence. Based on the temperature the springs can be divided into the following groups: cold springs (<17°C), sub-thermal springs (17-25°C) and thermal springs (>25°C). The electrical conductivity of all springs is between 250 and 650µS/cm. The water of *Gemlik kaplıca* (electrical conductivity: 410µS/cm) is one of the lowest mineralised thermal water throughout Northwestern Turkey.

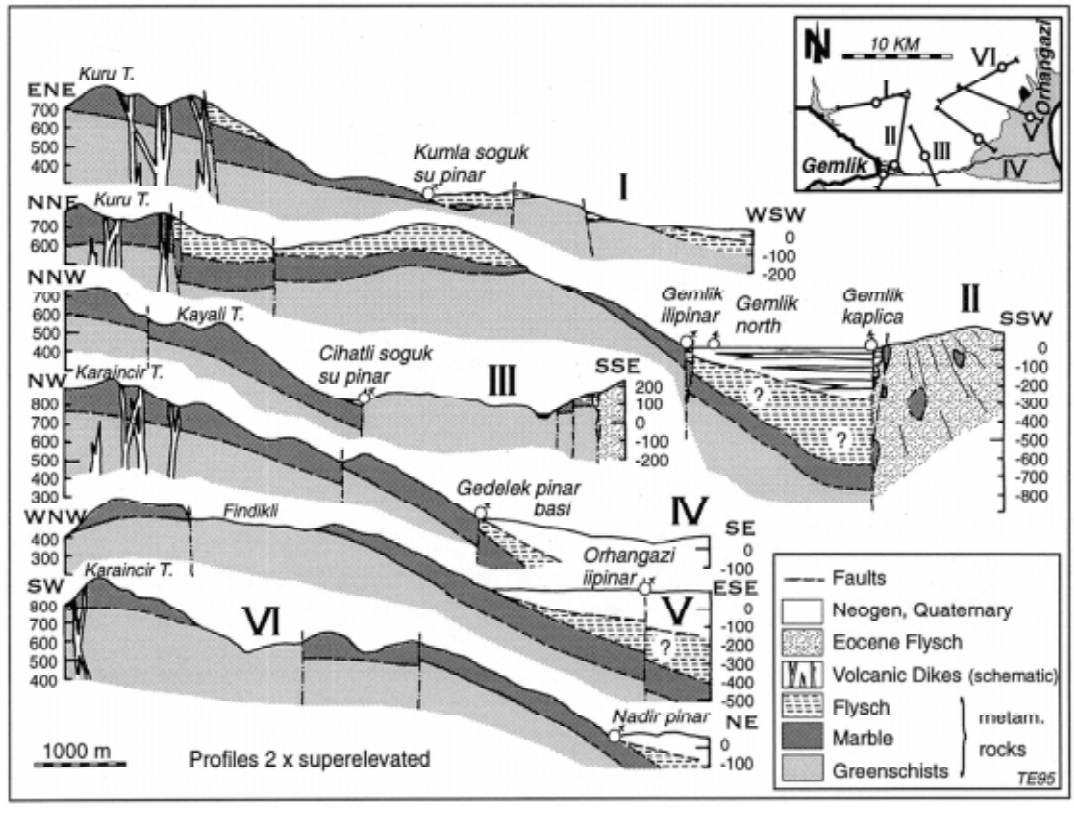


Figure 2: *Geological cross sections of the Gemlik-Orhangazi area. The orientation of the profiles (height scale doubled) is more or less parallel to the dipping direction of the schists.*

The discharge of *Gemlik kaplıca* is rather constant during the year. The discharge of the cold and subthermal springs, on the other hand, is between 2 and 6 times larger in April than in September. Nevertheless all springs have seasonal variations in temperature smaller than 1°C and variations in electrical conductivity smaller 30µS/cm. This behaviour can be explained by a pressure impulse caused by the intensive infiltration during winter months. A pressure impulse in a connected hydraulic system reaches the spring site much faster than the water itself.

The water of all the springs contains between 5 and 9mg/l dissolved oxygen (field titration). Water/gas samples (in evacuated glass bottles) from *Gemlik kaplıca*, *Gemlik north* and *Orhangazi İlıpınar* contained even between 7 and 15% oxygen which is typical for karstic springs (Eisenlohr 1995). In thermal springs usually contain no oxygen is observed. The gas composition of *Orhangazi İlıpınar* shows more or less the composition of air (70% air composition). The samples from *Gemlik kaplıca* and *Gemlik north* have a slight surplus of CO_2 (60 resp. 35% air composition). The surplus may be caused by CO_2 gas which rises up along tectonic faults. The spa of Gemlik is situated directly on a main branch of the NAFZ. A NS-orientated profile of soilgas measurements carried out some 100m east of the spa in 1992 showed a significant CO_2 peak on the expected fault line (Eisenlohr 1995). The amount of CO_2 gas in the soilgas rose from normal values of about 1% up to 16%. Nevertheless the content of dis-

solved CO_2 (negative p-value) measured directly in the thermal water (0.4-0.8mmol/l) is even slightly lower than in cold springs (0.7-1.5mmol/l). Compared to other thermal springs in Northwestern Turkey (Balderer et al. 1992, Greber 1992, Eisenlohr 1995) the thermal water of Gemlik seems to be little affected by uprising CO_2 gas.

The chemical composition of all the springs is similar and typical for karstic springs (Fig. 3). The waters can be classified as $\underline{Ca}Mg\underline{HCO_3}$ type. The balance of the most dominant ions Σ (Ca^{2+}, Mg^{2+}) and HCO_3^- indicates the dissolution of calcite and secondary dolomite. The sub-thermal and thermal springs show a little enrichment in Mg^{2+}, Na^+, Cl^- and SO_4^{2-} (Fig. 3), which may be caused by water-rock interaction. Compared to other thermal springs of the Marmara region (Balderer et al. 1992, Greber 1992, Eisenlohr 1995) this effect is almost negligible. A slight increase of Nitrate (NO_3^{2-}) in *Orhangazi İlıpınar* (9mg/l), *Gemlik İlıpınar* (7mg/l), *Cihatlı* (7mg/l) and *Karsak* (6mg/l) is most probably due to modern agriculture. Therefore local mixing with shallow groundwater can be assumed for these springs. Other chemical parameters and the isotopic composition confirm this assumption.

Gemlik kaplıca, *Gemlik north* and *Gemlik İlıpınar* have significant higher Mg^{2+} and lower Ca^{2+} contents compared to the other springs (Fig. 3). In the marbles of the Gemlik area dolomitic lenses occur. The significant change in the ionic proportion of Mg^{2+} and Ca^{2+} may be caused by dissolution of dolomite, thus confirming the assumption of a common reservoir rock for the sub-thermal and thermal springs of Gemlik. The chemical composition of *Gemlik north* and *Gemlik kaplıca* is almost identical. *Gemlik İlıpınar* differs slightly from the two others. The unconsolidated rocks of the plain consist mainly of well laminated gravels and clays (neogene, pliocene and quaternary). Up to 30m thick layers of impermeable clay prevent a vertical groundwater flow. Only at places where the layering is interrupted uprising thermal water can reach the surface. A fracturing of all sediments takes obviously place along the active fault zone at *Gemlik kaplıca*. *Gemlik north* is situated on a marginal alluvial fan. A lateral change in sedimentation by the coarse and highly permeable sediments of the alluvial fan can be expected in this area. The water of the spring *Gemlik İlıpınar,* on the contrary, flows directly out of the marble unit.

Stable isotope values (δD, $\delta\,^{18}O$) of all the springs align on a local meteoric waterline (MWL) defined as $\delta D = 8 * \delta\,^{18}O + 15$ (Eisenlohr et al. this volume). Therefore it can be assumed that the cold and thermal waters are part of the recent water cycle. With isotope analyses of samples from cold superficial springs (5-20l/min) it was possible to evaluate a correlation between altitude and deuterium for the investigation area (Fig. 4). This correlation allows a rough estimate of the mean infiltration altitudes. The mean infiltration altitude of the cold springs can be estimated between 800 and 1000m a.s.l. and the one of the Gemlik thermal water between 600 and 900m a.s.l. *Orhangazi İlıpınar* and *Karsak* infiltrate in lower altitudes. The evaluated altitudes of recharge are rather well in accordance with the estimates derived from geological observations like marble outcrops and sink holes.

The cold karstic and superficial springs are characterised by tritium contents between 14 and 18TU (1992). With increasing temperature the tritium contents decrease in sub-thermal and thermal springs. The lowest tritium concentration of 5TU was measured in *Gemlik kaplıca*. There are two different ways to explain this depletion. On the one hand it may represent a proper decay age which would indicate a mean residence time of about 30-40 years for *Gemlik kaplıca*. The modelling described in the next chapters of this paper showed clearly that this time is too short for the heat exchange. On the other hand the depletion may be caused by the mixing of cold karstic water with a water which contains no or only very little tritium. The chemical analyses indicate that highly mineralised deep groundwater and surface water can be excluded as a main mixing endmember. Therefore a mixture between cold karstic water (12°-15°C, 250-450µS/cm) and hot, stagnant karstic water (40°-50°C, 300-400µ S/cm) is proposed.

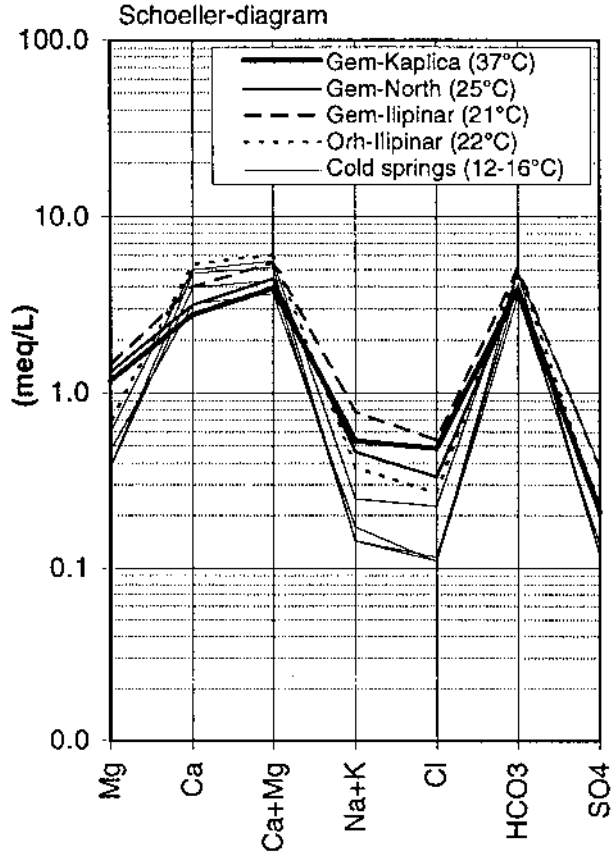


Figure 3: *Schoeller diagram (logarithmic plot of the concentration of the main ions) of the springs in the Gemlik-Orhangazi area.*

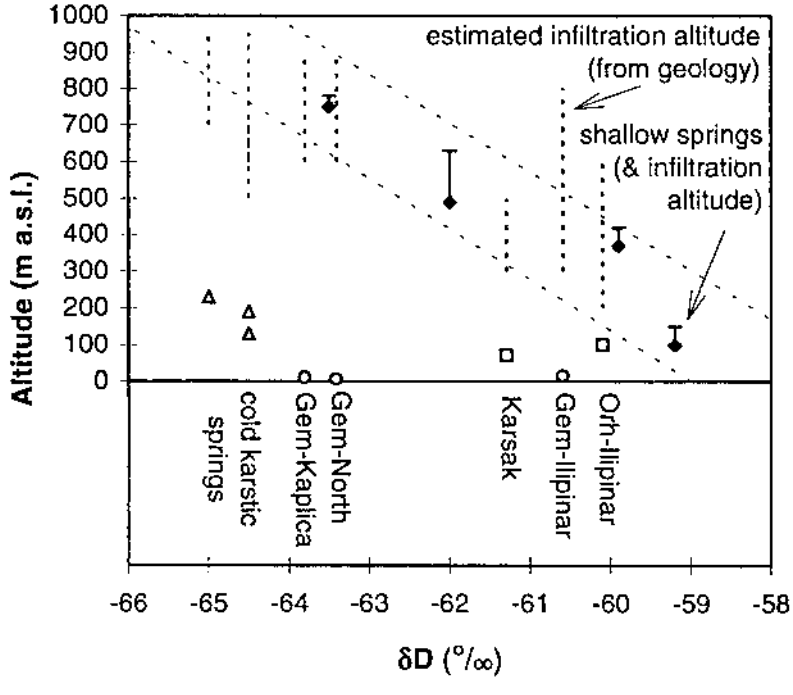


Figure 4: *Deuterium-altitude plot of karstic springs and shallow groundwaters. The local deuterium-altitude correlation allows an estimation of the mean infiltration altitude of cold and thermal karstic springs.*

Conceptual model of groundwater flow

The water of the cold, sub-thermal and thermal springs infiltrates into the mountain region north of Gemlik. The water flows in karstic systems of the marble unit dissolving calcite and dolomite. The temperature of the springs is controlled by the position of the marble unit in the underground. If the marble unit follows the surface, spring temperatures between 12° and 16°C result. Underneath the plains of Orhangazı and Gemlik the marbles are covered with thick layers of mostly impermeable rocks. In the karstic system mixing processes between cold, fast circulating karstic water and hot, stagnant karstic water takes place. The input of highly mineralised water and CO_2 gas into the karstic system has to be minimal. From the karstic system the heated water follows the fault zones to the surface. In the unconsolidated, sedimentary filling of Gemlik plain the water flows into permeable gravels layers from where it can reach the surface only through interruptions of the layering (fault zone, alluvial fan). At *Gemlik İlıpınar*, *Orhangazi İlıpınar*, *Karsak* and *Cihatlı* local mixing with shallow groundwater occurs.

Two-dimensional-quantitative numerical model

The hydrogeological conceptual flow model has been verified by quantitative model simulations. The numerical FE- (Finite Element) tool FRACTure (Kohl et al. 1993) allows fully coupled calculations of heat- and water-transport in saturated underground. The program code of FRACTure was changed with minor revisions to calculate transient tritium transport (Pfister 1995). The main physical transport mechanism of tritium is ground water movement. Further processes like radioactive decay, hydraulic dispersion effects and tritium boundary conditions (input by precipitation (IAEA 1981, 1983, 1990)) have been taken into account. The following differential equation describes the physical model of the transient tritium transport:

$$\frac{\partial H}{\partial t} = -v_f \nabla H + \nabla(D^* \nabla H) + \nabla\left(a_{ijkl} \frac{v_k - v_l}{\sqrt{v_k^2 - v_l^2}} \nabla H\right) - Z \cdot H + f$$

where:

H: tritium concentration [TU]
t: time [s]
v_f: particle velocity [m/s]
D^*: diffusion coefficient [m^2/s]
a_{ijkl}: dispersion components [m]
v_k, v_l: components of water velocity [m/s]
Z: decay constant [1/s]
f: boundary conditions (input by precipitation) [TU]

Geological profiles (Fig. 2) along the supposed flow pathes of the different springs were transformed into numerical grid-shape. 2D-elements (non-karstified marbles, greenschists, flysch) were combined with 1D-elements (karstic channels and faults). The representative elementary volume (REV) had a mean size of 50 to 100m. The karstic channels and faults are characterised by high hydraulic conductivity ($2.0*10^{-6}$m/s resp. $2.0*10^{-5}$m/s) in contrary to the surrounding marbles ($1.0*10^{-9}$m/s) and the units of very low permeability defined as ”country rock” (greenschists and flysch: $5.0*10^{-11}$m/s).

Based on heat flow investigations (Pfister et al. this volume) the bottom thermal boundary condition was set to 55mW/m^2. The surface thermal boundary condition was set to 4°C/km according to the regional atmospheric thermal gradient (Pfister 1995). Infiltration of rain water into the underground was defined according to the hydrogeological estimates to 15% of local precipitation on high permeable karstified marbles and 1.5% of local precipitation on low permeable "country rock".

The simulations for six different springs resulted in a comparison of measured and calculated temperature and tritium concentration for the year 1992 presented in Table 1. Mean temperature and mean tritium content have been calculated by using the same model parameters. A successful distinction between cold, sub-thermal and thermal waters could be achieved with respect to the temperature as well as to the tritium content of all the springs. The bigger differences in tritium contents between model results and measurements of the springs Gedelek and Cihatlı disappear by small changes in hydraulic conductivity.

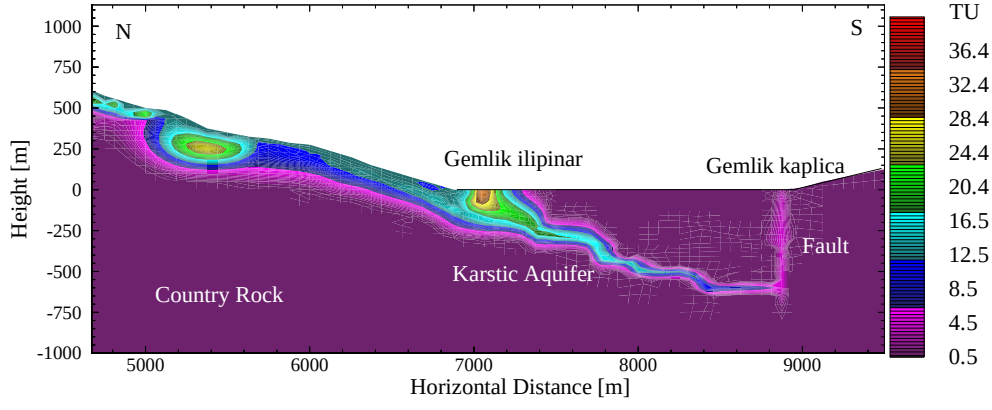


Figure 5: *Tritium distribution in the underground in 1992: model result for thermal springs Gemlik kaplıca and Gemlik İlıpınar. The tritium containing ground water is bound to karstified formations and their vicinity as well as to the fault zone.*

Spring	measured temperature, [°C]	modelled temperature, [°C]	measured tritium concentration, [TU]	modelled tritium concentration, [TU]
Gemlik kaplıca	36.9	33.0	4.7	3.7
Gemlik İlıpınar	21.5	20.7	11.3	11.3
Orhangazi İlıpınar	22.0	20.9	8.1	9.7
Cihatlı	16.0	16.9	17.2	26.0
Gedelek	14.8	15.8	17.1	23.6
Nadır	13.4	13.4	-	-

Table 1: *Measured and modelled temperature and tritium concentration of different springs in Gemlik-Orhangazi-region.*

Figure 5 shows the tritium distribution in the underground in the year 1992 of a selected cross section (Fig. 2). The tritium containing groundwater is strongly bound to the karst lithology and the fault zone. High water velocities in the range of 10^{-4}m/s result. The thermal water at *Gemlik kaplıca* and the sub-thermal water of *Gemlik İlıpınar* can be explained by a mixture of fast circulating karstic water with stagnant karstic water, rising at fault zones.

The time-dependent tritium contents of three typical springs were calculated (Fig. 6). The distribution of the anthropogenic tritium component is different: *Gemlik İlıpınar* shows rapid in-

crease in tritium concentration almost simoultaneous with the atmospheric input (boundary condition) due to circulation paths near the surface. This spring is strongly influenced by mixing phenomena with near-surface water which is also proposed by hydrochemical results. The spring *Gedelek* is characterised by a smoothed and retarded tritium signal which can be explained as a mainly radioactive decay signal and as a minimal mixture with shallow ground water. The thermal spa of *Gemlik kaplıca* shows only a weak tritium signal which results from a mixture of fast circulating water (high tritium contents) and stagnant, hot karstic water (very low tritium contents). A mixture with surface water which would be an additional tritium source can be excluded by the hydrochemical investigations.

Both the high water velocities in the karstic system compared to the normal ground water velocities of the country rock and the appearance of fracture zones are mainly responsible for this special situation of groundwater circulation. The results of the hydrogeologic investigations were nicely confirmed by these quantitative calculations.

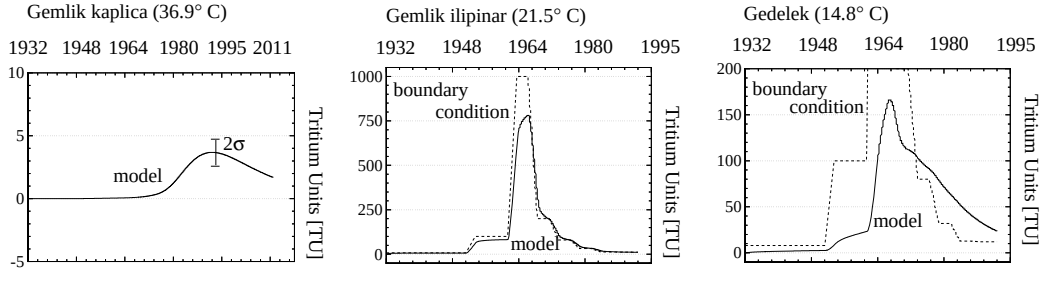


Figure 6: *Time dependent tritium concentration of three different springs. The hatched line represents the atmospheric boundary condition: tritium content of precipitation. Interpretation see text.*

Conclusions

Stable isotopes and tritium are very good parameters to obtain information about infiltration, flow paths and the residence time of groundwater. It was thus possible to characterise the different circulation patterns of the thermal springs. The calculation of the two independent parameters ‘temperature’ and ‘tritium’ allowed to verify the conceptual model and physical parameters such as ‘hydraulic conductivity’. The tritium signal in *Gemlik kaplıca* needs a certain amount of fast circulating ground water. It was necessary to introduce 1D-elements (karstic channel and fault zone) to simulate such high flow velocities. This seems to confirm the existence of open karstic channels even several hundred meters below sea level underneath the plain of Gemlik.

References

Balderer, W., Greber, E., Imbach, Th., Rauert, W., Trimborn, P. and Güler, S., 1992, Environmental Isotope Study of Thermal, Mineral and Normal Groundwater within the Bursa and Kuzuluk/Adapazari Areas in Northwestern Turkey, In: Isotope Techniques in Water Resources Development 1991, Proc. of a Symp., Vienna, 11-15 March 1991, IAEA Vienna, 720 – 724.

Eisenlohr, T., 1995, Die Thermalwässer der Armutlu-Halbinsel (NW-Türkei) und deren Beziehung zu Geologie und aktiver Tektonik, Thesis No. 11340 ETH Zürich, Switzerland, 165pp.

Eisenlohr, Th., this volume, The thermal springs of the Armutlu peninsula (NW Turkey) and their relationship to geology and tectonic.

Eisenlohr, T., Jeckelmann, J., Balderer, W., Bernasconi, S., Rauert, W. and Trimborn, P., this volume, Regional investigations of cold groundwater for determination of the recharge conditions in geothermal areas of Northwestern Turkey.

Greber, E., 1992, Das Geothermalfeld von Kuzuluk/Adapazarı (NW-Türkei), Geologie, aktive Tektonik, Hydrogeologie, Hydrochemie, Gase und Isotope, Diss. ETH Zürich, Nr. 9984, 213.

Greber, E., this volume, Deep circulation of CO_2-rich palaeowaters in a seismically active zone (Kuzuluk/Adapazarı, Northwestern Turkey).

IAEA, 1981, 1983, 1990, International Atomic Energy Agency, Technical reports series no. 206, 226, 311, Vienna, Austria.

Imbach, T., 1992, Thermalwässer von Bursa. Geologische und hydrogeologische Untersuchungen am Berg Uludag (NW-Türkei), Thesis No. 9988 ETH Zürich, Switzerland, 178pp.

Imbach, Th., this volume, Geology of Mount Uludağ with emphasis on the genesis of the Bursa thermal waters, Northwest Anatolia, Turkey.

Jeckelmann, Ch., 1996, Genese lokaler Thermalwasservorkommen in der Region Bergama/W-Türkei, Diss. ETH Zürich, Nr. 11990, 199p.

Kohl, Th., Hopkirk, R.J., Evans, K.F. and Rybach, L., 1993, FRACTure – a new tool to simulate coupled processes in geosciences, Proceedings for VIII. Intern. Conference on finite elements in fluids, Barcelona, 20. -24. Sept.

Mützenberg, St., 1991, Westliche Biga Halbinsel (Çanakkale, Türkei): Beziehung zwischen Geologie, Tektonik und Entwicklung der Thermalquellen, Mitteilungen aus dem geologischen Institut der Eidg. Technischen Hochschule und der Universität Zürich, Neue Folge, Nr. 287, 160p.

Mützenberg, St., this volume, Nature and origin of the thermal springs in the Tuzla area, Western Anatolia, Turkey.

Pfister, M., 1995, Geothermische Untersuchungen in der Region Marmara (NW-Türkei) – Kartierung des Wärmeflusses und hydrothermale Modellrechnungen, PhD-Thesis No. 11054 ETH Zürich, Switzerland, 231pp.

Pfister, M., Rybach, L. and Şimşek, Ş., this volume, Geothermal reconnaissance of the Marmara sea region.

Schindler, C., 1993, The MARMARA-Project: tectonics and recent crustal movements revealed by space-geodesy and their interaction with the circulation of groundwater, heat flow and seismicity in Northwestern Turkey, Terra Nova, 5, 164-173.

Yalçın, T., this volume, Hydrogeological investigation of the Gönen and Ekşidere thermal waters (NW Turkey).

Geology of Mount Uludağ with emphasis on the genesis of the Bursa thermal waters, Northwest Anatolia, Turkey

THOMAS IMBACH

Abstract

Faults related to the neotectonic stress regime of Northwestern Turkey permit the rise and outflow of thermal waters in two different districts in the city of Bursa. Based on their geographical, physical and chemical characterisation, two different circulation systems with maximal spring temperatures of 82°C (TDS=1207mg/l) and 46°C (TDS=504mg/l) can be distinguished. Isotopic data indicate different local recharge areas and residence times of at least 50 years. Water temperatures at depths are about 110°C and 50°C. Calcite dissolution and silicate hydrolysis are the dominant water-rock interactions. The dominant processes that affect both deep groundwater circulation systems are: mixing with shallow groundwater, loss of energy by heat conduction, and interaction with gases from the mantle, the crust and the atmosphere.

Introduction

This study is part of the interdisciplinary MARMARA Poly-Project realised by the Swiss Federal Institute of Technology (ETH) in Zürich (Schindler 1993). This project involves the study of tectonics, geology, hydrogeology, seismology, geodesy and geothermal prospects in the Marmara sea region. This paper focuses on deep groundwater circulation of thermal waters within a tectonically active area of high seismicity in and around Bursa. Every step of thermal water evolution from infiltration to outflow has been reconstructed, taking into account rock-water-gas interaction, gas exchange, heating, and mixing. Based on the resulting model, we discuss the protection of the Bursa thermal waters and improvement of their use.

The city of Bursa is situated to the south of the Marmara sea on the northern slope of the highest mountain in Western Turkey (Mount Uludağ, 2543m a.s.l.) on a large travertine complex. Thermal waters with temperatures up to 46°C and 82°C discharge within the two districts of Çekirge and Kükürtlü at the western end of Bursa just above the plain (100m a.s.l.) (Fig. 1). As with many other geothermal systems in Western Turkey, the circulation of the Bursa thermal waters is also closely related to a major fracture zone (Eisenlohr 1995, Greber 1992, Jeckelmann 1996, Mützenberg 1991).

Bursa was the first Ottoman capital (1326-1451), and has grown into one of the largest cities in Turkey, with a population of over 800,000. Once famous for the natural beauty of its environment, Bursa is today faced with environmental pollution caused by the expanding textile and automobile industry and the problem of its rapidly increasing population.

The semi-arid climate of Bursa is characterised by warm, dry summers and cold, wet winters. The mean annual temperature in Bursa is 14.4°C and the mean annual precipitation amounts to 710mm, with little snow during the winter time. The climate of Bursa is strongly influenced

by the high elevation of Mount Uludağ, with precipitation of about 1000-1600mm per year and a mean annual temperature of about 4.6°C at 1877m a.s.l (Gürer 1991). On Mount Uludağ, the Mediterranean vegetation of the plain changes to a deciduous forest, characteristic of semi-humid regions with increasing altitude. In the higher, more humid regions of Mount Uludağ, it is followed by mixed forest, humid coniferous forest, and Alpine vegetation at an altitude of more than 2000m a.s.l. (Rathjens 1952).

Geological setting

Introduction

As part of the Alpine-Himalayan orogenic belt, Turkey is a region of great tectonic complexity (Ketin 1966). Its geological and tectonic evolution has been dominated by the repeated opening and closing of the Paleozoic and Mesozoic oceans (Dewey and Şengör 1979, Jackson and McKenzie 1988, Şengör and Yılmaz 1981). Neotectonic activity and the lack of large-scale tectonic units make it very difficult to distinguish the effects of different orogenies within the study area.

It is generally proposed that most of the neotectonic activities in Anatolia were caused by the northerly movement of the Arabian plate towards Eurasia (McKenzie 1972). Due to this convergent zone in the east, crustal escape along major strike-slip faults, such as the North Anatolian Fault Zone (NAFZ), is observed. The high natural seismicity in the northwestern part of Turkey, and the existence of many hot water springs in this area, point to important active tectonic processes. The active fault segments of the western end of the NAFZ, and its transition into a complex system of restraining and releasing bends of strike-slip faults within and near the Marmara sea, are the dominant tectonic structures in the northwestern part of Turkey (Barka and Kadinsky-Cade 1988, Barka 1992).

The dominant tectonic structure of the Bursa area is the NAFZ's southern zone. Recent studies of the Poly-Project involving Global Positioning Systems (GPS) and measurements of the natural seismicity show that the strike-slip movements of the NAFZ, and its more extensional regime in the westernmost part, still affect the Bursa area (Straub 1996, Schindler 1993, Eyidoğan et al. 1991).

Stratigraphic units

Mount Uludağ consists mainly of high-grade regional metamorphic rocks, such as muscovite and biotite gneisses, garnet-bearing quartzites, muscovite-bearing calcite-marbles and amphibolites.

The highest peaks of Mount Uludağ consist mainly of muscovite-bearing calcite-marbles dipping to the south. North of the watershed dolomite-marbles with layers of kyanite-bearing tremolite-schists outcrop, dipping to the north. This structural and lithologic disconformity point to a sheared antiform as the main structure of Mount Uludağ. Structural analyses show that the fold axis of the antiform is folded and dips towards WNW. Within this high-grade metamorphic unit, a leucogranite of Oligocene age (Bingöl et al. 1982) outcrop and, close to the intrusion contact, clinozoisite and epidote (in metabasica), cordierite and fibrolithe (in metapelites), and grossularite, vesuvianite and epidote (in metacalcite) are observed.

Although the marbles of this high metamorphic unit show a strong recristallisation, one coral was found (6'73'900/44'47'850). This fossil proves at least a Post-Ordovician age. A Pre-Caledonian age, which has been postulated by Penck (1918) and Brinkmann (1966, 1968, 1971), can definitely be excluded.

Tectonic contacts separate the high-grade metamorphic rocks from rocks of low-grade metamorphism, such as micaschists, phyllites, calcite-marbles, epidote and glaucophane schists, serpentinites and greenschists.

East of Bursa, near the village of Kestel, the hills are covered by fusulinid-bearing limestone of Early Permian age. Under this fossiliferous limestone calcitic sandstones, basaltic layers, conglomerates and thick arcoses crop out. Because the basaltic layers contain blocks of limestone (no fossils have been observed) and because the stratigraphic contacts between the unmetamorphic sediments as well as the contact to the metamorphic basement is not clearly visible, it is difficult to separate those units strictly from each other and to characterise the whole section. The metamorphic basement consists here of muscovite schists and phyllites and contains dark marble blocks, too.

Although the age of one lithology, the Permian limestone, is well known, the age of the whole sequence is controversial. On the one hand, the Permian limestone is considered as a lithostratigraphic unit (Ketin 1947, Brinkmann 1966); on the other hand it is considered as sedimentary blocks of the Triadic Karakaya unit (Bingöl et al. 1975, Okay et al. 1991). Because there are no sedimentological evidences of the existence of Permian olistoliths in this area, the whole sequence is considered as a normal stratigraphic sequence of Late Palaeozoic age (Imbach 1992). The difficulties in correlating the Permian limestone in the field may be explained by neotectonic activity along some observed faults and not by sedimentological processes due to the Kimmerian orogeny.

Mesozoic sediments were not observed. In the western part of Mount Uludağ, sediments and vulcanites of Middle or Late Miocene age lie directly on low-grade metamorphic rocks. This Neogene unit consists of freshwater limestone, mica-bearing coloured sandstones and tuffites. The extension of these sediments is limited by tectonic contacts.

The Neogene sediments, which stay mostly in tectonic contact with the metamorphic rocks, can be interpreted as relicts of a late-Miocene basin structure. This structure extends in a northern direction under the plain of Bursa and is, as the hydrogeological investigation on Mount Uludağ shows, of great significance for hot and cold groundwater circulation (Imbach 1992 and in press).

At the northern border of Mount Uludağ, rock falls with volumes of up to $2\text{-}10*10^6 m^3$, large landslides, sags, alluvial fans and karstic springs accumulate the youngest sediments. Even moraines, which prove a former local glaciation to an altitude of about 1900m a.s.l., are observed north of the highest peaks of Mount Uludağ.

Paleotectonics

As mentioned at the beginning of this paper, strong neotectonic activities and the lack of large-scale tectonic units make it difficult to distinguish the effect of different orogenies within the study area. The new discussion of the evolution of the basement rocks began with the observation of Permian olistoliths in Western Turkey as part of a detritical series of Triassic age. Bingöl et al. (1975) called this lithostratigraphic unit the Karakaya formation. Due to the existence of this formation in Western Turkey, and due to the structural disconformity which separates this unit from the overlain Jurassic series, the Kimmerian orogeny was proposed in the

northern part of Anatolia (Şengör 1979a). Based on this new tectonic model, Şengör and Yılmaz (1981) interpreted the greenschist serie of the basement as sediments of the Karakaya marginal sea and defined the Karakaya complex as a new tectostratigraphic unit. As a result of this proposed model, most of the old studies were reinterpreted (Table 1). The postulated Kimmerian age of the metamorphic rocks on Mount Uludağ bases only on the definition of the proposed Karakaya complex and not on field observations. The only fossil which was found in the metamorphic rocks on Mount Uludağ proves a post-Ordovician age of the metamorphism (see this paper). Based on this fossil and based on the observed structural disconformity of pre-Permian age in the Kestel area a Hercynian orogeny has to be proposed.

Authors	Age of metamorphism							
	Amphibolite facies				Greenschist facies			
	Pre-C.	Caled.	Herc.	Kim.	Pre-C.	Caled.	Herc.	Kim.
PENCK 1918	x					(x)	x	
KETİN 1947							x	
VAN DER KAADEN 1959	(x)	x					x	
SCHULING 1959	(x)	x					x	
BRINKMANN 1966	x	(x)			(x)			
BRINKMANN 1968	x	(x)			x	(x)		
BRINKMANN 1971	x				x	(x)		
LISENBEE 1971						(x)	x	
VAN DER KAADEN 1971					(x)	x		
BINGÖL et al. 1975			..x				..x	
TEKELI 1981			(x)	x			(x)	x
KETİN 1984								x
GENÇ et al. 1986							..x	
DEMİRTASLI 1989								
KAYA et al. 1989								..x
YILMAZ 1990		x						x
OKAY et al. 1991				(x)				x
IMBACH 1992			..x				..x	

Pre-C: Pre-Caledonian; Caled: Caledonian; Herc: Hercynian; Kim: Kimmerian x = proposed ages;
(x) = expected ages; ..x = expected ages or older

Table 1: Ages of metamorphism on Mount Uludağ (Bursa, NW-Turkey) by different authors.

Neotectonics

Mount Uludağ is a zone of major tectonic uplift. A hiatus in metamorphism on Mount Uludağ, as well as the absence of unmetamorphic sediments in the central part, point to a considerable local elevation. To the North, the tectonic contact between the two metamorphic units runs mainly parallel to the marble layers of the northern limb of Mount Uludağ. Close to the tectonic contact, the marble layers of the central unit are strongly tectonised. Polished tectonic breccia, as well as polished iron precipitation, which are observed within the tectonised marble layers close to the village of Alaçam (6'94'900/44'42'800), trace normal faulting running concordant to the paleostructure of Mount Uludağ. At the location mentioned above, serpentinites make it possible to locate the contact between the two units within a range of some millimetres. In addition to the traces within the marble layers indicating normal faulting, serpentinites point to a dextral strike-slip movements along this contact.

The existence of foliated Neogene sediments close to fault planes at Çekirge indicate a postintrusive, starting in late Miocene age of the tectonic uplift, which may still be in process. However, the movement is not restricted to main faults (Imbach 1992). Terraced Neogene lithologies in the western part of Mount Uludağ, and the conspicuous stair-like topography of its northern slope, prove the existence of additional faults which cut the whole massif. According to the orientation of the main faults on Mount Uludağ, a NE-SW extension and a NW-SE compression has to be assumed. Due to numerous strike-slip faults, the local tectonics on Mount Uludağ may not be explained by a simple horst-graben fault model.

Most of the neotectonic activities in Anatolia are caused by the northerly movement of the Arabian plate towards Eurasia (McKenzie 1972). Based on the local observation and based on the regional strain analysis, it is proposed that Mount Uludağ is a convergent zone due to displacements along different fault systems, which may even define large tectonic units in Northwestern Turkey. The evaluation of the GPS data resulted in a deformation field which clearly shows that the main tectonic activity of a dextral strike-slip type takes place along NAFZ's northern zone, from the Mudurnu valley, passing the Marmara sea to the gulf of Saros. The displacement rates are 17mm/a on the average, with a gentle increase from E to W (16 to 18mm/a). Realistic horizontal errors are in the range of 4mm/a (Straub and Kahle, 1994, 1995). As part of the GPS regional network in the Bursa area, 14 GPS stations were installed. These recent GPS measurements confirm the proposed deformation field in the Bursa area. Preliminary results of this local network with baselines between 7.5km and 55.3km show that the displacement is not restricted to one single main fault.

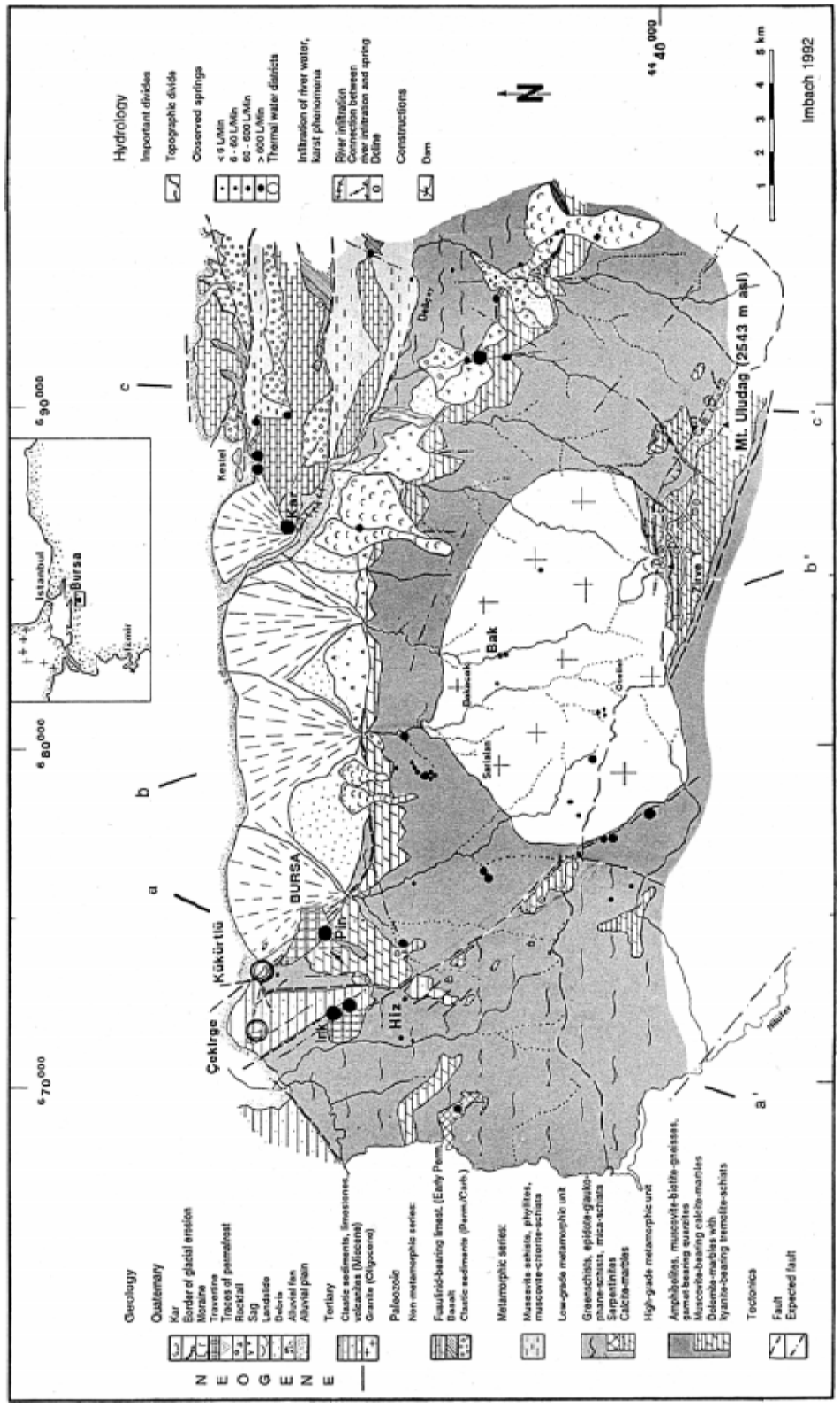


Figure 1: Geological map of Mount Uludağ (Bursa, NW-Turkey) with location of springs.

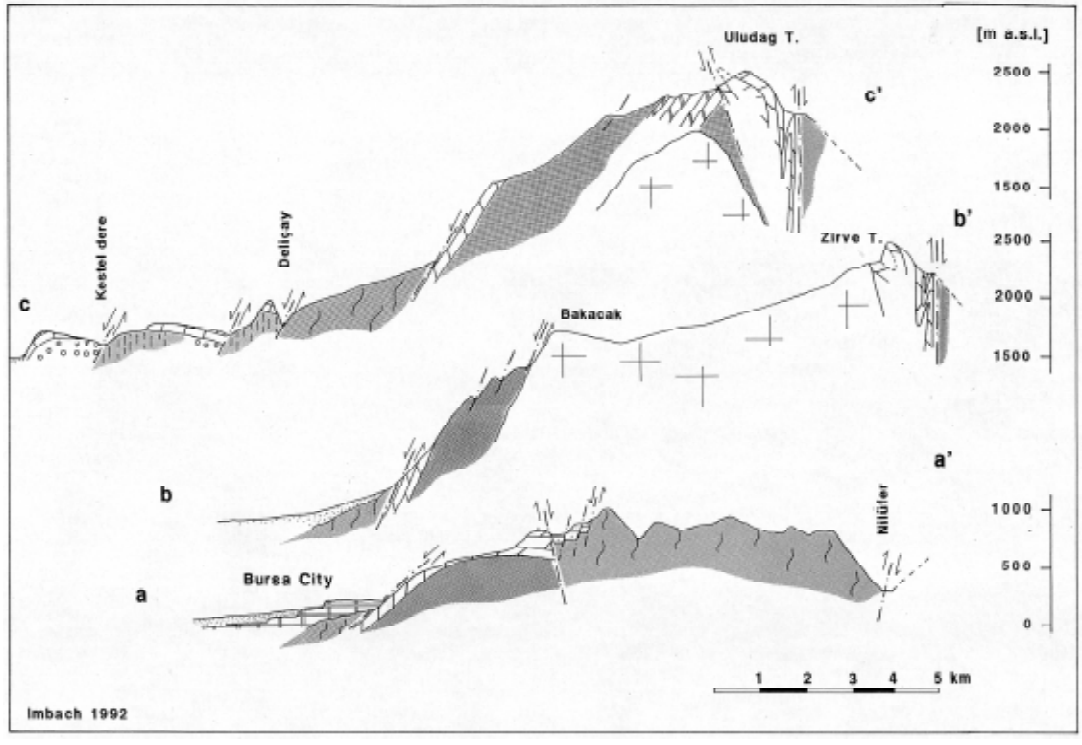


Figure 2: *Geological cross-sections of Mount Uludağ (Bursa, NW-Turkey).*

Hydrogeological setting

Thermal waters

Although several important normal faults separate Mount Uludağ from the plain, thermal waters discharge only in its westernmost part, in the two districts of Çekirge and Kükürtlü. There, post-Miocene tectonic contacts running in a N-S direction intersect with the normal faults separating Mount Uludağ from the plain and facilitate the outflow of deep-seated hot waters. Based on their geographical, physical and chemical characteristics, two different thermal water types can be distinguished. The Bursa thermal waters at Çekirge and Kükürtlü are now used for bathing and medicinal purposes. Due to the differences in water temperature and water chemistry, the two thermal water resorts have developed in different ways.

In Çekirge, low salinity thermal water flows from four springs and from some shallow excavations and boreholes within the Neogene unit (Fig. 3). The temperature varies only slightly, from 46°C (TDS~504mg/l) at the highest elevation of a small travertine complex to 31°C (TDS~485mg/l) in lower parts of the district. The outflow of thermal water is not restricted to the travertine complex and the freshwater limestone of the Neogene unit acts as a main aquifer close to the surface.

The bathing tradition in Çekirge can be traced back to the Roman-Byzantine period (Tchihatchef 1887, Fritsch 1882, Smith 1851). The ancient name of the *Eski Kaplıca*, the "Old public bath", was *Pythia* (the priestess of the temple of Apollo at Delphi). It was built around 500AD. The early development of a water distribution system in Çekirge made it possible to control and regulate the use of thermal water over many centuries. A well organised health re-

sort has been established, which nowadays impedes any additional use of thermal water by drilling (e.g. it is forbidden to use the thermal water from the *İpeker* drilling, which was drilled illegally). A common water distribution system shared by various private and state rehabilitation centres guarantees the controlled use of thermal water in this district. There are two main natural outflows: *Vakıfbahce* (Vak) and *Zeyni'nene* (Zey). The amount of water flowing from these, the hottest springs (Vak T=46°C, Zey T=44°C), cannot be measured precisely, but ranges between 700m^3 and 1700m^3 per day (for distribution network see Imbach 1992). The additional use of legally drilled artesian thermal waters with temperatures of about 35°C at present amounts to 600m^3 per day.

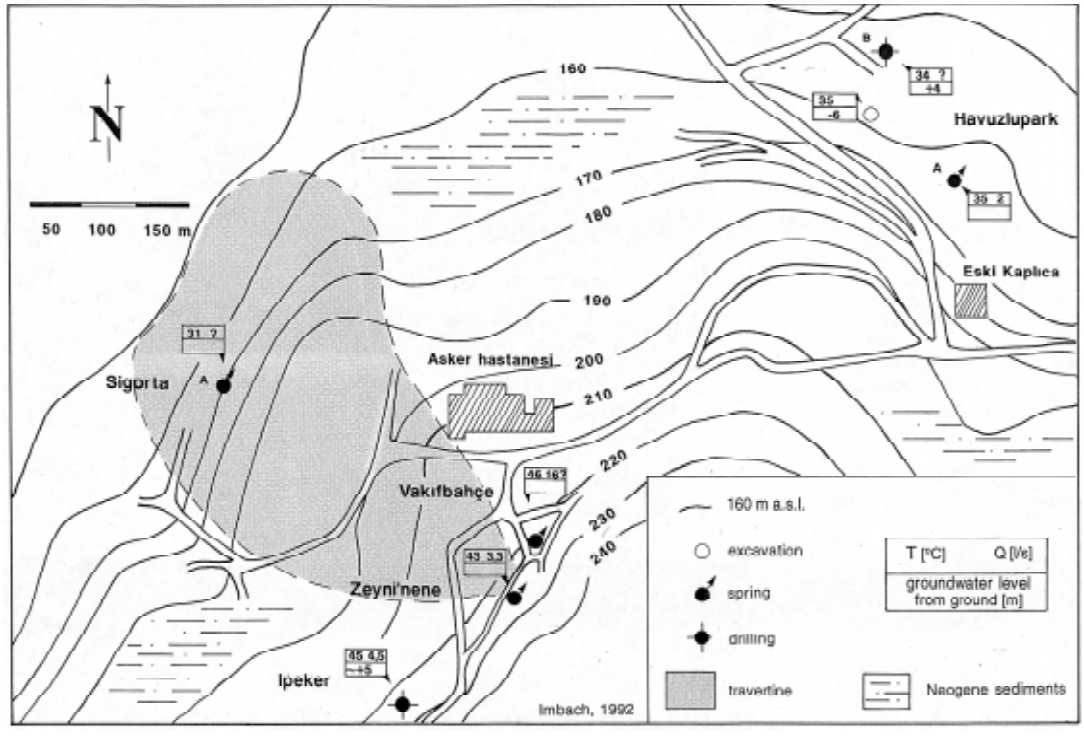


Figure 3: *Çekirge thermal water district.*

In Kükürtlü, which is situated two kilometers east of Çekirge towards the city-center of Bursa, thermal waters flow out within a small travertine complex, which covers a tectonic contact (Fig. 4). Temperature and mineralisation of the Kükürtlü thermal water vary with the different location. The hottest and most mineralised thermal waters discharge at the highest elevation of the travertine complex (e.g. the spring *Bağdemlibahçe* (Bag); T=82°C, TDS=1210mg/l). In shallow excavations and boreholes close to the plain, water temperatures of about 50°C (TDS~1088mg/l) are measured. Open cracks with vertical precipitation layers running parallel to the Neogene contact indicate that the thermal waters rise along this important fault zone.

The use of thermal water in Kükürtlü developed later under the Ottoman rulers (Hammer 1818). The *Yeni Kaplıca*, the "new public bath", was built in the 16th century and is still in use today. The hottest water within this district discharges at *Bağdemlibahçe* and is used for bathing purposes at the *Yeni Kaplıca*. The amount of water flowing from this spring is not precisely known but ranges between 150m^3 and 400m^3 per day. At all other localities a total of 200m^3 per day is pumped from shallow excavations or boreholes for bathing and heating, but also for car-washing. There is no arrangement between the different private and state users in this district.

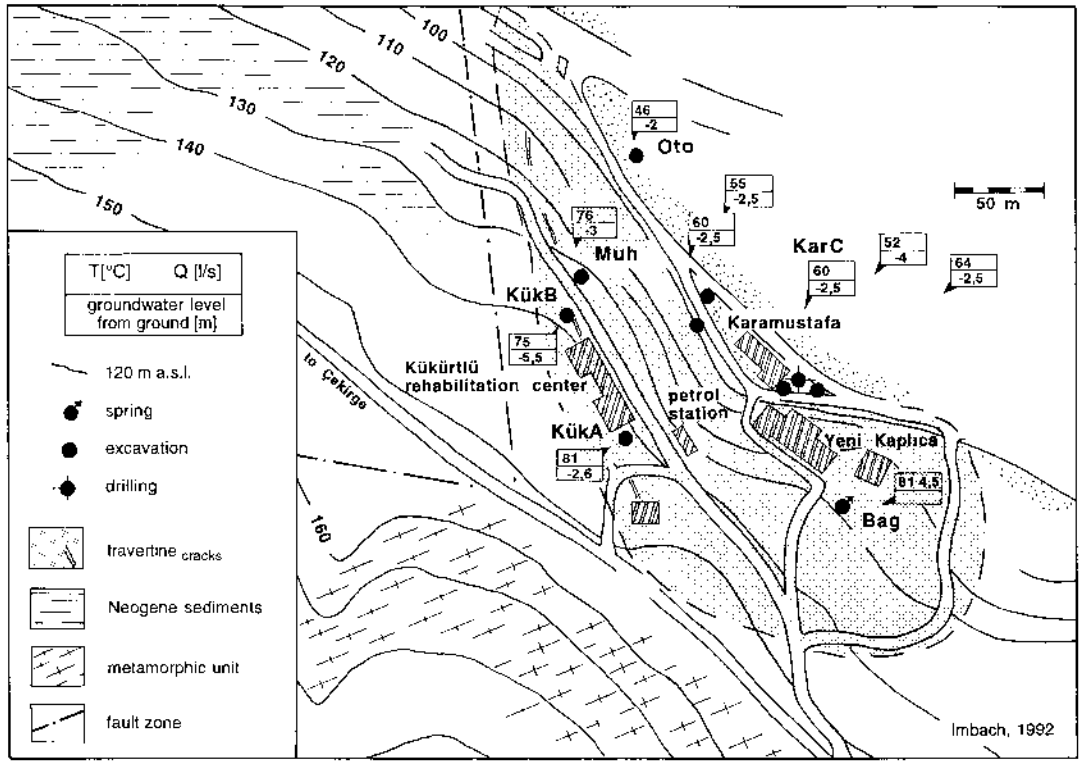


Figure 4: *Kükürtlü thermal water district.*

As the following quotations from Sandison show, the strong seismicity in this area affects the hot water systems:

(Sandison 1851, p. 19): "On the night of the 19th April, 1850, a shock of considerable violence occured at Brussa (means Bursa), lasting from eight to ten seconds...It was noticed that at Zehekerghé (means Çekirge) a momentary stoppage of the mineral springs accompanied the earthquake."

(Sandison 1855, p. 543): "By its resistless force, computed of about thirty seconds' duration (means the earthquake from 11th April, 1855), almost every stone-building left standing was overturned, or irreparably shattered... New streams of boiling water have burst out from the ground at the sites of the hot mineral baths, whilst the former currents there have been greatly increased in volume."

But although strong seismicity affects the hot water systems, a long-term change in water temperature is not observed, as old reports from Grisebach (1841), Smith (1851) and Fritsch (1882) prove.

Cold water

The Bursa area is rich in cold groundwater. The most important springwaters on Mount Uludağ are of Ca-HCO_3 type (TDS<600mg/l). They flow from strongly deformed marble layers at the northern foot of Mount Uludağ just above the plain (e.g. the karstic spring *Pınarbaşı* (Pın); Q_{max}=600l/s, TDS=321mg/l) and close to the main fault near the village of İnkaya (e.g. the karstic spring *İnkaya* (Ink), Q>100l/s, TDS=438mg/l); for their location see Fig. 1. Both springs have built large travertine complexes. The lower part of the large Pınarbaşı travertine

complex is mainly covered by alluvial fans and acts as an important aquifer within the Bursa plain.

Karstic marble layers at the topographic divide between Mount Uludağ and large dolines up to 100m in diameter are considered to be significant infiltration areas. Karstic springs are also related to river water infiltration (e.g. the karstic spring *Karapınar* (Kar); Q_{max}=1000l/s, TDS=314mg/l). In addition to these huge springs, which mainly discharge just above the plain, low salinity spring waters also emerge a few liters per minute from the gneiss unit at higher altitudes on Mount Uludağ (TDS<50mg/l). The central high plateau of Mount Uludağ above the timber line, where the granitic intrusion outcrops, must be considered the likely recharge area of these springs. In addition to deep-seated groundwater circulation on Mount Uludağ, shallow groundwater circulation takes place as a result of onion weathering and granular disintegration of granite (e.g. the spring *Bakaçak* (Bak); Q<1l/min, TDS=32mg/l). Within the deeply weathered low-grade metamorphic unit consisting of schists, phyllites, marbles and serpentinites, springs are rare and the groundwater is exploited by deep boreholes.

Main characteristics of cold and hot waters

Physical characteristics

The water temperature of the cold springs on Mount Uludağ (from 160 to 2310m a.s.l.) varies between 17.9° and 6.0°C, and electrical conductivities between 19 and 867µScm^{-1} were measured. Differences that correspond to the geological units have been observed (Table 2).

The Çekirge thermal water is characterised by low electrical conductivities between 570 and 531µScm^{-1} and by water temperatures between 46° and 34°C. The electrical conductivity and temperatures of the Kükürtlü thermal water vary between 1456 and 1142µScm^{-1} and between 81° and 46°C.

Geological unit	<x> µScm^{-1}	n	s µScm^{-1}	x_{max} µScm^{-1}	x_{min} µScm^{-1}
Granite	75	10	106	360	19
Gneisses and amphibolites	127	16	166	666	33
Marbles of high-grade metamorphism	353	16	159	573	142
Schists of low-grade metamorphism	404	19	113	867	95
Permian limestone	454	6	95	606	353

Table 2: Electrical conductivity of spring waters of Bursa area, Turkey, indicative of geological unit (<x>= mean value, n=number of springs, s = standard deviation, xmax= maximum value , xmin= minimum value).

Chemical characteristics

The chemistry of the cold groundwaters on Mount Uludağ is mainly dominated by Ca^{2+} and HCO_3^- ions (>50meq%) (Table 3). A classification of the, in part, very low salinity waters within the granite, gneisses and amphibolites is not possible because of the extreme variability of their constituents (Σ meq/l <1). The Ca^{2+} and HCO_3^- dominated groundwaters occur in

all geological units except for granite, and a classification according to geology is not possible. The chemical composition of the Çekirge thermal water clearly differs from that of the Kükürtlü thermal water (Fig. 5). Compared to the local cold groundwaters, both thermal water types, but especially the Kükürtlü thermal water, are enriched in Na and SO_4. (For chemical data see Table 3, Appendix 1 and Appendix 2).

The gas composition of both thermal water types is dominated by CO_2 and N_2. The gas from the hottest water within the Çekirge district is made up of CH_4 (0.02 vol.%), N_2 (39.2%), Ar (0.90%) and CO_2 (59.9%), in the Kükürtlü district it consists of CH_4 (0.01 vol.%), N_2 (10.4 %), O_2 (0.55%), Ar (0.26%), and CO_2 (88.8%).

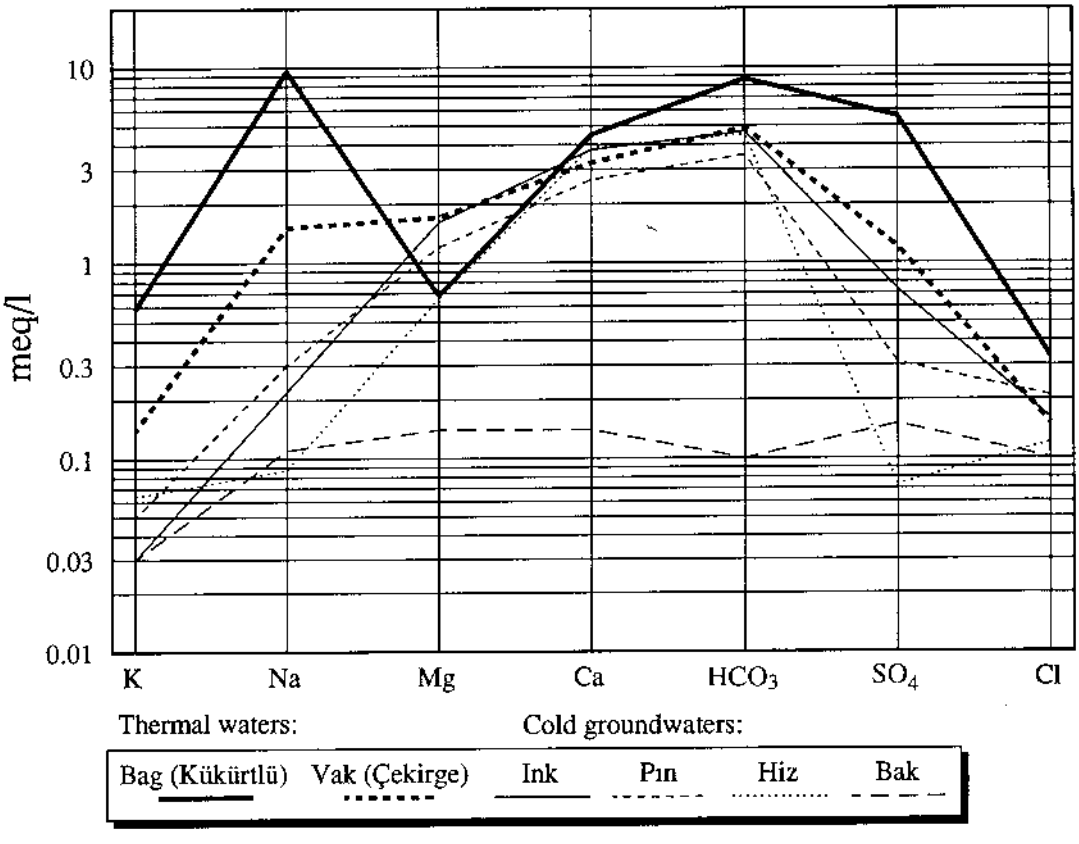


Figure 5: Main chemical composition of thermal waters and cold waters on Mount Uludağ.

Cold groundwaters	Ca Mg (Na) HCO_3 SO_4, Ca (Mg) HCO_3 (SO_4), Ca (Mg) HCO_3, Na Ca Cl	Ca Mg HCO_3 (SO_4), Ca Mg HCO_3, Ca HCO_3, Σ meq/l < 1
Çekirge thermal water	Ca Mg Na HCO_3 (SO_4)	
Kükürtlü thermal water	Na Ca HCO_3 SO_4	

Table 3: Chemical classification of groundwaters in the Bursa area (all ions >10meq% are mentioned; all >50meq% underlined and all <20meq% in parentheses) (Jäckli 1970).

Isotopic characteristics

The $\delta^{18}O$- and $\delta^{2}H$-values of cold groundwaters sampled on Mount Uludağ at altitudes between 140 and 2310m a.s.l. lie between the values of the Eastern Mediterranean meteoric water line (deuterium excess=22; IAEA 1981) and the continental water line of central Anatolia (deuterium excess=10; Şentürk et al. 1970) (Fig. 6). Compared to the isotope concentration of local rain, which was measured monthly by the Technical Research and Quality Control Department DSİ Ankara, the isotope concentration of local groundwater varies only slightly (Ertan 1987, Imbach 1992). This slight variation may be explained by selection processes, such as seasonal differences in groundwater recharge, or by water mixing within the unsaturated or saturated zones after single events of rainfall (Eichler 1965, Gat 1974, IAEA 1981). The isotopic values of local snow melt-water and river waters are similar to those of groundwaters. The tritium contents of local cold groundwater vary between 10.9 and 25.7TU. (For isotopic data see Table 4, Appendix 1 and Appendix 2).

The $\delta^{18}O$- and $\delta^{2}H$-values of the Çekirge thermal water are similar to those of local cold groundwaters (e.g. Ink), and the tritium values vary between 1.2 and 5.6TU. The isotopic characteristics of the Kükürtlü thermal water clearly differ from those of the Çekirge thermal water. The $\delta^{18}O$- and $\delta^{2}H$-values of the Kükürtlü thermal water are more negative in their $\delta^{2}H$-values. The tritium concentration, which is also very low, varies between 0.9 and 4.5TU.

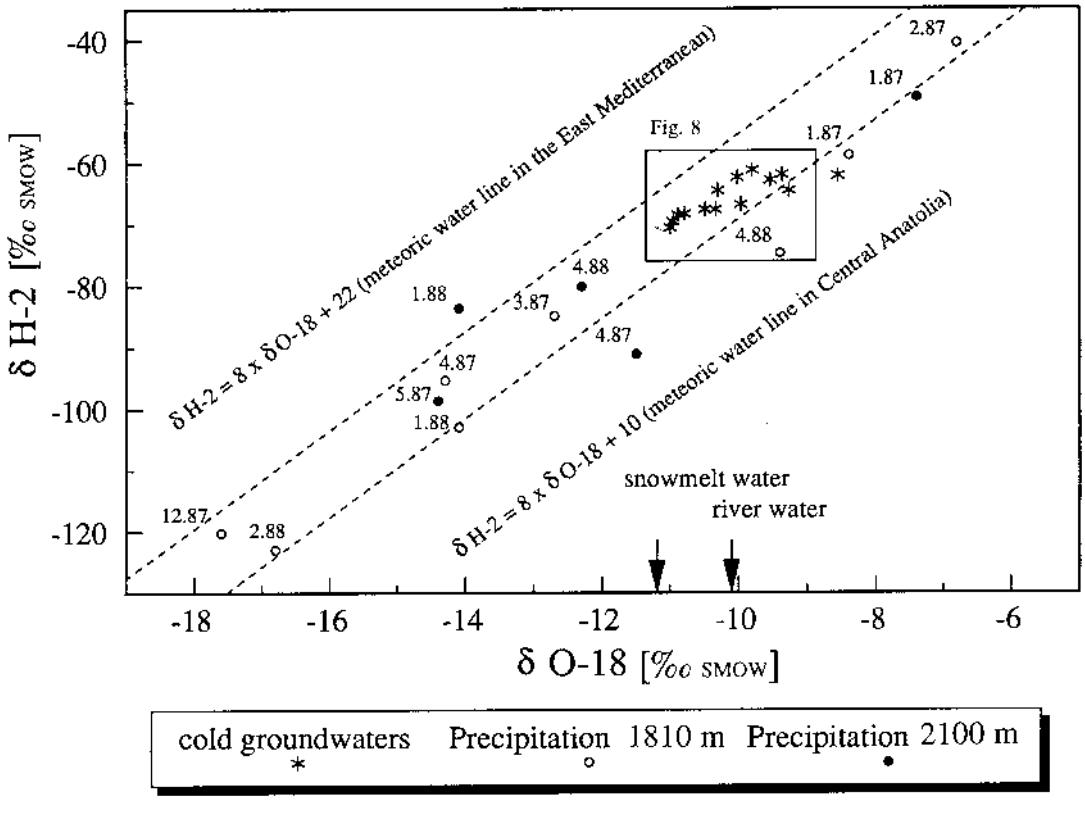


Figure 6: Isotopic data of cold groundwaters, precipitation, meltwater and riverwater sampled on Mount Uludağ at altitudes between 140 and 2310m a.s.l.

	Bursa thermal waters		Cold groundwaters			
	Kükürtlü	Çekirge	Mount Uludağ			
Sample name	Bag	Vak	Ink	Pin	His	Bak
Sampling date	89-Sept-05	89-Sept-06	89-Sept-08	89-Sept-08	89-Sept-12	89-Sept-11
Sampling altitude [m asl.]	130	220	450	250	810	1650
Field analyses						
T [°C]	81.1	45.7	14.8	15.0	11.2	7.3
$EC_{25°C}$ [µS/cm]	1456	541	484	502	392	30
Q [l/min]	270	960	6000	36000	30	0.5
pH	6.5	6.7	7.4	6.8	7.2	6.7
Alc [mmol/l]	8.2	4.8	5.7	4.0	4.3	0.2
Aci [mmol/l]	2.2	0.8	0.6	0.5	0.3	0.3
O_2 [mg/l]	0.4	1.3	9.1	7.2	7.1	8.1
Cations [mg/l]						
Li^+	0.68	<0.1	<0.1	<0.1	<0.1	<0.1
Na^+	220	35	5	7	2	3
K^+	22.8	5.6	1.2	1.9	0.8	0.5
Mg^{2+}	8	21	20	15	8	0
Ca^{2+}	90	65	76	53	78	2
Sr^{2+}	0.55	0.46	0.24	0.11	0.05	0.03
Ba^{2+}	0.07	0.10	0.02	0.02	0.02	0.01
Mn^{2+}	0.06	0.04	0.04	0.06	0.03	0.04
Fe^{2+}	0.52	0.23	0.20	0.07	0.11	0.11
Anions [mg/l]						
F^-	5.8	0.9	0.1	0.1	0.1	0.0
Cl^-	11.6	5.4	5.8	7.6	4.4	3.5
I^-	0.080	0.050	0.040	0.040	0.040	0.045
Br^-	<0.2	<0.2	<0.2	<0.2	<0.2	<0.2
HCO_3^-	531	296	284	215	275	9
NO_3^-	<0.08	0.2	5.0	2.2	1.9	0.2
PO_4^{3-}	0.50	0,38	0.25	0.27	0.21	0.14
SO_4^{2-}	268	58	35	15	7	5
Balance						
Cations [meq/l]	15.45	6.63	5.65	4.23	4.59	0.29
Anions [meq/l]	14.93	6.28	5.64	4.11	4.82	0.36
Non dissociat. [mg/l]						
As	0.13	0.04	0.05	0.03	0.02	0.02
B	1.70	0.07	<0.004	0.02	<0.004	<0.004
Si	45.37	15.35	5.35	3.76	2.97	7.84
TDS [mg/l]	1207	504	438	321	381	31
Environm. Isotopes						
^3H [TU]	0.9±0.7	1.2±0.7	12.1±0.9	18.1±1.4	25.6±1.8	15.4±1.3
δ^2H [‰ SMOW]	-72.3±1	-68.8±1	-68.3±1	-64.5±1	-64.5±1	-70.6±1
$\delta^{18}O$ [‰ SMOW]	-10.62±0.15	-10.75±0.15	-10.79±0.15	-9.27±0.15	-10.31±0,15	-11.00±0.15
$\delta^{34}S$ [‰ CD] in SO_4	13.9	6.0				
$\delta^{18}O$ [‰ SMOW] in SO_4	1.6	6.8				
Noble gases						
^3He [cm^3/g]	$1.19x10^{-13}$	$8.35 x10^{-13}$	$0.71 x10^{-13}$			
^4He [cm^3/g]	$17.9 x10^{-8}$	$118.2 x10^{-8}$	$(5.18 \pm 0.001) x10^{-8}$			
^{20}Ne [cm^3/g]	$4.89 x10^{-8}$	$24.75 x10^{-8}$	$(18.94 \pm 0.08) x10^{-8}$			
$^{20}Ne/^{22}Ne$	9.86	9.72	9.81 ± 0.05			

Table 4: *Physical, chemical and isotopic data of selected springs. The samples Vak and Bag represent the hottest waters of the thermal water districts. The samples Ink, Pin, His, and Bak represent different cold groundwater types on Mount Uludağ.*

Physical processes close to the atmosphere

Thermal water rising from depth loses its original characteristics, in part as a consequence of interaction with cold groundwaters and the atmosphere (Truesdell and Hulston 1980). The physical, chemical and isotopic data of the Çekirge and Kükürtlü thermal waters indicate the following processes within the outflow zone.

Cold water mixing, heat conduction and gas exchange within the outflow zone

The tritium concentrations of the Çekirge and Kükürtlü thermal waters vary between <1TU and 6TU. In both districts the tritium concentration of the thermal water correlates negatively with its temperature and electrical conductivity. This can be explained by mixing within the outflow zone (Fig. 7). The negative correlation between electrical conductivity and tritium concentration of the sampled thermal waters of each district allows us to determine the theoretical mixing endmembers. For both thermal provinces, an old, tritium-free deep-seated groundwater and a young, tritium-rich shallow groundwater can be assumed as endmembers of the thermal water mixing. The uniform chemical composition of the thermal waters within the Çekirge district points to similar compositions of the thermal and nonthermal mixing endmembers. This mixing model is consisted with the stable isotopic composition of the thermal waters within Çekirge (Fig. 8).

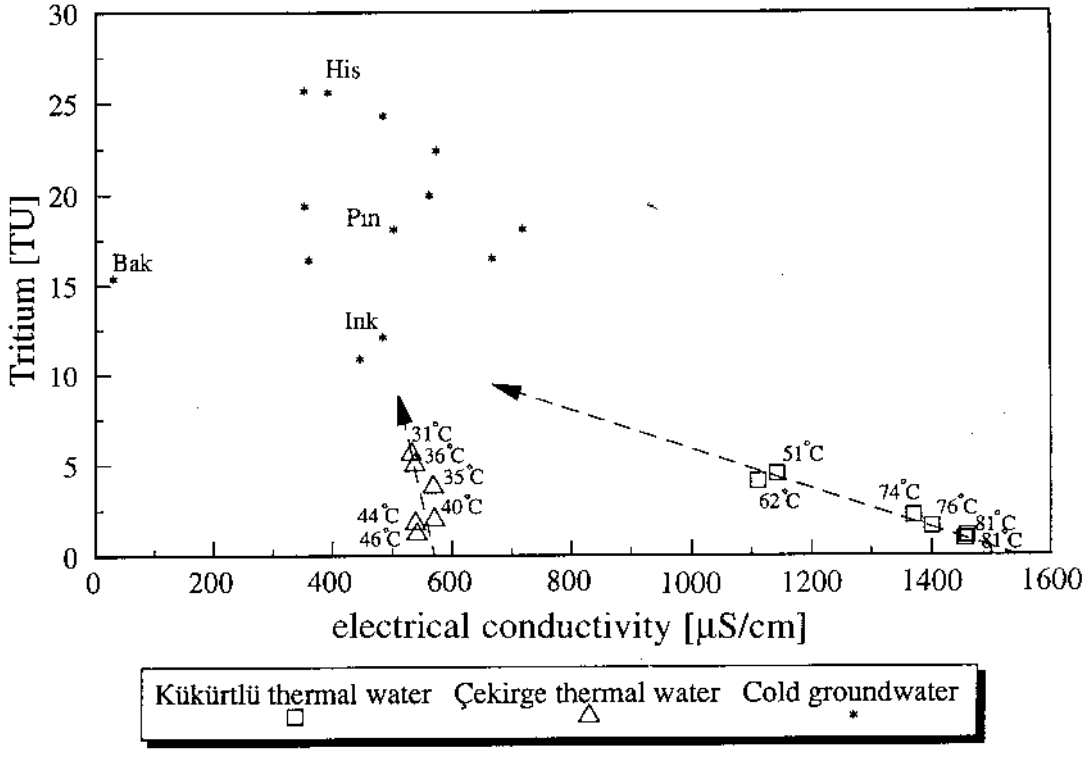


Figure 7: Electrical conductivity and tritium data of hot and cold waters, indicative of water mixing within the outflow zone of thermal water.

Based on this data, a linear correlation between chemical composition and temperature of the thermal waters must be expected in both districts. As Fig. 9 shows, thermal waters in the hotter district, Kükürtlü, deviate from the assumed range of water mixture. Water temperatures lower than expected indicate an additional loss of energy by heat conduction.

Helium and neon isotope measurements further indicate that the thermal waters rising from depth partly lose their original gas characteristics as a result of mixing with cold groundwater and of contact with the atmosphere (air) (Fig. 10). For further characterisation of the thermal waters, the different origins of helium (atmospheric, non-atmospheric (crust, mantle)) were calculated by separation of the measured helium according to the Equations 1-4 and 12 below. In the Çekirge thermal water atmospheric helium represents 6% (Ipe), 13% (Zey) and

16% (HavB), and in the Kükürtlü thermal water 8% (KükB) and 44% (KarC). (For the calculation method see Kipfer (1991) and Imbach (1992); for helium concentrations see Table 3, Appendix 1 and Appendix 2.)

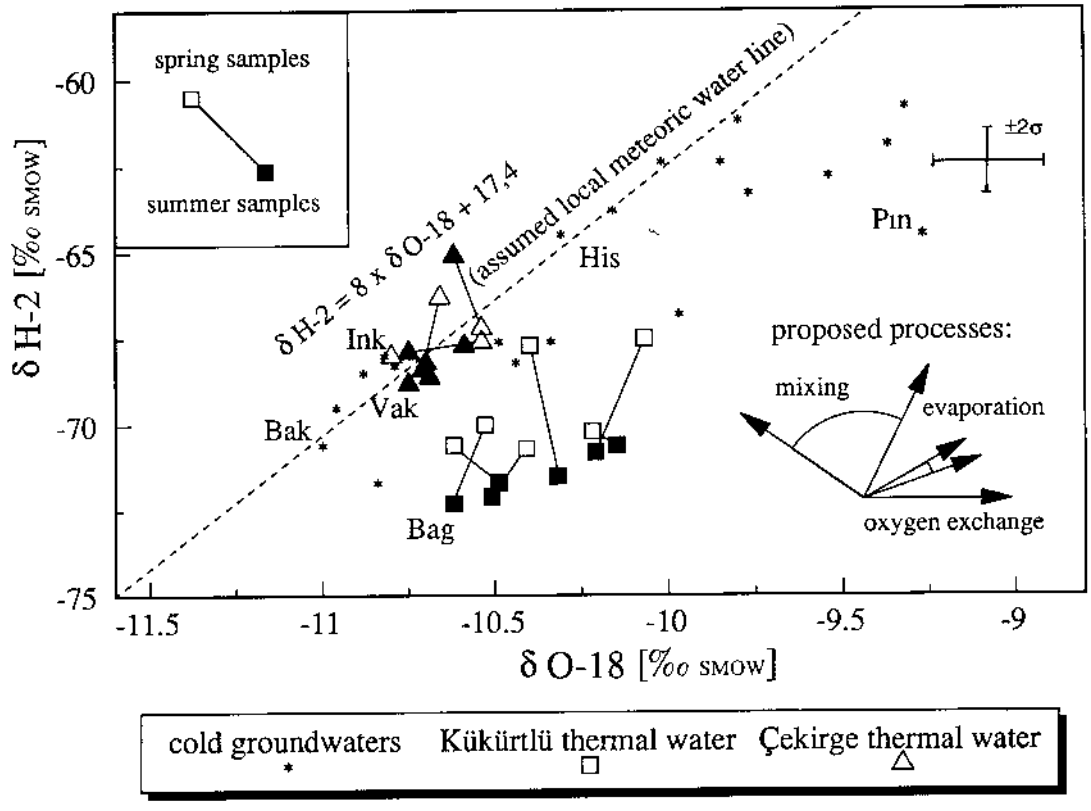


Figure 8: *Stable isotopic values of hot and cold groundwaters of Mount Uludağ. All the cold groundwaters were sampled in summer 1989, and each thermal water was sampled twice, once in summer 1989 at the end of the dry season, and once in spring 1990 at the end of the wet season. Error given at 1σ level.*

Separation of the measured helium concentration to an atmospheric and non atmospheric origin:

Definition:

$R_{meas}=(^3He/^4He)_{sample}$

$R_{atm}= (^3He/^4He)_{atmosphere}= (^3He/^4He)_{local\ groundwater\ sample}= 1.376x10^{-6}$

$(^4He/^{20}Ne)_{atm}= (^4He/^{20}Ne)_{local\ groundwater\ sample} = 0.274$

$R_{ex}= (^3He/^4He)_{non\text{-}atmospheric\ origin}$

Calculation of the helium concentration from the atmosphere (atm):

$$^3He_{atm}= R_{atm} x\ (^4He/^{20}Ne)_{atm} x\ ^{20}Ne_{meas} \quad [1]$$

$$^4He_{atm}= (^4He/^{20}Ne)_{atm} x\ ^{20}Ne_{meas} \quad [2]$$

Calculation of the helium concentration of non atmospheric origin (ex):

$$^3He_{ex}= {}^3He_{meas} - {}^3He_{atm} \quad [3]$$

$$^4He_{ex}= {}^4He_{meas} - {}^4He_{atm} \quad [4]$$

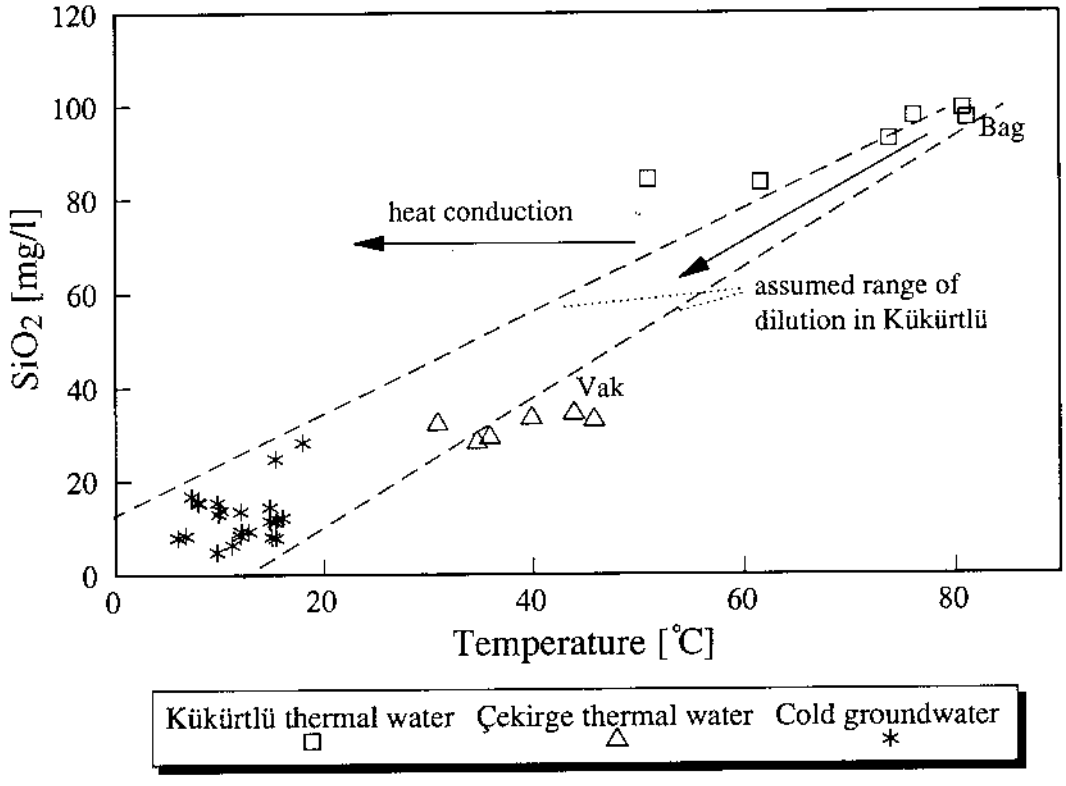


Figure 9: *Temperature and chemical composition of thermal waters indicative of additional loss of energy by heat conduction.*

Mobilisation of residual waters

Temperature and electrical conductivity of the hottest thermal waters and of huge coldwater near the thermal water provinces were measured every two weeks over a period of two years. Seasonal fluctuations were practically undetectable, but short-term increases in temperature and electrical conductivity up to 1.1°C and to 75µScm^{-1} were observed in the hottest thermal springs.

For example on October 18, 1989, one day after a heavy rainfall of about 180mm on Mount Uludağ, an increase in temperature and electrical conductivity of about 0.4°C and 35µScm^{-1} was measured in the Çekirge thermal water (Zey). At the same time, an increase of about 0.8°C and 50µScm^{-1} was observed in the Kükürtlü thermal water (Bag). This short-term increase of temperature and conductivity may be explained by a mobilisation of hot and highly mineralised residual water due to pressure transmission.

Water-rock interaction

Groundwaters in the study area are mainly dominated by Ca^{2+} and HCO_3^- ions, indicating the dominant role of calcite dissolution (Fig. 11). Its intensity, given the widespread availability of calcite, depends on temperature as well as on pH and pCO_2 (Stumm and Morgan 1981). With constant pCO_2 values, an equilibrium develops, which can be described by Equation 5.

$$2[Ca^{2+}] + [H^+] = [HCO_3^-] + 2[CO_3^{2-}] + [OH^-]; \text{ simplified: } 2[Ca^{2+}] \approx [HCO_3^-]; \text{ [mol/l]} \quad [5]$$

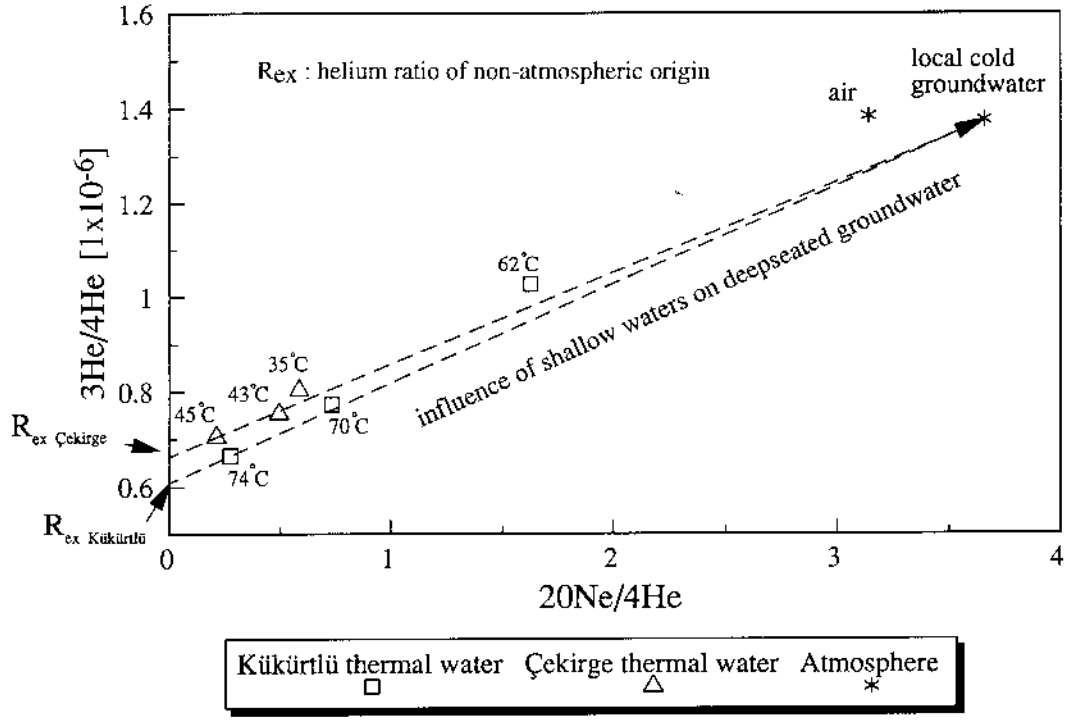


Figure 10: Helium ratios of thermal waters within the outflow zone confirm the mixing model and indicating gas exchange with the atmosphere.

The observed relation between Ca^{2+} and HCO_3^- ions ($2[Ca^{2+}] \approx [HCO_3^-]$ [mol/l]) in all cold groundwaters and the contribution of these ions to the TDS, which generally amounts to >25meq% each, implies that calcite dissolution is the dominant process in most of the groundwaters analysed. The CO_2 pressure of most of the cold groundwaters (except for some immature, very low salinity waters that lie below the calcite saturation line at 25°C) exceeds the atmospheric CO_2 pressure considerably. For these waters pCO_2 values between $10^{-2.5}$atm and $10^{-1.4}$atm have been calculated according to Equation 6 (Imbach 1992). For dissociation constants, see Plummer and Busenberg (1982).

$$\log pCO_{2(eq)} = \log[Ca^{2+}] + 2x\log[HCO_3^-] + \log K_2 - (\log K_1 + \log H_H + \log K_C) \quad [6]$$

Assuming equilibrium conditions, a CO_2 pressure of about $10^{-1.3}$atm respectively of about 1atm was calculated for the Çekirge respectively Kükürtlü thermal waters. The increased concentration of HCO_3^- in the Kükürtlü thermal water cannot be explained only by calcite dissolution. Due to the high CO_2 pressure of about 1atm an increased dissociation of carbonic acid takes place and, in addition to calcite dissolution, silicate hydrolysis has to be assumed. The high concentration of Na^+ in the thermal water of Kükürtlü, equal to >25meq%, and the crystalline basement host rock suggest silicate alteration, e.g. Equation 7. Both, the high CO_2 pressure and the relatively high temperature cause increased water-rock interaction, as the rich oxygen-18 content of the Kükürtlü thermal water shows (Fig. 8) (IAEA 1981, Blattner 1985).

$$2NaAlSi_3O_8 + 2H^+ + 9H_2O = Al_2Si_2O_5(OH)_4 + 4H_4SiO_4 + 2Na^+ \quad [7]$$

A maturity index MI<2 for both thermal waters (Giggenbach 1988) indicates that the chemical composition of the Çekirge and Kükürtlü thermal waters is dominated by isochemical rock dissolution and not by equilibrium reactions between fluid and minerals of the host rock.

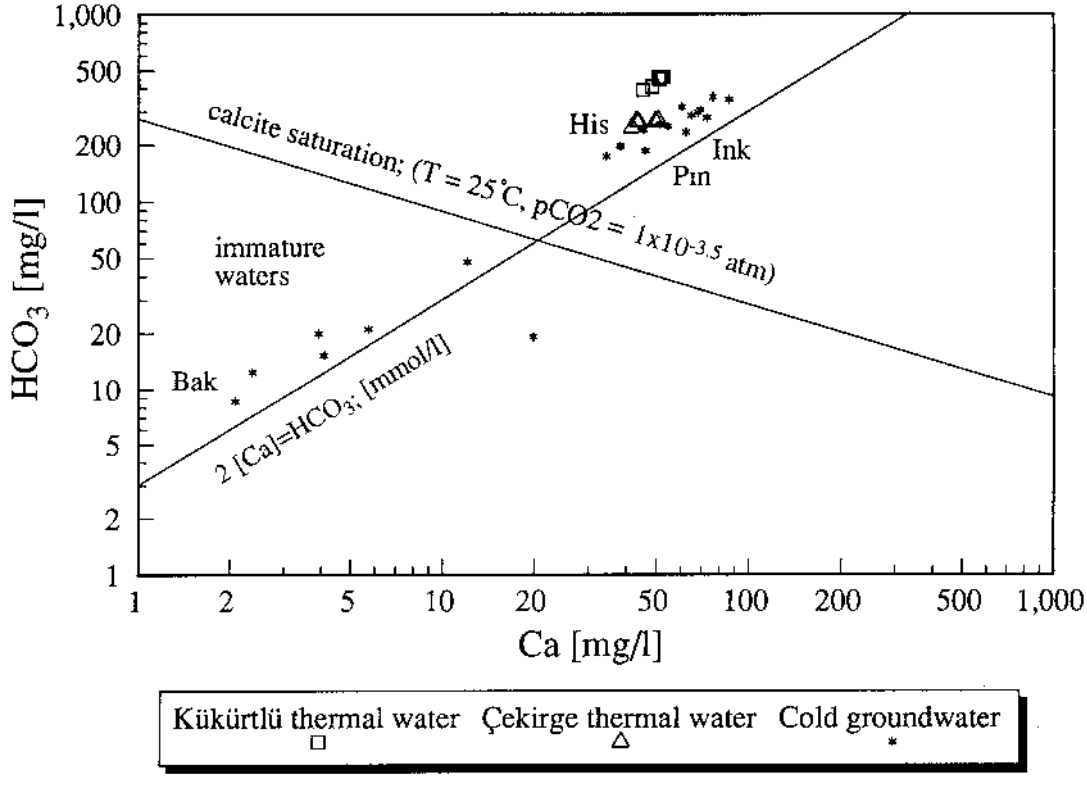


Figure 11: Calcite dissolution is the dominant process leading to the mineralisation of cold and hot groundwaters on Mount Uludağ. For the Kükürtlü thermal water an increased dissociation of carbonic acid has to be assumed due to CO_2 pressure of about 1atm.

Mixing with gases from crust and mantle

The helium concentrations of the thermal waters deviate from the values characteristic of local cold groundwaters. This proves an overprinting of the thermal waters by gases originating from crust and mantle. Based on the helium ratios of atmosphere, crust, and mantle and on the neon concentration of each sample, the helium content of the thermal water was separated according to its origin using Equations 8-11. (For calculation see Kipfer (1991) and Imbach (1992); for helium concentrations see Table 3, Appendix 1 and Appendix 2.)

Separation of the calculated non-atmospheric helium to its origin:

Definition:

$^4He_{ex}$, $^3He_{ex}$, according to Equations [3] and [4]

$R_{rad}=2 * 10^{-8}$, and $R_{man}=1 * 10^{-5}$ (Coon 1949, Ozima and Podesek 1983, Andrews 1985)

Calculation of the helium concentration from mantle (man) and crust (rad):

$$^3He_{man}= (^4He_{ex} – (R_{rad}^{-1} * {}^3He_{ex})) / (R_{man}^{-1} - R_{rad}^{-1}) \quad [8]$$

$$^4He_{man}= (^3He_{ex} – (R_{rad} * {}^4He_{ex})) / (R_{man} - R_{rad}) \quad [9]$$

$$^3He_{rad}= {}^3He_{ex} – {}^3He_{man} \quad [10]$$

$$^4He_{rad}= {}^4He_{ex} – {}^4He_{man} \quad [11]$$

Calculation of the helium content (%) originating from crust, mantle and atmosphere:

$He_{atm} / He_{meas} \sim {}^4He_{atm} / {}^4He_{meas}$

$He_{rad} / He_{meas} \sim {}^4He_{rad} / {}^4He_{meas}$

$He_{man} / He_{meas} \sim {}^4He_{man} / {}^4He_{meas}$ [12]

For the hottest thermal waters in Çekirge and Kükürtlü, at least 6-8% of the measured helium originates from the atmosphere, about 87-88% from the crust, and about 5-6% from the mantle.

As already pointed out, the hottest waters of Çekirge and Kükürtlü are almost identical with the deep-seated, tritium-free thermal water of each province at depth. The increasing $^3He/^4He$ ratio of the colder, less saline thermal waters within both thermal water districts proves cold water mixing and gas exchange with the atmosphere (Fig. 10). Nevertheless, the huge amount of helium originating from the crust and even the mantle indicates that an important gas exchange took place during the circulation of these deep-seated groundwaters.

Characterisation of the thermal waters at depth

Based on tritium and stable isotope investigations for the districts Kükürtlü and Çekirge, two different thermal water systems can be proposed. The negative correlation between tritium concentrations of the thermal waters and their physical and chemical parameters allow us to define the chemical composition of the original hot deep water of each province by means of extrapolation (Fig. 12).

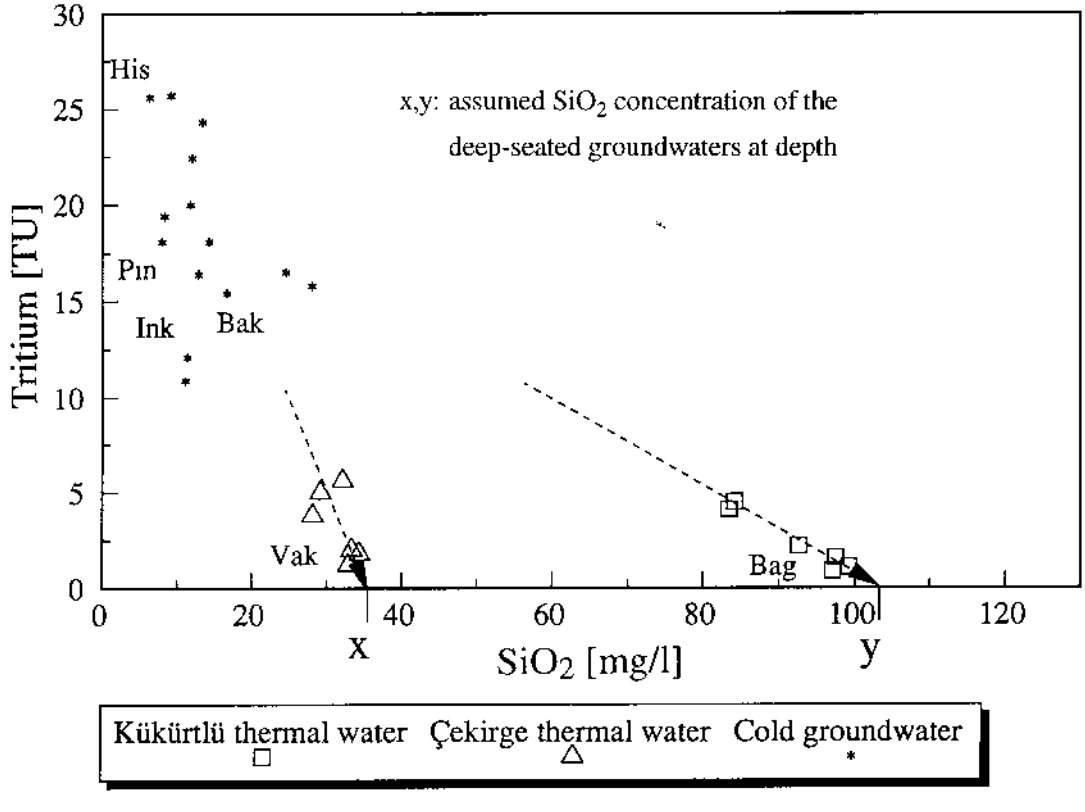


Figure 12: Characterisation of the hot deep water of each province by means of graphic extrapolation.

For the Kükürtlü hot water at depth an electrical conductivity of about 1600µScm^{-1} and total dissolved solids (TDS) of about 1300mg/l have to be assumed. Within the Çekirge district, the hottest thermal water is almost identical to the hot water at depth. An electrical conductivity of about 540µScm^{-1} and total dissolved solids (TDS) of about 500mg/l have to be expected. As the loss of energy by heat conduction is not taken into account by the graphic extrapolation, the reservoir temperatures must be calculated by geothermometers. The cation geothermometers based on Na^+, K^+, Mg^{2+} and Ca^{2+} cannot be applied, however, because the chemistry of both thermal waters is dominated by isochemical rock dissolution and not by equilibrium reactions between fluid and minerals of the host rock (Giggenbach 1988). As the amount of Cl^- in both thermal water types is very low (~10mg/l), temperatures of less than 200°C may be expected, and the chalcedony geothermometer was applied to the extrapolated tritium-free hot water endmembers of both thermal water districts (Truesdell 1975): For the Kükürtlü thermal water the result was a minimum reservoir temperature of about 111°C, and for the Çekirge thermal water a minimum reservoir temperature of about 52°C.

Recharge area of the Bursa thermal waters

According to the physical, chemical and isotopic data, mixing between the Çekirge and Kükürtlü thermal water can be excluded. Even a common origin for the Çekirge and Kükürtlü thermal water has to be negated. However, according to their isotopic characteristics, the Çekirge and Kükürtlü thermal water can both be related to recharge areas on Mount Uludağ. Based on the assumption that the altitude of shallow groundwater springs does not differ considerably from the altitude of the recharge area, a linear correlation between average altitude of groundwater infiltration and isotope concentration was graphically determined (Fig. 13) (Fontes 1980, IAEA 1981). Using the deuterium concentration of each province's hottest thermal water as tracer, it may be assumed that the Kükürtlü thermal water recharges at a higher elevation on Mount Uludağ (between 2500 and 1500m a.s.l.) and the Çekirge thermal water recharges in its lower parts (between 2000 and 1000m a.s.l.).

Hydrogeological circulation model

Physical, chemical, and isotopic investigation of hot and cold groundwaters made it possible to reconstruct the thermal water evolution from infiltration to discharge, including water-rock-gas interaction, gas exchange, heating, and shallow water mixing.

Meteoric waters (rain, meltwater) infiltrate on Mount Uludağ and recharge the thermal waters at Çekirge and Kükürtlü. During their residence times of at least 50 years the waters of the two different systems were mineralised by water-rock-gas interactions in the metamorphics of Mount Uludağ. Calcite dissolution and hydrolysis of silicates are the dominant water-rock interactions. Both waters interact with gases from crust and mantle during their circulation.

The Kükürtlü thermal water, infiltrating at the highest elevation on Mount Uludağ (most probably in the marbles on top of Mount Uludağ), is mineralised by water-rock-gas interactions governed by elevated CO_2-pressures at temperatures of less than 120°C. Residence times of at least 50 years or more are expected.

The Çekirge thermal water infiltrates in the lower parts of Mount Uludağ (probably the leucogranite in the region of the Uludağ plateau). This water is mineralised by water-rock-gas interactions governed by atmospheric CO_2-pressures in a low temperature environment of less than 50°C. Residence times of at least 50 years are expected.

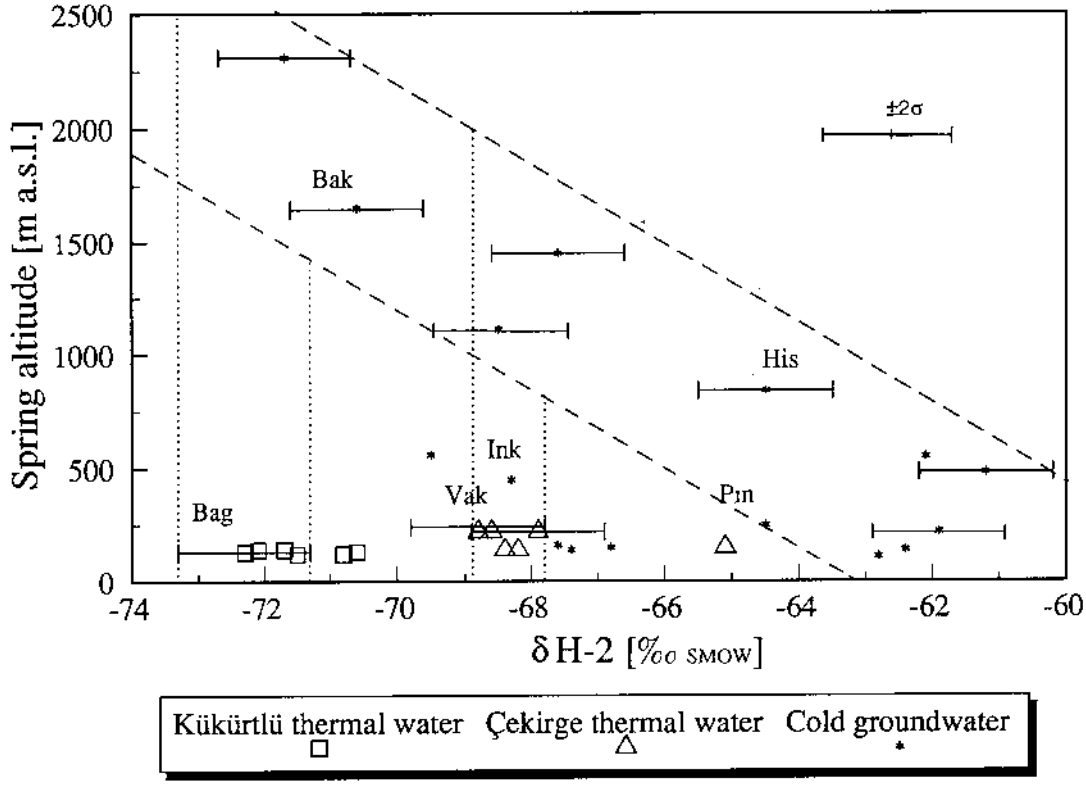


Figure 13: Graphic determination of recharge altitudes for the thermal waters of each province by means of isotopic data. Error given at 1σ level.

These thermal waters follow separate flow paths. The upflow of the two waters occurs in the westernmost part of Mount Uludağ along faults that are related to the neotectonic stress regime of Northwest Turkey. Within each thermal water district a travertine complex created by the thermal waters covers the upflow zone. During the upflow, especially in the travertine complex, the thermal water interacts with cold groundwater, rock and the atmosphere.

Final discussion: protection of thermal water and improvement of its use

On the basis of this conceptual model (Fig. 14) it is possible to discuss the additional use and protection of the thermal waters.

Thermal water of Kükürtlü

The thermal waters used in different spas within the Kükürtlü district have the same origin. Consequently, local use influences the entire occurrence of thermal water within the travertine aquifer. An overuse of the hot groundwater could impair or even drain the shallow excavations and springs situated on a higher level. Further deepening of existing excavations, on the other hand, would intensify drainage of the thermal water system. Direct use of thermal water by means of drilling into the travertine should be avoided, as the consequences for the entire thermal water system are incalculable. An unknown amount of thermal water flows

from the travertine complex into the alluvium of the Bursa plain. The use of thermal water within this plain offers an alternative to its capture within the travertine terrace. Instead of pumping thermal water out of the karstic travertine aquifer, hot water could be trapped within the unconsolidated sediments of the plain. This procedure would ensure considerable protection of the thermal water system. Protection of thermal waters from infiltration of polluted water is a further pre-condition for long-term use. Potential hazards, such as a petrol station that has already been installed within the travertine terrace without any safety measures, should be eliminated. This can only be achieved by legal procedures to protect the whole travertine complex. In view of an extensive use of thermal water, it also becomes imperative to protect the cold groundwater. To this day, the geothermal potential of the hot waters (P_{tot} ~1.5MW, Q=5l/s, T_{max}-10°C=70°C) is not exploited in a satisfactory way. In order to obtain a bathing temperature of approximately 40°C, the 80°C thermal water of Kükürtlü is cooled by addition of cold water. An application of heat exchangers would yield a geothermal power of about 0.8MW (Q=5l/s, T_{max}-40°C=40°C). This would avoid the consumption of expensive cold water, and at the same time would reduce or even eliminate oil-fired heating.

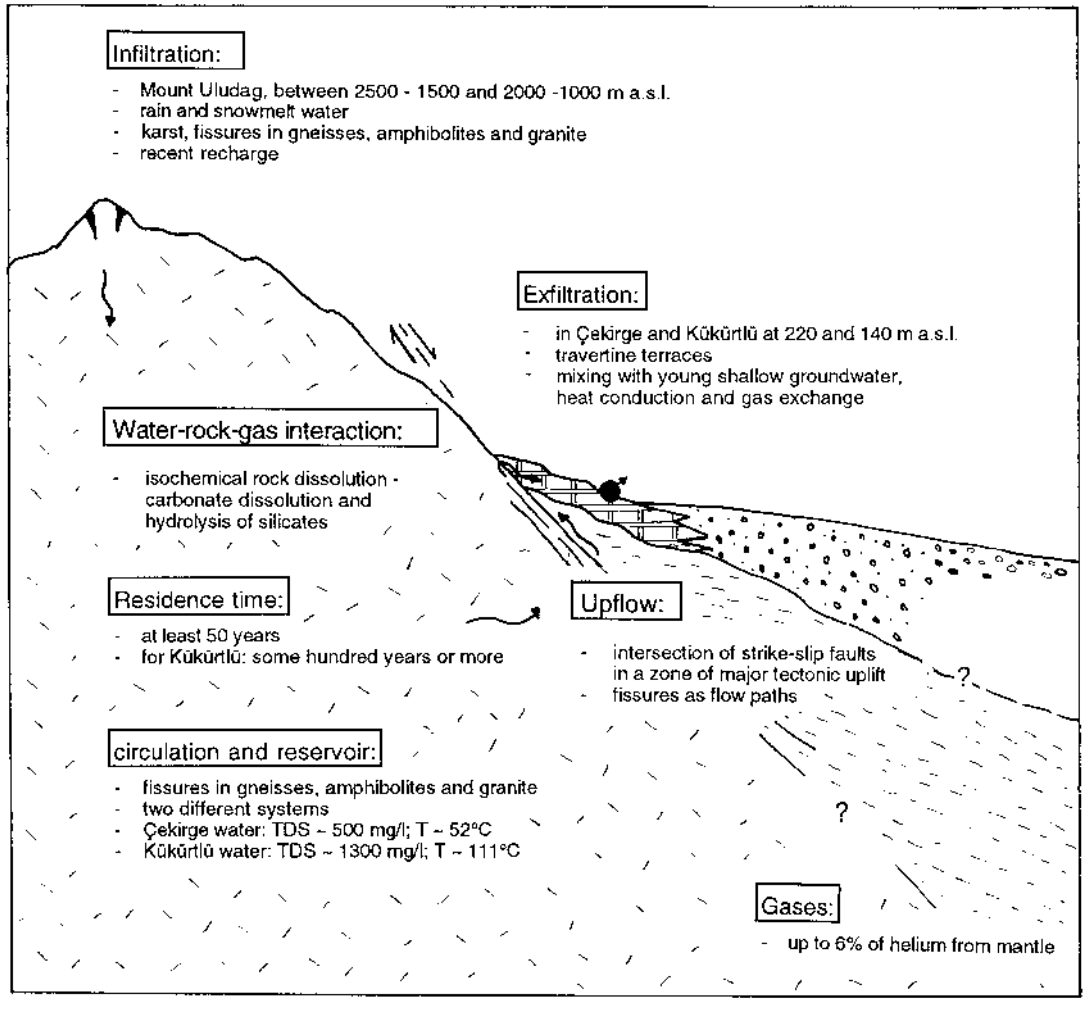


Figure 14: Conceptual model of the circulation of the Bursa thermal waters.

Thermal water of Çekirge

As in the case of Kükürtlü, the thermal waters sampled at different localities within the district of Çekirge are of the same origin, and consequently local overuse could influence the thermal water system as a whole. Where the thermal water is tapped by boreholes, a considerable decrease in hydraulic head could also have an impact on the thermal springs located at a higher topographic level. Based on the present outflow rates, the total geothermal potential of the Çekirge thermal water is about 2MW (Q=17l/s, T_{max}-10°C=30°C). Outside of the natural outflow area, but still within the Neogene unit of Çekirge, artesian thermal water is produced by boreholes. It can be assumed that the freshwater limestones represent the aquifer within the Neogene unit. As long as the natural outflow of thermal water is much higher than the amount made available through drilling, no negative effects should occur. However, any reduction of the natural thermal water outflow should first of all be taken as a signal of overuse of the thermal water system.

Acknowledgements

The author would like to thank C. Schindler (ETH Zürich), W. Balderer (ETH Zürich), and E. Yüzer (İstanbul Technical University) for supervising his PhD studies, as well as E. Greber and all other members of the MARMARA project for the good teamwork. Thanks are also extended to E. Saker and Y. İşleyen from DSİ Bursa for logistical support and to Turan Uçar for his hospitality. P. Signer and R. Kipfer (ETHZ), W. Rauert and P. Trimborn (National Centre for Environmental Sciences, D-Neuherberg), and P. Klöti (Swiss Federal Institute of Forest, Snow and Landscape Research, Birmensdorf) supported his isotopic and chemical investigations. Thanks are also due to F.D. Vuataz (Centre de Hydrogéologie, Neuchâtel) and to the reviewers and editors of *Geothermics* for their valuable suggestions concerning the hydrogeological part of this contribution, which appears in a slightly different form in that journal (Imbach 1997).The MARMARA Poly-Project was financed by the ETH Zürich and the author is especially grateful to R. Hütter, ETH Vice-President of Research and Development, for his support and personal interest in this interdisciplinary project.

References

Andrews, J.N., 1985, The Isotopic Composition of Radiogenic Helium and its Use to Study Groundwater Movement in Confined Aquifers, Chemical Geology 49, 339-351.

Barka, A.A., 1992, The North Anatolian fault zone, Annales Tectonicae, Suppl. to Vol. VI, 164-195.

Barka, A.A. and Kadinsky-Cade, K., 1988, Strike-slipe Fault Geometry in Turkey and its influence on earthquake activity, Tectonics 7, 663-684.

Bingöl, E., Akyürük, B. and Korkmazer, B., 1975, Geology of the Biga Peninsula and some Characteristics of the Karakaya Formation, Proc., Congress of Earth Sciences on the Occasion of the fiftieth Anniversary of the Turkish Republic, edited by: S. Doyuran, Maden Tetkik ve Arama Enştitüsü Ankara, 71-77.

Bingöl, E., Delaloye, M. and Ataman, G., 1982, Granitic Intrusions in Western Anatolia: A Contribution to the Geodynamic Study of this Area, Ecl. Geol. Helv. 75/2, 437-446.

Blattner, P., 1985, Isotope Shift Data and the Natural Evolution of Geothermal Systems, Chemical Geology 49, 187-203.

Brinkmann, R., 1966, Geotektonische Gliederung von Westanatolien, N. Jb. Geol. Paläont. Mh., Stuttgart, 603-618.

Brinkmann, R., 1968, Einige geologische Leitlinien von Anatolien, Geologica et Palaeontologica 2, 111-119.

Brinkmann, R., 1971, The Geology of Western Anatolia, in: Geology and History of Turkey, edited by: A.S. Campbell, The Petroleum Exploration Society of Libya on the Occasion of the 13th Annual Field Conference, Tripoli, Libya, 171-191.

Coon, J.H., 1949, ^{3}He Isotopic Abundance, Phys. Rev. 75, 1355-1357.

Demirtaslı, E., 1989, Stratigraphic Correlation Forms of Turkey, Rend. Soc. Geol. It. 12, 183-211.

Dewey, J.F. and Sengör A.M.C., 1979, Aegean and surrounding regions: Complex multiplate and continuum tectonics in a convergent zone, Geol. Soc. Am. Bull. 90, 80-92.

Eichler, R., 1965, Deuterium-Isotopengeochemie des Grund- und Oberflächenwassers, Geol. Rd. 55, 144-159.

Eisenlohr, T., 1995, Die Thermalwässer der Armutlu-Halbinsel (NW-Türkei) und deren Beziehung zu Geologie und aktiver Tektonik, PhD thesis ETH Zürich 11340, 165p.

Ertan, I., 1987, Determination of water equivalent of snow and the forecast of snowmelt runoff by means of isotopes in Turkey, in: Large Scale Effects of Seasonal Snow Cover, Proc. Symp. IAHS Vancouver, 1987, Publ. No. 166, 225-239.

Eyidoğan, H., Güçlü, U., Utku, Z. and Değirmenci, E., 1991, Türkiye Büyük Depremleri Makro-Sismik Rehberi (1900-1988), İstanbul Teknik Üniversitesi Maden Fakültesi Jeofizik Mühendisliği Bölümü, 199p.

Fontes, J.Ch., 1980, Environmental Isotopes in Groundwater Hydrology, in: Handbook of Isotope Geochemistry, edited by: P. Fritz and J.Ch. Fontes, Elsevier Amsterdam, Vol.1, 75-140.

Fritsch, K. von, 1882, Acht Tage in Kleinasien, Mitt. Ver. Erdk. H., 101-139.

Gat, J.R., 1974, Local Variability of the Isotope Composition of Groundwater, in: Isotope Techniques in Groundwater Hydrology 1974, Proc. Symp. IAEA Vienna, 1974, edited by: S.M. Freeman, Vol. 2, 51-60.

Genç, S., Akıncı, H. and Bilen, A., 1986, İznik-Uludağ (Bursa) arasında Kalan alanın jeolojisi, Maden Tetkik ve Arama Enştitüsü Ankara.

Giggenbach, W.F., 1988, Geothermal solute equilibria, Derivation of Na-K-Mg-Ca- geoindicators, Geochim. cosmochim. Acta, 52, 2749-2765.

Greber, E., 1992, Das Geothermalfeld von Kuzuluk/Adapazarı (NW-Türkei): Geologie, aktive Tektonik, Hydrogeologie, Hydrochemie, Gase und Isotope, Diss. ETH Zürich, Nr. 9984, 213.

Grisebach, U., 1841, Reise durch Rumelien und nach Brussa im Jahre 1839, Band 1, 361p. Bandenhoeck und Ruprecht, Göttingen.

Gürer, I., 1991, Kar erimesi ve akimi (Uludağ Örneği), Coğrafya Araştirmaları, sayı 3'den ayrıbasım, Ankara.

Hammer, J. von, 1818, Umblick auf einer Reise von Konstantinopel nach Brussa und dem Olympos und von da zurück über Nicäa und Nikomedien, Adolph Hertleben, Pesth, Wien, 200p.

IAEA, 1981, Stable Isotope Hydrology, Deuterium and Oxygen-18 in the Water Cycle, edited by: J.R. Gat and R. Gonfiantini, International Atomic Energy Agency Technical Reports Series 210, 339p.

Imbach, Th., 1992, Thermalwässer von Bursa: Geologische und hydrogeologische Untersuchungen am Berg Uludağ (NW-Türkei), PhD thesis ETH Zürich 9988, 178p.

Imbach, Th., 1997, Deep groundwater circulation in the tectonically active area of Bursa, Northwestern Anatolia, Turkey, Geothermics, Vol. 26, No. 2, 251-278

Jäckli, H., 1970, Kriterien zur Klassifikation von Grundwasservorkommen, Ecl. Geol. Helv. 63/2, 389-434.

Jackson, J.A. and McKenzie, D., 1988, The relationship between plate motions and seismic moment tensors and the rates of active deformation in the Mediterranean and the Middle East, Geophys. J.R. Astron. Soc. 93, 45-73.

Jeckelmann, Ch., 1996, Genese lokaler Thermalwasservorkommen in der Region Bergama/W-Türkei, Diss. ETH Zürich, Nr. 11990, 199p.

Kaya, O., Özkoçak, O. and Lisenbee, A., 1989, Stratigraphy of the Pre-Jurassic Blocky Sedimentary Rocks to the South of Bursa, NW Turkey, Bull Min. Res. Explor. Inst. Turkey, Foreign Edition 109, 15-24.

Kaaden, G. van der, 1959, Age Relations of Magmatic Activity and of Metamorphic processes in the Northwestern Part of Anatolia – Turkey, Bull. Min. Res. Explor. Inst. Turkey, Foreign Edition 52, 15-34.

Kaaden, G. van der, 1971, Basement rocks of Turkey, in: Geology and History of Turkey, edited by: A.S. Cambell, 191-207.

Ketin, I., 1947, Uludağ masifinin tektoniği hakkında (Über die Tektonik des Uludağ-Massivs), Türk. Jeol. Kur. Bült. 1, 61-88.

Ketin, I., 1966, Tectonic Units of Anatolia (Asia Minor), Bull. MTA 66, 23-34.

Ketin, I., 1984, Türkiye'nin bindirmeli-napli yapısında yeni gelişmeler ve bir Örnek: Uludağ Masifi, in: Proceedings on Ketin Symposium, Ankara, 20-21 February 1984, 19-36.

Kipfer, R., 1991, Primordiale Edelgase als Tracer für Fluide aus dem Erdmantel, PhD thesis ETH Zürich 9463, 223p.

Lisenbee, A.L., 1971, The Orhaneli Ultramafic-Gabbro Thrust Sheet and its Surroundings: A Progress Report, in: Geology and History of Turkey, edited by: A.S. Cambell, 349-368.

McKenzie, D.P., 1972, Active Tectonics of the Mediterranean Region, Geophs. J. Roy. Astron. Soc. 30, 109-185.

Mützenberg, S., 1991, Westliche Biga-Halbinsel (Çanakkale, Türkei): Beziehung zwischen Geologie, Tektonik und Entwicklung der Thermalquellen, Mitt. Geol. Inst. der ETH und der Univ. Zürich 287, 160p.

Okay, A.I., Siyako, M. and Bürkan, K.A., 1991, Geology and Tectonic Evolution of the Biga Peninsula, Northwestern Turkey, Bull. of the Technical University of İstanbul, 44/1,2.

Ozima, M. and Podesek, F.A., 1983, Noble Gas Geochemistry, Cambridge University Press, Cambridge, 367p.

Penck, W., 1918, Die tektonischen Grundzüge Westkleinasiens. Beiträge zur anatolischen Gebirgsgeschichte auf Grund eigener Reisen, Stuttgart, 21-55.

Plummer, L.N. and Busenberg, E., 1982, The solubilities of calcite, aragonite and vaterite in CO_2-H_2O solutions between 0 and 90°C, and an evaluation of the aqueous model for the system $CaCO_3$-CO_2-H_2O, Geochim. cosmochim. Acta, 46, 1011-1040.

Rathjens, C., 1952, Der Uludağ, Leben und Umwelt, 9, 66-72.

Sandison, D., 1851, Notice of the Occurrence of an Earthquake at Brussa, in: Proceedings of the Geological Society, Quart. J. Geol. Soc. Lond., 7/1, p19.

Sandison, D., 1855, Notice of the Earthquakes at Brussa, in: Proceedings of the Geological Society, Quart. J. Geol. Soc. Lond., 11, 543-544.

Schindler, C., 1993, The MARMARA Poly-Project – Tectonics and recent crustal movements revealed by space-geodesy and their interaction with the circulation of groundwater, heat flow and seismicity in Northwestern Turkey, Terra Nova 5/2, 164-173.

Schuling, R.D., 1959, Über eine prä-herzynische Faltungsphase im Kaz-Dağ Kristallin, Bull. Min. Res. Explor. Inst. Turkey, Foreign Edition, 53, 89-93.

Şengör, A.M.C., 1979a, The North Anatolian Transform Fault: Its Age, Offset and Tectonic Significance, J. Geol. Soc. Lond., 136, 269-282.

Şengör, A.M.C., 1979b, Mid-Mesozoic Closure of Permo-Triassic Tethys and its Implications, Nature 279, 590-593.

Şengör, A.M.C. and Yılmaz, Y., 1981, Tethyan evolution of Turkey: A plate tectonic approach, Tectonophysics 75, 181-241.

Şengör, A.M.C., 1985, Die Alpiden und die Kimmeriden: Die verdoppelte Geschichte der Tethys, Geol. Rd. 72/2, 181-213.

Şentürk, F., Bursalı, S., Omay, Y., Ertan, I., Güler, S., Yalçın, H. and Önhan, E., 1970, Isotope Techniques Applied to Groundwater Movement in the Konya Plain, in: Isotope Hydrology 1970, Proc. Symp. IAEA Vienna, 9-13 March 1970, 153-162.

Smith, J.L., 1851, On Some of the Thermal Waters of Asia Minor, Am. J. Sci. Art., second series 12, 10-16.

Straub, C., 1996, Recent Crustal Deformation and Strain Accumulation in the Marmara sea Region, N.W. Anatolia, inferred from GPS Measurements, PhD thesis ETH Zürich, 11614, 122p.

Straub, C. and Kahle, H.-G., 1994, GPS estimates of crustal deformation in the Marmara sea region, NW Anatolia, Earth Planet. Science Letters, 121, 495-502.

Straub, C. and Kahle, H.-G., 1995, Active Crustal deformation in the Marmara sea region, NW Anatolia, Inferred from GPS Measurements, Geophysical Research Letters 22/18, 2533-2536.

Stumm, W. and Morgan, J.J., 1981, Aquatic chemistry – an introduction emphasising chemical equilibra in natural waters, 2nd edition, Wiley-Interscience Publ., 780p.

Tchihatchef, P. de, 1887, Klein-Asien. Das Wissen der Gegenwart, Deutsche Universal-Bibliothek für Gebildete, 64.

Tekeli, O., 1981, Subduction Complex of Pre-Jurassic Age, Northern Anatolia, Turkey, Geology, 9, 68-72.

Truesdell, A.H., 1975, Summary of Section III. Geochemical Techniques in Exploration, in: Proc. 2nd U.N. Symp. Develop. Use Geothermal Resources, San Francisco, May 1975, 1, 1iii-ixiii.

Truesdell, A.H. and Hulston, 1980, Isotopic evidence on environments of geothermal systems, in: Handbook of isotope geochemistry, Vol.1, The terrestrial environment, edited by: P. Fritz and J.C. Fontes, Elsevier, Amsterdam, 179-225.

Yılmaz, Y., 1990, Allochthonous Terranes in the Tethyan Middle East: Anatolia and Surrounding regions, Phil. Trans. R. Soc. London, 331, 611-624.

Appendices

Sample name	Vak	Zey	Ipe	HavA	HavB	SigA
Sampling date	89-Sept-06	89-Sept-06	90-Sept-02	89-Oct-04	89-Sept-07	89-Sept-07
Sampling altitude [m a.s.l.]	220	220	220	160	150	170
Field analyses						
T [°C]	45.7	43.8	44.4	35.8	34.6	30.8
$EC_{25°C}$ [µS/cm]	541	538		537	568	531
Q [l/min]	960	198	270	120	60	
pH	6.7	7.1	7.0		7.0	7.7
Alc [mmol/l]	4.8	4.2	5.2		4.7	5.0
Aci [mmol/l]	0.8	1.1	0.8		1.3	0.7
O_2 [mg/l]	1.3	3.6	1.8		0.8	6.1
Cations [mg/l]						
Li^+	<0.1	<0.1	<0.1	<0.1	<0.1	<0.1
Na^+	35	32	35	30	28	29
K^+	5.6	4.6	6.5	4.9	4.8	6.1
Mg^{2+}	21	21	20	20	20	22
Ca^{2+}	65	66	64	75	77	62
Sr^{2+}	0.46	0.49		0.44	0.45	0.45
Ba^{2+}	0.10	0.11	0.11	0.10	0.09	0.10
Mn^{2+}	0.04	0.02	0.01			
Fe^{2+}	0.23	0.11	0.28			
Anions [mg/l]						
F^-	0.9	0.9	0.9	0.7	0.8	0.6
Cl^-	5.4	5.4	5.1	10.0	8.6	9.2
I^-	0.050	0.045		0.040	0.040	0.045
Br^-	<0.2	<0.2		<0.2	<0.2	<0.2
HCO_3^-	296	293	310	296	301	273
NO_3^-	0.2	0.2	<1.0	5.8	0.2	7.6
PO_4^{3-}	0,38	0.25	0.14	0.28	0.34	0.46
SO_4^{2-}	58	57	62	61	63	60
Balance						
Cations [meq/l]	6.63	6.49	6.52	6.82	6.79	6.32
Anions [meq/l]	6.28	6.20	6.57	6.55	6.54	6.16
Non dissociat. [mg/l]						
As	0.04	0.05		0.04	0.06	0.07
B	0.07	<0.07	0.10	0.05	0.05	0.14
Si	15.35	16.04	14.67	13.63	13.15	15.02
TDS [mg/l]	504	497	519	518	517	485
Environm. isotopes						
^3H [TU]	1.2±0.7	1.8±0.7	1.1±0.7	5.0±0.7	3.8±0.7	5.6±0.7
δ^2H [‰ SMOW]	-68.8±1	-67.9±1	-67.7±1	-68.2±1	-68.4±1	-65.1±1
$\delta^{18}O$ [‰ SMOW]	-10.75±0.15	-10.75±0.15	-10.59±0,15	-10.70±0,15	-10.71±0.15	-10.62±0.15
$\delta^{34}S$ [‰ CD] in SO_4	6.0	5.3				
$\delta^{18}O$ [‰ SMOW] in SO_4	6.8	6.0				
Noble gases						
^3He [cm^3/g]		$2.32x10^{-13}$	$8.35x10^{-13}$		$2.16x10^{-13}$	
^4He [cm^3/g]		$30.75x10^{-8}$	$118.2x10^{-8}$		$26.89x10^{-8}$	
^{20}Ne [cm^3/g]		$15.15x10^{-8}$	$24.75x10^{-8}$		$15.69x10^{-8}$	
$^{20}Ne/^{22}Ne$		9.73	9.72		9.79	

Appendix 1: Physical, chemical and isotopic data of the Çekirge thermal water.

Sample name	Bag	KükA	KükB	Muh	Oto	KarC
Sampling date	89-Sept-05	89-Sept-05	89-Sept-05	89-Sept-05	89-Sept-07	89-Sept-06
Sampling altitude [m a.s.l.]	130	140	140	130	110	110
Field analyses						
T [°C]	81.1	80.7	73.7	76.0	50.8	61.5
$EC_{25°C}$ [µS/cm]	1456	1460	1370	1400	1142	1110
Q [l/min]	270					
pH	6.5	6.3	6.5	6.5	7.0	6.8
Alc [mmol/l]	8.2	8.8	8.0	8.5	7.8	6.6
Aci [mmol/l]	2.2	4.7	3.0	4.1	2.1	1.7
O_2 [mg/l]	0.4	0.6	0.1	0.7	3.0	3.6
Cations [mg/l]						
Li^+	0.68	0.68	0.64	0.67	0.55	0.54
Na^+	220	223	210	218	198	185
K^+	22.8	23.0	22.8	22.8	20.0	19.0
Mg^{2+}	8	7	8	7	11	9
Ca^{2+}	90	92	90	93	84	77
Sr^{2+}	0.55	0.57	0.54	0.56	0.50	0.48
Ba^{2+}	0.07	0.07	0.07	0.07	0.05	0.05
Mn^{2+}	0.06	0.06	0.06	0.09	0.03	0.05
Fe^{2+}	0.52	0.28	0.62	0.68	0.04	0.05
Anions [mg/l]						
F^-	5.8	5.5	5.2	5.3	4.3	4.5
Cl^-	11.6	12.3	12.5	12.9	13.4	11.3
I^-	0.080	0.060	0.050	0.050	0.040	0.050
Br^-	<0.2	<0.2	<0.2	<0.2	<0.2	<0.2
HCO_3^-	531	529	516	534	468	449
NO_3^-	<0.08	0.6	<0.08	0.2	5.0	1.6
PO_4^{3-}	0.50	0.50	0.88	0.73	0.49	0.38
SO_4^{2-}	268	277	254	274	232	224
Balance						
Cations [meq/l]	15.45	15.59	15.02	15.45	14.31	13.21
Anions [meq/l]	14.93	15.10	14.40	15.13	13.22	12.62
Non dissociat. [mg/l]						
As	0.13	0.09	0.15	0.08	0.11	0.07
B	1.70	1.78	1.64	1.73	1.47	1.41
Si	45.37	46.37	43.29	45.57	39.36	39.00
TDS [mg/l]	1207	1220	1166	1217	1078	1022
Environm. isotopes						
^3H [TU]	0.9±0.7	1.1±0.7	2.2±0.7	1.6±0.7	4.5±0.7	4.1±0.7
δ^2H [‰ SMOW]	-72.3±1	-71.7±1	-72.1±1	-70.6±1	-70.8±1	-71.5±1
$\delta^{18}O$ [‰ SMOW]	-10.62±0.15	-10.49±0.15	-10.51±0,15	-10.15±0,15	-10.21±0.15	-10.32±0.15
$\delta^{34}S$ [‰ CD] in SO_4		13.9				
$\delta^{18}O$ [‰ SMOW] in SO_4		1.6				
Noble gases						
^3He [cm^3/g]			$1.19x10^{-13}$			$0.77x10^{-13}$
^4He [cm^3/g]			$17.9x10^{-8}$			$7.49x10^{-8}$
^{20}Ne [cm^3/g]			$4.89x10^{-8}$			$12.17x10^{-8}$
$^{20}Ne/^{22}Ne$			9.86			9.84

Appendix 2: Physical, chemical and isotopic data of the Kükürtlü thermal water.

Hydraulic level variations in a thermal water well: Impact of precipitation on the Çekirge thermal water system

EMIL GREBER, MARTIN PFISTER AND THOMAS IMBACH

Abstract

Hydraulic level measurements in a thermal water well were carried out in the Çekirge thermal water province of Bursa. The measurements cover two spring-summer seasons with limited precipitation and one autumn-spring season with abundant precipitation. During both dry and wet seasons, a general long-term decrease in hydraulic level was observed, which might be related to (1) the outflowing of a geothermal reservoir and/or (2) the vanishing effect of the shallow groundwater pressure on the total pressure of the geothermal system. This trend was interrupted by short-term increases, induced by heavy precipitation. Especially in the wet season, precipitation events led to marked peaks in hydraulic level with delays on the order of one to a few days. Long-term, stepwise and precipitation-independent increases in hydraulic level represent the recovering of the pressure field of the Çekirge geothermal system. This might be explained by complete filling of deeper subsurface cavities and/or joint systems.

Introduction

The Çekirge thermal water province in Bursa, consisting of several thermal springs and two thermal wells, is situated on the northern slope of Mount Uludağ. The geologic/tectonic and hydrogeological framework of this province is described in full detail by Imbach (1992, 1997 and this volume). For this reason, only the most relevant aspects of the system are mentioned in this paper. The altitude of the outflow zone is between 150 and 220m a.s.l., and that of the presumed recharge area between 1500 and 2100m a.s.l. The temperature range is between 30° and 45°C. Low tritium concentrations indicate bulk minimum residence times of 40 years. A limited mixing with shallow groundwaters is observed. The thermal springs flow out from fault-bounded Neogene, covered by young travertines.

At the end of April 1993, a gauge was installed in a 30m deep thermal water well in a walled garden located at the western upper margin of the Çekirge thermal spring province (Figure 1). Few data are available from the well. Neither core nor cutting descriptions exist. Furthermore, it is not clear if the aquifer is confined or not. The pressure is not artesian, as the water table is about 8 meters below ground level. During a 50 minute pumping test with a rate of 70l/min, the water temperature rose from an initial 19°C up to 29°C.

Measurements exist from three different periods: two spring-summer periods (26th April – 30th July 1993, 5th May – 20th July 1994) and one autumn-spring season (6th September 1993 – 26th March 1994). At the beginning of each measuring period, the gauge was set to zero. For this reason, the starting and ending levels of the three periods cannot be directly put into relation with each other. However, we know that the zero level for the first summer period (Figure 2) was 8.2m below ground level, whereas the zero level for the autumn-winter period was distinctly higher, at 7.3m below ground level (Figure 4). For the second summer period,

further information is missing. Relative level changes can be directly compared among the three periods and were measured with a relative precision of± 1-2cm.

Precipitation was measured at two stations, one on Mount Uludağ (1877m a.s.l.) and the other at the airport in the Bursa plain (100m a.s.l.). Most precipitation falls as rain or snow during the winter half-year (compare also with Imbach 1992).

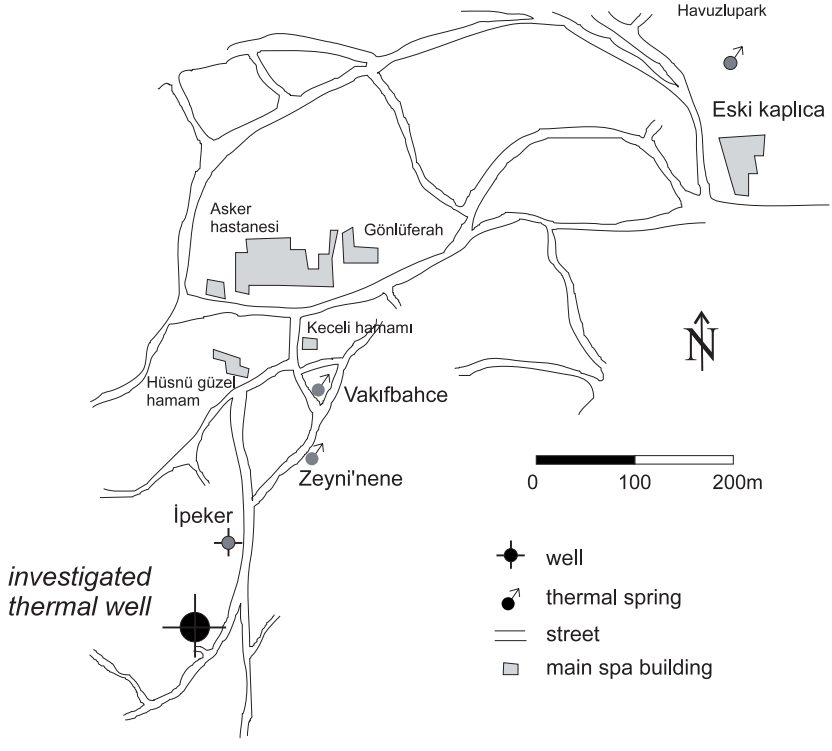


Figure 1: Geographic map of the Çekirge thermal spring area. The investigated thermal well is located at the western upper margin of the geothermal province. Compare also with Imbach (this volume, Figures 1 and 3)

As the main research activity of the Seismology group within the MARMARA Poly-Project was concentrated on the Bursa region, one principal aim of the gauge installation and observation was to record eventual hydraulic level changes of the geothermal water system coinciding with the deformation of the earth's crust and seismic signal behaviour. However, only minor seismic activity was detected over the time period of the project (Sellami et al. this volume). Therefore, no apparent influence of earthquakes on the thermal spring system of Çekirge was able to be observed at this stage.

Hydraulic level change behaviour

In the following, the three measurement data sets are described. For this purpose, they are separated into different intervals or sections of similar character or trend (notations in figures as A, B, C, A1, B1, C1 etc.). Distinct events are marked with numbers (e.g. 1-1').

Spring-Summer 1993 (26th April – 30th July 1993) (Fig. 2)

The level change curve can be divided into two main intervals, marked as A and B in Figure 2.

Interval A is characterised by a general decrease in level. This decrease is minor for periods of occasional precipitation (section A1) and steeper in times of missing precipitation (section A2). Section A3 represents a level decrease comparable with that of section A2, but is disturbed by considerable precipitation, especially on Mount Uludağ. The latter is responsible for a small but significant peak in hydraulic level (event 1), followed by an almost exponential decrease. The delay between maximum rainfall and the hydraulic peak is on the order of one day. It may be supposed that other smaller level peaks of interval A can also be attributed to brief times of precipitation.

In contrast to interval A, *interval B* is characterised by a general increase in level. This interval represents a three-step level increase (sections B1, B2 and B3). Each of these steps consists of a rather steep or rapid increase to a level maximum with a subsequent decrease. The strongest increase begins on 15th July and amounts to Δ36.4cm between 19th and 20th July (section B3). It should be stressed that interval B is a very precipitation-poor period. Of the two rainfall events, only one seems to induce a distinct peak in hydraulic level (event 2). Consequently, the general increase cannot be directly related to precipitation.

Spring-Summer 1994 (5th May – 20th July 1994) (Fig. 4)

Analogous to the Spring-Summer 1993 period described above, this gauge change curve can be divided into a long interval E with a general decrease, and a short interval F starting with a general increases in hydraulic level. The first interval E is superimposed on short-term increases clearly related to rainfall events.

Two main periods of heavy rainfall occurred during *interval E* (8th-13th May, event 7, and 7th-10th June, event 8, respectively). Section E1 represents a short period of gentle hydraulic level decrease. Then the first heavy rainfall led to a marked peak in hydraulic level (event 7), the time delay being on the order of three days. This peak is followed by a rather strong, roughly linear decrease in hydraulic level, interrupted by two intermediate peaks, which cannot be related to any rainfall events (section E2). The second, even heavier rainfall event (especially in Bursa with more than 40mm) led to a very strong and rapid increase in hydraulic level (event 8). This rather sharp peak is followed by a long and roughly exponential decrease (section E3). Two smaller rainfall events measured on Mount Uludağ might have led to the two small but sharp hydraulic level peaks in section E4.

Interval F began on 17th July with a strong increase in hydraulic level, some 20 days later in the summer than during the comparable interval B of the previous year. Unfortunately, the level measurements stopped on 20th July and therefore no additional information is available, however the measured increase is not related to any rainfall.

Autumn 1993-Spring 1994 (6th September 1993 – 26th March 1994) (Fig. 3)

The level curve of this more humid season can be divided into two intervals: C with a generally stronger decrease in hydraulic level and D with a weaker one. The mean level is about 1m higher than during the summer period of 1993! It is remarkable that this distinct rise in level happened during the dry months of July and August (compare also with interval B in Figure 2).

Interval C covers a time period with relatively little precipitation. The hydraulic level curve is characterised by a general decrease in hydraulic level, disturbed by several intermediate peaks. The first and most pronounced of these peaks might be related to precipitation ending on 8th September 1993 with a time delay of about one week (event 3). The shape of this peak is very sharp and is followed by a near-exponential decrease. The second, much broader peak might be attributed to precipitation between 30th September and 7th October (event 4). The last marked peak with a subsequent near-exponential decrease seems to be independent of precipitation (event 5).

The start of *interval D* is combined with heavy precipitation, which raises the hydraulic head to a distinctly higher level. The entire interval is characterised by frequent and abundant precipitation. The first three peaks in hydraulic level might be attributed to precipitation maxima, with time delays of one or two days (event 6). It should be stressed that both intervals C and D are characterised by distinctly higher frequencies than the spring-summer intervals. Even a different signal character between interval C and D is obvious; enhanced short-term fluctuations accompany frequent precipitation. The onset of the rainy season marks the boundary of the two intervals. The numerous single hydraulic level peaks can, in most cases, be related to precipitation events. However, the hydraulic level curve is not solely governed by precipitation, but shows a general trend towards a lower hydraulic level. A steep decrease in level is observed during diminishing precipitation (section D2).

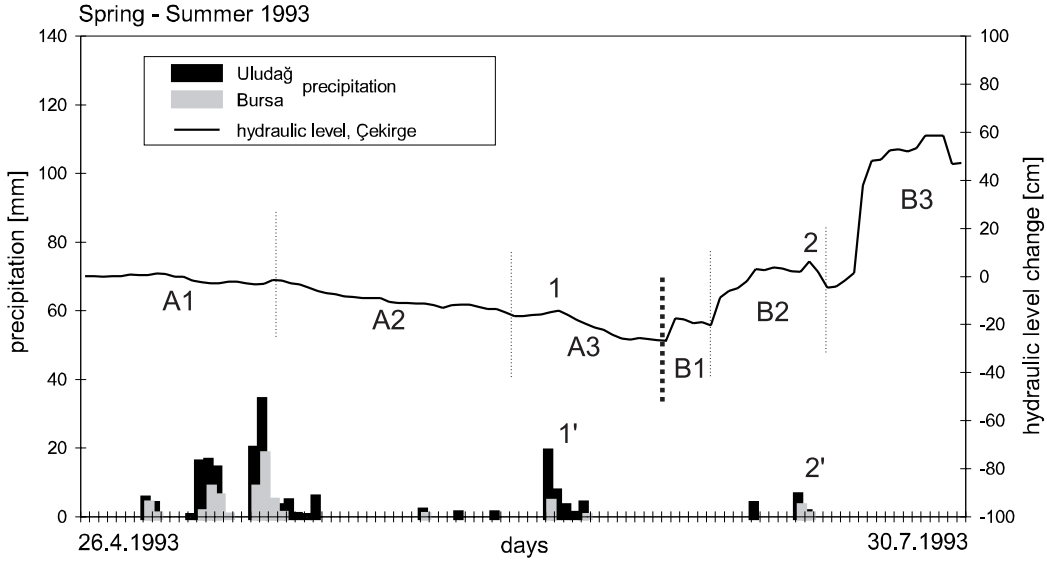


Figure 2: Hydraulic level and precipitation records during the time period Spring-Summer 1993 (26th April – 30th July 1993). The zero level was fixed at 8.2m below ground level, level changes are relative to this fixed point.

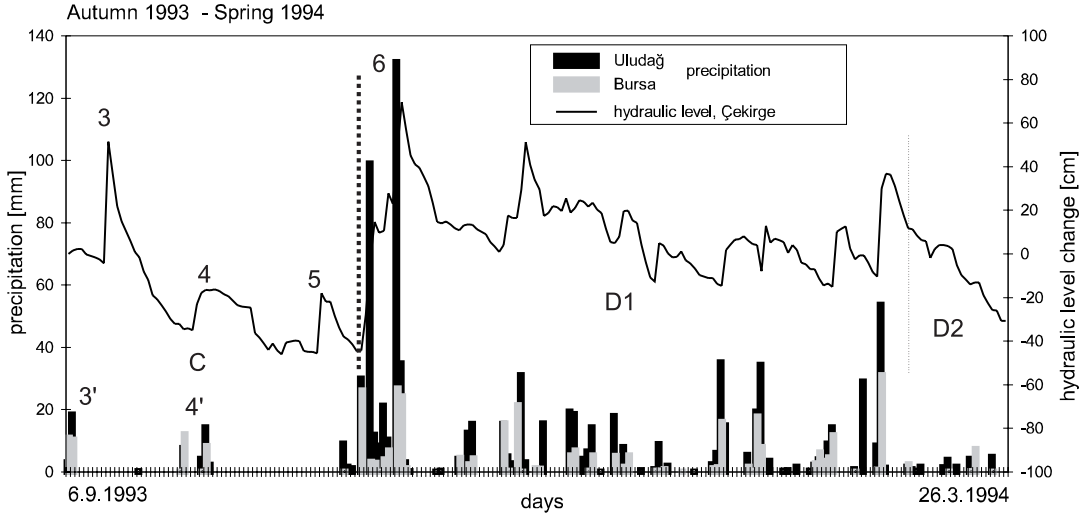


Figure 3: Hydraulic level and precipitation records during the time period Autumn 1993 – Spring 1994 (6th September 1993 – 26th March 1994). The zero level was fixed at 7.3m below ground level, level changes are relative to this fixed point.

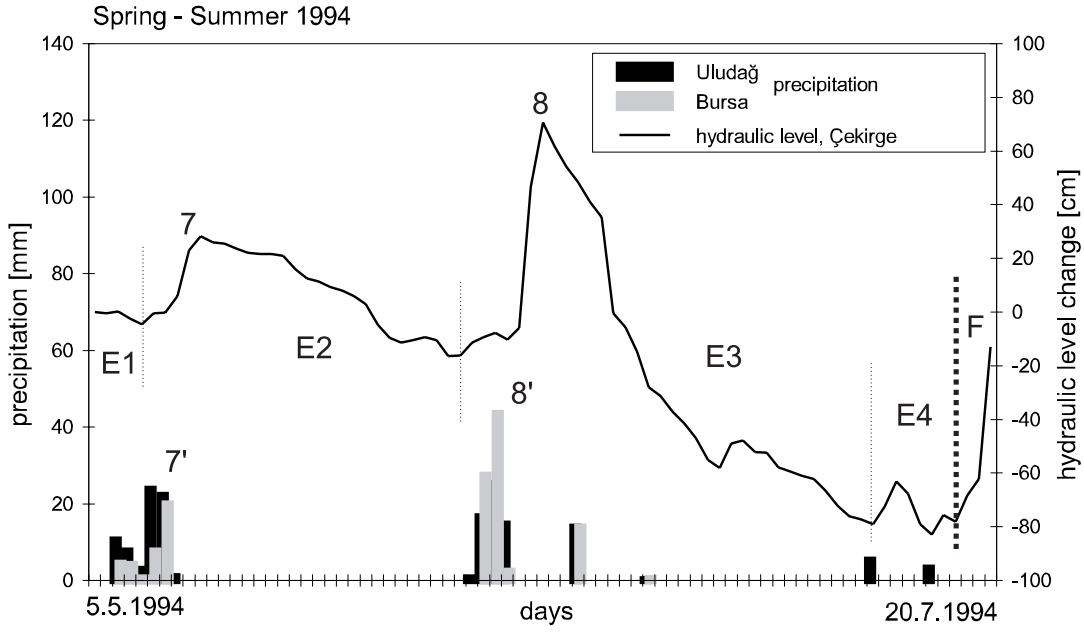


Figure 4: *Hydraulic level and precipitation records during the time period Spring-Summer 1994 (5th May – 20th July 1994). The zero level was fixed at a unknown depth below ground level, level changes are relative to this fixed point.*

Interpretation

A geothermal system is, without doubt, extremely complicated, and it is therefore difficult to explain the many observations made of hydraulic level time series, which describe only the final stage of the system, i.e. the outflow zone. Taking into account the long residence times of at least 40 years for the thermal water, we assume a smoothing effect on the seasonal recharge signature.

Obviously, there exists a relationship between precipitation and hydraulic level: heavy precipitation, measured either on Mount Uludağ or in the Bursa plain, results in hydraulic level peaks with time delays of between one and a few days. This phenomenon is especially evident in the rainy season, but can also be observed in the dry seasons. Furthermore, the hydraulic level is generally higher in rainy than in dry seasons. It can be argued that the precipitation-induced pressure waves have a positive effect on the outflow of the Çekirge thermal water. It is essential to realise that this effect can be explained without assuming mixing of the thermal water with a cold shallow groundwater (although the latter cannot be excluded).

The regional pressure field derived by 2D thermohydraulic modelling of the Bursa thermal spring system (Pfister 1995, Pfister et al. this volume) may be used to assist in understanding this phenomena: The short closed circulation system becomes important. Infiltration on Mount Uludağ is probably directly connected with the spring area by highly permeable zones, therefore an hydraulic pressure impulse due to precipitation on Mount Uludağ has a direct short-term influence on the thermal spring system (compare with Figure 15 in Pfister et al. this volume). Imbach (1992) detected a sudden temperature and electrical conductivity increase in the thermal water after heavy rainfall events in the Bursa and Mount Uludağ areas. But the response of the hydraulic level to precipitation shows different delay times, varying between

one and seven days. Effects of secondary porosity may trigger these delay times; cavities and/or joint systems must first be completely filled to enable the transmission of the initiated hydraulic pressure pulse.

Within this context, two main observations seem to be of special interest. First, the hydraulic level curve shows a general *long-term decrease* trend, which might be superimposed on occasional peaks induced by precipitation. Second, these long-term decrease trends are followed by *long-term increases* in hydraulic level, which cannot be directly related to precipitation.

Long-term hydraulic level decrease (wet and dry seasons, September – June)

The regional pressure field of the Çekirge geothermal system, which covers the whole area between the recharge and discharge areas and which is mainly influenced by the large altitude differences, loses more and more pressure. This might be explained by (1) the weakening impact of the shallow groundwater system on the geothermal system of Çekirge and/or (2) the outflowing of a geothermal reservoir.

Long-term increases in hydraulic level (only during dry seasons, July and August)

These periods seem to represent the recovering of the pressure field of the Çekirge geothermal system. Deeper in the subsurface, the suspected karstic cavities and joints are filled with water, which results in rising hydraulic level. The often step-wise character of the hydraulic level increases might indicate the existence of deep-lying interconnected karstic cavities and/or larger joint-rich zones serving as thermal water aquifers. The strong increases would thus represent the complete filling of such zones. Another explanation would be that of an impact by snowmelt. However, this effect would be expected some months earlier.

Conclusions

The regional pressure field of the Çekirge geothermal system is effectively influenced by the shallow groundwater system, which is directly influenced by the precipitation distribution. As a general rule, high water tables in the shallow aquifers enhance higher hydraulic levels in the observed thermal water well and thus probably facilitate the outflow of the thermal waters at the springs. In addition, a long-term effect is postulated representing the outflow and the recovery of the thermal system. It is not clear whether these long-term effects are related either to the impact of the shallow groundwater system or to some kind of reservoir behaviour and even a combination of these effects might be considered.

Acknowledgements

We would like to thank the local DSİ office for their continuous support during the field work and measuring period. Also, the local authorities permitted the access to this geothermal well. Finally, we thank Mrs. Gurtner for the work of digitising the field data.

References

Imbach, Th., 1992, Thermalwässer von Bursa: Geologische und hydrogeologische Untersuchungen am Berg Uludağ (NW-Türkei), Diss. ETHZ, Nr. 9988, 178p.

Imbach, Th., this volume, Geology of Mount Uludağ with emphasis on the genesis of the Bursa thermal waters, Northwest Anatolia, Turkey.

Imbach, Th., 1997, Deep groundwater circulation in the tectonically active area of Bursa, Northwestern Anatolia, Turkey, Geothermics, Vol. 26, No. 2, 251-278.

Pfister, M., 1995, Geothermische Untersuchungen in der Region MARMARA; Kartierung des Wärmeflusses und hydrothermale Modellrechnungen, Diss. ETHZ, Nr. 11054, 231p.

Pfister, M., Rybach, L. and Şimşek, Ş., this volume, Geothermal reconnaissance of the Marmara sea region.

Sellami, S., Pavoni, N., Mayer-Rosa, D., Mueller, St., Aktar, M., Eyidoğan, H., Gürbüz, C., Bariş, Ş and Yalcin, N., this volume, Seismicity and Seismotectonics of the Bursa region.

Hydrogeological investigation of the Gönen and Ekşidere thermal waters (NW Turkey)

TOLGA YALÇIN

Abstract

This hydrogeological investigation was carried out in and around the Gönen plain. Applications of stable isotope analyses of oxygen-18 and deuterium were used to study the origin of the Gönen and Ekşidere thermal waters together with the regional hydrogeology, chemical and gas composition of the water.

The investigation area is located in Gönen town of Balıkesir city, which is geographically in the Marmara region (NW Turkey) and geologically in the Sakarya zone of Pontides.

The Gönen thermal water has a temperature of 82°C and is chemically classified as a Na-SO_4-Cl-HCO_3 type. The Ekşidere thermal water has a temperature of 42°C and is chemically classified as a Ca-HCO_3 type.

The origin of both thermal waters is meteoric but the isotopic composition of the Gönen thermal water is related to old meteoric water (paleowater). The flow velocity of the Gönen thermal water was estimated by using the thermal profile and pressure-discharge test obtained from the thermal water wells. The isotopic composition of the sampled waters does not indicate a certain infiltration area but indicates cold climatic conditions during infiltration.

Introduction

Turkey is one of the areas richest in thermal water. Most of the thermal water resources have not been seriously investigated and their vast potential is, therefore, not very well known.

The Gönen geothermal region was selected for the investigation of the hydrogeologic conditions, the origin and the potential of the Gönen and Ekşidere thermal waters.

The Gönen thermal water is used for central heating and in spas. Approximately 1000 houses are heated by thermal water. The consumption of thermal water is around 50l/s. Gönen town is very active in domestic tourism due to the Gönen spa. The total bed capacity of the hotels is around 555. The use of the Ekşidere thermal water in the Ekşidere spa (Dağ Ilıcası) is developing but still limited.

The investigation area is located in Gönen town of Balıkesir city, geographically in the Marmara region, NW Turkey (Figure 1). The name of Gönen in antiquity was Artemea and the name of Gönen is derived from Germenon (Reman 1942). The center of the investigation area is the Gönen plain. The surface area of the plain (including the Sarıköy plain) is 187km^2 and its average altitude is 30m a.s.l. In the investigation area, the stream pattern was formed by the Gönen river (Aisepos) and its branches. The Marmara type climate prevails in the investigation area, which is a transitive climate between those of the Mediterranean and the Black seas. The annual average precipitation is 706mm and annual average temperature is 14.5°C.

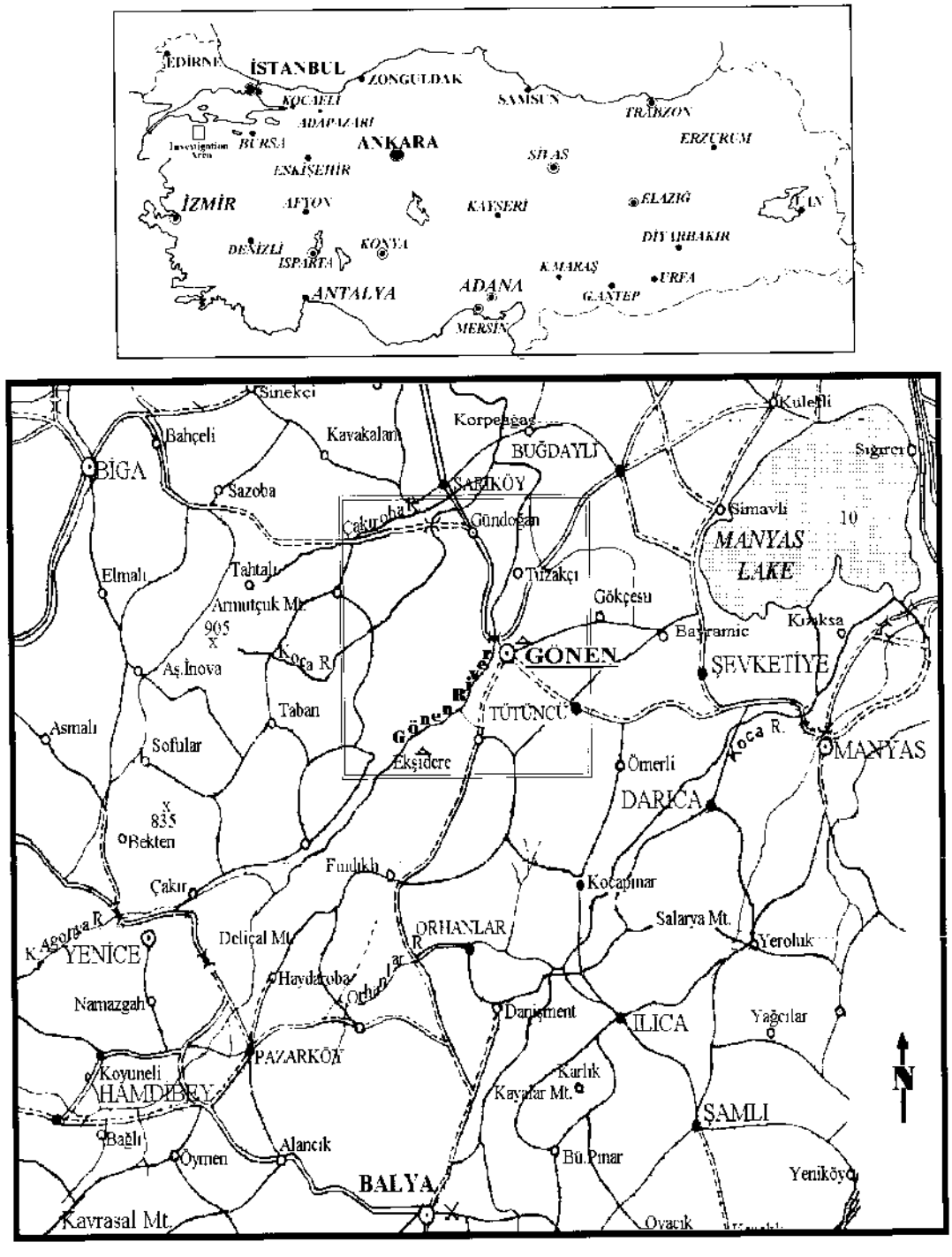


Figure 1: Location map of the investigation area.

The investigation consisted of geologic mapping to show geologic units, formation boundaries and major tectonic lines, and of collecting detailed hydrogeologic information. In-situ and laboratory works were carried out to determine the chemical, physical-chemical, gas and isotopic characteristics of the cold and hot waters. Samples of water for chemical, isotopic and gas analyses were collected from thermal water wells and hot and cold springs in different lo-

cations in and out of the investigation area. In the field, pH, electrical conductivity, Eh, temperature, alkalinity and acidity were measured. Chemical, isotopic and gas analyses were mainly carried out in Switzerland (laboratories of the ETH Zürich) and Germany (gsf, Neuherberg, Munich).

Geological setting

Stratigraphy

The stratigraphic sequence of the investigation area begins with the Karakaya complex. The Karakaya complex overlies the gneisses, amphibolites and marbles of the Kazdağ group outside of the investigation area (Okay et al. 1990).

The Karakaya complex crops out to the south of the Sarıköy plain (Figure 2). This unit was observed as an altered, foliated, green coloured sequence with an intercalation of marble and black chert, and identified as quartz-albite-muscovite schist, quartz-feldspar-muscovite schist (meta syenite porphyry) and metasiltstone (metatuff), according to thin section examinations. The Permian-aged limestone olistoliths of the Karakaya complex were exposed SE of the investigation area. The olistoliths are grey coloured and recrystallised limestone. The complex contains no fossils but Triassic age has been determined (Okay et al. 1990) based on results of regional tectonic considerations. The Karakaya complex is overlain unconformably by the Lower Jurassic-aged Bayırköy formation.

The Bayırköy formation was observed around Gündoğan, Hafızhüseyinbey and İncirli as a series of yellowish-brown-coloured, thin to thick-bedded, carbonate cemented conglomerate, sandstone, siltstone and marl. This formation is overlain by the Middle-Upper Jurassic-Lower Cretaceous aged Bilecik limestone.

The Bilecik limestone unit was observed around the villages of Hafızhüseyinbey, Dereköy, Çığmış, Babayaka, Akçapınar and İncirli, occurring as white-cream coloured, thick-bedded and oncolitic angular pebbly limestone at the base; black-light-brown coloured, medium-bedded and oolitic intercalated nodular (chert) sparitic limestone in the middle; and gray-black coloured, medium-bedded and micritic limestone at the top. This formation is overlain by the Upper Cretaceous-aged Vezirhan formation.

The Vezirhan formation was observed around Üçpınar as white, light-brown-coloured, thin to medium bedded, intensively fractured clayey limestone. The bottom of this formation was not seen in the investigation area, but this formation overlies the Bilecik limestone in several parts of the Biga peninsula (Okay et al. 1990). This formation is unconformably overlain by the Tertiary-aged deposits.

Miocene aged volcanic rocks, lacustine sediments and Quaternary-aged fluvial deposits were observed almost all over the investigation area. Lavas, commonly having andesitic composition, were dark gray and red-coloured and consisted of abundant plagioclase, biotite, pyroxene, amphibole and opaque microcrysts in a hylocrystalline porphyritic texture. In some places, feldspar minerals were extensively altered to form kaolin. Silicification and silicified zones were often observed. Tuffs were in the form of tuffite, sandy tuffite, agglomeratic tuffite and tuffaceous sandstone. They consisted of brownish-yellow, white and grey-coloured, commonly loose and sometimes compacted clay, silt, sand and tuff with plagioclase, biotite and amphibole crystals.

Lacustrine sedimentary rocks in the investigation area consisted of claystone with lignite, limestone, conglomerate, sandstone and marl. The volcanic, volcano-sedimentary and lacustrine sedimentary rocks are overlain by Quaternary-aged alluvium that was laid down by

the Gönen river and its branches. The thickness of the alluvium is generally 20m, but in some places reaches up to 100m. The total thickness of the Tertiary deposits is around 400m.

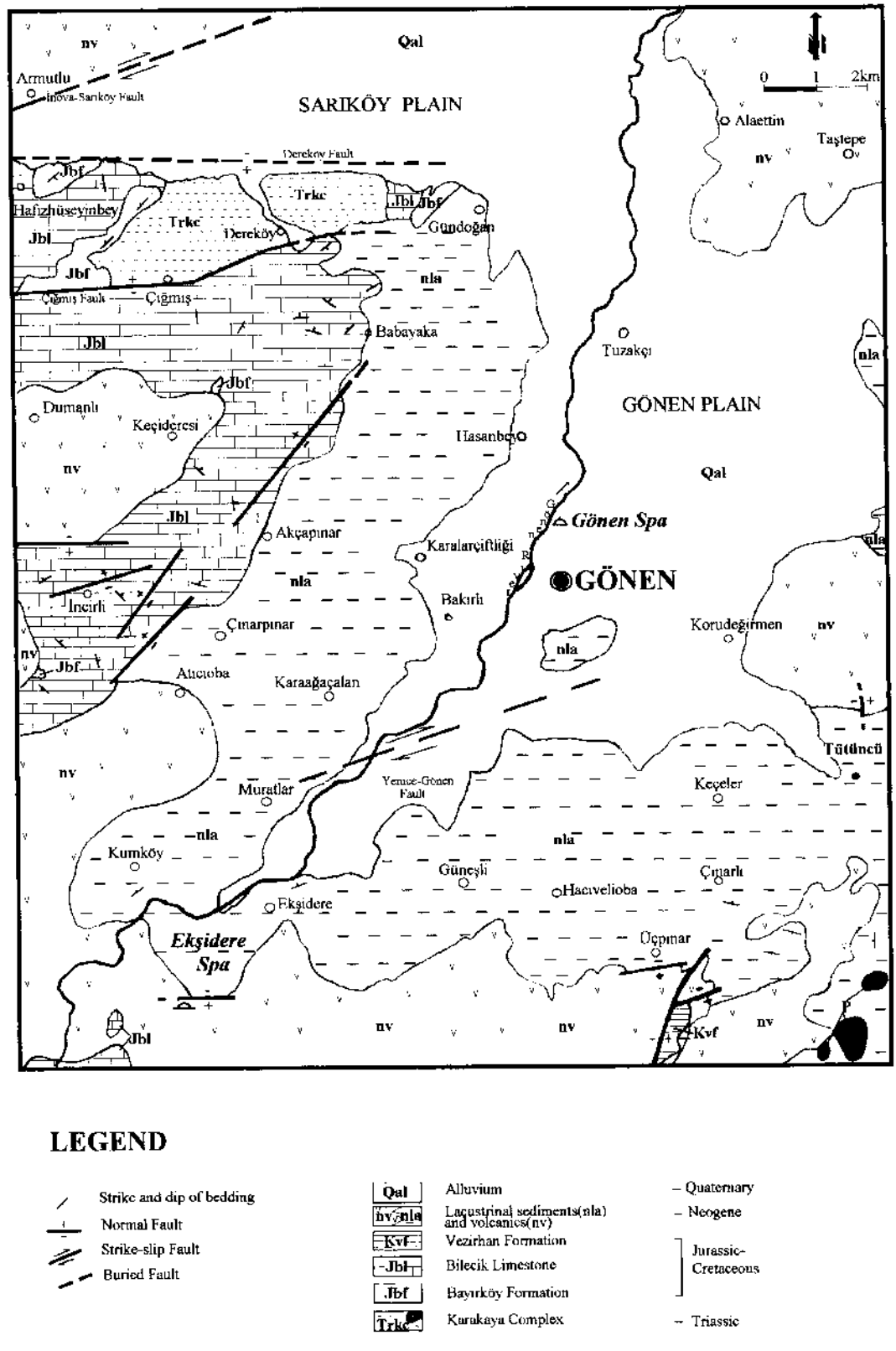


Figure 2: Simplified geological map of the investigation area.

Tectonics and structural features

Schistosity is observed in the Triassic-aged Karakaya complex which is metamorphosed in greenschist facies. Unconformities are seen among the Karakaya complex, the Bayırköy formation, the Bilecik limestone, the Vezirhan formation, the Neogene-aged units and the alluvium. The Bayırköy formation of Lower Jurassic age overlies the Karakaya complex transgressively and with an unconformity. The unconformity among the Bayırköy formation, the Bilecik limestone and the Vezirhan formation is a diastem. Gently folded structures are seen in the Jurassic-Lower Cretaceous-aged Bayırköy formation and Bilecik limestone. The evaluation of measured strikes and dips has yielded an average strike of fold axis of about 7NE, and a plunge of about 35NE. Generally flat-lying Neogene-aged sedimentary rocks display monoclines where the dips are locally steeper due to high angle faults in basement rocks.

The NE-SW oriented Sarıköy-İnova strike-slip fault forms the northern border of the Sarıköy plain. The Dereköy fault is an E-W oriented, buried, but easily interpreted as normal fault, that forms the southern border of the Sarıköy plain. The Yenice-Gönen strike-slip fault is located between Muratlar and Gönen, inside the investigation area and buried under the alluvium. The main features of this fault were examined by Ketin and Roesli (1953) after the earthquake which took place on March 18, 1953. The horizontal displacement was found 3.5-4m and the vertical displacement was 0.4-1m. The Ekşidere hot springs are located on a E-W striking normal fault between Neogene aged volcanic rocks and lacustrinel sediments. The main faulting in the investigation area is the western extension of the North Anatolian Fault Zone (NAFZ). The strike-slip faults move in a W-SW direction and E-W to NE-SW oriented normal faults form the graben, belonging to the Gönen-Bursa system, as a pull-apart basin (Herece 1990).

Seismicity

Gönen and its vicinity are a seismically active region that suffered serious structural damages and casualties during several recent earthquakes. The main cause of the earthquakes in this region is the movement of the NAFZ. The most destructive earthquake of recent years was the Yenice-Gönen earthquake that occurred on March 18, 1953. The intensity (I_0) of the earthquake has been determined as X in Gönen, the depth of focus has been calculated as 40-50km and the fault as a dextral strike-slip fault according to a focal mechanism solution (Eyidoğan 1991). Nearly 1750 earthquakes have been recorded for the period 1900-1990, between longitudes 26.0E-28.5E and latitudes 39.0N-40.5N. The list of earthquakes between 4.5 and 8.0 (M_S) is given in Table 1. Distribution of focal depths for the period 1986-1990 is given in Table 2.

Magnitude (M_S)	Number
4.5-5.0	22
5.0-5.5	23
5.5-6.0	16
6.0-6.5	14
6.5-7.0	7
7.0-7.5	0
7.5-8.0	3

Table 1: The number of earthquakes between 4.5 and 8.0 (Ms) occurring in the investigation area and its vicinity for the period 1900-1990 (H. Eyidoğan, pers. comm.).

Year	Number of earthquakes	non def.	0-2.5 km	2.5-5 km	5-7 km	7.5-10 km	10-12.5 km	12.5-15 km	>15 km
1986	208	21	3	11	10	49	4	1	1
1987	171	21	3	5	7	53	5	4	2
1988	144	29	5	8	6	45	3	2	2
1989	193	22	5	9	3	48	5	5	3
1990	106	4	8	15	12	45	3	5	8
Ave.	165	20	5	10	7	48	4	3	3

Table 2: Distribution of focus depths of the earthquakes occurring in and around the investigation area for the period 1986-1990 (data from H. Eyidoğan, pers. comm.).

Hydrogeological setting

Hydrogeological properties of the formations

The hydrogeological properties of the formations will be described in order from the oldest to youngest formations, in the area between Kazdağ mountain (or ancient Mount Ida) and Gönen.

The gneisses, amphibolites and marbles of the Kazdağ group which crop out around the Kazdağ mountain, outside of the investigation area, may be of importance for the occurrence of the Gönen thermal water. The solution channels and joints of marble should be sufficient to conduct water from the recharge area to Gönen. But there is still a question of whether the rocks of the Kazdağ group extend to Gönen or not. The opinion of A. Okay, who investigated the Biga peninsula in detail, is that the Kazdağ group is present under the Gönen region (pers.comm.). The Kazdağ group is supposed to be a poor aquifer.

The Karakaya complex that overlies the Kazdağ group is classified as a very poor aquifer due to its insufficient permeability. It is also relatively important for the occurrence of the Gönen thermal water, as its very low permeability acts as a caprock over the reservoir. But the huge limestone olistoliths of this unit become a second reservoir from which the Gönen thermal water is mainly exploited.

The Bayırköy formation has locally sufficient permeability to supply small quantities of water. The grains of this formation are generally tightly cemented, and, consequently, the permeability is low. The secondary porosity due to joints locally increases the permeability. This formation is classified as a local and individual aquifer.

From the Bilecik limestone, however, moderate quantities of water may be obtained locally. It yields moderate quantities of good quality water to springs, especially in areas where the limestone is karstified. Almost all of the important cold water springs in the investigation area yield from the Bilecik limestone. This formation is also classified as a local and individual aquifer.

The Neogene-aged sedimentary rocks are classified as poor and very poor aquifers. The data obtained from water well drillings indicate a specific capacity of less than 0.1l/s/m and hydraulic conductivity of about $2.3*10^{-6}$m/s. Fractured volcanic rocks which have specific capacity between 0.5-2l/s/m in drilled wells are classified as local and individual aquifer. The hydraulic conductivity is about $4.6*10^{-6}$m/s. The alluvia of the Sarıköy plain and the northern part of the Gönen plain are classified as a rich and extensive aquifer. The hydraulic conductiv-

ity of this aquifer ranges from $1.8*10^{-4}$ to $1.0*10^{-3}$m/s and its specific capacity is greater than 2l/s/m. Other alluvia of the plain are classified as poor and sometimes very poor aquifers according to pump tests obtained from water well drillings (unpublished DSİ records).

Water chemistry

Determinations of the temperature, pH, alkalinity, acidity, dissolved oxygen and electric conductivity (EC) were carried out in the field (Appendix 1), in order to avoid physical and chemical changes occurring with time. Analyses of anion and cation concentrations in the water samples were carried out in the laboratory (Appendix 2).

For classification purposes of the water resources, units of cation and anion concentrations were converted from mg/l to mval%, 100% referring to the equivalent sum of cations and anions, respectively. Cations and anions were sorted separately in descending order. Values of more than 10% were used for the classification. The ions found in the water samples of more than 50mval% are underlined and those of less than 20mval% are shown in parentheses. Table 3 gives the type of water according to the classification mentioned above.

Number of water sample	Type of water:
	Cold groundwater
S3	(Na) (Ca) Mg $\underline{SO_4}$ Cl
S4	$\underline{Ca}$ (Mg) $\underline{HCO_3}$
7933A	$\underline{Ca}$ Na Mg $\underline{HCO_3}$ Cl SO_4
7933B	$\underline{Na}$ $\underline{HCO_3}$ (SO_4) Cl
7471	$\underline{Ca}$ (Mg) Na $\underline{HCO_3}$
7473A	$\underline{Ca}$ (Na) Mg $\underline{HCO_3}$ (Cl) SO_4
7473B	$\underline{Ca}$ (Na) Mg $\underline{HCO_3}$ Cl
7469A	(Ca) (Mg) (Na) $\underline{HCO_3}$ (Cl)
7470A	$\underline{Ca}$ (Mg) Na $\underline{HCO_3}$ (Cl) SO_4
7470B	$\underline{Na}$ (Ca) (Mg) $\underline{HCO_3}$ (SO_4)
7475	(Mg) (Ca) Na $\underline{HCO_3}$ SO_4
7474A	$\underline{Ca}$ (Mg) Na $\underline{HCO_3}$ (Cl)
7474B	(Ca) (Na) (Mg) $\underline{HCO_3}$ SO4 Cl
Number of water sample	Typ of Water:
	Hot groundwater
G1	$\underline{Na}$ Ca (SO_4) (Cl) (HCO_3)
G2	$\underline{Na}$ Ca (SO_4) (Cl) (HCO_3)
G3	$\underline{Na}$ Ca (SO_4) (Cl) (HCO_3)
G4	$\underline{Na}$ Ca (SO_4) (Cl) (HCO_3)
S1	$\underline{Ca}$ (Mg) Na $\underline{HCO_3}$
S2	$\underline{Ca}$ (Mg) Na $\underline{HCO_3}$ Cl

Table 3: The classification of analysed water resources of the investigation area.

Geochemical modelling of the Gönen thermal water

Geochemical modelling based on equilibrium and irreversible thermodynamics is a well-recognised tool for understanding the process of water-rock interaction and predicting its consequences. For this purpose, a computer program, SOLMINEQ.88, was used in this study. This program computes the activity coefficients using Pitzer equations, pH and mineral solubilities. The principal computations carried out by this program are aqueous speciation and saturation states of minerals (Kharaka et al. 1988).

In-situ CO_2 concentrations of waters were found by acidimetric titration using 0.0227N NaOH to the phenolphthalein end point equal to pH≅8.3. An average of 14ml titrant were used for the titration procedure of Gönen (G1, G2, G3 and G4) samples and CO_2 concentrations were found to be 140mg/l (≈3.2mmol/l).

The program was used to compute ionic species and saturation indices (Figure 3, 4 and 5) of the Gönen thermal water at different temperatures and pressures. The first computation was carried out for 25°C and 0 bar pressure, reflecting the conditions of cooled thermal water. As a result of this computation, the cooled Gönen thermal water (sample G2) was found to be oversaturated in aragonite ($CaCO_3$), calcite ($CaCO_3$), chalcedony (SiO_2), cristobalite (SiO_2), dolomite ($CaMg(CO_3)_2$), quartz (SiO_2), and talc ($Mg_3Si_4O_{10}(OH)_2$) (Figure 3). As second computation was carried out for 82°C and 0 bar pressure and by adding the CO_2 lost to the concentration found by titration, reflecting the conditions of thermal water just before flowing out of the well. Under these conditions, the oversaturated minerals mentioned above become undersaturated, except for quartz (Figure 4). A third computation was carried out for 100°C and 100bars pressure with the CO_2 amount added previously, reflecting the conditions of thermal water at depth of 1km. Only dolomite becomes oversaturated and quartz is in equilibrium under these conditions (Figure 5).

The modelling helps to interpret the reason for low magnesium content in the Gönen thermal water while it cannot dissolve dolomite (or may precipitate from thermodynamic point of view) at depth. Due to the equilibrium with quartz at depth, the quartz geothermometer should give reasonable results for the computation of reservoir temperatures. Aragonite, which is one of the oversaturated mineral found by computations, was observed by the author around thermal water well drillings.

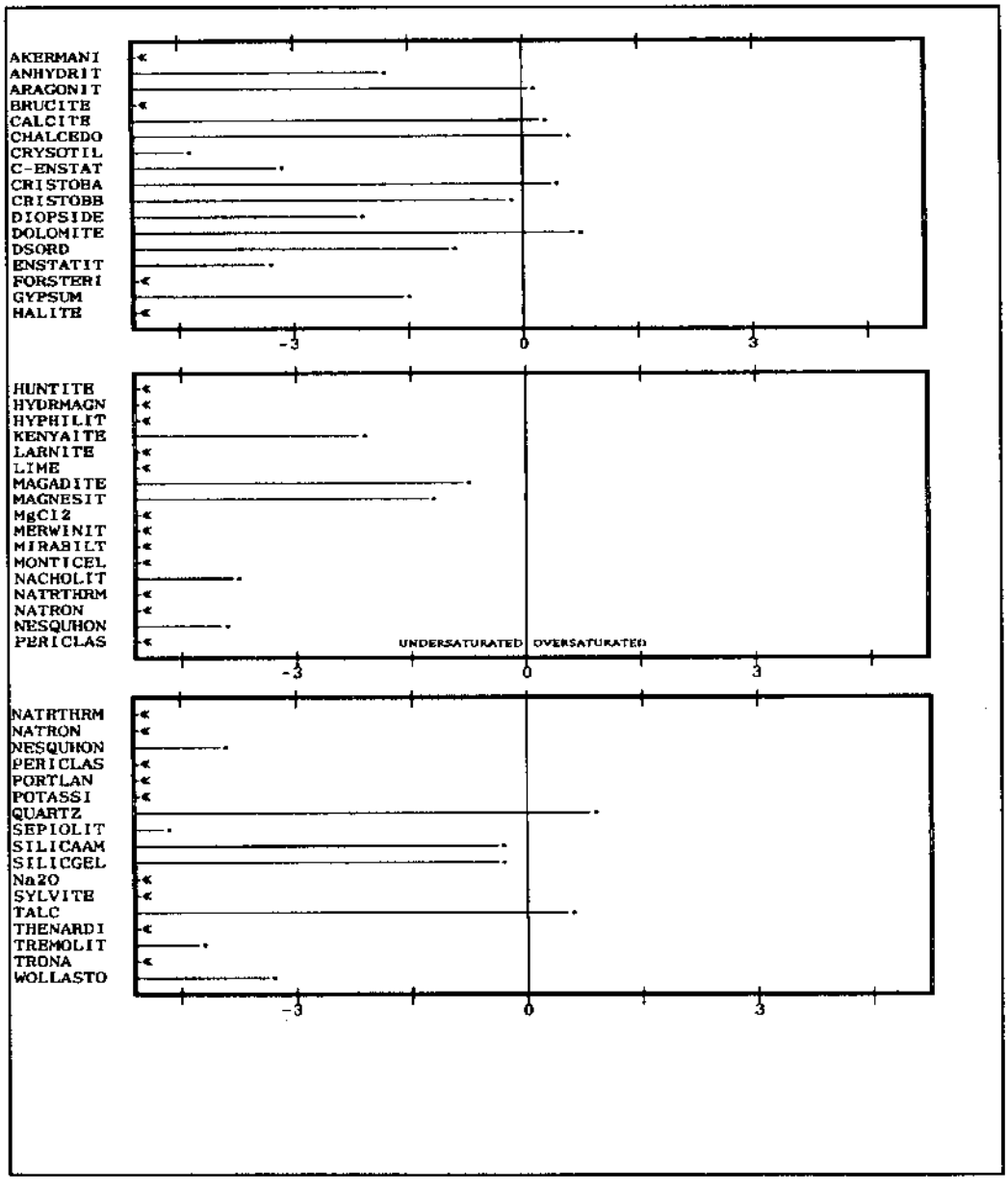


Figure 3: The saturation index plot of the Gönen thermal water at 25°C.

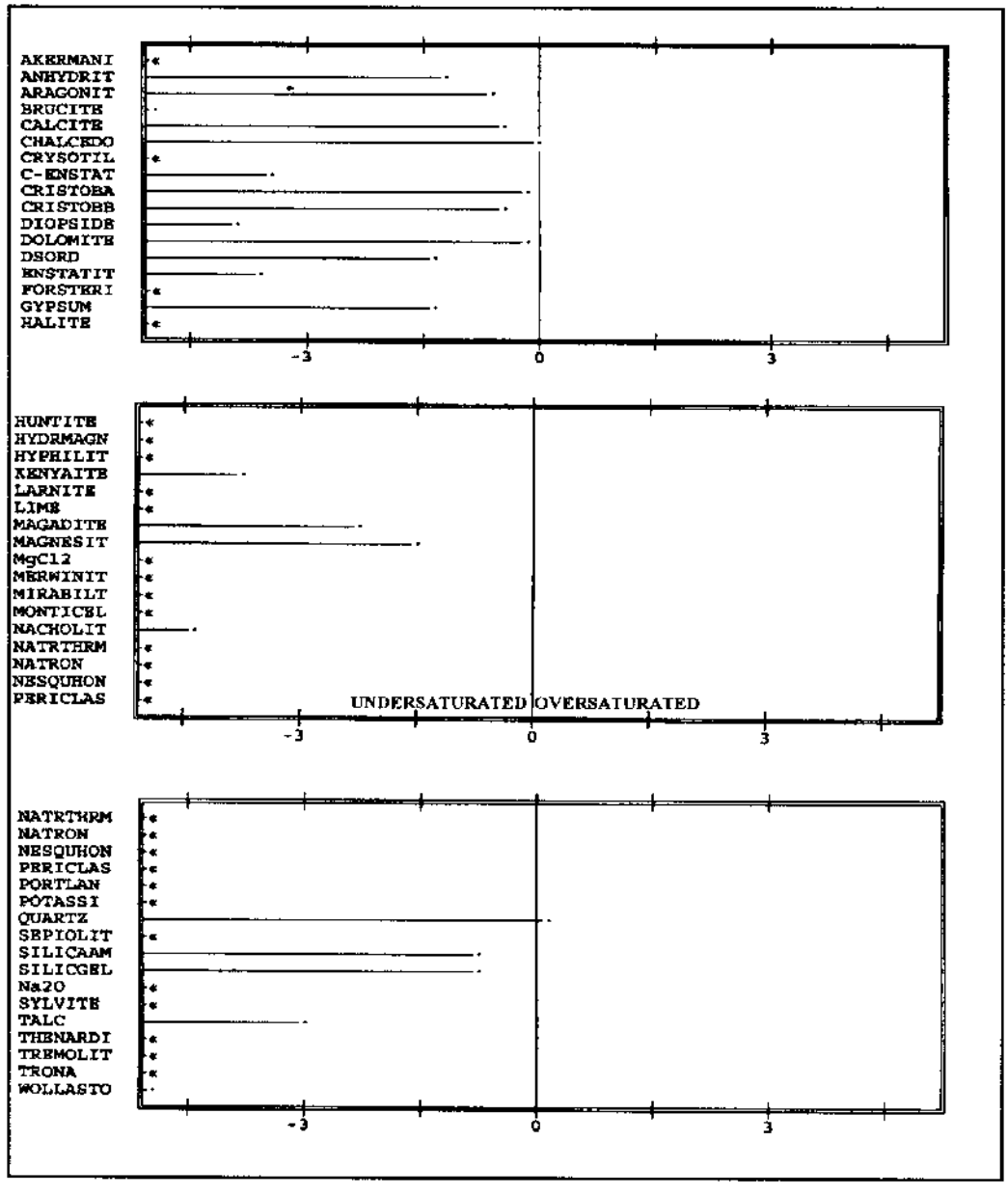


Figure 4: The saturation index plot of the Gönen thermal water at 82°C.

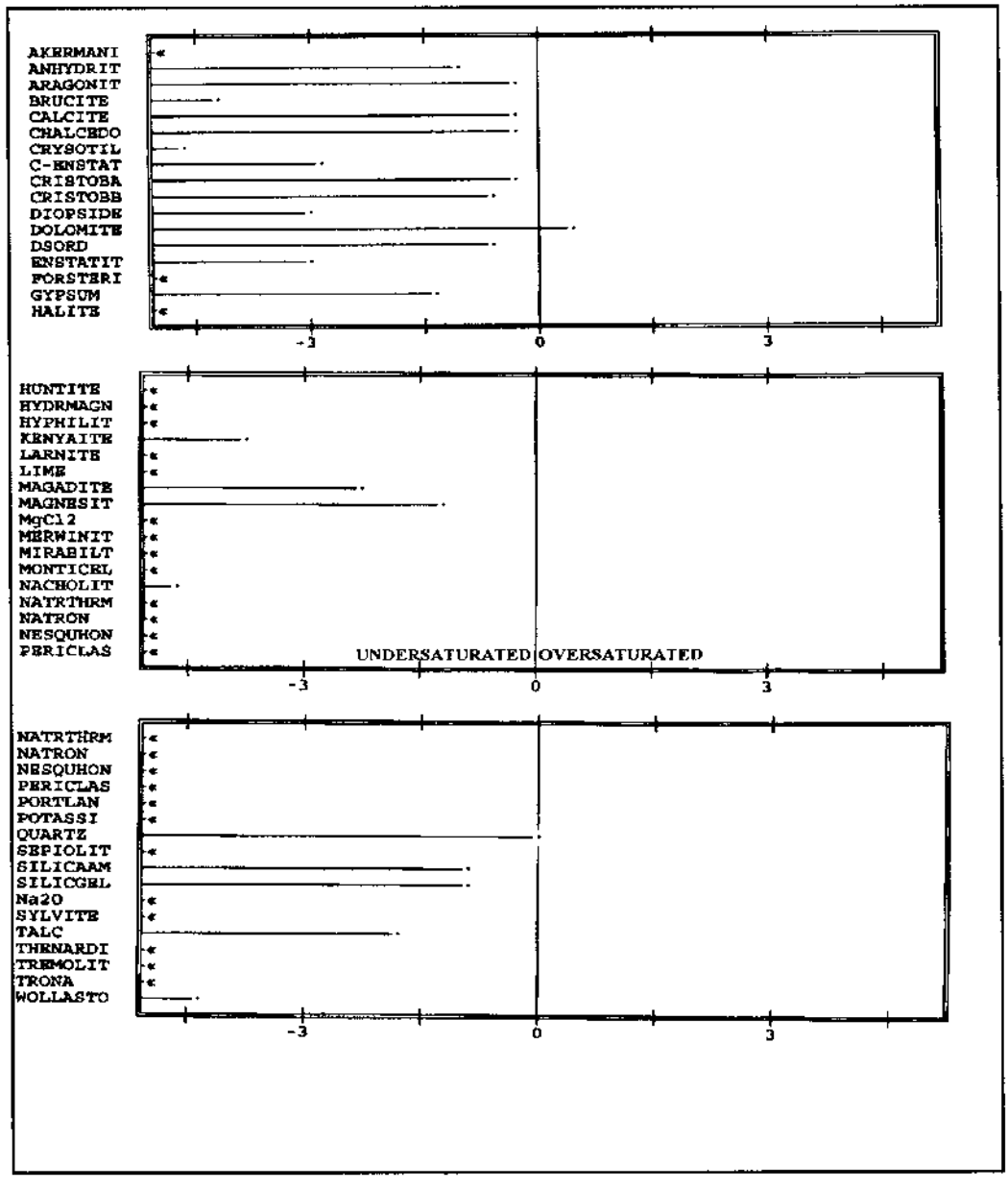


Figure 5: The saturation index plot of the Gönen thermal water at 100°C and 100bars.

Stable isotope composition of the sampled thermal waters

Oxygen and hydrogen isotope analyses are extremely useful in the study of the origin of thermal waters. Applications of stable isotope analyses of oxygen-18 and deuterium were used to study the origins of the Gönen and Ekşidere thermal waters together with regional hydrogeology, chemical and gas composition of the waters.

The water resources sampled for isotopic analyses in 1992 were S1, S2 (Ekşidere thermal waters), S3 (Gençlik suyu-acidic cold water), S4 (karstic cold spring), G2 (Gönen G2 thermal water well), G4 (Gönen G4 thermal water well) and Geyikli (acidic cold water near Geyikli village outside of the investigation area). The water samples from Gönen thermal water wells were found to be significantly lighter isotopically than other sampled waters. This difference has been the cause of sampling thermal waters extending to Kazdağ mountain. In 1994, thermal water samples were taken from G4, Hıd (Hıdırlar) and Top (Topaklar). Finally, in 1996,

samples were taken at different altitudes (1000-1700m a.s.l.) of Kazdağ mountain designated as GG (Gobaklıgediği), BK1 (Forester Hut 1), BK2 (Forester Hut 2), Toz (Tozlu), Kar (Kartalpınar) and from Kül (Külcüler thermal spring) near Kazdağ mountain. The locations of sampled waters are shown in Figure 6 and their isotopic compositions are given in Appendix 3.

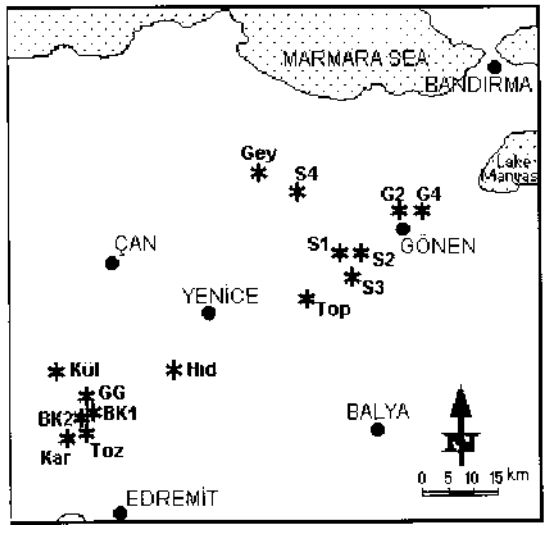


Figure 6: *Location map of sampled water resources for isotopic analyses. (Gey-Geyikli spring, Top-Topaklar thermal water, S1 and S2-Ekşidere thermal water, S3-Gençlik suyu spring, Kar-Kartalpınar spring, Toz-Tozlu spring, BK1 and BK2-Forester hut springs, GG-Gobaklıgediği spring, Kül-Külcüler thermal water).*

Gas composition of the Gönen and Ekşidere thermal waters

Gases dissolve in water in quantities varying with the nature of the gas, the temperature and the pressure. During infiltration, the water generally attains equilibrium with the air and dissolves atmospheric gases at the recharge area in the aeration zone of soil. Some gases of metamorphic and mantle origin may be dissolved in water during deep circulation. The samples were collected in August 1992 and the analyses were carried out at the Paul Scherrer Institute in December 1992. Table 4 gives the CH_4(methane), N_2(nitrogen), O_2(oxygen), Ar(argon) and CO_2(carbon dioxide) concentrations of the Gönen and Ekşidere thermal waters. Nitrogen and carbon dioxide predominate in these waters.

Nr		CH4		N2		O2		Ar		CO2	Total gas volume
	mg/kg	Vol%	mg/kg	Vol%	mg/kg	Vol%	mg/kg	Vol%	mmol/kg	Vol%	cm^3/kg
G2	0.79	1.53	39.8	44.1	-	-	1.00	0.78	1.7	53.6	72.1
G4	0.65	1.19	40.0	42.3	2.70	2.50	0.96	0.71	1.8	53.3	75.7
S2	-	-	16.0	42.0	1.82	4.20	0.56	1.04	0.7	52.7	30.4
Air (s.l.)		$2*10^{-4}$		78.8		20.9		0.9		0.03	

Table 4: *Gas concentrations of the Gönen and Ekşidere thermal waters and volumetric composition of air at sea level.*

The origin of the Gönen and Ekşidere thermal waters

At present, almost no problem concerning the origin of groundwater can be solved without the use of environmental isotope determinations.

The isotopic composition of present-day surface waters are well known and lies on a ”meteoric water line” that can be described by the general equation:

$\delta^2H = x*\delta^{18}O + d$

where the value of x is equal to 8 in all meteoric waters if it is not under the effect of evaporation, but the d parameter, which is described as deuterium excess, is equal to 10 in global and central Anatolian meteoric waters, 22 in eastern Mediterranean meteoric waters, 16 in Marmara meteoric waters (Eisenlohr 1995) and 1.2 in paleoclimatic waters (Moser et al. 1983).

The isotopic composition of the sampled waters is plotted on δ^2H -$\delta^{18}O$ diagram, where global and central Anatolian, eastern Mediterranean, Marmara and paleoclimatic water lines are also drawn (Figure 7). The samples of the Ekşidere thermal water (S1 and S2), the karstic spring (S4), Gençlik Suyu(S3) and the Hıdırlar thermal water (Hıd) are related to local meteoric water because their isotopic composition lies close to the Marmara meteoric line. The samples of the Topaklar thermal water (Top) and the Geyikli acidic spring (Gey) lie in-between the global and central Anatolian and Marmara water lines. The isotopic composition of the samples mentioned above lie in-between meteoric lines and their origin is certainly meteoric, therefore.

The meteoric water results from rain, snow and bodies of surface water that percolate in the rocks. The majority of the meteoric waters are generally recharged at high elevations in the margins of the basins. Recent evidence from stable isotope ratios of water indicates that meteoric water can percolate to great depths (up to 10km) in geothermal systems (Kharaka and Carothers 1986) and their circulation time may exceed thousands of years. This type of water is called old meteoric water.

The δ^2H content of the Gönen thermal water is the lowest among the sampled waters. The δ^2H and $\delta^{18}O$ composition of the Gönen thermal water is related to old meteoric water. Depleted δ^2H and $\delta^{18}O$ values indicate cold weather and/or higher recharge altitudes.

The isotopic composition of most deep geothermal waters is related to that of the local meteoric water but does not lie on the meteoric water line as they are usually enriched in ^{18}O. The $\delta^{18}O$ shift (Figure 7) in the Gönen thermal water is due to isotopic exchange that occurs between water and minerals at elevated temperatures (water-rock interaction). In waters,$\delta^{18}O$ shifts are more common than δ^2H shifts because hydrogen atoms are rarely found in minerals. The magnitude of oxygen isotope shift depends on the mineralogy of the rock, the temperature, the water/rock ratio and the time of contact. During circulation, the Gönen thermal water was shifted by +1‰ in ^{18}O composition by high temperature exchange with rock.

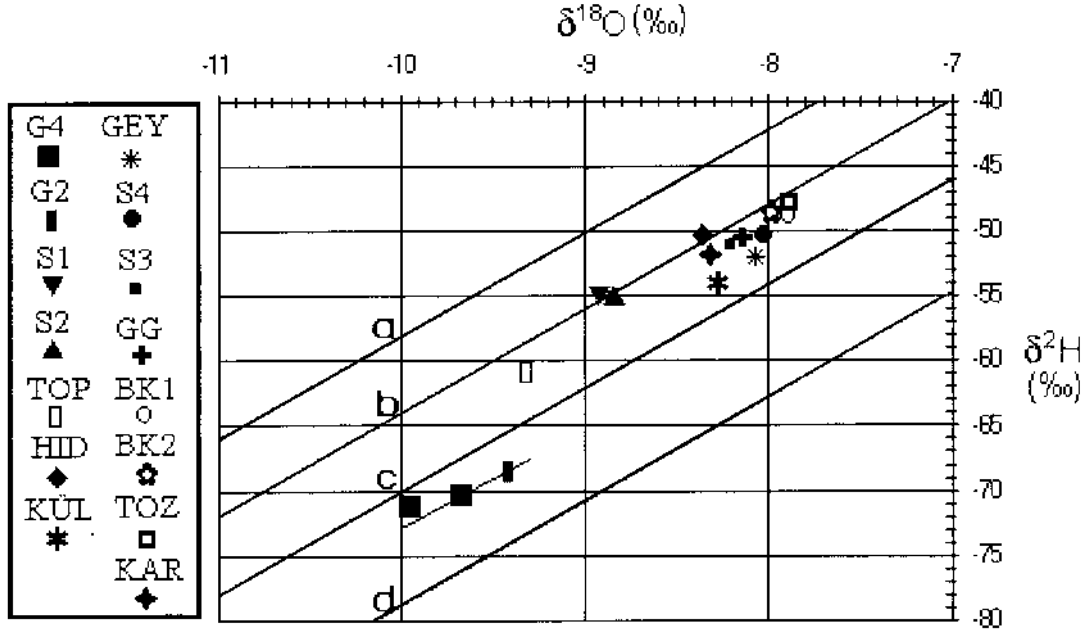


Figure 7: *The δ^2H -$\delta^{18}O$ plot of sampled waters. a) eastern Mediterranean δ^2H(‰) =8*$\delta^{18}O$+22, b) Marmara meteoric water line δ^2H(‰) =8*$\delta^{18}O$+16, c) global and central Anatolia meteoric water line δ^2H(‰) =8*$\delta^{18}O$+10, d) paleoclimatic water line δ^2H(‰) =8*$\delta^{18}O$+1.2).*

Recharge temperature and recharge area of the Gönen and Ekşidere thermal waters

The solubility of Argon in water is strongly temperature dependent. In other words, recharging water gets the temperature information when it equilibrates in the saturated zone. The recharge temperature of water can be found by using temperature dependent solubility of Argon (Mazor 1991). The Argon concentration of the Gönen and Ekşidere thermal waters is given in Table 5.

Sample Nr	Ar, in mg/kg	Ar, in cc_{Ar}/cc_{water}
G2	1.00	5.6×10^{-4}
G4	0.96	5.4×10^{-4}
S2	0.56	3.1×10^{-4}

Table 5: *Argon concentration of the Gönen and Ekşidere thermal waters.*

In order to compute the ambient temperature (or paleotemperature) in the water-recharge zone, the solubility diagram of atmospheric argon was used (Figure 8). The solubility of Ar in Figure 8 is given for 760mm Hg or at sea level. The recharge of the water should be at higher altitudes and a correction factor must be used before using Figure 8. The correction factor to sea level is given in Figure 9.

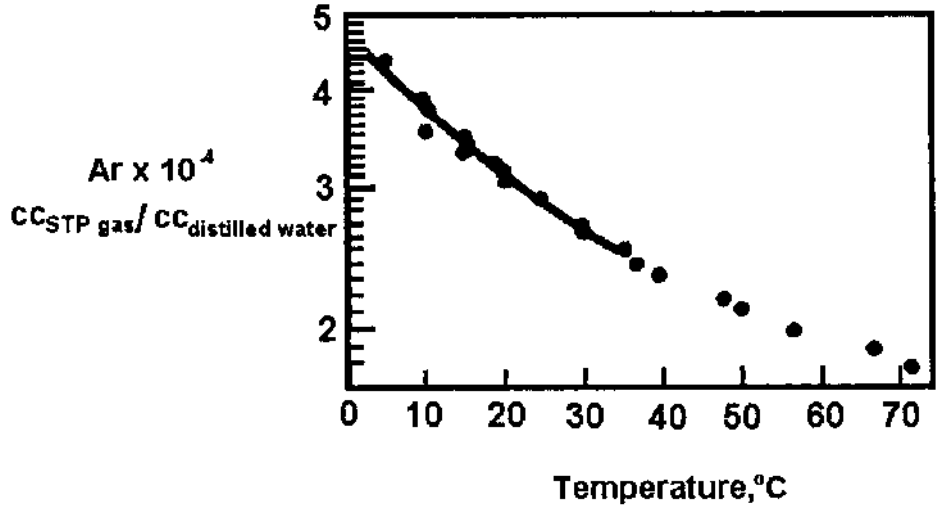


Figure 8: Solubility of atmospheric argon in fresh water at sea level, as a function of the ambient temperature (Mazor 1991).

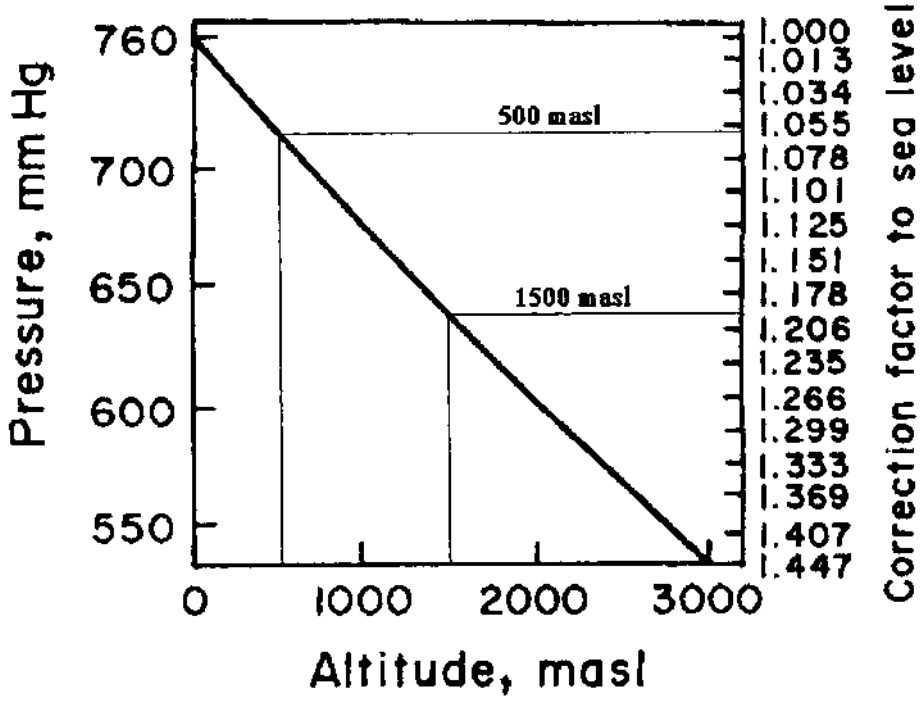


Figure 9: Atmospheric pressure variations as a function of altitude. Correction factor on the right axis serves to convert solubility values at sea level to values at desired altitude (dividing by the factor) or to normalise data at a given altitude to the corresponding value at 0m a.s.l. (multiplying by the factor) (Mazor 1991).

In the water samples of the Gönen thermal water, 5.4-5.6*10^{-4} cc_{Ar}/cc_{water} was found. The altitude selected was 1500m a.s.l. (considering Kazdağ mountain as the possible recharge area) and a correction factor of 1.19 was found from Figure 9. The Ar concentrations were divided by 1.19 and 4.7*10^{-4} cc_{Ar}/cc_{water} was calculated as an average value for 760mm Hg.

From Figure 8, the ambient temperature (or paleotemperature) at the water recharge zone was found to be about 0°C.

For the computation of ambient temperature at the water recharge zone for the Ekşidere thermal water the Ar concentration ($3.1*10^{-4}$ cc_{Ar}/cc_{water}) was divided by 1.055 (the altitude selected was 500m a.s.l.) and $3.0*10^{-4}$ cc_{Ar}/cc_{water} was found. The ambient temperature was found to be 23°C from Figure 8. This temperature is 10°C higher than the actual mean annual temperature of Gönen.

The recharge area of the Gönen thermal water might be Kazdağ mountain, which is the only area of high elevation around the Gönen thermal water. As the clouds move on into the continent or up a mountain, the produced rain becomes progressively depleted of the heavy isotopes. But isotopic compositions of the sampled waters (GG, BK1, BK2, Toz and Kar) from different elevations do not show a significant trend with respect to altitude. The stable isotope contents of young cold waters are almost the same over the whole area. Because of this result, it is not possible to define the recharge area as a function of altitude. The origin of depleted deuterium can only be explained by cold weather because the ambient temperature at the recharge zone was found to be about 0°C using argon concentration.

A trend was found in chlorine content and electrical conductivity among samples from Gönen, Topaklar, Hıdırlar and samples of Kazdağ (GG, BK1, BK2, Toz and Kar) as a function of distance from Kazdağ mountain (Figures 10 and 11). This trend indicates that chlorine concentration and electrical conductivity increase along the flow path from Kazdağ mountain to Gönen. Figure 12 shows that waters containing low chlorine and high deuterium, such as Hıdırlar (Hıd), Külcüler (Kül), Ekşidere (S1 and S2) and cold waters, indicate actual recharge conditions. In this case, Hıdırlar and Külcüler should be close to their recharge areas, which are also close to Kazdağ mountain.

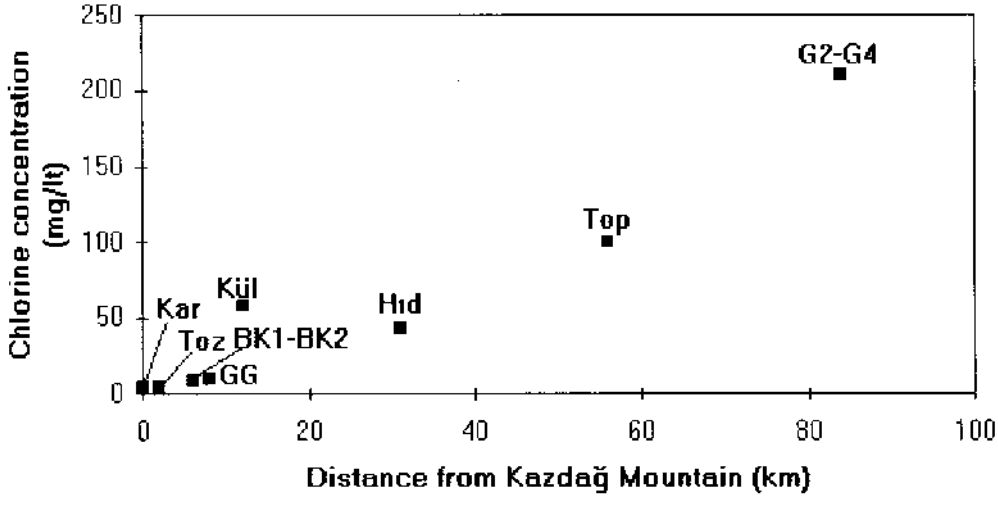


Figure 10: Plot of chlorine concentration versus distance from Kazdağ mountain.

The Ekşidere thermal water is different in temperature, chemical and isotopic composition from the Gönen thermal water. Its chemical composition ($CaHCO_3$ Type) and temperature (28.1-42.8°C) point to a shallow circulating system rather than to a deep circulating system. The ambient temperature found from argon concentration (23°C) indicates a warmer climate.

As a result, the recharge area of the Ekşidere thermal waters can be thought to be the hills seen at the southern edge of the thermal waters, where the average altitude is around 500m a.s.l.

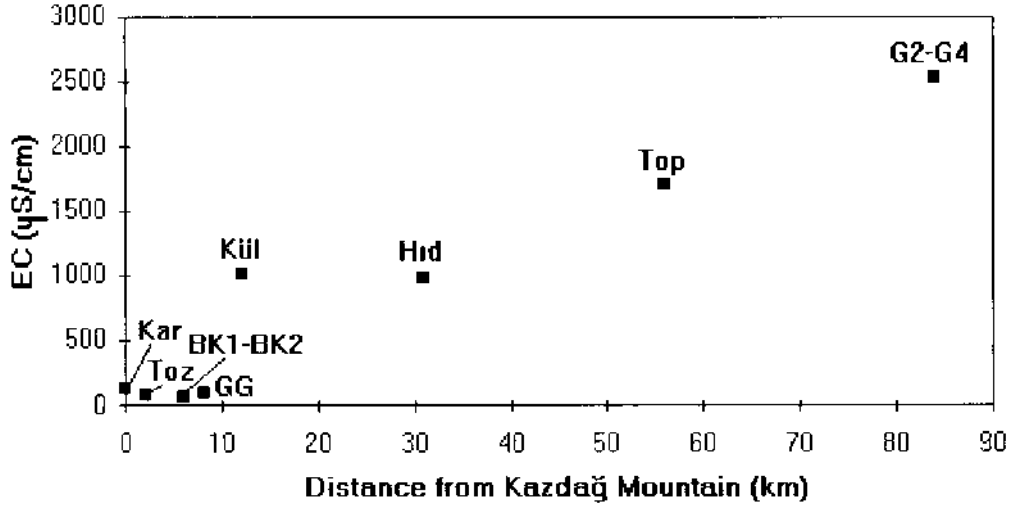


Figure 11: Plot of electrical conductivity versus distance from Kazdağ mountain.

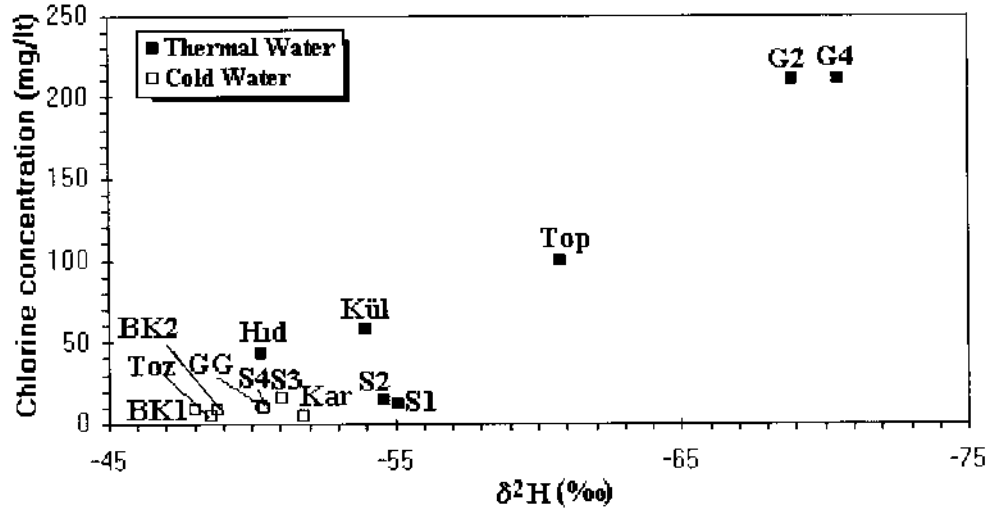


Figure 12: Plot of deuterium versus chlorine content.

Flow velocity and transit time of the Gönen thermal water

The best method to calculate the age or the transit time of water is the ^{14}C isotopic measurement method within 40,000 years. If the recharge area is known then the calculation of flow velocity is also possible.

The samples for ^{14}C isotopic age determination were collected from the Gönen, Hıdırlar and Topaklar thermal waters. A 30 liter carboy was used to precipitate CO_2 as $BaCO_3$ by using a saturated BaOH solution. The uncorrected age of Gönen thermal water is 23,000 years and that of Hıdırlar thermal water is 16,500 years according to ^{14}C and $\delta^{13}C$ values.

The tritium (^3H) concentration of water gives age information within 40 years. Tritium is the radioactive isotope of hydrogen. The concentration of tritium (^3H) in water is expressed by the ratio of ^3H atoms to ^1H atoms; a ratio of $^3H/^1H=10^{-18}$ is defined as 1 tritium unit (1TU). The tritium concentrations of all sampled waters are given in Appendix 3. All of the sampled thermal

waters have tritium concentrations below the detection limit. This indicates that the sampled thermal waters are at least older than 40 years.

An attempt was made to estimate the velocity of the thermal water by using a thermal profile (or temperature log) of the G4 thermal water well. The detailed temperature measurements in the well were carried out by MTA after completion of the drilling (Erzenoğlu and Uluşahin 1990). The temperature log of the G4 thermal water well is given in Figure 13.

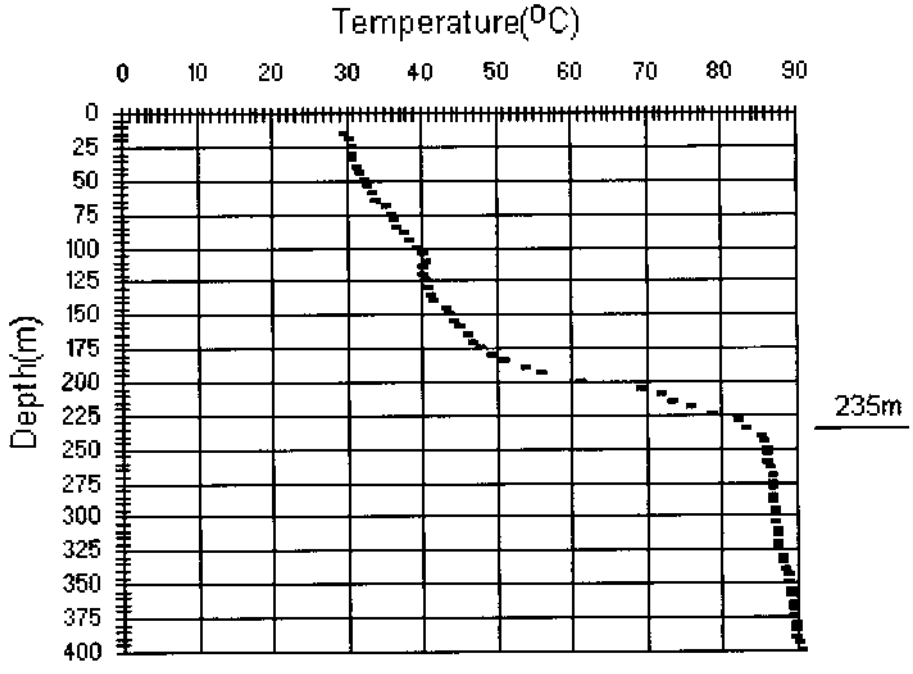


Figure 13: Temperature log of G4 thermal water well drilling.

The velocity estimation method using temperature logs obtained from thermal water wells is described in Dumlu and Yalçın (1991) according to the theory of Bredehoeft and Papadapulos (1965). They developed an analytical solution to estimate the rate of vertical groundwater movement by using thermal profiles. They used the following formula for heat and fluid which flows through an isotropic, homogenous and fully saturated porous medium:

$$\frac{\partial^2 T}{\partial z^2} - \frac{c\delta v}{K} \cdot \frac{\partial T}{\partial z} = 0$$

For boundary conditions $T_z=T_0$ at z=0 and $T_z=T_L$ at z=L the equation can be solved as (Bredehoeft and Papadapulos 1965):

$$f\left(\beta, {}^{z}\!/_{L}\right) = \frac{T_z - T_0}{T_L - T_0} = \frac{1 - e^{\frac{-\beta z}{L}}}{1 - e^{-\beta}} \qquad \left(\beta = \frac{c\rho v L}{K}\right)$$

where T is the temperature at any point (°C), z is the depth (cm), c is the specific capacity of the fluid (cal/gr*°C), ρ is the density of fluid (gr/cm^3), v is the vertical velocity of the fluid (cm/sec), K is the thermal conductivity of the solid-fluid complex (cal/cm*sec*°C), T_z is the temperature measurement at any depth z (°C), T_0 is the uppermost temperature measurement (°C), T_L is the lowermost temperature measurement (°C), L is the vertical distance between T_0 and T_L (cm).

In this method, β and v are estimated by matching a type curve [z/L; f(β,z/L)] and a field curve [z/L; $(T_z-T_0)/(T_L-T_0)$] and using the above mentioned equations.

The β value was checked for every computed v value. The average velocity was found to be $5.42*10^{-7}$ cm/s (Table 6), which is equal to 0.17 m/year. The actual groundwater velocity (v_a), assuming the porosity of the rock to be 2%, is: $v_a = \frac{0.17}{0.02} = 8.5$m/y.

The transit time can be calculated to be 10,000 years by using estimated flow velocities for the distance of 85km (near Kazdağ mountain).

Depth, z (m)	Temp.,Tz °(C)	v (cm/sec)	β=vL/K
240	85.0	5.20E-07	4.16
245	85.3	5.22E-07	4.18
250	85.4	5.16E-07	4.13
255	85.5	5.10E-07	4.08
260	85.5	5.00E-07	4.00
265	86.0	5.13E-07	4.11
270	86.1	5.08E-07	4.07
275	86.2	5.04E-07	4.03
280	86.3	5.00E-07	4.00
340	88.0	5.02E-07	4.01
345	88.3	5.18E-07	4.14
350	88.4	5.19E-07	4.15
355	88.6	5.31E-07	4.25
360	88.8	5.40E-07	4.36
365	88.9	5.49E-07	4.39
370	89.0	5.55E-07	4.44
375	89.2	5.77E-07	4.62
380	89.3	5.87E-07	4.70
385	89.4	6.00E-07	4.80
390	89.4	5.92E-07	4.73
395	89.8	7.23E-07	5.79
	average	5.42E-07	

Table 6: Estimated velocities from Tz at z, (values and average velocity.

Calculation of reservoir temperature and circulation depth of the Gönen and Ekşidere thermal waters

Thermal water rising to the surface may cool by various processes. The cooling may be conductive, adiabatic, boiling, mixing with cold water or a combination of these processes.

An important parameter to distinguish between adiabatic and conductive cooling processes is the flow rate of the thermal water. The calculations of the maximum rates of flow for conductive cooling and minimum rates of flow for adiabatic cooling of Truesdell and Fournier (1977) were used to understand the cooling process of the Gönen and Ekşidere thermal waters. Figure 14 shows the extrapolated correlation of the maximum rates of flow for conductive cooling versus depth and Figure 15 shows the extrapolated correlation of the minimum rates of flow for adiabatic cooling versus depth.

The measured maximum water temperature was about 90°C and the natural rate of flow is about 15l/s in the Gönen thermal water wells. The circulation depth of the Gönen thermal water can be calculated to be 3km by using the geothermal gradient if the initial temperature in the recharge zone is 0°C and measured maximum temperature is 90°C. The maximum rate of flow is found to be 1.25l/s for conductive cooling and the minimum rate of flow is found to be 11.5l/s for adiabatic cooling for a depth of 3km in Figures 14 and 15. These figures indicate that the cooling process of the Gönen thermal water may be adiabatic because the rate of flow of the Gönen thermal water is too high for conductive cooling.

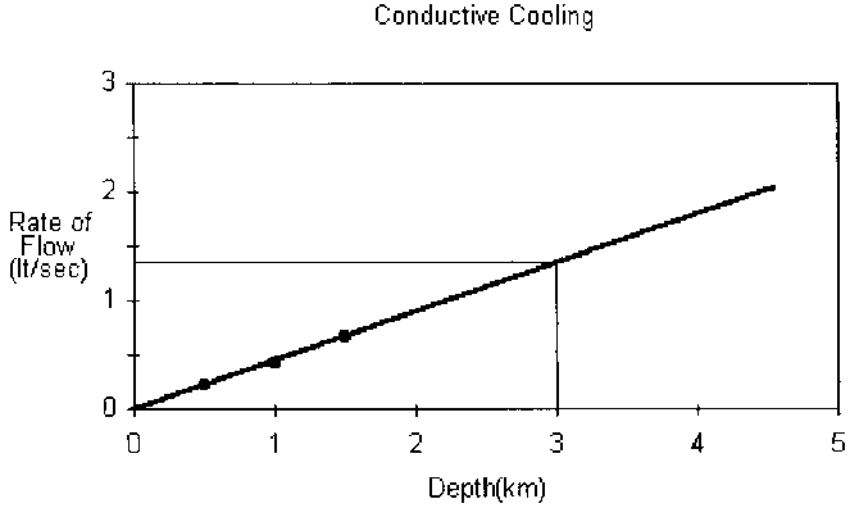


Figure 14: The extrapolated correlation of the maximum rates of flow versus depth for conductive cooling (dots are the calculated values from Truesdell and Fournier (1977)).

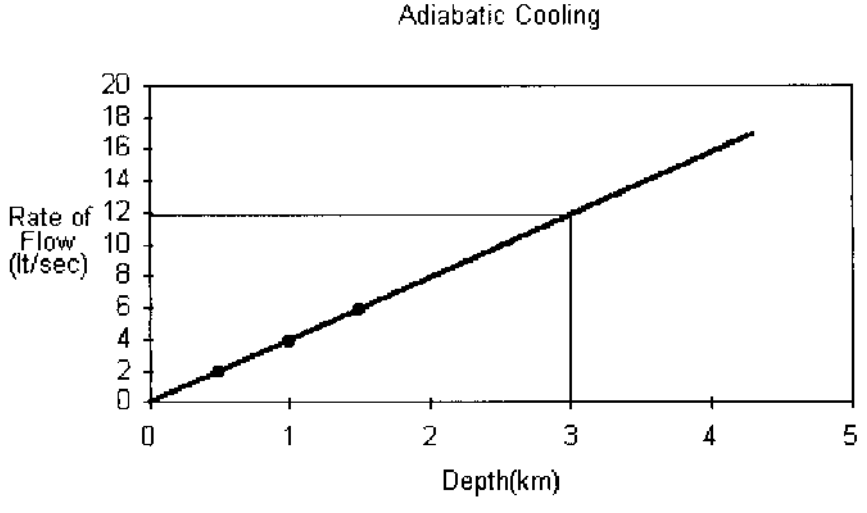


Figure 15: The extrapolated correlation of the minimum rates of flow versus depth for adiabatic cooling (dots are the calculated values from Truesdell and Fournier (1977)).

The rate of cooling due to expansion of water was calculated after Schoeller (1962) to be 0.57°C at every 100m. Using this calculation, the cooling of the Gönen thermal water at a depth of 3km can be calculated to be 17°C. The addition of cooling to the measured maximum temperature yields the minimum reservoir temperature of the Gönen thermal water of 99°C.

The rate of flow of the Ekşidere thermal waters is about 7l/s. Figures 14 and 15 indicate that the cooling of the Ekşidere thermal waters can also be adiabatic, unless if there is no horizontal flow at shallow depths.

Another widely-used method for the calculation of reservoir temperatures is chemical geothermometres. The calculated reservoir temperatures are given in Table 7.

Chemical Geothermometer	Equation	Calculated Reservoir Temperature ((C)	
		Gönen (G2)	Ekşidere (S1)
Quartz	$t = \frac{1309}{0.41 - \log k} - 273.15 \quad k = \frac{\alpha H_4 SiO_4}{\alpha H_2 O}$ α-activity	97.9	61.9
Na-K-Ca(β=1/3)	$t = \frac{699}{\log(Na/K) + \frac{1}{3}\left[\log(\sqrt{Ca}/Na) + 2.06\right] + 0.489} - 273.15$	120	147.3
Na-K-Ca(β=4/3)	$t = \frac{699}{\log(Na/K) + \frac{4}{3}\left[\log(\sqrt{Ca}/Na) + 2.06\right] + 0.489} - 273.15$	180.9	325.7
Na-K	$t = \frac{1180}{\log(Na/K) + 1.31} - 273.15$	169.5	-
Mg-Li	$t = \frac{2200}{\log(\sqrt{Mg}/Li) + 5.47} - 273.15$	68.5	-

Table 7: The calculated reservoir temperatures of the Gönen and Ekşidere thermal waters using chemical geothermometers (equations are after Kharaka et al. (1988)).

Hydrogeological circulation model

The circulation model of thermal waters is based on the regional hydrogeology, chemical, isotopic and gas composition of the sampled waters.

The origin of the Gönen thermal water is meteoric water infiltrated during the Pleistocene at a low temperature of about 0°C (≈10,000 years ago). The infiltrated water flows most probably through the Kazdağ metamorphic unit, and reaches a depth of 3-4km and is heated to approximately 100°C in the reservoir. The thermal water is in equilibrium with quartz and dolomite is oversaturated at a depth of 1km. The emergence of the water at the surface takes place where the permeability is increased due to fault zones. The cooling process is adiabatic. The surface temperature and rate of discharge are 82°C and 15-20l/s.

The origin of the Ekşidere thermal water is shallow circulating meteoric water much younger than the Gönen thermal water. The infiltrated water from the hills located at the southern side of the thermal water emerges at the surface through the fault zone between volcanic and sedimentary rocks of the Neogene. The impermeable sedimentary rocks cause the emergence of water above the plain level. The water does not equilibrate with any mineral during circulation. The surface temperature and rate of discharge are 42°C and 7l/s.

Conclusions

The geological and hydrogeological data were compiled from the possible recharge and discharge areas of the Gönen and Ekşidere thermal waters to understand the occurrence of the thermal waters.

The extensions of the North Anatolian Fault Zone (NAFZ) in and around the investigation area play an important role in the emergence of thermal waters.

The Gönen thermal water which discharges at a temperature of 82°C has been used for baths since ancient times and central heating since 1974. The water consumption is about 50l/s. The Ekşidere thermal water which discharges at a temperature of 42°C is used in baths.

The geochemical modeling of thermal waters is useful to estimate the possible chemical changes in water between the reservoir rock and the discharge point.

The stable isotope compositions of both thermal waters indicate a meteoric origin, but the Gönen thermal water is related to an old meteoric water (paleowater).

The Argon concentrations show that the Gönen thermal water infiltrated in a cold climate but that the Ekşidere thermal water infiltrated in a warm climate.

The recharge area of the Gönen thermal water is not certain, but Kazdağ mountain, which is 85km away from the discharge area, is the possible recharge area. The possible recharge area of the Ekşidere thermal water is near the hills located at the southern edge of the thermal waters.

The cooling process of the Gönen thermal water is adiabatic. The rate of cooling due to expansion was calculated to be 17°C and the reservoir temperature was found to be 99°C. The reservoir temperature was also calculated to be between 68.5 and 180.9°C by using chemical geothermometers. The quartz geothermometer gives a reservoir temperature of 97.9°C.

All the sampled thermal waters inside and outside of the investigation area are at least older than 40 years due to absence of tritium.

The estimated flow velocity of the Gönen thermal water is 8.5m/y by using the thermal profile method. The calculated age of the Gönen thermal water is 10,000 years by using a flow velocity estimation supposing that the water is recharging near Kazdağ mountain. The ^{14}C isotopic dating method gives 23,000 years as an uncorrected age.

The upflow mechanism of the thermal waters is mainly due to a piston effect. The emergence of the water at the surface takes place where the permeability is increased due to the fault zones.

References

Bredehoeft, J.D. and Papadopulos, I.S., 1965, Rates of Vertical Groundwater Movement Estimated from the Earth's Thermal Profile, Water Resources Research, vol.1, The American Geophysical Union, Washington DC,USA

Dumlu, O. and Yalçın,T., 1994, Termal Alanlarda Düşey Su Hızının Çeşitli Yöntemlerle Tahmini, Jeotermal Uygulamaları Sempozyumu '94 Bildiri Kitabı, 337-349

Eisenlohr, T., 1995, Die Thermalwässer der Armutlu-Halbinsel (NW-Türkei) und deren Beziehung zu Geologie und aktiver Tektonik, Diss. ETH-Zürich, Nr.11340

Erzenoğlu, Z. and Uluşahin, A., 1990, Gönen (Balıkesir) Kaplıcası G-4 ve G-4/A No.lu Sıcaksu Sondajları Kuyu Bitirme ve Korunma Alanları Raporu, MTA, Ankara (unpublished report)

Eyidoğan, H., 1991, Türkiye Büyük Depremleri Makro-Sismik Rehberi (1900-1988), İTÜ Maden Fakültesi, Kurtiş Matbaası, 198p.

Herece, E., 1990, 1953 Yenice-Gönen Deprem Kırığı ve Kuzey Anadolu Fay Sisteminin Biga Yarımadasındaki Uzantıları, MTA Dergisi, No. 111, Ankara, 47-59

Ketin, İ. and Rösli, F., 1953, Makroseismische Untersuchung Über das nordwestanatolische Beben vom 18. März 1953, Sonderausdruck aus Eclogae Geologicae Helvetica, Vol. 46, Nr. 2, E. Birkhäuser&Cie. A.G., Basel

Kharaka, Y.K. et al., 1988, SOLMINEQ.88: A Computer Program for Geochemical Modeling of Water-Rock Interactions, USGS Water-Resources Investigations Report 88-4227, Calif. USA, 420p.

Kharaka, Y.K. and Carothers, W.W., 1986, Oxygen and Hydrogen Isotope Geochemistry of Deep Basin Brines, in: Handbook of Environmental Geochemistry, edited by: D. Fritz and J.C. Fontes, Vol. 2, Elsevier, Netherlands, 305-353

Mazor, E., 1991, Applied Chemical and Isotopic Groundwater Hydrology, Open Univ. Press, Great Britain, 274p.

Moser, H. et al., 1983, Stable Isotope Studies on Paleowaters, in: Paleoclimates and paleowaters: A collection of environmental isotope studies, IAEA, Wien, 201-204.

Okay, A.İ., Siyako, M. and Bürkan, K.A., 1990, Biga Yarımadası'nın Jeolojisi ve Tektonik Evrimi, TPJD Bull., Vol. 2/1, Ankara, 83-121.

Reman, R., 1942, Şifalı Su Kullanmak İlmi (Balneoloji) ve Şifalı Kaynaklarımız, İstanbul Cumhuriyet Matbaası, 594p.

Schoeller, H., 1962, Les Eaux Souterraines,Masson&C^{ie}, Paris, 248p.

Truesdell, A.H. and Fournier, R.O., 1977, Procedure for Estimating the Temperature of a Hot-water Component in a Mixed Water Using a Plot of Dissolved Silica vs Entalpy, US Geol.Surv., J.Res., 5, 49-52.

Appendices

Date	Name or number of water resource	T(°C)	EC [1](μS/cm)	pH	Eh (mV)	Dissolved O_2 (mg/lt)	Alkalinity (mg/lt $CaCO_3$)	Acidity (mg/lt $CaCO_3$)	Discharge (lt/sec)
Aug.24,1990	Gönen River*	-	600	-	-	-	-	-	-
Aug.30,1990	S3	19.0	230	-	-	-	-	-	0.01
Aug.30,1990	S1	39.0	440	-	-	-	-	-	7
Aug.27,1991	Geyikli Spring[2]	21.3	197	3.75	189.6	-	70	-	-
Aug.28,1991	Gönen City Water[3]	-	425	-	-	-	280	71.3	-
Aug.29,1991	S5	16	462	7.50	-23.5	-	320	135	0.4
Aug.29,1990	S4	16	550	7.14	-3.2	-	390	135	7
Sep.04,1990	G3	70	2260	7.18	-6.9	-	297	140	-
Sep.04,1990	G1	-	2320	7.13	-4.5	-	135	-	-
Sep.04,1990	G4	62.8	2420	7.00	5.4	-	550	166	-
Sep.04,1990	G2	70.3	2370	7.13	-3.4	-	500	166	-
Mar.05,1992	S3	-	330	3.59	197.7	-	-	-	0.01
Mar.06,1992	S2	28.1	390	7.02	5.1	-	-	-	-
Aug.26,1992	G2	78.8	2530	7.80	-	0.8	550	90	-
Aug.26,1992	G4	73.8	2455	8.00	-	2.6	610	100	-
Aug.27,1992	S2	35.4	400	7.67	-	2.3	270	30	1
Aug.27,1992	S1	42.8	389	8.03	-	1.4	290	70	-
Aug.27,1992	S3	18.8	256	4.31	-	-	0	230	0.025
Aug.27,1992	S4	14.4	600	7.33	-	7.1	610	70	-
Aug.27,1992	Geyikli Spring**	25.2	213	4.20	-	5.2	-	210	-

[1]EC value is measured near the Gönen Bridge

[2]this spring is on the way to Geyikli village out of the investigation area

[3]Gönen city water comes from the Dumanalan Spring(S7)

Appendix 1: Some physical and chemical properties of water resources measured in the field.

Sample No	Date	CATIONS(mg/l)										ANIONS (mg/l)						
		B	Li^+	Na^+	K^+	Ca^{++}	Mg^{++}	Ba^{++}	Fe (total)	Al^{+++}	NH_4^+	Cl^-	HCO_3^-	$SO_4^=$	NO_3^-	F^-	I^-	SiO_2
G1 (3)	1974	7.6	-	460.0	24.0	46.0	2.2	-	0.1	-	1.1	262.0	354.0	473.0	-	3.8	0.4	68.0
G2 (3)	1976	-	4.0	440.0	22.0	49.0	1.6	-	0.2	-	1.2	270.0	394.0	491.0	0.3	4.3	-	46.0
G2 (2)	1992	7.2	-	403.0	25.6	43.2	2.4	0.051	0.2	0.2	-	209.7	-	381.4	0.3	-	-	-
G3 (3)	1985	7.6	-	460.0	26.2	48.0	3.2	-	0.1	-	0.3	261.0	397.0	459	0.8	3.4	-	80.0
G4 (1)	1991	3.0	1.5	365.6	26.5	49.0	2.9	-	0.5	-	1.4	252.0	384.3	-	-	-	-	68.0
G4 (2)	1992	7.1	-	414.0	26.4	45.8	3.1	0.044	0.1	0.2	-	209.3	-	380.2	0.3	-	-	-
S1 (3)	1985	0.4	<0.1	10.6	1.5	50.0	15.0	-	-	-	<0.1	12.0	195.0	28.4	2.1	0.3	-	35
S1 (2)	1992	<0.1	-	11.0	3.1	47.3	10.7	0.3	<0.1	0.3	-	9.6	-	17.8	0.3	-	-	-
S2 (3)	1985	<0.1	<0.1	11.4	2.1	49.0	11.0	-	0.1	-	0.1	14.7	177.0	41.0	2.0	0.4	<0.1	37
S2 (2)	1992	<0.1	-	10.8	2.9	47.3	9.4	0.2	<0.1	0.2	-	14.2	-	29.4	0.3	-	-	-
S3 (2)	1992	<0.1	-	7.6	1.6	6.6	2.0	<0.1	0.1	3.9	-	15.9	-	59.8	0.3	-	-	-
S4 (2)	1992	<0.1	-	6.0	1.7	76.0	12.8	<0.1	<0.1	0.2	-	11.3	-	9.3	8.2	-	-	-
7933A (4)	1966	-	-	27.4	2.7	84.0	11.4	-	-	-	-	41.2	260.9	39.0	-	-	-	-
7933B (4)	1966	-	-	207.0	2.7	24.0	8.4	-	-	-	-	42.6	388.5	132.0	-	-	-	-
7471 (4)	1966	-	-	16.8	2.7	46.0	13.2	-	-	-	-	12.8	212.3	17.3	-	-	-	-
7473A (4)	1966	-	-	54.0	3.5	90.0	14.4	-	-	-	-	69.6	286.5	60.5	-	-	-	-
7473B (4)	1966	-	-	32.9	16.4	76.0	15.6	-	-	-	-	42.6	298.6	25.4	-	-	-	-
7469A (4)	1966	-	-	49.9	3.5	76.0	28.8	-	-	-	-	100.8	295.2	37.5	-	-	-	-
7470A (4)	1966	-	-	19.8	3.1	66.0	13.2	-	-	-	-	34.8	208.4	34.5	-	-	-	-
7470B (4)	1966	-	-	64.4	2.3	24.0	13.2	-	-	-	-	16.3	174.1	68.1	-	-	-	-
7475 (4)	1966	-	-	19.8	2.7	38.0	25.2	-	-	-	-	23.4	190.0	39.8	-	-	-	-
7474A (4)	1966	-	-	27.8	3.5	86.0	20.4	-	-	-	-	53.9	319.6	25.9	-	-	-	-
7474B (4)	1966	-	-	64.4	3.5	67.0	19.8	-	-	-	-	49.0	283.0	89.8	-	-	-	-

(1) İTU Hydrogeology Lab.
(2) ETH Ingenieurgeologie Hydrolab.
(3) MTA
(4) DSı

Appendix 2: Cation and anion concentrations of water resources of the investigation area.

Sample name	Date of sampling	δ^2H(%0) Deuterium	δ^{18}O(%0) Oxygen18	^{3}H (TU) Tritium	Temperature °(C)	pH	EC μ(S/cm)	altitude (masl)
S1 Ekşidere West	Aug.27, 1992	-55.1	-8.84	<1.1	42.0	8.0	389	200
S2 Ekşidere East	Aug.27, 1992	-54.6	-8.92	<0.7	28.1	7.7	400	200
S3 Gençlik Suyu	Aug.27, 1992	-51.0	-8.21	11.6±1.2	19.0	4.3	256	200
S4 Hafız-hüseyinbey	Aug.26, 1992	-50.3	-8.04	20.0±1.4	14.4	7.3	600	200
G2 Gönen	Aug.26, 1992	-68.9	-9.41	<0.7	78.8	7.8	2530	35
G4 Gönen	Aug.26, 1992	-70.5	-9.68	<0.7	73.8	8.0	2455	35
Gey Geyikli	Aug.27, 1992	-52.1	-8.07	12.3±1.2	25.2	4.2	213	100
G4 Gönen	Sep.3, 1994	-71.4	-9.95	<1.7	75.0	7.1	2455	35
Hıd Hıdırlar	Sep.4, 1994	-50.3	-8.37	<0.7	84.2	6.6	980	300
Top Topaklar	Sep.4, 1994	-60.8	-9.31	<0.7	67.3	8.0	1700	150
GG Gobaklı-gediği	Aug.14,1996	-50.4	-8.18	-	8.5	6.3	92	1000
BK1 Forester hut 1	Aug.14,1996	-48.0	-7.89	-	10.5	7.7	65	1220
BK2 Forester hut 2	Aug.14,1996	-48.8	-7.96	-	7.5	8.4	65	1260
Toz Tozlu	Aug.15,1996	-48.6	-7.90	-	4.6	8.4	122	1480
Kar Kartal-pınar	Aug.15,1996	-51.8	-8.32	-	6.5	7.4	79	1700
Kül Külcüler	Aug.15,1996	-54.0	-8.29	-	34.7	6.9	1020	400

Appendix 3: Results of the isotopic analyses of the sampled waters (isotope analyses carried out by GSF,Neuherberg,Germany).

Nature and origin of the thermal springs in the Tuzla area, Western Anatolia, Turkey

STEFAN MÜTZENBERG

Abstract

The saline thermal springs in the Tuzla area, Western Anatolia, Turkey have been studied for their geological setting and their chemical and isotopic composition. From the regional structural features, the positions of the three thermal centres, Kestanbol kaplıca, Akçekeçili and Tuzla were identified at the intersections of three fault systems. At the surface, the waters reach temperatures between 35°C and 95°C and contain up to 65,000ppm total dissolved solids, mainly Na and Cl. As the ratios of the most soluble constituents are constant within all of the springs sampled, the presence of a common hot water aquifer can be postulated. The chemical and isotopic composition of the waters indicate the presence of a fossil, alterated seawater (connate water), which is diluted up to 70% with freshwater of meteoric origin. The thick sedimentary sequence in the Aegean basin is considered to be the host of the saline endmember. Deep circulation along major fault zones, the dilution with freshwater and zones of high vertical permeability lead to the buoyancy-driven ascent of the saline thermal water.

Introduction

Historical background

The area under study is located in the northwestern part of Anatolia on the Biga peninsula, known in antiquity as the Troas [1]. Along the western coast, three centres with thermal water discharges occur within a distance of 20km. The springs of Kestanbol kaplıca and Tuzla were described by Demetrios of Skepsis (born around 205BC) and the Greek geographer Strabo (63BC-26AD) (Leaf 1923). The springs of Tuzla, known as Tragasai in the antiquity, were of greater importance during this period. Thus, Strabo describes the extraction of salt in Tragasai, and also Galen (129AD-199AD) and Athenäus (ca. 200AD) mention the occurrence of salt in Tuzla (Tuzla meaning salt-works in Turkish).

Since classical times, the thermal springs of Kestanbol, Akçekeçili and Tuzla have been used as spas and ruins of the Roman period can be found at all three localities. Today, the spa of Kestanbol kaplıca (kaplıca meaning spa) is being enlarged, whereas the geothermal field in Tuzla is an object of interest for the use of geothermal energy.

Previous investigations

The earliest detailed information about the springs in Kestanbol kaplıca and Tuzla may be found in expedition reports and historical studies (Tchihatcheff 1853, Schliemann 1881 and Leaf 1923). Geological maps and stratigraphic sequences of the Biga peninsula were later

1. The famous city of »Troy« in Homer's Ilias lies within the Troas, 20 km north of the area under study.

published by Erguvanlı (1957), v.d. Kaaden (1959) and Bingöl et al. (1973). The work of Brinkmann (1966, 1971a, 1971b, 1971c) in key areas of Western Anatolia yielded further important information about the stratigraphy and the tectonic structure of the region. Geochronological and geodynamic studies on the volcanic rocks, which cover a large area of the Biga peninsula and adjoining areas, were carried out by Borsi et al. (1972).

The presented paper summarises the results of a regional study of the western part of the peninsula (Mützenberg 1990). Geological and structural data were combined with the results of hydrochemical and isotopic analyses of thermal and freshwater springs to give an overall picture of the hydrogeological conditions in the area under study.

Geological setting

Stratigraphic sequences

Metamorphic rocks are exposed in several outcrops along the western and northern border of a younger intrusive body. The metamorphic sequence consists of diopside-plagioclase schists, aktinolith-biotite schists, feldsparbearing and pure quartzites, sericite schists and marbles.

Strongly-folded slates and feldspar-bearing sandstones, probably of Carboniferous age, are exposed in a very small area south of Tavaklı. The stratigraphic and tectonic situation of this series is not recognised.

A 400 to 500m thick sequence of limestones, although extensively recrystallised, represents the earliest fossil-bearing sediments. They consist of shallow marine limestones with partly dolomitic and locally siliceous layers. Reddish, slightly marly layers contain abundant fossils. A dense community of the algae *Gymnocodium bellerophontis PIA* indicates a middle to upper Permian age (E. Flügel, pers. communication). Furthermore, the samples contain fusulinide foraminifera and gastropods. Fossil karstic channels with fillings of red clays or secondary calcification and active karstic systems are widespread within the limestone complexes.

The Kestanbol intrusive body[1] was intruded as lakkolite into the metamorphic basement and young paleozoic sediments. The age of intrusion is given by Fytikas et al. (1976) as 28m.y. (Oligocene). The exposed area of approximately 80km^2 is predominantly a biotite- and hornblende-bearing quartz-monzonite with phenocrysts of pink alkalifeldspars. The intrusion produced a very narrow thermal aureole, mainly with metasomatic reactions such as the formation of scapolite and garnet in metamorphic diopside-plagioclase schists and the development of skarns at the contact of the intrusion and adjacent Permian limestones.

During the lower and middle Miocene, Western Anatolia was dominated by calcalcaline volcanism (Borsi et al. 1972). Volcanic products of this period cover a large area of the southern Biga peninsula. They consist mainly of lava flows, lava domes and volcanic agglomerates. South of Tuzla, an extensive ignimbritic cover overlies older volcanic products.

In the coastal area, sediments of the Neogene overlie discordantly metamorphic rocks, Permian limestones and volcanic products. The sedimentary sequence starts with red coloured, terrestric-fluviatile sediments. North of Babadere, these sediments were deposited as scree deposits and contain boulders of mainly Quartz-Monzonite up to 2 meters in diameter. In the Tuzla region, the neogene sediments are composed of reddish or grey, tuffitic claystones,

1. Kestanbol refers to the former name of the village now named Uluköy.

siltstones and volcanic conglomerates. The occurrence of vertebrate fauna suggests a Turolian age (middle upper Miocene) for this unit (Kaya 1982).

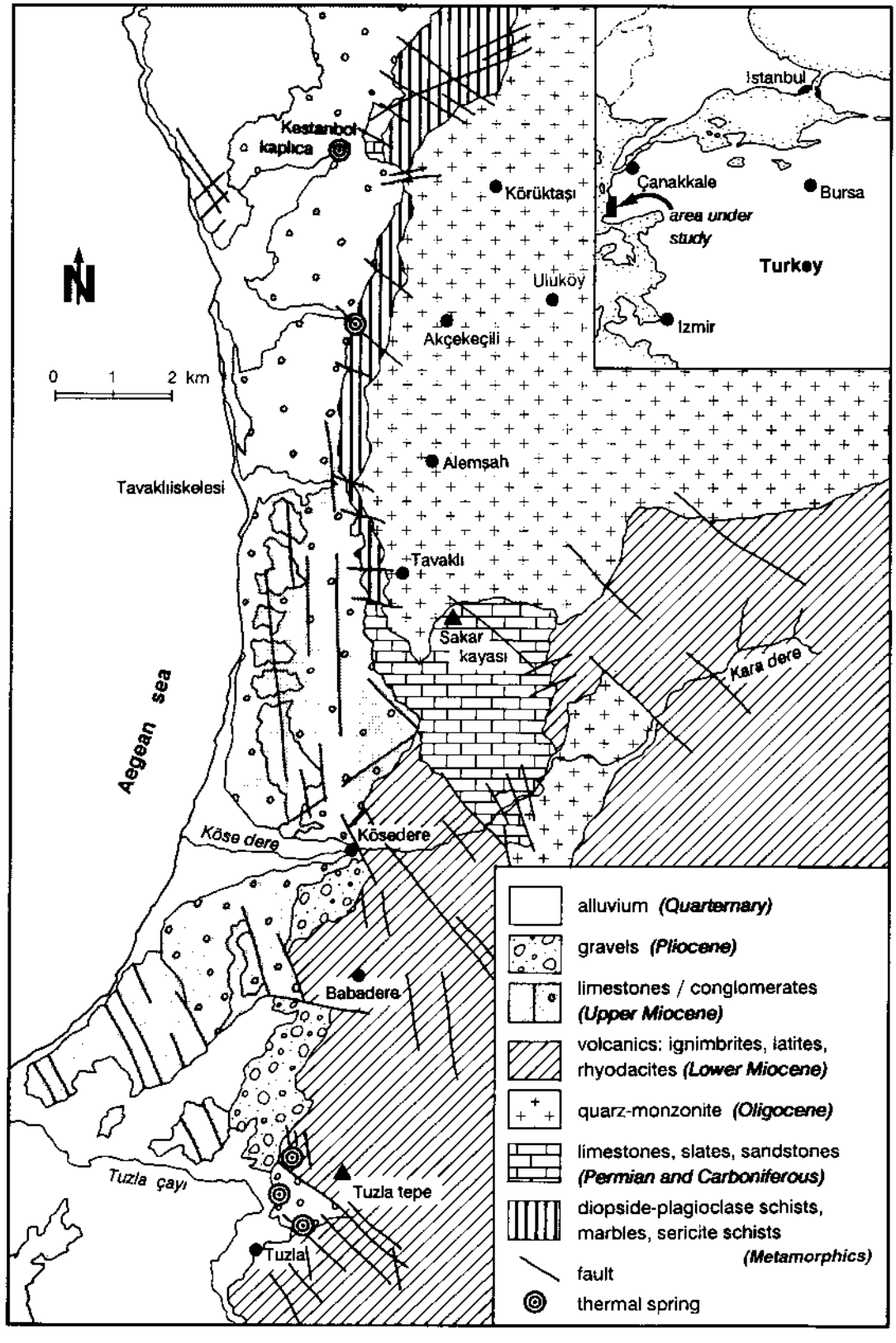


Figure 1: Geological map of the western Biga peninsula (simplified after Mützenberg 1990).

The overlying unit, also of upper Miocene age (Erguvanlı 1957), starts with a base conglomerate and continues upward with marine and brackish limestones, marls and shales.

During the Pliocene, light-coloured, poorly-sorted gravels were deposited. South of Kösedere, they cover upper Miocene sediments with a slight angular discordance.

Structural trends

Three main structural trends can be recognised on satellite images and areal photographs. After verification with field data, the following structural features can be identified:

- NNE-striking lineations corresponding to the strike of planar and linear structures in metamorphic rocks, tectonic boundaries within the paleozoic units and the direction of normal faults in the coastal area. During the Miocene, this fault system induced the depression of the Aegean sea (Kaya 1981, McKenzie 1970).
- The second important structural trend is oriented 55° NE-SW. Fault zones with this strike can be followed through Kestanbol kaplıca, Kösedere and Tuzla. The main geologic features are large-scale dragging of schistosity planes, plastic deformations, slickenslides and steps in the present day coastal line. They show dextral-normal displacements with a dip of the southern blocks. It is important to note that the shear sense and the strike of these faults are coherent with the North Anatolian Fault Zone (NAFZ) in Northwestern Anatolia (Dewey and Şengör 1979) and neotectonic movements in the Marmara sea region (Crampin and Evans 1986). In the Tuzla area, volcanic rocks of lower and middle Miocene age were affected by the displacements, whereas upper Miocene sediments show only minor deformation. Thus, the main activity along these faults is pre-upper Miocene. Along the fault zone through Tuzla, hydrothermal precipitations such as exhalation crusts, chalcedony and travertine are found within and covering the upper Miocene sedimentary sequence. They may indicate a later tectonic activity.
- Dense groups of NW-SE running lineations can best be observed on aerial photographs. In the field, the main deformation feature following this trend is brittle joint sets with only small displacements.

Hydrogeological setting

Along the western coast of the study area three localities with thermal water springs are found within a distance of 20km. In Kestanbol kaplıca, two springs emerge north of the small Ilıca dere valley from strongly fractured metamorphic rocks (Fig. 2). In 1975, a borehole was drilled in the valley resulting in artesian water with a temperature of more than 75°C. The water is used for a regional thermal spa and for the heating of several greenhouses.

The spring of Akçekeçili lies in a narrow gorge a few kilometres south of Kestanbol kaplıca. Only one small discharge in metamorphic rocks may be observed here.

In the Tuzla area, a great number of thermal springs emerge from Miocene volcanic rocks and sediments over an area of about 1km^2 (Fig. 3). Most springs emerge within small ponds, some of them with artesian discharge. Many diffuse water and gas discharges cover large areas, leaving white salt exhalations. Between 1982 and 1986, two boreholes were drilled to a depth of 800-1000m. From one borehole (TI) artesian water discharged with a temperature of 175°C (Şamilgil 1984). Unfortunately, the data of these drillings are sparse and have not been published. Presently, only one small spring is piped to supply a small thermal bath.

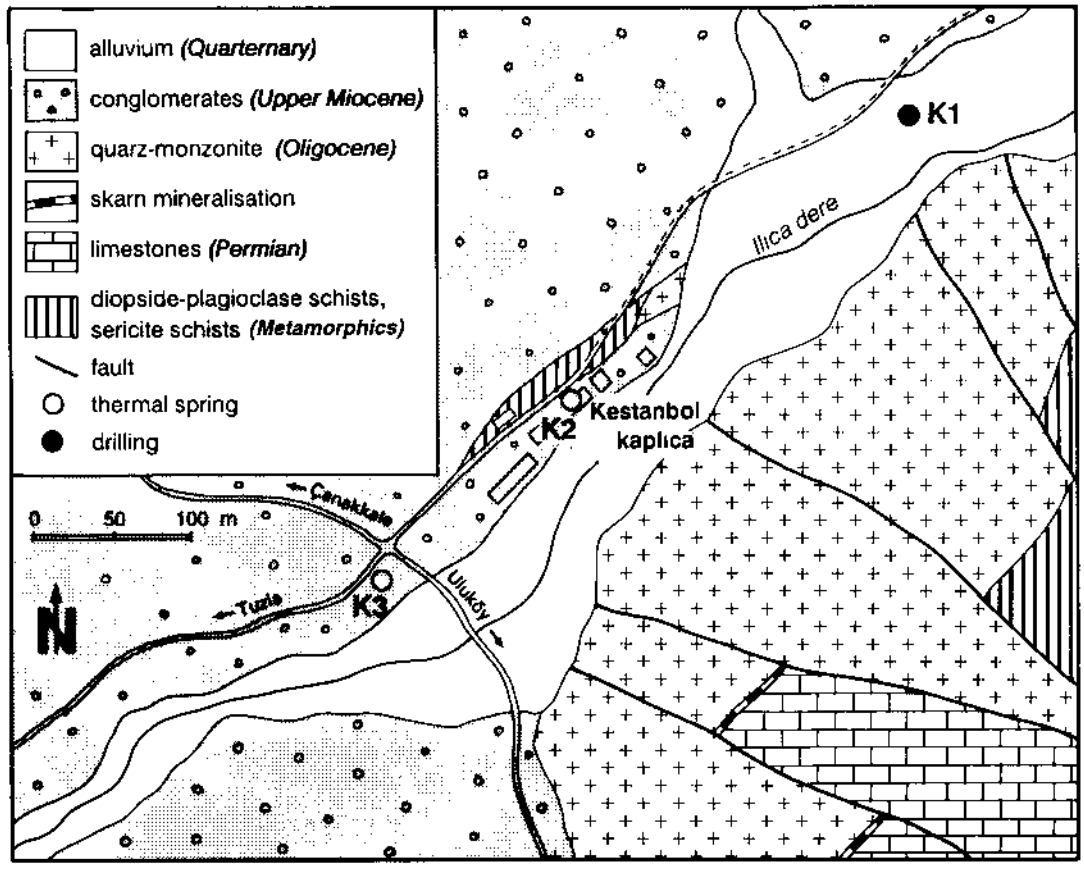


Figure 2: *Geological map and spring sites of the Kestanbol kaplıca thermal centre.*

In relation to the structural pattern, the positions of the three thermal areas are defined as follows:

i) The three areas with thermal spring activities are aligned along a major NNE-striking normal fault zone in the coastal area.

ii) NE-SW striking, right lateral strike slip faults cross the geothermal fields of Tuzla and Kestanbol kaplıca.

iii) NW-SE striking joint and fault sets cut through all three thermal areas.

From this position, it can be stated that the necessary vertical permeability, which gives rise to the thermal water, occurs at the intersection of these three major fault systems.

Chemical characteristics

The outflow of 14 thermal springs and one artesian borehole in the three areas with thermal water discharges were sampled at different seasons of the year in 1987 and 1988 (Table 1, Appendix). Based on the main constituents the water can be characterised as Na-Cl type with Na about 80mval % of total cations and Cl greater than 99mval % of total anions. The Ca content is generally greater than the K content. The waters have relatively low concentrations of Mg, SO_4, HCO_3.

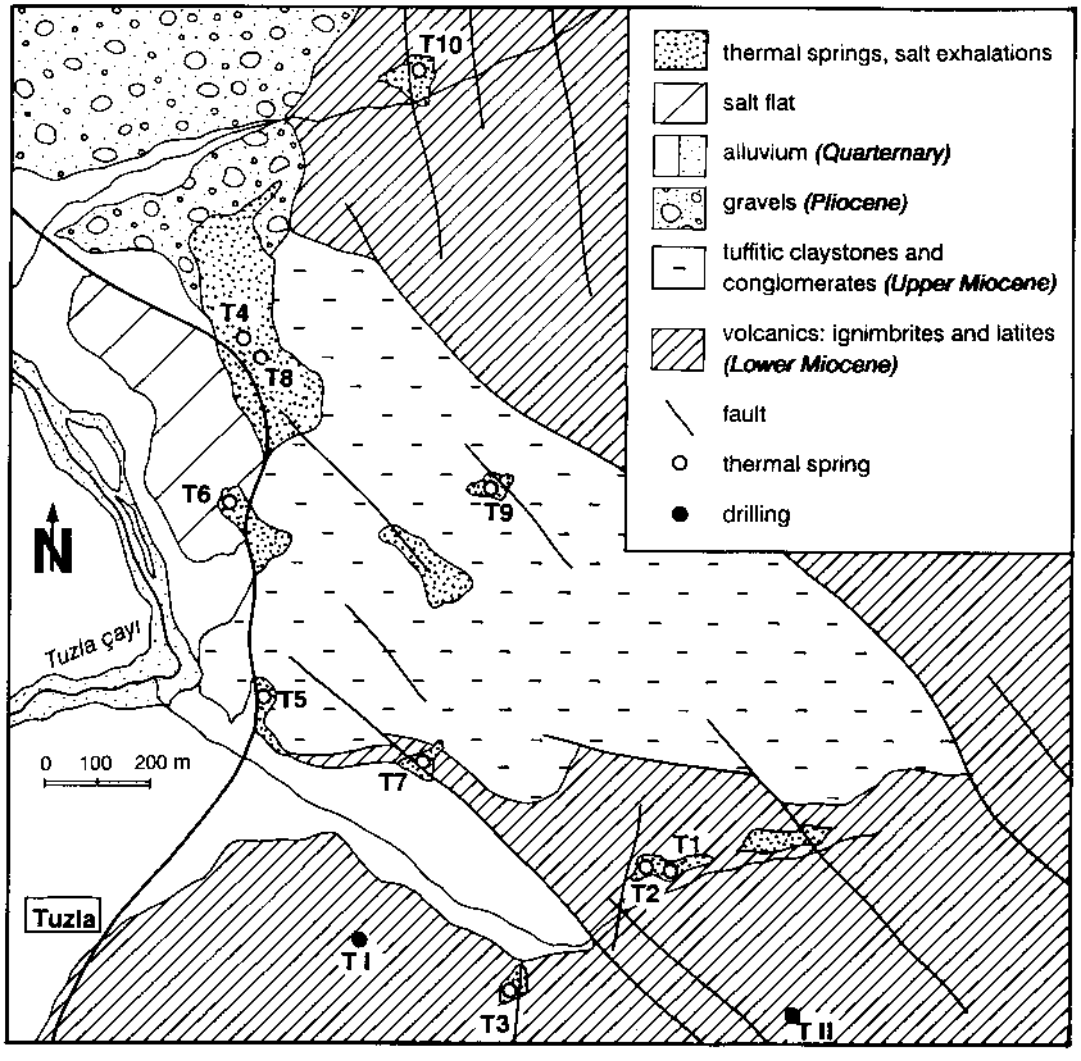


Figure 3: *Geological map and spring sites of the Tuzla thermal centre.*

Sample nr.	Locality	Approx. discharge in l/sec
K1	Kestanbol kaplıca borehole, 290m	25
K2	Kestanbol kaplıca «main spring» («ana kaynak»)	3
K3	Kestanbol kaplıca «second spring» («tali kaynak»)	1
A1	Akçekeçili thermal spring	<1
TI	Tuzla borehole, 800m (Şamilgil 1984)	-
T2	Tuzla artesian spring	1
T3	Tuzla captured artesian spring	3
T4	Tuzla south spring with roman bath	1
T5 – T10	Tuzla small springs around Ebe tepe	<<1
T11	Tuzla north spring with travertin	<1

Table 1: *List of samples (spring sites in Fig. 2 and 3).*

In Kestanbol kaplıca, the temperatures of the springs range from 63.6-76.2°C and the total mineralisation (TDS) varies between 20,875-23,535mg/l. The lowest temperatures (33.5°C) and the lowest mineralisation (16,070-16,230mg/l) were found in the small spring of Akçekeçili. With temperatures up to 95.6°C and TDS between 27,290-64,645mg/l, the highest temperatures and TDS were measured in the Tuzla area. The drilled discharge in Tuzla (TI), which was sampled in 1984 (Şamilgil 1984), yielded a value of 75'120mg/l. For comparison, the TDS-value for seawater is about 35,270mg/l.

The chemistry of the sampled thermal waters can best be visualised with reference to log-log plots of the characteristic dissolved ions vs. chloride (Fig. 4). For comparison, seawater and the dilution/evaporation line for seawater are also shown in the plots.

All the samples are aligned parallel to the dilution/evaporation line, thus the ratios vary little within the sampled waters. The Na/Cl plot shows similar ratios for seawater and the thermal waters, with a slight depletion of Na in the thermal waters. The Ca/Cl, K/C, Li/Cl and B/Cl ratios are increased with respect to seawater, whereas the Br/Cl ratio is slightly decreased.

In addition to the chemical composition of the water, upper Miocene ferromanganese crusts and recent red and ochre precipitation in open spring pools in Tuzla were analysed for their metal concentrations (Table 2). The most outstanding feature is high contents of Zn, Pb, As and Sb. Of these trace metals, Zn and Pb are known to build stable chloride complexes at high temperatures (White 1968). As and Sb can be used, in addition to NH_4 and B, to give a qualitative indication of the age of a geothermal system (Giggenbach and Goguel 1989). Since these volatile constituents evaporite in an early stage of a geothermal system, the relatively high concentrations in the present hydrothermal system of the Tuzla area may indicate a young age for this system, with a sufficient supply of fresh thermal water.

Sample number	1 Exh R	2 T6/1	3 T3/1
Si	$1.5x10^5 – 2x10^5$	$6x10^4 – 10^5$	$10^5 – 1.5x10^5$
Ca	7,000 – 10,000	$10^5 – 1.5x10^5$	$2x10^4 – 4x10^4$
Mn	700 – 900	2'000 – 3'000	1,000 – 3,000
Fe	$4x10^5 – 5x10^5$	$4x10^5 – 5x10^5$	$4x10^5 – 5x10^5$
Zn	700 – 900	3,000 – 5,000	2,000 – 4,000
As	500 – 700	3,000 – 4,000	3,000 – 5,000
Sb	n.d.	1,000 – 2,000	500 – 600
Ba	1,000 – 2,000	500 – 800	500 – 800
Pb	150 – 200	3,000 – 4,000	4,000 – 6,000
U.	300 – 500	n.d.	n.d.

Table 2: Metal concentrations in upper Miocene ferromanganese crusts and precipitation from present thermal springs in Tuzla (all in ppm). Chemical analyses by DSIR, New Zealand. [1: exhalation crusts in upper Miocene sediments from Tuzla, 2, 3: ochre precipitation in thermal water spring ponds in Tuzla (spring sites in Fig. 3), all values in ppm, n.d. = not detectable].

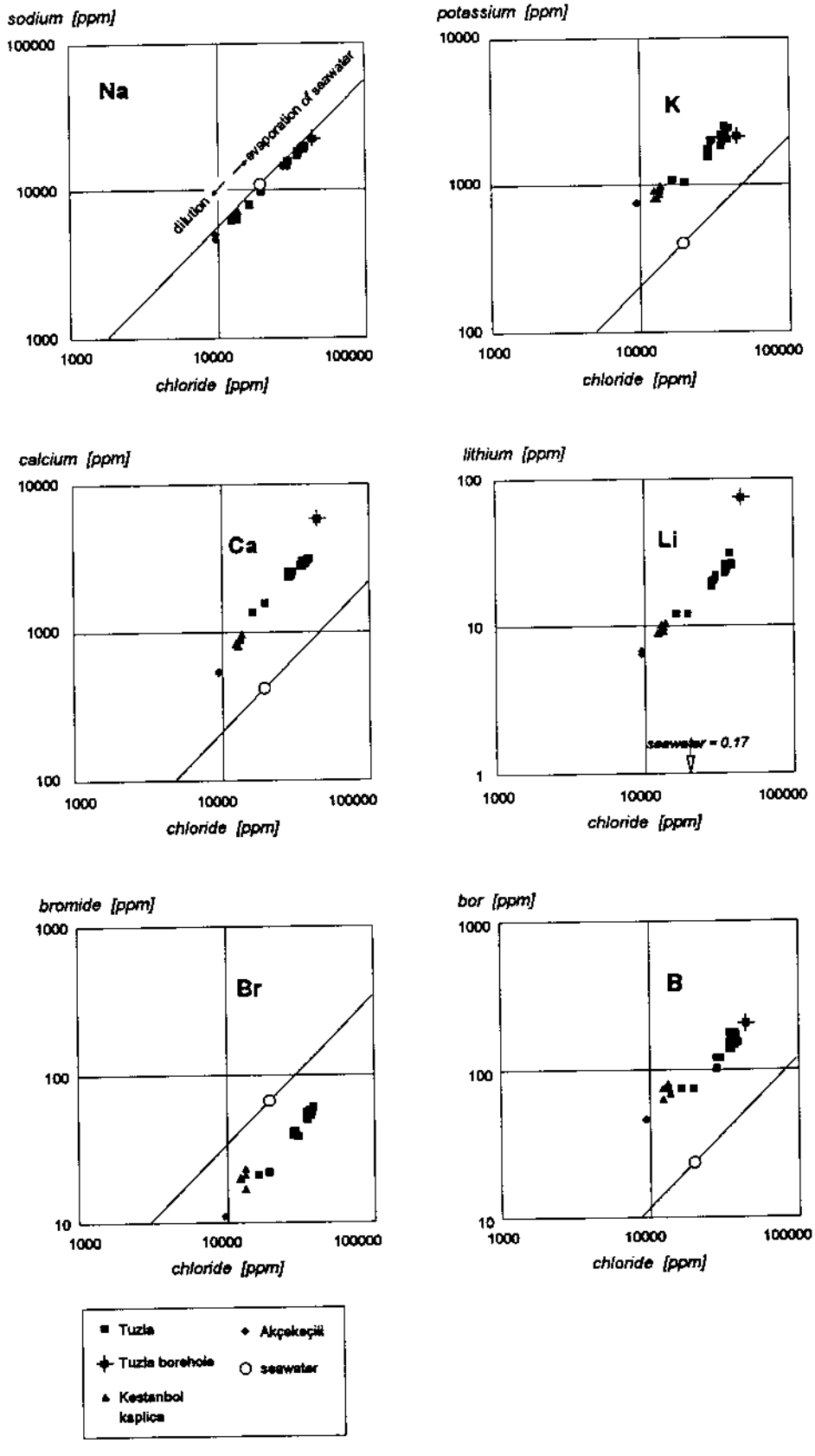


Figure 4: *The ratios of dissolved Na, K, Ca, Li, B and Br ions vs. chloride (all in ppm) are similar within all the samples and indicate the presence of a common hot water reservoir.*

Hydrochemical evolution

Since the ratios of non-reactive ions, in other words, ions which are not affected by secondary mineral formation, differ little within the sampled waters (Fig. 4), it can be assumed that they evolved from the same source and are a mixing series between a saline endmember (brine) and fresh water. Based on the chloride contents, the water in Kestanbol kaplıca is diluted with 70% freshwater with respect to the most saline water in Tuzla. For the lowest mineralised water in Akçekeçili a dilution with 80% freshwater can be calculated.

Similar Na/Cl ratios and only slightly differing Br/Cl and B/Cl ratios between seawater and the thermal waters suggest an alterated, fossil seawater (connate water) as the origin of the saline endmember.

The Br/Cl ratio is frequently used as a tracer for the origin of salinity, as both Br and Cl behave inertly in solution. High Br/Cl ratios are found in saline groundwaters in crystalline rocks (Frape and Fritz 1987) and oilfield brines (Collins 1980). On the other hand, bromide is depleted in brines which originate from the dissolution of marine evaporites (Edmunds et al. 1987). The analysed thermal waters show smaller Br/Cl ratios than seawater. This is an indication that the salinity of the water may partly result from the solution of marine evaporites or interstitial pore salts of marine sediments.

The chemical characteristics of the water can further be explained by diagenetic reactions in the sediments, such as dolomitisation ($Ca\uparrow$, $Mg\downarrow$) and rock-water interactions during circulation in volcanic and metamophic rocks, such as the albitisation of plagioclase ($Ca\uparrow$, $Na\downarrow$) and the leaching of biotite ($K\uparrow$, $Li\downarrow$).

Ion ratios of saline groundwaters are commonly used to characterise the water and determine the origin and evolution of the saline content (Table 3). Saline waters in crystalline rocks are generally governed by rock-water interaction and can be distinguished by high Ca/Na ratios, regardless of their deep origin. In contrast, deep, saline waters from the gulf of Mexico basin are considered as fossil seawater or connate waters (Kharaka and Carothers 1986). As these ion ratios show a very close similarity with the thermal saline waters from Tuzla, a similar hydrochemical evolution can be postulated. The subsequent circulation in crystalline and volcanic rocks in the Tuzla area can be recognised from the higher K/Na and Li/Na ratios of these waters.

Temperature at depth and cooling processes

The most frequently used geothermometers to calculate the underground temperature, as described by Ellis and Mahon (1977), utilise the relationship between the dissolved Na/K ratios and the discharge temperature of the water. Since these geothermometers are based only on the reaction between water and silica minerals, such as feldspar and muscovite, their application for alterated seawater is not possible.

More reliable underground temperatures may be calculated from silica concentrations (Truesdell 1975). But since the dilution with cooler water and the deposition of silica during the ascent and cooling of the water may reduce the silica content, the calculated temperatures give only a minimum value for the temperature at depth. For the sampled waters temperatures between 140°C and 160°C were calculated with the silica geothermometer.

Possible cooling processes during the ascent of the water to the surface can be derived by the relationship between the chloride content and the discharge temperature (Fig. 5). Most of the hot water springs in Tuzla have similar Cl-contents and discharge temperatures. The least concentrated waters in Akçekeçili and Tuzla show a dilution with cold freshwater. For several springs in Tuzla, a decrease in temperature is also due to conductive cooling during the ascent of the waters. In Kestanbol, the chloride content of the surface discharges is in-

creased with respect to the water from the drilled well. This may be due to evaporation processes near the surface and during the ascent of the water. An association between the thermal waters in Tuzla and in Kestanbol can be drawn by diluting the waters from Tuzla with heated freshwater.

Locality Sample number	Tuzla, Turkey T3	Lafayette, La [1] 77-GG-19	Houston, Tx [1] 76-GG-7	Canad. Shield [2] R 36	Cornwall [3] SC1
Ca/Na	.15	.13	.076	4.14	.523
K/Na	.11	.01	.02	.023	.043
Li/Na	.0013	.0002	.0004	.00002	.030
Mg/Ca	.0045	.015	.008	.055	.156
Na/Cl	.516	.545	.621	.103	.379
Br/Cl	.0014	.0029	.0012	.012	.0038
SO_4/Cl	.0039	.00005	.00006	.0028	.014
HCO_3/Cl	.002	.003	.011	.0007	.0065
B/Cl	.0008	.0003	.0008	--	.0015
TDS [4]	62,400	235,700	73,300	227,200	15,250

Table 3: *Ratios of dissolved species for saline waters from the Tuzla area and other saline waters of different origin. 1) connate water from the northern gulf of Mexico basin (Kharaka and Carothers 1986), 2) deep saline groundwater from the Canadian shield (Frape and Fritz 1987), 3) saline groundwater in the Carnmenellis granite, Cornwall (U.K.) (Edmunds et al. 1987), 4) Total dissolved solids in mg/l.*

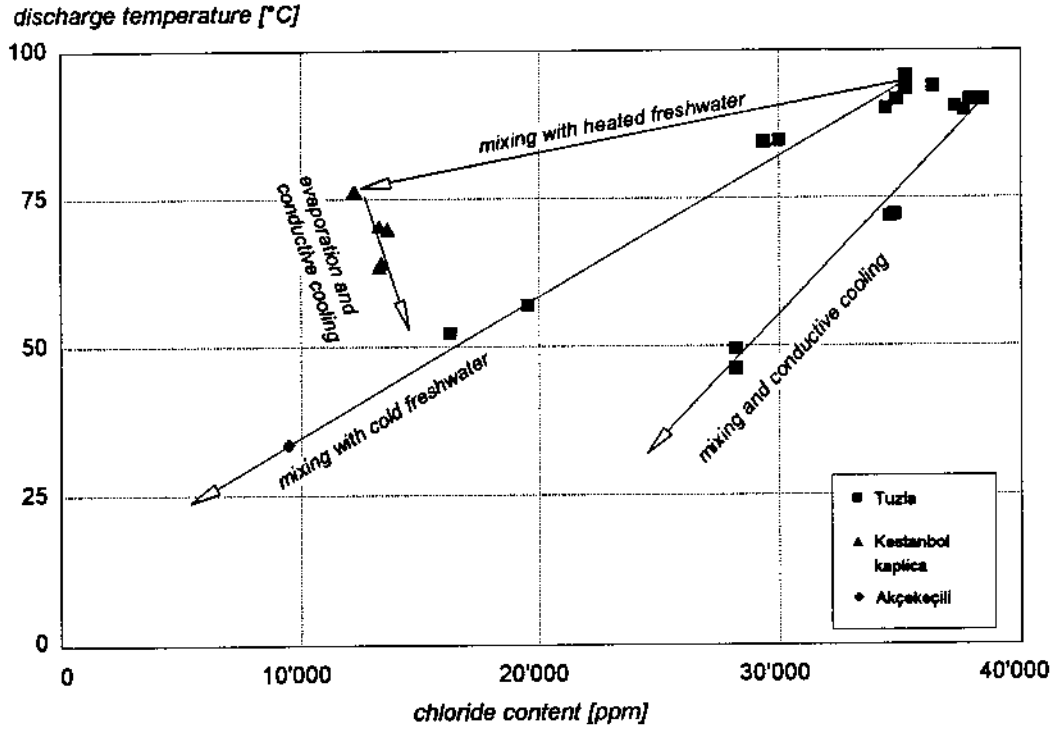


Figure 5: *The relationship between discharge temperatures and chloride contents indicates mixing with freshwater and conductive cooling during the ascent as the main cooling processes for the hot thermal brine.*

Isotope geochemistry

Introduction

As a first approach, it has been assumed that all samples taken can be considered to evolve from a common reservoir and result from the mixing of saline water (connate water) with freshwater. Further evidence of the origin and geochemical evolution of the endmembers can be obtained by the determination of natural stable and radioactive isotopes. Most geothermal waters related to local precipitation show characteristic oxygen shifts to higher $\delta^{18}O$ contents and $\delta^{2}H$ (deuterium) contents similar to local precipitation (Truesdell and Hulston 1980). In contrast, brines from many sedimentary basins vary both in $\delta^{18}O$ and $\delta^{2}H$ (Clayton et al. 1966).

In the present study, the contents of $\delta^{18}O$, deuterium and tritium of the thermal waters and the related freshwater springs were determined. In addition, $\delta^{34}S$ and $\delta^{18}O$ contents of the dissolved sulphates were measured for two samples, and one $^{3}He/^{4}He$ ratio was determined for a gas sample from Tuzla.

Deuterium, ^{18}O

On the $\delta^{2}H$ versus $\delta^{18}O$ diagram (Fig. 6) the values of the slightly mineralised shallow groundwaters are situated along the meteoric water line with the value $\delta^{2}H=8\times\delta^{18}O+10$. The values for the thermal waters fall below the meteoric water line and are generally more positive in $\delta^{18}O$ and $\delta^{2}H$ than the related freshwaters. Most of the samples in the three thermal areas fall on a line with a slightly lower slope than the meteoric water line. This line shows a mixing and dilution between the most concentrated brines of the Tuzla area and freshwater of meteoric origin. Thus, as already postulated in a previous chapter, the thermal waters of the three areas evolved from the same saline endmember and are diluted with local groundwater.

The same characteristics can be stated from the relationship between the chloride contents and the $\delta^{2}H$ and the $\delta^{18}O$ values (Fig. 7). Therefore, the most positive $\delta^{18}O$ and $\delta^{2}H$ values also correspond to the most saline water and the same mixing model for the isotopic and the chemical composition of the water can be derived.

Tritium

The tritium data reveal that only a small amount of the slightly mineralised groundwater of the freshwater springs contains anthropogenic tritium, whereas all of the mineralised thermal waters, except the spring in Akçekeçili, do not contain any measurable tritium (Fig. 7). In the thermal spring of Akçekeçili tritium is traceable to 3.5TU, a fact that emphasises the presence of recent freshwater.

^{34}S and ^{18}O in sulphates

The variation of the sulphur and oxygen isotopes in marine sulphates may document the age of the sulphates (Claypool et al. 1980) and the physicochemical factors which influence the sulphate contents in the water (Zak et al. 1980). For the present study only one sample from Kestanbol and one sample from Tuzla were analysed for their sulphur and oxygen isotope composition in the dissolved sulphate ions.

The values are $\delta^{34}S$ = 20.5‰ (CDT) and $\delta^{18}O$ = 7.55‰ (SMOW) for the sample K1 (Kestanbol kaplıca) and $\delta^{34}S$ = 12.63‰ (CDT) and $\delta^{18}O$ = 6.19‰ (SMOW) for T3 (Tuzla).

The rather low sulphate concentrations and different $\delta^{18}O$ $\delta^{34}S$ -values for evaporites (Claypool et al. 1980) exclude gypsum deposits as a possible sulphur source (Fig. 8).

The $\delta^{18}O$ $\delta^{34}S$ -values of the sample from Kestanbol are very similar to the measured values in tertiary interstitial waters from DSDP cores (Zak et al. 1980). The slight depletion of both isotopes may be due to the crystallisation of sulphates (gypsum, baryte) during the migration and the ascent of the thermal water. The sample from Tuzla shows no direct relation to the sample from Kestanbol or to any of the known sulphates. Low ^{34}S and ^{18}O values in sulphates, such as measured in this sample, are generally due to the dissolution and oxydation of metal sulphides. This may also be a process in the thermal water in the Tuzla area, where volcanic rocks with sulphide minerals are widespread.

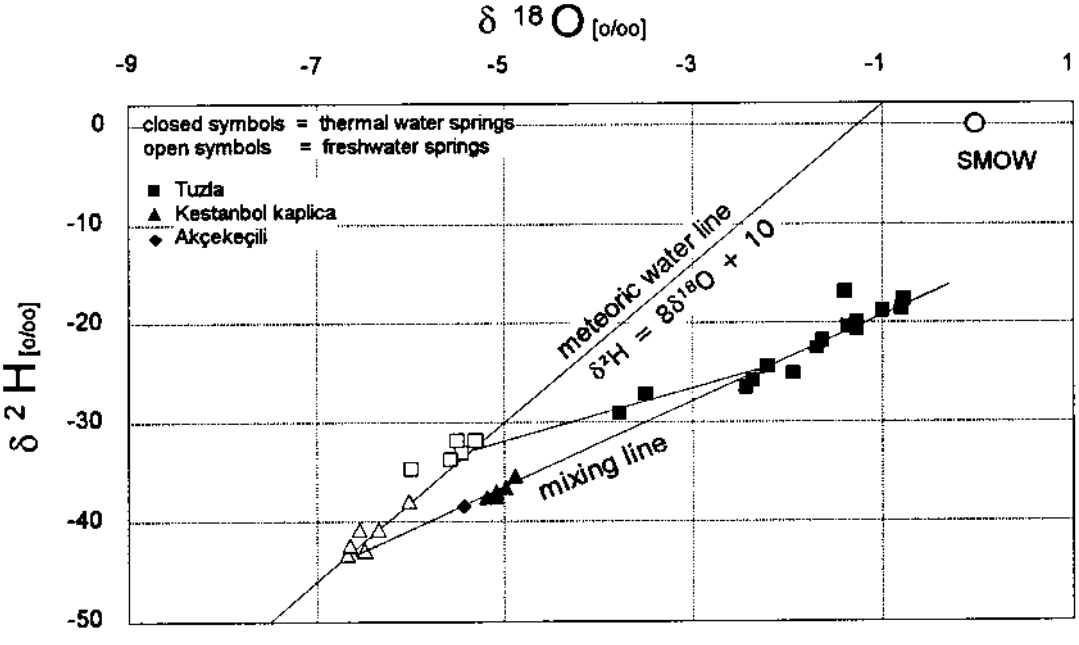


Figure 6: *The δ^2H and $\delta^{18}O$ values of the thermal waters are more positive with respect to related freshwater near the surface. The correlation of the different samples indicate a mixing with local meteoric water. Isotope analyses by gsf, Neuherberg, Germany.*

Helium isotopes

The isotope ^4He is produced in the continental crust through the radioactive decay of Uranium-238, Thorium-232 and their daughter products. On the other hand, only a minor amount of the isotope ^3He results from radioactive decay. The main contribution to the atmospheric $^3He/^4He$ -ratio of 1.4×10^{-6} is provided by premordial helium from the Earth's mantle or mantle helium (Mamyrin and Tolstikin 1984).

Helium isotopes in geothermal fluids are widely used to recognise active fault zones or generally mantle-crust interactions. High $^3He/^4He$ -ratios with respect to the atmospheric ratio, can be observed along active faults or in areas with volcanic activities.

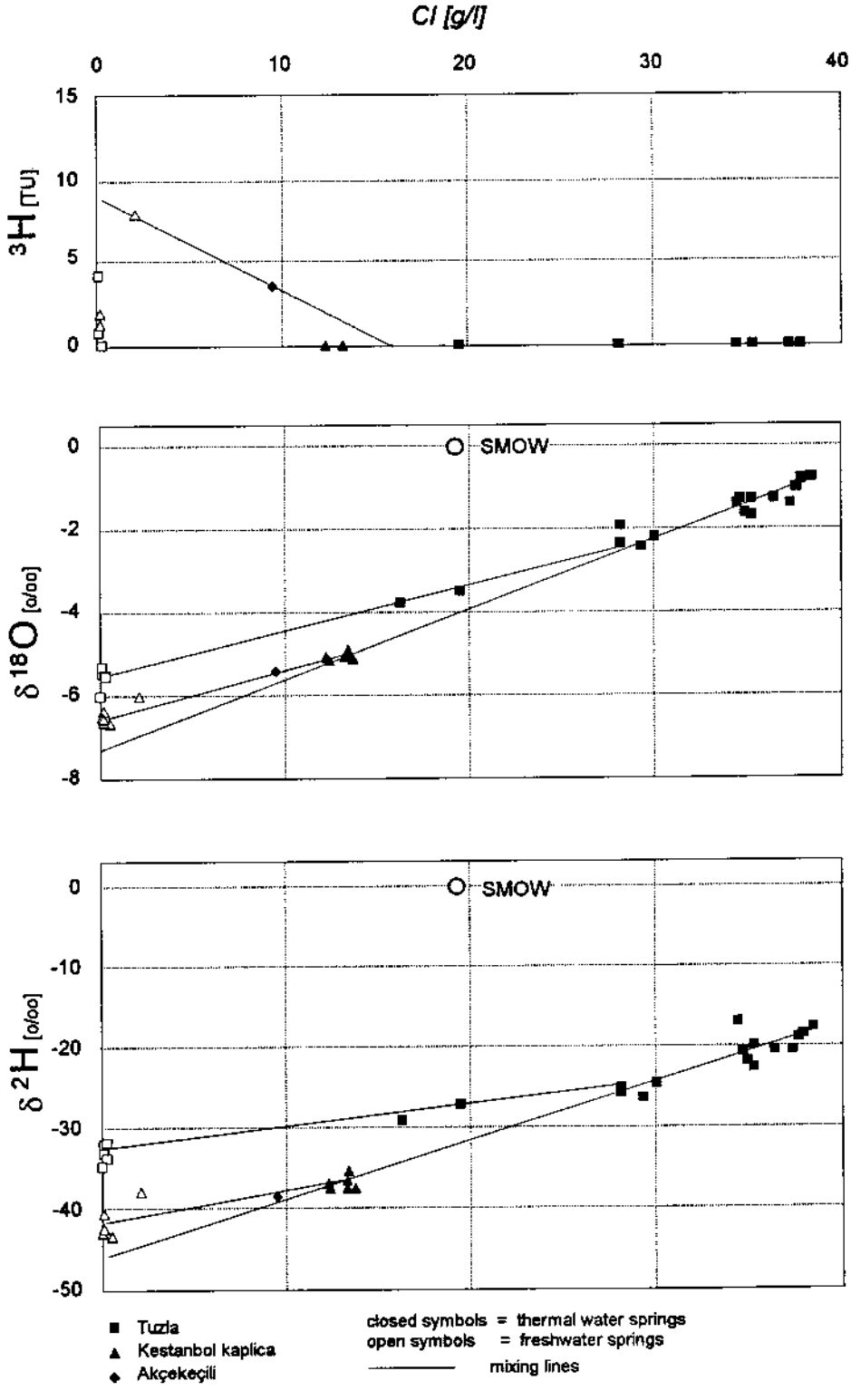


Figure 7: *Of the thermal waters tritium was detectable only in the slightly mineralised thermal water of Akçekeçili, indicating the presence of a young, freshwater near the surface. The $\delta^{18}O$ and δ^2H values elucidate the mixing of a chloride-rich endmember with $\delta^{18}O \approx 0‰$ (SMOW) and δ^2H greater than -20‰ (SMOW) and local freshwater of more negative $\delta^{18}O$ and δ^2H values. Isotope analyses by gsf, Neuherberg, Germany.*

In the Tuzla geothermal field one gas sample from a bubbling hot water pool was analysed for its $^3He/^4He$ ratio in the isotopic laboratory of the ETH Zürich. The recorded $^3He/^4He$ ratio of 2.03×10^{-6} is on the same order of magnitude with that reported from other geothermal areas in Western Turkey (Güleç 1988) and may indicate the presence of a mantle helium component in the thermal waters. In the Tuzla area the high $^3He/^4He$ ratio measured may thus be related to a deep, active fault zone.

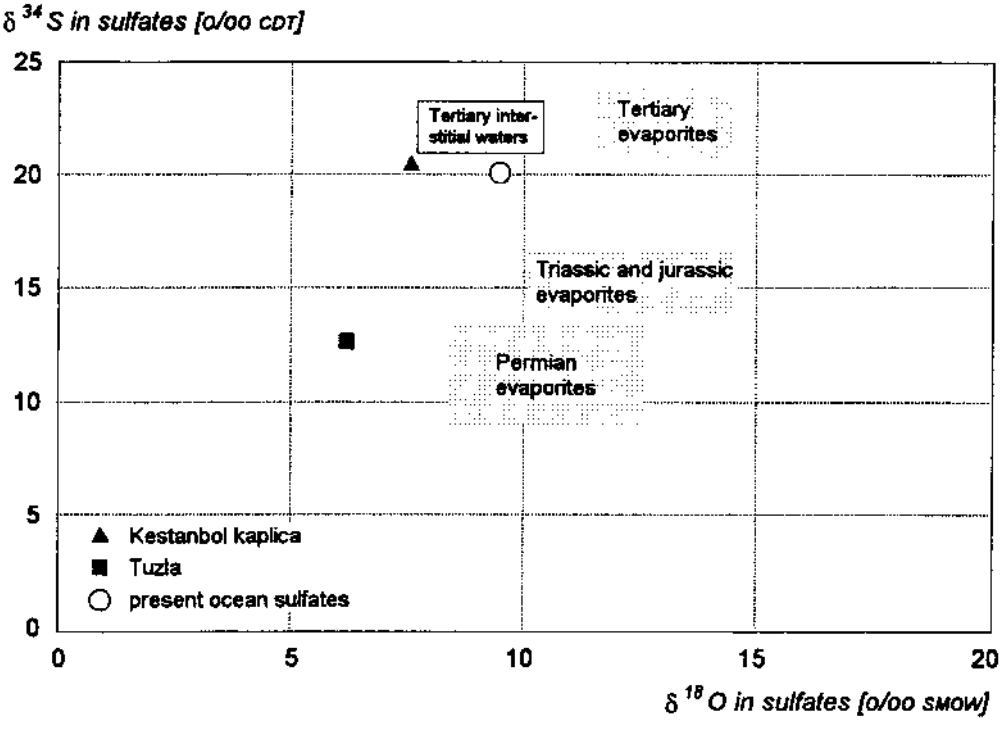


Figure 8: *Similar $\delta^{34}S$ and $\delta^{18}O$ in dissolved sulphates from the Kestanbol kaplıca thermal water and tertiary interstitial waters from DSDP cores (Zak et al. 1980) may indicate a similar origin for the thermal waters. For the sample of Tuzla additional water-rock interactions with metal sulphides is postulated. (evaporite data from Schmassmann et al. (1984) after Claypool et al. (1980)). Sulphate isotope analyses by university of Waterloo, environment isotope Lab.*

Hydrogeological circulation model

Based on the regional geological features and the chemical and isotopic data of the water, the following model for the origin, evolution and flow path of the thermal water in the western Biga peninsula is suggested:

(1) The Aegean sea can be considered as a classic example of a fast sinking basin in which a thick sequence of sediments and evaporitic layers have accumulated since the Miocene period. Fossil seawater trapped in these sediments is postulated to be the saline end-member of the hot mineral waters in the western Biga peninsula.

(2) The mineralisation of the fossil seawater increases due to diagenetic processes in the sediments and the dissolution of evaporitic layers.

(3) The existence of major fault zones in this area enhances the later mobilisation and migration of the saline water over large distances into metamorphic and plutonic rocks of the coastal area.

(4) Deeply-jointed and fractured volcanic and crystalline (metamorphic) rocks and Permian limestones build a deep reservoir for the saline water in the coastal area between Tuzla and Kestanbol. Miocene, loamy scree deposits which overlie the reservoir rocks act mostly as a impermeable cover.

(5) Rock-water interaction between silicate minerals of the reservoir rocks and the saline water increases the mineralisation only slightly. Due to the dilution with deep circulating freshwater, the salinity of the water in the reservoir decreases toward the north. Further dilution with freshwater of local meteoric origin occurs during the ascent of the hot saline water.

(6) The emergence of the water at the surface takes place where the impermeable cover is thin and the vertical permeability is increased due to the intersection of deep lateral and extensional faults.

Conclusions

With the presented study, the main geological and hydrogeological features of a geothermal area in the western Biga peninsula were recognised, based mainly on surface data. The interpretation of geological, hydrochemical and isotopic data shows good overall agreement. Unfortunately, only minimal sampling was carried out and only sparse data were obtained during former drillings, thus detailed information about the hydrogeological conditions at depth is limited.

The postulated circulation model with the mobilisation, large scale migration and upflow in the coastal area is rather extraordinary for a connate water, as such waters are generally sampled only from deep oil drillings in sedimentary basins. Nevertheless, the regional geological features, major active fault systems and many data from deep groundwater of other areas support this hypothesis. For further confirmation, however, additional sampling and investigation would be needed.

Acknowledgments

This work is part of a doctoral thesis carried out at the ETH Zürich and directed by Prof. Dr. C. Schindler, Engineering Geology. The research project was financed by the Direktion für Entwicklungszusammenarbeit und humanitäre Hilfe (DEH), Schweiz and the Gesellschaft für Strahlen- und Umweltforschung (gsf), Munich. It was the first study within the multidisciplinary MARMARA Poly-Project of the ETH Zürich.

I am very grateful to Prof. Dr. Conrad Schindler, to whom I owe the foundation of the project. His visits, along with his wife, in the field greatly helped me not only to understand the geology, but also to understand and love the Turkish people and the country. I am also very thankful to Prof. Dr. Kemal Erguvanlı and Prof. Dr. Erdoğan Yüzer for the opportunity to carry out this research in Turkey and for their help during the field work. I also thank PD Dr. Werner Balderer and Prof. Dr. Mark Grünenfelder for their visits in the field and stimulating discussions. I am also indebted to Prof. Dr. Terry Seward for the geochemical analyses, Prof. Dr. E. Flügel who produced the paleontological data on the limestones and Dr. Rolf Kipfer who analysed the helium isotopes.

References

Bingöl, T., Akyürek, B. and Korkmazer, B., 1973, Geology of the Biga Peninsula and some characteristics of the Karakaya Formation, Proc. Congr. Earth Sci. Ankara, 70-76.

Borsi, S., Ferrara, G., Innocenti, F. and Mazzuoli, R., 1972, Geochronology and Petrology of Recent Volcanics in the Eastern Aegean Sea (West Anatolia and Lesvos Island), Bull. volcanologique, 36/1 Napoli.

Brinkmann, R., 1966, Geotektonische Gliederung von West-Anatolen, N. Jb. Geol. Paläont., 10, 603-618.

Brinkmann, R., 1971a, Das kristalline Grundgebirge von Anatolien, Geol. Rundschau, Stuttgart, 60p.

Brinkmann, R., 1971b, Jungpaläozoikum und Älteres Mesozoikum in Nordwest-Anatolien, Bull. MTA 76, Ankara.

Brinkmann, R., 1971c, The Geology of Western Anatolia, in: Geology and History of Turkey, edited by: A.S. Campbell, Tripoli, 171-190.

Claypool, G.E., Holster, W.T., Kaplan, I.R., Sakai, H. and Zak, I., 1980, The age curve of sulphur and oxygen isotopes in marine sulphates und their mutual interpretation, Chem. Geol. 28, 199-260.

Clayton, R.N., Friedman, I., Graf, D.L., Mayeda, T.L., Meents, W.F. and Shimp, N.F., 1966, The origin of saline formation waters, Journal of Geophysical Research, 71/16.

Collins, A.G., 1980, Oilfield brines, in: Developments in Petroleum Geology 2, edited by: G.D. Hobson, Applied Science Publishers LTD, London, England.

Crampin, S. and Evans, R., 1986, Neotectonics of the Marmara Sea region of Turkey, Journ. Geol. Soc. London, 143, 349-353.

Dewey, J.F. and Şengör, A.M.C., 1979, Aegean and surrounding regions: Complex multiplate and continuum tectonics in a convergent zone, Bull. Geol. Soc. America, 90, 84-92.

Edmunds, W.M., Kay, R.L.F., Miles, D.L. and Cook, J.M., 1987, The origin of saline groundwaters in the Carnmenellis Granite, Cornwall (U.K.): further evidence from minor and trace elements, in: Saline water and gases in crystalline rocks, edited by: P. Fritz and S.L. Frape, Geol. Assoc. of Canada Special Paper, 33, 127-143.

Ellis, A. and Mahon, W., 1977, Chemistry and Geothermal systems, Academic Press, New York.

Erguvanlı, K., 1957, Outline of the Geology of the Dardanelles, Geol. Magazine, XCIV/ 1.

Frape, S.K. and Fritz, P., 1987, Geochemical trends for groundwaters from the Canadian Shield, in: Saline water and gases in crystalline rocks, edited by: P. Fritz and S.K. Frape, Geol. Assoc. of Canada Special Paper, 33, 19-38.

Fytikas, M., Giuliani, 0., Innocenti, F., Marinelli, G. and Mazzuoli, R., 1976, Geochronological data on recent magmatism of the Aegean sea, Tectonophysics, 31, 29-43.

Giggenbach, W.F. and Gougel, R.L., 1989, Collection and analysis of geothermal and volcanic water and gas discharges, Report No. CD 2401, Chemistry Division, DSIR, New Zealand.

Güleç, N., 1988, Helium-3 distribution in western Turkey, Bull. MTA, Ankara, 108.

Kaaden v.d., G., 1959, Age relations of magmatic activity and of metamorphic processes in the Northwestern part of Anatolia-Turkey, Bull. MTA, Ankara, 52, 15-33.

Kaya, 0., 1981, Miocene reference sections for the coastal parts of West Anatolia, Newsl. Stratigr., 10, 164-191.

Kaya, T., 1982, Gülpınar (Çanakkale) hipparionlarının odontolojik Özellikleri, Türkiye Jeoloji Kurumu Bülteni C.25, 127- 135.

Kharaka, Y.K. Carothers, W.W., 1986, Oxygen and hydrogen isotope Geochemistry of deep basin brines, in: Handbook of Environmental Isotope Geochemistry 2, edited by: P. Fritz. and J. Fontes.

Leaf, W., 1923, Strabo on the Troad, Book XIII, Cap.I, University press, Cambridge.

Mamyrin, B.A. and Tolstikhin, I.N., 1984, Developments in Geochemistry 3: Helium isotopes in Nature, Elsevier.

McKenzie, D.P., 1970, Plate Tectonics of the Mediterranean region, Nature 226, 239-243.

Mützenberg, S., 1990, Westliche Biga-Halbinsel (Çanakkale, Türkei) Beziehung zwischen Geologie, Tektonik und Entwicklung der Thermalquellen, PhD thesis, ETH-Zürich, No. 9113.

Şamilgil, E., 1984, Tuzla geothermal field (Canakkale/Turkey), MTA Ankara, unpublished report.

Schliemann, H.,1881, Reise in der Troas im Mai 1881, F.A. Brockhaus, Leipzig.

Schmassmann, H., Balderer, W., Kanz, W. und Pekdeger, A., 1984, Beschaffenheit der Tiefengrundwässer in der zentralen Nordschweiz und angrenzenden Gebieten, NAGRA Technischer Bericht, 84-21.

Tchihatcheff, P., 1853, Asie Mineure, Premiere Partie, Géographie physique, Paris.

Truesdell, A.H., 1975, Summary of Section III, Geochemical Techniques in Exploration, Proc. 2nd U.N. Symp. Develop. Use Geothermal Resources, Vol. 1. San Francisco.

Truesdell, A.H. and Hulston, J.R., 1980, Isotopic evidence on environments of geothermal systems, in: Handbook of environmental Isotope Geochemistry 1, edited by: P. Fritz and J. Fontes.

White, D.E., 1968, Environments and generations of some base-metal ore deposits, Econ. Geol., 63/4, 301-335.

Zak, I., Saki, H. and Kaplan, I.R., 1980, Factors controlling the $^{18}O/^{16}O$ and $^{34}S/^{32}S$ isotope ratios of ocean sulphates, evaporites and interstitial sulphates from modern deep sea sediments, in: Isotope Marine Chemistry, Geochemistry Research Association, edited by: E.D. Goldberg, Y. Horbie and K. Saruhashi, Tokio.

Appendices

Appendix 1: Chemical analyses of thermal waters

sample Nr.	K1/1	K1/2	K1/3	K2/1	K2/2	K3/1	K3/2	A1/1	A1/2
date	02.10.87	27.03.88	18.09.88	03.10.87	27.03.88	02.10.87	27.03.88	02.10.87	23.09.88
temp. [°C]	76.2	76.1	--	63.6	64.1	70.5	69.8	33.5	---
mS/cm	23.9	24.7	--	25.5	27.0	27.4	27.7	19.1	--
pH	5.9	--	6.5	6.2	--	5.9	--	6.4	6.6
Eh (Pt/AgC)	-80	-120	--	-55	-80	-50	-80	+5	--
cations [mg/l]									
Na	6570	6220	6920	6310	6910	6700	7200	4630	4920
K	804	904	799	866	949	903	981	741	749
Ca	828.7	835.7	807.2	882.8	927.9	938.7	959.9	540.5	534.7
Mg	61.8	45.0	59.3	62.6	49.8	68.0	52.3	38.3	36.5
Sr	--	47	--	--	52	--	53	---	--
Li	9.0	9.0	10.3	9.4	10.0	9.8	10.4	6.4	6.8
Ba	1.6	1.3	--	1.7	1.4	1.9	1.5	1.1	--
NH_4	8.5	6.9	--	7.9	6.4	9.0	7.7	6.0	--
anions [mg/l]									
Cl	12319	12230	12832	13294	13382	13269	13684	9483	9430
Br	20	20	--	17	21	23	3.6	11	--
I	0.94	0.83	--	0.8	.67	0.75	1.26	0.42	--
F	2.88	2.99	3.07	2.78	2.82	2.15	2.94	2.94	3.33
HCO_3	292.2	291.0	286.1	302.6	309.3	305.6	310.5	409.8	505.1
SO_2	96	77	103	92	67	91	80	42	43.2
SiO_2	139.3	115.7	--	124.3	109.3	132.9	109.3	111.4	--
H_3BO_3	74	63	--	74	74	80	69	46	--
Fe	1.1	6.2	--	1.2	2.8	1.2	9.2	0.8	--
Mn	1.4	1.3	--	1.5	1.5	1.9	1.6	1.2	--
TDS	21230	20875	21820	22050	22875	22540	23535	16070	16230
T-(SiO_2) [°C]	150.2	140.9	--	144.5	138.2	147.8	138.2	139.1	--
isotopes									
$\delta\ ^{2}H$ [‰]	-37.5	-37.0	--	-36.5	-35.4	-37.5	-37.6	-38.5	--
$\delta\ ^{18}O$ [‰]	-5.18	-5.09	--	-4.98	-4.88	-5.09	-5.11	-5.43	--
^{3}H [TU]	<0.9	--	--	<0.7	--	<1.2	--	3.5±0.7	--

Appendix 2: Chemical analyses of thermal waters

sample Nr.	TI	T2/1	T2/2	T3/1	T3/2	T3/3	T4/1	T4/2	T5/1	T5/2
date	09.82	03.10.87	24.03.88	03.10.87	26.03.88	19.09.88	03.10.87	24.03.88	02.09.87	24.03.88
temp. [°C]	173.0	95.6	84.6	90.5	94.0	--	57.0	52.3	90.1	91.6
mS/cm	57.0	62.6	51.2	65.2	65.1	--	36.9	31.8	59.4	61.7
pH	7	6.0	–	6.0	–	6.3	5.2	--	5.8	--
Eh (Pt/AgC)	–	-90	-60	-80	-60	--	+165	+210	-65	-25
cations [mg/l]										
Na	22250	18200	14660	19260	18900	19250	9640	7940	18140	17940
K	2125	1986	1990	2132	2500	2430	1028	1066	1842	2168
Ca	5716	2780.8	2408.8	2922.6	2992.0	2918.6	1576.7	1356.7	2806.4	2895.8
Mg	101	68.0	47.4	86.5	18.2	100.1	84.1	54.7	113.7	52.3
Sr	139	–	130	–	160	--	–	86	--	150
Li	74	23.4	20.4	25.2	25.2	31.1	12.0	12.0	22.9	24.0
Ba	4.1	6.4	4.3	1.0	4.8	--	2.9	2.5	4.0	3.2
NH_4	2.06	34.1	25.2	32.5	32.8	--	1.4	0.5	28.3	30.1
anions [mg/l]										
Cl	44140	35273	29335	37311	36425	37311	19498	16307	34430	34918
Br	–	50	42	53	58	--	22	21	51	57
I	1.0	1.6	0.88	2.0	1.76	--	2.5	0.23	0.41	0.83
F	4.3	1.99	1.92	2.11	2.11	2.2	0.53	0.52	--	1.37
HCO_3	55	86.6	99.4	77.5	84.8	92.1	85.4	157.4	160.4	173.9
SO_2	176	139	166	145	137	148	57	32	182	164
SiO_2	123	158.6	102.9	137.1	115.7	--	175.7	175.7	126.4	102.9
H_3BO_3	206	172	120	177	155	--	74	74	155	137.3
Fe	<0.1	2.9	3.2	3.0	1.2	--	1.3	0.2	2.2	8.4
Mn	5.7	6.4	5.3	7.0	6.9	--	4.6	5.3	5.8	6.5
TDS	75120	58990	49160	62400	61620	62280	32265	27290	58070	58835
T-(SiO_2) [°C]	143.9	156.8	135.3	149.3	140.9	--	162.3	162.3	145.3	135.3
isotopes										
$\delta\ ^2H$ [o/oo]	–	-22.6	-26.4	-20.5	-20.5	--	-27.2	-29.0	-16.9	-21.8
$\delta\ ^{18}O$ [o/oo]	–	-1.70	-2.44	-1.37	--1.27	--	-3.49	-3.77	-1.40	-1.63
^3H [TU]	–	<1.3	–	<1.1	–	--	<0.8	--	<1.40	--

Appendix 3: Chemical analyses of thermal waters

sample Nr.	T6/1	T6/2	T7/1	T7/2	T8/2	T9/2	T10/2	T11/1	T11/2	seawater
date	02.09.87	24.03.88	03.10.87	24.03.88	24.03.88	26.03.88	24.03.88	05.10.87	29.03.88	(TUREKIAN
temp. [°C]	91.7	91.5	72.0	71.8	89.7	93.6	84.9	46.0	49.5	1969)
mS/cm	65.8	66.5	59.5	59.6	67.8	59.6	53.7	54.2	49.6	
pH	6.1	--	6.2	–	--	--	--	5.8	--	
Eh (Pt/AgC)	-75	-95	-40	-25	-25	-50	+5	+20	--	
cations [mg/l]										
Na	19880	19620	17780	16760	18720	18140	15800	14440	14460	10800
K	2022	2434	2096	2180	2422	2182	1992	1510	1730	392
Ca	3031.7	3116.2	2999.6	2849.7	3038.1	2841.7	2537.1	2368.7	2551.1	411
Mg	121.5	137.3	132.7	70.5	48.6	65.6	9.72	122.5	18.2	1290
Sr	--	160	--	150	160	150	130	–	120	8.1
Li	25.2	26.0	26.0	24.8	26.4	24.8	22.0	18.5	20.0	0.17
Ba	5.6	4.5	3.3	2.4	3.9	4.1	2.8	1.9	1.4	0.021
NH_4	31.9	32.4	9.4	26.0	29.4	26.5	7.08	20.5	19.9	N: 16.17
anions [mg/l]										
Cl	37915	38463	34800	34652	37666	35273	30044	28183	28183	19400
Br	56	61	52	55	58	56	38	39	41	67.3
I	1.4	1.51	1.8	0.89	1.76	1.39	0.42	0.86	0.38	0.064
F	--	1.79	--	1.42	1.92	2.00	1.39	1.13	1.18	1.3
HCO_3	126.9	137.9	160.4	215.9	120.8	71.4	162.3	339.8	346.5	142
SO_2	170	166	161	164	134	172	159	212	200	2712
SiO_2	132.9	107.1	137.1	62.1	122.1	111.4	107.1	115.7	94.3	7.9
H_3BO_3	172	155	177	137	149	137	120	120	103	23
Fe	3.5	13.6	2.2	14.4	5.6	4.6	2.8	1.1	6.6	(0.0034)
Mn	7.2	7.6	6.5	5.4	7.7	4.5	5.4	5.6	5.5	(0.0004)
TDS	63700	64645	58545	57370	62715	59270	51140	47500	47900	35270
T-(SiO_2) [°C]	147.8	137.2	149.3	112.8	143.6	139.1	137.2	140.9	131.3	
isotopes										
$\delta\ ^2H$ [o/oo]	-18.5	-17.7	--	-20.6	-18.8	-19.9	--24.5	-25.2	-25.8	0
$\delta\ ^{18}O$ [o/oo]	-0.79	-0.77	--	-1.28	-0.99	-1.28	-2.2	-1.94	-2.36	0
^3H [TU]	<1.1	--	--	–	--	--	--	<0.9	--	

Regional investigation of cold groundwater for the determination of recharge conditions in geothermal areas of Northwestern Turkey

THOMAS EISENLOHR, CHRISTOF JECKELMANN, WERNER BALDERER, STEFANO BERNASCONI, WALTER RAUERT AND PETER TRIMBORN

Abstract

Cold groundwater systems in different geothermal areas of Northwestern Turkey have been characterised by chemical analysis, stable isotopes and tritium to determine the composition of the recharge of deep groundwater circulation. The δD and $\delta^{18}O$ values of the cold springs plot on a meteoric waterline (MWL: $\delta D = 8 \times \delta^{18}O + 15$), which is situated between the continental and the eastern Mediterranean MWL. A significant isotopic trend from west to east can be observed. In the western part, the ”heavy” atmospheric moisture of the Aegean sea influences the air masses. Infiltration water in the eastern part is more depleted and represents a more continental type. A correlation between infiltration altitude and deuterium content can be demonstrated locally. The gradient (δD/altitude) varies over the Marmara region from -0.6 to -1.7‰ δD/100m. On the Armutlu peninsula (eastern Marmara sea), cold springs close to the shoreline have higher chlorine contents due to salty sea spray. Furthermore, δD and $\delta^{18}O$ values on the outer peninsula are less depleted, which indicates a local influence of the surrounding sea on the atmospheric moisture. The tritium contents of the cold springs in the Marmara region increase from 4-15TU (1992) in the western part, and up to 14-24TU (1992) in the east. The main water reservoirs, the Aegean sea (2TU, 1994), the Marmara sea (14TU, 1993) and the Black sea (21TU, 1994), exhibit the same trend. The low values in the western part can be explained by a dilution of the air masses by atmospheric moisture from the Aegean sea. This influence decreases to the east, as has already been seen from stable isotopes. The rather high values in the Black sea region probably indicate an additional tritium source in the east. The investigations showed that the isotopic composition of the groundwater recharge varies significantly over the Marmara region. For the interpretation of the deep groundwater circulation it is therefore necessary to evaluate the local average input conditions.

Introduction

The main goal of the interdisciplinary MARMARA Poly-Project is the investigation of the relationship among deep groundwater circulation, active crustal movements, seismicity and heat flow in Northwestern Turkey (Schindler 1993). Hydrogeological investigations have focused on six limited areas with high geothermal activity (Fig. 1): Bergama (Jeckelmann 1996), Tuzla (Mützenberg this volume), Gönen (Yalcın this volume), Bursa (Imbach this volume), Armutlu (Eisenlohr this volume) and Kuzuluk (Greber this volume). In the different areas qualitative flow models of the thermal waters have been evaluated by geological mapping, field measurements at the spring sites and chemical and isotopic analyses of water and gas samples. Cold groundwaters can be used to constrain the isotopic composition of the recent recharge.

Therefore in each geothermal area some shallow groundwaters were sampled in addition to the thermal waters. The isotope analyses were carried out in Germany (GSF Institute of Hydrology, Neuherberg: $\delta^{18}O$, δD and tritium) and Zürich (Geological Institute, ETH Zürich: $\delta^{18}O$, δD). Oxygen and hydrogen data were normalised to the SMOW-SLAP scale. The analytical reproducibility (twofold standard deviation) is ±0.15‰ for oxygen, ±1‰ for hydrogen and ±1.1 to 1.7TU for tritium.

Climate

Northwestern Turkey is situated in a transition zone between the semiarid climate of the eastern Mediterranean, the continental climate of eastern Europe and the humid climate of the Black sea region. A pronounced climatic gradient exists across the Marmara region, as shown by the distribution of mean monthly precipitation at three representative stations (Fig. 1). Mean annual precipitation increases from about 600mm/year in the west to 900mm/year in the east, accompanied by a decrease in mean annual temperature from about 17° to 14°C. In the west, close to the Aegean sea, precipitation (and hence groundwater recharge) occurs mainly during the winter months, whereas rainfall is seasonally more evenly distributed in the Black sea region. The air masses responsible for precipitation enter the region of İstanbul during the winter months mostly from the west and during the rest of the year from the northwest (Erinc 1963-1964).

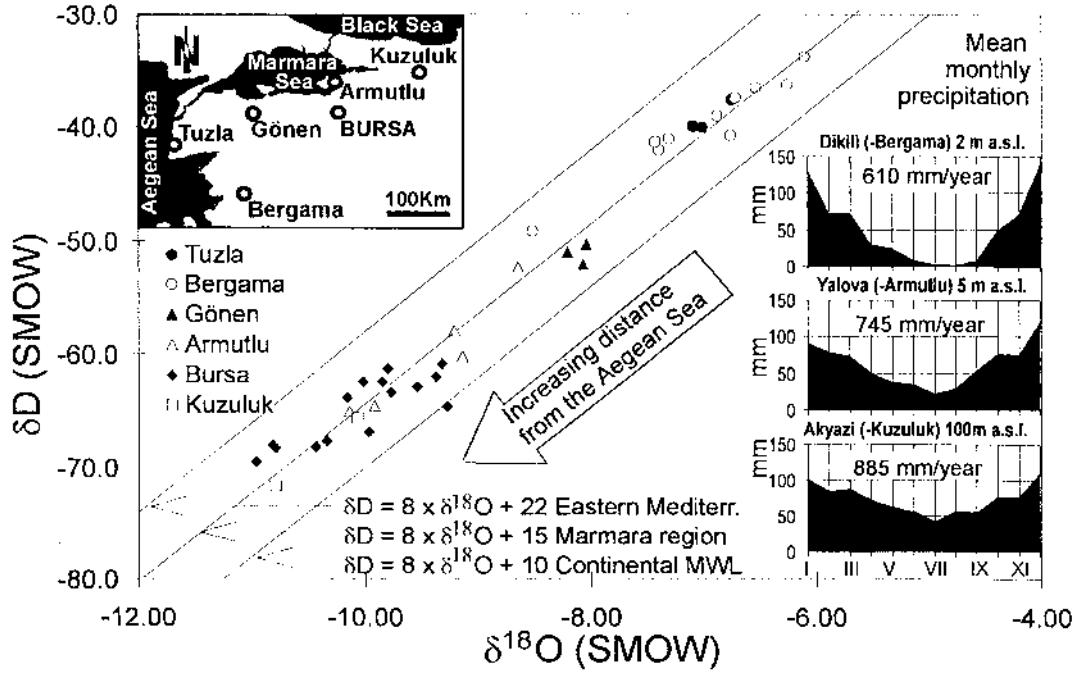


Figure 1: Location of the study areas, the mean monthly precipitation of three representative stations and the correlation of $\delta^{18}O$ and δD of cold groundwaters (spring discharge > 10l/min) in the Marmara region.

Isotopic composition of the cold groundwater

The δD and $\delta^{18}O$ values of cold groundwaters from the Marmara region plot on a meteoric waterline (MWL: $\delta D = 8 \times \delta^{18}O + 15$) which is situated between the continental and the eastern Mediterranean MWL (Gat, 1983) (Fig. 1). Springs with a discharge smaller than 10l/min show an ^{18}O enrichment due to evaporation and are therefore not included in Fig. 1. From west to east a significant isotopic trend can be observed. The δD values decrease from -35‰ to -70‰ and the $\delta^{18}O$ values from -6‰ to -11‰ as a result of the decreasing influence of atmospheric moisture from the Aegean sea. Owing to their upwind locations, the Aegean, the Marmara and the Black sea can be expected to have a significant influence on the isotopic composition of regional atmospheric moisture (see discussion of tritium, below). Isotopic data for samples from the three water bodies are presented in Table 1.

Water reservoir	Location (coastline, water surface)	Date of sampling	$\delta^{18}O$ [‰]	δD [‰]	Tritium [TU]
Aegean sea	Dikili near Bergama	Sept. 1994	+1.69	+8.7	1.5±1.1
Marmara sea	outer Armutlu peninsula	Aug. 1993	-1.75	-18.8	13.7×1.1
Black sea	upper Bosporus	Aug. 1994	-2.79	-25.1	21.4×1.7

Table 1: *$\delta^{18}O$, δD and tritium values of the main water reservoirs in the Marmara region (point measurements).*

In addition to regional trends, altitude effects on the stable isotope composition of precipitation are also evident at a local scale. For example, Fig. 2 shows data from the Bergama area, which has a gradient of about -1.3‰ δD/100m and the Armutlu peninsula, which has a gradient between -1.3 and -1.7‰ $\delta^{2}H$/100m. Deuterium values on the Armutlu peninsula show some spatial variation. On the outer peninsula, deuterium values are about 10‰ less depleted than in the southeastern part. For the determination of the local altitude-deuterium correlation it was necessary to distinguish three subareas (Fig. 2). Imbach (1992) observed a somewhat shallower gradient of about -0.6‰ δD/100m at Uludağ mountain near Bursa, which is more than 2500m high. A tendency exists for gradients to be steeper close to the sea, perhaps reflecting an enhancement of altitude effects by local rainout (i.e. ”continental”) effects.

The local deuterium-altitude correlation can be used to estimate the average altitude of the infiltration areas of thermal and karstic springs. The distinctly negative δD values of three karstic springs (see Fig. 2) in the southeastern part of the Armutlu peninsula, for example, indicate an infiltration area at about 800m a.s.l., which is well in accordance with geological observations.

The chemical and isotopic composition trends of the cold springs on the Armutlu peninsula indicate a direct influence from the sea. With increasing altitude and horizontal distance of the infiltration area from the shoreline, chlorine contents decrease from almost 100mg/l to values around 5mg/l (Fig. 3, left). Since no relationship between chlorine content and aquifer lithology is apparent, the enrichment in chlorine is most probably caused by salty sea spray. With increasing chlorine content the $\delta^{18}O$ value becomes more positive (Fig. 3, right). Owing to the most common wind direction in this region, a local influence of the surrounding sea on the atmospheric moisture can be expected.

Tritium contents of the shallow groundwaters also vary in the Marmara region. In 1992, shallow springs around Bergama were characterised by tritium contents between 4 and 15TU and on the Armutlu peninsula between 8 and 22TU. Measurements in 1990 around Kuzuluk yielded values between 16 and 28TU (Greber 1992). Values between 14 and 24TU result after correction for decay for 1990 to 1992. The only measured rain sample from the Armutlu peninsula (August 1994, 800m a.s.l) contained 21.1±1.7TU. Fig. 4 shows the existence of an

apparent relation among the tritium contents of the shallow groundwaters at Bergama, Armutlu, and Kuzuluk and the Aegean, Marmara, and Black seas, respectively, which suggests that local precipitation is strongly influenced by these water reservoirs. The low tritium values in the western part of the Marmara region can be explained by dilution of the air masses from western Europe with atmospheric moisture from the Aegean sea. The influence of the Aegean sea decreases more to the east, as has already been seen from stable isotopes. The tritium values in the central Marmara region are in the expected range of continental air masses. In the Black sea region, tritium values are rather high which may indicate an additional tritium source in the east.

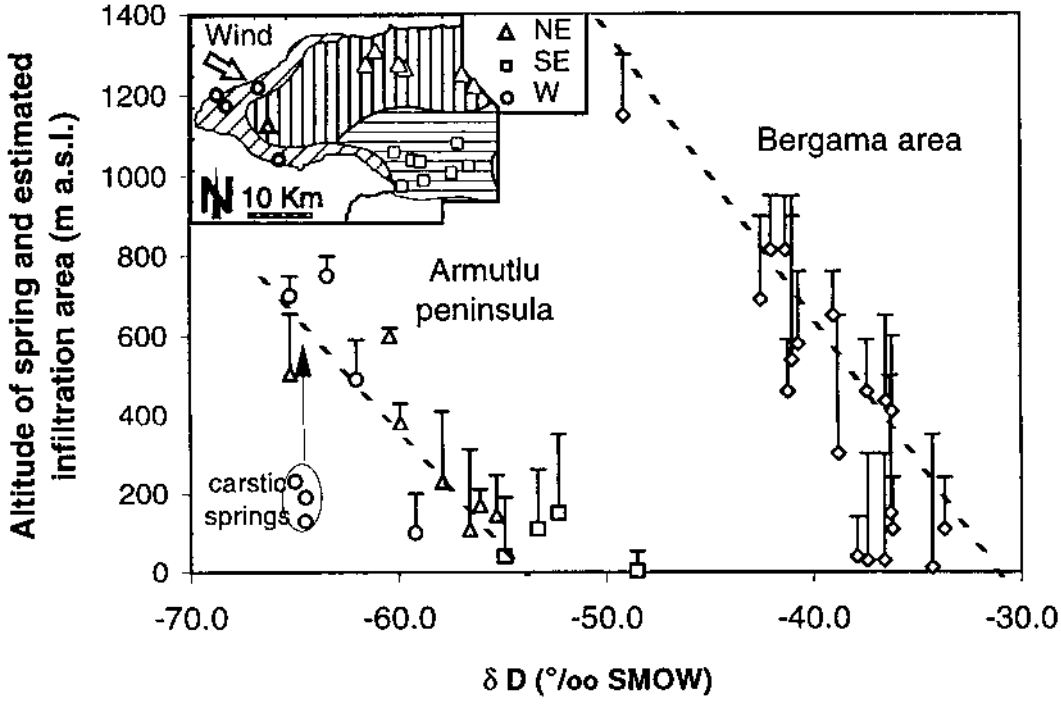


Figure 2: *Infiltration altitude – deuterium plot of cold springs in the Bergama area and on the Armutlu peninsula (correlations estimated); sampling locations on the Armutlu peninsula with three crosshatched subareas NE, SE and W (small map).*

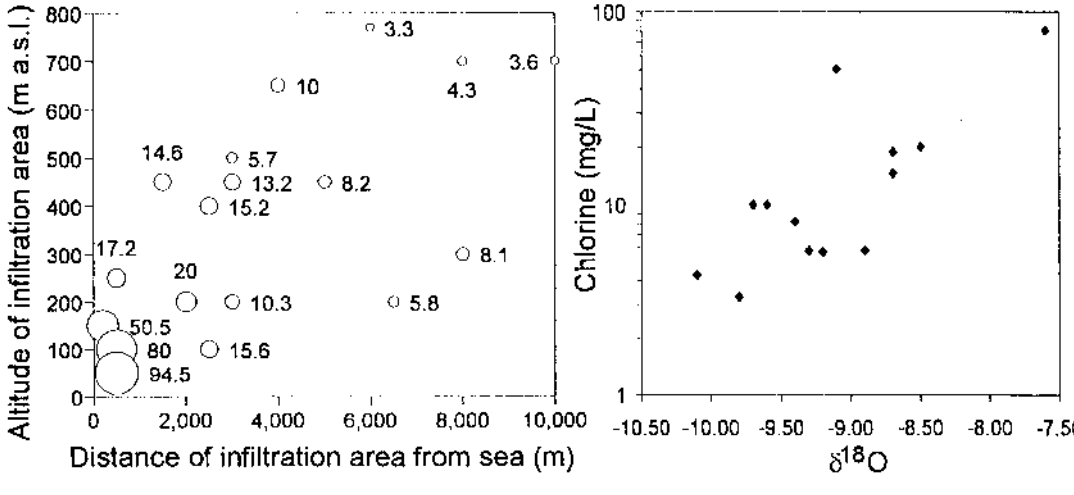


Figure 3: *Left: Chlorine contents (in mg/l) of cold springs on the Armutlu peninsula in relation to the infiltration altitude and the horizontal distance from the shoreline (shortest distance). Right: Chlorine (logarithmic scale) – $\delta^{18}O$ plot of cold springs on the Armutlu peninsula.*

The variations of tritium in shallow groundwater are rather important for the interpretation of deep groundwater circulation. While a tritium content of 5TU might be indicative of fairly recent recharge in the Bergama area, such a low value could indicate much older water in the eastern part of the Marmara region.

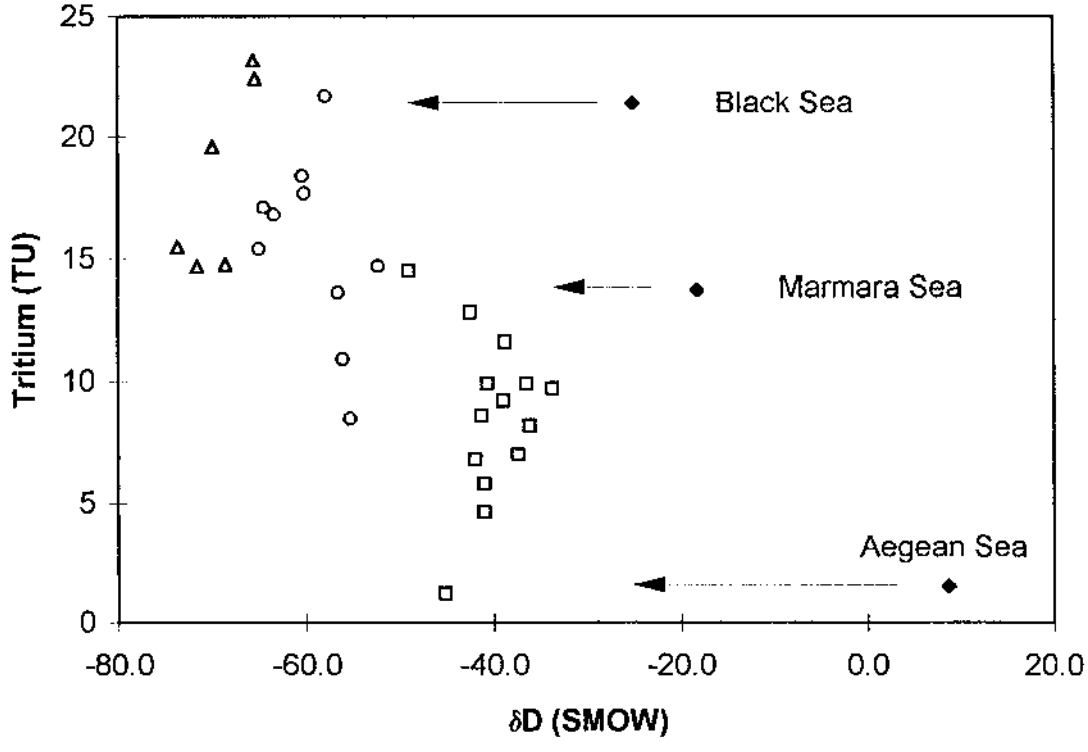


Figure 4: *Tritium – deuterium plot of the Aegean sea, the Marmara sea, the Black sea and cold springs (□ Bergama 1992, ○ Armutlu 1992, △ Kuzuluk decay-corrected from 1990 to 1992).*

Conclusions

The investigations of the MARMARA Poly-Project showed that the isotopic composition of cold groundwaters varies significantly over the Marmara region. The Turkish meteorological stations Ankara and Antalya are rather far away and are influenced by other local climates. Because of these strong local effects the data from these stations cannot be used for the Marmara region. For the interpretation of the deep groundwater circulation it is necessary to evaluate the local recharge conditions. Unlike rain and surface water, cold shallow groundwaters show very little seasonal variation in isotopic composition. Therefore, they are a good tool for the characterisation of the local average input conditions.

Acknowledgement

Thanks goes to the staffs of the GSF Institute of Hydrology, Neuherberg and the Institute of Geology of the ETH Zürich. We thank also Prof. Tom Edwards, Waterloo University, Canada, and our colleagues within the MARMARA Poly-Project for the good collaboration and fruitful discussions.

References

Eisenlohr, Th., this volume, The thermal springs of the Armutlu peninsula (NW Turkey) and their relationship to geology and tectonic.

Erinc, S., 1963-1964, Monthly Sequence and Frequencies of Weather Types in Istanbul, Rev. Geograph. Inst. University Istanbul, No. 9-10, 85-106.

Gat, J.R., 1983, Precipitation, groundwater and surface waters: Control of climate parameters on their isotopic composition and their utilisation as palaeoclimatological tools. Palaeoclimates and Palaeowaters: A Collection of Environmental Isotope Studies (Proc. Advisory Group Mtg Vienna, 1980), IAEA, Vienna, 3-12.

Greber, E., 1992, Das Geothermalfeld von Kuzuluk/Adapazarı (NW-Türkei), Geologie, aktive Tektonik, Hydrogeologie, Hydrochemie, Gase und Isotope, Diss. ETH Zürich, Nr. 9984, 213.

Greber, E., this volume, Deep circulation of CO_2-rich palaeowaters in a seismically active zone (Kuzuluk/Adapazarı, Northwestern Turkey).

Imbach, Th., 1992, Thermalwässer von Bursa, geologische und hydrogeologische Untersuchungen am Berg Uludağ (NW-Türkei), Diss. ETH Zürich, Nr. 9988, 178.

Imbach, Th., this volume, Geology of Mount Uludağ with emphasis on the genesis of the Bursa thermal waters, Northwest Anatolia, Turkey.

Jeckelmann, Ch., 1996, Genese lokaler Thermalwasservorkommen in der Region Bergama/W-Türkei, Diss. ETH Zürich, Nr. 11990, 199p.

Mützenberg, St., this volume, Nature and origin of the thermal springs in the Tuzla area, Western Anatolia, Turkey.

Schindler, C., 1993, The Marmara-Project: tectonics and recent crustal movements revealed by space-geodesy and their interaction with the circulation of groundwater, heat flow and seismicity in Northwestern Turkey, Terra Nova, 5 164-173.

Yalçın, T., this volume, Hydrogeological investigation of the Gönen and Ekşidere thermal waters (NW Turkey).

THEME 5

Contributions

Geology of Northwestern Turkey: Results of the MARMARA Poly-Project

CONRAD SCHINDLER

Abstract

In this paper, an evaluation of the geology of the 6 PhD theses of the MARMARA Poly-Project is given, completed by former investigations of Pavoni, Kopp and the author himself in Turkish Thrace. The synthesis takes into consideration numerous articles mostly published during the last decade. Within Theme 6 of this volume, the interrelations to the results of the other groups of the project are discussed.

As far as has been investigated, *Paleotectonics* started with two Paleozoic orogenic phases, both probably being *Variscan*. In three of our research areas, Permian sediments have an unconform, but stratigraphic, contact with the underlying metamorphic rocks. No statements are possible with regard to the question of a Late Triassic orogeny, as the single research area possibly situated in this zone yielded no key outcrops or fossils. The *Alpine cycle* started in the Lowermost Jurassic with the opening of a small northern branch of Neotethys. An important, early Alpine collision during the Late Cretaceous left an E-W oriented belt of metamorphic rocks. This belt becomes larger to the west, but east of the MARMARA research region it pinches out into the Intrapontide suture.

The zone with metamorphics later (at least temporarily) had a tendency for uplift while the adjoining areas on both sides subsided and were filled by flysch or other sediments. The compressive part of the Alpine cycle near the Oligocene-Miocene limit ended with moderate folding and faulting, best observed in Thrace.

Neotectonics began in the Middle Miocene (Langhian), probably connected with a new regime of subduction in the Eastern Mediterranean region. First, large areas broke up, than a part of Western Anatolia *rotated anticlockwise* for some 25°. Paleogeography dramatically changed: As proven by a transgression near the beginning of the Tortonian, the coastlines of the Marmara and Aegean seas already were similar those today. *Aegean extension,* including westernmost Anatolia, started in the Middle Miocene and – with at least one interruption – continued to the present. The *NAFZ* (*N*orth *A*natolian *F*ault *Z*one) progressed from east to west and reached the Marmara region in a *first phase of activity* during the Tortonian. The movements predominantly followed the southern zone, splitting west of İznik, then cutting the edge of the previously rotated block. More to the west they weakened and were lost before reaching the Aegean coast. A gentle phase of compression near the Miocene-Pliocene limit stopped all previous movements.

3-4m.y. ago, in the Middle Pliocene, Aegean extension and dextral movements resumed and still are going on. During the *second phase of NAFZ activity,* the displacements mainly followed the northern zone and progressed through the gulf of Saros into the Aegean sea. The movements were combined regionally with an anticlockwise rotation of 5° and the opening of a deep trough in the Marmara sea.

Are the *neotectonic* alignments *fixed* by *paleotectonics*? Obviously they frequently follow preexisting faults or zones of weakness as, e.g. the borders of the İznik metamorphics zone. The character and direction of the displacements, however, was changed. Even later, during neotectonics, the stress field varied and the movements were not continuous; NW Anatolia has to be regarded as a very unstable region. North of the NAFZ, however, conditions completely change: since the Middle Miocene, Thrace and the Kocaeli peninsula seem to be quiet.

Table of contents:

Introduction 330
Paleozoic 334
- Metamorphic series of the Uludağ, Ezine, Gönen and Kozak areas
- Permian sediments
- Age of the metamorphics and the metamorphose

Mesozoic and Paleocene 336
- Triassic, unmetamorphic Jurassic and Early Cretaceous, Gönen area
- Metamorphic Mesozoic series (İznik metamorphics), Kuzuluk, Armutlu and Şarköy areas
- Late Cretaceous and Paleocene sediments
- Tectonics from the Jurassic to the Paleocene

Eocene, Oligocene and Burdigalian (Lower Miocene) 339
- Eocene sediments
- Oligocene sediments
- Plutonites of Late Cretaceous to Burdigalian age
- Volcanics of Late Cretaceous to Burdigalian age
- Questions about intrusions, volcanics, uplift and erosion in the Ezine, Kozak and Uludağ areas
- Late Alpine compression in Thrace (Late Oligocene – Early Miocene)

Middle Miocene to Quaternary sediments and volcanics 345
- Middle and Late Miocene sediments
- Messinian (Uppermost Miocene)
- Pliocene sediments
- Quaternary sediments
- Volcanics since Middle Miocene

Neotectonics (Neo Alpine tectonics) 349
- Results of paleomagnetism, possibility of rotations
- Rotated zone in Northwestern Anatolia: borders and time of activity
- North Anatolian Fault System (NAFZ): First period of activity
- Messinian to Lowest Pliocene deformations
- Second phase of the NAFZ activity: Collected data
- Second phase of the NAFZ activity: Conclusions
- Neotectonic history of Uludağ

Conclusions 363
- Neotectonics: Movements, phases of activity, total displacements
- Average rate of movements
- Paleogeographic reconstruction, paleotectonics
- Relations between paleotectonics and neotectonics

Introduction

In the MARMARA Poly-Project, much attention has been paid to geology. The reason is that all of the other disciplines included in the project, such as hydrogeology, geodesy, seismology and geothermics, have to rely upon the current structures, processes and events. Geology analyses the current situation and, in addition, can give information on past development, thus furnishing a key to interpret the present. Therefore, the group working on geology and hydrogeology was formed of the most persons and began our activities in Turkey. The area covered by the project is very extensive (greatest extension 400km, average width 80km). It

was therefore impossible to cover all of it by detailed geological mapping and analysis. A limited number of restricted areas of special geological and hydrogeological interest were studied in detail (distribution see Fig. 3 in Theme 1 of this volume). Theme 4 of this volume gives a summary of all the individual contributions in the field of geology and hydrogeology. The PhD theses included in this project were all published in full, but they are available only in limited quantity at ETH Engineering Geology.

The various areas studied in detail proved to be very different from each other in geological and tectonical configuration. As results from Theme 4 of this volume show, a puzzle of information on geology and hydrogeology arises, already including some interrelations to the other disciplines of the project. However, this puzzle does not cover all of the stratigraphic or tectonic units present in NW Turkey. For instance, stratigraphic sequences covering the late stages of paleotectonics and much of neotectonics were incomplete, poorly exposed or heavily disturbed by tectonics. Looking around for more quiet and complete sections, southern Thrace proved to be a key region. This region was only marginally involved in the MARMARA project but detailed mapping and stratigraphic studies from Pavoni, the author and – especially for the Dardanelles peninsula – from Kopp could be relied upon. The results were partially published (Kopp 1964, Kopp, Pavoni and Schindler 1969).

In spite of numerous publications, mostly printed during the last decade, the actual knowledge of stratigraphy, tectonics and the structure of the lithosphere in Northwestern Turkey and the neighbouring areas still remains at a lower level than, for example, in Central Europe. As everybody working in this field will soon realise, controversial interpretations and open questions are quite common. This happens not only if older publications are compared with current ones but also if recent papers are compared. To furnish some direction in thus a quite confused situation, Table 1 was drafted, based on literature and the author's own results. This table should give rough outlines of the most probable solutions and timetables.

In Theme 3 of this volume, the papers of Yılmaz and Barka summarise the current stage of knowledge of stratigraphy and tectonics of Western Turkey, independent of the MARMARA project research. As they give an extensive literature list, only papers with reference to this text will be quoted in order to avoid repetitions. The same principle will be applied for the individual reports on geology and hydrogeology in Theme 4 of this volume.

As previously mentioned, the puzzle of information resulting from the MARMARA project has gaps. For example, no results were obtained for the controversial problem of a Triassic Karakaya trough. As the aim of this paper is to condense and evaluate the geological and tectonical results of *our project*, such questions will only be mentioned briefly. The reader will find some differences in the details of the interpretation of different authors of this volume as, e.g. between this paper, and those of Yılmaz or Barka concerning geology. Such contrasts were deliberately left open, as for the moment the most important thing is to collect as many facts and arguments as possible. The conclusions have to be regarded as open to discussion.

Reference maps for this paper are the sheets for İstanbul, Zonguldak and İzmir of the geological map of Turkey 1:500,000 (1964) and the geological map of Greece 1:500,000 (1983). The geological map of Turkey 1:2,000,000 (1989) gives additional and more recent general information. All of the locations cited in this paper can be found in the first theme of this volume, Figure 1.

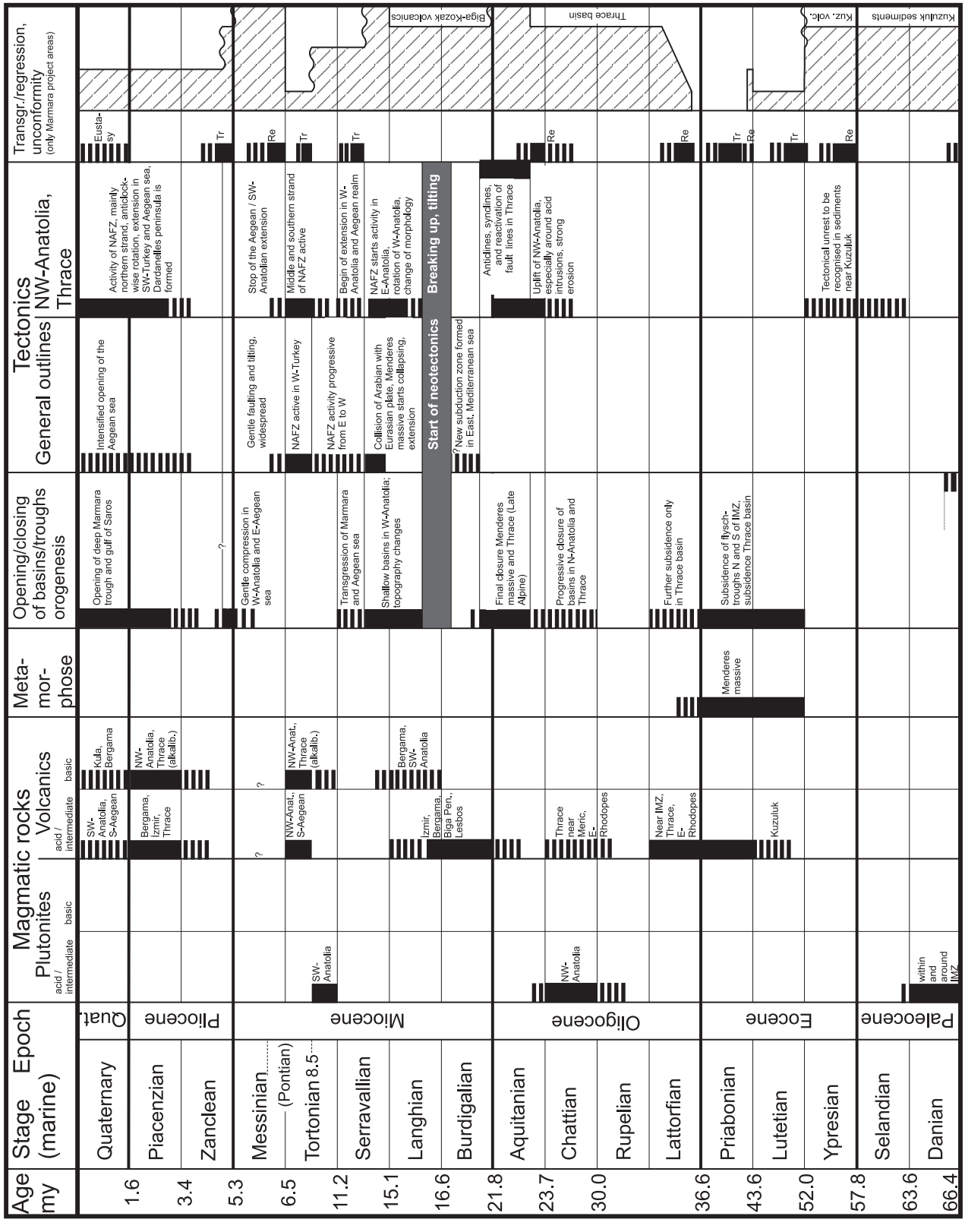
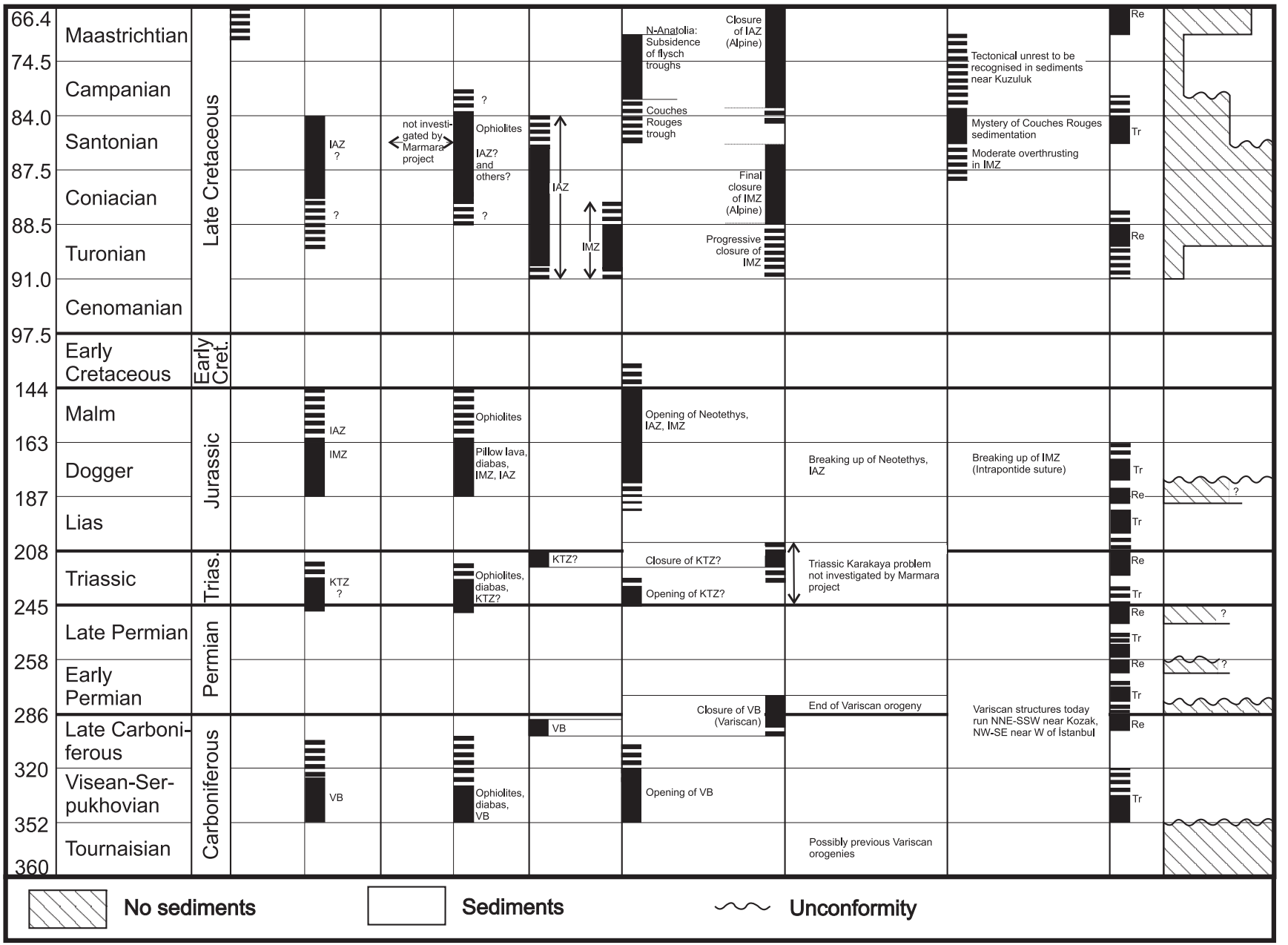


Table 1: Compilation of geological events in NW Turkey. VB = Variscan basins, KTZ = Karakaya Triassic zone, IAZ = İzmir-Ankara zone, IMZ = İznik metamorphics zone (Intrapontide suture). Absolute ages of the stages from: Geology, September 1983, page 504.


66.4
74.5
84.0
87.5
88.5
91.0
97.5
144
163
187
208
245
258
286
320
352
360
Maastrichtian
Campanian
Santonian
Coniacian
Turonian
Cenomanian
Early Cretaceous
Malm
Dogger
Lias
Triassic
Late Permian
Early Permian
Late Carboni-ferous
Visean-Ser-pukhovian
Tournaisian
Late Cretaceous
Early Cret.
Jurassic
Trias.
Permian
Carboniferous
IAZ ?
?
not investi-gated by Marmara project
?
Ophiolites
IAZ? and others?
?
IAZ
IMZ
N-Anatolia: Subsidence of flysch troughs
Closure of IAZ (Alpine)
Couches Rouges trough
Final closure of IMZ (Alpine)
Progressive closure of IMZ
Tectonical unrest to be recognised in sediments near Kuzuluk
Mystery of Couches Rouges sedimentation
Moderate overthrusting in IMZ
Re
Tr
Re
IAZ
IMZ
Ophiolites
Pillow lava, diabas, IMZ, IAZ
Opening of Neotethys, IAZ, IMZ
Breaking up of Neotethys, IAZ
Breaking up of IMZ (Intrapontide suture)
Tr
Re
Tr
?
KTZ ?
Ophiolites, diabas, KTZ?
KTZ?
Closure of KTZ?
Opening of KTZ?
Triassic Karakaya problem not investigated by Marmara project
Re
Tr
Re
Tr
Re
Tr
?
?
Closure of VB (Variscan)
End of Variscan orogeny
Variscan structures today run NNE-SSW near Kozak, NW-SE near W of İstanbul
Re
VB
Ophiolites, diabas, VB
Opening of VB
Tr
Possibly previous Variscan orogenies
No sediments
Sediments
Unconformity

Paleozoic

Metamorphic series of the Uludağ, Ezine, Gönen and Kozak areas

Several types of metamorphic series can be distinguished in those four working fields of the MARMARA project:

- *Highly metamorphic rocks* (amphibolite facies): Gneises, amphibolites and some quarzites, with thick persistant layers of marble (partly dolomitic) and a strong, ductile deformation. They were studied at Uludağ by Imbach (1992 and this volume). Similar sequences are known from Kazdağ, the Erdek peninsula and the Marmara islands. Eisenlohr (1995 and this volume) describes amphibolites and gneises from the western part of the Armutlu peninsula, but marbles are missing there. A correlation to the highly metamorphic Uludağ series cannot be proved.
- Basic to ultrabasic volcanics and plutonites, serpentinites, greenschists, micaschists and phyllites with thin layers of limestone marble. The deformation is predominantly of a ductile type. Such series occur north of Uludağ (tectonostatigraphic Nilüfer unit), in a few outcrops with huge marble bodies north of Gönen and to the northeast of Kozak (Çavdartepe formation) where it contains extensive lenses of marble (Jeckelmann 1996). The degree of metamorphism can be fixed near Uludağ and Kozak as higher *greenschist facies*.
- Chaotic, *intensively tectonised series*, predominantly detritic, with arcoses, greywackes, siltstones, shales, marls, phyllites, micaschists, cherts, but also with serpentinites and diabas. Characteristic for these flysch-type sequences are blocks and lenses of foreign material, mainly different types of recrystallised limestone. Light grey carbonates locally form huge lenses up to a length of more than 100m. Most authors interpret these inclusions as olistostromes glidden in a deep flysch-type trough, another explanation would be boudinage by intensive tectonic stress and squeezing. As Jeckelmann (1996) proved, the limestone bodies were deformed and partly marmorised during the mainly ductile, partly brittle orogeny affecting all of the series (Kınık formation) in the Kozak region. This type of chaotic tectonostratigraphic sequence was given the name Hodul unit by Bingöl et al. (1973). Good outcrops of it occur northwest of the Gönen research area. North of Uludağ (Imbach 1992 and this volume) and south of Tavaklı on the Biga peninsula (Mützenberg 1991 and this volume) the same type of sediments is outcropping. However, lenses of limestone are less common and smaller there.

Permian sediments

A central point of many discussions is the question of whether an outcrop of Permian still lies in the original stratigraphic position or whether it has to be interpreted as an olistostrome and once was glided into a flysch-type sequence of Triassic age. Both situations can occur, so the chosen solution is quite important for the interpretation of local tectonics.

North of Uludağ (Imbach 1992), northeast of Kozak (Jeckelmann 1996) and south of Tavaklı (Mützenberg 1991), stratigraphic sections and an *angular unconformity* with the underlying metamorphic series could be observed. In contrast to the intensive and mainly ductile deformation at the bottom, the Permian sediments lie much flatter and are only affected by brittle deformation, mostly by steep standing faults. Metamorphism is missing or is very low. As Jeckelmann (1996) shows, the difference between the two types of carbonatic rocks is obvious if a comparison is made by cathode luminescence.

Below the thick platform of Permian limestones lies a *basal sequence* of changing character and thickness. Locally, the transgression is marked by a basal conglomerate. Arcoses, calcareous sandstones and some basalt dykes or layers are typical. Kahler (1977) analysed the stratigraphy of the Permian around Bergama in detail. He found that the basal sequence originally included fossiliferous layers of Lower Permian limestones, but that they later were eroded and resedimentated. This explains the fact that north of Uludağ blocks of Permian limestones are found occasionally within the sandy basal sequence or even included in basalts (Imbach 1992, Brinkmann 1971). This, however, is clearly stratigraphic and no proof of an olistostrome.

The *carbonatic Permian platform* according to Brinkmann (1971) can reach a thickness of 500m, but the upper part was eroded in all outcrops studied in the MARMARA project. The series are fossiliferous, especially near the slightly sandy base, giving an age of Lower to Upper Permian.

North and northwest of Gönen, the slightly metamorphic Hodul unit contains huge lenses of light grey recrystallised limestone. They were interpreted by Yalçın (this volume) in accordance with other authors as olistostromes of Permian bedded in Triassic sediments. As fossils are missing here, further investigations should be made.

Age of the metamorphics and the metamorphose

The ages proposed in the literature for the rocks and the metamorphose vary between Precambrian and Mesozoic (Imbach this volume). There are obvious differences in the lithology of the series involved, but this is no clue for the age. Flysch-type sequences, for example, can be sedimentated several times during the geological history of a region, so overall solutions have to be excluded. For the MARMARA research areas of Uludağ, Ezine and Kozak, however, an upper time limit is given by the Lower Permian transgression. On the other hand, Imbach (1992 and this volume) found remains of a coral in the marbles of the amphibolitic series of Uludağ. The marbles age must be younger than Ordovician, as this fossil was confirmed by the paleontological institute at the university of Zürich and corals get generally frequent in Silurian. The flysch-type series below Permian unconformity probably were sedimentated in a *Variscan trough*. According to Brinkmann (1971), it opened during the Lower Carboniferous and was closed early in the Permian. The greenschist-carbonate series may be connected with the opening phase. For the three MARMARA research areas mentioned, it can tentatively be said that the series involved are Silurian to Devonian and Carboniferous in age and were deformed by Variscan orogenies. Unfortunately, all contacts between the different metamorphic units are tectonic. The series with amphibolite facies at some locations contain metagranites. Coğullu (1965) determined an age of 295m.y. in the western part of the Armutlu peninsula (Upper Carboniferous), Yılmaz (this volume) cites 272±3m.y. (Lowest Permian) from another source. It cannot be decided if there was only one phase of *Variscan metamorphism* near the Carboniferous/Permian limit or also earlier ones. North of the Marmara sea, slightly deformed, unmetamorphic sediments of Ordovician to Carboniferous age are outcropping.

The *tectonical structures* of the metamorphic series were affected by later displacements, but locally are well preserved. Imbach (1992) found a main trend running WNW-ESE in the Uludağ amphibolitic series, with weaker and younger, but still ductile deformations in a NNE-SSW direction. 10-20km east of Bursa, the detritic basal Permian sediments quickly change facies and thickness. The zones with identical conditions run E-W, this probably corresponding to Late Variscan structures. Jeckelmann (1996) observed predominantly NE-SW running structures in the metamorphics of the Kozak area.

Mesozoic and Paleocene

Triassic, unmetamorphic Jurassic and Early Cretaceous, Gönen area

These series are missing in the areas investigated by the MARMARA project with the exception of Gönen.

One of the often discussed, enigmatic problems in NW Anatolia is the postulated orogenic cycle starting near the end of the Permian and ending near the limit between the Triassic and the Liassic. Genç and Yılmaz (1995) describe as a key region a large area around Yenişehir, lying between our Armutlu and Uludağ areas, but outside of them. This Triassic Karakaya zone can be followed to the southwest to the gulf of Edremit and from Yenişehir to the ESE (Yılmaz, this volume, Fig. 2, Yenişehir Group). According to our results, this postulated belt of Triassic becomes narrower to the south (especially Kozak metamorphics are interpreted as paleozoic) but englobes the Gönen area.

Transgressive Liassic sediments unconformly cover older rocks. Unmetamorphic Liassic to Lower Cretaceous shallow water sediments once covered large areas south of the Marmara sea, of the Armutlu peninsula and of Geyve (Yılmaz et al. 1995, Yılmaz this volume). They later were mostly eroded, but were partly preserved in the Gönen area. Unfortunately, the outcrops there are of poor quality and gave no additional information.

Metamorphic Mesozoic series (İznik metamorphics), Kuzuluk, Armutlu and Şarköy areas

As described by Yılmaz et al. (1985) and Yılmaz in this volume, the Jurassic and Lower Cretaceous sediments change their character and become metamorphic north of the line Gemlik – İznik Lake – Geyve – Mudurnu valley. He named these series " İznik metamorphic association" and connected it with a postulated Intra-Pontide suture (Yılmaz this volume, Fig. 4A and B). As the meaning of the term "Intrapontide suture" is controversial (see Chapter *Tectonics from the Jurassic to the Paleocene)*, we will always speak of "İznik metamorphics". As may be seen in these figures, they englobe the western part of the Almacık lens with our Kuzuluk area and parts of the Armutlu area. According to the results of Eisenlohr (1995 and this volume), all of the most western part of the Armutlu peninsula should be included, so the northern limit of this zone should be curved to the region of Çınarcık in the WNW (Fig. 8 and 9). The Armutlu peninsula gives a key for the stratigraphy of İznik metamorphics. According to Eisenlohr, the sequence begins with an *angular unconformity* and some basal conglomerates, covering metamorphic rocks with *amphibolite facies* (Variscan?). Series with serpentinites, diabase, metavolcanics, greenschists and some sediments such as radiolarites and – at the top – quarzites follow. As proven by partly well-preserved pillow lavas and the radiolarites, the sequence predominantly corresponds to *deep water deposits*. The metamorphism reaches medium to upper greenschist facies. The sequence is covered by thick, partly *dolomitic limestones* alternating with some layers of micaschists. Kaya and Kozur (1987) found some fossil relicts indicating Dogger age. The sea seems to become very shallow, as the limestones are partly eroded and are locally covered by conglomerates. Sedimentation then turns to deep sea *flysch-type* with some layers of radiolarite. According to Kaya and Kozur (1987) some radiolarias could be determined and gave an age of Upper Jurassic. The youngest sediments of İznik metamorphics are *limestones* covered by massive *quarzites*. Metamorphism dropped to low degree facies.

Age determinations based on a few, not very well preserved fossils may be put in question. Yılmaz et al. (1995) give another stratigraphic interpretation based on lithology. However, data coming from the prolongation of İznik metamorphics far to the west (Fig. 8 and 9) give a rough confirmation for Jurassic to Lower Cretaceous age: Kopp (1964) found greenschist series with serpentinites and radiolarites covered in the upper part by black phyllites and partly marmorised limestones on the island of Samothrake. Corals near the top gave a Malm age. Outcrops on the mainland west of Alexandroupolis in slightly metamorphic rocks contained fossils indicating Malm to Lower Cretaceous.

Seen as a whole, the *outcrops of İznik metamorphics* seem to pinch out to the east in the western part of the Almacık lens and to get larger to the west, the general trend being E-W (see Figures 8 and 9). The very disturbed outcrops of Pre-Campanian rocks around Şarköy probably are part of this zone. Many serpentinites, but also greenschists, diabase, quarzites and partly marmorised limestones occur (Kopp, Pavoni and Schindler 1969).

In the Kuzuluk research area, the association is monotonous and contains no fossils (Greber 1992 and this volume): micaschists and quarzites, with thin layers and a few thick banks of partly marmorised limestones, the metamorphism probably reaching low greenschist facies. Looking to the *youngest rocks affected by metamorphism*, it is striking that east of the İstanbul – Mudanya line, 3-4 zones running approximately E-W can be distinguished from north to south:

- North of the Marmara sea – Adapazarı even Paleozoic is not metamorphic
- In İznik association, metamorphism ends in the middle or upper part of Cretaceous
- South of the gulf of Gemlik, İznik lake and Mudurnu valley, metamorphism is reported to englobe Triassic (e.g. Yılmaz et al. 1995).
- Near the north of Uludağ, Carboniferous, but not Permian rocks are metamorphic.
- The reason for the changes has to be tectonic and connected with orogenic cycles, as will be discussed later.

Late Cretaceous and Paleocene sediments

İznik metamorphics were deformed and cut by angular unconformity in all areas investigated by the MARMARA project, but more to the south the sequence of unmetamorphic Jurassic and Cretaceous lies more or less conformly (Yılmaz et al. 1995). West of the İstanbul – Bursa line outcrops of Upper Cretaceous are rare and isolated.

Within our research areas, the oldest preserved rocks of these series are fine-grained, partly clayey, red to greenish grey limestones with layers of radiolarite – a pelagic deep water facies known in the Alps as "*Couches Rouges*". Stratigraphic contacts to the base with coarse detritic material were observed at only two locations: west of Şarköy on serpentinites (Kopp, Pavoni and Schindler 1969) and in the southern part of the town of Gemlik on İznik metamorphics (Erk 1942). Couches Rouges, however, occur quite often as blocks or even olistostromes in younger Cretaceous or Eocene sediments within the Kuzuluk, Armutlu and Sarköy areas, but also outside of them. The age could be fixed by microfossils and varies between the Upper Santonian and Campanian/Maastrichtian limit. According to Görür and Okay (1996), isolated blocks found near Şarköy would be of Paleocene age.

South of the gulf of Gemlik – İznik lake line, Turonian limestones are covered by*coarse flysch of Upper Campanian to Lower Maastrichtian age*. The sediments seem to be furnished from the north, as Yılmaz et al. (1995) describe coarse, continental to littoral sediments of this age

to the east of the Armutlu peninsula. An isolated flysch-outcrop of the same age lies near Yalova (Akartuna 1968), others are known from the southern coast of the gulf of İzmit. During the upper part of Maastrichtian, flysch sedimentation ceased, the sea became shallow and then receded.

The Kuzuluk research area yielded an exceptional profile including Paleocene sediments as described by Greber (1992 and this volume): İznik metamorphics here are unconformly covered by extremely coarse breccias becoming finer at the top and interbedded there with arcoses, siltstones, marly limestones and echinodermic breccias. Fossils give an age of Campanian to Maastrichtian, an enclosed olistostrome of Couches Rouges indicates Late Santonian. These ages correspond to the data obtained from surrounding regions, but the facies shows the proximity of the border of the Upper Cretaceous flysch trough. These sediments are covered by shallow water, fossilferous limestones sedimentated in quiet conditions, *Upper Maastrichtian* to Lower Paleocene age. The following sediments, however, again demonstrate an unstable environment and contain breccias, sandstones and limestones with fossils proving *Middle and Upper Paleocene age*, maybe even reaching Lowest Eocene.

Tectonics from the Jurassic to the Paleocene

As far as they are preserved, the sediments of this age were not much deformed south of the Marmara sea and İznik lake. In the Gönen area, Yalçın (this volume) found gentle folding of unknown age with axes oriented NNE-SSW. Near the belt with metamorphic mesozoic sediments, conditions change abruptly *east of the İstanbul – Mudanya line*. The southern limit of İznik metamorphics later was mostly followed by large neotectonic fault lines. The northern limit often is hidden by younger sediments and was named "Intrapontide suture" by Şengör and Yılmaz (1981). They connected it with a narrow northern branch of Neotethys, opening during the Jurassic (Genç and Yılmaz 1995: in Liassic) and closing in the Upper Cretaceous; similar, but much smaller than the Neothethys ocean corresponding to the İzmir-Ankara zone. Some confusion arose, as the name Intrapontide suture was used by others (Barka 1992, Wong et al. 1995, Görür and Okay 1996) for the nearly identical line affecting the sedimentation of the Eocene and the Oligocene (see Chapter *Eocene sediments*). According to our interpretation, *İznik metamorphics* can be followed from the westernmost part of the Almacık lens in the east over the Armutlu peninsula to Samothrake and the region of Alexandroupolis in the west. They contain rocks of Jurassic and Lower Cretaceous age covering unconformly metamorphics of amphibolite facies (Variscan?) near Armutlu.

The highest, slightly metamorphic mesozoic rocks are cut by an *angular unconformity* and covered locally by Couches Rouges or younger Upper Cretaceous sediments. Metamorphism and the final closure of the trough therefore have to be older than Santonian. According to Yılmaz (this volume), age determinations of the *metamorphism* in the Ankara-İzmir zone gave values between 108 and 88m.y. (Albian-Turonian), which would be convenient for our zone too. He postulates that the *final closure* there happened in the Campanian or even later. As İznik metamorphics had to be compressed, partly eroded and than submerged previous to the Upper Santonian, the northern branch of Neotethys had to have closed earlier than the Ankara-İzmir zone.

Eisenlohr (1995 and this volume) deduced a main stress direction running NW-SE in the western part of the *Armutlu peninsula* from stretching lineations and an overthrusting to the southeast. As a whole, İznik metamorphics run E-W, so a N-S compression would be more likely. Possibly neotectonic rotation changed the original orientation (Chapter *Second phase of NAFZ activity: Conclusions)*.

The fact that the Couches Rouges could be sedimentated in apparently quiet deep sea conditions seems enigmatic. Following this episode, *relief suddenly became very pronounced* and flysch sedimentation started at least east of the line İstanbul-Bursa. We suppose that the zone underlain by mesozoic metamorphics experienced a tendency to uplift. Along the border zones, the sea bottom sank, so favourable conditions for flysch sedimentation arose. As described in the next chapter, similar and better-known conditions prevailed during the Eocene, connected with a S-N extension or compression (see Chapter *Paleogeographic reconstruction, paleotectonics*). During the Paleocene, with a few exceptions the sea retired from the areas investigated.

Eocene, Oligocene and Burdigalian (Lower Miocene)

Eocene sediments

Lower Eocene (Ypresian) is missing with the exception of the Kuzuluk area: Greber (1992 and this volume) found thick series of marine siltstones covered by continental volcanics over fossiliferous Upper Paleocene, both void of fossils, but conformly followed by nummulitic limestones of Lowest Lutetian age. The *Lutetian sea transgressed* over most of NW Turkey, but today Eocene sediments are very rare south of the Dardanelles – Marmara sea -Bursa – Eskişehir line. Eocene is outcropping in a large N-S belt in the eastern part of the Marmara region. According to the Geological Map of Turkey 1:500,000 (1964, see also Figure 8), north of the zone with İznik metamorphics *flysch facies* prevails. Very coarse and typical flysch is found along the southern shore of the gulf of İzmit. Eisenlohr (1995) describes such deposits at Esenköy which are separated from the İznik zone by a neotectonic fault system. South of this disturbance, Eocene is partly volcanic, partly detritic. The series were deposed under continental to marine conditions and contain some fossils. Near Kuzuluk, the approximately uninterrupted profile from the Upper Cretaceous to the Middle Eocene ends with Lutetian nummulitic limestones (Greber 1992 and this volume) and lies over metamorphics. The southern limit of this ancient high zone is disturbed practically everywhere by neotectonics. South of it, a relatively narrow belt with flysch facies follows (see Figure 8). At its northern border (Civek zone), Greber found chaotic sediments including flysch of supposed Eocene age. South and southeast of Gemlik, Erk mentioned fossiliferous Lutetian and Priabonian flysch in 1942.

The *neotectonic displacements* increase dramatically along the Gemlik – Marmara sea – Ganos fault – gulf of Saros line (see Chapter *Second phase of NAFZ activity: Conclusions* and Figure 6), so it becomes more difficult to find correlations across this limit. On the Anatolian side, Eocene was mostly eroded with exception of a few flysch outcrops west and northwest of Biga and on Bozcaada Island.

In *Thrace*, a large triangular basin is filled by Eocene, Oligocene and some younger sediments. Kopp, Pavoni and Schindler (1969) give an extensive description of these series. A compilation of the stratigraphy and of more recent publications is given in Görür and Okay (1996). In the northeast, Eocene reef and backreef sediments lie at the border of the İstranca mountains and partly cover them. The forereef deposits quickly get thicker toward the basin. To the east, the border with the Rhodope mountains is marked by different fault systems active during sedimentation (Figure 1). Similar, but hidden disturbances probably exist along the northeast border and within the basin (Schindler 1963, Perincek 1991). On the Greek side of the Meriç river, reefs and nummulitic limestones are interbedded with marls, sandstones and volcanics. In Ganosdağ and eastern Korudağ – to the south, but still on the basin side of the large neotectonic disturbances – very thick, partly silicified sequences of flysch occur.

They represent a continuous profile including Lutetian, Priabonian and even Lowest Oligocene. To the WNW, in the direction of Keşan, these sediments lose the flysch character, but remain coarse and thick. To the west, however, in western Korudağ, the facies quickly turns neritic, brackish and even continental. Between marls, sandstones and conglomerates lie intercalations of nummulitic limestones and some reefs. These indications of an ancient ridge running WNW-ESE are confirmed by Upper Cretaceous fossils found by Ternek (1949) near Mecidiye. Kopp, Pavoni and Schindler (1969) stated that they are mixed with Eocene fossils and therefore removed, but Cretaceous sediments must be very near.

South of the neotectonic Ganos fault, Eocene has neritic, brackish or in some layers even continental character too. *Around Şarköy*, internal unconformities and abrupt changes in the profile show that the basement was very unstable during the sedimentation. Most series are detritic here but, in addition, nummulitic limestones and reefs occur as on the famous Doluca Tepe. Near the Ganos fault, sediments locally become very coarse, chaotic and similar to flysch.

On the *Dardanelles peninsula*, Kopp (1964) found a less disturbed and more continuous Eocene. Most sediments are detritic, too, but predominantly fine grained. Besides some continental intercalations, neritic, partly fossiliferous sequences occur, including nummulitic limestones and isolated reefs. Western Korudag, Şarköy and Dardanelles profiles are similar and probably all cover a ridge underlain by İznik metamorphics.

Oligocene sediments

Oligocene sediments are, with the exception of Thrace, rare and mostly bare of fossils. The sea is *regressive*, so the conditions soon turn brackish, than continental. South of Gemlik, Erk (1942) stated that the Priabonian flysch was covered by marine sands and conglomerates. They rapidly become marly, bituminous and contain, near the top, lignites and gypsum. Greber (1992) supposed that the red-coloured claystones, sandstones and fine-grained breccias unconformly covering Lutetian limestones at Kuzuluk are of Oligocene age and of continental facies.

In contrast, the Oligocene is well represented in southern part of *Thrace*. There, a complete section up to Chattian or even Lower Aquitanian could be dated (Kopp, Pavoni and Schindler 1969). The basal part contains marine marls and partly conglomeratic sandstones, locally with flysch-facies. They are covered with a sharp limit by thick marls and shales (Serie Marneuse) of marine to brackish character. The highest, very thick sequence still contains some marls, but mainly sandstones which become conglomeratic at the top. These predominantly brackish to limnic sediments are of molasse type and contain some lignites (Lignitic Sandstones). To the northeastern and western borders of the Thrace basin, the series get thinner, no longer continuous and littoral.

The fact that the profile of Oligocene series is similar on both sides of the big neotectonic fault line – this in contrast to Eocene – is astonishing. The Lignitic Sandstones are missing due to erosion and flysch facies do not occur in the south. On the Dardanelles peninsula, Lower Oligocene is less sandy. All of these observations speak for quiet conditions in Thrace during the sedimentation of Oligocene, the supply of sediments coming mainly from the south. The conglomerates becoming frequent at the top were interpreted by Kopp (Kopp, Pavoni and Schindler 1969) as littoral, but probably have to be connected with the uplift, strong erosion and tectonical unrest in NW Anatolia (see Chapter *Late Alpine compression in Thrace*).

Plutonites of Late Cretaceous to Burdigalian age

For the moment, only the *age* of the unmetamorphic pluton and volcanics will be mentioned, the interrelation and the external conditions will be discussed later. As far as was investigated, the intrusions occurring during this period can be subdivided in two groups (see Figure 8):

Yılmaz et al. (1995) mention granites intruded in Upper Cretaceous sediments from the Mudurnu valley and from both sides of the Sakarya gorge and interprete them as *Uppermost Cretaceous to Paleocene*. To the west of the Armutlu peninsula, unmetamorphic granites are outcropping. As pebbles of these rocks lie in Eocene flysch (Eisenlohr 1995 and this volume), possible age varies between Late Cretaceous and Paleocene too. Bürküt (1966) found an age of 73m.y. (Maastrichtian) in granodiorites north of Bandırma, on the Kapıdağ peninsula.

Acidic Oligocene plutons are outcropping in large parts of the Ezine, Kozak and Uludağ MARMARA research areas. Fytikas et al. (1976) give an age of 28±0.9m.y. for the quarzmonzonites of Kestanbol southwest of Ezine (Chattian). Yılmaz (this volume) collected data for the granites of Kozak. The values vary extremely between 25.7 and 16.5m.y. (Aquitanian to Lowest Burdigalian) – how reliable are they? Uludağ granites were investigated by Bürküt (1966, 23.8m.y.) and Bingöl et al. (1982, 25-27m.y.), these values indicating Chattian. This group of acidic plutons occurring in NW Turkey in general have an age between 35 and 20m.y. (Yılmaz, this volume) which covers nearly all of the Oligocene.

Volcanics of Late Cretaceous to Burdigalian age

Volcanics with intermediate to acidic chemistry occur quite often in NW Turkey during this period, however the activity is not permanent and the focal points are changing. The following periods can be distinguished:

- Andesitic tuffs and tuffites are reported from *Campanian to Lower Maastrichtian* flysch, but do not occur in the MARMARA research areas.
- Greber (1992 and this volume) found thick andesitic subaerian volcanics in the upper part of *Lower Eocene* (Ypresian). The underlying marine siltstone series contain dykes and sills of these extrusives. The transgressive Middle Eocene limestone is totally free of tuffs. Going to the west, the Lower Eocene is not preserved, but intermediate to acidic volcanics are present in the Lutetian and especially in the Priabonian. In the flysch series north and south of the Armutlu peninsula, andesitic tuffs and tuffites are often included. In the central high zone, Eisenlohr (1995 and this volume) observed – interbedded with sediments – Eocene lavas, pyroclastic breccias, tuffs and some ignimbrites, so subaerian episodes have to be admitted between marine periods.
- In the Thrace basin and the Dardanelles peninsula, the volcanic activities cover the same period with a maximum during the Priabonian. Here, Tuff horizons subdivide the thick sediments (Kopp, Pavoni and Schindler 1969). On internal ridges and to the west of the Meriç river, lavas and pyroclastic breccias become common, with intermediate to acidic chemistry. Sümengen et al. (1987) found an age of 35±0.9m.y. (around the Eocene-Oligocene limit) for an andesite near Enez. The youngest volcanic activities of this cycle occur during *Middle Oligocene* and are restricted to the Thrace basin and to both sides of the Meriç river. Kopp, Pavoni and Schindler (1969) found tuffs and a bentonite interbedded with detritic sediments there. Two facts are striking for this period of intermediate to acidic volcanism: The outcrops lie along a belt oriented E-W, *N of 40° of latitude*, and – as a trend – the eruptions get younger to the west (see also Figure 8).

- South of this zone, on the Biga peninsula, Lesbos and southward to the region of İzmir, huge areas are covered by products of subaerial volcanism. They were studied in detail in the MARMARA research *areas of Kozak and Ezine*, where stratigraphic sequences valid for the local geology could be established (Jeckelmann 1996, Mützenberg 1991). The chemistry is calcalcaline (Yılmaz, this volume) and andesitic, but to the end of this phase of volcanism acidic and occasionally basic differenciates become frequent, so e.g. ignimbrites occur near the southwest corner of the Biga peninsula and on Lesbos. Around the Kozak area, age determinations compiled by Yılmaz (this volume) give values between 23.6 and 14.6m.y. (Aquitanian, Burdigalian and Langhian) for intermediate and acidic volcanics. Some basaltic lavas flowed out during the final period (16.7 to 13.6m.y.). For the Ezine area, Borsi et al. (1972) give ages between 21.5 and 16.8m.y. (Burdigalian) for the intermediate and acidic volcanics. As result, it can be stated that for the western part of the Biga peninsula, Lesbos and the Kozak area volcanism was very intensive and subaerial around *Burdigalian*. The age difference with the underlying pluton of similar chemistry is modest, some values even seem to coincide.
- The volcanics of post-Middle Miocene age will be discussed later.

Questions about intrusions, volcanics, uplift and erosion in the Ezine, Kozak and Uludağ areas

All three acidic plutons investigated by the MARMARA Poly-Project intruded during the Upper Oligocene through series previously affected by regional metamorphism: amphibolitic facies at Uludağ and greenschist to lower facies at Kestanbol and Kozak. Where the contacts are not disturbed, they often run parallel to pre-existing structures which were lifted and tilted by the intrusion. There is no doubt however, that the metamorphics were affected by previous strong dislocations connected with variscian orogeny as they are covered unconformly by much flatter, unmetamorphic Permian limestones.

Around the Kestanbol and Kozak plutons, *contact metamorphism* affects a zone only a few hundred meters wide and is not very pronounced (Mützenberg 1991 and this volume, Jeckelmann 1996). It could be more extensive at Uludağ, but there strong uplift movements along disturbances hide the interrelations (Chapter *Neotectonic history of Uludağ*). Near the pluton, Permian limestones are recrystallised, there and around Kestanbol. During the last stage of the intrusions, several hydrothermal or skarn ore deposits developed, the most important to be found at the Uludağ wolfram mines in contact with carbonates.

The acidic magmas probably *crystallised* at relatively *shallow depth*, but at a minimum of 2 to 3km. As in all three areas concerned, the top of the pluton is now outcropping, erosion reached at least 3km – but when did it happen? An answer is to be found in the Ezine and Kozak areas, as there the slightly younger, flat lying or tilted volcanics unconformly cover the partly eroded plutonites and the contact zone. The conditions can best be studied*around the Kestanbol intrusion*.

As described by Mützenberg (1991), quartzmonzonites cover a large surface there and can be followed at shallow depth to the south, as proved by a borehole at Tuzla. In several places, recrystallised, flat lying Permian limestones lie at the top of the pluton or near it and locally contain skarn minerals. Volcanics of Burdigalian age unconformly cover the different rock types, but also occur in numerous, steep standing dykes. Of special interest are outcrops in a Permian limestone quarry at Gökçebayır, 7km west of Ezine: The dykes there cut paleokarst filled by red-coloured, clayey-silty residual material! It has to be concluded that between the crystallisation of the pluton and the Burdigalian volcanic activity the erosional surface came down some 3km and even karstification had time to develop. According to the published age determinations, 6 to 7m.y. were available for this process, if main uplift started at the end of

the intrusion. What kind of rocks were eroded in the Ezine area? As Permian locally occurs near the top of the pluton, essentially unmetamorphic Mesozoic and Lower Tertiary sediments have to be expected higher up. As metamorphic Triassic Karakaya facies can be excluded here, the estimations of Brinkmann (1976) and Demirtaşlı (1989) may be reliable, giving a total thickness of 2000 to 3000m for Permian and Mesozoic in Western Turkey. On nearby Bozcaada island, Eocene in flysch facies is reported; such sediments probably covered the Kestanbol area, too.

In many ways, the conditions in the *Kozak area* are similar but less clear. Jeckelmann (1996) describes a strong uplift movement of the pluton along several steps of normal faults. No Permian covering of the granite was preserved. The range of the ages given for the pluton in the literature is very large and may not be completely reliable. It seems to be slightly younger than at Kestanbol, Aquitanian rather than Chattian. On the other hand, the oldest volcanics are reported to be Uppermost Oligocene, too. Even if we admit that some of the values given are not correct, the time available for the erosion of some 3km of rocks dwindles to a few m.y. during the Aquitanian, probably starting with the crystallisation of the granite. The rate of the average yearly erosion would reach values similar to current values in the Swiss Alps (1-2 mm/y).

There is no reason to believe that only the future areas of the plutons were once covered by Permian, Mesozoic and Eocene sediments, this at least for the western part of the Biga peninsula and the Bergama region. The erosion, however, was most active in the cover of the plutons. A *general*, pronounced *uplift movement* occurred during the *Upper Oligocene*. Where acidic plutons intruded, the upward movement was enforced by isostasy. As proven by steep standing dikes filled by aplites, hydrothermal deposits or Burdigalian volcanics, faults already existed and probably were active. Mützenberg (1991) reports that around Kestanbol pluton such dykes can be observed mostly along NW-SE running lineations, occasionally they are oriented NE-SW, too. According to Jeckelmann (1996), they have a predominantly NW-SE direction in the Kozak area. It can therefore be supposed that during the Late Oligocene and the beginning of the Miocene the apparent *main stress* was directed SE-NW, and the main extension SW-NE.

As discussed later in Chapter *Rotated zone in NW Anatolia*, limited uplift movements of the plutons are to be observed during the Neogene also, but today isostasy is near equilibrium as shown by the Bouguer gravity anomaly map. This is completely different in the Uludağ area, treated at the end of Chapter *Neotectonics*.

Late Alpine compression in Thrace (Late Oligocene – Early Miocene)

As described previously, flysch troughs were formed during the Lutetian north and south of the zone with İznik metamorphics, this connected with N-S extension or compression. The northern trough changes its character in the Thrace basin where thick sequences of Eocene and Oligocene sediments were deposed over a large area. Here lies the only region where the compression structures of late Alpine age can be well observed, as they were not disturbed by later neotectonic displacements.

The *frame and the bottom of the basin* consists – as far as it is known – of metamorphic and magmatic rocks. They were affected by different fault systems running WNW-ESE, NE-SW and approximately N-S (see Figure 1). Locally it can be proven that they were already active during sedimentation. The conditions in Thrace, however, were quiet, especially during the Oligocene up to the deposition of the conglomeratic upper part of the Lignitic Sandstones (Chattian or Early Aquitanian). All of these sediments were later folded, uplifted and partly eroded. The distribution and pattern of the *anticlines and synclines* is partly irregular (see Figure 1), which is often caused by pre-existing faults. The flanks of many anticlines are very steep and the crest disturbed (Kopp, Pavoni and Schindler 1969). In addition, some displacements by

wrench faults occur, but according to Perinçek (1991) they are more frequent in the northeastern part of the basin. Based on seismic investigations, he constructed complex structures predominantly running ESE-WNW, but hidden below an undisturbed Neogene cover. He found anticlines, synclines and normal faults, but in addition he proposed dextral shear faults causing relatively small displacements. A structural map including his interpretation in detail and the complete Thrace basin was published by Görür and Okay (1996). A high zone existed in *western Korudağ,* north of the gulf of Saros, which protected the area between Keşan, Meriç and Enez from strong deformations. Overlooking the distribution and direction of the structures in Figure 1, it can be concluded that they are the product of a strong compression coming from the south or SSE. There is no indication that the Dardanelles peninsula already existed (see also Chapter *Second phase of the NAFZ activity: Collected data*).

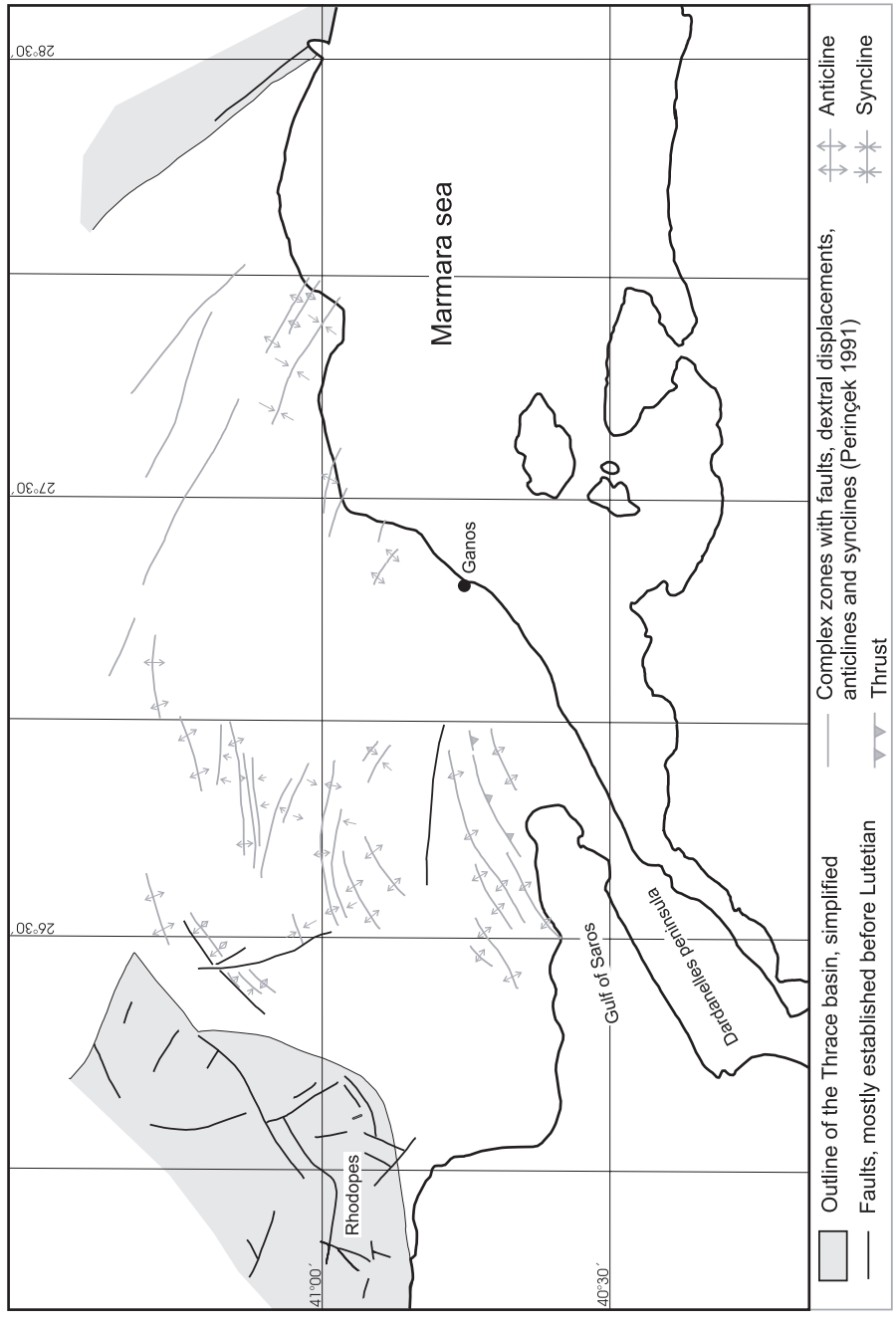


Figure 1: Thrace basin: Late Alpine deformations (Late Oligocene – Early Miocene).

The structures affecting the Eocene and Oligocene sediments are cut by a sharp *unconformity*. More than 2000m of sediments were eroded south of the Tekirdağ – Malkara – western Korudağ line, but also south of the neotectonic Ganos fault around Şarköy and on the Dardanelles peninsula. The unconformity was covered by Neogene sediments. Near the coast they become partly marine and fossiliferous, so *transgression* can be dated as Upper Serravallian to Lowest Tortonian (Middle to Upper Miocene). Folding in Thrace, therefore, had to occur between the Highest Aquitanian and the Lower Miocene (Burdigalian) and was connected with compression coming from the south to SSE and corresponds to a late phase of Alpine orogeny. At the same time, according to Yılmaz (this volume) compression affected Menderes massive for a last time before it collapsed. Perinçek (1991) discussed whether the structures he observed could be interpreted as neotectonic and correspond to an early activity of the North Anatolian Fault System. In our opinion, this solution has to be excluded.

The late Alpine orogeny compressed the Eocene flysch troughs too, but these structures were later affected by large scale neotectonic displacements.

Middle Miocene to Quaternary sediments and volcanics

Middle and Late Miocene sediments

(see Figure 2 and Barka, this volume, Fig. 6A)

The period of intensive erosion (Aquitanian in the south, in addition Lower Miocene in Thrace) and the continental conditions going on during the Lower and the Middle Miocene left no deposits in the MARMARA research areas except the Burdigalian volcanics southwest of the Marmara sea (Fig. 8). The distribution of Neogene sediments and especially the transgression around the end of the Middle Miocene show that *paleogeography changed* suddenly. Along the coasts of the Marmara sea, of the Dardanelles and the Aegean sea, we find littoral sediments proving that the extension of the seas was already similar to that today.

In *Thrace*, topography and the drainage system changed completely. During the Eocene and the Oligocene, the detritic material mainly came from the south, a very limited amount was supplied from the Rhodopes and İstranca mountains (Kopp, Pavoni and Schindler 1969). In the Miocene, deep cut valleys directed to the south or southwest were eroded near the coast and later filled by sediments. A large, low ridge marks the limit with the big flat Ergene basin to the north. This basin is drained to the west, near the confluence with the Meriç river, the Ergene river turns to the southwest. In western Anatolia, plenty of irregularly shaped basins filled with continental, limnic or occasionally brackish sediments can be observed. Many were completely isolated from the sea, others could have temporarily been connected with it but today are lying above sea level (e.g. the large E-W oriented basin including Uluabat and Kuş gölü).

The *partly marine sequences* are of special interest as they can be dated by fossils. Such series (see Figure 2) were investigated in Thrace and in the Armutlu and Ezine MARMARA research areas. In general, a predominantly detritic part underlies the clayey-sandy series with thin layers or banks of light-coloured limestones. The *lower sequence* shows marked influence from the nearby land. In the Şarköy-Dardanelles region and west of Ezine, red-coloured or variegated clays and marls often containing some gypsum are interbedded with sandstones, partly coarse conglomerates and occasional thin layers of limestone. Marine to brackish fossils, but also some remains of mammals, occur and indicate an age between Upper Serravallian and Lower Tortonian. The same series become continental and tuffitic at Tuzla and at the southwestern corner of the Biga peninsula (Mützenberg 1991). Near Yalova, they are represented by brownish-grey clays and marls with some crystals of gypsum. The upper part

of the detritic series is similar in all areas investigated: brownish, soft sands with some layers of pebbles, some marine to brackish fossils and occasionally mammal remains indicating Tortonian age.

Very typical and widespread are the *upper series* with clays and limestones. Green, white or brown clays and marls are interbedded with white sands and paper thin layers to thick banks of light-coloured limestone. In addition, some lumachellas occur (Mactra limestones). In contrast to the underlying series, swelling clays and white, tuffitic sands become common, this is probably connected with nearby acidic to intermediate volcanism. Some lignites occur as near as Yalova (Eisenlohr 1995 and this volume). Marine fossils point to Upper Tortonian age, the mammal remains to the corresponding continental stage of Pontian. The tendency is transgressive, so the sea in the upper part of the Miocene sequence reaches the confluence of the Meriç and Ergene rivers in Thrace (Kopp, Pavoni and Schindler 1969) and in brackish or intertidal facies the Cengiler pass between Yalova and Orhangazı (Eisenlohr 1995). Confusion arose due to the fact that in older literature Pontian was interpreted as Early Pliocene, but according to actual knowledge corresponds to the marine stages of Late Tortonian and Messinian. Mammal remains indicating Pontian are known from several locations as Cengiler pass (Akartuna 1968), Dardanelles aera, west of İstanbul, southwestern corner of the Biga peninsula etc. Engesser (1980) compiled and reviewed mammal remains from Western Anatolia with the target to subdivide the period. According to recent paleontological rules, the traditional name Pontian has to be given up in favour of 'Turolian'.

Continental to limnic deposits of Middle to Upper Miocene age are widespread, but hard to subdivide. Brown, reddish, green or white clays and marls, sands (often clayey) and intercalations with pebbles and limestones are typical. The series near the top are typical as white limestones become very frequent, sandstones are mostly tuffitic and in the clays (partly swelling) green and white colours predominate. Acidic to intermediate volcanism is documented, e.g. around Gönen (Yalcın this volume), by tuffs and some lavas. There and in other MARMARA areas banks of lignite occur and crystals of gypsum point to occasional lagoonal facies. Age determinations in principle would be possible by palynology, however, they are time consuming and the results are very difficult to correlate with marine stages. Research in the Soma lignite mines area east of Bergama by E.L.İ (1993) gave a thick sequence from the Lower Miocene to the Upper Pliocene. Unfortunately, reliable age determinations in the Neogene of NW Turkey are rare for the continental to limnic facies, so the stratigraphy is not well established (see Figure 6 in Yılmaz, this volume).

Messinian (Uppermost Miocene)

During this period, the climate turned out to be very dry and the sea receded. Jakobshagen (1986) mentions that a drillhole in the Aegean sea west of the Biga peninsula and south of the island of Limnos uncovered 800m of evaporitic sediments of this age. A gentle, but very widespread, compression caused uplift, tilting and folding of the sediments up to the Late Miocene. As in contrast the Pliocene is much less deformed (excepted for small zones affected by neotectonics), the series can be distinguished in favourable conditions by an unconformity. According to Barka (1992), in the Neogene basins occurring east of Bolu along the NAFZ, the lower, more disturbed Tortonian sediments are unconformly covered by Pliocene.

Pliocene sediments

(see Barka, this volume, Figure 6B)

Marine Pliocene is known to occur in the Marmara sea, the gulf of Saros and the Aegean sea. Outcrops within the MARMARA research areas are extremely rare. Jeckelmann (1996) found a partly silicified littoral sequence with some oolithes southwest of Dikilli (west of Bergama), age probably being Pliocene.

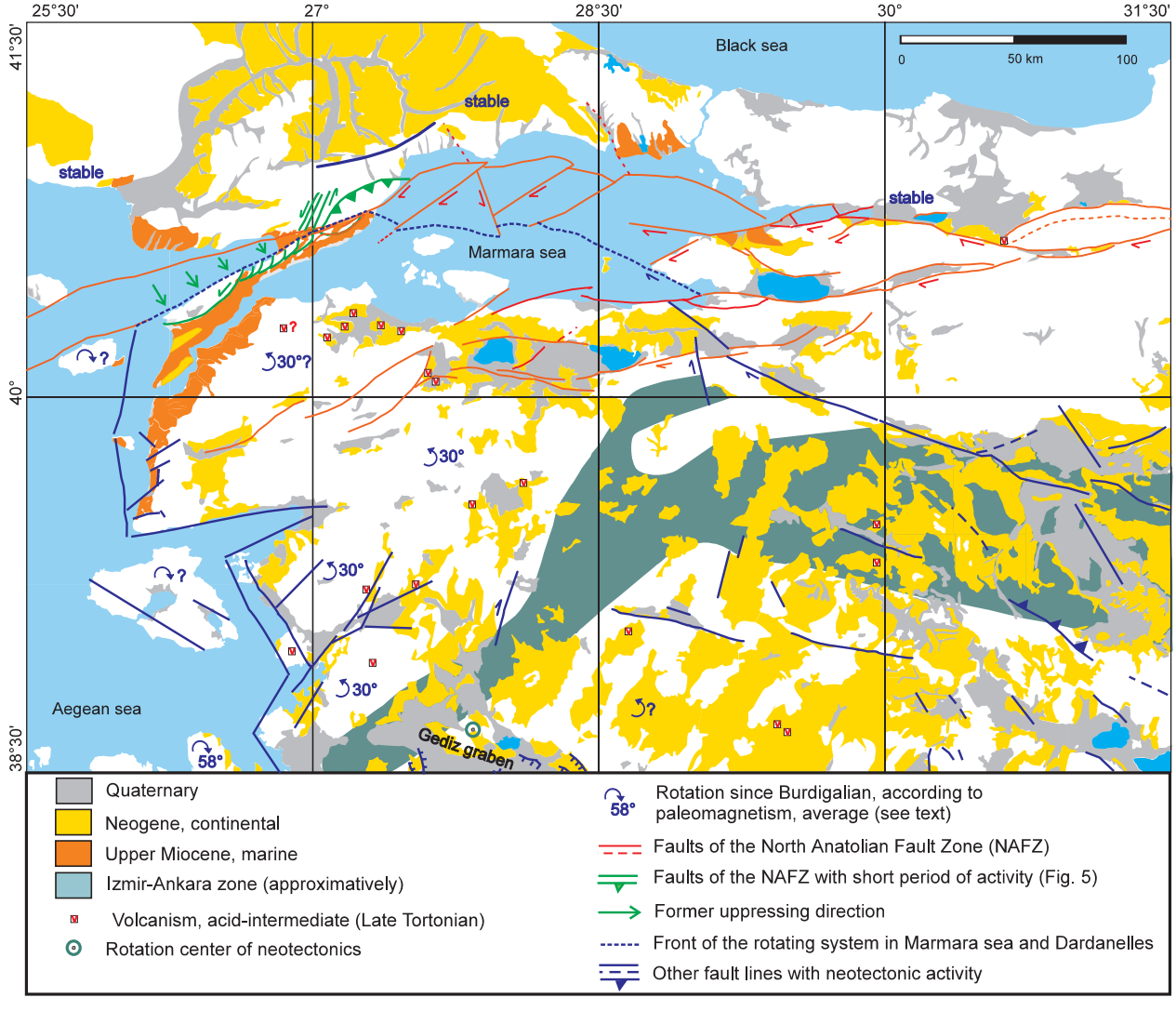


Figure 2: *Middle Miocene to Quaternary sediments, neotectonics.*

Continental to limnic Pliocene occurs in different facies. Around the Kuzuluk area (Mudurnu valley, north and west of the Almacık lens, north of the gorge of the Sakarya river), coarse fluvial deposits interbedded with sandy horizons can be observed (Greber 1992 and this volume). Similar, but much smaller outcrops with a marked basal unconformity were seen in the Armutlu and Ezine areas.

On the *Dardanelles peninsula*, detritic and partly very coarse sediments cover the Tortonian with a slight unconformity. According to Yaltırak (1995), their origin lies nearby in the northwestern part of the peninsula and they can be dated as Upper Pliocene, possibly even reach

Early Quaternary. The age of these predominantly continental series was – as far as we know – not proven by fossils, but would fit with our analysis of the neotectonics (Chapter *Second phase of the NAFZ activity: Conclusions*).

The Neogene series of the *Ergene basin* represent – according to palynology – the Upper Miocene and the Lower Pliocene (Perinçek 1991). These sediments are predominantly clayey to sandy, near the borders of the basin horizons with pebbles becoming frequent. During the Upper Pliocene erosion became prevalent, therefore the current rivers flow below the original level of the Ergene alluvial plain. More to the south, Oligocene and Eocene rocks outcrop. Sediments from the Pontian and the Pliocene occasionally fill some old valleys or depressions there, but in general are very thin or missing. A thin, sandy cover including pebbles up to 10cm and more diameter is quite common. It is lying on a kind of peneplain surface joining the Ergene plain, but is disturbed or cut to the southeast by neotectonics (Kopp, Pavoni and Schindler 1969). The age of the peneplain is supposed to be Middle to Upper Pliocene, the pebbles at the surface are interpreted as a relic from previous erosion.

In the research *areas of Uludağ, Gönen and Kozak*, the continental to limnic sediments of Pontian and Pliocene age have similar facies and are hard to distinguish. The less disturbed, younger sediments usually cover smaller areas compared with the extent of the Late Miocene. These flat basins are not identical with the range covered by Pontian deposits and can lie outside of them. In the Pliocene, lignites, layers of limestones and volcanics occur.

Quaternary sediments

(Barka, this volume, Fig. 6C)

In NW Turkey, the Quaternary is not of as much importance as it is in Switzerland. The marine deposits in the deep trough of the Marmara sea are partly known by seismic research (Wong et al. 1995). Some offshore boreholes were drilled in the past for petroleum research, however, the results were not published.

Fossile littoral terraces are known to occur along the coast between Ganos and Şarköy (Pfannenstiel 1944). As described by Kopp, Pavoni and Schindler (1969), they follow the actual topography reaching a thickness of 100m in deep valleys and occur at different levels, the highest lying at 170-180m. According to Barka (this volume), the sea never had a significantly higher level during the Quaternary than today, so a strong neotectonic uplift movement had to affect the region of Ganos-Şarköy. The age of the terraces is controversial, probably all belong to the Late Pleistocene. Depending on the interpretation, the average rate of uplift lies between 0.3 and 0.7mm/y. Similar terraces are reported to occur at a deeper level in some places around the Marmara sea (Pfannenstiel 1944, Ardel 1961, Göney 1964). On the other hand, the sea sank 80-90m below its current level during the last glaciation. Pfannenstiel (1944) analysed the relief of the bottom of the Marmara sea and proposed *submerged river beds*. Barka (this volume) gives an improved picture and proposed three main drainage systems to be followed below the sea. The rising water level at the end of the last glaciation submerged many deep cut valleys. They progressively were later filled by recent sediments, a very important fact, e.g., for the history of Troia.(Kraft, et al, 1980)

In the continental to limnic *interior basins*, the Quaternary deposits are very similar to Neogene. Of special interest for the hydrogeology are the numerous outcrops of travertine such as those around Bursa. In the highest part of the northern slope of Uludağ, beautiful *glacial features* can be observed such as kars, moraines, lakes and rocks polished by the ice. In addition, some periglacial deposits occur as block glaciers. These phenomena descend to an altitude of 1900-2000m above sea level, and with a few possible exceptions are fossil.

Volcanism since Middle Miocene

Acidic to intermediate, calcacaline volcanism: As already mentioned, this type of volcanism ceased activity in the Kozak and Ezine areas 15-14m.y. ago, during the Middle Miocene. According to Yılmaz (this volume), it rested for some 5m.y. and started eruptions again in the upper part of the Tortonian. As far as the areas investigated by the MARMARA project are concerned, this corresponds well with the fact that the sediments of the Lower Tortonian are brownish to variegated and do not contain volcanics. Then, especially in the continental facies of Pontian, they turn to mainly white and green and contain much swelling clays and tuffites. Greber (1992 and this volume) describes several layers of tuff and an ignimbrite from the Kuzuluk basin, Yalcın (this volume) found many intermediate to acidic tuffs and some lava flows southwest of Gönen. In contrast to these observations, no clear indications for an acidic to intermediate volcanic activity during the Pliocene or the Quaternary were found in the MARMARA research areas. Where are the centres of Pontian activity? Some of the steep standing dykes filled with andesite could be much younger than the surrounding volcanics of Eocene (Thrace, Armutlu area) or Lower Miocene (Kozak, Ezine areas) age, but this cannot be decided without radiometric dating. Going more to the south in Western Anatolia and in the Aegean sea, the periods with volcanic activity change. Kissel et al. (1989) report that two main periods with much activity can be distinguished there, the first period occurring in the Oligocene and the Miocene with a culmination 13m.y. ago (Serravallian), the second period starting 5m.y. ago (Lower Pliocene) and locally still active.

Young basalts are common in NW Turkey, but usually cover relatively small areas. All are of the alcaline type, most contain olivine. Their age was fixed in several samples by radiometric determination, other lavas can be dated by stratigraphic interrelations. In contrast to the acidic and intermediate volcanics, the results vary between Serravallian and Subrecent. Yılmaz (this volume) mentions ages for the Biga peninsula between Tortonian and Late Pliocene, for Balıkesir 13m.y (Serravallian) and for Gönen and Susurluk Late Pliocene. Upper Pliocene to Pleistocene basalts are described by Jeckelmann (1996) in the Bergama region and by Borsi et al. (1972) for Kula southeast of Bergama. Basalts are common in southern Thrace, too. Sümengen et al. (1987) found an age around 6.7m.y. (Uppermost Tortonian) for an outcrop between Tekirdağ and Çorlu. Many of the other not dated lavas could be Pliocene in age, a few even Quaternary, as they partly cover the peneplain surface.

Neotectonics (Neo Alpine tectonics)

One of the main aims of the MARMARA Poly-Project was to identify the recent deformations of the lithosphere, to analyse their effects and to find interrelations to hydrogeology, geothermics and seismicity. To better understand the present, we have to go back into the past with the methods of geology. The period with a similar type of deformations, comparable stress field and a resembling paleogeography can be summarised with "neotectonics". In the general sense of the term they still are Alpine, but quite different from the former events. The start of this sequence of events is coincident with the opening of the Aegean and Marmara seas, when the conditions suddenly became similar to those today. Most authors place the change in the middle part of the Miocene (LePichon and Angelier 1981: 13m.y., Yılmaz this volume: 15m.y., Mercier et al. 1989: 15-13.5m.y.). On the other hand, in NW Turkey we find a final phase of Alpine northward compression happening near the Oligocene to Miocene limit. This event clearly still is paleotectonic with conditions very different from current ones.

Results of paleomagnetism, possibility of rotations

Paleomagnetism is a valuable tool for recognition of former displacements and especially the rotation of rock bodies. During the last few years many samples of volcanic or plutonic rocks were analysed in NW Turkey and in Greece. However, they do not give a complete coverage of the areas of special interest. In addition, the exactitude of the results is limited and can be affected by several types of factors. An isolated value, therefore, is less reliable than the average of several measurements made in the same area on identical rocks. It is very important to know the period when the rock crystallised, as the deviation given by the paleomagnetic analysis summarises all deformations later affecting it. Eocene and Oligocene rocks, for example, give a result condensing complete neotectonics and the last paleotectonic event; Pliocene basalts, on the other hand, give an answer only for the last part of neotectonics. The published paleomagnetic results concerning declination will be summarised, subdivided into areas and the age of the samples.

North of the İznik Metamorphic zone (see Figures 8 and 9): Kondopoulos et al. (1996) report that the Rhodope mountains are subdivided by an important dextral wrench fault running from Kavala to Komotini and probably to the region of Edirne. NNW of this line, a pronounced clockwise rotation was observed. SSE of it, conditions apparently are quite different. Eocene and Oligocene volcanic samples collected between Komotini and the Meriç river gave no significant rotation. Tapırdamaz and Yaltırak (1996) worked on the Turkish side of the river on the same rocks near Enez, they also observed no obvious diversion. On the other hand, three samples of Oligocene volcanics taken between İpsala and Malkara showed clockwise rotations of 15, 37 and 48°. No geological observation speaks for an important neotectonic feature running between Enez and İpsala. The very scattered deviations in our opinion therefore are a product of the late Alpine folding of this region. Several samples of Pliocene basalts were taken by the same authors east of Çorlu in Thrace, showing, on the average, no rotation. Michel et al. (1995) published a few results from Eocene volcanics lying north of the NAFZ and east of Adapazarı. The deviations observed are not homogeneous, but do not show a significant rotation on the average.

The same authors took many samples in *the zone affected by the NAFZ* in Eocene rocks between the Almacık lens and Geyve (Figure 8). Some values clearly were influenced by nearby faults, but most showed a low to moderate anticlockwise rotation. The general clockwise deviation of 110° proposed for geological reasons by Şengör et al. (1985) for the Almacık lens was not confirmed. Sarıbudak et al. (1990) mentioned that a sample gave a paleomagnetic clockwise deviation of 212° (or 148° anticlockwise). Tatar et al. (1995) made paleomagnetic investigations north and northeast of İznik lake in Eocene rocks and obtained an average clockwise rotation of 14°. Eisenlohr predicted a clockwise diversion of 15-40° for the western part *of the Armutlu peninsula*, but unfortunately no paleomagnetic data exist here. With a clockwise rotation of 40° the main stress during the closure of the zone with İznik metamorphics would have an E-W direction, nearly parallel to the axis of the trough – an unlikely result.

Near the coast between Çanakkale and İzmir many samples of Lower Miocene volcanics were taken. Kissel et al. (1989) reported a homogenous anticlockwise rotation around 30°. Işseven et al. (1995) gave a similar, but more differentiated picture. In the north (Çanakkale and Çan), values of 36° were measured, sinking to 32° near Ezine and Tuzla and to 29° near the gulf of Edremit and Ayvalık. A sample from the region of Kozak gave an aberrant value with a 31° clockwise diversion. As all geological observations speak against an independently rotating Kozak block, an error is probable and additional measurements should be made. According to Kissel et al. (1989), a 10m.y. old basalt outcropping near Çanakkale showed no rotation, on the other hand Işseven et al. (1995) mentioned that four samples of Upper Miocene volcanics taken more to the south gave an anticlockwise rotation of 16° on

the average. South of the NAFZ, additional data only are available between Geyve and the Mudurnu valley. Michel et al. (1995) obtained no homogeneous results from Eocene volcanics; rotation seems to be anticlockwise and rather small.

The Aegean islands and the mainland of Greece give results very different from NW Anatolia and Thrace. No deviation or a small clockwise rotation is reported from Lower Miocene volcanics of Lesbos (Kissel et al. 1989, Westphal and Kondopoulos 1993). Rocks of the same age sampled on the Karaburun peninsula west of İzmir gave an astonishing clockwise rotation of 58°, but Upper Miocene volcanics showed no deviation at all (Kissel et al. 1989). According to the same authors, the clockwise rotation of Limnos island lies around 34°. According to the literature, the same trend exists on Eubeoa, Skyros island and – on the mainland – near Volos and on Chalkidike. According to Kissel et al. (1989), NW Greece rotated clockwise some 50° on the average since Lower Miocene – half of it earlier than the Upper Miocene, the other half during the Pliocene and the Quaternary.

The results of magnetometry show dispersion and are partly controversial. However, some *general trends* appear, especially if we take into consideration what geology suggests for neotectonics (Figure 2):

North of the NAFZ lies a quite stable zone without essential rotation since the Lower Miocene. The large zone locally affected by the NAFZ shows deviations due to nearby faults, but no trend concerning general clockwise rotation (Plazman et al. 1994, Michel et al. 1995). South of the NAFZ, rotation values east of Geyve are sparse and probably affected by late Alpine movements. It can be guessed that the neotectonic diversions were weak and anticlockwise. Well established is an anticlockwise rotation of some 30° for the large area between Çanakkale and İzmir, the essential part of it happening during the Miocene (compare Figure 2).

Looking at the geological maps of Turkey 1:500,000 (1964) and 1:2,000,000 (1989), a striking contrast can be observed: in NW Anatolia, west of 29° longitude, the *prevailing geological trends* ran NE-SW, but east of it and north of 40° latitude, the main structures are directed E-W to ENE-WSW. Philippson already remarked this contrast in 1918 and spoke of a separate tectonic unit in NW Anatolia lying between the Marmara sea and Ephesus. In conclusion, many facts speak for the rotation postulated by paleomagnetics.

On the other hand, it is obvious that conditions abruptly change near the Aegean coast. With the exception of Lesbos, all samples taken on Aegean islands and the Greek mainland east of Strimos river gave a marked clockwise rotation. If the Neogene rotations are eliminated, the geological structures in a regional scale seem to run approximately E-W (Figures 8 and 9).

Rotated zone in Northwestern Anatolia: Borders and time of activity

If an anticlockwise rotation of some 30° is accepted, we have to find the *borders of this zone*. If the southern edge of the deep trough in the Marmara sea, the Ganos fault and the southeastern border of the trench in the Saros gulf are joined, the line corresponds quite well to the sector of a circle – especially if later fault displacements are eliminated (Figures 2, 7 and 8). The circle has a radius of 220km and the center 60km ENE of İzmir, near the small Marmara lake (see Figure 2).

According to the completely different behaviour of Lesbos island and the Karaburun peninsula, the *western limit* of our rotating NW Anatolian block has to be located near the Aegean coast. Leaded by the relief of the sea floor, by fault systems recognised on land and by the distribution of microseismic epicenters, the outskirts of the block were sketched on Figure 2. The main faults recognised run NNE-SSW, ENE-WSW, NNW-SSE and approximately N-S.

The sector of the circle can be followed to the east to the region of Gemlik-Bursa, where the dextral movement apparently is transferred to the WNW-ESE running Eskişehir fault and to the N-S running Çekirge fault (Figure 2, 8 and Chapter *Neotectonic history of Uludağ*). More to the southeast, the movement could activate different fault systems and be transferred in a complex way to the tectonic triangle of Burdur. The active subduction zone located in the Eastern Mediterranean sea turns into Anatolia near Burdur (Reilinger and Barka 1996, Mueller et al. this volume). Overthrusting toward the WSW is typical for the SE flank of the triangle, subduction and complex structures for the southwestern flank. As the MARMARA project was not active southeast of Bursa, many questions have to be left open. The neotectonic problems concentrated around Uludağ will be discussed later. If the proposed borders of the block with some 30° anticlockwise rotation are correct, it includes not only the western part of the Sakarya continent, but also the Menderes massive and parts of the Ankara-İzmir zone.

How can *the period with active block rotation* be fixed? All samples showing anticlockwise rotation in the range of 30° around the Ezine area were taken in Lower Miocene volcanics. The eruptions ended with the deposition of a large cover of ignimbrites joining the southwestern corner of the Biga peninsula with Lesbos (Mützenberg 1991 and this volume). The massive faulting and tilting affecting the volcanics, the opening of the gulf of Edremit and the rotation must be younger than the ignimbrites (16.8m.y); according to the conditions in the Kozak area it could have started 15-16m.y. ago (Langhian) or later.

Marine Miocene sediments prove that after a long continental period the Aegean and Marmara seas opened for the first time with a transgression during the Upper Serravallian, some 11 to 13m.y. ago. The contrasts in the morphology increased. West of Ezine e.g., extremely coarse Tortonian sediments can be observed landward of the ancient coast line of the Aegean sea (Mützenberg 1991), the Kestanbol pluton being lifted again. On the European side of the Marmara sea, Middle and Upper Miocene sediments show that a high zone occurred to the NNW, but conditions were quiet and not affected by synsedimentary movements. This is remarkable as the Ganos fault (limit of the rotating block) is in direct contact with the series. An active rotation is therefore to be excluded between the Upper Serravallian and the end of the Tortonian, but can be older or younger.

Near Tuzla, silicified vertical water channels and intercalations with sediments of Early Tortonian age prove that the current *thermal springs* started their *activity* some 10 to 12m.y. ago (Mützenberg 1991). As thermal spring systems are extremely sensitive to changes in the tectonical configuration, conditions were already similar to those today at the beginning of the Tortonian. From all of these facts it can be concluded that the activity of the steep standing faults, the tilting of the blocks and the main part of the rotation are older than 12m.y., but younger than 16m.y. These events are directly connected with the birth of the Aegean and Marmara seas. During the same period, the Menderes massive collapsed according to Yılmaz (this volume) and extension in the Aegean region began. The initial development of the actual subduction zone from the Eastern Mediterranean sea to the Ionian sea is supposed to have happened concurrently (LePichon and Angelier 1981: 13m.y. ago, Mercier et al. 1989: 16-15m.y. ago in the Langhian). Less probable is the estimation of Kissel et al. (1989): Late Oligocene to Early Miocene. As a draft, the following *sequence of events* can be postulated for the rotating NW Anatolian block: breaking up during Langhian, the main part of the rotation during the Serravallian, marine transgression in the uppermost Serravallian. According to Mercier et al. (1989), Aegean extension started some 13.5m.y. ago.

North Anatolian Fault Zone (NAFZ): First period of activity

Barka (1992 and this volume) gives a general outlook and many details not reported here on the NAFZ. Our text will especially comment on the results to be deducted from the MARMARA project areas and from Thrace (Figures 2 and 6). The *origin of the NAFZ* is connected with the collision of the Arabian and African plates with Eurasia (Pavoni 1961, McKenzie 1972, Jackson and McKenzie 1988). The Anatolian plate moves westward from the zone of intensive convergence in eastern Turkey along the dextral NAFZ. East of Bolu, the displacements are concentrated on a small fault zone, but to the west the zone progressively splits up and becomes wider. The Kuzuluk research area lies at the western end of the first enlargement zone, the 80km long Almacık lens. It is surrounded by several curved faults. Southwest and west of Kuzuluk, the NAFZ definitively splits in two large, complex zones. Many authors, such as Barka (this volume), speak of three "strands", our southern zone being subdivided in a middle and southern strand. However they are hard to separate and show narrow interrelations. Both have a strong impact on the actual morphology and obviously were active during some periods of neotectonics. In the following it will be tried to place the active phases and the amount of displacement with the help of geology.

The beginning of the activity of the NAFZ can be connected with the sedimentation in Neogene basins in eastern Anatolia and has Upper Serravallian age, 12 to 14m.y. ago (Barka 1992). According to the same author, the movements progressed from east to west. In NW Anatolia the NAFZ is clearly younger than the main phase of rotation. The small, extensive *Kuzuluk basin* lies at the western end of the Almacık lens, both structures obviously being a product of the NAFZ. To the northwest and the southwest of the lens, coarse fluviatile sediments (Pliocene) are clearly younger than the start of the uplift of the lens. The depression of Kuzuluk is filled by acidic to intermediate volcanics interbedded with light coloured, mostly fine grained fluviatile sediments of Neogene type. As they contain volcanics and are covered unconformly by Pliocene gravels, Greber (1992 and this volume) supposes that they correspond to late Miocene (continental facies, Pontian). By silicified intercalations and subvertical channels included in these series, Greber could prove that the still active field of geothermal springs already started flowing during sedimentation (at least 7-8m.y. ago?). This gives a minimum age for the start of activity of the NAFZ here.

The *southern zone* west of the bifurcation near Kuzuluk, splitting to the west into several disturbances, will now be discussed. Many of these faults have a strong impact on morphology, but their activity cannot be fixed in detail in the numerous basins filled with Neogene and Quaternary sediments. West of 30° longitude, the southern zone of the NAFZ splits into three fault systems: the southern one runs south of the Uluabat and Kuş lakes, the middle one goes on to Gemlik and Bandırma. A third fault system can be found north of İznik lake, then deviates to WNW direction, crosses the Cengiler pass and ends near Yalova. All movements along the third system were dextral but, in addition, extension formed a shallow graben connecting İznik lake to Marmara sea region by a low saddle zone (Eisenlohr 1995). It was partly filled by Neogene, the fossiliferous limestones and marls of the Upper Tortonian/Pontian (Akartuna 1968) reaching from northwest the Cengiler pass. There again, the activity of the NAFZ can be proven to have started during the Tortonian. The Miocene sediments were later deformed and lifted here.

More to the west, the faults of the southern zone cut and displace the *border of the NW Anatolian rotation zone* between Bursa and Mudanya and continue to the west (Figure 2). Around Erdek and Gönen, however, the direction changes to WSW and the faults become weaker, the configuration indistinct. Most or all disturbances loose their identity before reaching the Aegean coast. As an example, in the Ezine research area, the frequent but weak faults running ENE-WSW could be suspected to belong to the NAFZ at first glance. Mützenberg (1991) describes them as dextral and extensive, but in several places he observed that some of

them were filled by hydrothermal chalcedony deposits. These deposits are completely different from the thermal spring deposits of Tuzla or Kestanbol and probably correspond to a final stage of the Burdigalian volcanism. This frequent fault system, therefore, is much older than the NAFZ; a small-scale reactivation during the Tortonian is however possible.

The total displacement along the southern zone was estimated by Barka (1992) to lie between 14 and 21km near Geyve (based on the deviation of the Sakarya river), to reach 20km in a cross profile south of İzmit and to dwindle slowly to the west, reaching some 12km near Gönen. Looking to the shift of the border of the rotated zone we obtain 18 to 20km of displacement, which is in agreement with Barka. What happens more to the west? The dextral displacements come progressively into contact with Aegean expansion and seem to fade away. The movement probably partly becomes extension along different fault systems and causes some rotation locally.

Messinian to Lowest Pliocene deformations

A not very spectacular widespread but gentle tilting, folding and faulting is to be observed in the northern Aegean region, NW Anatolia and far to the east along the NAFZ. This deformation affects all layers including the Upper Tortonian/Pontian, as may be observed along road cuts, e.g. west of Bursa or along the flat ridge lying between the Marmara sea and the depression between the Uluabat and Kuş lakes. The uplift of the Tortonian saddle zone between İznik lake and Yalova must be of the same age. In several outcrops, e.g. in the Kuzuluk and Ezine areas, the unconformity to flat lying Pliocene cover can be directly observed. The exact age of the deformations cannot be fixed, but they had to have happened between the Messinian and the Early Pliocene. LePichon and Angelier (1981) and Mercier et al. (1987) postulate a short-lived episode of compression for the Aegean region, but also as far to the west as Apulia, active during the Lowermost Pliocene and in the northeast possibly Late Messinian, too. As compression was the reason of the deformation, extension of northern Aegean sea and nearby Anatolia had to have been stopped for a while around the Miocene/Pliocene limit.

Second phase of the NAFZ activity: Collected data

Up to this point, the *northern zone of the NAFZ* has not been treated even though it is supposed to be the most prominent and active today. It can be followed from the bifurcation near Kuzuluk, westward to Sapanca lake, to the gulf of İzmit, to the deep trough within the Marmara sea, to the Ganos fault and to the trench of the gulf of Saros, then it continues into the Aegean sea (Figure 2 and Barka, this volume). Fortunately, the bottom of the Marmara sea is not only known by bathymetric maps but also by seismic research (Wong et al. 1995). The most interesting feature is a deep trough with a main axis running E-W, but also including oblique internal ridges. Pfannenstiel (1944) already supposed that they could correspond to faults. Seismic profiles showed that, in fact, the trough can be subdivided into internal basins and ridges (Wong et al. 1995, see also Barka this volume). The exact configuration of the faults and the amount of the dislocations, however, still is under discussion.

When did *the northern zone* of the NAFZ *begin its activity?* Two regions studied by us may provide a key: the north of the Armutlu peninsula on the Anatolian side and the borders of the northern zone in European Turkey, between Barbaros, south of Tekirdağ, and the western tip of the Dardanelles peninsula. In the northern *Armutlu peninsula*, Eisenlohr (1995) observed that a river once transported pebbles from the east or northeast of Yalova to the region of Armutlu in the west including unmetamorphic, reddish, quarzitic sandstones of supposed Triassic age. Since the deep trough of the Marmara sea and the gulf of İzmit opened, such a transport path is no longer possible, but a transport in the Tortonian can also be excluded too (depression connecting Yalova with İznik lake, Chapter *NAFZ: First period of activity*).

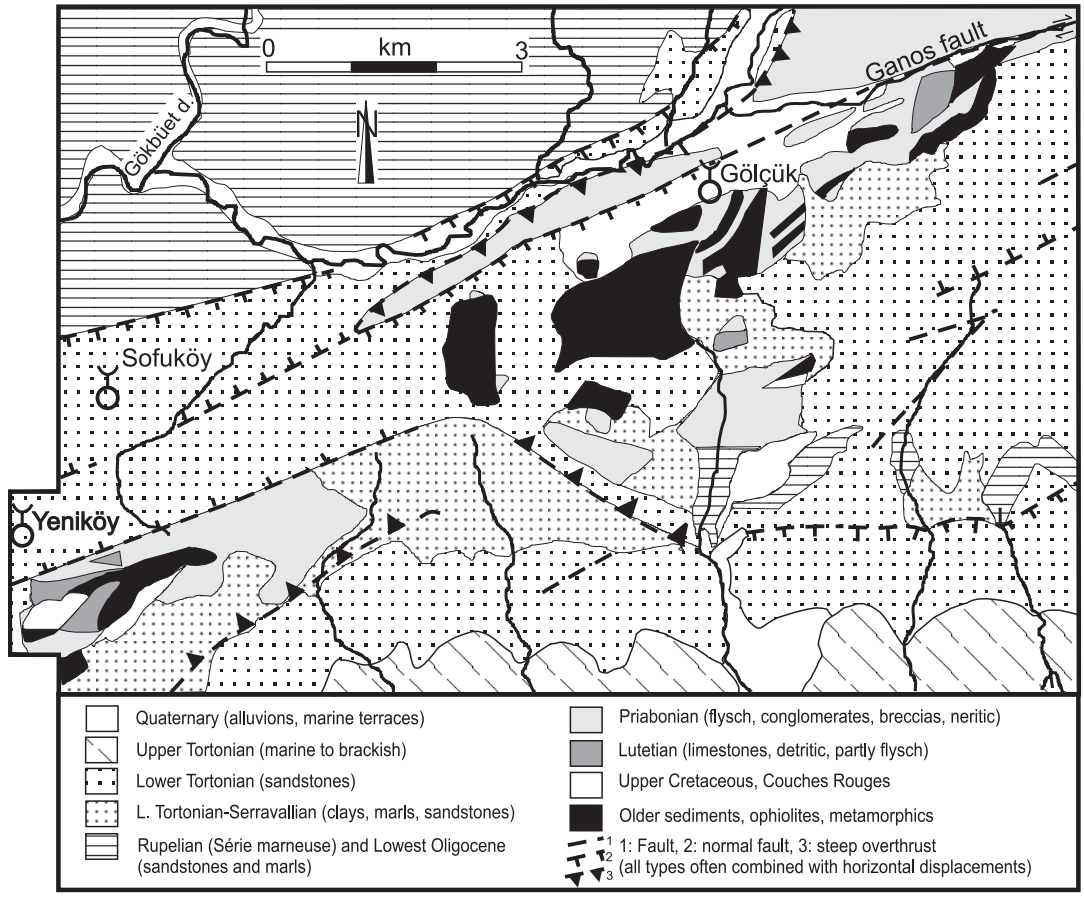


Figure 3: Detailed geology of the area north of Şarköy, simplified.

Wong et al. (1995) tried to fix the *beginning* of the sedimentation in the *deep Marmara trough* (in the Cınarcık basin northwest of Yalova). Based on the thickness of the young complex and average rates of sedimentation, they arrived at 3m.y. If this value is correct, the river transport to the WSW occurred during the Lower Pliocene and the Marmara trough opened in the Upper Pliocene.

In *European Turkey*, three typical configurations occur along the NAFZ: between Barbaros and Ganos, only the northwestern flank can be observed, as the opposite side of the fault now is part of the Marmara sea trough. Between Ganos and the eastern end of the gulf of Saros, both flanks are well preserved and lie on land. More to the WSW, the prolongation of the Ganos fault follows the northern coast of the Dardanelles peninsula, the northern flank being part of the deep Saros trench.

The *central and* large parts of the *eastern areas* were studied in detail by the author. As most of the results have been published (Schindler 1959, Kopp, Pavoni and Schindler 1969), we will give here only a summary with special attention to neotectonic events. Three figures are of special interest for the central areas: Figure 3 corresponds to a simplified reproduction of map B1 in Kopp, Pavoni and Schindler (1969). Figure 4 shows the Bouguer gravity anomalies north of Şarköy as measured by Seismos for the Marmara Petroleum Corp. nearly 40 years ago. Figure 21 of Barka (this volume) reproduces a spot image showing the region north of Gölçük (left lower corner) and Mürefte (right lower corner), with the Ganos fault as a diagonal. As may be recognised in Figure 3, the basement and all sediments older than Miocene are intensively disturbed and broken into blocks with irregular shape and mostly steep standing limits. Some are quite large, such as the 10km long Doluca Tepe block, others very small. These intensively

disturbed series were cut by an angular unconformity locally reaching 90° and covered by more flat lying sediments of Upper Serravallian and Tortonian.

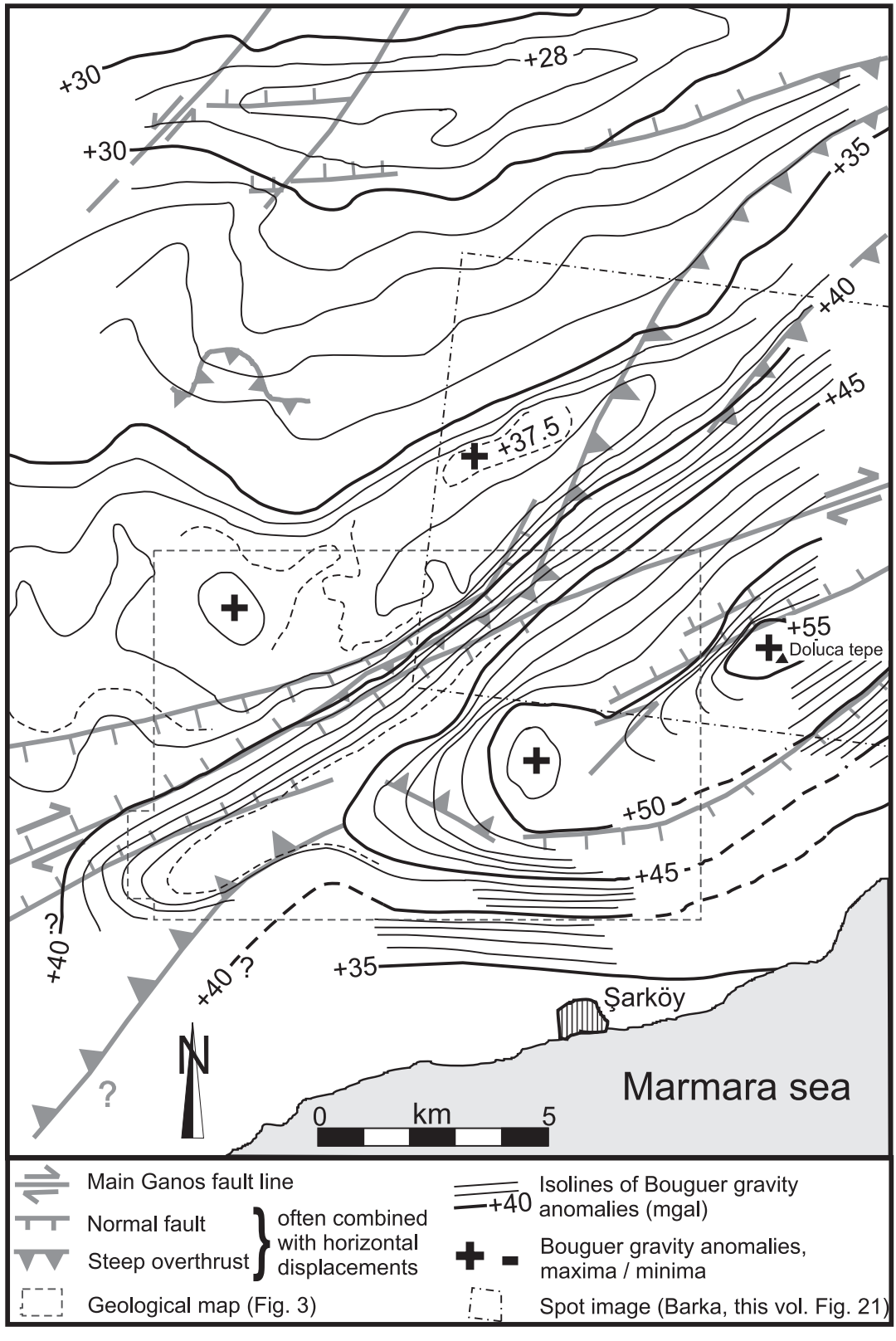


Figure 4: *Bouguer gravity anomalies compared with the main neotectonic features, Şarköy and Thrace regions.*

Why are the *rocks below the unconformity* in such a bad shape? They were not only affected by the late Alpine orogeny but by neotectonics too, as the border of the rotating zone was identical with the Ganos fault. Extensive dextral displacements affected it during the Middle Miocene. The slightly *younger deposits* of the Upper Serravallian and of the Tortonian do not show synsedimentary disturbances, but later were *tilted, faulted and deformed*. Tectonics are less brutal than below the unconformity, but still much more intensive than the usual effect of the Messinian to Lowermost Pliocene deformations. Strong dextral movements along steep standing structures are typical, especially along the Ganos fault. In addition, several narrow, partly-compressed grabens occur, but the most striking features are extensive rock bodies pressed up from the depths. Such *pop-up structures* can be observed all along the southern flank of the Ganos fault to the Dardanelles peninsula (Figure 5). In addition, the huge mass of Eocene and Oligocene flysch of *Ganosdağ* (north of the Ganos fault) was lifted and pushed over younger Oligocene sediments between Barbaros and Gölçuk. The limits of the uplifted bodies on the side opposite to the Ganos fault are curved and mostly steep. Most common are normal faults, but they often can change to steep overthrusting. All these facts prove that the dextral movement was combined with strong pressure. As may be recognised in Figures 3 and 5, the Saros gulf trench can be followed to the east as a graben becoming more and more narrow and pinching out in the southwestern corner of the Ganosdağ mass. The graben contain Miocene sediments, but they were pressed up to subvertical position, e.g. near Sofuköy. The compression zone, therefore, approximately reaches the actual eastern end of the Saros bay (Figure 5).

The map with *Bouguer gravity anomalies* (Figure 4) shows that the region north of Şarköy today is far from being in equilibrium. The pop-up structures as an entity correspond to a pronounced positive anomaly. The Ganos fault can be identified only in the southwest, where the uplifted mass of Ganosdağ pinched out. To the northeast, the border of the anomaly follows the main line of overthrusting (see Figure 5). A generalised, but much less detailed map of the Bouguer gravity anomalies in NW Turkey can be found in Şimşek (this volume, Figure 3). Southeast of the main neotectonic fault, a belt of positive anomalies can be followed there from Barbaros to the Dardanelles peninsula. The most prominent feature is a positive anomaly following the southeastern coast of the gulf of Saros, corresponding to the WSW prolongation of the Ganos fault.

Kopp (1964) worked on the *Dardanelles peninsula* and published a detailed map of the pre-Miocene outcrops. Along the southeastern coast of the gulf of Saros, strong compression coming from NNW caused folding and uplift. The oldest outcropping rocks are ophiolites and greenschists. The moderately deformed Eocene and Oligocene series to the southeast are abruptly relieved by Neogene, the contacts all being tectonic: steep standing normal faults or overthrusting to the southeast. As around Şarköy, the Miocene series were not affected by synsedimentary movements. Over a slight unconformity, they are covered by the coarse products of the nearby erosion of Paleogene series interpreted by Yaltırak (1995) as Upper Pliocene or even Lowermost Quaternary. The Dardanelles peninsula, therefore, seems to be very young and a product of the second active phase of the NAFZ.

The tectonic contacts between Paleogene and Neogene on the Dardanelles peninsula, but also in the direction of Ganos, are curved, the individual sectors of circles becoming narrower to the northeast and forming a funny garland (Figure 5). The most probable interpretation of this phenomenon is a sequence of (clockwise?) rotations progressing from southwest to northeast and caused by dextral transpression. Compression agrees very well with the observations east of the gulf of Saros, but becomes problematic where a trench lies immediately to the northwest as for at least 45km on the Dardanelles peninsula – the strain there probably is not active any more. The same considerations are valuable for *the eastern part of Ganosdağ*. For some 20km, the southeastern flank of the main fault sank down into the deep trough of the Marmara sea. Today, main compression oriented from Şarköy to the northwest seems to affect a large zone (Fig. 5).

As shown on Figure 5, neotectonic deformations reached *the northwestern foreland of the Ganos fault* also. North of the Ganosdağ, two young anticlines run oblique to Alpine structures. The peneplain of Thrace (Middle Pliocene?) was locally faulted and slightly deformed (Kopp, Pavoni and Schindler 1969). This caused the deviation of a valley originally running E-W and partly filled by Upper Tortonian sediments. The Gökbüet creek now turns to the south and to the gulf of Saros (Fig. 3 and 5). Probably due to ongoing deformations, the meandering river today crosses a saddle zone and eroded a small gorge.

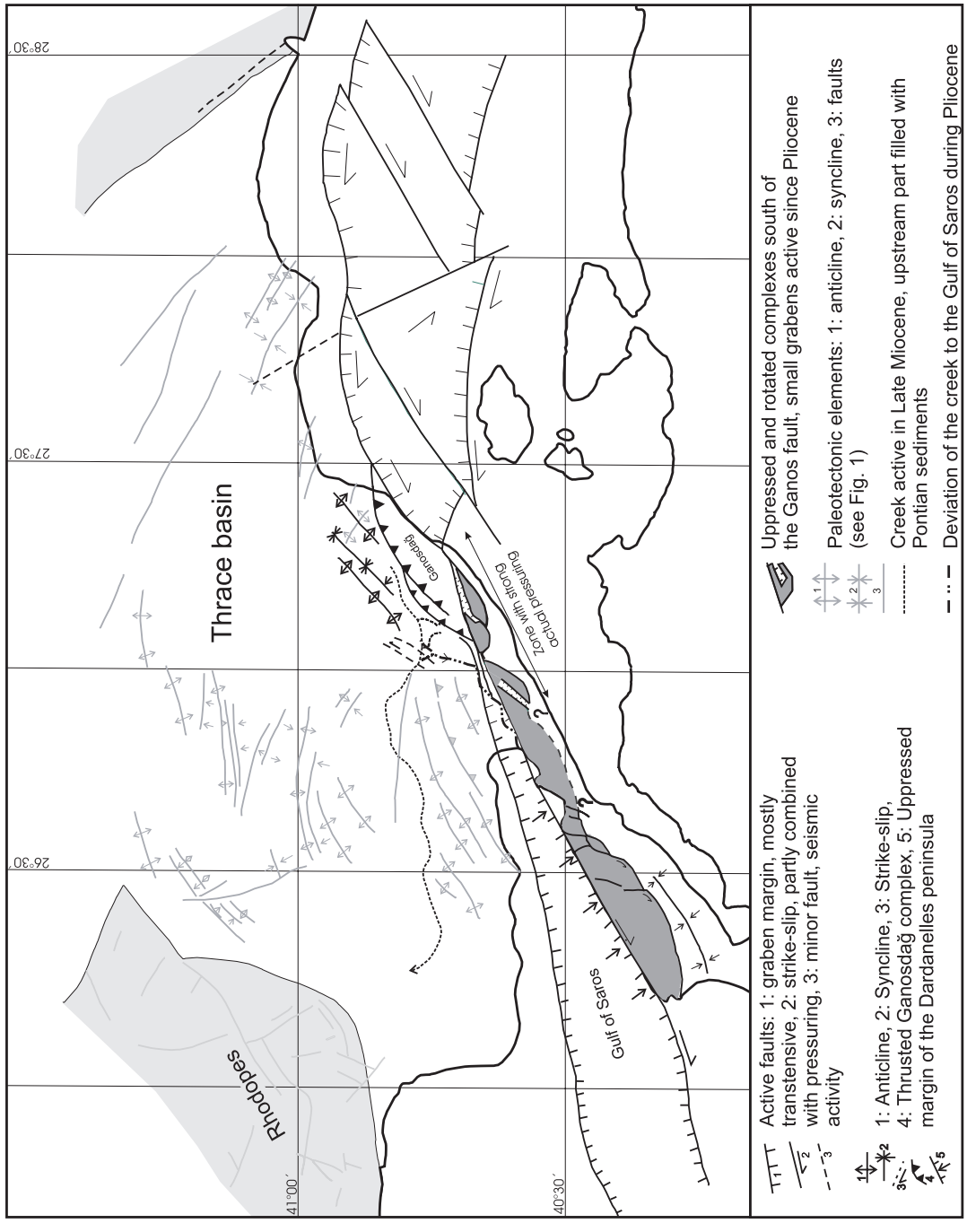


Figure 5: *Neotectonic activity since the Pliocene in European Turkey and the Marmara sea, compared with the Late Alpine structures.*

Second phase of the NAFZ activity: Conclusions

The *movements* still going on *started* in the middle or upper part of the Pliocene, *some 3 to 4m.y.* ago and were connected with the opening of the deep trough of the Marmara sea. The shape of the margins of the trough is very similar in the north and the south and can be joined by a 40km translatation to the WSW, parallel to the Ganos-Saros fault (Figures 6 and 7). Could the actual situation be explained by combining this translatation with a dextral E-W movement within the northern zone of the NAFZ? Using only these two kinds of movement, the attempt to reconstruct the conditions previous to the second phase of activity of the NAFZ fails. A much better approach to paleogeography, but also to the movements observed by geodesy (Straub and Kahle, this volume), results if a anticlockwise rotation of some 5° is added (Fig. 7). The northern border of the rotated area and the centre of the movement would be identical to those during the first phase of neotectonics, but the movements are much smaller. As this system was already active in the Middle Miocene, a revival is easily possible.

Based on these three presumptions, the *displacements* during the last 3 to 4m.y. can be estimated as follows (Figure 6):

- In the gulf of İzmit and more to the east, NAFZ was affected by a dextral movement of 55 to 60km.
- In the Marmara sea, the three types of movement are interacting, all in a dextral sense: E-W oriented northern zone of the NAFZ, translatation along faults running ENE-WSW for 40km, anticlockwise rotation of 5° causing a displacement of some 18km at the border.
- Along the Ganos fault and the gulf of Saros, all three movements joined in a dextral displacement of 55 to 60km to the WSW.
- In westernmost Anatolia and northern Aegean sea, a considerable extension in a N-S to NNE-SSW direction is active.
- The southern zone of the NAFZ, but also other faults, may in addition develop restricted activity.

Are these propositions compatible with the available data? On the *Dardanelles peninsula*, we found a compression zone no longer active today over a length of 45 to 50km, corresponding quite well to a dextral displacement of 55 to 60km away from the main zone of actual compression (Figure 5). The opening of a trench in the Saros gulf can at least partly be explained as an effect of the rotation. No problems arise along the Ganos fault and from the Ganosdağ.

In spite of recent seismic research, many questions still persist for *the deep trough of the Marmara sea,* e.g. concerning the exact position and function of the oblique faults proposed. The displacement of the borders of the trough by the ENE-WSW and NW-SE systems are probably in reality even smaller than that drawn in the figures. Our project was not carried out here and, therefore, cannot give additional information.

The proposed dextral displacements of 55 to 60km *between the gulf of İzmit and Kuzuluk* are much higher than the 15km proposed by Barka (this volume), but of the same order as the results from geodesy if the actual movement had continued at the same speed since the Middle Pliocene. According to an oral communication of G. Michel, the Turkish-German Earthquake Research Project working to the east of Kuzuluk came to dextral displacements on the same order as ours, this for the last 3 to 4m.y.

Large problems arise between the western part of the *Armutlu peninsula* and *Bursa*, where the two zones of the NAFZ came in direct contact at the border of the rotating zone. The southern zone cut and displaced this line in the Upper Miocene, the way for rotation is therefore now blocked (Fig. 2). The prominent, most southern fault of the *northern zone* follows the

northwestern coast of the Armutlu peninsula and reaches the rotation zone at the Boz Burun, west of Armutlu. Its dextral movement is essential for the opening of the deep Marmara sea trough. From the *Boz Burun to the vicinity of Bursa*, the ancient border of the rotation zone probably is no longer affected by shearing displacements, since it is blocked. There the dextral westward movement of the northern zone of the NAFZ is sustained by a dextral motion to the WNW of the anticlockwise displacement. This sector and its surroundings therefore have the function of a complex hinge (Fig. 6). For this restricted area, a purely geometric reconstruction of paleogeography cannot give satisfactory results. Movements between small blocks combined with some rotation may help to bridge the complex influences. In addition, some movements along the southern zone of the NAFZ are probable.

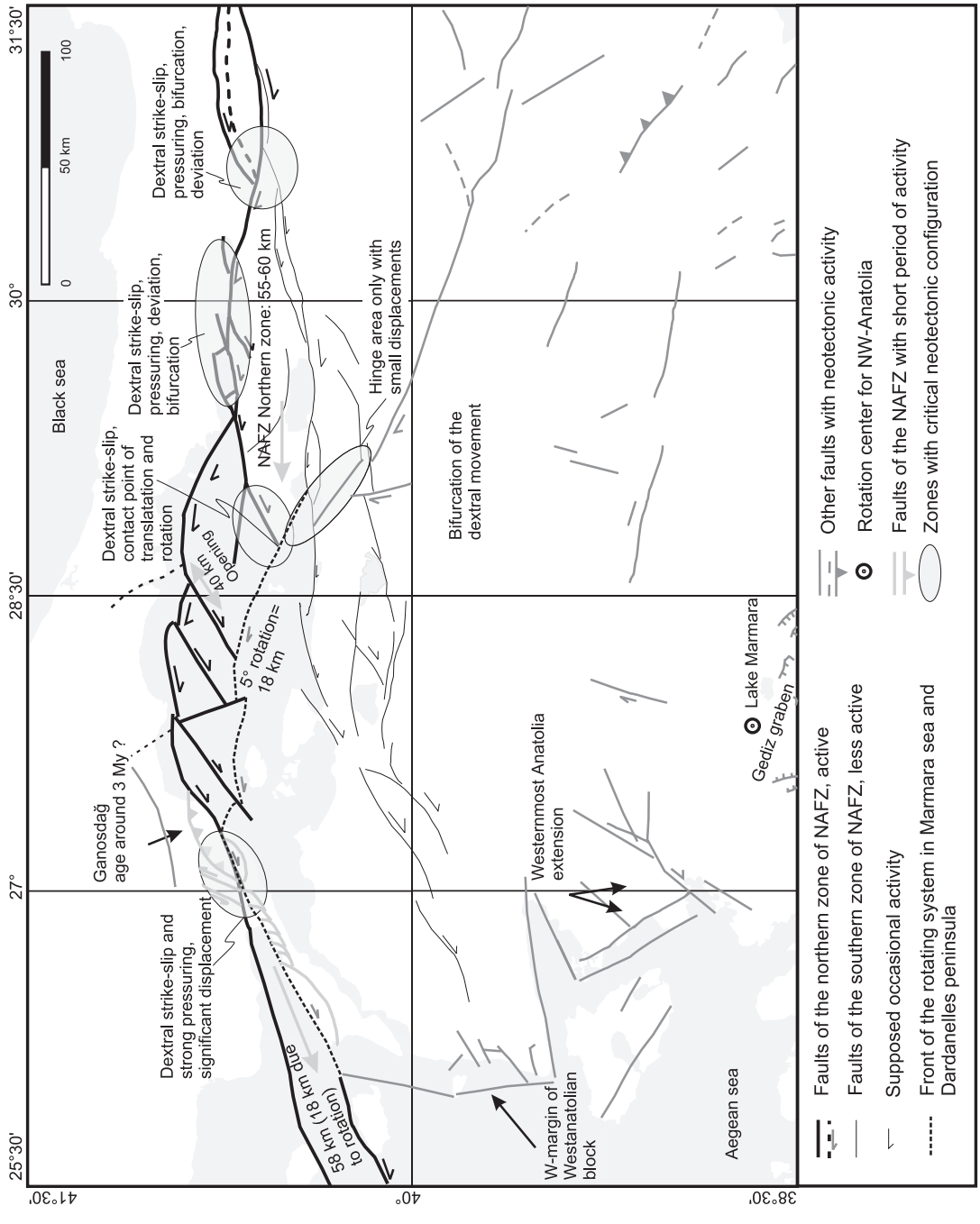


Figure 6: Neotectonic activities in NW Turkey since the Pliocene, critical configurations.

West of the fault line and the depression zone connecting İznik lake with Yalova, the*Armutlu peninsula* is exposed to a complex field of strains: large dextral movements to the WNW, smaller ones to the south, a hinge to the WSW, extension around İznik lake and WSW of it, compression east of Gemlik. Eisenlohr (1995 and this volume) postulated an internal deformation and a clockwise rotation of 15-40°. To obtain a convincing original direction for the late Alpine structures (N-S to NE-SW, see Fig. 9), the clockwise rotation should however reach at least 60° or the diversion has to change direction. This question cannot be solved without paleomagnetic measurements.

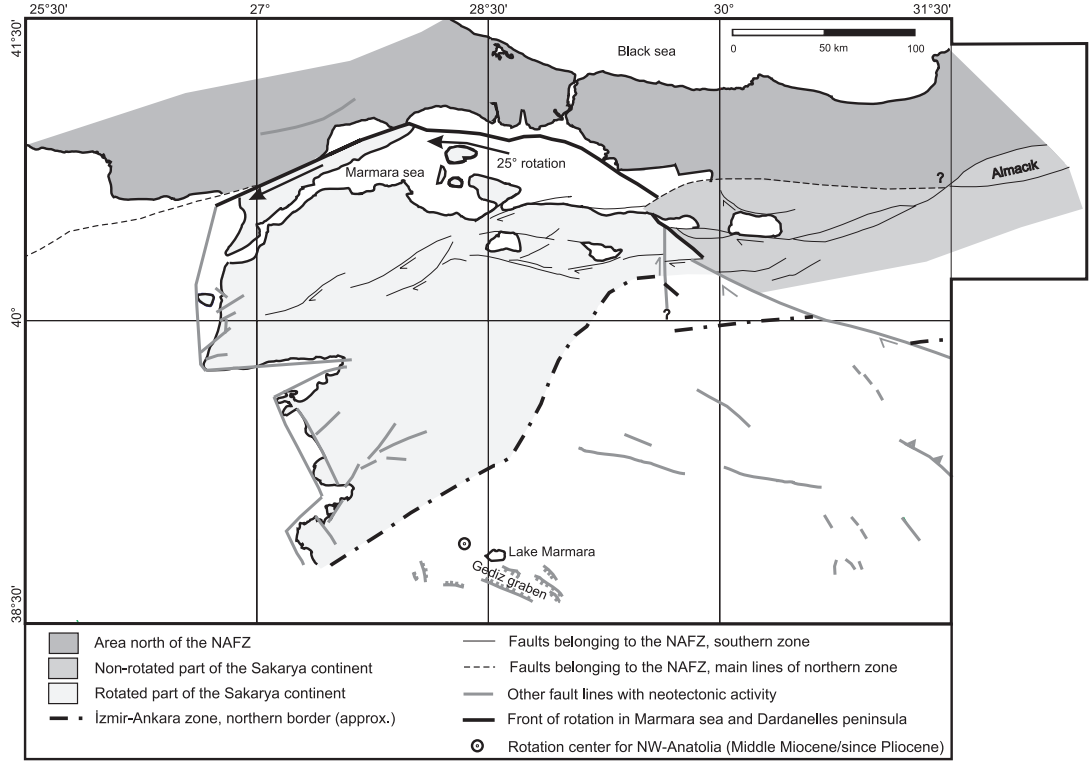


Figure 7: *Reconstruction of the paleogeography at the Miocene/Pliocene limit. To simplify orientation, the shorelines and – north of the northern zone of the NAFZ – the geographical grid correspond to the actual situation.*

Neotectonic history of Uludağ

During all three main phases of neotectonics, Uludağ was lying in an exposed situation, therefore it is not astonishing that its history is complex and still somewhat unclear. The paleotectonic events probably are very similar to what is known from the Ezine and Kozak areas: a granitic pluton intruded here 27 to 24m.y. ago during the Middle Oligocene, followed by quick uplift and strong erosion. At the end of the Oligocene, at least 3000m of cover had disappeared and the uplift became weak or stopped. A moderate uplift and tilting again affected the region around Kestanbol and Kozak plutons during the Middle to Upper Miocene. Since that time, no significant uplift movement has occurred there and the gravity field does not show marked anomalies.

The neotectonic history of Uludağ is quite different (Imbach 1992): near the western end of the massive it is subdivided by a prominent fault system which may followed from Çekirge near Bursa to the SSE. On its eastern side, highly metamorphic series and the granitic intru-

sion are outcropping; to the west lie very disturbed series with greenschist metamorphism. Many disturbances running approximately parallel to the main fault were observed on both sides. It is remarkable that east of the fault, the deformations are predominantly ductile, indicating great age (Variscan?). On the other hand, neotectonic activity is obvious. *West of the fault,* the relief is moderate and the morphology seems rather old. As described already by Ketin (1947), several terraces containing Neogene can be observed here, the lowest near the Bursa plain, the highest at an altitude of 900m. According to their facies, they very probably represent *Upper Tortonian/Pontian* and cover greenschists unconformly. This means that during sedimentation a continuous uplift occurred, but apparently stopped before the end of the Miocene (lowest terraces near the plain level). For 700m of uplift, a period of 2 to 4m.y. is available, the average rate being between 0.35 and 0.2mm/y.

East of the fault, such terraces are missing. Looking to the northern slope and to the crest of the massive, the morphology is quite ripe and relief moderate down to an altitude of around 1500m. Below it, the landscape abruptly changes character, a steep, quite uniform slope cut by narrow young gorges follows. Its shape is governed by a fault system striking approximately parallel to the slope and the stratification, inclined with 50-60° to the north. To the east, the system changes in an ESE direction, into the Eskişehir fault zone, and splits up into several steps. Normal, but also dextral movements can be deducted; the faults are transtensive. The foot of the steep slope is hidden by young rockfalls, landslides and cones, but in total the young movements along this group of faults caused an uplift of the southern flank of around 1000m. These movements still seem to be active, but when did they start?

As the period of Late Miocene uplift covers the same time interval as the first activity of the NAFZ, it may be speculated that the recent uplift could be parallel with the second phase of the NAFZ movements and have started 3 to 4m.y. ago. The average rate of uplift would be between 0.35 and 0.25mm/y – quite a reasonable value.

Uludağ has a very exposed position with regard to the anticlockwise rotation phases active during the Middle Miocene and since the Pliocene: To the WNW, the border of the displaced zone became approximately circular, to the ESE, the dextral movement was transmitted at least partly to the Eskişehir fault zone running WNW-ESE. As discussed in Chapter *Rotated zone in NW Anatolia*, a complex connection was proposed in addition, directed to the southeast and joining the Triangle of Burdur, but no details could be given. Looking around for a structure directed to the south or southeast and joining the labile İzmir-Ankara zone, the Çekirge fault zone could be a link. As already mentioned, its origin seems to be Variscan, but it was active again recently. This can be proven by a 3 to 4km dextral displacement cutting the most southern fault of the NAFZ (Figure 2 and 6), by its impact on morphology and by seismicity. On the map showing *Bouguer gravity anomalies* (Şimşek, this volume, Figure 3, as well as Klingelé and Medici, this volume, different figures) a spectacular negative anomaly roughly identical with Uludağ (but larger) can be observed. The external borders of the anomaly to the NNE and to the WSW are very steep and meet 12km southeast of Mudanya near the coast of the Marmara sea. The border running WNW-ESE is parallel to the Eskişehir fault zone, the other corresponds approximately to the Çekirge fault zone and can be followed to the south at least to 40° of latitude. The uplift tendency of the Uludağ area could be explained at least partly by isostasy.

It has to be supposed that the start of neotectonics during the Middle Miocene was very brutal and connected with heavy faulting, tilting and breaking up of existing structures. Very probably the *Çekirge fault zone* played a prominent part, especially during the initial phase of the rotation as conditions then were very favourable for dextral movements (see Figure 8). In the current phase of neotectonics, the Eskişehir and Çekirge fault systems limit a wedge pointing to the northwest. Both systems are affected by dextral movements. The anticlockwise rota-

tion typical for the southern border of the Marmara sea trough therefore must have been transformed and split by this wedge. Paleogeographic reconstruction (Figure 8) gives a very hypothetical total neotectonic dextral displacement of 40 to 50km along the Çekirge fault, 3 to 4km of it since the Pliocene.

What about the northwestern *prolongation of the Eskişehir fault*, cut by the southern zone of the NAFZ (Figure 2, between the Marmara sea near Mudanya and Kestel 12km ENE of Bursa)? It has no marked influence on morphology, but can easily be followed on the gravity map. As previously mentioned, the dextral movements along these disturbances were blocked by the first active phase of the NAFZ, during the Late Miocene. As all of the sediments outcropping along the fault are younger, large displacements cannot be expected at the surface.

An enigma is why Uludağ actually corresponds to a negative gravity anomaly – a problem which cannot be solved by surface geology.

Conclusions

Neotectonic displacements will be discussed first as they have a large influence on the reconstruction of the paleogeography and paleotectonics.

Neotectonics: Movements, phases of activity, average rates of displacement

(Table2)

The following sequence can be postulated for NW Turkey (based mainly on our results) and for the Northeastern Aegean area (based mainly on Mercier et al. 1989):

- *End of the Alpine compression* in Late Aquitanian or Early Burdigalian.
- *Start of neotectonics* in Langhian. A new subduction zone became active between the Eastern Mediterranean and the Ionian sea (Mercier et al. 1989). The paleogeography dramatically changes, regional faulting and tilting affects all of the MARMARA research areas except Thrace basin and probably the Kuzuluk area.
- An *anticlockwise rotation* reaching a total of 30° affects NW Anatolia. The limits of the rotating block can be followed from the Aegean sea (north of İzmir) to the Marmara sea near Mudanya. There it splits into the Eskişehir fault zone oriented ESE and the Çekirge fault zone oriented to the south. The prolongation of the limits to the south and southeast were not investigated by the MARMARA project. They probably are not identical with the southeastern border of the "Marmara block" defined by Crampin and Evans (1986), mainly fixed by high seismicity, but rather joining the Burdur triangle (Mueller et al. this volume). The centre of the anticlockwise rotation since the start of neotectonics is approximately stable and lies 60km ENE of İzmir near the small Marmara lake. As only 5° of rotation occurred since the Pliocene, the remaining 25° must have been bound to the *first phase of rotation*. It must be older than the marine transgression of the uppermost Serravallian to be observed near the coast of the current Marmara and Aegean seas and can be limited to the Middle Miocene. The displacement amounts to approx. 90km along the northern border of the rotating zone (Marmara sea, Ganos fault), a 220km distance from its centre.

- The *start of the Aegean extension* is possibly coincident with the start of the rotation. The first proof according to Mercier et al. (1989) is given by sediments with an age of 13.5m.y. (Middle Serravallian). Extension continues until the Messinian.
- *The NAFZ* progresses from east to west and reaches the MARMARA research area at the latest in the Upper Tortonian. West of Kuzuluk, the dextral movements during the *Upper Miocene* follow the *Southern zone of the NAFZ,* they cut and shift the border of the block rotated during the Middle Miocene. ENE of Bursa, the total displacements lie around 20km (an unknown part is of Pliocene to Quaternary age). More to the west, they progressively shrink and disappear near the Aegean coast. Mercier et al. (1989) constructed an Aegean extension directed NW-SE for Greek Thrace, Samothrake and Limnos in the Upper Miocene and concluded that under such conditions the dextral movements of the NAFZ could not progress into the Aegean sea.
- A gentle *phase of compression* caused some faulting, tilting and folding in NW Anatolia and far to the east. Its age has to correspond to the Messinian or the Lowermost Pliocene. Mercier et al. (1987) found witness of a short-lived compression as far to the west as Apulia and could fix the end of this period at 4.2m.y. (Lowermost Pliocene). Aegean extension, as well as the activity of the NAFZ in the MARMARA research area, were stopped previous to the end of the Messinian.
- During the *last 4m.y., Aegean extension,* according to Mercier et al. (1987, 1989), was again active, but 1.0-0.7m.y. ago (Lower Quaternary) the stress field changed after a short period of compression (not to be detected in MARMARA research area). They postulate that main extension near the Anatolian coast in the Pliocene had a NE-SW to NNE-SSW direction, but in the Quaternary turned 20-30° to the NNE-SSW and N-S. This actual orientation agrees with the results from the MARMARA project geodesy. According to Mercier et al. (1989), NAFZ movements reached the Aegean sea in the Upper Pliocene. The dextral movements of the northern zone progressed to the gulf of Saros and to the North Aegean Fault System, which combines shearing with extension.
- As previously discussed, the *NAFZ activity started again* 3-4m.y. ago, probably concurrent with Aegean extension. The main movements now follow the northern zone and are quite complex (see previous Chapter and Figure 6). The largest displacement is supposed to reach 55-60km and happened mainly along the Ganos fault and from the gulf of İzmit to the east. Some minor activities of the northern zone during the Late Miocene cannot be excluded, on the other hand, the southern zone of the NAFZ was not completely passive since the Pliocene, as proven by earthquakes and Geodesy (in Table 2 these movements are estimated to reach 10% of the total displacements). We suppose that this activity has rather to be seen as a reaction to the stress field governed by the northern zone of the NAFZ than as an autonomous revival.
- The *total displacement along the NAFZ since the Upper Miocene* for the region east of Kuzuluk results if the values from the northern and southern zone are added. The sum of 75-80km dextral movement is of the same order as the estimations published by Seymen (1975), Şengör (1979) and Westaway (1994).

In summary, it can be stated that the *neotectonic activity was not continuous* but interrupted by relatively quiet periods and even by at least one phase of slight compression. The character, the speed of the deformation and probably the stress field also changed from one active period to another.

	Stage (marine)	Age (m.y.)	Uncertainty (m.y.)	Main events	Max. displacement	Average rate
Quat.	Quaternary	1.6	3	Second phase activity NAFZ, W of Kuzuluk predominantly Northern zone + opening Marmara sea trough + 5° anticlockwise rotation + Extension in Aegean region *3-4m.y.*	NAFZ northern zone 55-60km + 5km(?) along southern zone	3m.y.: 2-2.2 cm/y 4m.y.: 1.5-1.7 cm/y
Pliocene	Late Pliocene	3.4	4		Opening Marmara trough 40km	3m.y.: 1.3cm/y 4m.y.: 1.0cm/y
Pliocene	Early Pliocene	5.3	5		Aegean ext. unknown	?
Miocene	Messinian	6.5	6	Gentle compression, folding, tilting. Previously and subsequently quiet periods. Extension in Aegean realm interrupted *1-3m.y., probably 1-2m.y.*	?	?
Miocene	Late Tortonian	11.2	8	First phase activity NAFZ, west of Kuzuluk predominantlly southern zone + extension in Aegean region *2-5m.y., probably 2.5-4m.y.*	NAFZ southern zone east of Bursa ~20km -5km(?) since Plioc.	2.5m.y.: 0.6cm/y 4m.y.: 0.4 cm/y
Miocene	Early Tortonian		11		Amount of extension unknown	?
Miocene	Serravallian	15.1	12	Extension in Aegean realm *1-6m.y., probably 2-4m.y.*	Amount of extension unknown	?
Miocene	Langhian	16.6	14	Start of extension in Aegean realm? 25° anticlockwise rotation breaking up and tilting *2-5m.y., probably 3-4m.y.*	Amount of extension unknown	?
Miocene	Burdigalian	21.8	16 17	End of Alpine compression	Marmara sea ~90km dextral movement	3m.y.: 3cm/y 4m.y.: 2.25cm/y

Table 2: Neotectonics in NW Turkey (MARMARA research areas and Thrace).

Average rate of movement

The rates are compiled in Table 2, but due to open questions with regard of the duration of the individual phases they can not be fixed exactly.

- *For the dextral movements* (partly connected with rotation), the largest average rates result from the rotation during the Middle Miocene, possibly reaching 3cm/y. The Upper Miocene displacements along the NAFZ are modest, as being around 0.6cm/y or lower. For the last phase of neotectonics (since the Pliocene) the movements increased again to 1.5-2.2cm/y – a value in the range of the 2.2cm/y resulting from the MARMARA geodesy research. This coincidence may be accidental or point to a very steady long-time behaviour. According to Reilinger and Barka (1996), a large-scale rotation model for the NAFZ would give an average displacement of 2.6cm/y, another calculation based on earthquakes yields a value of 3.8cm/y.
- The *southward extension* observed in Western Turkey and the Aegean region was more continuous than the activities of the NAFZ, but the amount of stretching cannot be deduced from the MARMARA project geology. The opening of the deep trough of the Marmara sea is not to be compared with Aegean conditions and lasted only 3-4m.y. The distance between both margins measured in an ENE-WSW direction increases 1.0-1.3cm/y.
- It is very difficult to estimate average rates for the *local uplift movements*. Near Bursa, tentative reconstruction gave values of 0.2-0.35mm/y for the western flank of the Çekirge fault for the Late Miocene and – more to the east – 0.25-0.35mm/y (?) for the Uludağ since the Middle Pliocene. Depending on the estimated age of Quaternary marine terraces near Şarköy, the uplift reaches 0.7mm/y, or more probably 0.3mm/y. The highest values of subsidence are actually expected to be in the Marmara sea basins and the gulf of Saros.
- *Previous to neotectonics*, uplift rates reaching 1mm/y were proposed during and immediately after the intrusion of acidic plutons in the Late Oligocene.

Paleogeographic reconstruction, paleotectonics

(Figure 8)

An attempt was made to reconstruct the conditions at the start of neotectonics, 16 to 17m.y. ago in the Late Burdigalian. To allow a better orientation, the area north of the NAFZ was assumed to be stable up to the geographic grid. In addition, the actual shorelines were drafted to aid in understanding. Where complex movements split up the displacements in unknown proportions, the original position of an area can no longer be fixed nearby: the Almacık lens probably has to be shifted more to the east, Uludağ possibly along the Eskişehir fault zone more to the ESE. For the islands of Imros and Lesbos, neither the location nor the amount of rotation are exactly known. In spite of possible further uncertainties, the following conclusions are possible:

- The *highly metamorphic series* (amphibolite facies) located south of the northern limit of the NAFZ originally had structures with prevalent ESE-WNW orientation (Uludağ, Kapı dağ, Marmara islands, Kazdağ?). As key horizons such as marbles are missing on the Armutlu peninsula, the structural conditions cannot be fixed there.
- Slightly metamorphic series (greenschist and lower facies) were obviously deformed during a late *Variscan orogeny*. In the Kozak area, the structures originally were oriented ENE-WSW. East of Bursa and north of the Eskişehir fault zone, a similar E-W direction was observed (see Chapter *Age of the metamorphics and of the metamorphose*). The deformations happened between the Late Carboniferous and the Lowermost Permian and obviously are younger than the structures affecting the highly metamorphic series, as they have another direction. The previous orogeny has to be older than the opening of the Carboniferous trough but younger than the coral found in Uludağ marbles. Probably it corresponds to an *early Variscan event* but Caledonian orogeny cannot be excluded.
- The youngest series affected by metamorphism do not have the same age everywhere. With sharp limits, different zones can be distinguished, all running approximately E-W (Fig. 8 and Chapter *Metamorphic Mesozoic series*).
- The youngest metamorphics occur in the *İznik Metamorphic zone* (Jurassic and large parts of Cretaceous). They lie in an E-W oriented belt affected by neotectonics (Fig. 9). The zone becomes larger towards the Aegean sea, but seems to pinch out in the direction of Bolu, where both flanks join the Intrapontide suture. The İznik metamorphics zone corresponds to the limit between the bulk of the Pontides to the north and the Sakarya "continent" to the south. Its closure in the Late Cretaceous corresponds to an*early Alpine event*.
- A large belt of acidic to intermediate, calcalcaline magmatics oriented E-W follows the zone with *İznik metamorphics* (northern half of Figure 8). Plutons of this group are proven or supposed to have intruded around the Cretaceous-Paleocene limit. The volcanics are younger and extruded between the Eocene and the Middle Oligocene, apparently progressing from east to west (Chapter *Volcanics of Late Cretaceous to Burdigalian age*).
- More to the south lies a belt with similar, but *younger magmatic rocks* concentrated west of 30° longitude (Fig. 8). Plutons of this group intruded during the Oligocene, the volcanics followed in the Early Miocene. The youngest eruptions may have happened in the Langhian, at the limit of neotectonics. The context, however, is still supposed to be*Late Alpine*.
- From the *uppermost Cretaceous to the early Oligocene*, the zone with İznik metamorphics was affected by uplift, erosion and tectonical unrest as proven by sedimentation and volcanics. To the north and the south, deep troughs arose and mostly were filled by flysch sediments, this from the Late Campanian to the early Maastrichtian (east of 29° longitude) and again from the Lutetian to the Priabonian (in Thrace to Lattorfian). A typical, often very coarse flysch is widespread, the clastic material being at least partly supported from the

high zone with İznik metamorphics. For the time in between (Upper Maastrichtian to early Eocene), nearly no sediments are preserved as conditions were continental. An exception is given by partly marine and fossiliferous series preserved in the Kuzuluk research area (Chapter *Late Cretaceous and Paleocene sediments*). They are affected by a pronounced tectonical unrest.

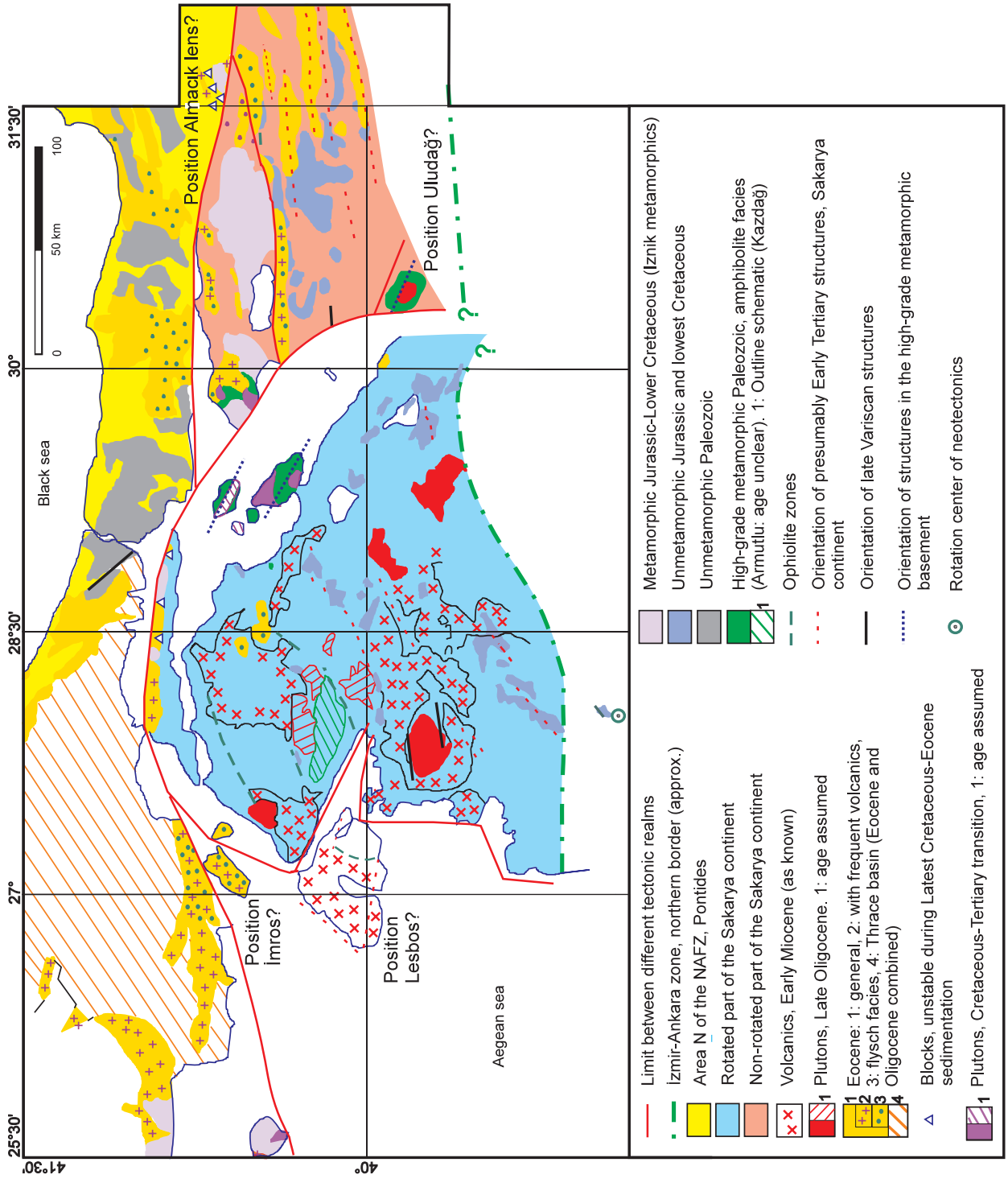


Figure 8: *Paleogeography at the start of neotectonics (Middle Miocene). To simplify orientation, the shorelines and – north of the northern zone of the NAFZ – the geographical grid correspond to the actual situation.*

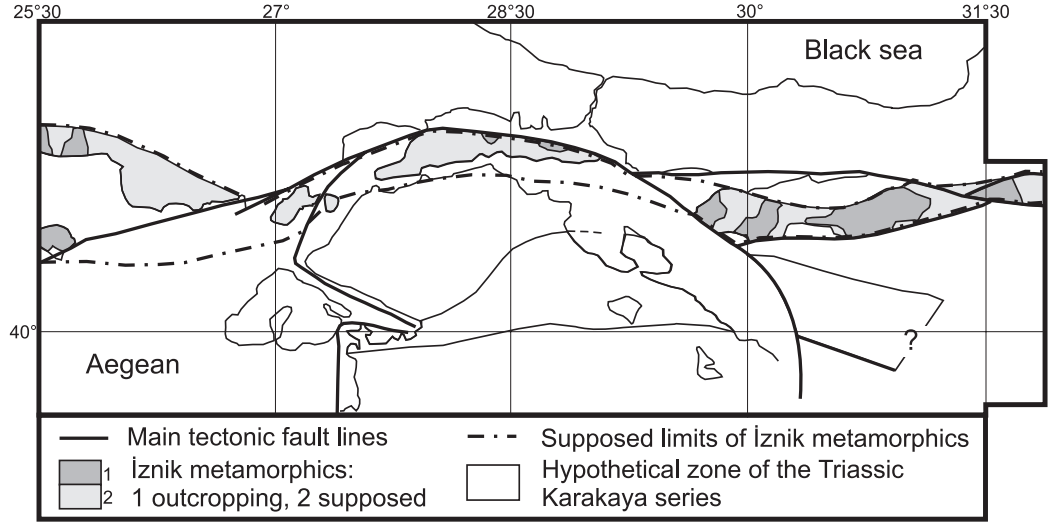


Figure 9: *Paleogeographic reconstruction showing the supposed extent of İznik metamorphics and main neotectonic fault lines. To simplify orientation, the shorelines and – north of the northern zone of NAFZ – the geographical grid correspond to the actual situation.*

- Why did the zone with İznik metamorphics show a tendency for uplift while the neighbouring areas (including the Thrace basin) subsided? Wong et al. (1995), Barka (this volume) and others postulate a phase of extension starting early in the Eocene or before. Another possible interpretation is to admit a varying, but uninterrupted *Alpine compression* for the Eocene and the Oligocene also. It would increase the relief by the formation of emerged ridges and deep, subsiding water bodies, but also be responsible for the foreland Thrace basin. The second interpretation agrees with Görür and Okay (1996) and Yılmaz (this volume), but also with observations in northern Greece (Mercier et al. 1989) and seems more probable to us.
- Folding and faulting during the Aquitanian (possibly continuing into the Lowermost Burdigalian) marks the *end of Alpine compression* in Thrace. To the east, neotectonic disturbances destroyed such structures, but they partly are preserved to the west and give a corresponding age (Mercier et al. 1989).
- Regional *uplift movements* combined with erosion are typical for the late Alpine period in NW Anatolia. They gently start in the Early Oligocene, but become much more intensive near the limit with the Miocene. Isostatic uplift caused by extensive acidic intrusions locally enforced this tendency. In Thrace, main uplift and erosion are connected with the final Alpine folding and faulting and, therefore, are slightly younger. Since that time, NW Anatolia and Thrace remained continental with the exception of some areas marginal to the Marmara and Aegean seas.
- Several sophisticated, but partly controversial, models in the past have tried to explain the very complex paleotectonic history of NW Turkey by *plate tectonics* (e.g. publications of Şengör et al. 1995, Yılmaz et al. 1995, Yılmaz this volume, Görür and Okay 1996). It was not the aim of the geological work of the MARMARA project to postulate an additional model, but to collect as many facts as possible. Supported by results coming from geophysics, they may help to find convincing answers in the future.
- For the *Alpine cycle,* however, some facts seem to be accepted by most of the specialists (see Table 1): Neotethys opened during the Lowermost Jurassic and had two branches, separated by the Sakarya "continent". The main trough corresponds to the İzmir Ankara

zone south of it, the minor trough in the north to the actual İznik metamorphics zone (where it pinches out: to the Intrapontide suture). Closure began around the Cenomanian (100-90m.y. ago) with a northward subduction of the oceanic crust below the continental crust. The collision between the continental masses seems to have happened first in the northern branch some 85m.y. ago (Santonian), later in the İzmir-Ankara zone, probably near the Cretaceous-Paleocene limit, some 65m.y. ago. Soon after the beginning of the Tertiary, all of NW Turkey would have been underlain by continental crust. Görür and Okay (1996) discuss the possibility that an oceanic belt could have been preserved south of the Thrace basin until the Oligocene. They suppose that the closure of the İznik metamorphics zone (their Intrapontide suture) during the early Alpine orogeny decreased from east to west, what could agree with our Figure 9. The metamorphism of the Jurassic and Early Cretaceous series on Samothrake and north of it, however, speaks against this hypothesis. Late Alpine compression ended near the Oligocene-Miocene limit and, according to Yılmaz (this volume), was effective mainly in the northern border region (Thrace and flysch troughs) and in southern Anatolia. According to different authors (e.g. Mercier et al. 1989, Kondopoulos et al. 1996) continental crust underlies all of Western Turkey and the Aegean sea.

Relations between paleotectonics and neotectonics

Paleotectonic structures are important for the MARMARA Poly-Project for several reasons: The pathway of cold or thermal groundwater in the case of karstic water circulation depends on the geometry and the extension of the carbonatic rocks, mostly fixed by paleotectonics. For hydrogeology, all kinds of brittle destruction of a rock are of interest, beginning with joints caused by the contraction of cooling down volcanics or plutonites and ending with major tectonic structures. As here we are looking for interrelations between paleo and neotectonics, only the major configurations and the age of the discontinuities will be considered, with special attention to the brittle structures. Work on these problems was an important task for all the detailed studies. To fix the age and history of the fault systems proved to be very difficult, however, many of them seem to be quite old and occasionally to have changed function.

In Thrace for example, faults running NW-SE, NE-SW and approximately N-S already were partly active during sedimentation in the Eocene and again had an influence on the late Alpine orogeny (Chapter *Late Alpine compression in Thrace*). In the Kozak, Uludağ and Ezine areas, the freshly-intruded plutons and the surrounding area were uplifted during the Upper Oligocene, this partly along normal faults. Dykes filled by aplites, volcanics or hydrothermal deposits in the Kozak, Ezine and Armutlu areas prove that several fault systems already existed previous to neotectonics. In some cases (as for andesitic dykes running NW-SE) Eocene (Armutlu area) to Lower Miocene (Kozak and Ezine areas) age is probable, but Upper Miocene to Pliocene cannot completely be excluded. After the main volcanic activity some late, local acidic to basic eruptions occurred during neotectonics.

At the *start of neotectonics,* a very widespread and brutal faulting or tilting occurred, combined with vertical displacements or rotation of small to very large entities. This best can be observed along the Aegean coast and landward of it, where many of the alignments already existed before (Mützenberg 1991, Jeckelmann 1996).

One of the most interesting questions is how *rotation* between Uludağ and the gulf of Saros could form a border corresponding approximately to the *sector of a circle.* Figure 9 shows that much of the way was made easy by the northern limit of İznik metamorphics and by the preexisting Çekirge fault zone. In between, the border had to cut obliquely through the metamorphics and through the hypothetical Karakaya zone.

The NAFZ to the east of the area covered by the MARMARA project is supposed by most of the authors to follow approximately the Intrapontide suture (e.g. Barka 1992). But what about the region west of Kuzuluk, where the NAFZ splits into two zones? Figures 8 and 9 show that between Kuzuluk and the Gebze – Gemlik line, the Eocene flysch basins south and north of the high zone with İznik metamorphics are of primordial importance. More to the west, the *northern zone* soon reaches the border of the rotated zone already activated in the Middle Miocene. The *southern zone* splits near İznik lake, the main branch following roughly the southern border of İznik metamorphics. A northern divergation obliquely cuts this zone. The only branch with a possible influence of the Triassic Karakaya zone runs more in the south through the region of Yenişehir. After cutting the border of the rotated block, the faults of the southern zone reach less labile areas. The propagation of the dextral movements there is more difficult, so the displacements westward become weaker and weaker. Steep standing, dextral faults running ENE-WSW may suggest that the southern zone of the NAFZ reaches the Aegean sea all the same. This cannot completely be excluded at a small scale, but detailed studies in the Ezine research area show that these faults already existed more than 10m.y. before the NAFZ reached the Biga peninsula (Chapter *NAFZ: First period of activity*).

As a *conclusion* it can be stated that neotectonic disturbances very often follow pre-existing faults or zones of weakness, such as the İznik metamorphics zone and its borders. If the pathway taken by the active tectonic zones is considered, paleotectonics have a predominant influence. The function of the pre-existing structures, however, mostly changed completely since the Lower Miocene, but even during the neotectonic history cannot be estimated to be stable. If we consider NW Turkey south of the northern border of the NAFZ, this large area is therefore highly labile from the geological point of view.

References

Akartuna, M., 1968, Armutlu yarımadasının jeolojisi, İstanbul Univ. Fen. Fak. Monogr., 20, 105p.

Ardel, A., 1961, Formation et Évolution de la mer Marmara pendant le Quaternaire, Rev. Geographic Inst. Univ. İstanbul, Nr. 7, 3-18.

Barka, A., 1992, The North Anatolian fault zone, Ann. Tectonicae, Special Issue, Suppl. to Vol. VI, 164-195.

Bingöl, E., Akyürek, B. and Korkmazer, B., 1973, Geology of the Biga Peninsula and some characteristics of the Karakaya Formation, Proc. Congr. Earth Sciences, Ankara, 70-76.

Bingöl, E., Delaloye, M. and Atama, G., 1982, Granitic intrusions in western Anatolia: A contribution to the geodynamic study of this area, Eclogae geol. Helv., Vol. 75/2, 437-446.

Borsi, S., Ferrara, G., Innocenti, F. and Mazzuoli, R., 1972, Geochronology and petrology of recent volcanics in the eastern Aegean sea (West Anatolia and Lesvos Island), Bull. volcanologique, 36, No. 1, 473-496.

Brinkmann, R., 1971, Jungpaläozoikum und Älteres Mesozoikum in Nordwest-Anatolien, Bull. of the mineral research and exploration Inst. of Turkey, foreign edition, 76, 55-67.

Brinkmann, R., 1976, Geology of Turkey, Ferdinand Enke Verlag, Stuttgart.

Bürküt, Y., 1966, Kuzebat, Anadoluda yerelan plütonların mukayeseli yenetik etüdü, Publ. Mining Eng. Fac. Tech. Univ. İstanbul.

Coğullu, E., 1967, Etude pétrographique de la région de Mihaliçik (Turquie), Bull. Suisse Min. Petr. 47. 683-824.

Crampin, S. and Evans, R., 1986, Neotectonics of the Marmara sea region of Turkey, Journal of the Geol. Soc. London, Vol. 143, 343-348.

Demirtaşli, E., 1989, Stratigraphic correlation forms of Turkey, Rend. Soc. geol. Italia, 12, 183-211.

Eisenlohr, Th., 1995, Die Thermalwässer der Armutlu-Halbinsel (NW-Türkei) und deren Beziehung zu Geologie und aktiver Tektonik, Diss. ETH Zürich, Nr. 11340.

E.L.I. (Ege linit işletmesi), 1993, Unpublished summary of the installations, statistics, Soma, Manisa, 16p.

Engesser, B., 1980, Insectivora und Chiroptera (Mammalia) aus dem Neogen der Türkei, Schweiz. Paläont. Abh., Vol. 102.

Erk, S.,1942, Etude géologique de la région entre Gemlik et Bursa (Turquie), Diss. Univ. Basel.

Fytikas, M., Giulani, O., Innocenti, F., Marinelli, G., Mazzueli, R., 1976, Geochronological data on recent magmatism of the Aegean sea, Tectonophysics 31, 29-34.

Fytikas, M., Innocenti, F., Manetti, P., Mazzuoli, R., Peccerillo, A. and Villari, L., 1984, Tertiary to Quaternary evolution of volcanism in the Aegean region, in: The Geological Evolution of Eastern Mediterranean, edited by: J.E. Dixon and A. Robertson, Geol. Soc., Blackwell Scientific Publ., 687-699.

Genç, S. and Yılmaz, Y., 1995, Evolution of the Triassic continental margin, Northwest Anatolia, Tectonophysics, 243, 193-207.

Göney, M., 1964, Some Pleistocene old shore lines in the vicinity of Karamürsel, Rev. Geographic Inst. Univ. İstanbul, Nr. 9-10, 153-160.

Görür, N. and Okay, A., 1996, A fore arc origin for the Thrace basin, NW-Turkey, Geol. Rundschau, 85, 662-668.

Greber, E., 1992, Das Geothermalfeld von Kuzuluk/Adapazarı (NW-Türkei), Geologie, aktive Tektonik, Hydrogeologie, Hydrochemie, Gase und Isotope, Diss ETH Zürich, Nr. 9984.

Imbach, Th., 1992, Thermalwässer von Bursa, geologische und hydrogeologische Untersuchungen am Berg Uludağ (NW-Türkei), Diss. ETH Zürich, Nr. 9988.

Işseven, T., Tapırdamaz, C., Özcep, F., Hisarlı, M. Orbay, N. and Sanver, M., 1995, Tectonics of Northwest Anatolia and Paleomagnetic Results, Jeofizik 9, 10, 201-212.

Jackson, J. and McKenzie, D., 1988, The relationship between plate motions and seismic moment tensors, and the rates deformation in the Mediterranean and Middle East, Geophys. Journal, 93. 45-73.

Jakobshagen, V. (ed.), 1986, Geologie von Griechenland, Beiträge zur regionalen Geologie der Erde, Bd. 19, Gebrüder Bornträger, Stuttgart.

Jeckelmann, Ch., 1996, Genese lokaler Thermalwasservorkommen in der Region Bergama/W-Türkei, Diss. ETH Zürich Nr. 11990.

Kahler, F. and G, 1977, Fusuliniden aus dem Karbon und Perm von Westanatolien und dem Iran, Mitt. Öster. Geol. Ges., 70, 187-269.

Kaya, O. and Kozur, H., 1987, A new and different jurassic to early creataceous sedimentary assemblage in Northwestern Turkey (Gemlik, Bursa): Implications for the pre-jurassic to early cretaceous tectonic evolution, Bull. of Earth Sc., Application and Research Center of Hacetepe Univ. 14, 253-268.

Ketin, I., 1947, Uludağ masifinin tektonigi hakkinda, Bull. Geol. Soc. of Turkey, 1, 61-88.

Kissel, C., Lay, C., Mazaud, A., Poisson, A., Savaşcin, Y., Simeakis, K., Fraissinet, C. and Mercier, J.L., 1989, Paleomagnetic study of the neogene formations of the Aegean area, in: Tectonic evolution of the Tethyan region, edited by: A.M.C. Şengör, NATO ASI series, Mathem. and Phys. Sc., Vol. 259, 159-189.

Kondopoulos, D., Atzemoglou, A. and Pavlides, S., 1996, Paleomagnetism as a tool for testing geodynamic models in the North Aegean: convergences, controversies and a further hypothesis, in: Paleomagnetism and Tectonics of the Mediterranean Region, edited by: A. Morris and D. Tarlin, Geol. Soc. Special Publications, No. 105, 277-288.

Kopp, K.O., 1964, Geologie Thrakiens II: Die Inseln und der Chersones, Neue Jahrbücher Geol. Paläont. Abh. 119/2, 172-214.

Kopp, K.O., Pavoni, N. und Schindler, C., 1969, Geologie Thrakien IV: Das Ergene Becken, Beihefte zum Geol. Jahrbuch Heft 76, Bundesanst. Bodenforschung u. Geol. Landesämter BRD, Hannover.

Kraft, J. Kayan, I. Erol, O., 1980, Geomorphic reconstructions in the environs of ancient Troy. Science 209, 776-782

Pavoni, N., 1961, Die nordanatolische Horizontalverschiebung, Geologische Rundschau, Bd. 51, 122-139.

Le Pichon, X. and Angelier, J., 1981, The Aegean Sea, Phil. Trans. R. Soc. London, A 300, 357-372.

McKenzie, D., 1972, Active Tectonics of the Mediterranean Region, Geophys. J. Royal Astron. Soc. 30, 109-185.

Mercier, J., Sorel, D. and Simeakis, K., 1987, Changes in the state of stress in the overriding plate of a subduction zone: the Aegean Arc from the Pliocene to the Present, Annales Tectonicae, Vol. 1, Nr. 1, 20-39.

Mercier, J., Sorel, D., Vergely, P. and Simeakis, K., 1989, Extensional tectonic regimes in the Aegean basins during the Cenozoic, Basin Research 2, 49-71.

Michel, G., Waldhör, M. Neugebauer, J. and Appel, E., 1995, Sequential rotation of stretching axes, and block rotations: a structural and paleomagnetic study along the North Anatolian Fault, Tectonophysics, 243, 97-118.

Mützenberg, St., 1991, Westliche Biga Halbinsel (Çanakkale, Türkei): Beziehung zwischen Geologie, Tektonik und Entwicklung der Thermalquellen, Mitt. Geol. Inst. ETH und Univ. Zürich, N.F., Nr 287.

Perinçek, D., 1991, Possible strand of the North Anatolian Fault in the Thrace Basin, Turkey – An Interpretation, Am. Ass. Petrol. Geol. Bull., V. 75, No 2, 241-257.

Pfannenstiel, M., 1944, Die diluvialen Entwicklungsstadien und die Urgeschichte von Dardanellen, Marmarameer und Bosporus, Geol. Rundschau, Bd XXXIV, Heft 7/8.

Philippson, A., 1918, Handbuch der regionalen Geologie, Carl Winters, Universitätsbuchhandlung, Heidelberg.

Platzman, E.S., Platt, J.P., Tapırdamaz, C., Sanver, M. and Rundle, C., 1994, Why are there no clockwise rotations along the North Anatolian Fault zone?, Journal Geophys. Res., Vol. 99, B11, 21705-21715.

Reilinger, R. and Barka, A., 1996, GPS constraints on fault slip rates in the Arabia-Africa-Eurasia Plate Collision Zone: Implications for Earthquake Recurrence Times.

Sarıbudak, M., Sanver, M., Şengör, A.M.C. and Görür, N., 1990, Paleomagnetic evidence for substancial rotation of the Almacık flake within the North Anatolian Fault zone, NW-Turkey, Geophys. J. Int., 102, 563-569.

Schindler, C., 1959, Die Störungszone von Gölçük (Türkisch-Thracien) und ihr Einfluss auf die Sedimentation des Alttertiärs, Eclog. geol. Helv. 52, 695-707.

Schindler, C., 1963, Zum geologischen Bau der europäischen Türkei, Bull. Ver. Schweiz. Petrol. Geol. und Ing. 29, 29-42.

Şengör, A.M.C., 1979, The North Anatolian transform fault: its age, offset and tectonic significance, J. geol. Soc. London, 136, 269-282.

Şengör, A.M.C. and Yılmaz, Y., 1981, Tethyan evolution of Turkey: a plate tectonic approach, Tectonophysics, 75, 181-241.

Şengör, A.M.C., Görur, N. and Saroğlu, F., 1985, Strike-slip faulting and related basin formation in zones of tectonic escape: Turkey as a case study. Soc. of Economic Paleont. and Miner., spec. ed., 227-264.

Seymen, I., 1975, Tectonic characteristics of the North Anatolian Fault zone in the Kelkit valley, PhD Thesis, İstanbul Tech. Univ.

Sümengen, M. ve diğ., 1987, Gelibolu yarımadası ve Güneybatı Trakya Tersiyer Havzası' nın stratigrafisi, sedimentolojisi ve tektoniği, MTA rap., No 8128.

Tapırdamaz, C. and Yaltırak, C., 1996, Results of Paleomagnetic study on young Volcanics in Thrace, Jeofizik, 9,10, 213-218.

Tatar, V., Ponat, E. and Işıkara, M., 1995, Paleomagnetism of volcanic rocks in the Armutlu Peninsula and Almacık Mountain, Jeofizik, 9,10, 219-228.

Ternek, Z., 1949, Geological study of the region of Keşan, Koru Dağ, Diss. Univ. İstanbul.

Westaway, R., 1994, Present day kinematics of the Middle East and eastern Mediterranean, Journal of Geophys. Res., Vol. 99, No. B6, 12071-12090.

Westphal, M. and Kondopoulou, D., 1993, Paleomagnetism of Miocene volcanics from Lemnos island (Northern Aegean): implications for block rotation in the vicinity of the North Aegean Trough, Annales Tectonicae, Vol. VII/2, 142-149.

Wong, H.K., Lüdmann, T., Ulug, A. and Görür, N., 1995, The sea of Marmara: a plate boundary sea in an escape tectonic regime, Tectonophysics 244, 231-250.

Yaltırak, C., 1995, Tectonic Mechanism controling the Plio-Quaternary sedimentation in the Gelibolu Peninsula, Jeofizik, 9,10, 103-106.

Yılmaz, Y., Genç, Ş., Yiğitbaş, E., Bozcu, M. and Yılmaz, K., 1995, Geological evolution of the late Mesozoic continental margin of Northwestern Anatolia, Tectonophysics 243, 155-171.

Maps

MTA, 1964, Geological map of Turkey 1:500,000, sheets İstanbul, Zonguldak, İzmir and Ankara

MTA, 1989, Geological map of Turkey 1:2,000,000

Institute of Geology and Mineral Exploration, Athens, 1983: Geological map of Greece 1:500,000

Mechanisms and processes of groundwater circulation in tectonically active areas

WERNER BALDERER

Abstract

From the results of the individual study areas as presented in Eisenlohr, Greber, Imbach, Mützenberg, Yalçin (all this volume) Jeckelmann (1996), a comprehensive overview of the characteristic hydrogeological features of the investigated areas is aimed by the present study with conclusions on groundwater circulation, flow paths and indication of deep processes, as derived from the applied methods of chemical and isotopic characterisation.

As indicated by the chemical constituents and isotopic composition of the investigated groundwaters, deep and long regional flow systems exist, but which also have interrelationships with local and intermediate flow systems. That indicates now deep flow systems which are interconnected locally by tectonic short cuts as resulting from deep faulting with open fractures (due to the observed extensional regime) with more shallow circulating groundwater of intermediate and local flow systems.

According to the chemical constituents and isotopic signatures of the investigated thermal and mineral waters the possibility exists to identify water bodies of different origin:

- groundwater of origin by infiltration in the surrounding areas of the thermal springs at higher altitudes (e.g. Uludağ, Kozak massif) with residence times in the range of the ^{14}C method of thousands to a few 10,000 years.
- brine of sedimentary origin derived from marine transgression periods invading temporarily coastal areas at low altitudes (depression zones). Such brines are in secular equilibrium for ^{36}Cl underground production, what means a residence time in the actual position within the rock of the actual flow system of at least / or more than 1.5 million years, respectively.
- brine yielding low $^{36}Cl/Cl$ ratios (of origin of evaporitic salt or remaining sea water of marine sediments) which is actively moving from sea shore areas into the continental basement. Such brines as flowing out at the Tuzla and Kestanbol thermal springs yield $^{36}Cl/Cl$ ratios which are not in secular equilibrium of underground production with the rock of the actual flow systems what infers residence times of less than 1.5 million years.
- deep groundwater of infiltration within the recharge areas in periods of changed climatic conditions.

Driving forces for the mobilised brines occurring in thermal waters are changes in the tectonic stress, eventually also other effects as change of hydraulic reference datum by sea level changes, gases, and pressurised deep fluids in more compressional zones (Kuzuluk, Gönen).

Observations on the influence of the tectonic activity and seismicity on the temperature, flow (hydraulic pressure head) and quality (as its chemical and isotopic composition) of the investigated thermal and mineral waters are reported for strong earthquakes for all investigated areas except the Gönen area.

Periodical and continuous monitoring of such kind of influences on thermal and mineral waters within the investigation period of the MARMARA project indicate that strong influences with respect to chemical composition (electrical conductivity) are observed as response to strong precipitation / storm events which lead to a sudden increase in hydraulic head within the recharge area causing a pressure pulse in the deeper part of the thermal water aquifer and the outflow (mobilisation) of deep seated higher mineralised thermal water. Such a rise is reported for the Bursa area by Imbach (this volume) with respect to electrical conductivity and for the Bergama area (with respect to the Na- and K- contents) by Jeckelmann (1996).

The same influence of recharge events on the hydraulic head results from water level measurements in the Bursa/Çekirge area on a confined thermal water aquifer connected to a shallow groundwater aquifer above (Greber et al. this volume).

From continuous recording of the pressure head of two artesian wells of the thermal water in the Kuzuluk area result a strong dependence on the CO_2 overpressure and the mechanical behaviour of the cap rock as confining cover of the thermal aquifer (Tschudi this volume).

From these observations result the conclusions, that an interdependence to external events exist, but that earthquakes as very rare events within other natural perturbations are only clearly detected for strong seismic events occurring within a relative close area with respect to the spring outflows or boreholes.

Tectonic situation and geological units: main hydrogeological properties of the investigated areas

Kuzuluk area

About 40 thermal and mineral waters arise in springs within the subsidence basin of the Kuzuluk area (Greber 1992, 1994, this volume). The main rock composition in this area consist of: andesites, micaschists, limestones and partly silicified fluvial deposits. The Kuzuluk basin is according to Greber (this volume) an extensional structure, separated by faults from the mountains in the north, east and south.

Bursa area

In this area (Imbach 1992, this volume), thermal springs arise within two locations near Kükürtlü/Bursa and Çekirge at the northern slope of the Uludağ massif (peak altitude of about 2500m) just above the valley plain (elevation 150m-200m). The Uludağ massif boarders the plain through an E-W striking fault zone, which is related to the North Anatolian Fault Zone (NAFZ). It is the southern border of a graben zone, which extends in an E-W direction from Bursa to the Ulubat lake – Manyas lake – up to the Gönen geothermal area.

Yalova/Armutlu/Gemlik area

The three main centres with thermal water discharges at Yalova, Armutlu and Gemlik kaplıca (Turkish meaning spa) occur at fault zones. The main faults related to these thermal springs are of N-S direction in the Yalova and Armutlu spas and of E-W direction in the Gemlik kaplıca area. The Armutlu peninsula mainly consists of metamorphic rocks. The main units are metamorphic gneisses, amphibolites, greenschists and marbles overlain by low grade metamorphic flysch units (Eisenlohr 1995, this volume).

Gönen/Yenice area

In the Gönen area, the largest medium to low temperature geothermal exploitation plant in Turkey exists (Yalçın this volume). This area is situated at the western part of the E-W striking graben structure extending up to Bursa. In this area, strong earthquakes occurred in 1953 (M=7.4) and 1969 (M=5.8). The geological features of this area are characterised by metabasic rocks and metamorphic volcanic sedimentary series, as well as thick neogene sedimentary deposits within the graben structures. According to current knowledge, the underlying bedrock is formed by metamorphic rocks supposed to be linked to the outcropping rocks in the Kazdağ massif (Yalçın this volume). Hot springs also occur from the southern area of Eksidere (Topaklar) to Yenice (Hıdırlar). These springs occur directly from volcanic rocks (mainly andesites) related to the existence of local fault systems (Yalçın this volume). For further comparison with respect to origin and evolution, the Manyas hot spring near the Manyas lake southeast of Gönen was also investigated.

Bergama/Kozak area

In the southern part, this area is dominated by the large plain of Bergama which is also characterised by the sedimentary filling of the NE-SW striking graben system limited by fault zones. At its eastern end near Turanlı, a possibly older, NNE-SSW striking, graben is morphologically well accentuated (Jeckelmann 1996). In this area, signs of several periods of volcanic and tectonic activities are visible as dykes, young lava flows and basaltic cones. At the northwestern part, this area is characterised by the granitic intrusion of the Kozak massif (Jeckelmann 1996). The investigated hot springs of 11 localities are situated within the Bakırçay-Bergama plain and the Kozak area: Kaynarca (as a geyser boiling hot spring), Nebiler İlıca (İlıca meaning spa) and the thermal spas of Paşa and of Kozak.

Kestanbol/Tuzla area

This area is located in the northwestern part of Anatolia along the western coast of the Biga peninsula. Here, two main centres with thermal water discharges named Kestanbol kaplıca (kaplıca meaning spa) and Tuzla occur. The thermal springs appear at an intrusive body of quartz-monzonite type in Kestanbol, or within a 600m thick volcanic sequence of calcaline volcanic and ignimbrites in the Tuzla area (Mützenberg 1991, this volume).

Information on fluids and gases: origin, interaction, residence time scale

Chemical composition of fluids

In the investigated areas of the MARMARA Poly-Project, the following main chemical compositions of mineral and thermal waters as represented in Table 1 were reported. These chemical compositions of the observed mineral and thermal waters are related to the following processes:

Dissolution of rock minerals (as a process of low temperature water-rock interaction) in contact with evaporitic minerals and mainly carbonate containing rocks, such as limestones and dolomites, which is a main process of the waters of the Gemlik/Orhangazi and Bursa-Çekirge areas. A special situation is presented by the very highly mineralised cold spring water of Adliye köyu (53g/l of TDS) originating in a small creek south of Gemlik. According to its isotopic composition (Eisenlohr 1995), this water is of meteoric origin (tritium content of 4.1±0.7TU) with shallow circulation and has acquired its mineralisation by water-rock interaction by the dissolution of gypsum and some salt contained within the observable evaporitic sequences of this area.

Hydrolysis of silicate minerals in crystalline rocks: This process is most probably involved in the thermal waters of Bursa, Yalova, Armutlu, Gönen and Bergama-Kozak.

Ion exchange: mainly Ca against Na in contact with clay minerals.

Redox processes: the dissolution and oxidation of sulfide minerals with the formation of sulphate (Yalova, Armutlu, Bergama, Kozak) was especially observed.

Additional interaction with CO2: supposed to occur at the Kuzuluk waters (in addition to low temperature water-rock interaction processes).

Mixing of waters with different origins: Kestanbol, Tuzla, Bademli (formation water / sea water).

Location	Chemical water type	Water temp (°C)	TDS (mg/l)	Main rock composition along flow path
Kuzuluk	Na-(Ca)-(Mg)-HCO_3-Cl	19.4-55 82 (borehole)	3000-7000	carbonates, volcanites, micaschists
Bursa	Na-Ca-HCO_3-SO_4	35-82	500-1220	gneis, schists, marble, granite
Yalova	Na-Ca-SO_4-(Cl)	60-75	1300	volcanic rocks (andesites) metamorphics
Armutlu	Na-Ca-SO_4-HCO_3-Cl	60-75	2000	epidot-chlorite schists metamorphics
Gemlik	Ca-Mg-(Na)-HCO_3-(Cl)	22-37	350	marble (limestone)
Gönen thermal	Na-Ca- SO_4-(Cl)-(HCO_3)	70-78	1700	gneis, amphibolite, marble volcanites
Topaklar	Na-Ca- SO_4-(Cl)-(HCO_3)	69	1011	gneis, amphibolite, marble volcanites
Hidirlar	Na-Ca- SO_4-(Cl)-(HCO_3)	40-81	719	gneis, amphibolite, marble volcanites
Eksidere	Ca-Mg-Na-HCO_3-(Cl)	28-39	346-363	limestones
Bergama	Na-Ca-HCO_3-SO_4-(Cl)	35	1509	granites, volcanites, alluvium
Kozak	Na-Ca-HCO_3-SO_4-(Cl)	52	873	crystalline (granite)
Bademli	Na-Cl	37-41	9500-11000	volcanite, metamorphics
Kestanbol	Na-Cl	70-76	22000	quarz-monzonite
Tuzla	Na-Cl	46-96	62375	volcanites, metamorphics, limestones

Table 1: Main chemical compositions of mineral and thermal waters of the MARMARA project.

Dissolved Gases

The contents of dissolved gases (as contained in outflowing water and captured by evacuated glass bottles filled with the water), the contained dissolved gases and also the gas bubbles without air contamination were analysed from samples of the investigated areas of Kuzuluk, Bursa, Yalova/Armutlu/Gemlik, Gönen and Bergama/Kozak. For the Kestanbol and Tuzla waters, no sampling for dissolved gases was possible because of the very high temperature of the water and the low gas contents of these highly mineralised hot brines.

The total gas contents and composition with respect to the main components (N_2, O_2, CO_2, H_2S, Ar and CH_4) of all investigated groundwaters, main mineral and thermal waters are presented in Fig. 1 in terms of absolute volumetric concentration (cm^3/kg). Figure 2 shows selected samples in terms of relative volumetric proportions of the total gas content (vol%) in the distribution of the investigated areas (for the exact description of the individual samples, see the respective contributions of Eisenlohr, Greber, Imbach, Jeckelmann, Mützenberg and Yalçın).

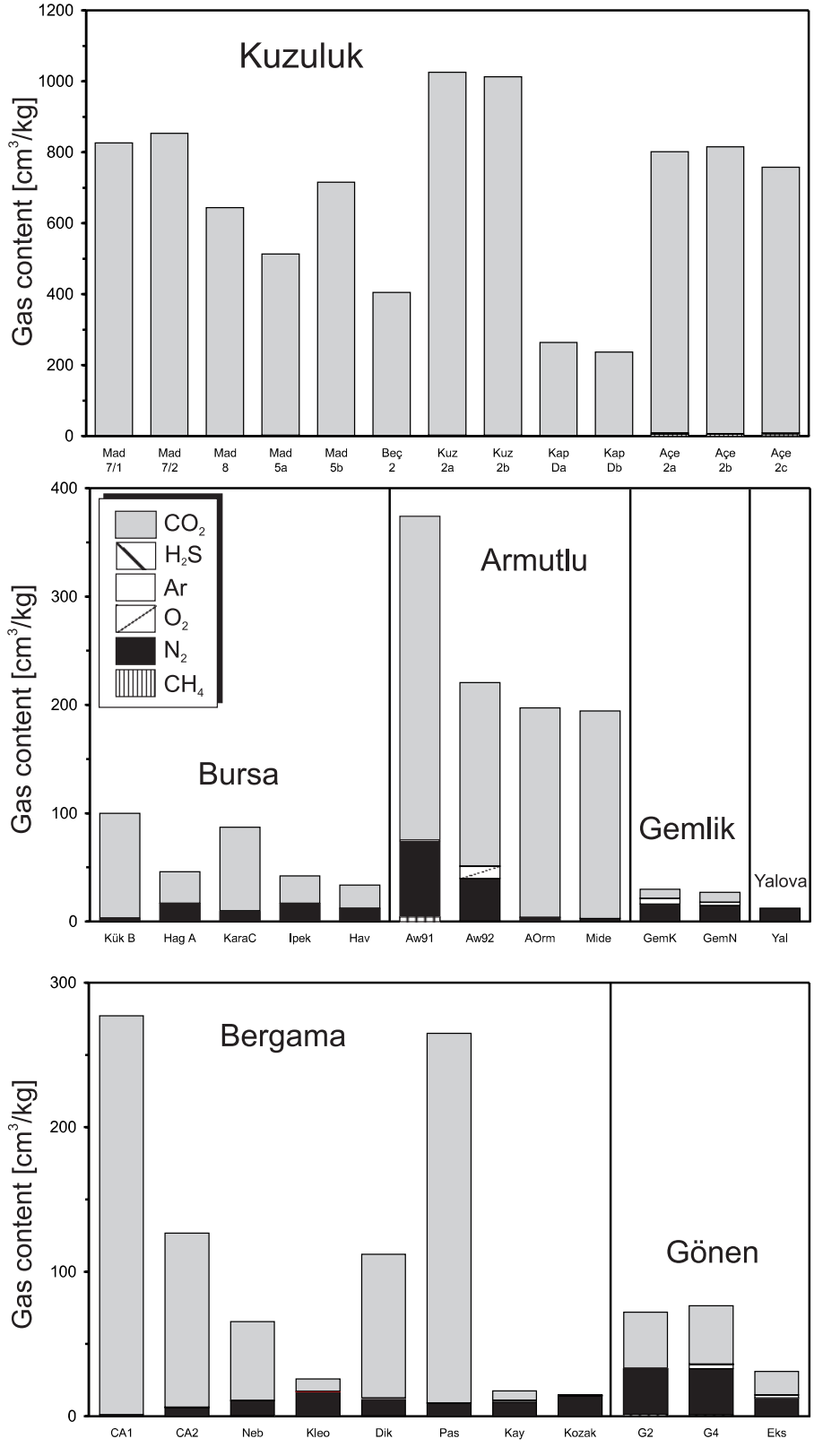


Figure 1: *Total gas contents (in terms of absolute volumetric concentration) and composition of the main components (N_2, O_2, CO_2, H_2S, Ar and CH_4) of the mineral and thermal waters of the investigated areas of the MARMARA project.*

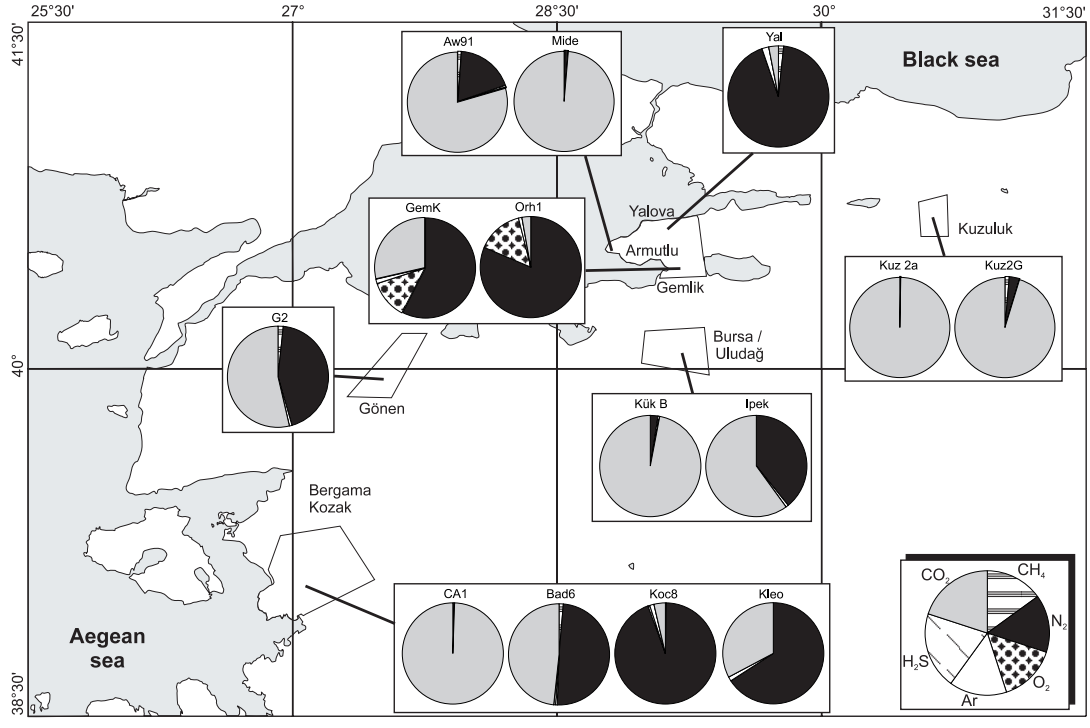


Figure 2: *Gas contents of thermal and mineral waters of the investigated areas of the MARMARA project (in terms of relative volumetric proportions of the total gas content [vol%]).*

From these diagrams in Figs. 1 and 2 it follows that gaseous CO_2 is the abundant component in most of the investigated thermal and mineral waters. Exceptions are the karstic thermal waters of Gemlik kaplıca (GemK), Gemlik north (GemN), the water of the springs of Orhangazi İlıpınar (Orh1) and also Keramet İlıca (not represented in Figs. 1 and 2), which contain a strong atmospheric component similar to the composition of air (Eisenlohr 1995). As a contamination of air during sampling can be excluded, the explanation is that all of these springs are outflows of karstic systems, where atmospheric air is entrapped during the recharge process in karstic channels. The same explanation can also be applied concerning the nitrogen content of the thermal waters of Bursa/Çekirge (Ipek and Hav). Some atmospheric influences may also be expected for the lower temperature water of Hagia Fontini A (Hag A).

The Kükürtlü sample (Kük B), with a temperature of 81°C, is the most representative of the hot thermal water of the Bursa Kükürtlü area. Its gas content of about 100cm^3/kg mainly consists of CO_2. For the other Kükürtlü sample of Karamustafa (KaraC) originating from a well which is fed by a fracture directly from the travertine rock (Imbach 1992), the higher N_2 content is also explained by some admixture of air. The low amount of gas in the Yalova water (Yal), which mainly consists of nitrogen without any oxygen, indicates that no contact with deep CO_2 exists and the dissolved gases are approximately in the amount which originates from the infiltration at the recharge area, which is also in agreement with the low carbonate water. The existence of small amounts of H_2S and CH_4 are indications of a reducing environment. For the analysed thermal waters of the Bergama area, only the samples of Kaynarca (Kay) and Kozak (Koc8) contain small amounts of oxygen, which can be explained by difficult sampling conditions. The varying amount of atmospheric gases in the thermal waters of this area are explained by recharge and circulation of these waters mainly in fractured crystalline rocks, according to the developed conceptual hydrogeological model (Jeckelmann 1996). Also for the thermal waters of the Gönen/Eksidere area, a circulation within fractured and also

partly through porous rocks, is indicated by the presence of atmospheric components. If now the total amount of gases are also considered (Fig. 1 and Fig. 3), it reveals that high volumes of gases in the waters above the limits of atmospheric saturation mainly consist of CO_2. The limits of atmospheric saturation at temperatures between 10 and 0°C and normal pressure conditions (STP) are between 23 and 30cm^3/kg or 35 and 47cm^3/kg in equilibrium with atmospheric CO_2 or with soil CO_2 respectively. This strong dependence results in a straight correlation as seen in Fig. 3, with a slope of almost 1:1. This observation now indicates that this amount of CO_2 above the limits of atmospheric concentration and possible biologic activity in the soil can only be derived by deep origin. Therefore, high CO_2 and total gas contents indicate admixture of CO_2 of deep sources along active (open) fault and fracture zones (Barnes et al. 1978). As demonstrated by the highest amounts of CO_2 observed within the Kuzuluk basin of up to about 1000cm^3/kg (STP), the most favourable hydrogeological situation is achieved within a deep aquifer pressurised by an almost impermeable cap-rock at the top leading to high artesian pressures.

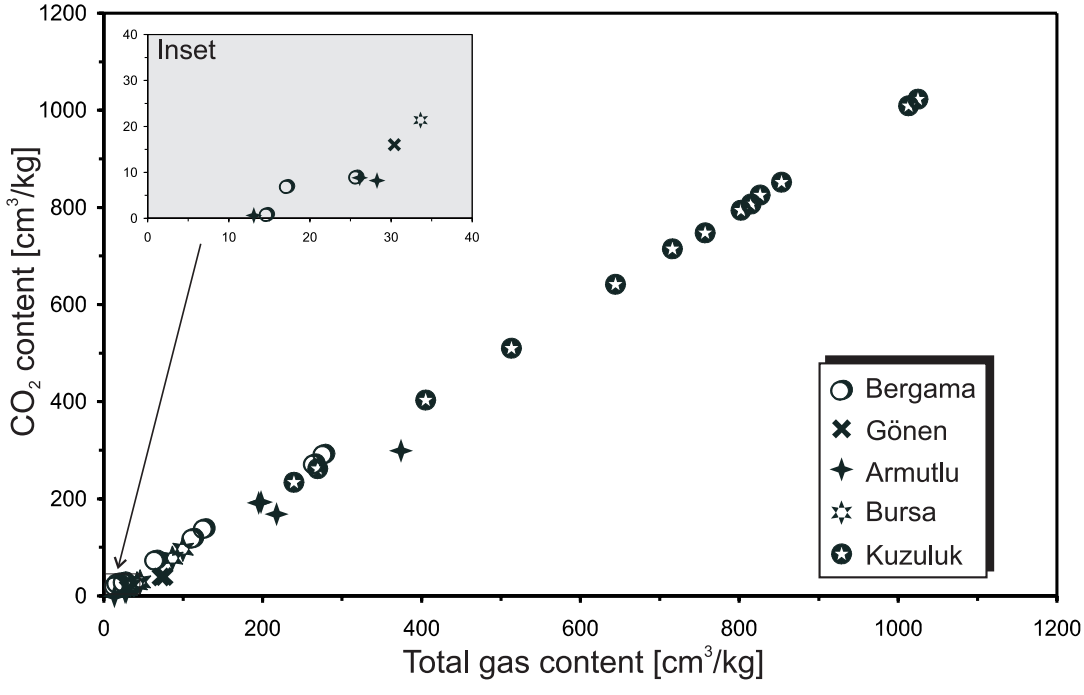


Figure 3: *CO_2 and total gas contents of the thermal- and mineral waters of the investigated areas of the MARMARA project.*

Isotopic composition: Stable isotopes δ^2H and $\delta^{18}O$ of cold groundwaters

The composition of waters with respect to the stable isotopes of deuterium and oxygen-18 is related to the conditions of recharge (infiltration, origin of air masses, isotopic composition of precipitation) and other physical processes occurring at shallow depth, such as evaporation and mixing.

The conditions of recharge of the shallow circulating, cold groundwaters are discussed in Mützenberg (1991), Greber (1992), Imbach (1992), Eisenlohr (1995), Jeckelmann (1996) and Yalçın (1997). From the existing data, various trends attributed to the continental effect (dependence of the stable isotope contents on the geographical position of the investigated

areas with respect to the Aegean, Marmara and Black seas) and the altitude effect (dependence of the stable isotope contents on the altitude of the areas of recharge of the investigated waters) can be noticed as presented in the δ^2H versus $\delta^{18}O$ plot of Fig. 1 in Eisenlohr et al. (this volume). According to the recent climatic conditions as revealed by the investigated shallow cold groundwaters and precipitation waters, a distinct meteoric water line with the equation: $\delta^2H = 8 * \delta^{18}O + 15$ (named Marmara MWL) characteristic for the recent infiltration conditions of the MARMARA project areas has been defined. This line is in Fig. 5 and in Fig. 1 of Eisenlohr et al. (this volume) situated between the Eastern Mediterranean and the Global Meteoric Water Line (GMWL). However, for each individual investigated area it is necessary to establish the locally prevailing conditions of recent recharge, as related to the local climatic and topographic conditions. Local linear relationships between the altitude of emergence of cold water springs (with restricted recharge area) and the values of δ^2H have been established for the areas of Bursa (Imbach this volume), the Armutlu peninsula (Eisenlohr 1995) and the Bergama area (Jeckelmann 1996) resulting in the following gradients:

Bursa (Kükürtlü and Çekirge):$\delta^2H / \Delta h = 0.64‰$ /100m (altitude range 1800m)

Yalova/Armutlu: $\delta^2H / \Delta h = 1.94‰$ /100m (altitude range 800m)

Gemlik/Orhangazi:$\delta^2H / \Delta h = 0.78‰$ /100m (altitude range 900m)

Bergama/Kozak:$\delta^2H / \Delta h = 1.27‰$ /100m (altitude range 1100m)

These established relationships now allow the deduction of the altitudes of infiltration of deep groundwaters within the corresponding investigated areas if it is admitted that their deuterium content is not influenced by secondary processes. If the deduced ranges of altitudes are in agreement with the current topography and hydrogeological situation of potential recharge areas, an infiltration under current climatic conditions is possible. But for the other areas of Kuzuluk, Gönen/Yenice and Tuzla/Kestanbol, nearly no relationship between altitude and deuterium content of the cold water spring exists. This indicates special climatic conditions with respect to the origin of air masses (humidity) and wind regime.

From the data reported in Greber (1992), Mützenberg (1991) and Yalçın (1997), the following total ranges of variation of the deuterium content within the altitude range of the sampled cold, freshwater springs result:

Kuzuluk: altitude range: 210m to 1330m, variation of $\delta^2H = 3.0‰$, (0.27‰/100m)

Gönen/Kazdağ: altitude range: 200m to 1700m, variation of $\delta^2H = 1.5‰$, (0.10‰/100m)

For these two areas, the scatter of the individual samples is of the same amount as the variation due to altitude, as shown in Fig. 4. The absence of the usually observed so-called altitude effect in isotope hydrological studies can be explained by the climatic and morphological situation of the areas. In the Gönen area, the humidity is produced most frequently from winds from a westward direction as a bulk mass to the whole area with very flat morphology. Therefore, the humid air masses are not affected much by the stepwise Rayleigh-kind fractionation process before merging at nearly the same time in the Kazdağ massif and also in the investigated area of Gönen/Eksidere and Yenice. As the stable isotope contents of the cold recent groundwaters now indicate a more or less uniform distribution over the whole investigated area, no further definition of recharge areas as a function of altitude is possible. That means that only a statement with respect to the range of δ^2H and $\delta^{18}O$ according to actual recent climatic conditions of the investigated area is possible.

For the Tuzla/Kestanbol area situated on the Biga peninsula near the shore of the Aegean sea special conditions with respect to the stable isotope contents of the cold lowly mineralised groundwater as sampled at naturally outflowing springs exist: altitude range: 50m to 75m, variation of $\delta^2H = 10.6‰$.

The observed variations of the deuterium content of the cold lowly mineralised waters is much greater than usually observed and more related to the areal distribution of the rain and the distance to the sea shore (continental effect), as the humid air masses in this area originate from the western part of the Mediterranean sea (Mützenberg 1991).

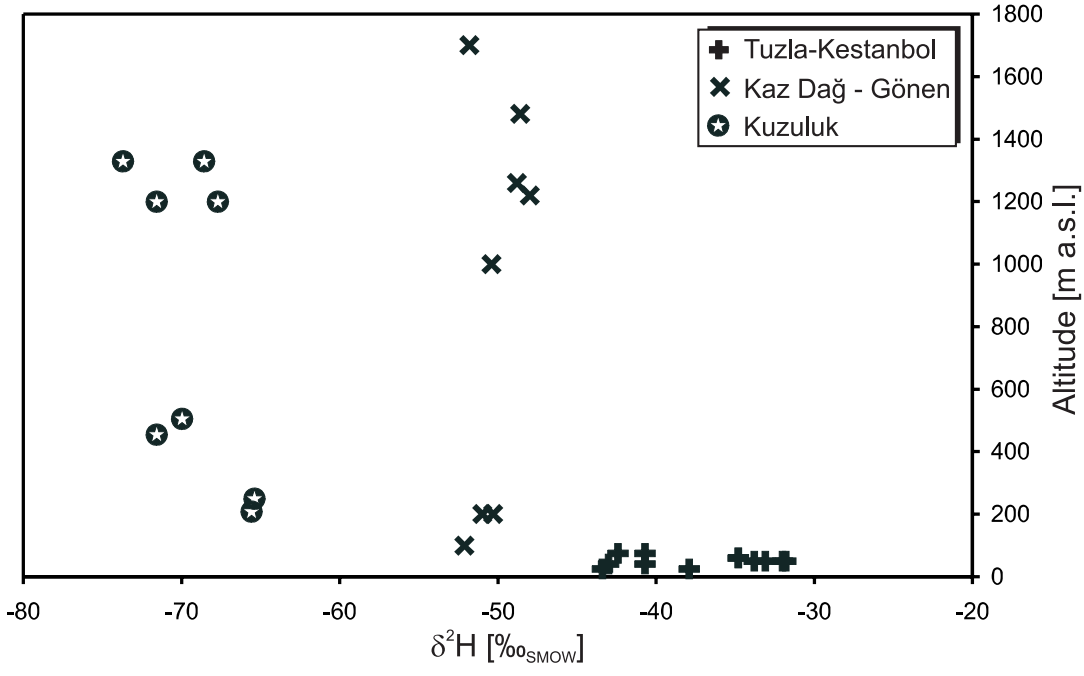


Figure 4: Diagram of the altitude of cold lowly mineralised springs and the corresponding δ^2H – values.

Isotopic composition: Stable isotopes δ^2H and $\delta^{18}O$ of deep circulating mineral and thermal waters

The δ^2H and $\delta^{18}O$ diagram in Fig. 5 summarises the isotope data of the mineral and thermal waters of the investigated geothermal areas of the Marmara project. This δ^2H versus $\delta^{18}O$ plot in Fig. 5 reveals indications with respect to the origin of the groundwater. δ^2H and $\delta^{18}O$ values near the meteoric water line indicate a normal origin by infiltration of meteoric precipitation water.

The position of the δ^2H and $\delta^{18}O$ values along the meteoric water line of a given groundwater depends on the altitude of infiltration but also on the current climatic conditions at the time of recharge. Colder climatic conditions yield lower (more depleted) stable isotope values, whereas higher temperature climatic conditions yield more enriched values of stable isotopes of the corresponding groundwater. For the investigated thermal and mineral waters of the MARMARA project the following observations are made:

Recharge conditions not distinguishable from recent climate conditions and altitude relationship: For the Bursa, Yalova, Armutlu and Gemlik thermal waters no systematic difference with the current shallow groundwaters of recent recharge of the corresponding recharge areas are observed.

R*echarge conditions different from actual climatic conditions:* The Kuzuluk mineral and thermal waters show δ^2H- values which are much more depleted as the groundwaters of recent recharge (even of the highest cold water spring at the Keremali mountain at about 1500m a.s.l.), therefore their formation likely occurred during a period of prevailing colder climatic

conditions (the $\delta^{18}O$- values are influenced by isotope exchange processes due to water-rock-gas interaction). For the water of the Gönen thermal wells G2 and G4, with respect to the stable isotope values of $\delta^{2}H$ and $\delta^{18}O$, all characteristics of a paleowater are fulfilled (as defined by Gat (1983) and A. Issar, pers. comm. 1995):

values much lower than the range of actual recharge (difference in $\delta^{2}H \geq 15‰$ and in $\delta^{18}O \geq 2‰$)

the $\delta^{2}H$ and $\delta^{18}O$ values are situated on the global meteoric waterline ($\delta^{2}H$ excess: d=10) or even on a meteoric water line with lower deuterium excess (in the range between d=10 and d=5, Gat 1983) and not on the Marmara meteoric water line (with d=15).

However, this second argument is rather weak, as oxygen isotope exchange at higher temperatures could have occurred to some extent (Yalçın this volume). For the$\delta^{2}H$ and $\delta^{18}O$ values of the Menteşe thermal waters (Bergama area), a much higher altitude of infiltration (about 1700 to 1800m a.s.l.) compared with the potential recharge areas also results (Jeckelmann 1996). Therefore, an infiltration under recent climatic conditions can nearly be excluded for the Menteşe thermal waters, also as the values show a deuterium excess lower than 10.

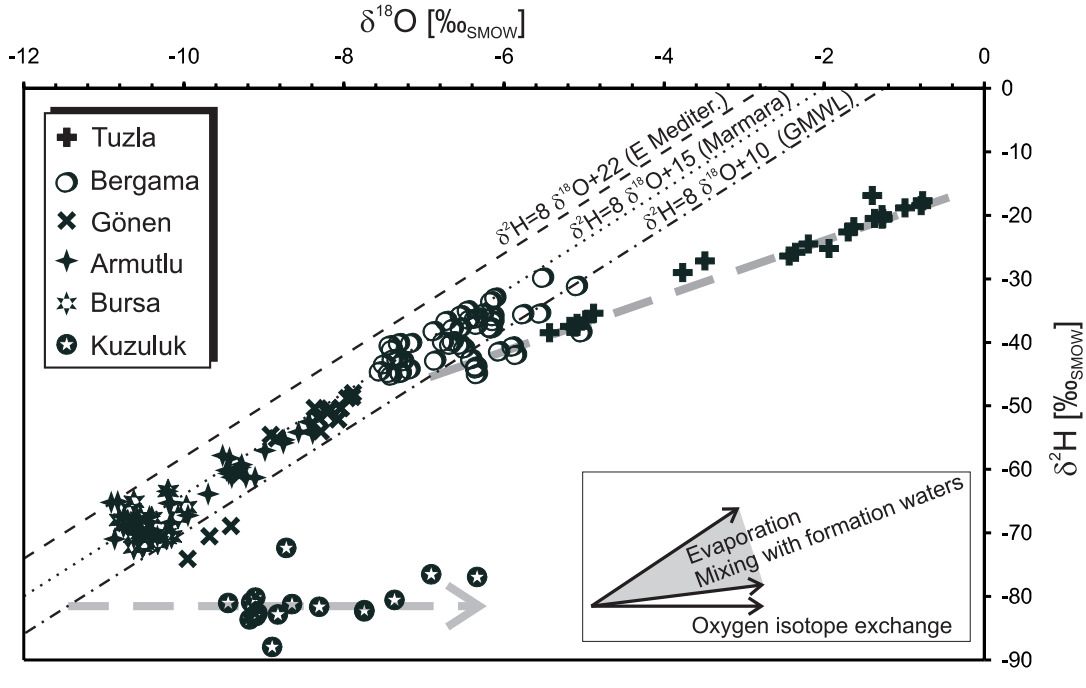


Figure 5: *$\delta^{2}H$ and $\delta^{18}O$ diagram of the values of mineral and thermal waters of the investigated areas of the MARMARA project. Deviation of the range of the meteoric water lines is due to evaporation, mixing with formation water/residual brine and isotope exchange processes.*

The $\delta^{2}H$ and $\delta^{18}O$ values of deep circulating mineral and especially thermal waters of longer residence time frequently reveal effects of additional processes occurring along the flow path in the underground which influence the stable isotopic composition and are visible on the$\delta^{2}H$ versus $\delta^{18}O$ plot as deviations from the above defined meteoric water lines. For the investigated mineral and thermal waters within the MARMARA project the following processes can be distinguished (Fig. 5):

Water-rock interaction at higher temperatures with oxygen isotope exchange between water and minerals: Such an effect is postulated for the Bursa-Kükürtlü thermal waters by Imbach

(1992). But this so-called oxygen shift is rather small for these waters. The same process is evoked for the hot thermal waters of Çamurlu and Kaynarca in the Bergama area in Jeckelmann (1996).

Water-rock-gas interaction with oxygen exchange between water, minerals and especially CO_2 gas at moderate to high temperatures: These two processes are evoked by Greber (1992, 1994) to explain the high amount of oxygen isotope exchange observed at the Kuzuluk mineral and thermal waters.

Influence of mixing of locally infiltrated groundwater with migrating deep brines (related to ancient formation waters): The δ^2H and $\delta^{18}O$ values of the Tuzla/Kestanbol thermal brines and of the Bademli thermal water are situated below the global meteoric water line and align on a straight line with a lower slope which presents a mixing line between local infiltrated fresh groundwater and a saline brine endmember (Mützenberg 1991, this volume, Jeckelmann 1996). This saline brine endmember most probably represents a formation water (Mützenberg 1991, Jeckelmann 1996, Hoeffs 1997). For the lower mineralised hot thermal waters which are situated on the same mixing line also a complex origin is admitted (Jeckelmann 1996).

Isotopic composition: Stable isotopes $\delta^{34}S$ and $\delta^{18}O$ of dissolved sulphates in deep circulating mineral and thermal waters

Stable isotopes $\delta^{34}S$ and $\delta^{18}O$ of dissolved sulphates in groundwaters are related to the origin of the sulphates as evaporites or to processes occurring within the sulphur cycle (Balderer 1985, Balderer et al. 1990, 1991). Based on the stable isotope contents and the sulphate concentration (Fig. 6 and Fig. 7) and also by considering the chemical evolution the following origins and processes are deduced for the investigated waters of the MARMARA project:

Sulphates of sedimentary origin of evaporitic sequences are dissolved by the infiltrating/percolating groundwater. One example of such an origin is the cold mineral water of Adliye köyu at the Armutlu peninsula (Eisenlohr this volume). The stable isotope $\delta^{34}S$ and $\delta^{18}O$ contents of dissolved sulphates in the groundwater reflect, in this case, the isotopic signature of the corresponding evaporitic formation of sedimentary evaporites. This is demonstrated directly for the water of Adliye köyu by the $\delta^{34}S$ and $\delta^{18}O$ contents of a gypsum sample which originated from a quarry in the area of this spring belonging to Oligocene deposits (according to Eisenlohr this volume).

Formation specific origin: The $\delta^{34}S$ and $\delta^{18}O$ contents of the dissolved sulphates in the saline thermal water of Kestanbol (sample K1 in Mützenberg 1991) can be directly related to remnant pore water of tertiary origin, whereas the dissolved sulphates of the Bademli thermal water (Bergama area) are linked whether to fossil pore water of Tertiary origin or even to recent sea water (as sulphates of remaining solution after precipitation of solid sulphates took place).

Origin by dissolution and successive oxidation of mineral sulphides of primary origin (mainly pyrites) within the crystalline rock environment which are oxidised by the local groundwater of meteoric origin to sulphate (Fontes and Michelot 1985, Michelot 1988). Such an origin of the dissolved sulphate is probable for low sulphate thermal and mineral waters in crystalline rocks (Figs. 6 and 7) of Kuzuluk, Bursa, Yalova, Armutlu and Gemlik (for which an origin of some amount of sulphate by direct oxidation H_2S gas seems also possible) and for most thermal waters of the Bergama area (thermal waters of Kozak, Bergama, Paşa, Nebiler and Menteşe).

Isotopic equilibration of SO4 with H2O due to higher temperatures: At normal ambient temperatures the theoretical isotopic equilibrium fractionation between water and aqueous sulphate, which would be about 31‰, has never been observed in cold natural groundwater systems (IAEA 1983), as the time required is extremely long due to very low reaction rate (Lloyd 1968). But the reaction rate is much enhanced at higher temperatures as prevailing in geothermal systems. According to Mizutani and Rafter (1969), this relationship can even be used as geothermometer. For the thermal waters of the MARMARA project, such an influence of gradual change towards isotopic equilibrium fractionation was observed. In Fig. 6, the samples originating from the Kuzuluk, Bursa, Armutlu, Yalova, Tuzla and Bergama area are situated within the $\delta^{34}S$ range of primary sulphides, but with $\delta^{18}O$ values in the range of 4 to 10‰. The use as a geothermometer was tested by Mützenberg (1991). For the thermal brine of Tuzla, a reservoir temperature on the order of 150°C resulted, comparable to the results gained by use of the chemical geothermometers.

Mixing processes of sulphates of sedimentary origin (or contained in residual fluids as formation water) with sulphates of origin by oxidation of primary sulphides contained in crystalline rocks. By this process, the whole range of observed isotopes values can be explained, as shown in Fig. 6. It is also an independent information regarding the presence of residual portions of an ancient formation water, which is flushed by young infiltrating groundwater of meteoric origin, or which is actively migrating from marine Tertiary sediments into the crystalline basement along the areas near the shore of the Aegean sea, as observed in the area of Tuzla/Kestanbol and probably also of Bademli/Bergama (some indications of such processes are also observed in the thermal waters of Kaynarca and Dikili/Çamurlu).

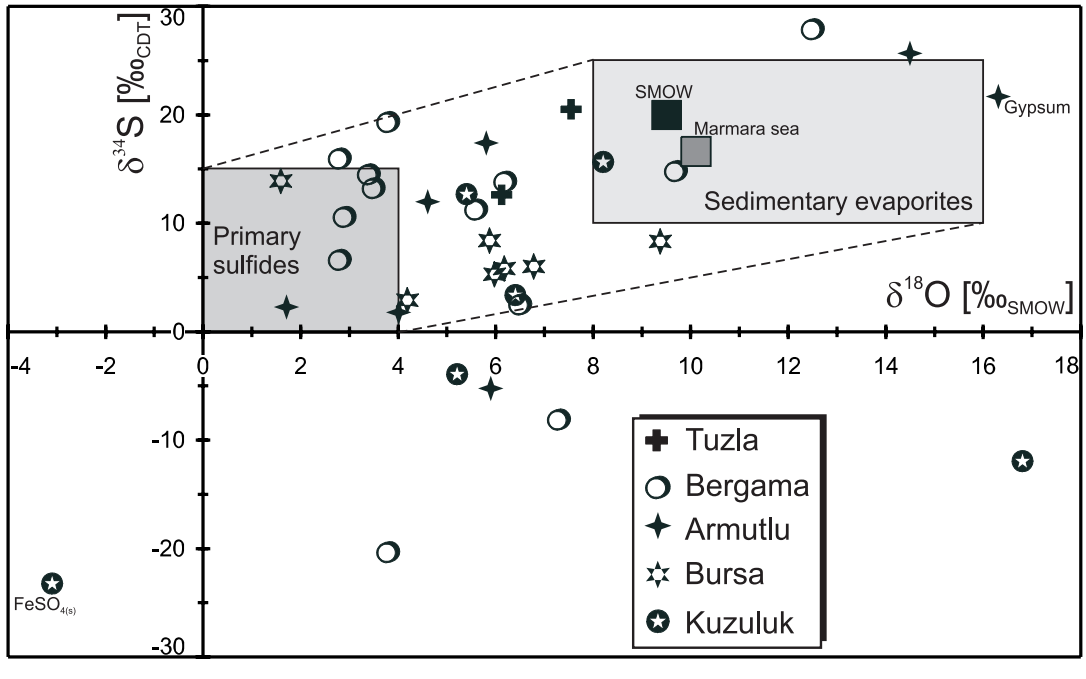


Figure 6: *Diagram of $\delta^{34}S$ versus $\delta^{18}O$ of dissolved sulphates of the thermal and mineral water of the MARMARA project.*

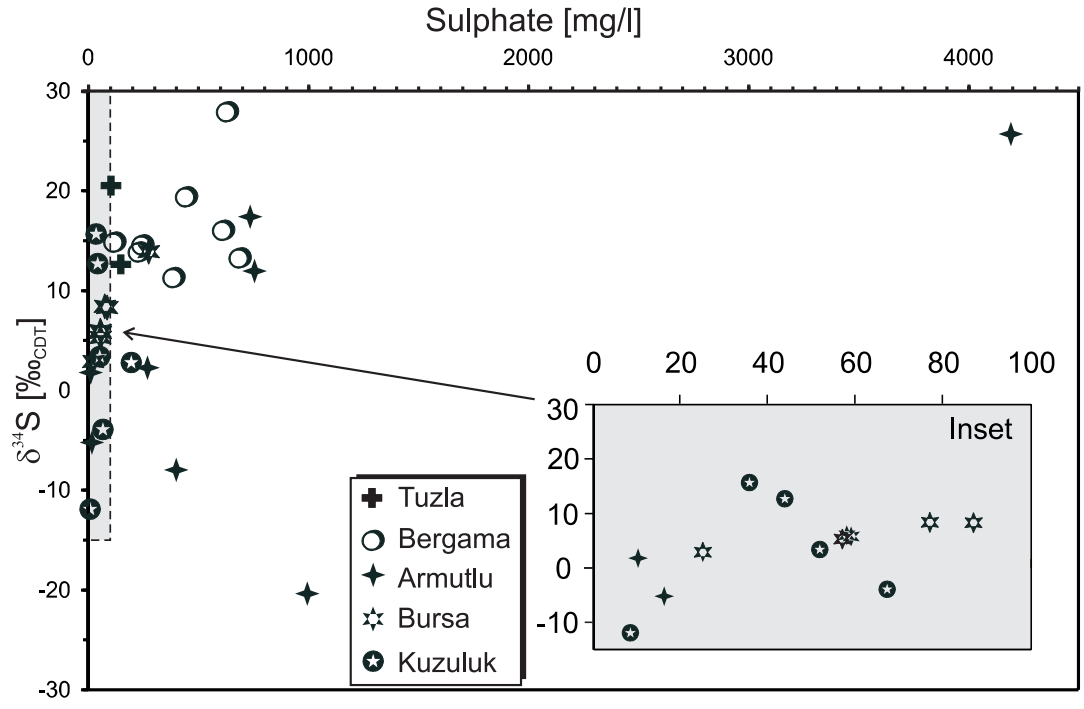


Figure 7: *Diagram of $\delta^{34}S$ versus sulphate contents of the thermal and mineral water of the MARMARA project. This figure indicates: mixing processes between sedimentary sulphates (with higher sulphate concentration) and sulphates of origin by oxidation of primary sulphide minerals (contained in crystalline rocks) of waters with low to moderate sulphate concentrations. Negative $\delta^{34}S$ values indicate secondary processes of bacterial sulphate reduction.*

Radionuclidic information on evolution and residence times

Tritium contents in normal and mineral and thermal waters

Shallow groundwaters of local origin also contain anthropogenic tritium in measurable amounts. As mentioned in Eisenlohr et al. (this volume (a)), the tritium content of the shallow groundwaters is also dependent on the geographical position of the investigated areas and the time of sampling. The tritium contents of the shallow groundwaters (which were chosen for the experimental definition of the $\delta^{2}H$ and $\delta^{18}O$ relationship of recharge) are in the range of the annual mean values of the precipitation (IAEA network), the residence times are generally on the order of some months to some years.

The tritium concentration measured in a sample from İznik lake (Eisenlohr 1995) was higher than expected for recent surface water. By hydrological model calculation a mean residence time of about 35 years results, which explains this measured tritium value. The investigated mineral and thermal waters generally yield tritium contents near the limit of detection, which indicates that no major component of anthropogenic tritium is present. Therefore, the residence time of these waters which were infiltrated before the nuclear test period is at least more than 40 years. As tritium is not affected by any chemical interactions with the aquifer, these residence times can be considered as the minimal 'ages'. In some waters, admixtures between shallow and deep groundwaters occur. Some thermal waters of origin in karstified rocks such as the Çekirge and the Gemlik/Orhangazi thermal waters reflect a gradual mixing of water components of short to long residence times (Imbach 1992, Eisenlohr et al. this volume (b)).

Radiocarbon in normal, mineral and thermal waters

As most of the thermal waters are influenced by the influx of deep produced CO_2, the radiocarbon method has to be applied with precautions and in combination with the stable isotope ^{13}C and the evaluation of the chemical evolution of the investigated waters. The measured values of ^{14}C and $\delta^{13}C$ of the analysed waters within the Gönen, Yalova/Armutlu/Gemlik and the Bergama areas are presented in Table 2.

Sample	Location	^{14}C(%)	±2 σ(%)	$\delta^{13}C$ (‰)	TIC (mmol/l)
Arm 8	Armutlu	4.7	0.2	-8.4	13.20
Gem 15	Gemlik	37.5	0.4	-14.1	4.20
Manyas	Manyas	36.2	0.4	-11.4	7.5
Hidirlar	Hidirlar	12.5	0.2	-16.2	1
G – 4	Gönen	5.7	0.1	-9.6	5
Be 01	Bergama	12.9	0.2	-10.3	11
Be 12	Bergama	22.8	0.4	-10.0	6.4
Ko 01	Kozak	27.1	0.3	-10.7	1.5
Ne 01	Nebiler	18.0	0.3	-10.1	11.3
Ne 03	Nebiler	56.2	0.6	-10.9	7.3

Table 2: *Result of the ^{14}C analyses. (AMS measurements made at the Institute of Particle Physics of PSI/ETH, sample preparation by Jeckelmann (1996))*

For the interpretation, the following correction model is applied:

Mass balance approach of Wigley (1975), as presented in Balderer (1985), for congruent dissolution:

$(A_i-A_M) / (A_a-A_M) = mC_1 / mC_2 = X_2$

with:

A_i = initial open system ^{14}C concentration at the end of the open system evolution versus the gas phase.

A_a = final ^{14}C concentration at the end of the closed system process and after the congruent dissolution evolution = initial value for the ^{14}C age determination (after correction for processes of chemical evolution without radioactive decay).

A_M = ^{14}C concentration of the rock carbonate, assumed to be zero.

mC_1 = initial concentration of the TDIC (Total Dissolved Inorganic Carbon) at the end of the open system evolution, equivalent to the TDIC of the selected shallow groundwater.

mC_2 = final concentration of the TDIC at the end of the closed system evolution, equivalent to the TDIC of the analysed thermal or mineral water.

The equation for the final calculation of the model age is:

$t = (T_{1/2} / \ln 2) * \ln (A_a / A_{TDIC}) = 5730/ \ln 2 * \ln (A_i * X / A_{TDIC})$

with:

A_{TDIC} = measured ^{14}C concentration in % modern of the TDIC of the groundwater sample

$T_{1/2}$ = half-life of ^{14}C, equal to 5730 years

t = ^{14}C – model age (years) for the considered evolution.

To apply this mass balance approach, values of shallow groundwaters representative of the initial recharge conditions with respect to the inorganic carbon cycle (mC_1) have to be selected. The corresponding values are given in Table 3. The ^{14}C concentration at the end of the open system evolution versus the gas phase A_1 is set as ≈ 100% modern carbon.

The evolution with respect to the initial conditions of the carbon cycle (Balderer et al. 1987, Reardon and Fritz 1978) starting from selected shallow groundwaters which represent the most probable origin of the analysed thermal and mineral waters can be checked by a second mass balance equation related to the stable carbon isotope ^{13}C (Wigley 1975):

$$mC_1 / mC_2 = X = (\delta^{13}C_2 - \delta^{13}C_{rock}) / (\delta^{13}C_1 - \delta^{13}C_{rock})$$

with:

$\delta^{13}C_1$ = initial open system ^{13}C concentration of the TDIC at the end of the open system evolution versus the gas phase. This value is related to the ^{13}C concentration $\delta^{13}C_g$ of the soil CO_2 by the following relation:

$$\delta^{13}C_1 = \delta^{13}C_g - \varepsilon_{g,s}$$

where $\varepsilon_{g,s}$ represents the additive isotope equilibrium fractionation factor between the gaseous CO_2 and the species of the dissolved inorganic carbon (TDIC) under open system conditions. It depends of the carbon species concentration in the groundwater and is therefore dependent on pH and temperature. In the following work it is calculated according to the relationship published in Wigley et al. (1978).

$\delta^{13}C_2$ = final ^{13}C concentration at the end of the congruent dissolution evolution equal to the analysed $\delta^{13}C$ value of the sampled thermal or mineral water for the ^{14}C age determination.

By setting up this second relationship beginning with the $\delta^{13}C_g$ of the gaseous CO_2 within the soil / root zone as starting value which presents a quite stable composition, depending only on the plant photosynthesis cycle CO_2, an independent check of the evolution of the groundwater with respect to the chemical conditions of the carbon cycle is possible.

For the most common plants, $\delta^{13}C_g$ values in the range of -26 ‰ to -21‰ are common according to literature (Stuiver and Polach 1977, Craig 1954, Fontes 1992). For the further calculations a value of $\delta^{13}C_g$ = -25 ‰ representative for the soil CO_2 of most common plants of modern environment (e.g. all trees and most of natural plants from temperate regions) is used for the further calculations as given in table 5. To apply the above described mass balance equation first the additive isotope fractionation factor for open system conditions $\varepsilon_{g,s}$ is determined using the measured pH and temperature values of the selected shallow groundwaters. As a next step the initial concentration of the shallow groundwater $\delta^{13}C_1$ is determined. By applying the ^{13}C mass balance equation with the measured values of the analysed groundwater samples $\delta^{13}C_2$, mC_1 and mC_2, finally the mean ^{13}C concentration of the rock carbonates $\delta^{13}C_{rock}$ dissolved by the investigated thermal and mineral waters during their evolution within the rock environment is possible. These values now yield an independent information of the isotopic composition of the rock carbonates which can be compared with the occurring main rock composition along the supposed flow paths.

In literature, the following $\delta^{13}C$- value ranges for rock carbonates are given (Hoeffs 1997, Balderer 1985, Balderer et al. 1987, Pearson and Balderer 1991):

Sedimentary carbonates of marine origin: 0 ‰ to +2‰

Metamorphic (marine) carbonates (marbles): 0 ‰ to +2‰

Carbonates of evolution in contact with magmatic CO_2: ≈ 0 ‰

Sedimentary carbonates of freshwater deposits: -5 ‰ to -2 ‰

Secondary calcites in crystalline rocks of NE -Switzerland: -5 ‰ to – 15 ‰

Sample	Location	Water Temp. (°C)	pH	TDIC (mmol/l)
Mec 92	Meceidiye	14.9	7.0	3.4
Ort 255	Ortaburun	11.2	5.3	0.4
Arm 87	Armutlu Picknick	13.5	7.0	3.4
Gem 190	Şahin Tepe (Gemlik)	17.2	6.4	3.3
W17	Susurluk (Manyas)	15	7.5	4
W18	Susurluk (Manyas)	15	8.2	5.3
GG	Kaz-Dağ	8.5	8.5	0.39
BK2	Kaz-Dağ	10.5	10.5	0.2
Tozlu	Kaz-Dğ	4.6	4.6	0.22
S27	Hafizhüseyinbey	15	15	4.5
Ov 03	Bergama/Ova Dere	11.7	1.1	1.5
Ov 04	Bergama/Ova Dere	12.3	0.2	0.5
Ma 01	Bergama/Madra Dağ	11.3	1.2	1.7
Ko 03	Bergama/Kozak	7.7	1.3	1.4

Table 3: *Selected groundwaters representative for of the initial recharge conditions with respect to the inorganic carbon cycle*

Discussion of the results of the application of the ^{14}C method to the following thermal and mineral waters (modelled by combined carbon and ^{13}C mass balance approach)

Armutlu kaplıca: The evolution from the two shallow groundwater samples Mec 92 and Arm 87 yield the same model age of about 14,000 years, whereas the evolution from a Ort 255 type water does not yield any age (negative value as resulting activity of final solution is lower than measured activity). This resulting model calculation (with A_a = 3% modern carbon) would mean a nearly complete loss of the active carbon (^{14}C) only through chemical processes, even without the process of radioactive decay. As the measured ^{14}C activity of the Armutlu thermal water is greater than this calculated value of modelled evolution starting from A_i = 100%, this would mean that this groundwater contained even anthropogenically produced ^{14}C. As the thermal water of Armutlu does not contain any anthropogenic tritium ($^3H < 1.0$) this possibility of evolution can be rejected. With respect to the results of the ^{13}C model the resulting $\delta^{13}C_{rock}$ values of -5.0‰ are within the value range of secondary calcites within crystalline rocks or of freshwater carbonates. As according to the geological mapping of Eisenlohr (1995) no carbonate rocks exist in this area of Armutlu, an evolution in contact with secondary calcites within the crystalline rocks for which a model age of about 14,000 years results would be even most probable. Such a residence time of more than 14,000 years means recharge under colder climatic conditions which is also not in contradiction with the established δ^2H- / $\delta^{18}O$- relationship of the area (Eisenlohr 1995, this volume).

Gemlik kaplıca: The resulting model age of about 6000 years is an indication for the old component of this thermal water for which a mixed origin of shallow and deep components is indicated also by the tritium content and the coupled hydrodynamic and thermal model calculations (Pfister 1995, Eisenlohr et al. 1995, this volume). The resulting $\delta^{13}C_{rock}$ value of +0.2‰ is within the range of marine sedimentary carbonates and marbles and confirms the hydrogeological observations of karst water circulation within the area of Gemlik Orhangazi (Eisenlohr this volume). The lower $\delta^{13}C_{CO2}$ value which had to be selected for the model calibration indicates a mixed type of vegetation in this karstified limestone area even nearly not used for agriculture.

Manyas: For this thermal water originating from a tectonic graben zone an evolution within sedimentary rocks (resulting $\delta^{13}C_{rock}$ = 0.9‰) or within freshwater carbonate rocks (resulting $\delta^{13}C_{rock}$ = -5‰) is possible. The resulting residence time according to the ^{14}C model ages is about 3000 to 5000 years, also in agreement with the other applied isotope methods.

Hidirlar: With respect to the low carbonate content of this thermal water an evolution entirely within crystalline rocks is probable. Such an evolution is also in agreement with the resulting value of $\delta^{13}C_{rock}$ of -16.5‰ to -12.5‰ and which yields a range of ^{14}C- model ages of about 4000 to 9000 years. This range of residence time is also in agreement with the $\delta^{2}H$- / $\delta^{18}O$ values which indicate recharge under recent climatic conditions.

Groundwater initial conditions	Groundwater final conditions	mC_1	mC_2	X	A_a (%mod.)	A_{TDIC} (%mod.)	t (years)
Mec 92	Armutlu	3.40	13.20	0.26	25.76	4.7	14063
Ort 255	Armutlu	0.40	13.20	0.03	3.03	4.7	-3628
Arm 87	Armutlu	3.40	13.20	0.26	25.76	4.7	14063
Gem 190	Gemlik	3.30	4.20	0.79	78.57	37.5	6115
W17	Manyas	4	7.5	0.53	53.33	36.2	3203
W18	Manyas	5.3	7.5	0.71	70.67	36.2	5530
GG	Hidirlar	0.39	1	0.39	39.00	12.5	9406
BK2	Hidirlar	0.2	1	0.20	20.00	12.5	3885
Tozlu	Hidirlar	0.22	1	0.22	22.00	12.5	4673
S27	G – 4	4.5	5	0.90	90.00	5.7	22811
GG	G – 4	0.39	5	0.08	7.80	5.7	2593
BK2	G – 4	0.2	5	0.04	4.00	5.7	-2928
Tozlu	G – 4	0.22	5	0.04	4.40	5.7	-2140
Ma 01	Be 01	1.7	11	0.15	15.45	12.9	1494
Ko 03	Be 01	1.4	11	0.13	12.73	12.9	-111
Ov 03	Be 01	1.5	11	0.14	13.64	12.9	459
Ma 01	Be 12	1.7	6.4	0.27	26.56	22.8	1263
Ko 03	Be 12	1.4	6.4	0.22	21.88	22.8	-342
Ov 03	Be 12	1.5	6.4	0.23	23.44	22.8	228
Ma 01	Ko 01	1.7	1.5	1.13	113.33	27.1	11828
Ko 03	Ko 01	1.4	1.5	0.93	93.33	22.8	11651
Ov 04	Ko 01	0.5	1.5	0.33	33.33	27.1	1711
Ma 01	Ne 01	1.7	11	0.15	15.45	18	-1260
Ko 03	Ne 01	1.4	11	0.13	12.73	18	-2865
Ov 03	Ne 01	1.5	11	0.14	13.64	18	-2295
Ma 01	Ne 03	1.7	7.3	0.23	23.29	56.2	-7283
Ko 03	Ne 03	1.4	7.3	0.19	19.18	56.2	-8888
Ov 03	Ne 03	1.5	7.3	0.21	20.55	56.2	-8318

Table 4: Resulting ^{14}C model calculation.

Groundwater initial conditions	Groundwater final conditions	$\delta^{13}C_{CO2}$ (‰)	$\varepsilon_{g,s}$(‰)	$\delta^{13}C_1$(‰)	$\delta^{13}C_2$(‰)	$\delta^{13}C_{rock}$(‰)
Mec 92	Armutlu	-25.0	-6.8	-18.2	-8.4	-5.0
Ort 255	Armutlu	-25.0	0.0	-25.0	-8.4	-7.9
Arm 87	Armutlu	-25.0	-6.8	-18.2	-8.4	-5.0
Gem 190	Gemlik	-22.0	-4.0	-18.0	-14.1	0.2
W17	Manyas	-25.0	-8.0	-17.0	-11.4	-5.0
W18	Manyas	-25.0	-8.5	-16.5	-11.4	0.9
GG	Hidirlar	-25.0	-3.0	-22.0	-16.2	-12.5
BK2	Hidirlar	-25.0	-8.5	-16.5	-16.2	-16.1
Tozlu	Hidirlar	-25.0	-9.8	-15.2	-16.2	-16.5
S27	G – 4	-18.5	-7.8	-10.7	-9.6	0.3
GG	G – 4	-18.5	-3.0	-15.5	-9.6	-9.1
BK2	G – 4	-18.5	-8.5	-10.0	-9.6	-9.6
Tozlu	G – 4	-18.5	-9.8	-8.7	-9.6	-9.6
Ma 01	Be 01	-25.0	-8.8	-16.2	-10.3	-9.2
Ko 03	Be 01	-25.0	-5.0	-20.0	-10.3	-8.9
Ov 03	Be 01	-25.0	-6.8	-18.2	-10.3	-9.1
Ma 01	Be 12	-25.0	-8.8	-16.2	-10.0	-7.8
Ko 03	Be 12	-25.0	-5.0	-20.0	-10.0	-7.2
Ov 03	Be 12	-25.0	-6.8	-18.2	-10.0	-7.5
Ma 01	Ko 01	-25.0	-8.8	-16.2	-10.7	-57.5
Ko 03	Ko 01	-25.0	-5.0	-20.0	-10.7	119.5
Ov 04	Ko 01	-25.0	-7.0	-18.0	-10.7	-7.1
Ma 01	Ne 01	-25.0	-8.8	-16.2	-10.1	-9.0
Ko 03	Ne 01	-25.0	-5.0	-20.0	-10.1	-8.7
Ov 03	Ne 01	-25.0	-6.8	-18.2	-10.1	-8.8
Ma 01	Ne 03	-25.0	-8.8	-16.2	-10.9	-9.3
Ko 03	Ne 03	-25.0	-5.0	-20.0	-10.9	-8.7
Ov 03	Ne 03	-25.0	-6.8	-18.2	-10.9	-9.0

Table 5: Resulting evolution with respect to the $\delta^{13}C$ of the dissolved rock carbonate.

For the *Gönen* area possible initial conditions are represented by the shallow groundwater of the well Hafizhüseynbey S27 (Yüzer this volume) and the shallow spring waters GG, BK2 and Tozlu of the Kazdağ area (Yalçın this volume, 1997). According to the results as presented in Table 4 and 5 an evolution with a water of the chemical composition of the Hafizhüseynbey S27 results for the Gönen thermal water a model ^{14}C-age of about 23000 years. This model age would be consistent with the indication of the stable isotopes δ^2H and $\delta^{18}O$ that this deep thermal groundwater could originate from recharge during pleistocene climatic conditions. With respect to the $\delta^{13}C$ mass balance calculation a $\delta^{13}C_{rock}$ value of 0.3‰ results (typical for marine carbonate rocks and marbles) if a $\delta^{13}C_{CO2}$ value of -18.5‰ is selected for the model initial conditions. Such a value of the soil CO_2 is lower than for the recent vegetation but typical for another type of vegetation (with e.g. Crassulacean plants, Fontes 1992) Such a vege-

tation could indicate changed climatic conditions with other types of plants or more influence of atmospheric CO_2 in soils with a less dense vegetation. For the other possibility of an evolution with a water of chemical composition similar to the shallow waters of the Kazdağ massif only with the water GG (Gobakli Gedigi) a positive model age of about 2600 years is resulting together with a $\delta^{13}C_{rock}$ value of -9.1‰ which is representative for an evolution by interaction within crystalline rocks only. But this second model of evolution yields a ^{14}C – model age which is not in agreement with the interpretation of the $\delta^{2}H$- / $\delta^{18}O$ values of the Gönen G-4 water which indicates an infiltration under colder climatic conditions. Therefore the first evolution model with interaction with marine or metamorphic carbonate rocks is more probable.

For the *Bergama* area the initial conditions are represented by the shallow groundwaters of Ova Dere (Ov 03 and Ov 04) originating of volcanites and of one spring at Madra Dağ (Ma 01) originating of metamorphic rocks and of a shallow sping at Kozak (Ko 03) originating of crystalline (granitic) rocks. The application of the above presented mass balance model for selected thermal waters of deep circulation (containing tritium near or at the limit of detection of < 0.7TU) yields the following interpretation based on the ^{14}C model ages:

For the thermal waters of the Bergama plain (Be 01 and Be 12) a residence time of more than 50 years (as containing no measurable tritium of anthropogenic origin) up to about 1000 years is resulting. The resulting $\delta^{13}C_{rock}$ values (Table 5) clearly indicate an evolution by interaction with secondary calcites within crystalline rocks.

For the Kozak thermal water (Ko 01) only with the initial conditions (for the carbon cycle) of the shallow groundwater Ov04 Bergama Ova Dere yields a plausible evolution for both carbon isotopes ^{14}C and ^{13}C. It results therefore the most consistent ^{14}C model age of about 1700 years for the Kozak thermal water.

For the Nebiler thermal water as represented by the water samples Ne 01 and Ne 03 none of the considered evolution from shallow groundwaters yield a positive model age, which is due to the fact that the calculated initial concentration corrected for chemical reactions is smaller than the measured ^{14}C concentration of these two thermal waters. Furthermore for both thermal waters Ne 01 and Ne 03 according to the results of the tritium analyses < 0.8TU and 0.8 ± 0.7 (2σ) TU a contribution of anthropogenic ^{14}C in greater amounts is not indicated. This fact could mean that these samples were affected by contamination during sampling with atmospheric CO_2, or that the real evolution is originating from a different initial groundwater than considered.

As general conclusion it can be stated that based on these ^{14}C model ages the residence time of thermal waters of the Bergama area are in the range of about more than 50 up to some 1000 years. As this kind of model calculation does not include any mixing consideration, this statement is therefore strictly valid only for a water of common origin. For the case that mixing with much older water components is occurring (according to Jeckelmann (1996) the presence of a component of an old formation water is indicated by the chemical constituents) this residene time is only valid for the potential younger component which is containing the active ^{14}C.

^{36}Cl in normal, mineral and thermal waters

^{36}Cl has a half-life of about 301'000 years. It has been used as a dating tool in various hydrologic systems since its detection by accelerator mass spectrometry (AMS) became possible. The principles of the ^{36}Cl method are well described by several authors as reviewed in Balderer and Synal (1996). The application of the ^{36}Cl method in groundwater studies needs, in principle, a detailed knowledge of all of the processes that occur within the water cycle and influence the ^{36}Cl concentration. This evolution can be solved by a three term mass balance approach (Balderer and Synal 1996). It can be applied, if the developed hydrogeological model is in agreement with following evolution:

- infiltration of water of atmospheric origin,
- subsequent decay of the atmospheric component,
- neutron activation of chlorine dissolved in the water phase and
- water rock interaction along the flow path of groundwater liberating chloride from the aquifer rock (contained in minerals, fluid inclusions and as intergranular salt in pore spaces), or by dissolution of limestones in contact with ascending CO_2.

A different approach has to be applied for the highly mineralised thermal waters encountered in the Tuzla/Kestanbol and the Bademli/Bergama areas. Following the results of hydrochemical investigations, as well as the results of isotopic studies (Mützenberg 1991, this volume, Jeckelmann 1996), the Tuzla and Kestanbol thermal brines, as well as the Bademli thermal water, present a mixing of two endmembers. One corresponds to a highly concentrated saline brine which is mixed with lowly mineralised water of local infiltration within the surrounding areas of the springs. The water of the second type originates directly from the infiltration in the crystalline complex itself. For the chloride of sedimentary origin of the residual brine endmember within the crystalline rock complex, an approximate residence time can be determined by application of a one-step equation for the underground production of ^{36}Cl (Balderer and Synal 1996). By a further approach, the mixing of two groundwater components is considered. The first component is a lowly mineralised recharge groundwater within the crystalline outcrops. The second component is a deep basin brine of sedimentary origin. This approach yields a distinct model age for the highly mineralised brine endmember.

The resulting model ages for the investigated thermal and mineral waters as represented in Fig. 8 (according to Balderer and Synal 1997) take into account the whole cycle of chloride in the groundwater cycle. They are valid under the assumptions given in Balderer and Synal (1997). The sometimes large errors in model age are dominated by the uncertainty of the $^{36}Cl/Cl$ ratio measured for the individual samples. However, in the case of the *Bursa/Kükürtlü* thermal water (Kük1), the resulting age range coincides in its lower part with the results of the hydrodynamic/geothermal modelling, which yields possible residence times on the order of 10^2 to some 10^4 years (Pfister 1995). The mineral and thermal waters of the *Kuzuluk* area, as also the deep thermal waters of the *Gönen* area, arise within topographically well-defined subsidence basins. The interpretation based on the δ^2H and $\delta^{18}O$ results of these thermal and mineral waters that the infiltration took place during a time period of changed (colder) climatic conditions is supported by the presented ^{36}Cl results in, at least a qualitative way. But the identification of a distinct colder climate period is not possible. For the thermal waters of *Yalova* and *Armutlu* the resulting ranges in model ages are not in contradiction with the already established hydrogeological conceptual model.

For the brine of the *Kestanbol* hot water, it can be stated that clearly no equilibrium of underground production is achieved for the deep brine endmember, even if the small amount of freshwater mixing component is deduced (Balderer and Synal 1996). The *Tuzla* hot brine seems to have a longer time of residence within the crystalline rocks. With respect to the overall uncertainties of the result, a residence time up to about 1m.y. is in agreement with the experimental data. These results of ^{36}Cl interpretation are in agreement with the resulting hydrogeological conceptual model for the *Kestanbol/Tuzla* area which indicates that the fossil pore water (within Neogene sediments of the Aegean basin) is actively migrating into the rocks of the crystalline basement along faults and is welling up in highly fractured zones. This process is caused by the tectonic activity of this area, which is evidenced by GPS measurements (Straub and Kahle this volume).

For the *Bergama* area, the hydrogeological conceptual model for the thermal waters of the thermal spas is quite similar to the situation of the *Bursa/Kükürtlü* thermal water. In the case

of the *Bademli* thermal brine, a process of active migration of seawater into the fissured rocks in the coastal area and mixing with local groundwater recharging in the surroundings of the Kozak high plateau is in agreement with the conceptual model based on hydrogeological, hydrochemical and stable isotope data (Jeckelmann 1996).

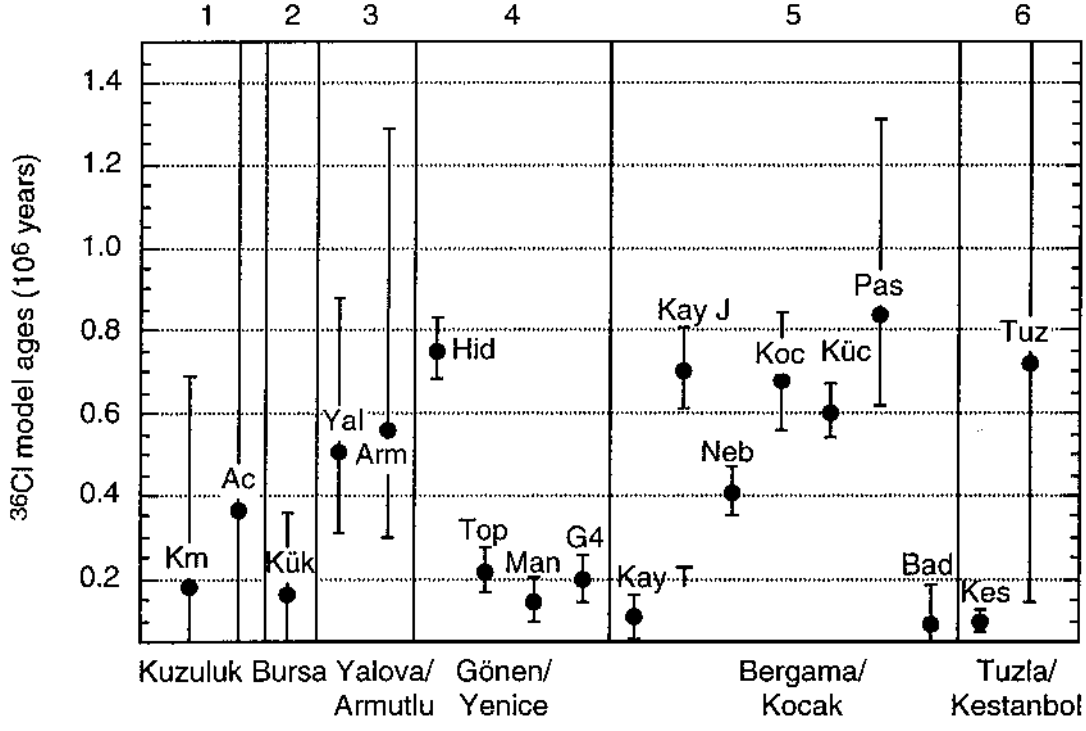


Figure 8: Resulting model ages for thermal and mineral water based on ^{36}Cl ivestigation.

Compared to the model ages resulting from the application of the ^{14}C method, the ^{36}Cl model ages are much larger by about one to two order of magnitudes. This first astonishing observation may be explained by the following considerations:

- Mixing effects are not considered in the applied isotope model approaches: a small mixing component of young groundwater containing high ^{14}C concentration (and a higher bicarbonate concentration) but which is low in chloride concentration may, if mixed with a groundwater of long residence time (containing no or only a small ^{14}C activity but still a measurable ^{36}Cl concentration), lead to such a result for residence time in the range of about 10,000 to about 200,000 years.
- As seen from this example, these two methods, which are different with respect to chemical behaviour and half-life, yield correct information but of different hydrogeological aspects for the same analysed deep groundwater.
- The sometimes large errors of the ^{36}Cl model age are dominated by the uncertainty of the ^{36}Cl/Cl ratio measured for the individual samples. But the precision of AMS measurements of low ^{36}Cl concentration will be further minimised in future by new AMS equipment and preparation techniques.

The conclusion that mixing components of different residence time are present in the same thermal water of deep origin indicates special hydrogeological features. These facts define flow regimes of deep groundwaters of deep and long regional flow systems which have interrelationships with local and intermediate flow systems, as indicated by the observed mixing

processes of chemical constituents and isotopes. This now indicates deep flow systems which are interconnected locally by tectonical short cuts resulting from deep faulting with open fractures (due to the observed extensional regime) with more shallow circulating groundwater of intermediate and local flow systems.

Gas Isotopes

^{18}O and ^{13}C in CO_2

For the Kuzuluk thermal and mineral waters, isotope analyses of the CO_2 gas of the Kuz2 well and of the total inorganic carbon (TIC) of 11 gas-water samples were carried out (Greber 1992, 1994, this volume). The result of the isotope analysis of the CO_2 of the gas sample is$\delta^{13}C$: -0.63‰ PDB and $\delta^{18}O$: 22.65‰ SMOW. According to these values, the origin of the CO_2 gas is most probably due to the production by a thermocatalytic reaction (Pezdic' et al. 1991) with carbonate rocks of sedimentary origin in depth (Greber 1992). The measured isotope values of the total inorganic carbon (TIC) of the 11 gas-water samples with $\delta^{13}C$ in the range of 6.59 to 2.74 ‰ PDB and $\delta^{18}O$ in the range of 31.51 to 33.76‰ SMOW are in agreement with such a process. The $\delta^{13}C$ of the CO_2 gas calculated for equilibrium fractionation with the TIC is in the range of -0.93 to -5.26‰ PDB. The lowest $\delta^{13}C$ values of about -5‰ PDB resulting for the Aci2 mineral spring are an indication that also some CO_2 of mantle origin is involved (Barnes et al. 1978). This hypothesis is supported by the helium isotope measurements which result in a mantle contribution of up to 8.5%, as CO_2 is acting as a carrier for the helium migration through the Earth's crust along active fault zones. Measurements of $\delta^{13}C$ and $\delta^{18}O$ of the CO_2 gas of thermal waters sampled as already mentioned in evacuated glass tubes were also performed for the thermal waters of Armutlu, Gemlik, Orhangazi and Keramet (Eisenlohr 1995, this volume).

The values of the CO_2 of the Armutlu thermal water (Mide suyu and well) of$\delta^{13}C$ of about -4‰ PDB and $\delta^{18}O$ of 32‰ SMOW also indicate a mixed sedimentary and mantle origin, whereas the samples from Gemlik ($\delta^{13}C$ of -17.6 and -13.4‰ PDB and $\delta^{18}O$ of about 32‰ SMOW) indicate a normal atmospheric origin by dissolution of atmospheric and soil CO_2 by the infiltrating water at recharge with subsequent dissolution of rock carbonate within the karstic limestone aquifer. The same origin also applies for the dissolved CO_2 within the waters of Orhangazi İlıpınar ($\delta^{13}C$ of -19.1‰ PDB and $\delta^{18}O$ of 22.5‰ SMOW) and Keramet İlıca ($\delta^{13}C$ of -10.7‰ PDB and $\delta^{18}O$ of 21.4‰ SMOW).

For the Bergama area, $\delta^{13}C$ values of the CO_2 gas in equilibrium with the analysed thermal waters are reported by Jeckelmann (1996). These values range from close to biogenic soil CO_2 gas (with $\delta^{13}C$ = -19.0‰ for Nebiler, Ne 03) to a range of mixed biogenitic and atmospheric origin (with about -12‰ to -7‰) for the thermal waters of Bergama (Be 01: $\delta^{13}C$ = -13.3‰), Nebiler (Ne 01: $\delta^{13}C$ = -11.8‰), Geyikli dere (Ge 01: $\delta^{13}C$ = -9.0‰), Kaynarca (Ka 01: $\delta^{13}C$ = -7.9‰) and Paşa İlıca (Pa 01: $\delta^{13}C$ = -7.9‰). This range overlaps the range of CO_2 gas of mantle origin with a range of -8‰ to -4‰ (Barnes et al. 1978), which also contains the $\delta^{13}C$ values of the samples from Bademli (Ba 01: $\delta^{13}C$ = -5.0‰) and Menteşe (Me 01: $\delta^{13}C$ = -4.4‰). The $\delta^{18}O$ (SMOW) values of the sampled CO_2 gas of the thermal waters of the Bergama area are all in a rather narrow range of 24‰ to 30‰ and are probably in equilibrium of fractionation with the corresponding waters as observed by Greber (1992) for the thermal water of Kuzuluk 2.

Isotopes of noble gases: ^{3}He, ^{4}He, ^{20}Ne, ^{21}Ne

Helium originates mainly from 3 sources, the atmosphere, the Earth's crust (^{4}He production through α decay of radionuclides contained in the rock) and the Earth's mantle which can be distinguished by the $^{3}He/^{4}He$ isotopic ratio (Fig. 7 in Pfister et al. this volume). To determine the amount of atmospheric contamination through inclusion of air during sampling, the Neon (^{20}Ne) content or the $^{20}Ne/^{21}Ne$ isotopic ratio is used (the exact correction procedure is described in Kipfer (1991)). Based on the following $^{3}He/^{4}He$ ratios of $1.364*10^{-6}$ for the atmosphere, $2*10^{-8}$ for the Earth's crust, and of $1*10^{-5}$ for the mantle, a helium contribution of the mantle of about 20% results for the Tuzla thermal spring (measured $^{3}He/^{4}He$ ratio $2.03*10^{-6}$, Mützenberg 1991). For the Kuzuluk thermal and mineral springs, measured $^{3}He/^{4}He$ ratios in the range of 0.856 to $1.006*10^{-6}$ result in mantle contributions of 6.9 to 8.5% (Greber 1992). For the Bursa area, the measured $^{3}He/^{4}He$ ratios have to be corrected for air contribution (Imbach this volume). According to the corrected $^{3}He/^{4}He$ ratios of 6.09 to $6.94*10^{-7}$, mantle contributions in the range of 5.9 to 6.7% result. For the Armutlu peninsula, mantle contributions of 3.0% for Armutlu, 3.6% for Yalova and 1.2% for Gemlik kaplıca and 2.4% for Orhangazi İlıpınar result from the measured $^{3}He/^{4}He$ ratios (corrected for atmospheric contribution and decay of tritium, Gemlik 4.3±0.33TU, Orhangazi 9.5±2.4TU, (Eisenlohr 1995, this volume). The higher $^{3}He/^{4}He$ ratio of the Orhangazi İlıpınar compared to the ratio of Gemlik kaplıca is, according to Eisenlohr (1995), due to the vicinity of a fault system. In the Bergama area, resulting mantle contributions of 12.0% for Paşa İlıca, 10.8% for Kozak İlıca, 6 to 8% for the Bergama plain, 6 to 6.5% for Kanarca and Geyikli Dere and the lowest value of only 0.8% for the Nebiler spa are reported by Jeckelmann (1996), based on the measured $^{3}He/^{4}He$ ratios.

Water-rock interactions and geothermometers

By the principal of application of chemical and isotope geothermometers, it is assumed that at the depth where the groundwater circulates very slowly or resides for a longer time a complete chemical and isotopic equilibrium between the minerals within the surrounding rock massif and water and contained gases is achieved. If the upflow of the water to the spring or wells is fast enough, the chemical equilibrium is still maintained in the water outflowing at the surface. By applying the laws of thermodynamic equilibria, the original reservoir temperature at depth can be reconstructed through the chemical and isotopic composition of the analysed groundwater.

As pointed out in Greber (1994), unfortunately CO_2 dominated systems such as the Kuzuluk area, are not really suitable for the application of classical cation geothermometers. By the application of the most reliable chalcedony geothermometer (Truesdell 1975), in-situ reservoir temperatures of about 120°C were calculated for the central Kuzuluk thermal waters. By the application of the ^{18}O water-sulphate geothermometer (Lloyd 1968, Mizutani and Rafter 1969), the following reservoir temperatures result for the central Kuzuluk thermal waters: central springs (Beç1, Çök2) t=96-124°C, borehole (Kuz1) t=120-134°C.

For the Bursa thermal area, the chalcedony geothermometer was also applied as being the most suitable. This resulted in the following equilibrium in-situ temperatures for the hottest springs of the two thermal provinces (Imbach 1992):

Bursa/Kükürtlü +(SiO_2) = 108°C (spring Bagdemlibahce/Yeni kaplıca)

Bursa/Çekirge +(SiO_2) = 52°C (drilling İpeker)

For the Yalova/Armutlu thermal area (Eisenlohr 1995), the quartz geothermometer (Fournier 1981) and also the chalcedony (Truesdell 1975) and the ^{18}O water/sulphate geothermometers (Mizutani and Rafter 1969) were applied, resulting in the following reservoir temperatures:

Yalova:	t = 70°-100°C
Armutlu	t = 100°-130°C

For the karstic thermal springs, only the quartz geothermometer (Fournier 1981) was applicable (Eisenlohr 1995), which resulted in reservoir temperatures quite similar to the actually observed spring temperatures:

Gemlik kaplıca	t = 53°C
Keramet	t = 60°C
Orhangazi İlıpınar	t = 37°C
Soguçak	t = 35°C

In the Kestanbol-Tuzla geothermal area, the chalcedony (SiO_2) geothermometer (Truesdell 1975) was also applied (Mützenberg 1991), resulting in the following ranges of reservoir temperatures:

Tuzla	t = 113°-162°C
Kestanbol	t = 138°-150°C

By the application of the ^{18}O water-sulphate geothermometer (Mizutani and Rafter 1969), reservoir temperatures of 228°C for Tuzla and 142°C for Kestanbol kaplıca result (Mützenberg 1991).

For the Gönen area, the quartz geothermometer (Kharaka and Carothers 1986) was also applied (Yalçın this volume), resulting in in-situ reservoir temperatures of 100°C for Gönen (thermal well G2) and of 62°C for Eksidere.

For the Bergama area the following reservoir temperatures result:

Kozak	t = 70° to 100°C
Kaynarca area	t = 150° to 170°C (which are the highest of this area, Jeckelmann 1996)

In Fig. 9, all of these resulting reservoir temperatures are presented against the measured values of the outflowing or pumped wells and springs. These resulting temperatures are also in good agreement with the modelled situations shown in Pfister (1995) for Bursa (thermal water occurrence through deep groundwater circulation which is cut short buy fault zones) and Gemlik/Orhangazi (system of mixing of karstic waters in deep karst structure with short cuts through fault zone).

Resulting origins and processes (origin and indications of flow paths)

Based on the presented results the following evolution is deduced for the thermal waters (brines) of the investigated areas (compare with Figure 2 in the Introduction to this volume).

Kuzuluk area

The occurring Na-HCO_3 type waters with very high CO_2 gas contents show a marked deviation with respect to $\delta^{18}O$ of the shallow groundwater of meteoric origin. This deviation of the cold mineral and thermal waters from the meteoric water line of the local shallow groundwaters can, with respect to the $\delta^{18}O$ values, be attributed to water-rock interaction and/or isotopic exchange with the uprising CO_2. This interaction with uprising CO_2 which also dominates the chemical composition of all the observed thermal and cold mineral waters would imply $\delta^{18}O$ values of $CO_{2(g)}$ in the range of marine carbonates or silica deposits. Additionally, the very low $\delta^{2}H$ values of these waters indicate a distinct origin not connected with the actual recharge groundwaters. The most likely explanation is that, for these waters, recharge occurred during a period of cooler climate (Pleistocene).

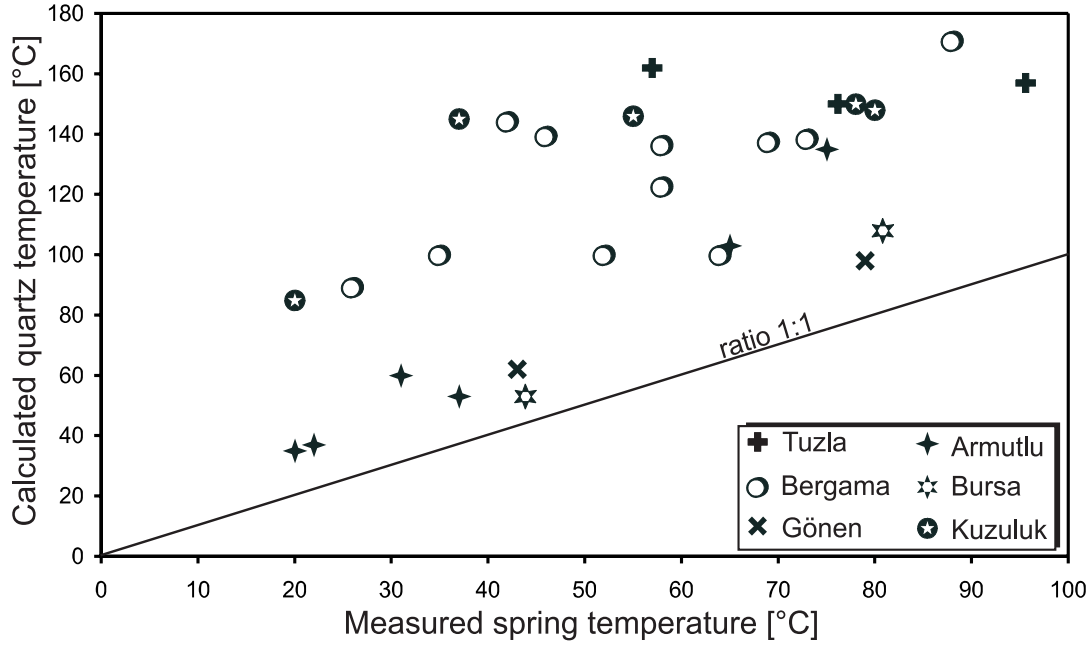


Figure 9: Reservoir temperatures based on SiO_2 geothermometers.

Bursa area

The groundwater recharge of the whole area (for cold as well as hot groundwaters) is concentrated on Mount Uludağ and dominated by heavy rainfall, snow, snow melt and successive infiltration during the winter (late autumn to spring) period. Based on the deuterium contents of the observed thermal waters combined with the deuterium-altitude relation of the local cold groundwaters (Imbach this volume) two different principal recharge areas may be distinguished: the Kükürtlü thermal waters correspond to waters recharged in the altitude range of 1500 to about 2500m up to the highest peaks of Mount Uludağ (most probably in the karstified marbles on top of Mount Uludağ). Whereas an altitude range of 1000 to 2000m would be adequate for the Çekirge thermal waters, which coincides with the leucogranite outcrops in the region of the Uludağ plateau (Imbach this volume). For both cases of Bursa/Kükürtlü and Çekirge, the outflowing thermal waters represent an actual water circulation system with known recharge and discharge areas. Considering the low mineralisation of these thermal waters, a very rapid ascent from depth along high permeable fault zones has to be assumed (Hydrogeological circulation model see Imbach this volume).

Yalova/Armutlu/Gemlik area

The three main centres with thermal water discharges at Yalova, Armutlu and Gemlik kaplıca occur at fault zones. The main faults related to these thermal springs are of a N-S direction in the Yalova and Armutlu spas and of an E-W direction in the Gemlik kaplıca area.

According to chemical composition, the waters of Yalova (Na-Ca-SO_4-(Cl) with 1300mg/l) and Armutlu (Na-Ca-SO_4-HCO_3-Cl with 2000mg/l total mineralisation) originate by the same processes of water-rock interaction (hydrolyse of silicates and oxidation of sulfides) within metamorphic and volcanic rocks (as andesites at Yalova and epidot-chlorite schists and amphibolites at Armutlu) leading to the same main composition of a Na-Ca-SO_4-(Cl) type water. For the water of Armutlu, the higher mineralisation can be explained by dissolution of carbonate minerals (calcite and dolomite, presence of calcareous schists encountered in the Armutlu borehole, Eisenlohr this volume) and an additional influence of NaCl for which the following possibilities exist: mixing with seawater, mixing with formation water of Tertiary origin or dissolution of airborne salt (sea spray) by the recharge water. The Gemlik Orhangazi water (Ca-Mg-(Na)-HCO_3-(Cl) with 350mg/l) shows the composition of a normal karstic water with dissolution of limestone and dolomite. The enhanced NaCl content most probably originates from the dissolution of evaporites present within the Oligocene (Tertiary) sequence (Eisenlohr this volume).

From the comparison of the stable isotopes δ^2H and $\delta^{18}O$ of recent cold groundwaters, an infiltration altitude of about 1000m a.s.l. is admitted for the thermal waters of Yalova and Armutlu. As such elevations exist in the central part of the Armutlu peninsula, an infiltration of the water under actual (recent) climatic conditions is possible. As these waters also yield about the same outflow temperatures of about 60 to 75°C and also nearly similar reservoir temperatures (100°C), about the same depth of circulation can be admitted. For the thermal to subthermal springs of Gemlik, Orhangazi, Soğucak and Keramet, altitudes of infiltration over a range of 600 to 800m result according to the recent relation of the stable isotopes δ^2H and $\delta^{18}O$ of cold groundwaters and springs.

Gönen/Yenice area

The geological structure of this area is characterised by metabasic rocks and metamorphic volcanic sedimentary series and also by deep neogene sedimentary deposits within the graben structures. According to present knowledge, the underlying bedrock was formed by metamorphic rocks as outcropping in the Kazdağ massif (Yalçın this volume). Hot springs also occur from the southern area of Eksidere (Topaklar) to Yenice (Hıdırlar). These springs emerge directly from crystalline rocks (mainly andesites) related to the existence of local fault systems.

For the Gönen thermal water (1700mg/l of total mineralisation), as also for the waters of the Manyas, Topaklar and Hıdırlar hot spring, an evolution by processes of water-rock interaction with metamorphic and volcanic rocks (gneiss, amphibolite, marble) by hydrolysis of silicates, oxidation of sulphides and dissolution of carbonates) is admitted, leading to a Na-Ca-SO_4-(Cl)-(HCO_3), to a Na-Ca-$\underline{HCO_3}$-(Cl)-(SO_4-) type water, respectively, for the Manyas spring. To account for the higher amount of NaCl, the presence of a mixing component of remnant brakish formation water of Neogene origin seems most probable. The Eksidere Ca-Mg-Na-HCO_3-(Cl) type water (with 346-363mg/l of total mineralisation) reflects the evolution of a karstic water in contact with carbonate rocks. The NaCl content could also result from some admixture of formation water.

To establish the recent recharge conditions, shallow cold groundwaters of the Gönen/Eksidere area and also at several altitude ranges at the Kazdağ massif (which presents also a potential infiltration area of the Gönen thermal waters) have been analysed with respect to the

stable isotope contents of ^{2}H and ^{18}O (cf. Chapter *Stable isotopes* in Yalçın this volume). As already mentioned in the section of stable isotopes and represented on Fig. 4, no significant trend of $\delta^{2}H$ and $\delta^{18}O$ with respect to the altitude of the sampled spring is apparent. The absence of the usually observed so called altitude effect is explained by the climatic and morphological situation of the area.

According to the position in the $\delta^{2}H$ versus $\delta^{18}O$ plot (Fig. 5) as stated by Yalçın (this volume), the thermal waters of Eksidere (S1 and S2), the karstic spring (S4), the Gençlik suyu (S3) mineral water and the Hıdırlar (Hid) thermal water can be related to recent infiltration conditions as their $\delta^{2}H$ and $\delta^{18}O$ value pairs are situated close to the Marmara meteoric water line (Fig. 7 in Yalçın this volume). Also, the waters of Topaklar thermal water (Top), the Geyikli acidic spring (Gey) and the Külcüler thermal spring (small spa in the vicinity of the Kazdağ massif at 350m in altitude) have to be attributed to recent meteoric origin, as their values are situated in the range of the Marmara and global meteoric water line. The water of the Gönen thermal wells G2 and G4 yields the lowest stable isotope values $\delta^{2}H$ and $\delta^{18}O$ and is related to recharge under colder climatic conditions.

Bergama/Kozak area

For the thermal waters of Kozak and Bergama the same processes of water-rock interaction within crystalline rocks (volcanites and granites) are assumed, mainly by the hydrolysis of silicates, interaction with a CO_2 gas phase and oxidation of primary sulphides contained within the crystalline rocks or oxydation of H_2S of deep origin in contact with the infiltrating air saturated water. The higher mineralisation of the Bergama water is due to the additional interaction with carbonates contained within the alluvial filling of the Bergama graben structure (Jeckelmann 1996). With respect to the stable isotope composition $\delta^{2}H$ and $\delta^{18}O$, the thermal waters of the Bergama/Kozak area reflect actual conditions of recharge, as referenced by the investigated cold (shallow) groundwaters (Eisenlohr et al. this volume (a), Jeckelmann 1996). By the existing altitude-$\delta^{2}H$ relationship, distinct areas of recharge can be attributed to the different investigated thermal springs, representing individual flow paths. Therefore, all thermal waters reflect active circulation with infiltration in the areas of the Kozak massif and with individual outflow zones in the plains of Bergama, Kocaoba, Kaynarca (Jeckelmann 1996). Except for one exception, the $\delta^{2}H$ and $\delta^{18}O$ present values for the Menteşe thermal waters (Bergama area) would lead to a much higher altitude of infiltration (about 1700 to 1800m a.s.l. according to the established $\delta^{2}H$ altitude relation of groundwaters of recent recharge) compared with the potential recharge areas (Jeckelmann 1996). Therefore, an infiltration under colder climatic conditions must be taken into account for the Menteşe thermal water also.

The very high NaCl concentration of the Bademli water indicates mixing with a highly mineralised formation water or sea water. As all thermal waters contain some higher amounts of NaCl, a small mixing component of such a highly mineralised water may potentially be assumed in the other investigated thermal waters of the Bergama area also (Jeckelmann 1996).

Kestanbol/Tuzla area

As the ratios of non-reactive species of the sampled thermal waters differ very little, it can be concluded that they evolved from a common saline endmember and represent mixing series with lowly mineralised fresh groundwater. The latter correspond either to shallow waters (containing anthropogenic tritium) or to heated regional groundwaters of meteoric origin. For the saline endmember, an evolution from a fossil altered seawater (connate water) is suggested based on the similar Na/Cl and only slightly differing Br/Cl and B/Cl ratios (Mützenberg et al. 1992).

The high salinity and the observed isotopic signatures can be explained by diagenetic reactions in the sediments (Clayton et al. 1966) and water-rock interactions at higher temperatures during circulation in volcanic/crystalline and metamorphic rocks (also involving oxygen isotope exchange reactions, Savin 1980, Kharaka and Carothers 1986, Balderer et al. 1991). Therefore, the actual composition of the present day outflowing hot waters of the observed springs can be explained by mixing processes with heated fresh water of regional aquifers and locally up to 85% with near surface groundwater of meteoric origin. The ascent of the saline thermal water results of the combined effect of (1) deep regional circulation and convection along major fault zones, (2) the dilution effect by mixing with lowly mineralised hot freshwater of low density which lead to the observed welling up of the hot brines due to the buoyancy effect along zones of high vertical permeability.

Resulting types of investigated groundwater systems (hydrogeological models and flow paths)

Kuzuluk area

The mineral and thermal waters of the Kuzuluk area, arising within a topographically well defined subsidence basin, are, with respect to their stable isotope contents clearly disconnected not only from the meteoric waterline showing a marked oxygen shift (^{18}O enrichment probably due to isotope exchange with CO_2, Greber this volume) but also disconnected, as proved by their much lower δ^2H values, from the actual local groundwater of recent recharge. The following different explanations for the origin of these waters are possible, which are of major importance for the understanding of the groundwater circulation in this tectonic active area):

(i) the evolution started from normal meteoric water infiltration. Subsequently, the water was heated up at greater depths within the fault system and would have undergone oxygen isotope exchange most probably in contact with CO_2 coming up from depth (Kipfer 1991, Greber this volume) or produced by thermocatalytic reaction (Pezdic' et al. 1991) with carbonate rocks at depth (Greber 1992). If, as usually admitted from experience in other geothermal areas also (Fontes 1976, Gonfiantini 1971, Giggenbach 1992), no deuterium exchange has to be taken into account, the only explanation for the observed low deuterium contents of these mineral and thermal waters would be that they correspond to the waters infiltrated under different climatic conditions (e.g. the cooler and more humid conditions of the Pleistocene epoch).

(ii) The second possibility of a connection with a process which would also lead to a depletion in the deuterium content, e. g. by separation of a steam phase of a deep hot water and condensation in a near surface local meteoric groundwater, is unlikely because of the very low tritium contents near or below detection limit and is also not supported by the hydrochemical composition of these waters (the oxygen isotope ratio seems in any case to be dominated by the large amount of uprising CO_2).

Also, the remaining possibility of an exchange with hydrogen contained in minerals, as stated by Blattner (1993) for hydrothermal fluids, seems not very likely to have occurred, as only moderate reservoir temperatures result from the applied geothemometers, as represented in Fig. 9. The presented isotopic signatures would lead to a conceptual model where a deep seated fluid exists, which is disconnected from actual recharge and is outflowing through fractures of the low permeable top layers of volcanic rocks and ignimbrites and silicified gravels (Greber 1992) not because of the usually admitted mechanism of the hydrologic cycle but because of the local tectonic configuration of the pressurising effect of the uprising CO_2 (in the

160m deep borehole hot thermal water at 82°C and a hydrostatic artesian overpressure of 3 bars and an additional 2 bars of CO_2 pressure was observed). In this case, not the normal situation of the hydrodynamic flow systems with flow in continuity but the lifting and emptying of a limited reservoir by the effect of upwelling/buoyancy due to the high CO_2 activity takes place.

Bursa area

From the presented results of isotope, hydrochemical and hydrogeological investigations and in consideration of the historical records (Imbach 1992) it results that the Bursa area represents a region of a stable thermal system. Normal regional terrestrial heat flow builds a boundary condition (Pfister et al. this volume (b)). Recharge in the fissured and partly karstified rocks of the Uludağ massif, deep vertical circulation due to tectonic structure and a high hydraulic gradient lead to the observed hot waters. These naturally occur at intersections of two fault systems (Imbach this volume). By the cooling process of the outflowing hot water, travertine deposits were formed by calcite precipitation beginning from the uppermost spring origins. The fact that the springs used today all originate within the altitude range of these travertine deposits indicates a decrease of hydraulic head with time.

Seasonal variations as shown by the tritium values and the stable isotopes are most probably attributed to mixing processes along the flow path inside the aquifer which are induced through change of hydraulic head, increased during the recharge period of autumn to spring and decreased in the summer period as mainly dry season (Greber et al. this volume). In the Bursa area, the outflowing hot thermal waters can be derived based on the stable isotopes by recharge of precipitation (rain and snow) within two distinct different altitudes ranges on Mount Uludağ (and the surrounding areas) which evolved in the deeper part of the descending pathways by oxygen isotope exchange as a result of the higher temperature.

Therefore, this area is good in agreement with the traditional model of regional groundwater flow with the properties needed for geothermal systems: long and deep groundwater circulation which is favoured by open fractures due to extensional tectonics, and fast ascent of the hot fluid by a high permeable regional fault zone.

Yalova/Armutlu/Gemlik area

The occurrences of the hot springs at Yalova and Armutlu are related to fault zones intersecting with morphological low level zones (within erosional valleys or canyons). They represent nearly unmixed deep groundwaters which evolved mainly by water-rock interaction processes. The Gemlik Orhangazi subthermal to thermal waters originate by the special tectonic structure of karstic systems below the valley level and rise up through tectonic fault zones (Eisenlohr et al. this volume (b), Eisenlohr this volume). Karstic processes of limestone dissolution are enhanced through uprising CO_2 along the fault zone.

Gönen area

Very old groundwaters exist within the Gönen graben area, as evidenced by the thermal waters G2 and G4 accessed by boreholes. The natural conditions are disturbed through the intense exploitation by the Gönen geothermal power plant. According to oral accounts, the former undisturbed situation was almost similar to that of the Kuzuluk area with naturally occurring springs at ground surface and CO_2 emanating in boiling ponds. Through the use of pumping in several boreholes, a pressure drop of about more than 10 bar occurred up to the present which has led to the installation of a reinjection facillity (Ş. Şimşek, pers. comm. 1996).

According to the presented results, the Gönen water originates from recharge during a period of Pleistocene climate, as evidenced by stable isotopes but also by the extremely low recharge temperature of about 0°C (probably infiltration of meltwater) resulting from the dissolved argon content (Yalçın 1997, this volume) and also in agreement with the resulting ^{14}C model age range in the order of 20,000 years. Compared with the thermal waters of Topaklar, Hıdırlar and Külcüler, an actual mixing process is assumed where younger recharged groundwaters occur within intermediate flow paths. Such a process is in agreement with the actual recharge conditions, as evidenced by the cold water springs of different altitude ranges of the Kazdağ massif (Yalçın this volume). For the waters of Eksidere, a different evolution mainly in contact with karstified carbonate rocks is admitted (Yalçın this volume).

Bergama/Kozak area

According to chemical and isotopic composition, the thermal waters of the Bergama/Kozak area reflect active flow systems with infiltration in the areas of the Kozak massif and with individual outflow zones in the plains of Bergama, Kocaoba, Kaynarca (Jeckelmann 1996). According to the very high NaCl concentration a mixing process with a highly mineralised formation water or sea water is assumed for the Bademli water. As several thermal waters contain some higher amounts of NaCl, a small mixing component of a highly mineralised water may potentially be assumed in other investigated thermal waters too (as formation water or remaining sea water of periods of sea water invasion during Tertiary periods (Schindler this volume); or as observed by the chemical composition by Jeckelmann (1996)). The discharge zones of the investigated hot waters are related to the combined effect of the intersection of fault zones combined with favourable areas of low topographic height, as in eroded valleys or gorges. The water of Bergama is outflowing along fault zones within the underlying bedrock also and accumulated within the sedimentary layers of higher hydraulic conductivity within the alluvial plain of Bergama. Therefore, hot water in different levels of these unconsolidated sediments of the infilling of the Bergama plain/graben structure exists (Jeckelmann 1996). The decrease in hydraulic head due to the active use of the groundwaters within the plain has, therefore, caused the dryout of the former historical thermal spring Güzelik Bergama (Kleopatra spa), which represented the natural overflow of this thermal water system. As shown in the conceptual hydrogeological interpretation model in Jeckelmann (1996), the following features favouring the geothermal activity of this area are:

- Shallow groundwater originated by local infiltration within the surrounding hills and high plateaus formed of crystalline rocks, such as the Kozak massif, Paleozoic schists, Tertiary sediments, Tertiary volcanites and Quaternary fillings of loose sediments , such as those existing in the Bergama plain.
- The shallow groundwater circulates to greater depths, as favoured by the observed systems of open fractures, and are mixed with deep-seated fluids of various origins, such as relict hydrothermal water (fluid inclusions), formation water or sea water of Tertiary flooding events.
- Also, admixtures with gases of deep origins are evidenced which indicate ascending deep pathways for fluids and gases.
- The fast ascent of the deep circulating thermal water is enhanced by conjugate steep fracture and fault zones leading to the observed natural outflow zones in the vicinity of the plain areas.

Tuzla/Kestanbol area

In the Tuzla/Kestanbol area on the Biga peninsula, the outflowing high concentrated thermal waters can, by their chemical and isotopic composition, be neither directly derived from infiltrated meteoric water nor from recent sea water (Mützenberg this volume). From the ob-

served chemical and isotopic composition of the water, it seems most probable that they represent mixtures between a deep lowly mineralised groundwater (containing no anthropogenic produced tritium) and a deep brine situated as connate water of probable marine origin at even greater depth. The mixed and heated water at greater circulation depth is driven to the surface by a buoyancy effect along the hydraulically conductive zones along the intersections of three major fault systems.

Clues for the interference of hot and mineral waters with tectonic activity and seismicity

It is now a quite new aspect to investigate the effects of active seismotectonic activity on the groundwater temperature, flow and quality (such as its chemical and isotopic composition). As such influences are short-term perturbations, the possible reactions consist of instationary, extremely time-dependent variations, or in abrupt but definitive changes of the observed parameters. The most reported known influences of earthquakes on groundwater systems concern changes of the hydrodynamic characteristics, such as changes of hydraulic head of wells (mainly artesian) and/or change of flow rate of springs and artesian wells. Such phenomenas are reported for all of the presented areas.

Origin, temperatures and flow rate: Cold groundwater / thermal water interrelation

Mixed waters which show interference of cold shallow and deep circulating thermal waters are observed if a kind of interface between the upwelling thermal water and the groundwater of local recharge exists. Such situations are described in Mützenberg (1991) and Mützenberg et al. (1992) for the *Tuzla* area as evidenced by the temperature and electrical conductivity. But by the comparison of the values of the stable isotopes δ^2H and δ^{18}O, and also of the tritium content, a distinct origin of local infiltration (on the local meteoric water line and containing anthropogenic tritium) or of deep fluid (deviated from the meteoric water line and containing no anthropogenic tritium) can be identified. Therefore, the theoretical definition of an unmixed endmember of deep origin is possible.

Within the investigated areas of *Bursa (including Çekirge),* mixing processes between shallow groundwaters of local infiltration and the occurring thermal waters are also described in Imbach (1992, this volume). With the parameters of electrical conductivity, tritium content and silica concentration, the unmixed tritium free endmembers of the thermal waters are determined.

Gradual mixing trends with respect to temperature, chemical composition (TDS), tritium content and stable isotopes are reported by Eisenlohr (1995) for the thermal and subthermal waters of the *Gemlik/Orhangazi* area circulating within karstic aquifers.

Mixing relations between local infiltrated shallow groundwater and the subthermal and thermal waters were also observed by Jeckelmann (1996) for the *Bergama* area based on the stable isotopes δ^2H and δ^{18}O and also on chemical composition.

Nearly unmixed thermal waters with very low tritium contents (near the detection limit) were observed for the almost naturally outflowing artesian thermal waters of the *Armutlu* and *Yalova* areas (Eisenlohr 1995).

In the *Kuzuluk* area, a nearly complete separation of the thermal and mineral waters and the shallow groundwaters was observed based on the stable isotopes (Greber 1992). Possible causes are: a) artesian overpressure, b) interaction with deep CO_2 and c) disconnection from the current day recharge. In this area, the natural undisturbed situation was still observed and described by Greber (1992). However, the situation may change under the recently begun forced artificial exploitation, as revealed by the investigations in the *Gönen* area (Yalçın 1997). Under such changed hydrodynamic conditions, long-term mixing processes are induced.

Short-term fluctuations: observations on electrical conductivity and temperature, seasonal variations

Short-term fluctuations of chemical and isotopic composition of groundwater other than the well-known influence of changing recharge conditions (e.g. due to precipitation events) on shallow groundwater systems as observed in, for example, karstic springs are not yet observed frequently enough. From the present studies, the following observations may be made:

For the *Bursa area,* Imbach (1992) reports periodical temperature and electrical conductivity measurements (with a 14 day interval) for one cold groundwater (Kültürpark) and 6 thermal springs of the Bursa Kükürtlü and Çekirge areas. In all of these waters, periodical variations of temperature and electrical conductivity were observed with a period of one year and maximal temperature and electrical conductivity values in August to September and minimal values in February and March (thermal waters of Hagia Fontini A, Bağhdemlibace, Zeyni'nene, Havuzlupark A and B), March to April (cold groundwater of Bursa Kültürpark) and May (thermal water of Oto kaplıca). The periodical variations in temperature can be explained by energy loss to the atmosphere, conductive cooling effects and mixing with shallow groundwaters within the discharge area of the naturally occurring springs or within the fissured travertine complex within the main spring outflow zones. The variation of the electrical conductivity is mainly due to mixing with small proportions of cold infiltration water, which explains some coincidence in the variations with the occurrence of precipitation. Some short-term fluctuations are also caused by hydraulic pressure change due to fast recharge within the Uludağ massif. Such a phenomenon is demonstrated by the strong storm event on 18 October 1989 which caused a sudden rise in the electric conductivity of the thermal waters of the Bursa area, which contain no anthropogenic tritium (Imbach 1992 and this volume).

The same kind of hydraulic phenomenon is discussed by Jeckelmann (1996) for the periodic (weekly) observations of Na and K contents (observation period 8.9.93 to 27.3.94) of the Çamurlu thermal waters. Such a rise in the Na and K contents, which coincide with the beginning of strong precipitation periods, can be explained by a sudden increase in hydraulic head within the recharge area leading to a pressure pulse in the deeper part of the thermal water aquifer causing the outflow (mobilisation) of deep seated more highly mineralised thermal water. However, the periodic (weekly) observations of the temperature variations (observation period 5.9.92 to 28.8.93) of the same Çamurlu thermal waters are more likely attributable to the saisonal variations in air (atmosphere) and soil temperature by conductive temperature loss (Jeckelmann 1996).

Also for the *Kuzuluk area,* periodic measurements of temperature (in a 14 days to one month rhythm) from September 1989 to September 1991 and of electrical conductivity were reported in Greber (1992). He observed two different kinds of temperature variations: periodic and non-periodic. The periodic fluctuations of 1° to 6°C are synchronous with regional air temperature fluctuations and can be explained by loss of temperature through conductive

cooling in the zone near the surface. As the variations of electrical conductivity of these investigated waters do not correlate with any of the observed temperature variations, mixing phenomena with cold shallow groundwater near the surface can be excluded. Also, the observed variations in the flow rate of these naturally outflowing springs do not correlate with either the temperature variations or with the observed variations of electrical conductivity. Therefore, with the exception of the conductive cooling in the areas of the rock near the surface, no other related processes seem to occur near the surface. However, the fact that variations of the flow rate, such as variations in electrical conductivity, exist indicate that other processes occur which are most likely related to the high amount of ascending CO_2 as evidenced by the observed outgassing at the surface in spring outflow areas (Greber 1992) and also the very high CO_2 gas overpressure in the Kuzuluk 2 borehole (Tschudi this volume).

For the *Yalova area*, the periodic measurements of temperature and electrical conductivity of the naturally outflowing thermal water (observation period July 1992 to September 1993, Eisenlohr 1995) show no influence of precipitation periods and only a slight influence of the seasonal variations of the atmospheric temperature caused by conductive cooling at the surface areas. Also, the periodic measurement of the temperature of the artesian well and the naturally outflowing thermal water of the Armutlu area (observation period March 1992 to September 1993, Eisenlohr 1995) reveals only slight influences of the seasonal variation of the atmospheric temperature caused by conductive cooling in the areas near the surface.

Historical observations: earlier signs of thermalism, change in place, altitude and chemistry, historical reports on influences of earthquakes on the situation of springs and flow rate

Tuzla area

The thermal activities around Tuzla cover a surface area of about $1km^2$. From the Upper Miocene to the Present, evidences of at least four thermal phases can be recognised in this area:

1. Red and black ferromanganese crusts intercalated in the Upper Miocene sediments with feeders along joint sets;
2. Silicified zones in sedimentary and volcanic rocks, probably associated with N-S striking faults;
3. Travertine terraces such as deposits of cooling water rich in carbonate;
4. Outflowing NaCl rich hot brines, which characterise the present hydrothermal activity.

Based on the structural pattern of the major fault systems (Fig. 1 of Mützenberg this volume), it can be recognised that the origins of the thermal springs within the three investigated areas coincide with the intersection of the following three systems: i) NNE-oriented dip-slip fault zones, ii) major NE-SW striking, right lateral strike-slip faults, iii) sets of NW-SE oriented joints/faults cutting through all three thermal areas.

From these observations, it may be concluded that, due to the resulting increase in vertical permeability, the intersections of these three major faults systems represent the actual flow path for the rise of the thermal water from the deep reservoir through the nearly impermeable cover of Miocene volcanics to the spring origins at the surface (Mützenberg this volume).

The outflow zones of the thermal brines are situated at about 20 to 30m in the Kestanbol area and at 20 to 80m above sea level in the Tuzla area. In both areas, springs of lowly mineralised fresh water at lower temperatures are observed at the same level or at slightly higher alti-

tudes. They represent the outflowing local groundwater recharged and circulating in the fissured rocks of the intrusion of the quartz-monzonite and eventually also in Miocene sediments in the Kestanbol, or in layers of increased permeability within the volcanic sediments in the Tuzla area, respectively. According to historical records, effects of earthquakes as displaced spring sites, but also the disappearance of an ancient geyser (probably caused by a drop in the hydraulic pressure head) in the Tuzla canyon are reported in Mützenberg (1991), at a place where today only some low outflowing hot springs remain. Since 1990 to 1996 a successive displacement of spring outflow areas is observed (Schindler pers. com.)

Bursa area

As pointed out by Imbach (1992), according to descriptions of the thermal springs by Grisebach (1841), Smith (1851) and Fritsch (1882) compared to his own observations, no change in spring outflow sites and temperature has occurred from the last century to the present. However, fluctuations over short periods were reported for earthquake activity in the years around 1850 (see Imbach this volume). In the long-term range from the Late Quaternary to the present and according to the geological evidence and the location of the travertine terraces, changes of the hydraulic head and flow rate displaced the most highly elevated spring outflow zones downward from the uppermost part of the travertine terraces more to the valley plain (Imbach 1992).

Kuzuluk area

From the geological investigations the change from a high temperature to a low temperature geothermal regime was reported by Greber (1992, 1994, this volume). Evidences for such phenomena are silicified wood and gravels cemented by chalcedony of Neogene age (Kuzuluk formation, Greber 1992). From historical records, it is known that ancient spring sites used for thermal spas have either disappeared (the springs dried up completely) after the strong earthquake event of 1967, or were displaced, as evidenced by thermal springs yielding at new locations. In the old spa area, some zones of high CO_2 emanations have been detected by E. Greber through soil gas measurements (Greber 1992).

Bergama area

A sudden emergence of steam and hot boiling water within the area of Kaynarca/Dikili was reported as a reaction to the strong earthquake event of 21 September 1937 (Birand 1940, Ketin 1948). Geological evidences of former tectonic and hydrothermal activities are mentioned in Jeckelmann (1996): silicified Pliocene sediments at Bademli springs and the occurrence of a travertine deposit within a higher elevated basalt flow of younger than Pleistocene age at Nebiler.

Armutlu peninsula

A substantial decrease in the flow rate of the springs of the Yalova spa as a reaction to the Çınarcik earthquake of 1963 (M=6.2) was reported.

Gönen area

Strong earthquakes occurred in 1953 (M=7.4) and 1969 (M=5.8). Although about 1750 earthquakes were recorded for the period of 1900 to 1990, a certain lack of information on hydrological phenomena may be due to the fact that the thermal springs are situated on fault zones within a graben structure in a depression basin. As in such a hydrological situation more short-term fluctuations have to be considered, it is not possible to figure out such changes in the thermal system caused by earthquakes without systematic periodic or even continuous observations.

Current short-term variations

The selection of sensitive spring sites was performed based on observed properties revealed by the periodic measurements. Change of chemical composition (such as electrical conductivity or concentration of specific ions) which coincide with beginning of strong precipitation periods can be explained by a sudden increase in hydraulic head within the recharge area leading to a pressure pulse in the deeper part of the thermal water aquifer causing the outflow (mobilisation) of deep seated, more highly mineralised thermal water.

The selected areas of observation were:

The Kuzuluk basin (area of the İTÜ/ETH MARMARA Poly-Project and of the Joint Turkish – German Earthquake Investigation Project) and the Bursa/Çekirge thermal provinces (area of the joint ITÜ/ETH Earthquake Investigation Project within the MARMARA project, compare this volume).

Kuzuluk basin

Piezometers were installed as part of the MARMARA project at two geothermal wells at Kuzuluk in order to monitor pressure variations in the active hydrothermal system. Both wells yielding artesian CO_2 rich thermal water at a temperature of about 82°C were pressurised in the closed state of the boreholes by about 2.5 bars and 6 bars, respectively. To monitor both, the occurring earthquakes but also the anthropogenic perturbations, an accelerometer was installed between the two boreholes situated at a distance of about 50m from each other.

The evaluation of the piezometric records of the water pressures of the two wells (Tschudi this volume) and of the accelerometer records lead to the following conclusions: The observed high frequency variations of the pressure data have to be explained by human activity influences (e.g. instability of electrical current of the official distribution network). The low frequency variations, which do not correlate with earth tides but only with the atmospherical tides S_1 and S_2, are explained to be most probably controlled by a complex reaction of the uppermost layers of the thermal aquifer (low permeable, confining beds acting as a so-called cap rock, which consist of ignimbrites, volcanic tuffs and tuffites as identified by Greber (this volume)).

This reaction of the bedrock with respect to the thermal water which is highly pressurised by the upwelling CO_2 from depth, may be a valve like behaviour, named a *geological valve system* by Tschudi (this volume). It is thought to act in the following manner: the hydraulic pressure is composed of the fluid and the CO_2 gas pressure, as at the shallow depth of the upper part of the thermal aquifer a separation of the gas water phase occurs caused by the high amount of CO_2, as evidenced by the boreholes 250 to 160m in depth. If the hydraulic total pressure increases above the hydraulic mechanical resistance of the caprock, some distinct fractures will be opened temporarily and therefore release some CO_2, but also some hot thermal water, until the pressure within the thermal aquifer is reduced to the remaining elastic resistance of the rock-fracture system, which will diminish the release of gas and fluid. As it is the pressure difference between the thermal water and CO_2 gas below the caprock and the atmosphere which acts as a threshold value for the mechanical/elastic behaviour of the caprock, these release events which are recorded as sudden pressure drops at the two thermal wells are linked to the atmospheric/meteorological pressure variations of the so-called atmospheric tides. As the Radon-222 noble gas moves with the CO_2 gas as a carrier, systematic links between pressure variations at the boreholes and the continuous ^{222}Rn monitoring of a spring site at Kuzuluk (installed by the Turkish-German-Earthquake Project, Woith 1996) were also checked. Within some unfortunately rare overlaps of the recording operation of the 2 monitoring stations, this systematic link was confirmed by some common anomalies (Tschudi this volume). But a direct relation of this valve-like behaviour with occurring earth-

quakes could not be confirmed. Reasons for this may be i) the occurrence of only small earthquakes in the successful period of observation and ii) events too far away, as also iii) the large amount of 'natural noise' caused by the action of the 'geological valve' and the sometimes high anthropogenic noise.

Bursa thermal province

The *Bağdemlibahce thermal spring* which feeds the thermal baths of Yeni kaplıca, was already observed by periodic measurements by Imbach (1992). Based on these observations, it was decided to install a permanent monitoring station. In two periods from Spring 1994 to Autumn 1995, and from Spring 1995 to Spring 1996, continuous measurements of temperature and electrical conductivity were carried out. However, in contrary to the aspect obtained by the periodic measurements as reported in Imbach (1992), no systematic variations which correlate either with meteorological records such as precipitation or air temperature or even with microearthquakes as recorded by the seismological group of the ETH/İTÜ MARMARA project during the observation period could be confirmed. The observed variations up to the present could not be interpreted, especially as external influences and disturbances such as electrical current instability and periodic manipulations (undertaken in the sense of maintenance of the electrodes of the conductivity measurement by the local technician of the spa), on the spring outflow and also on the electrical sensors and recording unit could not be excluded. Therefore, no final conclusion with respect to these continuous recordings can be made.

Çekirge thermal province

Through the installation of a continuous recording of the water level on an unused well belonging to the Turkish government (with confined but not artesian aquifer conditions) within the area of occurrence of the Çekirge thermal waters, it was possible to monitor changes in the groundwater level. According to the available records of the monitored variations of the groundwater level, it results that the Çekirge geothermal system is effectively influenced hydraulically by the shallow groundwater system (Greber et al. this volume). It directly reacts on distinct precipitation and recharge events. The observed short-term variations seem to be more influenced by the level changes of the directly overlaying shallow groundwater system, whereas the long-term variation are related to precipitation events of the whole recharge area (Mount Uludağ).

CO_2, water and gases in fault zones

As described for the Kuzuluk thermal water, CO_2 may be released from confined aquifers pressurised by CO_2 through a mechanical elastic release or the opening of fractures under pressure and acting as a so-called 'geological valve' as described for the interpretation of the pressure variations at the 2 Kuzuluk thermal boreholes (Tschudi this volume). If the thermal water is under artesian conditions, CO_2 gas and water will be released at the soil surface bringing about small springs as observed in the Kuzuluk area (Greber 1992, this volume). Under confined but not artesian conditions, only the CO_2 gas but no water will occur at the surface along major fracture zones. This fact can now be used to detect active fault zones by a systematic survey of the CO_2 gas concentration in the subsoil. This method to detect fault zones was successfully applied in the Kuzuluk, Bursa/Kükürtlü, and Gemlik/Orhangazi areas.

In the Kuzuluk area, this method was applied (using the Dräger Gas-Probe equipment) south of the Kay 18 spring with the aim of determining a potential NW-SE striking fault zone which was postulated according to the geological mapping, but was buried in the investigated area by alluvial sediments (Greber 1992). By this method it was possible to measure the CO_2 gas

concentration in the soil semi-quantitatively along a transversal profile. The measured CO_2 gas concentrations in the soil varied from about 2vol% (usual values for soils with biological activity) over the alluvial sediments to concentrations of up to 20 or even 30vol% at the crossing of the fault zone within an about 20m large area. Afterwards, at the other side more distant to the supposed fracture zone, the level fall on the initial concentration of about 2vol%.

A similar application was also made in the Bursa/Kükürtlü thermal area to determine a tectonic contact zone between different geological units. In that case, the soil was more loamy, which results in more difficult conditions for the uprising CO_2 gas. The measured values were in this case on the order of 1 to 2vol% in the normal soil zone, rising up to about 4 to 5vol% in the area of the supposed potential fracture zone only.

Another more successful application is described in Eisenlohr (1995), who applied this soil CO_2 gas method to localise a supposed fault zone in the plain of Gemlik, about 100m east of Gemlik kaplıca. According to the measured CO_2 profile a significant increase of the CO_2 in the soil gas of up to 18vol% was detected in the area of the fault zone, where the normal level in the areas not affected by the fault zone yielded CO_2 concentrations in the soil gas at the usual level of about 2vol%.

Conclusions

Indications of deep origin

In all of the investigated areas of Kuzuluk, Bursa, Yalova/Armutlu, Gönen, Bergama and Tuzla/ Kestanbol, in most of the thermal waters enhanced CO_2 gas concentrations were detected (Figs. 1, 2 and 3), which are signs of enhanced tectonic activity. According to the $^3He/^4He$ ratios of the dissolved helium, some amount of gases originating from the Earth's mantle of up to about 20% was present in the analysed thermal waters, as was also observed in thermal waters of other tectonic active areas (Marti et al. 1992, Balderer and Martinelli 1995, Güleç 1988). These conclusions are also confirmed by the isotopes of CO_2 and CH_4 (Jeckelmann 1996).

Waters

Old waters not connected to current recharge were observed in deep graben structures or depression basins, such as Kuzuluk and Gönen. For the Menteşe thermal water, the exact hydrogeological situation is not known well enough, but it seems to be situated in a local graben structure. Up to the investigated period, undisturbed conditions were prevailing within the Kuzuluk basin. In contrast, the Gönen deep thermal waters have been in use for over 10 years. The steady drop in the groundwater levels led to the installation of a reinjection facility in order to maintain the water balance of this deep groundwater.

The normal situation of a geothermal system with recharge in areas of higher altitudes, circulation to greater depth and fast ascent along fault zones leading to the formation of thermal springs in low altitude areas, such as gorges or valley flanks or deep lying plains, is observed in most of the investigated areas, i.e. Bursa, Yalova/Armutlu, Gemlik/Orhangazi and Bergama.

The occurrence of onshore highly concentrated hot brines was observed in the Tuzla/Kestanbol area and, to a much smaller extent, at the hot spring Bademli (Bergama) occurring in the shore area. These highly concentrated hot thermal waters are related to the migration of deep fluids (as formation water) from the Tertiary sediments within the shore area of the Aegean sea to the outcropping crystalline basement.

Current processes related to active tectonic

From the presented interpretation of the applied isotopic and hydrochemical methods, the following information results with respect to ongoing hydrodynamic processes and the relationship to the driving forces of the active tectonic:

- The hydrochemical and isotopic investigations (^{36}Cl method) of the Tuzla and Kestanbol thermal water indicate that these deep seated brines of sedimentary origin have been moving within the underlying crystalline rocks at least for about the last 1m.y.
- The brine (formation water or seawater encroachment) outflowing at the Bademli thermal spring yields a residence time for moving within the crystalline basement of about 10'000 years.
- Driving forces for the mobilised brines occurring in thermal waters are changes in the tectonic stress, and eventually other effects, such as change of hydraulic reference datum by sea level changes also.
- In the deep graben structure of Gönen the reverse process of slow replacement/dilution of the actual deep water (of recharge under colder climatic conditions) by water of recent infiltration (under recent climatic conditions) is observed. This reverse process of dilution of nearly stagnant deep groundwaters by post Pleistocene water would indicate a more accentuated defragmenting of the western part of the Marmara area by the extensional regime.
- Several indications point to ongoing mixing processes along the regional flow path of the deep thermal waters: the values of sulphate often present mixtures between sedimentary sulphate and sulphate originating by oxidation of primary sulphide minerals of crystalline origin!
- According to the chemical constituents and isotopic signatures of the investigated thermal and mineral waters, the possibility exists to separate different water bodies of different origin:

a) groundwater of local origin by infiltration in the surrounding areas of the thermal springs at higher altitudes (e.g. Uludağ)

b) a deep brine endmember of sedimentary origin (in secular equilibrium for ^{36}Cl underground production, which means a residence time in the current position within the rock of the actual flow system of more than 1.5m.y.). Such fluids can potentially be derived from marine transgression periods temporarily invading coastal areas at low altitudes (depression zones) and causing a sea water influx on the land surface (in Miocene to Pliocene period, Schindler this volume)

c) a brine of sedimentary origin (as formation water with low ^{36}Cl/Cl ratios as evaporite salt or seawater) which is actively moving from the seashore into the continental basement (yields ^{36}Cl/Cl ratios which are not in equilibrium with the rock of the actual flow system and inferred residence time of less than 1.5 million years)

d) deep groundwater of infiltration within the recharge areas in periods of changed climatic conditions which is actually diluted by young lowly mineralised water.

- These facts now define flow regimes of deep groundwaters of regional flow systems which show signs of interrelationships with local and intermediate flow systems, as indicated by the observed mixing processes of chemical constituents and isotopes. The deep flow systems are interconnected locally by tectonic short cuts resulting from deep faulting with open fractures (due to the observed extensional regime) which contribute more shallow circulating groundwater of intermediate and local flow systems.

- Hydrothermal activities are evidenced in the Tuzla/Kestanbol area since the Neogene period, at least since the last 6 to 8m.y. (Mützenberg 1990, this volume). However, the youngest geothermal cycle responsible for the present active occurrences of outflowing hot thermal brines is a recent process. By this process which could be caused by the compaction of the younger sediments within the Aegean sea sedimentary brines of the contained pore fluid are migrating into the underlying crystalline rocks.
- As seen, from this study, the application of several methods for the determination of the residence time with long-lived isotopes which are different in chemical behaviour and half-life can yield important information on different hydrogeological aspects of the same analysed deep groundwater.

References

Balderer, W., 1985, Sondierbohrung Böttstein: Ergebnisse der Isotopenuntersuchungen zur hydrogeologischen Charakterisierung der Tiefengrundwässer, Nagra, Tech. Ber. NTB 85-06, Nagra, Baden, Switzerland, 260p.

Balderer, W., Fontes, J.Ch. and Michelot, J.L., 1987, Isotopic investigations of the water-rock system in the deep crystalline rock of Northern Switzerland, in: Saline water and gases in crystalline rock, edited by: P. Fritz and S.K. Frape, Special paper 33, Geological Association of Canada.

Balderer, W., Pearson, F.J., Fontes, J.Ch., Michelot, J.L. and Soreau, S., 1990, ^{34}S and ^{18}O in SO_4 as Indicators of the Origin of Deep Groundwaters in Northern Switzerland, MEMOIRES of the 22nd Congress of IAH, Vol. XXII, Lausanne, 364-373.

Balderer, W., Pearson, F.J. and Soreau, S., 1991, Sulphur and Oxygen Isotopes in Sulphate and Sulphide, Chapter 7.1 in: Pearson, F.J., Balderer, W., Loosli, H.H., Lehmann, B.E., Matter, A., Peters, T., Schmassmann, H., Gautschi, A, Applied Isotope Hydrogeology – A Case Study in Northern Switzerland, in: Studies in Environmental Science 43, ELSEVIER, Amsterdam, Oxford, New York, Tokio 1991, 297-322.

Balderer, W. and Martinelli, G., 1995, Geochemistry of groundwaters and gases occurring in the November 23, 1980 earthquake area (South Italy), Journal of Geochemistry and Health, special volume.

Balderer, W. and Synal, H.-A., 1996, Application of the chlorine-36 method for the characterisation of the groundwater circulation in tectonically active areas: Examples from North Western Anatolia / Turkey. Terra Nova, 8, 324-333.

Balderer, W. and Synal, H.-A., 1997, Use of Chlorine-36 as Tracer for the Evolution of Waters in Geothermal and Tectonic Active Areas in Western Turkey. Nuclear Instruments and Methods in Physics Research, B (NIMB), Elsevier Science, B.V.

Barnes, I., Irwin, W.P. and White, D.E., 1978, Global distribution of Carbon Dioxide, discharges and major zones of seismicity, U.S. Geological Survey water resources investigations, Open-File report, 12, 78-79

Birand, S.A., 1940, Dikkili Zelzelsi . Yükseklik ziraat Enst. Calismalarindan, sayi 51, 19-26.

Blattner, P., 1993, "Andesitic" Water": a phantom of the isotopic evolution of water-silicate systems, Comment on "Isotopic shifts in waters from geothermal and volcanic systems along convergent plate boundaries and their origin" by W.F. Giggenbach, Earth and Planetary Science Letters 120 (1993) 511-511.

Clayton, R.N., Friedman, I., Graf, D.L., Mayeda, T.K., Meents, W.F. and Shimp, N.F., 1966, The origin of saline formation waters, J. Geophys. Res. 71/16.

Craig, H., 1954, Carbon-13 in plants and the relationship between carbon-13 and carbon-14 variations in nature, J. Geol., 62, 115.

Eisenlohr, Th., 1995, Die Thermalwässer der Armutlu-Halbinsel (NW-Türkei) und deren Beziehung zu Geologie und aktiver Tektonik, Diss. ETH-Zürich, Nr. 11340.

Eisenlohr, Th., this volume, The thermal springs of the Armutlu peninsula (NW Turkey) and their relationship to geology and tectonic.

Eisenlohr, T., Jeckelmann, Ch., Balderer, W., Bernasconi, S., Rauert, W. and Trimborn, P., this volume (a), Regional investigation of cold groundwater for the determination of the recharge conditions in geothermal areas of Northwestern Turkey, International symposium on Isotopes in Water Resources Management, IAEA-SM-336/22, International Atomic Energy Agency, Vienna, March 1996, Vol. 2, 431-437.

Eisenlohr, T., Pfister, M. and Balderer, W., this volume (b), Environmental isotope study and 2-D-modelling of cold and thermal karst within the Gemlik (Bursa) area of Northwestern Turkey.

Fontes, J.Ch., 1976, Isotopes du milieu et cycles des eaux naturelles: quelques aspects, Thèse de Doctorat dès-Sciences, Université P. et M. Curie, Paris, 228p.

Fontes, J.Ch. and Michelot, J.L., 1985, Stable isotope geochemistry of sulfur compounds, in: Hydrogeological and Hydrochemical Investigations in Boreholes, Final Report of the Phase 1 Geochemical Investigations of the Stripa Groundwaters, Nordstrom, D.K. Ed. Stripa Project Technical Report 85-06, SKB Stockholm, 7:1-7:17.

Fontes, J.Ch., 1992, Application des techniques isotopiques dans l'hydrogéologie, cours Université de Neuchâtel.

Fournier, R.O., 1981, Application of water geochemistry to geothermal exploration and reservoir engineering, in: Geothermal systems: Principles and Case Histories, edited by: L. Rybach and L.J.P. Muffler, Wiley New York, 109-143.

Fritsch, K. von, 1882, Acht Tage in Kleinasien, Mitt. Vereins Erdkunde zu Halle a./S., 101-139.

Gat, J.R., 1983, Precipitation, groundwater and surface waters: Control of climate parameters on their isotopic composition and their utilisation as paleoclimatological tools, in: Paleoclimates and Paleowaters: A collection of Environmental Isotope Studies, International Atomic Energy Agency, IAEA, Vienna, 3-12.

Giggenbach, W., F.,1992, Isotopic shifts in waters from geothermal and volcanic systems along convergent plate boundaries and their origin. Earth and Planetary Science Letters, 113 (1992) 495-510.

Gonfiantini, R., 1971, Notes on isotope hydrology, International Atomic Energy Agency, IAEA, Vienna, 45p.

Greber, E., 1992, Das Geothermalfeld von Kuzuluk / Adapazari (NW-Türkei), Geologie, aktive Tektonik, Hydrogeologie, Hydrochemie, Gase und Isotope, Diss. ETH-Zürich Nr. 9984.

Greber, E., 1994, Deep Circulation of CO_2-rich Paleowaters in a Seismically Active Zone (Kuzuluk/Adapazari, Northwestern Turkey). Geothermics, Vol. 23, No. 2, 151-174.

Greber, this volume: Stratigraphic evolution and tectonics in a area of high seismicity: Akyazi Adapazari (Pontides, Northwestern Turkey).

Greber, E., Pfister, M., and Imbach, Th., this volume, Hydraulic level variations in a thermal water well: Impact of precipitation on the Çekirge thermal water system.

Grisebach, U., 1841, Reise durch Rumelien und nach Brussa im Jahre 1839, Bd. 1 und 2, Göttingen.

Güleç, N., 1988, Helium-3 distribution in western Turkey, Bull. of the Mineral Research and Exploration, 108, 35-42.

Hoeffs, J., 1997, Stable Isotope Geochemistry, 4th ed., Springer.

IAEA, 1983, Isotope techniques in the hydrogeological assessment of potential sites for the disposal of high-level radioactive wastes, IAEA Technical Report Series No 228, Vienna.

IAEA, 1969, 1971, 1973, 1975, 1979, 1981, 1983, 1986, 1990, 1994, Environmental Isotope Data No. 1- 10: Survey of Isotope Concentration in Precipitation, International Atomic Energy Agency, Vienna.

Imbach, Th., 1992, Thermalwässer von Bursa. Geologische und hydrogeologische Untersuchungen am Berg Uludağ (NW-Türkei), Diss. ETH-Zürich Nr. 9988.

Imbach, Th., this volume, Geology of Mount Uludağ with emphasis on the genesis of the Bursa thermal waters, Northwestern Anatolia, Turkey.

Jeckelmann, Ch.,1996, Genese lokaler Thermalwasservorkommen in der Region Bergama/W Türkei, Diss ETH Zürich Nr. 11990.

Kharaka, Y.K. and Carothers, W., 1986, Oxygen and hydrogen isotope geochemistry of deep basin brines, in: The terrestrial environment, B., edited by: P. Fritz and J.C. Fontes, in the collection: Handbook of environmental isotope geochemistry, 5, 305-360.

Ketin, I.,1948, Die grossen anatolischen Erdbeben in den letzten zehn Jahren, Urania, Vol. 11/6, 230-235.

Kipfer, R., 1991, Primordiale Edelgase als Tracer für Fluide aus dem Erdmantel, Ph.D. thesis, ETH Zürich, 223p.

Lloyd, R.M.,1968, Oxygen Isotope Behaviour in the Sulphate-Water-System, J. Geophys. Res. 73/18, 6099-6110.

Marty, B., O'Nions, R.K., Oxburgh, E.R., Martel, D. and Lombardi, S., 1992, Helium Isotopes in Alpine Regions, Tectonophysics, 206, 71-78.

Michelot, J.L., 1988, Hydrologie Isotopique des Circulations Lentes en milieu cristallin fracturé: Essai Methodologique, Thèse de Doctorat dès Sciences Nr. 3446, Université de Paris-Sud, Orsay, France.

Mizutani, Y. and Rafter, T.A., 1969, Oxygen Isotopic Composition of sulphates – Part 3. Oxygen Isotopic Fractionation in the Bisulphate Ion water System, New Zealand J. of Sc., 12.

Mützenberg, S., this volume, Nature and origin of the thermal springs in the Tuzla area, Western Anatolia, Turkey.

Mützenberg, S., 1991, Westliche Biga-Halbinsel: Geologie,Tektonik und Thermalquellen (Canakkale,Türkei). Mitt. Geol. Inst. der ETH und der Universität Zürich, Nr. 287.

Mützenberg, S., Balderer, W. and Rauert, W., 1992, Environmental isotope study of saline geothermal systems in western Anatolia, Çannakkale, Turkey, Water-Rock Interaction, edited by: Kharaka and Maest, Balkema, Rotterdam. ISBN 90 5410 075 3, Vol. 2, 1317-1320

Pearson, F.J. and Balderer, W., 1991, Isotopic composition of carbonate minerals and water, in: Pearson, F.J., Balderer, W., Loosli, H.H., Lehmann, B.E., Matter, A., Peters, T., Schmassmann, H., Gautschi, A, Applied Isotope Hydrogeology – A Case Study in Northern Switzerland, in: Studies in Environmental Science 43, ELSEVIER, Amsterdam, Oxford, New York, Tokio 1991, 297-322.

Pearson, F.J., Balderer, W., Loosli, H.H., Lehmann, B.E., Matter, A., Peters, T., Schmassmann, H. and Gautschi, A, 1991, Applied Isotope Hydrogeology – A Case Study in Northern Switzerland, in: Studies in Environmental Science 43, ELSEVIER, Amsterdam, Oxford, New York, Tokio 1991, 297-322.

Pezdic', J., Dolonec, T., Zizek, D., Fritz, P. and Wolf, M., 1991, Origin and transport of CO_2 in the highly mineralised water system of the Pannonian Tertiary Basin (Northeast Slovenia), IAEA-SM-319/58P, International Atomic Energy Agency, IAEA, Vienna, 1992.

Pfister, M., 1995, Geothermische Untersuchungen in der Region Marmara, Kartierung des Wärmeflusses und hydrothermal Modellrechnungen, Diss. ETHZ Nr. 11054.

Pfister, M, Balderer, W., Greber, E., Kahle, H.-G., Mayer-Rosa, D., Mueller, St., Rybach, L., Sellami, S., Schindler, C. and Straub, C., this volume (a), Synthesis of the Poly-Project MARMARA.

Pfister, M., Rybach, L. and Şimşek, Ş., this volume (b), Geothermal reconnaissance of the Marmara sea region.

Reardon, E.J. and Fritz, P., 1978, Computer Modelling of Groundwater ^{13}C and ^{14}C Isotope Compositions, Journal of Hydrology, 36, 201-224.

Savin, S.M., 1980, Stable isotopes in climatic reconstruction, Eos, Transactions, American Geophysical Union. 61; 17, 249.

Schindler, C., this volume, Geology of NW Turkey: Results of MARMARA Poly-Project.

Smith, J.L., 1851, On Some of the Thermal Waters of Asia Minor, Am. J. Sci. Art., second series 12, 10-16.

Straub, Ch. and Kahle, H.-G., this volume, Recent crustal deformation and strain accumulation in the Marmara sea region, N.W. Anatolia, inferred from repeated GPS measurements.

Stuiver, M. and Polach, H.A., 1977, Discussion on Reporting of ^{14}C Data, Radiocarbon, Vol. 19, No. 3, 355-363.

Truesdell, A.H., 1975, Summary of Section-III- Geochemical Techniques in Exploration. – Second United Nations Symposium on the Development and Use of Geothermal Resources, San Francisco, May, 1975, 1, 1iii-1xiii.

Tschudi, S., this volume, Observed pressure variations and their causes in the geothermal field of Kuzuluk/NW Turkey

Wigley, T.M.L., 1975, Carbon-14 dating of groundwater from closed and open systems. Water Resources Res., 11, 324-328.

Wigley, T.M.L., Plummer, L.N. and Pearson, F.J., 1978, Mass transfer and carbon isotope evolution in natural water systems, Geochim. Et Cosmochim. Acta, Vol. 42, 1117.

Woith, H., 1996, Spatial and temporal variations of radon in ground air and ground water within the Mudurnu valley, NW Turkey, A contribution to the Turkish- German joint project on earthquake research, Dissertation Christian- Albrechts- Universität Kiel.

Yüzer, E., his volume, Hydrogeology of Northwestern Turkey.

Yalçın, T., this volume, Hydrogeological investigation of the Gönen and Ekşidere thermal waters (NW Turkey).

Yalçın, T., 1997, Hydrogeological investigation of Gönen and Ekşidere thermal waters (Balıkesir). Ph.D. thesis, ITÜ, Istanbul, Turkey.

follows the orientation of the northern fault line in the Marmara sea and its continuation towards the gulf of Saros. This area of highest shear corresponds well to the distribution of major historical seismic events (inset of Figure 27). In the central Marmara sea, there seems to be a local minimum of strain, this originates from the lack of data in this area. However, the deformation zone is wider than along the rest of the NAFZ and therefore the strain probably decreases.

The area around 40°N generally shows lower shearing processes. Hardly any shearing was detected on the Biga peninsula. However, considerable shear occurs near Bursa (29°E) and Gönen (27.5°E). These shears are caused mainly by a strong compressional component directing WNW. The compression near Gönen corresponds well with the fault plane solution of the March 3, 1969 earthquake. The complementary direction of strike, with sinistral sense of motion, is of less importance for the overall tectonic pattern. Nevertheless, the computed direction for sinistral shear (N-S, NW-SE) confirms sinistral motion along a fault structure in the Marmara sea that strikes in this direction, as suggested by Wong et al. (1995). The southernmost area (<39.5°N) is governed by strong extension, directing NW-SE in the east turning to almost N-S in the west. This extension is associated with minor left-lateral shear. At first sight, this seems to be strange behaviour. However, geologic field work (Jeckelmann 1996) and investigations of the complex system of normal faulting in western Turkey (Westaway 1994) indicate similar results. Westaway suggested bi-axial extension in western Turkey based on the multiple orientations of graben-structures. Unfortunately, the three southernmost GPS sites were reoccupied only once. In general, it must be stated that local findings might be influenced by deficiencies in the GPS results. Thus, the interpretation of local phenomena can be misleading. There certainly is a need for more repetitions of the GPS measurements.

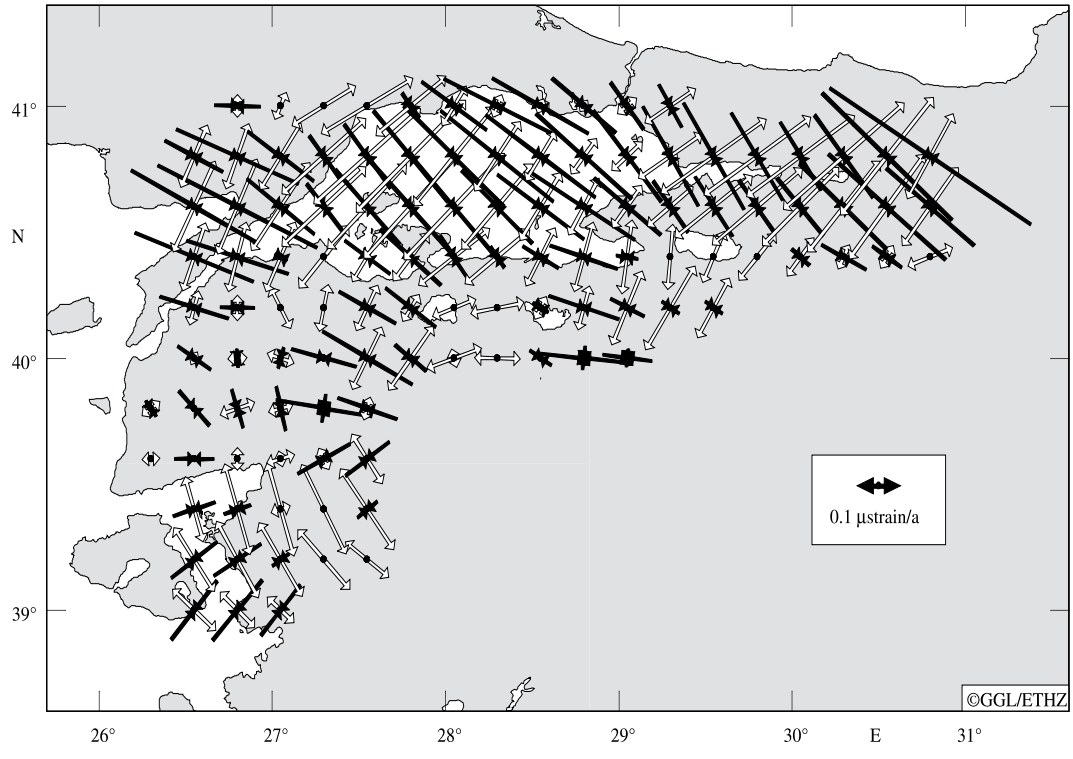


Figure 21: Normal strain rates derived from the GPS measurements. White arrows indicate extension; black arrows show compression. The length of the arrows indicate the strength of the strain rate. The average extension strain rate is 0.11µstrain/a (max. extension: 0.31µstrain/a). The average compression is -0.12µstrain/a (max. compression: -0.47µstrain/a). Points without arrows represent very low strain rates.

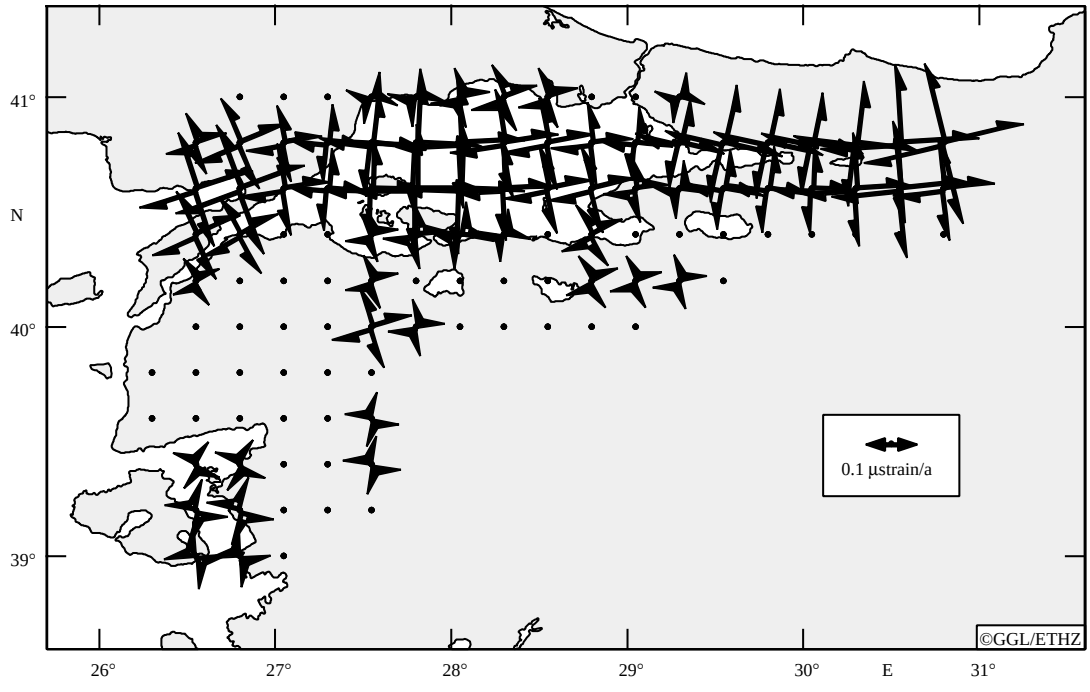


Figure 22: *Shear strain rates derived from the GPS measurements. The length of the arrows indicate the strength of the strain rate. The average shear strain rate is 0.11µstrain/a (maximum shear: 0.31µstrain/a). Points without arrows represent very low strain rates.*

Stress

The stress tensor was determined using the strain stress relationship. The elastic properties of the upper crust (≈10km) were determined using average seismic wave velocities (compressional: v_p=5.79km/s, shear: v_s=3.35km/s) and an average density (ρ=2.73g/cm^3) for western Anatolia (Alptekin et al. 1990). These properties were applied to the whole region. The calculations based on a homogenous material has led to similar results as the strain analysis. A more detailed division into regions of different material properties would be interesting but the data needed is not available. The stress presented corresponds to the time period between 1990 and 1996. One must keep in mind that the strain stress conversion can lead to stress in the third component (up-down). Thus, the shear stress (Figure 23) gives information where we can expect major contributions of normal faulting. Together with the normal strain, the type of faulting can be determined (extension or compression). Major extension can be seen near lake İznik (N-S) and lake Kuş (E-W) and east of Ayvalık/Edremit NW-SE). Compression is found west of Gönen (WNW-ESE).

The maximum shear stress and the density of strain energy are of great importance because they give information about the size of accumulated stress or energy and can be used as an indicator for areas of enhanced seismicity. However, the time interval of 6 years of observation is very short. Figure 24 displays the distribution of the amount of maximum shear stress in [kN/m^2]. This corresponds to the extreme values of the shear stress shown in Figure 23.

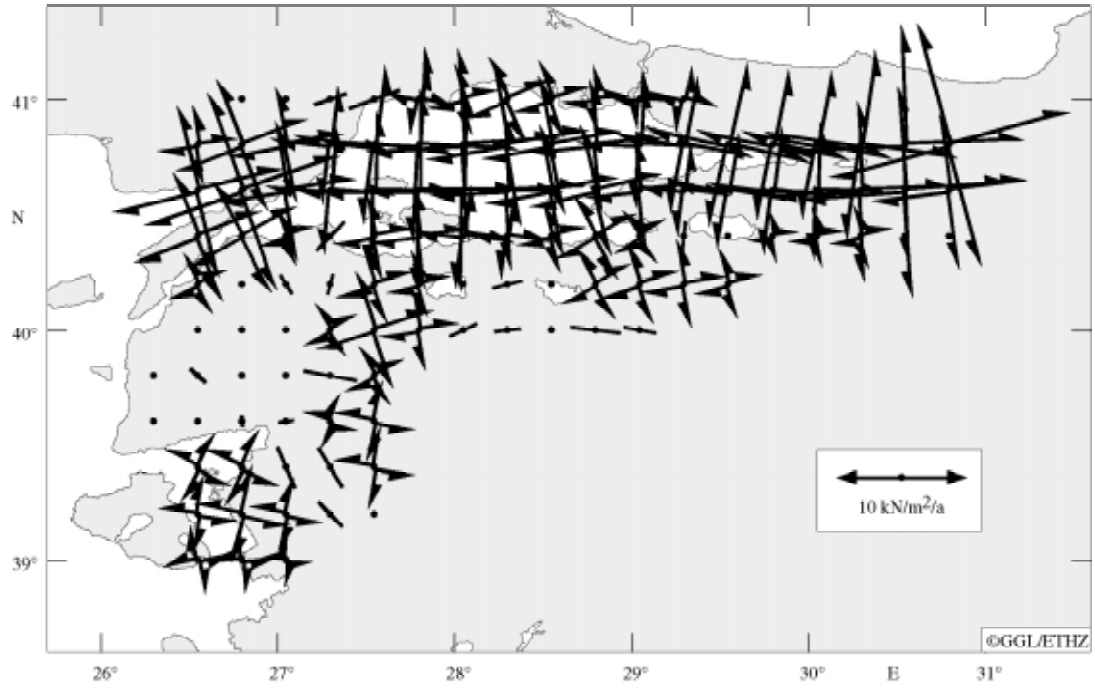


Figure 23: *Shear stress rates derived from the GPS measurements. The length of the arrows indicate the strength of the stress rate in [kN/m^2]. The average shear stress rate is 7.1kN/m^2 (max. shear: 19.2kN/m^2). Simple black bars without arrows indicate the direction of major normal faulting. Points without arrows represent very low strain rates.*

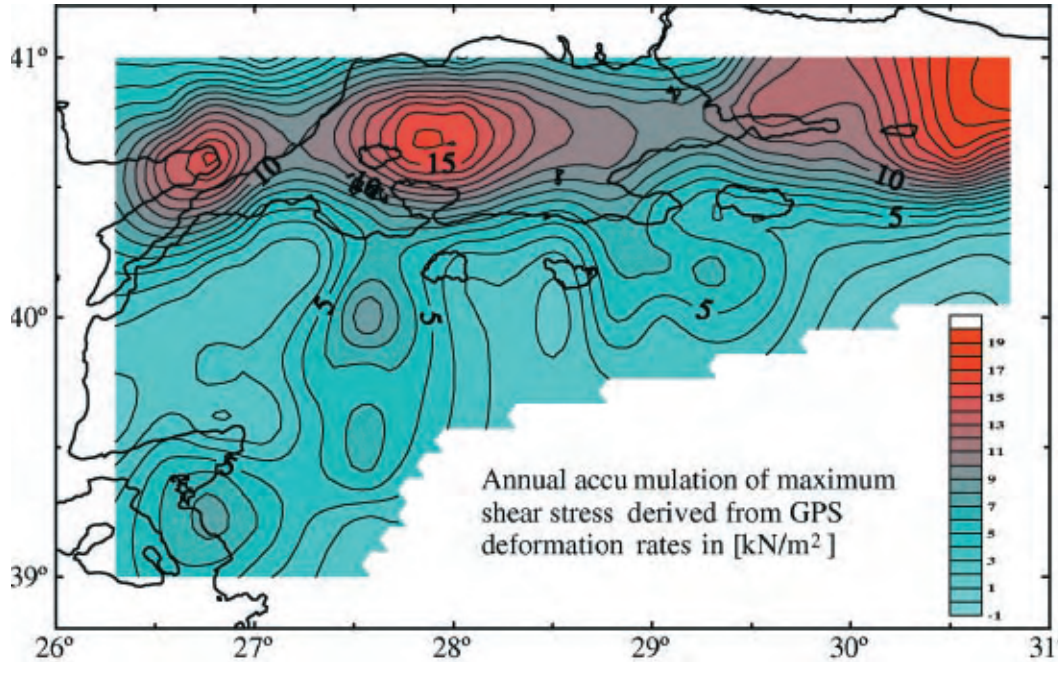


Figure 24: *Annual accumulation of maximum shear stress in [kN/m^2], showing the high stress along the northern zone of the splayed NAFZ. The average value is 7.1kN/m^2 (max. 19.2kN/m^2).*

The density of strain energy

The density of strain energy is given in Figure 25. The overall picture is similar to the distribution of shear stress. However, there are some important differences. The shift of the maximum in the south-western area reveals important contributions of normal faulting. The areas of high maximum shear stress are concentrated along the northern zone of the splayed NAFZ. The apparent local minimum in the Marmara sea is caused by the lack of information about this area. However, it can be expected that enhanced shear stress could be observed all along the northern zone of the NAFZ. The deformation zone in the Marmara sea (Figure 3) is considerably wider than further to the east or in the area of Şarköy and the gulf of Saros. Thus, the shear stress within the Marmara sea might not reach such extreme values as the ones in the east or the gulf of Saros.

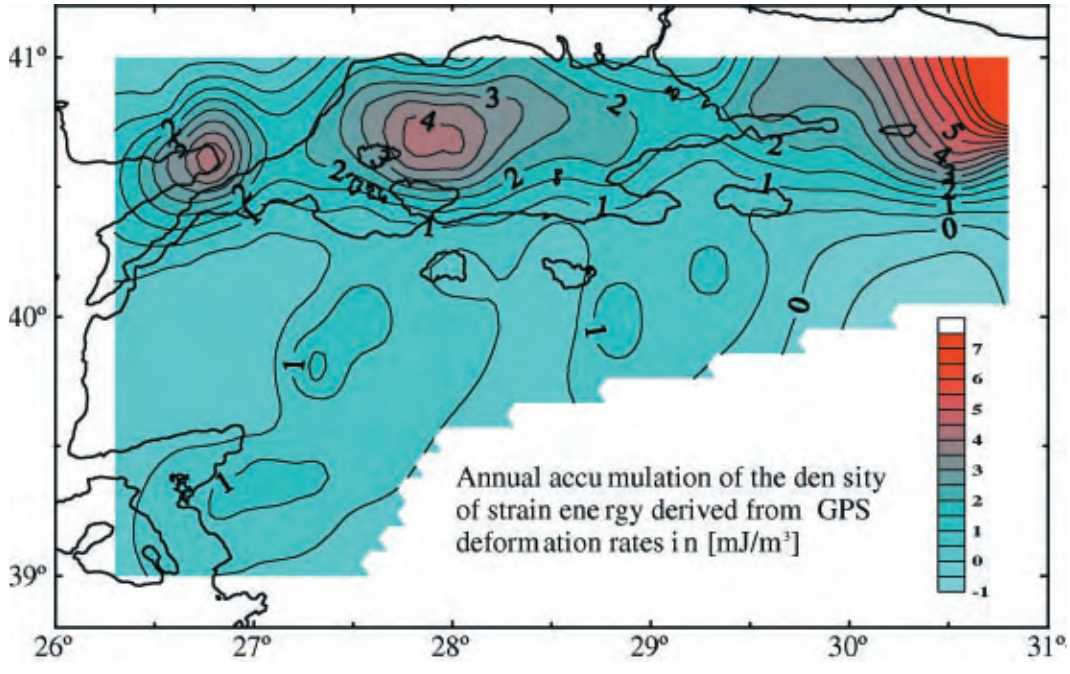


Figure 25: Annual accumulation of the density of strain energy in [mJ/m^3] between 1990 and 1996. Deviations from the shear stress indicate enhanced normal faulting (e.g. east of Ayvalık). The average value is 1.4mJ/m^3 (max. 9.1mJ/m^3).

Projection of the geodetic data onto the neotectonic structures

The kind and strength of motion along each fault has been determined by calculating the strain along the faults. Each fault is represented by a number of points which are at a distance of 5-10km from each other. The shear and the normal faulting part was determined for all these points. The fault lines were digitized to extract the fault direction. The results obtained are shown in the Figure 26 to 27. The interpretation of the results is restricted to the area inside the dashed line where GPS derived data are available because the least squares collocation does not allow us a sensible extrapolation. The scale given in Figure 27 is defined as follows: 1μstrain/a is equal to a relative motion of 1mm/a over a distance of 1km normal to the fault.

Figure 26 depicts the major sense of motion occurring along the individual faults. The neotectonic fault structures of the Marmara sea region are governed by dextral shearing and exten-

sion. The northern zone is clearly dominated by dextral shearing. Generally, extension becomes more important as we go from E to SW. The first indication for extension is found west of the bifurcation of the NAFZ (30.5°E). This correlates well with the FPS of the earthquake of July 30, 1967 (Barka this volume). The deformation patterns around lake İznik, Bursa, south of the eastern graben in the Marmara sea, between the Ulubat and Kuş lakes, and the gulf of Edremit are dominated by extension. Compression plays a major role at faults trending NE-SW.

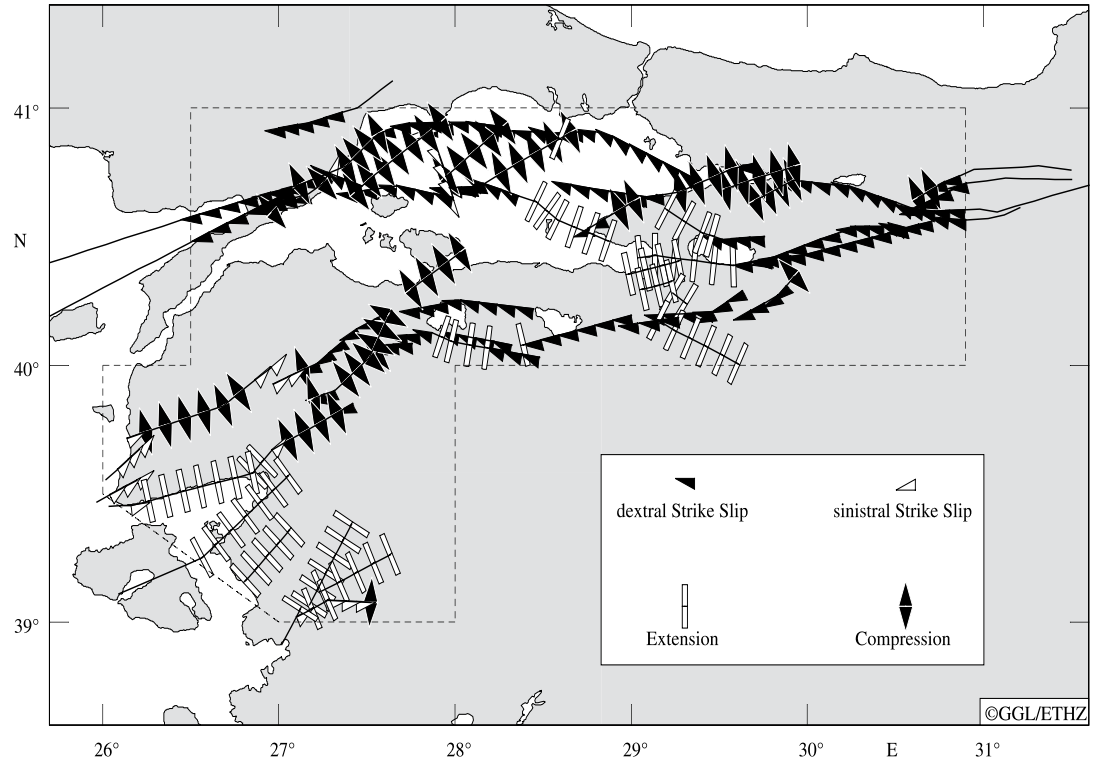


Figure 26: *Unscaled major kind of motion projected along the fault lines. The deformation pattern of the Marmara sea region is governed by dextral strike-slip and extension. The dashed line indicates the region investigated.*

Figure 27 shows the sense and strength of the occurring shear processes. This picture illustrates clearly that most of the shear occurs along the northern zone of the NAFZ. This GPS based deformation pattern is strongly supported by models of earthquake stress triggering along the NAFZ (Stein et al. 1997). The apparent low in the central Marmara sea is a lower boundary for the shear and normal strain rates along these faults. The introduction of additional rates assumed, in the north (0mm/a) and south (17mm/a westerly component) of the Marmara sea (Barka pers. comm.), slightly increased the compression along the NE-SW oriented faults as well as the dextral shear rates along the E-W trending faults in the Marmara sea. However, no fundamental changes were found. The southern zone undergoes far less shearing than the northern one. Almost no shear processes were found in the Bursa area, between the Ulubat and Kuş lakes, and on the Biga peninsula. Significant dextral shear was detected west of Bursa and around Gönen. Gönen lies in the area where the fault lines and velocity field change their direction from E-W to ENE-WSW. No clear shear direction could be deduced south of Edremit.Aegean extension

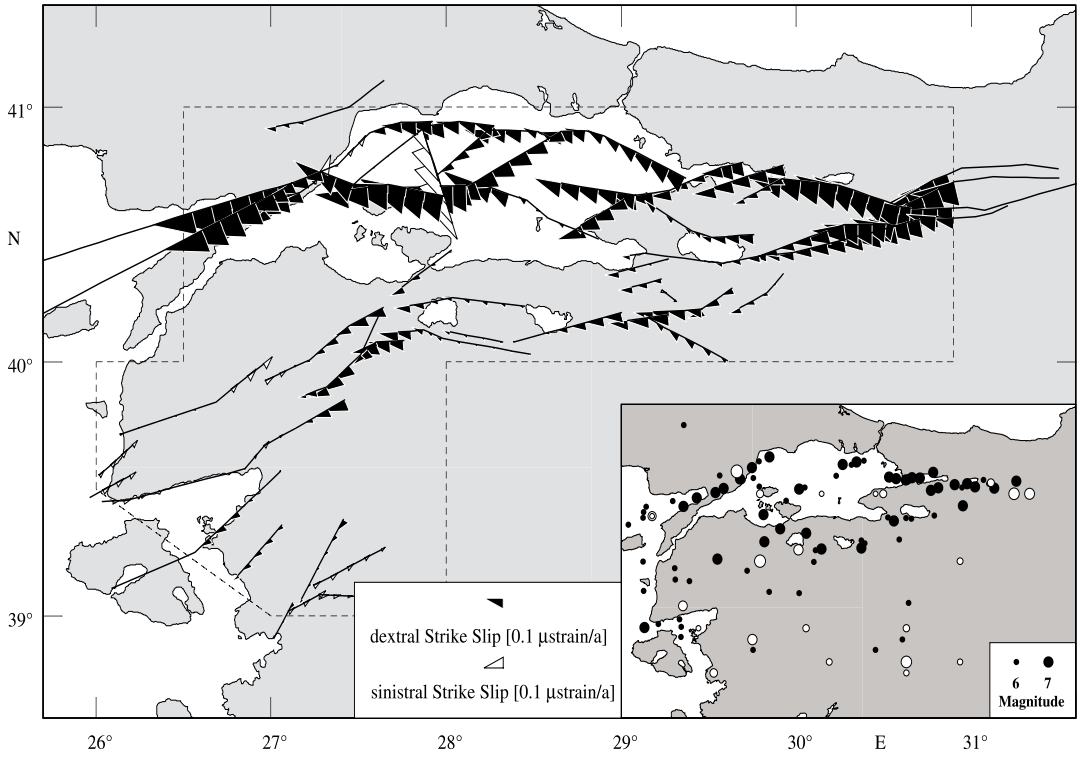


Figure 27: *Scaled and oriented sense of strike along the fault lines. Most activity occurs along the northern zone of the NAFZ and shows dextral sense of motion. Almost no shear can be revealed in the southern zone. The average dextral shear amounts to 0.10µstrain/a (329 out of 338 values, max. 0.28µstrain/a). The average sinistral shear is 0.05µstrain/a (65 out of 394 values, max. 0.22µstrain/a). The dashed line indicates the region investigated. The inset depicts the long-term seismicity of the Marmara sea region after Ambraseys and Finkel (1991) and NEIC (1990). Black dots show events before this century. This century's events are given as white dots.*

Conclusions

The GPS campaigns carried out in 1990, 1992, 1994, and 1996 were all completed successfully. In 1990, observations of excellent quality were gathered, considering the receiver technology available at that time. The quality of the data collected in 1992 was limited by the daytime observations and high temperatures. Fine data sets were achieved in 1994 and 1996. The detailed analysis of the GPS data presented led to a pattern of regional deformation that has revealed various new insights into the tectonics of the Marmara sea region. The westward motion relative to an assumed stable Eurasia gradually increases from N to S reaching a maximum of 22mm/a. This value can be regarded as the overall movement of Anatolia towards W. Around longitude 27.5°E, the strike of motion bends towards WSW.

Future re-occupations and a densification of the MARMARA network would be highly desirable in order to improve the estimates of the rates presented and to detect further details of the tectonics of the region. A network of permanent tracking stations could reveal the short period movements. Data collected by such a permanent network could lead to important findings of the strain accumulation before major seismic events. A dense permanent GPS network in the populated areas of İstanbul and Bursa (≈20 million inhabitants) should be constructed. Such a network is of great importance for a detailed seismic risk assessment.

The strain and stress analysis of the GPS derived deformation pattern has shown that the northern zone of the NAFZ is by far the most active zone. The motion is of a dextral sense and reaches values of up to 0.27 μstrain/a. No evidence was found that there is significant tectonic activity on the Biga peninsula. It is most probably inactive or locked. The Biga peninsula may even form a block of small internal deformation. The maximum activity of the eastern part of the southern zone is below 0.13μstrain/a. Further to the west, the southern zone is governed by thrust and normal faulting. The distinct bend of strike at longitude 27.5° E from E-W to ENE-WSW leads to clear compression directing WNW-ESE. The western-most part of the southern zone is associated with extension pointing NNW-SSE. The size of this extension unfortunately is not well constrained yet, because the southern-most sites have been re-occupied only once. The calculations of stress parameters give first estimates of the energy accumulated. The highest values of annual maximum shear stress accumulation (>14kN/m^2) are located along the northern zone. The compilation of the historical seismicity in the Marmara sea region shows that the strongest events are aligned along the northern zone of the NAFZ whereas far fewer earthquakes took place along the southern zone. This suggests that the deformation pattern obtained from four years of GPS observations represents the long-term behaviour of the neotectonic pattern of the Marmara sea region.

The strain rate components projected onto the major fault lines offer the possibility of predicting the kind and size of motion that can be expected. Thus, the individual faults can be classified. The motions derived can then be compared with neotectonic and seismotectonic results. A first evaluation of these independent data sets shows that a detailed analysis derived from geodetic observations is capable of predicting the type and size of motion in a given fault geometry. Yet, a detailed investigation should follow in cooperation with geologists who are familiar with the neotectonic pattern of the region.

Further comparisons with seismically derived strain rates suggest that about 60% of the deformation derived from the geodetic data is released by earthquakes. Recent investigations of seismic strain rates indicated that they account for 74% of regional SLR rates in NW Anatolia (Jackson et al. 1994). This result indicates a considerable amount of aseismic creep or a strain accumulation that might be released in future earthquakes. However, one must keep in mind that the time periods, both of geodetic and seismic data collection, are very short. They might not be representative for a longer time scale.

The strain and stress-analysis is based on the interpolation of the data using the method of least squares collocation. The calculations carried out also show some of the limitations of the interpolation method applied. The collocation is highly sensitive to the spatial distribution of the data. Thus, the interpolation of inhomogeneous data is difficult and must be interpreted with caution. The GPS network has a gap around the central part of the Marmara sea. It is, therefore, not clear whether the high dextral shear along the northern zone is lowered in the Marmara sea or not. It is not possible to give a clear estimate of the size of tectonic processes of the region unless the network is densified around the Marmara sea and on its islands. Such a densification is of great importance since the area in question is next to one of Anatolia's most populated areas (İstanbul and Bursa).

Acknowledgements

We thank all our partners who are working with us on the MARMARA Poly-Project. The Geodetic Institute of İstanbul Technical University (İTÜ, A. Aksoy, H. Denli) and the General Command of Mapping (GCM, İ. Kınık, O. Lenk), Ankara, are participating in the geodetic part of the project. Our partners at the ETH Zurich are the groups of Engineering Geology, Geothermics

and Seismology. We also appreciate the close cooperation with the Massachusetts Institute of Technology (MIT, USA). Fruitful discussions with R. Reilinger (MIT) and A. Barka (İTÜ) were particularly helpful in various scientific aspects of the project. We also thank C. Hasler for her help in editing the English version of the manuscript. The Marmara Project is financed by the ETH Zurich and we are especially grateful to R. Hütter, the former ETH vice-president of Research and Development, for his continuing help and support.

References

Alptekin, Ö., İlkışık, M., Ezen, Ü. and Üçer, B., 1990, Heat Flow, Seismicity, and the Crustal Structure of western Anatolia, Proceedings of IESCA Meeting İzmir Turkey, 8-2, 1-12.

Ambraseys N.N. and Finkel, C.F., 1991, Long-term seismicity of İstanbul and the Marmara Sea region, Terra Nova, 3, 527-539.

Ambraseys N.N. and Finkel, C.F., 1995, The seismicity of Turkey and adjacent areas, EREN Ltd İstanbul, ISBN 975-7622-38-9, 240p.

Barka, A.A., this volume, Neotectonics of the Marmara region.

Barka, A.A., 1992, The North Anatolian fault zone, Annales Tectonicae, Supp. to VI, 164-195.

Barka, A.A. and Kadinsky-Cade, K., 1988, Strike-Slip Fault Geometry in Turkey and its Influence on Earthquake Activity, Tectonics, 7:3, 663-684.

Beutler, G., Mueller, I.I. and Neilan, R., 1994, The international GPS Service for Geodynamics (IGS): Development and Start of Offical Service on 1 January 1994, Bulletin Geodésique, 68-1, 43-51.

Danuser, G., Geiger, A. and Müller, M., 1993, Modellierung von Verschiebungs- und Verzerrungsfeldern, Inst. für Geodäsie und Photogrammetrie (IGP), Publ. nr. 218, 176p.

Deniz, R., Aksoy, A., Yalın, D., Seeger, H., Franke, P., Hirsch, O. and Bautsch, P., 1993, Determination of Crustal movements in Turkey by terrestrial geodetic methods, J. Geodynamics,18, 13-22.

Eren, K., 1984, Strain analysis along the North Anatolian Fault by using geodetic surveys, Bull. Geodesique, 137-149.

Eyidoğan, H., 1988, Rates of crustal deformation in western Turkey as deduced from major earthquakes, Tectonophysics, 148, 83-92.

Jackson, J., Haines, J. and Holt, W., 1994, A comparison of satellite laser ranging and seismicity data in the Aegean region, Geophys. Res. Lett., 21, 2849-2852.

Jeckelmann, Ch., 1996, Genese lokaler Thermalwasservorkommen in der Region Bergama/W-Türkei, Diss. ETH Zürich Nr. 11990.

Kahle, H.-G., Straub, C., Müller, M.V., Kastens, K., Gilbert, L., Hurst, K. & G. Veis, 1996, Estimates of strain rates in the Eastern Mediterranean, inferred from GPS measurements (Abstract), Supp. to EOS Trans., 77-17, p. 573.

Kahle, H.-G., Müller, M.V., Geiger, A., Danuser, G., Mueller, St., Veis, G., Billiris, H. and Paradissis, D. , 1995, The strain field in NW Greece and the Ionian Islands: results inferred from GPS measurements, Tectonophysics, 249, 41-52.

Kiratzi, A. and Papazachos, C.B., 1995, Active crustal deformation from the Azores triple junction to the Middle East, Tectonophysics, 243, 1-24.

Kleusberg, A. and Teunissen, P. (eds.), 1996, GPS for Geodesy, Lecture Notes in Earth Sciences, 60, Springer , 408p.

Lenk, O., 1995, Space baced geodetic activities for geodynamics in Turkey, in: Proceedings of the First Turkish International Symposium on Deformations 1994, edited by: M. Şahin and P. A. Cross, 12-29.

Marti, U., Kahle, H.-G., Aksoy, A. and Deniz, R., 1991, GPS-Projekt Marmara: Dokumentation der ersten Messkampagne September 1990, Inst. für Geodäsie und Photogrammetrie (IGP), 179, 47p. plus appendix.

Mueller, St. and Kahle, H.-G., 1993, Crust-Mantle Evolution, Structure and Dynamics of the Mediterranean-Alpine Region, in: Contributions of Space Geodesy to Geodynamics: Crustal Dynamics, edited by: D. Smith and D. Turcotte, AGU Geodynamics Series , 23, 249-298.

Mueller, St., Kahle, H.-G. and Barka, A., this volume, Plate tectonic situation in the Anatolian-Aegean region.

NEIC, 1990, Global Hypocenter Data Base CD-ROM, USGS/NEIC.

Öztürk, E., Atasoy, V., Bektaş, S., Uysal, K. and Karahan, Z., 1987, Akyazı-Dokurcun Vadisinde kurulan Jeodezik Agda Yatay Kabuk Hareketlerinin Araştirilmasi, Türkiye 1. Harita Bilimsel ve Teknik Kurultayi, Ankara.

Reilinger, R., McClusky, S., Kahle, H.-G., Müller, M.V., Straub, C., Kastens, K., Gilbert, L., Hurst, K., M., Veis, G., Paradissis, D. and Barka, A., 1995, GPS evidence for westward continuation of dextral strike-slip motion from the North Anatolian Fault Zone across the North Aegean and North-Central Greece. Abstract. American Geophysical Union (AGU). EOS, Supplement, Nov. 7, F620-F621.

Reilinger, R., McClusky, S., Oral, B., King, R., Toksöz, M., Barka, A., Kınık, İ., Lenk, O. and Şanlı, İ., 1997, GPS measurements of present-day crustal movements in the Arabia-Africa-Eurasia Plate collision zone, J. Geophys.Res., 102, 9983-9999.

Rothacher, M. and Mervart, L., 1996, Bernese GPS Software Version 4.0, Print. Off. University of Berne Switzerland, 418p.

Saastamoinen, J., 1973, Contributions to the Theory of Atmospheric Refraction / Introduction to practical computation of Astronomical Refraction, Bulletin Geodésique, 105-107, 50p.

Schindler, C., this volume, Geology of NW Turkey: Results of the MARMARA Poly-Project.

Stein, R., Barka, A. and Dieterich, J., 1997, Progressive earthquake failure on the North Anatolian fault since 1939 by stress triggering, Geophys. J. Int., 128, 594-604.

Straub, C. and Kahle, H.-G., 1993, GPS Projekt MARMARA: Punktprotokolle Stand 1993, Inst. für Geodäsie und Photogrammetrie (IGP), 227, 56p.

Straub, C. and Kahle, H.-G., 1994, Global Positioning System (GPS) estimates of crustal deformation in the Marmara Sea region, NW Anatolia, EPSL, 121, 495-502.

Straub, C. and Kahle, H.-G., 1995, Active Crustal Deformation in the Marmara Sea region, NW Anatolia, inferred from GPS measurements, Geophys. Res. Lett., 22-18, 2533-2536.

Straub, C., 1996, Recent crustal deformation and strain accumulation in the Marmara Sea region, N.W. Anatolia, inferred from GPS measurements, Inst. of Geod. and Photog. ETHZ Mitteilungen, 58, 123p. plus appendix, ISBN 3-906513-82-3.

Thatcher, W., 1995, Microplate versus continuum descriptions of active tectonic deformation, J. Geophys. Res., 100, 3'885-3'894.

Uğur, E., 1974, Recent crustal movements in the Gerede-Cerkes region of the north Anatolian Fault zone by geodetic methods, Ph.D. Thesis, İTÜ İstanbul.

Westaway, R., 1994, Evidence for dynamic coupling of surface processes with isostatic compensation in the lower crust during active extension of western Turkey, J. Geophys. Res., 99, 20'203-20'223.

Wirth, B., 1990, Höhensysteme, Schwerepotentiale und Niveaufächen: Systematische Untersuchungen zur zukünftigen terrestrischen und GPS gestützten Höhenbestimmung in der Schweiz, Swiss Geodetic Commission, 42, 203p.

Wong, H.K., Lüdmann, E., Ulug, T. and Özel, E., 1995, The Sea of Marmara: a plate boundary sea in an escape tectonic regime, Tectonophysics, 244, 231-250.

Seismicity and seismotectonics of the Bursa region

SOUAD SELLAMI, NAZARIO PAVONI, DIETER MAYER-ROSA, STEPHAN MUELLER, HALUK EYIDOĞAN, MUSTAFA AKTAR, CEMİL GÜRBÜZ, ŞERİF BARİŞ, ORHAN POLAT AND NAMİK YALCİN.

Abstract

A sub-project 'Seismicity and seismotectonics of Bursa region' was initiated in the frame of the Marmara Poly-Project. During a three years period 12 seismic stations (weak and strong motions) were operated in the Bursa area. These stations were run by the different institutions involved in the sub-project. Although more then 2500 events have been registered, only a few exceeded a magnitude of 4.0. Local magnitudes (M_L) were assessed based on the duration of the seismic coda waves. The depth of most events was found being less than 15km. The seismicity showed a typical clustering behaviour which is very dependent on time. It has been shown by compiling the last 20 years data. These data have also been used to evaluate a preliminary seismic hazard for the Bursa Region. Fault-plane solutions in addition to station diagrams (a new method) were investigated. They confirm NE-SW to almost N-S oriented crustal extension and E-W dextral shear for the northern part of the area. Source parameters were determined from acceleration records and tripartite relationship between seismic moment size of the source and stress drop were obtained.

Introduction

The northwestern part of Turkey, referred to as the Marmara region, is intensely affected by recent tectonic activity (Figure 1). Therefore, active geological and geophysical processes, including pronounced hydrological, geothermal and seismological phenomena can be observed, particularly along the western branches of the North Anatolian Fault Zone (NAFZ). The region of Bursa (Figures 1 and 2) is located close to one such branch and demonstrates several typical aspects of the regional seismotectonic activity.

In the Marmara region, a series of research projects have been initiated through the co-operation of Turkish and Swiss scientific institutions within the framework of the "MARMARA Poly-Project". The topics covered geology, seismicity, geodesy, geothermics and hydrology. One of the general goals in the "MARMARA Poly-Project" is to bring together the results of the various disciplines in order to foster an integrated interpretation of the geological and geophysical phenomena. One sub-project in this framework is dedicated to the study of various aspects of the seismicity in the Bursa region

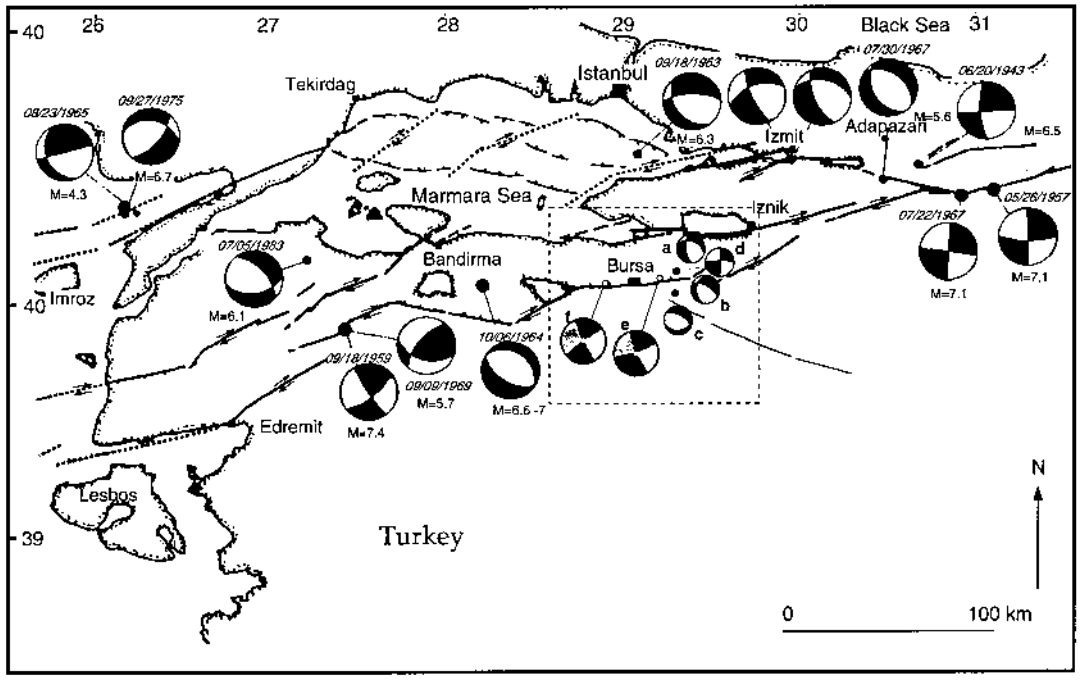


Figure 1: *Map of active faults of the Marmara region based on Barka (1992) and earthquake source mechanisms. The studied area is delineated by dotted lines. The source mechanisms are described in the text.*

The sub project "Seismicity and seismotectonics of the Bursa region" was carried out by the following institutions:

IGETH: Institute of Geophysics, Federal Institute of Technology Zürich (Switzerland)

DGİTU: Department of Geophysics, Mining Faculty of İstanbul Technical University (Turkey)

TÜBİTAK: Department of Earth Sciences, Marmara Research Institute of TÜBİTAK, Gebze (Turkey)

KOERİ: Kandilli Observatory and Earthquake Research Institute, Boğazıçı University, İstanbul (Turkey).

The sub-project was initially planned for two years (1992-1993) and later extended for another two years (1994-1995). The goal of the project was to install a seismic network to allow detailed monitoring of the earthquake activity in the area (dotted box in Figure 1).

In a very first phase of the project the study area was fixed to 39.90 – 40.50N and 28.80 – 29.30E (40x50km) (A_0) as shown on Figure 2. It turned out later that a relevant picture of the seismicity could only be obtained by enlarging this area further to the south ranging 39.75 – 40.50N and 28.50 – 29.50E (80x100km) (A_1), and so, including some of the most active part of the region. In order to study the historical seismicity in this area it was necessary to collect all data prior to the project period of the area covering the total of Figure 2 (39.2 – 41.0N and 28.0 – 30.0E).

Localities are shown on Figure 1 of Theme 1, Introduction to this volume.

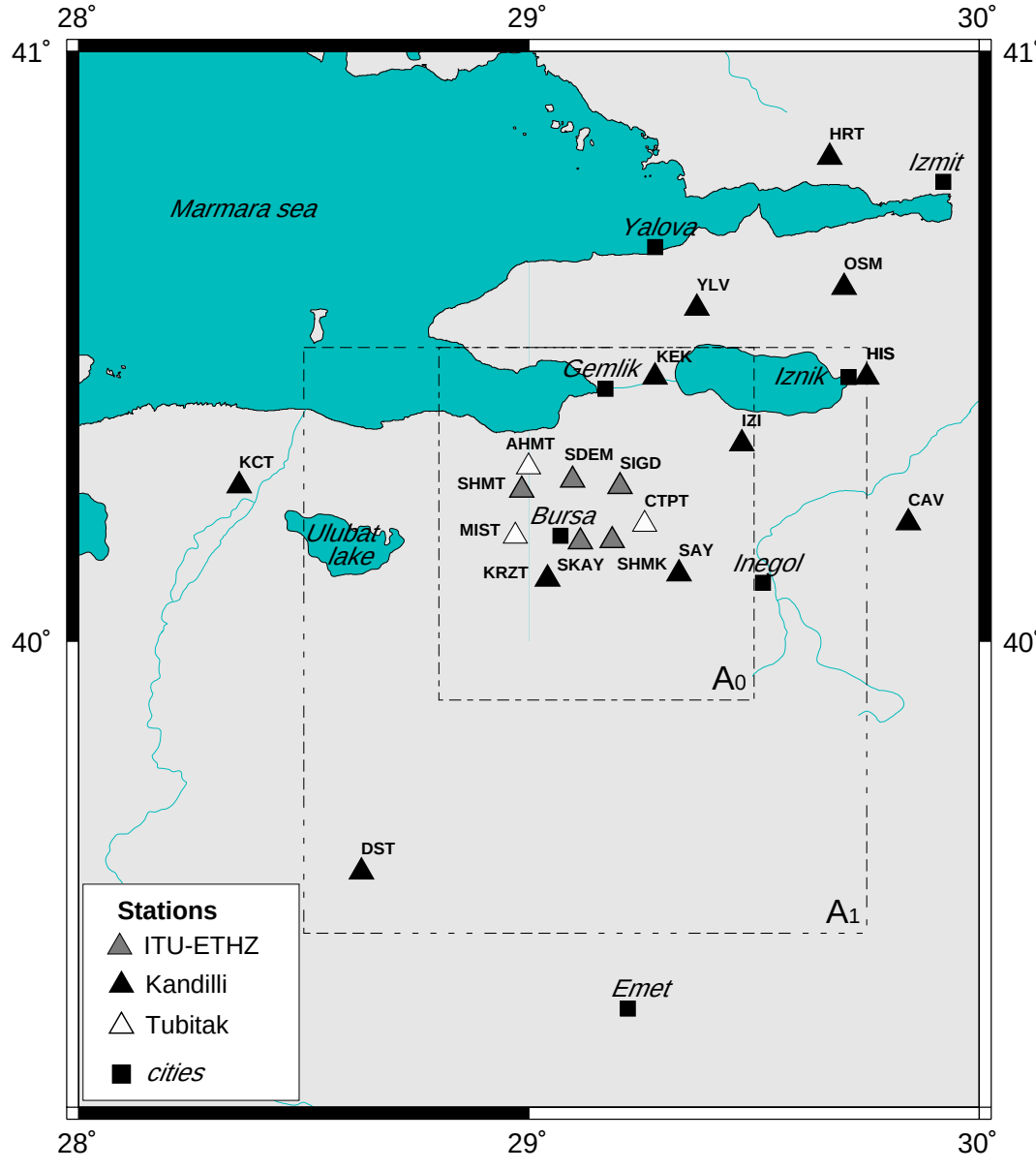


Figure 2: *The Bursa study area with the different regions of interest (A_0, A_1) and the location of the seismic stations.*

Seismotectonic setting and general seismicity of the Bursa region

Seismotectonic characteristics

The Marmara region is one of the neotectonic provinces of Turkey dominated by E-W dextral shear and NNE-SSW extension. The most prominent structural and morphological features of this province are several E-W oriented grabens (Gulf of İzmit, İznik, Gemlik, Yenişehir, Bursa, Manyas and Saros), cut by WSW-ENE trending dextral faults, with widths varying from a few km to a maximum of 20km. As the NAFZ approaches the Marmara sea, the fault splays

into several branches in and around the sea (Figure 1). The southern zone of the NAFZ extends 400km westward from Geyve to Edremit. It consists of both normal and dextral strike-slip faults.

Figure 1 depicts major active faults and compiled earthquake mechanisms in the Marmara region based on Barka (1992). For detailed discussion, the reader is referred to Theme 3 and 5 in this volume. The studied Bursa area is delineated by dotted lines in Figure 1, the source mechanisms obtained within this area are described further in a later paragraph.

Historical seismicity (prior to 1900)

The historical seismic activity of the Bursa region for the period prior to 1900 has been compiled by various authors. Table 1 gives a combined list of the historical earthquakes reported by Soysal et al. (1981) and Ambraseys and Finkel (1991). It is to be noted that the region experienced a large event in 1855 with intensity IX (MSK). The epicentre locations for these events are expected not to be very accurate.

Date year month day	O-Time Hr Min	Lat. N	Lon. E	Int. MSK	QL	Remarks
0029 11 24		40.4	29.7	IX	B	İznik, İzmit
0033		40.4	29.7	VIII	B	İznik, Kocaeli, Bursa
0069 01 02		40.4	29.7	VII	B	İznik, İzmit
0120		40.4	29.7	VIII	A	İznik, İzmit
0129		40.4	29.4	VIII	B	İznik, Zeytinbağ
0368 10 11		40.4	29.7	VII	B	İznik
0378		40.4	29.7	VI	C	İznik
0715		40.4	28.9	VIII	B	İznik, Bandirma, Erdek
0985 09 23		40.4	28.9	IX	A	İznik, İstanbul
1064 09 23		40.4	28.9	IX	A	İznik, Bandirma, Mürefte, İstanbul (Tsunami)
1417		40.2	29.1	VII	C	Bursa
1674		40.2	29.1	VII	C	Bursa
1855 02 28	03.00	40.2	29.0	IX	A	Bursa, Kemalpağa
1855 04 11	19.40	40.2	29.1	X	A	Bursa (fault occurence)
1855 12 15	21.30	40.2	29.1	VI	CB	Bursa, İstanbul
1858 04 19		40.2	29.0	VI	B	Bursa
1860 06 04		40.2	29.1	VII	A	Bursa vicinity (rock fall)
1862 01 11				VI	B	Bursa, Çanakkale
1863 11 06	10.00			IX	A	Gemlik Bay, Umurbey, Bursa,İstanbul,Gelibolu
1866 02 14	03.15	40.2	29.1	VI	B	Bursa vicinity
1866 09 22	10.00			VI	B	Usak, Bursa
1871 02 24	01.00	40.2	29.1	VI	B	Bursa vicinity
1872 01 17		40.2	29.1	VI	A	Bursa
1876 04 17		40.2	29.1	VI	B	Bursa vicinity
1881 12 30		40.2	29.1	V	B	Bursa vicinity
1884 02 01		40.2	29.1	VI	B	Bursa vicinity
1886 10 06		39.5	28.9	VIII	A	Gökcedağ, Balikesir, Tavşanlı, Küthya
1887 09		40.2	29.1	VI	B	Bursa vicinity
1895 01 21		40.4	29.7	V	B	Bursa vicinity
1897 03 14	09.30	40.4	29.1	V	C	Gemlik vicinity
1899 05		40.2	29.1	V	C	Bursa vicinity

Table 1: Historical earthquakes in the Bursa region (39.5-40.5N / 28.7-29.7E). QL: quality of data (A = good, B = fair, C = unreliable). Data compiled after Soysal et al. (1981).

Instrumental seismicity during 1900-1975

The seismicity for the instrumental period is studied for the smaller region confined by 39.5-40.5N and 28.5-29.5E. For the determination of source parameters up to 1975, only global and some regional networks were available. In the earthquake catalogues by Alsan et al.

(1975) and Ayhan et al. (1987), only three major earthquakes with M_s greater than 4.5 were found for this period. The 13 November 1948 earthquake, which was 7km away from Bursa city, had M_s = 5.6. In 1964 and 1969, two other events occurred with magnitudes less than 4.7. Table 2 shows significant events with M≥4.5 which occurred between 1900-1992 in the immediate vicinity of Bursa city (40.18N-29.07E). ATB denotes the catalogue by Alsan et al. (1975), ISC the data from the International Seismological Centre, İSK the data from the İstanbul Kandilli Observatory and Dist. the epicentral distances to Bursa city in km.

Ref.	Date d m y	Orig. time	Lat. N	Lon. E	Depth [km]	M_S	Dist. [km]
ATB	13 11 1948	04:44:50	40.23	29.02	60	5.6	7
ATB	02 04 1959	04:34:28	40.50	29.41	20	4.6	46
ISC	15 12 1964	21:03:15	40.02	28.79	26	4.5	30
ISC	01 02 1983	13:54:11	40.20	28.94	3	4.8	11
ISC	21 10 1983	20:34:49	40.14	29.35	12	4.9	24
ISC/ISK	28 10 1984	08:17:58	40.07	29.26	9	4.5	20
ISC/ISK	01 01 1988	11:21:51	40.14	29.23	6	4.5	14

Table 2: Instrumental earthquakes, M≥4.5.

Instrumental seismicity 1976 to 1992

In the period between 1976 and 1992 data were collected with local networks. The Kandilli Observatory and Earthquake Research Institute (KOERİ) began to install permanent seismic stations in 1976. After 1978, the regional radio-link seismic network (MARNET) was in operation. With the installation of seismic telemetry stations, data on micro-earthquake activity of the region could be collected. More than 1300 earthquakes were located within this 17 year period. The most important earthquake in this period was the İnegöl earthquake on 21 October 1983 with M_s = 4.9 (ISC) Kalafat (1989b). The role of this event in the course of the local seismic activity is illustrated in the graphs of strain energy release vs. time, as shown in Figure 3. There were three medium-sized earthquakes with a magnitude of M_s = 4.5 in the years 1983, 1984 and 1988 (Table 2). These earthquakes can be assumed to be the aftershocks of the İnegöl earthquake.

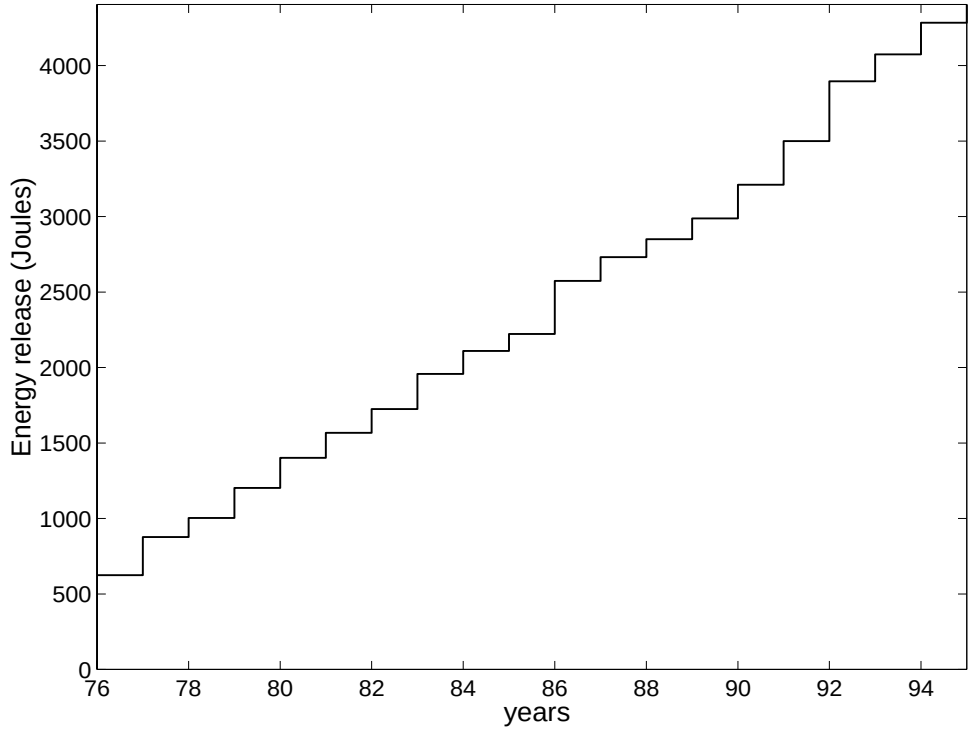


Figure 3: Annual cumulative strain energy release between 1976 and 1995 in the Bursa region.

The seismicity of Western Turkey is high and reveals swarm-type activity with remarkable clustering of low magnitude earthquakes in time and space (Üçer et al. 1985 and in Theme 3 of this volume). The epicentres and fault mechanisms are closely associated with major structures (Canitez and Üçer 1967, McKenzie 1972,1978, Jackson and McKenzie 1984). The focal depths of the earthquakes in Western Turkey range from 0 to 50km according to various bulletins and sources, but these have low reliability. The accurate determination of focal depths using joint hypocentre location techniques (Jackson and Fitch 1979) and modelling of the long period body waves (Eyidoğan and Jackson 1985) indicate that at least the hypocentres of the larger earthquakes in the region are not deeper than 10-15km.

Bursa region seismic network

Geological setting

The Bursa plain itself covers the area which is delimited approximately by the Tübitak and ETH-ITÜ seismic stations as shown on Figure 2. It is a basin filled with Quaternary deposits whose thickness varies from 80 to 300m. It is situated on a metamorphosed and highly deformed unit (for more details see Imbach, this volume). Abundant Permian limestones can be observed on the northern slopes of the Uludağ mountain (e.g. Kirazli village (KRZT)). The same limestone unit can also be observed at the hills bordering the Bursa plain to the north and on to the east (e.g. Çataltepe (CTPT) and Igdir (SIGD) villages). Volcanics, mainly spilitic basalt, are common around the Çataltepe village (CTPT). The metamorphic rocks are partly covered by Neogene clays and marls (thickness not known). Outcrops of these units can be

observed along the western part of the Bursa plain. The lesser hills appearing between the Bursa plain and the Marmara sea are formed by Neogene deposits.

The Mount Uludağ which limits the Bursa plain to the south is basically composed of highly metamorphosed pre-Triassic rocks (see Imbach this volume), such as amphibolites and gneisses, overlain by a thick marble unit. The marbles can be especially observed on the high plateau (2000-2500m) of the Uludağ mountain. They are intruded by granitic rocks of Carboniferous and Oligocene age.

Site selection, technical characteristics and operation

A digital network of 12 stations was planned for the detailed monitoring of the seismicity of the Bursa region A_o (Figure 2). The installation and operation of these stations were partitioned among several institutions. The DGİTU/IGETH operated five strong motion stations, the TÜBITAK operated four, and the KOERİ three weak motion stations.

The nine stations operated by the DGİTU/IGETH and the TÜBITAK and one station of the KOERİ were installed during the project period while two other KOERİ stations already existed. A site selection study was carried out by a joint DGİTU and TÜBİTAK team in order to obtain the most suitable network configuration. The main criteria for the site selection were (1) to distribute the stations optimally along the perimeter of the Bursa plain and (2) to ensure low seismic noise and (3) the existence of suitable infrastructure (availability of AC power, telephone lines, easy access, etc.).

In addition to the 12 stations mentioned above, the TÜBİTAK temporarily deployed two additional weak motion recorders at Iğdır (SIGD) and Kaplıkaya (SKAY). Also, two additional weak motion instruments with velocity sensors were temporarily installed by the DGİTU/IGETH at Hamamlıkazık (SHMT) and Demirtaş (SDEM).

Upon completion of the first and second stage of the project, each institution made available the raw data in common ("GSE") format. Table 3-5 show the various station networks which were operated by the different institutions.

Stations operated by DGİTU/IGETH

The DGİTU/IGETH operated 5 accelerographs (BUSNET) in the Bursa region during this project period. Additionally, two MLR-II velocity recorders were run temporarily for a period of 6 months in 1993-1994 in order to check the activity of micro earthquakes below the threshold of the strong-motion stations. All station co-ordinates and site characteristics are given in Table 3.

Station Name	Code	Instr. Type	Lat. N	Long. E	Elev [m]	Sens.	Formation	Inst.
Demirtaş	SDEM	SIG	40 16.50	29 05.82	110	SM2	Sandstone	6/8/92
Hamamlıkazık	SHMK	SIG	40 10.32	29 11.10	350	SM2	Slope Dep.	7/8/92
Hamitler	SHMT	SIG	40 15.48	28 59.04	110	SM2	Greywacke	6/8/93
Iğdır	SIGD	SIG	40 15.84	29 12.12	140	SM2	Limestone	3/4/93
Kaplıkaya	SKAY	SIG	40 10.20	29 06.84	350	SM2	Marble	7/8/92
Demirtaş	TDEM	MLRII	40 16.50	29 05.82	110	L4C	Sandstone	1/7/93
Hamamlıkazık	THMK	MLRII	40 10.32	29 11.10	350	L4C	Slope Dep.	1/7/93

Table 3: DGİTU – IGETH stations.

The stations were visited by DGİTU personnel periodically every month to retrieve the data, and to calibrate and test the equipment manually. In addition, the results of an automatic periodic test every 7 days were kept in memory. The pre and post event times were adjusted to 15sec and 20sec, respectively. The sensor was set to 200mg full-scale for stations SHMK, SHMT, SIGD and SKAY, and to 500mg for SDEM. The trigger levels were set to 0.4mg for the Iğdır (SIGD) and Kaplıkaya (SKAY) stations, 0.6mg for Hamamlıkazık (SHMK), and 0.5mg for the Hamitler (SHMT) station. The trigger level for the Demirtaş (SDEM) station was changed to 1.5mg from June 1994 onwards to avoid false triggers due to environmental noise.

Stations operated by TÜBİTAK

The Earth Science Department of the Marmara Research Centre of the TÜBİTAK was responsible for the installation and operation of 4 weak motion seismic stations within the framework of the project (Table 4). The sensors for the stations consisted of 3-dimensional L4-C type velocity transducers. The connected MIDAS recorders were developed in the TÜBİTAK department. Apart from these 4 basic stations the TÜBİTAK also operated 2 temporary stations at varying locations and times. For these additional stations a 1-dimensional version of the same type of sensor was used. The recorders in this case were the RefTek 72A-06 type commercial instruments. The description of the station sites, the technical characteristics of the instrumentation and the data collection procedures are described below.

The sites for the weak motion stations were chosen in such a way that complete coverage of the Bursa plain was achieved. From a technical point of view further restriction came from the fact that the MIDAS stations permitted remote access via telephone lines, therefore the availability of local telecommunication services was important. To minimise lightning and other hazard related to aerial telephone lines, the stations were located in villages with a 'PBX' centre. A suitable sheltered location was found for three of the stations (AHMT, MIST, KRZT) and an independent shelter had to be built at one station (CTPT). The co-ordinates, starting date of operation, sensor positions and formation types are shown in Table 4.

Station Name	Code	Instr.	Lat. N	Long. E	Elev [m]	Sensor	Formation	Inst.
Ahmetbey	AHMT	Midas	40 17.78	28 59.81	200	L4C3D	Neogene	5/9/92
Misi	MIST	Midas	40 10.68	28 57.87	150	L4C3D	Limestone	5/9/92
Kirazli	KRZT	Midas	40 00.61	29 02.35	900	L4C3D	Limestone	5/9/92
Çataltepe	CTPT	Midas	40 12.05	29 15.32	350	L4C3D	Quartzite	5/9/92
Iğdır	IGDT	Reftek	40 15.84	29 12.12	140	L4C	Limestone	IGDT
Kaplıkaya	KAPT	Reftek	40 10.20	29 06.84	350	L4C3D	Marble	

Table 4: TÜBİTAK stations.

The MIDAS recorders can be monitored via telephone lines using a dial-up modem. Therefore, the operation of these stations is essentially based on this feature. The MIDAS recorders use a STA/LTA algorithm for the detection procedurestoring data on internal hard disk whenever the threshold is exceeded, for local events, teleseismic events or even transient noise. The data can be retrieved later via telephone line or by direct connection when the site is visited. Apart from this basic operation, daily monitoring was carried out using the dial-up modem function for the following operations:

a. Checking the normal operation of various functions

b. Checking the number of events recorded in the last 24 hours

c. Checking the size of events recorded in the last 24 hours

d. Downloading one data file once every week for checking of wave forms

e. Downloading any other data file if required

f. Measuring the drift in the internal clock

g. Synchronising the internal clock

It must be pointed out that during the telephone connection and the carrying out of the above functions, the data acquisition process was not interrupted and continued as usual. Whenever the data stored exceeded 15MB, which roughly corresponds to 3 months of recording, or whenever an operational error was detected the site was to be visited. Apart from the high stability of the internal clock, the output from a DCF receiver was recorded simultaneously on a fourth channel. A comparison of the trigger times at each station was performed off-line at the base station.

Stations operated by KOERİ

Seven PC-based telemetered seismic stations have been in operation since September 1992 around the İznik-Mekece fault, which is one of the main branches of the NAFZ in the Marmara region. This network consists of one base station (İZİ) near İznik town and six outstations located around İznik-Mekece fault. The seismic network with these seven stations is termed İZİNET (Üçer et al. 1995). The geographical co-ordinates of all stations were determined by using a portable GPS receiver. The locations and technical descriptions of the KOERİ stations are given below. The installation of the seismic network began on July 20, 1992 and five sites were in operation by August 10, 1992. Two more stations in Kekliktepe (KEK) and Hisarcık (HIS) were added to the network specifically for this project in the summer of 1993.

The sites for the İZİNET stations were chosen in such a way as to cover the İznik-Mekece fault segment of the NAFZ. The location of stations were selected at places with direct sight to the base station at Kibletepe (İZİ). In addition, places having electricity and low background noise were looked for. The co-ordinates, elevations, installation dates and bedrock formation are given in Table 5.

The İZİNET network consisted of one base station and several remote stations. Each remote station was equipped with a vertical component short period (2Hz) seismometer (L22) except Sayfiye (SAY), near the city of Bursa, which has a 1Hz Willmore Mark IIIA sensor. At the base station, three component seismometers (L-22) were installed. The signals of the remote stations are transmitted via radio-link (457 MHz, 2.5 W) to the base station.

The seismic signals from all stations were digitised with a 16 channel AD- converter (12 bit) and pre-processed on a PC at the base station. MDETECT software based on LTA/STA detection ratio (Tottingham et al. 1989) is used for real-time data acquisition. A sample frequency of 100Hz was chosen in order to obtain the high frequency content of local seismic signals. The data were stored on a removable hard disk with a capacity of 350MB. This hard disk was replaced by a spare one nearly every month. The system was monitored by dial-up from time to time using a telephone connection via modem.

The seismic network had a very accurate timing system based on satellite transmitted universal time codes, which were recorded by a GPS receiver with an accuracy better than 10ms. A DCF 77KHz receiver was connected separately to the PC through a RS-232C port, synchronising the CPU time of the PC every 24 hours. In order to ensure uninterrupted operation, a battery buffered power supply was used for the entire system at the base station.

Station Name	Abbr.	Instr.	Lat. N	Long. E	Elev [m]	Sensor	Formation
Çavuşköy*	CAV	Tele.	40 12.13	29 50.55	460	L22	Limestone.
Gülveren*	GUL	Tele.	40 25.94	30 30.90	930	L22	Limestone.
Hisarcık*	HIS	Tele.	40 28.12	29 55.88	970	L22	Siltstone
İznik*	IZI	BASE	40 20.97	29 27.68	930	L22	Limestone
Kekliktepe*	KEK	Tele.	40 29.12	29 14.53	950	L22	Limestone
Orhaniye*	ORH	Tele.	40 51.61	30 04.24	320		
Osmaniye*	OSM	Tele.	40 36.13	29 42.01	820	L22	Granit
Sayfiye*	SAY	Tele.	40 07.00	29 20.07	850	L22	Schist
Altintaş	ALT	Perm.	39 03.31	30 06.62	1060		Limestone
Bandirma	BNT	Tele.	40 21.36	27 55.20	353		Limestone
Çatalca	CTT	Tele.	41 08.84	28 25.78	324		Sandstone
Demirköy	DMK	Perm.	41 49.28	27 45.44	315		Granite
Dursunbey	DST	Perm.	39 36.33	28 37.68	625		Limestone
Edincik	EDC	Perm.	40 20.81	27 50.00	269		Granite
Eskiyayla	EYL	Tele.	40 33.96	30 09.45	1160		Limestone
Ezine	EZN	Perm.	39 49.55	26 19.52	49		Serpentine
Gölpazarı	GPA	Perm.	40 17.33	30 18.56	560		Limestone
Hereke	HRT	Tele.	40 49.30	29 40.08	645		Limestone
Kandilli	ISK	Perm.	41 03.94	29 03.55	132		Greywack
Karaçabey	KCT	Tele.	40 15.93	28 21.39	451		Sandstone
Karabiga	KGT	Tele.	40 27.09	27 18.20	185		Limestone
Karahallı	KHL	Perm.	38 19.39	29 31.39	940		Sandstone
Mürefte	MFT	Tele.	40 47.20	27 16.87	924		Sandstone
Yalova	YLV	Tele.	40 34.00	29 22.37	829		

Table 5: KOERİ İZİNET(*) and MARNET permanent stations.

Data evaluation: Velocity models and relocation

Crustal velocity

A quarry-blast near Kestel (about 10km west of Cataltepe (CTPT)) was used for the determination of crustal velocities in the project area. It was recorded on 27. April 1993 at a total of nine seismic stations operated by TÜBITAK and KOERİ. One station (Reftek) was deployed at the source site to obtain the origin time. The quarry blast did not trigger the Marnet system. Table 6 contains the travel times for P and S waves at each station.

Station Name	Coordinates Lat. N-Long. E	Elev. [m]	Dist. [km]	Azimuth	P-travel-time [s]	S-travel-time [s]
Çataltepe	40.01 – 29.25	350	2.12	68.5	0.37	1.02
Dudakli	40.23 – 29.30	630	7.86	54.3	1.51	2.79
Sayfiye	40.12 – 29.33	850	12.26	131.7	2.14	4.16
Kirazli	40.10 – 29.04	900	25.50	218.2	3.43	5.96
Misi	40.18 – 28.96	150	22.22	266.2	3.86	7.56
Ahmetli	40.29 – 28.99	200	22.62	301.0	3.97	8.41
Iznik	40.35 – 29.46	930	26.68	48.8	4.60	8.74
Yalova	40.57 – 29.37	829	43.48	16.7	7.63	13.43
Osmaniye	40.60 – 29.70	820	60.86	41.4	10.24	17.85

Table 6: List of stations with P- and S-wave travel-times.

Arrival times of P and S waves were read with an accuracy of 0.1s. An elevation correction for the individual stations was applied by reducing the observed travel-time data to sea level elevation with the uppermost layer velocity obtained from the raw data. A new travel time – distance plot was constructed. From the plane layer interpretation of the data, the following four-layer model was obtained.

P and S wave velocity model obtained from travel time analysis of Kestel quarry blast:

LAYER 1	V_p0 = 3.5 km/s
H = 1.0km	V_s0 = 2.0 km/s
LAYER 2	V_p1 = 5.7 km/s
H = 7.0km	V_s1 = 2.8 km/s
LAYER 3	V_p2 = 6.8 km/s
H = 24.0km	Vs2 = 3.9 km/s
HALFSPACE	V_p3 = 7.8 km/s
	V_s3 = 4.5 km/s

The velocity of the second layer is apparent since no reverse shooting was available. It was also not possible to estimate the dip of the refractor. Since the stations are not positioned along a linear profile, but moreover cover a wide azimuthal range (Table 6). The velocity structure, therefore, has to be regarded as very preliminary and approximate. The maximum observable signal range for this charge is about 60km. A superficial weathered layer with a thickness of 1km and a MOHO depth of 32km had to be introduced to obtain a useful crustal model.

The localisation of known quarry blasts constitutes a check for the validity of the obtained crustal model. There is one large quarry near the Hamamlıkazık (SHMK) and Çataltepe (CTPT) stations. Other smaller ones exist near the Iğdır (SIGD) station. The recordings from blasts have been identified by analysing the waveforms at the above stations. The epicentre

locations of 48 recorded blasts provided solutions which are clustered around the true quarry locations (Figure 4) and thereby showing the uncertainty of source locations due to the velocity model used. This test shows that the model is a realistic one, despite its poor determination.

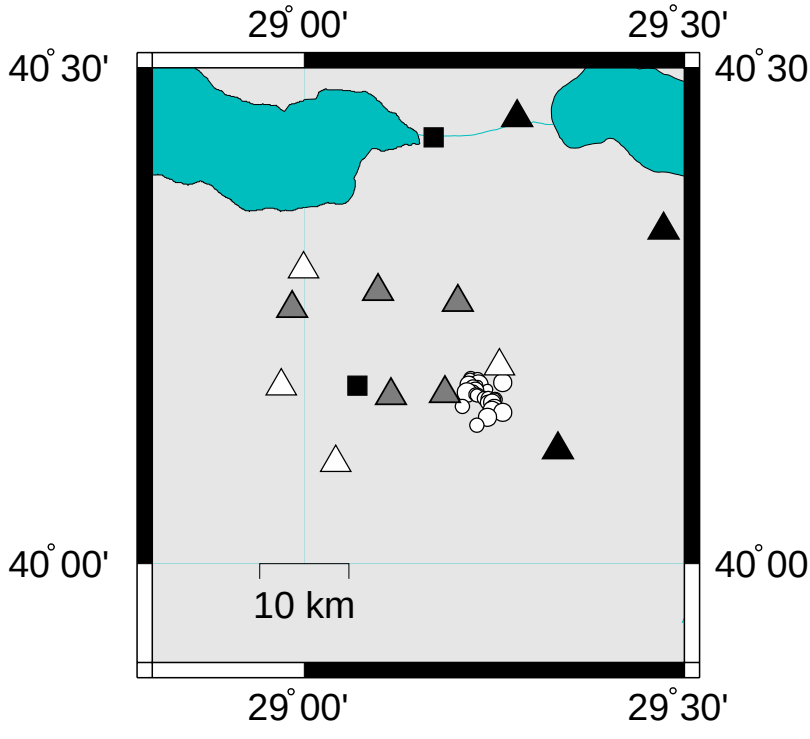


Figure 4: *Identified quarry blast locations (region A_0 on Figure 2).*

Localisation and magnitude assessment

All events recorded throughout the project period were localised using the Hypo 71 program (Lee and Lahr 1972) but the above-mentioned time corrections for elevation in the ”Kestel” model were applied only to the earthquakes in the Bursa area.

The magnitudes (M_L) were calculated by using magnitude relations determined by Kalafat (1989a) for the KOERİ stations in the Marmara region, which are based on the duration of the seismic coda waves (Lee et al. 1972). The magnitude of an earthquake was first calculated at each station separately and later averaged over all the recording stations. Table 7 contains the magnitude-duration relationships for the KOERİ stations.

T is the duration (in seconds) from the first P wave arrival up to the background noise level of the coda-waves and D is the epicentral distance (km). The last column shows correlation coefficients for each equation. The coefficients for each station were incorporated in the subroutine related to the magnitude determinations of the HYPO71 program (Lee and Lahr 1972). Thus, instead of using a single magnitude equation for the whole network, magnitude estimations were performed at each station separately. If the magnitude of an earthquake was greater than 4.5, a different group of magnitude equations were used in the calculations (Kalafat 1989a).

Station Name	duration – magnitude – relationships
IZI:	M_L = 1.401 + 0.448 Log T + 0.0010 D (0.95)
YLV:	M_L = 1.594 + 0.413 Log T + 0.0005 D (0.97)
KCT:	M_L = 1.650 + 0.416 Log T + 0.0008 D (0.86)
DST:	M_L = 1.444 + 0.416 Log T + 0.0004 D (0.94)
GPA:	M_L = 2.096 + 0.342 Log T + 0.0009 D (0.96)
ALT:	M_L = 1.923 + 0.352 Log T + 0.0009 D (0.93)
EY_L:	M_L = 1.767 + 0.358 Log T + 0.0005 D (0.90)
HRT:	M_L = 1.733 + 0.359 Log T + 0.0009 D (0.97)
ISK:	M_L = 2.048 + 0.351 Log T + 0.0009 D (0.96)
CTT:	M_L = 1.816 + 0.341 Log T + 0.0015 D (0.96)
BNT:	M_L = 1.548 + 0.441 Log T + 0.0008 D (0.96)
EDC:	M_L = 1.769 + 0.418 Log T + 0.0004 D (0.96)

Table 7: Duration dependent magnitude equation obtained for MARNET stations (confidence levels in brackets).

Duration magnitude equations were also determined for the four TÜBİTAK stations AHMT, KRZT, MIST, CTPT using the KOERİ's M_L magnitudes as reference magnitudes. For this purpose, the constants a, b and c of the general relationship below were calculated by regression analysis.

$M_L = a + b \log T + c D$

where T is the duration [s] and D the epicentral distance [km] for the TÜBITAK stations. The results of the regression analysis are seen in Table 8:

Station Name	duration – magnitude – relationships
AHMT	M_L = 0.244(±0.24) + 1.599(±0.17)Log T + 0.0018(±0.0006) D
KRZT	M_L = 0.608(±0.14) + 1.265(±0.11)Log T + 0.0025(±0.0003) D
CTPT	M_L = 0.394(±0.15) + 1.361(±0.10)Log T + 0.0026(±0.0003) D
MIST	M_L = 0.231(±0.17) + 1.518(±0.11)Log T + 0.0021(±0.0004) D

Table 8: Duration magnitude equations for the TÜBİTAK stations.

The standard deviation for each constant is put in parenthesis. Table 9 gives the limitations of the above magnitude equations, such as correlation coefficients, minimum and maximum magnitude intervals, minimum and maximum epicentral distances and, finally, the amount of data used in this calculation.

Code	Num	Cor.	M_L (min)	M_L (max)	Dist (min)	Dist (max)
AHMT	300	0.96	1.8	4.4	8 km	403 km
KRZT	710	0.95	1.8	4.6	1 km	389 km
CTPT	744	0.96	1.6	4.6	1 km	407 km
MIST	611	0.95	1.8	4.6	1 km	48 km

Table 9: Limitations of the TÜBİTAK magnitude equations.

Magnitude equations were solved with a large amount of data (see Table 9) covering a reasonable magnitude range. However, magnitude values smaller than 2.0 are not well represented.

In this study, Wood-Anderson seismograms were simulated by using two horizontal components of the Kibletepe base station of the İZİNET. For the conversion procedure, the original seismic signal was first band-filtered between 0.5 and 15Hz. After Fourier transformation, the ground motion spectrum was calculated by taking into account the transfer function of the seismograph. Finally, the time series were simulated by using the transfer function and phase response of the Wood-Anderson seismograph.

Local magnitude (M_L) was calculated from the maximum trace amplitude (A) and distant dependent attenuation values (A_0) were obtain by the following well known formula.

$M_L = \log A - \log A_0$

$\log A_0$ is determined from the equations (Eaton 1992).

$\log A_0 = 0.15 - 1.60\ D$, for $D < 200$km

$\log A_0 = 3.38 - 3.00\ D$, for $D > 200$km

These calculations were carried out for each component and an arithmetic average was calculated to obtain the M_L magnitude. Wood-Anderson seismograms of fifteen recordings were calculated in order to compare differences between the magnitude obtained by the duration dependent equation and that simulated by W-A seismograms. The differences found were not larger than 0.2 magnitude unit, however, simulated seismograms give more reliable results for short distance and small magnitudes. This is very useful for small size networks and the determination of small magnitudes, such as in the Bursa network.

Data evaluation: Seismicity observation

Distribution in space

A general evaluation of the seismic activity during the period September 1992 – May 1995 reveals three main earthquake cluster zones (Figure 5):

- the Gemlik bay activity,

- the Emet zone activity and

- the activity on the Bursa-İnegöl plain, with which this project is mostly concerned.

Relatively low seismic areas separate these zones. Each of the active zones are described individually in the following paragraphs, mentioned localities are shown on Figure 1 of Theme 1, Introduction to this volume.

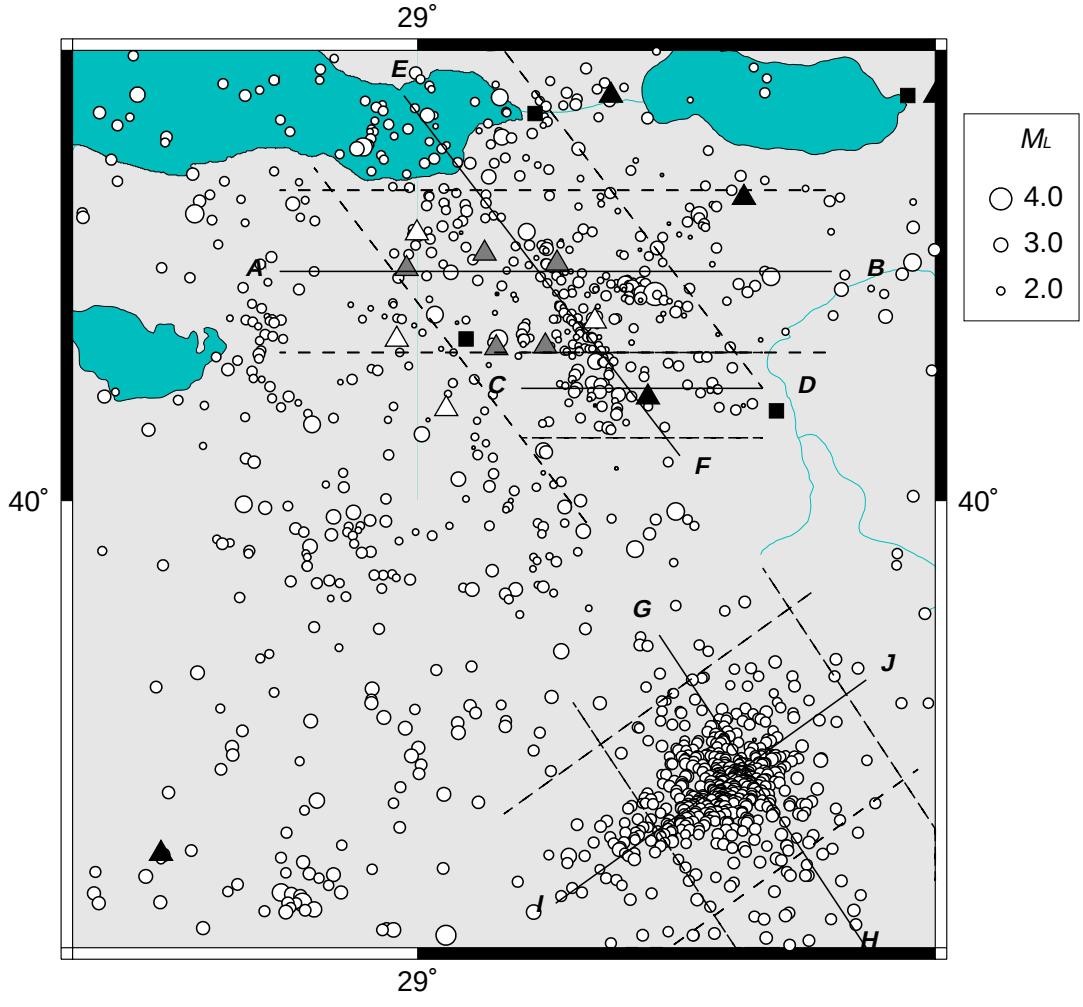


Figure 5: *The epicentral distribution of the earthquakes located in this study (1992-1995) (region A_1 of Figure 2).*

Gemlik bay: The northernmost cluster is the Gemlik bay activity. It is associated with the southern zone of the western extensions of the NAFZ, i.e. that which passes through the İznik-Mekece valley, along the southern shore of lake İznik and which penetrates into Gemlik bay near the town of Gemlik. This fault zone, which essentially shows a right lateral strike-slip mechanism to the east, is expected to have a strong normal component inside Gemlik bay. This region is outside the area of the Bursa project and the station distribution is not favourable to provide a reliable picture of the source properties.

The Emet zone: The southernmost clustering is also outside the study area of this project. The seismicity is reflected by an intense clustering around Tavşanlı and known to have existed for at least the last 10 years. It has been proposed that this clustering marks the northwestern end of the Kütahya fault, which is known for its recent activity. As for Gemlik bay, the station geometry is not suitable for a very detailed study of this active spot.

The Bursa-İnegöl plain: The main goal of this project was to study the seismic activity of the Bursa-İnegöl plain and its vicinity. It is noteworthy that the plain itself shows only very minor seismic activity, except the distinct earthquake clusters at Sayfiye, Çataltepe and Ulubat, described in the following.

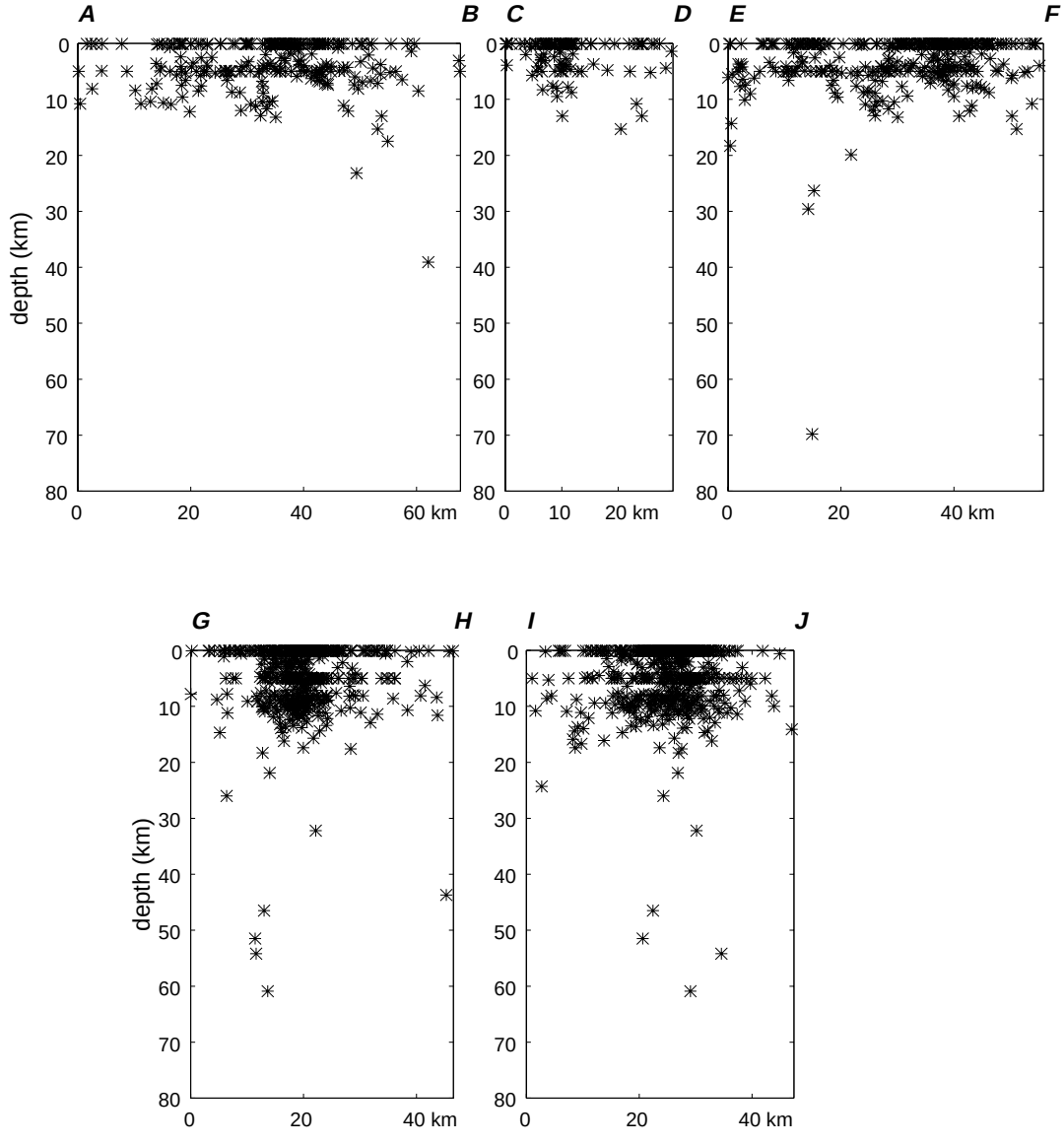


Figure 6: Hypocentral depth distributions along profiles indicated in Figure 5.

- *The Çataltepe clustering:* The Çataltepe clustering corresponds to the large event which occurred on 21 February 1994 (M_L=4.1). Apart from this event, no noticeable activity was observed in this locality. This relatively large event and its aftershocks are examined more closely below. Furthermore, this earthquake is obviously the largest event which occurred during the observation period in the study area. The hypocentre location of the main event is quite reliable (RMS: 0.35s), which cannot be said for all of the aftershocks. Nevertheless, all of the epicentres were clustered in a small area of approximately 2km x 2km. The main event was located at a depth of 5km, while the aftershocks tended to be at 6-8km (Figure 6 A-B). There were 3 foreshocks and 25 aftershocks associated with this event (see Table 10). The total activity was concentrated over a period of 15 days and no other microearthquake activity was observed in this location before or afterwards. In fact, if a seismicity map is redrawn with this event and the aftershocks removed, there is no evidence for a fault at this location. The fault plane solution of this event is discussed in a subsequent chapter on source mechanisms (see also Figure 15d).

Date year	Mo Day	O-time h m s	Lat. N	Lon. E	Depth [km]	M_S	
1994	02 20	04 23 34.1	40.222	29.300	9	3.0	foreshock
1994	02 20	06 04 40.3	40.231	29.330	9	2.4	foreshock
1994	02 20	07 44 32.7	40.227	29.297	15	2.9	foreshock
1994	02 21	04 36 22.5	40.232	29.344	5F	4.2	main shock
1994	02 21	04 51 38.4	40.218	29.319	7	1.4	aftershock
1994	02 21	04 57 22.3	40.214	29.320	8	1.4	aftershock
1994	02 21	05 12 12.4	40.217	29.335	0F	1.7	aftershock
1994	02 21	05 14 36.0	40.228	29.317	0F	1.9	aftershock
1994	02 21	05 25 06.4	40.217	29.321	8	1.4	aftershock
1994	02 21	07 42 21.0	40.236	29.341	12	1.5	aftershock
1994	02 21	08 27 04.0	40.220	29.217	7	1.6	aftershock
1994	02 21	08 46 50.8	40.209	29.295	5	1.5	aftershock
1994	02 21	09 14 16.2	40.238	29.386	6	2.1	aftershock
1994	02 21	12 41 39.8	40.229	29.246	5	1.8	aftershock
1994	02 21	20 56 50.0	40.241	29.284	7	1.6	aftershock
1994	02 21	22 10 43.8	40.223	29.310	2	1.5	aftershock
1994	02 21	22 24 27.0	40.204	29.202	7	2.1	aftershock
1994	02 22	08 12 17.2	40.260	29.398	0F	2.1	aftershock
1994	02 22	14 57 47.2	40.211	29.264	11	1.7	aftershock
1994	02 23	07 45 10.4	40.236	29.295	8	2.1	aftershock
1994	02 23	10 05 42.9	40.220	29.283	7	2.5	aftershock
1994	02 24	18 48 30.5	40.220	29.396	6	1.0	aftershock
1994	02 27	03 25 18.9	40.210	29.328	8		aftershock
1994	03 01	17 26 34.3	40.222	29.308	6	1.9	aftershock
1994	03 06	17 44 04.6	40.284	29.341	5	2.0	aftershock
1994	03 06	20 10 23.5	40.274	29.345	2	2.2	aftershock

Table 10: Main event of 21 February 1994 and associated foreshock/aftershock activity.

- *The Sayfiye clustering:* The clustering near Sayfiye is known to have existed for a long time on the eastern slopes of the Uludağ mountain. No local data are available for the past several decades, except for during a three month observation campaign in 1983 during which an intense activity at exactly the same location was also observed. Most of the events were located in the upper crust (h<15km) and, therefore, often felt locally (Figure 6 C-D). Inhabitants of this region are also aware of this activity and indicate that there has been a noticeable increase over the last decade. It has been proposed that this location is the intersection point of the Eskişehir fault and the southernmost branch of the NAF (Schindler this volume). However, at the moment there is no seismological evidence to support this hypothesis.

- *The Ulubat activity:* There is no striking feature which can be interpreted in terms of local faulting. One exception to this is the NE-SW alignment of epicentres along the southeast coast of Ulubat lake. This alignment can most probably be associated with the Ulubat fault which is traceable through geomorphological features at the surface.

Finally, as far as the town of Bursa and its vicinity is concerned, there exists no noticeable activity associated with any of the known local faults. No particular seismic activity has been observed in the zone directly where the hydrothermal sources are aligned. The events located to the east of Kaplıkaya are the only ones appearing in this zone. However, they also could possibly be linked to the mislocated local quarry blasts. Although most of the events due to artificial sources have been identified as such using the near stations (CTPT, KAPT, IGDT), it is highly probable that very few doubtful traces were misinterpreted as natural events and were not eliminated.

Magnitude distribution

The magnitude distribution in the study area was also investigated for the earthquakes over the period 1976 – 1995 by adopting a linear Gutenberg-Richter relationship with the following result

$\log N = 5.55\ (\pm 0.1) - 1.15\ (\pm 0.1)\ M_L$

where N is the frequency of earthquakes in a certain magnitude interval, a and b are constants and the terms within the parentheses are estimated standard deviations of these constants. The magnitude threshold for this period is $M_L = 2.6$ (Figure 7).

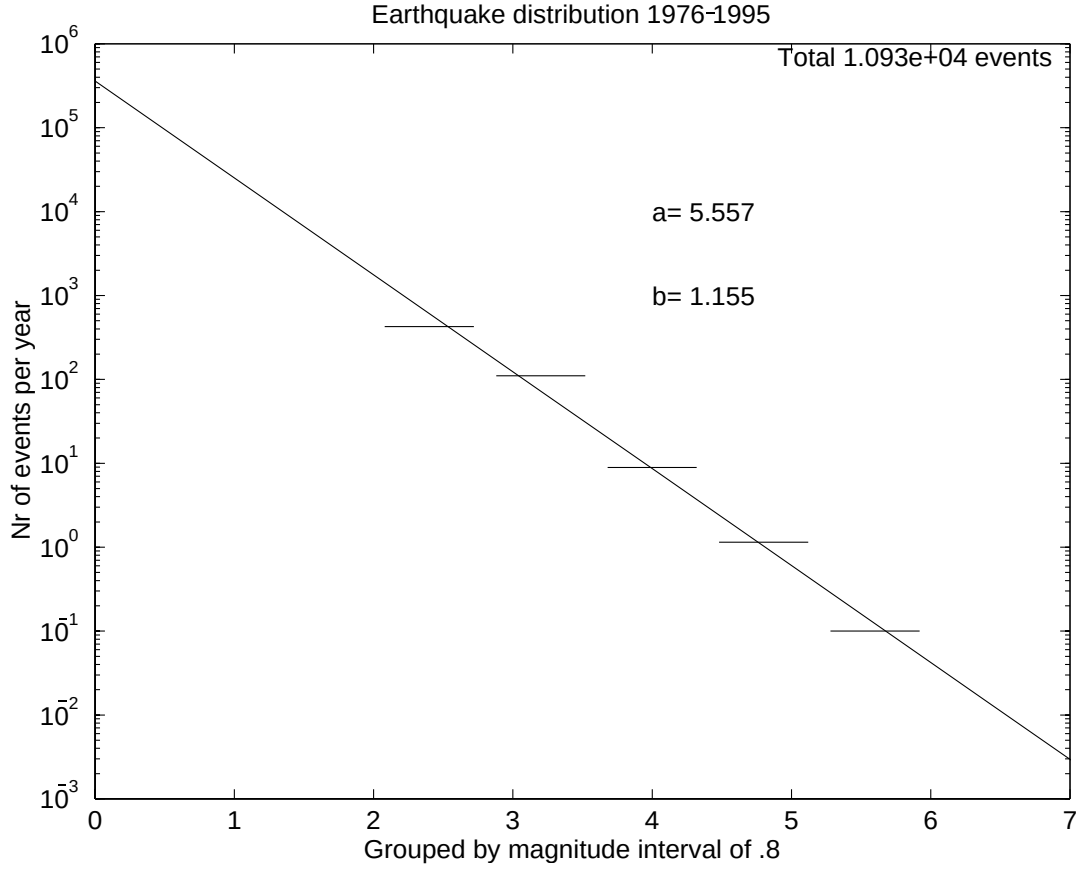


Figure 7: Gutenberg-Richter log N = a – b M graph for the period of 1976 – 1995 in the Bursa region.

Distribution in time

The occurrence of earthquakes over the period 1976 – 1995 varies quite strongly with time, as can be seen from Figures 8 and 9.

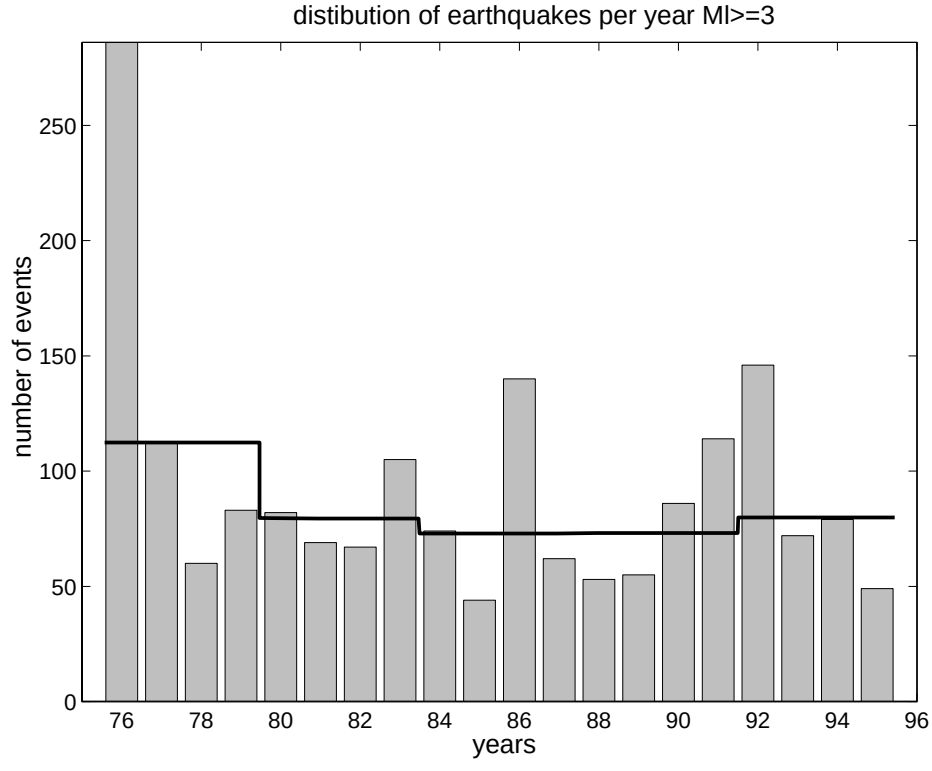


Figure 8: Number of earthquakes 1976 – 1995 M_L(≥3.0) in the Bursa study area.

The activity is obviously also migrating within the chosen space window. The number of earthquakes per year for the whole window (Figure 9) indicates rather normal behaviour, which can be seen in many other areas of the world. The number of earthquakes (M≥3.0) is changing within a certain range (50-150 events/year), but the average trend is stable and between 70-80 events/year. This feature was already observed in the strain energy release curve in Figure 3, in which a remarkably steady linear trend is seen over the past 20 years. All of this indicates that the window chosen in this study is rather independent from the surroundings with respect to seismic energy release. Figure 9 shows the clustering of events. Each of the clusters is active during a certain time period, ranging from 1 to 5 years.

Seismic hazard in Bursa

A seismic hazard study for the city of Bursa was carried out using the standard SEISRISK III computer code by Perkins and Bender (1987). For this study, only the most recent earthquake catalogue for the time period 1976-1995 was used. The dimension of the study area for the delineation of seismic source zones around Bursa (170km x 200km) was chosen in such a way that the ground motion of larger earthquakes with a magnitude of 5 still produce significant ground motions in Bursa (e.g. larger than 0.0001g, when applying standard attenuation models). After designing the seismic sources, the respective seismicity parameters (frequency of occurrence and Gutenberg-Richter gradient) were determined.

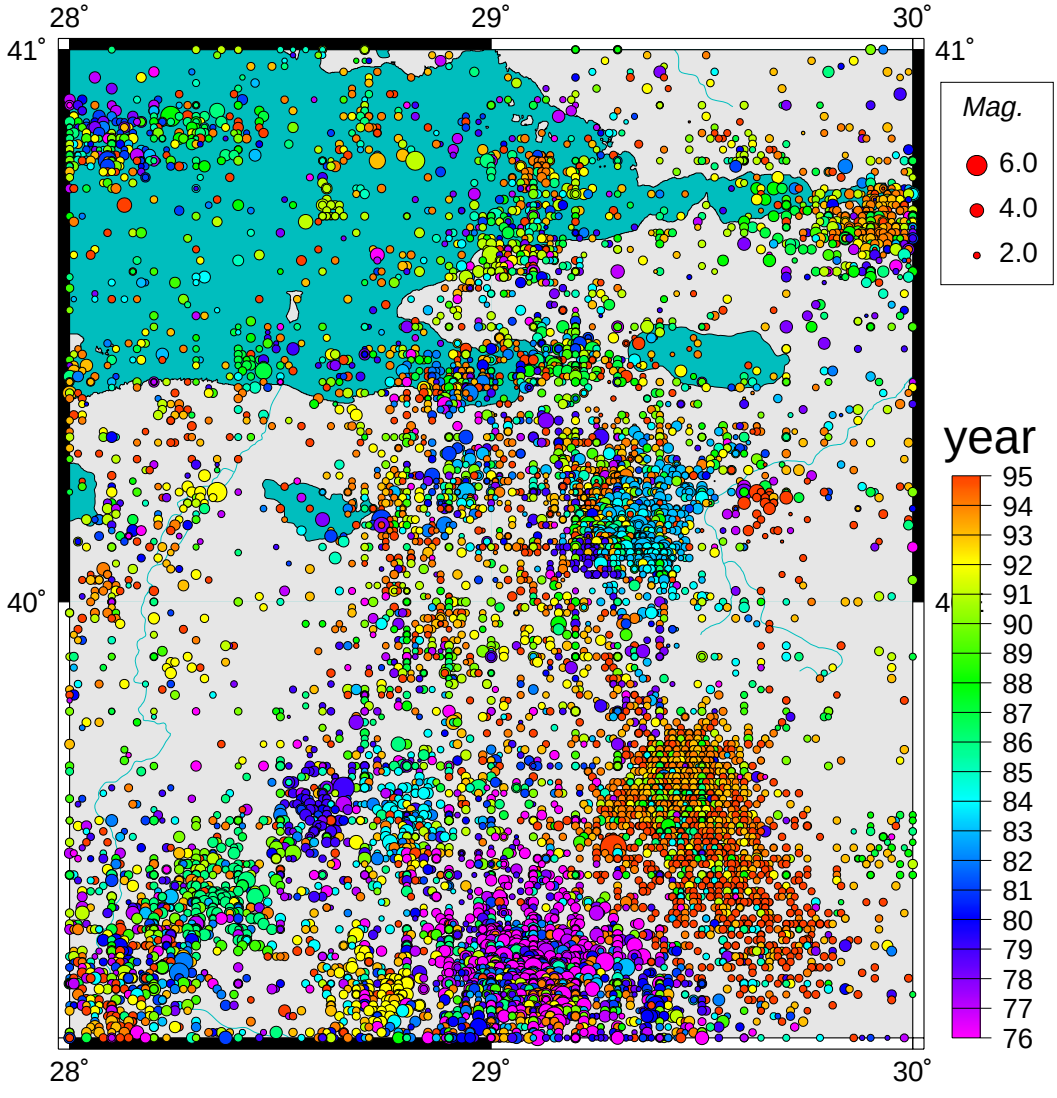


Figure 9: *Epicentre distribution for 1976 – 1995 showing the clustering in time (the area corresponds to the Figure 2).*

In total, 8 seismic sources were defined by identifying the most active regions around Bursa for which the activity is clearly above average. Figure 10 shows the distribution of the sources. All activity is associated with areal sources, no specific faults have been assumed within the window. This procedure seems to be justified because of the very scattered distribution of the epicentres, which cannot be associated with one specific mapped fault without any doubt. This procedure is preferable to the delineation of "active faults" with more or less supposed activity concentrated on them. The design of areal sources also takes the inevitable location errors during this time period into account, which is certainly on the order of 10km for the first ten years. This procedure normally leads to a rather smoothed distribution of hazard. In this case it is not significant how the hazard is presented outside the studied Bursa site. However, when mapping is of concern, the classification of areal and linear sources should be reconsidered.

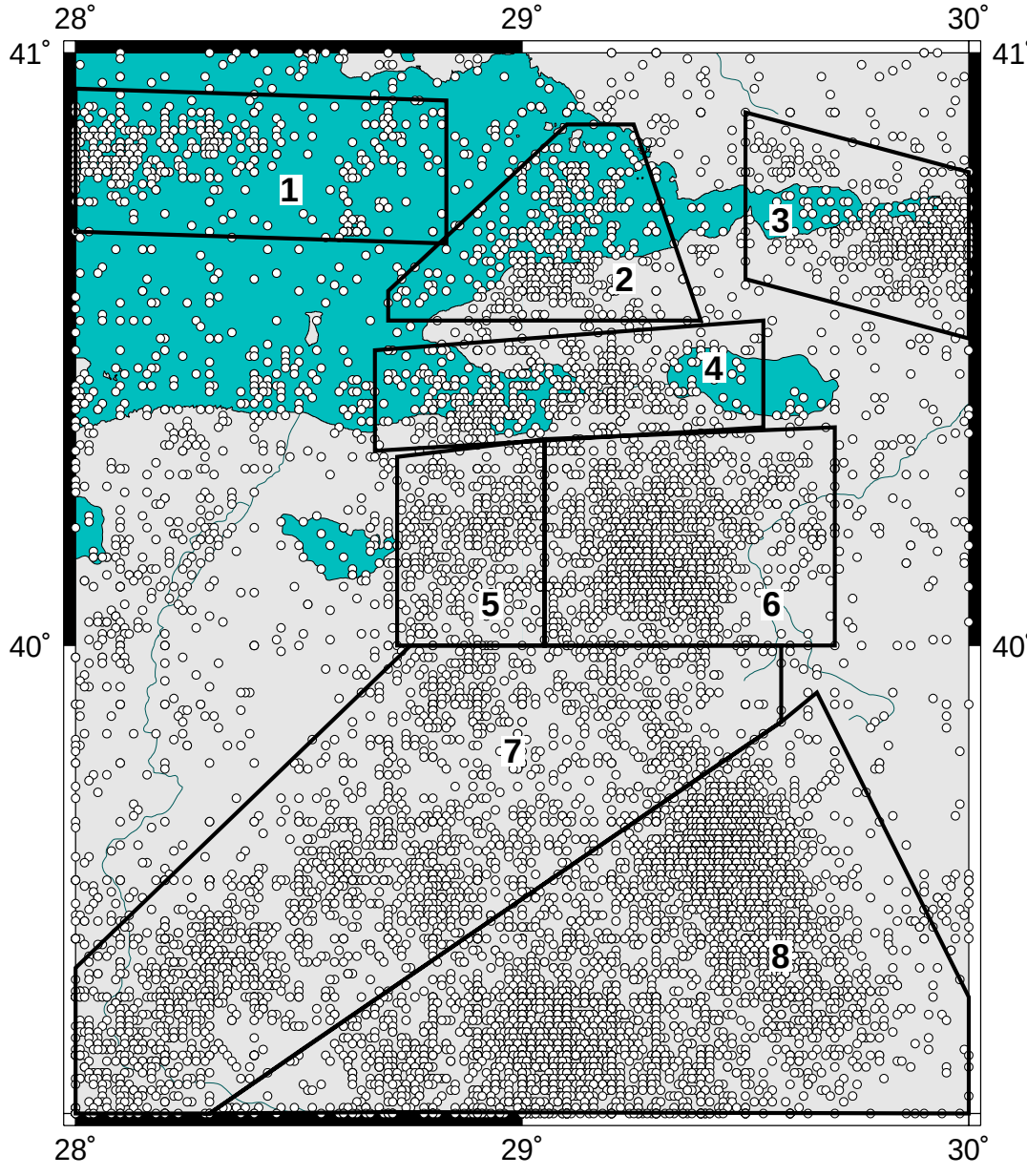


Figure 10: The eight seismic source zones delineated within the window chosen for the Bursa City hazard study (Figure 9: earthquake activity from 1976 – 1995).

The magnitude distribution is plotted in Figure 11 for each of the seismic sources 1 through 8. The remarkable result of this exercise was that all b-values range from 0.9 to 1.1, which can be considered as "normal" behaviour compared to the average worldwide b-value of 1.0. This finding is particularly noteworthy since the magnitude range due to the relative short time window of 20 years is narrow (2.0 to 5.0) and the time variation within the time window is large with respect to the source areas. This time-space variance was described in the preceding chapter.

For the hazard calculation, a linear extrapolation was done up to magnitude 7 in the <LogN – M> graphs (see Figure 11). This procedure must be considered conservative with respect to the calculated results. An upper bound of magnitude 7.2 (for a magnitude window of ±0.2) is sufficient as long as return periods of less than 500 years are considered. For larger return

periods the upper bound magnitudes have to be re-evaluated in the context of the tectonic situation. Guiding parameters for the maximum possible earthquake are maximum fault lengths and maximum slip rates in the seismotectonic province of Bursa.

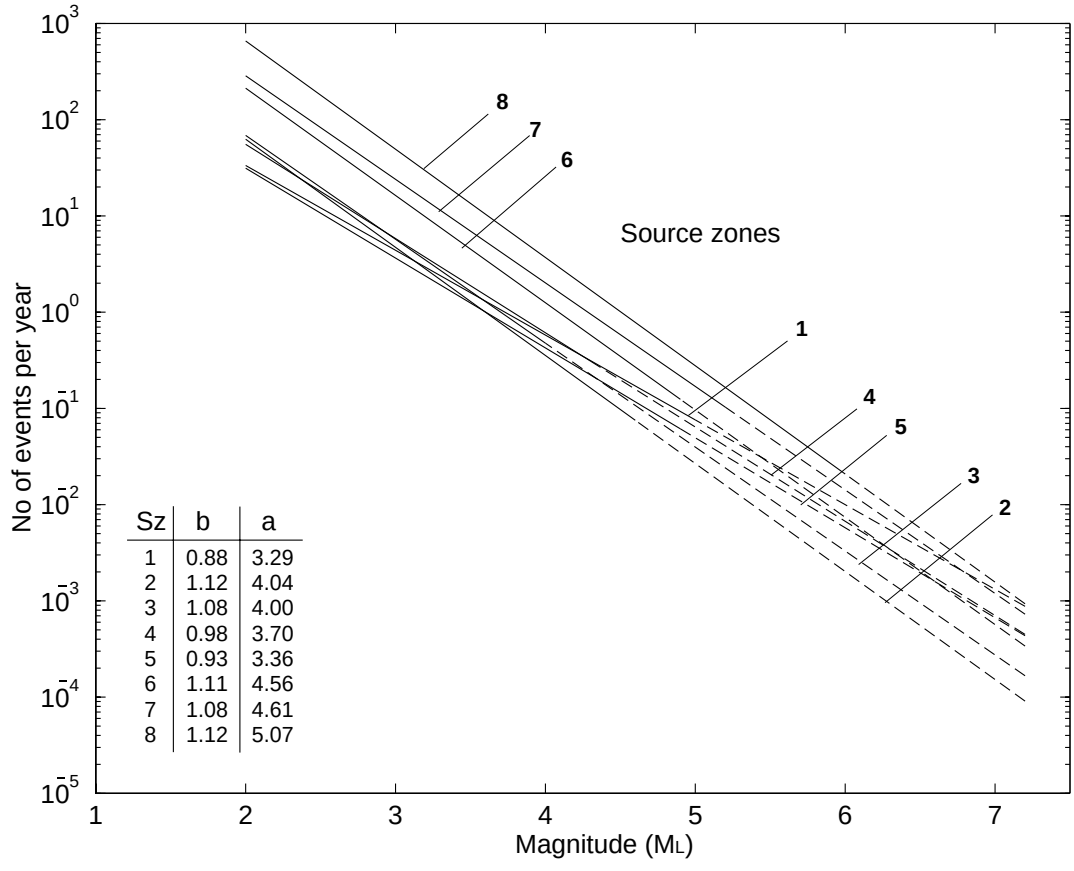


Figure 11: Magnitude distribution for the eight source zones in Figure 10.

For the calculation of hazard at a certain site, regionally valid attenuation models for the ground motion have to be used. Since no specific strong motion data for the Bursa area were available, a model introduced by Joyner and Boore (1991), based on worldwide data, was adopted for the calculation. These attenuation models had to be tabulated for the SEISRISK III-input file. The peak acceleration was chosen as the representative parameter for ground motion. This is in agreement with engineering practice, but it is well-known that peak values are rather loosely related to the damaging power of an earthquake. Other parameters, e.g. duration of strong shaking and frequency contents, are of at least equivalent importance.

For the Bursa hazard calculation, SEISRISK III requires input parameters for the ground motion attenuation model as well as for earthquake rates (yearly occurrence of earthquakes of a certain level of magnitude) with respect to magnitudes. Figure 12 shows the attenuation of acceleration used for the Bursa area. This model is used in many areas of the world, however, it is not specially adapted to Turkey. The model is valid between magnitudes of 3.0 to 7.6, and for a distance range of up to 200km.

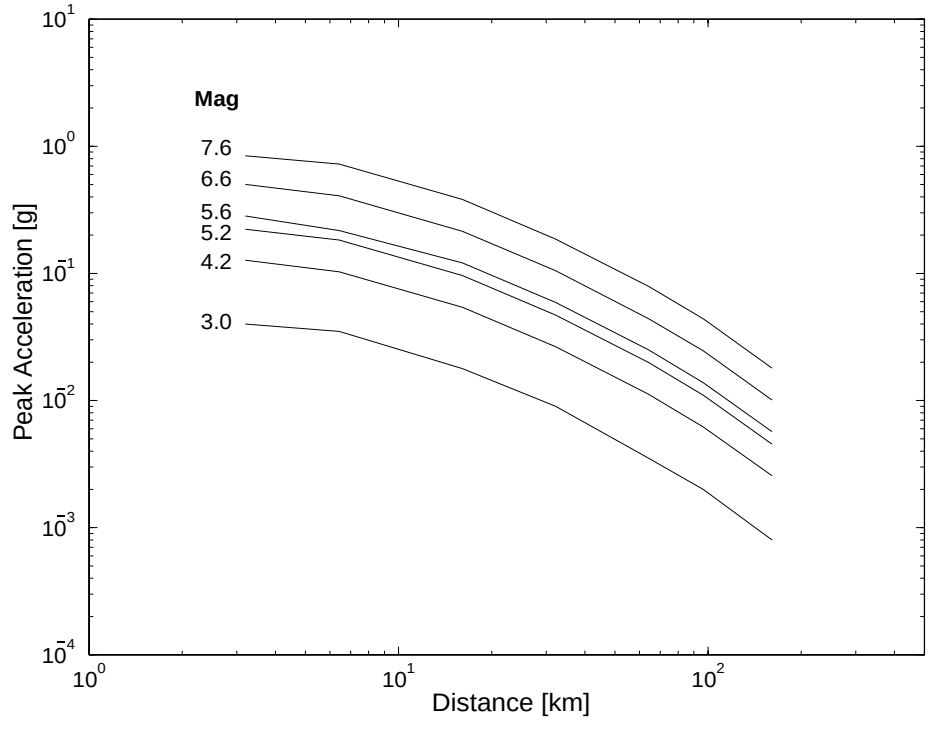


Figure 12: Attenuation model (Joyner and Boore 1991) used for the seismic hazard calculations for Bursa (mean values).

Figure 13 shows in graphical form the two parameters, a and b, of the Gutenberg-Richter relationship for the source zone 1-8. The rate of activity (a) is normalised to 1km^2 to accommodate for the different source size.

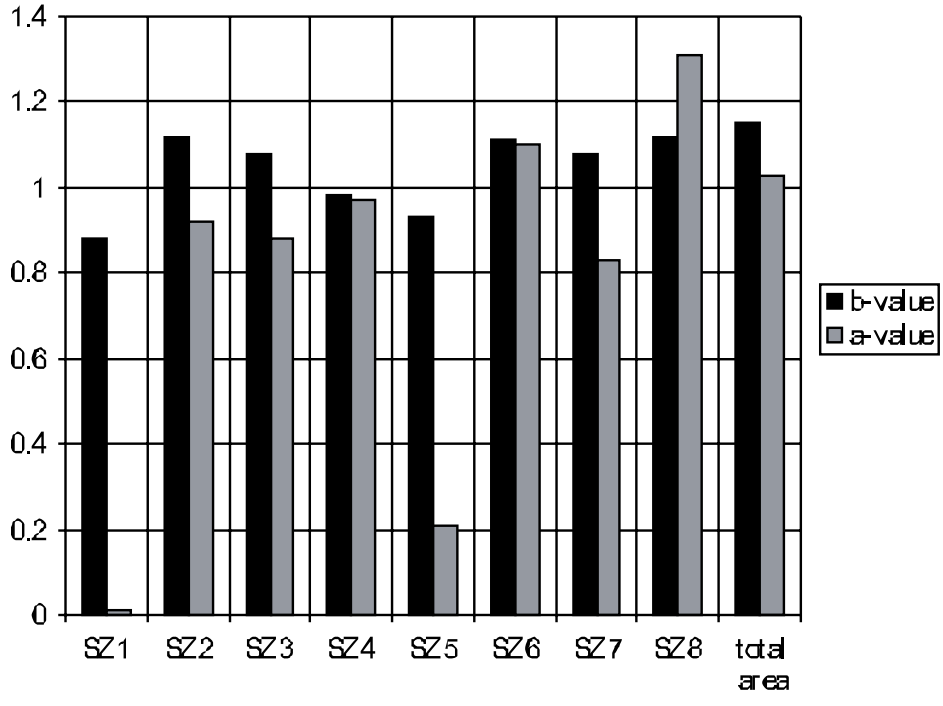


Figure 13: Graphical display of a- and b-values in the Gutenberg-Richter relations for source zones 1-8 (see Figure 10). The values of the total Bursa area are included for comparison. The rates (a-values) are normalised to 1km^2.

Source zones 1 and 5 show low seismicity and therefore do not noticeably contribute to the seismic hazard in Bursa. The same may be said for those areas which are not transformed into source zones because of their low seismicity. The undoubtedly highest contribution comes from source zone 6, where Bursa is situated. Any change in the parameters of this zone will dominate the output of the calculations.

SEISRISK III: Results of hazard calculations, Bursa site at Long = 29.1N, Lat = 40.2E

Attenuation variability: sigma=0.0			Attenuation variability: sigma=0.5	
G.M.	occ./yr	R (years)	occ./yr	R (years)
.02	76.12969	0.2	74.51785	0.2
.04	3.14166	1.1	4.03011	0.6
.06	.60926	3.6	.97248	1.6
.08	.15970	8.5	.33214	3.3
.10	.06337	18.5	.13961	6.0
.12	.02517	34.7	.06776	10.2
.14	.01393	67.1	.03640	16.3
.16	.00671	122.0	.02103	24.8
.18	.00346	211.2	.01284	36.5
.20	.00181	342.2	.00819	52.0
.22	.00103	529.2	.00541	72.4
.24	.00062	785.1	.00368	98.7
.26	.00036	1096.4	.00257	132.2
.28	.00026	1522.4	.00182	174.1
.30	.00018	2084.7	.00132	226.1

Table 11: Occurrence and return periods of ground acceleration levels (G.M.) for the city of Bursa.

The habitual manner in which the hazard at a site is expressed, is to indicate the ground motion which is not exceeded with 90% probability over a certain period. The results below give the ground acceleration (in g = earth acceleration) for three different time windows. The 90% nonexceedance probability in 50 years, for example, corresponds to a statistical return period of 475 years, which is the level adopted in the new unified 'European Building Code 8'. Values for a rather conservative figure of sigma = 0.5 represent a more realistic output than for sigma = 0.0, since the scatter of the input data is relatively high. This is certainly true for the attenuation relationship used in this study.

For different assumed life expectancies of buildings (10, 50 and 100 years) the ground acceleration is calculated for a probability of 90% that these values will not be exceeded. The results are as follows:

90% non-exceedance probability with sigma = 0.0:

0.15g in 10 years

0.22g in 50 years

0.25g in 100 years

90% non-exceedance probability with sigma = 0.5:

0.24g in 10 years

0.36g in 50 years

0.43g in 100 years

It should be mentioned here that the calculation of seismic hazard on the basis of an extremely short earthquake catalogue of only 20 years runs the risk of large uncertainties when extrapolating over a return period of more than 100 years. In the above tables and graphs, such results must be interpreted with necessary care. The uncertainty is significant in these results. However, a comparison with previous hazard studies carried out for the entire western part of Turkey shows that the values obtained here are reasonable and can be adopted as preliminary figures.

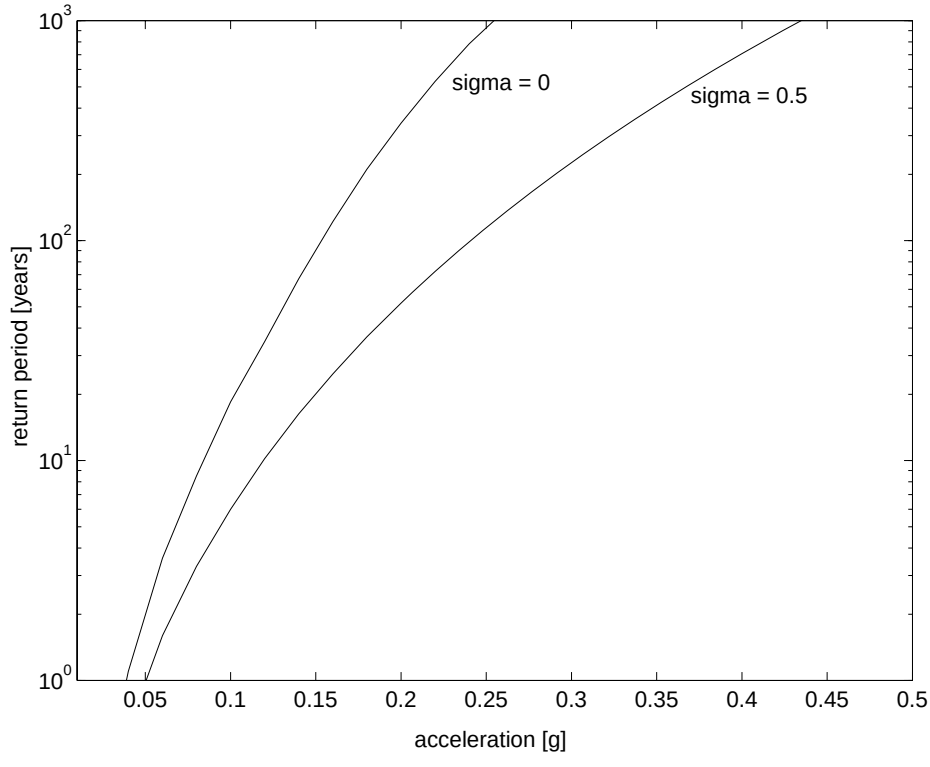


Figure 14: Return period for ground accelerations for the Bursa site. The two relations consider two different sigma-values, 0.0 and 0.5, respectively.

Data evaluation: Source mechanisms and spectra

Fault-plane solutions and station diagrams

The relationship between seismicity and local tectonics was investigated by looking at fault-plane solutions of selected earthquakes in the Bursa area and two station diagrams of seismic stations of the Bursa seismic network. Because of low seismic activity during the project

period, only a limited number of fault-plane solutions could be established for earthquakes with sufficiently large magnitudes to enable reading of reliable first motion. The fault-plane solutions for the four earthquakes studied are shown in Figure 15.

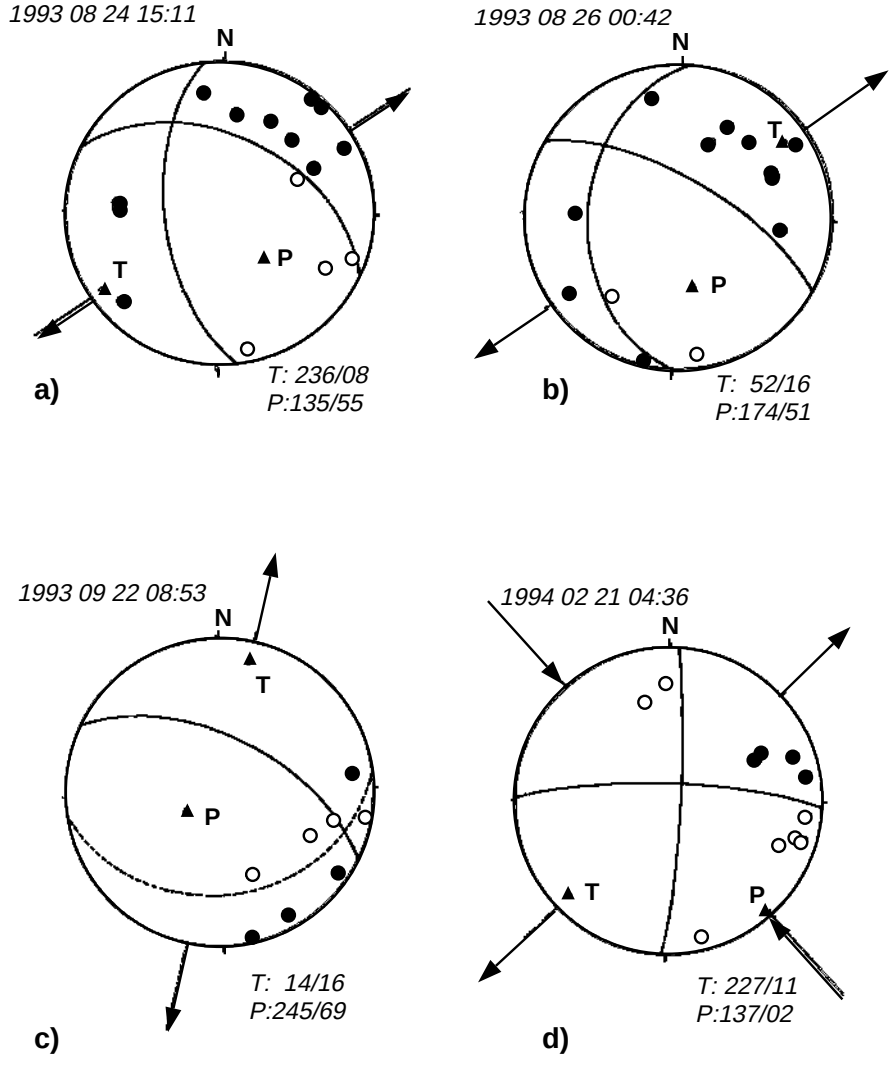


Figure 15: Fault plane solution for 4 different earthquakes.

The focal mechanisms of the events of August 24, 1993 (Fig. 15a), August 26, 1993 (Fig. 15b) and September 22, 1993 (Fig. 15c) are of normal faulting type with a minor component of lateral shear. The nearly horizontal T-axes of these earthquakes are oriented NNE-SSW (N14E) to NE-SW (N56E). The P-axes, i. e. the orientations of maximum compression, are aligned on a nearly vertical plane, striking NW-SE. The mechanism of the February 21, 1994, earthquake (Fig. 1, Fig. 15d) is of strike-slip type, with a NS striking sinistral and an EW striking dextral fault-plane. The T-axis is oriented SW-NE (N227E), the P-axis NW-SE (N137E).

Another way to investigate the local tectonic trend is to construct so-called station diagrams (Pavoni 1984). Station diagrams are local seismicity maps, centred at a particular seismic station, in which the epicentres are represented by the polarity of the first arrival recorded at the respective station. Particularly in regions of predominantly strike-slip tectonics, these diagrams can be used to obtain the orientation of the principal horizontal stress components. If the tectonic stress field in the region is homogeneous, azimuthal distribution of compression

(C) and dilatation (D) should become apparent in the station diagram. Station diagrams are especially useful if many small earthquakes are recorded, but representative fault-plane solutions cannot be constructed because of insufficient number/quality of recordings for single events.

Figure 16 shows the diagrams for the CTPT and MIST stations. For these graphs, which cover the period 1992- 1995, only earthquakes with magnitudes M_L greater than 2.5 and distances from 10 to 100 km were selected. In the two station diagrams, sectors can be identified which contain predominantly compressional or predominantly dilatational readings. Only sectors with dark shading were used for interpretation. For further information and details about the construction and interpretation of station diagrams see Pavoni (1984), Roth (1986), Roth et al. (1992).

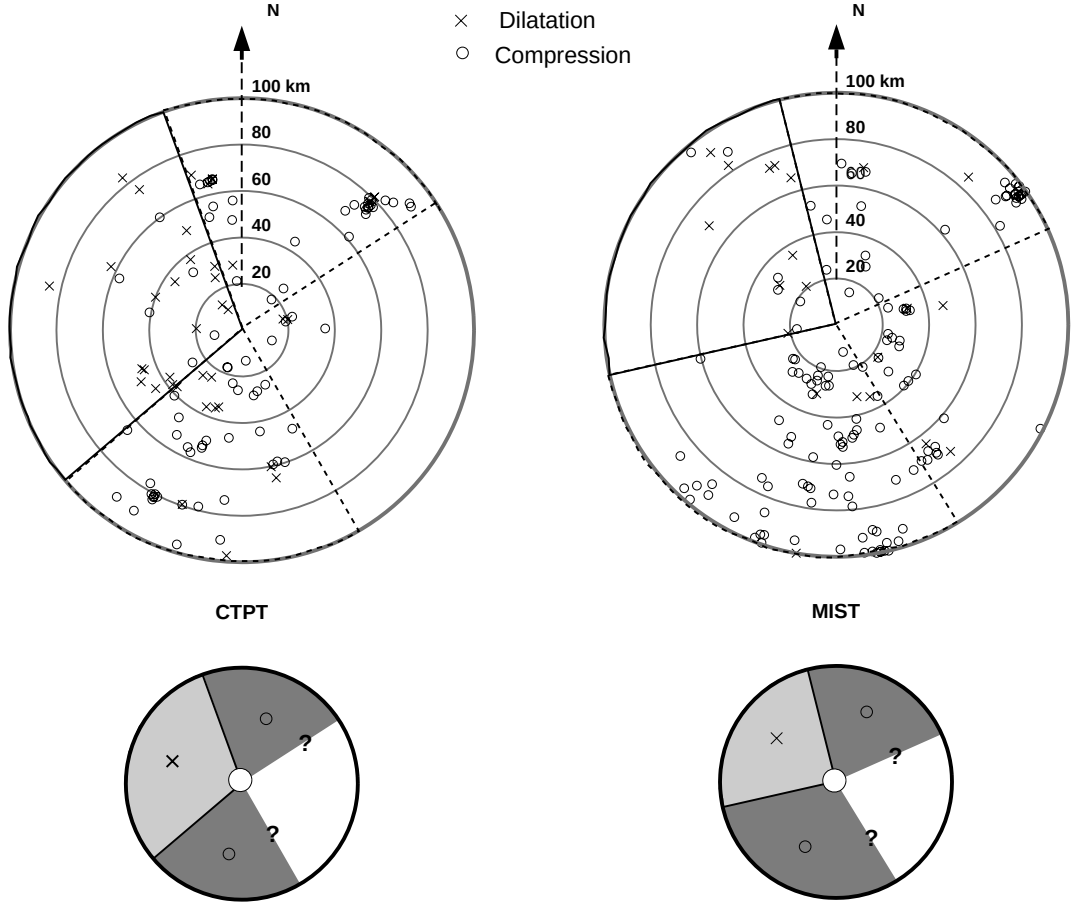


Figure 16: Station diagrams for two locations (CTPT and MIST) and earthquakes of $M_L^{\geq 2.5}$.

Seismotectonics, crustal deformation and present stress state

The fault-plane solutions (Fig. 1, Fig. 15) as well as the two station diagrams MIST and CTPT (Fig. 1, Fig. 16) allow a first statement about the present deformation and deviatoric stress of the Earth crust in the Bursa region and adjacent areas.

The four fault-plane solutions reveal a tectonic stress regime with NE-SW maximum horizontal crustal extension (MHE) and NW-SE maximum horizontal crustal shortening (MHS). Evidently, the earthquakes of August 24 and 26, 1993 (Figs. 15a and 15b), are associated with faulting along the Eskişehir fault zone. The WNW-ESE striking nodal planes, with a dextral

component of lateral displacement, correspond well with the strike of this major fault zone. The event of September 22, 1993 (Fig. 15c), is probably associated with the fault zone along the northern slope of Uludağ. The location of the event and the WNW-ESE striking, NNE dipping nodal plane of the solution correspond well with the zone of young normal faults bordering the Uludağ to the Northeast (Imbach 1992). The February 21, 1994, event (M_L=4.2) belongs to the cluster of earthquakes located near the Gölbaşı lake. Here, the Hamidiye fault, an ENE-WSW trending, dextral strike-slip fault which borders the Yenişehir basin to the Northwest, joins the Eskişehir fault zone. The cluster of earthquakes in the Gölbaşı district seems to be related with tectonic activity at the intersection of the Hamidiye and the Eskişehir fault zones.

The same tectonic stress regime, as inferred from the fault-plane solutions, is indicated by the two station diagrams MIST and CTPT (Fig. 16). The stations MIST and CTPT are located 25km apart, to the west and east of city of Bursa. The station diagrams show the polarities of first arrivals of local events recorded at the two stations during 1992-1995. Maximum horizontal crustal shortening, as derived from the western sectors of the station diagrams, is oriented WNW to NW. Accordingly, MHE is oriented NNE to NE. These trends correspond with the orientations of P- and T-axes of the fault-plane solutions (Fig. 15). The rather regular pattern of P- and T-axes allows the construction of P- and T-trajectories. It is of special interest to note that the results of seismotectonic investigations in the Bursa region fit well into the regional seismotectonic picture of the wider Marmara sea region (Fig. 1).

Apart from the seismological investigations, additional information about the present crustal deformation and stress state is obtained from geological, geomorphologic and geodetic studies. Neotectonic and geomorphologic studies supply important information and estimates of the long term crustal strain, whereas seismological and geodetic measurements supply precise information about the short term behaviour of crustal strain. An integrated observation program can utilise the strengths of each method and overcome their separate spatial or temporal biases. Therefore, a multidisciplinary approach is of great significance for a comprehensive understanding of the deformation process.

As indicated above, it may be convenient to construct trajectories of crustal deformation in order to illustrate and compare the results of the different fields of research. In an actively deforming region, such as the Bursa region, the orientation and pattern of MHE- and T-trajectories on the one hand, and the MHS- and P-trajectories on the other hand, should be directly comparable. An early attempt to construct MHS-trajectories, based on a kinematic analysis of active strike-slip faults in Anatolia and the Middle East, was presented by Pavoni (1969), Fig. 17. According to this analysis, MHE is oriented N33E in the Bursa region. This MHE orientation corresponds with the NE-SW trend of T-axes of the four FPS (Fig. 15). Indeed, the P- and T-orientations, derived from the seismological investigations during the period 1992-1995, fit well into the long-term deformation picture based on neotectonics and geomorphology.

Geodetic studies have been carried out by means of repeated Global Positioning System (GPS) measurements in order to determine crustal deformation within the western part of the NAFZ (Straub and Kahle 1995, Straub 1996). The patterns of normal and shear components of strain derived from the displacements observed between 1990-1994 agree remarkably well with the results of seismological investigations and neotectonic analyses. The distribution of active faults, the spatial distribution of seismicity, as well as the results of GPS measurements, convincingly show that the deformation of the crust and the upper, seismogenic part of the lithosphere in NW Anatolia is characterised by distributed shear (Pavoni 1995). The Marmara region cannot be regarded as part of a rigid Anatolian plate.

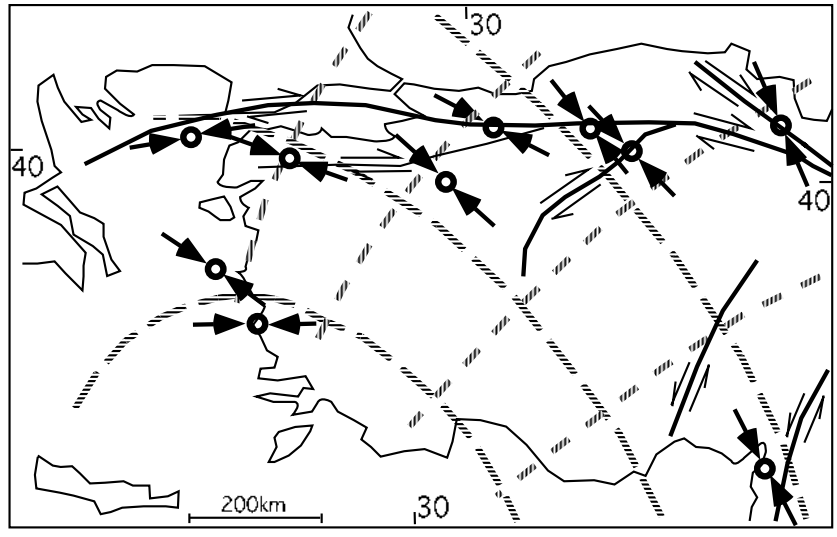


Figure 17: Crustal deformation in Anatolia (redrawn from Pavoni 1969). Solid lines with arrows: major active dextral and sinistral strike-slip faults. Dashed lines: trajectories of maximum horizontal crustal shortening (MHS) and maximum horizontal crustal extension (MHE), derived from active stike-slip faults. Circles: epicentres of major earthquakes with orientation of P-axis (pair of arrows) after Shirokova (1968).

Seismic source spectra

In recent years, numerous studies concerning the kinematic and dynamic source parameters, and the spectral scaling of small to large earthquakes, have been published. Studying the displacement amplitude spectrum of the body wave seismograms, corrected for instrument and path effects, became a common tool to obtain specific source parameters, such as seismic moment, size of source and stress drop.

Commonly adopted source models include the ones proposed by Haskell (1964), Aki (1967) and Brune (1970). The Haskell model is the most prevalent among the kinematic models. The fault is described by five source parameters: the fault length, the fault width, the average dislocation, the rise time of the rupture and the rupture velocity. Since Haskell's source model assumes coherent rupture radiation, this theory may not work for source models with regard to large irregularities in the slip rupture process due to high frequency radiation from the source. Haskell (1964) and Aki (1967) proposed ω^2 and ω^3 models and Aki (1967) developed the ω^2 statistical model even further. Brune (1970) proposed a relatively simple model of faulting that concerns three independent spectral parameters namely: long period spectral level, Ω_0, the spectral corner frequency, f_C and the spectral decay parameter, γ. ω_0, f_C and γ are parameters proportional to seismic moment, source size and source type, respectively. Savage (1972) discussed the differences in source models developed by Brune (1970) and Haskell (1964). Both theories provide a spectrum in which the average trend in the middle frequencies is proportional to ω_1, but the cause of this intermediate trend is entirely different in the two models. Aki (1967) suggested that the corner frequencies at the spectrum of theΩ^2 model depends on the coherence length and the coherence time rather than on the total fault length and the rupture time for large earthquakes.

These results show that the study of the source characteristics of small earthquakes should give important clues about the relationship between source size and temporal development of the rupture, which may in turn help to simulate the source process of large earthquakes. In

the light of the present source models, it is generally believed that the spectral displacement decreases beyond f_C at a rate proportional to ω^2. Savage (1972) examined the effect of stress drop 'completeness' on Brune's spectrum. He proposed an alternative source spectrum in which two corner frequencies appear, depending on the size of the inequality between the effective stress and stress drop values. Hanks (1982) and Papageorgiou and Aki (1983) discussed the existence of a second corner frequency, namely f_{max}, beyond which the decay of the frequencies depart from the ω^2 and ω^3 models. f_{max} was attributed by Hanks (1982) to the effect of absorption due to near surface structures. Originally, Papageorgiou and Aki (1983) attributed f_{max} to the source effect, without considering the site effect. Later, Papageorgiou (1988) showed in the case of the San Fernando earthquake that f_{max} was not significantly different for a soil site or a rock site. In many investigations, the spectral characteristics of f_{max} have been determined, but the origin of f_{max} can not be explained as yet.

Data processing and source spectra

Conventionally, the spectral source parameters of earthquakes are determined from the corrected spectrum of the displacement records of P and S waves. Near earthquakes are recorded by velocity or acceleration seismographs due to the instrumental shortcomings of displacement seismographs. Integrating the velocity and acceleration traces of many earthquakes i.e. to obtain realistic displacement seismograms, is a cumbersome process since it calls for special attention to proper detrending and windowing of the time series. In the case of processing the acceleration traces, the two-fold integration increases the possibility of systematic errors which may finally distort the calculated ground motion record. Concurrently with developments in seismical instrumentation, state of the art accelerometers have a wider spectral band and high dynamic range. This makes an accelerometer a reliable tool for the study of earthquake source processes, not only for larger but also for smaller earthquakes. This study aims therefore 1) to use the acceleration records as well as the displacement traces to determine the spectral source parameters described above, 2) to show the possibility of obtaining the corner frequency without converting acceleration traces into displacement and 3) to find evidences of the parameter f_{max}.

Polat (1995) analysed the three-component digital accelograms of 42 small earthquakes (Table 12) which were recorded by the accelerograph network, having epicentral distances less than 100km in the Bursa area, in order to determine spectral source parameters based on the assumption of Brune's source model. Duration magnitude (M_d) of the earthquakes studied here range from 1.7 to 3.5.

The NS and EW components of the acceleration records were rotated into transverse (SH) and radial (SV) components using the back azimuth of the stations. The frequency range between 0.2Hz and 30Hz is used since the response of the <SM2> accelerometer is flat in this frequency interval. The horizontal S-phase accelerograms were integrated twice to obtain the displacement record. The FFT spectra were calculated for both acceleration and displacement using a cosine tapering of 0.1. SH acceleration and displacement spectra were carefully examined and their patterns correlated with each other to extract the spectral parameters from the acceleration traces. The spectra were also examined to determine the cut off frequency f_{max}, beyond which the spectral amplitudes noticeably decays. The validity of the corner frequency and f_{max} was tested in the spectral domain of both acceleration and displacement (Figure 18).

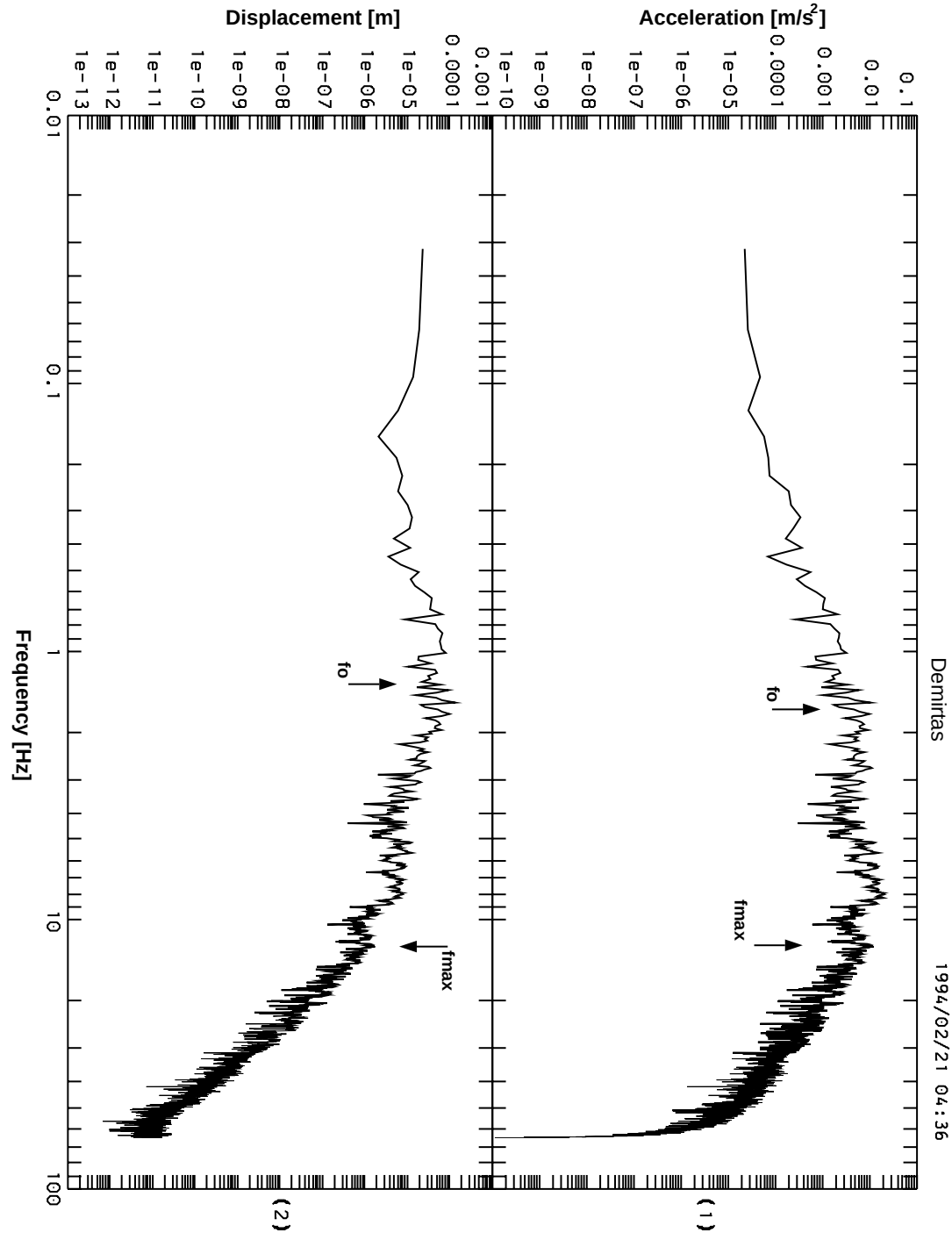


Figure 18: The acceleration and displacement source spectra of the 21 February 1994 earthquake calculated for the stations Demirtaş.

No	Date Year Mo Dy	O-time h m s	Lat. N	Lon. E	Depth [km]	ML	RMS [s]	Q
1	1992 11 18	08 20 08.8	40.15	29.26	14	2.5	.66	C
2	1993 01 19	13 50 30.2	40.07	28.89	6	2.8	.56	D
3	1993 04 23	00 22 34.0	39.94	28.95	12	2.3	.68	D
4	1993 04 26	08 05 56.5	39.90	28.92	5	2.4	.79	D
5	1993 04 28	13 58 58.1	40.12	28.93	15	2.2	.51	C
6	1993 05 01	08 08 13.6	40.13	29.22	10	2.6	.65	D
7	1993 06 07	12 15 21.1	39.98	28.88	13	2.6	.51	D
8	1993 06 08	03 02 24.5	40.11	29.20	12	2.7	.33	D
9	1993 06 18	23 14 47.2	40.18	29.05	11	1.7	.53	C
10	1993 06 26	00 27 15.7	40.17	29.16	7	2.3	.43	C
11	1993 06 26	01 16 56.5	40.17	29.15	5	2.1	.43	C
12	1993 06 27	11 41 45.7	40.18	29.15	6	2.3	.38	C
13	1993 06 27	11 56 34.9	40.18	29.15	5	2.2	.31	C
14	1993 06 29	07 29 52.8	40.17	29.17	3	1.7	.27	C
15	1993 06 29	19 00 42.5	40.15	29.17	5	1.8	.44	C
16	1993 06 29	23 15 52.6	40.18	29.15	8	1.7	.33	C
17	1993 06 29	23 18 19.6	40.20	29.15	1		.08	C
18	1993 07 05	03 35 00.3	40.28	29.16	10	2.5	.48	D
19	1993 07 20	06 21 59.8	40.40	29.02	24	2.7	.49	D
20	1993 07 21	13 56 29.2	40.20	29.13	5	2.4	.12	C
21	1993 07 23	20 36 54.5	40.12	29.25	14	2.3	.51	D
22	1993 07 25	16 19 30.7	40.20	29.26	8	2.2	.75	D
23	1993 07 31	21 35 39.7	40.11	29.25	15	2.4	.63	D
24	1993 08 06	01 15 56.5	40.06	28.92	15	2.6	.41	C
25	1993 08 22	07 05 39.3	40.09	29.08	10	2.4	.52	D
26	1993 08 22	07 22 00.7	40.13	29.09	7	2.0	.58	D
27	1993 08 24	15 11 30.7	40.21	29.29	9	2.5	.40	C
28	1993 08 26	00 42 09.2	40.23	29.27	9	2.5	.35	C
29	1993 08 26	11 47 28.6	40.03	29.17	15	2.7	.65	D
30	1993 10 02	03 05 00.7	40.26	29.19	11	1.7	.39	D
31	1993 10 02	13 10 42.9	40.03	29.08	10	1.8	.50	D
32	1993 10 09	01 14 20.1	40.42	29.07	18	1.9	.49	D
33	1993 10 19	23 18 13.0	40.12	29.24	11		.36	D
34	1993 10 19	23 18 46.4	40.15	29.21	10	3.0	.62	D
35	1993 10 23	07 58 38.3	40.25	29.36	12	2.7	.43	D
36	1993 10 30	21 34 22.3	40.28	29.29	12	2.2	.35	C
37	1993 11 17	02 19 08.2	40.27	29.21	16	2.3	.59	C
38	1993 11 17	04 34 52.7	40.27	29.19	13	1.7	.29	B
39	1993 11 23	17 05 21.1	40.14	29.22	15	2.3	.50	D
40	1993 12 14	22 05 06.8	40.25	29.19	10	2.3	.85	D
41	1993 12 14	22 59 26.5	40.27	29.18	10	2.1	.49	C
42	1994 02 21	04 36 22.1	40.22	29.32	1	3.5	.37	C

Table 12: Earthquakes in the Bursa area, recorded by the accelerograph network.

The effect of frequency-independent Q models on the observed SH spectra were also studied. In most of the acceleration spectra, a second corner frequency, namely f_{max}, can be observed. Correction of spectra for assumed Q-factors representing the base rock site did not change the position of f_{max}, implying that the origin of f_{max} is a source rather than a site or path effect.

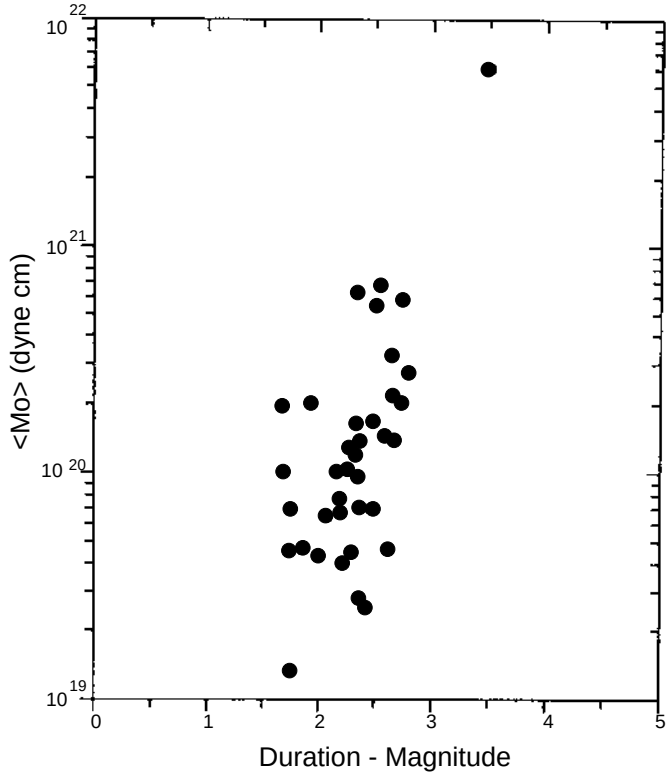


Figure 19: The relation between duration magnitude and seismic moment obtained from the displacement spectra for the earthquakes given in Table 12. Since only one earthquake with a magnitude larger than 3.0 could be considered, a gap exists in the seismic moment range between 10^{21} and 10^{22}dyne-cm.

The source parameters were calculated using the formulas inferred from Brune's source model, even if some of the spectra are not in agreement with that model. The seismic moments range from 10^{19} to 10^{21} dyne-cm. The relation between seismic moments and source radii obtained from the displacement traces is given in Figure 19. The SH-wave energies of earthquakes range between 10^{13}-10^{15}ergs. Corner frequencies vary between 2-13Hz in the acceleration spectra and range from 2-10Hz in the displacement spectra. The radii of the earthquake sources were calculated to range between 90m and 560m, according to the acceleration spectra, and between 120 and 520m according to the displacement spectra. Figure 20a and 20b illustrate the relationship among spectral parameters, source radii, seismic moment and stress-drop values which were calculated from acceleration and displacement records, respectively.

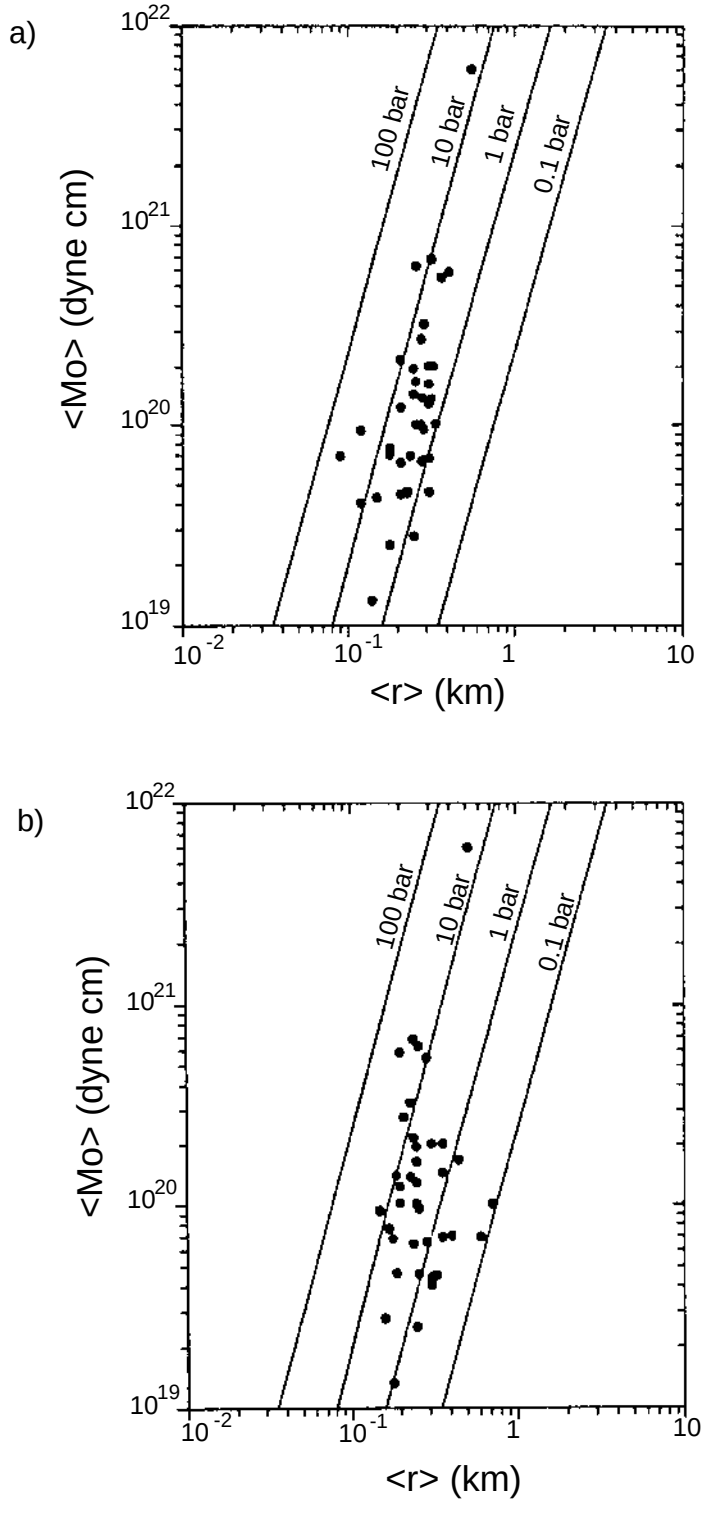


Figure 20: The tripartite relation among seismic moment, stress drop and source size, obtained from a) acceleration and b) displacement spectra.

Synthesis and future prospects

In the frame of the sub-project seismicity of Bursa, 12 seismic stations have been operated during a three years period (1992-1995) in the Bursa area. These stations were managed by the different institutions involved in the sub-project. This initiated a very fruitful collaboration between the different institutions and allowed to acquire experience in the exchange and joint evaluation of data. It is planned that these stations remain in the area for further studies, since possible large earthquake ($M \geq 5.0$) have not been recorded during the project period.

During the three year observational period, the seismicity in the area was rather low compared to the period prior to the study. From September 1992 to May 1995, only one event reached a magnitude of 4.0 out of a total of more than 1900 events. In May and August 1995 three events occurred with magnitudes greater than 4.0. However they were located in the larger region (A_1) about 50km from Bursa. Among them a M=6.0 event probably related to the cluster in the Emet region, which was strongly felt in Bursa.

The magnitudes (M_L) were assessed based on the duration of the seismic coda waves, using a large amount of data covering the magnitude range from 2.0 to 4.0. Therefore Wood-Anderson seismograms were simulated in order to compare duration magnitude with W-A magnitudes.

In the greater Bursa area these recordings complemented the almost 20 year period of instrumental observation and verified the existence of characteristic earthquake clustering behaviour. The clusters change their activity within the studied window, where different spots have been active during different time sections. The most active region is in the south, around Emet. It can not be concluded from the observed data if the time and space distributions are quasi periodical or rather stochastic. The identified clusters have to be observed during a much longer period for a better understanding of their basic space-time occurrence patterns.

The earthquake foci are, in general, rather shallow and show deepening trend towards the south. In fact, 90% of the events occurred above 15km depth and only a very few deeper than 25km. A three layer model, confirmed by large chemical explosion has been used, with a Moho depth of 32km. Still, the crustal structure of the Bursa plain is poorly defined. It is of great importance to investigate this point in detail by refraction and reflection studies in the future.

The city of Bursa is one of the 5 largest cities in Turkey. The population exceeds 1 million of inhabitants and many important industries are concentrated on the Bursa plain. The hazard study carried out for the Bursa city shows values of ground motion which are, in general, in accordance with previous studies and confirm the high risk of the area. It is essential to acquire more strong motion data to obtain valid attenuation models to improve further hazard study.

The general regime of a NE-SW to N-S oriented crustal extension and E-W oriented dextral shear is confirmed by fault plane solutions of the larger earthquakes in the observation period and also by the newly defined ”station diagrams” of a larger number of smaller earthquakes for which polarity of first movement with respect to a specific station could be determined. The general orientation of the principal horizontal stresses are in accordance with tectonic fault models of previous investigations, with the geological interpretation by Schindler (this volume) and also with GPS measurements carried out during the project (Straub and Kahle this volume)

The spatial distribution of earthquakes demonstrates the distributed pattern of crustal deformation along a large number of active faults. However more seismic stations should be added to have an appropriate network for a detailed study of the faults mechanisms. This would also allow a more reliable depth determination of the earthquake foci.

Using the acceleration records as well as the displacement traces, spectral source parameters were determined. The main finding of this investigation is the possibility of obtaining the corner frequencies necessary for the estimation of the moment magnitude and source dimension, without converting to displacement seismograms. Thus a well known source of errors could be eliminated. It could be shown that the corner frequencies rather depend on the source itself and to a lesser extent on site and path effects.

Acknowledgements

This work is the result from the collaboration between several institutions. We would like to thank for their support in Turkey the İstanbul Technical University, the TÜBİTAK research centres and the Boğazıcı observatory through its director Prof. Ahmet Işıkara. The collaberators who helped in the installation and the collection of data in Turkey: Bulent Kaypak İTÜ, Mehmet Ergin, Faruk Bicmen, Ahmet Yoruk from TÜBİTAK. Mr. Osman Geleri, Director of Bursa Public Work showed a deep interest and provided assistance on the field. We are indebted to Balamir Ücer for preparing the seismic catalogs and to Patrick Smit from ETH-Zürich who not only installed the strong motion instruments but also developed a data base for the strong motion data and developped the conversion software to GSE format.

References

Aki, K., 1967, Scaling law of seismic spectrum, J. Geophys. Res., 72, 4, 1217-1231.

Alsan, E., Tezçan, L. and Bath, M., 1975, An Earthquake Catalogue for Turkey for the interval 1913-1970, Kandilli Observatory, İstanbul and Seism. Inst. of Uppsala Univ. Rep. No. 7-75, 166p.

Ambraseys, N.N. and Finkel, C.F., 1991, Long-term seismicity of İstanbul and of the Marmara sea region, Terra Nova, 3, 527-539.

Ayhan, E., Alsan, E., Sancakli, N. and Üçer, S.B., 1987, Earthquake Catalogue for Turkey and surrounding area, 1881-1980, Publ. of Kandilli Observatory, Space and Earth Sciences Research and Development Centre.

Barka, A., 1992, The North Anatolian fault zone, Ann. Tectonicae, Special Issue, Suppl. to Vol. VI, 164-195.

Bender, B and Perkins, D.M., 1987, Seisrisk III: A computer program for seismic hazard estimation. U.S. Geological Survey Bulletin 1772, Denver, Colorado.

Brune, J.N., 1970, Tectonic stress and the spectra of seismic shear waves from earthquakes, J. Geophys. Res., 75, 4997-5009.

Canitez, N. and Üçer, S.B., 1967, Computer determinations for the fault-plane solutions in and near Anatolia, Tectonophysics, 4, 235-244.

Eaton, J.P., 1992, Development of Earthquake Magnitude Scales, U. S. Geol. Surv., Open-File Report 92-441, 281-315.

Eyidoğan, H. and Jackson, J., 1985, A seismological study of normal faulting in the Demirci, Alaşehir and Gediz earthquakes of 1969-1970 in Western Turkey: implications for the nature and geometry of deformation in the continental crust, Geophys. J. R. Astron. Soc., 81, 569-637.

Hanks, T.C., 1982, f_{max}, BSSA, 72, 6, 1867-1879.

Haskell, N.A., 1964, Total energy and energy spectral density of elastic wave radiation from propagating faults, BSSA, 54, 1811-1841.

Imbach, Th., 1992, Thermalwasser von Bursa, geologische und hydrogeologische Untersuchungen am Berg Uludağ (NW-Türkei), PH.D. Thesis, ETH Zürich, 178p.

Imbach, Th., this volume, Geology of Mount Uludağ with emphasis on the genesis of the Bursa thermal karst within the Gemlik (Bursa) area of Northwestern Turkey.

Jackson, J. and Fitch, T., 1979, Seismotectonic implications of relocated aftershock sequences in Iran and Turkey, Geophys. J. R. Astron. Soc., 57, 209-229.

Jackson, J. and McKenzie, D.P., 1984, Active tectonics of the Alpine-Himalayan belt between Western Turkey and Pakistan, Geopys. J. R. Astron. Soc., 77, 185-264.

Joyner, W.B. and Boore, D.M., 1981, Peak horizontal acceleration and velocity from strong motion records including records from the 1979 Imperial Valley, California earthquake. Bull. Seism. Soc. Am., vol. 71, 2011-2038.

Kalafat, D.,1989a, Batı Anadolu'da yeralan sismik istasyonlarin süreye baılı yerel manyitüd denklemlerinin Çikartilmasi, Deprem Araştırma Bülteni, 65, Nisan, 1989, 83-94.

Kalafat, D., 1989b, Son yillarda olmuş bazı büyük depremlerin odak mekanizması açısınndan irdelenmesi, Deprem Araştırma Bülteni, 66, Temmuz, 1989, 6-33.

Lee, W.H.K. and Lahr, L.C., 1972, A computer program for determining hypocenter, magnitude and first motion pattern of local earthquakes, U.S. Geol. Surv., Open-File Report, 100p.

Lee, W.H.K., Bennett, K.E.R. and Meagher, K.L., 1972, A method of estimating magnitude of local earthquakes from signal duration, U.S. Geol. Surv., Open-File Report, 28p.

McKenzie, D.P., 1972, Active Tectonics of Mediterranean region, Geophys. J. R. Astron. Soc., 30, 109-185.

McKenzie, D.P., 1978, Active tectonics of the Alpin-Himalayan belt; the Aegean Sea and surrounding regions, Geophys. J. R. Astron. Soc., 55, 217-254.

Okay, A., 1984, Kueybati Anadoluda yer alan Metamorfik Kusaklar, Proc. Ihsan Ketin Semposium, TJK, 63-92.

Papageorgiou, A.S. and Aki, K., 1983, A specific barrier model for the quantitative description of inhomogeneous faulting and the prediction of strong-ground motion, Part II, Applications of the model, BSSA, 73, 953-978.

Papageorgiou, A.S., 1988, On two characteristics frequencies of acceleration spectra: path corner frequency and f_{max}, BSSA, 78, 2, 509-528.

Pavoni, N., 1969, Zonen lateraler horizontaler Verschiebung in der Erdkruste und daraus ableitbare Aussagen zur globalen Tektonik, Geol. Rdsch., 59, 56-77.

Pavoni, N., 1984, Seismotektonik Nordschweiz, Technischer Bericht, NTB 84-45, NAGRA, Baden, 45p.

Pavoni, N., 1995, Crustal deformation in Anatolia – concepts and prospects. In: M. Sahin & P. A. Cross (eds.), Proceedings of the First Turkish International Symposium on Deformations, Istanbul 1994, tome 1, 30-39.

Perkins, D.M. and Bender, B., 1987, SEISRISK III; a computer program for seismic hazard estimation, U. S. Geological Survey, Reston, VA, United States, 48p.

Polat, O.D., 1995, Bursa ve Çevrsindeki küçük depremlerin ivme kayitlarinin incelenmesi, Master Tezi, İTÜ Maden Fakültesi, 125p.

Roth, Ph., 1986, Untersuchungen über den gegenwärtigen Deformations- und Spannungszustand der Erdkruste im Gebiet der Schweiz mit Hilfe von Nahbeben-Stationsdiagrammen. Diplomarbeit, Institut für Geophysik, ETH Zürich.

Roth, P., Pavoni, N. and Deichmann, N., 1992, Seismotectonics of the eastern Swiss Alps and evidence for precipitation-induced variations of seismic activity, Tectonophysics, 207, 183-197.

Savage, J.C., 1972, Relation of corner frequency to fault dimensions, J. Geophys. Res., 77, 20, 3788-3795.

Shirokova, E. I., 1968, General features in the orientation of principal stresses in earthquake foci in the mediterranean-Asian belt. Izv., Earth Physics, 1, 22-36, 1967. (Engl. Transl. 12-22, 1968).

Soysal, H., Sipahioglu, S., Kolçak, D. and Altinok, Y., 1981, Türkiye ve Çevresinin tarihsel deprem katalogu. TÜBITAK, Proje No. TBAG, 341p.

Schindler, C., this volume, Geology of NW Turkey: Results of the MARMARA Poly-Project.

Straub, Ch., 1996, Recent crustal deformation and strain accumulation in the Marmara Sea region, N.W. Anatolia, inferred from GPS Measurements. Ph.D. Thesis, IGP, ETH Zürich, Mitt. Nr. 58.

Straub, Ch., and Kahle, H.-G., 1995, Active crustal deformation in the Marmara Sea region, NW Anatolia, inferred from GPS measurements. Geophys. Res. Lett., 22, 2533-2536.

Straub, Ch. and Kahle, H.-G., this volume, Recent crustal deformation and strain accumulation in the Marmara sea region, N.W. Anatolia, inferred from repeated GPS measurements.

Tottingham D.M., Lee, W.H.K. and Rogers, J.A., 1989, User manual for MDETECT, IASPEI Software Library, Vol. 1, 49-88.

Üçer, S.B., Crampin, S., Evans, R., Miller, A. and Kafadar, N., 1985, The MARNET radio-linked seismometer network spanning the Marmara Sea and the Seismicity of Western Turkey, Geophys. J.R. Ast. Soc., 83, 17-30.

Üçer, S.B., Gürbüz, C., Kafadar, N., Alçik, H.A., Barka, S., Türkelli, N. and İşıkara, A.M., 1995,. PC-Based Telemetered Digital Seismic Network (IZINET) and Micro-Seismicity along the Western Branches of the North Anatolian Fault Zone, in: Multidisciplinary Research on Fault Activity in the Western Part of North Anatolian Fault Zone (5), edited by: Y. Honkura and A.M. İşıkara, Boğazıçı University, 33-40.

Gravimetric studies of the Marmara sea region

EMILE KLINGELÉ AND FAUSTO MEDICI

Abstract

The Bouguer anomaly map of the Marmara sea region, computed with a density of 2500 kgm^{-3} (Ekingen 1971, 1978, Şimşek this volume, Figure 3), was analysed. New maps of isostatic anomalies and Bouguer anomalies were processed and interpreted. The main result was the determination of the depth of the crust-mantle boundary which differs significantly from the depth of the Mohorovicic discontinuity given by Hurtig et al. (1991). The mean depth obtained for the discontinuity is around 30 km instead of 34 km as given previously. The maximum depth is around 32 km instead of 37 km in the south of the study area and the NW-SE gradient is stronger in the model proposed here. The residual field does not show any particular correlation between the anomalies and the known seismo-tectonic features excepted, may be, in the region of Uludağ (Bursa) where a cluster of earthquakes epicenters appear on the flank of the -70 mgal anomaly.

Introduction

One of the most common applications of gravimetry is the determination of lateral density distribution at depth as, for example, the determination of the size of an intrusive body, the thickness of the sediments filling a basin or, last but not the least, the depth of the crust-mantle boundary.

Gravimetry involves the measurements of the regional variations of the Earth's gravity field. The observations are normally made within a few decimeters above the Earth's surface. The observed minute changes in the main gravity field are mainly a result of variations in density of the subsurface. To detect the gravity changes in an area of interest field work is carried out on land by gravity readings at selected stations. Each of these readings will generally be influenced by four factors: 1) latitude, 2) elevation, 3) topography of the surrounding terrain and 4) density changes within the subsurface material.

Fortunately, the first three effects can be computed with sufficient accuracy thus allowing the determination of the gravity effect caused by the density variation within the subsurface material. A possible difference between the measured and the calculated gravity of the model

$$\Delta g = g_{measured} - g_{model} \qquad [1]$$

is called the gravity anomaly Δg. Resulting gravity anomalies enable the interpretation and modelling of the density distribution within the subsurface material.

The Bouguer model

Both the rotation of the Earth and its slight equatorial bulge produce an increase of gravity with latitude. Assuming that the Earth is very close in shape to a rotational ellipsoid, it is possible to express the theoretical value of gravity g_0 at sea level as a function of latitude φ. The mathematical form of the latitude correction is

$$g_0 = g_e (1 + a \cdot \sin^2 \varphi + b \cdot \sin^2 2\varphi) \quad [2]$$

where g_e is the gravity at the equator (9.7803185 ms^{-2}), a = 0.0053024, b = 0.0000059.

Because the measurement points are not located on the reference ellipsoid, it is necessary to correct the model for changes in elevation. The first depends only on the distance between the ellipsoid and the station elevation. The free-air correction Δg_{FA} is obtained by

$$\Delta g_{FA} = \frac{\partial \bar{g}}{\partial z} \Delta H \quad [3]$$

where Δg_{FA} is the variation of gravity caused by the elevation above the ellipsoid, $\frac{\partial \bar{g}}{\partial z}$ is the mean vertical free-air gradient (-0.3086 mgal/m, 1 mgal = 10^{-5} ms^{-2}) and ΔH is the altitude (z) above the ellipsoid. This correction is subtracted from the model gravity when the station is above the ellipsoid and added to the model value when below it.

The second correction is necessary to take into account the attraction of material between the station and the ellipsoid, which is ignored in the free-air correction. To simplify the computation the material below the station is assumed to be a homogeneous horizontal slab with infinite lateral extent or a spherical shell with a given limited radius. The so called Bouguer correction Δg_B is given by

$$\Delta g_B = G \cdot \rho \cdot 2\pi \cdot z \quad [4]$$

where G is the universal gravity constant ($6.67 \cdot 10^{-11}$ Nm^2kg^{-2}). The total altitude correction can then be written as ([z] = m, [ρ] = kgm^{-3}):

$$\Delta g_{Alt} = \Delta g_{FA} + \Delta g_B = -0.3086 \cdot z + G \cdot \rho \cdot 2\pi \cdot z = -0.3086 \cdot z + 0.0419 \cdot \rho \cdot z \quad [5]$$

Two simplifying assumptions are normally made in using the Bouguer correction: first that the slab has a uniform density, second that it is of curved extent without any kind of irregularities in shape. Neither of these assumptions can be considered as valid. The influence of density variations occurring in the subsurface material leads to gravity anomalies. The effect of topography (shape irregularities) is taken into account in the following correction.

The role of topographic corrections is to allow for the effect of irregularities such as mountains and valleys in the vicinity of a gravity station. Topographic corrections are always subtracted from the model gravity, which is due to the fact that mountains as well as valleys affect the measurements in the same sense. There are several methods to compute the topographic corrections. The most commonly used methods divide the surrounding topography of a station by a set of small square prisms or geographic trapezoids. The total topographic correction can be then written as

$$\Delta g_{Topo} = \rho \cdot T \quad [6]$$

where ρ is the average density assumed for the surface rocks and T is the sum of the individual effects of each prism computed for 1 kgm^{-3}. Finally, the Bouguer gravity anomaly $\Delta g_{Bouguer}$ can be expressed as

$$\Delta g_{Bouguer} = g_{measured} - [g_o - \Delta g_{FA} + \Delta g_B - \Delta g_{Topo}] \quad [7]$$

A local variation in density – the significant parameter in gravity interpretation – is the source of the anomaly. The term $\Delta g_{Bouguer}$ contains the crucial information which together with additional geological and geophysical data allows the interpreter to infer the density distribution of interest within the subsurface material. A negative anomaly can be attributed to an existing mass deficiency in the model, whereas a positive anomaly indicates a mass excess.

In case of very rugged topography it is necessary to transfer the anomaly values from their location to a horizontal surface in order to minimise the effect of the altitude differences between the stations.

The isostatic model (after Airy)

Isostasy is a condition of static equilibrium of the Earth's crust. According to this idea, the Earth's crust is "floating" on a denser substratum, and the weights of irregular topographies, such as mountains and oceans, are supported by hydrostatic buoyancy. Airy (1855) proposed that the mountains are compensated by roots formed of crustal material sinking into the denser upper-mantle material. These roots produce a mass deficit which induces negative gravity anomalies. The opposite is also valid for oceanic areas where anti-roots of upper mantle material produce positive gravity anomalies. The thickness of these roots and anti-roots are proportional to the height of the mountains or depth of the oceans and of the difference of density between crustal and upper-mantle material.

To compute an Airy's isostatic anomaly it is necessary to compute first the depth of the crust-mantle interface and then to subtract the gravity effect of the deficit/excess of mass from the Bouguer anomaly. From the anomaly values and also from some geological hypothesis it is possible to compute the shape and the density of a disturbing body. The interpretation of the data can be performed either by trial-and-error modeling techniques or, in case of simple disturbing bodies, by inversion techniques.

The aim of the gravimetry part of the MARMARA Poly-Project was to provide primarily, a qualitative interpretation mainly by looking at the correlation existing between the anomalies and the different geological units or between the anomalies and some other geophysical data. The aim was to formulate hypotheses about the geodynamic process related to isostatic anomalies and to produce an improved map of the depth to the crust-mantle boundary in Western Anatolia.

Data processing

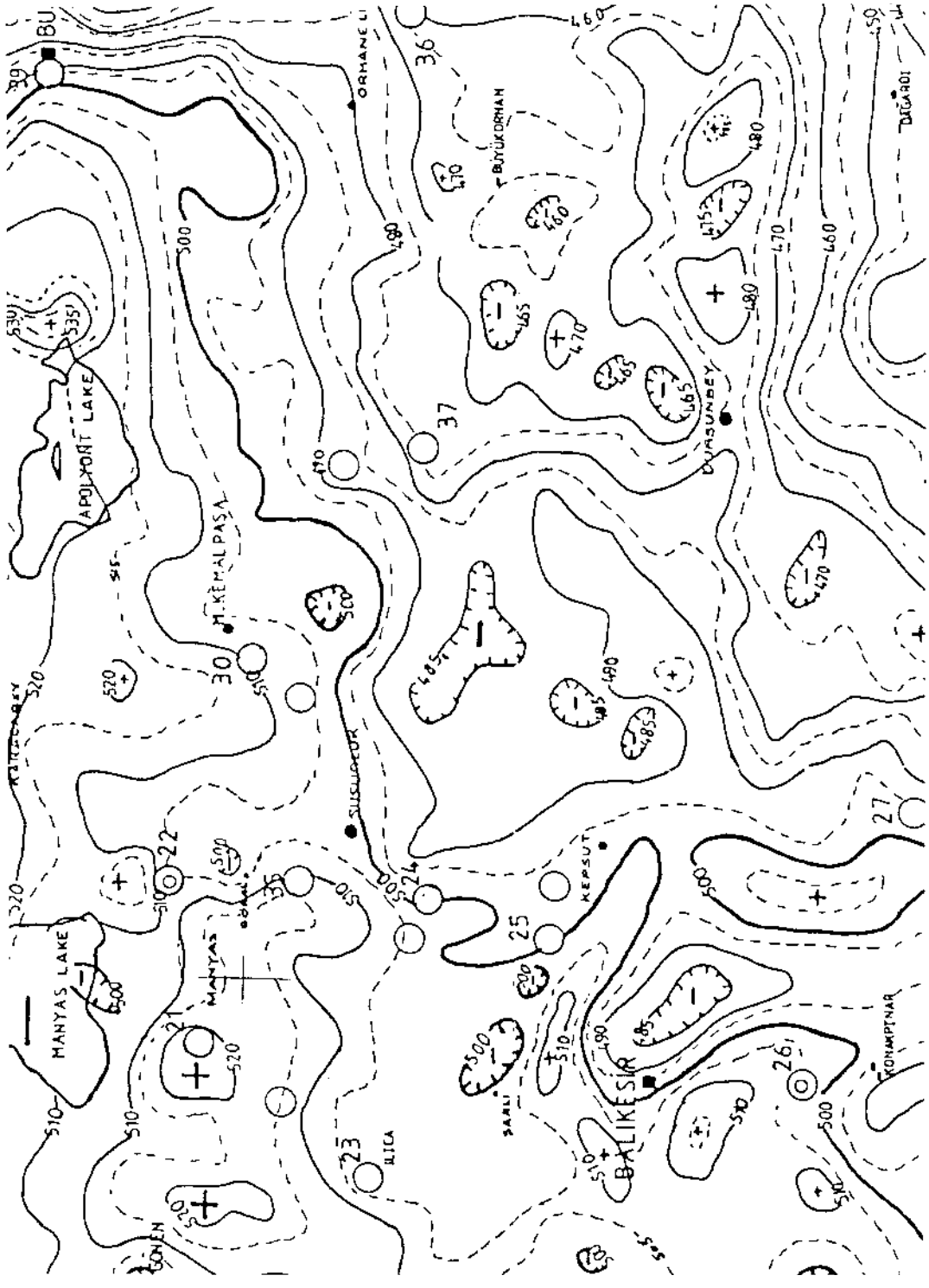


Figure 1: *Part of the Bouguer anomaly map after Ekingen (1971, 1978) and Şimşek (this volume, Figure 3). Density used for the topographic corrections: 2500 kgm^{-3}. Maximal distance for the correction: unknown.*

Preprocessing

Since only a hand-drawn map of Bouguer anomaly, computed with a density of 2500 kgm^{-3} (Ekingen 1971 and 1978, Şimşek this volume, Figure 3) without information about its projection was at our disposal, some general processing was necessary at the beginning in order to obtain a map with an acceptable degree of regionality. Figure 1 shows a part of the gravity map of Anatolia from which the regional map was produced.

In a first step the isolines of the original map were digitised to form a dense network of polygonal lines. The result of this work was around 16,000 Bouguer anomaly values associated with local x,y coordinates. Because the Bouguer map shows anomalies ranging from 560 mgal to 430 mgal, a constant value of 500 mgal was subtracted in order to obtain realistic anomalies. To find the kind of projection used by Şimşek (this volume), this was compared by superposition to the geologic map of Turkey at the same scale (1/500,000) which is in UTM projection with 27° east central meridian. From this comparison, it was possible to conclude that the gravity map was based on the same projection.

Before the transformation of the digitised points in both UTM and geographic coordinates was carried out, the UTM grid was determined and drawn by using 16 well representative points of both the geologic and gravimetric maps. In order to obtain a map with a reasonable degree of regionality these 16,000 points were used to produce, by interpolation, a subset of 8000 x, y, Bouguer values corresponding to the nodes of six different grids. The mesh sizes of these six grids were chosen depending on the size and the number of the individual anomalies present on the original map. A completion of the data was then achieved by adding to each point the altitude of the corresponding 5' by 5' mean altitude.

A small data bank was also created containing the mean 5' by 5' elevations of an area extending from 38° N to 44° N and 24° E to 32° E by extracting data from the TUG87 world elevation data bank. A flow chart of these procedures is shown in Figure 2.

Map production

In a first step the isostatic anomaly was computed for each of the 8000 Bouguer anomaly points following the scheme of Airy (Heiskanen and Vening-Meinesz 1970). The parameters of the model were: 30 km for the thickness of the normal crust, 2670 kgm^{-3} for the density of the crust and 3270 kgm^{-3} for the density of the mantle.

This computation produced a new set of points containing the x,y coordinates, the elevation, the Bouguer and the isostatic anomalies. From this data two basic maps were produced; one of the Bouguer anomaly and one of the Airy isostatic anomaly. To produce these maps it was necessary to create a grid of values by interpolating the irregularly distributed data.

The gridding was done in two steps. In the first one, a coarse grid consisting of square meshes with sides of 5 by 5 km was calculated. To do this, a method similar to that described by La Porte (1962) was used: The experimental points inside a circle of radius R_0 centred on the point to be interpolated are approximated by a second-order polynomial of the type

$$F(x,y)=a_0 + a_1x^2 + a_2x + a_3y + a_4xy + a_5y^2 \quad [8]$$

in a least-squares fit procedure. Before performing this operation a weighting procedure is used, based on the term R^{-2} in order to reduce the effect of distant values. The weight attributed to a point P_i is (Figure 3):

$$W_i = \left(\frac{R_0^2 - d_i^2}{d_i^2 - h^2} \right)^2 \quad [9]$$

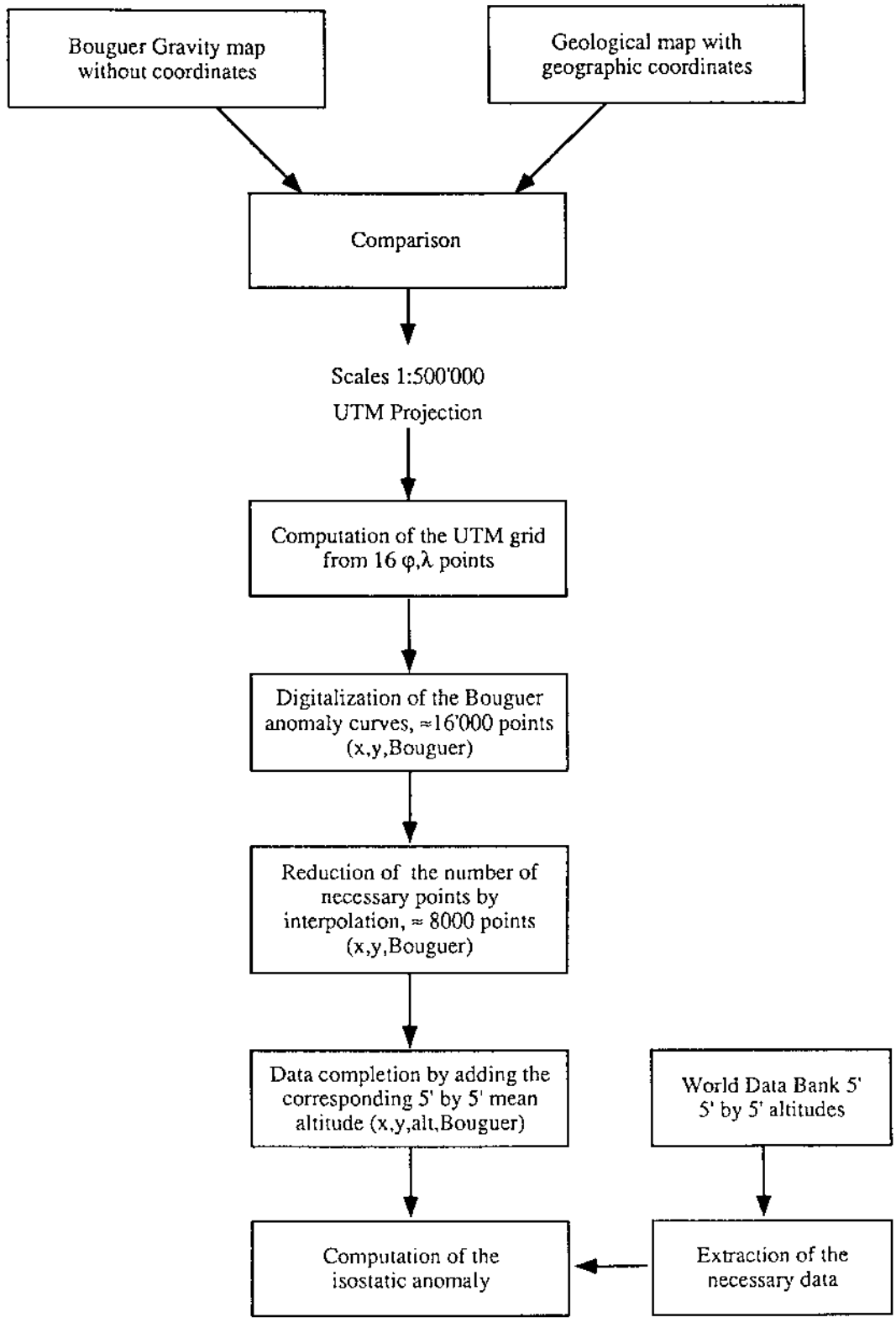


Figure 2: Flow chart of the procedures used to construct the regional Bouguer anomaly map and the isostatic anomaly map.

where d_i is the distance between the center of the circle and the point P_i , h is a smoothing factor and R_0 the radius of the area around P_i where the experimental points are taken into account. In our procedure the smoothing factor h is not given as an absolute value but as a function of the search radius R_0 (Klingelé and Olivier 1980, Klingelé et al. 1995).

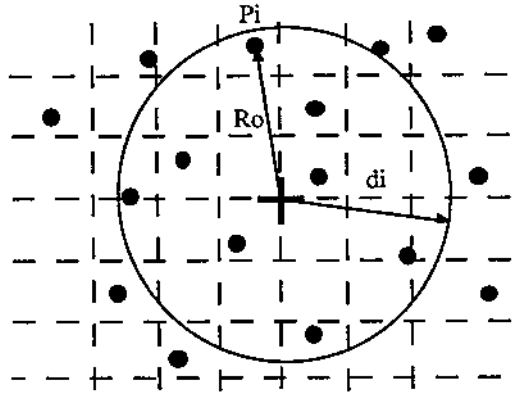


Figure 3: Data selection to compute the coarse grid.

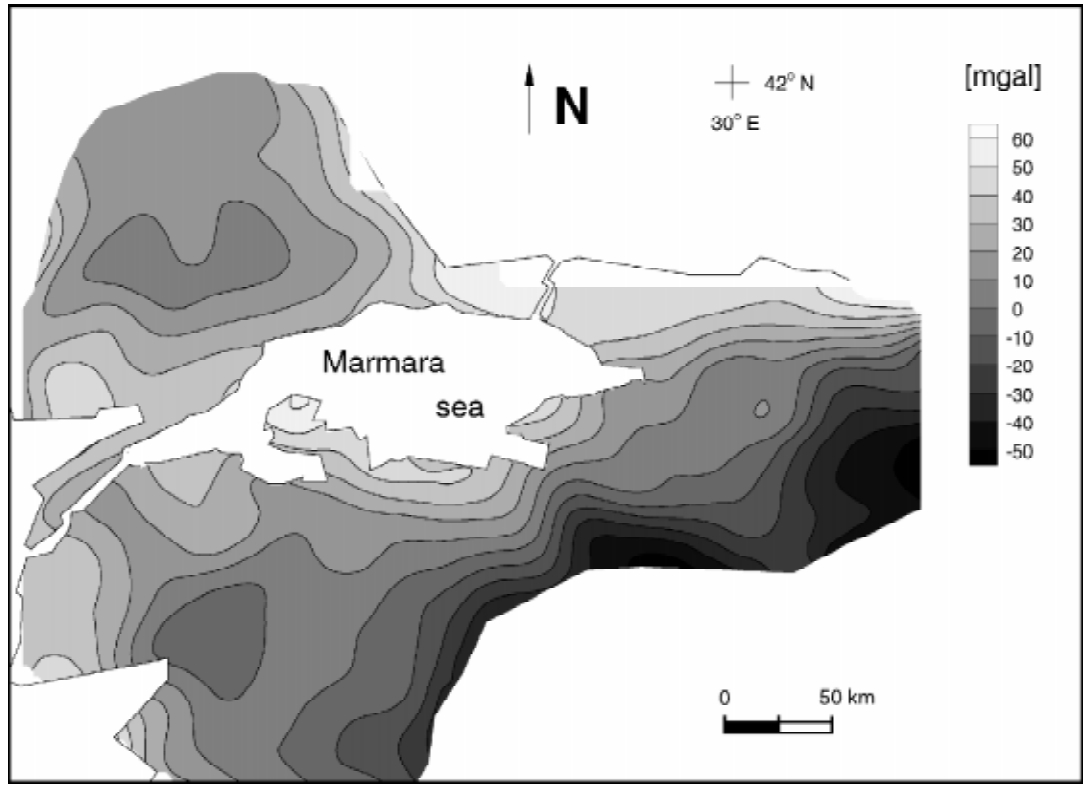


Figure 4: Regional Bouguer anomaly map produced by means of the procedure described in Figure 2. The source data are from Ekingen (1971 and 1978) and Şimşek (this volume, Figure 3).

The second step allows the refining of the initial grid to obtain a much finer one, needed for a good-quality tracing. To save computing time, the interpolation is done first line by line on the initial grid. A rectangular grid is thus obtained with the smallest dimensions, equal to 1/K times the original grid size, coinciding with the horizontal axis. Secondly, one proceeds to an interpolation column by column on the previously obtained intermediate grid. This twofold unidimensional interpolation uses a spline under tension whose variations of the stress factor allows an interpolation ranging from a broken line to a classical bi-cubic spline (Cline 1974). The fine grid has a size of M (K -1) by N (K-1), where M and N are the dimensions of the large-scale grid, and K is the refinement factor.

Finally these grids were used by the mapping package TECPLOT for producing anomaly maps (Figures 4 and 5). The depth of the crust-mantle boundary as given by Hurtig et al. (1991) is also plotted on the isostatic anomaly map (Figures 5).

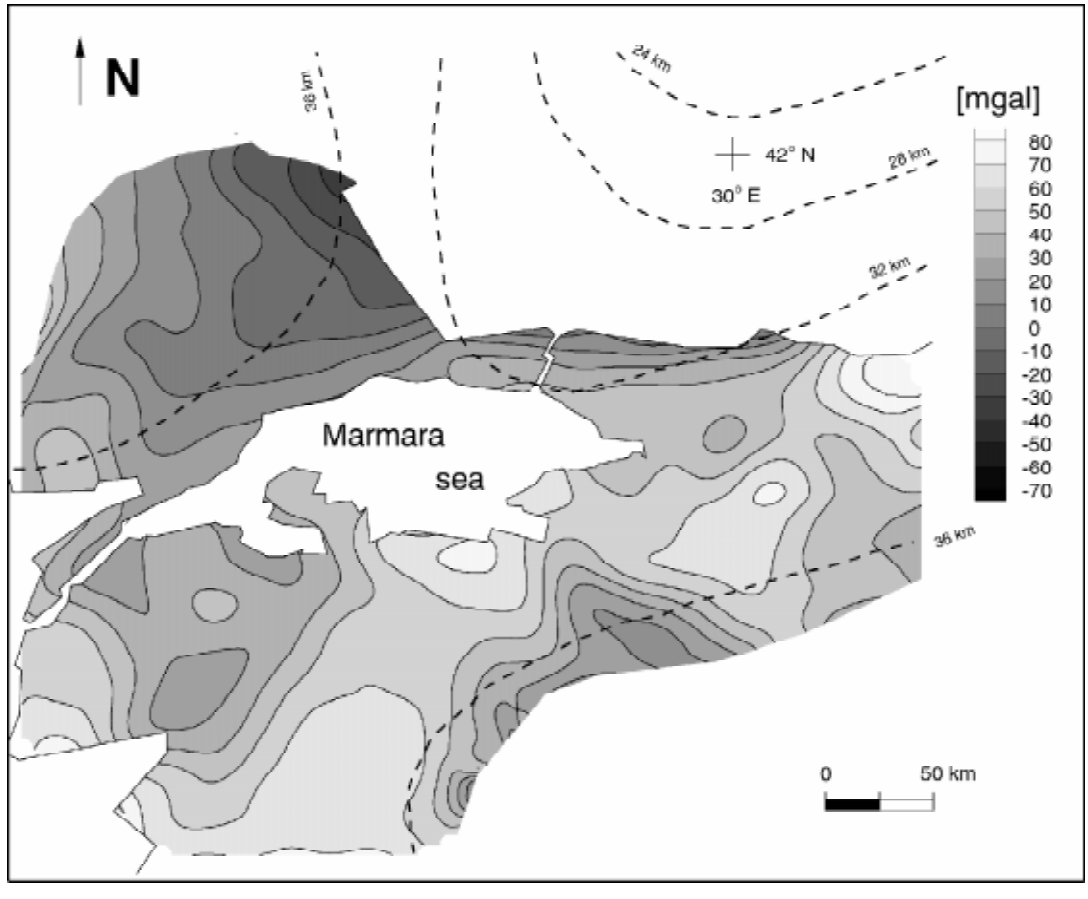


Figure 5: *Map of the isostatic anomaly computed with the model of Airy for a normal thickness of the Earth's crust of 30 km. The dashed lines represent the Moho depth after Hurtig et al. (1991).*

Analysis of the results

In the computation of the Bouguer anomaly the density plays an essential role. The part between brackets in Formula 7 can be written in a different form such that the density ρ appears more clearly:

$$\Delta g_{Model} = g_0 - \Delta g_{FA} + \rho (2\pi Gz - T) \qquad [10]$$

in the last term; T is always smaller than $2\pi Gz$. Therefore, if the density chosen for the computation of the model is higher than the real density of the material of the surrounding area, the Bouguer anomaly will be to small (too negative or too less positive). In the opposite case if the density chosen is too low the Bouguer anomaly will be too high (too less negative or too positive).

Now by looking at Figure 6 it is easy to see that in some parts of the study area a strong correlation exists between the anomalies and the topography. It is particularly the case for the zones marked A, B, C and D in Figure 7. The zones B and C belong to the highest part of the area which is formed mostly by ultrabasites, plutonites and metamorphites (see Geological Map of Turkey, 1/2,000,000, by E. Bingöl, 1989). These rocks have a density much higher than 2500 kgm^{-3} and therefore they are producing these negative gravity "spots".

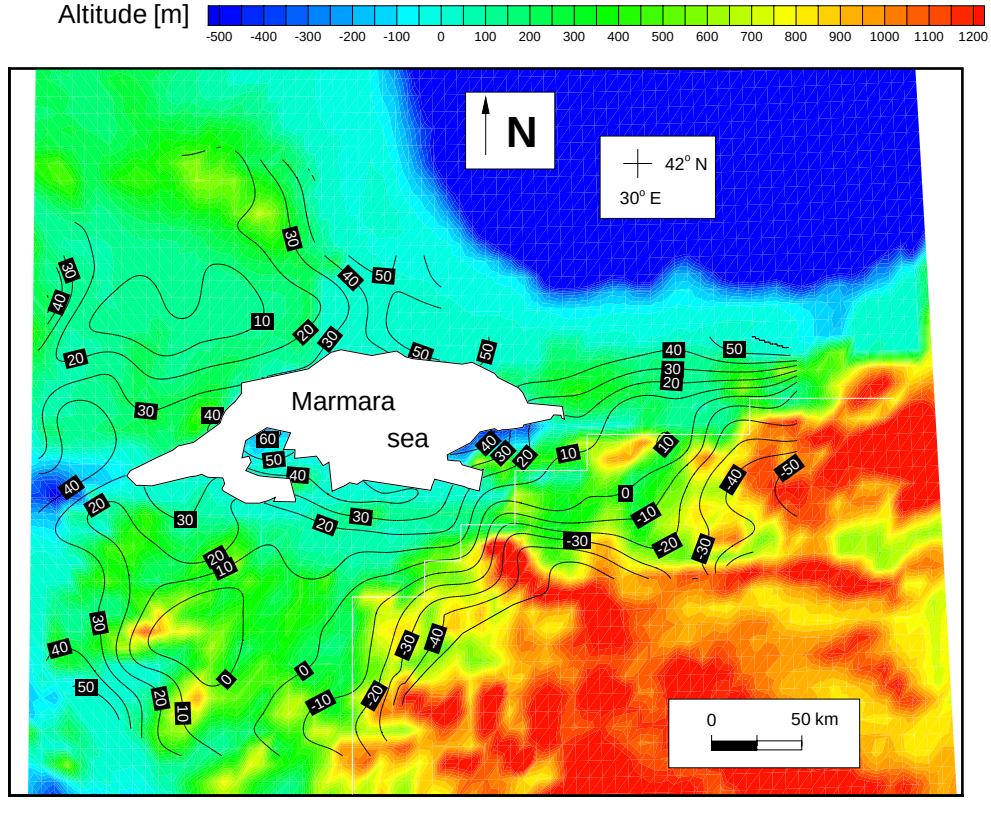


Figure 6: *Map of the Bouguer anomaly and topography.*

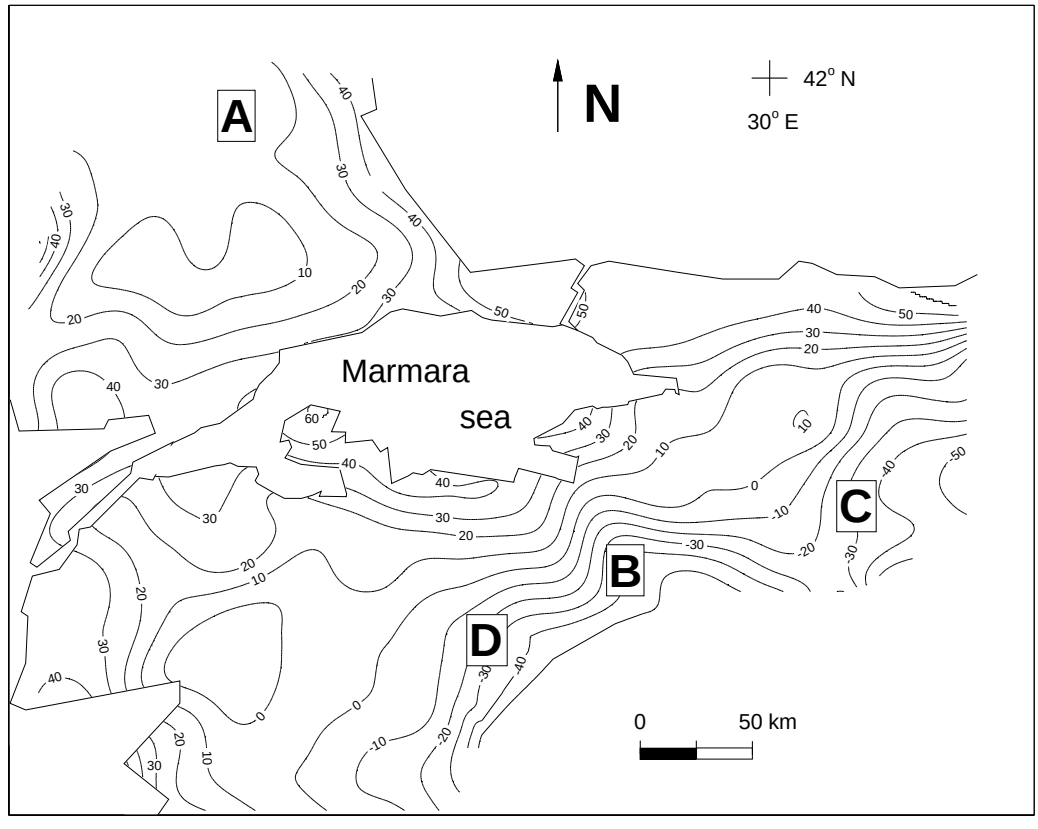


Figure 7: *Map of the Bouguer anomaly computed with r = 2500 kgm^{-3} with the zones (A,B,C,D) showing a strong correlation between local anomalies and elevation.*

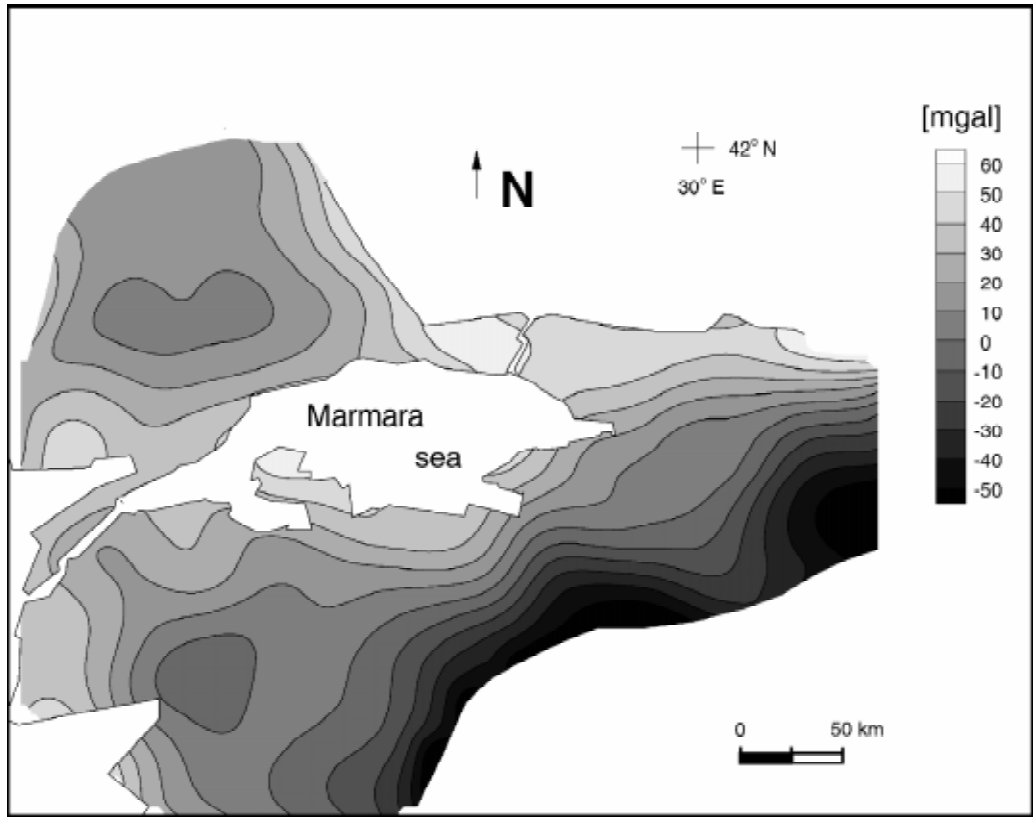


Figure 8: *Map of the Bouguer anomaly corrected for the effect of the topographic masses having a density higher than 2500 kgm^{-3}.*

Assuming a mean density of 2850 kgm^{-3} for the rocks forming the topography of zones B, C and D a supplementary correction was applied to the Bouguer and the isostatic anomaly data of the zone located south of the white line in Figure 6. For this, each terrain column was taken with a density of 350 kgm^{-3} and their effects subtracted from the grid points forming the Bouguer anomaly map. The results of these corrections are presented in Figure 8. On this map the local medium wavelength Bouguer anomalies located in the front of the mountainous area are strongly reduced and the map has a more regional character which is better fitted for the inversion procedure applied for determining the crust-mantle boundary depth.

Because of its depth, the relief of the crust-mantle discontinuity produces always anomalies with very long wavelengths which can be considered as regional effect. In order to find this component the Bouguer anomaly was divided into two components: a local and a regional one represented by an algebraic polynomial in x and y of degree three of the form:

$$P(x,y) = a_0 + a_1x + a_2y + a_3x^2 + a_4xy + a_5y^2 + a_6x^3 + a_7x^2y + a_8xy^2 + a_9y^3 \quad [11]$$

The coefficients of this polynomial were determined by means of a least-squares procedure (Klingelé et al. 1995). The values of the a_i coefficients are:

$a_0 = 1.75750957570845 \circ 10^{+5}$ $a_1 = -0.321939752952049 \circ 10^{-1}$

$a_2 = -0.115572246440641$ $a_3 = -0.164123985150611 \circ 10^{-7}$

$a_4 = 0.160657774521339 \circ 10^{-7}$ $a_5 = 0.253368174368386 \circ 10^{-7}$

$a_6 = -0.275575387069506 \circ 10^{-14}$ $a_7 = 0.468600738773182 \circ 10^{-14}$

$a_8 = -0.210976520443868 \circ 10^{-14}$ $a_9 = -0.184618291554396 \circ 10^{-14}$

A map of the regional field and one of the local field are presented in Figures 9 and 10. The regional field shows a clear correlation with the depth of the crust-mantle boundary given in Figure 4, while the residual field shows anomalies of medium wavelength and small amplitudes correlated with the most prominent topographic features. Different kinds of information were added to the residual map in order to facilitate a qualitative interpretation. These information are the major faults and the epicenters of the earthquakes with magnitudes larger than 3.5 for the period 1975-1991. The computed regional field can be considered as representing the gravimetric effect of the variation in depth of the crust-mantle boundary.

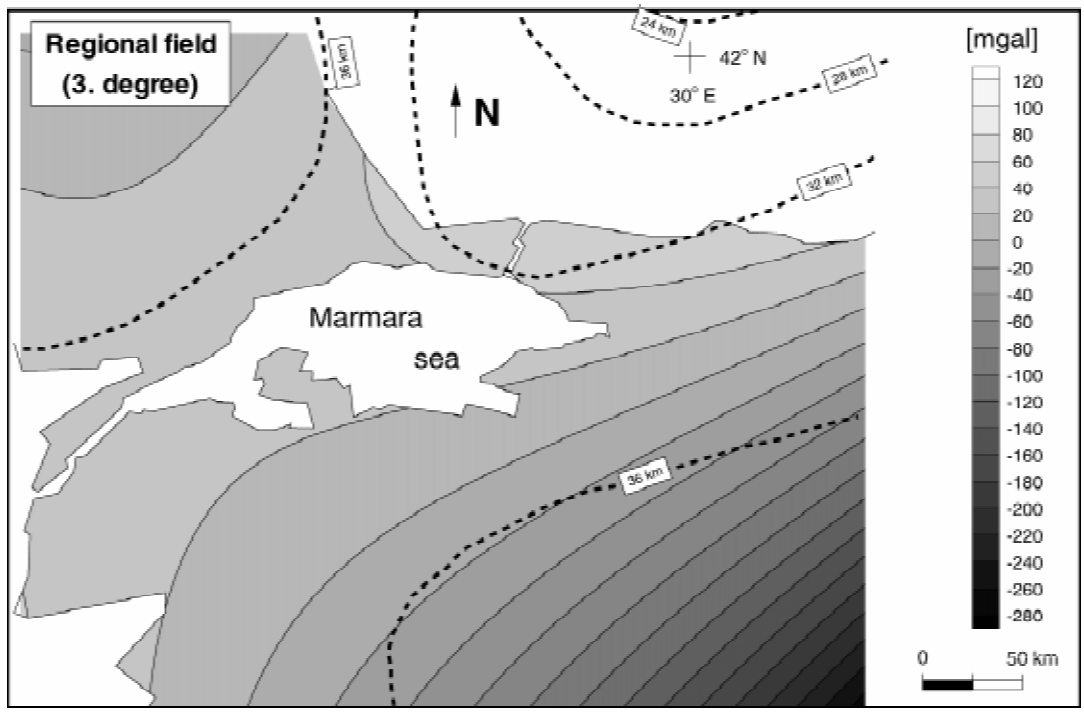


Figure 9: *Regional part of the Bouguer anomaly field given by an algebraic polynomial of degree 3. The dashed lines represent the Moho depth after Hurtig et al. (1991).*

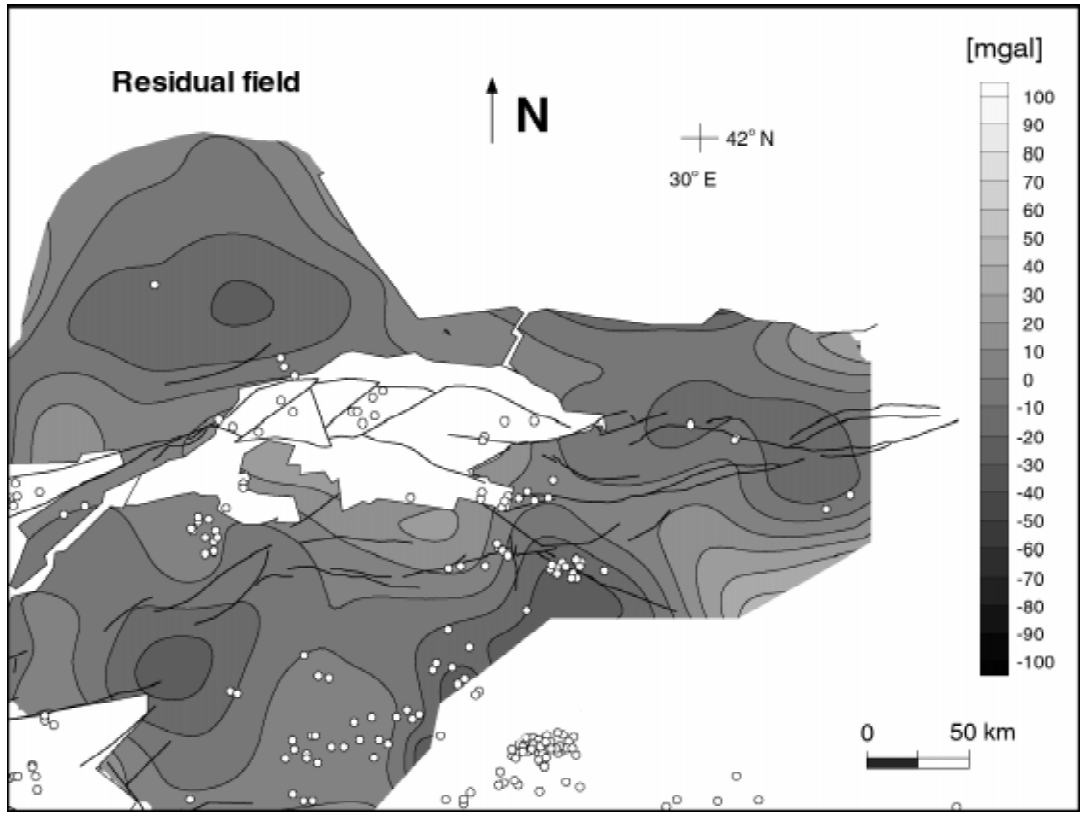


Figure 10: *Residual part of the Bouguer anomaly field. The major faults are represented by the wide black lines and the epicentres of the earthquakes with magnitudes larger than 3.5 are marked by open dots (period 1975-1991).*

Determination of the crust-mantle boundary depth

For this determination an iterative inversion procedure was applied to the regional gravity field previously computed. This method is able to find one interface of a disturbing body of constant density, if the second one is known. The disturbing body is approximated by "welded" vertical prisms of square cross section. The method consists of adjusting the depth of the unknown interface until the produced anomaly fits the observed anomaly to a given tolerance. It is an automated "trial and error" method. In the first iteration the depth of the interface is computed with the formula of the infinite horizontal layer with constant density. Then the effect of this body is computed on each grid point. Generally, the computed field differs from the experimental field of a quantity $\Delta g_1 = g_{exp} - g_{calc,1}$. This residual field serves to improve the depth of the unknown interface. To do this, the field at the depth of the interface is computed using the two following relationships:

a) $$\frac{1}{2}\left[g(+z)-g(-z)\right] = g(0) - z^2\frac{\partial^2 g(0)}{\partial z^2} + \frac{z^4}{3^2}\frac{\partial^4 g(0)}{\partial z^4} - \frac{z^6}{(3.5)^2}\frac{\partial^6 g(0)}{\partial z^6} + \qquad [12]$$

b) $$g(z) = \frac{1}{2\pi}\int_{-\infty}^{+\infty}\int_{-\infty}^{+\infty}\frac{g(0)\cdot z}{(x^2+y^2+z^2)^{\frac{3}{2}}}\,dxdy \qquad [13]$$

With this downward continued residual field it is possible to compute (again with the formula of an infinite horizontal layer of constant density) for each grid point an improvement of the unknown depth. The new computed surface then allows to compute a new gravimetric effect and then a new residual $\Delta g_2 = g_{exp} - g_{calc,2}$. This procedure is repeated until the residual is smaller than a pre-set threshold ε.

This procedure has been applied on the regional field of Western Anatolia represented in Figure 9. The lower crust was approximated by right vertical prisms of square cross section of 10 km side, having their top at 30 km for the continental areas and for marine areas their bottom at the same depth. After seven iterations, a stable depth was obtained for the interface between the lower crust and the upper mantle. The depth of this interface is shown in Figure 11. At the end of the inversion procedure the effect of the roots and anti-roots found, was computed and compared with the regional field used for the calculation. The spatial distribution of the differences between these two fields is shown in Figure 12. The RMS of these differences is 1.20 mgal.

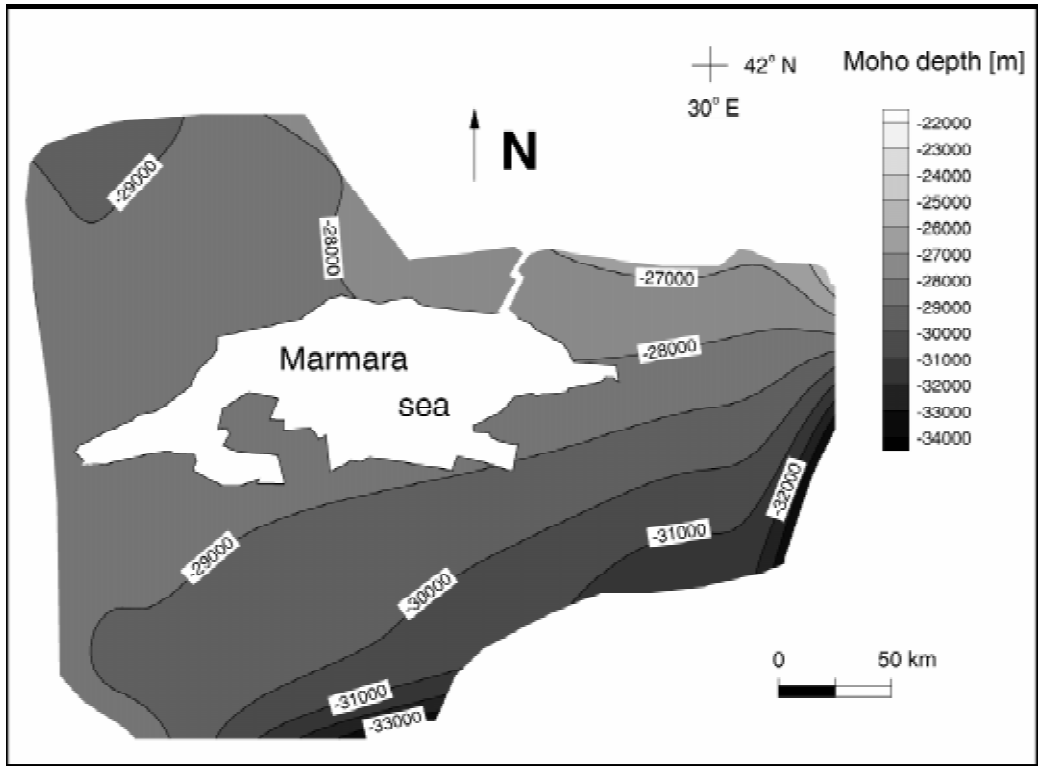


Figure 11: *Map of the depth of the crust-mantle obtained after seven iteration of the inversion of the regional Bouguer anomaly field of Figure 9. The density difference between the materials forming the crust and the upper mantle was taken as 600 kgm^{-3}. The RMS of the difference between the regional field of Figure 9 and the effect of the depth shown in this figure is 1.20 mgal.*

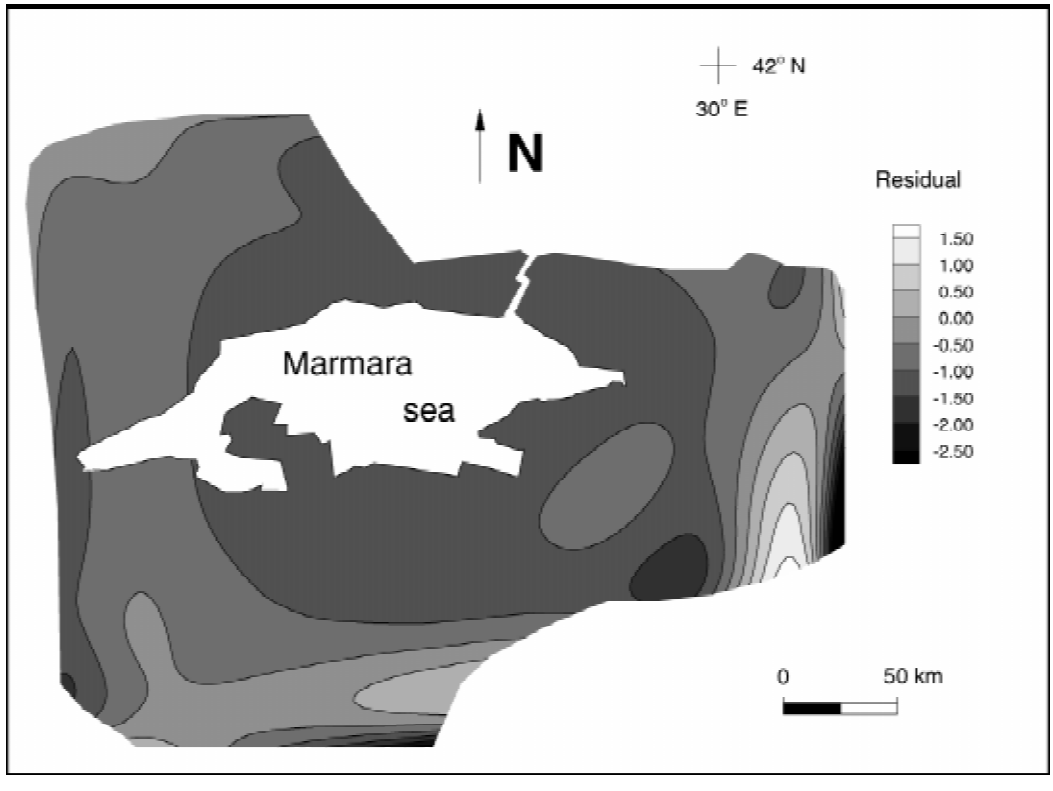


Figure 12: *Spatial distribution of the difference in mgal between the regional field used for the inversion (Fig. 9) and the effect of the roots and anti-roots obtained after this inversion (Fig. 11).*

Conclusions

The depth of the crust-mantle boundary obtained here differs significantly from the depth of the Mohorovicic discontinuity given by Hurtig et al. (1991). The mean depth obtained for the discontinuity is around 30 km instead of 34 km as given previously. The maximum depth is around 32 km instead of 37 km in the south of the study area and the NW-SE gradient is stronger in the model proposed here. The residual field does not show any particular correlation between the anomalies and the known seismo-tectonic features excepted, may be, in the region B of Figure 7 where a cluster of earthquakes epicenters appear on the flank of the -70 mgal anomaly.

To be interpretable in terms of superficial seismo-tectonic structures the residual field should have a less regional character. For that it would be necessary to reprocess the original field data, to take into account the local variations of the density, to create a new grid with finer mesh and finally to use more elaborated prost-processing techniques.

References

Airy, G.B., 1855, On the computations of the effect of the attraction of the mountain masses as disturbing he apparent astronomical latitude of stations in geodetic surveys, Phil. Trans. R. Soc. Lond., 145, 101-104.

Bingöl, E., 1989, Geological Map of Turkey, 1:2,000,000. General Directorate of Mineral Research, Ankara.

Cline, A.K., 1974, Scalar and Planar Curve Fitting using Spline under Tension, Comm. of ACM, 17, 4, 218-223.

Ekingen, A., 1971, Gravimetric Method in Geothermal Field Explorations and its Application in Turkey, Proceedings of I. Geothermal Energy Symposium of Turkey, 60-74.

Ekingen, A., 1978, Gravity gradient of Biga peninsula, Geothermal Energy Assoc. Publ. No. 6, MTA Ankara, 2-6.

Heiskanen, W.A., and F.A. Vening-Meinesz, 1970, The Earth and its Gravity Field, Mac Graw Hill, New York, 470p.

Hurtig, E., Cermak, C., Haenel, R. and V. Zui, 1991, Geothermal Atlas of Europe, Map 21.2 East Europe, Depth of the Crust-Mantle Boundary, scale 1/5,000,000.

Klingelé, E.E. and Olivier, R., 1980, La Nouvelle Carte Gravimetrique de la Suisse, Materiaux pour la Geologie de la Suisse, Serie Géophysique, 96 Pages, 9 Figures, 4 Tables, 1 Carte.

Klingelé, E.E., Wyss, T.M., and F. Arnet, 1995, PROGRAV, Fortran Programs for Processing and Interpretation of Gravimetric Data. Institut für Geodäsie und Photogrammetrie, IGP-Publications No. 250, ISBN 3-906513-71-8, ETH Zürich, Switzerland, July 1995.

LaPorte, M., 1962, Elaboration rapide des cartes gravimétriques déduites de l'anomalie de Bouguer à l'aide de la calculatrice Électronique. Geophys. Prosp., 10, 238-257.

Şimşek, Ş, this volume, Geothermal potential in Northwestern Turkey.

Geothermal reconnaissance of the Marmara sea region

MARTIN PFISTER, LADISLAUS RYBACH AND ŞAKİR ŞIMŞEK

Abstract

Northwestern Anatolia is an area of significant neotectonic activity. The Northern Anatolian Fault Zone (NAFZ) splits into different branches and the tectonic regime changes from translation to a combination of extension and translation. High seismicity, as well as frequent and in places large hot springs are related to these tectonic features. The present study aimed at characterising the geothermal situation of this area by detailed heat flow density mapping and thermal spring studies.

High resolution temperature logs and measurements of rock thermal conductivity were used to determine the terrestrial heat flow density. Because of the shallowness of the available drillholes (maximum depth of 200m), hydraulic influences on the thermal profiles had to be taken into account. Conductive heat flow density was calculated considering possible convective effects due to water movements. In spite of these hydraulic influences, the temperature distribution showed stability over a time period of at least one year. Stationary models were, therefore, applied. Terrestrial surface heat flow density varies regionally from 35 to 115mW/m^2, with a mean value of 60mW/m^2. Estimates about paleoclimatic effects on geothermal gradient lead to the conclusion that these shallow heat flow densities have to be corrected by +5 to +25%.

The heat flow density map shows that the extensional tectonics of the region south of the Marmara sea is characterised by higher heat flow density values. Regions with low tectonic activity, such as parts of European Turkey, or regions with compressional and translational tectonics have average or slightly lower values.

Numerical calculations based on FD and FE codes were used to evaluate the applicability of conceptional circulation models on the basis of hydrogeological data.

The thermal springs of Bursa are geologically explained by a fault zone with higher permeabilities. The system was interpreted by a ‘closed circuit’ circulation system. Fast circulation allows the precipitation to infiltrate to depths of 1000m b.s.l. and to rise again to the surface. The thermal springs of the Gemlik-Orhangazi region show water components which travelled from the infiltration area to the spring area in less than 40 years. A coupled model of groundwater, heat and tritium transport reveals that the circulation paths of these springwaters are bound to karstic lithologies and, in the spring area, to tectonic fault lines. The heat flow density values of 50 – 70mW/m^2 in both regions, near the regional average, are not in contradiction with the high spring temperatures. High permeabilities permit hot water to rise quickly and to transport heat to the surface from greater depths.

The spatial pattern of thermal springs in the Marmara sea region does not coincide with the terrestrial heat flow density distribution. Their appearance is bound to neotectonic faults (=locally enhanced vertical permeabilities).

Introduction

The Marmara sea region of NW Turkey is a tectonically extremely active area. Large, and also frequent, earthquakes are triggered by the influence of the westward moving Anatolian platform along the Northern Anatolian Fault Zone (*NAFZ*) and the extensional part of the Aegean plate which combine to form a transtensional tectonic regime. Up to 23 strong earthquakes with magnitudes greater than 5.9 have occurred in the Marmara area since 1899 (Ambraseys and Finkel 1991, compare also Barka, Fig. 2, this volume).

Furthermore, large thermal springs occur all over the described region. Figure 1 displays the distribution of hot springs, which are classified by their thermal energy output. This energy output is calculated using outflow rate and temperature, the latter reduced by the mean surface temperature of 16°C (Equation 1). The entire region is covered by thermal springs, but large hot springs with an energy output of several megawatt occur in distinct areas only. Estimates of the total thermal energy output from drillholes are about 100MW (Şimşek this volume) and, from natural thermal springs, about 60 to 130MW (based on Şimşek this volume and Pfister 1995). Added together, the possible amount of thermal energy output (230MW) distributed over the investigation area (85,000km^2) corresponds to a theoretical convective heat flow component of ca. 2.5mW/m^2. Therefore, the geothermal areas of Northwestern Anatolia form significant anomalies only locally. The distribution of hot springs according to temperature is shown in Şimşek (this volume, Figure 3).

$$E = (T_{measured} - T_0) \cdot Q \cdot c \cdot \rho \qquad [1]$$

where:

E: thermal energy output [W]
T_0: mean surface temperature [16°C (from Pfister 1995)]
$T_{measured}$: spring temperature [°C]
c: heat capacity of water[J/kg°C]
ρ: water density[kg/m^3]
Q: outflow rate [l/s]

The basic question about the thermal boundary conditions, within the Earth's crust, of this geothermal potential has not yet been answered. Preliminary investigations on terrestrial heat flow density distribution have been documented by Tezcan and Turgay (1991), İlkışık (1995) and Tezcan (1995) (compare Figure 8, Mueller et al. this volume). All these studies rely on estimates of rock thermal conductivity as well as to the greater part on estimates of the temperature distribution in the underground. Generally all studies obtained rather high values in the region south of the Marmara sea compared to the global average continental heat flow density.

The present study aimed at characterising the geothermal situation of this area by detailed heat flow density mapping and geothermal modelling studies. For these purposes, temperature profiles in shallow drillholes (up to 200m depth range) were measured. Rock thermal conductivity from local samples were also obtained. These two parameters permitted the calculation of terrestrial heat flow density. Advective / convective heat transfer had to be considered by means of Peclet-number analysis because of the shallow data-depth-range. Temperature profiles of oil wells partly permitted a comparison of deep and shallow heat flow densities. Thermal water wells and their temperature profiles were interpreted by simple physical models based on vertical water movement over a certain depth range and basal heat flow density values.

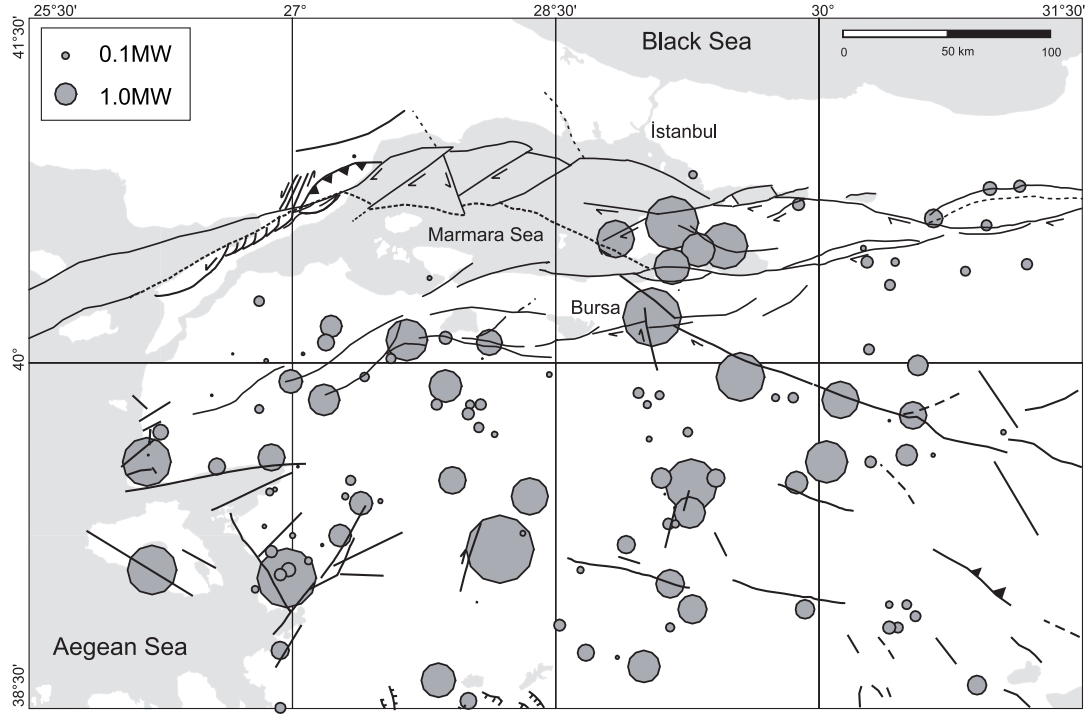


Figure 1: *Natural thermal springs of the Marmara sea region and the neotectonic regime: Circles are proportional to the energy output of thermal springs according to Equation 1.*

The study described below leads to a consistent picture of the geothermal map considering all obtained information about terrestrial heat flow density, which is an indispensable boundary condition for modelling geothermal processes in the uppermost part of the Earth's crust.

Data acquisition

The search for available and suitable drillholes was mainly made possible with the help of the following national organisations with offices in different cities: The DSİ (State Hydraulic Works) and Köy Hizmetleri (Rural Services). A first selection of unused or abandoned wells (which are especially suitable due to the absence of disturbing water flow caused by pumping) had to be checked by personal field trips. Three field measuring campaigns during the summers of 1991, 1992 and 1993 led to valuable temperature data for 44 shallow water wells. The temperatures were recorded using two measurement equipments with different resolutions: +/-0.1°C and +/-0.02°C, respectively, and with different depth sample intervals of 4m and 0.1m, respectively. High resolution temperature logging is described in detail in Pfister and Rybach (1995, 1996). 9 selected records are shown in Figure 2, the complete measurements are presented in Pfister (1995). The selected data records show representatively the character of the temperature profiles for shallow depths. Water movement is interpreted as the main cause for nonlinear temperature increase with depth. Changes in thermal conductivity of the underground are considered as secondary effects over these small depth ranges. Most of the locations showed constant lithology over the whole measurable depth range. Repeated measurements at the same drill sites were also performed (Figure 3 a,b). In spite of the hydraulic influences, the temperature distributions showed stability over a time period of at least one year. Stationary models were, therefore, applied.

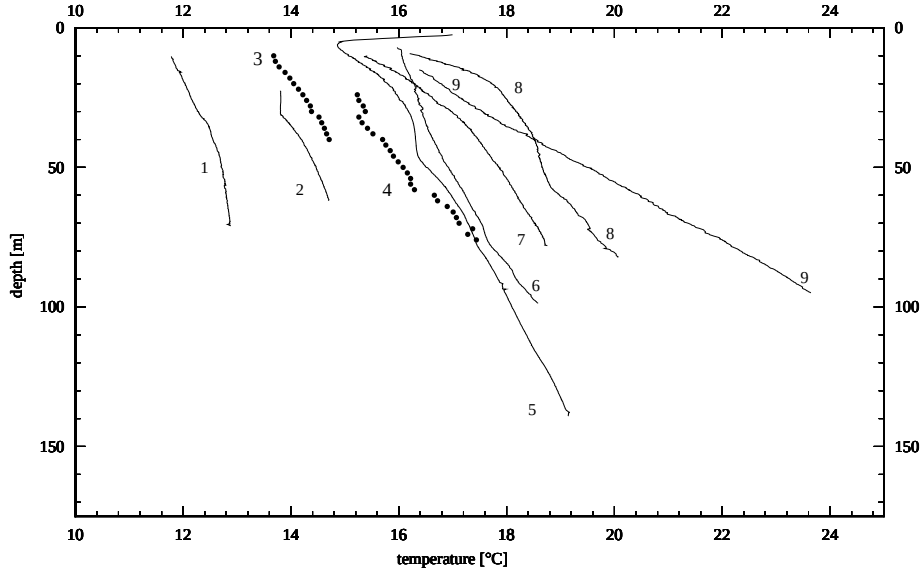


Figure 2: *Selected temperature profiles (1-9) measured in shallow wells. Water movement is interpreted as the main cause for nonlinear temperature increase with depth. Changes of thermal conductivity of the underground are considered as secondary effects over these small depth ranges.*

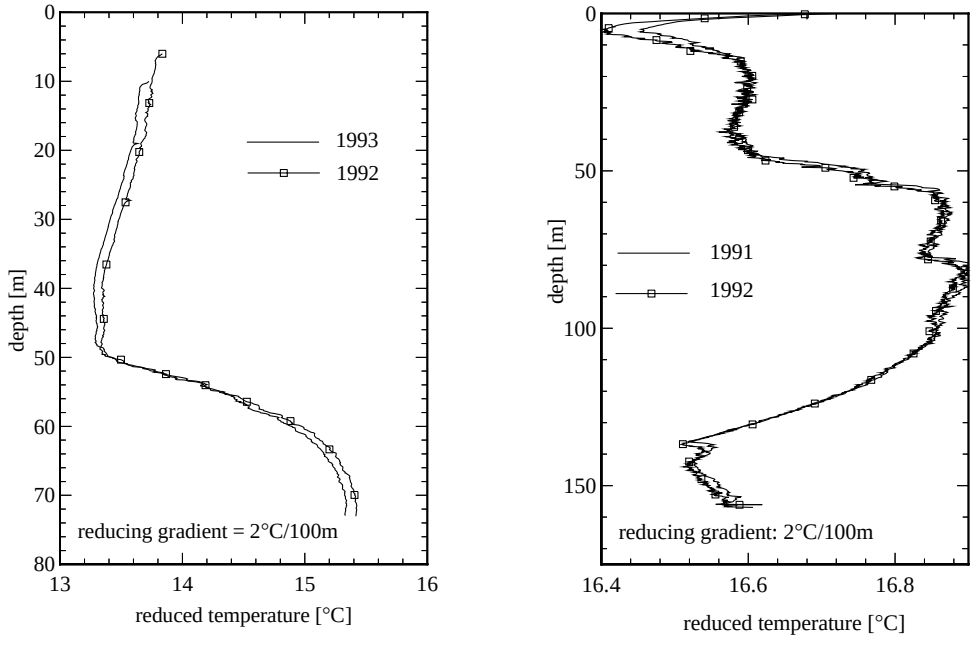


Figure 3: *Repeated measurements of the temperature profile at two different drill sites, Soğuksu (3a) and Kite (3b), both near the city of Bursa. Note the stable conditions over one year (reduced temperature scale).*

High resolution digital temperature logging is even able to resolve convection cells of the water within the drillhole. Gretener (1967) as well as Diment and Urban (1983) describe typical relationships of such cells. Pfister and Rybach (1995) observed and analysed convection cells in a well in northern Switzerland. According to Diment and Urban (1983), the cells show the following relation:

$$R = A \cdot G' \cdot a \qquad [2]$$

where:

R: maximal temperature difference within the convection cell [°C]
A: cell aspect ratio, height/drillhole radius
G': geothermal gradient [°C/m]
a: drillhole radius [m]

Figure 4 shows several temperature logs from the study area with typical convection cell patterns depending on drillhole diameter and temperature gradient. The cell sizes show greater vertical dimensions at larger well diameters and larger temperature ranges at higher geothermal gradients, as described by Equation 2.

Furthermore, temperature records from a total of nine oil wells (data from the Turkish Petroleum Agency, TPAO Ankara) reaching depths up to 2500m were obtained. Figure 5 shows temperature profiles for five onshore wells digitised with a depth interval of 25m from analogue data on paper. These data, as well as the BHT data of four other offshore wells, were used to calculate mean geothermal gradients as listed in Appendix 1.

Temperature records from four thermal water wells (data from the General Directorate of Mineral Research and Exploration, MTA Ankara) show the strong influence of fast rising water in hot spring areas (compare Figure 8). The accuracy of such records lies in the range of +/- 10°C, because measurements were taken at the wellhead (mud data).

Rock samples from surface outcrops were collected at the specific drill sites of the shallow wells. Thermal conductivities of these samples were measured at ambient temperatures and water saturated conditions. Pribnow (1994) describes, in detail, different measuring methods. For our purposes, the transient method of a heated line source (Carslaw and Jaeger 1959) was applied. This theory is easily changed into a model of a heated line source over a half space; the source temperature is compared to the logarithm of heating time. Thermal conductivity λ is calculated according to Equation 3 at large times t:

$$\lambda = \frac{Q}{2\pi} \cdot \frac{\Delta t}{\Delta T} \qquad [3]$$

where:

λ: thermal conductivity [$Wm^{-1}K^{-1}$]
Q: produced heat per unit line length and time [$Wm^{-1}s^{-1}$]
ΔT: measured temperature difference [K]
Δt: time difference [s]

An approximation of the heating curve according to Erbas (1985), based on Blackwell (1954), is used to calculate the final values of thermal conductivity. Two equipment were used: a *QTM* and a *TK04*. The sample size was typically ca. 9cm in diameter with a minimum thickness of 3cm. Erbas (1985) gives penetrating depths of 2 to 3cm of the heat wave into the sample size using a *TK04*.

The different lithologies show a wide range of values but group reasonably well (Figure 6). Each dot in the plot represents a different sample from one specific outcrop. Usually, up to 10 measurements were performed on each sample. The standard deviations of the measurements range from +/-0.02 to +/-0.4$Wm^{-1}K^{-1}$. Thermal conductivities of sandstones vary strongly due to differing contents of salt and clay. Limestones appear generally with higher values, granitic rocks show intermediate values whereas volcanic rocks (andesites, ignimbrites and tuffites) yield lower values.

The data set described above requires careful analysis and special treatment of the temperature data. The shallow underground, up to 200m in depth, is often dominated by groundwater flow. The following chapter describes the necessary calculation procedures to extract reliable information about terrestrial heat flow density, even from severly disturbed temperature logs.

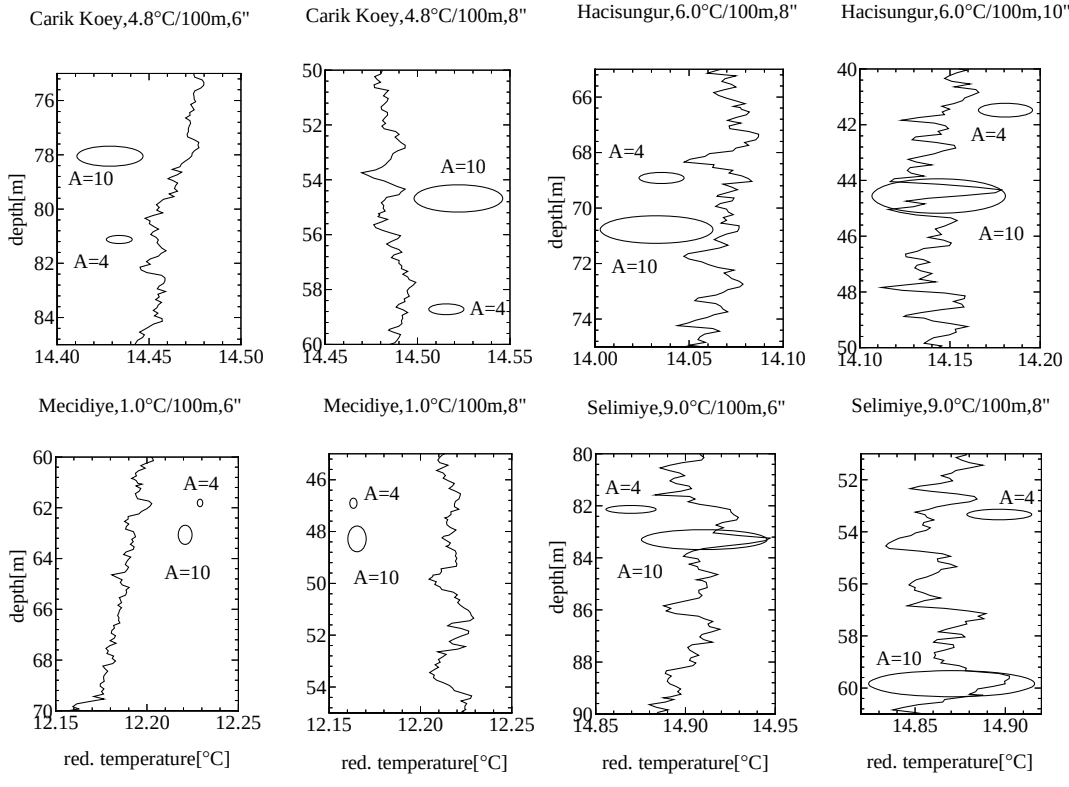


Figure 4: *Observations of convection cells in drillholes: 8 different graphs show convection cells which depend on the drillhole radius a and the geothermal gradient G'. The temperature scale of each graph is reduced by the local geothermal gradient (indicated in the top line). The drillhole site and name are indicated at the top of each figure (cf. Appendix 2) and two examples of convection cell sizes (heights and temperature amplitudes) are plotted for each example. The convection cell sizes are calculated by Equation 2 for different values of A, 4 and 10. The measurements show a good agreement with the criterion of Diment and Urban (1983), see text.*

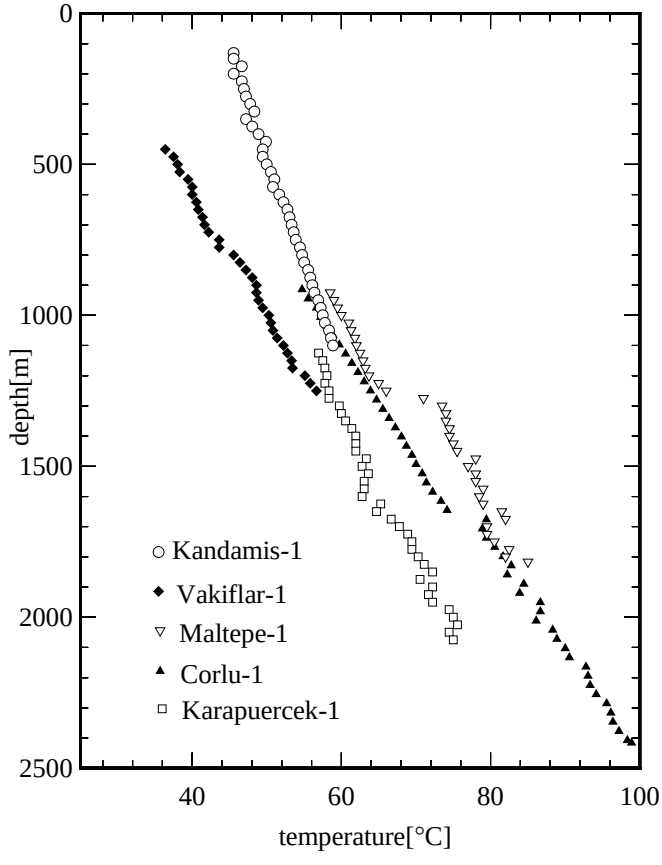


Figure 5: Temperature logs of five oil wells in Thrace. The logs are digitised with a sampling interval of 25m from analogue data on paper.

Convective/advective heat transport by water movement

Vertical terrestrial heat flow density is defined according to Equation 4, which is based on the physical model of purely conductive heat transfer:

$$q_z = -\lambda \cdot \frac{\partial T}{\partial z} \qquad [4]$$

where:

q_z: terrestrial heat flow density [mW/m^2]
λ: thermal conductivity [WK^{-1}m^{-1}]
$\partial T/\partial z$: temperature gradient [°C/km]

In shallow depth ranges, this model is often violated: moving groundwater can also easily transport heat too. This effect can be detected by the nonlinearity of the measured temperature profile. Figure 7 shows three different cases of moving groundwater and its influence on the temperature profile. These three conceptual models (FLOW, BETA, RAM) are consecu-

tively described according to their mathematical solution. The main goal of this treatment is to obtain information about conductive heat flow density at the deepest point of the observed depth range.

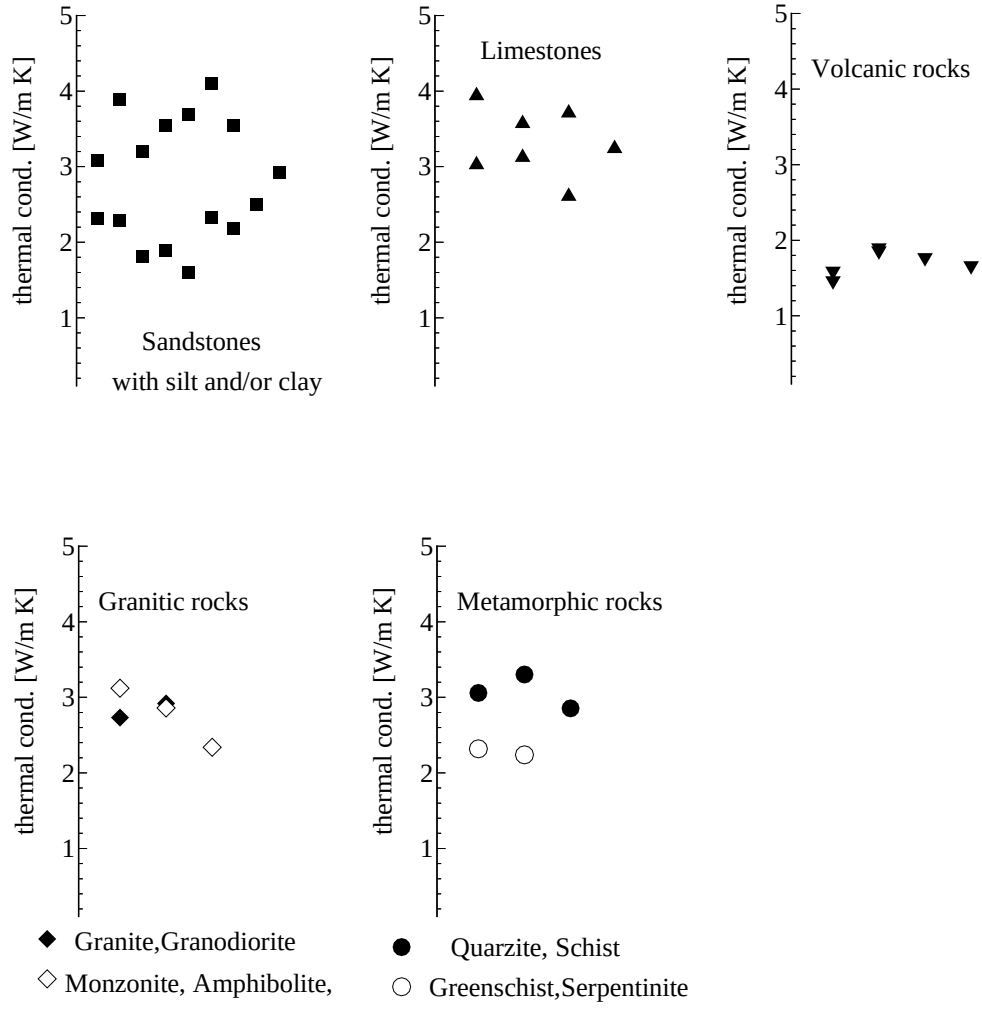


Figure 6: Thermal conductivities for different lithologies of rock samples from surface outcrops.

Convective and/or advective heat transfer is considered here, regardless of whether this fluid movement is caused by hydraulic gradients (forced convection, "advection") or by temperature-dependent fluid densities leading to buoyancy (free convection, "convection").

Generally, the measured temperature profiles are simulated by the analytical solutions of the physical models FLOW, BETA and RAM. Then, terrestrial (conductive) heat flow is determined by different approaches: either by a linear regression of ln(q) versus depth (model FLOW), by varying the parameter "heat flow" until the simulated temperature profile fits the measurement well (model BETA) or by varying the parameter "geothermal gradient" until the model fit is satisfying (model RAM).

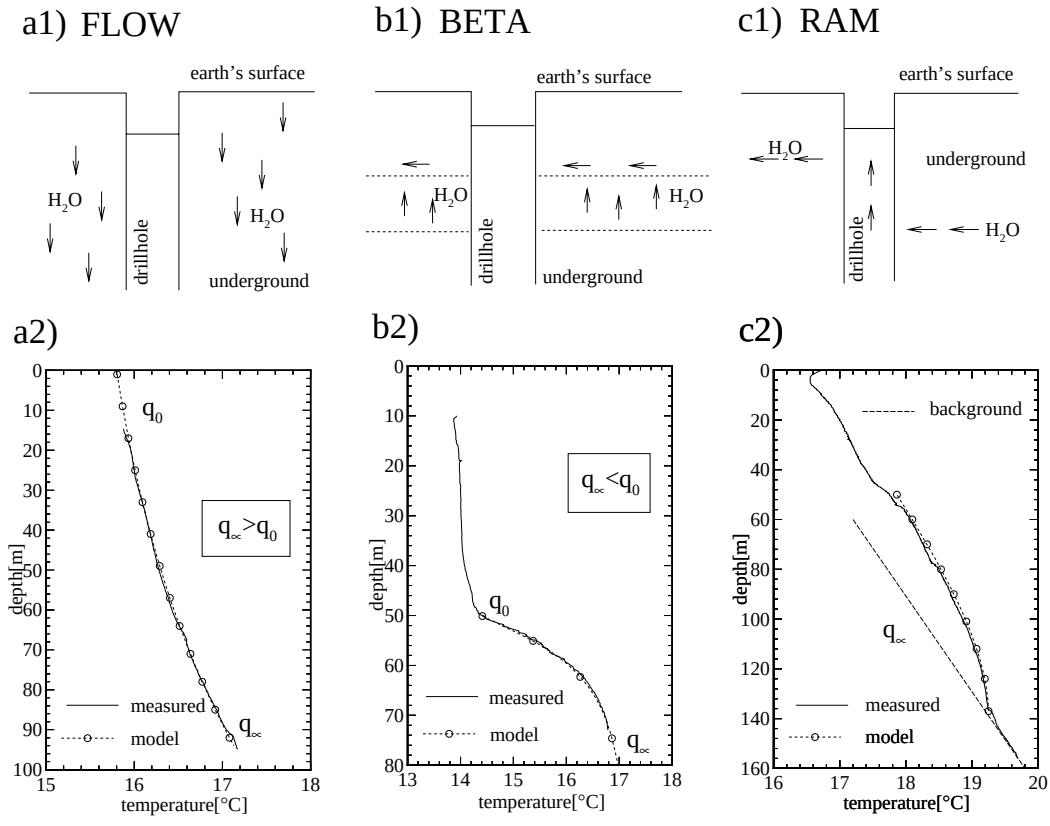


Figure 7: *Three different models of water movement in the underground. The sketches a1 to c1 describe the water flow situations which have been measured by temperature logs and modelled according to a2 to c2.*

Linyıtleri a: FLOW		Soğuksu b: BETA		Kite c: RAM	
q(0)	14mW/m^2	-	-	gradient	2.6°C/m
q(95)	50mW/m^2	q(76)	56mW/m^2	q(138)	52mW/m^2
Peclet no.	1.3	Peclet no.	-2.2	time	20-25 years
L	95m	l	22m	depth	50-138m
λ	2.0WK^{-1}m^{-1}	λ	2.60WK^{-1}m^{-1}	λ	2.00WK^{-1}m^{-1}
T(0)	15.8°C	T(49)	14.2°C	inflow Temp.	19.2°C
-	-	h	54m	κ	1*10^{-6} m^2/s
				water vel.	0.3mm/s

Table 1: *Model input parameters for simulations of Figure 7.*

FLOW: vertical water movement over the whole observed depth range

In this model, groundwater moves vertically over the whole observed depth range (Figure 7, Sketch a1). Bredehoeft and Papadopulos (1965) described a method to calculate the velocity of the moving groundwater. They considered an isotropic, homogenous and permeable un-

derground with an incompressible fluid (groundwater). The differential equation for this physical model can be written as (Equation 5):

$$\frac{\partial^2 T}{\partial z^2} = \frac{c \cdot \rho \cdot v_D}{\lambda} \cdot \frac{\partial T}{\partial z} \quad [5]$$

where:

T: temperature [°C]

z: variable of depth [m]

c: heat capacity of water [[J/kg K]

ρ: density of water [kg/m^3]

v_D: Darcy velocity [m/s]

λ: rock thermal conductivity [WK^{-1}m^{-1}]

z-axis is positive downwards, c, ρ and λ are independent of z.

The solution to this differential equation for a layer with a top at depth z_1 (temperature T_1) and a bottom at depth z_2 (temperature T_2) is the following (Bredehoeft and Papadopulos 1965):

$$T(z) = T_1 + \left(\frac{T_2 - T_1}{e^{\beta(z_2 - z_1)} - 1} \right) \cdot \left[e^{\beta(z - z_1)} - 1 \right] \quad [6]$$

$$\beta = \frac{c \cdot \rho \cdot v_D}{\lambda} = \frac{Pe}{L}$$

Pe: Peclet number (dimensionless)
L: vertical distance of water movement [m]

The total energy flow E_1 at the layer top (z_1) can be defined using Equation 7 (Mansure and Reiter 1979):

$$E_1 = -\lambda \cdot \left. \frac{\partial T}{\partial z} \right|_{z_1} + c \cdot \rho \cdot v_D \cdot T_1 \quad [7]$$

Equation 6 is modified to become Equation 8:

$$T(z) = T_1 + \left(\frac{-E_1}{\lambda \cdot \beta} + T_1 \right) \cdot \left[e^{\beta(z - z_1)} - 1 \right] \quad [8]$$

Clauser and Villinger (1990) showed that, in such a case, the conductive heat flow density q(z) is depth dependent:

$$q(z) = q(0) \cdot e^{\beta(z - z_0)} \quad [9]$$

q(z) can be calculated from the measured temperature profile at different depths. The linear regression of ln q(z) versus z yields the value of ln q(0) at the surface (depth z_0=0) and, from the slope of the regression line, the value β. Furthermore, q(z_1) can be calculated. q(z_1) and β are to be inserted into Equation 7 to yield the value of E_1. The new temperature profile is calculated beginning at depth z1 using Equation 8.

This kind of interpretation of temperature-depth profiles is also called a Peclet number analysis. The Peclet number Pe = β * L describes the relation between advective/convective and conductive heat transport. L is the length over which water circulation is effective and, for the present case, is assumed to be $|z_2\text{-}z|$. There is no evidence for larger L values, although this can not be excluded. Conductive heat flow in this case is given by $q_\infty = q_{z=L}$.

For a layered medium with N layers with different thermal conductivities λ_j, as j=1→N, Equation 8 becomes Equation 10:

$$T(z) = T_j + \left(\frac{-E_j}{\lambda_j \cdot \beta} + T_j \right) \cdot \left[e^{\beta (z - z_j)} - 1 \right] \qquad [10]$$

and Equation 7 becomes:

$$E_j = -\lambda_{j-1} \cdot \left. \frac{\partial T_{j-1}}{\partial z} \right|_{z_j} + c \cdot \rho \cdot v_D \cdot T_j \qquad [11]$$

All necessary parameters for the model a2 of Figure 7 are listed in Table 1.

BETA: vertical water movement within a certain depth range (”layer”)

In many cases, groundwater moves vertically only over a certain depth range (Figure 7, Sketch b1). This behaviour is treated by the following model, which is based on three "layers" and a homogeneous isotropic medium. The top and bottom "layers" are defined by only conductive heat transport, whereas in the middle "layer", an incompressible fluid is able to move vertically. Because of 1D model considerations, the differential equation for layers 1 and 3 (top and bottom) is the following:

$$\lambda_{1,3} \cdot \frac{\partial^2 T_{1,3}}{\partial z^2} = 0 \qquad [12]$$

Valid for depth ranges: -0- (surface) up to -h- (top of middle layer); and -h+l- (bottom of middle layer) up to -∞-.

The differential equation for layer 2 (middle) is identical to Equation 5, but in this case only valid for depth ranges -h- (top of middle layer) to -h+l- (bottom of middle layer, l = layer 2 thickness).

The continuity at the layer boundaries of the temperatures, as well as the temperature gradients, is required. The continuity of the conductive heat flow density is, therefore, guaranteed. Water is able to enter or leave the middle layer at depth -h- or -h+l- with the respective temperatures at these layer boundaries.

According to the following three equations (13 to 15) the temperature profiles ($T_1(z)$, $T_2(z)$ and $T_3(z)$) can be calculated. Boundary values are the surface temperature $T_1(0)$ and the conductive heat flow q_∞ at depth z = ∞. All necessary parameters for the model b2 of Figure 7 are listed in Table 1.

$$T_1(z) = T_0 + \frac{q_\infty}{\lambda_3} \cdot e^{-Pe} \cdot z \quad 0 \le z \le h \qquad [13]$$

$$T_2(z) = T_0 + \frac{q_\infty}{\lambda_3}\left[e^{-Pe\left(h - \frac{l}{Pe}\right)} + \frac{l}{Pe} \cdot e^{-Pe\left(\frac{h}{l} + l - \frac{z}{l}\right)}\right] \quad h \le z \le h+l \qquad [14]$$

$$T_3(z) = T_0 + \frac{q_\infty}{\lambda_3}\left[e^{-Pe\left(h - \frac{l}{Pe}\right)} + \frac{l}{Pe}\right] + \frac{q_\infty}{\lambda_3} \cdot [z - h - l] \quad h+l \le z \le \infty \qquad [15]$$

The parameters q_∞, Pe and l are varied until a satisfactory fit of the measured temperature profile is achieved. Then q_∞ serves as the value for the regional terrestrial heat flow field.

RAM: vertical water movement within the drillhole casing

Groundwater is able to enter a drillhole where the casing has a filter section or below the casing shoe. The water can leave at the collar or, eventually, deeper, e.g. through a fracture (Figure 7, Sketch c1). The constant background temperature gradient of the underground vanishes in the temperature records of the drillhole (Figure 7, temperature profile c2). An analytical solution to describe this water movement within the drillhole was given by Ramey (1962). The temperatures in the drillhole below (or above) the entry point of the water are given by Equation 16, depending on the water flows downward (+) or upward (-). All necessary parameters for the model c2 of Figure 7 are listed in Table 1.

$$T(z) = T(i) + z \cdot \frac{\partial T}{\partial z} \pm \left[e^{(-z/A)} - 1\right] \cdot A \cdot \frac{\partial T}{\partial z} \qquad [16]$$

where:

T(i): temperature at the entry point of the water [°C]
$\partial T/\partial z$: undisturbed temperature gradient, below water entry [°C/m]
A: $=v*\rho*c*r^2*f(t)/2\lambda$
v: water velocity [m/s]
c: heat capacity of water [J/kg K]
r: drillhole radius [m]
λ: thermal conductivity of the surrounding rocks [$WK^{-1}m^{-1}$]

f(t): $f(t) = -\ln\left(\frac{r}{2\sqrt{\kappa^t}}\right) - 0.290$

κ: thermal diffusivity of the underground [m^2/s]
t: total duration of the water movement in the drillhole [s]

The parameter "undisturbed temperature gradient" is varied until a good simulation of the measured temperature profile is achieved. Then, this geothermal gradient serves for calculating q_∞, the regional terrestrial heat flow.

Figure 7 shows different model fits, along with the measured temperature profiles. In all three cases (FLOW, BETA, RAM), the basal (conductive) heat flow density can be determined. Appendix 2 lists all the investigated drillholes, also indicating the treatment method used to determine the undisturbed heat flow density.

Interpretation of thermal drillholes

The thermal spring area of Armutlu on the Yalova peninsula was investigated and the hydrogeology and geology of the region was documented by Eisenlohr (1995 and this volume). A thermal drillhole was deepened within the spring area. Figure 8 shows the measured temperatures (dots), the lithology profile, outflow temperatures of several springs and the analytical simulation of the measured temperature profile.

The simulation was carried out using model BETA described above. A zone with a top at a depth of 150m and a thickness of 50m enables the water to rise vertically and advective/convective, as well as conductive, heat transport is possible over this depth range. Above and below this zone, conductive heat transport only takes place. Further model input parameters are listed in Table 2.

The thermal water of the springs shows temperatures similar to those of the moving groundwater at a depth of 150 to 200m and apparently has its origin outside of this depth range. Heat flow density is not elevated (65mW/m^2) below this upflow zone. Above this zone, very high temperature gradients of up to 30°C/100m and therefore high conductive heat flow density of up to 600mW/m^2 occurs. As a main conclusion it follows that the relatively fast movement of groundwater in certain depth ranges is able to transport heat near to the surface and enables the building up locally of thermal springs where flow paths to the surface are available.

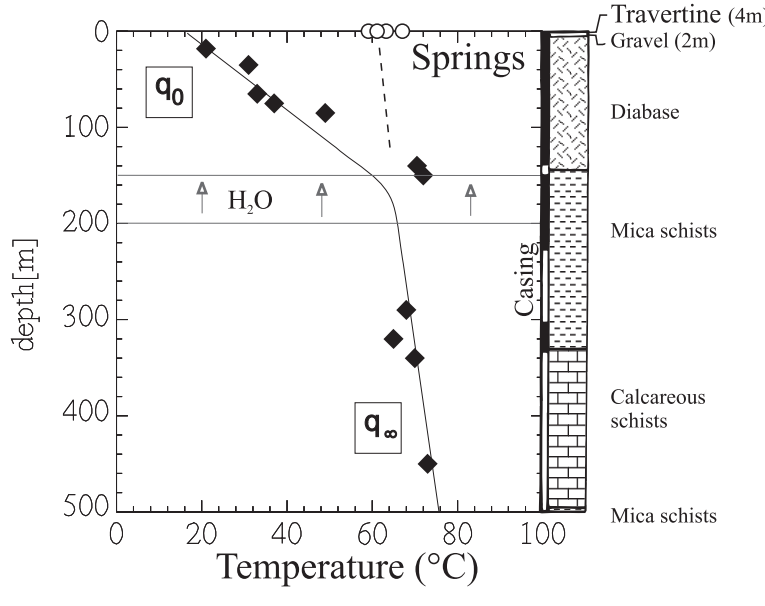


Figure 8: Measured (symbols) and modelled (line) temperatures of the Armutlu thermal water well. The depth of the zone with vertical water movement is indicated by two parallel lines. q_0: surface heat flow (600mW/m^2), q_∞: basal heat flow (65mW/m^2)

Armutlu b: BETA	
Darcy-Velocity	0.5 m/year
q(0)	ca. 600mW/m^2
q(500)	65mW/m^2
Peclet no.	-2.2
l	50m
λ	2.0WK^{-1}m^{-1}
T(0)	16°C
h	150m

Table 2: Model input parameters for Armutlu well simulation.

Heat flow density map and paleoclimatic effects

A total of 44 shallow wells and their temperature records were processed for heat flow density calculation (Appendix 2). Constant gradients served for heat flow density calculation according to Equation 4 (definition of heat flow density). Convective / advective effects of the groundwater movement were considered according to the previously described 1D models. Measured temperatures were simulated using the models FLOW, BETA or RAM, respectively, over a depth range for each log individually selected. At the base of such observed / modelled depth intervals, heat flow density was determined (listed in Appendix 2, q_∞).

It must be emphasised here that the heat flow density so determined characterises only near surface conditions. In the heat flow signal, however, the influence of integrated geological processes of the deeper crust, and even the upper mantle of the Earth, is present.

The data set of shallow heat flow built the base for mapping by geostatistical methods. The kriging method described below was used for isoline interpolation.

Semivariance analysis (Davis 1986) describes the spatial dependence of the heat flow density data (q_∞). Values of two points with a distance larger than 'a' have no statistical relation to each other (Figure 9, semivariogram). This value 'a' and the valueσ are used for kriging interpolation. A spherical model according to Equation 17 simulates the semivariogram (line in Figure 9).

$$\gamma_{h\Delta} = \sigma_0^2 \cdot \left(\frac{3h\Delta}{2a} - \frac{(h\Delta)^3}{2a^3} \right) \qquad [17]$$

where:

a: span or range [° geograph. length]
σ_0^2: variance [mW^2/m^4]
Δ: 0.5° geograph. length (42.5km)
h: 1,2,3...

The 44 heat flow density values (q_∞) were interpolated using the kriging method with the parameters a = 150km, Δ = 0.5° (42.5km) and σ_0^2 = 3557mW^2/m^4. The map in Figure 10 contains the 44 well locations with the specific heat flow density values. The isolines delimit four

intervals: 35-55mW/m^2, 55-75mW/m^2, 75-95mW/m^2 and 95-115mW/m^2. Analysis of oil wells in the Thrace region (Appendix 1 and Figure 5) reveals similar range of values for this region. Temperature gradients based on singular BHT data (Appendix 1) are very uncertain and cannot be used for heat flow density calculations. The interpretation of thermal well data (one example in Figure 8) yields heat flow density values (q_∞) which fit well into the regional field. The histogram of the data from the 44 shallow wells shows a mean value of 60mW/m^2 and a variation range of +/- 50mW/m^2 (Figure 10). The heat flow density distribution of the Marmara sea region cannot be regarded as generally high. Only selected areas show elevated surface heat flow density of up to 100mW/m^2, such as regions south of the Marmara sea. The Thrace area (north of the Marmara sea), as well as the İstanbul and Bursa regions, are characterised by normal values of up to 55 mW/m^2.

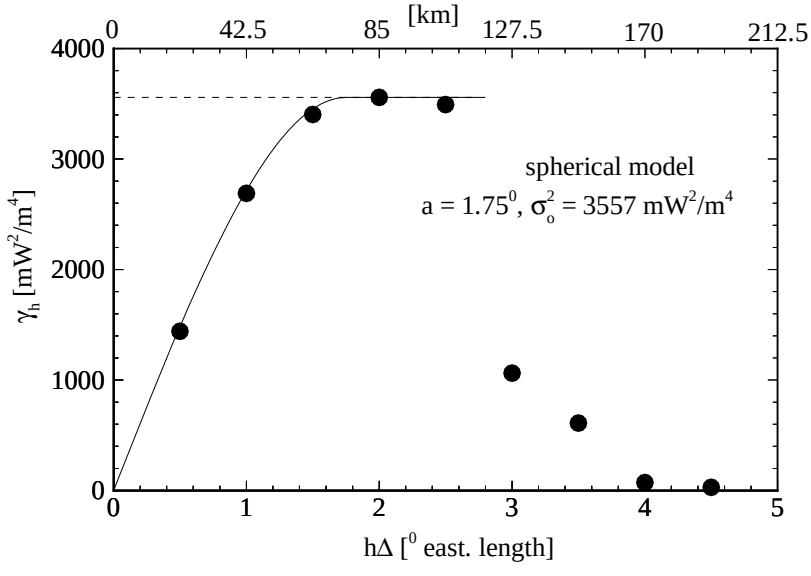


Figure 9: *Semivariogram for heat flow values from shallow depths. The line shows a spherical model, calculated with the values Δ = 0.5° (42.5km), a = 1.75° (150km) and variance σ_0^2 = 3557mW^2/m^4 (dashed line).*

The near surface conditions provoke a further thermal signal which has to be considered before the interpretation of deeper processes. Recently new thermal data from deep drillholes have become available, e.g. super deep drillholes in Russia (Kola, Ural) or in Germany (KTB). Substantial differences between shallow and deep terrestrial heat flow data led to reconsidering paleoclimatic effects on the heat flow data (IHFC, 1996). Considering these new findings that a paleoclimatic influence of up to 30% or even 60% in the shallow depth levels of the Earth's crust is possible, we try to estimate this influence for the Marmara sea region.

During the last ice age ground temperatures were lowered by several degrees, even in Mediterranean or Aegean regions (Farrand 1971). Bodmer and Rybach (1984) described the application of a paleoclimatic model for correction of subsurface temperatures in Alpine regions (Switzerland). Our model for the Marmara sea region (Figure 11) is a combination of the model of Bodmer and Rybach (1984) with the knowledge about paleoclimatic history in Mediterranean region (Farrand 1971, 1980, Cita and Ryan 1978, Roberts and Wright 1993, Grove and Conterio 1994). We assume the same paleoclimatic history for recent time (up to 10,000 y. B.P.) but a similar trend for the ice ages with smaller amplitudes of the temperature difference time series compared to Alpine regions.

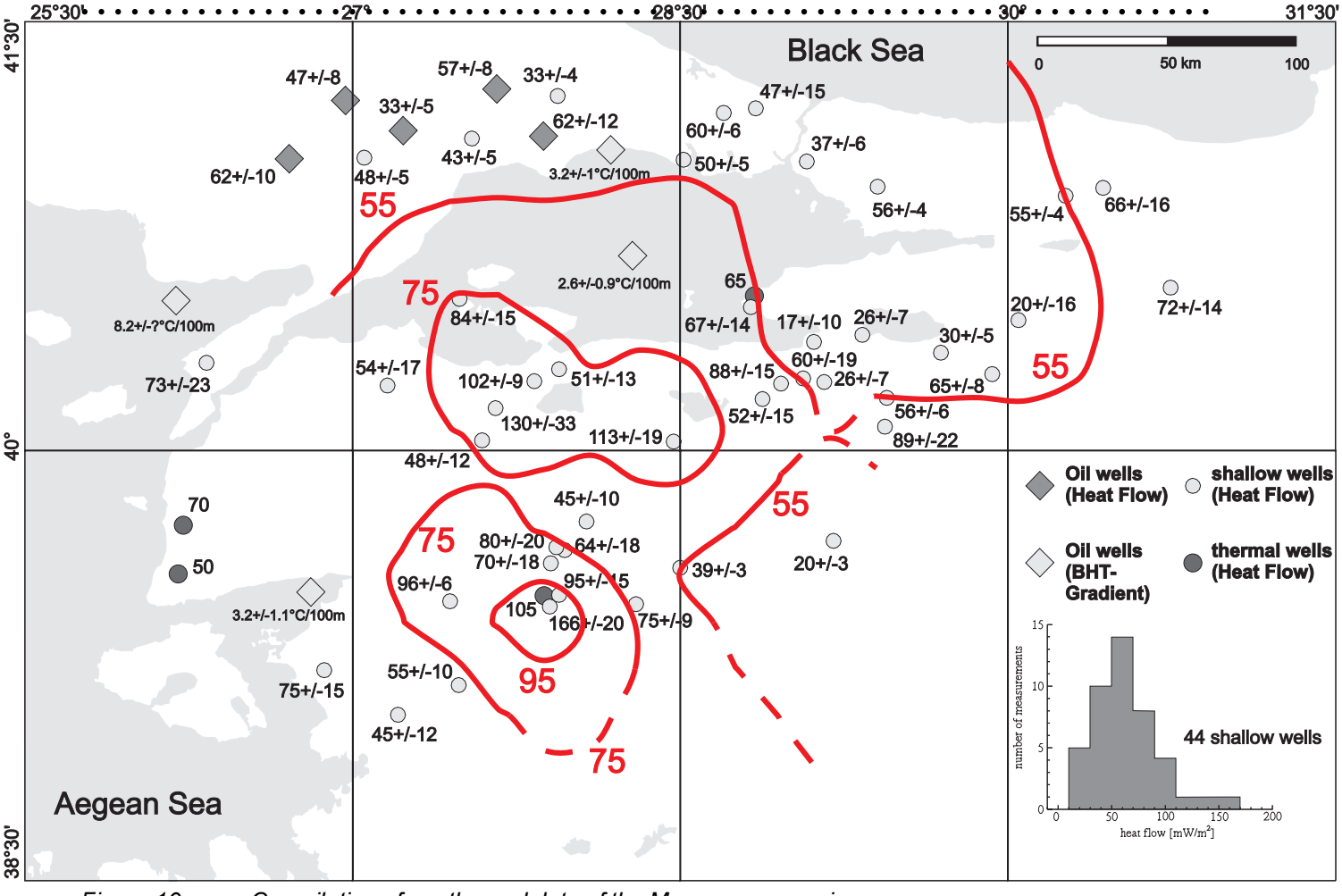


Figure 10: *Compilation of geothermal data of the Marmara sea region.*

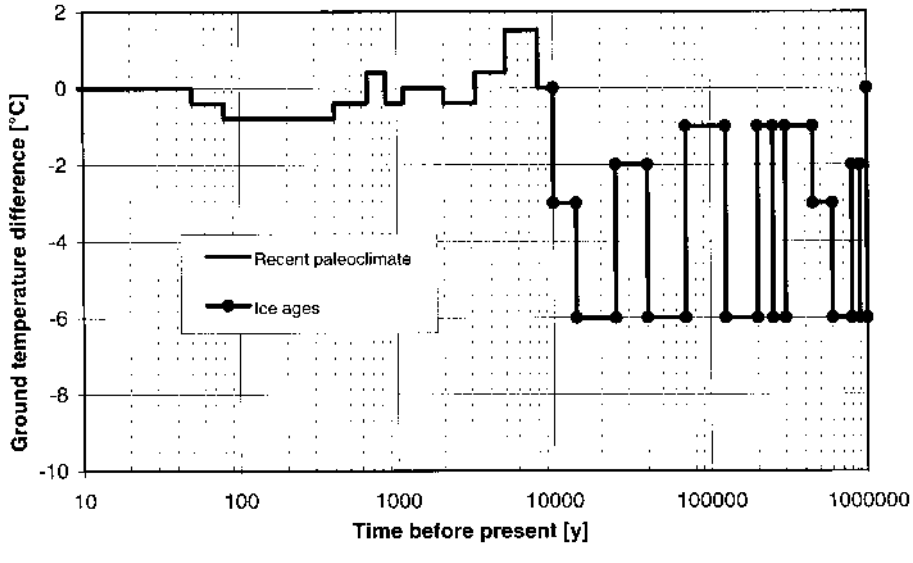


Figure 11: *Paleoclimatic model of surface temperature for the Eastern Mediterranean sea region. Sources: Farrand (1971, 1980), Cita and Ryan (1978), Roberts and Wright (1993), Grove and Conterio (1994) and Bodmer and Rybach (1984).*

The temperature effect at any depth z, caused by a single step change in surface temperature, can be found by solving the 1D heat conduction equation $\delta^2T / \delta z^2 = (1/K)\, \delta T / \delta z$ with the time dependent difference $\Delta T_{S(i)}$ to the surface temperature of today $T_{S(1)}$ as a boundary. Applying this, Equation 18 describes the change in temperature gradient at a given depth z for n time steps (Birch 1948)

$$\Delta g(z) = \sum_{i=1}^{n} \left\{ \Delta T_{s(i)} \cdot \left[\left(1/\sqrt{\pi\kappa t_i}\right) \cdot \exp\left(-z^2/\sqrt{4\kappa t_i}\right) - \left(1/\sqrt{\pi\kappa t_{i+1}}\right) \cdot \exp\left(-z^2/\sqrt{4\kappa t_{i+1}}\right) \right] \right\} \quad [18]$$

where:

$\Delta g(z)$: change in geothermal gradient [°C/m]
$\Delta T_{S(i)}$: temperature difference to the surface temperature of today, time step i [K]
κ: thermal diffusivity [varied between 0.7 and $1.5*10^{-6}$ m^2/s]
t_i: time for step i [s]

Figure 12 shows calculated temperature gradient differences using the paleoclimatic model of Figure 11. Three data sets explain the influence of the whole paleoclimatic model but with varying thermal diffusivity κ. Three further sets show the influence of the ice ages with different time lengths but without considering recent history. It is clearly to be seen that recent paleoclimatic changes disturb significantly the shallow temperature gradients. However, the maximum influence of the ice ages does not exceed |4°C/km|. Especially in the 100m to 200m depth range this maximum amplitude has to be considered. We estimate therefore a possible maximum (and very probable) paleoclimatic influence on shallow heat flow data by the following procedure: Using calculated heat flow values and measured thermal conductivity data, a geothermal gradient is to be calculated. This gradient is corrected by adding a value of 4°C/km (maximum possible influence by paleoclimate within the depth range of 100m to 200m, which is the depth range of heat flow in this study). The resulting new gradient is used again to calculate corrected heat flow values (in Appendix 2 corrected heat flow values are listed as well as the percentage of this correction). Figure 13 shows these maximum corrections in percent of observed heat flow, determined for all shallow values. It can be concluded that lower heat flow densities require a larger paleoclimatic correction than higher values. Therefore, mean heat flow densities of 60mW/m^2 have to be corrected by 12 to 20%.

Applying a correction for paleoclimate, as described above, also a better coincidence of deep and shallow data within the Thrace area can be achieved. The generally lower values out of the shallow depth range get closer towards the higher values out of the deeper depth range (oil wells). The range of all corrected values is narrower (23mW/m^2) compared to that of all uncorrected values (29mW/m^2). The correction is large for shallow data, whereas it becomes smaller for deeper data. This conclusion follows directly from Figure 12.

Generally, for extrapolation to greater depths, the paleoclimatic influence on shallow data has to be taken into account within a probable range of 5 to 25%!

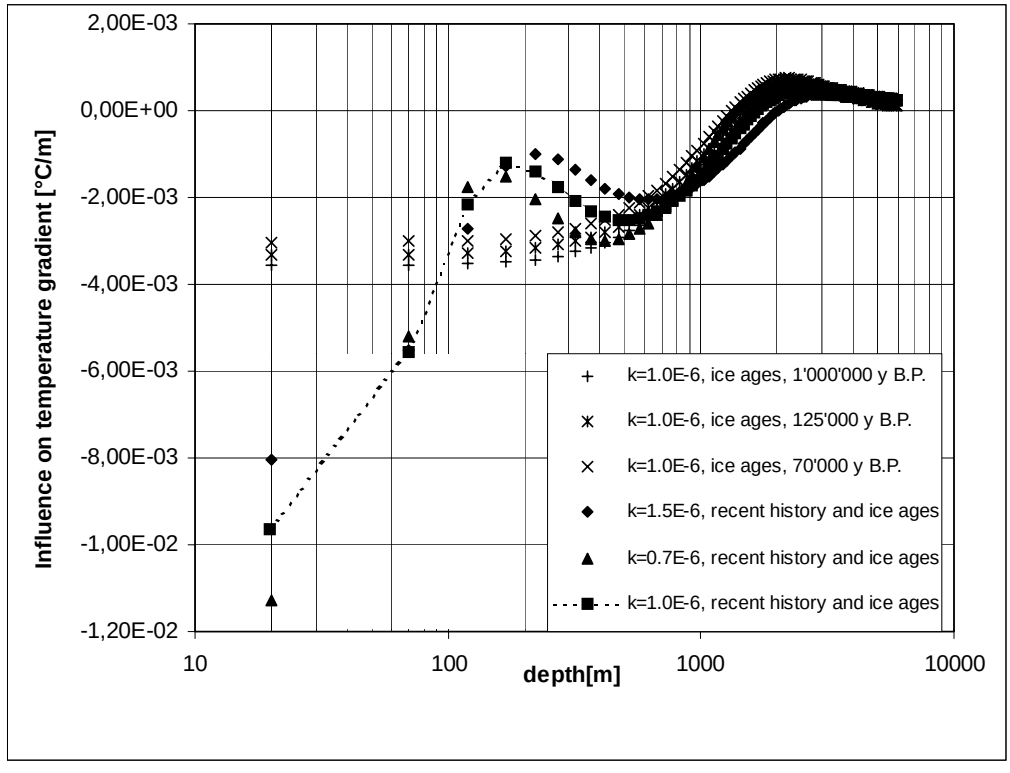


Figure 12: *Influence of paleotemperatures on the geothermal gradient. Different paleotemperature models were used: Complete model of Figure 11 with varying thermal diffusivity κ in the Figure written as k and three models describing only the influence of ice ages with different time lengths neglecting recent history.*

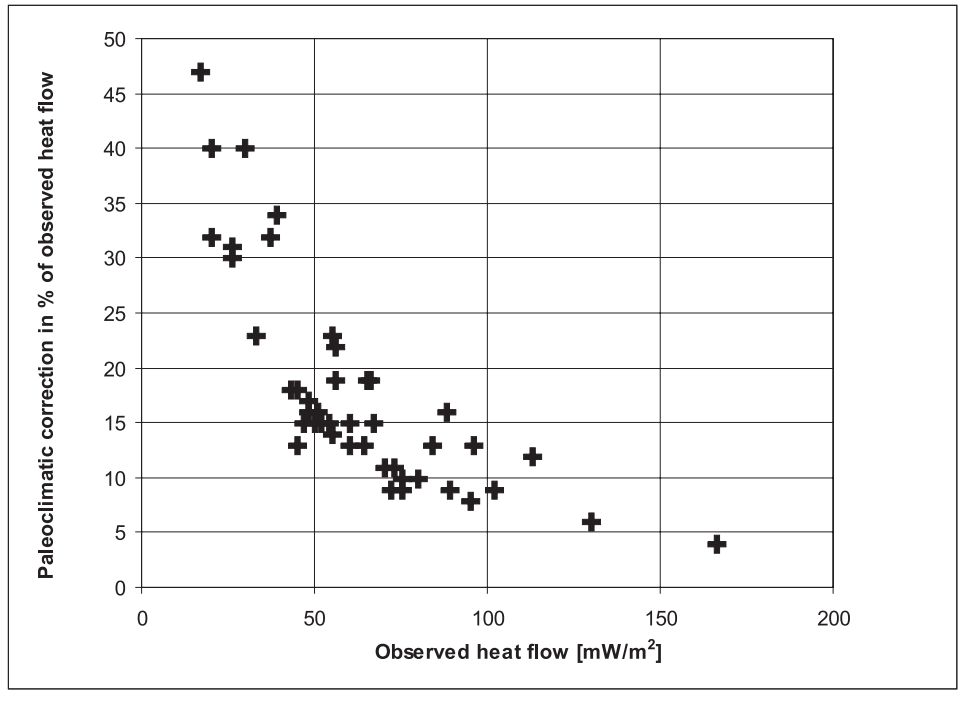


Figure 13: *Observed heat flow values (shallow depth range) and their maximum correction for paleoclimate in percent of observed values.*

Numerical modelling of hydro-thermal circulation pattern:

Thermal springs of Bursa and Gemlik-Orhangazi

The numerous thermal spring occurrences are characteristic of the study area. The presence of a thermal spring requires a peculiar, permeability-governed circulation which enables infiltration of precipitation, its descent to depths where the water can be heated up (accompanied by water-rock-gas interaction of different extent), and finally the ascent to the surface.

Numerical simulations of thermal and hydraulic processes along such pathways follow through to verify postulated circulation patterns conceptually derived from hydrogeological investigations. The coupling of heat transport mechanisms with groundwater transport and the consideration of groundwater and heat sources at the surface (precipitation and surface temperature), as well as in the crust (radioactive heat production, basal heat flow density), offers the opportunity to arrive at a more comprehensive picture of the thermal and hydraulic fields over a certain depth range. The assumption of steady state conditions is certainly a simplification. However, the models investigated represent only a limited window in space and time. The limited depth range of the models (in this case up to 5km b.s.l.) justifies this simplification. The results of the numerical calculations can be compared with field measurements and, therefore, justify the heat flow density field near the surface which acts as a boundary condition for further thermo-tectonic considerations.

Imbach (1992 and this volume) and Eisenlohr (1995 and Eisenlohr et al. this volume) investigated the geothermal areas of Bursa and Gemlik-Orhangazi, respectively. Their qualitative circulation models are to be confirmed or questioned by the numerical calculations. As mentioned before the main question was to obtain information about the thermal boundary conditions in the underground and the basal terrestrial heat flow density.

The following three physical models were used for this purpose and constituted the basis for these simulations: hydraulic groundwater transport based on Darcy's law, heat transport in water saturated underground and transport of the radiogenic isotope tritium (^{3}H) by groundwater movement.

Physical models

Transport of Groundwater

The general mass balance equation describes the change of mass in a certain volume. For a water-saturated and porous medium, Equation 19 describes the balance of mass change in a certain volume (left side of equation) and of inflow and outflow into/out of this volume:

$$\frac{\partial(\Phi\rho)}{\partial t} = -\nabla(\rho\underline{v}) \qquad [19]$$

where:

ϕ: porosity [%]
ρ: fluid density [kg/m^3]
$\underline{v}$: Darcy velocity [m/s]

The driving force of Darcy flow is a pressure difference, which is commonly known as Darcy equation (20):

$$\underline{q} = -K\left(\nabla P + \rho g \nabla z\right) \quad [20]$$

where:

$\underline{q}$: Darcy velocity [m/s]
$K=k/\mu$
K: hydraulic conductivity [m^2/Pa s]
k: permeability [m^2]
μ: dynamic viscosity of fluid [Pa s]
g: gravity [m/s^2]
z: 'z'-directional vector
ρ: density [kg/m^3]
P: pressure [Pa]

It follows that $\underline{v} = \underline{q}$ (Darcy velocity) and $v_f = \underline{q} / \Phi$ (particle velocity or filter velocity). Kohl (1992) describes the transformation of the flow equation (Equation 21) of a laminar fluid flow beginning from the mass balance equation (Equation 19). Here a further possible driving mechanism of the hydraulic system, the linear temperature dependence of the fluid density, as well as the special hydraulic height h_g (often used in hydrogeology) is introduced. This hydraulic height is a combination of the outer pression and of the hydrostatic water level. The left side of Equation 21 becomes zero in the following examples for steady state (intransient) groundwater transport calculations.

$$S_g \frac{\partial h}{\partial t} = \nabla\left[K_g\left(\nabla h_g - \nabla z \beta_f \Delta T\right)\right] + W \quad [21]$$

where:

$S_g = \rho * g * S$
S: specific storage coefficient [1/Pa = kg^{-1} s^2 m]
S_g: specific storage coefficient in groundwater hydraulics [1/m]
β_f: linear expansion coefficient of the fluid [1/K]
K_g: $k * \rho * g / \mu$, hydraulic permeability [m/s]
h_g: hydraulic head [m]
ΔT: temperature difference with respect to the undisturbed condition [K]
W: fluid source term [1/s]

Definition of hydraulic head: $$h_g = \frac{P}{\rho g} + z \quad [22]$$

Transport of Heat

Transport of heat in a water-saturated and porous underground is described by Equation 23. It is considered that the temperature of the fluid is the same as that of the surrounding rock. The left side of Equation 23 becomes zero in the following examples for steady state (intransient) heat transport calculations.

$$\overline{\rho c} \frac{\partial T}{\partial t} = -\rho_f c_f \Phi \underline{v}_f \nabla T + \nabla(\overline{\lambda} \nabla T) + \overline{f} \quad [23]$$

where:

Φ: porosity [%]
v_f: water filter velocity [m/s]
$\rho_{f,s}$: density of fluid/solid phase [kg/m^3]

f: heat source [J/s m^3]

$$\overline{\rho c} = (1-\Phi)\rho_s c_s + \Phi \rho_f c_f$$

whereas: $c_{f,s}$: specific heat capacity of fluid/solid phase [J/kg K]

$$\overline{\lambda} = \lambda_s^{1-\Phi} \cdot \lambda_f^{\Phi}$$

whereas: $\lambda_{f,s}$: thermal conductivity of fluid/solid phase [W/K m]

Transport of Tritium [^{3}H]

Transport of the radiogenic isotope ^{3}H (Tritium) in a porous medium can be described by Equation 24. The time dependent Tritium concentration depends mainly on transport by water flow, molecule diffusion, mechanical dispersion, radioactive decay and eventual sources. Tritium exhibits a conservative behaviour and no considerable reaction other than radioactive decay (Freeze and Cherry 1979, Matthess 1990). Tritium is usually measured in "Tritium units" (TU), where 1TU is defined as 1 atom of ^{3}H per 10^{18} atoms of ^{1}H, or 3.19 picocuries [pCi] or 118 milliBecquerel [mBq] per litre of water (IAEA 1981).

$$\frac{\partial H}{\partial t} = -\underline{v}_f \nabla H + \nabla\left(D^* \nabla H\right) + \nabla\left(a_{ijkl} \frac{v_k - v_l}{\sqrt{v_k^2 - v_l^2}} \nabla H\right) - Z \cdot H + \overline{f} \qquad [24]$$

where:

H: tritium concentration, [TU]
$\underline{v}_f$: particle velocity [m/s]
D^*: coefficient of diffusion [m^2/s]
a_{ijkl}: components of dispersivity [m]
v_k, v_l: components of particle velocity [m/s]
Z: radioactive decay constant [1/s]
f: tritium source

FE (Finite-Element) and FD (Finite-Difference) numerical procedures build the base for solving the previously described transport equations. Two computer codes were used: The FE package FRACTure (Kohl 1992, Kohl and Hopkirk 1995) and the FD package SHEMAT (Clauser 1988, Clauser and Villinger 1990). Both codes serve for the simulation of coupled heat / groundwater transport as described by Equations 21 and 23. Furthermore, the tritium transport equation (Equation 24) can be solved with FRACTure.

The computer code SHEMAT was installed on a VAX8600 and CPU time reached values of 1 minute (2D, stationary simulations). FRACTure was installed on a HP-7000 UNIX workstation and CPU time reached values up to 6 hours for the 2D, transient simulations. The generation of the largest grid (ca. 7500 elements) required a CPU time of one hour.

Bursa example: "closed circuit" deep circulation pattern

Introduction

Two dimensional analyses of the qualitative hydrogeological circulation model of thermal springs in Bursa were performed by FD calculations. The 2D grid consisted of 2160 rectangular elements. Finer discretisation was set for simulation of fracture zones and/or simulation of karstic features. The hydrogeological investigations of Imbach (1992 and this volume) led to the following quantitative models (two simulation cases can be differentiated): First, model A, with uniform geology (country rock) within a mountaneous region, shows the general picture of groundwater circulation and heat transport. Second, model B, with karstic features and fracture zones, leads to a kind of "closed circuit" of infiltration area and spring area and to rapid groundwater circulation with the occurrence of thermal springs at the surface. The karstified and fractured zones were simulated by homogenous, permeable media with higher permeabilities than the surrounding country rock. No further geological differentiation could be made. The boundary values and model parameters were set according to Appendix 3.

Model A, Figure 14

The character of groundwater circulation in mountaneous regions is clearly shown. The figure shows a 2D vertical section in a north-south direction from the plain of Bursa to the mountain of Uludağ. At the mountain / plain boundary (region of Bursa city and Çekirge) groundwater rises and appears at the surface as springs. Mainly conductive heat transport can be observed. Main Peclet numbers according to Equation 6 result in approximately 0.6 with L = 4km (vertical circulation distance). Heat flow in shallow depths below the plain of Bursa becomes 70mW/m^2. This value has to be compared with the measured values (55 to 60mW/m^2) corrected for paleoclimatic effects. Just below the spring area, heat flow is strongly disturbed by convective/advective transport processes up to depths of 1km. Permeability is mainly responsible for increasing the influence of convective/advective heat transport. Further simulations with higher permeabilities revealed that convective/advective heat transport has a strong influence starting at values higher than 10^{-16}m^2.

Model B, Figure 15

The picture shows the same profile as Figure 14. Geological and hydrogeological investigations by Imbach (1992 and this volume) indicated a close connection between the thermal waters in Bursa and Çekirge and the infiltration conditions at Uludağ. Direct and fast circulation of the groundwater was even postulated. Large karstic features in the infiltration region and permeable fracture zones caused by strong tectonic activity are thought to build the main flow paths. This conceptual and qualitative model was simulated by high permeable zones situated within a low permeable background (country rock). Figure 15 shows the result of the numerical calculation. Groundwater circulates faster in more highly permeable zones. This fast circulation is able to transport hot water from a certain depth to the surface and to form thermal springs at the surface with outflow temperatures of up to 60°C. Rapid infiltration lowers the temperatures in the underground of the mountain. Residence time can be estimated in the order of 10^2 to 10^4 years. Normal heat flow of 60mW/m^2 at a depth of 5km b.s.l. is the necessary boundary condition.

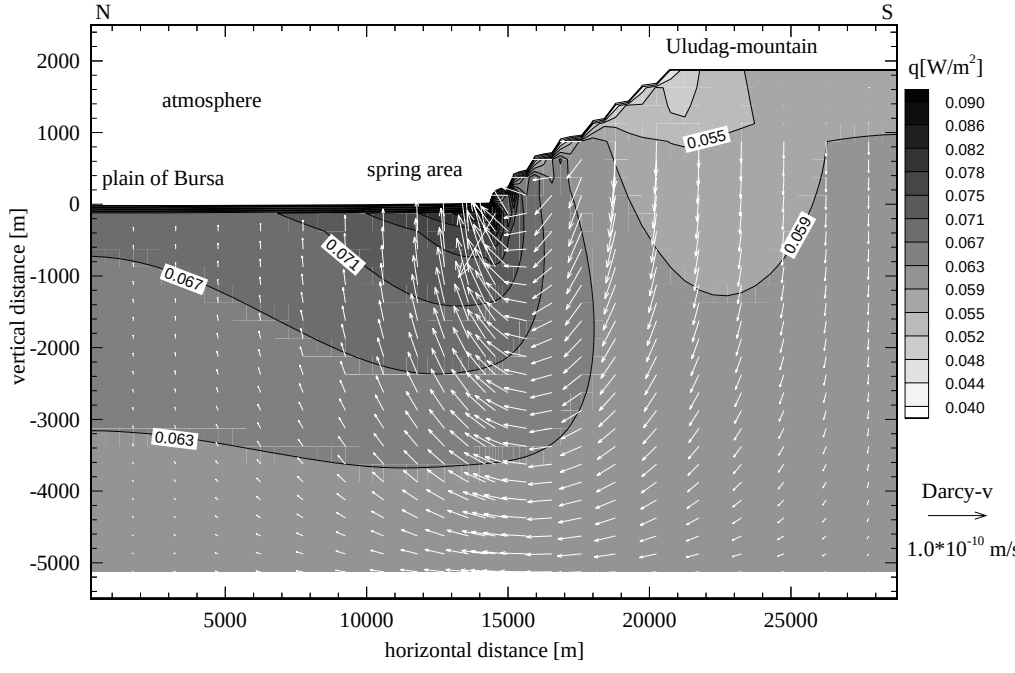


Figure 14: 2D thermohydraulic modelling of the Uludağ region (Bursa), model A (temperature and flow fields). With low permeabilities (this model $10^{-17}m^2$) the heat flow distribution in the underground is dominated by conductive heat transport. The possible spring area is characterised by the upflow zone at the mountain / plain boundary.

This "closed circuit" deep circulation system is able to move heat from greater depths to the surface. Imbach (1992) and Greber et al. (this volume) detected and describe a direct response of the thermal springs at the onset of high precipitation within a time lapse of several hours to days. Residence times of the thermal waters were estimated to be more than 40 years. Therefore, the explanation is a pressure pulse, which can only exist by direct hydraulic connection between the infiltration area and the spring area.

Gemlik example: Thermal karstic water with water components younger than 40 years

Introduction

The thermal waters of Gemlik-Orhangazi were hydrogeologically investigated by Eisenlohr (1995 and Eisenlohr et al. this volume). This work shows circulation models of karstic groundwater in detail with extended flow pathways and the occurrence of cold, subthermal and thermal springs. The question arises concerning the thermal boundary condition of these springs. Tritium contents indicate water components which are younger than 40 years, and high flow velocities are expected.

Numerical simulation of the groundwater and heat transport was performed to simulate quantitatively these qualitative circulation models. Two-dimensional geological profiles along the flow path (Eisenlohr et al. this volume, Figure 2) were translated into 2D FE grids. Figure 16 shows the numerical grid for the modelling of the thermal spa of Gemlik kaplıca. The finer dis-

cretisation of the active karstic formations is clearly visible. At these positions, 1D linear elements, not distinguishable in Figure 16, were introduced for the simulation of such active karstic channels and, also, fracture zones. The presented model consisted of approximately 7500 elements.

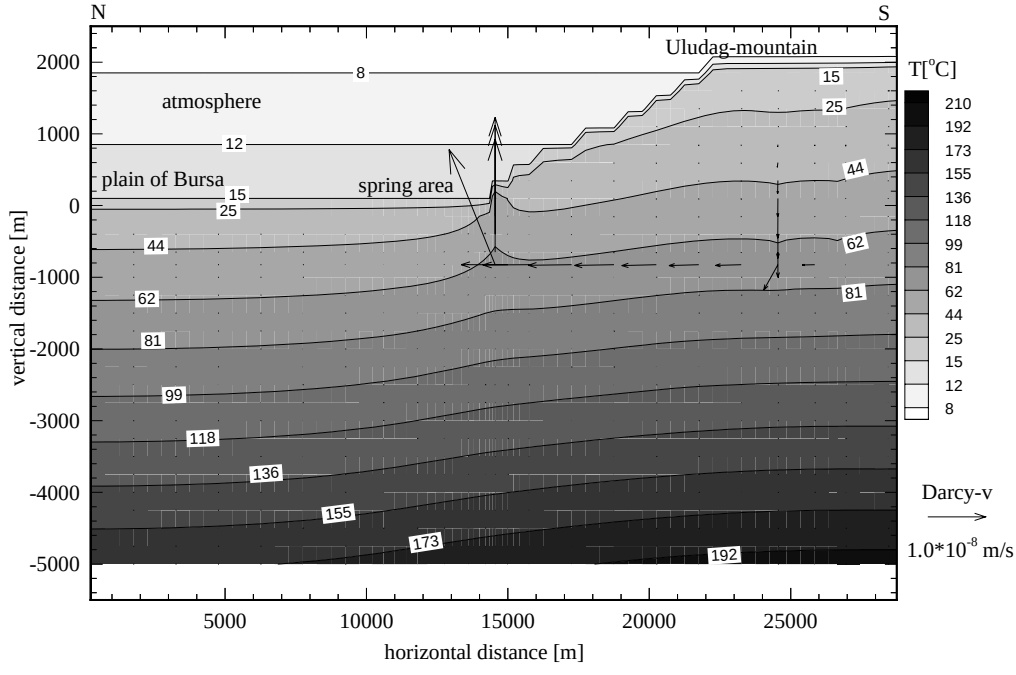


Figure 15: 2D thermohydraulic modelling of the Uludağ region (Bursa), model B (temperature and flow fields). The circulation system characterised by "channels" (karstic features, tectonic faults) with high permeabilities (this model $10^{-15}m^2$, country rock: $10^{-17}m^2$) permits a faster water circulation. Hot water is able to rise with higher velocities and forms thermal springs at the mountain / plain boundary.

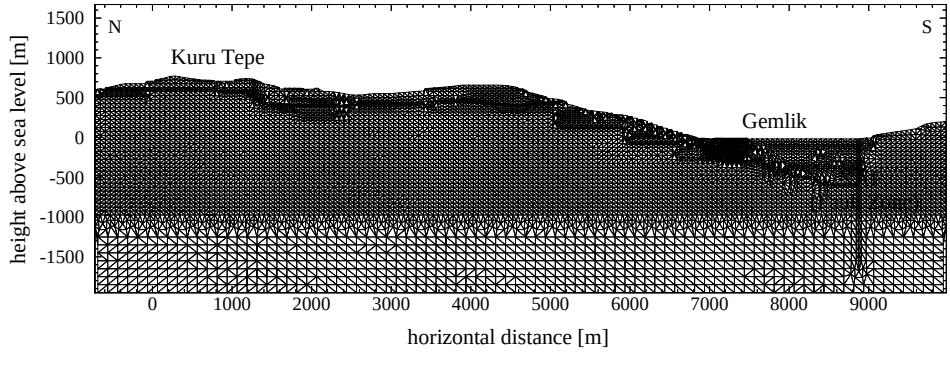


Figure 16: 2D discretisation for the simulation of transport processes for Gemlik kaplıca area. Note the finer grid of the karst lithology and the fracture zone (for comparison see also Eisenlohr et al. this volume, Figure 2).

The simulation of stationary heat transport and transient tritium transport were coupled with stationary groundwater transport by numerical FE calculations. Appendix 4 lists all necessary input parameters. The thermal boundary value was set to 55mW/m^2 at the bottom of the model and the ground temperature gradient was set to -4°C/km. Mean ground temperature at 0m a.s.l. was set to 15°C. Two different infiltration rates were selected: 15% of precipitation (142mm/year) over karstic terrain and 1.5% of precipitation over normal terrain (country rock). High infiltration rates are only possible over karstified terrain, whereas high infiltration rates over country rock would lead to anomalous cooling of the underground. Tritium input by precipitation was defined according to the published values of Freeze and Cherry (1979) and IAEA (1981, 1983, 1990), Figure 17.

Discussion of model parameters and results

Sensitivity analyses of hydraulic conductivity (Pfister 1995) led to this set of parameters (Appendix 4), which is able to describe all different cold, subthermal as well as thermal springs of this area reasonably. Figure 18 is based on the results also listed in Table 1 of Eisenlohr et al. (this volume) and compares measured and modelled temperatures as well as tritium concentrations of these springs. Most solutions appear near the 1:1 dashed line which indicates perfect agreement between measured and modelled values. Only two tritium measurements could not be sufficiently explained with the parameter set of Appendix 4. However, slight changes in the hydraulic conductivity of the karstic channels by less than a factor of five would allow these two values to fit also. The great advantage of such a model procedure was that different circulation models individually selected for each spring and simulated with individual FE grids, but with identical model parameters, led to a consistent overall picture.

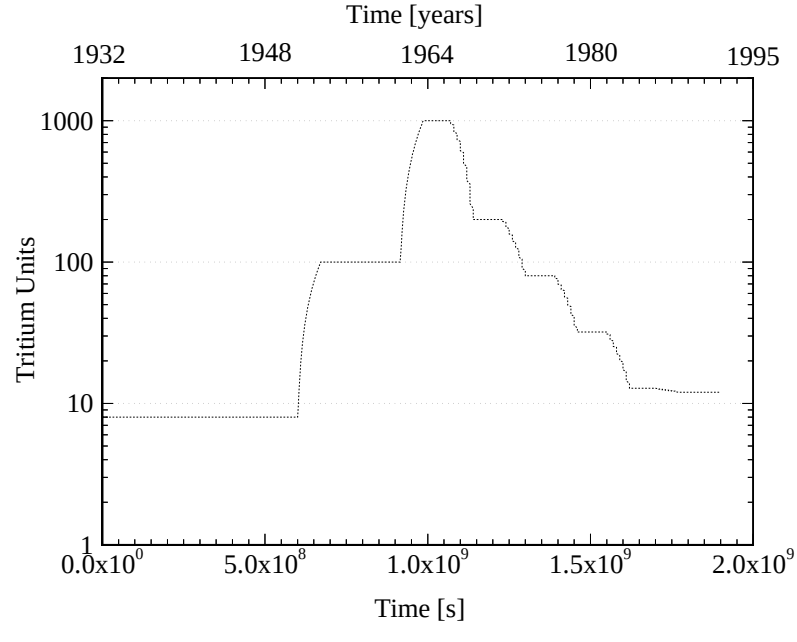


Figure 17: Tritium concentration in precipitation for the Marmara sea region over the last 60 years (after Freeze and Cherry (1979) and IAEA (1981, 1983 and 1990). The bottom axis shows the modeling time range of the FE calculations in seconds.

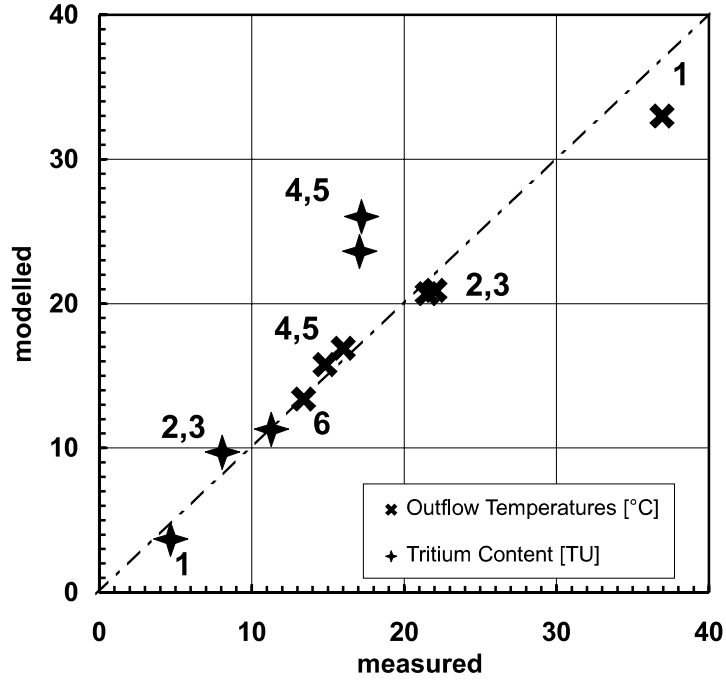


Figure 18: *Modelled and measured tritium contents and temperatures of different karstic springs in the Gemlik-Orhangazi region. Numbers refer to the following sites: 1 Gemlik kaplıca, 2 Gemlik İlıpınar, 3 Orhangazi İlıpınar, 4 Çihatlı, 5 Gedelek, 6 Nadir pınar. The model runs have been performed with the identical parameter set but with individual grids for each flow path model of the different springs.*

Water velocities within the karstic channels on the order of 10^{-4}m/s (Figure 19) lead to minimum mean residence times in the range of 200 days to 18 months (mean flow distances between 2 and 5km). This estimation seems reasonable, but residence times in the range of hours to several days are typical for most karstic terrains all over the world and should be taken into consideration as well. The limit between laminar and turbulent flow is described by the non-dimensional Reynolds number Re for fracture flow, Equation 25 (see also Kohl, 1992). Turbulent flow can be assumed when Re is greater than 2300.

$$\mathrm{Re} = \frac{2 a_h v_f \rho_f}{\mu} \qquad [25]$$

where:

a_h: hydraulic fracture width, 0.1m or 0.02m
v_f: particle velocity, 10^{-4}m/s
ρ_f: fluid density, 1000kg/m^3
μ: viscosity, $7*10^{-4}$Pa s at 30°C

The values listed above yield Reynolds numbers in the range of 6 to 30. The utilisation of a laminar flow law within the 1D linear elements to simulate karstic channels can be taken as correct. Particle velocities of almost two orders of magnitude higher would cause serious numerical problems. Then, turbulent flow laws would have to be taken into consideration.

Figure 19 shows the calculated temperature distribution in the underground of the 2D profile Gemlik kaplıca and Gemlik İlıpınar. At the fault zone (NAF), hot water is able to rise quickly and builds thermal springs at the surface. Within the karstic lithologies and the fault zone wa-

ter velocities of up to 10^{-4}m/s result. The slower water velocities within the country rock are not distinguishable in this figure. The temperature field is generally strongly influenced by the topography and the high infiltration rate caused by the karstic lithologies which touch the surface. Basal heat flow of 55mW/m^2 is the sufficient thermal boundary condition at a depth of 2km. Further observations are discussed in Eisenlohr et al. (this volume), e.g. calculated tritium distribution in the underground in 1992 in the surroundings of the Gemlik kaplıca and Gemlik İlıpınar springs as well as modelled time dependence of the tritium concentration in different spring waters.

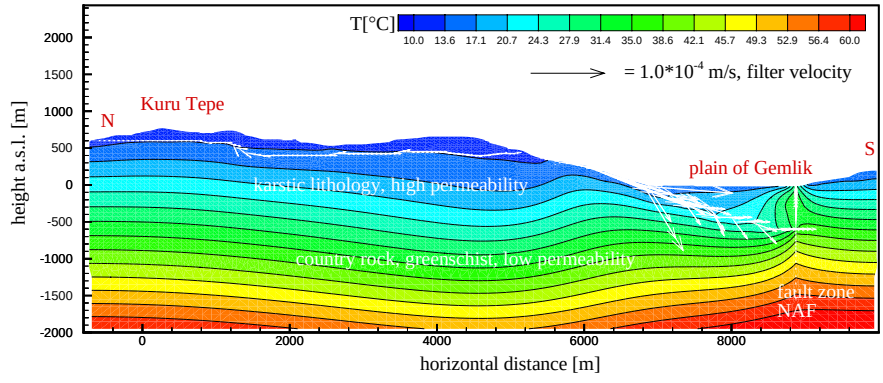


Figure 19: 2D FE modelling results of the Gemlik İlıpınar and Gemlik kaplıca springs (temperature and flow fields). Temperature distribution in the underground is influenced by topography as well as by the infiltration of cold karstic water. Thermal water rises in the fracture zone (NAF) to the surface.

Discussion and conclusions

The compilation of geothermal data of the Marmara sea region leads to the following conclusive reflections:

The described temperature measurements in shallow drillholes do not yield an ideal base for heat flow calculations. The strong influence of water movement on the temperature profile due to advective and convective heat transport needs to be carefully considered in order to extract the undisturbed heat flow density signal from the data. The determination of terrestrial heat flow density by data from shallow depth ranges requires therefore detailed considerations of the physical thermal transport model. In following this procedure, no contradiction was found between the shallow and deep heat flow data. In the northern part of the investigation area, these shallow values were confirmed by data from oil wells within depths of up to 2500m (Figure 10).

The surface heat flow distribution of the Marmara sea region shows values ranging from 35 to 115mW/m^2, with a mean value of 60mW/m^2. Two different areas can be distinguished on Figure 10: the part south of Marmara sea with 75 to 95mW/m^2 and the other areas in the eastern and northern part of the investigation area with up to 55mW/m^2. Applying paleoclimatic corrections to this data set, according to Figure 13, two different heat flow regimes can be attributed to these areas with different tectonic characteristics: Increased values (80-110mW/m^2) in the area south of the Marmara sea correspond to the general extensional tectonic regime of this region (Straub and Kahle, Schindler, Barka, all this volume). Normal heat flow values (60-72mW/m^2) occur in the northern and eastern part of the investigation area (Bursa, İznik, İzmit and Thrace region), where stable or compressional components appear in the tectonic regime (Straub and Kahle this volume; Crampin and Evans 1986).

On the other hand, the distribution of thermal springs according to their energy output can not be related to the terrestrial heat flow density field in the area of investigation (Figures 1 and 10). The occurrence of the springs is much more bound to active tectonic fault lines. Large thermal springs occur more frequently where translational and extensional tectonics appear together, within a so-called transtensional tectonical regime.

The conceptual models of the hydrogeological investigations of the MARMARA Poly-Project provided the basic input for the numerical calculations of coupled heat / groundwater and tritium transport. Generally, these conceptual models were confirmed. The combination of two independent parameters, such as tritium and temperature, within a quantitative model yielded a significant consolidation of the flowpath models. Tritium transport is mainly influenced by near surface processes, whereas heat transport is dominated by deeper heat sources. The thermal springs of Bursa and Gemlik-Orhangazi are related to zones with higher permeability where groundwater is able to circulate rapidly. Heat supply is provided by normal heat flow values of around 60mW/m^2 at depths of 2000m to 5000m. At Gemlik-Orhangazi, precipitation water infiltrates and circulates rapidly (< 40 years) over distances up to 10km through active karstic formations to maximum depths of 600m below sea level, where mixture with stagnant hot karstic water occurs and a fast common rise of this thermal water is bound to active steep faults. The tritium content of the springs shows the anthropogenic influence of the last 40 years. At Bursa, deep circulation of precipitation water at depths of 1000m to 2000m below sea level and the fast rise of this thermal water in tectonic fault zones causes the huge thermal springs of Çekirge and Kükürtlü thermal areas. The local shallow heat flow field is strongly influenced by the circulation of thermal waters.

These observations were generally confirmed by simple 1D model calculations to simulate temperature depth profiles of selected thermal wells (Figure 8) in shallow depth ranges. The lower boundary values (conductive heat flow density q_∞) of the 1D model approaches fit well with the overall distribution of values determined by the other shallow measurements (Figure 10). Finally, the basal thermal boundary of all different model approaches (in different dimensions) confirmed the interpolated heat flow field determined by measurements in shallow drillholes.

Northwestern Anatolia is characterised by normal to locally elevated terrestrial heat flow density compared to a normal value defined by the world wide continental mean value of 65mW/m^2 (Pollack et al. 1993). The abundance and distribution of hot springs, especially the very large ones, and geothermal fields in this region can only be explained by local zones of strongly elevated vertical hydraulic permeability due to active transtensional faulting of the crust. The importance, within this context, of the combination of strike slip and normal faults (transtensional regime) will be further clarified and confirmed by the ongoing interdisciplinary approach within this volume.

Acknowledgements

We would like to thank the General Directorate, as well as the local offices, of the state organisations DSİ (State Hydraulic Works) and of Köy Hizmetleri (Rural Services) in different cities of Northwestern Anatolia for their kind collaboration. For three years they allowed us free access to convenient drillholes for our purposes. We also thank the General Directorate of MTA (Mineral Research and Exploration). Thanks are also to all our partners working with us on the MARMARA Poly-Project. We are especially grateful to Prof. R. Hütter, ETH Vice-President for Research, for his continuing help and support in many aspects of this Poly-Project. Fruitful discussions with Ch. Clauser (Hannover, Germany) and Th. Kohl (Zürich, Switzerland) were helpful for various scientific aspects of our work.

References

Ambraseys, N.N. and Finkel, C.F., 1991, Long-term seismicity of İstanbul and of the Marmara sea region, Terra Nova, 3, 527-539.

Barka, A.A., this volume, Neotectonics of the Marmara sea region.

Birch, F., 1948, The effects of Pleistocene climatic variations upon geothermal gradients, American Journal of Science, December 1948, 729-760.

Blackwell, J., 1954, A transient flow method for determination of thermal constants of insulating materials in bulk, Journal of Applied Physics, 25, 137-144.

Bodmer, Ph. and Rybach, L., 1984, Geothermal map of Switzerland, Kümmerly & Frey, Geographischer Verlag, Bern.

Bredehoeft, J.D. and Papadopulos, I.S., 1965, Rates of vertical groundwater movement estimated from Earth's thermal profile, Water Resources Research, Vol.1, No.2, 325-328.

Carslaw, H.S. and Jaeger, J.C., 1959, Conduction of heat in solids, 2nd ed., Clarendon Press, Oxford, 510p.

Cita, M.B. and Ryan, W.B.F., 1978, The deep-sea record of the Eastern Mediterranean in the last 150,000 years, in: Thera and the Aegean world, edited by: C. Doumas, 45-60.

Clauser, C., 1988, Untersuchungen zur Trennung der konduktiven Anteile im Wärmetransport in einem Sedimentbecken am Beispiel des Oberrheingrabens, Fortschrittberichte VDI, Reihe 19, Wärmetechnik/ Kältetechnik, Nr. 28, VDI-Verlag Düsseldorf, 124p.

Clauser, C. and Villinger, H., 1990, Analysis of conductive and convective heat transfer in a sedimentary basin, demonstrated for the Rheingraben, Geophys. J. Int. 100, 393-414.

Crampin, S. and Evans, R., 1986, Neotectonics of the Marmara sea region of Turkey, Journal of the Geological Society, London, Vol. 143, 343-348.

Davis, J.C., 1986, Statistics and data analysis in geology, Kansas Geological Survey, John Wiley and Sons, New York, 646p.

Diment, W.H., and Urban, Th.C.,1983, A simple method for detecting anomalous fluid motions in boreholes from continuous temperature logs, Geothermal Resources Council. Transactions Vol. 7, October 1983, 485-490.

Eisenlohr, Th., 1995, Die Thermalwässer der Armutlu-Halbinsel (NW-Türkei) und deren Beziehung zu Geologie und aktiver Tektonik, Diss. ETHZ, Nr. 11340, 165p.

Eisenlohr, Th., this volume, The thermal springs of the Armutlu Peninsula (NW-Turkey) and their relationship to geology and tectonic.

Eisenlohr, Th., Pfister, M. and Balderer, W., this volume, Environmental isotope study and 2D-Modelling of cold and thermal karst within the Gemlik (Bursa) area of Northwestern Turkey.

Erbas, A.K., 1985, Bestimmung der Wärmeleitfähigkeit von Festkörpern mit einer Halbraum-Linien-Quellen-Apparatur, Diplomarbeit, Technische Universität Berlin, Institut für angewandte Geophysik, Petrologie und Lagerstättenforschung, 72p.

Farrand, W.R., 1971, Late Quaternary paleoclimates of the Eastern Mediterranean area, in: The late Cenozoic glacial ages, Yale Univ. Press, New-Haven London, 529-564.

Farrand, W.R., 1980, Pluvial climates and frost action during the last glacial cycle in the Eastern Mediterranean – evidence from archaeological sites, in: Quaternary paleoclimate, edited by: W.C. Mahaney, GEO abstracts, Norwich, England, 393-410.

Freeze, R.A. and Cherry, J.A., 1979, Groundwater, Prentice Hall, Englewood Cliffs, New Jersey 07632, U.S.A., 604p.

Greber, E., Imbach, Th., Pfister, M. and Sellami, S., this volume, Hydraulic level variations in a thermal water well: Impact of precipitation on the Çekirge thermal water system.

Gretener, P.E., 1967, On the thermal instability of large diameter wells – an observational report, Geophysics, Vol. XXXII, No. 4, 727-738.

Grove, J.M and Conterio, A., 1994, Climate in the Eastern and central Mediterranean, 1675 to 1715, in: Climate trends and anomalies in Europe 1675-1715, edited by: B. Frenzel and G. Fischer, Verlag, Stuttgart, 275-285.

IAEA, 1981, Statistical treatment of environmental isotope data in precipitation, Technical reports series no. 206, International Atomic Energy Agency, Vienna, Austria.

IAEA, 1983, Environmental isotope data no. 7, world survey of isotope concentration in precipitation (1976-1979), Technical reports series no. 226, International Atomic Energy Agency, Vienna, Austria.

IAEA, 1990, Environmental isotope data no. 9, world survey of isotope concentration in precipitation (1984-1987), Technical reports series no. 311, International Atomic Energy Agency, Vienna, Austria.

IHFC, 1996, International heat flow commission, Fourth international workshop on heat flow and the structure of the lithosphere, June 9-15, Trest-Castle, Trest, Czech Republic.

İlkışık, O.M., 1995, Regional heat flow in Western Anatolia using silica temperature estimates from thermal springs, Tectonophysics, 244, 175-184.

Imbach, Th., 1992, Thermalwässer von Bursa. Geologische und hydrogeologische Untersuchungen am Berg Uludağ (NW-Türkei), Diss. ETHZ, Nr. 9988, 178p.

Imbach, Th., this volume, Geology of Mount Uludağ with emphasis on the genesis of the Bursa thermal waters, Northwest Anatolia, Turkey.

Kohl, T., 1992, Modellsimulation gekoppelter Vorgänge beim Wärmeentzug aus heissem Tiefengestein, Diss. ETH Zürich, Nr. 9802, 149p.

Kohl, T. and Hopkirk, R.J., 1995, The finite element program 'FRACTure' for the simulation of hot dry rock reservoir behaviour, Geothermics, 24, 345-359.

Mansure, A.J. and Reiter, M., 1979, A vertical groundwater movement correction for heat flow, Journal of Geophysical Research, Vol. 84, No. b7, 3490-3496.

Matthess, G., 1990, Die Beschaffenheit des Grundwassers, Lehrbuch der Hydrogeologie, Gebrüder Borntraeger, Berlin – Stuttgart, 498p.

Mueller, St, Kahle, H.G. and Barka, A., 1997, Plate tectonic situation in the Anatolian-Aegean region, this volume.

Pfister, M., 1995, Geothermische Untersuchungen in der Region MARMARA; Kartierung des Wärmeflusses und hydrothermale Modellrechnungen, Diss. ETHZ, Nr. 11054, 231p.

Pfister, M. and Rybach, L., 1995, High-resolution digital temperature logging in areas with significant convective heat transfer, Geothermics, 24, 1, 95-100.

Pfister, M. and Rybach, L., 1996, High-resolution temperature logging in shallow drillholes for the determination of terrestrial heat flow: field examples and analysis, Tectonophysics, 257, 93-99.

Pollack, H.N., Hurter, S.J. and Johnson, J.R., 1993, Heat Loss from the Earth's Interior: Analysis of the Global Data Set, Reviews of Geophysics, Vol. 31, 3, 267-280.

Pribnow, D., 1994, Ein Vergleich von Bestimmungsmethoden der Wärmeleitfähigkeit unter der Berücksichtigung von Gesteinsgefügen und Anisotropie, VDI Verlag, Reihe 19, Wärmetechnik / Kältetechnik, Nr. 75, Düsseldorf, 111p.

Ramey, H.J., 1962, Wellbore heat transmission, Journal of Petroleum Technology, April 1962, 427-435.

Roberts, N. and Wright, H.E., 1993, Vegetational, lake-level, and climatic history of the near east and southwest Asia, in: Global climates since the last glacial maximum, edited by: H.E. Wright, Jr. et al., University of Minnesota Press, 194-220.

Schindler, C., this volume, Geology of NW-Turkey: Results of the MARMARA Poly-Project.

Schön, J., 1983, Petrophysik, Akademie Verlag, Berlin, Deutschland, 405p.

Şimşek, Ş., this volume, Geothermal potential in Northwestern Turkey.

Skagius, K. and Neretnieks, I., 1982, Diffusion in crystalline rocks of some sorbing and nonsorbing species, SKBF KBS Teknisk Rapport 82-12, Royal Institute of Technology Department of Chemical Engineering, Stockholm, Sweden, 1982-03-01, 44p.

Straub, Ch. and Kahle, H.-G., this volume, Recent crustal deformation and strain accumulation in the Marmara sea region, N.W. Anatolia, inferred from repeated GPS measurements.

Tezcan, A.K. and Turgay, M.I., 1991, Geothermal atlas of Europe, catalogue of heat flow density data: Turkey, in: Geothermal Atlas of Europe, edited by: E. Hurtig, V. Cermák, R. Haenel and V. Zui, 84-85.

Tezcan, A.K., 1995, Geothermal Explorations and Heat Flow in Turkey, in: Terrestrial Heat Flow and Geothermal Energy in Asia, edited by: L. Mohan Gupta and Makoto Yamano, A.A.Balkema/ Rotterdam, 23-42.

Appendices

East. Long.	North. Lat.	Name	Gradient	Stratigraphy	Thermal Conductivity	Heat Flow
26.9806	41.2252	Karapürcek 1	2.05+/-0.06	Oligocene	2.3+/-0.3	47+/-8
27.8759	41.1005	Corlu 1	2.71+/-0.13	Oligocene	2.3+/-0.3	62+/-12
26.7108	41.0214	Maltepe 1	2.01+/-0.17	Eocene	3.1+/-0.2	62+/-10
27.2328	41.1197	Kandamis 1	1.42+/-0.02	Oligocene	2.3+/-0.3	33+/-5
27.6633	41.265	Vakiflar 1	2.46+/-0.04	Oligocene	2.3+/-0.3	57+/-8
28.2859	40.6835	Marmara 1	2.6+/-0.9 (BHT)	?	?	?
28.1851	41.0524	Kmarmara 1	3.2+/-1.0 (BHT)	?	?	?
26.8099	39.5107	Edremit 1	3.2+/-1.1 (BHT)	?	?	?
26.1919	40.5266	Saros 1	8.2+/-? (BHT)	?	?	?

Appendix 1: Temperature gradients (°C/100m, with standard deviations), stratigraphy, respective thermal conductivities (W/m,K, with standard deviations) and calculated heat flow values (mW/m^2, with standard deviations) of oil wells in Thrace region (northwestern Marmara).

No.	East [°]	North [°]	Name	Meth.	Int. [m]	Depth [m]	λ±σ [W/K m]	q±σ [mW/m^2]	Paleo [mW/m^2]	[%]
2	28.8765	40.1982	Kite	R	80	140	2.0±0.5	52±15	60	15
3	29.4382	40.1059	İnegöl	F	120	130	2.0±0.5	89±22	97	9
5	28.9618	40.2522	Linyıtleri	F	76	96	3.5±0.6	88±15	102	16
7	29.1588	40.2579	Kazıklı	G	46	96	2.0±0.5	60±19	68	13
11	29.0632	40.2703	Demirtaş	F	70	80	2.0±0.5	26±7	34	30
12	29.0800	41.0300	İst. Cam.	G	80	100	3.0±0.2	37±6	49	32
13	27.9060	39.6239	Çaiyrhısar	F	120	140	2.0±0.5	80±20	88	10
15	27.9700	39.6700	Köseler	G	110	130	2.0±0.5	64±18	72	13
18	27.6559	40.1802	Gönen	G	72	112	2.0±0.5	130±33	138	6
21	27.5926	40.0541	Gön. Balçı	F	30	40	2.0±0.5	48±12	56	16
22	27.9441	40.3029	Bandırma	F	40	50	2.0±0.5	51±13	59	16
25	27.1588	40.2455	Biga	G	30	40	2.0±0.5	54±17	62	15
101	28.4706	40.0495	Mustafak.	B	28	84	3.5±0.6	113±19	127	12
104	29.1118	40.3986	Ask. Vet.	G	21	85	2.0±0.5	17±10	25	47
106	29.9294	40.2860	Çumalı	G	15	25	2.9±0.2	65±8	77	19
107	29.6941	40.3604	Mecidiye	G	30	70	3.0±0.2	30±5	42	40
108	29.2020	39.7030	Okçular	B	30	70	1.6±0.2	20±3	26	32
109	29.3353	40.4234	Akharım	G	20	76	2.0±0.5	26±7	34	31
110	29.4471	40.2027	Soğuksu	B	22	72	2.6±0.3	56±6	66	19
118	27.4448	39.4910	İv. Kayapa	B	62	102	3.2±0.2	96±6	109	13
119	27.8309	40.2613	Çarık	F	80	90	2.3±0.2	102±9	111	9
120	28.2971	39.4820	Turfullar	G	110	120	1.7±0.2	75±9	82	9
131	28.8460	41.2160	Kisirm.	B	56	96	1.8±0.2	47±15	54	15
136	27.9383	41.2590	Veliköy	B	12	68	1.9±0.2	33±4	41	23
140	27.9324	39.6802	Anad. Lis.	B	74	84	2.0±0.5	70±18	78	11
142	27.9015	39.4730	Selimiye	G	86	96	1.7±0.2	166±20	173	4
150	26.3350	40.3190	Yolagzi	F	90	100	2.0±0.5	73±23	81	11
201	27.4844	39.1977	Sarıcalar	G	50	150	1.9±0.2	55±10	63	14
203	28.8235	40.5205	Armutlu	B	70	80	2.5±0.5	67±14	77	15
206	30.2664	40.9099	Kaymaz	B	10	45	3.1±0.2	55±4	67	23
207	28.0698	39.7703	Kürse	G	58	68	1.5±0.2	45±10	51	13
208	28.5000	39.6081	Çamköy	F	45	75	3.3±0.2	39±3	52	34
209	27.9441	39.5135	İnkaya	G	48	78	1.9±0.2	95±15	103	8
210	27.4882	40.5495	Ekinlik Ada	G	30	50	2.7±0.2	84±15	95	13
211	27.2063	39.0946	Bergama	B	30	100	2.0±0.5	45±12	53	18
212	30.0500	40.4750	Pamukova	G	20	60	2.0±0.5	20±16	28	40
213	30.4375	40.9369	Fındıklı	G	60	100	3.1±0.2	66±16	78	19
214	29.4048	40.9414	Akfırat	B	63	78	3.1±0.2	56±4	68	22
215	28.6988	41.2000	Taşoluk	F	130	150	2.3±0.2	60±6	69	15
216	28.5151	41.0360	Türkobasi	B	110	145	1.9±0.2	50±5	58	15
217	27.0521	41.0428	Yörgüç	G	45	75	2.0±0.5	48±15	56	17
218	27.5452	41.1104	Kepenekli	B	35	165	1.9±0.2	43±5	51	18
219	26.8692	39.2500	Beşiktepe	G	15	115	1.8±0.3	75±15	82	10
220	30.7460	40.589	Samanpaz.	G	20	40	1.6±0.2	72±14	78	9

Appendix 2: Characteristics of 44 wells: number (No.) and coordinates of well location (East and North); location name (Name); method of heat flow calculation: F = model a (FLOW), B = model b (BETA), R = model c (RAM), G = linear gradient model (Equation 4); observation interval length in depth scale (Int), depth of heat flow determination (Depth), thermal conductivity value (λ) and heat flow value q (both with standard error), paleoclimate corrected heat flow value (Paleo) and percentage of correction (%).

Parameters	Values
Basal heat flow	60 mW/m^2
No fluid- or heat-flow through left/right side boundaries	
Surface temperature at 0 m a.s.l.	15°C
Surface temperature gradient	-4°C/km
Hydraulic heads	according to topography
Mountaineous water level	1500 m a.s.l.
Permeability (country rock)	10^{-17} m^2
Permeability (fractures and karst)	- (Model A) 10^{-15} m^2 (Model B)
Thermal conductivity	2.8 WK^{-1}m^{-1}
Heat production rate	$1.2*10^{-6}$ W/m^3

Appendix 3: Boundary values and model parameters for numerical simulation of Bursa-Çekirge thermal springs.

Best fit model parameters	country rock (Greenschist, Flysch)	active karst (Marble), 1D a_h = 0.1 m	palaeo-karst (Marble)	fault 1D, a_h = 0.02 m	plain (Neogen, Quaternary)
Groundwater Transport					
Hydraulic conductivity, Kg [m/s]	$5.0*10^{-11}$	$2.0*10^{-6}$	$1.0*10^{-9}$	$2.0*10^{-5}$	$5.0*10^{-8}$
Porosity, Φ [%]	10	10	10	10	10
Heat Transport					
Thermal conductivity, λ [W/K m], measured	2.7	2.9	2.9	2.7	2.0
Linear expansion coefficient [1/K], from Kohl 1992	$1.0*10^{-5}$	$1.0*10^{-5}$	$1.0*10^{-5}$	$1.0*10^{-5}$	$1.0*10^{-5}$
Heat production [W/m^3], measured by F. Medici (1994, pers. comm.)	$1.0*10^{-6}$	$0.3*10^{-6}$	$0.3*10^{-6}$	$1.0*10^{-6}$	$1.0*10^{-6}$
Volumetric heat capacity, fluid $\rho * c_f$ [J/m^3 K], from Schön (1983)	$4.2*10^6$	$4.2*10^6$	$4.2*10^6$	$4.2*10^6$	$4.2*10^6$
Volumetric heat capacity, solid $\rho * c_s$ [J/m^3 K], from Schön (1983)	$2.3*10^6$	$2.3*10^6$	$2.3*10^6$	$2.3*10^6$	$2.3*10^6$
Tritium Transport:					
Diffusivity, D* (water) [m^2/s], from Skagius and Neretnieks (1982)	$2.4*10^{-9}$	$2.4*10^{-9}$	$2.4*10^{-9}$	$2.4*10^{-9}$	$2.4*10^{-9}$
Diffusivity, D* (rock) [m^2/s], from Skagius and Neretnieks (1982)	$1.5*10^{-13}$	$1.5*10^{-13}$	$1.5*10^{-13}$	$1.5*10^{-13}$	$1.5*10^{-13}$
Longitudinal dispersivity, α_l [m]	100	100	100	100	100
Transversal dispersivity, α_t [m]	20	20	20	20	20

Appendix 4: Boundary values and model parameters for numerical simulation of Gemlik-Orhangazi thermal springs.

THEME 6

Synthesis

Synthesis of the MARMARA Poly-Project

MARTIN PFISTER, WERNER BALDERER, EMIL GREBER, HANS-GERT KAHLE, DIETER MAYER-ROSA, STEPHAN MUELLER, LADISLAUS RYBACH, CONRAD SCHINDLER, SOUAD SELLAMI AND CHRISTIAN STRAUB

Introduction

Northwestern Anatolia shows prominent neotectonic activity, including seismicity and crustal deformation. Groundwater circulation in this area manifests itself by large thermal springs. The MARMARA Poly-Project provides a multidisciplinary scientific approach. Thus, the combination of manifold methods and the specific investigation area yielded new results in various topics. This knowledge will be integrated within this synthesis. Based on the actual plate tectonic situation in the Anatolian-Aegean region (Mueller et al. this volume), on general summaries provided by the different disciplines, on regional geological-hydrogeological investigations and on newly established regional connections (Themes 3, 4 and 5 of this volume), this conclusive chapter aims to combine all results within a geodynamic interpretation.

This final Theme 6 consists of three parts: a summary of "key observable quantities", the description of selected geodynamic processes and, finally, a conclusive interpretation.

The definition of so-called "key observable quantities" aims to identify the most important parameters and models which resulted from the numerous works of different authors described within this volume. These observations can be understood as keys to open the door to a geodynamic synthesis and interpretation. On the one hand, we use the conclusive scheme of geology (Schindler this volume) exemplified by the distribution of active faults in Northwestern Anatolia, which itself portrays the bulk of geologic, tectonic, geodetic, gravimetric and paleomagnetic observations. On the other hand, we integrate measured parameters, e.g. the conductive terrestrial heat flow density at the surface or the distribution of seismicity over magnitude, space and time.

The description of integrative physical processes and models follows as a second step. The interaction between the key observable quantities is described by (1) deep groundwater circulation bound to active faults and mainly taking part in an upper level of the Earth's crust and (2) the quasi-continuous extension of the lithosphere, which is dominated by processes within the lower Earth's crust and the upper mantle.

Finally, we present our main conclusions focusing on the North Anatolian Fault Zone (NAFZ) with respect to its northern and southern marginal areas in the Marmara sea region.

Key observable quantities

Geological synthesis, active faults

Barka (this volume) presents an introduction and summary of neotectonics in the Marmara sea region. Based on this detailed work, the geologic interpretation and the conclusions by Schindler (this volume) contribute to an up-to-date definition of active faults within the MAR-

MARA project working area (Fig. 2 in Schindler this volume). Various modern geologic and geodetic studies of our Poly-Project as well as recent paleomagnetic interpretations (e.g. Morris and Tarling 1996), complete the background to this synthetic picture. Due to the location of the MARMARA Poly-Project investigation area, the definition of active faults can be considered as quite accurate in the area close to the Marmara sea, to the North Anatolian Fault Zone (NAFZ) and to the Aegean sea. Less information is available in the area further south around Simav, Gediz and Emet, where we had to rely on published geological maps. Schindler (this volume) lists the main tectonic and geologic events since the Carboniferous (ca. 360m.y. ago) in detail. A reconstruction of the tectonic activity since Middle Miocene times (ca. 15-17m.y. ago) leads to the actual pattern of neotectonic movements in the Marmara sea region starting 3-4m.y. ago in the Pliocene. It contains three main components: a dextral movement controlled by the westward motion of the Anatolian block along the NAFZ, the Aegean extension directed to the S or SSE and an anticlockwise rotation of some 5° around a pole situated 38.7°N and 27.8°E (Schindler this volume). The limits of the rotating block to the south and southeast are still unknown, as well as the relations to the "Marmara block" as defined by Crampin and Evans (1986).

The actual movements take place mainly along reactivated older structures and faults, which can be regarded as the first hint to the predominant influence of older weak zones within the Earth's crust. Schindler shows that the major neotectonic events are bound to older tectonic units; the Earth's crust is breaking along pre-existing weak zones. The distribution of active faults provides a background for all of the following interpretations, e.g. comparison with seismicity and thermal spring abundance (Figures 1, 2 and 3), as well as GPS strain field calculation.

The major current tectonic regimes can roughly be separated and differentiated in the following manner: Large-scale extension is observed almost in the entire area, mainly within the Marmara sea as well as south of it. West of Kuzuluk (30.5°E) regional extension starts to increase (Greber this volume). Compressional and strike-slip tectonics prevail to the southeast of the investigation area at approx. 31°E and 39°N (near Afyon). Also, at the western end of the Marmara sea, near Şarköy at approx. 27.5°E and 40.75°N, huge pushed-up lenses are evidence of compressional forces. Strong dextral strike-slip movements, frequently combined with compressional and extensional forces, occur all along the so-called northern zone of the NAFZ (Straub and Kahle this volume). North of it, the Kocaeli peninsula and Thrace seem to be stable at the present time from a tectonic and geodetic point of view.

Recent seismicity

The basis for the following considerations is the NEIC earthquake data set (CD-ROM by USGS) for the time span starting in 1975, which was assumed to be reasonably complete and homogeneous for the whole area under consideration (Northwestern Turkey). This data set was completed for the time after 1988 (the last year contained on the CD-ROM) with the stronger earthquakes ($m_b > 4.0$) found in the latest NEIC and ISC earthquake catalogues. Figures 1 and 2 represent this data set, where Figure 1 shows the distribution of larger earthquakes ($m_b \geq 4$) and Figure 2 the clustering of smaller events ($m_b \leq 4$). The data set in Figure 2 was considered sufficiently illustrative for this purpose and, therefore, was not completed for earthquakes occurring after 1988.

The different distributions of larger and smaller earthquakes reveal, in both cases, a remarkable clustering of epicentres in space. The clusters are, furthermore, built up during relatively short time periods. It is obvious that most clusters show correlation with the active tectonic features in the area, as far as the mapped faults allow such a conclusion. This is certainly the

question for the southeastern part (south of 40°N and east of 28°E) in both figures, in which the tectonic features have not been investigated in the same way as for the area close to the Marmara and Aegean seas.

The distribution of smaller earthquakes (Fig. 2) leads further to the conclusion that regions with strong extensional tectonics (see Schindler this volume) are predominantly marked with concentrations of microearthquake activity, as in the central and western part of the Marmara sea, the gulf of Saros, the Bursa-Gemlik region and Lesbos. If this finding holds, then the concentrations in the southern part below 40°N should also be associated with extensional tectonics. On the contrary, the zones with predominantly compressional and/or strike-slip tectonics (e.g., NAFZ east of Kuzuluk, Şarköy area, Gönen area) do not show this mentioned seismicity feature. Rather, they have been affected by the strongest earthquakes ($m_b > 7$) in the 20^{th} century (Ambraseys and Finkel 1991, Barka this volume).

The investigation of the depth of earthquake foci does not give any evidence of the tectonic processes. In general, the uncertain depth distribution of hypocentres for this data set does not allow the differentiation of areas with respect to this aspect. This uncertainty is mainly caused by insufficient coverage of recording station in the whole area, even for the time period after 1975. While the errors in the epicentre location can be assumed to be smaller than 5km in general, the depth estimation is, only in the best cases, 5km and, realistically, closer to 10km or worse. It therefore can only be stated with confidence that the majority of seismic activity takes place in the upper part of the Earth's crust, i.e. between 5 and 15km in depth. In addition, a much smaller part of the activity extends to greater depths, up to 30km.

The much more detailed investigation of the seismicity in the Bursa area (Sellami et al. this volume) reveals a somewhat more detailed and reliable picture, but only for a much smaller area, confirming the general finding of a predominantly upper crust activity with minor activity in the lower crust. However, a still significant number of earthquakes are occurring in the epicentre clusters down to the Moho depth (about 30km). Earthquakes at still greater depth are very uncertain regarding their location. They should not be considered for any interpretation of tectonic processes.

Üçer et al. (this volume), presenting current knowledge on earthquake activity in the western NAFZ, also reach the conclusion that the majority of hypocentres is concentrated within the upper 15km of the crust. They also do not differentiate among certain regions with respect to the depth distribution of seismic activity. Zanchi and Angelier (1993), in their compilation of earthquakes for the area, show a distribution of earthquake where the main concentration of hypocenters is found to lie at a depth of between 20 and 30km. This is in certain contrast to the results described above and most probably caused by different localisation algorithms.

It is without doubt that the hitherto existing data are not sufficient to draw any conclusions on the fine structure of the crust and related tectonic features. For this purpose, a much denser station network must be operated for a longer time in the area under investigation. This was clearly outside of the framework of the seismic part of the MARMARA project.

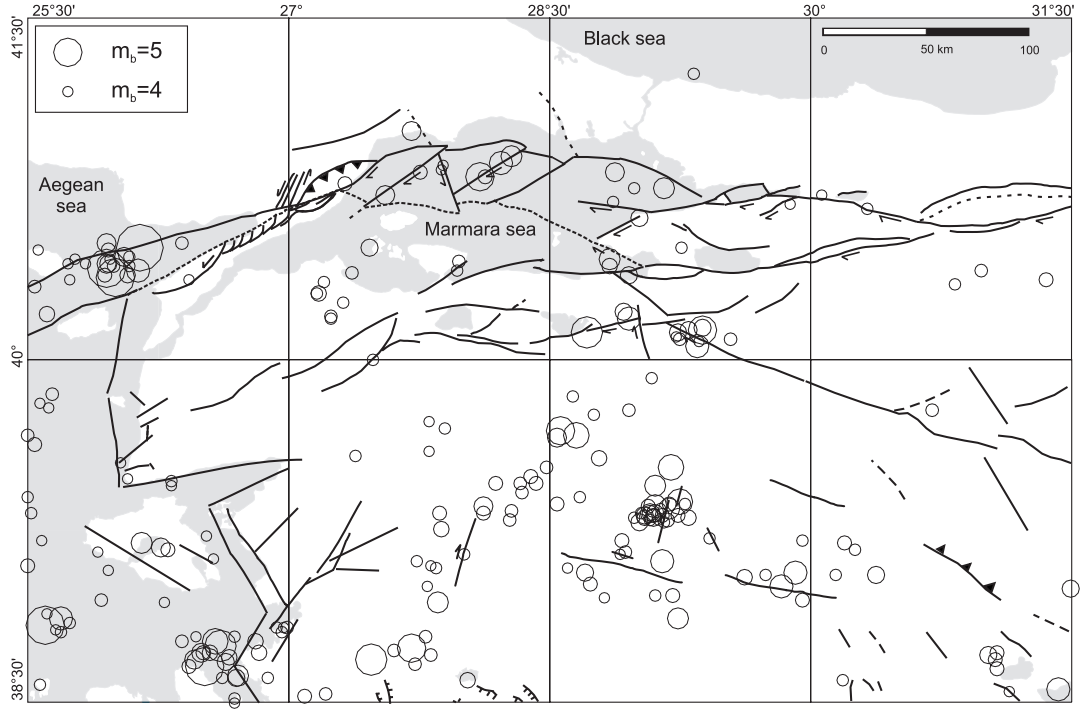


Figure 1: *Active faults according to the results of the geological investigations by different authors of the Marmara project (summarised by Schindler in this volume). Earthquakes (m_b = 4 to 6) for the time period 1975 – 1995 have been compiled from NEIC and ISC catalogues.*

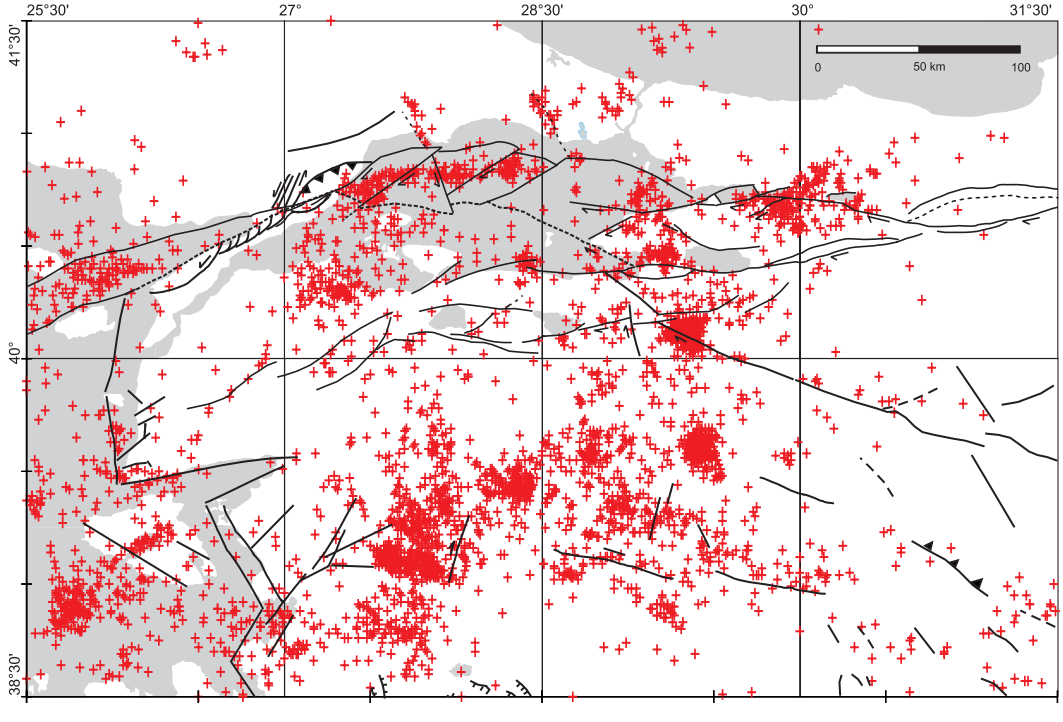


Figure 2: *Microearthquake activity ($m_b \leq 4$) for the time period 1975 – 1988 (NEIC catalogues) in relation to active faults (same as in Fig. 2).*

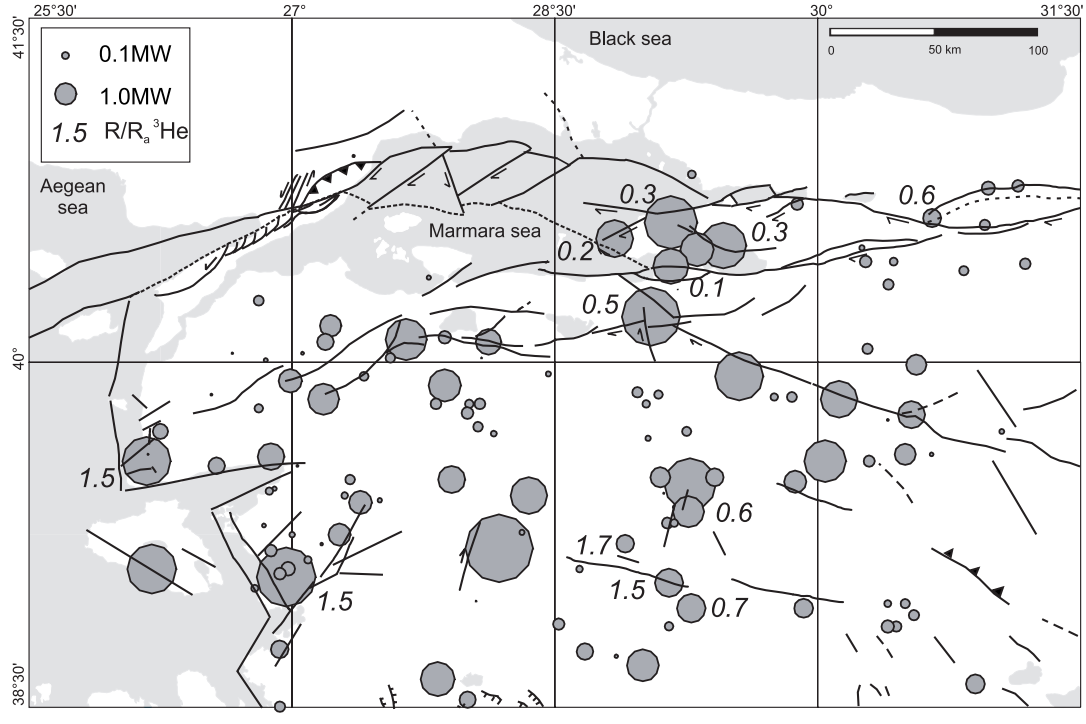


Figure 3: *Thermal spring distribution of the Marmara sea region. Active faults after Schindler (this volume) and thermal springs of the Marmara sea region according to their energy output. Italic numbers indicate helium R/R_A values measured in selected thermal springs.*

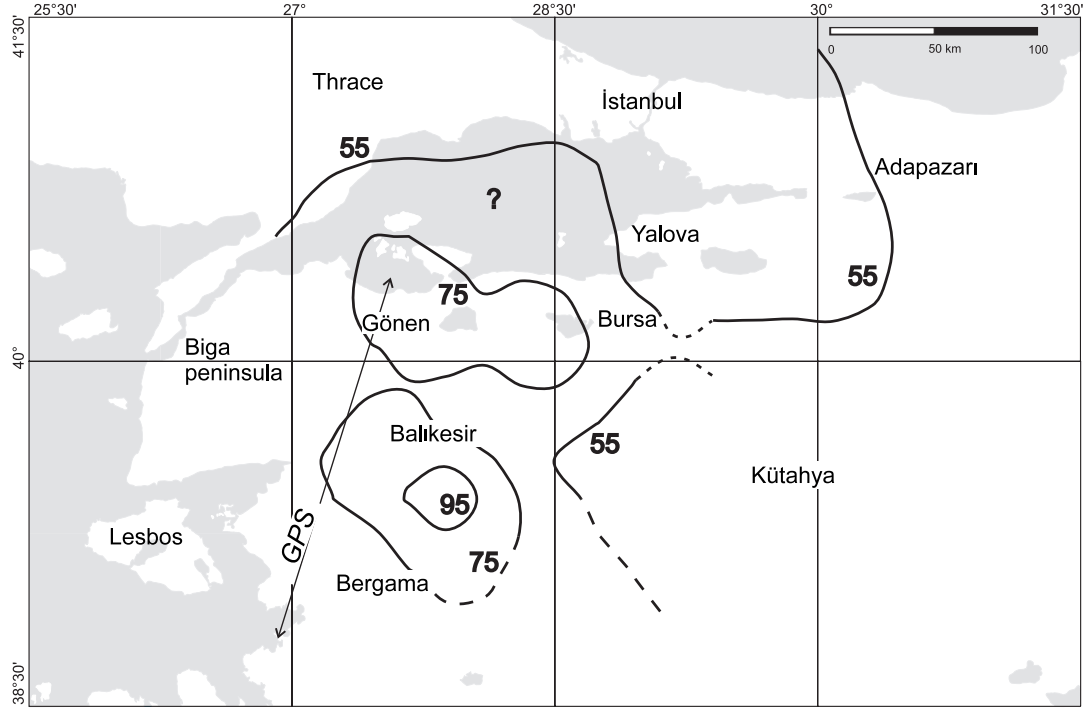


Figure 4: *Terrestrial heat flow density contours (Pfister et al. this volume), labelled in mW/m^{-2}; profile trace of strain calculation from the deformation field derived by GPS measurements (Straub and Kahle this volume), labelled by GPS.*

Crustal strain

One important quantity for a better understanding of tectonically active regions is the strain rate tensor. There are two independent methods for the determination of strain rates: geodetic assessments of the velocity field and summation of seismic moment tensors. The differences are compiled in Table 1.

	Geodetic determination	Seismic moment tensor summation
model	derivatives of velocity field	Kostrov (1974), refined
observed strain rates	sum of elastic and inelastic	elastic
time span of available data	<10 years	<100 years
data acquisition	active	passive
area covered	depending on point distribution	depending on distribution of major earthquakes
time resolution	repetition of measurements	recurrence interval of seismic events

Table 1: Comparison of geodetic and seismic methods for the determination of strain rates.

Currently, the determination of seismic strain rates is based on the summation of seismic moment tensors following Kostrov's original (1974) or slightly refined formulae. It offers a tool for the determination of elastic strain rates. Therefore, the average fault plane mechanism, the seismic release, the rigidity of the rocks and the deformed volume of major earthquakes must be known or estimated. Thus, the determination of seismic strain rates is directly dependent on the occurrence of major events (commonly $M_b \geq 5.5$). Time clusters of major events or seismic gaps may distort the estimation significantly. The spatial and time resolution depends on the occurrence of major earthquakes and can, therefore, not be influenced. Recent estimates of seismic strain rates include data from a time window of 40 to 60 years. Recurrence intervals of large seismic events in the Marmara region are expected to vary between 100 and 1000 years (Barka this volume).

Geodetic strain rates are deduced by deriving the deformation field obtained from GPS measurements. Thus, the total strain rate over the given time interval is observed. So far, precise geodetic networks span a time interval of only less than ten years. Nevertheless, the deformation pattern derived from geodetic observations has proved to be surprisingly constant in most cases. Frequent repetitions of geodetic observations and dense networks supply detailed information about the spatial and time behaviour of the strain rates.

Theoretically, the geodetic strain rates should be larger than the corresponding seismic rate. The difference should lead to the inelastic part of the strain rate (seismic strain deficit).

Many estimates of deformation rates along the NAFZ based on geologic, seismologic, and geodetic data have been published during the last 35 years with extreme values of 4 and 110mm/a. Most recent studies average on a value in the range of 16 to 30mm/a which nowadays is widely accepted. Table 2 compiles the most recent seismic and geodetic estimates of deformation and normal and shear strain rates in the Marmara region. The seismic strain rates of the different authors are based on calculations with varying size of area and time frame. The corresponding shear components range from 5 to 16%/m.y. Thus, they reach 40 to 100% of the geodetically observed values. The geodetic observations allow for a detailed spatial resolution of the strain rates in the Marmara region (Straub and Kahle this volume). The geodetic strain rates clearly show that the Marmara region should be divided into a northern and a southern zone. The mean strain rates in the north (comp. 19%/m.y.; ext. 16%/m.y.) are roughly twice as large as the ones in the south (comp. 8%/m.y.; ext. 8%/m.y.). Based on the highly coherent regional deformation pattern (e.g., Reilinger et al. 1997), we assume that

the geodetically observed deformation rates must be representative for the bulk of the Earth's crust in the investigated area. In general, it is concluded that the geodetic values yield higher strain rates than the seismic determinations – a result which is in good agreement with the theoretical assumptions. However, it is an open question whether the ratio between the elastic and inelastic parts follow clearly defined rules or are dependent on time and/or region.

Region	Source	Velocity [mm/a]	Extensional strain rate [%/m.y.] and azimuth	Compressional strain rate [%/m.y.] and azimuth	Shear strain rate [%/m.y.]	Reference
Marmara	seism.	24	12; 37°	11; 127°	11	Eyidoğan (1988)
NAFZ	seism.	40				Jackson and McKenzie (1988)
W NAFZ	seism.	16	11; 39°	11; 129°	11	Kiratzi (1993)
Marmara	seism.		8; 17°	5;117°	6	Jackson et al. (1994)
NAFZ	geod.	30				Robbins et al. (1995)
Marmara	seism.	12.1	7; 25°	6; 117°	5	Kiratzi and Papazachos (1995)
NAFZ	geod.	25				Oral et al. (1995)
NAFZ	geod.	22.9				Noomen et al. (1996)
W/E-Marmara	seism.	20	9/18; 25°	7/14; 116°	8/16	Papazachos and Kiratzi (1996)
NAFZ	geod.	26				Reilinger et al. (1997)
Marmara	geod.	22	av. 11 (max. 31); 42°	av. 12 (max. 47); 130°	av. 11 (max 31)	Straub and Kahle (this volume)

Table 2: Estimates of velocity and strain rates in the westernmost part of the NAFZ resp. Marmara region. The strain rates are given in [%/m.y.]. 100%/m.y. equals 1μstrain/a and corresponds to a change of distance of 1mm per km and year or is equivalent to $3.17 \cdot 10^{-14}$ /s.

Gravity field and crustal thickness

The inversion of Bouguer gravity anomalies allowed the contouring of the crust-mantle boundary (Klingelé and Medici this volume). The extensional areas in the south show thinner crust. Old, currently stable areas of Thrace or the eastern areas pointing to Central Anatolia are associated with a slightly thicker crust. Towards the Black sea near İstanbul, the crust is thinned as a result of a paleorift tectonic process (Late Cretaceous to Early Eocene according to Okay et al. 1994).

The residual field of the Bouguer gravity anomaly certainly shows a topographic influence, but distinct tectonic structures of the upper crust contribute to the signal. This is demonstrated for the Şarköy area (Schindler this volume), where detailed gravity data are available. The onset of the Ganos fault as part of the mainly active northern zone of the NAFZ is trapped by a distinct lineament of the gravity anomaly. Steeply inclined mass movement along the fault in the upper crust seems to be the process responsible.

In the Bursa region, the Uludağ massif (compare Imbach this volume) reveals a strong negative Bouguer gravity anomaly which cannot only be explained by topography alone. Schindler (this volume) considers this anomaly, too, and explains the critical tectonic situation of the Uludağ area. At the surface, active tectonic fault structures are observed which surround this massif to the NE, N and W. Geological observations give hints of uplift mechanisms of this massif and it may be plausible that an isostatic rise of this large body is happening today. But nevertheless, the reason for the negative anomaly remains unknown.

The evidence that strike-slip faults with vertical components can give rise to a gravity anomaly indicates that these structures may influence large parts of the crust and, therefore, may reach deep into the lower levels of the crust.

The more general picture of the isostatic anomaly may point to slight subsidence of the region south of the Marmara sea which would coincide with the general tectonic extension of this area.

Thermal springs / water-gas-rock interaction

The distribution of thermal springs in the Marmara sea region displays a clear pattern. Figure 3 shows 127 registered springs according to their thermal energy output (compare Pfister et al. this volume). Large springs with several MW energy output occur. No springs are detectable north of 41°N (Thrace area, Tekirdağ, İstanbul area, northern Adapazarı region). Zones with significant compressional tectonics (e.g., Şarköy, Afyon areas) or regions with clear strike-slip tectonics (Mudurnu valley) are characterised by no or lower thermal water activity. On the other hand, extension tectonics are clearly associated with significant thermal spring activity (e.g., Bursa – Gemlik area, Bergama area, Tuzla, Lesbos). The largest springs flow out in tectonically active zones where extension faults intersect strike-slip faults. This can be observed in detail at outcrops which are mentioned by different authors in Theme 4 of this volume, or in a more regional sense (e.g., Figure 3). In Kuzuluk, the thermal waters are bound to a local extensional basin (Greber this volume and 1994) and to a geologically extraordinary structure, the zone of İznik metamorphics, an older suture which can be defined as a tectonically "weak" structure (Schindler this volume).

Among other chemical and physical parameters, helium isotopes have a special importance for geodynamic considerations. Primordial ^{3}He was trapped in the Earth's mantle and can be detected today at the surface in thermal spring waters. The ratio R/R_a describes the quotient of measured (corrected for atmospheric influences) $^3He/^4He$-ratio to the $^3He/^4He$-ratio of the atmosphere. Commonly, the different helium reservoirs are defined by their distinct R-values (atmosphere: $R_a \sim 10^{-6}$, crust: $R_c \sim 10^{-8}$, mantle: $R_m \sim 10^{-5}$, Mamyrin and Tolstikhin 1984). High values of R/R_a are interpreted, therefore, as the influence of magmatic gases from the Earth's mantle. R/R_a values of 0.6-1.5 indicate ca. 8%-20% of mantle contribution, whereas R/R_a values of 0.1-0.6 indicate ca. 5%-8%. The R/R_a values presented in Figure 3 result from different studies (Eisenlohr 1995, Greber 1992, Güleç 1988, Imbach 1992 and 1997, Jeckelmann 1996, Mützenberg 1991).

In the large zone affected by the NAFZ, the mantle contribution is only slightly elevated and has been observed near the southern border at Bursa and to the east where the zone becomes much narrower at Kuzuluk. The highest values, however, have been observed south of the NAFZ. This increase of ^{3}He in thermal waters is assumed to be connected with stronger extension tectonics which enable enhanced gas migration from mantle or lower crustal levels to upper crustal levels. One could assume strongly elevated R/R_a values in the deep Marmara sea trough, too, as the most significant actual stretching of the crust occurs there, but this assumption cannot be verified due to lack of data.

Selected geothermal areas were investigated in detail by hydrogeological methods (Greber, Imbach, Eisenlohr, Mützenberg, Yalçın (all this volume), Jeckelmann 1996). The graphical representation of δD versus $\delta^{18}O$ isotopes of different geothermal springs in the Marmara sea region as a summary (Figure 5 of Balderer this volume) points towards recent infiltration of most spring waters. Deviation from the Marmara meteoric water line to more positive $\delta^{18}O$ values indicates possible water-rock interaction at high (>130°C) temperatures with eventu-

ally long residence times. Greber (this volume and 1994) gives different explanations for the $\delta^{18}O$ shift of the Kuzuluk waters: either long residence times at relatively low temperatures which give chance to water-rock interaction or an ^{18}O exchange with CO_2 gas. Mützenberg (this volume) explains the smaller slope of the mixing line compared to the meteoric water line with mixing processes of a saline brine endmember with fresh groundwater.

Generally, no significant water-rock interaction takes place in the investigated area. Most of the thermal waters can be attributed as part of the hydrologic cycle with residence times t_R on the order of 10^2-10^4 years. Exceptions are the thermal brines of Tuzla and Kestanbol (Mützenberg this volume, Balderer and Synal 1996), as well as the fossil waters with $t_R>10^4$y. of Kuzuluk (Greber this volume, Balderer and Synal 1996) and Gönen (Yalcın this volume, Balderer and Synal 1996).

Furthermore, chemical analysis of spring waters detected possible lithologies as subsurface flow paths or reservoir rocks. Using this information, geothermometers are applicable resulting in maximum temperatures of the individual thermal groundwater. The maximum SiO_2 reservoir temperatures were 160°C at Tuzla (Mützenberg this volume) and 150-170°C at Bergama-Kaynarca (Jeckelmann 1996). In combination with the temperature field of the crust based on heat flow investigations, maximum circulation depths can be calculated, e.g. in the Bergama area in the range of 6 to 8km (Jeckelmann 1996).

Surface heat flow density

The main result of the geothermal investigations is represented by a detailed measured surface heat flow density distribution (Pfister et al. this volume). In principle, two different realms can be separated (Fig. 4): regions with about 50mW/m^2 and regions with slightly elevated values of about 75-95mW/m^2. Because of the shallow depth range of temperature data possible paleoclimatic corrections have to be taken into account (Pfister et al. this volume). A possible maximal climatic influence range from about +15% for elevated values, to +20% for normal and low values, respectively, has been estimated. Applying these corrections, two regimes of terrestrial surface heat flow can be separated: one with 60mW/m^2, which is only slightly increased relative to a stable continental crust (40-55mW/m^2 Morgan 1995), and the second with 85-110mW/m^2, which is typical for continental rifting areas (Morgan 1995). The worldwide mean value for continental crust is 65mW/m^2 according to Pollack et al. (1993).

Higher heat flow is generally associated with thinned crust. This correlation seems to be generally valid for the regions surrounding the Marmara sea. No information is available about the Marmara sea itself, which tends towards a strongly thinned crust. The general extension in this area is documented by GPS data (Straub and Kahle this volume) and by gravity data (Klingelé and Medici this volume), but also supported by geological models (Schindler this volume). Approaching the Black sea region, the heat flow contour lines can no longer be correlated with the Moho contours. Strongly thinned crust there coincides with very low heat flow densities (Hurtig et al. 1991). The newest results of 50-55mW/m^2 were presented by Kutas et al. (1996) after applying correction for sedimentation. This low heat flow is due to the older tectonic history of this region. The extension of the western Black sea basin is thought to have occurred during the Late Cretaceous till the Early Eocene (ca. 80 to 55m.y. ago (Okay et al. 1994)). The thermal signal of this extension process is no longer detectable. On the other hand, the thinned crust still persists with time in the gravity signal.

Crustal radioactive heat production

Tectonic processes of the lithosphere are triggered by the thermal regime at its base. Only surface heat flow density can be directly determined, therefore, crustal contribution to the heat budget becomes an important variable which may be estimated using seismic p-wave velocities. Little is known about these seismic parameters in the investigation area. Nevertheless, the study of Alptekin et al. (1990) resulted in some ideas concerning the depth distribution of V_p. This study was based on seismic surface wave investigations. Applying the method described by Rybach and Buntebarth (1992), a vertical profile of heat production can be estimated. The mean values are approximately $1.5\mu Wm^{-3}$ and obviously are subject to a certain variance. The main contribution of this heat production comes from the uppermost 15km of the crust.

Harris et al. (1994) analysed the geochemistry of intrusive rocks in the region of Orhaneli, south of Bursa. Based on their results estimations of radioactive heat production of these rocks give a median value of $1.5\mu Wm^{-3}$ ($\sigma = \pm 0.8\mu Wm^{-3}$).

These estimates of radioactive heat production will later be used to calculate temperature-depth profiles of the crust and give reason to account for the crustal heat flow contribution in the range of ca. $25mW/m^2$ (Fig. 5). Possible future investigations in determining crustal p-wave velocities, as well as geochemical characterisations of surface rocks, will give more exact solutions to these questions. Considering a possible paleoclimate correction to the near surface heat flow determinations, two different heat flow regimes with a source in the upper mantle can be differentiated (see Figure 5): first, basal heat flux from the asthenosphere (q_A) of ca. $35mW/m^2$ in the northern and eastern part of the Marmara sea region and second, elevated heat flow in the southwestern part of the region (q_R of 60 to $85mW/m^2$). Lachenbruch and Sass (1987) describe different models to explain stretching processes of the lithosphere. The heat budget explained above mainly follows their instructions: q_R is to be understood as reduced heat flow. In the static conduction case with a stable lithosphere, q_R equals q_A.

The values in Figure 5 symbolise the general budget of the conductive heat transport regime for the two main and different tectonic areas. The stretched lithosphere shows significantly elevated basal heat flow (q_R) by a factor of ca. 2 compared to the region not mainly influenced by extensional forces (q_A). This significant difference in basal heat flux will be used later for considerations of steady state stretching processes of the lithosphere.

Correlation of thermal spring energy with seismicity and crustal deformation

A visual comparison of Figures 1 and 3 reveals some correlation between geothermal energy output of the springs and recent seismicity. Most of the significant geothermal sites are bound to active fault lines and lie near regions with elevated seismicity. The upper crust is fractured and enables, therefore, an enhanced circulation of groundwater to depths of several kilometers. Thus, a possible correlation of thermal spring energy with seismic energy release and crustal deformation was investigated.

Within the area covered by GPS measurements (Straub and Kahle this volume), the 18 most significant springs with thermal energy output of >1MW were selected. The thermal energy output Q_i according to Figure 3 (details in Pfister et al. this volume) was set as a dependent variable. Microseismicity of magnitude larger than 3.5 between 1975 and 1995 within the sur-

rounding area of each individual spring was determined (60km maximum distance from the spring). Equations 1 and 2 (Gutenberg and Richter 1956) were used to calculate the logarithmic seismic energy E_S based on surface wave magnitudes and a distance criterion.

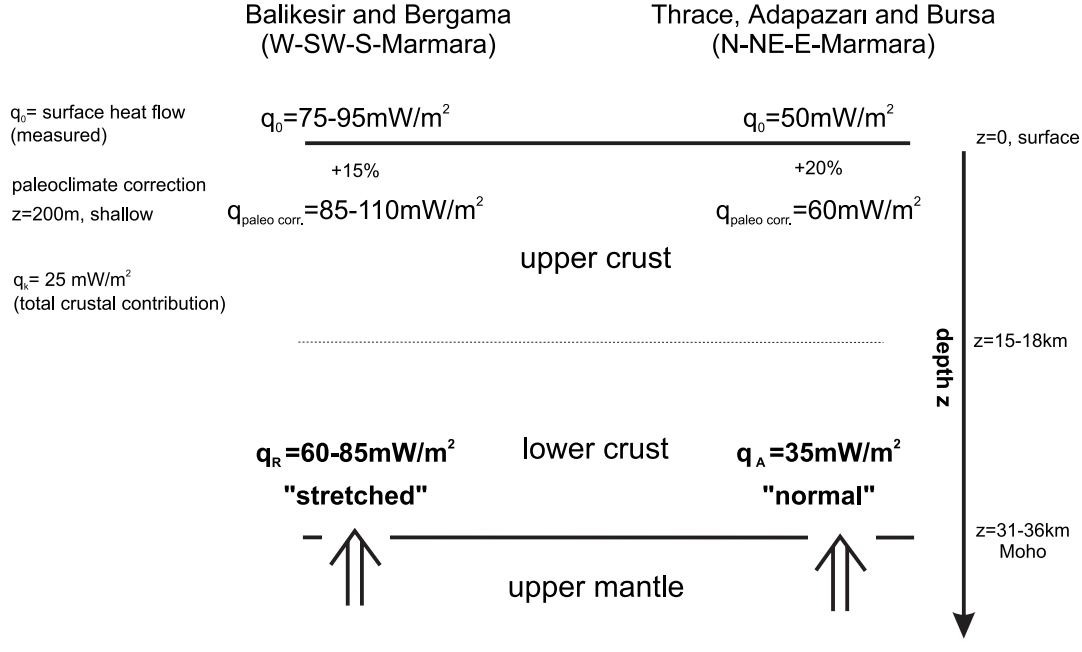


Figure 5: *Sketch of heat budget through the crust. The stretched lithosphere shows significantly elevated basal heat flow by a factor of ca. 2 (q_R, Balıkesir and Bergama) compared to the region not mainly influenced by extensional forces (q_A, Thrace, Adapazarı) or less influenced (Bursa). The upper crust contribution to the budget was estimated using the Vp-depth distribution given by Alptekin et al. (1990) and the relationship between seismic velocities and crustal heat production (Rybach and Buntebarth 1992).*

$$(m_b)_i = 2.5 + 0.63 \cdot (M_S)_i \qquad [1]$$

where:

m_b: body wave magnitude

M_S: surface wave magnitude

$$(E_S)_j = \sum_i \left[\left(1 - \frac{x_i^2}{R^2} \right)^2 \right] \cdot \left[4.8 + (1.5 \cdot (M_S)_i) \right] \qquad [2]$$

where:

E_s: logarithmic seismic energy release within the influence radius
x: distance epicentre-spring
R: influence radius, varied between 20 and 60km
M_S: surface wave magnitude
j: index variable for thermal spring
i: index variable for earthquake within the influence radius

A single regression calculation between thermal spring energy and seismic energy should define the most significant distance criteria R (Pfister 1997). Varying this parameter R between values of 20km and 60km, the best regression fit resulted using an influence radius R of 40km. This value was used for all further calculations.

Volume dilatation [Φ] was determined at each spring site using the crustal deformation field (Straub and Kahle this volume). A significant linear correlation between the mentioned parameter as expressed in Equation 3 was found and tested using a regression calculation with normally distributed residuals E_j. It was tested whether the variables $(E_s)_j$[1] as seismic energy and Φ_j[2] as volume dilatation contribute significant information to the model or not. A detailed analysis of model residuals was performed and resulted in the final model described by Equation 3 (Pfister 1997).

$$\log(Q_j) = \alpha + \beta_1 \cdot (E_s)_j^{(1)} + \beta_2 \cdot (E_s)_j^{(1)} \Phi_j^{(2)} + E_j \qquad [3]$$

where:

Q_j: thermal spring energy
$(E_s)_j$: logarithmic seismic energy
Φ_j: volume dilatation
$E_j \sim N(0,\sigma^2)$: residuals
$\alpha \pm \sigma$, $\beta_1 \pm \sigma$, $\beta_2 \pm \sigma$: intercept and coefficients

The variables seismic energy $(E_S)_j$ and the combination of seismic energy with volume dilatation $(E_S\,\Phi)_j$ cannot be neglected according to a 5% level (p-value of the test is 0.0002, 18 largest springs with a thermal energy output $\geq$ 1MW). The calculated values are: $\alpha \pm \sigma$: -.25$\pm$0.33, $\beta_1 \pm \sigma$: +0.42$\pm$0.09, $\beta_2 \pm \sigma$: -1.03$\pm$0.27. This evidence may confirm the geological observations or interpretations that huge thermal springs are bound to significant neotectonic structures dominated by frequent seismicity and a certain amount of extension. Within this analysis, it turned out that shear strain does not contribute any further significant information (Pfister 1997).

Obviously, a certain combination of seismicity and crustal deformation may be necessary for the largest spring occurrence. Looking for the theoretical background of the described correlation, two main contributions must be shortly summarised at this stage:

Hill (1977) introduced a model for earthquake swarm activity. He described this model for magmatic dike intrusions triggering the release of earthquakes, but he also mentioned the possibility for water under pressure which effectively forms a distribution of 'dikes' with long dimensions on the order of several hundreds of meters. Sibson (1992) described the complex interaction between rupture nucleation or recurrence and fluid flow in the crust. Strong indications were found for episodic events. Fluid pressure and fault failure occurred within a cycle process.

The stable outflow conditions of the thermal springs during the observed time period of our studies (e.g., Theme 4) do not seem to be representative for the mentioned cycles. We have strong indications from field studies, as well as from hydrothermal modelling studies, that the thermal groundwater shows a constant flow regime over several decades, whereas the swarm activity possesses a certain variability in time and space (compare Fig. 9 in Sellami et al. this volume). It cannot be answered here how far the thermal waters, as well as the temperature anomaly in the crust, are responsible for opening or closing of existing systems or even for faulting. But detailed, careful and coincident observation of thermal water outflow and seismic behaviour in such regions is highly promising to determine such unknowns. So far, no direct connections were observed between changes in thermal water discharge and (nearby) seismic events during the project period, whereas older historical reports describe

the influence of strong earthquakes on the thermal spring occurrence (Greber this volume Imbach this volume, Balderer this volume). But a possible consideration of the strongest earthquakes during this century (compare Barka this volume, Figure 2) seems to support the correlation described above.

Interdependence matrix

As we differentiated between selected key observable quantities, a certain influence of such "elements" on the whole system of an actively deforming crust could be detected and demonstrated. However, the cybernetic role of an element within a system cannot be elucidated by the analysis of the element itself. The interdependencies with the other elements can define the importance and influence of that particular element.

We try to define the role of the major system elements (e.g. key observable quantities) with the instrument of an interdependence matrix (Vester 1988). This method separates system elements by identifying the "active", "reactive-passive", "critical" and "neutral" elements (Table 3). An active element is largely independent of all other elements which depend strongly on it. On the other hand, the reactive or passive element is strongly dependent on all other elements but these are largely independent of it. The critical element is strongly dependent on the other elements but these are also strongly dependent on it. Finally, the neutral element is largely independent of the other elements and these are also largely independent of it. The interactions between the individual element pairs are tentatively defined by effectiveness factors from 0 (no effect) to 3 (strong effect). The active and passive sums (AS and PS, see Table 3) characterise the elements: the active element has the highest Q=AS/PS, the reactive element the lowest Q; the critical element the highest P=AS*PS, the neutral element the lowest P.

		1	2	3	4	5	6	7	AS	AS: active sum (horizontal)
Active faults	1		3	0	1	3	3	1	11	effectiveness factors:
Recent seismicity	2	1		0	0	1	2	0	4	0: no effect
Surface heat flow density	3	0	1		1	0	1	1	4	1: small effect
Gravity field	4	1	0	0		1	0	2	4	2: medium effect
Crustal strain	5	2	2	2	1		2	3	12	3: strong effect
Thermal springs	6	1	1	0	0	0		0	2	
Crustal thickness	7	1	1	3	3	1	0		9	
	PS	6	8	5	6	6	8	7		PS: passive sum (vertical)
	Q	1.83	0.5	0.8	0.67	2	0.3	1.3		Q: Quotient AS/PS
	P	66	32	20	24	72	16	63		P: Product AS*PS

Table 3: Interdependence matrix with key observable quantities for active tectonics in the Marmara sea region as elements (project period since 1990). The active, as well as critical, element turned out to be "crustal strain" (No. 5), the passive or reactive, as well as, neutral element is "thermal springs" (No. 6). The effectiveness factor range was set from 0 (no effect) to 3 (strong effect).

The most active element turned out to be "crustal strain" (No. 5), the most passive or reactive element is "thermal springs" (No. 6), the most critical element is again "crustal strain" and the most neutral element again "thermal springs". Slightly diverse effectiveness estimations may result from different analyses. Nevertheless, Figure 6 shows the relative position of the elements in a 2D field. The reactive and neutral element "thermal springs" (6) plots close to the elements "gravity field" (4), "surface heat flow density" (3) and "recent seismicity" (2), but seems to be more reactive than the three latter elements. This indicates the importance of ongoing observation of thermal spring activity to detect possible triggering by neotectonic activity.

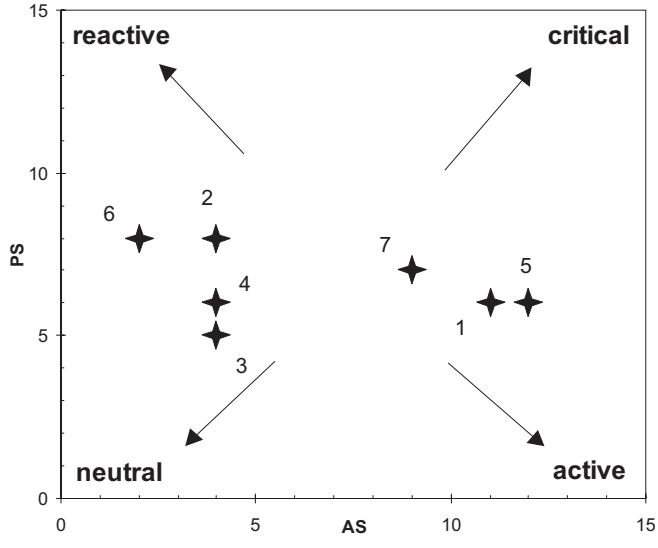


Figure 6: *Solution of interdependence matrix: The elements do not show large variation in the vertical direction. (1) active faults, (2) recent seismicity, (3) surface heat flow density, (4) gravity field, (5) crustal strain, (6) thermal springs, (7) crustal thickness. For interpretation see text.*

The most active but also the most critical component of "crustal strain" symbolises, significantly, the "motor" of the neotectonic activity based on the general plate tectonic regime in the Aegean-Anatolian region. The "active faults" (No. 1) plots close to "crustal strain" and is probably closely related to it. The "crustal thickness" (No. 7) plays a role between the active and neutral elements.

This method is only a simple step to elucidate the complex interplay of the system "Neotectonics of the Marmara sea region". Nevertheless, it confirms the importance of time series observation of parameters such as thermal spring behaviour or crustal strain rates in tectonic active areas. Tschudi (this volume), as well as Greber et al. (this volume), observed mainly atmospheric influence on the outflow characteristics of the thermal waters; the observation period turned out to be too short to detect tectonic influences. On the other hand, historical documents confirm the possibility of detection (Balderer this volume). Therefore, we repeat our previous statement that it is highly necessary to develop long-term observation records of nearly undisturbed natural conditions of a geothermal system over 10 to 20 years or even more which may reveal the tectonic or seismic influence directly. Detailed, careful and coincident observation of thermal water outflow, crustal strain rate development and seismic behaviour in this region would be highly promising. We suggest areas like Tuzla (Mützenberg this volume) or Çekirge (Imbach this volume) for this purpose, which show nearly undisturbed natural conditions.

Models and processes

Kinematic analyses of neotectonic structural features (Barka, Schindler, both this volume), the distribution of active faults (Barka, Schindler, both this volume), the spatial distribution of seismicity (Üçer et al, Sellami et al., both this volume), regional regularities of the orientation of P- and T- axes as determined from fault-plane solutions of earthquakes (Sellami et al. this volume), as well as results of GPS measurements (Straub and Kahle this volume) convincingly show, that the deformation of the crust and the upper, seismogenic part of the lithosphere is characterised by distributed shear. The large-scale deformation of the lithosphere as a whole may be more adequately described by the deformation of a continuum, i.e. by a continuous velocity field, than by rigid microplate motion. According to this style of tectonic deformation in NW Turkey, the presented key observable quantities allow now a characterisation of "Active tectonics and its interaction with groundwater circulation, terrestrial heat flow and seismicity in the Marmara sea region", which was the central target of our project.

Two general processes can be differentiated: first, deep groundwater circulation in the upper levels of the crust with involvement of deeper sources in a tectonic environment of distributed shear; second, the large-scale extension of the lithosphere caused by the general plate tectonic regime of the Aegean-Anatolian region as a model of deformation of a continuum.

Deep groundwater circulation

All hydrogeological investigations within the Marmara sea region revealed a similar circulation pattern for the thermal waters: Recent components within the water cycle turned out to be dominant. Generally limited water-rock interaction at high temperatures was observed. Deviations from the Marmara meteoric water line were observed at three different thermal spring areas. They can be explained by (1) water-gas interaction due to elevated CO_2 pressures or water-rock interaction at low temperatures but during long residence times (Kuzuluk: Greber this volume) and (2) mixture with brines (Tuzla: Mützenberg this volume, Bergama: Jeckelmann 1996). The upper brittle crust can be regarded as partially strongly fractured and the circulation of the thermal water is mainly bound to an anisotropic configuration of hydraulic conductivity, not only within the discharge area, but also in recharge areas. Strong infiltration into the underground is due to distinct topography (mainly elevated terrains) and along highly permeable zones (e.g., highly weathered rock surfaces, karst and fault structures). Paleoinfiltration during the Late Pleistocene should be considered as well (Balderer this volume). Circulation of deep groundwater within the range of months, years or up to several thousand years can be observed and/or postulated. Short-term fluctuations of physical parameters have been observed. These findings point to circulation depths mainly within the uppermost 6km of the crust. This depth range results from the mentioned geothermometer estimates of reservoir temperatures combined with the geothermal temperature gradient within the area.

Within the Bergama area, one of the most active of the investigated areas, evidence was found that steep strike-slip faults generally are functioning as vertical flow paths for infiltration as well as for the rise of fluids. The combination of translational tectonics with extensional forces ("transtension") becomes a main mechanism for the thermal spring occurrence. Advective forces, convection, density layering as well as buoyancy effects due to gas appearance and temperature differences, are the main rising mechanisms for the deep fluids. The following observations of gas tracers of very deep origin in the geothermal waters support this view and indicate the presence of deep fault structures.

Gas tracers of very deep origin

Carbon dioxide sources in the Earth's crust are characterised by different, partly overlapping $\delta^{13}C$-ranges. The $\delta^{13}C$ measurements on $CO_{2(g)}$ and $CH_{4(g)}$ samples from the Marmara sea region (Fig. 7) indicate gas origins in the deeper crust as well as in the mantle, besides superficial lithologies such as carbonates or organic matter. The presence of primordial helium, as indicated by the $^3He/^4He$ ratio within the thermal waters, also indicate admixtures of gases of mantle origin (Figures 3 and 7). Furthermore, high CO_2 content is often observed in tectonically active areas and points to inorganic CO_2 origins (Fig. 8).

These findings point to deeper extents of the fault structures even to lower crustal levels. The combined determination of helium, as well as of CO_2 and CH_4 origin as revealed by their isotopic composition, decodes the main gas origins (Figure 7). We conclude that the main part of the thermal springs is influenced by gas admixture from the Earth's mantle. The trend towards mantle influenced gases is most significantly detected within the Bergama region. But furthermore, thermal waters with CO_2 components from marine carbonates and probably from organic sediments are also evident. The thermal springs of Nebiler and of city of Bergama (compare Figure 7 and 8: Neb01, Neb03 and Berg) certainly show a source of the gases in organic matter and/or some mixture with inorganic CO_2 gas. Other geothermal areas in the Marmara sea region show similar behaviour individually. The karstic springs of Orhangazi and Gemlik point towards organic CO_2 sources in the soil zone of the infiltration area (Eisenlohr this volume); the Kuzuluk springs indicate an origin from marine carbonates (Greber this volume and 1994).

Within the context of active tectonics, the importance of these gases pointing towards mantle origin is their ability to develop high fluid pressures at depth which could reduce the effective frictional strength of rocks. If the pressure were maintained at a sufficiently high level, the fault behaviour might be characterised by frequent small earthquakes and/or fault creep, as we may observe in the thermal spring regions or generally in Northwestern Anatolia. Irwin and Barnes (1980) describe worldwide observations of CO_2 rich springs in tectonically active areas.

These influences may help to explain the observed correlation between microseismicity energy release, crustal deformation and thermal spring occurrence as previously described. The enhanced fluid circulation in the crust can depend on frequently existing faults and on acting extensional forces which would again lead to frequent micro-earthquake occurrence. A correlation among all these phenomena is certain, however, which is the main trigger force and which is the main reaction cannot yet be distinguished at this stage.

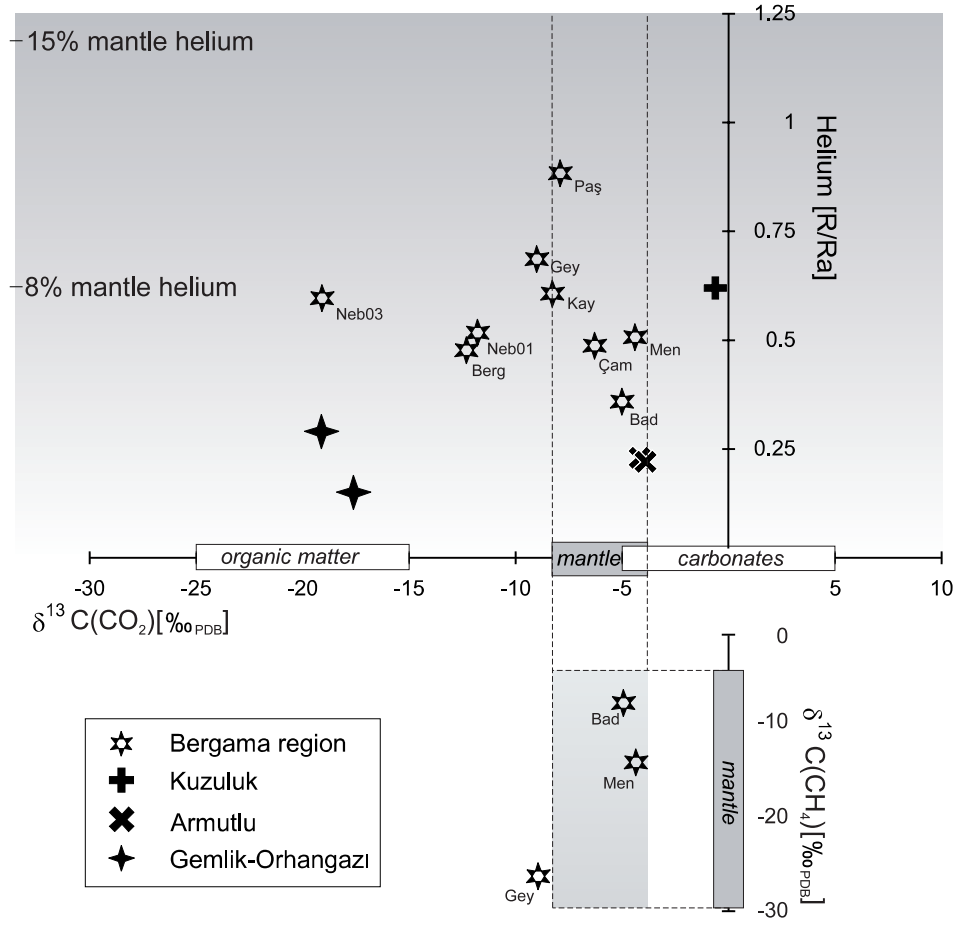


Figure 7: *Helium R/R_a and $\delta^{13}C$ values of selected thermal springs in the Marmara sea region. Mantle gas admixture is prominent. Limited influence by marine carbonates or organic matter has to be considered. Areas defining gas source range with $\delta^{13}C$-values are taken mainly from Dai et al. (1996), Deines (1980) and Barnes et al. (1978). Grey shading symbolises increasing percentage of mantle gases. Notice that in the Bergama region three springs (Bademli, Menteşe and Geyikli) have been sampled for $\delta^{13}C$ in CO_2 as well as in CH_4 gas. Bergama region: Bad = Bademli, Neb01, Neb03 = Nebiler, Gey = Geyikli, Kay = Kaynarca, Çam = Çamurlu-Dikili, Berg = city of Bergama, Men = Menteşe, Paş = Paşa İlıca (Jeckelmann 1996) Kuzuluk (Greber 1992), Armutlu and Gemlik-Orhangazi (Eisenlohr 1995).*

Models of extending lithosphere: implications from helium and heat flow

Large-scale continental extension can be seen and interpreted in terms of a thermal and a gas signal observed at the surface of the Earth by measuring terrestrial heat flow density and primordial ^{3}He concentrations in geothermal fluids. The respective models were introduced by Lachenbruch and Sass (1978):

Generally the crust is thinned by extensional forces and the isostatic compensation is possible by three different main processes: underplating of mantle melt at the base of the lithosphere, intrusion of mantle melt into the lithosphere and simple stretching of the lithosphere with accretion of crystalline material at mantle temperatures. All three processes add heat and primordial ^{3}He gas to the base of the crust from where they migrate to the surface. Under-

plating contributes the largest amount of heat and helium. While stretching contributes only a significant amount of heat, helium addition can be regarded as small and locally caused by limited intrusiva. Combined occurrence of underplating, intrusion and simple stretching has to be taken into account, too, but generally is not resolvable at this stage of work. The timescale of a physical transport through the crust can be estimated by the following relationship:

$$\frac{\kappa^{T,He} \cdot t}{L^2} = a \qquad [4]$$

where:

κ^T =diffusion coefficient of heat transport, $10^{-6} m^2 s^{-1}$.
κ^{He} =diffusion coefficient of helium transport, $10^{-8} m^2 s^{-1}$ (after Torgersen 1993)
t =time since the initiation of the event [s]
L =depth of the event [m]
a =1

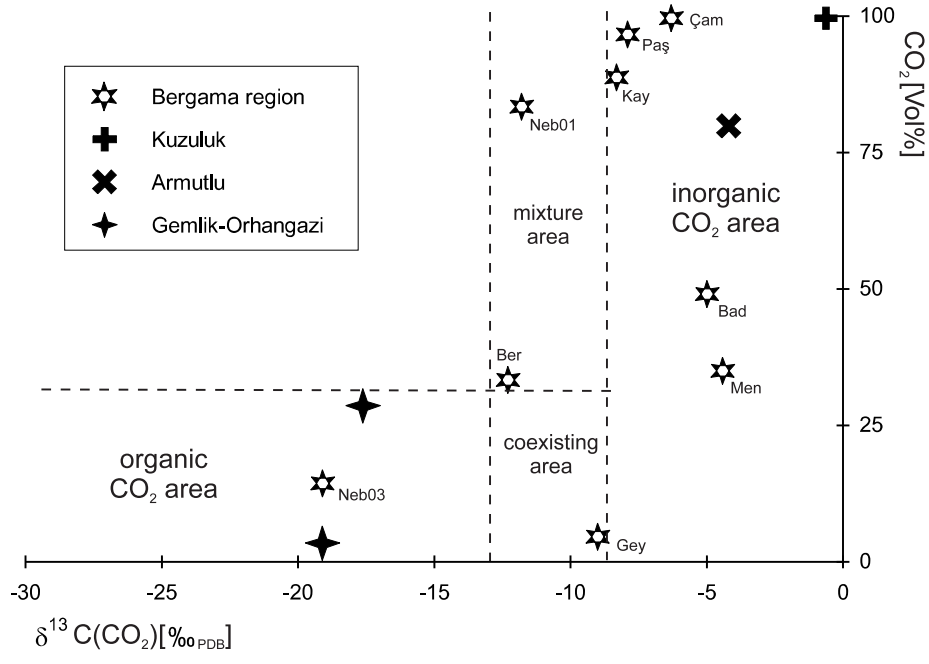


Figure 8: *$\delta^{13}C(CO_2)$ versus CO_2 content of the gas phase in the thermal waters of the Marmara sea region. High CO_2 content is often observed in tectonic active areas and points to inorganic CO_2 origin. The springs of Gemlik-Orhangazi, Nebiler and Bergama city are strongly influenced by mixture with organic gases.*
Bergama region: Bad = Bademli, Neb = Nebiler, Gey = Geyikli, Kay = Kaynarca, Çam = Çamurlu-Dikili, Berg = city of Bergama, Men = Menteşe, Paş = Paşa İlıca (Jeckelmann 1996), Kuzuluk (Greber 1992), Armutlu and Gemlik-Orhangazi (Eisenlohr 1995).

Lachenbruch and Sass (1978) defined a=0.25 to detect these processes at surface. With L=40km and t=15m.y., a value of "a" in the range of 0.3 results for the thermal transport process. Assuming that the extensional process started 15m.y. ago, steady state calculations may be applied to quantify the amount of extension and their surface signals within the Marmara sea region. Schindler and Yılmaz (both this volume) and many other authors emphasise the onset of extension at that time. With respect to the smaller diffusion coefficients of the he-

lium transport process, steady state assumptions can only be assumed for processes starting at depth levels of L≅4km. Therefore, we mainly follow Torgersen's (1993) argumentation:

First, underplating or intrusion cannot be regarded as the main continental extension mechanism based on the observations in old extensional basins. These two processes would require such an enhanced contribution of mantle material to explain the heat flow anomalies at the surface that this would lead to an elevated ^{3}He signal at the surface which cannot be observed in any older crustal extensional region. Second, the R/R_a values between 0.5 and 1.5, measured in the southern part of Northwestern Turkey, describe the typical range of values for extensional basins. Such values can be explained by local and limited magmatic intrusions into the upper level of the crust. Small intrusions do not show any thermal signal in the far field.

For the Marmara sea region, gas movements in the crust bound to highly permeable fault zones due to extensional tectonics may be a much more reasonable process to transport ^{3}He rapidly from the mantle to the surface.

Consequently, we would explain the extension south of the NAFZ with a simple stretching model of the continental crust. The rate of extension is calculated on a baseline through a main part of the investigation area (Fig. 4, GPS-line, data from Straub (1996). Considering only the onshore part, compression and extension varies along this profile, but a mean value of +3%/m.y. results, meaning that extension overwhelms compression. Consequently, we assume that this mean strain rate was generally constant over the last 15m.y., which can be confirmed by geology for the last 3-4m.y. at the most (Schindler this volume). Previously, even a short-term interval with regional compression was known in the southern part of Northwestern Turkey, but for 15m.y. extension was the overwhelming tectonic force (Mercier et al. 1987), with the main impact on the thermal profile of the lithosphere. The rate of deformation during the Miocene, however, is unknown.

Following the heat budget defined in Figure 5, a heat flow ratio q_R/q_A of about 2 results. Applying the simple stretching model (Equation 5, after Lachenbruch and Sass 1978) these observable quantities point to a crustal extension with a lithosphere thickness of about 40km (Fig. 9).

$$q(0,R,\beta,q_A) = q_A e^{R^2/2\beta^2} + A_0 D \qquad [5]$$

where:

$q(0,R,\beta,q_A)$: surface heat flow density at z=0

$$\beta^2 = \frac{K}{s\rho c}$$

K: thermal conductivity, $2.7 Wm^{-1}K^{-1}$
s: extension strain rate, 3%/m.y.
$\rho \cdot c$: volumetric specific heat capacity, $2.5*10^6 Jm^{-3}K^{-1}$
A_0: radioactive heat production at surface, $1.5*10^{-6} \mu Wm^{-3}$
D: characteristic depth for radioactive heat production, $15*10^3$m
R: "lithosphere thickness", depth to dry solidus, [m]
q_A: basal heat flux from the asthenosphere

Therefore, it has to be emphasised that the main thermal signal of crustal extension, which is measured in the terrestrial surface heat flow density, is assumed to be caused by simple stretching of the lithosphere and accretion of crystalline material at mantle temperatures balancing isostasy. It may be possible that limited intrusiva would occur at well-defined localities

where, for example, combined extensional and translational tectonics can be observed. Outcrops of very rare young volcanics favour this interpretation of shallow intrusions of only limited volume and without any long term influence on surface heat flow density (e.g. basalts of Quaternary age near Kula 120km E of İzmir, compare Yılmaz this volume; or young basaltic cones in the Bergama area, compare Jeckelmann 1996).

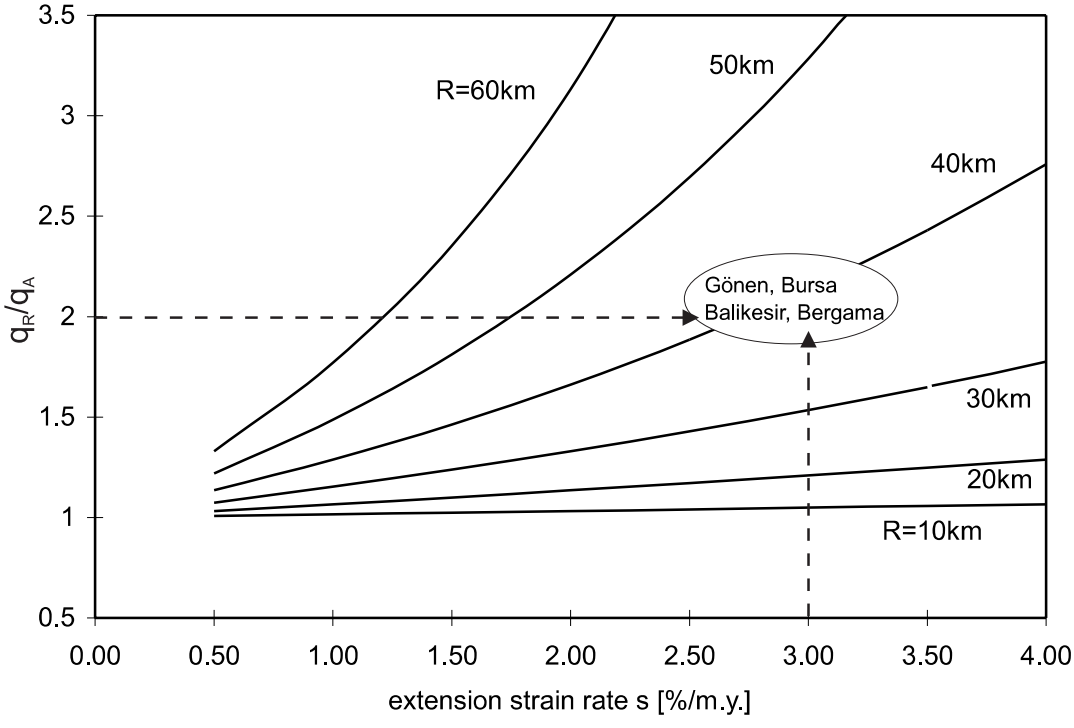


Figure 9: Effect on heat flow of stretching of a lithosphere of thickness R. Reduced heat flow is q_R, conductive heat flux at the top of the asthenosphere is q_A, extension strain rate in %/m.y. (Equation 5, after Lachenbruch and Sass 1978).

Thermal profile of the lithosphere

The main controlling factor of the reflections formulated above is defined by the modelled temperature profile of the lithosphere based on the main parameters basal heat flow q_A and lithosphere thickness R. The temperature-depth curve should cut the dry solidus at the appropriate depth (z=R). Equation 6 describes the temperature-depth function for a stretched lithosphere.

$$T(z,R,\beta,q_A) = e^{R^2/2\beta^2} q_A \frac{\beta}{K}\left(\frac{\pi}{2}\right)^{1/2} erf\left(\frac{z^2}{2\beta^2}\right)^{1/2} + \frac{A_0 D^2}{K}\left[1-e^{-z/D}\right] \qquad [6]$$

(same symbols as Equation 5, z: depth [m])

Figure 10 shows the calculated temperature depth curves (1, 2, 3) for three different basal heat flow values q_A (25, 35, 45mW/m^2). Further input values are λ=2.7WK^{-1}m^{-1} for the whole depth profile and A_0=1.5μWm^{-3} with a characteristic depth range of D=15km mainly based on the depth distribution of seismic p-velocities derived by Alptekin et al. (1990). The stretching case is dependent of the lithosphere thickness (R); the static conduction case considering no tectonic strain is shown for comparison, too. Independently, the numerical modelling of ther-

mal groundwater circulation revealed temperature depth distributions for the uppermost part of the crust. According to these models (Pfister et al. this volume) in the region of Bursa, temperatures of around 190°C have to be taken into account at depths of ca. 6km. In the region of Gemlik, temperatures of around 60 to 70°C occur at depths of ca. 2km. These values agree with the general trend of the temperatures at the border between a stretched and a stable lithosphere (stars in Figure 10).

The very dramatic effect of stretching the lithosphere by 3%/m.y. during ca. the last 15m.y. becomes obvious by considering that these models propose that the asthenosphere top reached very shallow depth ranges of about 40 to 50km! The Marmara sea itself could possess an even thinner lithosphere. Seismic tomography results also indicate a similar strongly-thinned lithosphere and shallow reaching partial melting (Figures 5 and 6 in Theme 2, Mueller et al. this volume).

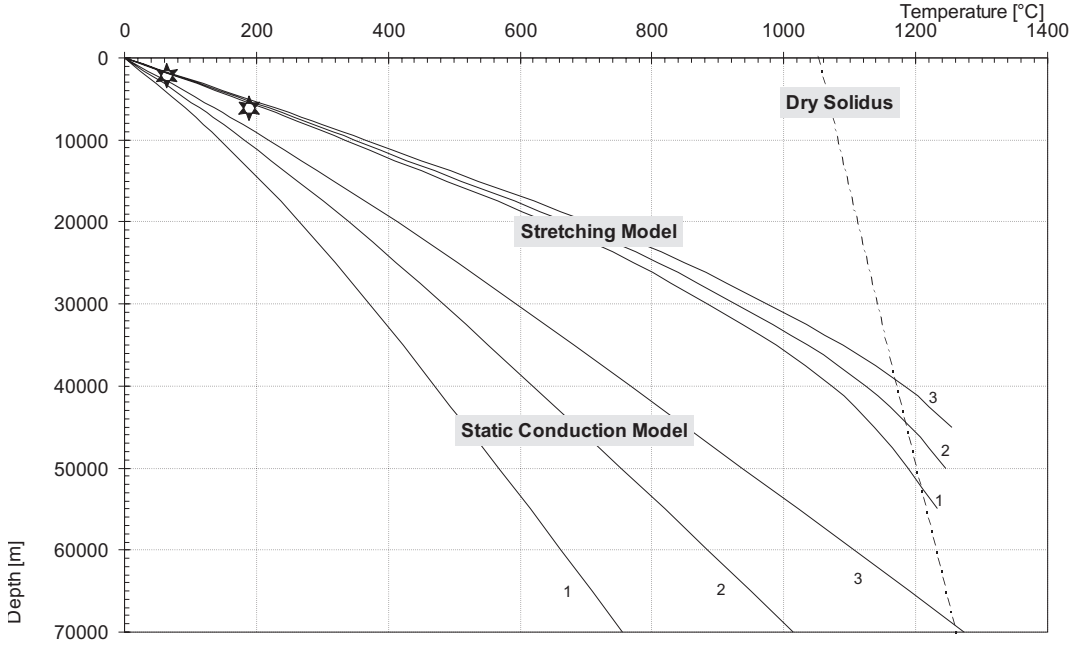


Figure 10: Calculated geotherms of the lithosphere based on the stretching model (Equation 6) with different q_a (1: 25, 2: 35, 3: 45mWm^2) and static conduction model with different $q_R = q_A$ (1: 25, 2: 35, 3: 45mWm^2). For comparison, the results from numerical thermohydraulic modelling of spring systems (Pfister et al. this volume): at Bursa a temperature of 190°C prevails in 6km depth, at Gemlik a 60-70°C is reached in 2km depth (stars).

Concluding remarks

From geological evidence, it has been shown that the last phase of neotectonics started 3-4m.y. ago, during the Pliocene, and that it is still active (Schindler this volume). Considering this recent phase, Northwestern Anatolia can be divided into three main tectonic units: the North Anatolian Fault Zone (NAFZ), the Anatolian – Aegean extension zone and the Thrace – Black sea block north of the Marmara sea (Fig. 11).

The Thrace – Black sea block

From surface geology, paleomagnetic results, seismicity data and the absence of thermal springs, the Thrace-Black sea block is considered to be a stable unit. Also, space geodetic data are indicative of a non-deforming zone. In fact, all GPS stations along the northern shore of the Marmara sea show negligible motion in a Europe-fixed reference system. This holds also true for the Satellite Laser Ranging station Askites in Thrace, northern Greece, and Yığılca on the Black sea block. Geothermics permits observation of no thermal springs and a normal terrestrial heat flow density field, which is typical for stable continental crust.

The Anatolian – Aegean extension zone

The Anatolian – Aegean extension zone has a longer and more continuous record of activity than the NAFZ, reaching back to the Middle Miocene. As the Geodesy project was restricted to the adjacent regions of the Marmara sea, the amount of southward oriented stretching could only be estimated and the eastern limit of the Anatolian – Aegean extension zone could not be exactly determined. The GPS data indicate progressively increasing N-S extension and bending of the crustal motion to the SW. Furthermore, heat flow density, enhanced thermal spring occurrence and elevated microseismicity indicate strong regional extension tectonics. Helium and carbon isotope signals of geothermal areas have their origin in deeper crustal levels; the ascent of these gases is probably caused by the acting extensional forces.

The North Anatolian Fault Zone

Here we discuss the westward prolongation of the NAFZ between the Mudurnu valley (MV) and the Biga block. This zone is divided into two subzones. As they diverge towards the west, the wedge in between them broadens until the Biga block can be distinguished as a separate unit. In general, it is noted that the orientation of the individual faults plays a major role for the resulting deformation field within the subzones.

The northern zone

The northern zone of the NAFZ is by far the most active unit in the Marmara sea region. This is seen both in the GPS displacement rates (Straub and Kahle this volume) and seismicity (Fig. 1 and 2). Because extension is observed onshore in local and restricted areas only, no elevated heat flow signal could be detected. But it may not be excluded in the offshore area of the deep Marmara sea through. Limited thermal spring occurrence is bound to local extensional basins (e.g., Kuzuluk, Greber this volume). Starting in the east, the northern zone can be divided into the following sections (compare also with Fig. 11):

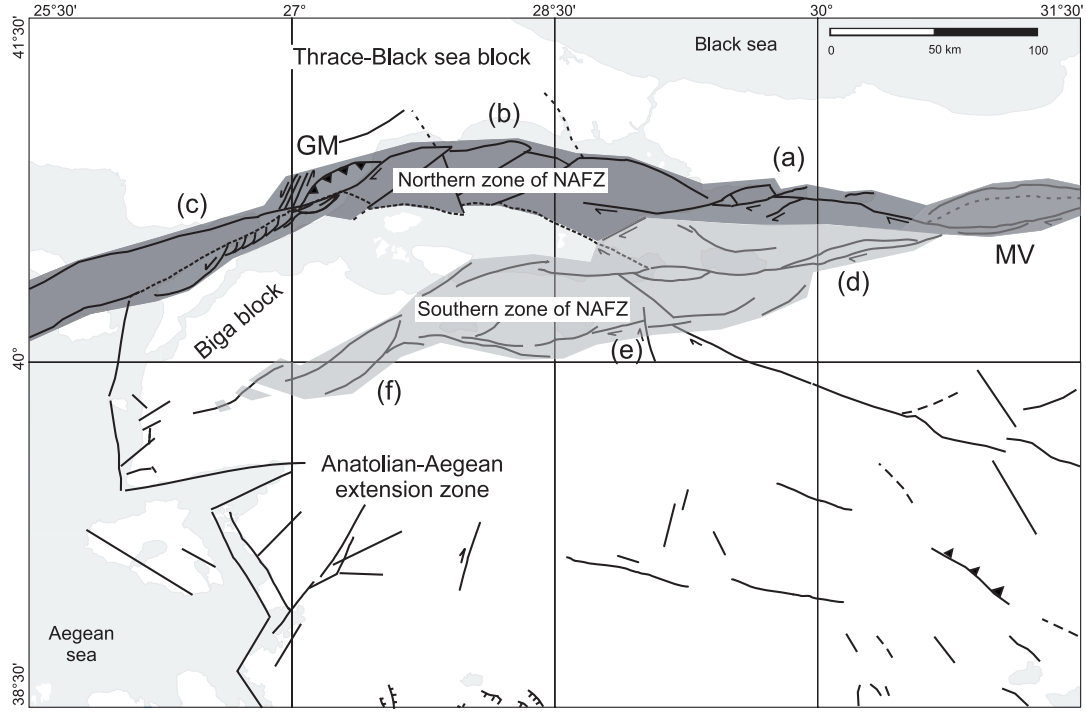


Figure 11: Major definition of tectonic realms in the Marmara sea region. For further discussion see text. (GM: Ganos mountains, MV: Mudurnu valley).

a) From the Mudurnu valley to the region of Gebze around the gulf of İzmit, dextral movements are prevalent in a relatively narrow belt. The total offset is estimated to be 55-60km, which accumulated over the last 3-4m.y. (Schindler this volume). The geodetic displacement rates confirm the strong dextral shear motion along this section with shear rates of almost 20%/m.y. The fault line between the Mudurnu valley and İzmit is associated with slight extension which is also confirmed by earthquake focal mechanisms (Barka, Üçer et al., both this volume). The ENE-WSW oriented faults within the gulf of İzmit are associated with slight compression.

b) The northern zone broadens between Gebze and the Ganos mountains (GM). In this region it forms the trough of the Marmara sea. Here it is bounded by E-W oriented faults (the northern boundary extending from Gebze to the Ganos mountains; the southern boundary extending from the Armutlu peninsula to the Ganos mountains). Furthermore, it is subdivided into several basins transected by dextral NE-SW and sinistral NW-SE oriented faults. This system resembles a pull-apart type extensional stress regime, which has opened a basin with an extent of about 40km during the last 3-4m.y.

c) Southwest of Ganos, the zone narrows again attaining a distinct dextral sense of motion and reaching a total amount of offset of 55-60km. At the same time, it is associated with strong compression which pushed up the Ganos mountains to an altitude of 900m. Near the western end, at the gulf of Saros, the strike-slip type of motion follows mainly the easternmost end of the northern Aegean trough where, finally, the compressional activity changes to extension. The dextral sense of motion with maximum shear strain rates (20%/m.y.) and clear compression has also been identified by the GPS measurements. Barka (this volume, Figure 24) presents a summary of focal solutions of the major earthquakes which occurred during this century in that region. The 1985 event (magnitude 4.4) clearly evidenced compressional forces in the Ganos mountain region, whereas further west in the Saros trough, the 1965 and 1975 events (magnitudes 4.3 and 6.7) revealed extensional components.

The southern zone

The southern zone is less distinct and less active than the northern zone as far as displacements and seismicity are concerned. The amount of 20km of dextral displacement estimated from geologic evidence for the area east of Bursa (Barka, Schindler, both this volume) is mainly attributed to older processes during the Late Miocene. To the west, the displacement diminishes strongly. The GPS deformation rates fully confirm that the southern zone currently is undergoing only minor deformation compared to the strong activity along the northern zone. Nevertheless, large thermal springs occur all over this zone mainly due to the increasing influence of Aegean extension in the south. Primordial helium gas from the mantle was detected in these springs which indicates deep reaching fault zones and extensional forces, too. This southern zone can be divided into the following sections:

d) From geological evidence it is estimated that the dextral displacements between the Mudurnu valley and İznik have not exceeded 5km since the Pliocene. There are indications, however, from GPS observations that the current rate of crustal motion is slightly higher (on the order of 5mm/y). This area is associated with compression rather than extension.

e) The southern zone broadens between İznik and Gönen where dextral movements are mainly associated with extension. The seismicity increases especially in the area between Yalova, Boz Burun (western tip of Armutlu peninsula), Bursa and İnegöl (compare below). The GPS results suggest that this zone is dominated by extension. The shearing process is relatively small. However, along the fault structures west of 29°E, some dextral motion and extension was detected from the GPS measurements and from the fault plane solution of the major earthquake in 1964 east of Kuş gölü (Manyas lake), compare with Figure 1 in Üçer et al. (this volume).

f) Near Gönen, the E-W oriented southern zone turns into a ENE-WSW direction, and the overall dextral motion is associated with compression. The indications of both the dextral shear and compression are corroborated by the GPS data. The strong compression is caused by the distinct change of strike of the fault system from E-W to ENE-WSW around 27.5°E. Further west, the southern zone of the NAFZ is no longer identifiable and disappears near the Aegean coast.

The Armutlu-Bursa area

The features between Yalova, Boz Burun, Bursa and İnegöl are most enigmatic. Thermal spring activity reaches its maximum as far as the southern zone of the NAFZ is concerned. Different structures of dextral type of motion join each other in this region. To the west, the southern margin of the Marmara sea trough rotated anticlockwise by about 5° since the Pliocene around a pole located near the Marmara lake (Schindler this volume). This corresponds to 18km displacement. To the east, shearing deformations are supposed to follow the northern and southern zone of the NAFZ. Between Boz Burun and the region of Bursa, SE-NW oriented dextral movements are assumed to be blocked by an intricate hinge system. South and east of Bursa, a transition is encountered along the dextral S-N running Çekirge fault zone (3-4km since the Pliocene?), the ESE-WNW running Eskişehir fault zone (displacement unknown) and, to the ENE, the southern zone of the NAFZ (displacement less than 5km?). The position of the Armutlu peninsula, located SW of the still active fault connecting Orhangazi with Yalova, is extremely exposed.

The entire area forms the junction between several tectonic elements and is associated with distinct clusters of seismic activity (mostly microseismicity), see Figs. 1 and 2.

The Biga block

On the Biga block, no striking neotectonic features are known and the seismicity is low. This relatively stable zone is associated with a positive Bouguer gravity anomaly (Şimşek, Klingelé and Medici, both this volume). No remarkable thermal spring activity is observed and terrestrial heat flow tends towards normal values of stable continental crust. To the north and south, the Biga block is bounded by two compressional belts ((f) and eastern part of (c)). Going eastward, conditions change to extension (western part of (e) and (b)). The easternmost part of the Biga block lying in between is characterised by a diffuse cluster of frequent microseismicity and a few larger earthquakes (Figs. 1 and 2). The Biga peninsula is densely occupied by GPS sites. Only marginal internal deformation was found. It is suggested that this region is a rather rigid unit. At the present time, almost no data are available for the eastern prolongation of the Biga block mostly hidden below the sea.

We conclude that the limit between the stable Thrace – Black sea block and the northern extension of the NAFZ is relatively sharp and the motion pattern is well defined. North of this limit, seismicity and thermal spring activity are almost lacking, south of this limit, neotectonic activity is well established. The westward motion of the Anatolian block is clearly seen in SLR solutions for the motion of Yozgat and Melengiclik (Robbins et al. 1995) and in extensive GPS networks established by Reilinger et al. (1997) and Straub and Kahle (1995). This average westward motion of the Anatolian plate in the Marmara sea region is 22mm/y relative to the Eurasian plate. West of 27.5°E the motion turns to ENE-WSW. Most of the deformation occurs along the northern zone which passes through the Marmara sea. Further south, around the Biga block and the southern extension zone of the NAFZ, the relative motion is smaller, less expressed and partly combined with differential displacements, such as rotations of smaller blocks.

References

Alptekin, Ö., Ilkisik, O.M., Ezen, Ü. and Ücer, S.B., 1990, Heat flow, Seismicity and the crustal structure of Western Anatolia, International Earth Sciences Congress on Aegean Regions, 1-6 October, İzmir, Turkey.

Ambraseys, N.N. and Finkel, C.F., 1991, Long-term seismicity of İstanbul and of the Marmara sea region, Terra Nova, 3, 527-539.

Balderer, W. and Synal, H.-A., 1996, Application of the chlorine-36 method for the characterisation of the groundwater circulation in tectonically active areas: Examples from North Western Anatolia / Turkey. Terra Nova, 8, 324-333.

Balderer, W., this volume, Mechanisms and processes of groundwater circulation in tectonic active areas.

Barnes, I., Irwin, W.P. and White, D.E., 1978, Global distribution of Carbon Dioxide, discharges and major zones of seismicity, U.S. Geological Survey water resources investigations, Open-File report, 12, 78-79.

Barka, A., this volume, Neotectonics of the Marmara sea region.

Crampin, S. and Evans, R., 1986, Neotectonics of the Marmara sea region of Turkey, Journal of the Geological Society, London, Vol. 143, 343-348.

Dai, J.X., Song, Y., Dai, Ch.S. and Wang, D.R., 1996, Geochemistry and accumulation of carbon dioxide gases in China, AAPG Bulletin, Vol. 80, No. 10, 1615-1626.

Deines, P., 1980, The isotopic composition of reduced organic carbon, in: Handbook of environmental isotope geochemistry 1: The terrestrial environment, edited by: P. Fritz and J.C. Fontes, Elsevier, Amsterdam, 329-406.

Eydoğan, H., 1988, Rates of crustal deformation in Western Turkey as deduced from major earthquakes, Tectonophysics, 148, 83-92.

Eisenlohr, Th., 1995, Die Thermalwässer der Armutlu-Halbinsel (NW-Türkei) und deren Beziehung zu Geologie und aktiver Tektonik, Diss. ETH Zürich Nr. 11340, 165.

Eisenlohr, Th., this volume, The thermal springs of the Armutlu peninsula (NW Turkey) and their relationship to geology and tectonic.

Greber, E., 1992, Das Geothermalfeld von Kuzuluk/Adapazari (NW-Türkei), Geologie, aktive Tektonik, Hydrogeologie, Hydrochemie, Gase und Isotope, Diss. ETH Zürich, Nr. 9984, 213.

Greber, E., 1994, Deep circulation of CO_2-rich palaeowaters in a seismically active zone (Kuzuluk/Adapazarı, Northwestern Turkey), Geothermics, Vol. 23, No. 2, 151-174.

Greber, E., this volume (a), Stratigraphic evolution and tectonics in an area of high seismicity: Akyazı / Adapazarı (Pontides, Northwestern Turkey).

Greber, E., this volume (b), Deep circulation of CO_2-rich palaeowaters in a seismically active zone (Kuzuluk / Adapazarı, Northwestern Turkey).

Greber, E., Pfister, M. and Imbach, Th., this volume, Hydraulic level variations in a thermal water well: Impact of precipitation on the Çekirge thermal water system.

Güleç, N., 1988, Helium-3 distribution in Western Turkey, Mineral Res. Expl. Bull., 108, 35-42.

Gutenberg, B. and Richter, C.F., 1956, Earthquakes, magnitude, energy and acceleration, Bull. Seism. Soc. Am., Vol. 46, 105-145.

Harris, N.B.W., Kelley, S. and Okay, A.I., 1994, Post-collision magmatism and tectonics in Northwest Anatolia, Contrib. Mineral. Petrol., 117, 241-252.

Hill, D.P., 1977, A Model for Earthquake Swarms, Journal of Geophysical Research, Vol. 82, No.8.

Hurtig, E., Cermak, V., Haenel, R. and Zui, V., 1991, Geothermal Atlas of Europe, Hermann Haack Verlagsgesellschaft mbH, Geographisch-Kartographische Anstalt Gotha, Germany, 156, 36 maps.

Imbach, Th., 1992, Thermalwässer von Bursa, geologische und hydrogeologische Untersuchungen am Berg Uludağ (NW-Türkei), Diss. ETH Zürich, Nr. 9988, 178p.

Imbach, Th., 1997, Deep groundwater circulation in the tectonically active area of Bursa, Northwestern Anatolia, Turkey, Geothermics, Vol. 26, No. 2, 251-278.

Imbach, Th., this volume, Geology of Mount Uludağ with emphasis on the genesis of the Bursa thermal waters, Northwestern Anatolia, Turkey.

Irwin, W.P. and Barnes, I., 1980, Tectonic relations of carbon dioxide discharges and earthquakes, JGR, Vol. 85, No. B6, 3115-3121.

Jackson, J.A. and McKenzie, D.P., 1988, The relationship between plate motions and seismic moment tensors, and the rates of active deformation in the Mediterranean and the Middle East, Geophys. J. R. Astr. Soc., 93, 45-73.

Jackson, J.A., Haines, J. and Holt, W., 1994, A comparison of satellite laser ranging and seismicity data in the Aegean region, Geophys. Res. Lett., 21, 2849-2852.

Jeckelmann, Ch., 1996, Genese lokaler Thermalwasservorkommen in der Region Bergama/W-Türkei, Diss. ETH Zürich, Nr. 11990, 199p.

Kiratzi, A., 1993, A study on the active crustal deformation of the North and East Anatolian Fault Zones, Tectonophysics, 225, 191-203.

Kiratzi, A. and Papazachos, C.B., 1995, Active crustal deformation from the Azores triple junction to the Middle East, Tectonophysics, 243, 1-24.

Klingelé, E. and Medici, F., this volume, Gravimetric studies of the Marmara sea region.

Kostrov, V., 1974, Seismic moment and energy of earthquakes, and seismic flow of rock, Izv. Acad. Sci. USSR Phys. Solid Earth, Engl. Transl., 1, 23-44.

Kutas, R.I., Kobalev, V.P. and Tsvyaschenko, V.A., 1996, Heat Flow and Geothermal Model of the Black Sea Depression, 4th International Workshop on Heat Flow and the Structure of the Lithosphere, Trest Castle, Czech Republic, June 9-15.

Lachenbruch, A.H. and Sass, J.H., 1978, Models of extending lithosphere and heat flow in the Basin and Range province, Geological Society of America, Memoir 152, 209-250.

Mamyrin, B.A. and Tolstikhin, L.N., 1984, Helium Isotopes in Nature, Developments in Geochemistry, 3, Elsevier, 273p.

Mercier, J., Sorel, D. and Simeakis, K., 1987, Changes in the state of stress, Ann. Tectonicae, 1, 20-39.

Morgan, P., 1995, Heat Flow in Rifts, in: Continental Rifts: Evolution, Structure, Tectonics, edited by: K.H. Olsen, Developments in Geotectonics, 25, Elsevier.

Morris, A. and Tarling, D.H. (eds), 1996, Paleomagnetism and Tectonics of the Mediterranean Region, Geological Society Special Publication No. 105, 1-18.

Mueller, St., Kahle, H.-G. and Barka, A., this volume, Plate tectonic situation in the Aegean region.

Mützenberg, St., 1991, Westliche Biga Halbinsel (Çanakkale, Türkei): Beziehung zwischen Geologie, Tektonik und Entwicklung der Thermalquellen, Mitteilungen aus dem geologischen Institut der Eidg. Technischen Hochschule und der Universität Zürich, Neue Folge, Nr. 287, 160p.

Mützenberg, St., this volume, Nature and origin of the thermal springs in the Tuzla area, Western Anatolia, Turkey.

Noomen, R., Springer, T., Ambrosius, B., Herzberger, K., Kuijper, D., Mets, G., Overgauauw, B. and Wakker, K, 1996, Crustal deformations in the Mediterranean area computed from SLR and GPS observations, J. of Geodynamics, Vol. 21, 1, 73-96.

Okay, A.I., Şengör, A.M.C. and Görür, N.,1994, Kinematic history of the opening of the Black Sea and its effect on the surrounding regions, Geology, 22, 267-270.

Oral, B., Reilinger, R., Toksöz, M.N., King, R.W., Barka, A., Kınık, İ. and Lenk, O., 1995, Global positioning system offers evidence of plate motions in Eastern Mediterranean, EOS Trans., Vol. 76, 2, 9-10.

Papazachos, C.B. and Kiratzi, A.A., 1996, A detailed study of the active crustal deformation in the Aegean and surrounding area, Tectonophysics, 253, 129-153.

Pfister, M., 1997, Thermalquellen und ihre Beziehung zu Seismizität und aktiver Tektonik in Nordwest Anatolien: Zusätzliche Evidenzen aus Regressionsmodellen, Projektarbeit am Seminar für Statistik ETH Zürich, 13p.

Pfister, M., Rybach, L. and Şimşek, Ş., this volume, Geothermal reconnaissance of the Marmara sea region.

Pollack, H.N., Hurter, S.J. and Johnson, J.R., 1993, Heat Loss from the Earth's Interior: Analysis of the Global Data Set, Reviews of Geophysics, Vol. 31, 3, 267-280.

Reilinger, R., McClusky, S., Oral, B., King, R., Toksöz, M., Barka, A., Kınık, İ., Lenk, O. and Şanlı, İ., 1997, GPS measurements of present-day crustal movements in the Arabia-Africa-Eurasia Plate collision zone, J. Geophys. Res., in press.

Robbins, J., Dunn, P.J., Torrence, M.H. and Smith, D.E., 1995, Deformation in the Eastern Mediterranean, Proceedings of the First Turkish International Symposium on Deformations 1994, edited by M. Sahin and P.A. Cross, 738-745.

Rybach, L. and Buntebarth, 1982, Relationships between the petrophysical properties density, seismic velocity, heat generation, and mineralogical constitution, Earth and Planetary Science Letters, 57, 367-376.

Schindler, C., this volume, Geology of NW Turkey: Results of the MARMARA Poly-Project.

Sellami, S., Pavoni, N., Mayer-Rosa, D., Mueller, St., Aktar, M., Eyidoğan, H., Gürbüz, C., Bariş, Ş and Yalcin, N., this volume, Seismicity and Seismotectonics of the Bursa region.

Sibson, R.H., 1992, Implications of fault-valve behaviour for rupture nucleation and recurrence, Tectonophysics, 211, 283-293.

Straub, Ch., 1996, Recent crustal deformation and strain accumulation in the Marmara sea region, NW-Anatolia, inferred from GPS measurements, Diss. ETH Zürich, Nr. 11614, 123p.

Straub, C. and Kahle, H.-G., 1995, Active crustal deformation in the Marmara Sea region, NW Anatolia, inferred from GPS measurements, Geophysical Research Letters, 22, 18, 2'533-2'536.

Straub, Ch. and Kahle, H.-G., this volume, Recent crustal deformation and strain accumulation in the Marmara sea region, NW Anatolia, inferred from repeated GPS measurements.

Torgersen, Th., 1993, Defining the Role of Magmatism in Extensional Tectonics: Helium 3 Fluxes in Extensional Basins, Journal of Geophysical Research, Vol. 98, No. B9, 16'257-16'269.

Tschudi, S., this volume, Observed pressure variations and their causes in the geothermal field of Kuzuluk / NW Turkey.

Üçer, B., Eyidoğan, H., Gürbüz, C, Barka, A. and Bariş, Ş., this volume, Seismic investigations of the Marmara region.

Vester, F., 1988, Unsere Welt – ein vernetztes System, Deutscher Taschenbuch Verlag, München.

Yalçın, T., this volume, Hydrogeological investigation of the Gönen and Ekşidere thermal waters (NW Turkey).

Yılmaz, Y., this volume, Geology of Western Anatolia.

Zanchi, A. and Angelier, J., 1993, Seismotectonics of western Anatolia: regional stress orientation from geophysical and geological data, Tectonophysics, 222, 259-274.

Index

Numerics
1D-element 234
2D-element 234

A
accelerometer 188
acid to intermediate volcanics 302, 341, 349, 353, 366
active element (interdependence matrix) 552
active faults 63,354, 442, 539
advective heat transfer 504, 510
Aegean extension 352, 364, 433, 443, 556
Airy's isostatic anomaly 489
Aksartepe limestones 146
Almacık lens 156, 336, 350, 353, 366
Altındere detrital series 149
amphibolite metamorphic facies 200, 240, 334, 366
amplitude tide spectra 191
Anatolian - Aegean extension zone 560
ancient formation water 309, 315, 386
andesitic rocks 43, 148, 201, 277, 341, 349
Armutlu (thermal system) 206, 376
Armutlu peninsula 67, 198, 336, 338, 350, 354, 359
Armutlu-Bursa area 562
asthenosphere 19, 559
atmospheric tides 190

B
basal heat flow 22, 529, 549
basic volcanics 43, 201, 241, 334, 341, 349
Bayırköy formation 280
Benioff zone 16
BHT data 507
Biga block 563
Biga peninsula 77, 301, 341, 350, 394, 453
Bilecik limestone 280
block rotation 204, 350, 357
Bouguer correction 488
Bouguer gravity 114, 357, 362, 488
Bouguer model 488
breccias series of Şarkbeynevit 147
brine 311, 375, 385, 394, 405
brittle deformation 203, 334, 369, 418, 553
Büyük Menderes graben 49
Bursa 239

C
cap rock 117, 192
carbon dioxide 336, 378, 402, 554
carbonate dissolution 169, 213, 232, 254
carbon-dioxide discharge 178, 554
Çekirge fault zone 239, 352, 362
Cemalbey fault 157
chemistry of groundwater 37, 113, 129, 135, 166, 211, 248, 281, 305
chlor-36 method 393
Civek zone 153
climate 125, 322
closed circuit deep circulation system 258, 271, 525
CO_2 Water and gases in fault zones 186, 410, 554
cold karstic spring 210, 232, 387, 399, 400
compression phase near limit Miocene - Pliocene 25, 346, 354, 364
conceptual flow model 180, 236, 260, 296, 314
conductive heat transport 168, 513
confined fluids 186
connate water 315
continental climate 322
continental extension 16, 555
continental rift systems 21
convective heat transfer 504, 507, 510
correlation of thermal springs and seismicity 548
Couches Rouges 146, 201, 337, 339
coupled transport processes 234, 523, 546, 553
crustal and upper mantle structure 5, 18, 20, 55, 90, 497, 499
crustal deformation rates 435
crustal radioactive heat production 548
crustal strain 544

D
Dağdibi clastic series 145
Darcy flow 234, 522
Dardanelles peninsula 62, 72, 340, 344, 347, 357
deep groundwater circulation 2, 31, 180, 236, 295, 385, 411, 553, 554
deformation analysis (geodetic) 104, 438
density of strain energy 442
deuterium 172, 215, 232, 250, 287, 311, 323, 381
diagenetic processes 309, 314
diffusion 523, 556
dilution/evaporation 307
dissolution of rock minerals 169, 211, 231, 254, 282, 309, 377, 397
dissolved gases 178, 218, 256, 312, 378, 554
ductile deformation 202, 418, 555

E
early Alpine tectonics 155, 202, 338
Earth tides 190
Earth's mantle 178, 218, 312
earthquake activity 13, 21, 47, 63, 89, 418, 449
earthquake clustering 90, 462, 550
electroneutrality 169
ellipsoid 488
Eocene and Oligocene sediments 39, 146, 201, 339, 341
epicenter 15, 71, 79, 94, 97, 418, 463, 468, 498, 542
Eskişehir fault zone 15, 352, 362, 366, 476
evaporites 201, 340, 346, 385

exhalation crust 304
exploration well (geothermal) 117, 505

F
ferromanganese crust 307
finite Element 234, 523
finite-Difference 523
flysch 153, 201, 334, 366, 370
focal mechanism 17, 57, 67, 74, 76, 89, 450, 474
formation specific origin 385
fossil groundwater 180, 314, 385
FRACTure 234
free-air correction 488
frequency (spectral) 191, 478

G
Ganos fault and environment 72, 339, 351, 354
gas analyses 186, 214, 249, 258, 378, 396, 410
gas bubbles 166, 191, 194
gases from crust and mantle 179, 218, 256, 312, 546, 554
gauge 267
gauge change curve 269
Gediz graben 49
Gemlik 67, 206, 353, 361
geochemical modelling 282
geoelectrical studies 116
geological events time table 331
geostatistical method 516
geothermal area 112, 114, 504, 546
geothermal energy 111, 112, 117, 305, 504
geothermometer 176, 213, 258, 309, 397, 547
Global Positioning System 23, 420
Gönen 275, 336, 349, 377
GPS (campaigns, network) 23, 420
gravity data 116, 355, 362, 487, 545
greenschist metamorphic sequence 36, 143, 200, 241, 334, 361
gulf of Saros 15, 72, 93, 357, 364

H
Haraklı fault 156
heat flow density 22, 504, 516, 543, 547, 549
heat transport 168, 235, 252, 260, 504, 507, 510, 522, 527
heated line source 507
helium 21, 167, 218, 252, 312, 397, 546
Hellenic arc 13
high frequency trembling 189
high frequency variations 189
high resolution temperature logging 505
historical seismicity 3, 69, 91, 444
hydraulic conductivity 235
hydraulic dispersion 234
hydraulic level change behaviour 268, 272
hydrochemical evolution 165, 211, 249, 282, 305, 309
hydrogeologic map of NW Turkey 128
hydrogeological circulation model 180, 220, 229, 252, 257, 295, 314, 402, 527
hydrology of NW Turkey 126
hydrolysis of silicates 258, 377
hydrothermal precipitation 214, 232, 259, 282, 304, 307
hydrothermal system of Kuzuluk 189
hydrothermal valve 192, 194
hypocenter 21, 464

I
ignimbrite 302, 341, 349
infiltration area 179, 220, 229, 248, 258, 280, 323
interaction 551
interdependence matrix 551
Intrapontide suture 32, 143, 198, 336, 338, 366, 370
inversion procedure 499
isotope analysis 173, 215, 233, 253, 287, 323, 385, 546
İstanbul zone 143
İzmir-Ankara suture zone 39, 338
İznik metamorphics 37, 336, 366

J
joint system 193, 204, 272

K
Karakaya complex 31, 241, 277, 336, 369
karstic phenomenas 206, 230, 234, 248, 272, 342, 526
Kazdağ group 280
Keremali mountains 158
Kestanbol thermal system 301, 377
key observable quantities 539
kinematic fault plane solutions 16, 57, 67, 74, 76, 89, 456, 473, 474
kinematic field 23, 435
kriging interpolation 516
Kükürtlü thermal system 239, 376
Kuzuluk thermal system 162, 376
Kuzuluk basin 150, 157, 164
Kuzuluk series 150

L
laminar flow groundwater 528
Late Alpine compressive tectonics 40 135, 343, 366
Late Cretaceous metamorphism 39, 201, 339
lithosphere 18, 557
lithosphere-asthenosphere system 18, 549, 555
low-temperature thermal field 165

M
magmatic rocks 43, 341, 349
main-Alpine tectonics 40, 155, 343, 360
mantle 18, 252, 499, 545, 548
mantle helium 21, 167, 218, 252, 312, 397, 546
mantle-crust interaction 312, 499, 545, 548
marine late Tertiary sediments 43, 60, 80, 345, 352, 386
Marmara and Aegean sea

age 60, 345, 352, 364
Marmara sea trough 55, 78, 355, 360
mass balance equation 521
mechanical dispersion 523
mechanical properties 192, 438, 555
Menderes massif 39
metamorphic rocks 31, 143, 198, 240, 277, 302, 334, 336, 366
meteoric waterline 322
meteorological event 194
microgeodetic network 102
mineral water 115, 164, 214, 383, 405
molecule diffusion 523
Mount Uludağ 7, 33, 239, 334, 341, 361, 449, 524
Mudurnu fault 70, 90, 141, 155
Mudurnu river bend 153

N
NAFZ east of Kuzuluk 155, 353, 364, 442
NAFZ northern zone 63, 72, 78,203, 364, 370, 442
NAFZ southern zone 9, 77, 67, 203, 243, 279, 353, 370, 442
Neo (alpine) tectonics 14, 55, 101, 155, 203, 243, 279, 304, 351, 362, 368, 435, 442, 539, 542, 560
Neogene 41, 60, 150, 202, 241, 277, 302, 345, 357, 362
neon 167, 218
neotectonic events and deformation time table 364
Neotethys 47, 338, 368
numerical model of groundwater circulation 234, 321
Nummulitic limestones 149, 339

O
Orhangazi (thermal system) 67, 206

P
paleo-Alpine tectonics 155, 202, 338
Paleocene sediments 39, 146, 337
paleoclimatic effect 517
paleogeographic reconstruction for Middle Miocene 60, 361, 366
paleomagnetic data 350
paleo-stress field 204, 338, 343, 366
paleotectonics 31, 39, 47, 241, 335, 338, 343, 366
paleowater 174, 280, 296, 314, 385
Pazarköy series 145
Peclet number analysis 292, 504, 513
Permian unconformity and sediments 33, 241, 302, 334
physical transport mechanism 234
physical water characteristics 248
piston flow model 216
plate tectonics 13, 31, 368, 561
plutons 43, 153, 201, 240, 302, 334, 341, 365, 555
potential of large earthquakes 81, 97
precipitation 125, 191
premordial helium 21, 167, 218, 252, 312, 397, 546
pressure field 271, 272, 438
pull-apart structure 57, 59, 97

R
radioactive decay 234, 523
radiogenic isotope 174, 216, 234, 255, 291, 313, 325, 388, 555
radon variations 190
reactive element 552
Recent seismicity 13, 55, 89, 279, 407, 417, 449, 540
relations paleotectonics / neotectonics 349, 369
repeat time of large earthquakes 72
reservoir rock 176, 315
reservoir temperature 176, 216, 258, 296, 309, 397, 525, 546
residence time 180, 258, 272, 296, 314, 387, 524, 546
resistivity survey 120
Reynolds number 528
Riedel-fault 204
rock thermal conductivity 504
rock-water interaction 171, 206, 254, 315, 377, 397
rotation of NW Anatolia 18, 25, 359, 369

S
Sakarya continent 31, 143, 198, 352
saline brine 311, 375, 385, 394, 405
sea ridge in Marmara sea 78
seasonal influence on groundwater 192, 325
secondary porosity (karstic) 272
seismic energy 95, 454, 550
seismic gap 81, 97
seismic moment 438
seismic velocities 90, 458
seismicity 13, 47, 63, 89, 178, 418, 444
semiarid climate 125, 322
semivariance analysis 516
Serravallian transgression 345, 356
shear stress 440
short closed circulation system 258, 271, 525
short-term fluctuations 406
simple stretching 555
single regression 550
skarn 302, 342
slip rate 65
stable isotopes 166, 215, 232, 258, 285, 311, 381
stable lithosphere 559
strain analysis 93, 104, 438, 454
stress analysis 24, 438
stretched lithosphere 558
sulphur isotope 175, 217, 311, 385
surface heat flow density 22, 504, 516, 543, 547, 549
synthesis 539

T
Tauride Anatolide platform 31, 47
terrestrial heat flow density 22, 509
thermal boundary condition 530
thermal conductivity 505, 508
Thermal profile of the lithosphere 558
thermal spring distribution 115, 504, 543
thermal spring energy 550
thermal springs start of activity 165, 307, 352, 353,
thermal water evolution 165, 220, 258, 307
thermal water well 112, 117, 267, 507, 515
Thrace - Black sea block 560
Thrace basin 331, 340, 350, 368
tomography (seismic) 19
transient tritium transport 234, 527
transport of groundwater 180, 234, 260, 292, 314, 509, 521
transport of heat 5, 168, 235, 25, 260, 504, 507, 510, 522
travertine 245, 304
tritium 167, 216, 231, 257, 311, 323, 387
Troas 301
troposphere parameters 427
turbulent flow groundwater 528
Tuzla 301, 352, 377

U
Uludağ 7, 33, 239, 334, 342, 348, 361, 449, 524
underplating 555
unmetamorphic mesozoic sediments 36, 277, 336
uplift / erosion Late Oligocene / Early Miocene 368
upper crust levels 553
use of thermal water 111, 117, 179, 259, 275, 296

V
volume dilatation 550

W
water chemistry 113, 123, 135, 166, 211, 248, 281, 305, 377
water-gas interaction 180, 191, 215, 258, 378, 402, 553
water-rock interaction 171, 206, 254, 315, 377, 397
well pressure analysis 188

Y
Yalova 66, 206, 345, 353, 354
Yeniköy siltstone series 147

Main contributors and authors:

Name	Institution	Adress	e-mail
Prof. Dr. A. Aksoy	İnşaat Fakültesi İTÜ	İTÜ Ayazağa Kampüsü TR-80626 Maslak, İstanbul	aksoy@ sariyer.cc.itu.edu.tr
Prof. Dr. M. Aktar	TÜBİTAK Research Centre	TÜBİTAK Marmara Araştirma Merkezi, PK 21 TR-4170 Gebze Kocaeli	aktar@mam.gov.tr
PD Dr. W. Balderer	Engineering Geology ETH Zürich	ETH Hönggerberg CH-8093 Zürich	balderer@ erdw.ethz.ch
Dr. Ş. Bariş	Kandilli Rasathanesi ve Deprem Araştirma Enstitüsü	Boğaziçi Üniversitesi TR-Çengelköy, İstanbul	baris@ hamlin.cc.boun.edu.tr
Prof. Dr. A. Barka	Maden Fakültesi İTÜ	İTÜ Ayazağa Kampüsü TR-80626 Maslak, İstanbul	barka@ sariyer.cc.itu.edu.tr
Dr. R. Deniz	İnşaat Fakültesi İTÜ	İTÜ Ayazağa Kampüsü TR-80626 Maslak, İstanbul	
Dr. Th. Eisenlohr	H. Jäckli AG Zürich, Switzerland	Bettenstr. 44 (private) CH-8400 Winterthur	
Prof. Dr. H. Eyidoğan	Jeofizik Mühendisliği Bölümü İTÜ	İTÜ Ayazağa Kampüsü TR-80626 Maslak, İstanbul	mdeyido@ cc.itu.edu.tr
Dr. E. Greber	Geoform Winterthur, Switzerland	Dienerstr. 36 (private) CH-8004 Zürich	
Prof. Dr. C. Gürbüz	Kandilli Rasathanesi ve Deprem Arastirma Enstitüsü	Boğaziçi Üniversitesi TR-Çengelköy, İstanbul	gurbuz@ hamlin.cc.boun. edu.tr
Dr. Ch. Jeckelmann	CSD Aarau, Switzerland	Hönggerstr. 41 (private) CH-8037 Zürich	
Dr. Th. Imbach	H. Jäckli AG Zürich, Switzerland	Limmatstr. 211 (private) CH-8005 Zürich	101744.2744@ com-puserve.com
Prof. Dr. H.-G. Kahle	Institute of Geodesy ETH Zürich	ETH Hönggerberg CH-8093 Zürich	hans-gert.kahle@ geod. ethz.ch
Prof. Dr. E. Klingelé	Institute of Geophysics ETH Zürich	ETH Hönggerberg CH-8093 Zürich	emile.klingele@ geod.ethz.ch
Dr. D. Mayer-Rosa	Institute of Geophysics ETH Zürich	ETH Hönggerberg CH-8093 Zürich	mayer-rosa@ seismo.ifg. ethz.ch
Prof. Dr. St. Mueller †	Institute of Geophysics ETH Zürich	Frohburgstr. 138 (private) CH-8057 Zürich	
Dr. St. Mützenberg	H. Jäckli AG Zürich, Switzerland	Pfaffenzielstr. 16 (private) CH-5300 Ennetturgi	
Dr. N. Pavoni	Institute of Geophysics ETH Zürich	Sonnenbergstr. 11 (private) CH-8134 Adliswil	
Dr. M. Pfister	GSF München, Insitute of Hydrology	Palmstrasse 4 (private) D-80496 München	martin.pfister@gsf.de
Prof. Dr. L. Rybach	Institute of Geophysics ETH Zürich	ETH Hönggerberg CH-8093 Zürich	rybach@ geo.phys.ethz.ch
Prof. Dr. C. Schindler	Engineering Geology ETH Zürich	Schwerzestr. 7 (private) CH-8616 Oetwil am See	
Dr. S. Sellami	Institute of Geophysics ETH Zürich	ETH Hönggerberg CH-8093 Zürich	sellami@ seismo.ifg.ethz.ch
Dr. Ch. Straub	Institute of Geodesy ETH Zürich	Weihermattstr. 3 (private) CH-8902 Urdorf	christian_straub@union-re.com

Errata

Figure 10 on page 518 should be replaced by this figure:

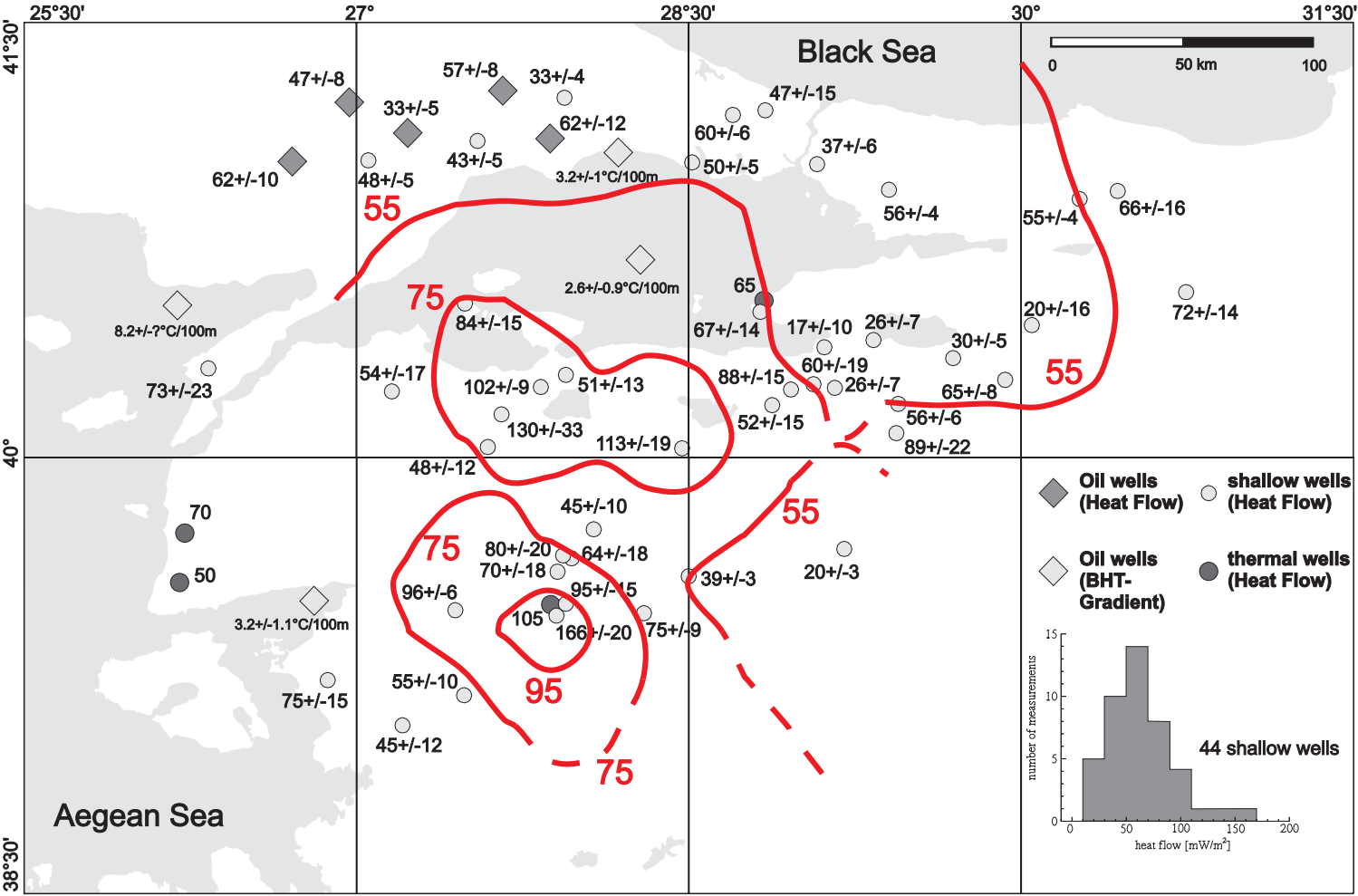


Figure 10: Compilation of geothermal data of the Marmara sea region